Downloaded From : www.EasyEngineering.net

SECOND EDITION

PAVEMENT ANALYSIS AND DESIGN



YANG H. HUANG

Downloaded From : www.EasyEngineering.net

Downloaded From : www.EasyEngineering.net



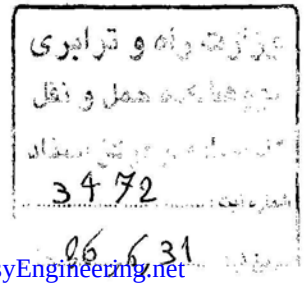
Pavement Analysis and Design

Second Edition

Yang H. Huang
University of Kentucky

PEARSON
Prentice Hall

Upper Saddle River, NJ 07458



Downloaded From : www.EasyEngineering.net

Downloaded From : www.EasyEngineering.net

Library of Congress Cataloging-in-Publication Data Available

Vice President and Editorial Director, ECS: *Marcia Horton*
Acquisitions Editor: *Laura Fischer*
Editorial Assistant: *Andrea Messineo*
Vice President and Director of Production and Manufacturing, ESM: *David W. Riccardi*
Executive Managing Editor: *Vince O'Brien*
Managing Editor: *David A. George*
Production Editor: *Rose Kernan*
Director of Creative Services: *Paul Belfanti*
Creative Director: *Carole Anson*
Art Director: *Jayne Conte*
Art Editor: *Gregory Dulles*
Cover Designer: *Bruce Kenselaar*
Manufacturing Manager: *Trudy Pisciotti*
Manufacturing Buyer: *Lisa McDowell*
Marketing Manager: *Holly Stark*



2004 by Pearson Education, Inc.
Pearson Prentice Hall
Pearson Education, Inc.
Upper Saddle River, NJ 07458

All rights reserved. No part of this book may be reproduced in any form or by any means, without permission in writing from the publisher.

Pearson Prentice Hall® is a trademark of Pearson Education, Inc.

The author and publisher of this book have used their best efforts in preparing this book. These efforts include the development, research, and testing of the theories and programs to determine their effectiveness. The author and publisher make no warranty of any kind, expressed or implied, with regard to these programs or the documentation contained in this book. The author and publisher shall not be liable in any event for incidental or consequential damages in connection with, or arising out of, the furnishing, performance, or use of these programs.

Printed in the United States of America

10 9 8 7 6 5

ISBN 0-13-142473-4

Pearson Education Ltd., *London*
Pearson Education Australia Pty. Ltd., *Sydney*
Pearson Education Singapore, Pte. Ltd.
Pearson Education North Asia Ltd., *Hong Kong*
Pearson Education Canada, Inc., *Toronto*
Pearson Educación de Mexico, S.A. de C.V.
Pearson Education—Japan, *Tokyo*
Pearson Education Malaysia, Pte. Ltd.
Pearson Education, Inc., *Upper Saddle River, New Jersey*

Downloaded From : www.EasyEngineering.net

Downloaded From : www.EasyEngineering.net

Contents

Preface to Second Edition ix
Preface to First Edition xi

CHAPTER 1 Introduction 1

1.1 Historical Developments 1
1.2 Pavement Types 8
1.3 Road Tests 19
1.4 Design Factors 26
1.5 Highway Pavements, Airport Pavements, and Railroad Trackbeds 37
Summary 41
Problems and Questions 43

CHAPTER 2 Stresses and Strains in Flexible Pavements 45

2.1 Homogeneous Mass 45
2.2 Layered Systems 57
2.3 Viscoelastic Solutions 76
Summary 89
Problems 90

CHAPTER 3 KENLAYER Computer Program 94

3.1 Theoretical Developments 94
3.2 Program Description 106
3.3 Comparison with Available Solutions 109
3.4 Sensitivity Analysis 130
Summary 141
Problems 143

CHAPTER 4 Stresses and Deflections in Rigid Pavements 147

4.1 Stresses Due to Curling 147
4.2 Stresses and Deflections Due to Loading 153

Downloaded From : www.EasyEngineering.net

Downloaded From : www.EasyEngineering.net

4.3	Stresses Due to Friction	164
4.4	Design of Dowels and Joints	171
	Summary	180
	Problems	182

CHAPTER 5 KENSLABS Computer Program **186**

5.1	Theoretical Developments	186
5.2	Program Description	206
5.3	Comparison with Available Solutions	213
5.4	Sensitivity Analysis	226
	Summary	234
	Problems	236

CHAPTER 6 Traffic Loading and Volume **244**

6.1	Design Procedures	244
6.2	Equivalent Single-Wheel Load	245
6.3	Equivalent Axle Load Factor	256
6.4	Traffic Analysis	265
	Summary	275
	Problems	276

CHAPTER 7 Material Characterization **279**

7.1	Resilient Modulus	279
7.2	Dynamic Modulus of Bituminous Mixtures	297
7.3	Fatigue Characteristics	309
7.4	Permanent Deformation Parameters	316
7.5	Other Properties	326
	Summary	330
	Problems	331

CHAPTER 8 Drainage Design **334**

8.1	General Consideration	334
8.2	Drainage Materials	340
8.3	Design Procedures	351
	Summary	365
	Problems	366

CHAPTER 9 Pavement Performance **368**

9.1	Distress	368
9.2	Serviceability	388
9.3	Surface Friction	401

Downloaded From : www.EasyEngineering.net

Downloaded From : www.EasyEngineering.net

	9.4	Nondestructive Deflection Testing	410
	9.5	Pavement Performance	424
		Summary	436
		Problems	438
CHAPTER 10	**Reliability**		**441**
	10.1	Statistical Concepts	441
	10.2	Probabilistic Methods	451
	10.3	Variability	460
	10.4	Rosenblueth Method	466
		Summary	469
		Problems	470
CHAPTER 11	**Flexible Pavement Design**		**472**
	11.1	Calibrated Mechanistic Design Procedure	472
	11.2	Asphalt Institute Method	487
	11.3	AASHTO Method	505
	11.4	Design of Flexible Pavement Shoulders	522
		Summary	528
		Problems	530
CHAPTER 12	**Rigid Pavement Design**		**533**
	12.1	Calibrated Mechanistic Design Procedure	533
	12.2	Portland Cement Association Method	545
	12.3	AASHTO Method	568
	12.4	Continuous Reinforced Concrete Pavements	583
	12.5	Design of Rigid Pavement Shoulders	592
		Summary	596
		Problems	598
CHAPTER 13	**Design of Overlays**		**600**
	13.1	Types of Overlays	600
	13.2	Design Methodologies	605
	13.3	Asphalt Institute Method	608
	13.4	Portland Cement Association Method	620
	13.5	AASHTO Method	627
		Summary	650
		Problems	652
APPENDIX A	**Theory of Viscoelasticity**		**655**
	A.1	Differential Operators	655
	A.2	Elastic–Viscoelastic Correspondence Principle	657

Downloaded From : www.EasyEngineering.net

Downloaded From : www.EasyEngineering.net

	A.3	Method of Successive Residuals	662
	A.4	Complex Modulus	666
APPENDIX B	**Theory of Elastic Layer Systems**		**671**
	B.1	Differential Equations	671
	B.2	Circular Loaded Area	673
	B.3	Boundary and Continuity Conditions	674
	B.4	Extension to Concentrated Load	676
APPENDIX C	**KENPAVE Software**		**677**
	C.1	Software Installation	677
	C.2	Main Screen	678
	C.3	LAYERINP	679
	C.4	SLABSINP	681
APPENDIX D	**An Introduction to Superpave**		**682**
	D.1	Asphalt Binder Grading System	682
	D.2	Aggregates in HMA	684
	D.3	Asphalt Mix Design	689
		Summary	692
		Problems	693
APPENDIX E	**Pavement Management Systems**		**694**
	E.1	PMS Activity Levels	694
	E.2	Network-Level Elements	695
	E.3	Project-Level Elements	700
	E.4	Life-Cycle Cost Analysis	703
	E.5	PMS Data and Software	711
	E.6	Infrastructure and Asset Management	713
	E.7	Pavement Preservation	714
		Summary	714
		Problems	714
APPENDIX F	**A Preview of 2002 Design Guide**		**716**
	F.1	General Features	716
	F.2	Design inputs	717
	F.3	Distress Prediction Models	722
		Summary	727
APPENDIX G	**List of Symbols**		**728**
APPENDIX H	**References**		**741**
Author Index			**761**
Subject Index			**767**

Downloaded From : www.EasyEngineering.net

Downloaded From : www.EasyEngineering.net

Preface to Second Edition

The first edition of *Pavement Analysis and Design* was published in 1993. The widespread adoption of this book by so many colleges as an undergraduate or graduate text has encouraged me to write this second edition. A major event during the past decade was the completion of the Strategic Highway Research Program (SHRP), which led to the development of the highly publicized 2002 Pavement Design Guide. However, at the time of this writing, the final draft of the 2002 Guide is still not available. It will likely be a few more years before the Guide is approved and implemented by the American Association of State Highway and Transportation Officials (AASHTO). For this reason, only a brief preview of the 2002 Pavement Design Guide is presented, in an appendix.

Other than those improvements in the computer programs that necessitate changes in the text, not much is changed in the theoretical part of this book. Although new procedures were developed by SHRP for material characterization and pavement evaluation, these procedures, such as Superpave, are still in the developmental stage and will be subject to change as more experience is gained in their use. In this second edition, Superpave is presented in an appendix. To extend the usefulness of the book, a new appendix on Pavement Management System is added. It is hoped that a more extensive revision will be made in the third edition, after the 2002 Pavement Design Guide is fully implemented and all the testing and evaluation procedures are finalized. Major changes made in this edition are the following:

1. The floppy disk containing the four DOS programs is replaced by a CD containing a Windows program called KENPAVE, which combines the original KENLAYER, LAYERINP, KENSLABS, and SLABSINP into a single package, together with the addition of some computer graphics. The software was written in Microsoft Visual Basic 6.0 and can be run on any computer with Windows 95 or higher. Detailed instructions on the use of KENPAVE can be found in the software program.
2. Section 13.5 on the AASHTO method of overlay design has been totally revised. The 1986 AASHTO Design Guide was used in the first edition. The guide was revised in 1993 with practically no change in the design of new pavements, but the design of overlay was completely rewritten.
3. New developments and information from the literature have been added to keep the book current. A new method based on the Mohr–Coulomb failure criterion

Downloaded From : www.EasyEngineering.net

Downloaded From : www.EasyEngineering.net

has been added in KENLAYER for nonlinear analysis, and new comparisons are made between KENLAYER and the latest Windows version of MICH-PAVE.

4. Three new appendices have been added: Appendix D—An Introduction to Superpave; Appendix E—Pavement Management Systems; and Appendix F—A Preview of 2002 Design Guide. Appendix C is combined with Appendix B; a new Appendix C contains a brief description of KENPAVE.
5. To provide room for the above additions, Sections 3.4.3 (on contained rock asphalt mats) and 10.5 (on probabilistic computer programs) have been deleted. Also deleted from the appendices are the description of the input programs and the programming details of KENLAYER and KENSLABS, such as subroutines and flowcharts. The description of input and output parameters in Chapters 3 and 5 and the illustrative examples in the appendices also have been removed, because they can now be found in the software program.

I wish to acknowledge gratefully the contribution of my colleague, Dr. Kamyar C. Mahboub, who wrote the appendices on Superpave and Pavement Management Systems. These new additions broaden the scope of this book and make it more suitable for a wider audience. I also want to offer my heartfelt thanks to AASHTO, the Transportation Research Board, the Federal Highway Administration, the Asphalt Institute, the Portland Cement Associations, and many others who have permitted the use of the information they developed. Finally, I would like to thank my wife Jane for her support in the use of our retirement time on this book.

YANG H. HUANG, Sc. D., P. E.
Professor Emeritus of Civil Engineering
University of Kentucky

Apprise Education, Reprise Innovations

Downloaded From : www.EasyEngineering.net

Downloaded From : www.EasyEngineering.net

Preface to First Edition

During the past two decades, I have been teaching a course on pavement analysis and design to both seniors and graduate students at the University of Kentucky. I had difficulty finding a suitable textbook for the course because very few are available. There are at least two reasons that a professor does not like to write a textbook on pavement analysis and design. First, the subject is very broad. It covers both highway and airport pavements and involves analysis, design, performance, evaluation, maintenance, rehabilitation, and management. It is difficult, if not impossible, to cover all these topics in sufficient detail to serve as a textbook with enough illustrative examples and homework problems for the students. Second, empirical methods have been used most frequently for pavement analysis and design, and a book based on empirical procedures becomes out of date within a short time. No one is willing to write a book with such a short life. Because of the above difficulties, I have written this book as an alternative. I have limited the content to the structural analysis and design of highway pavements and covered essentially the mechanistic–empirical design procedures rather than the purely empirical methods.

To facilitate the teaching of mechanistic–empirical methods, I have included two computer programs that I developed for pavement analysis and design. These programs have been used by my students for more than ten years and have been constantly updated and improved. They are original and contain salient features not available elsewhere. For example, the KENLAYER program for flexible pavements can be applied to a multilayered system under stationary or moving multiple wheel loads with each layer being either linear elastic, nonlinear elastic, or viscoelastic. The KENSLABS program for rigid pavements can be applied to multiple slabs fully or partially supported on a liquid, solid, or layered foundation with moment or shear transfer across the joints. Both programs can perform damage analysis by dividing a year into a number of periods, each having a different set of material properties and subjected to varying repetitions of different axle loads. These programs were originally written for an IBM mainframe, but were later adapted to an IBM-PC and can be run by using the disk provided with this book.

In addition to the documentation of the computer programs, this book presents the theory of pavement design and reviews the methods developed by several organizations, such as the American Association of State Highway and Transportation Officials (AASHTO), the Asphalt Institute (AI), and the Portland Cement Association (PCA). Because most of the advanced theory and detailed information are presented

Downloaded From : www.EasyEngineering.net

Downloaded From : www.EasyEngineering.net

in the appendices, the book can be used as a text either for an undergraduate course (by skipping the appendices) or for an advanced or graduate course (by including them). Although this book covers only the analysis and design of highway pavements, the same principles can be applied to airport pavements and railroad trackbeds.

This book is divided into 13 chapters. Chapter 1 introduces the historical development of pavement design, the major road tests, the various design factors, and the differences in design concepts among highway pavements, airport pavements, and railroad trackbeds. Chapter 2 discusses stresses and strains in flexible pavements, including the analysis of homogeneous mass and layered systems composed of linear elastic, nonlinear elastic, and linear viscoelastic materials. Simplified charts and tables for determining stresses and strains are also presented. Chapter 3 presents the KENLAYER computer program, based on Burmister's layered theory, including theoretical developments, program description, comparison with available solutions, and sensitivity analysis on the effect of various factors on pavement responses. Chapter 4 discusses stresses and deflections in rigid pavements due to curling, loading, and friction, plus the design of dowels and joints. Influence charts for determining stresses and deflections are also presented. Chapter 5 presents the KENSLABS computer program, based on the finite-element method, including theoretical developments, program description, comparison with available solutions, and sensitivity analysis. Chapter 6 discusses the concept of equivalent single-wheel and single-axle loads and the prediction of traffic. Chapter 7 describes the material characterization for mechanistic–empirical methods of pavement design, including the determination of resilient modulus, of fatigue and permanent deformation properties, and of the modulus of subgrade reaction. Their correlations with other empirical tests are also presented. Chapter 8 outlines the subdrainage design, including general principles, drainage materials, and design procedures. Chapter 9 discusses pavement performance, including distress, serviceability, skid resistance, nondestructive testing, and the evaluation of pavement performance. Chapter 10 illustrates the reliability concept of pavement design in which the variabilities of traffic, material, and geometric parameters are all taken into consideration. A simple and powerful probabilistic procedure, originally developed by Rosenblueth, is described, and two probabilistic computer programs—VESYS (for flexible pavements) and PMRPD (for rigid pavements)—are discussed. Chapter 11 outlines an idealistic mechanistic method of flexible pavement design and presents in detail the Asphalt Institute method and the AASHTO method, plus the design of flexible pavement shoulders. Chapter 12 outlines an idealistic mechanistic method of rigid pavement design and presents in detail the Portland Cement Association method and the AASHTO method. The design of continuous reinforced concrete pavements and rigid pavement shoulders is also included. Chapter 13 outlines methods of design of overlays on both flexible and rigid pavements, including the AASHTO, the AI, and the PCA procedures. More advanced theory and detailed information related to some of the chapters, plus a list of symbols and references, are included in the appendices.

Other than the empirical AASHTO methods used by many state highway departments, this book emphasizes principally the mechanistic-empirical method of design. With the availability of personal computers and of sophisticated methods of material testing, the trend toward mechanistic–empirical methods is quite apparent. It is believed that a book based on mechanistic–empirical methods is more interesting

Downloaded From : www.EasyEngineering.net

Downloaded From : www.EasyEngineering.net

and challenging than one based on empirical methods. This book, with the accompanying computer programs and the large number of illustrative examples, will serve as a classroom text and useful reference for people interested in learning about the structural analysis and design of highway pavements.

Although considerable portions of the materials presented in this book were developed by myself through years of research, teaching, and engineering practice, much information was obtained from the published literature. Grateful acknowledgment is offered to AASHTO, the Asphalt Institute, the Federal Highway Administration, the Portland Cement Association, the Transportation Research Board, and many other organizations and individuals that have permitted me to use the information they developed. The many helpful comments by James Lai, Professor of Civil Engineering, Georgia Institute of Technology, are highly appreciated.

YANG H. HUANG, Sc. D., P. E.
Professor of Civil Engineering
University of Kentucky

Downloaded From : www.EasyEngineering.net

Downloaded From : www.EasyEngineering.net

CHAPTER 1

Introduction

1.1 HISTORICAL DEVELOPMENTS

Although pavement design has gradually evolved from art to science, empiricism still plays an important role even up to the present day. Prior to the early 1920s, the thickness of pavement was based purely on experience. The same thickness was used for a section of highway even though widely different soils were encountered. As experience was gained throughout the years, various methods were developed by different agencies for determining the thickness of pavement required. It is neither feasible nor desirable to document all the methods that have been used so far. Only a few typical methods will be cited to indicate the trend.

Some technical terms will be used in this introductory and review chapter. It is presumed that the students using this book as a text are seniors or graduate students who have taken courses in transportation engineering, civil engineering materials, and soil mechanics and are familiar with these terms. In case this is not true, these terms can be ignored for the time being, because most are explained and clarified in later chapters.

1.1.1 Flexible Pavements

Flexible pavements are constructed of bituminous and granular materials. The first asphalt roadway in the United States was constructed in 1870 at Newark, New Jersey. The first sheet-asphalt pavement, which is a hot mixture of asphalt cement with clean, angular, graded sand and mineral filler, was laid in 1876 on Pennsylvania Avenue in Washington, D.C., with imported asphalt from Trinidad Lake. As of 2001 (FHWA, 2001), there are about 2.5 million miles of paved roads in the United States, of which 94% are asphalt surfaced.

Design Methods Methods of flexible pavement design can be classified into five categories: empirical method with or without a soil strength test, limiting shear failure method, limiting deflection method, regression method based on pavement performance or road test, and mechanistic–empirical method.

Downloaded From : www.EasyEngineering.net

Downloaded From : www.EasyEngineering.net

Empirical Methods The use of the empirical method without a strength test dates back to the development of the Public Roads (PR) soil classification system (Hogentogler and Terzaghi, 1929), in which the subgrade was classified as uniform from A-1 to A-8 and nonuniform from B-1 to B-3. The PR system was later modified by the Highway Research Board (HRB, 1945), in which soils were grouped from A-1 to A-7 and a group index was added to differentiate the soil within each group. Steele (1945) discussed the application of HRB classification and group index in estimating the subbase and total pavement thickness without a strength test. The empirical method with a strength test was first used by the California Highway Department in 1929 (Porter, 1950). The thickness of pavements was related to the California Bearing Ratio (CBR), defined as the penetration resistance of a subgrade soil relative to a standard crushed rock. The CBR method of design was studied extensively by the U.S. Corps of Engineers during World War II and became a very popular method after the war.

The disadvantage of an empirical method is that it can be applied only to a given set of environmental, material, and loading conditions. If these conditions are changed, the design is no longer valid, and a new method must be developed through trial and error to be conformant to the new conditions.

Limiting Shear Failure Methods The limiting shear failure method is used to determine the thickness of pavements so that shear failures will not occur. The major properties of pavement components and subgrade soils to be considered are their cohesion and angle of internal friction. Barber (1946) applied Terzaghi's bearing capacity formula (Terzaghi, 1943) to determine pavement thickness. McLeod (1953) advocated the use of logarithmic spirals to determine the bearing capacity of pavements. These methods were reviewed by Yoder (1959) in his book *Principles of Pavement Design*, but were not even mentioned in the second edition (Yoder and Witczak, 1975). This is not surprising because, with the ever increasing speed and volume of traffic, pavements should be designed for riding comfort rather than for barely preventing shear failures.

Limiting Deflection Methods The limiting deflection method is used to determine the thickness of pavements so that the vertical deflection will not exceed the allowable limit. The Kansas State Highway Commission (1947) modified Boussinesq's equation (Boussinesq, 1885) and limited the deflection of subgrade to 0.1 in. (2.54 mm). The U.S. Navy (1953) applied Burmister's two-layer theory (Burmister, 1943) and limited the surface deflection to 0.25 in. (6.35 mm). The use of deflection as a design criterion has the apparent advantage that it can be easily measured in the field. Unfortunately, pavement failures are caused by excessive stresses and strains instead of deflections.

Regression Methods Based on Pavement Performance or Road Tests A good example of the use of regression equations for pavement design is the AASHTO method based on the results of road tests. The disadvantage of the method is that the design equations can be applied only to the conditions at the road test site. For conditions other than those under which the equations were developed, extensive modifications based on theory or experience are needed. Regression equations can also be developed from the performance of existing pavements, such as those used in the pavement evaluation systems COPES (Darter *et al.*, 1985) and EXPEAR (Hall *et al.*, 1989). Unlike pavements

Downloaded From : www.EasyEngineering.net

Downloaded From : www.EasyEngineering.net

subjected to road tests, the materials and construction of these pavements were not well controlled, so a wide scatter of data and a large standard error are expected. Although these equations can illustrate the effect of various factors on pavement performance, their usefulness in pavement design is limited because of the many uncertainties involved.

Mechanistic–Empirical Methods The mechanistic–empirical method of design is based on the mechanics of materials that relates an input, such as a wheel load, to an output or pavement response, such as stress or strain. The response values are used to predict distress from laboratory-test and field-performance data. Dependence on observed performance is necessary because theory alone has not proven sufficient to design pavements realistically.

Kerkhoven and Dormon (1953) first suggested the use of vertical compressive strain on the surface of subgrade as a failure criterion to reduce permanent deformation: Saal and Pell (1960) recommended the use of horizontal tensile strain at the bottom of asphalt layer to minimize fatigue cracking, as shown in Figure 1.1. The use of the above concepts for pavement design was first presented in the United States by Dormon and Metcalf (1965).

The use of vertical compressive strain to control permanent deformation is based on the fact that plastic strains are proportional to elastic strains in paving materials. Thus, by limiting the elastic strains on the subgrade, the elastic strains in other components above the subgrade will also be controlled; hence, the magnitude of permanent deformation on the pavement surface will be controlled in turn. These two criteria have since been adopted by Shell Petroleum International (Claussen *et al.*, 1977) and by the Asphalt Institute (Shook *et al.*, 1982) in their mechanistic–empirical methods of design. The advantages of mechanistic methods are the improvement in the reliability of a design, the ability to predict the types of distress, and the feasibility to extrapolate from limited field and laboratory data.

The term "hot mix asphalt" in Figure 1.1 is synonymous with the commonly used "asphalt concrete." It is an asphalt aggregate mixture produced at a batch or drum mixing facility that must be mixed, spread, and compacted at an elevated temperature. To avoid the confusion between portland cement concrete (PCC) and asphalt concrete (AC), the term hot mix concrete (HMA) will be used frequently throughout this book in place of asphalt concrete.

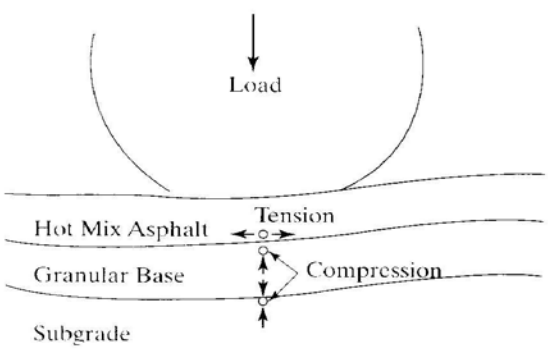


FIGURE 1.1
Tensile and compressive strains in flexible pavements.

Downloaded From : www.EasyEngineering.net

Downloaded From : www.EasyEngineering.net

Other Developments Other developments in flexible pavement design include the application of computer programs, the incorporation of serviceability and reliability, and the consideration of dynamic loading.

Computer Programs Various computer programs based on Burmister's layered theory have been developed. The earliest and the best known is the CHEV program developed by the Chevron Research Company (Warren and Dieckmann, 1963). The program can be applied only to linear elastic materials but was modified by the Asphalt Institute in the DAMA program to account for nonlinear elastic granular materials (Hwang and Witczak, 1979). Another well-publicized program is BISAR, developed by Shell, which considers not only vertical loads but also horizontal loads (De Jong *et al.*, 1973). Another program, originally developed at the University of California, Berkeley, and later adapted to microcomputers, is ELSYM5, for elastic five-layer systems under multiple wheel loads (Kopperman *et al.*, 1986). Using the layered theory with stress-dependent material properties, Finn *et al.* (1986) developed a computer program named PDMAP (Probabilistic Distress Models for Asphalt Pavements) for predicting the fatigue cracking and rutting in asphalt pavements. They found that the critical responses obtained from PDMAP compared favorably with SAPIV, which is a finite-element stress analysis program developed at the University of California, Berkeley.

Khazanovich and Ioannides (1995) developed a computer program (called DIPLOMAT) in which the Burmister's multilayered system was extended to include a number of elastic plates and spring beds. The program in its present form deals only with interior loading and is therefore of limited application, because a rigid layer of concrete can be considered as one of the multilayers, as illustrated in Section 5.3.4, and there is really no need to treat the concrete slab as a separate plate unless the load is applied near an edge or a discontinuous boundary.

A major disadvantage of the layered theory is the assumption that each layer is homogeneous with the same properties throughout the layer. This assumption makes it difficult to analyze layered systems composed of nonlinear materials, such as untreated granular bases and subbases. The elastic modulus of these materials is stress dependent and varies throughout the layer, so a question immediately arises: Which point in the nonlinear layer should be selected to represent the entire layer? If only the most critical stress, strain, or deflection is desired, as is usually the case in pavement design, a point near to the applied load can be reasonably selected. However, if the stresses, strains, or deflections at different points, some near to and some far away from the load, are desired, it will be difficult to use the layered theory for analyzing nonlinear materials. This difficulty can be overcome by using the finite-element method.

Duncan *et al.* (1968) first applied the finite-element method for the analysis of flexible pavements. The method was later incorporated in the ILLI-PAVE computer program (Raad and Figueroa, 1980). The large amount of computer time and storage required means that the program has not been used for routine design purposes. However, a number of regression equations, based on the responses obtained by ILLI-PAVE, were developed for use in design (Thompson and Elliot, 1985; Gomez-Achecar and Thompson, 1986). The nonlinear finite-element method was also used in the MICH-PAVE computer program developed at Michigan State University (Harichandran *et al.*, 1989). More information about ILLI-PAVE and MICH-PAVE is presented in Section 3.3.2.

Downloaded From : www.EasyEngineering.net

Downloaded From : www.EasyEngineering.net

Serviceability and Reliability As a result of the AASHO Road Test, Carey and Irick (1960) developed the pavement serviceability performance concept and indicated that pavement thickness should also depend on the terminal serviceability index required. Lemer and Moavenzadeh (1971) presented the concept of reliability as a pavement design factor, and a probabilistic computer program called VESYS was developed for analyzing a three-layer viscoelastic pavement system (Moavenzadeh *et al.*, 1974). This program, which incorporated the concepts of serviceability and reliability, was modified by the Federal Highway Administration (FHWA, 1978; Kenis, 1977), and several versions of the VESYS program were developed (Lai, 1977; Rauhut and Jordahl, 1979; Von Quintus, *et al.*, 1988; Jordahl and Rauhut, 1983; Brademeyer, 1988). The reliability concept was also incorporated in the Texas flexible pavement design system (Darter *et al.*, 1973b) and in the AASHTO Design Guide (AASHTO, 1986). Although the AASHTO procedures are basically empirical, the replacements of the empirical soil support value by the subgrade resilient modulus and the empirical layer coefficients by the resilient modulus of each layer clearly indicate the trend toward mechanistic methods. The resilient modulus is the elastic modulus under repeated loads; it can be determined by laboratory tests. Details about resilient modulus are presented in Section 7.1, serviceability in Section 9.2, and reliability in Chapter 10.

Dynamic Loads All of the methods discussed so far are based on static or moving loads and do not consider the inertia effects due to dynamic loads. Mamlouk (1987) described a computer program capable of considering the inertial effect and indicated that the effect is most pronounced when shallow bedrock or frozen subgrade is encountered; it becomes more important for vibratory than for impulse loading. The program requires a large amount of computer time to run and is limited to the analysis of linear elastic materials. The inclusion of inertial effect for routine pavement design involving nonlinear elastic and viscoelastic materials is still a dream to be realized in the future.

Research by Monismith *et al.* (1988) showed that, for asphalt concrete pavements, it was unnecessary to perform a complete dynamic analysis. Inertia effects can be ignored and the local dynamic response can thus be determined by an essentially static method using material properties compatible with the rate of loading. However, under impulse loading, a dynamic problem of more immediate interest is the effect of vehicle dynamics on pavement design. Current design procedures do not consider the damage caused by pavement roughness. As trucks become larger and heavier, some benefits can be gained by designing proper suspension systems to minimize the damage effect.

1.1.2 Rigid Pavements

Rigid pavements are constructed of Portland cement concrete. The first concrete pavement was built in Bellefontaine, Ohio in 1893 (Fitch, 1996), 15 years earlier than the one constructed in Detroit, Michigan, in 1908, as mentioned in the first edition. As of 2001, there were about 59,000 miles (95,000 km) of rigid pavements in the United States. The development of design methods for rigid pavements is not as dramatic as that of flexible pavements, because the flexural stress in concrete has long been considered as a major, or even the only, design factor.

Downloaded From : www.EasyEngineering.net

Downloaded From : www.EasyEngineering.net

Analytical Solutions Analytical solutions ranging from simple closed-form formulas to complex derivations are available for determining the stresses and deflections in concrete pavements.

Goldbeck's Formula By treating the pavement as a cantilever beam with a load concentrated at the corner, Goldbeck (1919) developed a simple equation for the design of rigid pavements, as indicated by Eq. 4.12 in Chapter 4. The same equation was applied by Older (1924) in the Bates Road Test.

Westergaard's Analysis Based on Liquid Foundations The most extensive theoretical studies on the stresses and deflections in concrete pavements were made by Westergaard (1926a, 1926b, 1927, 1933, 1939, 1943, 1948), who developed equations due to temperature curling as well as three cases of loading: load applied near the corner of a large slab, load applied near the edge of a large slab but at a considerable distance from any corner, and load applied at the interior of a large slab at a considerable distance from any edge. The analysis was based on the simplifying assumption that the reactive pressure between the slab and the subgrade at any given point is proportional to the deflection at that point, independent of the deflections at any other points. This type of foundation is called a liquid or Winkler foundation. Westergaard also assumed that the slab and subgrade were in full contact.

In conjunction with Westergaard's investigation, the U.S. Bureau of Public Roads conducted, at the Arlington Experimental Farm, Virginia, an extensive investigation on the structural behavior of concrete pavements. The results were published in *Public Roads* from 1935 to 1943 as a series of six papers and reprinted as a single volume for wider distribution (Teller and Sutherland, 1935–1943).

In comparing the critical corner stress obtained from Westergaard's corner formula with that from field measurements, Pickett found that Westergaard's corner formula, based on the assumption that the slab and subgrade were in full contact, always yielded a stress that was too small. By assuming that part of the slab was not in contact with the subgrade, he developed a semiempirical formula that was in good agreement with experimental results. Pickett's corner formula (PCA, 1951), with a 20% allowance for load transfer, was used by the Portland Cement Association until 1966, when a new method based on the stress at the transverse joint was developed (PCA, 1966).

The PCA method was based on Westergaard's analysis. However, in determining the stress at the joint, the PCA assumed that there was no load transfer across the joint, so the stress thus determined was similar to the case of edge loading with a different tire orientation. The replacement of corner loading by the stress at the joint was due to the use of a 12-ft-wide (3.63-m) lane with most traffic moving away from the corner. The PCA method was revised again in 1984, in which an erosion criterion based on the corner deflection, in addition to the fatigue criterion based on the edge stress, was employed (PCA, 1984).

Pickett's Analysis Based on Solid Foundations In view of the fact that the actual subgrade behaved more like an elastic solid than a dense liquid, Pickett *et al.* (1951) developed theoretical solutions for concrete slabs on an elastic half-space. The complexities of the mathematics involved have denied this refined method the attention it

Downloaded From : www.EasyEngineering.net

Downloaded From : www.EasyEngineering.net

merits. However, a simple influence chart based on solid foundations was developed by Pickett and Badaruddin (1956) for determining the edge stress, which is presented in Section 5.3.2.

Numerical Solutions All the analytical solutions mentioned above were based on the assumption that the slab and the subgrade are in full contact. It is well known that, due to pumping, temperature curling, and moisture warping, the slab and subgrade are usually not in contact. With the advent of computers and numerical methods, some analyses based on partial contact were developed.

Discrete-Element Methods Hudson and Matlock (1966) applied the discrete-element method by assuming the subgrade to be a dense liquid. The discrete-element method is more or less similar to the finite-difference method in that the slab is seen as an assemblage of elastic joints, rigid bars, and torsional bars. The method was later extended by Saxena (1973) for analyzing slabs on an elastic solid foundation.

Finite-Element Methods With the development of the powerful finite-element method, a break-through was made in the analysis of rigid pavements. Cheung and Zienkiewicz (1965) developed finite-element methods for analyzing slabs on elastic foundations of both liquid and solid types. The methods were applied to jointed slabs on liquid foundations by Huang and Wang (1973, 1974) and on solid foundations by Huang (1974a). In collaboration with Huang (Chou and Huang, 1979, 1981, 1982), Chou (1981) developed finite-element computer programs named WESLIQID and WESLAYER for the analysis of liquid and layered foundations, respectively. The consideration of foundation as a layered system is more realistic when layers of base and subbase exist above the subgrade. Other finite-element computer programs available include ILLI-SLAB developed at the University of Illinois (Tabatabaie and Barenberg, 1979, 1980), JSLAB developed by the Portland Cement Association (Tayabji and Colley, 1986), and RISC developed by Resource International, Inc. (Majidzadeh et al., 1984). The general-purpose 3-D finite-element package ABAQUS (1993) was used in simulating pavements involving nonlinear subgrade under dynamic loading (Zaghloul and White, 1994) and in investigating the effects of discontinuity on the response of a jointed plain concrete pavement under a standard falling weight deflectometer load (Uddin *et al.*, 1995).

Other Developments Even though theoretical methods are helpful in improving and extrapolating design procedures, the knowledge gained from pavement performance is the most important. Westergaard (1927), who contributed so much to the theory of concrete pavement design, was one of the first to recognize that theoretical results need to be checked against pavement performance. In addition to the above theoretical developments, the following events are worthy of note.

Fatigue of Concrete An extensive study was made by the Illinois Division of Highways during the Bates Road Test on the fatigue properties of concrete (Clemmer, 1923). It was found that an induced flexural stress could be repeated indefinitely without causing rupture, provided the intensity of extreme fiber stress did not exceed

Downloaded From : www.EasyEngineering.net

Downloaded From : www.EasyEngineering.net

approximately 50% of the modulus of rupture, and that, if the stress ratio was above 50%, the allowable number of stress repetitions to cause failures decreased drastically as the stress ratio increased. Although the arbitrary use of 50% stress ratio as a dividing line was not actually proved, this assumption has been used most frequently as a basis for rigid pavement design. To obtain a smoother fatigue curve, the current PCA method assumes a stress ratio of 0.45, below which no fatigue damage need be considered.

Pumping With increasing truck traffic, particularly just before World War II, it became evident that subgrade type played an important role in pavement performance. The phenomenon of pumping, which is the ejection of water and subgrade soils through joints and cracks and along the pavement edge, was first described by Gage (1932). After pavement pumping became critical during the war, rigid pavements were constructed on granular base courses of varying thickness to protect against loss of subgrade support due to pumping. Many studies were made on the design of base courses for the correction of pumping.

Probabilistic Methods The application of probabilistic concepts to rigid pavement design was presented by Kher and Darter (1973), and the concepts were incorporated into the AASHTO design guide (AASHTO, 1986). Huang and Sharpe (1989) developed a finite-element probabilistic computer program for the design of rigid pavements and showed that the use of a cracking index in a reliability context was far superior to the current deterministic approach.

1.2 PAVEMENT TYPES

There are three major types of pavements: flexible or asphalt pavements, rigid or concrete pavements, and composite pavements.

1.2.1 Flexible Pavements

Flexible pavements can be analyzed by Burmister's layered theory, which is discussed in Chapters 2 and 3. A major limitation of the theory is the assumption of a layered system infinite in areal extent. This assumption makes the theory inapplicable to rigid pavements with transverse joints. Nor can the layered theory be applied to rigid pavements when the wheel loads are less than 2 or 3 ft (0.6 or 0.9 m) from the pavement edge, because discontinuity causes a large stress at the edge. Its application to flexible pavements is validated by the limited area of stress distribution through flexible materials. As long as the wheel load is more than 2 ft (0.61 m) from the edge, the discontinuity at the edge has very little effect on the critical stresses and strains obtained.

Conventional Flexible Pavements Conventional flexible pavements are layered systems with better materials on top where the intensity of stress is high and inferior materials at the bottom where the intensity is low. Adherence to this design principle makes possible the use of local materials and usually results in a most economical design. This is particularly true in regions where high-quality materials are expensive but local materials of inferior quality are readily available.

Downloaded From : www.EasyEngineering.net

Downloaded From : www.EasyEngineering.net

Figure 1.2 shows the cross section of a conventional flexible pavement. Starting from the top, the pavement consists of seal coat, surface course, tack coat, binder course, prime coat, base course, subbase course, compacted subgrade, and natural subgrade. The use of the various courses is based on either necessity or economy, and some of the courses may be omitted.

Seal Coat Seal coat is a thin asphalt surface treatment used to waterproof the surface or to provide skid resistance where the aggregates in the surface course could be polished by traffic and become slippery. Depending on the purpose, seal coats might or might not be covered with aggregate. Details about skid resistance are presented in Section 9.3.

Surface Course The surface course is the top course of an asphalt pavement, sometimes called the wearing course. It is usually constructed of dense graded HMA. It must be tough to resist distortion under traffic and provide a smooth and skid-resistant riding surface. It must be waterproof to protect the entire pavement and subgrade from the weakening effect of water. If the above requirements cannot be met, the use of a seal coat is recommended.

Binder Course The binder course, sometimes called the asphalt base course, is the asphalt layer below the surface course. There are two reasons that a binder course is used in addition to the surface course. First, the HMA is too thick to be compacted in one layer, so it must be placed in two layers. Second, the binder course generally consists of larger aggregates and less asphalt and does not require as high a quality as the surface course, so replacing a part of the surface course by the binder course results in a more economical design. If the binder course is more than 3 in. (76 mm), it is generally placed in two layers.

Tack Coat and Prime Coat A tack coat is a very light application of asphalt, usually asphalt emulsion diluted with water, used to ensure a bond between the surface being paved and the overlying course. It is important that each layer in an asphalt

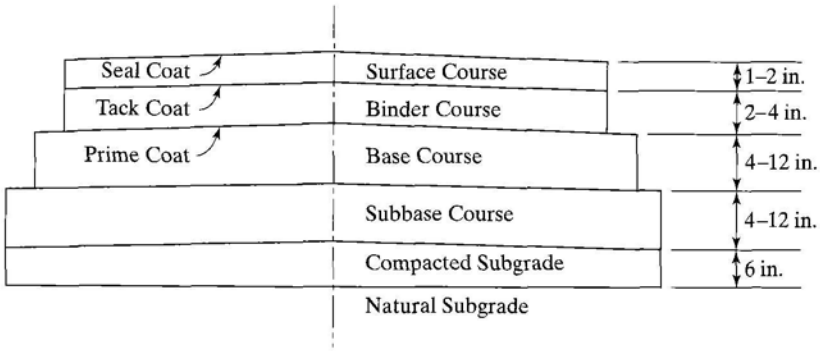


FIGURE 1.2

Typical cross section of a conventional flexible pavement (1 in. = 25.4 mm).

Downloaded From : www.EasyEngineering.net

Downloaded From : www.EasyEngineering.net

pavement be bonded to the layer below. Tack coats are also used to bond the asphalt layer to a PCC base or an old asphalt pavement. The three essential requirements of a tack coat are that it must be very thin, it must uniformly cover the entire surface to be paved, and it must be allowed to break or cure before the HMA is laid.

A prime coat is an application of low-viscosity cutback asphalt to an absorbent surface, such as an untreated granular base on which an asphalt layer will be placed. Its purpose is to bind the granular base to the asphalt layer. The difference between a tack coat and a prime coat is that a tack coat does not require the penetration of asphalt into the underlying layer, whereas a prime coat penetrates into the underlying layer, plugs the voids, and forms a watertight surface. Although the type and quantity of asphalt used are quite different, both are spray applications.

Base Course and Subbase Course The base course is the layer of material immediately beneath the surface or binder course. It can be composed of crushed stone, crushed slag, or other untreated or stabilized materials. The subbase course is the layer of material beneath the base course. The reason that two different granular materials are used is for economy. Instead of using the more expensive base course material for the entire layer, local and cheaper materials can be used as a subbase course on top of the subgrade. If the base course is open graded, the subbase course with more fines can serve as a filter between the subgrade and the base course.

Subgrade The top 6 in. (152 mm) of subgrade should be scarified and compacted to the desirable density near the optimum moisture content. This compacted subgrade may be the in-situ soil or a layer of selected material.

Full-Depth Asphalt Pavements Full-depth asphalt pavements are constructed by placing one or more layers of HMA directly on the subgrade or improved subgrade. This concept was conceived by the Asphalt Institute in 1960 and is generally considered the most cost-effective and dependable type of asphalt pavement for heavy traffic. This type of construction is quite popular in areas where local materials are not available. It is more convenient to purchase only one material, i.e., HMA, rather than several materials from different sources, thus minimizing the administration and equipment costs.

Figure 1.3 shows the typical cross section for a full-depth asphalt pavement. The asphalt base course in the full-depth construction is the same as the binder course in conventional pavement. As with conventional pavement, a tack coat must be applied between two asphalt layers to bind them together.

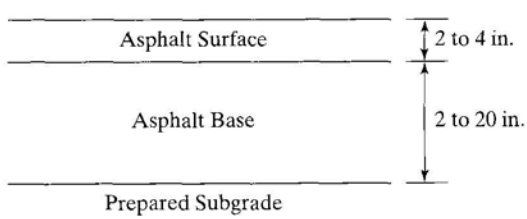


FIGURE 1.3
Typical cross-section of a full-depth asphalt pavement (1 in. = 25.4 mm).

Downloaded From : www.EasyEngineering.net

Downloaded From : www.EasyEngineering.net

According to the Asphalt Institute (AI, 1987), full-depth asphalt pavements have the following advantages:

1. They have no permeable granular layers to entrap water and impair performance.
2. Time required for construction is reduced. On widening projects, where adjacent traffic flow must usually be maintained, full-depth asphalt can be especially advantageous.
3. When placed in a thick lift of 4 in. (102 mm) or more, construction seasons may be extended.
4. They provide and retain uniformity in the pavement structure.
5. They are less affected by moisture or frost.
6. According to limited studies, moisture contents do not build up in subgrades under full-depth asphalt pavement structures as they do under pavements with granular bases. Thus, there is little or no reduction in subgrade strength.

1.2.2 Rigid Pavements

Rigid pavements are constructed of portland cement concrete and should be analyzed by the plate theory, instead of the layered theory. Plate theory is a simplified version of the layered theory that assumes the concrete slab to be a medium thick plate with a plane before bending which remains a plane after bending. If the wheel load is applied in the interior of a slab, either plate or layered theory can be used and both should yield nearly the same flexural stress or strain, as discussed in Section 5.3.4. If the wheel load is applied near to the slab edge, say less than 2 ft (0.61 m) from the edge, only the plate theory can be used for rigid pavements. The reason that the layered theory is applicable to flexible pavements but not to rigid pavements is that PCC is much stiffer than HMA and distributes the load over a much wider area. Therefore, a distance of 2 ft (0.61 m) from the edge is considered quite far in a flexible pavement but not far enough in a rigid pavement. The existence of joints in rigid pavements also makes the layered theory inapplicable. Details of plate theory are presented in Chapters 4 and 5.

Figure 1.4 shows a typical cross section for rigid pavements. In contrast to flexible pavements, rigid pavements are placed either directly on the prepared subgrade or on a single layer of granular or stablized material. Because there is only one layer of material under the concrete and above the subgrade, some call it a base course, others a subbase.

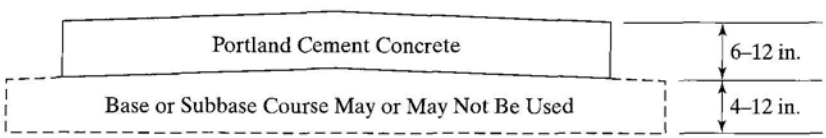


FIGURE 1.4

Typical cross section of a rigid pavement (1 in. = 25.4 mm).

Downloaded From : www.EasyEngineering.net

Downloaded From : www.EasyEngineering.net

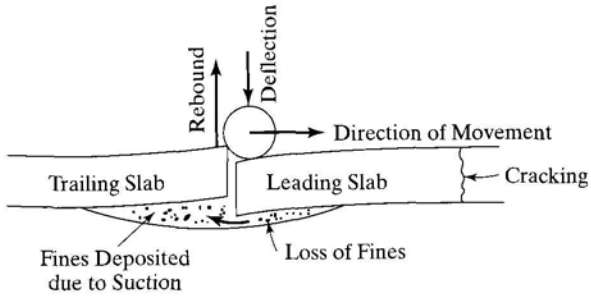


FIGURE 1.5
Pumping of rigid pavement.

Use of Base Course Early concrete pavements were constructed directly on the subgrade without a base course. As the weight and volume of traffic increased, pumping began to occur, and the use of a granular base course became quite popular. When pavements are subject to a large number of very heavy wheel loads with free water on top of the base course, even granular materials can be eroded by the pulsative action of water. For heavily traveled pavements, the use of a cement-treated or asphalt-treated base course has now become a common practice.

Although the use of a base course can reduce the critical stress in the concrete, it is uneconomical to build a base course for the purpose of reducing the concrete stress. Because the strength of concrete is much greater than that of the base course, the same critical stress in the concrete slab can be obtained without a base course by slightly increasing the concrete thickness. The following reasons have been frequently cited for using a base course.

Control of Pumping Pumping is defined as the ejection of water and subgrade soil through joints and cracks and along the edges of pavements, caused by downward slab movements due to heavy axle loads. The sequence of events leading to pumping includes the creation of void space under the pavement caused by the temperature curling of the slab and the plastic deformation of the subgrade, the entrance of water, the ejection of muddy water, the enlargement of void space, and finally the faulting and cracking of the leading slab ahead of traffic. Pumping occurs under the leading slab when the trailing slab rebounds, which creates a vacuum and sucks the fine material from underneath the leading slab, as shown in Figure 1.5. The corrective measures for pumping include joint sealing, undersealing with asphalt cements, and muck jacking with soil cement.

Three factors must exist simultaneously to produce pumping:

1. The material under the concrete slab must be saturated with free water. If the material is well drained, no pumping will occur. Therefore, good drainage is one of the most efficient ways to prevent pumping.
2. There must be frequent passage of heavy wheel loads. Pumping will take place only under heavy wheel loads with large slab deflections. Even under very heavy loads, pumping will occur only after a large number of load repetitions.
3. The material under the concrete slab must be erodible. The erodibility of a material depends on the hydrodynamic forces created by the dynamic action of moving

Downloaded From : www.EasyEngineering.net

Downloaded From : www.EasyEngineering.net

wheel loads. Any untreated granular materials, and even some weakly cemented materials, are erodible because the large hydrodynamic pressure will transport the fine particles in the subbase or subgrade to the surface. These fine particles will go into suspension and cause pumping.

Control of Frost Action Frost action is detrimental to pavement performance. It results in frost heave, which causes concrete slabs to break and softens the subgrade during the frost-melt period. In northern climates, frost heave can reach several inches or more than one foot. The increase in volume of 9% when water becomes frozen is not the real cause of frost heave. For example, if a soil has a porosity of 0.5 and is subjected to a frost penetration of 3 ft (0.91 m), the amount of heave due to 9% increase in volume is $0.09 \times 3 \times 0.5 = 0.135$ ft or 1.62 in. (41 mm), which is much smaller than the 6 in. (152 mm) or more of heave experienced in such climate.

Frost heave is caused by the formation and continuing expansion of ice lenses. After a period of freezing weather, frost penetrates into the pavement and subgrade, as indicated by the depth of frost penetration in Figure 1.6. Above the frost line, the temperature is below the ordinary freezing point for water. The water will freeze in the larger voids but not in the smaller voids where the freezing point may be depressed as low as 23°F (−5°C).

When water freezes in the larger voids, the amount of liquid water at that point decreases. The moisture deficiency and the lower temperature in the freezing zone increase the capillary tension and induce flow toward the newly formed ice. The adjacent small voids are still unfrozen and act as conduits to deliver the water to the ice. If there is no water table or if the subgrade is above the capillary zone, only scattered and small ice lenses can be formed. If the subgrade is above the frost line and within the capillary fringe of the groundwater table, the capillary tension induced by freezing sucks up water from the water table below. The result is a great increase in the amount of water in the freezing zone and the segregation of water into ice lenses. The amount of heave is at least as much as the combined lens thicknesses.

Three factors must be present simultaneously to produce frost action:

1. The soil within the depth of frost penetration must be frost susceptible. It should be recognized that silt is more frost susceptible than clay because it has both high

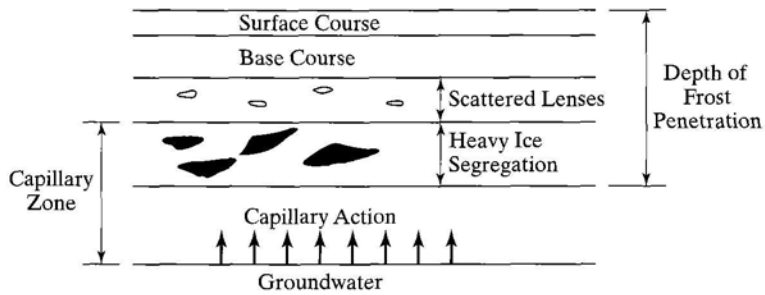


FIGURE 1.6

Formation of ice lenses, due to frost action.

Downloaded From : www.EasyEngineering.net

Downloaded From : www.EasyEngineering.net

capillarity and high permeability. Although clay has a very high capillarity, its permeability is so low that very little water can be attracted from the water table to form ice lenses during the freezing period. Soils with more than 3% finer than 0.02 mm are generally frost susceptible, except that uniform fine sands with more than 10% finer than 0.02 mm are frost susceptible.

2. There must be a supply of water. A high water table can provide a continuous supply of water to the freezing zone by capillary action. Lowering the water table by subsurface drainage is an effective method to minimize frost action.
3. The temperature must remain freezing for a sufficient period of time. Due to the very low permeability of frost-susceptible soils, it takes time for the capillary water to flow from the water table to the location where the ice lenses are formed. A quick freeze does not have sufficient time to form ice lenses of any significant size.

Improvement of Drainage When the water table is high and close to the ground surface, a base course can raise the pavement to a desirable elevation above the water table. When water seeps through pavement cracks and joints, an open-graded base course can carry it away to the road side. Cedergren (1988) recommends the use of an open-graded base course under every important pavement to provide an internal drainage system capable of rapidly removing all water that enters.

Control of Shrinkage and Swell When moisture changes cause the subgrade to shrink and swell, the base course can serve as a surcharge load to reduce the amount of shrinkage and swell. A dense-graded or stabilized base course can serve as a water-proofing layer, and an open-graded base course can serve as a drainage layer. Thus, the reduction of water entering the subgrade further reduces the shrinkage and swell potentials.

Expedition of Construction A base course can be used as a working platform for heavy construction equipment. Under inclement weather conditions, a base course can keep the surface clean and dry and facilitate the construction work.

As can be seen from the above reasoning, there is always a necessity to build a base course. Consequently, base courses have been widely used for rigid pavements.

Types of Concrete Pavement Concrete pavements can be classified into four types: jointed plain concrete pavement (JPCP), jointed reinforced concrete pavement (JRCP), continuous reinforced concrete pavement (CRCP), and prestressed concrete pavement (PCP). Except for PCP with lateral prestressing, a longitudinal joint should be installed between two traffic lanes to prevent longitudinal cracking. Figure 1.7 shows the major characteristics of these four types of pavements.

Jointed Plain Concrete Pavements All plain concrete pavements should be constructed with closely spaced contraction joints. Dowels or aggregate interlocks may be used for load transfer across the joints. The practice of using or not using dowels varies among the states. Dowels are used most frequently in the southeastern states, aggregate interlocks in the western and southwestern states, and both are used in other

Downloaded From : www.EasyEngineering.net

Downloaded From : www.EasyEngineering.net

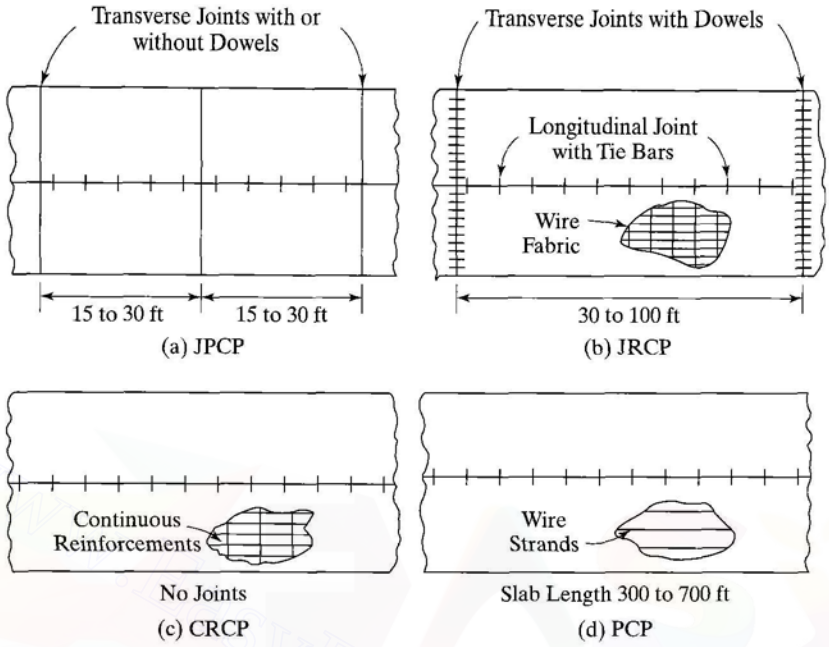


FIGURE 1.7

Four types of concrete pavements (1 ft = 0.305 m).

areas. Depending on the type of aggregate, climate, and prior experience, joint spacings between 15 and 30 ft (4.6 and 9.1 m) have been used. However, as the joint spacing increases, the aggregate interlock decreases, and there is also an increased risk of cracking. Based on the results of a performance survey, Nussbaum and Lokken (1978) recommended maximum joint spacings of 20 ft (6.1 m) for doweled joints and 15 ft (4.6 m) for undoweled joints.

Jointed Reinforced Concrete Pavements Steel reinforcements in the form of wire mesh or deformed bars do not increase the structural capacity of pavements but allow the use of longer joint spacings. This type of pavement is used most frequently in the northeastern and north central part of the United States. Joint spacings vary from 30 to 100 ft (9.1 to 30 m). Because of the longer panel length, dowels are required for load transfer across the joints.

The amount of distributed steel in JRCP increases with the increase in joint spacing and is designed to hold the slab together after cracking. However, the number of joints and dowel costs decrease with the increase in joint spacing. Based on the unit costs of sawing, mesh, dowels, and joint sealants, Nussbaum and Lokken (1978) found that the most economical joint spacing was about 40 ft (12.2 m). Maintenance costs generally increase with the increase in joint spacing, so the selection of 40 ft (12.2 m) as the maximum joint spacing appears to be warranted.

Continuous Reinforced Concrete Pavements It was the elimination of joints that prompted the first experimental use of CRCP in 1921 on Columbia Pike near

Downloaded From : www.EasyEngineering.net

Downloaded From : www.EasyEngineering.net

Washington, D.C. The advantages of the joint-free design were widely accepted by many states, and more than two dozen states have used CRCP with a two-lane mileage totaling over 20,000 miles (32,000 km). It was originally reasoned that joints were the weak spots in rigid pavements and that the elimination of joints would decrease the thickness of pavement required. As a result, the thickness of CRCP has been empirically reduced by 1 to 2 in. (25 to 50 mm) or arbitrarily taken as 70 to 80% of the conventional pavement.

The formation of transverse cracks at relatively close intervals is a distinctive characteristic of CRCP. These cracks are held tightly by the reinforcements and should be of no concern as long as they are uniformly spaced. The distress that occurs most frequently in CRCP is punchout at the pavement edge. This type of distress takes place between two parallel random transverse cracks or at the intersection of Y cracks. If failures occur at the pavement edge instead of at the joint, there is no reason for a thinner CRCP to be used. The 1986 AASHTO design guide suggests using the same equation or nomograph for determining the thickness of JRCP and CRCP. However, the recommended load-transfer coefficients for CRCP are slightly smaller than those for JPCP or JRCP and so result in a slightly smaller thickness of CRCP. The amount of longitudinal reinforcing steel should be designed to control the spacing and width of cracks and the maximum stress in the steel. Details on the design of CRCP are presented in Section 12.4.

Prestressed Concrete Pavements Concrete is weak in tension but strong in compression. The thickness of concrete pavement required is governed by its modulus of rupture, which varies with the tensile strength of the concrete. The preapplication of a compressive stress to the concrete greatly reduces the tensile stress caused by the traffic loads and thus decreases the thickness of concrete required. The prestressed concrete pavements have less probability of cracking and fewer transverse joints and therefore result in less maintenance and longer pavement life.

The first known prestressed highway pavement in the United States was a 300-ft (91-m) pavement in Delaware built in 1971 (*Roads and Streets*, 1971). This was followed in the same year by a demonstration project on a 3200-ft (976-m) access road at Dulles International Airport (Pasko, 1972). In 1973, a 2.5-mile (4-km) demonstration project was constructed in Pennsylvania (Brunner, 1975). These projects were preceded by a construction and testing program on an experimental prestressed pavement constructed in 1956 at Pittsburgh, Pennsylvania (Moreell, 1958). These projects have the following features:

1. Slab length varied from 300 to 760 ft (91 to 232 m).
2. Slab thickness was 6 in. (152 mm) on all projects.
3. A post-tension method with seven wire steel strands was used for all projects. In the post-tension method, the compressive stress was imposed after the concrete had gained sufficient strength to withstand the applied forces.
4. Longitudinal prestress varied from 200 to 331 psi (1.4 to 2.3 MPa) and no transverse or diagonal prestressing was used.

Prestressed concrete has been used more frequently for airport pavements than for highway pavements because the saving in thickness for airport pavements is much

Downloaded From : www.EasyEngineering.net

Downloaded From : www.EasyEngineering.net

greater than that for highway pavements. The thickness of prestressed highway pavements has generally been selected as the minimum necessary to provide sufficient cover for the prestressing steel (Hanna et al., 1976). Prestressed concrete pavements are still at the experimental stage, and their design arises primarily from the application of experience and engineering judgment, so they will not be discussed further in this book.

1.2.3 Composite Pavements

A composite pavement is composed of both HMA and PCC. The use of PCC as a bottom layer and HMA as a top layer results in an ideal pavement with the most desirable characteristics. The PCC provides a strong base and the HMA provides a smooth and nonreflective surface. However, this type of pavement is very expensive and is rarely used as a new construction. As of 2001, there are about 97,000 miles (155,000 km) of composite pavements in the United States, practically all of which are the rehabilitation of concrete pavements using asphalt overlays. The design of overlay is discussed in Chapter 13.

Design Methods When an asphalt overlay is placed over a concrete pavement, the major load-carrying component is the concrete, so the plate theory should be used. Assuming that the HMA is bonded to the concrete, an equivalent section can be used with the plate theory to determine the flexural stress in the concrete slab, as is described in Section 5.1.2. If the wheel load is applied near to the pavement edge or joint, only the plate theory can be used. If the wheel load is applied in the interior of the pavement far from the edges and joints, either layered or plate theory can be used. The concrete pavement can be either JPCP, JRCP, or CRCP.

Composite pavements also include asphalt pavements with stabilized bases. For flexible pavements with untreated bases, the most critical tensile stress or strain is located at the bottom of the asphalt layer; for asphalt pavements with stabilized bases, the most critical location is at the bottom of the stabilized bases.

Pavement Sections The design of composite pavements varies a great deal. Figure 1.8 shows two different cross sections that have been used. Section (*a*) (Ryell and Corkill, 1973) shows the HMA placed directly on the PCC base, which is a more conventional type of construction. A disadvantage of this construction is the occurrence of reflection cracks on the asphalt surface that are due to the joints and cracks in the concrete base. The open-graded HMA serves as a buffer to reduce the amount of reflection cracking. Placing thick layers of granular materials between the concrete base and the asphalt layer, as in Section (*b*) (Baker, 1973), can eliminate reflection cracks, but the placement of a stronger concrete base under a weaker granular material can be an ineffective design. The use of a 6-in. (152-mm) dense-graded crushed-stone base beneath the more rigid macadam base, consisting of 2.5-in. (64-mm) stone choked with stone screenings, prevents reflection cracking. The 3.5-in. (89-mm) HMA is composed of a 1.5-in. (38-mm) surface course and a 2-in. (51-mm) binder course.

Figure 1.9 shows the composite structures recommended for premium pavements (Von Quintus *et al.*, 1980). Section (*a*) shows the composite pavement with a jointed plain concrete base, and Section (*b*) shows the composite pavement with a continuous reinforced

Downloaded From : www.EasyEngineering.net

Downloaded From : www.EasyEngineering.net

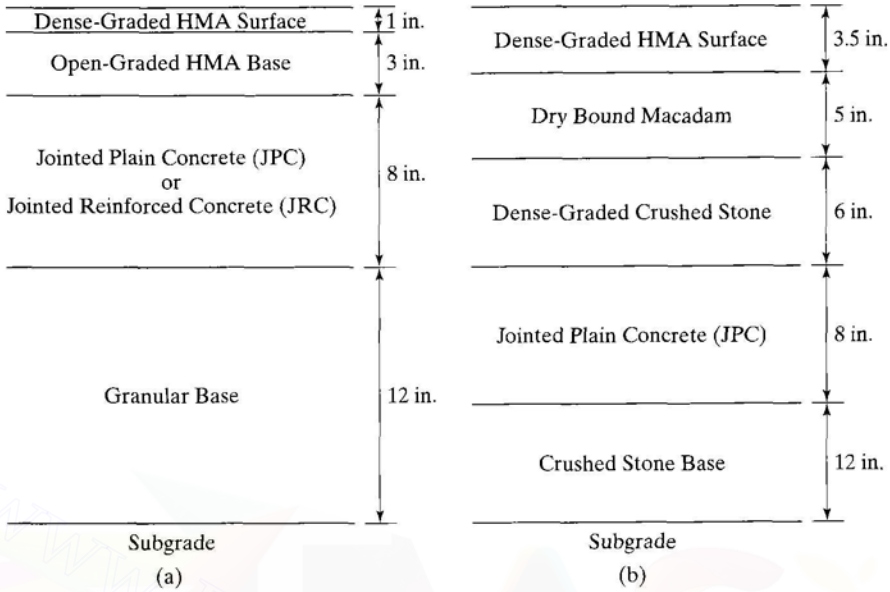


FIGURE 1.8

Two different cross-sections for composite pavements (1 in. = 25.4 mm).

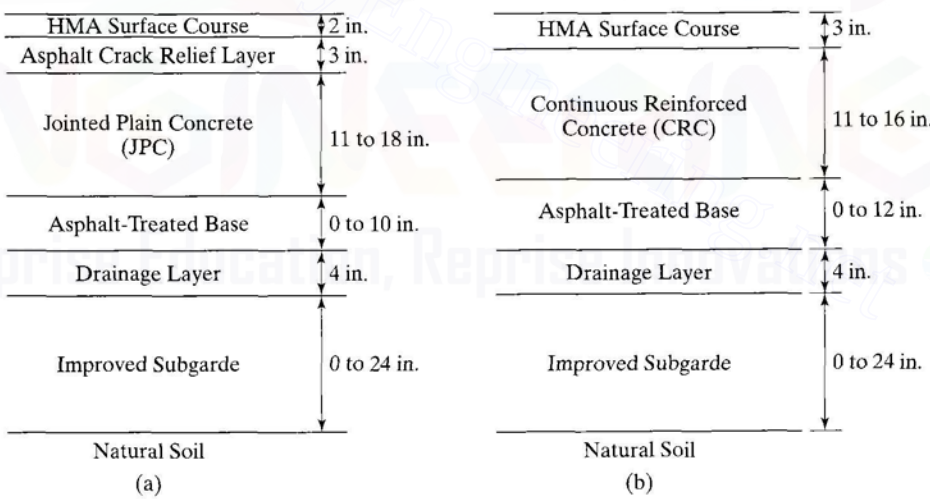


FIGURE 1.9

Typical cross-sections for premium composite pavements (1 in. = 25.4 mm). (After Von Quintus et al. (1980).)

concrete base. Premium pavements are also called zero-maintenance pavements. They are designed to carry very heavy traffic with no maintenance required during the first 20 years and normal maintenance for the next 10 years before resurfacing. The ranges of thickness indicated in the figure depend on traffic, climate, and subgrade conditions.

Downloaded From : www.EasyEngineering.net

Downloaded From : www.EasyEngineering.net

A salient feature of the design is the 4-in. (102-mm) drainage layer on top of the natural or improved subgrade. The drainage layer is a blanket extending full width between shoulder edges. In addition, a perforated collector pipe should be placed longitudinally along the edge of the pavement. The pipe should be placed in a trench section cut in the subgrade. Filter materials should be placed between the drainage layer and the subgrade, if needed. Because the concrete base is protected by the HMA, a leaner concrete with a modulus of rupture from 450 to 550 psi (3.1 to 3.8 MPa) may be used. Note that a 3-in. (7.6-mm) asphalt crack-relief layer should be placed above the jointed plain concrete base. This is a layer of coarse open-graded HMA containing 25 to 35% interconnecting voids and made up of 100% crushed material. It is designed to reduce reflection cracking. Because of the large amount of interconnecting voids, this crack-relief layer provides a medium that resists the transmission of differential movements of the underlying slab. The asphalt relief layer is not required for continuous reinforced concrete base. When the subgrade is poor, an asphalt-treated base might be required beneath the concrete slab.

1.3 ROAD TESTS

Because the observed performance under actual conditions is the final criterion to judge the adequacy of a design method, three major road tests under controlled conditions were conducted by the Highway Research Board from the mid-1940s to the early 1960s.

1.3.1 Maryland Road Test

The objective of this project was to determine the relative effects of four different axle loadings on a particular concrete pavement (HRB, 1952). The tests were conducted on a 1.1-mile (1.76-km) section of concrete pavement constructed in 1941 on US 301 approximately 9 miles (14.4 km) south of La Plata, Maryland.

General Layout The pavement consisted of two 12-ft (3.66-m) lanes having a 9–7–9-in. (229–178–229-mm) thickened-edge cross section and reinforced with wire mesh. The soils under the pavement ranged from A-1 to A-7-6, with the A-6 group predominant. There were four separate test sections. The west and east lanes of the southern 0.5 mile (0.8 km) were subjected to 18,000 and 22,400 lb (80 and 100 kN) single-axle loads, respectively; the west and east lanes of the northern 0.6 mile (0.96 km) were subjected to 32,000 and 44,800 lb (142 and 200 kN) tandem-axle loads, respectively, as shown in Figure 1.10. Controlled traffic tests were conducted from June through December 1950. The total cost of the project was $245,000.

It should be noted that thickened-edge pavements were very popular at the time of the road test but are rarely in use today. This type of pavement is more costly to construct because of the grading operations required at the thickened edge. Thickened-edge pavements were popular in the old days when pavement widths were in the neighborhood of 18 to 20 ft (5.5 to 6.1 m) and most trucks traveled very close to the pavement edge. With current 24-ft (7.3-m) wide pavements, traffic concentration is between 3 and 4 ft (0.91 to 1.22 m) from the edge, thus significantly reducing the stress at the edge.

Downloaded From : www.EasyEngineering.net

Downloaded From : www.EasyEngineering.net

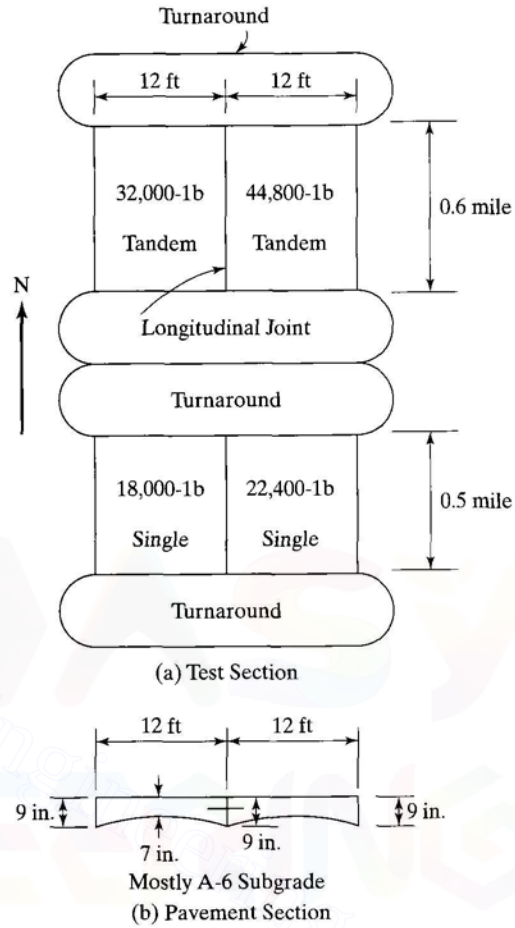


FIGURE 1.10

Maryland Road Test (1 in. = 25.4 mm, 1 ft = 0.305 m, 1 mile = 1.6 km, 1 lb = 4.45 N).

Major Findings

1. Both the average cracking and the average settlement of slab at the joint increased in this order: 18,000-lb (80-kN) single axle, 32,000-lb (142-kN) tandem axle, 22,400-lb (100-kN) single axle, and 44,800-lb (200-kN) tandem axle.
2. Pumping occurred on plastic clay soils but not on granular subgrades with low percentages of silt and clay. Prior to the development of pumping, the stresses for all cases of loading investigated were below generally accepted design limits—that is, 50% of the modulus of rupture of the concrete. Pumping and the accompanying loss of subgrade support caused large increases in the stresses for the corner case of loading.
3. Under creep speed, the deflections for the corner loading averaged approximately 0.025 in. (0.64 mm), those for the edge loading approximately 0.014 in. (0.36 mm). After pumping developed, the maximum deflections increased considerably. In some instances, the corner deflection approached 0.2 in. (5 mm) before cracking

Downloaded From : www.EasyEngineering.net

Downloaded From : www.EasyEngineering.net

occurred. The failure of the slabs on the fine-grained soil can be explained by the fact that the deflections of these slabs under all of the test loads were sufficient to cause pumping when the other requisites for pumping were present. As pumping developed, the deflections increased with corresponding more rapid increase of stress to a magnitude sufficient to cause rupture of the slab.

4. With the exception of the corner case of loading for pumping soils, the stress and deflection resulting at vehicle speed of 40 mph (64 km/h) averaged approximately 20% less than those at creep speed. For pumping slabs under corner loading, the stresses averaged approximately the same for both vehicle speeds.
5. The stresses and deflections caused by loads acting at the corners and edges of slabs were influenced to a marked degree by temperature curling. For the corner loading, the stresses and deflections for a severe downward curled condition were observed to be only approximately one-third of those for the critical upward curled condition. For the case of edge loading, the effect of temperature curling, although appreciable, was not as pronounced as for the case of corner loading.

1.3.2 WASHO Road Test

After the successful completion of the Maryland Road Test sponsored by the eleven midwestern and eastern states, the Western Association of State Highway Officials (WASHO) conducted a similar test, but on sections of flexible pavements in Malad, Idaho, with the same objective in mind (HRB, 1955).

General Layout Two identical test loops were constructed, each having two 1900-ft (580-m) tangents made up of five 300-ft (92-m) test sections separated by four 100-ft (30-m) transition sections, as shown in Figure 1.11. One tangent in each loop was surfaced with 4 in. (102 mm) of HMA and 2 in. (51 mm) of crushed gravel base; the other tangent was surfaced with 2 in. (51 mm) of HMA and 4 in. (102 mm) of crushed gravel base. The thicknesses of the gravel subbase were 0, 4, 8, 12, and 16 in. (0, 102, 203, 205, and 406 mm). Thus, the total thickness of pavement over the A-4 basement soil varied from 6 to 22 in. (152 to 559 mm) in 4-in. (102-mm) increments for the five test sections. In one loop, 18,000-lb (80-kN) single-axle loads were operated in the inner lane and 22,400 lb (100 kN) in the outer lane. In the other loop, 32,000-lb (142-kN) tandem-axle loads were in the inner lane and 40,000 lb (178 kN) in the outer lane.

Construction began in April 1952, and the completed pavement was accepted on September 30, 1952. On November 6, 1952, after completion of preliminary testing and installation of instruments, regular traffic operation was started. Except for one spring and two winter periods, it was continued until May 29, 1954. The total cost of the project was $840,000.

Major Findings

1. The amount of damage to the pavement increased in the following order: 18,000-lb (80-kN) single axle, 32,000-lb (142-kN) tandem axle, 22,400-lb (100-kN) single axle, and 40,000-lb (178-kN) tandem axle. For example, the results of an analysis showed that the minimum thicknesses of pavement with 2-in. (51-mm) HMA

Downloaded From : www.EasyEngineering.net

Downloaded From : www.EasyEngineering.net

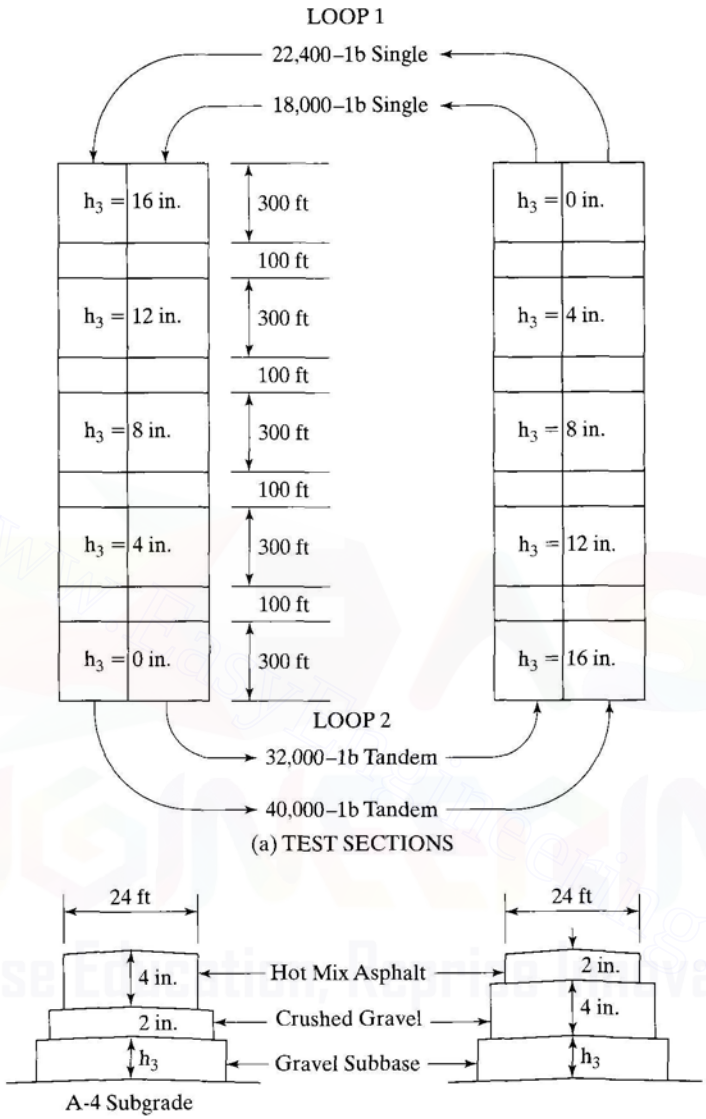


FIGURE 1.11

WASHO Road Test (1 in. = 25.4 mm, 1 ft = 0.305 m, 1 lb = 4.45 N).

that would have been adequate to carry the 238,000 applications of the above loads were 16, 17, 19, and 20 in. (406, 432, 483, and 508 mm), respectively.

2. The behavior of the pavement with 4-in. (102-mm) HMA was far superior to that of equal total thickness with 2-in. (51-mm) HMA.
3. Distress in the outer wheelpath was more than that in the inner wheelpath. Surfacing of the shoulders in three of the test sections in July 1953 proved to be highly

Downloaded From : www.EasyEngineering.net

Downloaded From : www.EasyEngineering.net

effective in retarding distress in the outer wheelpath. Both facts suggest that the outer wheelpath with paved shoulders is the equivalent of the inner wheelpath and testify to the advantages of shoulder paving.

4. Development of structural distress was confined largely to two critical periods of traffic operation. One period was from June 11 to July 7, 1953, in which 27% of the total distress developed under 0.7% of the total load applications. The second period was from February 17 to April 7, 1954, in which 40% of the total distress developed under 13% of the total applications.
5. On the basis of pavement distress, a tandem axle with a total load about 1.5 times that of a single-axle load is equivalent to the single-axle load; whereas a tandem axle with a total load about 1.8 times a single-axle load produced equal maximum deflections.
6. Deflection of the pavement surface under traffic was influenced by vehicle speed, temperature of the surfacing, load, and moisture content of the top layers of basement soil. The deflection was maximum under a static load. Deflection decreased as speed increased up to about 15 mph (24 km/h), after which deflections decreased only slightly as speed increased. Deflections were greater as temperature of surfacing increased. Deflections of the pavement surface under traffic were approximately proportional to the applied load. When the moisture content at the basement soil exceeded 22%, deflections increased with increase in moisture content.
7. For the type of loading employed, there was no significant difference between the magnitudes of the wheel loads transmitted in the outer wheelpath and those in the inner wheelpath that was due to the crown of the pavement.

1.3.3 AASHO Road Test

The objective of this project was to determine any significant relationship between the number of repetitions of specified axle loads of different magnitudes and arrangements and the performance of different thicknesses of flexible and rigid pavements (HRB, 1962). The test facility was constructed along the alignment of Interstate 80 near Ottawa, Illinois, about 80 miles (128 km) southwest of Chicago.

General Layout The test consisted of four large loops, numbered 3 through 6, and two smaller loops, 1 and 2. Each loop was a segment of a four-lane divided highway whose parallel roadways, or tangents, were connected by a turnaround at each end. Tangent lengths were 6800 ft (2070 m) in loops 3 through 6, 4400 ft (1340 m) in loop 2, and 2000 ft (610 m) in loop 1. In all loops, the north tangents were surfaced with HMA and south tangents with PCC. Centerlines divided the pavements into inner and outer lanes, called lane 1 and lane 2. Each tangent was constructed as a succession of pavement sections called structural sections. Pavement designs varied from section to section. The minimum length of a section was 100 ft (30.5 m) in loops 2 through 6 and 15 ft (4.6 m) in loop 1. The axle loads on each loop and lane are shown in Table 1.1.

Construction began in August 1956, and test traffic was inaugurated on October 15, 1958. Test traffic was operated until November 30, 1960, at which time 1,114,000 axle loads had been applied. The total cost of the project was $27,000,000.

Downloaded From : www.EasyEngineering.net

Downloaded From : www.EasyEngineering.net

TABLE 1.1 Applications of Axle Loads on Various Lanes at AASHO Road Test

Loop no.	1		2		3	
Lane no.	1	2	1	2	1	2
Axle load (lb)	None	None	2000 single	6000 single	12,000 single	24,000 tandem
Loop no.	4		5		6	
Lane no.	1	2	1	2	1	2
Axle load (lb)	18,000 single	32,000 tandem	22,400 single	40,000 tandem	30,000 single	48,000 tandem

Note: 1 lb = 4.45 N.

Major Findings One important contribution of the AASHO Road Test was the development of the pavement serviceability concept, which is discussed in Section 9.2.1 together with the equations relating serviceability, load, and thickness design of both flexible and rigid pavements. Major findings for flexible and rigid pavements are summarized separately as follows.

Flexible Pavements

1. The superiority of the four types of base under study fell in the following order: bituminous treated, cement treated, crushed stone, and gravel. Most of the sections containing the gravel base failed very early in the test, and their performance was definitely inferior to that of the sections with crushed-stone base.
2. The pavement needed to maintain a certain serviceability at a given number of axle-load applications would be considerably thinner in the inner than in the outer wheelpath.
3. Rutting of the pavement was due principally to decrease in thickness of the component layers. About 91% of the rutting occurred in the pavement itself: 32% in the surface, 14% in the base, and 45% in the subbase. Thus, only 9% of a surface rut could be accounted for by rutting of the embankment. Data also showed that changes in thickness of the component layers were caused not by the increase in density, but primarily by lateral movements of the materials.
4. More surface cracking occurred during periods when the pavement was in a relatively cold state than during periods of warm weather. Generally, cracking was more prevalent in sections having deeper ruts than in sections with shallower ruts.
5. The deflection occurring within the pavement structure (surface, base, and subbase), as well as that at the top of the embankment soil, was greater in the spring than during the succeeding summer months. This effect was due to the higher moisture contents of the base, subbase, and embankment soil that existed in the spring. A high degree of correlation was found between the deflection at the top of the embankment and the total surface deflection and one between deflection and rutting. A pronounced reduction in deflection accompanied an increase in

Downloaded From : www.EasyEngineering.net

Downloaded From : www.EasyEngineering.net

vehicle speed. Increasing the speed from 2 to 35 mph (3.2 to 56 km/h) reduced the total deflection 38% and the embankment deflection 35%.

Rigid Pavements

1. Of the three design variables, viz., reinforcement or panel length, subbase thickness, and slab thickness, only slab thickness has an appreciable effect on measured strains.
2. Inspections of the pavements were made weekly and after each rain. Faulting occasionally occurred at cracks, never at the transverse joints, because all joints were doweled. No part of the cracking in the traffic loops was attributed solely to environmental changes, because no cracks appeared in the nontraffic loop, or loop 1. (*Note:* although no cracks appeared during and immediately after the road test, cracks did occur many years later.)
3. Pumping of subbase material, including the coarser fractions, was the major factor causing failures of sections with subbase. The amount of materials pumped through joints and cracks was negligible when compared with the amount ejected along the edge.
4. Twenty-four-hour studies of the effect of fluctuating air temperature showed that the deflection of panel corners under vehicles traveling near the pavement edge might increase severalfold from afternoon to early morning. Edge strains and deflections were affected to a lesser extent.
5. Corner deflections of a 40-ft (12.2-m) reinforced panel usually exceeded those of a 15-ft (4.6-m) nonreinforced panel, if all other conditions were the same. Edge deflections and strains were not affected significantly by panel length or reinforcement. An increase in vehicle speed from 2 to 60 mph (3.2 to 96 km/h) resulted in a decrease in strain or deflection of about 29%.

1.3.4 Strategic Highway Research Program (SHRP)

The strategic Highway Research Program was approved by U.S. Congress in 1987 as a five-year, $150 million research program to improve highways and make them safer for both motorists and highway workers. It was a new program, intended not to duplicate any ongoing research activities but rather to focus on some long-neglected needs for improving basic technologies and material properties. The research was conducted by independent contractors and targeted in four areas: highway operations, concrete and structures, asphalt, and long-term pavement performance. The 1991 Intermodal Surface Transportation Efficiency Act (ISTEA) authorized an additional $108 million for SHRP implementation and for continuation of the 20-year long-term pavement-performance program.

Asphalt and long-term pavement performance are the two areas directly related to pavement design. Research on asphalt resulted in the development of Superpave (Al, 1998, 2002), as described in Appendix D. One of the basic goals of the *long-term* pavement-performance (LTPP) program is to establish a national pavement-performance data base (NPPDB) to store all the data collected and generated under the LTPP program. These data, which include inventory, materials testing, profile, deflection by falling

Downloaded From : www.EasyEngineering.net

Downloaded From : www.EasyEngineering.net

weight deflectometer (FWD), cross profile, distress, friction, maintenance, rehabilitation, climate, and traffic, will provide researchers with reliable data for pavement design and performance studies. The data were collected from 777 general pavement studies (GPS) sections and 234 specific pavement studies (SPS) sections throughout the United States. The GPS program focuses on existing pavements; the SPS program includes specially constructed pavement that will help develop a better understanding of the effects on performance of a few targeted factors not widely covered in the GPS. Since its inception, the LTPP program has been international in scope. Fifteen countries are participating, conducting research on 666 international sites and forwarding data to the LTPP program. In July 1992, responsibility for the on-going LTPP research and data-collection effort was assumed by the Federal Highway Administration (FHWA). The Transportation Research Board (TRB) was made responsible for maintaining the NPPDB.

The nine pavement types for GPS are as follows:

GPS-1: Asphalt concrete (AC) on granular base
GSP-2: AC on stabilized base
GPS-3: Jointed plain concrete pavement (JPCP)
GPS-4: Jointed reinforced concrete pavement (JRCP)
GPS-5: Continuous reinforced concrete pavement (CRCP)
GPS-6: AC overlay of AC pavement
GPS-7: AC overlay of jointed concrete pavement (JCP)
GPS-8: Bonded JCP overlay of concrete pavement
GPS-9: Unbonded JCP overlay of concrete pavement

The nine experiments for SPS are as follows:

SPS-1: Strategic study of structural factors for flexible pavement
SPS-2: Strategic study of structural factors for rigid pavement
SPS-3: Preventive-maintenance effectiveness for flexible pavement
SPS-4: Preventive-maintenance effectiveness for rigid pavement
SPS-5: Rehabilitation of AC pavement
SPS-6: Rehabilitation of JCP
SPS-7: Bonded concrete overlay of concrete pavement
SPS-8: Study of environmental effects in the absence of heavy loads
SPS-9: Validation of SHRP asphalt specifications and mix design and innovations in asphalt pavement

The LTPP program is still going on and the collection of data is not complete, so any conclusions or findings based on the short-term data are tentative and subject to changes and therefore are not reported here at this time.

1.4 DESIGN FACTORS

Design factors can be divided into four broad categories: traffic and loading, environment, materials, and failure criteria. The factors to be considered in each category will

Downloaded From : www.EasyEngineering.net

Downloaded From : www.EasyEngineering.net

be described, and how the design process fits into an overall pavement management system will be discussed.

1.4.1 Traffic and Loading

The traffic and loading to be considered include axle loads, the number of load repetitions, tire-contact areas, and vehicle speeds.

Axle Loads Figure 1.12 shows the wheel spacing for a typical semitrailer consisting of single axle with single tires, single axle with dual tires, and tandem axles with dual tires. For special heavy-duty haul trucks, tridem axles consisting of a set of three axles, each spaced at 48 to 54 in. (1.22 to 1.37 m) apart, also exist.

The spacings of 23 and 13 ft (7 and 4 m) shown in Figure 1.12 should have no effect on pavement design because the wheels are so far apart that their effect on stresses and strains should be considered independently. Unless an equivalent single-axle load is used, the consideration of multiple axles is not a simple matter. The design may be unsafe if the tandem and tridem axles are treated as a group and considered as one repetition. The design is too conservative if each axle is treated independently and considered as one repetition. A method for analyzing multiple-axle loads is presented in Section 3.1.3.

In the design of flexible pavements by layered theory, only the wheels on one side, say at the outer wheelpath, need be considered; in the design of rigid pavements by plate theory, the wheels on both sides, even at a distance of more than 6 ft (1.8 m) apart, are usually considered.

Number of Repetitions With the use of a high-speed computer, it is no problem to consider the number of load repetitions for each axle load and evaluate its damage. The method of dividing axle loads into a number of groups has been used frequently for the design of rigid pavements, as illustrated by the PCA method in Section 12.2. However, its application to flexible pavements is not widespread, because of the empirical nature of the design and of the large amount of computer time required.

Instead of analyzing the stresses and strains due to each axle-load group, a simplified and widely accepted procedure is to develop equivalent factors and convert each load group into an equivalent 18-kip (80-kN) single-axle load, as illustrated by the

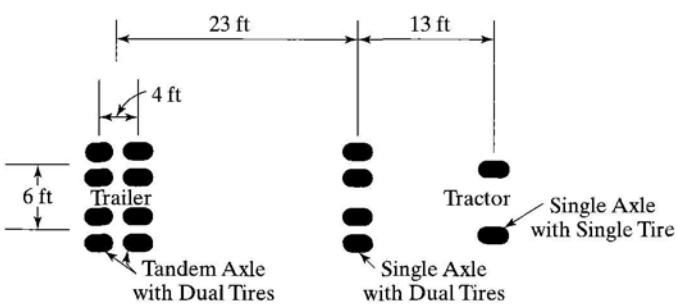


FIGURE 1.12
Wheel configurations for typical semitrailer units (1 ft = 0.305 m).

Downloaded From : www.EasyEngineering.net

Downloaded From : www.EasyEngineering.net

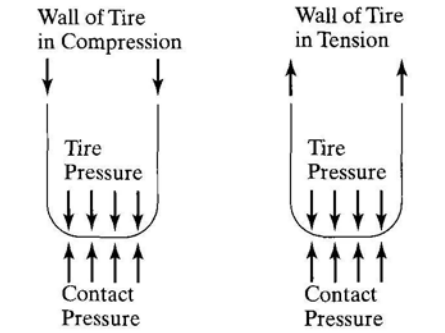


FIGURE 1.13
Relationship between contact pressure and tire pressure.

Asphalt Institute method in Section 11.2 and the AASHTO method in Sections 11.3 and 12.3. It should be noted that the equivalency between two different loads depends on the failure criterion employed. Equivalent factors based on fatigue cracking could be different from those based on permanent deformation. Therefore, the use of a single equivalent factor for analyzing different types of distress is empirical and should be considered as approximate only.

Contact Area In the mechanistic method of design, it is necessary to know the contact area between tire and pavement, so the axle load can be assumed to be uniformly distributed over the contact area. The size of contact area depends on the contact pressure. As indicated by Figure 1.13, the contact pressure is greater than the tire pressure for low-pressure tires, because the wall of tires is in compression and the sum of vertical forces due to wall and tire pressure must be equal to the force due to contact pressure; the contact pressure is smaller than the tire pressure for high-pressure tires, because the wall of tires is in tension. However, in pavement design, the contact pressure is generally assumed to be equal to the tire pressure. Because heavier axle loads have higher tire pressures and more destructive effects on pavements, the use of tire pressure as the contact pressure is therefore on the safe side.

Heavier axle loads are always applied on dual tires. Figure 1.14a shows the approximate shape of contact area for each tire, which is composed of a rectangle and two semicircles. By assuming length L and width $0.6L$, the area of contact $A_c = \pi(0.3L)^2 + (0.4L)(0.6L) = 0.5227L^2$, or

$$L = \sqrt{\frac{A_c}{0.5227}} \tag{1.1}$$

in which A_c = contact area, which can be obtained by dividing the load on each tire by the tire pressure.

The contact area shown in Figure 1.14a was used previously by PCA (1966) for the design of rigid pavements. The current PCA (1984) method is based on the finite-element procedure, and a rectangular area is assumed with length $0.8712L$ and width $0.6L$, which has the same area of $0.5227L^2$, as shown in Figure 1.14b. These contact areas are not axisymmetric and cannot be used with the layered theory. When the

Downloaded From : www.EasyEngineering.net

Downloaded From : www.EasyEngineering.net

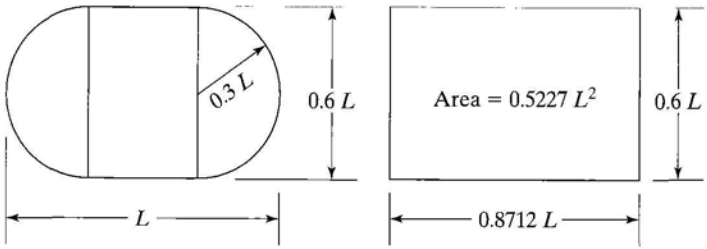


Figure 1.14
Dimension of tire contact area.

layered theory is used for flexible pavement design, it is assumed that each tire has a circular contact area. This assumption is not correct, but the error incurred is believed to be small. To simplify the analysis of flexible pavements, a single circle with the same contact area as the duals is frequently used to represent a set of dual tires, instead of using two circular areas. This practice usually results in a more conservative design, but could become unconservative for thin asphalt surface because the horizontal tensile strain at the bottom of asphalt layer under the larger contact radius of single wheel is smaller than that under the smaller contact radius of dual wheels, as is illustrated in Section 3.4.1. For rigid pavements, it is more reasonable to use a larger circular area to represent a set of duals, as discussed in Section 4.2.1.

Example 1.1:

Draw the most realistic contact area for an 18-kip (80-kN) single-axle load with a tire pressure of 80 psi (552 kPa). What are the other configurations of contact area that have been used for pavement design?

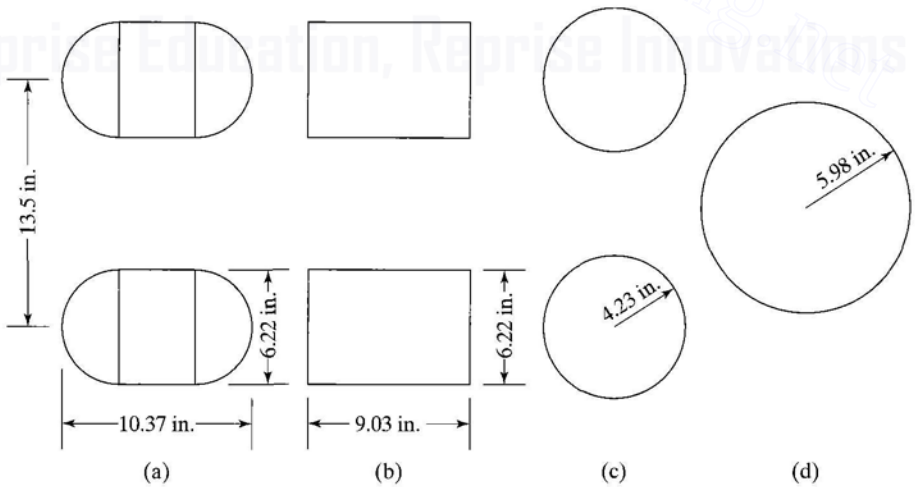


FIGURE 1.15
Example 1.1 (1 in. = 25.4 mm).

Downloaded From : www.EasyEngineering.net

Downloaded From : www.EasyEngineering.net

Solution: The 18-kip (80-kN) single-axle load is applied over four tires, each having a load of 4500 lb (20 kN). The contact area of each tire is $A_c = 4500/80 = 56.25$ in.^{2} (3.6×10^4 mm^2). From Eq. 1.1, $L = \sqrt{56.25/0.5227} = 10.37$ in. (263 mm). The width of the tire is $0.6L = 0.6 \times 10.37 = 6.22$ in. (158 mm). The configuration of various contact areas is shown in Figure 1.15.

Figure 1.15a is the most realistic contact area consisting of a rectangle and two semicircles, as used previously by PCA (1966). Figure 1.15b is the rectangular contact area for use in the finite-element analysis of rigid pavements with length $0.8712L$, or 9.03 in. (229 mm), and width 6.22 in. (158 mm). Figure 1.15c shows the contact area as two circles, each having a radius of $\sqrt{56.25/\pi}$, or 4.23 in. (107 mm). This assumption was also made by the Asphalt Institute (AI, 1981a), although they used a tire pressure of 70 psi (483 kPa) and a contact radius of 4.52 in. (115 mm). Figure 1.15d considers the contact area as a single circle with contact radius $\sqrt{2 \times 56.25/\pi} = 5.98$ in. (152 mm). This contact area was used in VESYS (FHWA, 1978).

Vehicle Speed Another factor related to traffic is the speed of traveling vehicles. If the viscoelastic theory is used, such as in VESYS and KENLAYER, speed is directly related to the duration of loading. If the elastic theory is used, the resilient modulus of each paving material should be properly selected to be commensurate with the vehicle speed. Generally, the greater the speed, the larger the modulus, and the smaller the strains in the pavement.

1.4.2 Environment

The environmental factors that influence pavement design include temperature and precipitation, both affecting the elastic moduli of the various layers. In the mechanistic–empirical method of design, each year can be divided into a number of periods, each having a different set of layer moduli. The damage during each period is evaluated and summed throughout the year to determine the design life.

Temperature The effect of temperature on asphalt pavements is different from that on concrete pavements. Temperature affects the resilient modulus of asphalt layers and induces curling of concrete slabs. In cold climates, the resilient moduli of unstabilized materials also vary with the freeze–thaw cycles. The severity of cold climate is indicated by the freezing index, which can be correlated with the depth of frost penetration.

Effect on Asphalt Layer The elastic and viscoelastic properties of HMA are affected significantly by pavement temperature. Any mechanistic methods of flexible pavement design must consider pavement temperature, which can be related to air temperature. During the winter, when temperature is low, the HMA becomes rigid and reduces the strains in the pavement. However, stiffer HMA has less fatigue life, which may neutralize the beneficial effect of smaller strains. Low temperature can cause asphalt pavements to crack.

Effect on Concrete Slab The temperature gradient in concrete pavements affects not only the curling stress but also the slab–subgrade contact. During the day, when the temperature at top is higher than that at bottom, the slab curls down so that its interior may not be in contact with the subgrade. At night, when the temperature at top is lower than that at bottom, the slab curls upward so that its edge and corner may be out of

Downloaded From : www.EasyEngineering.net

Downloaded From : www.EasyEngineering.net

contact with the subgrade. The loss of subgrade contact will affect the stresses in concrete due to wheel loads. The change between maximum and minimum temperatures also determines the joint and crack openings and affects the efficiency of load transfer.

Frost Penetration Another effect of temperature on pavement design in cold climate is the frost penetration, which results in a stronger subgrade in the winter but a much weaker subgrade in the spring. Figure 1.16 shows the maximum depth of frost penetration in the United States. Although frost heave causes differential settlements and pavement roughness, the most detrimental effect of frost penetration occurs during the spring breakup period, when the ice melts and the subgrade is in a saturated condition. It is desirable to protect the subgrade by using non-frost-susceptible materials within the zone of frost penetration. If this cannot be done, the design method should take into consideration the weakening of the subgrade during spring breakup.

Freezing Index The severity of frost in a given region can be expressed as a freezing index in terms of degree days. A negative one-degree day represents one day with a mean air temperature one degree below freezing; a positive one-degree day indicates one day with a mean air temperature one degree above freezing. The mean air temperature for a given day is the average of high and low temperatures during that day. If the mean air temperature is 25°F on the first day and 22°F on the second and third days, the total degree days for the three-day period are $(25 - 32) + 2 \times (22 - 32) = -27$ degree days. Given the mean air temperature of each day, the degree days for each month can be similarly calculated. A plot of cumulative degree days versus time results in a curve, as shown in Figure 1.17. The difference between the maximum and minimum

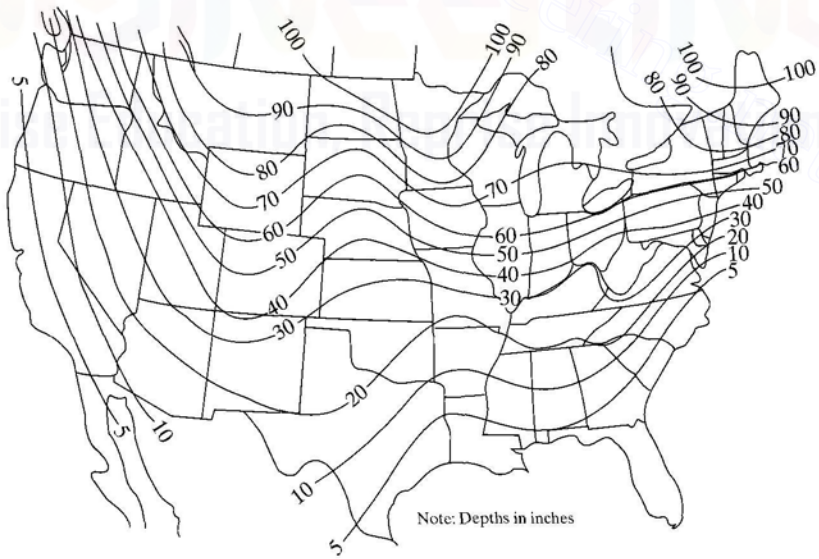


FIGURE 1.16

Maximum depth of frost penetration in the United States (1 in. = 25.4 mm).

Downloaded From : www.EasyEngineering.net

Downloaded From : www.EasyEngineering.net

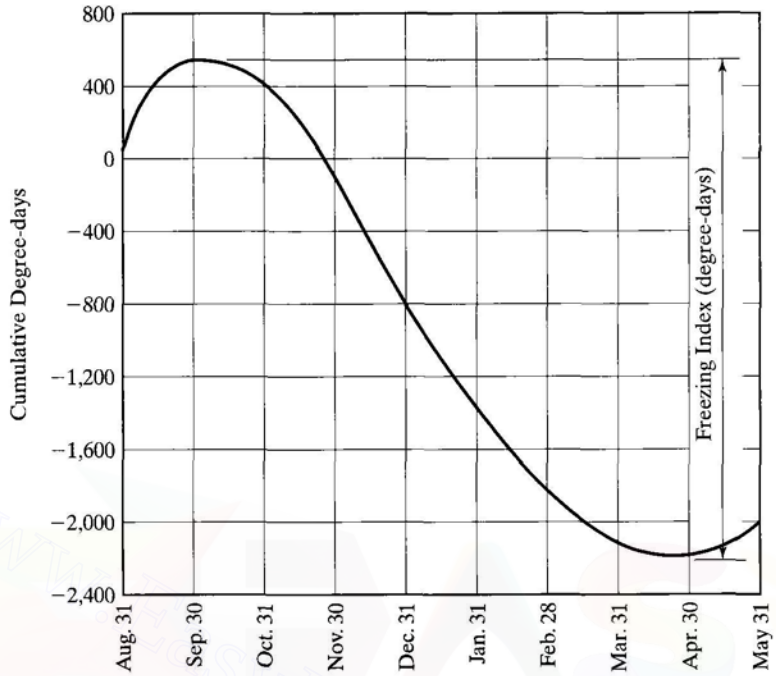


FIGURE 1.17
Determination of freezing index.

points on the curve during one year is called the freezing index for that year. The freezing index has been correlated with the depth of frost penetration and can be used as a factor of pavement design and evaluation.

Example 1.2:

The monthly degree-day data are September, 540; October, −130; November, −450; December, −770; January, −540; February, −450; March, −290; April, −70; and May, 170. Calculate the freezing index.

TABLE 1.2 Monthly and Cumulative Degree Days

	Degree days (°F)	
Month	Monthly	Cumulative
September	540	540
October	−130	410
November	−450	−40
December	−770	−810
January	−540	−1350
February	−450	−1800
March	−290	−2090
April	−70	−2160
May	170	−1990

Downloaded From : www.EasyEngineering.net

Downloaded From : www.EasyEngineering.net

Solution: The monthly and cumulative degree day data are shown in Table 1.2. The cumulative degree days are plotted in Figure 1.17. Freezing index = 2160 + 540 = 2700 degree days, which can be calculated from the table or measured from Figure 1.17.

Precipitation The precipitation from rain and snow affects the quantity of surface water infiltrating into the subgrade and the location of the groundwater table. Every effort should be made to improve drainage and alleviate the detrimental effect of water. If water from rainfalls can be drained out within a short time, its effect can be minimized, even in regions of high precipitation.

The location of the groundwater table is also important. The water table should be kept at least 3 ft (0.91 m) below the pavement surface. In seasonal frost areas, the depth from the pavement surface to the groundwater table should be much greater. For example, the recommended minimum depths are 7 ft (2.1 m) in Massachusetts, 5 ft (1.5 m) in Michigan and Minnesota, 8 to 12 ft (2.4 to 3.7 m) in Saskatchewan, and 3 to 7 ft (0.9 to 2.1 m) in Nebraska (Ridgeway, 1982).

If proper drainage cannot be provided, smaller elastic moduli must be selected for the component layers affected by poor drainage. However, this measure might not solve the problem, because poor drainage could still incur damages other than the lack of shear strength, such as the pumping and the loss of support. Details about drainage are presented in Chapter 8.

1.4.3 Materials

In the mechanistic–empirical methods of design, the properties of materials must be specified, so that the responses of the pavement, such as stresses, strains, and displacements in the critical components, can be determined. These responses are then used with the failure criteria to predict whether failures will occur or the probability that failures will occur. Details of material characterization are presented in Chapter 7.

General Properties The following general material properties should be specified for both flexible and rigid pavements:

1. When pavements are considered as linear elastic, the elastic moduli and Poisson ratios of the subgrade and each component layer must be specified. The Poisson ratios have relatively small effects on pavement responses, so their values can be reasonably assumed.
2. If the elastic modulus of a material varies with the time of loading, the resilient modulus, which is the elastic modulus under repeated loads, must be selected in accordance with a load duration corresponding to the vehicle speed.
3. When a material is considered nonlinear elastic, the constitutive equation relating the resilient modulus to the state of stresses must be provided.

Flexible Pavements The following properties may be specified for flexible pavements:

1. When the HMA is considered linear viscoelastic, the creep compliance, which is the reciprocal of the moduli at various loading times, must be specified. If the temperature at the creep test is not the same as the temperature used for pavement design,

Downloaded From : www.EasyEngineering.net

Downloaded From : www.EasyEngineering.net

the time–temperature shift factor, which indicates the sensitivity of asphalt mixtures to temperature as described in Section 2.3.2, must also be provided.

2. If the design is based on fatigue cracking, the fatigue properties of asphalt mixtures, as described in Section 7.3.1, must be specified.
3. If the design is based on rut depth by summing the permanent deformations over all layers, the permanent deformation parameters of each layer must be specified. These parameters can be obtained from permanent deformation tests, as described in Section 7.4.2.
4. If other distresses, such as low-temperature cracking, are used as a basis for design, appropriate properties, such as the asphalt stiffness at the winter design temperature, should be specified.

Rigid Pavements The following properties may be specified for rigid pavements:

1. For rigid pavements on liquid foundations, the modulus of subgrade reaction, as described in Section 7.5.1, must be specified.
2. To consider the effect of temperature curling, the coefficient of thermal expansion of the concrete must be specified.
3. The most common distress in rigid pavements is fatigue cracking, so the modulus of rupture and the fatigue properties of concrete, as described in Section 7.3.2, must be specified.
4. If other distresses, such as faulting caused by excessive bearing stress on dowel bars, are used as a basis for design, appropriate properties, such as the diameter and spacing of dowels, must be specified.

1.4.4 Failure Criteria

In the mechanistic–empirical methods of pavement design, a number of failure criteria, each directed to a specific type of distress, must be established. This is in contrast to the AASHTO method, which uses the present serviceability index (PSI) to indicate the general pavement conditions. The failure criteria for mechanistic–empirical methods are described next.

Flexible Pavements It is generally agreed that fatigue cracking, rutting, and low-temperature cracking are the three principal types of distress to be considered for flexible pavement design. These criteria are fully discussed in Section 11.1.4 and are briefly described below.

Fatigue Cracking The fatigue cracking of flexible pavements is based on the horizontal tensile strain at the bottom of HMA. The failure criterion relates the allowable number of load repetitions to the tensile strain, through the laboratory fatigue test on small HMA specimens. The difference in geometric and loading conditions makes the allowable number of repetitions for actual pavements much greater than that obtained from laboratory tests. Therefore, the failure criterion must incorporate a shift factor to account for the difference.

Downloaded From : www.EasyEngineering.net

Downloaded From : www.EasyEngineering.net

Rutting Rutting occurs only on flexible pavements, as indicated by the permanent deformation or rut depth along the wheelpaths. Two design methods have been used to control rutting: one limit the vertical compressive strain on the top of subgrade, and the other limit the rutting to a tolerable amount, say, 0.5 in. (13 mm).

The first method, which requires a failure criterion based on correlations with road tests or field performance, is much easier to apply and has been used by Shell Petroleum (Claussen *et al.*, 1977) and the Asphalt Institute (Shook *et al.*, 1982). This method is based on the contention that, if the quality of the surface and base courses is well controlled, rutting can be reduced to a tolerable amount by limiting the vertical compressive strain on the subgrade.

The second method, which computes the rut depth directly, can be based on empirical correlations with road tests, as used in PDMAP (Finn et al., 1986) and MICH-PAVE (Harichandran et al., 1989) or on theoretical computations from the permanent-deformation parameters of each component layer, as incorporated in VESYS (FHWA, 1978). The Shell method also includes a procedure for estimating the rut depth in HMA (Shell, 1978). If rutting is due primarily to the decrease in thickness of the component layers above the subgrade, as was found in the AASHO Road Test, the use of this method should be more appropriate.

Thermal Cracking This type of distress includes both low-temperature cracking and thermal fatigue cracking. Low-temperature cracking is usually associated with flexible pavements in northern regions of the United States and much of Canada, where winter temperatures can fall below −10°F(−23°C). Thermal fatigue cracking can occur in much milder regions if an excessively hard asphalt is used or the asphalt becomes hardened by aging.

The most comprehensive study on low-temperature cracking has been conducted in Canada, as reported by Christison *et al.* (1972). The potential of low-temperature cracking for a given pavement can be evaluated if the mix stiffness and fracture-strength characteristics as a function of temperature and time of loading are known and if temperature data on the site are available. The pavement will crack when the computed thermal stress is greater than the fracture strength.

Thermal fatigue cracking is similar to the fatigue cracking caused by repeated loads. It is caused by the tensile strain in the asphalt layer that is due to daily temperature cycle. The cumulative damage can be evaluated by Miner's hypothesis.

Rigid Pavements Fatigue cracking has long been considered the major or only criterion for rigid pavement design. Only recently has pumping or erosion been considered. Other criteria under consideration include faulting and joint deterioration of JPCP and JRCP and edge punchout of CRCP. These criteria are fully discussed in Sections 12.1.2 through 12.1.6 and are briefly described below.

Fatigue Cracking Fatigue cracking is most likely caused by the edge stress at the midslab. The allowable number of load repetitions to cause fatigue cracking depends on the stress ratio between flexural tensile stress and the concrete modulus of rupture. Because the design is based on the edge loading and only a small portion of the traffic loads is applied at the pavement edge, the total number of load repetitions must be

Downloaded From : www.EasyEngineering.net

Downloaded From : www.EasyEngineering.net

reduced to an equivalent number of edge loads so that the same fatigue damage is obtained. This approach is different from the fatigue analysis of flexible pavements, in which a shift factor is used to adjust the allowable number of load repetitions.

Pumping or Erosion Although permanent deformation are not considered in rigid pavement design, the resilient deformation under repeated wheel loads will cause pumping of the slabs. Consequently, corner deflections have been used in the latest version of the PCA method (PCA, 1984) as an erosion criterion in addition to the fatigue criterion. The applicability of the PCA method is quite limited because it is based on the results of the AASHO Road Test, which employed a highly erodible subbase. Pumping is caused by many other factors, such as types of subbase and subgrade, precipitation, and drainage, so a more rational method for analyzing pumping is needed.

Other Criteria Other major types of distress in rigid pavements include faulting, spalling, and joint deterioration. These distresses are difficult to analyze mechanistically, and a great effort has been made recently in developing regression models to predict them. These empirical models are applicable only under the conditions from which the models were derived. Unless an extensive data base containing a sufficient number of pavement sections with widely different design characteristics is available, the usefulness of these models in practice could be limited by the large amount of error involved.

1.4.5 Reliability

In view of the fact that the predicted distress at the end of a design period varies a great deal, depending on the variability of predicted traffic and the quality control on materials and construction, it is more reasonable to use a probabilistic approach based on the reliability concept. If PSI is used as a failure criterion, the reliability of the design, or the probability that the PSI is greater than the terminal serviceability index, can be determined by assuming the PSI at the end of a design period to be a normal distribution with a mean and a standard deviation. Conversely, given the required reliability and terminal serviceability index, the acceptable PSI at the end of the design period can be computed. More details about reliability are presented in Chapter 10.

1.4.6 Pavement Management Systems

It has long been recognized that pavement design is a part of the total pavement management process, which includes planning, design, construction, maintenance, evaluation, and rehabilitation. With the use of a computer, a pavement management system (PMS) can be developed to assist decision makers in finding optimum strategies for providing, evaluating, and maintaining pavements in a serviceable condition over a given period of time. Pavement management can be divided into two generalized levels: network and project. At the network level, the pavement management system provides information on the development of an overall program of new construction, maintenance, or rehabilitation that will optimize the use of available resources. At the project level, consideration is given to alternative design, construction, maintenance, or rehabilitation activities for a particular project within the overall program.

Downloaded From : www.EasyEngineering.net

Downloaded From : www.EasyEngineering.net

Figure 1.18 is a flowchart for a project-level pavement management system (AASHTO, 1986). The traffic and loading, environment, and materials are the design factors that have just been discussed. Models of pavement structure may be a mechanistic or an empirical model for flexible or rigid pavements. Behavior is characterized by stresses, strains, or deformations; distress is evaluated by failure criteria; and performance is based on PSI. For a given reliability, the life of the pavement before the serviceability index drops below the minimum acceptable value can be evaluated. Even if the life is less than the design period, say 20 years, the option is still open, because an overlay at a later date will bring the serviceability index up and prolong the life of the pavement to more than 20 years. As long as the design meets the constraints, it will move on to the life-cycle costs block of the process.

Life-cycle costs refer to all costs, including construction, maintenance, and rehabilitation costs, all benefits, and indirect costs. An economic evaluation will be made on all possible options and an optimized design at the lowest overall cost will be selected. After the pavement has been constructed, information on performance, such as distress, roughness, traffic loading, skid characteristic, and deflection, should be monitored and put into a data bank. The feedback of these performance data into the PMS information system is crucial to the development of mechanistic–empirical design procedures. More about PMS is presented in Appendix E.

It should be noted that pavement design is a critical part of pavement management. Poor design practice will result in higher pavement maintenance and rehabilitation costs throughout the years and has by far the greatest effect on life-cycle costs. Recent developments in pavement technology, such as the improvement in laboratory and field testing equipment and the availability of high-speed microcomputers, have provided pavement designers with more tools to evaluate the consequences of design alternatives on life-cycle costs.

1.5 HIGHWAY PAVEMENTS, AIRPORT PAVEMENTS, AND RAILROAD TRACKBEDS

The principles used for the design of highway pavements can also be applied to those of airport pavements and railroad trackbeds, with some modifications.

1.5.1 Highway Versus Airport

Airport pavements are generally thicker than highway pavements and require better surfacing materials, because the loading and tire pressure of aircraft are much greater than those of highway vehicles. The effect of loading and tire pressure can be taken care of automatically in any mechanistic method of design, whether the pavement is used for a highway or an airport. However, the following differences should be noted in applying the mechanistic methods:

1. The number of load repetitions on airport pavements is usually smaller that on highway pavements. On airport pavements, due to the wander of aircraft, several passages of a set of gears are counted as one repetition, whereas on highway pavements, the passage of one axle is considered as one repetition. The fact that highway loadings are not really applied at the same location is considered in the

Downloaded From : www.EasyEngineering.net

Downloaded From : www.EasyEngineering.net

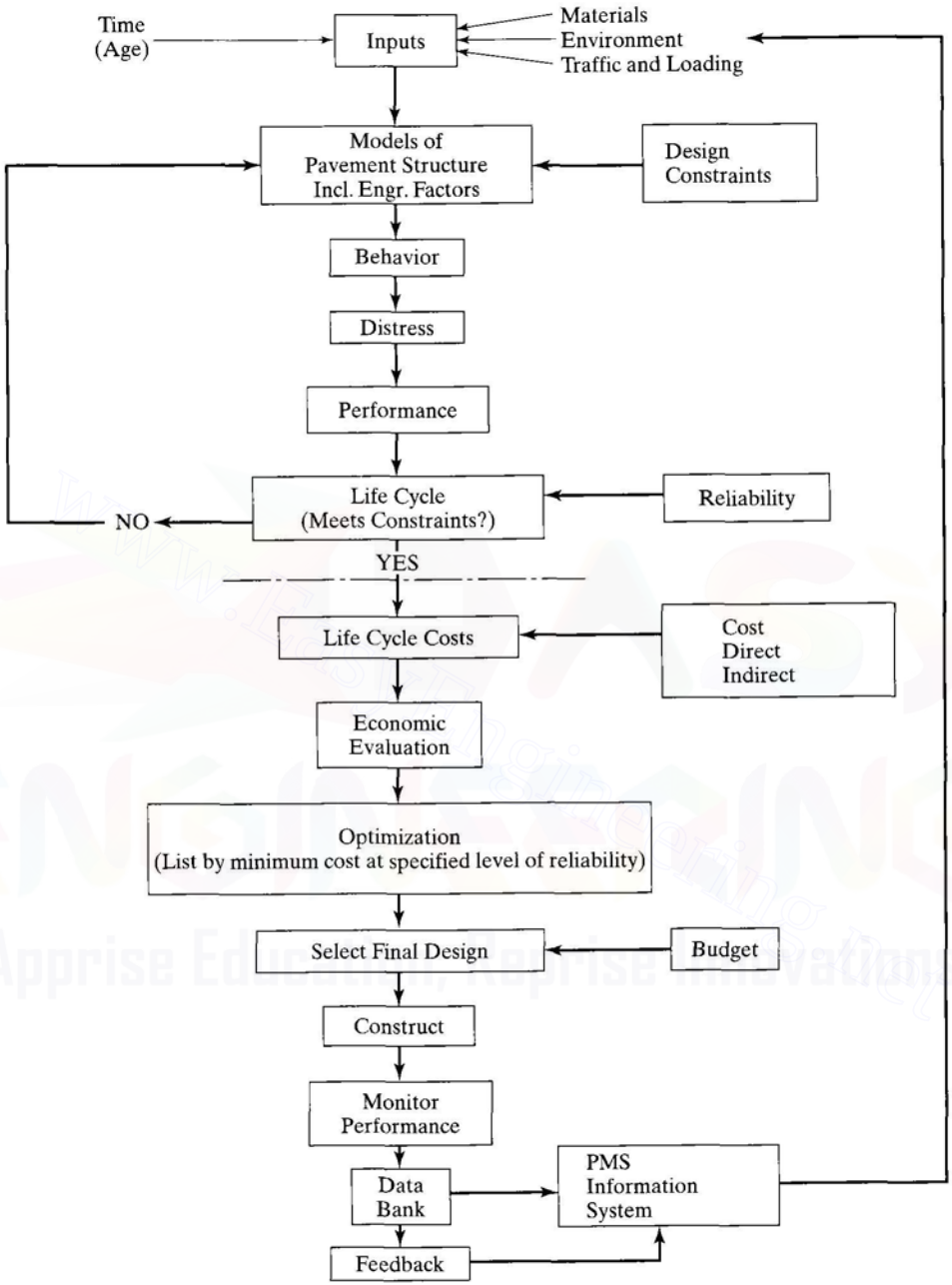


FIGURE 1.18

Flow diagram of a project-level pavement management system. (From the *AASHTO Guide for Design of Pavement Structures*. Copyright 1986. American Association of State Highway and Transportation Officials, Washington, DC. Used by permission.)

Downloaded From : www.EasyEngineering.net

Downloaded From : www.EasyEngineering.net

failure criteria by increasing the allowable number of load repetitions, such as the incorporation of a shift factor for the fatigue of flexible pavements, as described in Section 7.3.1, and an equivalent damage ratio for the fatigue of rigid pavements, as described in Section 12.1.2.

2. The design of highway pavements is based on moving loads with the loading duration as an input for viscoelastic behaviors and the resilient modulus under repeated loads for elastic behaviors. The design of airport pavements is based on moving loads in the interior of runways but stationary loads at the end of runways. As a result, thicker pavements are used at the runway end than in the interior.
3. Although loads are applied near to the edge of highway pavements but far away from the outside edge of airport pavements, this fact is not considered in the design of flexible pavements. It is assumed that the edge effect is insignificant if a load is at a distance of 2 to 3 ft (0.6 to 0.9 m) from the edge, so the layered theory can still be applied. However, this fact should be considered in the design of rigid pavements. The Portland Cement Association employs edge loading for the design of highway pavements (PCA, 1984), but interior loading for the design of airport pavements (PCA, 1955). The Federal Aviation Administration considers edge loading, but the edge stress is reduced by 25% to account for load transfer across the joint (FAA, 1988), so the loading is applied at the longitudinal joint, not really at the outside pavement edge. Even if the loads can be applied near the outside edge of airport pavements in certain situations, the number of load repetitions is small and may be neglected. The above contention is based on the assumption that the design is based on fatigue and the fact that the stresses at the edge and the interior are greater than those at the joints. This is not true if the design is based on the erosion caused by the corner deflection at the joints.

1.5.2 Highway Versus Railroad

Two methods have been used to incorporate HMA in railroad trackbeds, as shown in Figure 1.19. The first method, which is similar to the construction of flexible highway pavements, is called overlayment. The HMA is placed on top of the subgrade or above a layer of base course, and the ties are placed directly on the asphalt mat. In the second method, called underlayment, the asphalt mat is placed under the ballast.

Based on the same design principles as used in highway pavements, Huang et al. (1984b) developed a computer model called KENTRACK for the design of HMA railroad trackbeds. The design considers traffic and loading, environment, and materials as the major factors and applies Burmister's layered theory and Miner's hypothesis of cumulative damage (Miner, 1945). However, there is a major difference between a highway pavement and a railroad trackbed, namely, the distribution of wheel loads to the layered system. On highway pavements, wheel loads are applied over small areas and the magnitude of loads on each area is a constant independent of the stiffness of the layered system. On railroad trackbeds, wheel loads are distributed through rails and ties over a large area and the load on the most critical tie under the heaviest wheel load depends strongly on the stiffness of the layered system. Therefore, the use of thicker

Downloaded From : www.EasyEngineering.net

Downloaded From : www.EasyEngineering.net

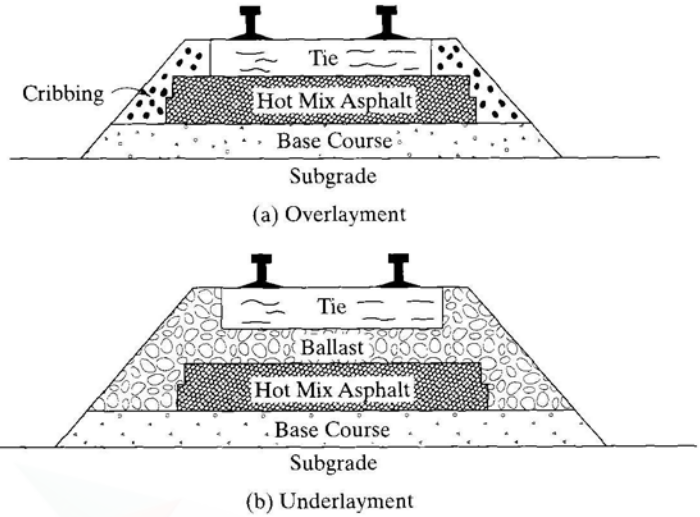


FIGURE 1.19
Hot-mix-asphalt railroad trackbeds.

HMA for highway pavements is very effective in reducing both the tensile strain at the bottom of HMA and the compressive strain on the top of subgrade, but not very effective for railroad trackbeds. In fact, for an underlayment with a given combined thickness of ballast and HMA, the tensile strain increases as the HMA thickness increases, which indicates that the use of ballast is more effective than the use of HMA in reducing tensile strains (Huang et al., 1985). That the replacements of ballast by HMA increases the tensile strain is due to the load concentration, as indicated by the tremendous increase in the maximum contact pressure between tie and ballast caused by the stiffer trackbed.

It was also found that overlayment cannot be used for heavy-haul trackbeds, because the required thickness of asphalt mat is just too excessive, while an underlayment with a thick layer of ballast and a thin layer of HMA can easily satisfy the design requirements (Huang *et al.*, 1987). For the same reason, the use of full-depth construction, which is popular for highway pavements, is not recommended for railroad trackbeds. Although the vertical compressive strain on the top of subgrade has been used most frequently for the design of highway pavements, it was found that the use of vertical compressive stress is more appropriate for railroad trackbeds (Huang *et al.*, 1984a, 1986a).

Portland cement concrete can be used for the construction of slab tracks. The design of slab tracks is similar to that of rigid highway pavements, except that loads are applied to the rails connected directly to the concrete slab or through rubber-booted block ties. The KENTRACK computer program, originally developed for the design of HMA and conventional ballasted trackbeds, was later expanded for the design of slab tracks via the finite-element method and the fatigue principle (Huang *et al.*, 1986b).

Downloaded From : www.EasyEngineering.net

Downloaded From : www.EasyEngineering.net

SUMMARY

This chapter provides an introduction to pavement analysis and design. It covers five major sections: historical development, pavement types, road tests, design factors, and the differences between highway pavements and airport pavements and between highway pavements and railroad trackbeds. The three major road tests constitute an important part of historical development but are presented in a separate section after pavement types, so that the conclusions drawn from the road tests can be more easily understood. Also included is a brief description of the recently completed Strategic Highway Research Program (SHRP).

Important Points Discussed in Chapter 1

1. There has been a dramatic change in the design methods for flexible pavements, from the early purely empirical methods to the modern mechanistic–empirical methods. With the availability of high-speed microcomputers and sophisticated testing methods, the trend toward mechanistic methods is apparent.
2. The most practical and widely used mechanistic–empirical method for flexible pavement design is based on Burmister's elastic layered theory of limiting the horizontal tensile strain at the bottom of asphalt layer and the vertical compressive strain on the surface of subgrade. With modifications, the method can be applied to layered systems consisting of viscoelastic and nonlinear elastic materials.
3. Westergaard's plate theory has been used for the design of rigid pavements since the 1920s. The method can be applied only to a single slab on a liquid foundation with full slab–subgrade contact. Most design methods are based on the flexural stress in the concrete. Earlier designs considered stress due to corner loading to be the most critical. With wider traffic lanes and more efficient load transfer, edge stress due to edge loadings near the midslab is now being considered more critical. The current PCA method considers both the edge stress to prevent fatigue cracking and the corner deflection to minimize pumping or erosion of the subgrade.
4. The most practical method to analyze multiple slabs on a layer foundation with partial slab–foundation contact is by the finite-element computer programs. With the increase in speed and storage of modern computers, it is no longer necessary to consider the foundation as a liquid. More use of solid or layer foundation in design is expected in years to come.
5. There are two major types of pavements: flexible and rigid. The design of flexible pavements is based on the layered theory by assuming that the layers are infinite in areal extent with no discontinuities. Because of the rigidity of the slab and the existence of joints, the design of rigid pavements is based on the plate theory. Layered theory can also be applied to rigid pavements if the loads are applied in the interior of a slab. A third type of pavement is called the composite pavement. Composite pavements should be designed by the plate theory, because concrete is the main load-carrying component.
6. The two types of flexible pavements in common use are conventional and full-depth. Conventional pavements are layer systems with better materials on top and are most suited to regions where local materials are available. Full-depth

Downloaded From : www.EasyEngineering.net

Downloaded From : www.EasyEngineering.net

asphalt pavements, though more expensive, have gained popularity because of their many advantages over conventional pavements.

7. The four types of rigid pavements are jointed plain concrete pavement (JPCP), jointed reinforced concrete pavement (JRCP), continuous reinforced concrete pavement (CRCP), and prestressed concrete pavement (PCP). The most economical construction is JPCP with closely spaced joints. Steel reinforcements in JRCP do not increase its structural capacity, but allow the use of longer joint spacings; if the pavement cracks, the steel can tie the concrete together. The advantage of CRCP is the complete elimination of transverse joints. Previous experience has indicated that the thickness required for CRCP should be the same as that for JPCP and JRCP. Although several experimental projects have been constructed in the United States, the use of PCP for highway pavements is limited, because the savings in materials is not sufficient to compensate for the extensive labor required.
8. The three major road tests conducted from the mid-1940s to the early 1960s are the Maryland Road Test for rigid pavements, the WASHO Road Test for flexible pavements, and the AASHO Road Test for both flexible and rigid pavements. The first two tests were initiated for taxation purposes to determine the relative effects of four different axle loads on pavement distress; the last test was more comprehensive and involved the development of equations for design purposes.
9. A significant outcome for each test is summarized as follows: The Maryland Road Test indicated that pumping was the major cause of distress for pavements on fine-grained soils and that the stresses for all cases of loading were less than 50% of the modulus of rupture of the concrete prior to the development of pumping, but increased tremendously after pumping and caused the rupture of the slab. The WASHO Road Test indicated that the distress in the outer wheelpath was more than that in the inner wheelpath and that the outer wheelpath with paved shoulders was the equivalent of the inner wheelpath, thus testifying to the advantage of shoulder paving. The AASHO Road Test developed the pavement serviceability concept and the equations relating the change in serviceability to the number of load repetitions, thus adding a new dimension to pavement design.
10. Most of the design methods in use today are based on the 18-kip equivalent single-axle load and a fixed set of material properties for the entire design period. However, with the use of modern computers and the mechanistic–empirical methods, these limitations and approximations can be overcome. Each axle-load group can be considered separately, and each year can be divided into a number of periods with widely different material properties for damage analysis.
11. Many of the mechanistic–empirical methods for flexible pavement design are based on the horizontal tensile strain at the bottom of the asphalt layer and the vertical compressive strain on the surface of subgrade. With heavier axle loads and higher tire pressures, much of the permanent deformation occurs in the upper layers above the subgrade. Consequently, the determination of permanent deformation in each individual layer, instead of the vertical compressive strain on the subgrade, is a better approach.

Downloaded From : www.EasyEngineering.net

Downloaded From : www.EasyEngineering.net

12. The fatigue principle has long been used throughout the world for the design of concrete pavements. In view of the fact that pumping is the main cause of distress, the inclusion of corner deflection as a failure criterion, in addition to fatigue cracking, is warranted.
13. Other than the AASHTO empirical methods, the concepts of serviceability and reliability have not been widely accepted in current methods of pavement design. As more research is directed to these concepts and more efficient computer programs are developed, it is expected that these concepts will become more popular and widely accepted in future mechanistic–empirical methods.
14. With the availability of high-speed computers and the improvement in laboratory and field testing equipment, pavement design should be integrated into the pavement management system, so that the consequences of design alternatives on life-cycle costs can be evaluated.
15. The design principles used for highway pavements can be equally applied to airport pavements with only a few exceptions, such as the consideration of aircraft wandering on the number of load repetitions and the use of stationary loads at the end of runways.
16. The use of full-depth asphalt, which is popular for highway pavements, is ineffective for railroad trackbeds. It is more economical to place the HMA under the ballast rather than over the ballast.

PROBLEMS AND QUESTIONS

1.1 Sketch and show the dimensions of the most realistic contact areas for a dual-tandem axle load of 40,000 lb with a tire pressure of 100 psi. If the contact areas are assumed as rectangles, what should be the dimension of the rectangular area? [Answer: most realistic area consisting of a rectangle and two semicircles with a length of 9.78 in. and a width of 5.87 in.; rectangular area with a length of 8.52 in. and a width of 5.87 in.]

1.2 Mean monthly temperatures at a given paving project are September, 50°F; October, 32°F; November, 24°F; December, −3°F; January, 14°F; February, 16°F; March, 22°F; April, 25°F; and May, 40°F. Calculate the freezing index. Is this value likely to be different from the freezing index calculated from mean daily temperature? [Answer: 2851 degree days]

1.3 Why is the limiting shear failure method of flexible pavement design rarely in use today? Under what situations could the method be used?

1.4 What is meant by the mechanistic–empirical method of pavement design? Is it possible to develop a wholly mechanistic method of pavement design? Why?

1.5 What are the purposes of using a seal coat?

1.6 What is the difference between a tack coat and a prime coat? Which requires the use of a less viscous asphalt?

1.7 Why are flexible pavements generally built in layers with better materials on top?

1.8 What is the difference between a surface course and a binder course? Under what conditions should a binder course be used?

1.9 What are the advantages of placing a layer of HMA under a granular base or subbase?

1.10 Describe the mechanics of pumping.

1.11 Explain why rigid pavements pump, whereas very few flexible pavements do so. Under what conditions would a flexible pavement result in pumping?

1.12 Which is more frost susceptible, silt or clay? Why?

Downloaded From : www.EasyEngineering.net

Downloaded From : www.EasyEngineering.net

1.13 Is frost heave due solely to the 9% volume expansion of soil water during freezing? Why?
1.14 Discuss the pros and cons of JPCP versus JRCP.
1.15 Discuss the pros and cons of JRCP versus CRCP.
1.16 What are the advantages and disadvantages of prestressed pavements?
1.17 What is the major distress in a composite pavement? How can it be prevented?
1.18 Why are modern concrete pavements no longer built with a thickened edge?
1.19 List any two conclusions from the Maryland Road Test that are similar to those found in the AASHO Road Test.
1.20 List any two conclusions from the WASHO Road Test that are similar to those found in the AASHO Road Test.
1.21 List any two conclusions from the Maryland Road Test on rigid pavements that are similar to the WASHO Road Test on flexible pavements.
1.22 Explain why, for a high-pressure tire, contact pressure is smaller than tire pressure.
1.23 Why is the shape of contact area used for the design of flexible pavements different from that for rigid pavements?
1.24 On which pavement does pumping occur more frequently, airport or highway?
1.25 For a given wheel load, which should be thicker, a highway or an airport pavement? Why?
1.26 Discuss the basic design differences between an airport and a highway pavement.
1.27 Discuss the basic design differences between a highway pavement and a railroad trackbed.
1.28 What is meant by full-depth construction? Why is full-depth construction not recommended for railroad trackbeds?

Downloaded From : www.EasyEngineering.net

Downloaded From : www.EasyEngineering.net

CHAPTER 2

Stresses and Strains in Flexible Pavements

2.1 HOMOGENEOUS MASS

The simplest way to characterize the behavior of a flexible pavement under wheel loads is to consider it as a homogeneous half-space. A half-space has an infinitely large area and an infinite depth with a top plane on which the loads are applied. The original Boussinesq (1885) theory was based on a concentrated load applied on an elastic half-space. The stresses, strains, and deflections due to a concentrated load can be integrated to obtain those due to a circular loaded area. Before the development of layered theory by Burmister (1943), much attention was paid to Boussinesq solutions because they were the only ones available. The theory can be used to determine the stresses, strains, and deflections in the subgrade if the modulus ratio between the pavement and the subgrade is close to unity, as exemplified by a thin asphalt surface and a thin granular base. If the modulus ratio is much greater than unity, the equation must be modified, as demonstrated by the earlier Kansas design method (Kansas State Highway Commission, 1947).

Figure 2.1 shows a homogeneous half-space subjected to a circular load with a radius a and a uniform pressure q. The half-space has an elastic modulus E and a Poisson ratio v. A small cylindrical element with center at a distance z below the surface and r from the axis of symmetry is shown. Because of axisymmetry, there are only three normal stresses, σ_z, σ_r, and σ_t, and one shear stress, τ_{rz}, which is equal to τ_{zr}. These stresses are functions of q, r/a, and z/a.

2.1.1 Solutions by Charts

Foster and Ahlvin (1954) presented charts for determining vertical stress σ_z, radial stress σ_r, tangential stress σ_t, shear stress τ_{rz}, and vertical deflection w, as shown in Figures 2.2 through 2.6. The load is applied over a circular area with a radius a—and an

Downloaded From : www.EasyEngineering.net

Downloaded From : www.EasyEngineering.net

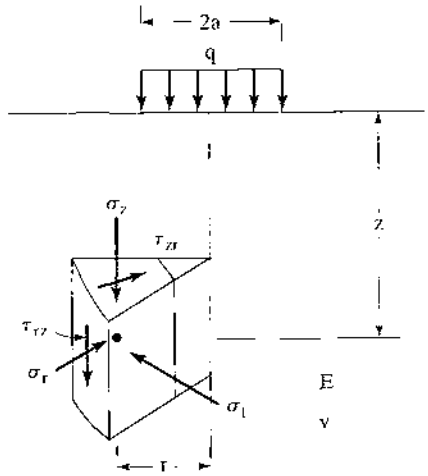


FIGURE 2.1

Component of stresses under axisymmetric loading.

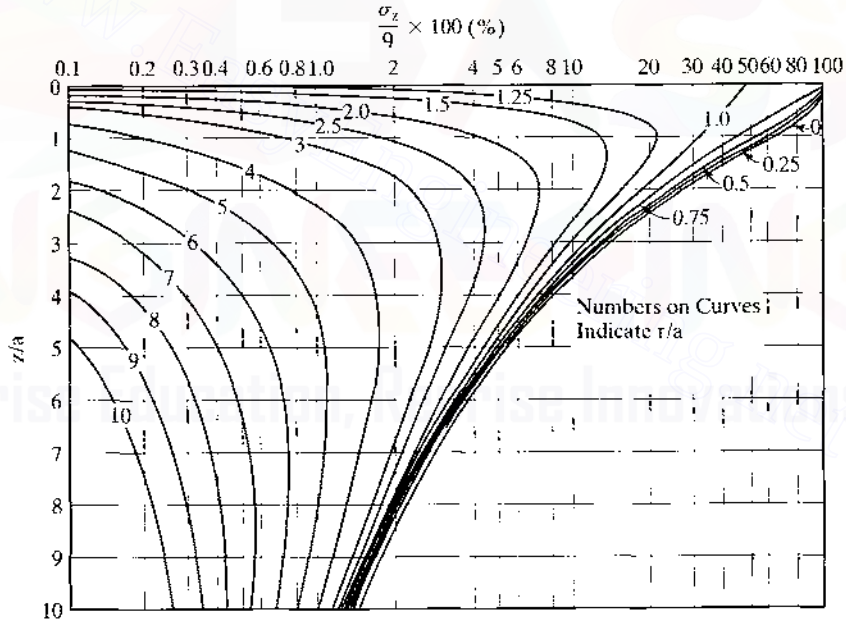


FIGURE 2.2

Vertical stresses due to circular loading. (After Foster and Ahlvin (1954).)

intensity q. Because Poisson ratio has a relatively small effect on stresses and deflections, Foster and Ahlvin assumed the half-space to be incompressible with a Poisson ratio of 0.5, so only one set of charts is needed instead of one for each Poisson ratio. This work was later refined by Ahlvin and Ulery (1962) who presented a series of

Downloaded From : www.EasyEngineering.net

Downloaded From : www.EasyEngineering.net

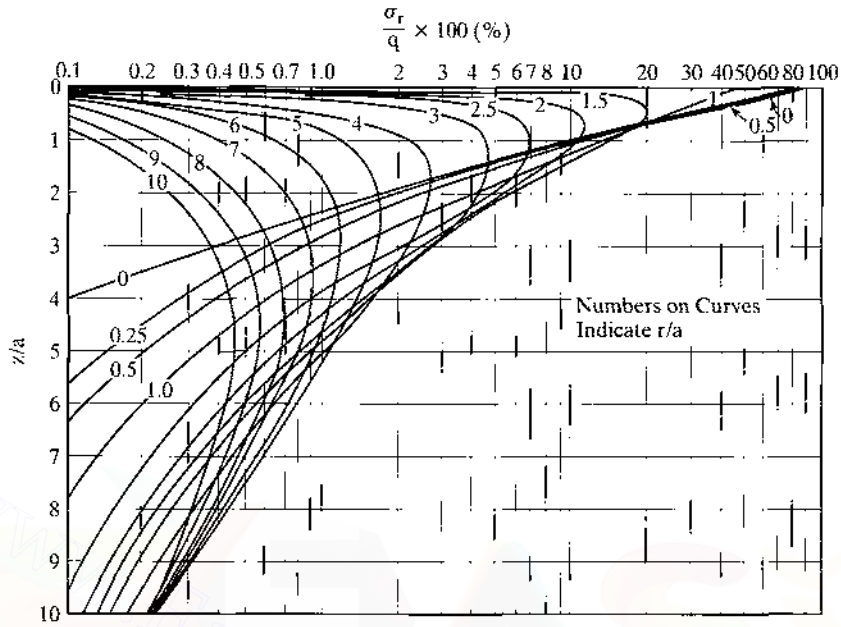


FIGURE 2.3

Radial stresses due to circular loading. (After Foster and Ahlvin, (1954).)

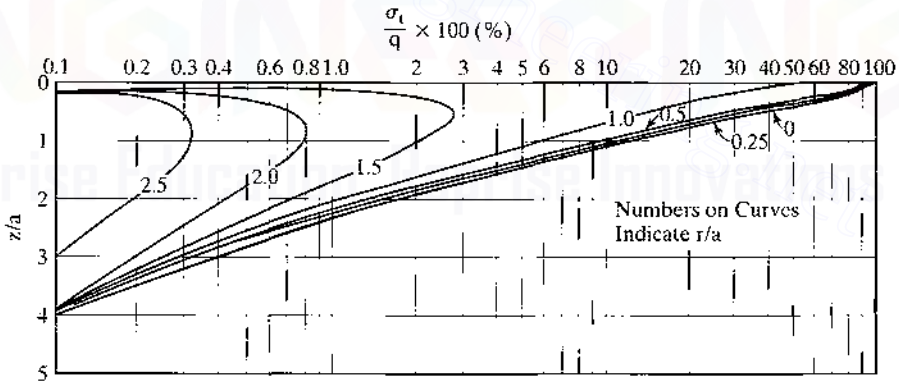


FIGURE 2.4

Tangential stresses due to circular loading. (After Foster and Ahlvin (1954).)

equations and tables so that the stresses, strains, and deflections for any given Poisson ratio can be computed. These equations and tables are not presented here because the solutions can be easily obtained from KENLAYER by assuming the homogeneous half-space to be a two-layer system, one of any thickness, but having the same elastic modulus and Poisson ratio for both layers.

Downloaded From : www.EasyEngineering.net

Downloaded From : www.EasyEngineering.net

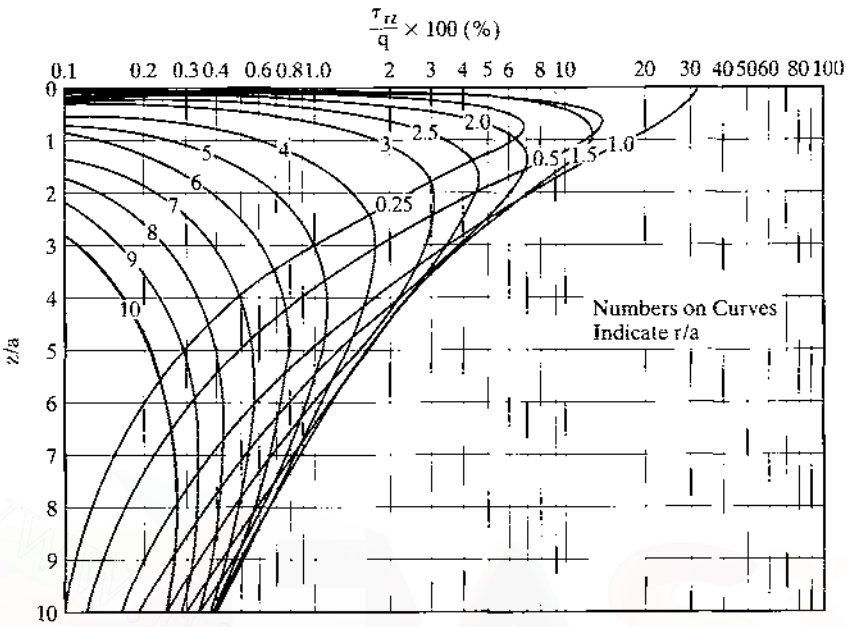


FIGURE 2.5

Shear stresses due to circular loading. (After Foster and Ahlvin (1954).)

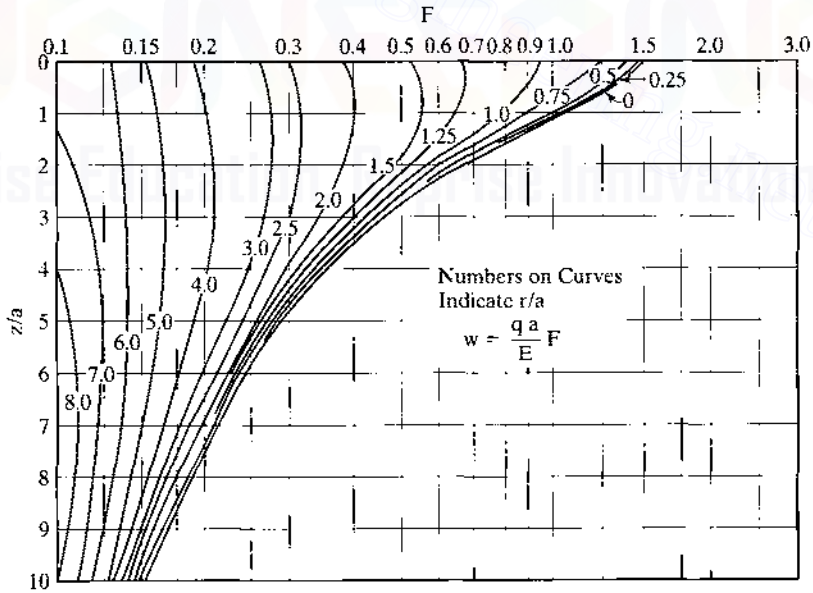


FIGURE 2.6

Vertical deflections due to circular loading. (After Foster and Ahlvin (1954).)

Downloaded From : www.EasyEngineering.net

Downloaded From : www.EasyEngineering.net

After the stresses are obtained from the charts, the strains can be obtained from

$$\epsilon_z = \frac{1}{E}[\sigma_z - v(\sigma_r + \sigma_t)] \tag{2.1a}$$

$$\epsilon_r = \frac{1}{E}[\sigma_r - v(\sigma_t + \sigma_z)] \tag{2.1b}$$

$$\epsilon_t = \frac{1}{E}[\sigma_t - v(\sigma_z + \sigma_r)] \tag{2.1c}$$

If the contact area consists of two circles, the stresses and strains can be computed by superposition.

Example 2.1:

Figure 2.7 shows a homogeneous half-space subjected to two circular loads, each 10 in. (254 mm) in diameter and spaced at 20 in. (508 mm) on centers. The pressure on the circular area is 50 psi (345 kPa). The half-space has elastic modulus 10,000 psi (69 MPa) and Poisson ratio 0.5. Determine the vertical stress, strain, and deflection at point A, which is located 10 in. (254 mm) below the center of one circle.

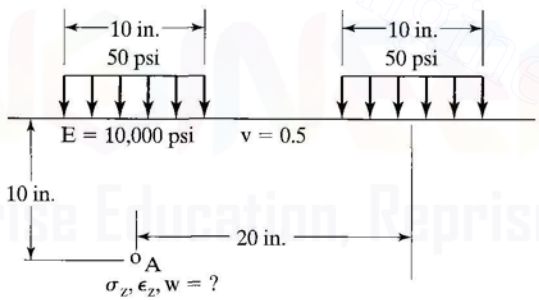


FIGURE 2.7
Example 2.1 (1 in. = 25.4 mm, psi = 6.9 kPa).

Solution: Given $a = 5$ in. (127 mm), $q = 50$ psi (345 kPa), and $z = 10$ in. (254 mm), from Figures 2.2, 2.3, and 2.4, the stresses at point A due to the left load with $r/a = 0$ and $z/a = 10/5 = 2$ are $\sigma_z = 0.28 \times 50 = 14.0$ psi (96.6 kPa) and $\sigma_r = \sigma_t = 0.016 \times 50 = 0.8$ psi (5.5 kPa); and those due to the right load with $r/a = 20/5 = 4$ and $z/a = 2$ are $\sigma_z = 0.0076 \times 50 = 0.38$ *psi (2.6 kPa)*, $\sigma_r = 0.026 \times 50 = 1.3$ psi (9.0 kPa), and $\sigma_t = 0$. By superposition, $\sigma_z = 14.0 + 0.38 = 14.38$ psi (99.2 kPa), $\sigma_r = 0.8 + 1.3 = 2.10$ psi (14.5 kPa), and $\sigma_t = 0.8$ psi (5.5 kPa). From Eq. 2.1*a*, $\epsilon_z = [14.38 - 0.5(2.10 + 0.8)]/10{,}000 = 0.00129$. From Figure 2.6, the deflection factor at point A due to the left load is 0.68 and that due to the right load is 0.21. The total deflection $w = (0.68 + 0.21) \times 50 \times 5/10{,}000 = 0.022$ in. (0.56 mm). The final answer is $\sigma_z = 14.38$ psi (99.2 kPa), $\epsilon_z = 0.00129$, and $w = 0.022$ in. (0.56 mm). The results obtained from KENLAYER are $\sigma_z = 14.6$ psi (100.7 kPa), $\epsilon_z = 0.00132$, and $w = 0.0218$ in. (0.554 mm), which check closely with those from the charts.

Downloaded From : www.EasyEngineering.net

Downloaded From : www.EasyEngineering.net

In applying Boussinesq's solutions, it is usually assumed that the pavement above the subgrade has no deformation, so the deflection on the pavement surface is equal to that on the top of the subgrade. In the above example, if the pavement thickness is 10 in. (254 mm) and point A is located on the surface of the subgrade, the deflection on the pavement surface is 0.022 in. (0.56 mm).

2.1.2 Solutions at Axis of Symmetry

When the load is applied over a single circular loaded area, the most critical stress, strain, and deflection occur under the center of the circular area on the axis of symmetry, where $\tau_{rz} = 0$ and $\sigma_r = \sigma_t$, so σ_z and σ_r are the principal stresses.

Flexible Plate The load applied from tire to pavement is similar to a flexible plate with a radius a and a uniform pressure q. The stresses beneath the center of the plate can be determined from

$$\sigma_z = q\left[1 - \frac{z^3}{(a^2 + z^2)^{1.5}}\right] \tag{2.2}$$

$$\sigma_r = \frac{q}{2}\left[1 + 2v - \frac{2(1 + v)z}{(a^2 + z^2)^{0.5}} + \frac{z^3}{(a^2 + z^2)^{1.5}}\right] \tag{2.3}$$

Note that σ_z is independent of E and v, and σ_r is independent of E. From Eq. 2.1,

$$\epsilon_z = \frac{(1 + v)q}{E}\left[1 - 2v + \frac{2vz}{(a^2 + z^2)^{0.5}} - \frac{z^3}{(a^2 + z^2)^{1.5}}\right] \tag{2.4}$$

$$\epsilon_r = \frac{(1 + v)q}{2E}\left[1 - 2v - \frac{2(1 - v)z}{(a^2 + z^2)^{0.5}} + \frac{z^3}{(a^2 + z^2)^{1.5}}\right] \tag{2.5}$$

The vertical deflection w can be determined from

$$w = \frac{(1 + v)qa}{E}\left\{\frac{a}{(a^2 + z^2)^{0.5}} + \frac{1 - 2v}{a}\left[(a^2 + z^2)^{0.5} - z\right]\right\} \tag{2.6}$$

When $v = 0.5$, Eq. 2.6 can be simplified to

$$w = \frac{3qa^2}{2E(a^2 + z^2)^{0.5}} \tag{2.7}$$

On the surface of the half-space, $z = 0$; from Eq. 2.6,

$$w_0 = \frac{2(1 - v^2)qa}{E} \tag{2.8}$$

Downloaded From : www.EasyEngineering.net

Downloaded From : www.EasyEngineering.net

Example 2.2:

Same as Example 2.1, except that only the left loaded area exists and the Poisson ratio is 0.3, as shown in Figure 2.8. Determine the stresses, strains, and deflection at point A.

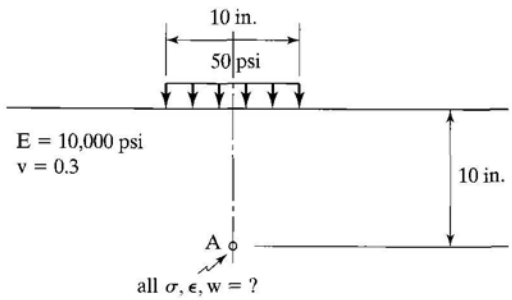


FIGURE 2.8

Example 2.2 (1 in. = 25.4 mm, 1 psi = 6.9 kPa).

Solution: Given $a = 5$ in. (127 mm), $q = 50$ psi (345 kPa), and $z = 10$ in. (254 mm), from Eq. 2.2, $\sigma_z = 50[1 - 1000/(25 + 100)^{1.5}] = 14.2$ psi (98.0 kPa). With $v = 0.3$, from Eq. 2.3, $\sigma_r = 25[1 + 0.6 - 2.6 \times 10/(125)^{0.5} + 1000/(125)^{1.5}] = -0.25$ psi (-1.7 kPa). The negative sign indicates tension, which is in contrast to a compressive stress of 0.8 psi (5.5 kPa) when $v = 0.5$. From Eq. 2.4, $\epsilon_z = 1.3 \times 50/10{,}000\,[1 - 0.6 + 0.6 \times 10/(125)^{0.5} - 1000/(125)^{1.5}] = 0.00144$. From Eq. 2.5, $\epsilon_r = 1.3 \times 50/20{,}000\,[1 - 0.6 - 1.4 \times 10/(125)^{0.5} + 1000/(125)^{1.5}] = -0.00044$. From Eq. 2.6, $w = 1.3 \times 50 \times 5/10{,}000\,\{5/(125)^{0.5} + 0.4/5[(125)^{0.5} - 10]\} = 0.0176$ in. (0.447 mm). The results obtained from KENLAYER are $\sigma_z = 14.2$ psi (98.0 kPa), $\sigma_r = -0.249$ psi (-1.72 kPa), $\epsilon_z = 0.00144$, $\epsilon_r = -0.000444$, and $w = 0.0176$ in. (0.447 mm), which are nearly the same as those derived from the formulas.

Rigid Plate All the above analyses are based on the assumption that the load is applied on a flexible plate, such as a rubber tire. If the load is applied on a rigid plate, such as that used in a plate loading test, the deflection is the same at all points on the plate, but the pressure distribution under the plate is not uniform. The differences between a flexible and a rigid plate are shown in Figure 2.9.

The pressure distribution under a rigid plate can be expressed as (Ullidtz, 1987)

$$q(r) = \frac{qa}{2(a^2 - r^2)^{0.5}} \tag{2.9}$$

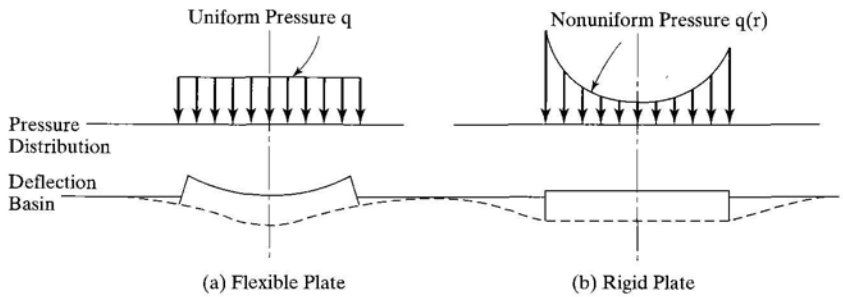


FIGURE 2.9

Differences between flexible and rigid plates.

Downloaded From : www.EasyEngineering.net

Downloaded From : www.EasyEngineering.net

in which r is the distance from center to the point where pressure is to be determined and q is the average pressure, which is equal to the total load divided by the area. The smallest pressure is at the center and equal to one-half of the average pressure. The pressure at the edge of the plate is infinity. By integrating the point load over the area, it can be shown that the deflection of the plate is

$$w_0 = \frac{\pi(1 - v^2)qa}{2E} \tag{2.10}$$

A comparison of Eq. 2.10 with Eq. 2.8 indicates that the surface deflection under a rigid plate is only 79% of that under the center of a uniformly distributed load. This is reasonable because the pressure under the rigid plate is smaller near the center of the loaded area but greater near the edge. The pressure near the center has a greater effect on the surface deflection at the center. Although Eqs. 2.8 and 2.10 are based on a homogeneous half-space, the same factor, 0.79, can be applied if the plates are placed on a layer system, as indicated by Yoder and Witczak (1975).

Example 2.3:

A plate loading test using a plate of 12-in. (305-mm) diameter was performed on the surface of the subgrade, as shown in Figure 2.10. A total load of 8000 lb (35.6 kN) was applied to the plate, and a deflection of 0.1 in. (2.54 mm) was measured. Assuming that the subgrade has Poisson ratio 0.4, determine the elastic modulus of the subgrade.

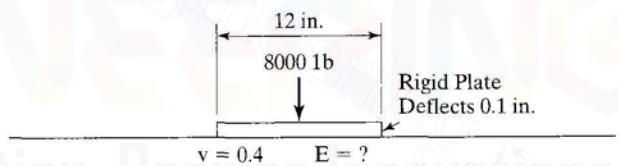


FIGURE 2.10
Example 2.3 (1 = 25.4 mm, 1 lb = 4.45 N).

Solution: The average pressure on the plate is $q = 8000/(36\pi) = 70.74$ psi (488 kPa). From Eq. 2.10, $E = \pi(1 - 0.16) \times 70.74 \times 6/(2 \times 0.1) = 5600$ psi (38.6 MPa).

2.1.3 Nonlinear Mass

Boussinesq's solutions are based on the assumption that the material that constitutes the half-space is linear elastic. It is well known that subgrade soils are not elastic and undergo permanent deformation under stationary loads. However, under the repeated application of moving traffic loads, most of the deformations are recoverable and can be considered elastic. It is therefore possible to select a reasonable elastic modulus commensurate with the speed of moving loads. Linearity implies the applicability of the superposition principle, so the elastic constant must not vary with the state of stresses. In other words, the axial deformation of a linear elastic material under an axial stress should be independent of the confining pressure. This is evidently not true for

Downloaded From : www.EasyEngineering.net

Downloaded From : www.EasyEngineering.net

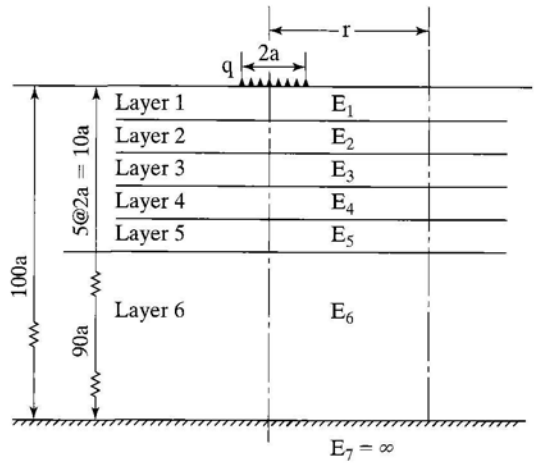


FIGURE 2.11
Division of half-space into a seven-layer system.

soils, because their axial deformation depends strongly on the magnitude of confining pressures. Consequently, the effect of nonlinearity on Boussinesq's solution is of practical interest.

Iterative Method To show the effect of nonlinearity of granular materials on vertical stresses and deflections, Huang (1968a) divided the half-space into seven layers, as shown in Figure 2.11, and applied Burmister's layered theory to determine the stresses at the midheight of each layer. Note that the lowest layer is a rigid base with a very large elastic modulus.

After the stresses are obtained, the elastic modulus of each layer is determined from

$$E = E_0(1 + \beta\theta) \tag{2.11}$$

in which θ is the stress invariant, or the sum of three normal stresses; E is the elastic modulus under the given stress invariant; E_0 is the initial elastic modulus, or the modulus when the stress invariant is zero; and β is a soil constant indicating the increase in elastic modulus per unit increase in stress invariant. Note that the stress invariant should include both the effects of the applied load and the geostatic stresses; it can be expressed as

$$\theta = \sigma_z + \sigma_r + \sigma_t + \gamma z(1 + 2K_0) \tag{2.12}$$

in which σ_z, σ_r, and σ_t are the vertical, radial, and tangential stresses due to loading; γ is the unit weight of soil; z is the distance below ground surface at which the stress invariant is computed; and K_0 is the coefficient of earth pressure at rest. The problem can be solved by a method of successive approximations. First, an elastic modulus is assumed for each layer and the stresses are obtained from the layered theory. Given

Downloaded From : www.EasyEngineering.net

Downloaded From : www.EasyEngineering.net

the stresses thus obtained, a new set of moduli is determined from Eq. 2.11 and a new set of stresses is then computed. The process is repeated until the moduli between two consecutive iterations converge to a specified tolerance.

In applying the layered theory for nonlinear analysis, a question immediately arises: Which radial distance r should be used to determine the stresses and the moduli? Huang (1968a) showed that the vertical stresses are not affected significantly by whether the stresses at $r = 0$ or $r = \infty$ are used to determine the elastic modulus, but the vertical displacements are tremendously affected. He later used the finite-element method and found that the nonlinear behavior of soils has a large effect on vertical and radial displacements, an intermediate effect on radial and tangential stresses, and a very small effect on vertical and shear stresses (Huang, 1969a). Depending on the depth of the point in question, the vertical stresses based on nonlinear theory may be greater or smaller than those based on linear theory and, at a certain depth, both theories could yield the same stresses. This may explain why Boussinesq's solutions for vertical stress based on linear theory have been applied to soils with varying degrees of success, even though soils themselves are basically nonlinear.

Approximate Method One approximate method to analyze a nonlinear half-space is to divide it into a number of layers and determine the stresses at the midheight of each layer by Boussinesq's equations based on linear theory. From the stresses thus obtained, the elastic modulus E for each layer is determined from Eq. 2.11. The deformation of each layer, which is the difference in deflection between the top and bottom of each layer based on the given E, can then be obtained. Starting from the rigid base, or a depth far from the surface where the vertical displacement can be assumed zero, the deformations are added to obtain the deflections at various depths. The assumption of Boussinesq's stress distribution was used by Vesic and Domaschuk (1964) to predict the shape of deflection basins on highway pavements, and satisfactory agreements were reported.

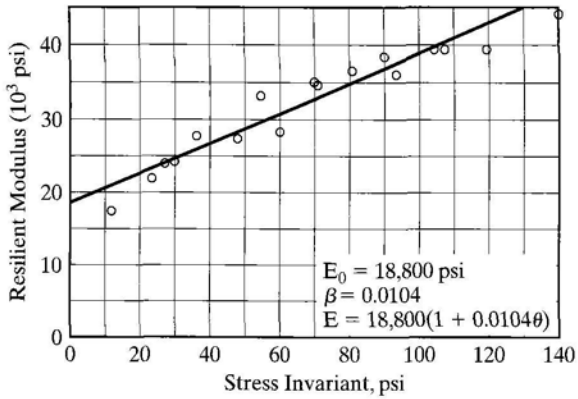
It should be noted that Eq. 2.11 is one of the many constitutive equations for sands. Uzan (1985), Pezo *et al.* (1992), and Pezo (1993) assumed that the modulus of granular materials depended not only on the stress invariant, θ, but also on the deviator stress, which is the difference between major and minor principal stresses. This concept has been used in the 2002 Design Guide, as presented in Appendix F. Other constitutive relationships for sands or clays can also be used, as discussed in Section 3.1.4.

Example 2.4:

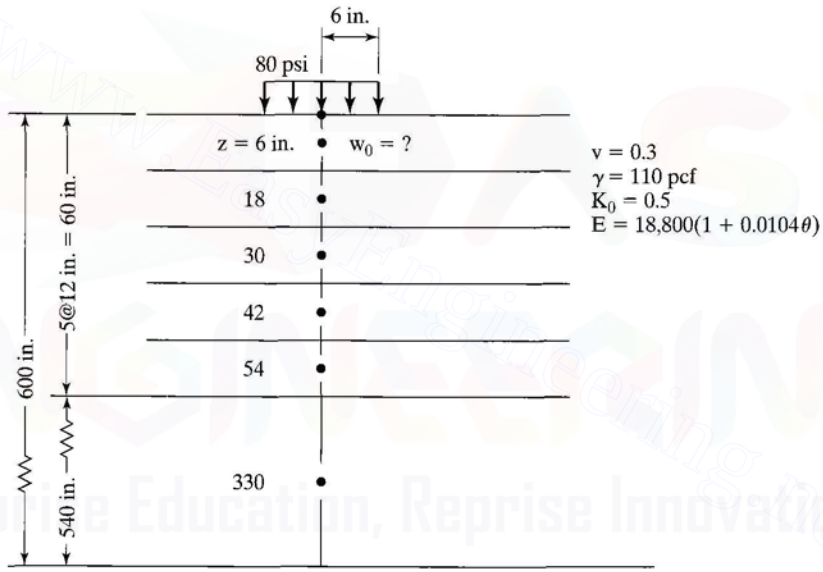
A circular load having radius 6 in. (152 mm) and contact pressure 80 psi (552 kPa) is applied on the surface of a subgrade. The subgrade soil is a sand with the relationship between the elastic modulus and the stress invariant shown in Figure 2.12*a*. The soil has Poisson ratio 0.3, the mass unit weight is 110 pcf (17.3 kN/m^3), and the coefficient of earth pressure at rest is 0.5. The soil is divided into six layers, as shown in Figure 2.12*b*. Determine the vertical surface displacement at the axis of symmetry.

Downloaded From : www.EasyEngineering.net

Downloaded From : www.EasyEngineering.net



(a) Resilient Modulus



(b) Layer Subdivision

FIGURE 2.12

Example 2.4 (1 in. = 25.4 mm, 1 psi = 6.9 kPa, 1 pcf = 157.1 N/m^3).

Solution: At the midheight of layer 1, $z = 6$ in. (152 mm). From Eq. 2.2, $\sigma_z = 80[1 - 216/(36 + 36)^{1.5}] = 51.7$ psi (357 kPa). From Eq. 2.3, $\sigma_r = \sigma_t = 40\,[1 + 2 \times 0.3 - 2.6 \times 6/(72)^{0.5} + 216/(72)^{1.5}] = 4.60$ psi (31.7 kPa). From Eq. 2.12, $\theta = 51.7 + 4.6 + 4.6 + 110 \times 6\,(1 + 2 \times 0.5)/(12)^3 = 61.7$ psi (426 kPa). From Eq. 2.11 with $E_0 = 18{,}800$ psi (130 MPa) and $\beta = 0.0104$, as shown in Figure 2.12*a*, $E = 18{,}800\,(1 + 0.0104 \times 61.7) = 30{,}900$ psi (213 MPa). From Eq. 2.6, the deflection at top, when $z = 0$, $w = 1.3 \times 80 \times 6\,(1 + 1 - 0.6)/30{,}900 = 0.0283$ in. (0.719 mm), and the deflection at bottom, when $z = 12$ in. (305 mm), $w = 1.3 \times 80 \times 6\,\{6/(36 + 144)^{0.5} + 0.4[(180)^{0.5} - 12]/6\}/30{,}900 = 0.0109$ in. (0.277 mm). The deformation for layer 1 is $0.0283 - 0.0109 = 0.0174$ in. (0.442 mm). The deformations for other layers can be determined similarly, and the results are tabulated in Table 2.1.

Downloaded From : www.EasyEngineering.net

Downloaded From : www.EasyEngineering.net

TABLE 2.1 Computation of Deformation for Each Layer

Layer no.	Thickness (in.)	z at mid-height (in.)	σ_z (psi)	σ_r (psi)	θ (psi)		E (psi)	wE (lb/in.)	Deformation (in.)
					Loading	Geostatic			
								873.6	
1	12	6	51.72	4.60	60.92	0.76	30,860		0.0174
								338.0	
2	12	18	11.69	−0.51	10.67	2.29	21,330		0.0073
								182.1	
3	12	30	4.57	−0.27	4.03	3.82	20,330		0.0029
								123.2	
4	12	42	2.39	−0.15	2.09	5.35	20,250		0.0015
								92.9	
5	12	54	1.46	−0.09	1.28	6.88	20,400		0.0009
								74.5	
6	540	330	0.04	0.00	0.04	42.01	27,020		0.0025
								7.5	
							Total		0.0325

Note. 1 in. = 25.4 mm, 1 psi = 6.9 kPa, 1 lb/in. = 175 N/m.

To compute the deformation of each layer, the product of w and E at each layer interface is first determined from Eq. 2.6. The difference in wE between the two interfaces divided by E gives the deformation of the layer. The surface deflection is the sum of all layer deformations and equals to 0.0325 in. (0.826 mm). It is interesting to note that the stress invariant θ due to the applied load decreases with depth, while that due to geostatic stresses increases with depth. As a result, the elastic moduli for all layers, except layers 1 and 6, become nearly the same. Note also that more than 50% of the surface deflections are contributed by the deformation in the top 12 in. (305 mm).

The same problem was solved by KENLAYER after the incorporation of Eq. 2.11 into the program. The differences in stress distribution between Boussinesq and Burmister theory and the resulting moduli are shown in Table 2.2. It can be seen that the two solutions correspond well. The surface deflection based on layered theory

TABLE 2.2 Differences in Stresses and Moduli between Boussinesq and Burmister Solutions

z at midheight (in.)	Boussinesq			Burmister		
	σ_z (psi)	σ_r (psi)	E (psi)	σ_z (psi)	σ_r (psi)	E (psi)
6	51.72	4.60	30,860	50.46	4.50	30,580
18	11.69	−0.51	21,330	10.61	−0.65	21,070
30	4.57	−0.27	20,330	4.26	−0.27	20,280
42	2.39	−0.15	20,250	2.31	−0.11	20,260
54	1.46	−0.09	20,400	1.47	0.01	20,440
330	0.04	0.00	27,020	0.04	0.00	27,020

Note. 1 in. = 25.4 mm, 1 psi = 6.9 kPa.

Downloaded From : www.EasyEngineering.net

Downloaded From : www.EasyEngineering.net

is 0.0310 in. (0.787 mm), which also agrees with the 0.0325 in. (0.826 mm) from Boussinesq theory.

2.2 LAYERED SYSTEMS

Flexible pavements are layered systems with better materials on top and cannot be represented by a homogeneous mass, so the use of Burmister's layered theory is more appropriate. Burmister (1943) first developed solutions for a two-layer system and then extended them to a three-layer system (Burmister, 1945). With the advent of computers, the theory can be applied to a multilayer system with any number of layers (Huang, 1967, 1968a).

Figure 2.13 shows an n-layer system. The basic assumptions to be satisfied are:

1. Each layer is homogeneous, isotropic, and linearly elastic with an elastic modulus E and a Poisson ratio ν.
2. The material is weightless and infinite in areal extent.
3. Each layer has a finite thickness h, except that the lowest layer is infinite in thickness.
4. A uniform pressure q is applied on the surface over a circular area of radius a.
5. Continuity conditions are satisfied at the layer interfaces, as indicated by the same vertical stress, shear stress, vertical displacement, and radial displacement. For frictionless interface, the continuity of shear stress and radial displacement is replaced by zero shear stress at each side of the interface.

In this section, only some of the solutions on two- and three-layer systems with bonded interfaces are presented. The theoretical development of multilayer systems is discussed in Appendix B.

2.2.1 Two-Layer Systems

The exact case of a two-layer system is the full-depth construction in which a thick layer of HMA is placed directly on the subgrade. If a pavement is composed of three

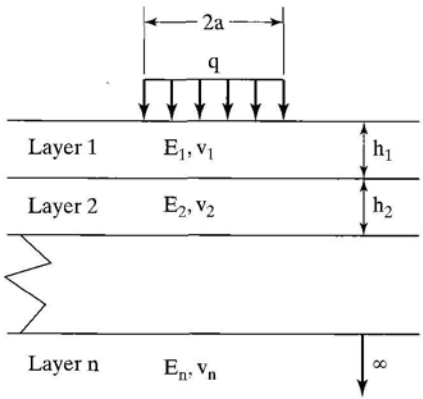


FIGURE 2.13
An n-layer system subjected to a circular load.

Downloaded From : www.EasyEngineering.net

Downloaded From : www.EasyEngineering.net

layers (e.g., an asphalt surface course, a granular base course, and a subgrade), it is necessary to combine the base course and the subgrade into a single layer for computing the stresses and strains in the asphalt layer or to combine the asphalt surface course and base course for computing the stresses and strains in the subgrade.

Vertical Stress The vertical stress on the top of subgrade is an important factor in pavement design. The function of a pavement is to reduce the vertical stress on the subgrade so that detrimental pavement deformations will not occur. The allowable vertical stress on a given subgrade depends on the strength or modulus of the subgrade. To combine the effect of stress and strength, the vertical compressive strain has been used most frequently as a design criterion. This simplification is valid for highway and airport pavements because the vertical strain is caused primarily by the vertical stress and the effect of horizontal stress is relatively small. As pointed out in Section 1.5.2, the design of railroad trackbeds should be based on vertical stress instead of vertical strain, because the large horizontal stress caused by the distribution of wheel loads through rails and ties over a large area makes the vertical strain a poor indicator of the vertical stress.

The stresses in a two-layer system depend on the modulus ratio E_1/E_2 and the thickness–radius ratio h_1/a. Figure 2.14 shows the effect of a pavement layer on the distribution of vertical stresses under the center of a circular loaded area. The chart is applicable to the case when the thickness h_1 of layer 1 is equal to the radius of contact area, or $h_1/a = 1$. As in all charts presented in this section, a Poisson ratio of 0.5 is assumed for all layers. It can be seen that the vertical stresses decrease significantly with the increase in modulus ratio. At the pavement–subgrade interface, the vertical stress is about 68% of the applied pressure if $E_1/E_2 = 1$, as indicated by Boussinesq's stress distribution, and reduces to about 8% of the applied pressure if $E_1/E_2 = 100$.

Figure 2.15 shows the effect of pavement thickness and modulus ratio on the vertical stress σ_c at the pavement–subgrade interface under the center of a circular loaded area. For a given applied pressure q, the vertical stress increases with the increase in contact radius and decreases with the increase in thickness. The reason that the ratio a/h_1 instead of h_1/a was used is for the purpose of preparing influence charts (Huang, 1969b) for two-layer elastic foundations.

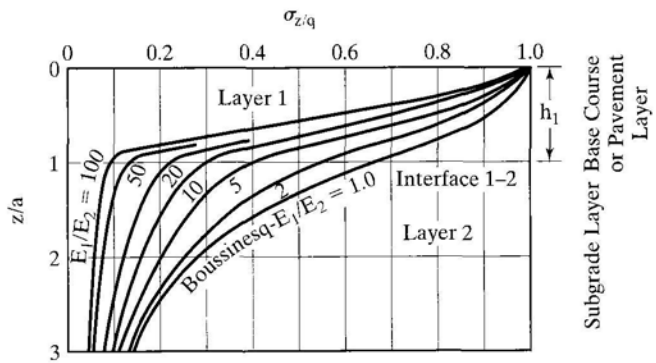


FIGURE 2.14

Vertical stress distribution in a two-layer system. (After Burmister (1958).)

Downloaded From : www.EasyEngineering.net

Downloaded From : www.EasyEngineering.net

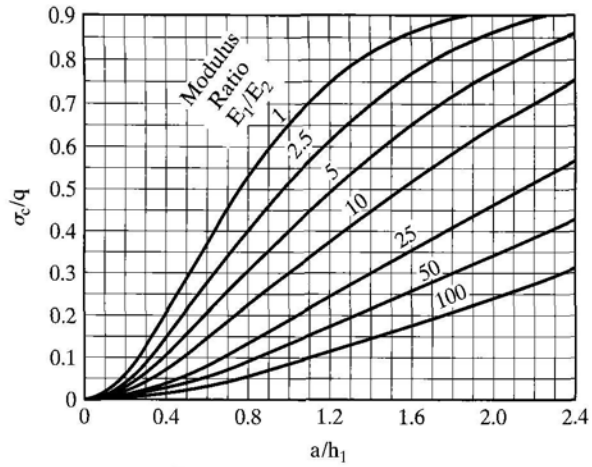


FIGURE 2.15

Vertical interface stresses for two-layer systems. (After Huang (1969b).)

Example 2.5:

A circular load having radius 6 in. (152 mm) and uniform pressure 80 psi (552 kPa) is applied on a two-layer system, as shown in Figure 2.16. The subgrade has elastic modulus 5000 psi (35 MPa) and can support a maximum vertical stress of 8 psi (55 kPa). If the HMA has elastic modulus 500,000 psi (3.45 GPa), what is the required thickness of a full-depth pavement? If a thin surface treatment is applied on a granular base with elastic modulus 25,000 psi (173 MPa), what is the thickness of base course required?

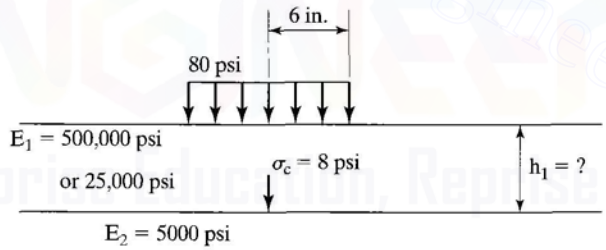


FIGURE 2.16

Example 2.5 (1 in. = 25.4 mm, 1 psi = 6.9 kPa).

Solution: Given $E_1/E_2 = 500{,}000/5000 = 100$ and $\sigma_c/q = 8/80 = 0.1$, from Figure 2.15, $a/h_1 = 1.15$, or $h_1 = 6/1.15 = 5.2$ in. (132 mm), which is the minimum thickness for full depth. Given $E_1/E_2 = 25{,}000/5000 = 5$ and $\sigma_c/q = 0.1$, from Figure 2.15, $a/h_1 = 0.4$, or $h_1 = 6/0.4 = 15$ in. (381 mm), which is the minimum thickness of granular base required.

In this example, an allowable vertical stress of 8 psi (55 kPa) is arbitrarily selected to show the effect of the modulus of the reinforced layer on the thickness required. The allowable vertical stress should depend on the number of load repetitions. Using the Shell design criterion and the AASHTO equation, Huang et al. (1984b) developed the relationship

$$N_d = 4.873 \times 10^{-5}\, \sigma_c^{-3.734}\, E_2^{3.583} \tag{2.13}$$

in which N_d is the allowable number of stress repetitions to limit permanent deformation, σ_c is the vertical compressive stress on the surface of the subgrade in psi, and E_2 is

Downloaded From : www.EasyEngineering.net

Downloaded From : www.EasyEngineering.net

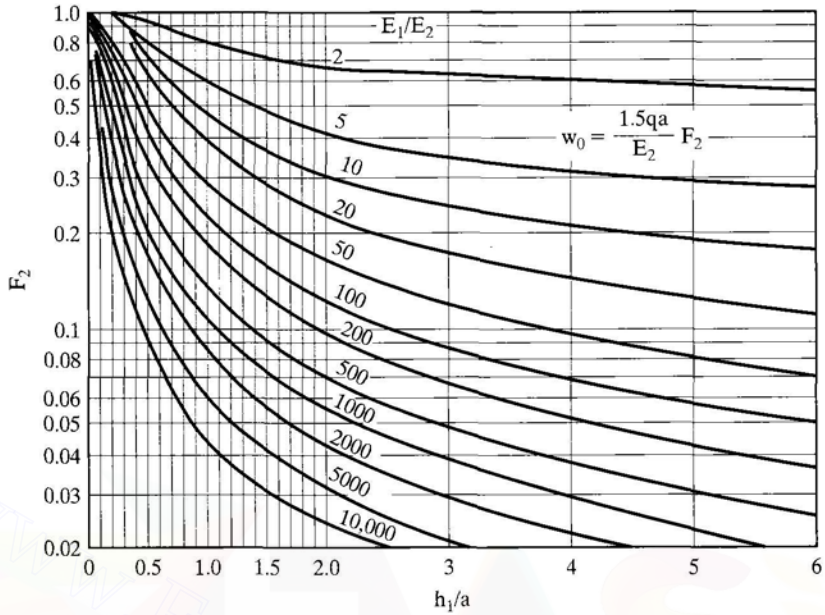


FIGURE 2.17

Vertical surface deflections for two-layer systems. (After Burmister (1943).)

the elastic modulus of the subgrade in psi. For a stress of 8 psi (5 kPa) and an elastic modulus of 5000 psi (35 MPa), the allowable number of repetitions is 3.7×10^5.

Vertical Surface Deflection Vertical surface deflections have been used as a criterion of pavement design. Figure 2.17 can be used to determine the surface deflections for two-layer systems. The deflection is expressed in terms of the deflection factor F_2 by

$$w_0 = \frac{1.5qa}{E_2} F_2 \tag{2.14}$$

The deflection factor is a function of E_1/E_2 and h_1/a. For a homogeneous half-space with $h_1/a = 0$, $F_2 = 1$, so Eq. 2.14 is identical to Eq. 2.8 when $v = 0.5$. If the load is applied by a rigid plate, then, from Eq 2.10,

$$w_0 = \frac{1.18qa}{E_2} F_2 \tag{2.15}$$

Example 2.6:

A total load of 20,000 lb (89 kN) was applied on the surface of a two-layer system through a rigid plate 12 in. (305 mm) in diameter, as shown in Figure 2.18. Layer 1 has a thickness of 8 in. (203 mm) and layer 2 has an elastic modulus of 6400 psi (44.2 MPa). Both layers are incompressible with a Poisson ratio of 0.5. If the deflection of the plate is 0.1 in. (2.54 mm), determine the elastic modulus of layer 1.

Downloaded From : www.EasyEngineering.net

Downloaded From : www.EasyEngineering.net

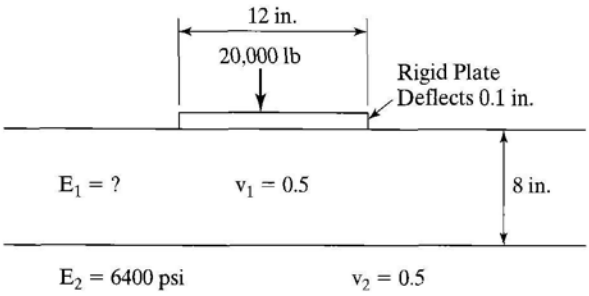


FIGURE 2.18

Example 2.6 (in. = 25.4 mm, 1 psi = 6.9 kPa, 1 lb = 4.45 N).

Solution: The average pressure on the plate is $q = 20{,}000/(36\pi) = 176.8$ psi (1.22 MPa). From Eq. 2.15, $F_2 = 0.1 \times 6400/(1.18 \times 176.8 \times 6) = 0.511$. Given $h_1/a = 8/6 = 1.333$, from Figure 2.17, $E_1/E_2 = 5$, or $E_1 = 5 \times 6400 = 32{,}000$ psi (221 MPa).

Vertical Interface Deflection The vertical interface deflection has also been used as a design criterion. Figure 2.19 can be used to determine the vertical interface deflection in a two-layer system (Huang, 1969c). The deflection is expressed in terms of the deflection factor F by

$$w = \frac{qa}{E_2}F \tag{2.16}$$

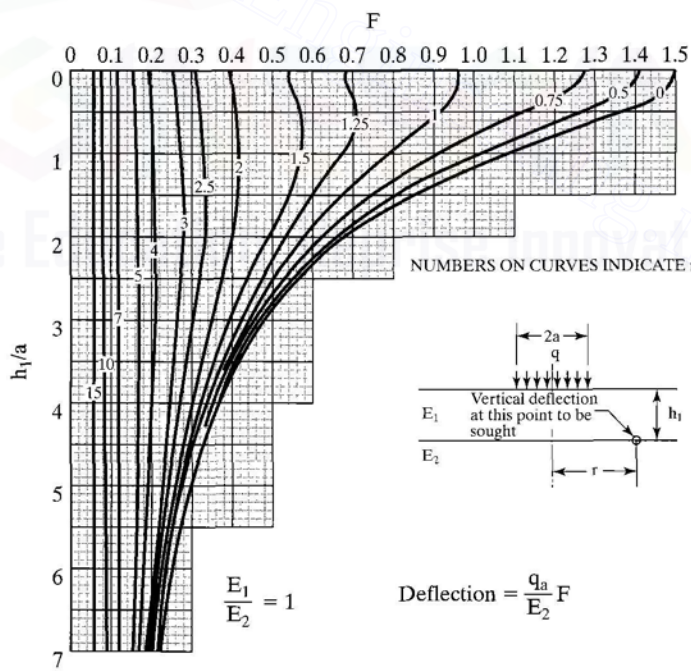


FIGURE 2.19

Vertical interface deflections for two-layer systems. (After Huang (1969c).)

Downloaded From : www.EasyEngineering.net

Downloaded From : www.EasyEngineering.net

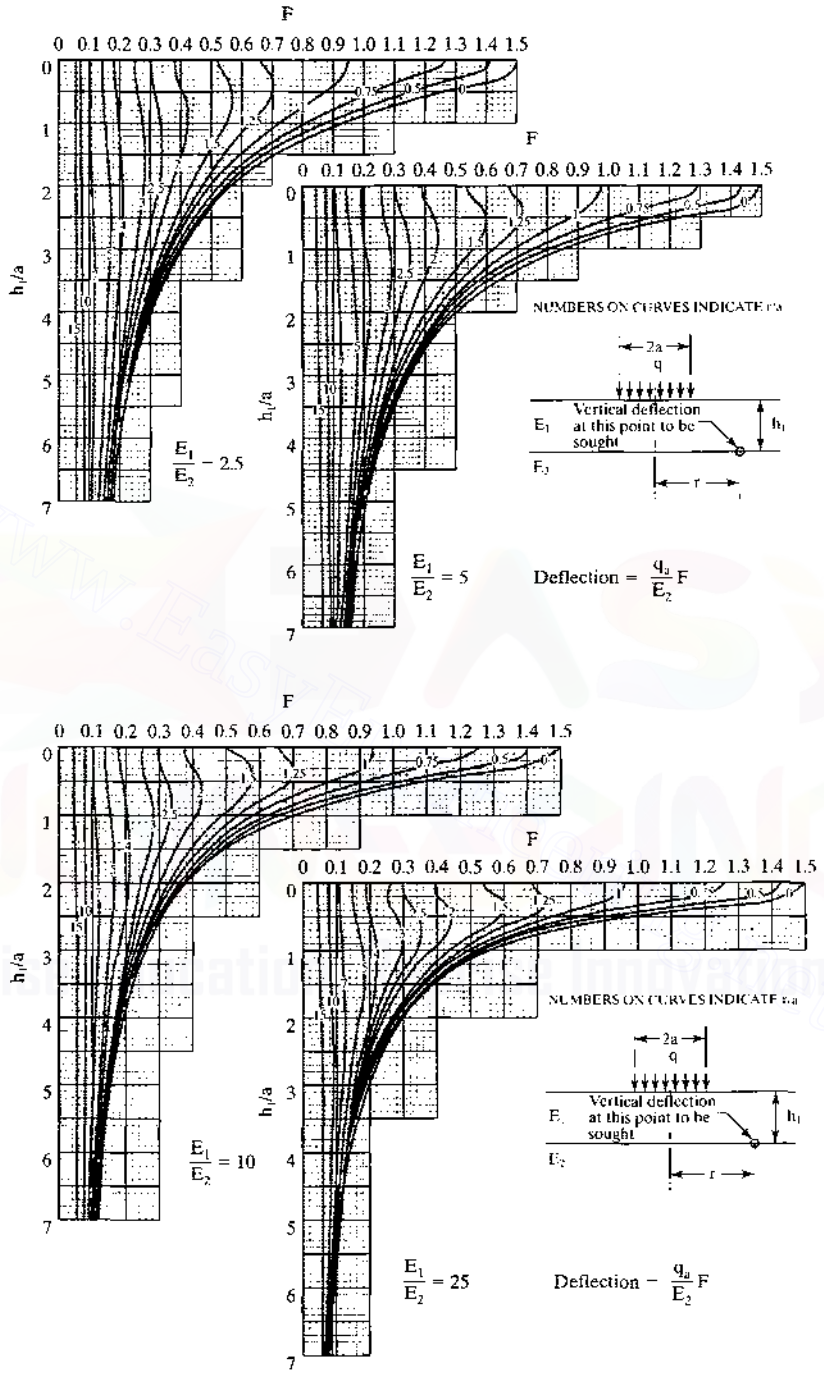


FIGURE 2.19 (Continued)

Downloaded From : www.EasyEngineering.net

Downloaded From : www.EasyEngineering.net

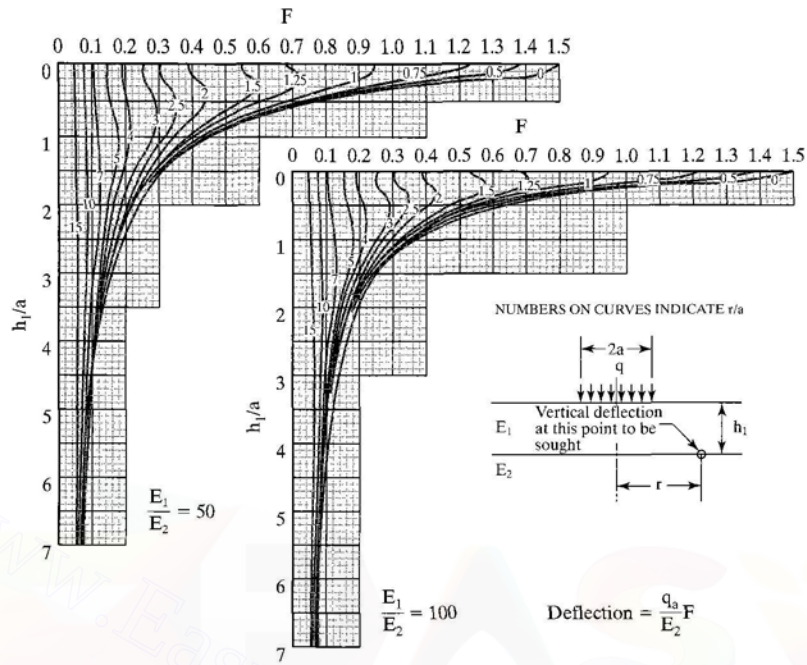


FIGURE 2.19 (Continued)

Note that F in Eq. 2.16 is different from F_2 in Eq. 2.14 by the factor 1.5. The deflection factor is a function of E_1/E_2, h_1/a, and r/a, where r is the radial distance from the center of loaded area. Seven sets of charts for the modulus ratios 1, 2.5, 5, 10, 25, 50, and 100, are shown; the deflection for any intermediate modulus ratio can be obtained by interpolation. The case of $E_1/E_2 = 1$ is Boussinesq's solution.

Example 2.7:

Figure 2.20 shows a set of dual tires, each having contact radius 4.52 in. (115 mm) and contact pressure 70 psi (483 kPa). The center-to-center spacing of the dual is 13.5 in. (343 mm). Layer 1 has thickness 6 in. (152 mm) and elastic modulus 100,000 psi (690 MPa); layer 2 has elastic modulus 10,000 psi (69 MPa). Determine the vertical deflection at point A, which is on the interface beneath the center of one loaded area.

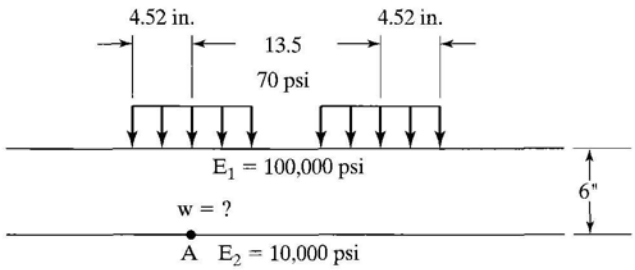


FIGURE 2.20
Example 2.7 (1 in. = 25.4 mm, 1 psi = 6.9 kPa).

Downloaded From : www.EasyEngineering.net

Downloaded From : www.EasyEngineering.net

Solution: Given $E_1/E_2 = 100{,}000/10{,}000 = 10$ and $h_1/a = 6/4.52 = 1.33$, from Figure 2.19, the deflection factor at point A due to the left load with $r/a = 0$ is 0.56 and that due to the right load with $r/a = 13.5/4.52 = 2.99$ is 0.28. By superposition, $F = 0.56 + 0.28 = 0.84$. From Eq. 2.16, $w = 70 \times 4.52/10{,}000 \times 0.84 = 0.027$ in. (0.69 mm). The interface deflection obtained from KENLAYER is 0.0281 in. (0.714 mm), which checks well with the chart solution.

It should be pointed out that the maximum interface deflection under dual tires might not occur at point A. To determine the maximum interface deflection, it is necessary to compute the deflection at several points, say one under the center of one tire, one at the center between two tires, and the other under the edge of one tire, and find out which is maximum.

Critical Tensile Strain The tensile strains at the bottom of asphalt layer have been used as a design criterion to prevent fatigue cracking. Two types of principal strains could be considered. One is the overall principal strain based on all six components of normal and shear stresses. The other, which is more popular and was used in KENLAYER, is the horizontal principal strain based on the horizontal normal and shear stresses only. The overall principal strain is slightly greater than the horizontal principal strain, so the use of overall principal strain is on the safe side.

Huang (1973a) developed charts for determining the critical tensile strain at the bottom of layer 1 for a two-layer system. The critical tensile strain is the overall strain and can be determined from

$$e = \frac{q}{E_1} F_e \tag{2.17}$$

in which e is the critical tensile strain and F_e is the strain factor, which can be determined from the charts.

Single Wheel Figure 2.21 presents the strain factor for a two-layer system under a circular loaded area. In most cases, the critical tensile strain occurs under the center

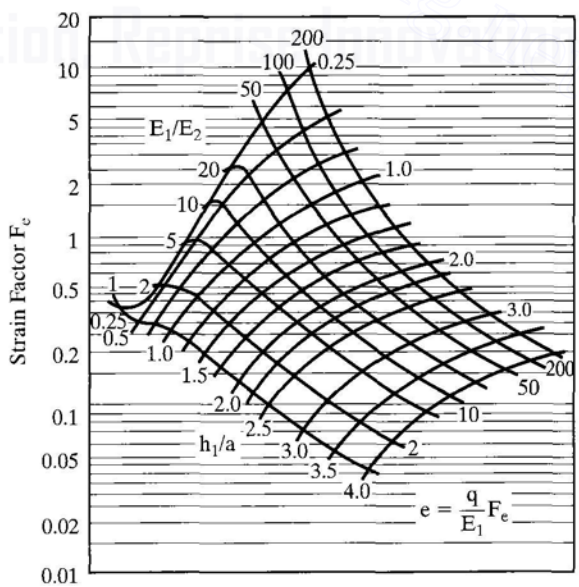


FIGURE 2.21

Strain factor for single wheel. (After Huang (1973a).)

Downloaded From : www.EasyEngineering.net

Downloaded From : www.EasyEngineering.net

of the loaded area, where the shear stress is zero. However, when both h_1/a and E_1/E_2 are small, the critical tensile strain occurs at some distance from the center, as the predominant effect of the shear stress. Under such situations, the principal tensile strains at the radial distances 0, $0.5a$, a, and $1.5a$ from the center were computed, and the critical value was obtained and plotted in Figure 2.21.

Example 2.8:

Figure 2.22 shows a full-depth asphalt pavement 8 in. (203 mm) thick subjected to a single-wheel load of 9000 lb (40 kN) having contact pressure 67.7 psi (467 kPa). If the elastic modulus of the asphalt layer is 150,000 psi (1.04 GPa) and that of the subgrade is 15,000 psi (104 MPa), determine the critical tensile strain in the asphalt layer.

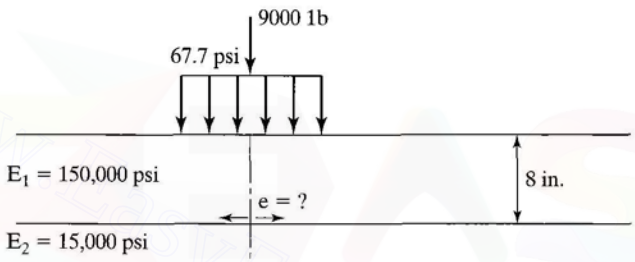


FIGURE 2.22

Example 2.8 (1 in. = 25.4 mm, 1 psi = 6.9 kPa, 1 lb = 4.45 N).

Solution: Given $a = \sqrt{9000/(\pi \times 67.7)} = 6.5$ in. (165 mm), $h_1/a = 8/6.5 = 1.23$, and $E_1/E_2 = 150{,}000/15{,}000 = 10$, from Figure 2.21, $F_e = 0.72$. From Eq. 2.17, the critical tensile strain $e = 67.7 \times 0.72/150{,}000 = 3.25 \times 10^{-4}$, which checks well with the 3.36×10^{-4} obtained by KENLAYER.

It is interesting to note that the bonded interface makes the horizontal tensile strain at the bottom of layer 1 equal to the horizontal tensile strain at the top of layer 2. If layer 2 is incompressible and the critical tensile strain occurs on the axis of symmetry, then the vertical compressive strain is equal to twice the horizontal strain, as shown by Eq. 2.21 (as is discussed later). Therefore, Figure 2.21 can be used to determine the vertical compressive strain on the surface of the subgrade as well.

Dual Wheels Because the strain factor for dual wheels with a contact radius a and a dual spacing S_d depends on S_d/a in addition to E_1/E_2 and h_1/a, the most direct method is to present charts similar to Figure 2.21, one for each value of S_d/a. However, this approach requires a series of charts, and the interpolation could be quite time-consuming. To avoid these difficulties, a unique method was developed that requires only one chart, as shown in Figure 2.23.

In this method, the dual wheels are replaced by a single wheel with the same contact radius a, so that Figure 2.21 can still be used. Because the strain factor for dual wheels is generally greater than that for a single wheel, a conversion factor C, which is the ratio between dual- and single-wheel strain factors, must be determined. Multiplication of

Downloaded From : www.EasyEngineering.net

Downloaded From : www.EasyEngineering.net

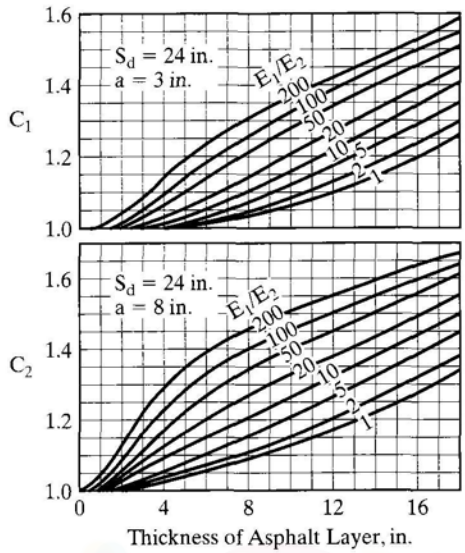


FIGURE 2.23
Conversion factor for dual wheel (1 in. = 25.4 mm). (After Huang (1973a).)

the conversion factor by the strain factor obtained from Figure 2.21 will yield the strain factor for dual wheels.

The two-layer theory indicates that the strain factor for dual wheels depends on h_1/a, S_d/a, and E_1/E_2. As long as the ratios h_1/a and S_d/a remain the same, the strain factor will be the same, no matter how large or small the contact radius a may be. Consider a set of dual wheels with $S_d = 24$ in. (610 mm) and $a = 3$ in. (76 mm). The strain factors for various values of h_1 and E_1/E_2 were calculated and the conversion factors were obtained and plotted as a set of curves on the upper part of Figure 2.23. Another set of curves based on the same S_d but with $a = 8$ in. (203 mm) is plotted at the bottom. It can be seen that, for the same dual spacing, the larger the contact radius, the larger the conversion factor. However, the change in conversion factor due to the change in contact radius is not very large, so a straight-line interpolation should give a fairly accurate conversion factor for any other contact radii. Although Figure 2.23 is based on $S_d = 24$ in. (610 mm), it can be applied to any given S_d by simply changing a and h_1 in proportion to the change in S_d, so that the ratios h_1/a and S_d/a remain the same. The procedure can be summarized as follows:

1. From the given S_d, h_1, and a, determine the modified radius a' and the modified thickness h_1':

$$a' = \frac{24}{S_d} a \tag{2.18a}$$

$$h_1' = \frac{24}{S_d} h_1 \tag{2.18b}$$

2. Using h_1' as the pavement thickness, find conversion factors C_1 and C_2 from Figure 2.23.

Downloaded From : www.EasyEngineering.net

Downloaded From : www.EasyEngineering.net

3. Determine the conversion factor for a' by a straight-line interpolation between 3 and 8 in. (76 and 203 mm), or

$$C = C_1 + 0.2 \times (a' - 3) \times (C_2 - C_1) \tag{2.19}$$

Example 2.9:

For the same pavement as in Example 2.8, if the 9000-lb (40-kN) load is applied over a set of dual tires with a center-to-center spacing of 11.5 in. (292 mm) and a contact pressure of 67.7 psi (467 kPa), as shown in Figure 2.24, determine the critical tensile strain in the asphalt layer.

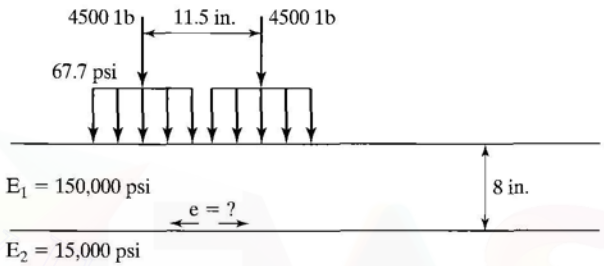


FIGURE 2.24

Example 2.9 (1 in. = 25.4 mm, 1 psi = 6.9 kPa, 1 lb = 4.45 N).

Solution: Given $a = \sqrt{4500/(\pi \times 67.7)} = 4.6$ in. (117 mm), $S_d = 11.5$ in. (292 mm), and $h_1 = 8$ in. (203 mm), from Eq. 2.18, $a' = 24 \times 4.6/11.5 = 9.6$ in. (244 mm) and $h_1' = 24 \times 8/11.5 = 16.7$ in. (424 mm). With $E_1/E_2 = 10$ and an asphalt layer thickness of 16.7 in. (424 mm), from Figure 2.23, $C_1 = 1.35$ and $C_2 = 1.46$. From Eq. 2.19, $C = 1.35 + 0.2\,(9.6 - 3)(1.46 - 1.35) = 1.50$. From Figure 2.21, the strain factor for a single wheel = 0.47 and that for dual wheels = $1.50 \times 0.47 = 0.705$, so the critical tensile strain $e = 67.7 \times 0.705/150{,}000 = 3.18 \times 10^{-4}$, which checks closely with the 3.21×10^{-4} obtained by KENLAYER.

By comparing the results of Examples 2.8 and 2.9, it can be seen that, in this particular case (when the asphalt layer is thick and the dual spacing is small), a load applied on a set of dual tires yields a critical strain that is not very different from that on a single wheel. However, this is not true when thin asphalt layers or large dual spacings are involved.

Huang (1972) also presented a simple chart for determining directly the maximum tensile strain in a two-layer system subjected to a set of dual tires spaced at a distance of $3a$ on center. A series of charts relating tensile strains to curvatures was also developed, so that the tensile strain under a design dual-wheel load can be evaluated in the field by simply measuring the curvature on the surface (Huang, 1971).

Dual-Tandem Wheels Charts similar to Figure 2.23 with dual spacing S_d of 24 in. (610 mm) and tandem spacings S_t of 24 in. (610 mm), 48 in. (1220 mm), and 72 in. (1830 mm) were developed for determining the conversion factor due to dual-tandem wheels, as shown in Figures 2.25, 2.26, and 2.27. The use of these charts is similar to the use of Figure 2.23. Because the conversion factor for dual-tandem wheels depends on h_1/a, S_d/a, and S_t/a, and because the actual S_d may not be equal to 24 in. (610 mm), it is

Downloaded From : www.EasyEngineering.net

Downloaded From : www.EasyEngineering.net

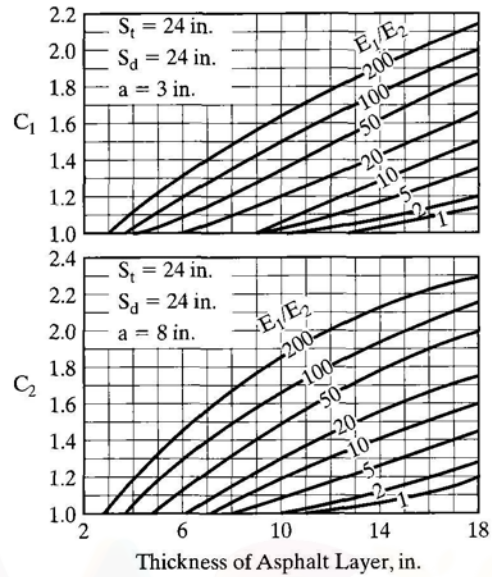


FIGURE 2.25

Conversion factor for dual-tandem wheels with 24-in. tandem spacing (1 in. = 25.4 mm). (After Huang (1973a).)

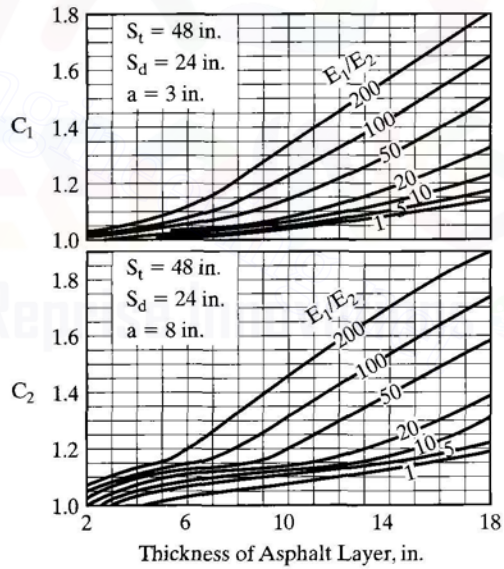


FIGURE 2.26

Conversion factor for dual-tandem wheels with 48-in. tandem spacing (1 in. = 25.4 mm). (After Huang (1973a).)

necessary to change S_d to 24 in. (610 mm) and then change the contact radius a proportionately according to Eq. 2.18*a*, thus keeping the ratio S_d/a unchanged.

The values of h_1 and S_t must also be changed accordingly to keep h_1/a and S_t/a unchanged. Therefore, the original problem is changed to a new problem with S_d = 24 in. (610 mm) and a new S_t. The conversion factor for S_t = 24, 48, and 72 in. (0.61, 1.22, and 1.83 m) can be obtained from the charts; that for other values of S_t can be determined by interpolation.

Downloaded From : www.EasyEngineering.net

Downloaded From : www.EasyEngineering.net

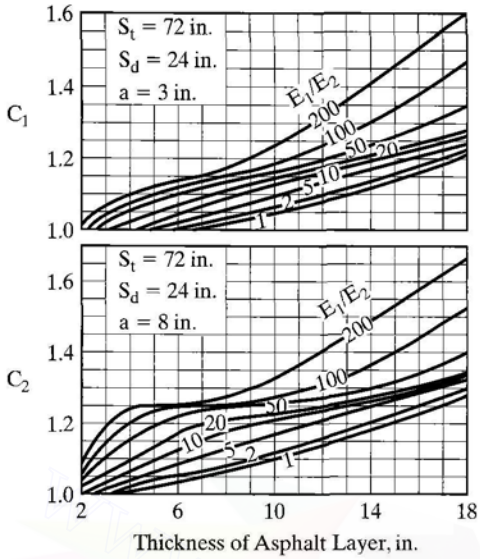


FIGURE 2.27

Conversion factor for dual-tandem wheels with 72-in. tandem spacing (1 in. = 25.4 mm). (After Huang (1973a).)

If the new values of S_t are greater than 72 in. (1.83 m), Figure 2.23, based on dual wheels can be used for interpolation. In fact, Figure 2.23 is a special case of dual-tandem wheels when the tandem spacing approaches infinity. It was found that, when S_t = 120 in. (3.05 m) the conversion factor due to dual-tandem wheels does not differ significantly from that due to dual wheels alone, so Figure 2.23 can be considered to have a tandem spacing of 120 in. (3.05 m).

A comparison of Figure 2.23 with Figures 2.25 through 2.27 clearly indicates that, in many cases, the addition of tandem wheels reduces the conversion factor, thus decreasing the critical tensile strain. This is due to the compensative effect caused by the additional wheels. The interaction among these wheels is quite unpredictable, as indicated by the irregular shape of the curves in the lower part of Figures 2.26 and 2.27.

Example 2.10:

Same as example 2.9, except that an identical set of duals is added to form dual-tandem wheels having the tandem spacing 49 in. (1.25 m), as shown in Figure 2.28.

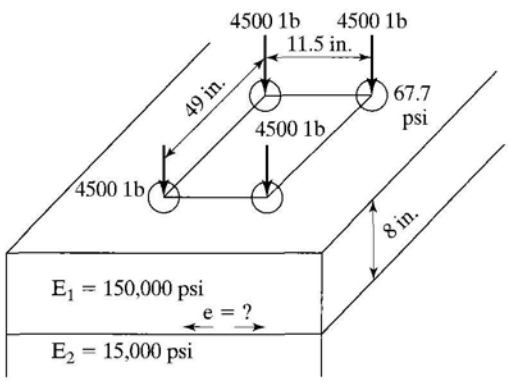


FIGURE 2.28

Example 2.10 (1 in. = 25.4 mm, 1 psi = 6.9 kPa, 1 lb = 4.45 N).

Downloaded From : www.EasyEngineering.net

Downloaded From : www.EasyEngineering.net

Solution: Given S_d = 11.5 in. (292 mm) and S_t = 49 in. (1.25 m), modified tandem spacing = 49 × 24/11.5 = 102.3 in. (2.60 m). Values of a' and h' are the same as in Example 2.8. When S_t = 72 in. (1.83 m), a' = 9.6 in. (244 mm), and h_1' = 16.7 in. (424 mm), from Figure 2.27, C = 1.23 + 0.2 (9.6 − 3)(1.30 − 1.23) = 1.32, which is smaller than the 1.5 for the dual wheels alone. With a conversion factor of 1.32 for S_t = 72 in. (1.83 m) and 1.50 for S_t = 120 in. (3.05 m), by straight-line interpolation, C = 1.32 + (1.50 − 1.32)(102.3 − 72)/(120 − 72) = 1.43. The strain factor due to dual-tandem wheels = 1.43 × 0.47 = 0.672. Critical tensile strain = 67.7 × 0.672/150,000 = 3.03 × 10^{-4}, which checks closely with the 3.05 × 10^{-4} obtained from KENLAYER.

2.2.2 Three-Layer Systems

Figure 2.29 shows a three-layer system and the stresses at the interfaces on the axis of symmetry. These stresses include vertical stress at interface 1, σ_{z1}, vertical stress at interface 2, σ_{z2}, radial stress at bottom of layer 1, σ_{r1}, radial stress at top of layer 2, σ'_{r1}, radial stress at bottom of layer 2, σ_{r2}, and radial stress at top of layer 3, σ'_{r2}. Note that, on the axis of symmetry, tangential and radial stresses are identical and the sheer stress is equal to 0.

When the Poisson ratio is 0.5, we have, from Eq. 2.1,

$$\epsilon_z = \frac{1}{E}(\sigma_z - \sigma_r) \tag{2.20a}$$

$$\epsilon_r = \frac{1}{2E}(\sigma_r - \sigma_z) \tag{2.20b}$$

Equation 2.20 indicates that the radial strain equals one-half of the vertical strain and is opposite in sign, or

$$\epsilon_z = -2\epsilon_r \tag{2.21}$$

Equation 2.21 can be visualized physically from the fact that, when a material is incompressible and has the Poisson ratio 0.5, the horizontal strain is equal to one-half of the vertical strain and the sum of ϵ_z, ϵ_r, and ϵ_t must be equal to 0.

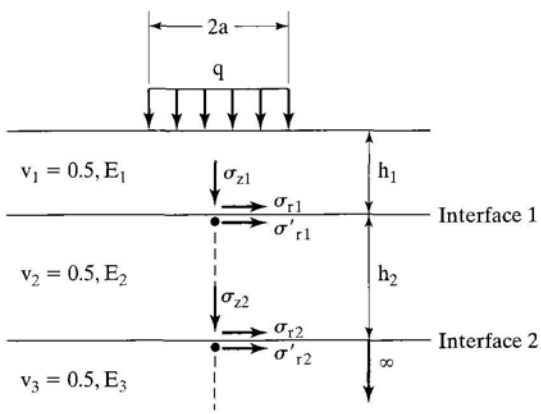


FIGURE 2.29
Stresses at interfaces of a three-layer system.

Downloaded From : www.EasyEngineering.net

Downloaded From : www.EasyEngineering.net

Jones' Tables The stresses in a three-layer system depend on the ratios k_1, k_2, A, and H, defined as

$$k_1 = \frac{E_1}{E_2} \qquad k_2 = \frac{E_2}{E_3} \tag{2.22a}$$

$$A = \frac{a}{h_2} \qquad H = \frac{h_1}{h_2} \tag{2.22b}$$

Jones (1962) presented a series of tables for determining σ_{z1}, $\sigma_{z1} - \sigma_{r1}$, σ_{z2}, and $\sigma_{z2} - \sigma_{r2}$. His tables also include values of $\sigma_{z1} - \sigma'_{r1}$ at the top of layer 2 and $\sigma_{z2} - \sigma'_{r2}$ at the top of layer 3, but these tabulations are actually not necessary because they can be easily determined from those at the bottom of layers 1 and 2. The continuity of horizontal displacement at the interface implies that the radial strains at the bottom of one layer are equal to that at the top of the next layer, or, from Eq. 2.20*b*,

$$\sigma_{z1} - \sigma'_{r1} = \frac{\sigma_{z1} - \sigma_{r1}}{k_1} \tag{2.23a}$$

$$\sigma_{z2} - \sigma'_{r2} = \frac{\sigma_{z2} - \sigma_{r2}}{k_2} \tag{2.23b}$$

The tables presented by Jones consist of four values of k_1 and k_2 (0.2, 2, 20, and 200), so solutions for intermediate values of k_1 and k_2 can be obtained by interpolation. In view of the fact that solutions for three-layer systems can be easily obtained by KENLAYER and the interpolation from the tables is impractical and requires a large amount of time and effort, only the more realistic cases (k_1 = 2, 20, and 200, and k_2 = 2 and 20) are presented, to conserve space.

Table 2.3 presents the stress factors for three-layer systems. The sign convention is positive in compression and negative in tension. Four sets of stress factors,—ZZ1, ZZ2, ZZ1 − RR1, and ZZ2 − RR2—are shown. The product of the contact pressure and the stress factors gives the stresses:

$$\sigma_{z1} = q\,(\text{ZZ1}) \tag{2.24a}$$

$$\sigma_{z2} = q\,(\text{ZZ2}) \tag{2.24b}$$

$$\sigma_{z1} - \sigma_{r1} = q\,(\text{ZZ1} - \text{RR1}) \tag{2.24c}$$

$$\sigma_{z2} - \sigma_{r2} = q\,(\text{ZZ2} - \text{RR2}) \tag{2.24d}$$

Example 2.11:

Given the three-layer system shown in Figure 2.30 with a = 4.8 in. (122 mm), q = 120 psi (828 kPa), h_1 = 6 in. (152 mm), h_2 = 6 in. (203 mm), E_1 = 400,000 psi (2.8 GPa), E_2 = 20,000 psi (138 MPa), and E_3 = 10,000 psi (69 MPa), determine all the stresses and strains at the two interfaces on the axis of symmetry.

Downloaded From : www.EasyEngineering.net

TABLE 2.3 Stress Factors for Three-Layer Systems

			$k_1 = 2$				$k_1 = 20$				$k_1 = 200$			
H	k_2	A	ZZ1	ZZ2	(ZZ1 − RR1)	(ZZ2 − RR2)	ZZ1	ZZ2	(ZZ1 − RR1)	(ZZ2 − RR2)	ZZ1	ZZ2	(ZZ1 − RR1)	(ZZ2 − RR2)
0.125	2	0.1	0.42950	0.00896	0.70622	0.01716	0.14529	0.00810	1.81178	0.01542	0.03481	0.00549	3.02259	0.00969
		0.2	0.78424	0.03493	0.97956	0.06647	0.38799	0.03170	3.76886	0.06003	0.11491	0.02167	8.02452	0.03812
		0.4	0.98044	0.12667	0.70970	0.23531	0.78651	0.11650	5.16717	0.21640	0.33218	0.08229	17.64175	0.14286
		0.8	0.99434	0.36932	0.22319	0.63003	1.02218	0.34941	3.43631	0.60493	0.72695	0.27307	27.27701	0.45208
		1.6	0.99364	0.72113	−0.19982	0.97707	0.99060	0.69014	1.15211	0.97146	1.00203	0.63916	23.38638	0.90861
		3.2	0.99922	0.96148	−0.28916	0.84030	0.99893	0.93487	−0.06894	0.88358	1.00828	0.92560	11.87014	0.91469
	20	0.1	0.43022	0.00228	0.69332	0.03467	0.14447	0.00182	1.80664	0.02985	0.03336	0.00128	3.17763	0.01980
		0.2	0.78414	0.00899	0.92086	0.13541	0.38469	0.00716	3.74573	0.11697	0.10928	0.00509	8.66097	0.07827
		0.4	0.97493	0.03392	0.46583	0.49523	0.77394	0.02710	5.05489	0.43263	0.31094	0.01972	20.12259	0.29887
		0.8	0.97806	0.11350	−0.66535	1.49612	0.98610	0.09061	2.92533	1.33736	0.65934	0.07045	36.29943	1.01694
		1.6	0.96921	0.31263	−2.82859	3.28512	0.93712	0.24528	−1.27093	2.99215	0.87931	0.20963	49.40857	2.64313
		3.2	0.98591	0.68433	−5.27906	5.05952	0.96330	0.55490	−7.35384	5.06489	0.93309	0.49938	57.84369	4.89895
0.25	2	0.1	0.15524	0.00710	0.28362	0.01353	0.04381	0.00530	0.63215	0.00962	0.00909	0.00259	0.96553	0.00407
		0.2	0.42809	0.02783	0.70225	0.05278	0.14282	0.02091	1.83766	0.03781	0.03269	0.01027	3.10763	0.01611
		0.4	0.77939	0.10306	0.96634	0.19178	0.37882	0.07933	3.86779	0.14159	0.10684	0.04000	8.37852	0.06221
		0.8	0.96703	0.31771	0.66885	0.55211	0.75904	0.26278	5.50796	0.44710	0.30477	0.14513	18.95534	0.21860
		1.6	0.98156	0.66753	0.17331	0.95080	0.98743	0.61673	4.24281	0.90115	0.66786	0.42940	31.18909	0.58553
		3.2	0.99840	0.93798	−0.05691	0.89390	1.00064	0.91258	1.97494	0.93254	0.98447	0.84545	28.98500	0.89191
	20	0.1	0.15436	0.00179	0.25780	0.02728	0.04236	0.00123	0.65003	0.01930	0.00776	0.00065	1.08738	0.00861
		0.2	0.42462	0.00706	0.67115	0.10710	0.13708	0.00488	1.90693	0.07623	0.02741	0.00257	3.59448	0.03421
		0.4	0.76647	0.02697	0.84462	0.39919	0.35716	0.01888	4.13976	0.29072	0.08634	0.01014	10.30923	0.13365
		0.8	0.92757	0.09285	0.21951	1.26565	0.68947	0.06741	6.48948	0.98565	0.23137	0.03844	26.41442	0.49135
		1.6	0.91393	0.26454	−1.22411	2.94860	0.85490	0.20115	6.95639	2.55231	0.46835	0.13148	57.46409	1.53833
		3.2	0.95243	0.60754	−3.04320	4.89878	0.90325	0.48647	6.05854	4.76234	0.71083	0.37342	99.29034	3.60964
0.5	2	0.1	0.04330	0.00465	0.08250	0.00878	0.01122	0.00259	0.17997	0.00440	0.00215	0.00094	0.26620	0.00128
		0.2	0.15325	0.01836	0.28318	0.03454	0.04172	0.01028	0.64779	0.01744	0.00826	0.00373	0.98772	0.00509
		0.4	0.42077	0.06974	0.70119	0.12954	0.13480	0.03998	1.89817	0.06722	0.02946	0.01474	3.19580	0.01996
		0.8	0.75683	0.23256	0.96681	0.41187	0.35175	0.14419	4.09592	0.23476	0.09508	0.05622	8.71973	0.07434
		1.6	0.93447	0.56298	0.70726	0.85930	0.70221	0.42106	6.22002	0.62046	0.27135	0.19358	20.15765	0.23838
		3.2	0.98801	0.88655	0.33878	0.96353	0.97420	0.82256	5.41828	0.93831	0.62399	0.52912	34.25229	0.54931
	20	0.1	0.04193	0.00117	0.08044	0.01778	0.00990	0.00063	0.19872	0.00911	0.00149	0.00023	0.31847	0.00257
		0.2	0.14808	0.00464	0.27574	0.07027	0.03648	0.00251	0.72264	0.03620	0.00564	0.00094	1.19598	0.01025
		0.4	0.40086	0.01799	0.67174	0.26817	0.11448	0.00988	2.19520	0.14116	0.01911	0.00372	1.02732	0.04047
		0.8	0.69098	0.06476	0.86191	0.91168	0.27934	0.03731	5.24726	0.51585	0.05574	0.01453	12.00885	0.15452
		1.6	0.79338	0.19803	0.39588	2.38377	0.50790	0.12654	10.30212	1.59341	0.13946	0.05399	32.77028	0.53836
		3.2	0.85940	0.49238	−0.41078	4.47022	0.70903	0.35807	16.38520	3.69109	0.30247	0.18091	77.62943	1.56409

Downloaded From : www.EasyEngineering.net
Downloaded From : www.EasyEngineering.net

1	2	0.1	0.01083	0.00241	0.02179	0.00453	0.00263	0.00100	0.04751	0.00160	0.00049	0.00029	0.06883	0.00035
		0.2	0.04176	0.00958	0.08337	0.01797	0.01029	0.00347	0.18481	0.00637	0.00195	0.00116	0.26966	0.00138
		0.4	0.14665	0.03724	0.28491	0.06934	0.03810	0.01565	0.66727	0.02498	0.00746	0.00460	1.00131	0.00545
		0.8	0.39942	0.13401	0.71341	0.24250	0.12173	0.05938	1.97428	0.09268	0.02647	0.01797	3.24971	0.02092
		1.6	0.71032	0.38690	1.02680	0.63631	0.31575	0.20098	4.37407	0.29253	0.08556	0.06671	8.92442	0.07335
		3.2	0.92112	0.75805	0.90482	0.97509	0.66041	0.53398	6.97695	0.65446	0.25186	0.22047	20.83387	0.21288
	20	0.1	0.00963	0.00061	0.02249	0.00920	0.00193	0.00024	0.05737	0.00322	0.00027	0.00007	0.08469	0.00062
		0.2	0.03697	0.00241	0.08618	0.03654	0.00751	0.00098	0.22418	0.01283	0.00104	0.00028	0.33312	0.00248
		0.4	0.12805	0.00950	0.29640	0.14241	0.02713	0.00387	0.82430	0.05063	0.00384	0.00110	1.25495	0.00985
		0.8	0.33263	0.03578	0.76292	0.51815	0.08027	0.01507	2.59672	0.19267	0.01236	0.00436	4.26100	0.03825
		1.6	0.52721	0.12007	1.25168	1.56503	0.17961	0.05549	6.77014	0.66326	0.03379	0.01683	12.91809	0.13989
		3.2	0.65530	0.33669	1.70723	3.51128	0.34355	0.18344	15.23252	1.88634	0.08859	0.06167	36.04291	0.45544
2	2	0.1	0.00250	0.00100	0.00555	0.00188	0.00059	0.00033	0.01219	0.00051	0.00011	0.00008	0.01737	0.00009
		0.2	0.00991	0.00397	0.02199	0.00750	0.00235	0.00130	0.04843	0.00203	0.00045	0.00033	0.06913	0.00036
		0.4	0.03832	0.01569	0.08465	0.02950	0.00922	0.00518	0.18857	0.00803	0.00179	0.00131	0.27103	0.00142
		0.8	0.13516	0.05974	0.29365	0.11080	0.03412	0.02023	0.68382	0.03093	0.00685	0.00520	1.00808	0.00553
		1.6	0.36644	0.20145	0.75087	0.35515	0.10918	0.07444	2.04134	0.10864	0.02441	0.02003	3.27590	0.02043
		3.2	0.67384	0.51156	1.17294	0.77434	0.29183	0.23852	4.60426	0.30709	0.08061	0.07248	9.02195	0.06638
	20	0.1	0.00181	0.00025	0.00652	0.00378	0.00033	0.00008	0.01568	0.00094	0.00005	0.00002	0.02160	0.00014
		0.2	0.00716	0.00099	0.02586	0.01507	0.00130	0.00031	0.06236	0.00374	0.00018	0.00007	0.08604	0.00058
		0.4	0.02746	0.00394	0.10017	0.05958	0.00503	0.00123	0.24425	0.01486	0.00071	0.00030	0.33866	0.00229
		0.8	0.09396	0.01535	0.35641	0.22795	0.01782	0.00485	0.90594	0.05789	0.00261	0.00119	1.27835	0.00901
		1.6	0.23065	0.05599	1.00785	0.78347	0.05012	0.01862	2.91994	0.21190	0.00819	0.00467	4.35311	0.03390
		3.2	0.37001	0.17843	2.16033	2.13215	0.11331	0.06728	7.95104	0.67732	0.02341	0.01784	13.26873	0.11666
4	2	0.1	0.00057	0.00034	0.00147	0.00065	0.00013	0.00010	0.00312	0.00015	0.00003	0.00002	0.00437	0.00002
		0.2	0.00228	0.00137	0.00587	0.00260	0.00054	0.00039	0.01245	0.00029	0.00011	0.00009	0.01746	0.00009
		0.4	0.00905	0.00544	0.02324	0.01032	0.00214	0.00154	0.04944	0.00235	0.00042	0.00036	0.06947	0.00036
		0.8	0.03500	0.02135	0.08957	0.04031	0.00837	0.00610	0.19247	0.00924	0.00168	0.00142	0.27221	0.00144
		1.6	0.12354	0.07972	0.31215	0.14735	0.03109	0.02358	0.69749	0.03488	0.00646	0.00560	1.01140	0.00553
		3.2	0.34121	0.25441	0.81908	0.43632	0.10140	0.08444	2.09049	0.11553	0.02332	0.02126	3.28913	0.01951
	20	0.1	0.00030	0.00008	0.00201	0.00128	0.00005	0.00002	0.00413	0.00025	0.00001	0.00000	0.00545	0.00003
		0.2	0.00119	0.00034	0.00803	0.00510	0.00021	0.00009	0.01651	0.00099	0.00003	0.00002	0.02178	0.00014
		0.4	0.00469	0.00134	0.03191	0.02032	0.00083	0.00035	0.06569	0.00396	0.00013	0.00008	0.08673	0.00054
		0.8	0.01790	0.00532	0.12427	0.07991	0.00321	0.00138	0.25739	0.01565	0.00050	0.00031	0.34131	0.00215
		1.6	0.06045	0.02049	0.45100	0.29991	0.01130	0.00542	0.95622	0.05993	0.00186	0.00124	1.28773	0.00833
		3.2	0.14979	0.07294	1.36427	0.97701	0.03258	0.02061	3.10980	0.20906	0.00612	0.00483	4.38974	0.03010

Source. After Jones (1962).

Downloaded From : www.EasyEngineering.net

Downloaded From : www.EasyEngineering.net

Downloaded From : www.EasyEngineering.net

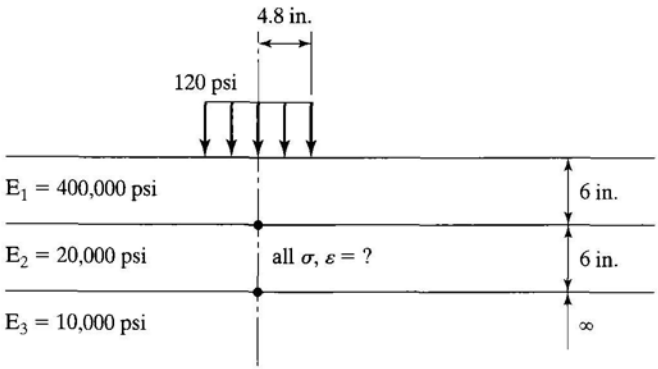


FIGURE 2.30

Example 2.11 (1 in. = 25.4 mm, 1 psi = 6.9 kPa).

Solution: Given $k_1 = 400{,}000/20{,}000 = 20$, $k_2 = 20{,}000/10{,}000 = 2$, $A = 4.8/6 = 0.8$, and $H = 6/6 = 1.0$, from Table 2.3, ZZ1 = 0.12173, ZZ2 = 0.05938, ZZ1 − RR1 = 1.97428, and ZZ2 − RR2 = 0.09268. From Eq. 2.24, $\sigma_{z1} = 120 \times 0.12173 = 14.61$ psi (101 kPa), $\sigma_{z2} = 120 \times 0.05938 = 7.12$ psi (49.1 kPa), $\sigma_{z1} - \sigma_{r1} = 120 \times 1.97428 = 236.91$ psi (1.63 MPa), and $\sigma_{z2} - \sigma_{r2} = 120 \times 0.09268 = 11.12$ psi (76.7 kPa). From Eq. 2.23, $\sigma_{z1} - \sigma'_{r1} = 236.91/20 = 11.85$ psi (81.8 kPa) and $\sigma_{z2} - \sigma'_{r2} = 11.12/2 = 5.56$ psi (38.4 kPa). At bottom of layer 1: $\sigma_{r1} = 14.61 - 236.91 = -222.3$ psi (−1.53 MPa), from Eq. 2.20, $\epsilon_z = 236.91/400{,}000 = 5.92 \times 10^{-4}$ and $\epsilon_r = -2.96 \times 10^{-4}$. At top of layer 2: $\sigma'_{r1} = 14.61 - 11.85 = 2.76$ psi (19.0 kPa), $\epsilon_z = 11.85/20{,}000 = 5.92 \times 10^{-4}$, and $\sigma_r = -2.96 \times 10^{-4}$. At bottom of layer 2: $\sigma_{r2} = 7.12 - 11.12 = -4.0$ psi (−28 kPa), $\epsilon_z = 11.12/20{,}000 = 5.56 \times 10^{-4}$, and $\epsilon_r = -2.78 \times 10^{-4}$. At top of layer 3: $\sigma'_{r2} = 7.12 - 5.56 = 1.56$ psi (10.8 kPa), $\epsilon_z = 5.56/10{,}000 = 5.56 \times 10^{-4}$ and $\epsilon_r = -2.78 \times 10^{-4}$.

In the foregoing example, the parameters k_1, k_2, A, and H are exactly the same as those shown in the table, so no interpolation is needed. Because each interpolation requires three points, the interpolation of only one parameter requires at least three times the effort. If all four parameters are different from those in the table, the total effort required will be $3 \times 3 \times 3 \times 3$, or 81 times.

Peattie's Charts Peattie (1962) plotted Jones' table in graphical forms. Figure 2.31 shows one set of charts for radial strain factors, (RR1 − ZZ1)/2, at the bottom of layer 1. As indicated by Eq. 2.20*b*, the radial strain can be determined from

$$\epsilon_r = \frac{q}{E}\left(\frac{\text{RR1} - \text{ZZ1}}{2}\right) \tag{2.25}$$

The radial strains at the bottom of layer 1 should be in tension. Although the solutions obtained from the charts are not as accurate as those from the table, the chart has the advantage that interpolation for A and H can be easily done. However, interpolation for k_1 and k_2 is still cumbersome.

Downloaded From : www.EasyEngineering.net

Downloaded From : www.EasyEngineering.net

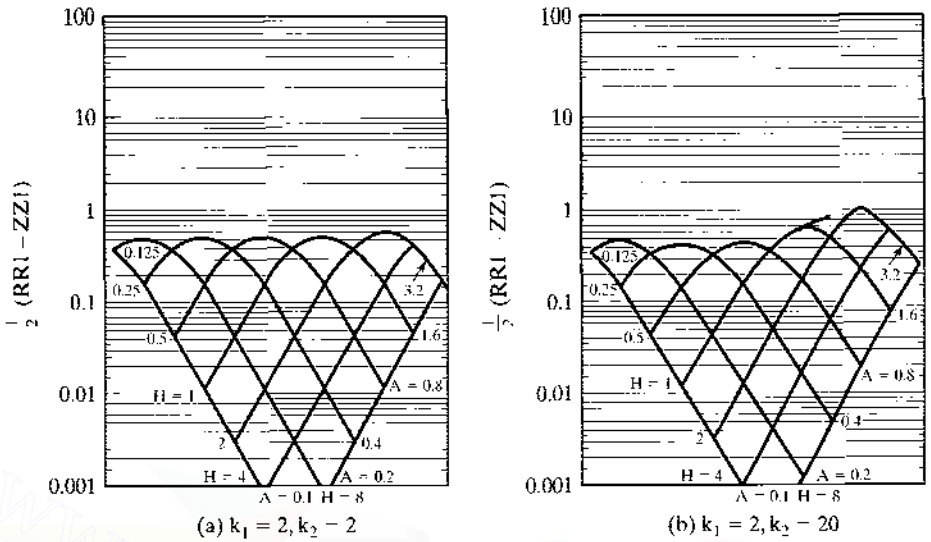


FIGURE 2.31

Charts for horizontal strain factors at bottom of layer 1. (After Peattie (1962).)

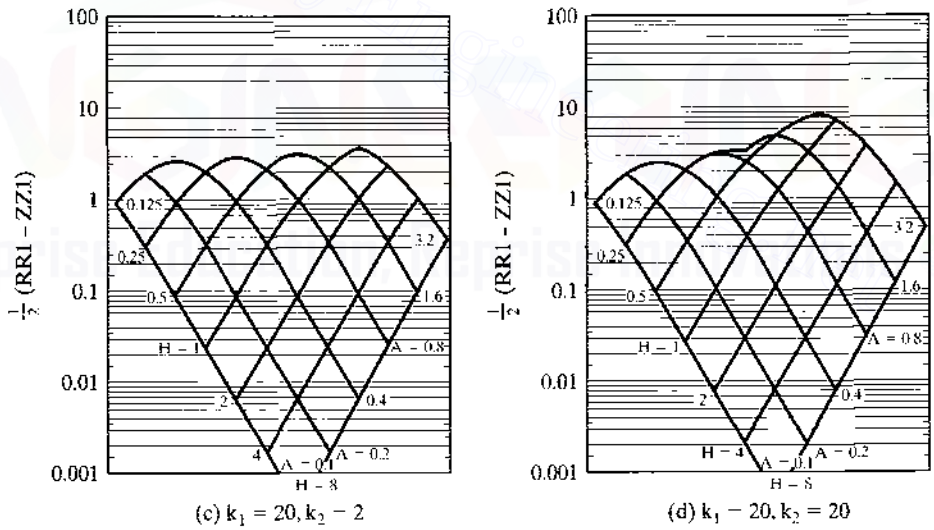


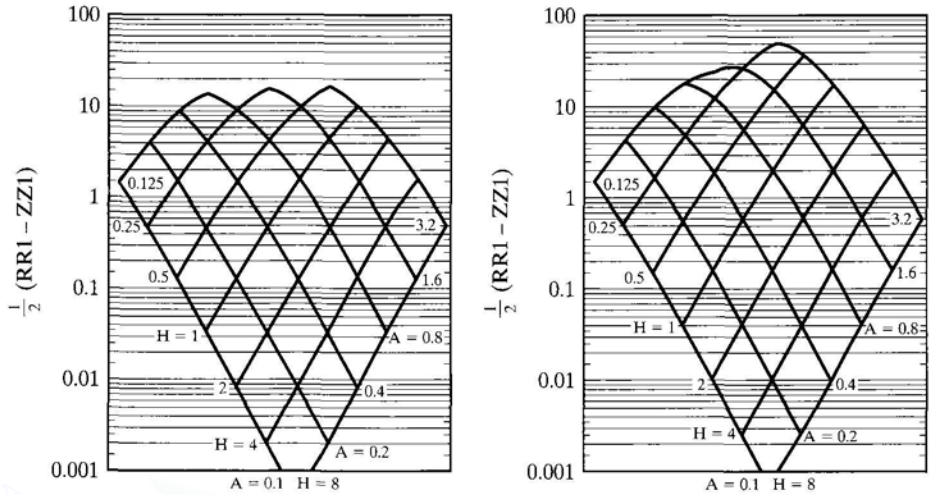
FIGURE 2.31 (Continued)

Example 2.12:

For the same case as Example 2.11, determine the radial strain at the bottom of layer 1, as shown in Figure 2.32. If $h_2 = 8$ in. (203 mm), what is the radial strain at the bottom of layer 1?

Downloaded From : www.EasyEngineering.net

Downloaded From : www.EasyEngineering.net



(e) $k_1 = 200, k_2 = 2$ (f) $k_1 = 200, k_2 = 2$

FIGURE 2.31 (Continued)

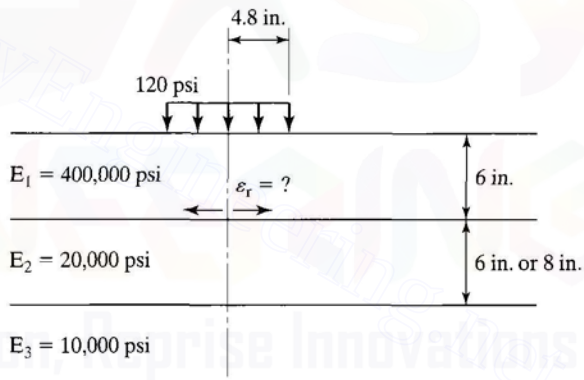


FIGURE 2.32

Example 2.12 (1 in = 25.5 mm, 1 psi = 6.9 kPa).

Solution: Given $k_1 = 20, k_2 = 2, A = 0.8$, and $H = 1.0$, from Figure 2.31*c*, (RR1 − ZZ1)/2 = 1. From Eq. 2.25, $\epsilon_r = 120/400{,}000 = 3 \times 10^{-4}$ (tension), which checks closely with the 2.96×10^{-4} from the table. Given $h_2 = 8$ in. (203 mm), $A = 4.8/8 = 0.6$, and $H = 6/8 = 0.75$, from Figure 2.31*c*, the strain factor is still close to 1, indicating that the thickness of layer 2 has very little effect on the tensile strain due to the predominant effect of layer 1. The radial strain obtained from KENLAYER is 2.91×10^{-4}.

2.3 VISCOELASTIC SOLUTIONS

A viscoelastic material possesses both the elastic property of a solid and the viscous behavior of a liquid. Suppose that a material is formed into a ball. If the ball is thrown on the floor and rebounds, it is said to be elastic. If the ball is left on the table and begins to flow and flatten gradually under its own weight, it is said to be viscous. The viscous component makes the behavior of viscoelastic materials time dependent: the longer the time,

Downloaded From : www.EasyEngineering.net

Downloaded From : www.EasyEngineering.net

the more the material flows. HMA is a viscoelastic material whose behavior depends on the time of loading, so it is natural to apply the theory of viscoelasticity to the analysis of layered systems. The general procedure is based on the elastic–viscoelastic correspondence principle by applying the Laplace transform to remove the time variable t with a transformed variable p, thus changing a viscoelastic problem to an associated elastic problem. The Laplace inversion of the associated elastic problem from the transformed variable p to the time variable t results in the viscoelastic solutions. Details about the theory of viscoelasticity are presented in Appendix A. A simple collocation method to obtain the viscoelastic solutions from the elastic solutions is presented in this section.

2.3.1 Material Characterization

There are two general methods for characterizing viscoelastic materials: one by a mechanical model, the other by a creep-compliance curve. The latter is used in KENLAYER because of its simplicity. Because Poisson ratio v has a relatively small effect on pavement behavior, it is assumed to be elastic independent of time. Therefore, only modulus E is considered to be viscoelastic and time dependent.

Mechanical Models Figure 2.33 shows various mechanical models for characterizing viscoelastic materials. The models are formed of two basic elements: a spring and a dashpot.

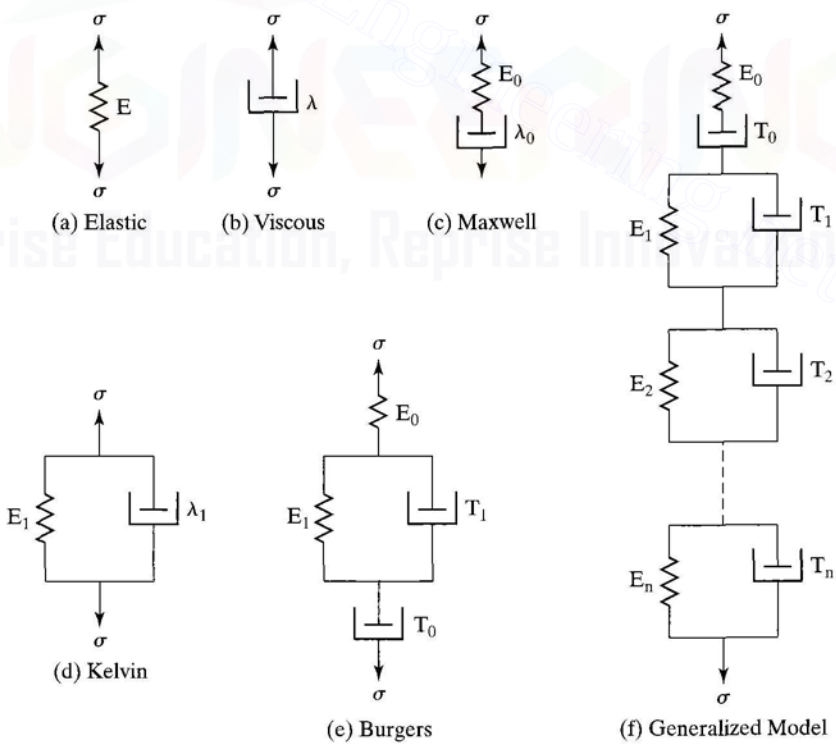


FIGURE 2.33

Mechanical models for viscoelastic materials.

Downloaded From : www.EasyEngineering.net

Downloaded From : www.EasyEngineering.net

Basic Models An elastic material is characterized by a spring, as indicated in Figure 2.33*a*, and obeys Hooke's law, which asserts that stress is proportional to strain:

$$\sigma = E\epsilon \tag{2.26}$$

Here, σ is stress, ϵ is strain, and E is the elastic modulus.

A viscous material is characterized by a dashpot, as indicated in Figure 2.33*b*, and obeys Newton's law, according to which stress is proportional to the time rate of strain:

$$\sigma = \lambda \frac{\partial \epsilon}{\partial t} \tag{2.27}$$

In this equation, λ is viscosity and t is time. Under a constant stress, Eq. 2.27 can easily be integrated to become

$$\epsilon = \frac{\sigma t}{\lambda} \tag{2.28}$$

Maxwell Model A Maxwell model is a combination of spring and dashpot in series, as indicated in Figure 2.33*c*. Under a constant stress, the total strain is the sum of the strains of both spring and dashpot, or, from Eqs. 2.26 and 2.28,

$$\epsilon = \frac{\sigma}{E_0} + \frac{\sigma t}{\lambda_0} = \frac{\sigma}{E_0}\left(1 + \frac{t}{T_0}\right) \tag{2.29}$$

in which $T_0 = \lambda_0/E_0$ = relaxation time. A subscript 0 is used to indicate a Maxwell model. If a stress σ_0 is applied instantaneously to the model, the spring will experience an instantaneous strain, σ_0/E_0. If this strain is kept constant, the stress will gradually relax and, after a long period of time, will become zero. This can be shown by solving the differential equation

$$\frac{\partial \epsilon}{\partial t} = \frac{1}{E_0}\frac{\partial \sigma}{\partial t} + \frac{\sigma}{\lambda_0} \tag{2.30}$$

The first term on the right side of Eq. 2.30 is the rate of strain due to the spring, the second term that due to the dashpot. If strain is kept constant, $\partial\epsilon/\partial t = 0$, or, after integration,

$$\sigma = \sigma_0 \exp\left(-\frac{t}{T_0}\right) \tag{2.31}$$

It can be seen from Eq. 2.31 that when $t = 0, \sigma = \sigma_0$; when $t = \infty, \sigma = 0$; and when $t = T_0, \sigma = 0.368\,\sigma_0$. Consequently, the relaxation time T_0 of a Maxwell model is the time required for the stress to reduce to 36.8% of the original value. It is more convenient to specify relaxation time than viscosity, because of its physical meaning. A relaxation time of 10 min gives an idea that the stress will relax to 36.8% of the original value in 10 min.

Kelvin Model A Kelvin model is a combination of spring and dashpot in parallel, as indicated in Figure 2.33*d*. Both the spring and the dashpot have the same strain, but the total stress is the sum of the two stresses, or, using subscript 1 to indicate a Kelvin model,

$$\sigma = E_1\epsilon + \lambda_1 \frac{\partial \epsilon}{\partial t}$$

Downloaded From : www.EasyEngineering.net

Downloaded From : www.EasyEngineering.net

If a constant stress is applied, then

$$\int_0^{\epsilon} \frac{d\epsilon}{\sigma - E_1\epsilon} = \int_0^t \frac{dt}{\lambda_1}$$

or

$$\epsilon = \frac{\sigma}{E_1}\left[1 - \exp\left(-\frac{t}{T_1}\right)\right] \tag{2.32}$$

in which $T_1 = \lambda_1/E_1$ = retardation time. It can be seen from Eq. 2.32 that when $t = 0, \epsilon = 0$; when $t = \infty, \epsilon = \sigma/E_1$, or the spring is fully stretched to its total retarded strain; and when $t = T_1, \epsilon = 0.632\sigma/E_1$. Thus, the retardation time T_1 of a Kelvin model is the time to reach 63.2% of the total retarded strain.

Burgers Model A Burgers model is a combination of Maxwell and Kelvin models in series, as indicated in Figure 2.33*e*. Under a constant stress, from Eqs. 2.29 and 2.32,

$$\epsilon = \frac{\sigma}{E_0}\left(1 + \frac{t}{T_0}\right) + \frac{\sigma}{E_1}\left[1 - \exp\left(-\frac{t}{T_1}\right)\right] \tag{2.33}$$

The total strain is composed of three parts: an instantaneous elastic strain, a viscous strain, and a retarded elastic strain, as shown in Figure 2.34. Qualitatively, a Burgers model well represents the behavior of a viscoelastic material. Quantitatively, a single Kelvin model is usually not sufficient to cover the long period of time over which the retarded strain takes place, and a number of Kelvin models could be needed.

Generalized Model Figure 2.33*f* shows a generalized model that can be used to characterize any viscoelastic material. Under a constant stress, the strain of a generalized model can be written as

$$\epsilon = \frac{\sigma}{E_0}\left(1 + \frac{t}{T_0}\right) + \sum_{i=1}^{n} \frac{\sigma}{E_i}\left[1 - \exp\left(-\frac{t}{T_i}\right)\right] \tag{2.34}$$

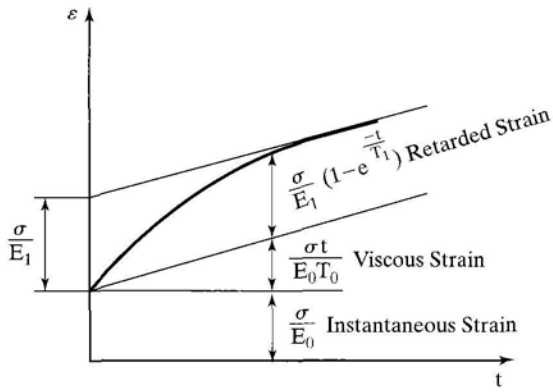


FIGURE 2.34
Three components of strain for a Burgers model.

Downloaded From : www.EasyEngineering.net

Downloaded From : www.EasyEngineering.net

in which n is the number of Kelvin models. This model explains the effect of load duration on pavement responses. Under a single load application, the instantaneous and the retarded elastic strains predominate, and the viscous strain is negligible. However, under a large number of load repetitions, the accumulation of viscous strains is the cause of permanent deformation.

Creep Compliance Another method to characterize viscoelastic materials is the creep compliance at various times, $D(t)$, defined as

$$D(t) = \frac{\epsilon(t)}{\sigma} \tag{2.35}$$

in which $\epsilon(t)$ is the time-dependent strain under a constant stress.

Under a constant stress, the creep compliance is the reciprocal of Young's modulus. For the generalized model, the creep compliance can be expressed as

$$D(t) = \frac{1}{E_0}\left(1 + \frac{t}{T_0}\right) + \sum_{i=1}^{n} \frac{1}{E_i}\left[1 - \exp\left(-\frac{t}{T_i}\right)\right] \tag{2.36}$$

Given the various viscoelastic constants, E_0, T_0, E_i, and T_i, for a generalized model, the creep compliances at various times can be computed from Eq. 2.36.

Example 2.13:

A viscoelastic material is characterized by one Maxwell model and three Kelvin models connected in series with the viscoelastic constants shown in Figure 2.35*a*. Determine the creep compliance at various times, and plot the creep-compliance curve.

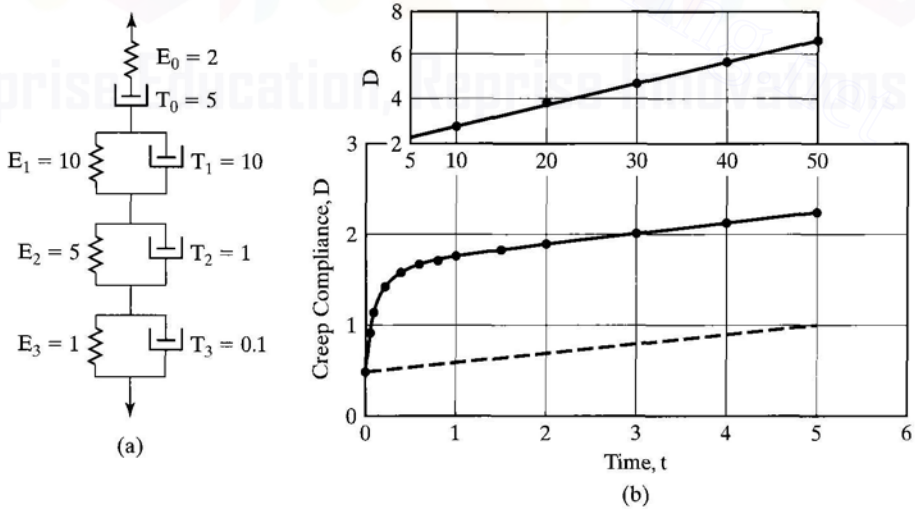


FIGURE 2.35
Example 2.13.

Downloaded From : www.EasyEngineering.net

Downloaded From : www.EasyEngineering.net

TABLE 2.4 Creep Compliance at Various Times

Time	Creep compliance	Time	Creep compliance
0	0.500	2	1.891
0.05	0.909	3	2.016
0.1	1.162	4	2.129
0.2	1.423	5	2.238
0.4	1.592	10	2.763
0.6	1.654	20	3.786
0.8	1.697	30	4.795
1.0	1.736	40	5.798
1.5	1.819	50	6.799

Solution: In Figure 2.35*a*, no units are given for the viscoelastic constants. If E is in lb/in^2, then the creep compliance is in in.^{2}/lb. If E is in kN/m^2, then the creep compliance is in m^2/kN. If T is in seconds, then the actual time t is also in seconds. From Eq. 2.36, when $t = 0, D = 1/E_0 = \frac{1}{2} = 0.5$; and when $t = 0.1, D = 0.5\,(1 + 0.1/5) + 0.1\,(1 - e^{-0.01}) + 0.2\,(1 - e^{-0.1}) + (1 - e^{-1}) = 1.162$. The creep compliances at various times are tabulated in Table 2.4 and plotted in Figure 2.35*b*. It can be seen that, after $t = 5$, all the retarded strains have nearly completed and only the viscous strains exist, as indicated by a straight line. If the retarded strain lasts much longer, more Kelvin models with longer retardation times will be needed.

If a creep compliance curve is given, the viscoelastic constants of a generalized model can be determined by the method of successive residuals, as described in Appendix A. However, it is more convenient to use an approximate method of collocation, as described below.

2.3.2 Collocation Method

The collocation method is an approximate method to collocate the computed and actual responses at a predetermined number of time durations. Instead of determining both E_i and T_i by the method of successive residuals, several values of T_i are arbitrarily assumed, and the corresponding E_i values are determined by solving a system of simultaneous equations. The method can also be used to obtain the viscoelastic solutions from the elastic solutions.

Elastic Solutions Given the creep compliance of each viscoelastic material at a given time, the viscoelastic solutions at that time can be easily obtained from the elastic solutions, as is illustrated by the following example.

Example 2.14:

Figure 2.36 shows a viscoelastic two-layer system under a circular loaded area having radius 10 in. (254 mm) and uniform pressure 100 psi (690 kPa). The thickness of layer 1 is 10 in. (254 mm), and both layers are incompressible, with Poisson ratio 0.5. The creep compliances of the two materials at five different times are tabulated in Table 2.5. Determine the surface deflection under the center of the loaded area at the given times.

Downloaded From : www.EasyEngineering.net

Downloaded From : www.EasyEngineering.net

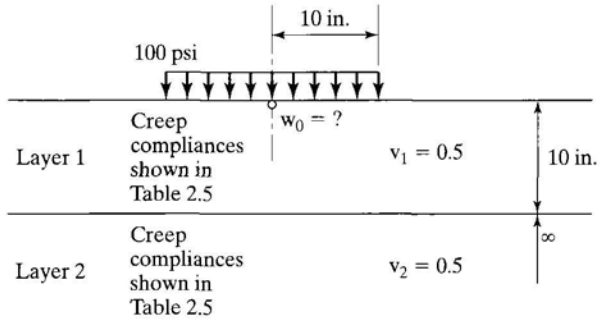


FIGURE 2.36
Example 2.14 (1 in. = 25.4 mm, 1 psi = 6.9 kPa).

Solution: If the modulus ratio is greater than 1, the surface deflection w_0 at any given time can be determined from Figure 2.17. Take $t = 1$ s, for example. The elastic modulus is the reciprocal of creep compliance. For layer 1, $E_1 = 1/(2.683 \times 10^{-6}) = 3.727 \times 10^5$ psi (2.57 GPa) and for layer 2, $E_2 = 1/(19.52 \times 10^{-6}) = 5.123 \times 10^4$ psi (353 MPa), so $E_1/E_2 = 3.727 \times 10^5/(5.123 \times 10^4) = 7.27$. From Figure 2.17, $F_2 = 0.54$, so $w_0 = 1.5 \times 100 \times 10 \times 0.54/(5.123 \times 10^4) = 0.016$ in. (4.1 mm). The same procedure can be applied to other time durations and the results are shown in Table 2.5.

TABLE 2.5 Creep Compliances and Surface Deflections

Time (s)	0.01	0.1	1	10	100
Layer 1 $D(t)$ (10^{-6}/psi)	1.021	1.205	2.683	9.273	18.320
Layer 2 $D(t)$ (10^{-6}/psi)	1.052	7.316	19.520	73.210	110.000
Deflection w_0 (in.)	0.0016	0.0064	0.016	0.059	0.096

Note. 1 psi = 6.9 kPa, 1 in. = 25.4 mm.

It should be noted that the above procedure is not the exact viscoelastic solution. It is a quasi-elastic solution that provides a close approximation to the viscoelastic solution.

Dirichlet Series Pavement design is based on moving loads with a short duration. The creep compliance $D(t)$ caused by the viscous strain is negligible, so Eq. 2.36 can be written as

$$D(t) = \frac{1}{E_0} + \sum_{i=1}^{n} \frac{1}{E_i}\left[1 - \exp\left(-\frac{t}{T_i}\right)\right] \tag{2.37}$$

It is therefore convenient to express the creep compliance as a Dirichlet series, or

$$D(t) = \sum_{i=1}^{n} G_i \exp\left(-\frac{t}{T_i}\right) \tag{2.38}$$

Downloaded From : www.EasyEngineering.net

Downloaded From : www.EasyEngineering.net

A comparison of Eqs. 2.37 and 2.38 with $T_n = \infty$ shows that

$$G_i = -\frac{1}{E_i} \tag{2.39a}$$

$$G_n = \frac{1}{E_0} + \sum_{i=1}^{n} \frac{1}{E_i} \tag{2.39b}$$

In KENLAYER, the collocation method is applied at two occasions. First, the creep compliances at a reference temperature are specified at a number of time durations and fitted with a Dirichlet series, so that the compliances at any other temperature can be obtained by the time–temperature superposition principle. Second, the elastic solutions obtained at these durations are fitted with a Dirichlet series to be used later for analyzing moving loads.

Collocation of Creep Compliances The creep compliances of viscoelastic materials are determined from creep tests. A 1000-s creep test with compliances measured at 11 different time durations (0.001, 0.003, 0.01, 0.03, 0.1, 0.3, 1, 3, 10, 30 and 100 s) is recommended (FHWA, 1978) to cover all possible range of interest. This range from 0.001 to 100 s should be able to take care of moving loads with both short and long duration as well as the change in creep compliances with temperature.

Because moving loads usually have a very short duration, retardation times T_i of 0.01, 0.03, 0.1, 1, 10, 30, and ∞ seconds are specified in KENLAYER. If creep compliances are specified at seven durations, the coefficients G_1 through G_7 can be determined from Eq. 2.38 by solving 7 simultaneous equations. If the creep compliances are specified at 11 time durations, there are 11 equations but 7 unknowns, so the 11 equations must be reduced to 7 equations by multiplying both sides with a 7×11 matrix, which is the transpose of the 11×7 matrix, or

$$\begin{bmatrix} \exp\left(-\frac{t_1}{T_1}\right) \dots \exp\left(-\frac{t_{11}}{T_1}\right) \\ \vdots\ 7 \times 11 \text{ matrix} \ \vdots \\ \exp\left(-\frac{t_1}{T_7}\right) \dots \exp\left(-\frac{t_{11}}{T_7}\right) \end{bmatrix} \begin{bmatrix} \exp\left(-\frac{t_1}{T_1}\right) \dots \exp\left(-\frac{t_1}{T_7}\right) \\ \vdots\ 11 \times 7 \text{ matrix} \ \vdots \\ \exp\left(-\frac{t_{11}}{T_1}\right) \dots \exp\left(-\frac{t_{11}}{T_7}\right) \end{bmatrix} \begin{Bmatrix} G_1 \\ \vdots \\ G_7 \end{Bmatrix}$$

$$= \begin{bmatrix} \exp\left(-\frac{t_1}{T_1}\right) \dots \exp\left(-\frac{t_{11}}{T_1}\right) \\ \vdots\ 7 \times 11 \text{ matrix} \ \vdots \\ \exp\left(-\frac{t_1}{T_7}\right) \dots \exp\left(-\frac{t_{11}}{T_7}\right) \end{bmatrix} \begin{Bmatrix} D_1 \\ \vdots \\ D_{11} \end{Bmatrix} \tag{2.40}$$

After coefficients G_1 through G_7 are obtained, the creep compliance at any time t can be computed by Eq. 2.38. The use of 7 equations and 7 unknowns, instead of 11 equations and 11 unknowns, not only saves the computer time but also smooths out the results of creep tests.

Downloaded From : www.EasyEngineering.net

Downloaded From : www.EasyEngineering.net

Example 2.15:

It is assumed that the creep compliance of a viscoelastic material is represented by

$$D(t) = G_1 \exp(-10t) + G_2 \tag{2.41}$$

If the creep compliances at $t = 0.01$, 0.07, and 0.4 s are 9.516×10^{-5}, 5.034×10^{-4} and 9.817×10^{-4} in.^{2}/lb (13.8, 72.9, and 142.3 mm^2/kN), respectively, determine the coefficients G_1 and G_2.

Solution: With $t_1 = 0.01, t_2 = 0.07, t_3 = 0.4, T_1 = 0.1, T_2 = \infty, D_1 = 9.516 \times 10^{-5}, D_2 = 5.034 \times 10^{-4}$, and $D_3 = 9.817 \times 10^{-4}$. From Eq. 2.40,

$$\begin{bmatrix} e^{-0.1} & e^{-0.7} & e^{-4} \\ 1 & 1 & 1 \end{bmatrix} \begin{bmatrix} e^{-0.1} & 1 \\ e^{-0.7} & 1 \\ e^{-4} & 1 \end{bmatrix} \begin{Bmatrix} G_1 \\ G_2 \end{Bmatrix} = \begin{bmatrix} e^{-0.1} & e^{-0.7} & e^{-4} \\ 1 & 1 & 1 \end{bmatrix} \begin{Bmatrix} 9.516 \times 10^{-5} \\ 5.034 \times 10^{-4} \\ 9.817 \times 10^{-4} \end{Bmatrix}$$

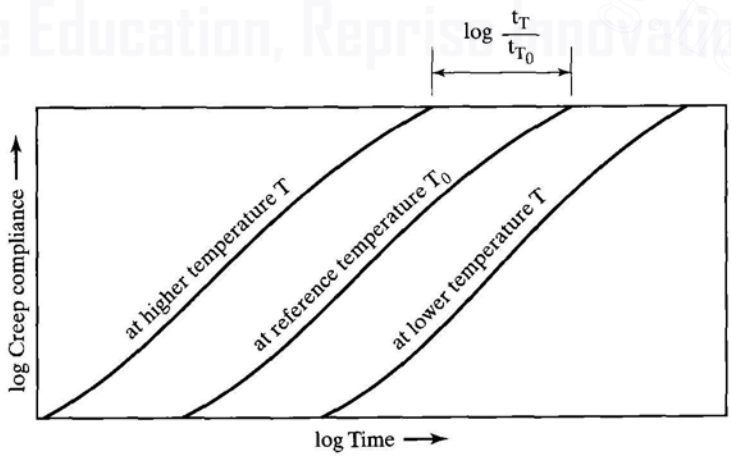
or

$$\begin{bmatrix} 1.066 & 1.420 \\ 1.420 & 3.000 \end{bmatrix} \begin{Bmatrix} G_1 \\ G_2 \end{Bmatrix} = \begin{Bmatrix} 3.541 \times 10^{-4} \\ 1.580 \times 10^{-3} \end{Bmatrix} \tag{2.42}$$

The solution of Eq. 2.42 is $G_1 = -0.001$ in.^{2}/lb (-145 mm^2/kN) and $G_2 = 0.001$ in.^{2}/lb (145 mm^2/kN), which is as expected because the given creep compliances are actually computed from a Kelvin model with

$$D(t) = 0.001\,(1 - e^{-10t}) \tag{2.43}$$

Time–Temperature Superposition It has been demonstrated that asphalt mixes subjected to a temperature increase experience an accelerated deformation as if the time scale were compressed. Figure 2.37 shows the plot of creep compliance D versus time t



FIGUR E 2.37

Creep compliance at different temperatures.

Downloaded From : www.EasyEngineering.net

Downloaded From : www.EasyEngineering.net

on log scales. At a given time, the creep compliance at a lower temperature is smaller than that at a higher temperature. There is a parallel shift between the curves at various temperatures.

If the creep compliances under a reference temperature T_0 are known, those under any given temperature T can be obtained by using a time–temperature shift factor a_T, defined (Pagen, 1965) as

$$a_T = \frac{t_T}{t_{T_0}} \tag{2.44}$$

in which t_T is the time to obtain a creep compliance at temperature T and t_{T_0} is the time to obtain a creep compliance at reference temperature T_0.

Various laboratory tests on asphalt mixes have shown that a plot of log a_T versus temperature results in a straight line, as shown in Figure 2.38. The slope of the straight line β varies from 0.061 to 0.170, with an average about 0.113 (FHWA, 1978). From Figure 2.38,

$$\beta = \frac{\log(t_T/t_{T_0})}{T - T_0} \tag{2.45}$$

or

$$t_T = t_{T_0} \exp[2.3026\beta(T - T_0)] \tag{2.46}$$

If the creep compliance based on the reference temperature T_0 is

$$D(t) = \sum_{i=1}^{n} G_i \exp\left(-\frac{t_{T_0}}{T_i}\right) \tag{2.47}$$

then the creep compliance based on temperature T is

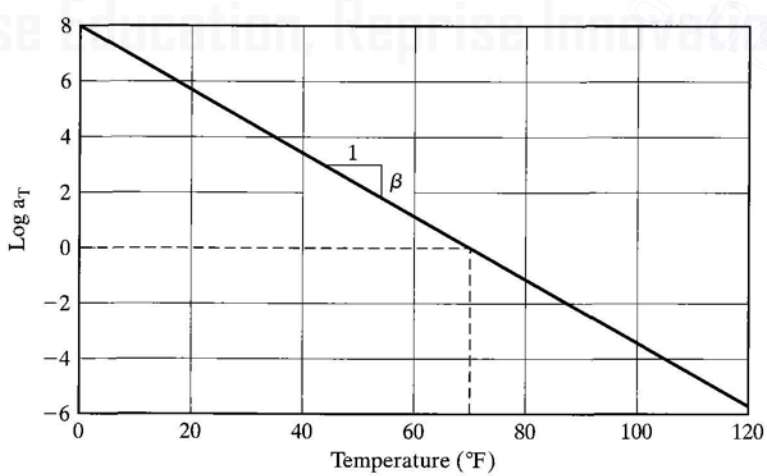


FIGURE 2.38

Shift factor versus temperature.

Downloaded From : www.EasyEngineering.net

Downloaded From : www.EasyEngineering.net

$$D(t) = \sum_{i=1}^{n} G_i \exp\left(-\frac{t_T}{T_i}\right) \tag{2.48}$$

The relationship between t_T and t_{T_0} is indicated by Eq. 2.46.

Example 2.16:

The expression for the creep compliance at 70°F (21.1°C) is represented by Eq. 2.43. What is the expression for creep compliance at 50°F (10°C) if the time–temperature shift factor β is 0.113?

Solution: From Eq. 2.46, $t_T = t_{T_0} \exp[2.3026 \times 0.113 \times (50 - 70)] = 0.0055 t_{T_0}$. From Eq. 2.43, $D(t) = 0.001[1 - \exp(-0.055t)]$. It can be seen that the creep compliance at 50°F (10°C) is much smaller than that at 70°F (21.1°C).

Collocation for Viscoelastic Solutions Even though the exact viscoelastic solutions is not known, the viscoelastic response R can always be expressed approximately as a Dirichlet series:

$$R = \sum_{i=1}^{7} c_i \exp\left(-\frac{t}{T_i}\right) \tag{2.49}$$

If elastic solutions at 11 time durations are obtained, Eq. 2.40 can be applied to reduce the number of equations to seven, which is the number of unknowns to be solved. If the responses at seven time durations are obtained from the elastic solutions, the coefficients c_1 through c_7 can be solved directly by

$$\begin{bmatrix} e^{-\frac{0.01}{0.01}} & e^{-\frac{0.01}{0.03}} & e^{-\frac{0.01}{0.1}} & e^{-\frac{0.01}{1}} & e^{-\frac{0.01}{10}} & e^{-\frac{0.01}{30}} & 1 \\ e^{-\frac{0.03}{0.01}} & e^{-\frac{0.03}{0.03}} & e^{-\frac{0.03}{0.1}} & e^{-\frac{0.03}{1}} & e^{-\frac{0.03}{10}} & e^{-\frac{0.03}{30}} & 1 \\ e^{-\frac{0.1}{0.01}} & e^{-\frac{0.1}{0.03}} & e^{-\frac{0.1}{0.1}} & e^{-\frac{0.1}{1}} & e^{-\frac{0.1}{10}} & e^{-\frac{0.1}{30}} & 1 \\ e^{-\frac{1}{0.01}} & e^{-\frac{1}{0.03}} & e^{-\frac{1}{0.1}} & e^{-\frac{1}{1}} & e^{-\frac{1}{10}} & e^{-\frac{1}{30}} & 1 \\ e^{-\frac{10}{0.01}} & e^{-\frac{10}{0.03}} & e^{-\frac{10}{0.1}} & e^{-\frac{10}{1}} & e^{-\frac{10}{10}} & e^{-\frac{10}{30}} & 1 \\ e^{-\frac{30}{0.01}} & e^{-\frac{30}{0.03}} & e^{-\frac{30}{0.1}} & e^{-\frac{30}{1}} & e^{-\frac{30}{10}} & e^{-\frac{30}{30}} & 1 \\ 1 & 1 & 1 & 1 & 1 & 1 & 1 \end{bmatrix} \begin{Bmatrix} c_1 \\ c_2 \\ c_3 \\ c_4 \\ c_5 \\ c_6 \\ c_7 \end{Bmatrix} = \begin{Bmatrix} (R)_{0.01} \\ (R)_{0.03} \\ (R)_{0.1} \\ (R)_1 \\ (R)_{10} \\ (R)_{30} \\ (R)_\infty \end{Bmatrix} \tag{2.50}$$

After the coefficients c_i are obtained, the viscoelastic response can be determined by Eq. 2.49.

Example 2.17:

The creep compliance of a homogeneous half-space is expressed as a Dirichlet series shown by Eq. 2.41 with $G_1 = -0.001$ in.^{2}/lb (-145 mm^2/kN), $G_2 = 0.001$ in.^{2}/lb (145 mm^2/kN), $T_1 = 0.1$ s, and $T_2 = \infty$. Assuming that the half-space has Poisson ratio 0.5 and is subjected to a circular load with contact radius 6 in. (152 mm) and contact pressure 80 psi (552 kPa), as shown in Figure 2.39, determine the maximum surface deflection after a loading time of 0.1 s by the collocation method.

Downloaded From : www.EasyEngineering.net

Downloaded From : www.EasyEngineering.net

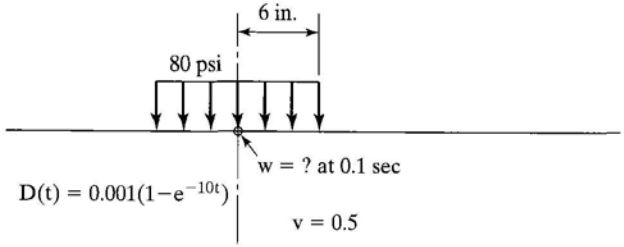


FIGURE 2.39
Example 2.15 (1 in. = 25.4 mm, 1 psi = 6.9 kPa).

Solution: The maximum deflection occurs under the center of the loaded area. With $v = 0.5$, from Eq. 2.8,

$$w_0 = \frac{1.5qa}{E} = 1.5qaD(t) \tag{2.51}$$

Substituting Eq. 2.43 and the values of q and a into Eq. 2.51 yields

$$w_0 = 0.72(1 - e^{-10t}) \tag{2.52}$$

When $t = 0.1$, from Eq. 2.52, then $w_0 = 0.455$ in. (11.6 mm).

The above solution is simple and straightforward. However, to illustrate the collocation method, it is assumed that the surface deflections are expressed as a Dirichlet series, as shown by Eq. 2.49. The elastic response on the right side of Eq. 2.53 is obtained from Eq. 2.52. From Eq. 2.50,

$$\begin{bmatrix} 0.368 & 0.717 & 0.905 & 0.990 & 0.999 & 1.000 & 1 \\ 0.050 & 0.368 & 0.741 & 0.970 & 0.997 & 0.999 & 1 \\ 0.000 & 0.036 & 0.368 & 0.905 & 0.990 & 0.997 & 1 \\ 0.000 & 0.000 & 0.000 & 0.368 & 0.905 & 0.967 & 1 \\ 0.000 & 0.000 & 0.030 & 0.000 & 0.368 & 0.717 & 1 \\ 0.000 & 0.000 & 0.000 & 0.000 & 0.050 & 0.368 & 1 \\ 1 & 1 & 1 & 1 & 1 & 1 & 1 \end{bmatrix} \begin{Bmatrix} c_1 \\ c_2 \\ c_3 \\ c_4 \\ c_5 \\ c_6 \\ c_7 \end{Bmatrix} = \begin{Bmatrix} 0.069 \\ 0.187 \\ 0.455 \\ 0.720 \\ 0.720 \\ 0.720 \\ 0.720 \end{Bmatrix} \tag{2.53}$$

The solution of Eq. 2.53 is $c_1 = 2.186$, $c_2 = -3.260$, $c_3 = 2.214$, $c_4 = -2.055$, $c_5 = 2.446$, $c_6 = -2.229$, and $c_7 = 1.418$. From Eq. 2.49, the surface deflection can be expressed as

$$w_0 = 2.186e^{-t/0.01} - 3.260e^{-t/0.03} + 2.214e^{-t/0.1} - 2.055e^{-t} + 2.446e^{-t/10} - 2.229e^{-t/30} + 1.418 \tag{2.54}$$

When $t = 0.1$, then $w_0 = 0 - 0.116 + 0.814 - 1.859 + 2.422 - 2.222 + 1.418 = 0.457$ in. (11.6 mm), which checks with the exact solution of 0.455 in. (11.6 mm).

2.3.3 Analysis of Moving Loads

The elastic–viscoelastic correspondence principle can be applied directly to moving loads, as indicated by Perloff and Moavenzadeh (1967) for determining the surface deflection of a viscoelastic half-space, by Chou and Larew (1969) for the stresses and displacements in a viscoelastic two-layer system, by Elliott and Moavenzadeh (1971) in a three-layer system, and by Huang (1973b) in a multilayer system. The complexities of the analysis and

Downloaded From : www.EasyEngineering.net

Downloaded From : www.EasyEngineering.net

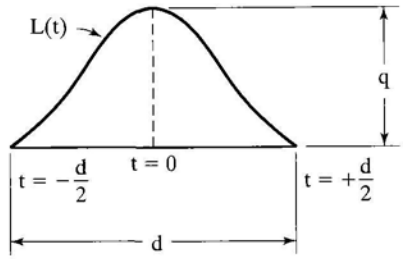


FIGURE 2.40
Moving load as a function of time.

the large amount of computer time required make these methods unsuited for practical use. Therefore, a simplified method has been used in both VESYS and KENLAYER.

In this method, it is assumed that the intensity of load varies with time according to a haversine function, as shown in Figure 2.40. With $t = 0$ at the peak, the load function is expressed as

$$L(t) = q \sin^2\left(\frac{\pi}{2} + \frac{\pi t}{d}\right) \tag{2.55}$$

in which d is the duration of load. When the load is at a considerable distance from a given point, or $t = \pm d/2$, the load above the point is zero, or $L(t) = 0$. When the load is directly above the given point, or $t = 0$, the load intensity is q.

The duration of load depends on the vehicle speed s and the tire contact radius a. A reasonable assumption is that the load has practically no effect when it is at a distance of $6a$ from the point, or

$$d = \frac{12a}{s} \tag{2.56}$$

If $a = 6$ in. and $s = 40$ mph (64 km/h) $= 58.7$ ft/s (17.9 m/s), $d = 0.1$ s.

The response under static load can be expressed as a Dirichlet series:

$$R(t) = \sum_{i=1}^{7} c_i \exp\left(-\frac{t}{T_i}\right) \tag{2.49}$$

The response under moving load can be obtained by Boltzmann's superposition principle:

$$R = \int_{-d/2}^{0} R(t) \frac{dL}{dt} dt \tag{2.57}$$

From Eq. 2.55,

$$\frac{dL}{dt} = -\frac{q\pi}{d} \sin\left(\frac{2\pi t}{d}\right) \tag{2.58}$$

Substituting Eqs. 2.49 and 2.58 into Eq. 2.57 and integrating yields

$$R = \frac{q\pi^2}{2} \sum_{i=1}^{n} c_i \frac{1 + \exp(-d/2T_i)}{\pi^2 + (d/2T_i)^2} \tag{2.59}$$

Downloaded From : www.EasyEngineering.net

Downloaded From : www.EasyEngineering.net

Example 2.18:

Same as the problem in Example 2.17, but the load is moving at 40 mph (64 km/h). Determine the maximum deflection.

Solution: According to Eq. 2.52 in Example 2.17, the surface deflection under a static load can be expressed as

$$w = 0.72(1 - e^{-10t}) \tag{2.52}$$

The first term is independent of time and therefore remains the same regardless of whether the load is moving. From Eq. 2.59, the second term with $T = 0.1$ and $d = 0.1$ s for 40 mph (64 km/h) should be changed to $0.5 \times \pi^2 \times 0.72\,(1 + e^{-0.5})/(\pi^2 + 0.25) = 0.564$ in. (14.3 mm), so maximum deflection $= 0.72 - 0.564 = 0.156$ in. (3.96 mm).

SUMMARY

This chapter discusses the stresses and strains in flexible pavements and their determinations. An understanding of this subject is indispensable for any mechanistic methods of design.

Important Points Discussed in Chapter 2

1. Boussinesq theory can be applied only to an elastic homogeneous half-space, such as the analysis of a plate bearing test on a subgrade or of a wheel load on a thin pavement.
2. An approximate method to determine the deflection on the surface of a nonlinear elastic half-space, in which the elastic modulus varies with the state of stresses, is to assume the same stress distribution as in the linear theory but vary the moduli according to the state of stresses.
3. The most practical mechanistic method for analyzing flexible pavements is Burmister's layered theory. Based on two-layer elastic systems, various charts were developed for determining pavement responses. The vertical interface stress beneath the center of a circular loaded area can be determined from Figure 2.15, the vertical interface deflection at various radial distances from Figure 2.19. The critical tensile strain at the bottom of layer 1 under a single wheel can be determined from Figure 2.21, under dual wheels from Figure 2.23, and under dual tandem wheels from Figures 2.25, 2.26, and 2.27. For three-layer elastic systems, the stresses and strains at the interfaces beneath the center of a circular loaded area can be determined from Table 2.3 and Figure 2.31.
4. Two methods can be used to characterize viscoelastic materials: a mechanical model and a creep-compliance curve. Both are closely related, and each can be converted to the other. The advantage of using a mechanical model is that the stress–strain relationship can be visualized physically to develop the governing differential equations; the advantage of using a creep-compliance curve is that it can easily be obtained by a laboratory creep test.
5. The elastic–viscoelastic correspondence principle based on Laplace transforms, described in Appendix A, can be used to analyze layered systems consisting of viscoelastic materials. However, a more convenient method is to obtain the elastic solutions at a number of time durations and fit them with a Dirichlet series as a function of time.
6. Instead of using the method of successive residuals, described in Appendix A, a collocation method can be applied to convert the creep compliance to a mechanical model, as indicated by a Dirichlet series. The time–temperature superposition principle, as indicated by Eqs. 2.46 and 2.48, can then be applied to convert the creep compliance from a reference temperature to any given temperature.

Downloaded From : www.EasyEngineering.net

Downloaded From : www.EasyEngineering.net

7. The responses of viscoelastic layered systems under moving loads can be obtained from those under static loads by applying Boltzmann's superposition principle, in which the moving load is expressed as a haversine function and the static response as a Dirichlet series.

PROBLEMS

2.1 A uniformly distributed load of intensity q is applied through a circular area of radius a on the surface of an incompressible ($v = 0.5$) homogeneous half-space with an elastic modulus E, as shown in Figure P2.1. In terms of q, a, and E, determine the vertical displacement, three principal stresses, and three principal strains at a point $2a$ below the surface under the edge ($r = a$) of the loaded area. [Answer: $w = 0.58\,qa/E$, $\sigma_1 = 0.221q$, $\sigma_2 = 0.011q$, $\sigma_3 = 0.004q$, $\varepsilon_1 = 0.214q/E$, $\varepsilon_2 = -0.102q/E$, $\varepsilon_3 = -0.112q/E$]

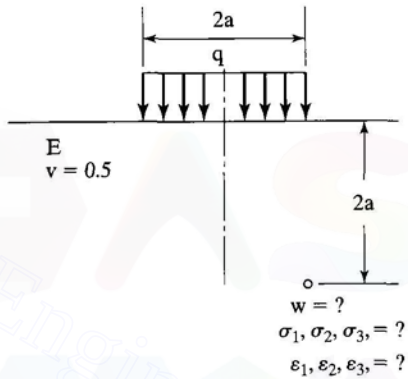


FIGURE P2.1

2.2 A 100-psi pressure is applied through a circular area 12 in. in diameter on a granular half-space, as shown in Figure P2.2. The half-space has mass unit weight its 110 pcf, coefficient of earth pressure at rest is 0.6, its Poisson ratio is 0.35, and its elastic modulus varies with the sum of normal stresses according to the equation shown in the figure. Assuming that the Boussinesq stress distribution is valid and that the stresses at a point 12 in. below the center of the loaded area are used to compute the elastic modulus, determine the maximum surface displacement. [Answer: 0.054 in.]

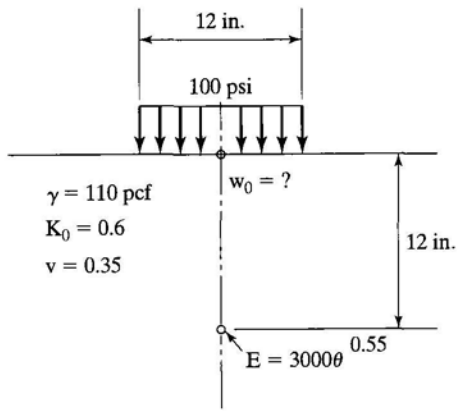


FIGURE P2.2

Downloaded From : www.EasyEngineering.net

Downloaded From : www.EasyEngineering.net

2.3 A plate bearing test using a 12-in.-diameter rigid plate is made on a subgrade, as shown in Figure P2.3*a*. The total load required to cause settling by 0.2 in. is 10,600 lb. After 10 in. of gravel base course is placed on the subgrade, a plate bearing test is made on the top of the base course, as shown in Figure P2.3*b*. The total load required to cause settling by 0.2 in. is 21,200 lb. Assuming a Poisson ratio of 0.5, determine the thickness of base course required to sustain a 50,000-lb tire exerting a contact pressure of 100 psi over a circular area, as shown in Figure P2.3*c*, yet maintain a deflection of no more than 0.2 in. [Answer: 70 in.]

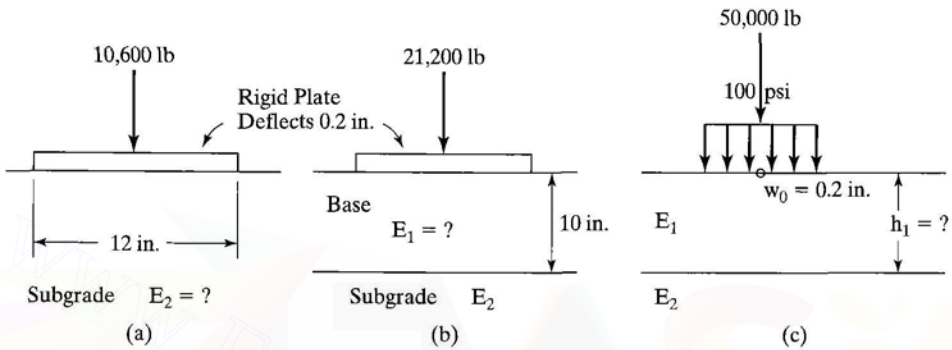


FIGURE P2.3

2.4 A 10,000-lb wheel load exerting contact pressure of 80 psi is applied on an elastic two-layer system, as shown in Figure P2.4. Layer 1 has elastic modulus 200,000 psi and thickness 8 in. Layer 2 has elastic modulus 10,000 psi. Both layers are incompressible, with Poisson ratio 0.5. Assuming that the loaded area is a single circle, determine the maximum surface deflection, interface deflection, and interface stress. [Answer: 0.025 in., 0.024 in., 11 psi]

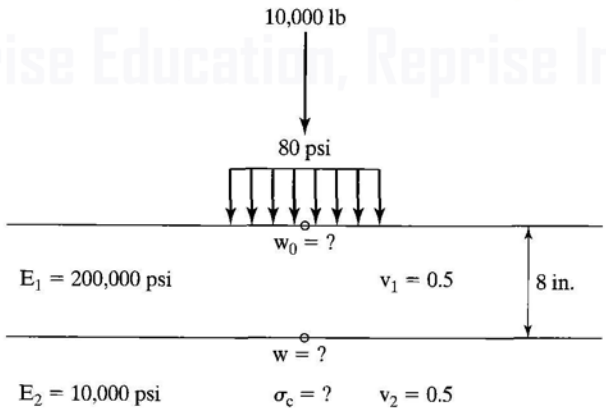


FIGURE P2.4

2.5 A full-depth asphalt pavement, consisting of an 8-in.-thick asphalt layer with elastic modulus 1,500,000 psi and a soil subgrade with elastic modulus 30,000 psi, is subjected to dual-tandem wheel loads, as shown in Figure P2.5. Each load weighs 50,000 lb, with a tire pressure of 100 psi and center-to-center spacings of 28 in. between dual and 60 in. between

Downloaded From : www.EasyEngineering.net

Downloaded From : www.EasyEngineering.net

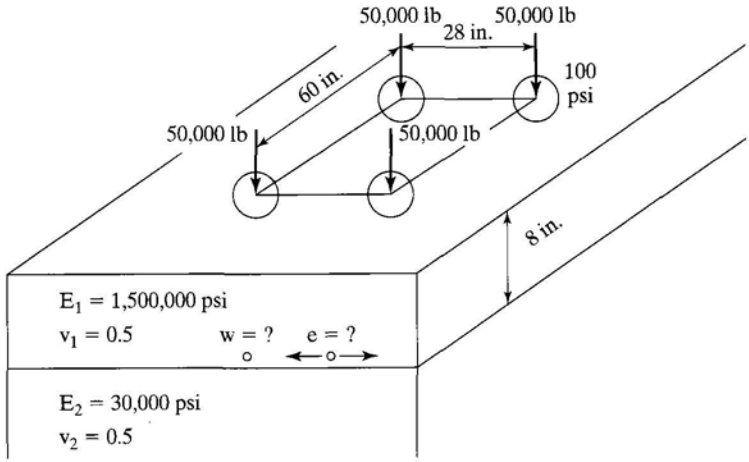


FIGURE P2.5

tandem. Assuming a Poisson ratio of 0.5, determine the maximum tensile strain at the bottom of asphalt layer under the center of one wheel and the vertical deflection on the surface of subgrade under the center of one wheel. [Answer: 2.05×10^{-4}, 0.057 in.]

2.6 Figure P2.6 shows a pavement structure composed of the following three layers: 5.75 in. HMA with elastic modulus 400,000 psi, 23 in. granular base with elastic modulus 20,000 psi, and a subgrade with elastic modulus 10,000 psi. All layers are assumed to have a Poisson ratio of 0.5. Calculate the maximum horizontal tensile strain at the bottom of HMA and the maximum vertical compressive strain on the top of subgrade under a 40,000-lb wheel load and 150-psi contact pressure, assuming that the contact area is a circle. [Answer: -7.25×10^{-4}, 1.06×10^{-3}]

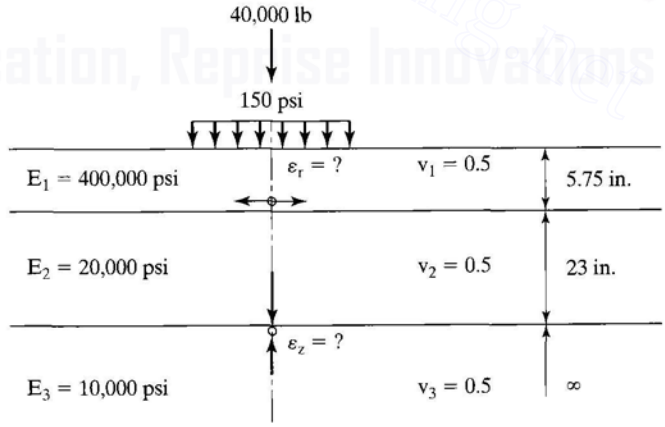


FIGURE P2.6

2.7 In Problem 2-6, if the base and subgrade are combined as one layer, as shown in Figure P2.7*a*, what should be the equivalent elastic modulus of this combined layer so that the same tensile strain at the bottom of HMA can be obtained? If the HMA and base are combined as

Downloaded From : www.EasyEngineering.net

Downloaded From : www.EasyEngineering.net

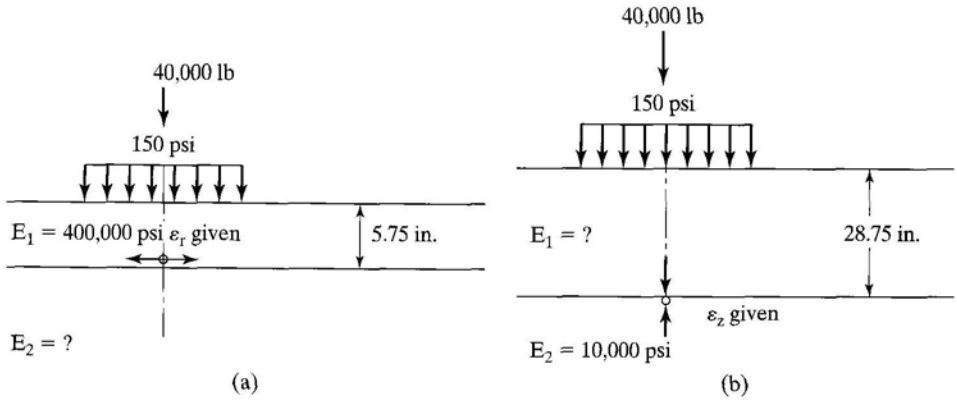


FIGURE P2.7

one layer with the same total thickness of 28.75 in., as shown in Figure 2.7*b*, what should be the equivalent elastic modulus of this combined layer so that the same compressive strain on the top of subgrade can be obtained? [Answer: 20,000 psi, 35,000 psi]

2.8 A circular load of intensity 80 psi and radius 6 in. moves over point *A* on the surface of a homogeneous half-space. The half-space has a Poisson ratio of 0.3 and a modulus characterized by the Maxwell model shown in Figure P2.8. If the intensity of load varies with time according to the triangular function with duration 10 s, determine the surface deflection when the load arrives at point *A*. If the variation of load is a haversine function indicated by Eq. 2.55, determine the surface deflection. [Answer: 0.109 in., 0.109 in.]

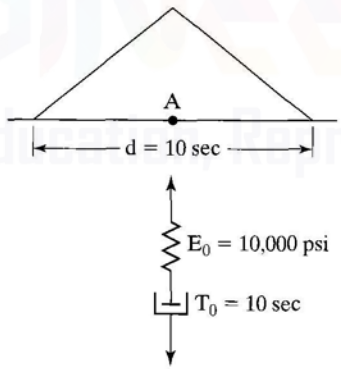


FIGURE P2.8

Downloaded From : www.EasyEngineering.net

Downloaded From : www.EasyEngineering.net

CHAPTER 3

KENLAYER Computer Program

3.1 THEORETICAL DEVELOPMENTS

The KENLAYER computer program applies only to flexible pavements with no joints or rigid layers. For pavements with rigid layers, such as PCC and composite pavements, the KENSLABS program described in Chapter 5 should be used. The backbone of KENLAYER is the solution for an elastic multilayer system under a circular loaded area. The solutions are superimposed for multiple wheels, applied iteratively for nonlinear layers, and collocated at various times for viscoelastic layers. As a result, KENLAYER can be applied to layered systems under single, dual, dual-tandem, or dual-tridem wheels with each layer behaving differently, either linear elastic, nonlinear elastic, or viscoelastic. Damage analysis can be made by dividing each year into a maximum of 12 periods, each with a different set of material properties. Each period can have a maximum of 12 load groups, either single or multiple. The damage caused by fatigue cracking and permanent deformation in each period over all load groups is summed up to evaluate the design life.

3.1.1 Elastic Multilayer System

Figure 3.1 shows an n-layer system in cylindrical coordinates, the nth layer being of infinite thickness. The modulus of elasticity and the Poisson ratio of the ith layer are E_i and v_i, respectively.

For axisymmetric problems in elasticity, a convenient method is to assume a stress function that satisfies the governing differential equation and the boundary and continuity conditions. After the stress function is found, the stresses and displacements can be determined (Timoshenko and Goodier, 1951).

The governing differential equation to be satisfied is a fourth-order differential equation, as described in Appendix B. The stress function for each layer has four constants

Downloaded From : www.EasyEngineering.net

Downloaded From : www.EasyEngineering.net

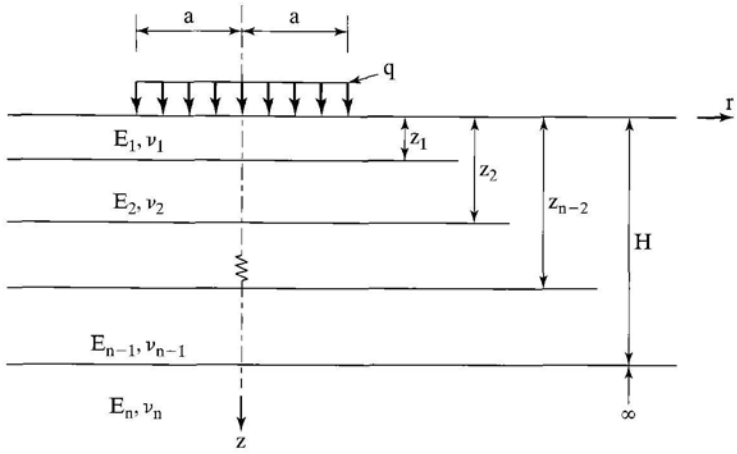


FIGURE 3.1

An n-layer system in cylindrical coordinates.

of integration, A_i, B_i, C_i, and D_i, where the subscript i is the layer number. Because the stress function must vanish at an infinite depth, the constants A_n and C_n should be equal to zero, i.e., the bottom most layer has only two constants. For an n-layer system, the total number of constants or unknowns is $4n - 2$, which must be evaluated by two boundary conditions and $4(n - 1)$ continuity conditions. The two boundary conditions are that the vertical stress under the circular loaded area be equal to q and that the surface be free of shear stress. The four conditions at each of the $n - 1$ interfaces are the continuity of vertical stress, of vertical displacement, of shear stress, and of radial displacement. If the interface is frictionless, the continuity of shear stress and radial displacement is replaced by the vanish of shear stress both above and below the interface. The equations to be used in KENLAYER for computing the stresses and displacement in a multilayer system under a circular loaded area are presented in Appendix B.

3.1.2 Superposition of Wheel Loads

Solutions for elastic multilayer systems under a single load can be extended to cases involving multiple loads by applying the superposition principle. Figure 3.2*a* shows the plan view of a set of dual-tandem wheels. The vertical stress and vertical displacement under point A due to the four loads can be easily obtained by adding those due to each of the loads, because they are all in the same vertical, or z, direction. However, the radial stress σ_r, the tangential stress σ_t, and the shear stress τ_{rz}, due to each load cannot be added directly, because they are not in the same direction, as is indicated by the four different radial directions at point A. Therefore, σ_r, σ_t, and τ_{rz} must be resolved into components in the x and y directions, as shown in Figure 3.2*b* for stresses at Point A due to load at point B. The use of point A is for illustrative purposes, and other points should also be tried in order to find the maximum stresses.

Downloaded From : www.EasyEngineering.net

Downloaded From : www.EasyEngineering.net

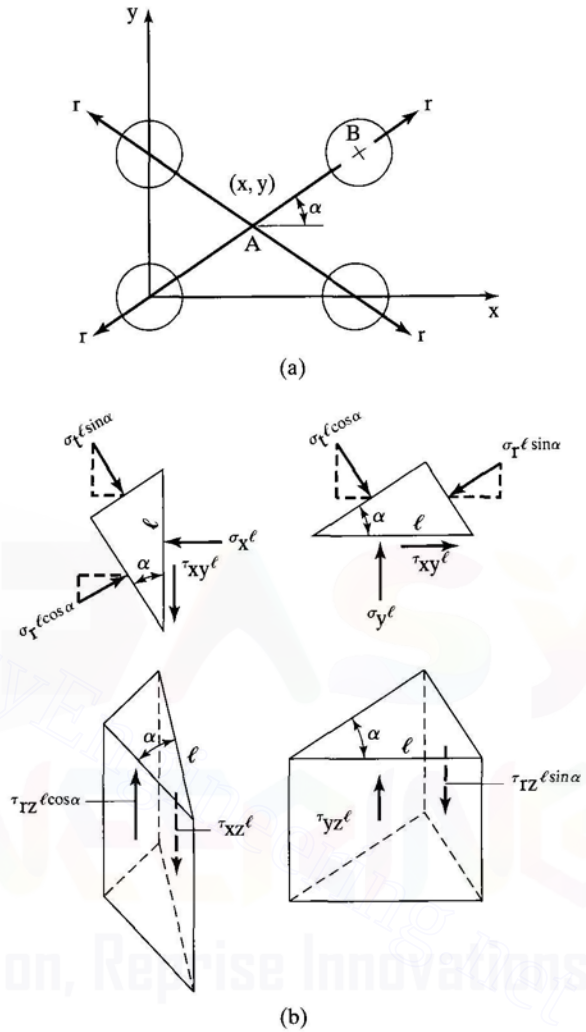


FIGURE 3.2
Superposition of stresses for multiple wheels.

Resolution of Stresses into *X* and *Y* Components By equating the forces in the x and y directions to zero, it can be easily proven from Figure 3.2*b* that

$$\sigma_x = \sigma_r \cos^2 \alpha + \sigma_t \sin^2 \alpha \tag{3.1a}$$

$$\sigma_y = \sigma_r \sin^2 \alpha + \sigma_t \cos^2 \alpha \tag{3.1b}$$

$$\tau_{xy} = (\sigma_r - \sigma_t) \sin \alpha \cos \alpha \tag{3.1c}$$

$$\tau_{yz} = \tau_{rz} \sin \alpha \tag{3.1d}$$

$$\tau_{xz} = \tau_{rz} \cos \alpha \tag{3.1e}$$

Downloaded From : www.EasyEngineering.net

Downloaded From : www.EasyEngineering.net

After resolving the stresses due to each load into σ_x, σ_y, τ_{xy}, τ_{yz}, and τ_{xz} components, those due to multiple loads can be obtained by superposition. During superposition, care should be taken in determining the proper sign of each stress.

Computation of Principal Stresses and Strains After σ_x, σ_y, σ_z, τ_{xy}, τ_{yz}, and τ_{xz} are obtained by superposition, the three principal stresses, σ_1, σ_2, and σ_3, can be determined by solving the following cubic equation:

$$\sigma^3 - (\sigma_x + \sigma_y + \sigma_z)\sigma^2 + (\sigma_x\sigma_y + \sigma_y\sigma_z + \sigma_x\sigma_z - \tau_{yz}^2 - \tau_{xz}^2 - \tau_{xy}^2)\sigma - (\sigma_x\sigma_y\sigma_z + 2\tau_{yz}\tau_{xz}\tau_{xy} - \sigma_x\tau_{yz}^2 - \sigma_y\tau_{xz}^2 - \sigma_z\tau_{xy}^2) = 0 \quad (3.2)$$

These principal stresses can be used for nonlinear analysis. The principal strains, ϵ_1, ϵ_2, and ϵ_3, are then determined from

$$\epsilon_1 = \frac{1}{E}[\sigma_1 - \nu(\sigma_2 + \sigma_3)] \quad (3.3a)$$

$$\epsilon_2 = \frac{1}{E}[\sigma_2 - \nu(\sigma_3 + \sigma_1)] \quad (3.3b)$$

$$\epsilon_3 = \frac{1}{E}[\sigma_3 - \nu(\sigma_1 + \sigma_2)] \quad (3.3c)$$

In the fatigue analysis, the horizontal minor principal strain, instead of the overall minor principal strain, is used. The strain is called minor because tensile strain is considered negative. Horizontal principal tensile strain is used because it is the strain that causes the crack to initiate at the bottom of asphalt layer. The horizontal principal tensile strain is determined from

$$\epsilon_t = \frac{\epsilon_x + \epsilon_y}{2} - \sqrt{\left(\frac{\epsilon_x - \epsilon_y}{2}\right)^2 + \gamma_{xy}^2} \quad (3.4)$$

in which ϵ_t is the horizontal principal tensile strain at the bottom of asphalt layer, ϵ_x is the strain in the x direction, ϵ_y is the strain in the y direction, γ_{xy} is the shear strain on the x plane in the y direction, and

$$\epsilon_x = \frac{1}{E}[\sigma_x - \nu(\sigma_y + \sigma_z)] \quad (3.5a)$$

$$\epsilon_y = \frac{1}{E}[(\sigma_y - \nu(\sigma_x + \sigma_z)] \quad (3.5b)$$

$$\gamma_{xy} = \frac{2(1 + \nu)}{E}\tau_{xy} \quad (3.5c)$$

3.1.3 Damage Analysis

Damage analysis is performed for both fatigue cracking and permanent deformation.

Downloaded From : www.EasyEngineering.net

Downloaded From : www.EasyEngineering.net

Failure Criteria The failure criterion for fatigue cracking is expressed as

$$N_f = f_1(\epsilon_t)^{-f_2}(E_1)^{-f_3} \tag{3.6}$$

in which N_f is the allowable number of load repetitions to prevent fatigue cracking; ϵ_t is the tensile strain at the bottom of asphalt layer; E_1 is the elastic modulus of asphalt layer; and f_1, f_2, and f_3 are constants determined from laboratory fatigue tests, with f_1 modified to correlate with field performance observations. The Asphalt Institute used 0.0796, 3.291, and 0.854 for f_1, f_2, and f_3, respectively, in their analytically based design procedure; the corresponding values used by Shell are 0.0685, 5.671, and 2.363 (Shook *et al.*, 1982). In view of the fact that the number of load repetitions required to progress from the onset of cracking to limiting failure conditions is fewer for thin asphalt layers than for thicker layers, Craus *et al.* (1984) suggested that f_1 in the Asphalt Institute criterion be reduced to 0.0636 for HMA layers less than 4 in. (102 mm) in thickness.

The failure criterion for permanent deformation is expressed as

$$N_d = f_4(\epsilon_c)^{-f_5} \tag{3.7}$$

in which N_d is the allowable number of load repetitions to limit permanent deformation, ϵ_c is the compressive strain on the top of subgrade, and f_4 and f_5 are constants determined from road tests or field performance. Values of f_4 and f_5 are suggested as 1.365×10^{-9} and 4.477 by the Asphalt Institute (AI, 1982), 6.15×10^{-7} and 4.0 by Shell (Claussen *et al.*, 1977), and 1.13×10^{-6} and 3.571 by the University of Nottingham (Brown *et al.*, 1977).

It should be noted that the use of compressive strain on the top of subgrade as a failure criterion is valid only when the permanent deformation is caused by the weak subgrade rather than by the overlying layers. In two test pavements on sand subgrade, one with a 6-in. (15-mm) gravel AC and the other with a 3-in. (8-mm) gravel AC, Groenendijk *et al.* (1997) found that all rutting could be ascribed to subgrade deformation with practically no shear deformation within the asphalt layer, and that the Shell permanent deformation criterion, originally based on a terminal serviceability index of 2.5, corresponded to a rut depth of 0.7 in. (18 mm).

Multiple Axles The large spacing between two axles causes the critical tensile and compressive strains under multiple axles to be only slightly different from those under a single axle. If the passage of each set of multiple axles is assumed to be one repetition, the damage caused by an 18-kip (80-kN) single axle is nearly the same as that caused by 36-kip (160-kN) tandem axles or 54-kip (240-kN) tridem axles. If one passage of tandem axles is assumed to be two repetitions and that of tridem axles to be three repetitions, the damage caused by 36-kip (160-kN) tandem and 54-kip (240-kN) tridem axles are two and three times greater than that by an 18-kip (80-kN) single axle. Both assumptions are apparently incorrect. The equivalent factors suggested by the Asphalt Institute are 1.38 for tandem axles and 1.66 for tridem axles, as indicated in Table 6.4.

The following procedure is used in KENLAYER to analyze damage due to tandem-axle loads. First, determine the tensile and compressive strains at three points under dual-tandem wheels, as shown in Figure 3.3*a*, and find out which point results in the maximum tensile strain and which point results in the maximum compressive strain. These maximum strains are then used with Eqs. 3.6 and 3.7 to determine the allowable number of load repetitions due to the first axle load.

Downloaded From : www.EasyEngineering.net

Downloaded From : www.EasyEngineering.net

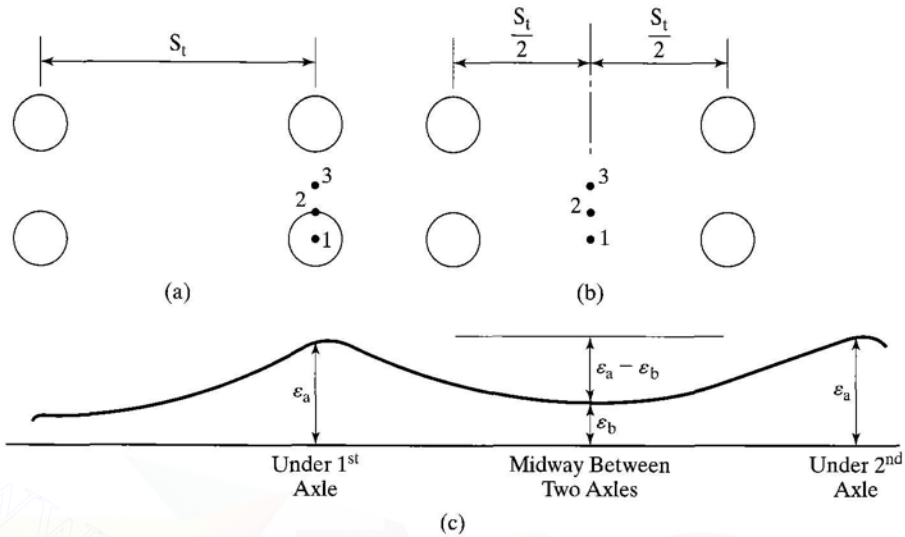


FIGURE 3.3

Damage analysis of tandem-axle loads.

Next, determine the tensile and compressive strains at the corresponding point that lies midway between the two axles, as shown in Figure 3.3*b*. The strain for damage analysis due to the second axle load is $\epsilon_a - \epsilon_b$, where ϵ_a is the strain due to the loading shown in Figure 3.3*a* and ϵ_b is the strain due to the loading shown in Figure 3.3*b*. This can be easily explained in Figure 3.3*c*, where the strain due to the second axle load is $\epsilon_a - \epsilon_b$. The same procedure was incorporated in VESYS (Jordahl and Rauhut, 1983), although VESYS can be applied only to a single tire and the point under the center of the load is used to determine the strains.

A similar but more approximate procedure is used for tridem axles. First, determine the maximum strain ϵ_a by comparing the strains at three points, as shown in Figure 3.4*a*. Then, determine the corresponding strain ϵ_b, as shown in Figure 3.4*b*. The strains to be used for the damage analysis of the three axle loads are ϵ_a, $\epsilon_a - \epsilon_b$, and $\epsilon_a - \epsilon_b$, respectively.

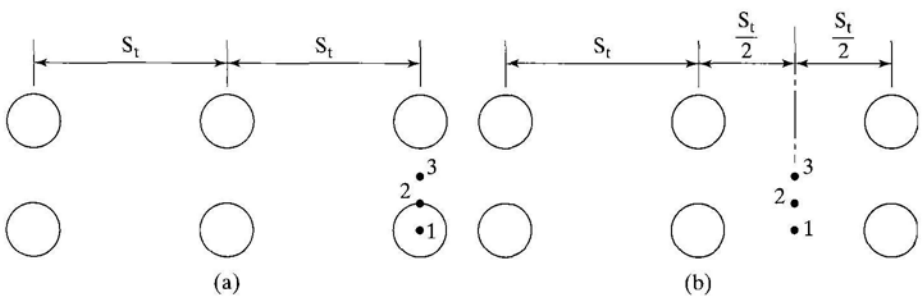


FIGURE 3.4

Damage analysis of tridem-axle loads.

Downloaded From : www.EasyEngineering.net

Downloaded From : www.EasyEngineering.net

3.1.4 Nonlinear Layers

It is well known that granular materials and subgrade soils are nonlinear with an elastic modulus varying with the level of stresses. The elastic modulus to be used with the layered systems is the resilient modulus obtained from repeated unconfined or triaxial compression tests. Details about resilient modulus are presented in Section 7.1. The resilient modulus of granular materials increases with the increase in stress intensity; that of fine-grained soils decreases with the increase in stress intensity. If the relationship between the resilient modulus and the state of stresses is given, a method of successive approximations can be used, as explained previously for the nonlinear homogeneous mass in Section 2.1.3. The nonlinear material properties, which have been incorporated in KENLAYER, are described below.

Granular Materials The resilient modulus of granular materials increases with the increase in the first stress invariant, as indicated by Eq. 2.11. However, KENLAYER employs a more popular relationship, which is described next.

Constitutive Relationship A simple relationship between resilient modulus and the first stress invariant can be expressed as

$$E = K_1 \theta^{K_2} \tag{3.8}$$

in which K_1 and K_2 are experimentally derived constants and θ is the stress invariant, which can be either the sum of three normal stresses, σ_x, σ_y, and σ_z, or the sum of three principal stresses, σ_1, σ_2, and σ_3:

$$\theta = \sigma_1 + \sigma_2 + \sigma_3 = \sigma_x + \sigma_y + \sigma_z \tag{3.9}$$

Including the weight of a layered system gives

$$\theta = \sigma_x + \sigma_y + \sigma_z + \gamma z(1 + 2K_0) \tag{3.10}$$

in which γ is the average unit weight, z is the distance below surface at which the modulus is to be determined, and K_0 is the coefficient of earth pressure at rest. The reason σ_1, σ_2, and σ_3 are not used in Eq. 3.10 is that they may not be in the same direction as the geostatic stresses. In contrast to other computer programs, KENLAYER uses the soil mechanics sign convention for stresses and strains. Therefore, θ is positive when in compression and negative when in tension.

Typical Values Summarizing a statistical analysis of published data, Rada and Witczak (1981) presented the mean and standard deviation of resilient modulus for several granular materials, as shown in Table 3.1. It was reported (Finn *et al.*, 1986) that the resilient moduli of base and subbase aggregates in the AASHO Road Test can be represented by Eq. 3.8 with K_2 equal to 0.6 and K_1 ranging from 3200 to 8000 psi, depending on the moisture contents. Other reported values of K_1 and K_2 are shown in Table 3.2.

Downloaded From : www.EasyEngineering.net

Downloaded From : www.EasyEngineering.net

TABLE 3.1 Nonlinear Constants K_1 and K_2 for Granular Materials

Material type	No. of data points	K_1 (psi) Mean	K_1 (psi) Standard deviation	K_2 Mean	K_2 Standard deviation
Silty sand	8	1620	78	0.62	0.13
Sand-gravel	37	4480	4300	0.53	0.17
Sand-aggregate blend	78	4350	2630	0.59	0.13
Crushed stone	115	7210	7490	0.45	0.23

Note. 1 psi = 6.9 kPa.
Source. After Rada and Witczak (1981).

TABLE 3.2 Ranges of K_1 and K_2 for Untreated Granular Materials

Reference	Material	K_1 (psi)	K_2
Hicks (1970)	Partially crushed gravel, crushed rock	1600–5000	0.57–0.73
Hicks and Finn (1970)	Untreated base at San Diego Test Road	2100–5400	0.61
Allen (1973)	Gravel, crushed stone	1800–8000	0.32–0.70
Kalcheff and Hicks (1973)	Crushed stone	4000–9000	0.46–0.64
Boyce et al. (1976)	Well-graded crushed limestone	8000	0.67
Monismith and Witczak (1980)	In service base and subbase materials	2900–7750	0.46–0.65

Note. 1 psi = 6.9 kPa.
Source. After Shook *et al.* (1982).

Fine-Grained Soils The resilient modulus of fine-grained soils decreases with the increase in deviator stress σ_d. In laboratory triaxial tests, $\sigma_2 = \sigma_3$, so the deviator stress is defined as

$$\sigma_d = \sigma_1 - \sigma_3 \tag{3.11}$$

In a layered system, σ_2 may not be equal to σ_3, so the average of σ_2 and σ_3 is considered as σ_3. Including the weight of layered system yields

$$\sigma_d = \sigma_1 - 0.5(\sigma_2 + \sigma_3) + \gamma z(1 - K_0) \tag{3.12}$$

Equation 3.12 is not theoretically correct because the principal loading stresses may not be in the same direction as the geostatic stresses. Because the loading stresses in the subgrade are usually small and do not have significant effect on the computed modulus, KENLAYER uses the three normal stresses, σ_x, σ_y, and σ_z, to replace the three principal stresses, σ_1, σ_2, and σ_3 in Eq. 3.12. If the point selected for computing the modulus is on the axis of symmetry for a single tire or on the plane of symmetry between two dual tires, the three normal stresses and the three principal stresses are identical.

Figure 3.5 shows the general relationship between resilient modulus and deviator stress of fine-grained soils obtained from laboratory repeated-load tests. The bilinear behavior can be expressed as

$$E = K_1 + K_3(K_2 - \sigma_d) \qquad \text{when } \sigma_d < K_2 \tag{3.13a}$$

$$E = K_1 - K_4(\sigma_d - K_2) \qquad \text{when } \sigma_d > K_2 \tag{3.13b}$$

in which K_1, K_2, K_3, and K_4 are material constants.

Downloaded From : www.EasyEngineering.net

Downloaded From : www.EasyEngineering.net

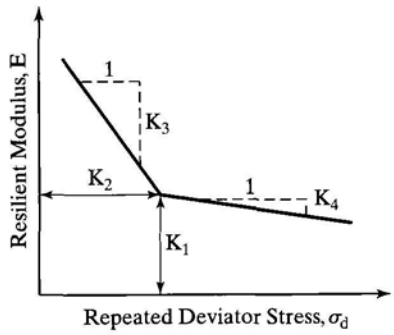


FIGURE 3.5

General relationship between resilient modulus and deviator stress for fine-grained soils.

Thompson and Elliott (1985) indicated that the value of resilient modulus at the breakpoint in the bilinear curve, as indicated by K_1 in Figure 3.5, is a good indicator of resilient behavior, while other constants, K_2, K_3, and K_4, display less variability and influence pavement response to a smaller degree than K_1. They classified fine-grained soils into four types, viz., very soft, soft, medium, and stiff, with the resilient-modulus–deviator-stress relationship shown in Figure 3.6. The maximum resilient modulus is governed by a deviator stress of 2 psi (13.8 kPa). The minimum resilient modulus is limited by the unconfined compressive strengths, which are assumed to be 6.21 psi (42.8 kPa), 12.90 psi (89.0 kPa), 22.85 psi (157 kPa), and 32.8 psi (226 kPa) for the four soils. Equation 3.13 has also been incorporated in KENLAYER. (Note that the K_1 and

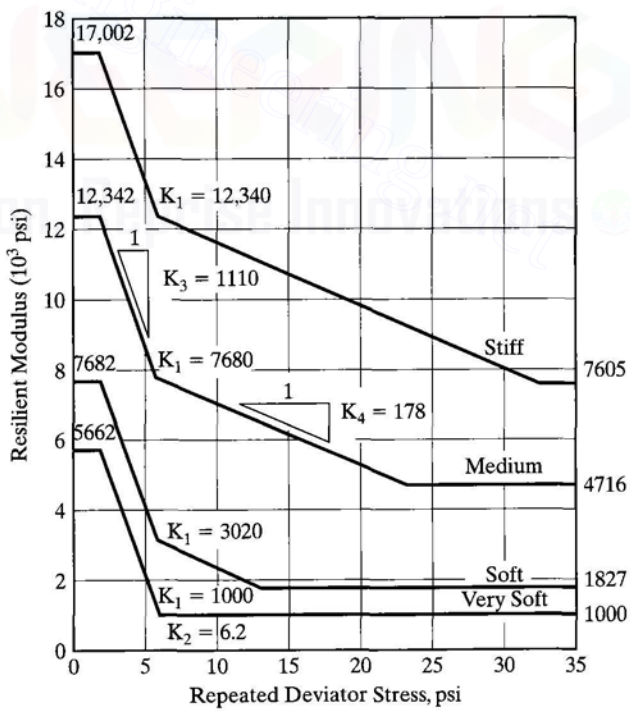


FIGURE 3.6

Resilient-modulus–deviator-stress relationship for four types of subgrade (1 psi = 6.9 kPa). (After Thompson and Elliott (1985).)

Downloaded From : www.EasyEngineering.net

Downloaded From : www.EasyEngineering.net

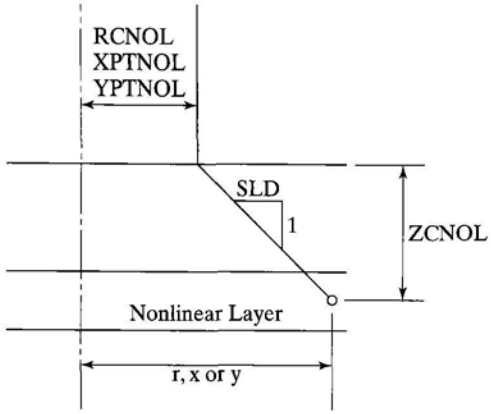


FIGURE 3.7
Loacation of stress point for nonlinear layer.

K_2 defined herein are different from those used by Thompson and Elliott, in that they are interchanged in meaning.)

Stress Point for Nonlinear Layer The elastic modulus of each nonlinear layer is determined from the stresses at a designated point according to Eq. 3.8 or 3.13. This point is called a stress point and is defined by a point on the pavement surface, by a slope of load distribution, SLD, and by a z coordinate, ZCNOL, as is shown in Figure 3.7.

The point on the surface can be located by the radial coordinate, RCNOL, for a single wheel or by the x and y coordinates, XCNOL and YCNOL, for multiple wheels. For a given ZCNOL, the r coordinate of the stress point is

$$r = \text{RCNOL} + (\text{SLD})(\text{ZCNOL}) \tag{3.14}$$

and the x and y coordinates of the stress point are

$$x = \text{XPTNOL} + (\text{SLD})(\text{ZCNOL}) \tag{3.15}$$

$$y = \text{YPTNOL} + (\text{SLD})(\text{ZCNOL}) \tag{3.16}$$

If only the maximum stresses, strains, or deflections are required, then the stress point should be located under the center of a single wheel with RCNOL = 0 and SLD = 0 or between the center of two duals with XPTNOL = 0, YPTNOL = YW/2, and SLD = 0. Note that YW is the center-to-center spacing between the duals, as shown in Figure 3.8. If the average responses, such as the deflection basin under a circular area, are required, then the use of RCNOL = a, where a is the radius of loaded area, and SLD = 0.5 is recommended. This is based on the general assumption that, starting from the edge of loaded area, the load is distributed downward at a slope of 0.5.

Stress Adjustment for Computing Modulus It is well known that most granular materials cannot take any tension. Unfortunately, when they are used as a base or subbase on a weaker subgrade, the horizontal stresses due to applied loads are most likely to be in tension. However, these materials can still take tension if the tension is smaller than the precompression caused by geostatic or other in situ stresses. The elastic modulus of granular materials depends not on the loading stress alone but on the combination of

Downloaded From : www.EasyEngineering.net

Downloaded From : www.EasyEngineering.net

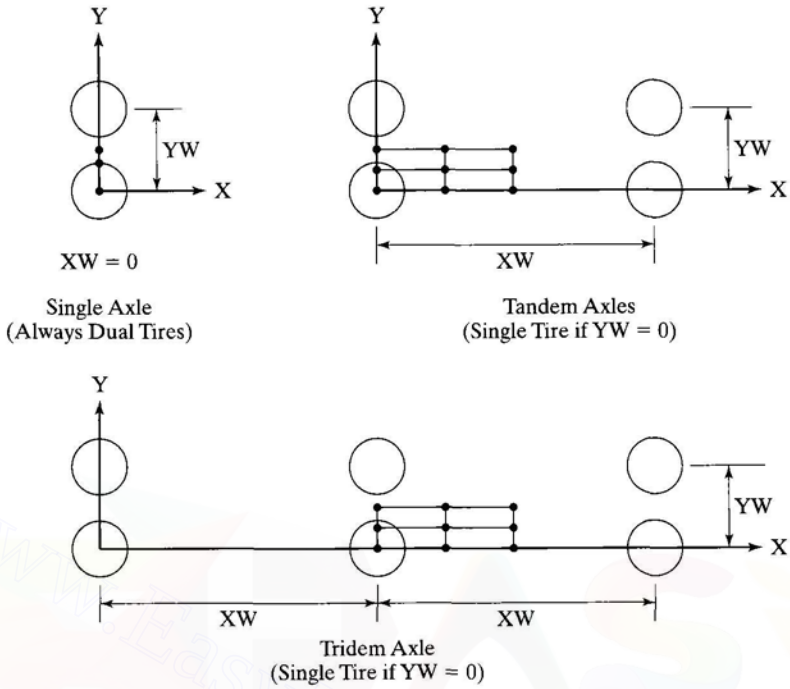


FIGURE 3.8

Plan view of multiple wheels.

the loading stress and the precompression. It is not possible that the combined horizontal stress will become negative, because, when it is reduced to 0, the particles separate and no stress will exist. A review of the results computed by KENLAYER reveals that the combined horizontal stresses at most of the stress points in granular layers are negative. This might indicate that the usual practice of using K_o from 0.5 to 1 (based on the active earth pressure theory) to compute the geostatic stress is too conservative and that a much larger K_o (based on the passive earth pressure) might have to be used. Using experiments conducted with a layer of sand on a soft clay, Selig *et al.* (1986) indicated that the development of horizontal residual stresses under repeated loads is the key to the stability of the two-layer system. Because the actual precompression varies a great deal and is difficult to determine, it is reasonable to adjust the combined stresses so that the actual stress will not exceed the strength of the material. This adjustment applies only to the determination of the modulus of granular materials, and no actual changes in the state of stresses due to loading are attempted.

Three methods have been incorporated into KENLAYER for nonlinear analysis. The first two methods were described in the first edition; the third method is a new addition based on Mohr–Coulomb theory. The method to be used depends on the value of input parameter PHI, ϕ. If PHI is assigned 0, method 1 is used; if PHI is a large value representing the minimum modulus of the granular material, method 2 is implied; if PHI is the angle of internal friction of the granular material (with a value between 0 and 90), method 3 is indicated.

Downloaded From : www.EasyEngineering.net

Downloaded From : www.EasyEngineering.net

Method 1 In method 1, the nonlinear granular layer is subdivided into a number of layers, and the stresses at the mid-depth of each layer are used to determine the modulus. If the horizontal stress, including the geostatic stress, is negative or in tension, it is set to 0. This stress modification is necessary to avoid negative θ. With the two horizontal stresses equal to 0, the elastic modulus is dependent on the vertical stress only, with no contributions from the horizontal stresses. The vertical stress at a stress point near to the load is always positive, so the modulus will also be positive, and no minimum modulus need be specified.

Method 2 In method 2, the granular layer is considered as a single layer, and an appropriate stress point, usually between the upper quarter and upper third of the layer, is selected to compute the modulus. Because the stress point is near to the load at the upper part of the layer, there is no chance that the stress invariant, θ, will become negative, so no stress modification is needed. In other words, the negative horizontal stresses are used to compute θ. To avoid the use of an unreasonably low modulus, a minimum modulus, indicated by the value of PHI, must be specified. If the computed modulus is smaller than PHI, PHI will be used as the modulus of the layer. It is suggested that K1 of the granular material be used as PHI, so that the computed modulus will never be smaller than K1; this relationship is always true, unless θ is smaller than 1 psi (6.9 kPa).

Method 3 In method 3, the granular layer is considered as a single layer with the stress point at the midheight of the layer. The negative or small horizontal stresses are modified according to the Mohr–Coulomb theory of failure so that the strength of the materials will not be exceeded. This method was originally proposed by Raad and Figueroa (1980) and was later incorporated in the ILLI-PAVE and MICH-PAVE computer programs. The case to be considered in KENLAYER is much simpler than that in those finite-element programs, because the stress points are located under or very near to the load; therefore, the vertical stress can be considered as the major principal stress and the horizontal stress as the minor principal stress. Because the horizontal stresses at the stress point in the subgrade are always positive and satisfy the Mohr–Coulomb failure criterion, no adjustments for fine-grained soils are needed. To adjust the horizontal stress in granular materials, it is assumed that the material has an angle of internal friction, ϕ, with the failure envelope shown in Figure 3.9. When failure occurs, the Mohr's circle based on the

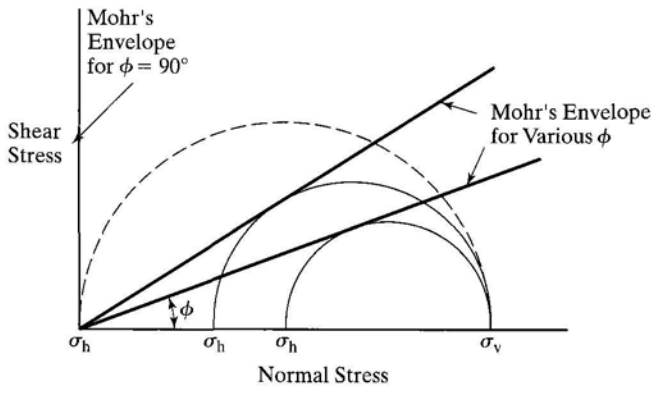


FIGURE 3.9
Adjustment of horizontal stress at stress point.

Downloaded From : www.EasyEngineering.net

Downloaded From : www.EasyEngineering.net

major and minor principal stresses must be tangent to the failure envelope. It can easily be proven by geometry that

$$\sigma_h = \sigma_v \tan^2\left(45° - \frac{\phi}{2}\right) \tag{3.17}$$

in which σ_h is the combined horizontal stress, σ_v is the combined vertical stress, and ϕ is the angle of internal friction. No circle should cut and lie outside the envelope, so no horizontal stress should be smaller than the σ_h computed by Eq. 3.17.

It can be seen, from Figure 3.9 or Eq. 3.17, that, for a given σ_v, the actual σ_h to be used for computing the elastic modulus depends solely on the value of ϕ. When ϕ is assigned 0, $\sigma_h = \sigma_v$; when ϕ is assigned 90°, as indicated in the figure by the dashed circle, $\sigma_h = 0$. By simply varying ϕ, the adjusted σ_h can be given any value between 0 and σ_v. It is suggested that a PHI value of 40 be used for a weak subgrade with a modulus less than 10,000 psi (69 MPa) and that a larger PHI, say, up to 60, be used for a stiff subgrade.

The case of $\phi = 90°$ is the same as method 1, with the implication that $\sigma_h = 0$. Instead of using an awkward PHI value (90) to indicate method 1, the value 0 may be used for simplicity. When PHI is inputted as 0, KENLAYER will automatically change it to 90°, substitute it into Eq. 3.17, and thus produce a zero σ_h. As presented in Section 3.3.2, if the granular base is divided into several layers, the use of PHI = 0, or method 1, checks most closely with the more accurate finite-element solutions by MICH-PAVE; by contrast, if the base is considered a single layer, either method 2 or 3 can be used.

3.2 PROGRAM DESCRIPTION

KENLAYER, together with input program LAYERINP and graphic program LGRAPH, is part of a computer package called KENPAVE. In its present dimensions, it can be applied to a maximum of 19 layers with output at 10 different radial coordinates and 19 different vertical coordinates, or a total of 190 points. For multiple wheels, in addition to the 19 vertical coordinates, solutions can be obtained at a total of 25 points by specifying the x and y coordinates of each point. Creep compliances can be specified at a maximum of 15 time durations. Damage analysis can be made by dividing each year into a maximum of 12 periods, each with a maximum of 12 load groups.

To facilitate entering and editing data, a program named LAYERINP can be used. The program uses menus and data entry forms to create and edit the data file. Although the large number of input parameters appears overwhelming, default values are provided to many of them, so only a limited number of inputs will be required. More about LAYERINP is presented in Appendix C.

3.2.1 General Features

The capabilities of KENLAYER can be demonstrated by the following four input parameters, which must be specified at the very outset:

MATL = 1 for linear elastic, 2 for nonlinear elastic, 3 for linear viscoelastic, and 4 for combination of nonlinear elastic and linear viscoelastic.

Downloaded From : www.EasyEngineering.net

Downloaded From : www.EasyEngineering.net

NDAMA = 0 for no damage analysis, 1 for damage analysis with summary printout, and 2 for damage analysis with detailed printout.

NPY = number of periods per year.

NLG = number of load groups.

Materials Unless indicated otherwise, all layers are assumed to be linear elastic with a constant elastic modulus. For the linear elastic case, solutions for multiple wheels are obtained by superposition of those due to single wheels.

For the nonlinear elastic case, the elastic moduli of some layers are stress dependent, and these layers must be identified. An iterative procedure is used, in which the moduli of nonlinear layers are adjusted as the stresses vary, while the moduli of linear layers remain the same. During each iteration, a constant set of moduli is computed from the stresses obtained from the previous iteration, so the problem is considered linear and the superposition principle can still be applied to multiple wheels. After the stresses due to single or multiple wheels are determined, the elastic moduli of nonlinear layers are recalculated, and a new set of stresses is determined. The process is repeated until the moduli converge to a specified tolerance.

For the linear viscoelastic case, the viscoelastic layers must be identified and their creep compliances specified, while the other layers are linear elastic. Solutions due to either moving or stationary loads can be obtained. Moving loads require the input of creep compliances at 11 times from 0.001 to 100 sec, so that a Dirichlet series can be obtained by collocation, which, in combination with a haversine function, can be used to compute the stresses and strains, as indicated by Eq. 2.55. If stationary loads are specified and there is no conversion of temperature, no Dirichlet series are needed, so any number of times can be specified; KENLAYER will simply take the reciprocal of creep compliances as the elastic moduli to determine the elastic solution at each specified time. However, if pavement temperature is different from that used for the creep test, KENLAYER will use the specified creep times as the retardation times to collocate the creep compliances at these times. The number of equations is equal to the number of unknowns, so Eq. 2.38 can be used directly to determine the coefficients of the Dirichlet series.

For a case that is a combination of nonlinear elastic and linear viscoelastic, some layers are nonlinear elastic, some are viscoelastic, and the remaining, if any, are linear elastic. If only one layer is viscoelastic, the stresses in every layer will be time dependent. The stresses to be used for determining the modulus of nonlinear layer are the peak stresses at $t = 0$ under a moving load, as shown in Figure 2.40, or the stresses at the last time duration under a stationary load.

Damage Analysis Damage analysis is based on the horizontal tensile strain at the bottom of specified layers, usually the HMA or layer 1, and on the vertical compressive strain on the top of specified layers, usually the subgrade or the lowest layer. Instead of reading in the z coordinates, simply specifying the total number of layers for bottom tension (NLBT), the total number of layers for top compression (NLTC), the layer number for bottom tension (LNBT), and the layer number for top compression (LNTC), the program will determine the z coordinates of all necessary points and compute the required

Downloaded From : www.EasyEngineering.net

Downloaded From : www.EasyEngineering.net

strains. If several radial coordinate points are specified under a single wheel or several x and y coordinate points under multiple wheels, the program will compare the strains at these points and select the most critical ones for damage analysis.

Each year can be divided into a maximum of 12 periods. The elastic modulus, nonlinear coefficient K_1, and creep compliance can differ from period to period. The predicted number of load repetitions for each load group is specified for each period. The allowable number of load repetitions for fatigue cracking is determined by Eq. 3.6 and that for permanent deformation by Eq. 3.7. The elastic modulus of the viscoelastic layer to be used in Eq. 3.6 is computed from the three principal stresses and the minor principal strain (minor because tension is negative) by

$$E = \frac{\sigma_3 - \nu(\sigma_1 + \sigma_2)}{\epsilon_3} \tag{3.18a}$$

The same E is obtained if the major principal strain is used:

$$E = \frac{\sigma_1 - \nu(\sigma_2 + \sigma_3)}{\epsilon_1} \tag{3.18b}$$

The damage ratio, which is the ratio between the predicted and allowable number of repetitions, is computed for each load group in each period and summed over the year by

$$D_r = \sum_{i=1}^{p} \sum_{j=1}^{m} \frac{n_{i,j}}{N_{i,j}} \tag{3.19}$$

in which D_r is the damage ratio at the end of a year, $n_{i,j}$ is the predicted number of load repetitions for load j in period i, $N_{i,j}$ is the allowable number of load repetitions based on Eqs. 3.6 and 3.7, p is the number of periods in each year, and m is the number of load groups. The design life, which is equal to $1/D_r$, is evaluated both for fatigue cracking and for permanent deformation, and the one with a shorter life controls the design.

Number of Periods Per Year The number of periods per year (NPY) is used mainly for damage analysis. Each year can be considered as one period with the same material properties throughout the year or divided into four seasons or 12 months, each with a different set of material properties. If no damage analysis is to be made, or NDAMA = 0, NPY is usually specified as 1. However, NPY can be more than 1 even if no damage analysis is required. In this case, NPY should be interpreted as the number of material properties, so several different sets of material properties can be run one after the other.

Some of the material properties that do not change over the periods are entered first. The properties that vary with each period will then be read in. To avoid the input of creep compliances for each period, the creep compliances are specified at a reference temperature and fitted with a Dirichlet series, as shown by Eq. 2.38. The creep compliances at any other temperature are obtained by the time–temperature superposition principle, as indicated by Eqs. 2.46 and 2.48. If creep compliances are used directly with no temperature conversions needed, an arbitrary reference temperature the same as the actual temperature can be specified, or a zero-temperature shift coefficient, BETA, can be used.

Downloaded From : www.EasyEngineering.net

Downloaded From : www.EasyEngineering.net

Loads Whether a load has a single wheel or multiple wheels is identified by the parameter LOAD, with 0 for single wheel, 1 for single axle with dual tires, 2 for tandem axles, and 3 for tridem axles. The two dual tires must be oriented in the y direction with dual spacing YW. If YW is specified as 0, the tandem- or tridem-axle loads are applied on a single tire; otherwise, they are applied on dual tires.

For a single-wheel load, NR radial distances and NZ vertical distances must be specified, so solutions at NR $\times$ NZ points can be obtained. For example, if a point is located by the coordinates (r, z) and it is desired to obtain solutions at two points, (0, 0) and (10, 10), then two radial coordinates of 0 and 10 and two vertical coordinates of 0 and 10 must be specified, and solutions at (0, 0), (0, 10), (10, 0), and (10, 10) will be obtained, even though the ones at (0, 10) and (10, 0) are not needed. The extra time required for these unnecessary points is small, because KENLAYER computes all points at the same time and a large part of the program is the same no matter how many radial and vertical coordinates are used. To save the computer time for numerical integration, each point is checked for convergence. If the results at any given point have converged to the desired tolerance, no more integration will be performed at that point.

For multiple wheels, instead of radial distances, the x and y coordinates of each point must be specified. Figure 3.8 shows a plan view of multiple wheels. It is required to use the center of the left and lowest wheel as the origin for x and y coordinates. The dual wheels must be oriented along the y axis. The spacing YW must be specified for dual tires and XW for multiple axles. The (x, y) coordinates of all points at which solutions are to be sought are also needed. In Figure 3.8, three points are specified for dual wheels and nine points for tandem and tridem axles. Based on these coordinates, the radial distances from each point to each of the multiple wheels are determined, and the solutions due to all single-wheel loads are computed at the same time. These solutions are then superimposed to obtain those caused by multiple wheels.

3.3 COMPARISON WITH AVAILABLE SOLUTIONS

KENLAYER can be applied to a homogeneous half-space by assuming that all layers have the same elastic modulus and Poisson ratio. As indicated in Section 2.1, the solutions obtained by KENLAYER checked very closely with the Boussinesq solutions for a homogeneous half-space. In this section, the solutions obtained by KENLAYER are compared with ELSYM5 for multiple wheels, MICH-PAVE for nonlinear layers, VESYS for moving loads, and DAMA for damage analysis.

3.3.1 Multiple Wheels

The computation of principal stresses under multiple wheels is complex and requires the resolution of stresses into x and y components before superposition, as described in Section 3.1.2. To be sure that the solutions are correct, a comparison of solutions was made between KENLAYER and ELSYM5 (Kopperman *et al.*, 1986). ELSYM5 is a linear elastic layer system composed of a maximum up to five layers. The pavement may be loaded with one or more identical uniform circular loads normal to the surface. The program superimposes the various loads and computes the stresses, strains, and displacements in three dimensions, along with the three principal stresses and strains, at locations specified by the user.

Downloaded From : www.EasyEngineering.net

Downloaded From : www.EasyEngineering.net

An elastic three-layer system, with the thicknesses, elastic moduli, and Poisson ratios shown in Figure 3.10*a*, is subjected to six-wheel loads, as shown in Figure 3.10*b*. Each loaded area has a radius of 4 in. (102 mm) and a contact pressure of 100 psi (690 kPa). The vertical displacements at each layer interface, the principal tensile strains at the bottom of the asphalt layer and the vertical compressive strains on the top of the subgrade under the four points shown in Figure 3.10*b*, were determined by both KENLAYER and ELSYM5 and are tabulated in Table 3.3. Also shown in Table 3.3 are the three principal stresses used to determine the strains. Values without parentheses were obtained by KENLAYER; those within parentheses were obtained by ELSYM5. It can be seen that the two solutions check quite closely, with a maximum discrepancy not over 2%.

It should be noted that any computer solutions based on Burmister's layered theory are not exact and involve the numerical integration of an infinite series. Because the accuracy of the solutions depends on the interval and tolerance specified for the integration, the solutions obtained from the two programs are not expected to be exactly the same.

3.3.2 Nonlinear Layers

The extension of linear elastic layered systems to include nonlinear, or stress-sensitive, materials is certainly an improvement of practical significance. However, the use of the stresses at a single point in each nonlinear layer to compute the modulus of the layer is not theoretically correct. As the stresses vary with the radial distance from the load, the modulus should also change with the radial distance and is not uniform throughout the layer. Theoretically, this problem could be solved more accurately by the finite-element method, such as the ILLI-PAVE program developed at the University of Illinois (Raad and Figueroa, 1980) and the MICH-PAVE program developed at the Michigan State University (Harichandran *et al.*, 1989). If only the most critical tensile strain at the bottom of the asphalt layer and the most critical compressive strain on the top of the subgrade are required, it should be possible to select a point in each nonlinear layer to compute the modulus so that these critical strains obtained from KENLAYER can match reasonably well with those from the finite-element programs, as will be demonstrated later.

IIII-PAVE Model The ILLI-PAVE computer program considers the pavement as an axisymmetric solid of revolution and divides it into a number of finite elements, each as

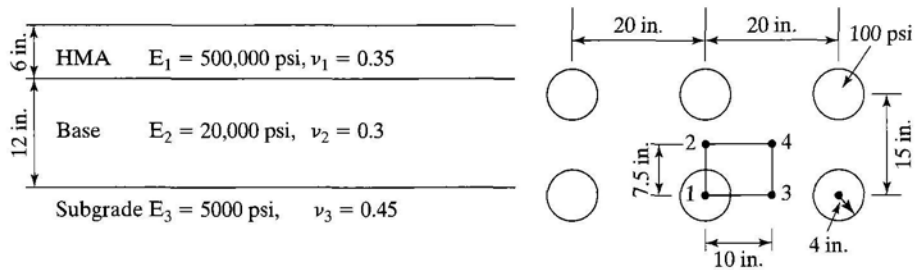


FIGURE 3.10

A layer system under six circular loaded areas (1 in. = 25.4 mm, 1 psi = 6.9 kPa).

Downloaded From : www.EasyEngineering.net

Downloaded From : www.EasyEngineering.net

TABLE 3.3 Comparison of Results Between KENLAYER and ELSYM5

Point	Vertical coordinate	Vertical deflection (10^{-3} in.)	Strain (10^{-6})		Principal stress (psi)		
			Vertical	Horizontal	Major	Intermediate	Minor
1	6.00	70.50	244.3	−241.4	13.9	−143.3	−166.0
		(70.67)	(243.3)	(−240.7)	(13.9)	(−142.7)	(−165.4)
	18.01	63.83	962.7	−502.7	6.1	1.4	0.9
		(64.06)	(949.3)	(−496.4)	(6.1)	(1.5)	(0.9)
2	6.00	72.20	175.0	−157.3	11.8	−104.9	−111.2
		(72.08)	(175.2)	(−157.5)	(11.8)	(−105.0)	(−111.4)
	18.01	65.45	1038.0	−515.8	6.3	1.6	1.0
		(65.32)	(1039.0)	(−516.7)	(6.3)	(1.5)	(1.0)
3	6.00	67.81	119.5	−184.4	9.2	−41.6	−103.5
		(67.79)	(119.6)	(−184.5)	(9.2)	(−41.6)	(−103.6)
	18.01	62.19	906.8	−482.7	5.9	1.4	0.9
		(62.17)	(907.8)	(−483.2)	(5.9)	(1.4)	(0.9)
4	6.00	69.76	125.3	−173.7	9.6	−50.5	−101.2
		(69.77)	(125.3)	(−173.6)	(9.6)	(−50.6)	(−101.2)
	18.01	63.75	979.3	−496.0	6.1	1.5	0.9
		(63.75)	(979.8)	(−496.2)	(6.1)	(1.5)	(0.9)

Note. Values without parentheses are obtained by KENLAYER, those within parentheses by ELSYM5. Compression is positive, tension negative. 1 in. = 25.4 mm, 1 psi = 6.9 kPa.

a section of concentric rings. Incorporated in ILLI-PAVE are the stress-dependent resilient modulus and the failure criteria for granular materials and fine-grained soils. The principal stresses in the granular and subgrade layers are modified at the end of each iteration, so that they do not exceed the strength of the materials, as defined by the Mohr–Coulomb theory of failure (Raad and Figueroa, 1980).

Stress Modification The procedure for stress modification incorporated into ILLI-PAVE and MICH-PAVE can best be illustrated by a granular material with cohesion 0 and angle of internal friction ϕ. The Mohr–Coulomb failure criterion can be written as

$$s = \sigma \tan \phi \tag{3.20}$$

in which s is the shear strength, or the shear stress at the time of failure, σ is the normal stress, and ϕ is the angle of internal friction. Under a vertical loading stress σ_z and a vertical geostatic stress γz, the total vertical stress σ_v is

$$\sigma_v = \sigma_z + \gamma z \tag{3.21}$$

The minimum and maximum allowable principal stresses $(\sigma_3)_{\min}$ and $(\sigma_1)_{\max}$ can be determined from the Mohr's circles, as shown by circles A and B in Figure 3.11 and expressed as

$$(\sigma_3)_{\min} = \sigma_v \tan^2\left(45° - \frac{\phi}{2}\right) \tag{3.22}$$

$$(\sigma_1)_{\max} = \sigma_v \tan^2\left(45° + \frac{\phi}{2}\right) \tag{3.23}$$

Downloaded From : www.EasyEngineering.net

Downloaded From : www.EasyEngineering.net

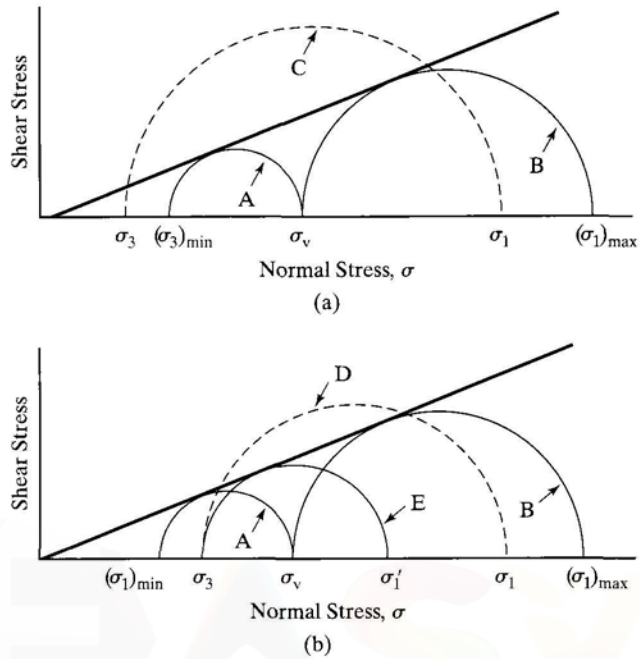


FIGURE 3.11

Stress modification to satisfy Mohr–Coulomb failure criterion.

If the computed minor principal stress σ_3, including the horizontal geostatic stress, is smaller than $(\sigma_3)_{min}$, as shown by circle C in Figure 3.10*a*, it must be increased to $(\sigma_3)_{min}$, so that circle C is reduced to circle A with $\sigma_3 = (\sigma_3)_{min}$ and $\sigma_1 = \sigma_v$. If the minor principal stress σ_3 is greater than $(\sigma_3)_{min}$, as shown by circle D in Figure 3.10*b*, the maximum allowable major principal stress can be determined by circle E and expressed as

$$\sigma_1' = \sigma_3 \tan^2\left(45° + \frac{\phi}{2}\right) \tag{3.24}$$

If σ_1 is greater than σ_1', it must be reduced to σ_1', so circle D is reduced to circle E. If the computed σ_1 is smaller than σ_1', then the computed σ_1 should be used.

ILLI-PAVE Algorithms In view of the fact that the computational techniques of ILLI-PAVE are too costly, complex, and cumbersome to be used for routine design, Thompson and Elliott (1985) developed simple regression equations or algorithms for predicting the responses of typical flexible pavements. The resilient modulus of the crushed stone base is represented by Eq. 3.8 with $K_1 = 9000$ psi (62 MPa) and $K_2 = 0.33$. The relationship between resilient modulus and deviator stress for four different subgrade soils is shown by Eq. 3.13 and Figure 3.6. Because parameters K_2, K_3, and K_4 are the same for all soils, the only soil property represented in the regression equation is K_1, which is the resilient modulus at the breakpoint. To apply the Mohr–Coulomb failure criteria, the crushed-stone base is assumed to be cohesionless and have a friction angle of 40°, while the stiff, medium, soft, and very soft subgrade soils have a zero

Downloaded From : www.EasyEngineering.net

Downloaded From : www.EasyEngineering.net

TABLE 3.4 Some Material Properties for Developing ILLI-PAVE Algorithms

Property	Hot mix asphalt			Crushed stone base	Sungrade soils			
	40°F	70°F	100°F		Stiff	Medium	Soft	Very soft
Unit weight (pcf)	145.0	145.0	145.0	135.0	125.0	120.0	115.0	110.0
Coefficient of earth pressure at rest	0.37	0.67	0.85	0.60	0.82	0.82	0.82	0.82
Poisson ratio	0.27	0.40	0.46	0.38	0.45	0.45	0.45	0.45
Modulus (10^3 psi)	1400	500	100	$9000\theta^{0.33}$	See Figure 3.6			

Note. 1 psi = 6.9 kPa, 1 pcf = 157.1 N/m^3.
Source. After Thompson and Elliott (1985).

friction angle and cohesions of 16.4, 11.425, 6.45, and 3.105 psi (113, 78.8, 44.5, and 21.4 kPa), respectively, each equal to one-half of its unconfined compressive strength. Other material properties are shown in Table 3.4.

The regression equations were based on a 9000-lb (40.1-kN) circular load having a contact pressure of 80 psi (552 kPa), which represents one dual wheel of the standard 18,000-lb (81-kN) single-axle load. A total of 168 pavement configurations were solved by ILLI-PAVE, with thicknesses ranging from 1.5 to 8 in. (38 to 203 mm) for HMA and from 4 to 24 in. (102 to 610 mm) for the granular base. The factors included in the analysis as independent variables are the thickness and modulus of HMA, the thickness of granular base, and the subgrade K_1. The predicted responses include radial strain at the bottom of HMA, vertical strain on the top of subgrade, subgrade deviator stress, surface deflection, and subgrade deflection. Only algorithms for the HMA tensile strain ϵ_t and the subgrade compressive strain ϵ_c are presented below.

$$\log \epsilon_t = 2.9496 + 0.1289h_1 - \frac{0.5195}{h_1} \log h_2 - 0.0807h_1 \log E_1 - 0.0408 \log K_1 \tag{3.25}$$

$$\log \epsilon_c = 4.5040 - 0.0738h_1 - 0.0334h_2 - 0.3267 \log E_1 - 0.0231K_1 \tag{3.26}$$

in which ϵ_t and ϵ_c are in microinch per inch, or 10^{-6}, h_1 is the HMA thickness in inches, h_2 is the base thickness in inches, E_1 is the HMA modulus in ksi, and K_1 is the breakpoint resilient modulus of subgrade in ksi.

Example 3.1:

A three-layer system has an HMA surface with $h_1 = 5$ in. (127 mm) and $E_1 = 500{,}000$ psi (3.5 GPa); a granular base with $h_2 = 12$ in. (305 mm) and $K_1 = 9000$ psi (62 MPa); and a soft subgrade with $K_1 = 3020$ psi (21 MPa). Determine the tensile strains at the bottom of asphalt layer and the compressive strain on the top of subgrade with the ILLI-PAVE algorithm.

Solution: From Eq. 3.25, $\log \varepsilon_t = 2.9496 + 0.1289 \times 5 - (0.5195/5) \log 12 - 0.0807 \times 5 \times \log 500 - 0.0408 \log 3.02 = 2.373$, or $\varepsilon_t = 236 \times 10^{-6}$. From Eq. 3.26, $\log \varepsilon_c = 4.5040 - 0.0738 \times 5 - 0.0334 \times 12 - 0.3267 \times \log 500 - 0.0231 \times 3.02 = 2.783$, or $\varepsilon_c = 606 \times 10^{-6}$.

Downloaded From : www.EasyEngineering.net

Downloaded From : www.EasyEngineering.net

It should be noted that the solutions given by the ILLI-PAVE algorithm are only approximate, because of the inaccuracy in the DOS version of ILLI-PAVE. Solutions of Example 3.1 by the new Windows version of MICH-PAVE, which is considered much more accurate, result in tensile strain calculated as 279×10^{-6} and compressive strain calculated as 665×10^{-6}.

MICH-PAVE Model The MICH-PAVE computer program is very similar to ILLI-PAVE and uses the same methods to characterize granular materials and fine-grained soils and the same Mohr–Coulomb failure criteria to adjust the state of stresses. A major improvement is the use of a flexible boundary at a limited depth beneath the surface of subgrade, instead of a rigid boundary at a large depth below the surface. The subgrade below the flexible boundary is considered as a homogeneous half-space, whose stiffness matrix can be determined and superimposed to the stiffness matrix of the pavement above the flexible boundary to form the overall stiffness matrix. This procedure is quite similar to the case of slabs on solid foundation, as described in Section 5.1.1. The use of a flexible boundary greatly reduces the number of finite elements required, especially those oblong elements at the bottom. Consequently, the storage requirement is significantly reduced and the program can be implemented on personal computers. The fewer number of simultaneous equations to be solved and the elimination of those oblong elements also yield more accurate results.

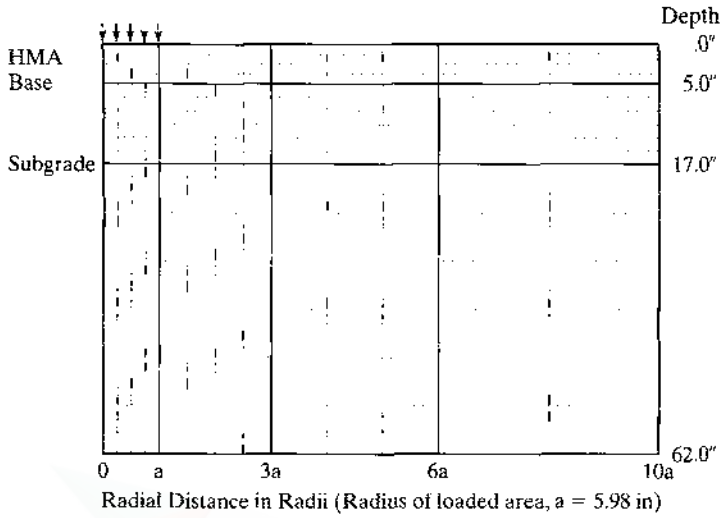
In the first edition, a comparison of solutions based on linear elastic materials was made among ILLI-PAVE, MICH-PAVE, and KENLAYER. It was found that the tensile strains at the bottom of HMA obtained by the two finite-element programs differed somewhat from those obtained by KENLAYER when the HMA was less than 2.5 in. (63 mm) thick and that the compressive strains on the top of the subgrade obtained by the finite-element programs were about 20 percent smaller than those obtained by KENLAYER. The reason for this error was the use of insufficient elements in these DOS programs. The Windows-based Michigan Flexible Pavement Design System (MFPDS) developed recently by Harichandran *et al.* (2001) increases by several times the number of elements; its results check closely with those from KENLAYER.

To show the difference in the finite-element mesh used for the three-layer system in Example 3.1, the computer plot obtained from the old DOS MICH-PAVE is compared with that from the new Windows MICH-PAVE, as shown in Figure 3.12. It can be seen that only 208 elements were used in DOS, because of storage limitations, but 1768 elements were used in Windows.

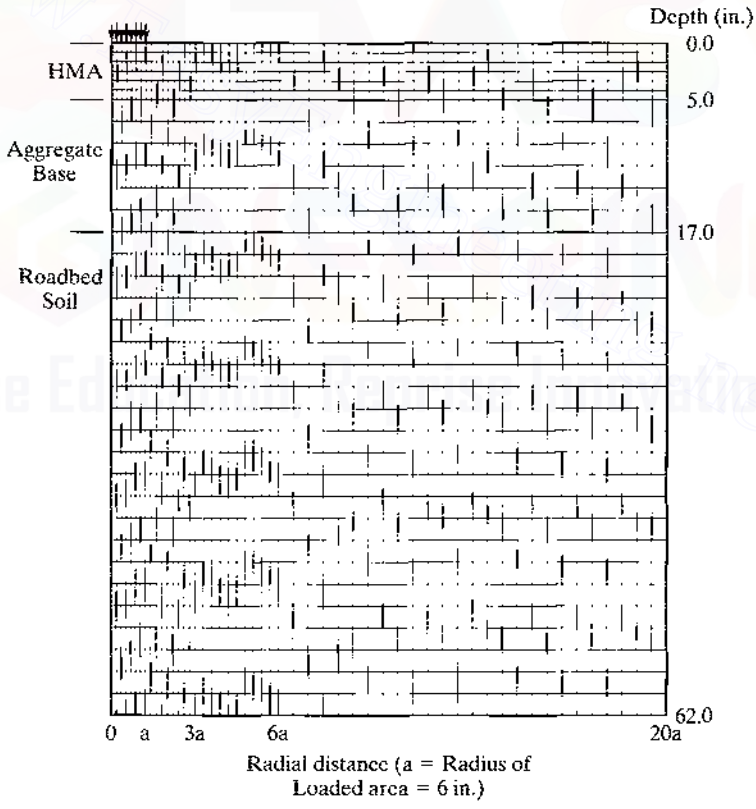
Linear Analysis Figure 3.13 shows the cross section of a three-layer system subjected to a circular load with a contact radius of 6 in. (152 mm) and a contact pressure of 80 psi (552 kPa). All three layers are linear elastic. Layer 1, which ranges in thickness from 1 to 10 in. (25 to 254 mm), has an elastic modulus of 500,000 psi (3.5 GPa) and a Poisson's ratio of 0.4. Layer 2 has a thickness of 12 in. (305 mm), an elastic modulus of 20,000 psi (138 MPa), and a Poisson's ratio of 0.38. Layer 3 has an elastic modulus of 8000 psi (55 MPa) and a Poisson's ratio of 0.45. The tensile strains, ε_t, at the bottom of layer 1 and the compressive strains, ε_c, at the top of layer 3 for various thicknesses of layer 1 are obtained by both MICH-PAVE and KENLAYER and presented in Figure 3.14.

Downloaded From : www.EasyEngineering.net

Downloaded From : www.EasyEngineering.net



(a) DOS Version



(b) Windows Version

FIGURE 3.12

Finite-element mesh used by MICH-PAVE (1 in. = 25.4 mm).

Downloaded From : www.EasyEngineering.net

Downloaded From : www.EasyEngineering.net

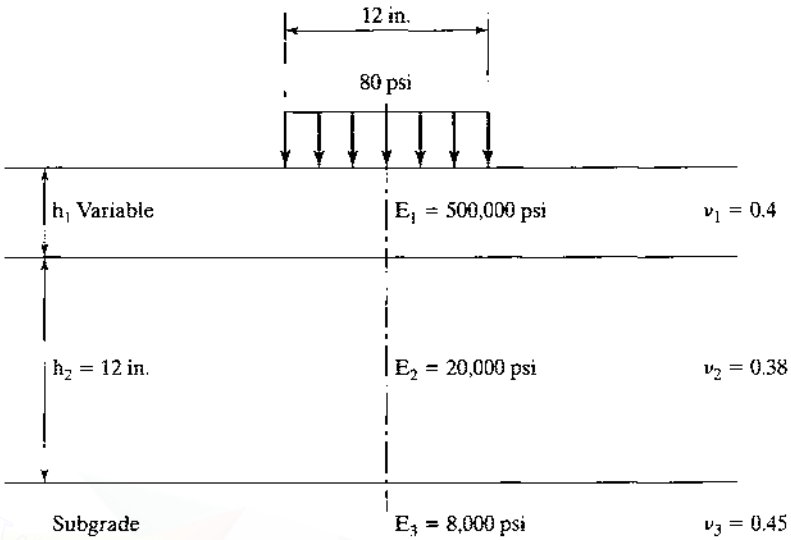


FIGURE 3.13

Cross-section of a three-layer system (1 in. = 25.4 mm, 1 psi = 6.9 kPa).

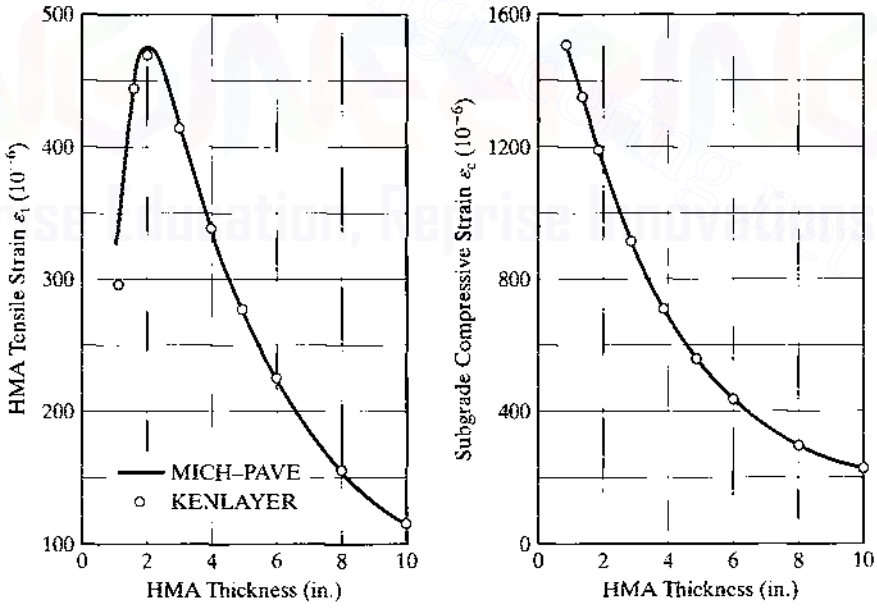


FIGURE 3.14

Comparison of linear solutions between MICH-PAVE and KENLAYER (1 in. = 25.4 mm).

Downloaded From : www.EasyEngineering.net

Downloaded From : www.EasyEngineering.net

A cursory inspection of the figure might suggest that the two programs correspond very well. However, a closer review reveals considerable differences in the HMA tensile strains when the HMA has a thickness of less than 2 in. (51 mm). Take the extreme case of 1-in. (25-mm) HMA, for example; the tensile strain obtained by both KENLAYER and ELSYM5 is 294 $\times$ 10^{-6}, but that from MICH-PAVE is 335 $\times$ 10^{-6}, a difference of 14 percent. The differences are reduced to 5 percent for the 1.5-in. (38-mm) HMA and only 2 percent for the 2-in. (51-mm) HMA. In MICH-PAVE, the HMA is divided into six layers of finite elements. In order to satisfy the required aspect ratio of not more than 4:1, the thinner the HMA is, the more oblong are the elements and the greater is the number of elements (and thus the less accurate are the results).

Nonlinear Analysis The same pavement section shown in Figure 3.13 for linear analysis was used for nonlinear analyses by considering layer 1 to be linear with the same elastic modulus and Poisson ratio used in the linear analysis, layer 2 to be a nonlinear granular base with K_1 = 9000 psi (62 MPa) and K_2 = 0.33, and layer 3 to be a nonlinear soft subgrade with K_1 = 3020 psi (20.8 MPa). Because MICH-PAVE assumes a bilinear relationship between resilient modulus and deviator stress for fine-grained soils, similar to Figure 3.6, but with no maximum and minimum limits, a very large EMAX and a zero EMIN were used in KENLAYER. Other properties are the same as those in Table 3.4 for developing the ILLI-PAVE algorithms.

In applying KENLAYER, the 12-in. (305-mm) granular layer can be divided into six layers, each 2 in. (51 mm) thick, as shown in Figure 3.15, or considered as a single

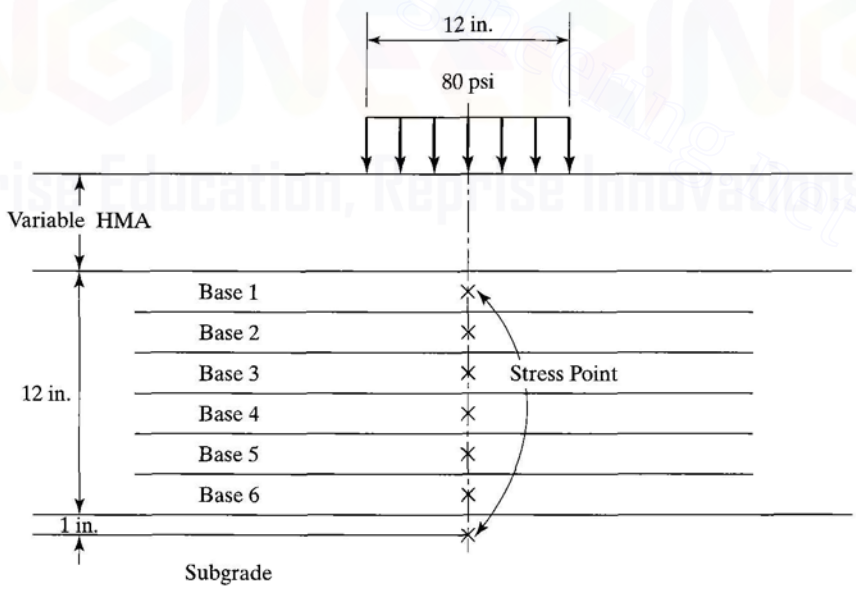


FIGURE 3.15

Division of granular base into six nonlinear layers (1 in. = 25.4 mm, 1 psi = 6.9 kPa).

Downloaded From : www.EasyEngineering.net

Downloaded From : www.EasyEngineering.net

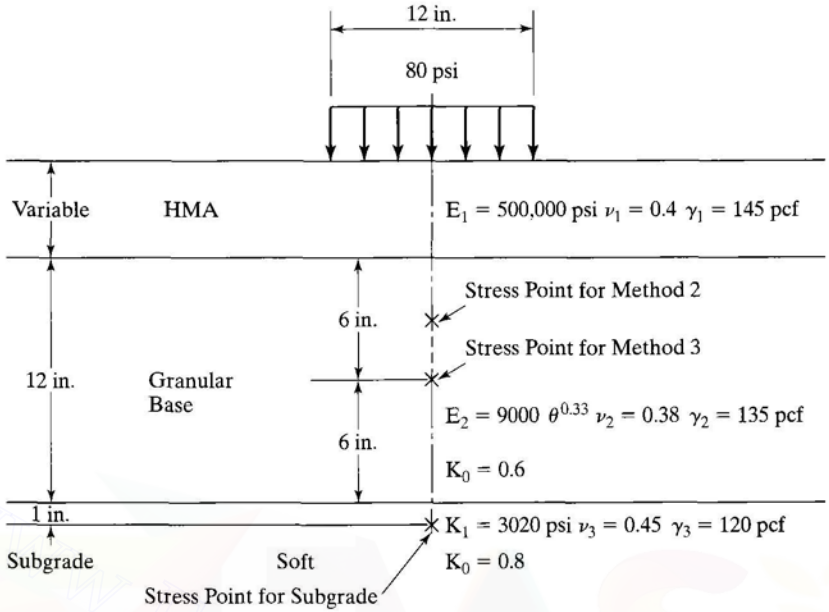


FIGURE 3.16

Consideration of granular base as a single nonlinear layer (1 in. = 25.4 mm, 1 psi = 6.9 kPa).

12-in. (305-mm) layer, as shown in Figure 3.16. The following six cases were considered and compared with MICH-PAVE:

1. The granular base is divided into 2-in. layers with the stress points at the midheight of each layer and PHI = 0. This case assumes zero horizontal stresses when the granular material is in tension and is designated as method 1 in Section 3.1.4.
2. This case is the same as case 1, except that PHI is assigned 40 instead of 0. A friction angle of 40° is typical for granular base and was used to develop ILLI-PAVE algorithms and also to run MICH-PAVE. The use of the Mohr–Coulomb failure criterion with $\phi = 40°$ results in a much larger horizontal stress and thus a greater modulus, compared with method 1.
3. The granular base is considered to be a single 12-in. (305-mm) layer with the stress point at the upper quarter of the layer. There is no adjustment of horizontal stresses, as described for method 2 in Section 3.1.4.
4. This case is the same as case 3, except that the stress point is located at the upper third, instead of at the upper quarter.
5. The granular base is considered to be a single 12-in. (305-mm) layer, with the stress point at the midheight of the layer and PHI = 0.
6. This case, designated as method 3 in Section 3.1.4, is the same as case 5 except that PHI is assigned 40 instead of 0.

Downloaded From : www.EasyEngineering.net

Downloaded From : www.EasyEngineering.net

A comparison of results between MICH-PAVE and the six cases of KENLAYER for various thicknesses of HMA is presented in Figure 3.17, where the results from MICH-PAVE are shown by the smooth curve, those from KENLAYER by the individual symbols. If several symbols are so close together that they cannot be individually plotted, some are shifted sidewise, so their actual location should be moved horizontally to the thickness indicated. When the HMA is 5 in. (127 mm) or more in thickness, all six symbols are very close together and check well with the curve from MICH-PAVE, so only case 1 is plotted.

As can be seen from Figure 3.17, when the HMA is less than 5 in. (127 mm) thick, some discrepancies exist among the various cases with some above and some below the curve. The scattering is much more pronounced in HMA tensile strains than in subgrade compressive strains. It appears that the use of six layers and PHI = 0, or method 1, checks most closely with MICH-PAVE in both strains, so method 1 is recommended for use in nonlinear analysis. Except for HMA thickness of 1.5 in. (38 mm), the strains obtained by method 2 with the stress point at the upper quarter lie below the curve produced by MICH-PAVE, and those with the stress point at the upper third lie above, so method 2 can also yield satisfactory results when a proper stress point is selected. The use of method 3 with one single layer and a PHI of 40° gives the best fit in

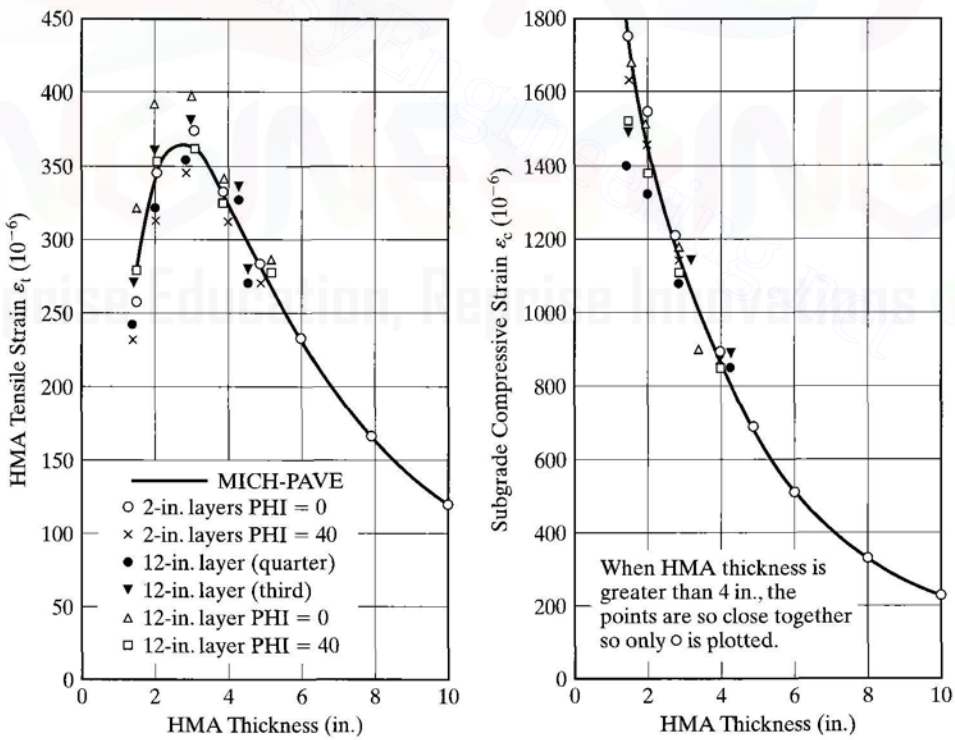


FIGURE 3.17

Comparison of nonlinear solutions between MICH-PAVE and KENLAYER (1 in. = 25.4 mm).

Downloaded From : www.EasyEngineering.net

Downloaded From : www.EasyEngineering.net

HMA tensile strains, but the match in the subgrade compressive strains is poor when the asphalt layer is thin. The problem with a single layer is its failure to represent the actual case of decreasing modulus with depth, so the use of a single layer with the same modulus throughout the layer just cannot reproduce the same responses in both tensile and compressive strains as those obtained by multiple layers or MICH-PAVE.

Deflection Basins All previous comparisons between MICH-PAVE and KENLAYER are based on the critical strains at some given points under the axis of symmetry. Another important usage of the KENLAYER program is to backcalculate the modulus of various layers, so that the deflection basin obtained by the program can match with field measurements. It will be interesting to compare deflection basins between MICH-PAVE and KENLAYER for nonlinear analysis.

The pavement used for comparison is the same as that used for nonlinear analysis. Only the case of 1.5-in. HMA is considered, because the effects of base and subgrade on surface deflections are more pronounced when the pavement is thin. To simulate the Dynatest FWD test system described by Chua and Lytton (1985), the contact pressure under the 12-in. (305-mm) loading plate is increased to 100 psi (690 kPa), and deflections are computed at seven locations: 0, 7.9, 11.8, 23.6, 47.2, 70.9, and 94.5 in. (0, 0.2, 0.3, 0.6, 1.2, 1.8, and 2.4 m) from the center of load. Figure 3.18 shows the cross section of the pavement for analysis.

As indicated previously, the stress points for computing the maximum strains are located on the axis of symmetry—at RCNOL = 0 and SLD = 0. However, for analyzing deflection basins, average layer moduli based on RCNOL = 6 in. (152 mm) and SLD = 0.5 are recommended. The stress point for the subgrade is assumed at a depth of 24 in. (0.61 m) below the top of subgrade, instead of at 1 in. (25 mm), for computing maximum strains. To avoid crowdedness, only four of the six cases, as described in the nonlinear analysis, were investigated and compared with MICH-PAVE. It was found that the use of a stress point at 24 in. (0.61 m) below the top of the subgrade results in an average subgrade modulus of 8011 psi (55.2 MPa), but the use of one at 1 in. (25 mm) results in 5870 psi (40.5 MPa). The deflection at point 7, which is the farthest point from the load, is inversely proportional to the modulus of the subgrade, independent of all the overlying layers, so the use of a stress point 1 in. (25 mm) from the top of the subgrade results in too large a deflection at point 7 when compared with MICH-PAVE.

Figure 3.19 is a comparison between MICH-PAVE and the four cases of KENLAYER. It can be seen that all four cases check well with MICH-PAVE, but the case using 6 layers and PHI = 0 still gives the best fit. The discrepancies in deflections among the various cases are not as pronounced as those in the strains. When the point is far from the load, all four cases yield about the same deflections, so only the circles are shown in the figure.

3.3.3 Moving Loads

The use of KENLAYER for the analysis of viscoelastic layered systems under a moving load involves several steps. First, the creep compliances of HMA at several time durations are specified at a reference temperature. The compliances are then fitted with a Dirichlet series, and the time–temperature superposition principle is applied to obtain

Downloaded From : www.EasyEngineering.net

Downloaded From : www.EasyEngineering.net

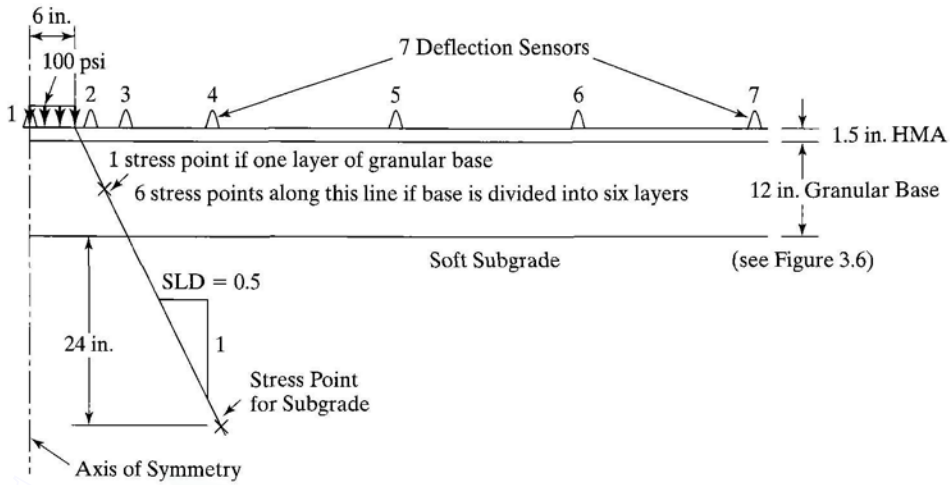


FIGURE 3.18

Cross section used for comparing deflection basins (1 in. = 25.4 mm, 1 psi = 6.9 kPa, 1 pcf = 157.1 N/m^3).

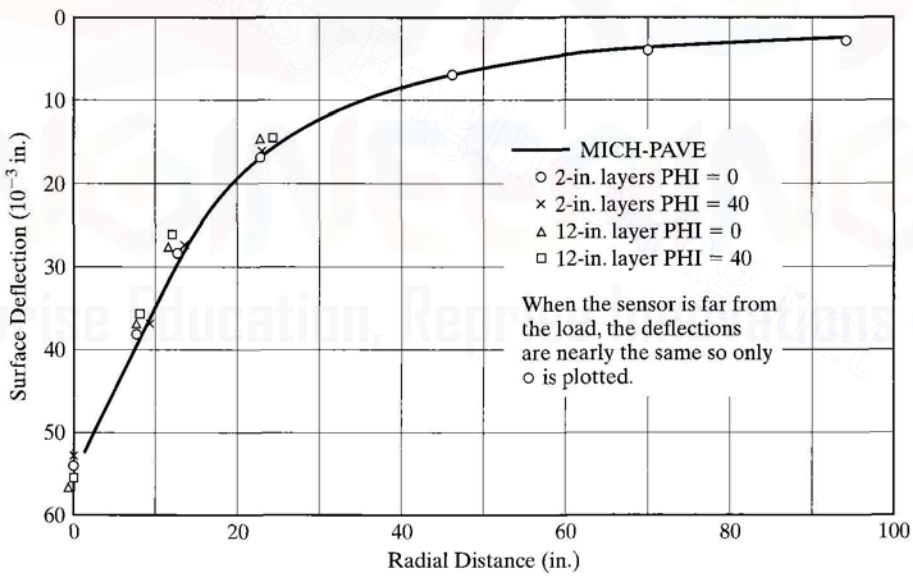


FIGURE 3.19

Comparison of deflection basin between MICH-PAVE and KENLAYER (1 in. = 25.4 mm).

the compliances at any given temperature and time. Next, the viscoelastic responses under a static load are determined and expressed again as a Dirichlet series, and Boltzmann's superposition principle is then applied to obtain the responses under a moving load. Because these procedures are complex and repeatedly invoke the approximate

Downloaded From : www.EasyEngineering.net

Downloaded From : www.EasyEngineering.net

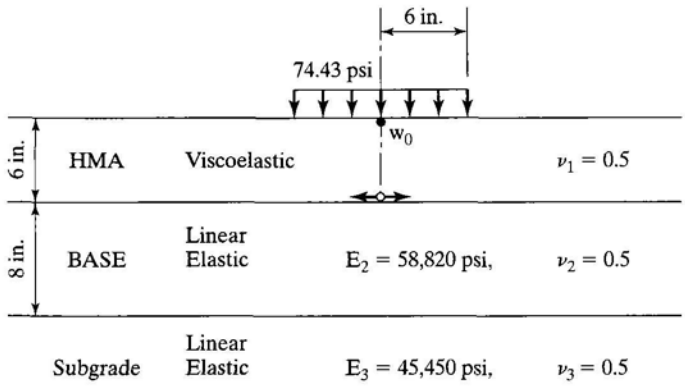


FIGURE 3.20

A viscoelastic three layer system under a moving load (1 in. = 25.4 mm, 1 psi = 6.9 kPa).

method of collocation, it is desirable to check the entire process from the input of creep compliances at a reference temperature to the output of responses under moving loads at various pavement temperatures. This can be accomplished by comparing the solutions between KENLAYER and VESYS.

Figure 3.20 shows a viscoelastic three-layer system subjected to a moving load of duration 0.1 s. The load is applied over a circular area with radius 6 in. (152 mm) and contact pressure 74.43 psi (514 kPa). The HMA layer is considered viscoelastic, with its creep compliances specified for 11 time durations at reference temperature 70°F (21°C). The base and the subgrade are considered linear elastic, with their moduli shown in the figure.

The system shown in Figure 3.20 was employed by Kenis (1977) to illustrate the application of VESYS. Each year was divided into 12 months, and the maximum deflections on the pavement surface and the radial tensile strains at the bottom of the asphalt layer at 12 different temperatures were presented and are tabulated in Table 3.5. Also shown in Table 3.5 are the solutions obtained by KENLAYER. It can be seen that some solutions by VESYS are nearly the same as those by KENLAYER, while others are somewhat different. However, the discrepancies are not more than 5%. In view of the approximate nature of the procedures employed by both programs, these discrepancies are expected and should be considered acceptable.

3.3.4 Damage Analysis

The DAMA computer program developed by the Asphalt Institute also employs the damage concept to determine the design life. It is interesting to compare the results obtained from DAMA with those from KENLAYER.

Chen et al. (1995) made an assessment of five computer programs (*viz.*, ILLI-PAVE, MICH-PAVE, ABAQUS, DAMA, and KENLAYER) and concluded that DAMA was probably the most appropriate among the five for routine structural analysis of flexible pavements. Note that both DAMA and KENLAYER are based on the Burmister layer theory and should yield nearly the same results for linear analysis. However, Chen et al. showed that DAMA and KENLAYER matched very well on surface displacements and tensile strains at the bottom of the asphalt layer, but that the

Downloaded From : www.EasyEngineering.net

Downloaded From : www.EasyEngineering.net

TABLE 3.5 Comparison of VESYS and KENLAYER

Pavement temperature (°F)	Deflection (10^{-3} in.)		Radial strain (10^{-6})	
	VESYS	KENLAYER	VESYS	KENLAYER
49.7	3.884	3.764	38.86	36.89
53.3	3.922	3.816	39.97	38.20
59.5	4.152	4.152	46.82	46.69
68.6	5.526	5.615	90.16	90.89
75.2	6.827	7.160	141.9	147.8
81.6	8.232	8.753	201.0	210.5
84.6	8.861	9.335	226.5	237.9
84.7	8.882	9.359	227.3	238.7
78.9	7.658	8.081	177.2	184.8
70.1	5.824	5.950	100.8	102.2
59.1	4.126	4.116	46.01	45.73
52.3	3.908	3.795	39.55	37.70

Note. Radial strains are in tension but negative signs are not shown. 1 in. = 25.4 mm.

compressive strains at the top of the subgrade obtained by KENLAYER were unrealistically small. This discrepancy was caused by their misuse of KENLAYER. They forgot to add 0.0001 or a small amount to the depth of interface, so the compressive strains on the top of the subgrade that they reported were actually those for the bottom of the granular base. They also compared the vertical stress on the surface and showed that only DAMA and MICH-PAVE gave a vertical stress exactly equal to the contact pressure; all the other programs were way off the mark. It should be noted that the vertical stress on the surface of pavement within a loaded area should theoretically be equal to the tire contact pressure. However, this can be achieved even approximately only after numerous cycles of numerical integration. Now, this stress is already known, and it is not used as a criterion for pavement design, so it is not worthwhile to spend the extra computer time just for the purpose of showing that the stress is nearly equal to the contact pressure. For numerical methods, it is not possible to obtain a vertical stress exactly equal to the contact pressure. It is believed that DAMA and MICH-PAVE did not get the vertical stress numerically, but simply assigned the contact pressure to it. To avoid confusion, KENLAYER was changed by setting the vertical pressure inside the loaded area exactly equal to the contact pressure and assigning zero to that outside the loaded area.

DAMA Model The DAMA computer program can be used to analyze a multilayer elastic pavement structure by cumulative-damage techniques for a single- or dual-wheel system. Any pavement structure comprised of hot-mix asphalt, emulsified asphalt mixtures, untreated granular materials, and subgrade soils can be analyzed, provided that the maximum number of layers does not exceed five. Environmental effects are characterized by input variables: mean monthly temperatures and variable monthly material modulus.

Pavement Temperature The air-temperature data are used to account for the effect of temperature on moduli of asphalt mixtures. The relationship between mean

Downloaded From : www.EasyEngineering.net

Downloaded From : www.EasyEngineering.net

pavement temperature M_p and mean monthly air temperature M_a varies with the depth below pavement surface in accordance with the formula

$$M_p = M_a\left(1 + \frac{1}{z+4}\right) - \frac{34}{z+4} + 6 \tag{3.27}$$

in which z is the depth below surface in inches. The temperature at the upper third point of each layer is used as the weighted-average pavement temperature.

The capability to account for monthly variations in the properties of base, subbase, and subgrade allows one to assess the effects of freeze–thaw or variable moisture conditions on pavement life. For pavements using emulsified asphalt stabilized materials, the effect of modulus change over any specified cure time is also considered in the damage analysis.

Nonlinear Analysis In DAMA, the subgrade and all asphalt-stabilized layers are considered to be linear elastic, the untreated granular base nonlinear elastic. The consideration of subgrade as linear elastic is a reasonable approximation because the variation of modulus due to the change of subgrade stresses is usually quite small and a reasonable subgrade modulus can be assumed. Instead of using the more accurate method of iterations and Eq. 3.8 to determine the modulus of granular layer, the following predictive equation based on multiple regression is used to account for stress dependency (Smith and Witczak, 1981):

$$E_2 = 10.447 h_1^{-0.471} h_2^{-0.041} E_1^{-0.139} E_3^{0.287} K_1^{0.868} \tag{3.28}$$

In this equation, E_1, E_2, and E_3 are the modulus of asphalt layer, granular base, and subgrade, respectively; h_1 and h_2 are the thickness of the asphalt layer and granular base, respectively; and K_1 is the nonlinear constant in Eq. 3.8 with the exponent K_2 equal to 0.5.

Equation 3.28 was developed from pavement structures composed of only three layers under an 18,000-lb (80-kN) single-axle load. When two different asphalt-stabilized layers with thicknesses h_{1a} and h_{1b} and moduli E_{1a} and E_{1b} are present above the aggregate layer, the equivalent modulus E_1 of the combined asphalt layer (with thickness $h_{1a} + h_{1b}$) is determined by

$$E_1 = \left[\frac{h_{1a}(E_{1a})^{1/3} + h_{1b}(E_{1b})^{1/3}}{h_{1a} + h_{1b}}\right]^3 \tag{3.29}$$

Example 3.2:

For the four-layer system shown in Figure 3.21, with moduli of 966,000 psi (6.7 GPa) for the surface course, 1,025,000 psi (7.1 GPa) for the binder course, and 12,000 psi (8.3 MPa) for the subgrade, determine the modulus of the granular layer by Eq. 3.28 for a K_1 of 8000 psi (55 MPa).

Downloaded From : www.EasyEngineering.net

Downloaded From : www.EasyEngineering.net

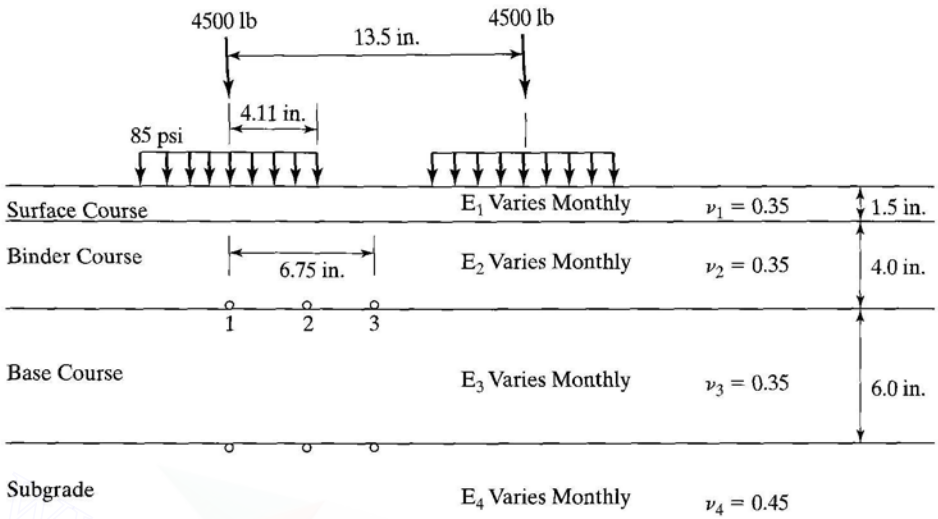


FIGURE 3.21

A four-layer linear system for damage analysis (1 in. = 25.4 mm, 1 psi = 6.9 kPa, 1 lb = 4.45 N).

Solution: In Eq. 3.28, E_1 is the equivalent modulus for the surface and binder courses combined and can be determined from Eq. 3.29: $E_1 = \{[1.5 \times \sqrt[3]{966{,}000} + 4.0 \times \sqrt[3]{1{,}025{,}000}]/(1.5 + 4.0)\}^3 = 1{,}009{,}000$ psi (7.0 GPa). From Eq. 3.28 with $h_1 = 1.5 + 4.0 = 5.5$ in. (140 mm), the modulus of the granular base $= 10.447 \times (5.5)^{-0.471} \times (6)^{-0.041} \times (1{,}009{,}000)^{-0.139} \times (12{,}000)^{0.287} \times (8000)^{0.868} = 23{,}040$ psi (159 MPa).

Comparison of Strains by Linear Analysis Figure 3.21 shows a four-layer linear system subjected to a 9000-lb (40-kN) dual-wheel load exerting a contact pressure of 85 psi (587 kPa). Using the Asphalt Institute's failure criteria, as shown in Eqs. 3.6 and 3.7 with $f_1 = 0.0796$, $f_2 = 3.291$, $f_3 = 0.854$, $f_4 = 1.365 \times 10^{-9}$, and $f_5 = 4.477$, a damage analysis was made by both DAMA and KENLAYER, and the results were compared.

Table 3.6 shows a comparison of tensile strains at the bottom of the HMA binder course and the compressive strains on the top of subgrade between DAMA and KENLAYER. It can be seen that the two solutions correspond very well.

Comments on Table 3.6

1. The monthly air temperature is used to determine the HMA modulus, which is described in Section 7.2.3. These are the temperatures in South Carolina and were applied by the Asphalt Institute to develop design charts.
2. The granular base is assumed nonlinear. The nonlinear constants K_1 vary throughout the year and are used to determine the modulus of the granular base. The value of K_1 is 8000 in normal months, but can increase to 400% in the winter and decrease to 25% during the spring breakup. After these values are entered,

Downloaded From : www.EasyEngineering.net

TABLE 3.6 Comparison of Strains Determined by DAMA and KENLAYER

Month	Air temperature (°F)	Granular base K_1	Modulus (psi)				Tensile strain (10^{-6})		Compressive strain (10^{-6})	
			HMA surface	HMA binder	Granular base	Sub-grade	DAMA	KENLAYER	DAMA	KENLAYER
Jan	45	8000	1,436,929	1,478,458	21,870	12,000	106.1	106.2	286.2	285.6
Feb	38	16,000	1,875,179	1,891,803	50,610	31,000	67.2	67.2	152.8	153.0
Mar	43	24,000	1,561,968	1,598,808	84,539	50,000	61.9	61.9	123.9	124.2
Apr	45	2000	1,436,929	1,478,458	5670	7200	128.9	129.7	308.8	307.2
May	56	3500	878,127	937,209	10,277	8400	171.1	171.1	410.1	409.4
Jun	70	5000	415,886	473,105	16,042	9600	250.7	250.6	553.0	553.8
Jul	78	6500	254,835	302,849	22,206	10,800	295.8	295.8	613.3	613.5
Aug	81	8000	209,688	253,517	28,111	12,000	292.9	293.2	599.4	599.5
Sep	78	8000	254,835	302,849	27,408	12,000	271.3	271.5	568.2	568.3
Oct	73	8000	347,698	402,234	26,322	12,000	236.5	236.6	516.2	516.9
Nov	58	8000	798,268	857,035	23,630	12,000	152.7	152.7	377.0	377.1
Dec	54	8000	965,976	1,024,883	23,039	12,000	136.2	136.2	346.0	345.9

Note. Negative signs for tensile strains not shown. 1 psi = 6.9 kPa.

Downloaded From : www.EasyEngineering.net
Downloaded From : www.EasyEngineering.net

Downloaded From : www.EasyEngineering.net

DAMA computes the modulus for each month from Eqs. 3.28 and 3.29. A modulus of 23,039 psi (159 MPa) computed for December checks with Example 3.2.

3. The moduli of HMA surface and binder courses are based on a standard mix and vary with the pavement temperature. Although the same mix properties are specified for surface and binder courses, there is a slight difference between the moduli due to the difference in pavement temperatures at different depths.
4. The subgrade is considered linear elastic. The modulus of the subgrade is 12,000 psi (82.8 MPa) in normal months, but can range from 7200 to 50,000 psi (50 to 345 MPa).
5. The tensile strains at the bottom of the binder course and the compressive strains on the top of the subgrade were computed at three points: one under the center of one wheel, one at the edge of one wheel, and the third at the center between the two duals, as shown in Figure 3.21. Only the maximum of the three is presented in the table. It is not necessary to compute the strains at the bottom of the surface course, because they are not critical and could be in compression.
6. The tensile strain for DAMA is the overall principal strain, but that for KENLAYER is the horizontal principal strain. As can be seen, the two strains check very closely. However, this is not true at the bottom of the HMA surface course, where a large difference exists between the two. It was found that the overall principal strain at the bottom of the surface course was in tension, but the horizontal principal strain was in compression. If the surface and binder courses are combined as a unit, the bottom of the thinner surface course lies above the neutral axis and should be in compression. This is the reason the horizontal principal strain is used for fatigue analysis. For multiple wheels, KENLAYER prints out both the overall principal strain and the horizontal principal strain, but only the horizontal strain is used for damage analysis.
7. KENLAYER solutions are based on linear elastic layers using the modulus values obtained from DAMA, as shown in the table. The close agreement between DAMA and KENLAYER indicates the correctness of the linear elastic solutions.

Comparison of Damage Ratios by Nonlinear Analysis Table 3.7 is a comparison of damage ratios between DAMA and KENLAYER. The number of axle-load repetitions during each month is assumed to be 5000. For each month, the damage ratios are computed at three points, as indicated in Figure 3.21, and the maximum of the three is shown in the table. In applying KENLAYER, both the HMA layers and the subgrade are assumed to be linear elastic, having the same modulus values as in DAMA, but the granular base is assumed to be nonlinear elastic, with its modulus obtained by iterations based on the monthly K_1 values specified.

Three methods can be used with KENLAYER, as shown in Figure 3.22. In method 1, the granular base is divided into three layers, each 2 in. (51 mm) thick with PHI = 0. In method 2, the granular base is considered as one layer, with the stress point at the upper quarter and PHI = K1. In method 3, the granular base is considered as one layer, but with the stress point at the midheight and a PHI of 40. The load is applied over dual wheels; another wheel, in the transverse (or y) direction, is not shown in the figure. The stress points are placed between the dual wheels with XPTNOL = 0, YPTNOL = 6.75 in. (171 mm), and SLD = 0.

Downloaded From : www.EasyEngineering.net

TABLE 3.7 Comparison of Damage Ratios between DAMA and KENLAYER

	Base Modulus (psi)				Damage Ratio for ε_t (%)				Damage Ratio for ε_c (%)			
Month	DAMA	Method 1	Method 2	Method 3	DAMA	Method 1	Method 2	Method 3	DAMA	Method 1	Method 2	Method 3
Jan	21,870	21,960 18,800	21,740	23,060	0.0972	0.1000	0.0979	0.0956	0.0502	0.0487	0.0495	0.0509
Feb	50,610	50,660 43,140	50,220	53,010	0.0267	0.0276	0.0268	0.0259	0.0030	0.0030	0.0030	0.0031
Mar	84,539	85,320 70,910	83,310	89,510	0.0176	0.0185	0.0179	0.0168	0.0012	0.0012	0.0012	0.0012
Apr	5670	5514 5365	5493	5420	0.1844	0.1900	0.1896	0.1901	0.0705	0.0654	0.0663	0.0652
May	10,277	10,430 9440	10,340	10,200	0.3172	0.3205	0.3167	0.3182	0.2510	0.2439	0.2503	0.2475
Jun	16,042	16,540 13,900	16,310	17,430	0.6225	0.6351	0.6149	0.5885	0.9509	0.9639	0.9681	0.9831
Jul	22,206	23,720 19,620	22,180	24,960	0.7313	0.7347	0.7335	0.6477	1.5220	1.5640	1.5240	0.1486
Aug	28,111	30,450 24,920	27,610	31,890	0.6098	0.6014	0.6258	0.5164	1.3730	1.4220	1.3840	1.2950
Sep	27,408	29,530 24,370	26,990	31,120	0.5515	0.5476	0.5624	0.4748	1.0810	1.1160	1.0860	1.0330
Oct	26,322	28,070 23,430	26,030	29,810	0.4473	0.4488	0.4525	0.3961	0.7018	0.7272	0.7089	0.6885
Nov	23,630	24,160 20,590	23,530	25,920	0.2023	0.2073	0.2026	0.1912	0.1722	0.1729	0.1722	0.1756
Dec	23,039	23,320 19,950	22,950	24,980	0.1617	0.1660	0.1620	0.1550	0.1173	0.1165	0.1169	0.1198
Sum of Damage Ratios (%)					3.9695	3.9970	4.0020	3.6160	6.2941	6.4460	6.3310	6.1490

Note. 1 psi = 6.9 kPa

Downloaded From : www.EasyEngineering.net

Downloaded From : www.EasyEngineering.net

Downloaded From : www.EasyEngineering.net

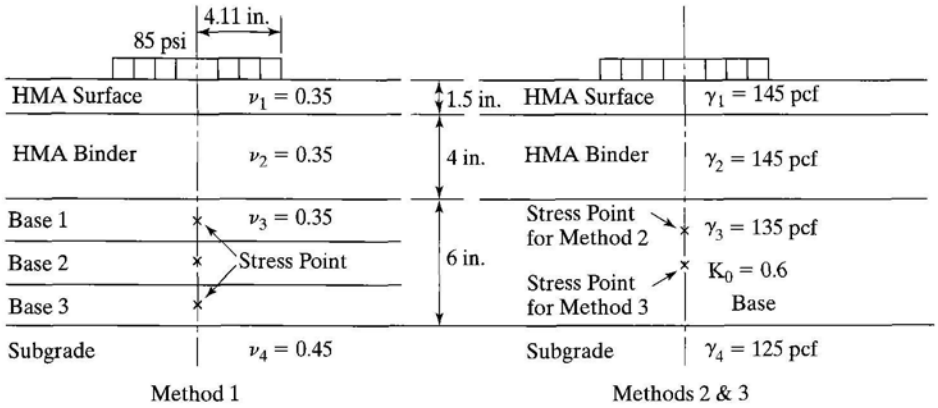


FIGURE 3.22

Three methods for characterizing nonlinear granular layers (1 in. = 25.4 mm, 1 pcf = 157.1 N/m^3).

Comments on Table 3.7

1. From the K_1 of the base course material, DAMA computes the base modulus by Eqs. 3.28 and 3.29; KENLAYER determines the modulus by iterations. Two base moduli are shown for method 1: the top value for the top layer, the bottom value for the bottom layer. The modulus of the middle layer lies between the two and is not presented.
2. During each month, DAMA computes the damage ratios for fatigue cracking and permanent deformation at three points. These monthly ratios are summed separately over a year, and the maximum ratio among the three at the end of one year is used to determine the design life. Because the maximum damage ratio for each month does not occur at the same point, the maximum damage ratios at the end of a year as obtained by DAMA are actually 3.943% for fatigue cracking and 6.244% for permanent deformation, which are slightly smaller than the sums 3.970 and 6.294% shown in Table 3.7.
3. The damage analysis by KENLAYER is not limited to dual wheels with three fixed points but can also be applied to a combination of single-, dual-, and multiple-wheel loads; the maximum damage ratio during each month for each load group is determined and summed over the year to compute the design life. This procedure, although not theoretically correct, does give a clear picture of the damage during each month for each load group. The analysis is more conservative, because the maximum damage ratio during each month for each load group might not occur at the same point.
4. The damage ratios obtained from KENLAYER by using methods 1 and 2 check closely with those from DAMA, but those obtained by method 3 with PHI = 40 are somewhat smaller. An inspection of the table reveals that, during the spring months (April, May, and June), when the modulus of the subgrade is below 10,000 psi (6.9 MPa), the modulus and damage ratios obtained by method 3 check closely with those obtained by methods 1 and 2, but their discrepancies increase

Downloaded From : www.EasyEngineering.net

Downloaded From : www.EasyEngineering.net

as the subgrade modulus increases. Consequently, a larger PHI might have to be used for a stronger subgrade.

5. Theoretically, KENLAYER should be more accurate than DAMA, because it uses direct iterations instead of the indirect regressions based on the results of iterations. Therefore, the prime interest is not in the comparison between DAMA and KENLAYER, but rather in the comparison among the three methods. If PHI in method 3 is changed to 60, the damage ratio for fatigue cracking will be increased to 3.969%, which checks well with the 3.997% from method 1; however, the match of damage ratio for permanent deformation will not be as good, as indicated by damage ratios at 6.272 vs 6.446%. If the granular base is divided into several layers, the tensile strain at the bottom of HMA is affected most significantly by the modulus of the uppermost layer, and the compressive strain on the top of the subgrade by that of the lowest layer. If the modulus of a single layer is selected so that the tensile strain at the bottom of HMA checks well against that obtained from multiple layers, a different and smaller modulus is needed to match the compressive strain on the subgrade. Unless the asphalt layer is thick and the effect of the granular base is not very significant, it is just impossible to replace multiple granular layers by a single layer and expect both to match closely in tensile and in compressive strains.

3.4 SENSITIVITY ANALYSIS

With the use of KENLAYER, sensitivity analyses were made on both three-and four-layer systems to illustrate the effect of various parameters on pavement responses. The complex interactions among the large number of parameters make it difficult to present a concise, but accurate, picture on the effect of a given parameter, because the effect depends not only on the parameter itself, but also on all other parameters. Conclusions based on a set of parameters could be invalid if some of the other parameters are changed. The best approach is to fix all other parameters at their most reasonable values while varying the parameter in question, to show its effect.

3.4.1 Linear Analysis

This analysis is based on the assumption that all layers are linear elastic. Although HMA layers are viscoelastic and granular layers are nonlinear elastic, an approximate procedure is to assume them to be linear elastic by selecting appropriate moduli for HMA, based on vehicle speeds and pavement temperatures, and for granular materials, based on the level of loading.

Three-Layer Systems To illustrate the effect of some design factors on pavement responses, an elastic three-layer system is used, as shown in Figure 3.23. The variables to be considered include layer thicknesses h_1 and h_2 and layer moduli E_1, E_2, and E_3. Two types of wheel loads are considered: one on a single tire and the other on a set of dual tires with a dual spacing of 13.5 in. (343 mm). A contact radius a of 5.35 in. (136 mm) is assumed for a single tire, 3.78 in. (96 mm) for dual tires. These radii are based on an 18-kip (80-kN) single-axle load exerting a contact pressure of 100 psi (690 kPa). The Poisson

Downloaded From : www.EasyEngineering.net

Downloaded From : www.EasyEngineering.net

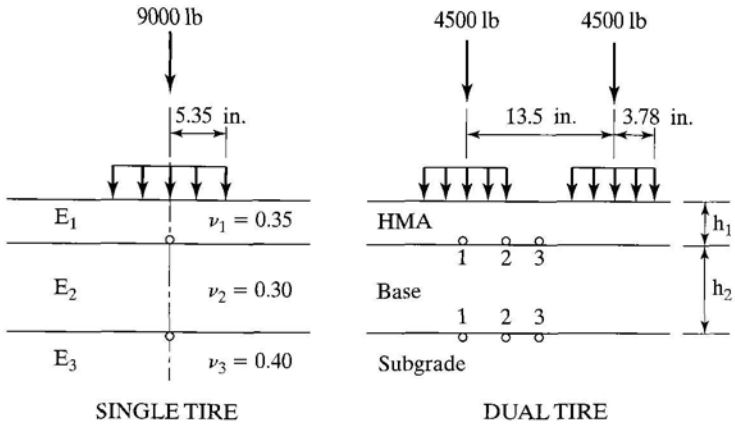


FIGURE 3.23

Three-layer systems subjected to single- and dual-wheel loads (1 in. = 25.4 mm, 1 lb = 4.45 N).

ratios for the three layers are 0.35, 0.3, and 0.4, respectively. For a single tire, the critical strains occur under the center of the loaded area. For a set of dual tires, the strains at points 1, 2, and 3, as shown in Figure 3.23, are computed, and the largest among the three is selected as the most critical.

Effect of Layer Thickness The effect of HMA thickness h_1 and base thickness h_2 on the tensile strain ϵ_t at the bottom of asphalt layer and the compressive strain ϵ_c at the top of subgrade was investigated.

Figure 3.24 shows the effect of h_1 on ϵ_t and ϵ_c when E_1 = 500,000 psi (34.5 GPa), E_2 = 20,000 psi (138 MPa), E_3 = 7500 psi (51.8 MPa), and h_2 = 4 or 16 in. (102 or 406 mm). The reason that two different thicknesses h_2 are used is to check whether the trend on a very thin base is also applicable to that on a thick base. The legend for various cases and a typical cross section are shown on the right side of the figure. A review of Figure 3.24 reveals the following trends:

1. For the same total load and contact pressure, single-wheel loads always result in greater ϵ_c, but not necessarily greater ϵ_t. When the asphalt surface is very thin, ϵ_t under dual-wheel loads is greater than under a single-wheel load. Therefore, the use of a single tire to replace a set of duals, as has been practiced in ILLI-PAVE and MICH-PAVE, is unsafe when analyzing the fatigue cracking of a thin asphalt surface.
2. Under a single-wheel load, there is a critical thickness at which ϵ_t is maximum. Above the critical thickness, the thicker the asphalt layer, the smaller is the tensile strain; below this critical thickness, the thinner the asphalt layer, the smaller is the strain. The same trend is shown in Figures 2.21 and 3.14 and was also reported by Freeme and Marais (1973), who indicated that fatigue cracking could be minimized by keeping the asphalt surface as thin as possible. The critical thickness is not as pronounced under dual wheels as it's under single wheels.

Downloaded From : www.EasyEngineering.net

Downloaded From : www.EasyEngineering.net

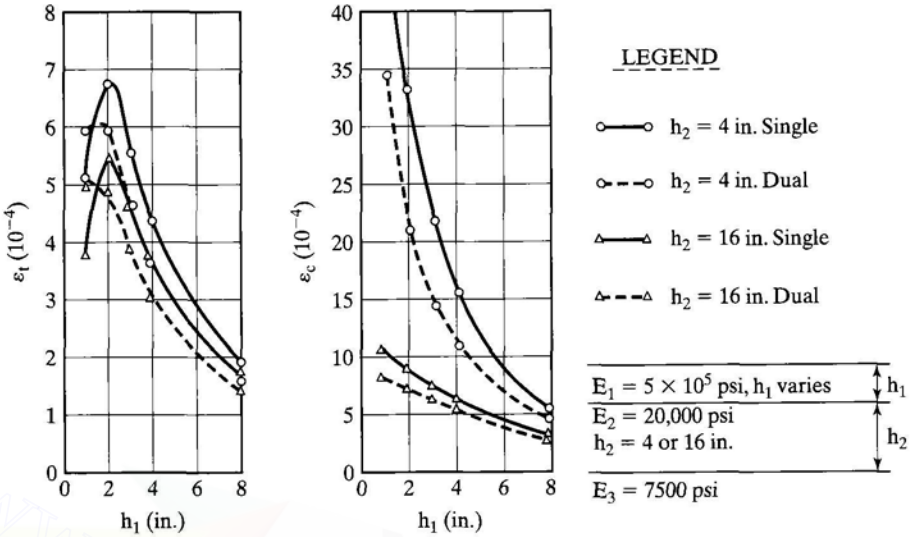


FIGURE 3.24
Effect of HMA thickness on pavement responses (1 in. = 25.4 mm, 1 psi = 6.9 kPa).

3. Above the critical thickness, increasing h_1 is very effective in reducing ϵ_t, regardless of the base thickness. Unless the asphalt surface is less than 2 in. (51 mm) thick, the most effective way to prolong the fatigue life is to increase the HMA thickness.
4. Increasing h_1 is effective in reducing ϵ_c only when the base course is thin, not when the base course is thick.

Figure 3.25 shows the effect of h_2 on ϵ_t and ϵ_c when E_1 = 500,000 psi (34.5 GPa), E_2 = 20,000 (138 MPa), E_3 = 7500 psi (51.8 MPa), and h_1 = 2 or 8 in. (51 and 203 mm). The following trends can be found in Figure 3.25:

1. When h_1 is 2 in. (51 mm) or more, the replacement of dual wheels by a single wheel increases both ϵ_t and ϵ_c.
2. An increase in h_2 does not cause a significant decrease in ϵ_t, especially when h_1 is large.
3. An increase in h_2 causes a significant decrease in ϵ_c only when h_1 is small. Unless a full-depth or thick layer of HMA is used, the most effective way to reduce ϵ_c is to increase h_2.

Effect of Layer Modulus The effect of the base modulus E_2 and subgrade modulus E_3 on the tensile strain ϵ_t and the compressive strain ϵ_c is now discussed. The effect of HMA modulus E_1 is not presented, because it is well known that an increase in E_1 results in a decrease in ϵ_t and ϵ_c. However, an increase in E_1 also causes a decrease in the allowable number of repetitions for fatigue cracking, as is indicated by Eq. 3.6.

Downloaded From : www.EasyEngineering.net

Downloaded From : www.EasyEngineering.net

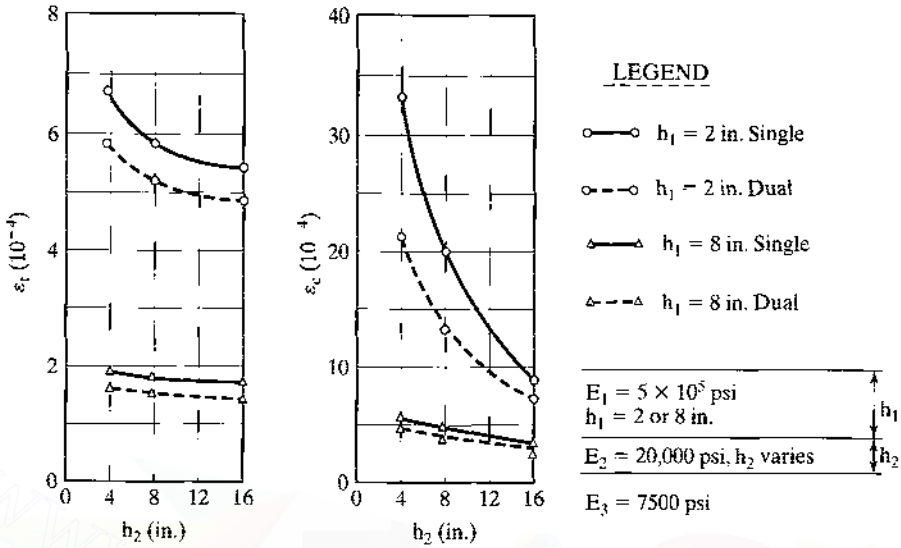


FIGURE 3.25

Effect of base thickness on pavement responses (1 in. = 25.4 mm, 1 psi = 6.9 kPa.)

Whether a smaller ϵ_t due to a larger E_1 should increase or decrease the fatigue life depends on the material properties and failure criterion.

Figure 3.26 shows the effect of E_2 on ϵ_t and ϵ_c when $h_1 = 4$ in. (102 mm), $h_2 = 8$ in. (203 mm), $E_1 = 200{,}000$ or 1,000,000 psi (1.4 or 6.9 GPa), and $E_3 = 7500$ psi

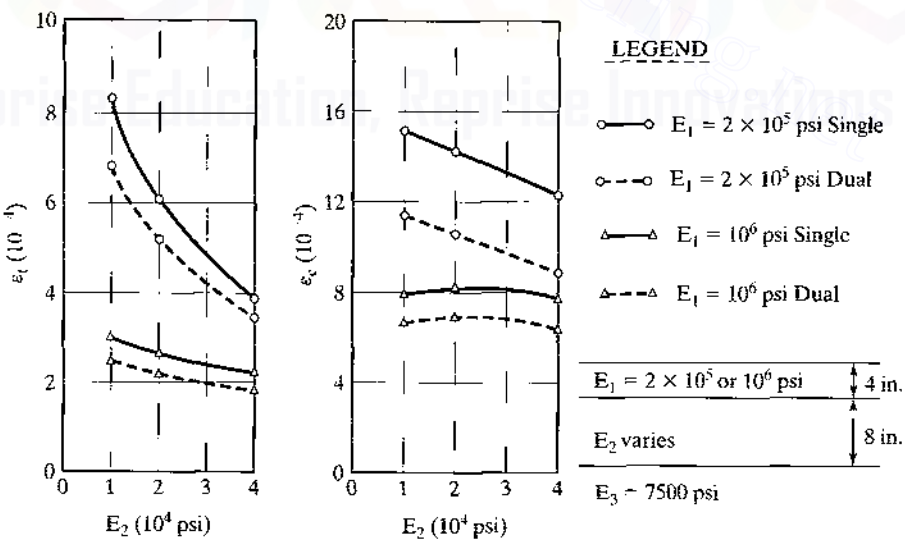


FIGURE 3.26

Effect of base modulus on pavement responses (1 in. = 25.4 mm, 1 psi = 6.9 kPa.).

Downloaded From : www.EasyEngineering.net

Downloaded From : www.EasyEngineering.net

(51.8 MPa). It can be seen that E_2 has more effect on ϵ_t than on ϵ_c and that the effect is greater when E_1 is smaller.

Figure 3.27 shows the effect of E_3 on ϵ_t and ϵ_c when $h_1 = 4$ in. (102 mm), $h_2 = 8$ in. (203 mm), $E_1 = 200{,}000$ or 1,000,000 psi (1.4 or 6.9 GPa), and $E_2 = 20{,}000$ psi (138 MPa). It can be seen that E_3 has a large effect on ϵ_c but a very small effect on ϵ_t. The effect of E_3 is nearly the same, no matter how large or small E_1 is.

Four-Layer Systems Figure 3.28 shows a standard pavement consisting of 4 in. (102 mm) of hot-mix asphalt surface course, 8 in. (203 mm) of crushed-stone base course, and 8 in. (203 mm) of gravel subbase course, which is subjected to a 9000-lb (40-kN)

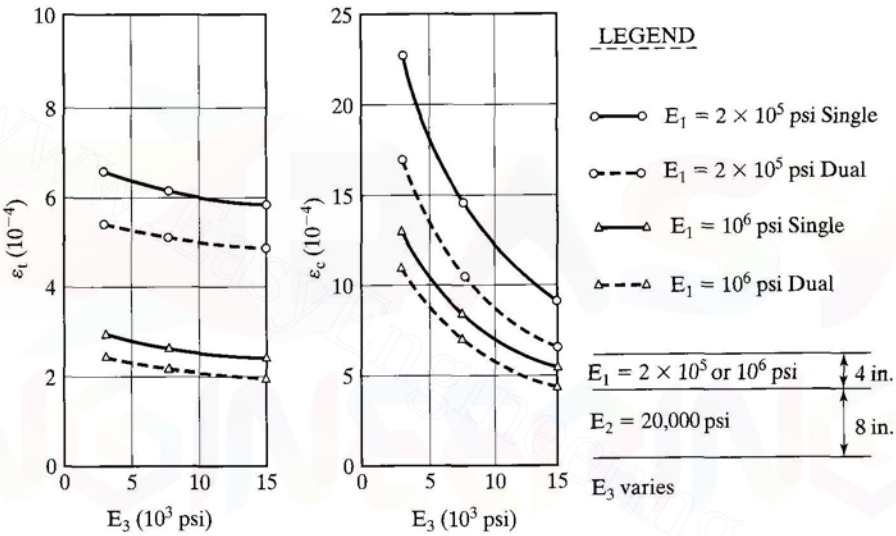


FIGURE 3.27
Effect of subgrade modulus on pavement responses (1 in. = 25.4 mm, 1 psi = 6.9 kPa).

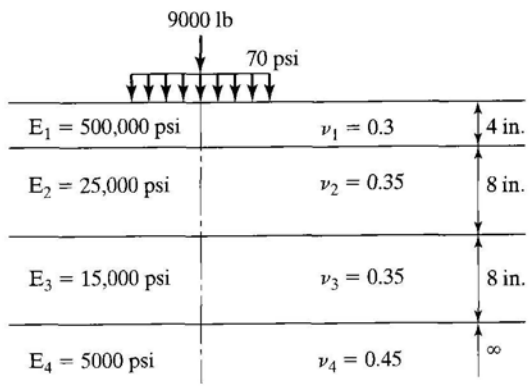


FIGURE 3.28
Four-layer elastic system for sensitivity analysis (1 in. = 25.4 mm, 1 psi = 6.9 kPa, 1 lb = 4.45 N).

Downloaded From : www.EasyEngineering.net

Downloaded From : www.EasyEngineering.net

single-wheel load exerting a contact pressure of 70 psi (483 kPa). The elastic modulus and Poisson ratio of each layer are shown in the figure.

In addition to the standard case, six nonstandard cases, each with only one parameter different from the standard case, were also analyzed. The results are presented in Table 3.8. Case 1 has the same total load as the standard case but the contact pressure is doubled, thus resulting in a smaller contact radius. Case 2 has a strong subgrade with an elastic modulus three times greater than the standard case. In case 3, all layers are assumed incompressible with a Poisson ratio of 0.5. The granular base is replaced by an asphalt base in case 4 and by a cement-treated base in case 5. Theoretically, the Poisson ratio of these treated bases should be different from that of the granular base; however, because the effect of Poisson ratio is small, the same Poisson ratio, 0.35, is used. Case 6 is a five-layer system with the top 6 in. (152 mm) of subgrade replaced by a lime-stabilized layer with the same Poisson ratio of 0.45. The values in parentheses were obtained from the ELSYM5 (Kopperman *et al.*, 1986) program, as reported by ERES Consultant, Inc. (1987). It can be seen that the solutions obtained from KENLAYER check closely with those from ELSYM5.

The responses to be compared include the surface deflection w_0, the radial stress σ_r and the tensile strain ϵ_t at the bottom of the HMA, the vertical stress σ_z at the top of each layer, the radial stress at the top and bottom of each layer, the vertical compressive strain ϵ_c at the top of the subgrade, and the vertical and radial stresses in the subgrade 36 in. (914 mm) below the surface. The surface deflection is a good indication of the overall strength of a pavement. The tensile strain at the bottom of the asphalt layer and the compressive strain at the top of the subgrade have frequently been used as design criteria. The vertical stresses contribute to the consolidation of each layer and the rutting on the surface. The radial stresses are important because they cause the rupture of rigid layers and control the resilient modulus of unbounded granular layers.

Comments on Table 3.8

1. A comparison of case 1 with the standard case indicates that the effect of contact pressure or contact radius is significant only in the top layers. If the design is governed by the radial tensile strain at the bottom of the asphalt layer, case 1 results in a radial strain 45% greater than the standard case, thus requiring the use of thicker or better HMA to prevent fatigue cracking. If the design is governed by the vertical compressive strain at the top of subgrade, case 1 has a vertical strain only 3.6% greater than the standard case, so the effect of contact radius is insignificant.
2. A comparison of case 2 with the standard case indicates that a strong subgrade reduces the surface deflection by 38%, but the tensile strain at the bottom of the asphalt layer by only 4.1%. The stiffer foundation cause the vertical and radial compressive stresses to increase and the radial tensile stesses to decrease. The effect is most significant in the subbase, which lies directly above the subgrade, and diminishes in the layers that are farther away from the subgrade. Because the granular base and subbase are actually nonlinear, the change in vertical and radial stresses will increase their resilient moduli, so the effect of a stronger subgrade on the tensile strain at the bottom of the asphalt layer should be greater than the 4% obtained from the linear theory.

Downloaded From : www.EasyEngineering.net

TABLE 3.8 Sensitivity Analysis of Elastic Multilayer Systems

Location	Response	Standard case	Case 1 high pressure q = 140 psi	Case 2 strong subgrade E_1 = 15,000 psi	Case 3 v = 0.5	Case 4 asphalt base E_2 = 300,000 psi	Case 5 cement base E_2 = 1,000,000 psi	Case 6 6 in. lime E_4 = 50,000 psi E_5 = 5000 psi
Top of HMA	w_0 (in.)	0.0341 (0.034)	0.0360 (0.036)	0.0212 (0.021)	0.0336 (0.034)	0.0202 (0.021)	0.0161 (0.017)	0.0290 (0.029)
Bottom of HMA	σ_r (psi)	−199.9 (−200)	−291.4 (−291.0)	−190.8 (−191)	−269.6 (−270)	6.51 (6.3)	39.1 (38.4)	−188.1 (−188)
	$\epsilon_t(10^{-6})$	−295.7 (−296)	−428.7 (−429)	−283.5 (−284)	−293.8 (−294)	−21.16 (−21.5)	19.77 (18.8)	−279.8 (−280)
Top of base	σ_z (psi)	26.48 (26.5)	34.5 (34.4)	27.28 (27.3)	24.21 (24.2)	50.44 (50.4)	58.18 (58.2)	27.35 (27.4)
	σ_r (psi)	2.88	2.07	3.79	9.51	6.51	61.74	3.97
Bottom of base	σ_1 (psi)	−6.95 (−7.0)	−7.56 (−7.4)	−4.29 (−4.3)	−7.67 (−7.7)	−61.08 (−60.6)	−102.1 (−100)	−3.99 (−3.9)
Top of subbase	σ_z (psi)	8.59 (8.6)	9.30 (9.3)	10.62 (10.6)	8.42 (8.4)	3.77 (3.7)	2.21 (2.2)	10.45 (10.5)
	σ_r (psi)	−2.32	−2.53	−0.29	−1.24	−1.13	−0.36	−0.15
Bottom of subbase	σ_r (psi)	−5.25 (−5.3)	−5.47 (−5.3)	−0.56 (−0.6)	−5.92 (5.9)	2.22 (−2.2)	−1.20 (−1.1)	0.92 (1.0)
Top of subgrade	σ_z (psi)	3.48 (3.5)	3.58 (3.5)	5.66 (5.7)	3.49 (3.5)	1.74 (1.7)	1.22 (1.2)	2.13 (2.2)
	σ_r (psi)	0.39	0.02	3.65	0.35	0.18	0.26	0.40
	$\epsilon_v(10^{-6})$	688.8	713.8	355.2	627.4	314.9	196.0	354.8
36 in. below surface	σ_z (psi)	1.59 (1.6)	1.61 (1.6)	2.41 (2.4)	1.66 (1.6)	0.99 (0.9)	0.78 (0.7)	1.44 (1.4)
	σ_r (psi)	0.03	0.03	0.05	1.37	0.11	0.14	0.16

Note. Numbers in parentheses were reported by ERES Consultant, Inc. using ELSYM5. 1 in. = 25.4 mm. 1 psi = 6.9 kPa.

Downloaded From : www.EasyEngineering.net
Downloaded From : www.EasyEngineering.net

Downloaded From : www.EasyEngineering.net

3. A comparison of case 3 with the standard case indicates that the Poisson ratios have very little effect on the surface deflection, the vertical stresses, and the radial tensile strain at the bottom of the asphalt layer, but a significant effect on the radial stresses. The vertical compression strain at the top of the subgrade is reduced by 9.1% by the greater Poisson ratio.
4. The replacement of granular base by asphalt base, as shown in case 4, results in a significant decrease in the surface deflection and the stresses in the subbase and subgrade. The radial stress at the bottom of the HMA surface course changes from tension to compression, so the most critical tensile strain occurs at the bottom of the asphalt base course, instead of the surface course.
5. The replacement of granular base by cement base, as shown in case 5, further reduces the surface deflection and the stresses in the subbase and subgrade, as compared to case 4. The radial tensile stress at the bottom of the base course increases with the rigidity of the base.
6. A comparison of case 6 with the standard case indicates that the placement of a 6-in. (152-mm) lime-stabilized layer above the subgrade reduces the tensile strain at the bottom of layer 1 by only 5.4%. The effect is similar to case 2 with a stronger subgrade.
7. The radial stresses in the subgrade are always in compression, while those in the subbase and at the bottom of the base are in tension. One exception is in case 6, where the radial stress at the bottom of the subbase is in compression as a result of the existence of a very stiff lime-stabilized layer underneath.

3.4.2 Nonlinear Analysis

This analysis is based on the assumption that one or more layers are nonlinear elastic with a stress-dependent resilient modulus. The nonlinear granular layer can be considered as a single layer or subdivided into a number of layers, each not over 2 in. (51 mm) thick.

Three-Layer Systems Figure 3.29 shows a three-layer system subjected to a total load P, which is applied by a single tire and a set of dual tires. Under a given contact radius, the stresses, strains, and deflections in a linear system are proportional to the contact pressure or the magnitude of the total load, P. However, for a nonlinear system with stress-sensitive granular materials, the increase in responses is not as rapid as the increase in load due to the stiffening effect of granular materials under greater loads. The purpose herein is to find the effect of load magnitude on pavement responses. The information necessary for the analysis is shown in the figure.

Figure 3.30 illustrates the effect of P on ϵ_t and ϵ_c when $h_1 = 2$ or 8 in. (51 or 203 mm). The granular base is divided into six layers with PHI = 0. The reason the subgrade is considered linear elastic instead of nonlinear elastic is that the nonlinear effect is usually quite small and can be neglected.

Downloaded From : www.EasyEngineering.net

Downloaded From : www.EasyEngineering.net

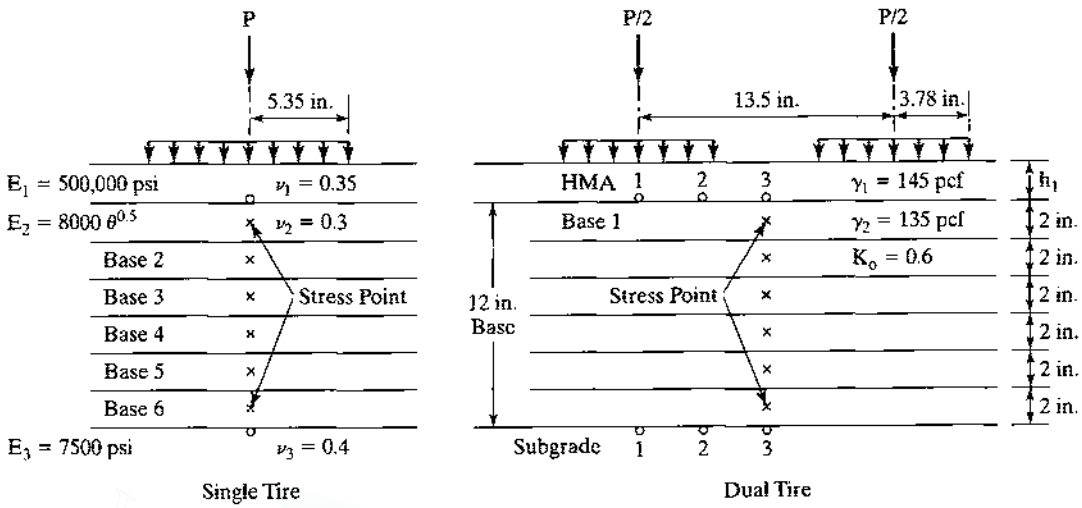


FIGURE 3.29

Pavement section for nonlinear analysis (1 in. = 25.4 mm, 1 psi = 6.9 kPa, 1 pcf = 157.1 N/m^3).

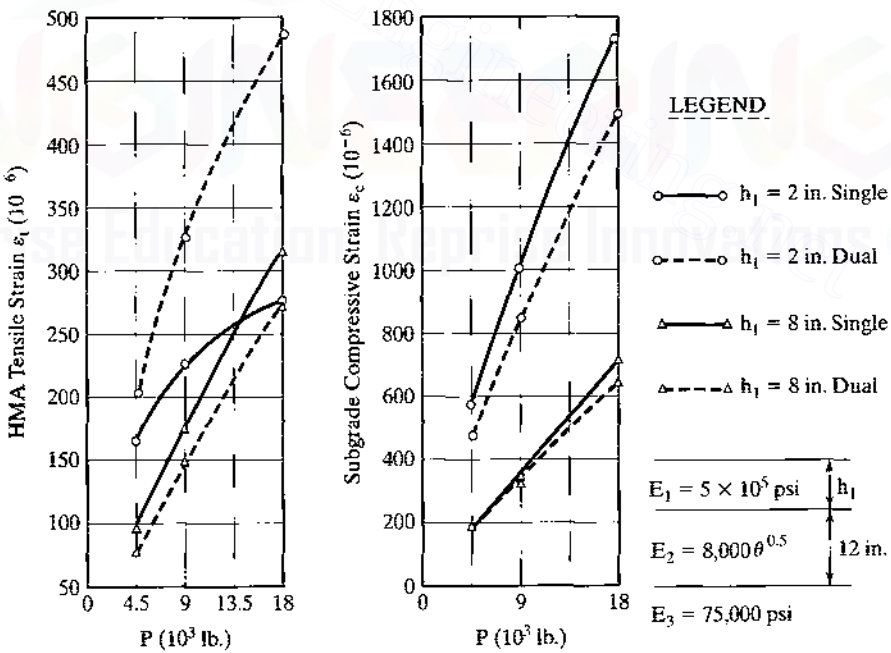


FIGURE 3.30

Effect of wheel loads on nonlinear responses (1 in. = 25.4 mm, 1 psi = 6.9 kPa).

Downloaded From : www.EasyEngineering.net

Downloaded From : www.EasyEngineering.net

Comments on Figure 3.30

1. For a thin HMA layer with $h_1 = 2$ in. (51 mm), ϵ_t under dual-wheel loads is greater than under a single-wheel load. This trend is noted in Figure 3.24, but is more pronounced when the base is nonlinear. Figure 3.30 further shows that the greater the load, the more difference there is in ϵ_t between single and dual wheels. This is because the single-wheel load results in greater stresses in the granular base and makes the base stronger, thus further decreasing ϵ_t.
2. The nonlinear effect, as indicated by the curvilinear relationship between ϵ_t and P, is more pronounced for thinner HMA than for thicker HMA. For thicker HMA with $h_1 = 8$ in. (203 mm), the relationship between ϵ_c and P is nearly linear.
3. The differences in responses between single and dual wheels are more significant when the HMA is thin and become less significant as the HMA thickness increases.

Four-Layer Systems Figure 3.31 is the standard case for a nonlinear elastic system similar to the linear system shown in Figure 3.28. Even though layer 1 is actually viscoelastic, it is always possible to find a vehicle speed or load duration such that the modulus is equal to 500,000 psi (3.5 GPa). The elastic modulus of base, subbase, and subgrade are stress dependent, as is indicated by the equations shown in the figure. For fine-grained subgrade soil, only the equation for a deviator stress smaller than 6.2 psi (42.8 kPa) is shown, because the actual stress is always smaller than this value. The constants in these nonlinear equations were selected so that the same moduli as in the linear system could be obtained. To achieve a modulus of 25,000 psi (173 MPa) for

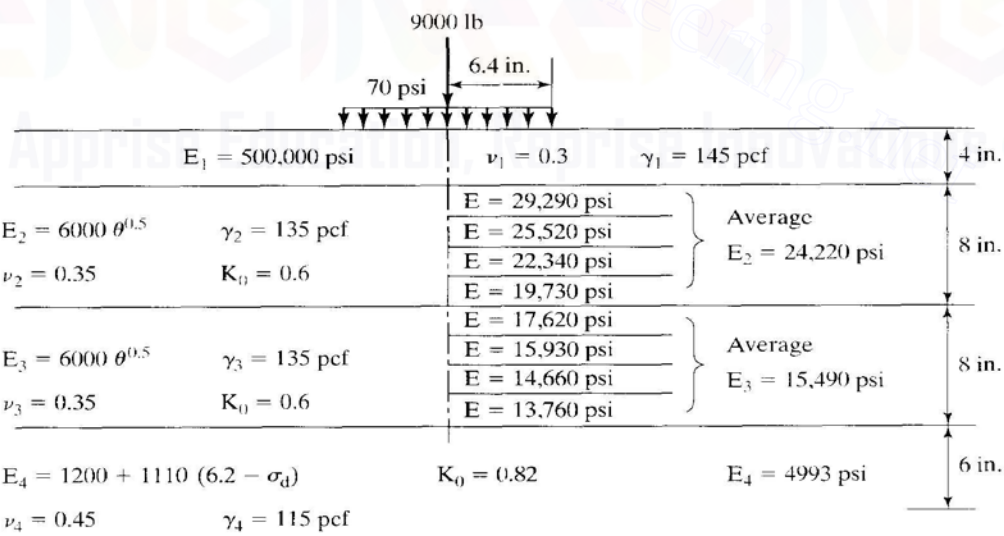


FIGURE 3.31

Four-layer nonlinear elastic system for sensitivity analysis (1 in. = 25.4 mm, 1 psi = 6.9 kPa, 1 lb = 4.45 N, 1 pcf = 151.7 N/m^3).

Downloaded From : www.EasyEngineering.net

Downloaded From : www.EasyEngineering.net

TABLE 3.9 Sensitivity Analysis of Nonlinear Elastic Multilayer Systems

Response	Standard case	Case 1 high pressure q = 140 psi	Case 2 strong subgrade[1]	Case 3 strong base[2]	Case 4 strong base K_2 = 0.7	Case 5 strong surface $E_1 = 10^6$ psi	Case 6 subgrade K_0 = 0.4
Avg E_2 (psi)	24,220	26,360	25,870	53,000	46,110	20,740	24,020
Avg E_3 (psi)	15,490	15,720	17,930	30,090	21,600	14,510	15,160
E_4 (psi)	4993	4984	14,700	5514	5359	5211	4277
w_0 (in.)	0.0341 (0.0341)	0.354 (0.0360)	0.0205 (0.0212)	0.0252	0.0277	0.0307	0.0371
ϵ_t (10^{-6})	−290.0 (−295.7)	−403.4 (−428.7)	−267.5 (−283.5)	−173.6	−193.2	−218.9	−293.4
ϵ_c (10^{-6})	691.0 (688.8)	704.5 (713.8)	357.6 (355.2)	507.5	564.0	584.4	748.7

Note. Figures in parentheses are from Table 3.8 based on the elastic system. 1 psi = 6.9 kPa, 1 in. = 25.4 mm.
[1] Subgrade K_1 = 12,340 psi
[2] Base K_1 = 12,000 psi

the base and 15,000 psi (104 MPa) for the subbase, the same K_1 of 6000 should be used. The base and subbase courses are each subdivided into four layers. The modulus of each layer, as obtained by KENLAYER, is shown in the figure.

In addition to the standard case shown in Figure 3.31, six more cases, each with only one parameter different from the standard case, were also analyzed. The results are presented in Table 3.9. The responses include the average base and subbase moduli E_2 and E_3, the subgrade modulus E_4, the surface deflection w_0, the radial tensile strain ϵ_t at the bottom of layer 1, and the vertical compressive strain ϵ_c at the top of the subgrade. For comparison, the corresponding w_0, ϵ_t, and ϵ_c based on the linear theory, as presented in Table 3.8, are shown in parentheses.

Comments on Table 3.9

1. The standard case for nonlinear analysis is very similar to that for linear analysis, with nearly the same layer moduli. A comparison between linear and nonlinear solutions shows that the nonlinear solution results in the same w_0, a slightly smaller ϵ_t, and a slightly greater ϵ_c. These results are reasonable because w_0 depends on the average moduli, ϵ_t depends to a large extent on the modulus of the material immediately under the asphalt layer, and ϵ_c depends on the modulus of the material immediately above the subgrade. Although the average moduli of the nonlinear system are the same as those of the linear system, the modulus of the granular layer immediately below the asphalt layer is 29,290 psi (201 MPa), which is greater than the average base modulus of 24,220 psi (167 MPa), and the modulus of the granular layer immediately above the subgrade is 13,760 psi (95 MPa), which is smaller than the average subbase modulus of 15,490 psi (107 MPa). The greater the base modulus immediately below the asphalt layer, the smaller is the ϵ_t; the smaller the subbase modulus immediately above the subgrade, the greater is the ϵ_c.

Downloaded From : www.EasyEngineering.net

Downloaded From : www.EasyEngineering.net

2. With the same total load, an increase in tire pressure causes an increase in E_2 but has practically no effect on E_3 and E_4. This is reasonable because the subbase and subgrade are quite far away from the load and are not affected by contact pressure, as long as the total load is the same. Furthermore, the relatively large geostatic stress in the subbase and subgrade also reduces the effect of loading stress on the resilient modulus. Given the increase in E_2, the nonlinear analysis results in a smaller w_0, ϵ_t, and ϵ_c, compared with the linear analysis.
3. A strong subgrade causes an appreciable increase in E_2 and E_3. An increase of E_4 from 4993 psi (34.5 MPa) to 14,700 psi (101.4 MPa) results in a 16% increase in E_3 and 7% increase in E_2. Consequently, the nonlinear analysis results in a reduction of ϵ_t by 7.8% compared to the 4.1% in the linear analysis.
4. A stronger base or subbase can be obtained by increasing the nonlinear coefficients K_1 and K_2. The effect of K_1 and K_2 is more significant on ϵ_t than on ϵ_c.
5. A strong surface course causes a decrease in E_2, a slight decrease in E_3 and E_4, and a significant decrease in w_0, ϵ_t, and ϵ_c.
6. A decrease in the K_0 of the subgrade reduces E_4 and ϵ_c, but has practically no effect on E_2, E_3, and ϵ_t. Because the horizontal stresses at all the stress points in the granular layers are in tension, which must be set to 0 to compute the stress invariant, the K_0 of the granular materials in the base and subbase has no effect on the analysis.
7. The large effect of geostatic stress makes the modulus of the subgrade less sensitive to the loading stress or the moduli of the overlying layers. It appears reasonable to assume the subgrade to be linear with an elastic modulus independent of the state of stresses. This is not true for bases and subbases, because their elastic moduli depend strongly on the stiffness of subgrade.

SUMMARY

This chapter describes some features of the KENLAYER computer program. The theory presented in Chapter 2 and Section 3.1 was used in developing KENLAYER.

Important Points Discussed in Chapter 3

1. The basic component of KENLAYER is the elastic multilayer system under a circular loaded area. Each layer is linear elastic, homogeneous, isotropic, and infinite in areal extent. The problem is axisymmetric, and the solutions are in terms of cylindrical coordinates r and z.
2. For multiple wheels involving two to six circular loaded areas, the superposition principle can be applied, because the system is linear. The stresses at a given point due to each of these loaded areas are not in the same direction, so they must be resolved into x and y components and then superimposed.
3. The same superposition principle can also be applied to a nonlinear elastic system by a method of successive approximations. First, the system is considered to be linear, and the stresses due to multiple-wheel loads are superimposed. From the stresses thus computed, a new set of moduli for each nonlinear layer is then

Downloaded From : www.EasyEngineering.net

Downloaded From : www.EasyEngineering.net

determined. The system is considered linear again, and the process is repeated until the moduli converge to a specified tolerance.

4. Because the most critical strains occur directly under or near the load, a point under the center of a single wheel or between the centers of dual wheels can be selected for computing the elastic modulus of each nonlinear layer.
5. Three methods can be used in KENLAYER to adjust the horizontal stresses for determining the modulus of granular layers. In method 1, the granular layer is subdivided into a number of layers, each of maximum thickness 2 in. (51 mm), and the stress points are located at the midheight of each layer, with PHI = 0. In method 2, the granular base or subbase is not subdivided, and the stress point is located at the upper quarter or upper third of the layer with PHI = K1, which is the nonlinear coefficient of the granular material. In method 3, the layer is not subdivided, the stress point is at the midheight, and PHI is equal to the angle of internal friction of the granular material. A comparison with the results from MICH-PAVE indicates that method 1 yields the best results. For pavements with a thick layer of HMA, where the effect of granular layer is not very significant, the use of a single layer, via method 2 or 3, might also give reasonable results. However, for a thick granular layer under a thin HMA, the use of method 1 (subdividing the granular base or subbase into 2-in. (51-mm) layers) is recommended. The problem with a single layer is its failure to represent the actual case of decreasing modulus with depth so, no matter what modulus is assumed, it is just impossible to get a good match with multiple layers or MICH-PAVE in both the tensile strain at the bottom of HMA and the compressive strain at the top of the subgrade.
6. If the layered system is viscoelastic, the responses under a static load can be expressed as a seven-term Dirichlet series, as indicated by Eq. 2.49, using the following seven T_i values: 0.01, 0.03, 0.1, 1, 10, 30, and ∞ seconds. The responses under a moving load are obtained by assuming the loading to be a haversine function and applying Boltzmann's superposition principle to the Dirichlet series, as indicated by Eq. 2.59.
7. A direct method for analyzing viscoelastic layer systems under static loads is to assume the viscoelastic layer to be elastic with a modulus varying with the loading time. For a given loading time, the elastic modulus is the reciprocal of the creep compliance at that loading time.
8. KENLAYER can be applied to layer systems with a maximum of 19 layers, each being either linear elastic, nonlinear elastic, or linear viscoelastic. If the layer is linear elastic, the modulus is a constant, so no further work need be done to determine its value. If the layer is nonlinear elastic, the modulus varies with the state of stresses; a method of successive approximations is then applied until it converges. If the layer is viscoelastic, elastic solutions under static loads are obtained at a specified number of time durations, usually 11, and then fitted with a Dirichlet series.
9. Damage analysis is based on the horizontal tensile strain at the bottom of a specified asphalt layer and the vertical compressive strain on the surface of a specified layer, usually the subgrade. To determine the allowable number of repetitions to prevent fatigue cracking, it is necessary to know the elastic modulus of the hot-mix asphalt. If the hot-mix asphalt is specified as viscoelastic, its elastic modulus is not

Downloaded From : www.EasyEngineering.net

Downloaded From : www.EasyEngineering.net

a constant but depends on the duration of loading and can be determined by Eq. 3.18.

10. In damage analysis, each year can be divided into several periods and each period can have a number of load groups. For tandem and tridem load groups, the allowable number of load repetitions for the first axle load is based on the total strain, that for each additional axle on the difference between maximum and minimum strains. The damage ratios for fatigue cracking and permanent deformation in each season under each load group are evaluated and summed over a year, and the one with a larger damage ratio controls the design. The reciprocal of the damage ratio is the design life of the pavement.
11. The results obtained by KENLAYER compare well with those from other layer-system programs, such as ELSYM5, VESYS, and DAMA and with those from the windows version of MICH-PAVE using the finite-element method.
12. For thin asphalt surfaces, say less than 2 in. (51 mm) thick, the use of a single tire to replace the actual dual tires results in a smaller tensile strain and is unsafe for the prediction of fatigue cracking.
13. The most effective way to decrease the tensile strain at the bottom of the asphalt layer is to increase the HMA thickness or the modulus of the base course; the most effective way to decrease the compressive strain on top of the subgrade is to increase the thickness of the granular base and subbase or the modulus of the subgrade.
14. A sensitivity analysis of elastic layered systems indicates that the incorporation of a stiff layer reduces the stresses and strains appreciably in its underlying layers, but, among its overlying layers, only the one lying immediately above the stiff layer will be affected to a significant degree. For example, a strong subgrade significantly reduces the tensile stress in the subbase but not in the asphalt layer. However, a sensitivity analysis of nonlinear layered systems indicates that the above conclusion is only paritally true. A strong subgrade increases the moduli of base and subbase and has more effect in reducing the tensile stress and strain in the asphalt layer than that predicted by the linear theory.
15. The result of nonlinear analysis indicates that the modulus of the subgrade is not affected significantly by the moduli of the base and the subbase, but the moduli of the base and the subbase depend strongly on the modulus of the subgrade. In pavement design, it appears reasonable to assume the base and subbase to be nonlinear elastic and the subgrade to be linear elastic.

PROBLEMS

Note: On the Editor screen of KENPAVE, there is an Examples menu with six examples (LAY1 to LAY6). It is suggested that these examples be carefully studied before you work on the following problems. Either English or SI units can be used, so it is suggested that some of these problems be converted to SI units and run with KENLAYER.

3.1 Solve Problem 2-2 by KENLAYER. (*Hint:* Use a two-layer system with two nonlinear layers, the same nonlinear properties, the same ZCNOL for each layer, ITENOL = 2, and RELAX = 1.0). [Answer: 0.0534 in.]

3.2 Solve Problem 2-4 by KENLAYER. [Answer: 0.0251 in., 0.0235 in., 11.4 psi]

3.3 Solve Problem 2-5 by KENLAYER. [Answer: 2.065×10^{-4}, 0.0571 in.]

Downloaded From : www.EasyEngineering.net

Downloaded From : www.EasyEngineering.net

3.4 Solve Problem 2-6 by KENLAYER. [Answer: -7.26×10^{-4}, 1.06×10^{-3}]

3.5 Figure P3.5 shows a three-layer system under a single-wheel load. Layer 1 is linear elastic, layers 2 and 3 nonlinear elastic. The loading, thicknesses, and material properties are shown in the figure. With the use of KENLAYER, determine the maximum tensile strain at the bottom of layer 1 and the maximum compressive strain at the top of layer 3 by (a) method 1 in which layer 2 is subdivided into two layers, each 2 in. thick, and (b) method 2 in which layer 2 is considered as one layer and the stress at the upper quarter point of layer 2 is used to determine E_2. [Answer: (a) 1.02×10^{-4}, 2.85×10^{-4}; (b) 1.04×10^{-4}, 2.85×10^{-4}]

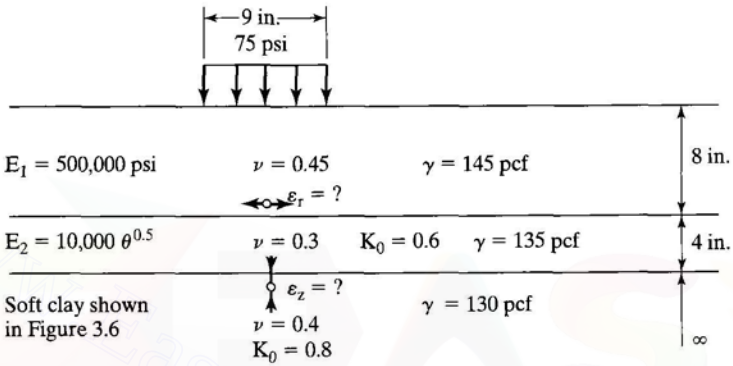


FIGURE P3.5

3.6 Figure P3.6 shows a three-layer system under a set of dual-wheel loads. Layers 1 and 3 are linear elastic, layer 2 nonlinear elastic. The loading, thicknesses, and material properties are shown in the figure. The stresses at the upper quarter of layer 2 between the two wheels are used to evaluate E_2. The maximum tensile strain at the bottom of layer 1 and the maximum compressive strain at the top of layer 3 are determined by comparing the results at three locations: one under the center of one wheel, one under the edge of one wheel, and the other at the center between two wheels. If the actual number of repetitions

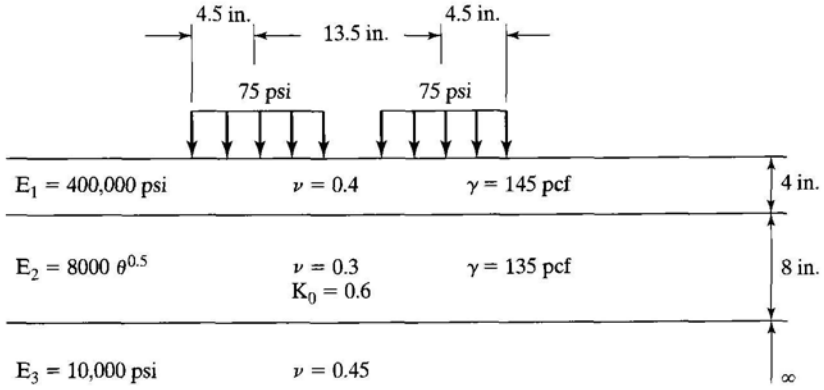


FIGURE P3.6

Downloaded From : www.EasyEngineering.net

Downloaded From : www.EasyEngineering.net

is 100 per day and the Asphalt Institute's failure criteria are used, determine the life of the pavement by KENLAYER. What should be the number of repetitions per day for a design life of 20 years? [Answer: 5.49 years, 27.5 per day]

3.7 Same as Problem 3-6, except that layer 2 is subdivided into four layers, each 2 in. thick, and the stresses at the midheight of each layer are used to determine the modulus of each layer. [Answer: 5.08 years, 25.4 per day]

3.8 For the three-layer system shown in Figure P3.6, predict the modulus of layer 2 via Eq. 3.28. Compare the modulus with that obtained by KENLAYER, using the stress point at the upper quarter of layer 2 between the dual, and determine the three principal stresses at the stress point. [Answer: 28,550 versus 29,560 psi, 14.00 psi, 1.13 psi, −3.08 psi]

3.9 A two-layer system is subjected to a circular load having radius of 6 in. and contact pressure of 75 psi. The thickness of layer 1 is 8 in. Layer 1 is viscoelastic, and layer 2 is elastic, with their stress–strain relationship characterized by the models shown in Figure P3.9. Both layers are incompressible, with Poisson ratio 0.5. If the load is stationary, determine the maximum vertical displacements at 0, 0.01, 0.1, 1, 10, and 100 s by KENLAYER. Check the displacement at 100 s by Figure 2.17. [Answer: 0.0156, 0.0166, 0.0196, 0.0206, 0.0209, 0.0209 in.]

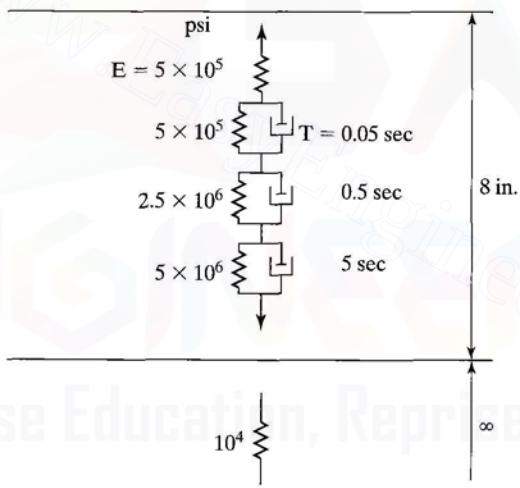


FIGURE P3.9

3.10 If the load in Problem 3-9 is moving with a duration of 0.1 s and the number of load repetitions per year is 100,000, determine the life of the pavement from the Asphalt Institute's failure criteria. [Answer: 21.0 years]

3.11 The pavement system and loading are the same as Example 1 (LAY1) in KENPAVE. Edit file LAY1.DAT via LAYERINP and rename it P311.DAT. What is the design life if the tandem load is repeated 200,000 times per year? Which criterion controls the design life? What percentage of damage is caused by maximum tensile strain at the bottom of asphalt layer (layer 1) and what percentage by the differential tensile strain? [Answer: 19.09 years, 83.2%, 16.8%]

3.12 The pavement system and loading are the same as Example 2 (LAY2), and the load is repeated 1000 times per year. Determine the design life based on permanent deformation by (a) method 1, (b) method 2 with stress point at the upper third, and (c) method 3 with PHI = 40. Review the text file and explain why there is such a large difference in design life among the three methods. [Answer: 1.89, 24.22, 7.75 years]

Downloaded From : www.EasyEngineering.net

Downloaded From : www.EasyEngineering.net

3.13 The pavement system and loading are the same as Example 3 (LAY3). The load is repeated 60,000 times per year. What are the two design lives if the load is moving at durations of 0.1 and 0.2 sec? Run both cases at the same time with NPROB = 2. [Answer: 11.62, 7.54 years]

3.14 The pavement system and loading are the same as Example 6 (LAY6), except that the 8-in. granular layer is subdivided into four 2-in. layers with PHI = 0. [Answer: 25.15 years]

Downloaded From : www.EasyEngineering.net

Downloaded From : www.EasyEngineering.net

CHAPTER 4

Stresses and Deflections in Rigid Pavements

4.1 STRESSES DUE TO CURLING

During the day, when the temperature on the top of the slab is greater than that at the bottom, the top tends to expand with respect to the neutral axis, while the bottom tends to contract. However, the weight of the slab restrains it from expansion and contraction; thus, compressive stresses are induced at the top, tensile stresses at the bottom. At night, when the temperature on the top of the slab is lower than that at the bottom, the top tends to contract with respect to the bottom; thus, tensile stresses are induced at the top and compressive stresses at the bottom.

Another explanation of curling stress can be made in terms of the theory of a plate on a Winkler, or liquid, foundation. A Winkler foundation is characterized by a series of springs attached to the plate, as shown in Figure 4.1. When the temperature on the top is greater than that at the bottom, the top is longer than the bottom and the slab curls downward. The springs at the outside edge are in compression and push the slab up, while the springs in the interior are in tension and pull the slab down. As a result, the top of the slab is in compression and the bottom is in tension. When the temperature on the top is lower than that at the bottom, the slab curls upward. The exterior springs pull the slab down while the interior springs push the slab up, thus resulting in tension at the top and compression at the bottom. Westergaard (1926a) developed equations for determining the curling stress in concrete pavements, based on the plate theory. The equations are very complex and are not presented here.

4.1.1 Bending of Infinite Plate

The difference between a beam and a plate is that the beam is stressed in only one direction, the plate in two directions. For stresses in two directions, the strain ϵ_x in the

Downloaded From : www.EasyEngineering.net

Downloaded From : www.EasyEngineering.net

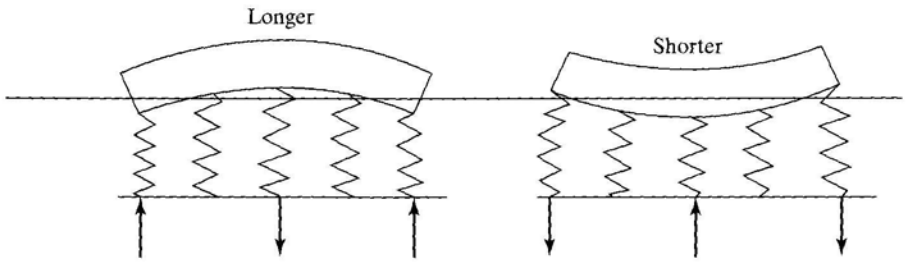


FIGURE 4.1

Curling of slab due to temperature gradient.

x direction can be determined by the generalized Hooke's law,

$$\epsilon_x = \frac{\sigma_x}{E} - v\frac{\sigma_y}{E} \tag{4.1}$$

in which E is the elastic modulus of concrete. In this chapter, when only a Winkler foundation is considered, E is used to denote the elastic modulus of concrete. In later chapters involving plates on a solid foundation, the elastic modulus of concrete is denoted by E_c to distinguish it from the elastic modulus of foundation E_f.

The first term on the right side of Eq. 4.1 indicates the strain in the x direction caused by stress in the x direction; the second term indicates the strain in the x direction caused by stress in the y direction. Similarly,

$$\epsilon_y = \frac{\sigma_y}{E} - v\frac{\sigma_x}{E} \tag{4.2}$$

When the plate is bent in the x direction, ϵ_y should be equal to 0 because the plate is so wide and well restrained that no strain should ever occur unless near the very edge. Setting Eq. 4.2 to 0 yields

$$\sigma_y = v\sigma_x \tag{4.3}$$

Substituting Eq. 4.3 into Eq. 4.1 and solving for σ_x gives

$$\sigma_x = \frac{E\epsilon_x}{1 - v^2} \tag{4.4}$$

Eq. 4.4 indicates the stress in the bending direction, Eq. 4.3 the stress in the direction perpendicular to bending.

When bending occurs in both the x and y directions, as is the case for temperature curling, the stresses in both directions must be superimposed to obtain the total stress. The maximum stress in an infinite slab due to temperature curling can be obtained by assuming that the slab is completely restrained in both x and y directions.

Let Δt be the temperature differential between the top and the bottom of the slab and α_t be the coefficient of thermal expansion of concrete. If the slab is free to

Downloaded From : www.EasyEngineering.net

Downloaded From : www.EasyEngineering.net

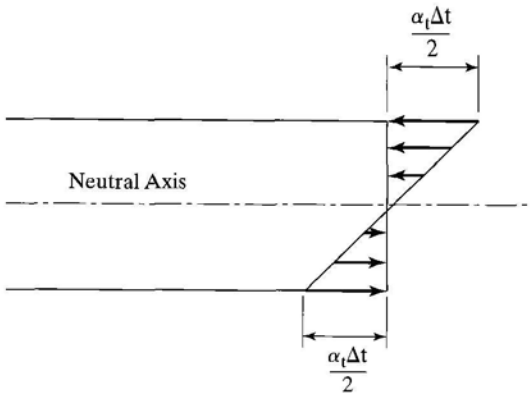


FIGURE 4.2
Temperature gradient in concrete slab.

move and the temperature at the top is greater than that at the bottom, the top will expand by a strain of $\alpha_t \Delta t/2$ and the bottom will contract by the same strain, as shown in Figure 4.2. If the slab is completely restrained and prevented from moving, a compressive strain will result at the top and a tensile strain at the bottom. The maximum strain is

$$\epsilon_x = \epsilon_y = \frac{\alpha_t \Delta t}{2} \tag{4.5}$$

From Eq. 4.4, the stress in the x direction due to bending in the x direction is

$$\sigma_x = \frac{E\alpha_t \Delta t}{2(1 - v^2)} \tag{4.6}$$

Because Eq. 4.6 is also the stress in the y direction due to bending in the y direction, from Eq. 4.3, the stress in the x direction due to bending in the y direction is

$$\sigma_x = \frac{vE\alpha_t \Delta t}{2(1 - v^2)} \tag{4.7}$$

The total stress is the sum of Eqs. 4.6 and 4.7:

$$\sigma_x = \frac{E\alpha_t \Delta t}{2(1 - v^2)}(1 + v) = \frac{E\alpha_t \Delta t}{2(1 - v)} \tag{4.8}$$

The preceding analysis is based on the assumption that the temperature distribution is linear throughout the depth of the slab. This is an approximation, because the actual temperature distribution is nonlinear, as revealed by field measurements in Illinois (Thompson *et al.*, 1987) and in Florida (Richardson and Armaghani, 1987). Numerical methods were developed by Harik *et al.* (1994) for calculating the effect of nonlinear gradient on curling stresses, and a closed-form solution was introduced by Mohamed and Hansen (1997).

Downloaded From : www.EasyEngineering.net

Downloaded From : www.EasyEngineering.net

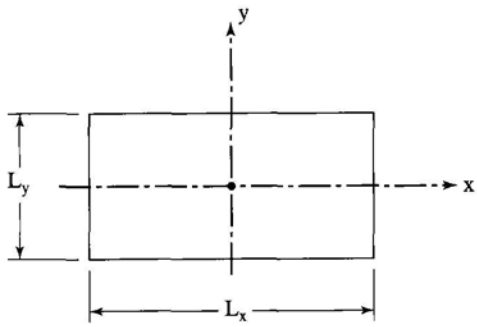


FIGURE 4.3
A finite slab.

4.1.2 Curling Stresses in Finite Slab

Figure 4.3 shows a finite slab with lengths L_x in the x direction and L_y in the y direction. The total stress in the x direction can be expressed as

$$\sigma_x = \frac{C_x E \alpha_t \Delta t}{2(1-v^2)} + \frac{C_y v E \alpha_t \Delta t}{2(1-v^2)} = \frac{E \alpha_t \Delta t}{2(1-v^2)}(C_x + vC_y) \tag{4.9a}$$

in which C_x and C_y are correction factors for a finite slab. The first term in Eq. 4.9*a* is the stress due to bending in the x direction and the second term is the stress due to bending in the y direction. Similarly, the stress in the y direction is

$$\sigma_y = \frac{E \alpha_t \Delta t}{2(1-v^2)}(C_y + vC_x) \tag{4.9b}$$

Using Westergaard's analysis, Bradbury (1938) developed a simple chart for determining C_x and C_y, as shown in Figure 4.4. The correction factor C_x depends on L_x/ℓ

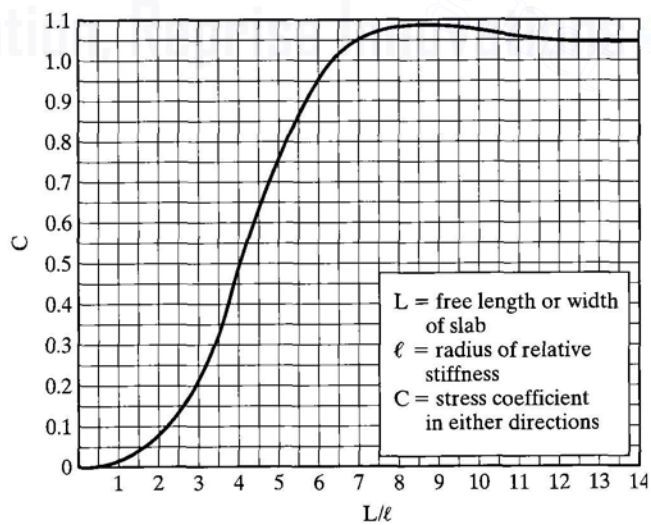


FIGURE 4.4
Stress correction factor for finite slab. (After Bradbury (1938).)

Downloaded From : www.EasyEngineering.net

Downloaded From : www.EasyEngineering.net

and the correction factor C_y depends on L_y/ℓ, where ℓ is the radius of relative stiffness, defined as

$$\ell = \left[\frac{Eh^3}{12(1 - v^2)k}\right]^{0.25} \tag{4.10}$$

in which E is the modulus of elasticity of concrete, h is the thickness of the slab, v is Poisson ratio of concrete, and k is the modulus of subgrade reaction.

In all the examples presented in this chapter, a modulus of 4×10^6 psi (27.6 GPa) and a Poisson ratio of 0.15 are assumed for the concrete. Equation 4.9 gives the maximum interior stress at the center of a slab. The edge stress at the midspan of the slab can be determined by

$$\sigma = \frac{CE\alpha_t \Delta t}{2} \tag{4.11}$$

in which σ may be σ_x or σ_y depending on whether C is C_x or C_y. Note that Eq. 4.11 is the same as Eq. 4.9 when the Poisson ratio at the edge is taken as 0.

It can be seen from Figure 4.4 that the correction factor C increases as the ratio L/ℓ increases, having a value of $C = 1.0$ for $L = 6.7\ell$, reaching a maximum value of 1.084 for $L = 8.5\ell$, and then decreasing to 1 as L/ℓ approaches infinity. That the coefficient C can have a value greater than unity may be explained by the fact that in slabs longer than about 6.7ℓ the subgrade reaction actually reverses slightly the curvature that temperature curling tends to produce. However, this additional effect is relatively minor; the increase in stress is no more than 8.4% compared with that based on the assumption of zero curvature.

Example 4.1:

Figure 4.5 shows a concrete slab, 25 ft (7.62 m) long, 12 ft (3.66 m) wide, and 8 in. (203 mm) thick, subjected to a temperature differential of 20°F (11.1°C). Assuming that $k = 200$ pci (54.2 MN/m^3) and $\alpha_t = 5 \times 10^{-6}$ in./in./°F (9×10^{-6} mm/mm/°C), determine the maximum curling stress in the interior and at the edge of the slab.

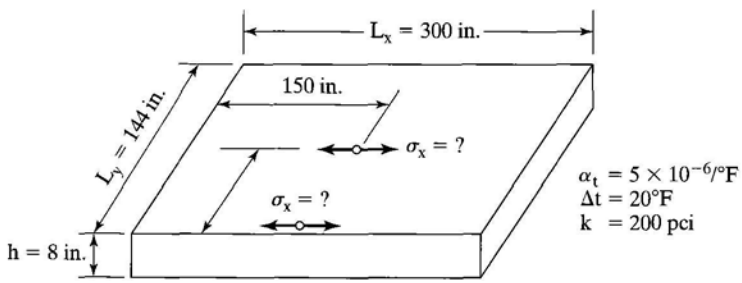


FIGURE 4.5

Example 4.1 (1 in. = 25.4 mm, 1 pci = 271.3 kN/m^3).

Downloaded From : www.EasyEngineering.net

Downloaded From : www.EasyEngineering.net

Solution: From Eq. 4.10, $\ell = [4 \times 10^6 \times 512/(12 \times 0.9775 \times 200)]^{0.25} = 30.57$ in. (776 mm). With $L_x/\ell = 25 \times 12/30.57 = 9.81$ and $L_y/\ell = 12 \times 12/30.57 = 4.71$, from Figure 4.4, $C_x = 1.07$ and $C_y = 0.63$. From Eq. 4.9*a*, the maximum stress in the interior is in the x direction, or $\sigma_x = 4 \times 10^6 \times 5 \times 10^{-6} \times 20(1.07 + 0.15 \times 0.63)/1.955 = 238$ psi (1.64 MPa). From Eq. 4.11, the maximum stress at an edge is also in the x direction, or $\sigma_x = 1.07 \times 4 \times 10^6 \times 5 \times 10^{-6} \times 20/2 = 214$ psi (1.48 MPa).

4.1.3 Temperature Differentials

Curling stresses in concrete pavements vary with the temperature differentials between the top and bottom of a slab. Unless actual field measurements are made, it is reasonable to assume a maximum temperature gradient of 2.5 to 3.5°F per inch of slab (0.055 to 0.077°C/mm) during the day and about half the above values at night.

In the Arlington Road Test, the maximum temperature differentials between the top and bottom surfaces of slabs were measured during the months of April and May, when there was probably as much curling as at any time during the year (Teller and Sutherland, 1935–1943). If the largest five measurements were averaged, the maximum temperature differential of a 6-in. (152-mm) slab was 22°F (12.2°C) and that of a 9-in. (229-mm) slab was 31°F (17.2°C); these values correspond to temperature gradients of 3.7°F/in. (0.080°C/mm) and 3.4°F/in. (0.074°C/mm), respectively.

In the AASHO Road Test (HRB, 1962), temperatures were measured in a 6.5-in. (165-mm) slab. The temperature at a point 0.25 in. (6.4 mm) below the top surface of the 6.5-in. (165-mm) slab minus the temperature at a point 0.5 in. (12.7 mm) above the bottom surface was referred to as the standard temperature differential. The maximum standard temperature differential for the months of June and July averaged about 18.5°F (10.2°C) when the slab curled down and −8.8°F (−4.9°C) when it curled up; these values correspond to temperature gradients of 3.2°F/in. (0.07°C/mm) and 1.5°F/in. (0.03°C/mm), respectively. Temperature measurements in slabs of other thicknesses at the AASHO test site also showed that the temperature differential was not proportional to the thickness of slab and that the increase in temperature differential was not as rapid as the increase in thickness. Therefore, greater temperature gradients should be used for thinner slabs.

4.1.4 Combined Stresses

Even though curling stresses can be quite large and can cause concrete to crack when combined with loading stresses, they are usually not considered in the thickness design for the following reasons:

1. Joints and steel are used to relieve and take care of curling stresses. Curling stresses are relieved when the concrete cracks. Minute cracks will not affect the load-carrying capacity of pavements as long as the load transfer across cracks can be maintained.
2. When the fatigue principle is used for design, it is not practical to combine loading and curling stresses. A pavement might be subjected to millions of load repetitions during the design period, but the number of stress reversals due to curling is quite limited.

Downloaded From : www.EasyEngineering.net

Downloaded From : www.EasyEngineering.net

3. Curling stresses may be added to or subtracted from loading stresses to obtain the combined stresses. If the design is governed by the edge stress, curling stresses should be added to loading stresses during the day but subtracted from the loading stresses at night. Due to this compensative effect and the fact that a large number of heavy trucks are driven at night, it may not be critical if curling stresses are ignored.

Whether the curling stress should be considered in pavement design is quite controversial. The Portland Cement Association does not consider curling stress in fatigue analysis, but many others indicate that it should be considered. Past experience has demonstrated that more cracks appear in longer slabs because longer slabs have much greater curling stress than shorter slabs. The nontraffic loop in the AASHO site did not have any cracks during the road test. However, when the site was surveyed after 16 years most of the 40-ft (12.2-m) long slabs had cracks, but not the 15-ft (4.6-m) slabs (Darter and Barenberg, 1977).

In designing zero-maintenance jointed plain concrete pavements, Darter and Barenberg (1977) suggested the inclusion of curling stress with loading stress for fatigue analysis. This is necessary because curling stresses are so large that, when combined with the loading stresses, they might cause the concrete to crack even under a few repetitions. The cracking of the slab will require proper maintenance, thus defeating the zero-maintenance concept. If curling stresses are really so important, it is more reasonable to consider the fatigue damage due to loading and curling separately and then combined, similar to the analysis of thermal cracking in flexible pavements described in Section 11.1.4.

The moisture gradient in concrete slabs also induces warping stresses. Determining the moisture gradient is difficult because it depends on a variety of factors, such as the ambient relative humidity at the surface, the free water in the concrete, and the moisture content of the subbase or subgrade. The moisture content at the top of a slab is generally lower than that at the bottom, so the bottom of a slab is in compression, which compensates for the tensile stresses caused by edge loading. Furthermore, the moisture effect is seasonal and remains constant for a long time, thus resulting in very few stress reversals and very low fatigue damage. For this reason, warping stresses due to moisture gradient are not considered in the design of concrete pavements.

4.2 STRESSES AND DEFLECTIONS DUE TO LOADING

Three methods can be used to determine the stresses and deflections in concrete pavements: closed-form formulas, influence charts, and finite-element computer programs. The formulas originally developed by Westergaard can be applied only to a single-wheel load with a circular, semicircular, elliptical, or semielliptical contact area. The influence charts developed by Pickett and Ray (1951) can be applied to multiple-wheel loads of any configuration. Both methods are applicable only to a large slab on a liquid foundation. If the loads are applied to multiple slabs on a liquid, solid, or layer foundation with load transfer across the joints, the finite-element method should be used. The liquid foundation assumes the subgrade to be a set of independent springs. Deflection at any given point is proportional to the force at that point and independent of the forces at all other points. This assumption is unrealistic and does not represent soil behaviors. Due to its simplicity, it was used in Westergaard's analysis. However, with

Downloaded From : www.EasyEngineering.net

Downloaded From : www.EasyEngineering.net

the ever-increasing speed and storage of personal computers, it is no longer necessary to assume the foundation to be a liquid with a fictitious k value. The more realistic solid or layer foundation can be used. The KENSLABS computer program based on the finite-element method and the various types of foundations are presented in Chapter 5.

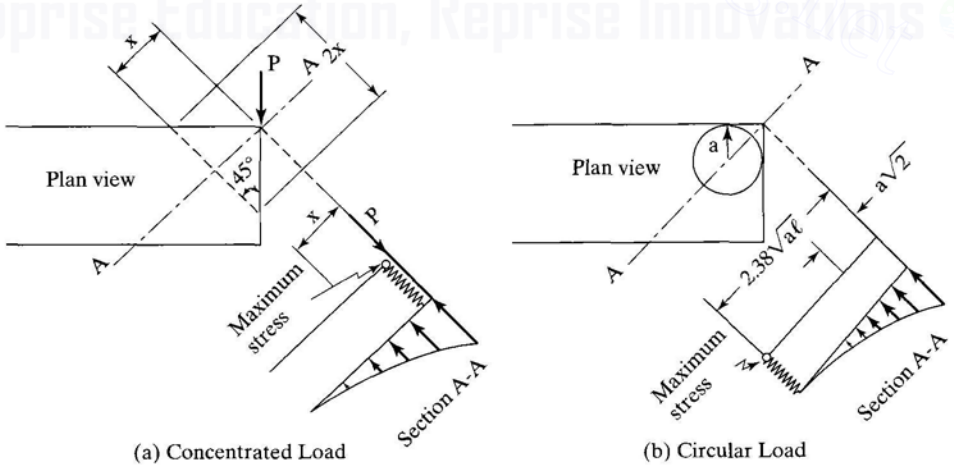
4.2.1 Closed-Form Formulas

These formulas are applicable only to a very large slab with a single-wheel load applied near the corner, in the interior of a slab at a considerable distance from any edge, and near the edge far from any corner.

Corner Loading The Goldbeck (1919) and Older (1924) formula is the earliest one for use in concrete pavement design. The formula is based on a concentrated load P applied at the slab corner, as shown in Figure 4.6*a*. When a load is applied at the corner, the stress in the slab is symmetrical with respect to the diagonal. For a cross section at a distance x from the corner, the bending moment is Px and the width of section is $2x$. When the subgrade support is neglected and the slab is considered as a cantilever beam, the tensile stress on top of the slab is

$$\sigma_c = \frac{Px}{\frac{1}{6}(2x)\,h^2} = \frac{3P}{h^2} \tag{4.12}$$

in which σ_c is the stress due to corner loading, P is the concentrated load, and h is the thickness of the slab. Note that σ_c is independent of x. In other words, every cross section, no matter how far from the corner, will have the same stress, as indicated by Eq. 4.12. If the load is really a concentrated load applied at the very corner, Eq. 4.12 is an exact solution, because, at a cross section near to the load, with x approaching 0, the subgrade reaction is very small and can be neglected.



(a) Concentrated Load (b) Circular Load

FIGURE 4.6

A slab subjected to corner load.

Downloaded From : www.EasyEngineering.net

Downloaded From : www.EasyEngineering.net

Figure 4.6*b* shows a circular load applied near the corner of a slab. Because the section of maximum stress is not near the corner, the total subgrade reactive force is quite large and cannot be neglected. Westergaard (1926b) applied a method of successive approximations and obtained the formulas

$$\sigma_c = \frac{3P}{h^2}\left[1 - \left(\frac{a\sqrt{2}}{\ell}\right)^{0.6}\right] \tag{4.13}$$

and

$$\Delta_c = \frac{P}{k\ell^2}\left[1.1 - 0.88\left(\frac{a\sqrt{2}}{\ell}\right)\right] \tag{4.14}$$

in which Δ_c is the corner deflection, ℓ is the radius of relative stiffness, a is the contact radius, and k is the modulus of subgrade reaction. He also found that the maximum moment occurs at a distance of $2.38\sqrt{a\ell}$ from the corner. For a concentrated load with $a = 0$, Eqs. 4.13 and 4.12 are identical.

Ioannides *et al.* (1985) applied the finite-element method to evaluate Westergaard's solutions. They suggested the use of the relationships

$$\sigma_c = \frac{3P}{h^2}\left[1 - \left(\frac{c}{\ell}\right)^{0.72}\right] \tag{4.15}$$

and

$$\Delta_c = \frac{P}{k\ell^2}\left[1.205 - 0.69\left(\frac{c}{\ell}\right)\right] \tag{4.16}$$

in which c is the side length of a square contact area. They found that the maximum moment occurs at a distance of $1.80c^{0.32}\ell^{0.59}$ from the corner. If a load is applied over a circular area, the value of c must be selected so that the square and the circle have the same contact area:

$$c = 1.772a \tag{4.17}$$

Example 4.2:

Figure 4.7 shows a concrete slab subjected to a corner loading. Given $k = 100$ pci (27.2 MN/m^3), $h = 10$ in. (254 mm), $a = 6$ in. (152 mm), and $P = 10{,}000$ lb (44.5 kN), determine the maximum stress and deflection due to corner loading by Eqs. 4.13 through 4.16.

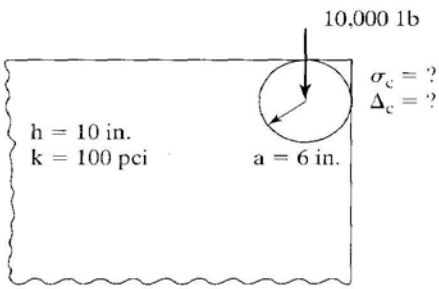


FIGURE 4.7

Example 4.2 (1 in. = 25.4 mm, 1 *lb* = 4.45 N, 1 pci = 271.3 kN/m^3).

Downloaded From : www.EasyEngineering.net

Downloaded From : www.EasyEngineering.net

Solution: From Eq. 4.10, $\ell = [4 \times 10^6 \times 1000/(12 \times 0.9775 \times 100)]^{0.25} = 42.97$ in. (1.09 m). From Eq. 4.13, $\sigma_c = 3 \times 10{,}000/100 \times [1 - (6\sqrt{2}/42.97)^{0.6}] = 186.6$ psi (1.29 MPa). From Eq. 4.14, $\Delta_c = 10{,}000/(100 \times 1846.4)[1.1 - 0.88(6\sqrt{2}/42.97)] = 0.0502$ in. (1.27 mm). From Eqs. 4.15 and 4.17, $\sigma_c = 3 \times 10{,}000/100[1 - (1.772 \times 6/42.97)^{0.72}] = 190.3$ psi (1.31 MPa), which is 2% larger than the value obtained from Eq. 4.13. From Eqs. 4.16 and 4.17, $\Delta_c = 10{,}000/(100 \times 1846.4)[1.205 - 0.69(1.772 \times 6/42.97)] = 0.0560$ in. (1.42 mm), which is 11% greater than the value obtained from Eq. 4.14.

Interior Loading The earliest formula developed by Westergaard (1926b) for the stress in the interior of a slab under a circular loaded area of radius a is

$$\sigma_i = \frac{3(1+v)P}{2\pi h^2}\left(\ln\frac{\ell}{b} + 0.6159\right) \tag{4.18}$$

in which ℓ is the radius of relative stiffness and

$$b = a \qquad \text{when } a \geq 1.724h \tag{4.19a}$$

$$b = \sqrt{1.6a^2 + h^2} - 0.675h \qquad \text{when } a < 1.724h \tag{4.19b}$$

For a Poisson ratio of 0.15 and in terms of base-10 logarithms, Eq. 4.18 can be written as

$$\sigma_i = \frac{0.316P}{h^2}\left[4\log\left(\frac{\ell}{b}\right) + 1.069\right] \tag{4.20}$$

The deflection equation due to interior loading (Westergaard, 1939) is

$$\Delta_i = \frac{P}{8k\ell^2}\left\{1 + \frac{1}{2\pi}\left[\ln\left(\frac{a}{2\ell}\right) - 0.673\right]\left(\frac{a}{\ell}\right)^2\right\} \tag{4.21}$$

Example 4.3:

Same as Example 4.2 except that the load is applied in the interior, as shown in Figure 4.8. Determine the maximum stress and deflection due to interior loading.

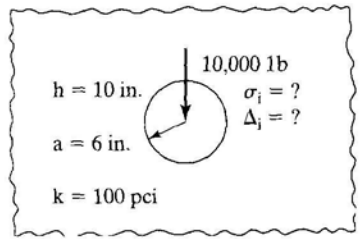


FIGURE 4.8

Example 4.3 (1 in. = 25.4 mm, 1 lb = 4.45 N, 1 pci = 271.3 kN/m^3).

Downloaded From : www.EasyEngineering.net

Downloaded From : www.EasyEngineering.net

Solution: From Eq. 4.19*b*, $b = \sqrt{1.6 \times 36 + 100} - 0.675 \times 10 = 5.804$ in. (147 mm). From Eq. 4.20, $\sigma_i = 0.316 \times 10{,}000/100 \times [4 \log(42.97/5.804) + 1.069] = 143.7$ psi (992 kPa). The same result is obtained if Eq. 4.18 is used. From Eq. 4.21, $\Delta_i = 10{,}000/(8 \times 100 \times 1846.1)\{1 + (1/2\pi) \times [\ln(6/85.94) - 0.673] \times (6/42.97)^2\} = 0.0067$ in. (0.17 mm). Compared with the Westergaard solutions due to corner loading, the stress due to interior loading is 77% of that due to corner loading, while the deflection is only 13%. This is true only when there is no load transfer across the joint at the corner. If sufficient load transfer is provided, the stress due to corner loading will be smaller than that due to interior loading but the deflection at the corner will still be greater.

Edge Loading The stress due to edge loading was presented by Westergaard (1926b, 1933, 1948) in several different papers. In his 1948 paper, he presented generalized solutions for maximum stress and deflection produced by elliptical and semielliptical areas placed at the slab edge. Setting the length of both major and minor semiaxes of the ellipse to the contact radius a leads to the corresponding solutions for a circular or semicircular loaded area. In the case of a semicircle, its straight edge is in line with the edge of the slab. The results obtained from these new formulas differ significantly from those of the previous formulas. According to Ioannides *et al.* (1985), the following equations are the correct ones to use:

$$\sigma_{e\,(\text{circle})} = \frac{3(1+\nu)P}{\pi(3+\nu)h^2}\left[\ln\left(\frac{Eh^3}{100ka^4}\right) + 1.84 - \frac{4\nu}{3} + \frac{1-\nu}{2} + \frac{1.18(1+2\nu)a}{\ell}\right] \tag{4.22}$$

$$\sigma_{e\,(\text{semicircle})} = \frac{3(1+\nu)P}{\pi(3+\nu)h^2}\left[\ln\left(\frac{Eh^3}{100ka^4}\right) + 3.84 - \frac{4\nu}{3} + \frac{(1+2\nu)a}{2\ell}\right] \tag{4.23}$$

$$\Delta_{e\,(\text{circle})} = \frac{\sqrt{2+1.2\nu}P}{\sqrt{Eh^3k}}\left[1 - \frac{(0.76+0.4\nu)a}{\ell}\right] \tag{4.24}$$

$$\Delta_{e\,(\text{semicircle})} = \frac{\sqrt{2+1.2\nu}P}{\sqrt{Eh^3k}}\left[1 - \frac{(0.323+0.17\nu)a}{\ell}\right] \tag{4.25}$$

For $\nu = 0.15$, Eqs. 4.22 to 4.25 can be written as

$$\sigma_{e\,(\text{circle})} = \frac{0.803P}{h^2}\left[4\log\left(\frac{\ell}{a}\right) + 0.666\left(\frac{a}{\ell}\right) - 0.034\right] \tag{4.26}$$

$$\sigma_{e\,(\text{semicircle})} = \frac{0.803P}{h^2}\left[4\log\left(\frac{\ell}{a}\right) + 0.282\left(\frac{a}{\ell}\right) + 0.650\right] \tag{4.27}$$

$$\Delta_{e\,(\text{circle})} = \frac{0.431P}{k\ell^2}\left[1 - 0.82\left(\frac{a}{\ell}\right)\right] \tag{4.28}$$

$$\Delta_{e\,(\text{semicircle})} = \frac{0.431P}{k\ell^2}\left[1 - 0.349\left(\frac{a}{\ell}\right)\right] \tag{4.29}$$

A recent search of the archives at the Waterways Experiment Station revealed that, shortly before his untimely death in 1950, Westergaard had submitted a report to

Downloaded From : www.EasyEngineering.net

Downloaded From : www.EasyEngineering.net

the Corps of Engineers (authored by Skarlatos (1949), under Westergaard's supervision) in which an analytical solution of edge-load transfer was developed. This solution was neither widely disseminated nor put into practical use. With the help of modern computational tools, loannides and Hammons (1996) derived closed-form formulas of maximum stress and deflections on the unloaded side of slab, akin to those on the free edge, thus constituting a complete solution of the edge-load transfer problem.

Example 4.4:

Same as Example 4.2, except that the load is applied to the slab edge, as shown in Figure 4.9. Determine the maximum stress and deflection under both circular and semicircular loaded areas.

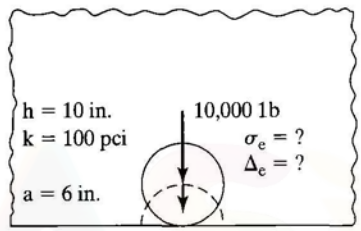


FIGURE 4.9

Example 4.4 (1 in. = 25.4 mm, 1 lb = 4.45 N, 1 pci = 271.3 kN/m^3).

Solution: For a circular area, from Eq. 4.26, $\sigma_e = 0.803 \times 10{,}000/100 \times [4 \log(42.97/6) + 0.666(6/42.97) - 0.034] = 279.4$ psi (1.93 MPa); from Eq. 4.28, $\Delta_e = 0.431 \times 10{,}000/(100 \times 1846.4) \times [1 - 0.82(6/42.97)] = 0.0207$ in. (0.525 mm). For a semicircular area, from Eq. 4.27, $\sigma_e = 0.803 \times 10{,}000/100 \times [4 \log(42.97/6) + 0.282(6/42.97) + 0.650] = 330.0$ psi (2.28 MPa); from Eq. 4.29, $\Delta_e = 0.431 \times 10{,}000/(100 \times 1846.4) \times [1 - 0.349(6/42.97)] = 0.0222$ in. (0.564 mm). It can be seen that the maximum stress due to edge loading is greater than that due to corner and interior loadings and that the maximum deflection due to edge loading is greater than that due to interior loading but much smaller than that due to corner loading. The fact that both the stress and deflection are greater under a semicircular loaded area than those under a circular area is reasonable: The centroid of a semicircle is closer to the pavement edge than is that of a circle.

Dual Tires With the exception of Eqs. 4.23, 4.25, 4.27, and 4.29 for a semicircular loaded area, all of the closed-form formulas presented so far are based on a circular loaded area. When a load is applied over a set of dual tires, it is necessary to convert it into a circular area, so that the equations based on a circular loaded area can be applied. If the total load is the same but the contact area of the circle is equal to that of the duals, as has been frequently assumed for flexible pavements, the resulting stresses and deflection will be too large. Therefore, for a given total load, a much larger circular area should be used for rigid pavements.

Figure 4.10 shows a set of dual tires. It has been found that satisfactory results can be obtained if the circle has an area equal to the contact area of the duals plus the area between the duals, as indicated by the hatched area shown in the figure. If P_d is the load on one tire and q is the contact pressure, the area of each tire is

$$\frac{P_d}{q} = \pi(0.3L)^2 + (0.4L)(0.6L) = 0.5227L^2$$

Downloaded From : www.EasyEngineering.net

Downloaded From : www.EasyEngineering.net

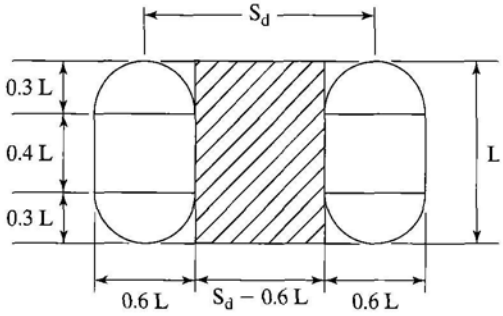


FIGURE 4.10
Method for converting duals into a circular area.

or

$$L = \sqrt{\frac{P_d}{0.5227q}} \tag{4.30}$$

The area of an equivalent circle is

$$\pi a^2 = 2 \times 0.5227L^2 + (S_d - 0.6L)L = 0.4454L^2 + S_dL$$

Substituting L from Eq. 4.30 yields

$$\pi a^2 = \frac{0.8521P_d}{q} + S_d\sqrt{\frac{P_d}{0.5227q}}$$

So the radius of contact area is

$$a = \sqrt{\frac{0.8521P_d}{q\pi} + \frac{S_d}{\pi}\left(\frac{P_d}{0.5227q}\right)^{1/2}} \tag{4.31}$$

Example 4.5:

Using Westergaard's formulas, determine the maximum stress in Examples 4.2, 4.3, and 4.4 if the 10,000-lb (44.5-kN) load is applied on a set of duals spaced at 14 in. (356 mm) on centers, as shown in Figure 4.11, instead of over a 6-in. (152-mm) circular area.

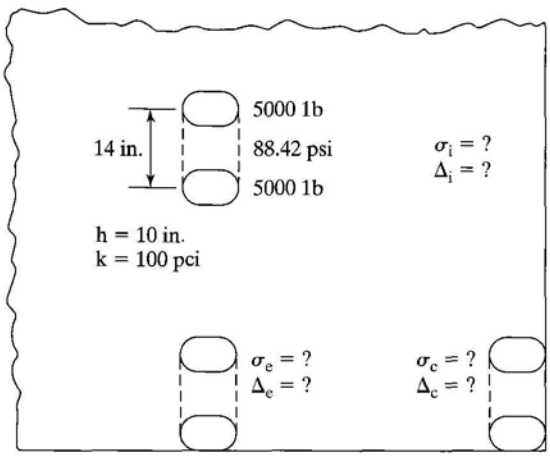


FIGURE 4.11
Example 4.5 (1 in. = 25.4 mm, 1 lb = 4.45 N, 1 pci = 271.3 kN/m^3).

Downloaded From : www.EasyEngineering.net

Downloaded From : www.EasyEngineering.net

Solution: With S_d = 14 in. (356 mm), q = 10,000/(36π) = 88.42 psi (610 kPa), and P_d = 5000 lb (22.3 kN), from Eq. 4.31,

$$a = \sqrt{\frac{0.8521 \times 5000}{88.42\pi} + \frac{14}{\pi}\left(\frac{5000}{0.5227 \times 88.42}\right)^{1/2}} = 7.85 \text{ in. (199 mm)}$$

which is greater than the original 6 in. (152 mm). From Eq. 4.13, $\sigma_c = 3 \times 10{,}000/100 \times [1 - (7.85\sqrt{2}/42.97)^{0.6}] = 166.8$ psi (1.15 MPa), which is about 89% of the stress in Example 4.2. From Eq. 4.19*b*, $b = \sqrt{1.6 \times 61.62 + 100} - 0.675 \times 10 = 7.34$ in. (186 mm). From Eq. 4.20, $\sigma_i = 0.316 \times 10{,}000/100 \times [4 \log(42.97/7.34) + 1.069] = 130.8$ psi (902 kPa), which is about 91% of the stress in Example 4.3. From Eq. 4.26, $\sigma_e = 0.803 \times 10{,}000/100 \times [4 \log(42.97/7.85) + 0.666(7.85/42.97) - 0.034] = 244.2$ psi (1.68 MPa), which is about 87% of the stress in Example 4.4.

4.2.2 Influence Charts

Influence charts based on liquid foundations (Pickett and Ray, 1951) were used previously by the Portland Cement Association for rigid pavement design. The charts are based on Westergaard's theory with a Poisson ratio of 0.15 for the concrete slab. Only charts for interior and edge loadings are available, the interior loading being used for the design of airport pavements (PCA, 1955) and the edge loading for the design of highway pavements (PCA, 1966).

Interior Loading Figure 4.12 shows the applications of influence charts for determining the moment at the interior of slab. The moment is at point O in the n direction. To use the chart, it is necessary to determine the radius of relative stiffness ℓ according to Eq. 4.10. For example, if ℓ is 57.1 in. (1.45 m), the scale on the top of Figure 4.12 is 57.1 in. (1.45 m). This scale should be used to draw the configuration of the contact area. If the actual length of tire imprint is 22.6 in. (574 mm), the length to be drawn on the influence chart is 22.6/57.1 or 39.6% of the length shown by the scale ℓ. The location of other tires is based on the same scale. By counting the number of blocks N covered by the tire imprints, the moment in the n direction M can be determined from

$$M = \frac{q\ell^2 N}{10{,}000} \tag{4.32a}$$

in which q is the contact pressure. The stress is determined by dividing the moment by the section modulus:

$$\sigma_i = \frac{6M}{h^2} \tag{4.32b}$$

For the tire imprints shown in Figure 4.12, the moment is under the center of the lower left tire in the lateral direction. If the moment in the longitudinal direction is desired, the tire assembly must rotate 90° clockwise so that two of the tires lie in the zone of negative blocks, and the moment becomes much smaller.

Figure 4.13 shows the influence chart for deflection due to interior loading. The chart is axisymmetric, and the blocks are formed by concentric circles and radial lines.

Downloaded From : www.EasyEngineering.net

Downloaded From : www.EasyEngineering.net

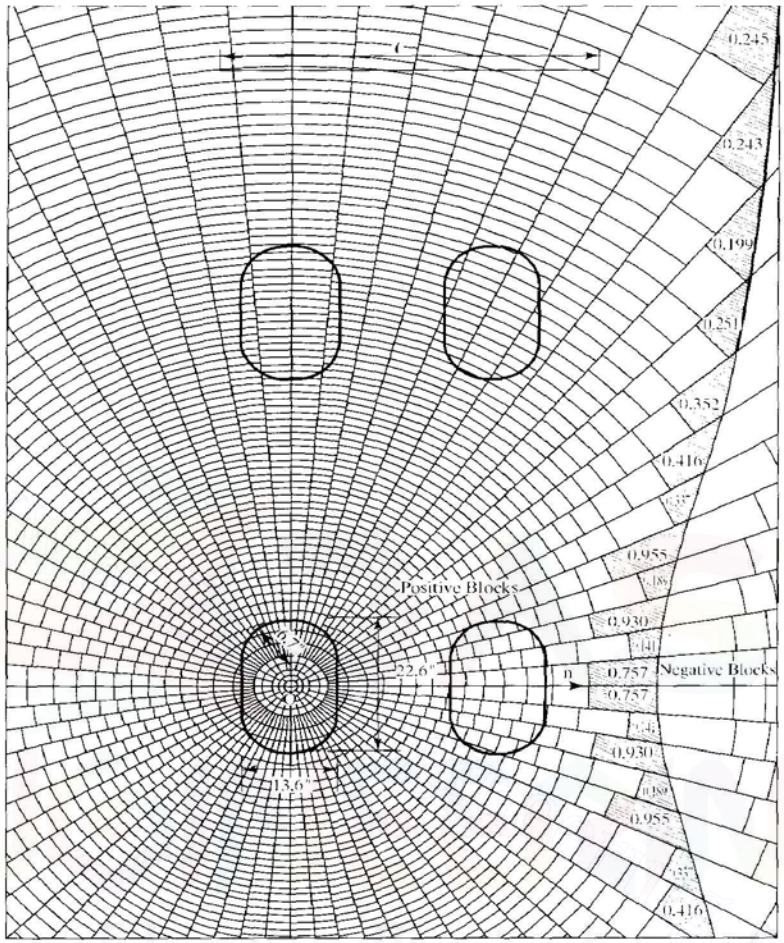


FIGURE 4.12

Application of influence chart for determining moment (1 in. = 25.4 mm). (After Pickett and Ray (1951).)

The deflection is at the center of the circles. The use of the chart is similar to that of Figure 4.12. After the number of blocks covered by the tire imprint are counted, the deflection can be determined as

$$\Delta_i = \frac{0.0005 q \ell^4 N}{D} \tag{4.33}$$

in which D is the modulus of rigidity:

$$D = \frac{Eh^3}{12(1 - \nu^2)} \tag{4.34}$$

Downloaded From : www.EasyEngineering.net

Downloaded From : www.EasyEngineering.net

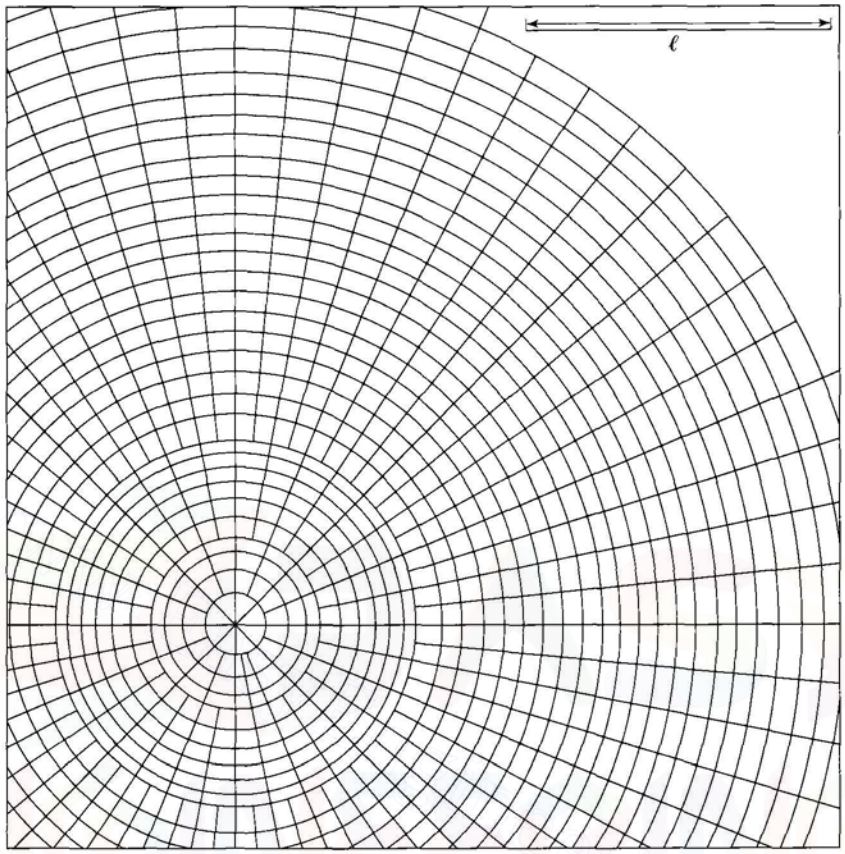


FIGURE 4.13

Influence chart for deflection due to interior loading. (After Pickett and Ray (1951).)

Example 4.6:

Same as Example 4.3. Determine the maximum stress and deflection due to interior loading by the influence charts shown in Figures 4.13 and 4.14.

Solution: With $\ell = 42.97$ in. (1.09 m); the scale at the top of Figure 4.14 is 42.97 in. (1.09 m). The radius of contact area $a = 6$ in. (152 mm), or $a/\ell = 6/42.97 = 0.14$. The number of blocks covered by a circle with center at 0 and a radius equal to 0.14ℓ is 148 and can be found from Figure 4.14. From symmetry, only the blocks within one-quarter of the circle need be counted and the result is then multiplied by 4. With $q = 10{,}000/(\pi \times 36) = 88.42$ psi (610 kPa), from Eq. 4.32*a*, $M = 88.42 \times (42.97)^2 \times 148/10{,}000 = 2416$ in.-lb/in. (10.8 m-kN/m), and from Eq. 4.32*b*, $\sigma_i = 6 \times 2416/100 = 145.0$ psi (1.0 MPa), which checks with the 143.7 psi (992 kPa) obtained in Example 4.3. The number of blocks for deflection is 16 and can be found from Figure 4.13. From Eq. 4.34, $D = 4 \times 10^6 \times 10^3/(12 \times 0.9775) = 3.41 \times 10^8$ in.-lb (38.5 m-MN). From Eq. 4.33, $\Delta_i = 0.0005 \times 88.42 \times (42.97)^4 \times 16/(3.41 \times 10^8) = 0.0071$ in. (0.18 mm), which checks with the 0.0067 in. (0.17 mm) obtained in Example 4.3.

Downloaded From : www.EasyEngineering.net

Downloaded From : www.EasyEngineering.net

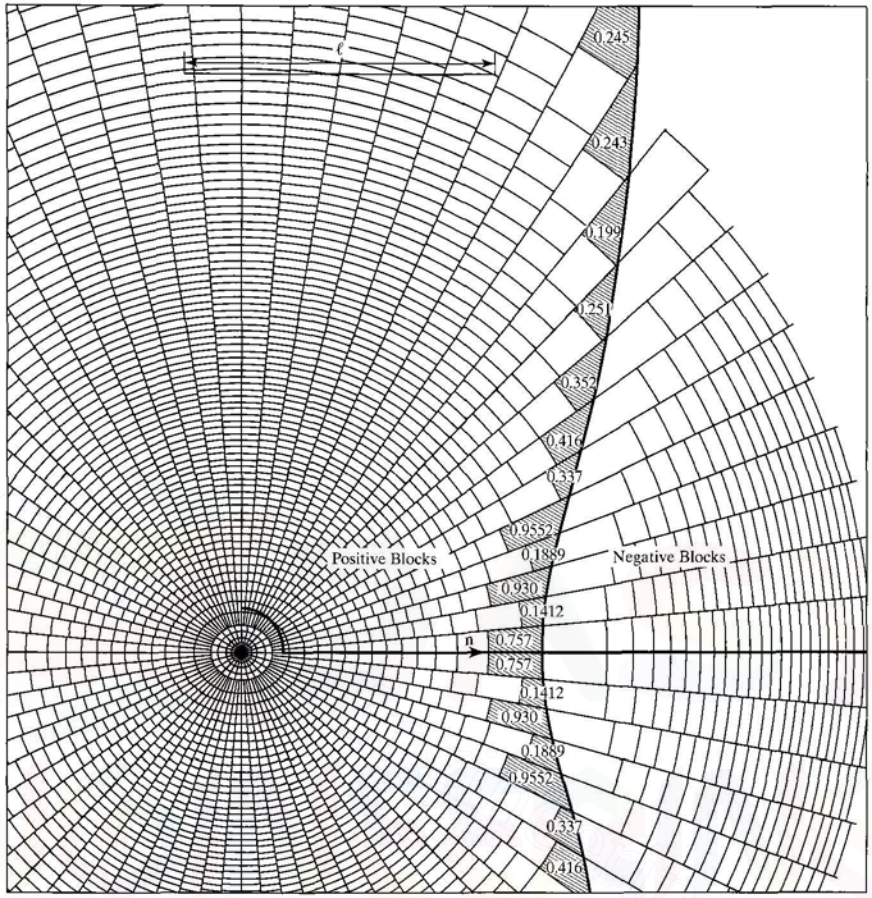


FIGURE 4.14
Influence chart for moment due to interior loading. (After Pickett and Ray (1951).)

Edge Loading Figures 4.15 and 4.16 show the influence charts for moment and deflection at point O on the edge of slab. The use of the charts is similar to the case of interior loading and the same formulas, Eqs. 4.32 to 4.34, apply.

Example 4.7:

Same as Example 4.4. Determine the maximum stress and deflection due to the circular loaded area tangent to the pavement edge.

Solution: By drawing a circle tangent to the edge at point O with a radius of 0.14ℓ, the number of blocks is 282 for moment and 46 for deflection. Because the stress and deflection are proportional to N, from Example 4.6, $\sigma_e = 145.0 \times 282/148 = 276.3$ psi (1.91 MPa), which checks with the 279.4 psi (1.93 MPa) obtained in Example 4.4, and $\Delta_e = 0.0071 \times 46/16 = 0.0204$ in. (0.518 mm), which checks with the 0.0207 in. (0.525 mm) in Example 4.4.

Downloaded From : www.EasyEngineering.net

Downloaded From : www.EasyEngineering.net

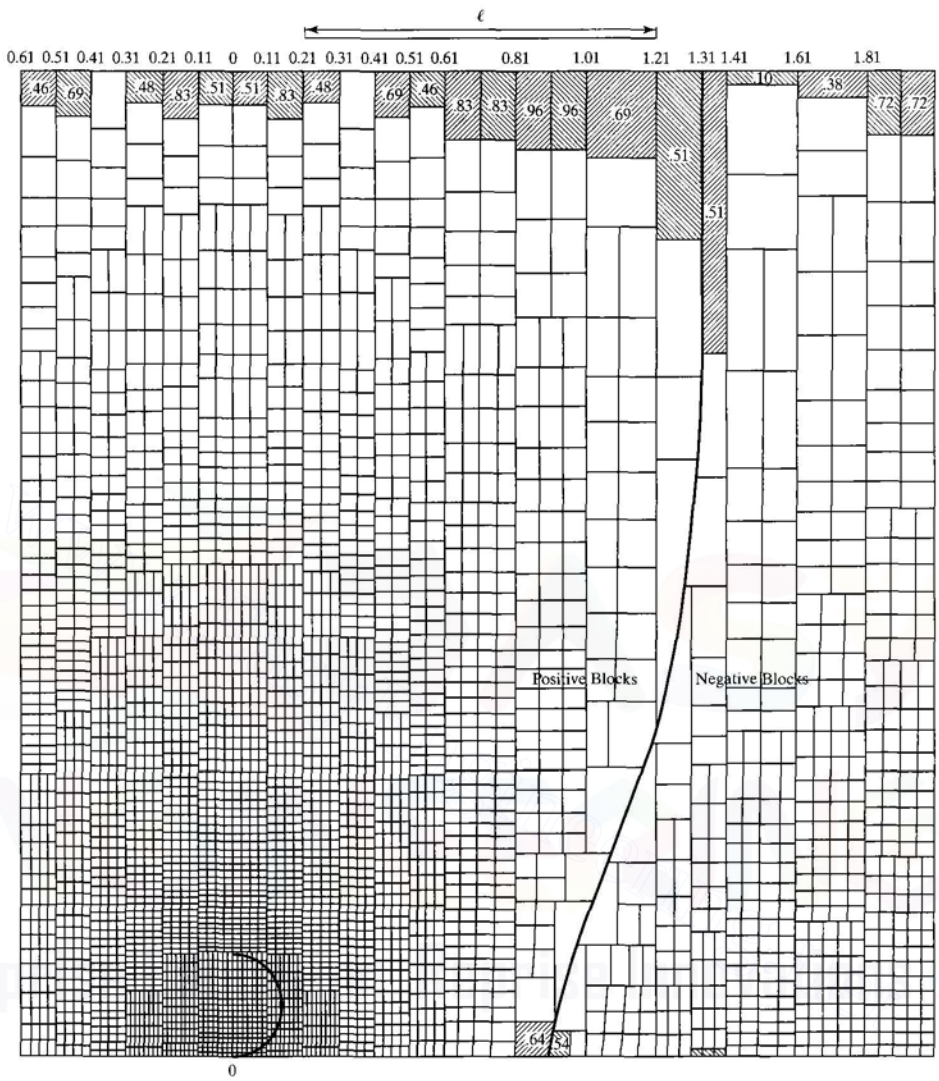


FIGURE 4.15

Influence chart for moment due to edge loading. (After Pickett and Ray (1951).)

4.3 STRESSES DUE TO FRICTION

The friction between a concrete slab and its foundation causes tensile stresses in the concrete, in the steel reinforcements, if any, and in the tie bars. For plain concrete pavements, the spacing between contraction joints must be so chosen that the stresses due to friction will not cause the concrete to crack. For longer joint spacings, steel reinforcements must be provided to take care of the stresses caused by friction. The number of tie bars required is also controlled by the friction. Figure 4.17 shows the arrangement of joints and steel in concrete pavements.

Downloaded From : www.EasyEngineering.net

Downloaded From : www.EasyEngineering.net

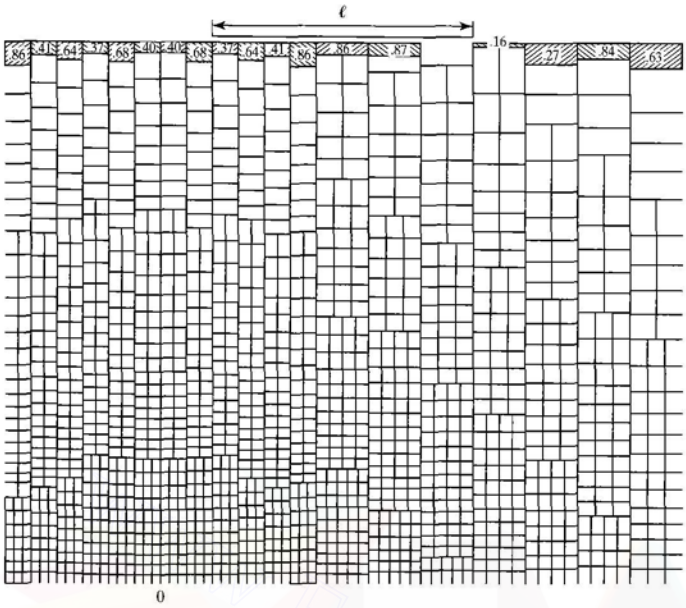


FIGURE 4.16

Influence chart for deflection due to edge loading. (After Pickett and Ray (1951).)

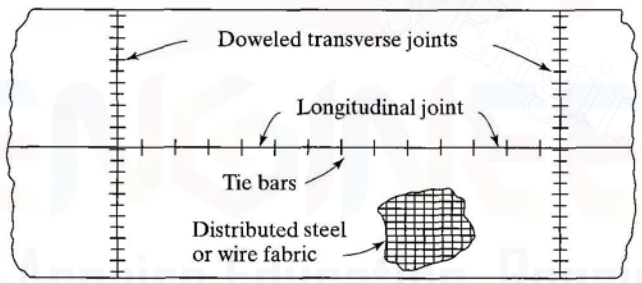


FIGURE 4.17

Steel and joints in concrete pavements.

4.3.1 Effect of Volume Change on Concrete

The volume change caused by the variation of temperature and moisture has two important effects on concrete. First, it induces tensile stresses and causes the concrete to crack. Second, it causes the joint to open and decreases the efficiency of load transfer.

Concrete Stress Figure 4.18 shows a concrete pavement subject to a decrease in temperature. Due to symmetry, the slab tends to move from both ends toward the center, but the subgrade prevents it from moving; thus, frictional stresses are developed between the slab and the subgrade. The amount of friction depends on the relative movement, being zero at the center where no movement occurs and maximum at some distance from the center where the movement is fully mobilized, as shown in Figure 4.18*b*. For practical purposes, an average coefficient of friction f_a may be assumed. The tensile stress in the concrete is greatest at the center and can be determined by equating the

Downloaded From : www.EasyEngineering.net

Downloaded From : www.EasyEngineering.net

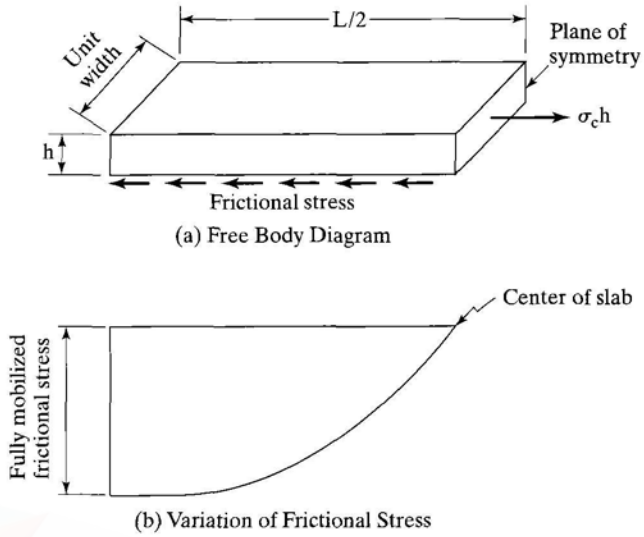


FIGURE 4.18
Stresses due to friction.

frictional force per unit width of slab, $\gamma_c h L f_a/2$, to the tensile force $\sigma_c h$, as shown in Figure 4.18*a*:

$$\sigma_c = \frac{\gamma_c L f_a}{2} \tag{4.35}$$

in which σ_c is the stress in the concrete, γ_c is the unit weight of the concrete, L is the length of the slab, and f_a is the average coefficient of friction between slab and subgrade, usually taken as 1.5. Equation 4.35 implies that the stress in the concrete due to friction is independent of the slab thickness.

Example 4.8:

Given a concrete pavement with a joint spacing of 25 ft (7.6 m) and a coefficient of friction of 1.5, as shown in Figure 4.19, determine the stress in concrete due to friction.

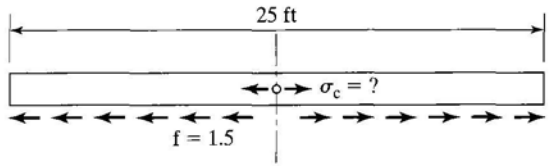


FIGURE 4.19
Example 4.8 (1 ft = 0.305 m).

Solution: With γ_c = 150 pcf = 0.0868 pci (23.6 kN/m^3), L = 25 ft = 300 in. (7.6 m), and f_a = 1.5, from Eq. 4.35, σ_c = 0.0868 × 300 × 1.5/2 = 19.5 psi (135 kPa).

The tensile strength of concrete ranges from $3\sqrt{f'_c}$ to $5\sqrt{f'_c}$, where f'_c is the compressive strength of concrete (Winter and Nilson, 1979). If f'_c = 3000 psi (13.8 MPa), the tensile strength is from 164 to 274 psi (1.13 to 1.89 MPa), which is much greater than the tensile stress of 19.5 psi

Downloaded From : www.EasyEngineering.net

Downloaded From : www.EasyEngineering.net

(135 kPa). Therefore, it does not appear that joint spacings in plain concrete pavements are dictated by the concrete stress due to friction.

Joint Opening The spacing of joints in plain concrete pavements depends more on the shrinkage characteristics of the concrete rather than on the stress in the concrete. Longer joint spacings cause the joint to open wider and decrease the efficiency of load transfer. The opening of a joint can be computed approximately by (Darter and Barenberg, 1977)

$$\Delta L = CL(\alpha_t \Delta T + \epsilon) \tag{4.36}$$

in which ΔL is the joint opening caused by temperature change and drying shrinkage of concrete; α_t is the coefficient of thermal expansion of concrete, generally 5 to 6×10^{-6}/°F (9 to 10.8×10^{-6}/°C); ϵ is the drying shrinkage coefficient of concrete, approximately 0.5 to 2.5×10^{-4}; L is the joint spacing or slab length; ΔT is the temperature range, which is the temperature at placement minus the lowest mean monthly temperature; and C is the adjustment factor due to slab-subbase friction, 0.65 for stabilized base and 0.8 for granular subbase.

Example 4.9:

Given $\Delta T = 60$°F (33°C), $\alpha_t = 5.5 \times 10^{-6}$/°F ($9.9 \times 10^{-6}$/°C), $\epsilon = 1.0 \times 10^{-4}$, $C = 0.65$, and the allowable joint openings for undoweled and doweled joints are 0.05 and 0.25 in. (1.3 and 6.4 mm), respectively, determine the maximum allowable joint spacing.

Solution: From Eq. 4.36, $L = \Delta L/[C(\alpha_t \Delta T + \epsilon)] = \Delta L/[0.65(5.5 \times 10^{-6} \times 60 + 0.0001)] = \Delta L/0.00028$. For the undoweled joint, $L = 0.05/0.00028 = 178.6$ in. $= 14.9$ ft(4.5 m). For the doweled joint, $L = 0.25/0.00028 = 892.9$ in. $= 74.4$ ft(22.7 m).

4.3.2 Steel Stress

Steel is used in concrete pavements as reinforcements, tie bars, and dowel bars. The design of longitudinal and transverse reinforcements and of the tie bars across longitudinal joints is based on the stresses due to friction and is presented in this section. The design of dowel bars is not based on the stresses due to friction and is presented in Section 4.4.1.

Reinforcements Wire fabric or bar mats may be used in concrete slabs for control of temperature cracking. These reinforcements do not increase the structural capacity of the slab but are used for two purposes: to increase the joint spacing and to tie the cracked concrete together and maintain load transfers through aggregate interlock. When steel reinforcements are used, it is assumed that all tensile stresses are taken by the steel alone, so $\sigma_c h$ in Figure 4.18*a* must be replaced by $A_s f_s$, and Eq. 4.35 becomes

$$A_s = \frac{\gamma_c h L f_a}{2 f_s} \tag{4.37}$$

in which A_s is the area of steel required per unit width and f_s is the allowable stress in steel. Equation 4.37 indicates that the amount of steel required is proportional to the length of slab.

Downloaded From : www.EasyEngineering.net

Downloaded From : www.EasyEngineering.net

TABLE 4.1 Yield Strength and Allowable Stress for Steel

Type and grade of steel	Yield strength (psi)	Allowable stress (psi)
Billet steel, intermediate grade	40,000	27,000
Rail steel or hard grade of billet steel	50,000	33,000
Rail steel, special grade	60,000	40,000
Billet steel, 60,000 psi minimum yield	60,000	40,000
Cold drawn wire (smooth)	65,000	43,000
Cold drawn wire (deformed)	70,000	46,000

Note. 1 psi = 6.9 kPa.

The steel is usually placed at the middepth of the slab and discontinued at the joint. The amount of steel obtained from Eq. 4.37 is at the center of the slab and can be reduced toward the end. However, in actual practice the same amount of steel is used throughout the length of the slab.

Table 4.1 gives the allowable stress for different types and grades of steel. The allowable stress is generally taken as two-thirds of the yield strength. Table 4.2 shows the weight and dimensions of reinforcing bars and Table 4.3 shows those of welded wire fabric.

Welded wire fabric is prefabricated reinforcement consisting of parallel series of high-strength, cold-drawn wires welded together in square or rectangular grids. The spacings and sizes of wires are identified by "style." A typical style designation is $6 \times 12 - W8 \times W6$, in which the spacing of longitudinal wires is 6 in. (152 mm), the spacing of transverse wires is 12 in. (305 mm), the size of longitudinal wire is W8 with a cross-sectional area of 0.08 in.^{2} (51.6 mm^2), and the size of transverse wires is W6 with a cross sectional area of 0.06 in.^{2} (38.7 mm^2). The typical style with deformed welded wire fabric is $6 \times 12 - D8 \times D6$. The following standard practices on wire sizes, spacings, laps, and clearances are recommended by the Wire Reinforcement Institute (WRI, 1975):

TABLE 4.2 Weights and Dimensions of Standard Reinforcing Bars

		Nominal dimensions, round sections		
Bar size designation	Weight (lb/ft)	Diameter (in.)	Cross-sectional area (in.^{2})	Perimeter (in.)
No. 3	0.376	0.375	0.11	1.178
No. 4	0.668	0.500	0.20	1.571
No. 5	1.043	0.625	0.31	1.963
No. 6	1.502	0.750	0.44	2.356
No. 7	2.044	0.875	0.60	2.749
No. 8	2.670	1.000	0.79	3.142
No. 9	3.400	1.128	1.00	3.544
No. 10	4.303	1.270	1.27	3.990
No. 11	5.313	1.410	1.56	4.430

Note. 1 in. = 25.4 mm, 1 lb = 4.45 N, 1 ft = 0.305 m.

Downloaded From : www.EasyEngineering.net

Downloaded From : www.EasyEngineering.net

TABLE 4.3 Weights and Dimensions of Welded Wire Fabric

Wire size no.		Diameter	Weight	Cross-sectional area (in.^{2}/ft) center-to-center spacing (in.)						
Smooth	Deformed	(in.)	lb/ft	2	3	4	6	8	10	12
W31	D31	0.628	1.054	1.86	1.24	.93	.62	.465	.372	.31
W30	D30	0.618	1.020	1.80	1.20	.90	.60	.45	.36	.30
W28	D28	0.597	.952	1.68	1.12	.84	.56	.42	.336	.28
W26	D26	0.575	.934	1.56	1.04	.78	.52	.39	.312	.26
W24	D24	0.553	.816	1.44	.96	.72	.48	.36	.288	.24
W22	D22	0.529	.748	1.32	.88	.66	.44	.33	.264	.22
W20	D20	0.504	.680	1.20	.80	.60	.40	.30	.24	.20
W18	D18	0.478	.612	1.08	.72	.54	.36	.27	.216	.18
W16	D16	0.451	.544	.96	.64	.48	.32	.24	.192	.16
W14	D14	0.422	.476	.84	.56	.42	.28	.21	.168	.14
W12	D12	0.390	.408	.72	.48	.36	.24	.18	.144	.12
W11	D11	0.374	.374	.66	.44	.33	.22	.165	.132	.11
W10.5		0.366	.357	.63	.42	.315	.21	.157	.126	.105
W10	D10	0.356	.340	.60	.40	.30	.20	.15	.12	.10
W9.5		0.348	.323	.57	.38	.285	.19	.142	.114	.095
W9	D9	0.338	.306	.54	.36	.27	.18	.135	.108	.09
W8.5		0.329	.289	.51	.34	.255	.17	.127	.102	.085
W8	D8	0.319	.272	.48	.32	.24	.16	.12	.096	.08
W7.5		0.309	.255	.45	.30	.225	.15	.112	.09	.075
W7	D7	0.298	.238	.42	.28	.21	.14	.105	.084	.07
W6.5		0.288	.221	.39	.26	.195	.13	.097	.078	.065
W6	D6	0.276	.204	.36	.24	.18	.12	.09	.072	.06
W5.5		0.264	.187	.33	.22	.165	.11	.082	.066	.055
W5	D5	0.252	.170	.30	.20	.15	.10	.075	.06	.05
W4.5		0.240	.153	.27	.18	.135	.09	.067	.054	.045
W4	D4	0.225	.136	.24	.16	.12	.08	.06	.048	.04

Note. Wire sizes other than those listed above may be produced provided the quantity required is sufficient to justify manufacture. 1 in. = 25.4 mm, 1 lb = 4.45 N, 1 ft = 0.305 m.

Source. After WRI (1975).

1. Because the fabric is subjected to bending stresses as well as tensile stresses at cracks, neither the longitudinal nor the transverse wires should be less than W4 or D4.
2. To provide generous opening between wires to permit placement and vibration of concrete, the minimum spacing between wires should not be less than 4 in. (102 mm). The maximum spacing should not be greater than 12 in. (305 mm) between longitudinal wires and 24 in. (610 mm) between transverse wires.
3. Because the dimensions of a concrete slab are usually greater than those of the welded wire fabric, the fabric should be installed with end and side laps. The end lap should be about 30 times the longitudinal wire diameter but not less than 12 in. (305 mm). The side laps should be about 20 times the transverse wire diameter but not less than 6 in. (152 mm).
4. The fabric should extend to about 2 in. (51 mm) but not more than 6 in. (152 mm) from the slab edges. The depth from the top of slab should not be less than 2.5 in. (64 mm) or more than middepth.

Downloaded From : www.EasyEngineering.net

Downloaded From : www.EasyEngineering.net

Example 4.10:

Determine the wire fabric required for a two-lane concrete pavement, 8 in. (203 mm) thick, 60 ft (18.3 m) long, and 24 ft (7.3 m) wide, with a longitudinal joint at the center, as shown in Figure 4.20.

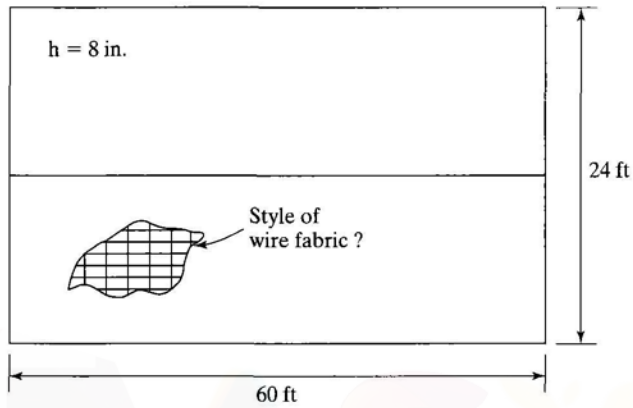


FIGURE 4.20
Example 4.10 (1 in. = 25.4 mm, 1 ft = 0.305 m).

Solution: With $\gamma_c = 0.0868$ pci (23.6 kN/m^3), $h_c = 8$ in. (203 mm), $L = 60$ ft = 720 in. (18.3 m), $f_a = 1.5$, and $f_s = 43{,}000$ psi (297 MPa), from Eq. 4.37, the required longitudinal steel is $A_s = 0.0868 \times 8 \times 720 \times 1.5/(2 \times 43{,}000) = 0.00872$ in.^{2}/in. $= 0.105$ in.^{2}/ft (222 mm^2/m). The required transverse steel is $A_s = 0.0868 \times 8 \times 24 \times 12 \times 1.5/(2 \times 43{,}000) = 0.00349$ in.^{2}/in. $= 0.042$ in.^{2}/ft (88.9 mm^2/m). From Table 4.3, use 6 × 12 − W5.5 × W4.5 with cross-sectional areas of 0.11 in.^{2} (71 mm^2) for longitudinal wires and 0.045 in.^{2} (29 mm^2) for transverse wires.

If the concrete pavement is used for a four-lane highway with all four slabs tied together at the three longitudinal joints, the transverse reinforcements in the two inside lanes should be doubled, because the length L in Eq. 4.37 should be 48 ft (14.6 m) instead of 24 ft (7.3 m).

Tie Bars Tie bars are placed along the longitudinal joint to tie the two slabs together so that the joint will be tightly closed and the load transfer across the joint can be ensured. The amount of steel required for tie bars can be determined in the same way as the longitudinal or transverse reinforcements by slightly modifying Eq. 4.37:

$$A_s = \frac{\gamma_c h L' f_a}{f_s} \tag{4.38}$$

in which A_s is the area of steel required per unit length of slab and L' is the distance from the longitudinal joint to the free edge where no tie bars exist. For two- or three-lane highways, L' is the lane width. If tie bars are used in all three longitudinal joints of a four-lane highway, L' is equal to the lane width for the two outer joints and twice the lane width for the inner joint.

The length of tie bars is governed by the allowable bond stress. For deformed bars, an allowable bond stress of 350 psi (2.4 MPa) may be assumed. The length of bar

Downloaded From : www.EasyEngineering.net

Downloaded From : www.EasyEngineering.net

should be based on the full strength of the bar, namely,

$$t = 2\left(\frac{A_1 f_s}{\mu \Sigma o}\right) \tag{4.39}$$

in which t is the length of the tie bar, μ is the allowable bond stress, A_1 is the area of one bar, and Σo is the bar perimeter. For a given bar diameter d, $A_1 = \pi d^2/4$ and $\Sigma o = \pi d$, so Eq. 4.39 can be simplified to

$$t = \frac{1}{2}\left(\frac{f_s d}{\mu}\right) \tag{4.40}$$

The length t should be increased by 3 in. (76 mm) for misalignment.

It should be noted that many agencies use a standard tie-bar design to simplify the construction. Tie bars 0.5 in. (13 mm) in diameter by 36 in. (914 mm) long spaced at intervals of 30 to 40 in. (762 to 1016 mm) are most commonly used.

Example 4.11:

Same pavement as Example 4.10. Determine the diameter, spacing, and length of the tie bars required, as shown in Figure 4.21.

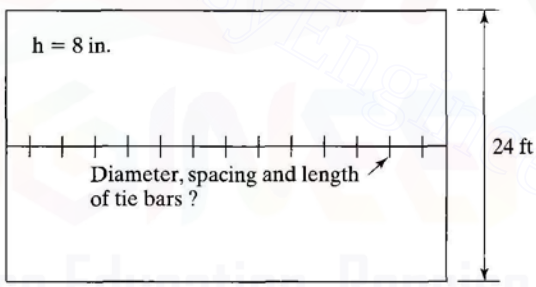


FIGURE 4.21
Example 4.11 (1 in. = 25.4 mm, 1 ft = 0.305 m).

Solution: Assume f_s = 27,000 psi (186 MPa) for billet steel (see Table 4.1). With L' = 12 ft = 144 in. (3.66 m), from Eq. 4.38, $A_s = 0.0868 \times 8 \times 144 \times 1.5/27{,}000 = 0.00556$ in.^{2}/in. If No. 4 (0.5 in. or 1.2 mm) bars are used, from Table 4.2, the cross-sectional area of one bar is 0.2 in.^{2} (129 mm^2). The spacing of the bar = 0.2/0.00556 = 36 in. (914 mm).

Assume that μ = 350 psi (24 MPa), from Eq. 4.40, $t = 0.5 \times 27{,}000 \times 0.5/350 = 19.3$ in. (353 mm). After adding 3 in. (76 mm), $t = 19.3 + 3 = 22.3$ in. (use 24 in. or 610 mm). The design selected is No. 4 deformed bars, 24 in. (610 mm) long and 3 ft (0.9 m) on centers.

4.4 DESIGN OF DOWELS AND JOINTS

The design of dowels and joints is mostly based on experience, although some theoretical methods on the design of dowels are available. The size of dowels to be used depends on the thickness of slab. Table 4.4 shows the size and length of dowels for different slab thicknesses as recommended by PCA (1975). It can be seen that the diameter of dowels is equal to one-eighth of the slab thickness. In a recent edition of joint design, PCA (1991) recommended the use of 1.25 in. (32 mm) diameter dowels for highway pavements less

Downloaded From : www.EasyEngineering.net

Downloaded From : www.EasyEngineering.net

TABLE 4.4 Recommended Dowel Size and Length

Slab thickness (in.)	Dowel diameter (in.)	Dowel length (in.)
5	$\frac{5}{8}$	12
6	$\frac{3}{4}$	14
7	$\frac{7}{8}$	14
8	1	14
9	$1\frac{1}{8}$	16
10	$1\frac{1}{4}$	18
11	$1\frac{3}{8}$	18
12	$1\frac{1}{2}$	20

Note. All dowels spaced at 12 in. on centers, 1 in. = 25.4 mm.
Source. After PCA (1975).

than 10 in. (254 mm) thick and 1.5 in. (38 mm) diameter dowels for pavements 10 in. (254 mm) thick or greater. A minimum dowel diameter of 1.25 to 1.5 in. (32 to 38 mm) is needed to control faulting by reducing the bearing stress in concrete.

4.4.1 Design of Dowels

Dowel bars are usually used across a transverse joint to transfer the loads to the adjoining slab. The stress and deflection at the joint are much smaller when the loads are carried by two slabs, instead of by one slab alone. The use of dowels can minimize faulting and pumping which has been considered by the Portland Cement Association (PCA, 1984) as a factor for thickness design.

Allowable Bearing Stress Because concrete is much weaker than steel, the size and spacing of dowels required are governed by the bearing stress between dowel and concrete. The allowable bearing stress can be determined by Eq. 4.41 (American Concrete Institute, 1956),

$$f_b = \left(\frac{4 - d}{3}\right) f'_c \tag{4.41}$$

in which f_b is the allowable bearing stress in psi, d is the dowel diameter in inches, and f'_c is the ultimate compressive strength of concrete.

Bearing Stress on One Dowel If the load applied to one dowel is known, the maximum bearing stress can be determined theoretically by assuming the dowel to be a beam and the concrete to be a Winkler foundation. Using the original solution by Timoshenko, Friberg (1940) indicated that the maximum deformation of concrete under the dowel, as shown by y_0 in Figure 4.22, can be expressed by

$$y_0 = \frac{P_t(2 + \beta z)}{4\beta^3 E_d I_d} \tag{4.42}$$

in which y_0 is the deformation of the dowel at the face of the joint, P_t is the load on one dowel, z is the joint width, E_d is Young's modulus of the dowel, I_d is the moment of

Downloaded From : www.EasyEngineering.net

Downloaded From : www.EasyEngineering.net

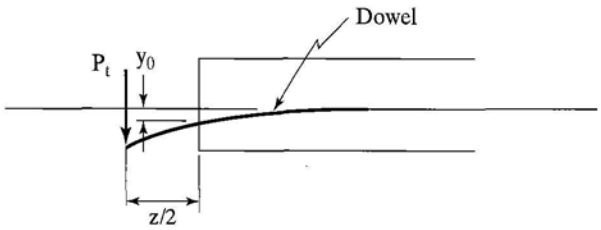


FIGURE 4.22
Dowel deformation under load.

inertia of the dowel, and β is the relative stiffness of a dowel embedded in concrete. Note that

$$I_d = \frac{1}{64}\pi d^4 \tag{4.43}$$

and

$$\beta = \sqrt[4]{\frac{Kd}{4E_d I_d}} \tag{4.44}$$

in which K is the modulus of dowel support, which ranges from 300,000 to 1,500,000 pci (81.5 to 409 GN/m^3), and d is the diameter of dowel. The bearing stress σ_b is proportional to the deformation:

$$\sigma_b = Ky_0 = \frac{KP_t(2 + \beta z)}{4\beta^3 E_d I_d} \tag{4.45}$$

The bearing stress obtained from Eq. 4.45 should compare with the allowable bearing stress computed by Eq. 4.41. If the actual bearing stress is greater than allowable, then larger dowel bars or smaller dowel spacing should be used. Recent studies have also shown that the bearing stress is related to the faulting of slabs, as described in Section 12.1.4. By limiting the bearing stress, the amount of faulting can be reduced to the allowable limit.

Dowel Group Action When a load W is applied on one slab near the joint, as shown in Figure 4.23, part of the load will be transferred to the adjacent slab through the dowel group. If the dowels are 100% efficient, both slabs will deflect the same amount and the reactive forces under both slabs will be the same, each equal to $0.5W$, which is also the total shear force transferred by the dowel group. If the dowels are less than 100% efficient, as in the case of old pavements where some dowels become loose, the reactive forces under the loaded slab will be greater than $0.5W$, while those under the unloaded slab will be smaller

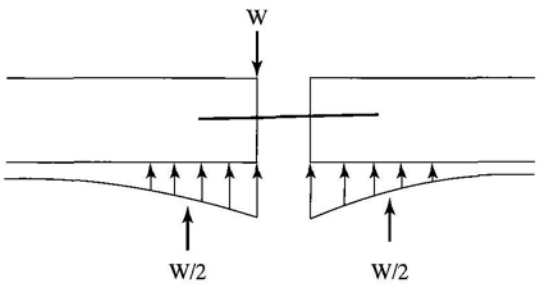


FIGURE 4.23
Load transfer through dowel group.

Downloaded From : www.EasyEngineering.net

Downloaded From : www.EasyEngineering.net

than 0.5W. As a result, the total shear force on the dowels is smaller than 0.5W. Therefore, the use of 0.5W for the design of dowels is more conservative.

Based on Westergaard's solutions, Friberg (1940) found that the maximum negative moment for both interior and edge loadings occurs at a distance of 1.8ℓ from the load, where ℓ is the radius of relative stiffness defined by Eq. 4.10. When the moment is maximum, the shear force is equal to zero. It is therefore reasonable to assume that the shear in each dowel decreases inversely with the distance of the dowel from the point of loading, being maximum for the dowel under or nearest to the point of loading and zero at a distance of 1.8ℓ. The application of the above principle for dowel design can be best illustrated by the following examples.

Example 4.12:

Figure 4.24 shows a concrete pavement 8 in. (203 mm) thick having a joint width of 0.2 in. (5.1 mm), a modulus of subgrade reaction of 100 pci (27 kN/m^3), and a modulus of dowel support of 1.5 × 10^6 pci (407 GN/m^3). A load of 9000 lb (40 kN) is applied over the outermost dowel at a distance of 6 in. (152 mm) from the edge. The dowels are $\frac{3}{4}$ in. (19 mm) in diameter and 12 in. (305 mm) on centers. Determine the maximum bearing stress between dowel and concrete.

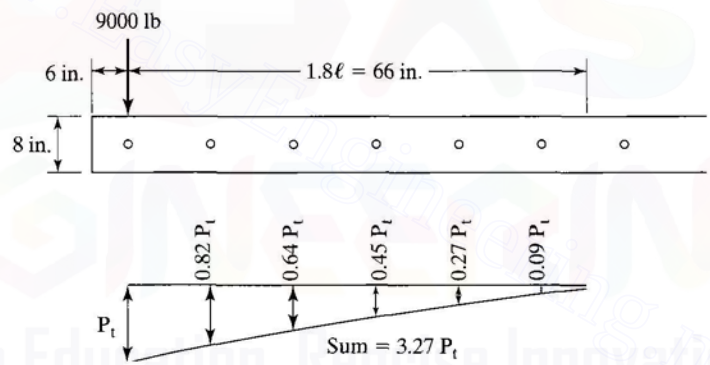


FIGURE 4.24

Example 4.12 (1 in. = 25.4 mm, 1 lb = 4.45 N).

Solution: From Eq. 4.10, $\ell = [4 \times 10^6 \times 512/(12 \times 0.9775 \times 100)]^{0.25} = 36.35$ in. (427 mm). If the dowel directly under the load is subjected to a shear force P_t, the forces on the dowels within a distance of 1.8ℓ, or 66 in. (1.68 m), can be determined by assuming a straight-line variation, as shown in Figure 4.24. The sum of the forces on all dowels is 3.27P_t, which must be equal to one-half of the applied load based on 100% joint efficiency, or $P_t = 4500/3.27 = 1376$ lb (6.1 kN). From Eq. 4.43, $I_d = \pi(0.75)^4/64 = 0.0155$ in.^{4} (6450 mm^4). From Eq. 4.44, $\beta = [1.5 \times 10^6 \times 0.75/(4 \times 29 \times 10^6 \times 0.0155)]^{0.25} = 0.889$ in. (22.6 mm). From Eq. 4.45, $\sigma_b = 1.5 \times 10^6 \times 1376(2 + 0.889 \times 0.2)/(4 \times 0.703 \times 29 \times 10^6 \times 0.0155) = 3556$ psi (24.5 MPa). For a 3000-psi (20.7-MPa) concrete, the allowable bearing stress obtained from Eq. 4.41 is $f_b = (4 - 0.75) \times 3000/3 = 3250$ psi (22.4 MPa). Because the actual bearing stress is about 10% greater than the allowable, the design is not considered satisfactory.

In this example, only the left-wheel load near the pavement edge is considered. The right-wheel load is at least 6 ft (1.83 m) from the left-wheel load, which is greater than 1.8ℓ, so the right

Downloaded From : www.EasyEngineering.net

Downloaded From : www.EasyEngineering.net

wheel has no effect on the maximum force P_t on the dowel near the pavement edge. If the slab is thicker and stronger and the foundation is weaker, ℓ may become much larger and both wheels must be considered in determining the force P_t on the most critical dowel.

Example 4.13:

Figure 4.25*a* shows a 9.5-in. (241-mm) slab resting on a foundation with $k = 50$ pci (13.6 MN/m^3). Twelve dowels at 12 in. (305 mm) on centers are placed at the joint on the 12-ft

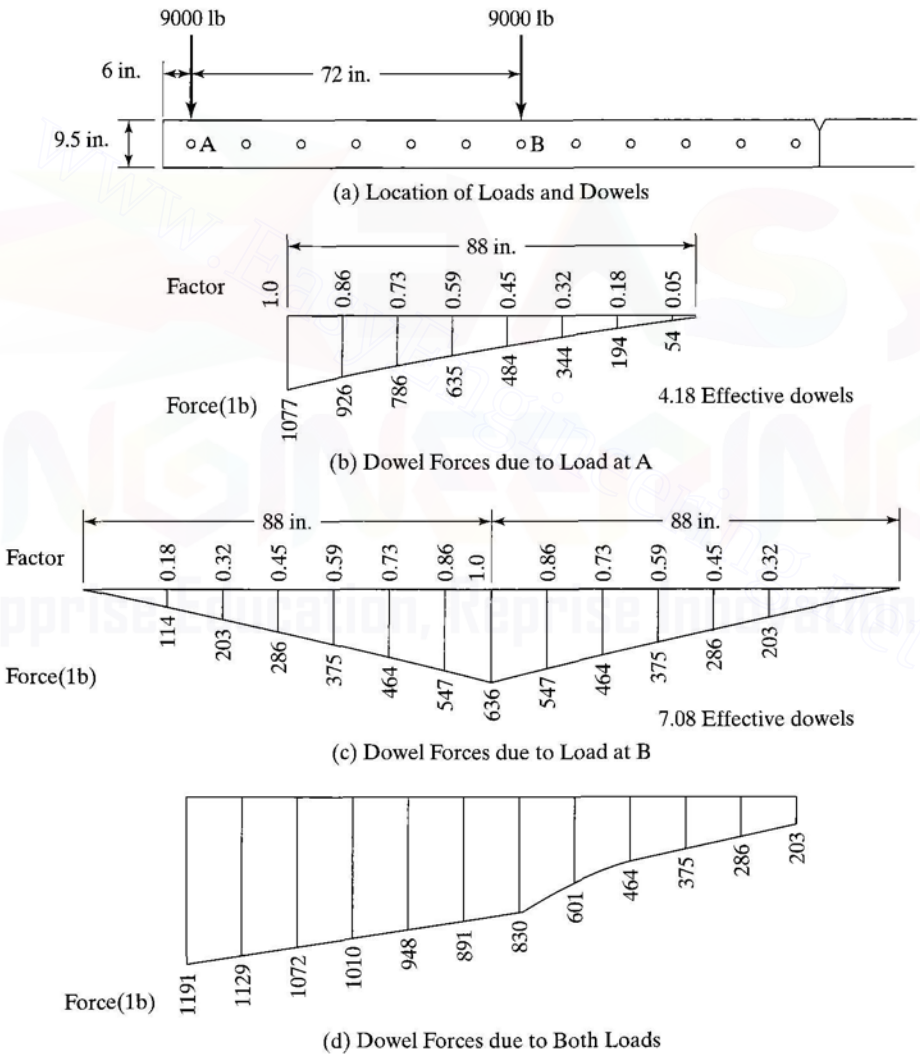


FIGURE 4.25

Example 4.13 (1 in. = 25.4 mm, 1 lb = 4.45 N).

Downloaded From : www.EasyEngineering.net

Downloaded From : www.EasyEngineering.net

(3.66-m) lane. Two 9000-lb (40-kN) wheel loads are applied at points A and B. Determine the maximum load on one dowel.

Solution: From Eq. 4.10, $\ell = [4 \times 10^6 \times (9.5)^3/(12 \times 0.9775 \times 50)]^{0.25} = 49.17$ in. (1.25 m), so $1.8\ell = 88$ in. (2.24 m). First, consider the 9000-lb (40-kN) load at A. If the dowel at A has a load factor of 1, the load factors at other dowels can be determined from similar triangles, as shown in Figure 4.25*b*. The sum of these factors results in 4.18 effective dowels, so the load carried by the dowel at A is 4500/4.18 or 1077 lb (4.8 kN). The loads carried by other dowels can be determined by proportion. Next, consider the 9000-lb (40-kN) load at B. If the dowel at B has a load factor of 1, the load factors at other dowels can be determined from the triangular distribution, as shown in Figure 4.25*c*. The sum of these factors results in 7.08 effective dowels. Note that the dowels on the other side of the longitudinal joint are not considered effective in carrying the load. The load carried by the dowel at B is 4500/7.08 or 636 lb (2.8 kN), and those carried by other dowels can be determined by proportion. Figure 4.25*d* shows the forces on each dowel due to the combined effect of both loads. It can be seen that the dowel nearest to the pavement edge is the most critical and should be used for design purposes. The load carried by this dowel can be determined directly by $P_t = 4500/4.18 + 0.18 \times 4500/7.08 = 1191$ lb (5.3 kN).

The above examples are based on the assumption that the maximum negative moment occurs at a distance of 1.8ℓ from the load. Recent studies by Heinrichs et al. (1989) have shown that the maximum negative moment occurs at 1.0ℓ, so the load carried by the most critical dowel should be larger than those shown in the examples. This has been proved by comparing the results with the KENSLABS computer program.

4.4.2 Design of Joints

Joints should be provided in concrete pavements so premature cracks due to temperature or moisture changes will not occur. There are four types of joints in common use: contraction, expansion, construction, and longitudinal.

Contraction Joints Contraction joints are transverse joints used to relieve tensile stresses. The spacing of joints should be based on local experience since a change in coarse aggregate types may have a significant effect on the concrete thermal coefficient and consequently the acceptable joint spacing. As a rough guide, the joint spacing in feet for plain concrete pavements should not greatly exceed twice the slab thickness in inches. For example, the maximum joint spacing for an 8-in. (203-mm) slab is 16 ft (4.9 m). Also, as a general guideline, the ratio of slab width to length should not exceed 1.25 (AASHTO, 1986).

Figure 4.26 shows typical contraction joints. In Figure 4.26*a*, a dummy groove is formed by placing a metal strip on the fresh concrete, which is later removed, or by sawing after the concrete is set. The groove is then sealed with a plastic material. If the joint spacing is small, the load transfer across the joint can be achieved by the aggregate interlock and no dowels may be needed. However, dowels are needed if the joint spacing is large or if the short panels are located near the end of the pavement. In such cases, the joint may open up and the load transfer through aggregate interlock may be lost. In lieu of a dummy groove, joints can be formed by placing a felt, asphalt ribbon, or asphalt board strip in the fresh concrete and leaving it there permanently, as shown in Figure 4.26*b*.

Downloaded From : www.EasyEngineering.net

Downloaded From : www.EasyEngineering.net

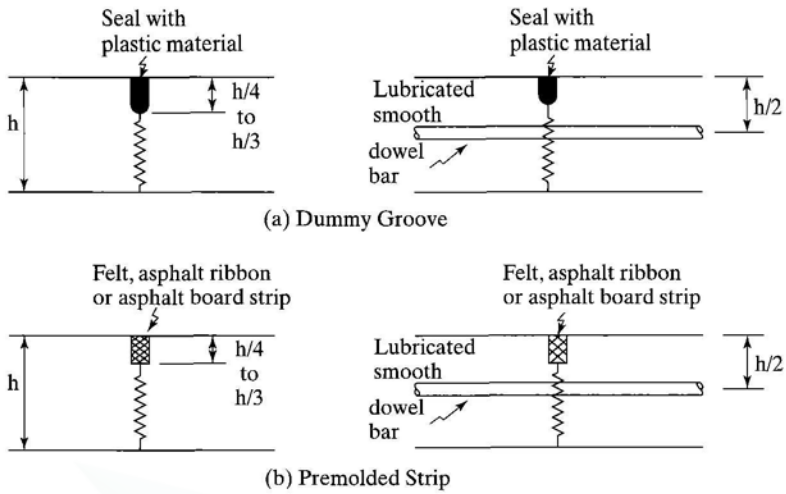


FIGURE 4.26

Typical contraction joints.

The sealant used in the joints must be capable of withstanding repeated extension and compression as the temperature and moisture in the slabs change. Sealants can be classified as field molded and preformed. Field-molded sealants are those applied in liquid or semiliquid form, and preformed sealants are shaped during manufacturing. Figure 4.27 shows the design of joint sealant reservoir for field-molded sealants. To maintain an effective field-molded seal, the sealant reservoir must have the proper shape factor or depth-to-width ratio. The common practice is to have the ratio between 0.5 to 1. Table 4.5 shows the reservoir dimensions for field-molded sealants, and Table 4.6 shows the joint and sealant widths for preformed seals as recommended by PCA (1975).

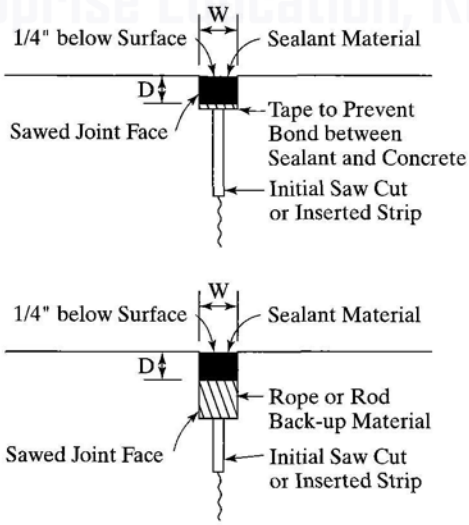


FIGURE 4.27

Design of joint sealant reservoir (1 in. = 25.4 mm). (After PCA (1975).)

Downloaded From : www.EasyEngineering.net

Downloaded From : www.EasyEngineering.net

TABLE 4.5 Reservoir Dimensions for Field-Molded Sealants

Joint spacing (ft)	Reservoir width (in.)	Reservoir depth (in.)
15 or less	$\frac{1}{4}$	$\frac{1}{2}$ minimum
20	$\frac{3}{8}$	$\frac{1}{2}$ minimum
30	$\frac{1}{2}$	$\frac{1}{2}$ minimum
40	$\frac{5}{8}$	$\frac{5}{8}$

Note. 1 ft = 0.305 m, 1 in. = 25.4 mm.
Source. After PCA (1975).

TABLE 4.6 Joint and Sealant Width for Preformed Seals

Joint spacing (ft)	Joint width (in.)	Sealant width (in.)
20 or less	$\frac{1}{4}$	$\frac{7}{16}$
30	$\frac{3}{8}$	$\frac{5}{8}$
40	$\frac{7}{16}$	$\frac{3}{4}$
50	$\frac{1}{2}$	$\frac{7}{8}$

Note. 1 ft = 0.305 m, 1 in. = 25.4 mm.
Source. After PCA (1975).

The preformed sealant is the type most recommended to achieve long-term performance. Preformed sealants can do an excellent job of keeping out incompressibles over a long period of time, but might not be completely water tight compared to the field-molded sealants. The preformed sealants should be so designed that the seal will always be compressed at least 20% in the joint. The maximum allowable compression of the seal is 50%. Thus, the seal working range is 20 to 50% (Darter and Barenberg, 1977).

Example 4.14:

A concrete pavement 15 ft (4.6 m) long is placed on a gravel subbase. If the joint width is $\frac{1}{4}$ in. (6.4 mm), the design temperature range ΔT is 100°F (55.6°C), the coefficient of thermal expansion α_t is 5×10^{-6}/°F (9×10^{-6}/°C), and the drying shrinkage coefficient ϵ is 1.0×10^{-4}, determine the width of preformed sealant required.

Solution: From Eq. 4.36, the joint opening due to temperature change is $\Delta L = 0.65 \times 15 \times 12(0.000005 \times 100 + 0.0001) = 0.07$ in. (1.8 mm). Try $\frac{7}{16}$ or 0.4375 in. (11.1 mm) sealant installed in summer, so the joint would not be further compressed. Check maximum compression of sealant: $(0.4375 - 0.25)/0.4375 = 0.43 < 50\%$, OK. Check minimum compression of sealant: $(0.4375 - 0.25 - 0.07)/0.4375 = 0.27 > 20\%$, OK. Therefore, the use of $\frac{7}{16}$ in. (11.1 mm) sealant for a $\frac{1}{4}$-in. (6.4-mm) joint is satisfactory, as shown in Table 4.6.

Downloaded From : www.EasyEngineering.net

Downloaded From : www.EasyEngineering.net

Contraction joints are usually placed at regular intervals perpendicular to the center line of pavements. However, skewed joints with randomized spacings, say 13–19–18–12 ft (4.0–5.8–5.5–3.7 m), have also been used. The obtuse angle at the outside pavement edge should be ahead of the joint in the direction of traffic, since that corner receives the greatest impact from the sudden application of wheel loads. The advantage of skewed joints is that the right and left wheels do not arrive at the joint simultaneously, thus minimizing the annoyance of faulted joints. The use of randomized spacings can further reduce the resonance and improve the riding comfort.

Expansion Joints Expansion joints are transverse joints for the relief of compressive stress. Because expansion joints are difficult to maintain and susceptible to pumping, they are no longer in use today except at the connection between pavement and structure. Experience has shown that the blowups of concrete pavements are related to a certain source and type of coarse aggregates. If proper precaution is exercised in selecting the aggregates, distress due to blowups can be minimized. The plastic flow of concrete can gradually relieve compressive stress, if any, so it is not necessary to install an expansion joint except at bridge ends.

Figure 4.28 shows a typical expansion joint. The minimum width of joint is $\frac{3}{4}$ in. (19 mm). Smooth dowel bars lubricated at least on one side must be used for load transfer. An expansion cap must be installed at the free end to provide space for dowel movements. Nonextruding fillers, including fibrous and bituminous materials or cork, must be placed in the joint and the top sealed with a plastic material.

Construction Joints If at all possible, the transverse construction joint should be placed at the location of the contraction joint, as shown by the butt joint in Figure 4.29*a*. If the work must stop due to an emergency or machine breakdown, the key joint shown in Figure 4.29*b* may be used. This joint should be placed only in the middle third of a normal joint interval. Key joints have not performed well and many failures have occurred.

Longitudinal Joints Longitudinal joints are used in highway pavements to relieve curling and warping stresses. Different types of longitudinal joints are used, depending on whether the construction is full width or lane-at-a-time.

In the full-width construction, as shown in Figure 4.30, the most convenient type is the dummy groove joint, in which tie bars are used to make certain that aggregate interlock is maintained, as shown in Figure 4.30*a*. These bars may be shoved into the wet concrete before the final finishing and placement of the dummy groove. The joint

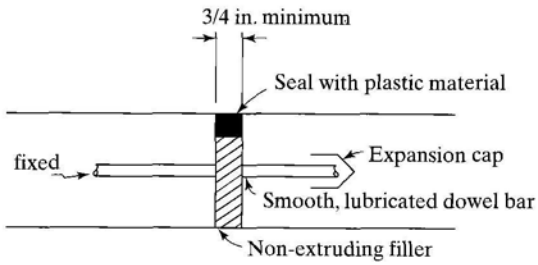
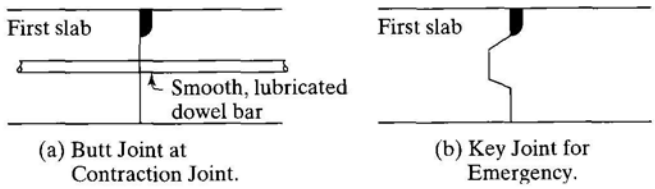


FIGURE 4.28
Expansion joint (1 in. = 25.4 mm).

Downloaded From : www.EasyEngineering.net

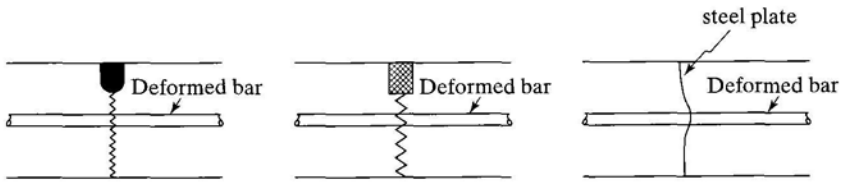
Downloaded From : www.EasyEngineering.net



(a) Butt Joint at Contraction Joint.

(b) Key Joint for Emergency.

FIGURE 4.29
Construction joints.



(a) Dummy Groove.

(b) Ribbon or Premolded Strip.

(c) Deformed Plate.

FIGURE 4.30
Longitudinal joints for full-width construction.

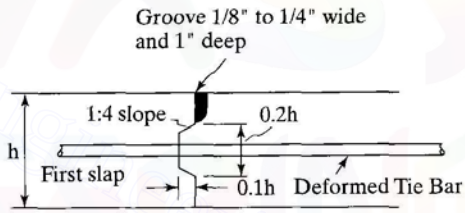


FIGURE 4.31
Longitudinal joints for lane-at-a-time construction (1 in. = 25.4 mm).

can also be formed by inserting a premolded strip into the fresh concrete and leaving it there permanently as an integral part of the warping joint, as shown in Figure 4.30*b*. Another method is to install deformed steel plates and tie bars at the center line before the pour of concrete, as shown in Figure 4.30*c*.

Lane-at-a-time construction is used when it is necessary to maintain traffic on the other lane. To insure load transfer, key joints are usually used, as shown in Figure 4.31. In most cases, the keyed joints are tied together with tie bars. However, tie bars may be omitted if the longitudinal joint is at the interior of a multilane pavement and there is very little chance that the joint will be wide open.

Butt joints have also been used for lane-at-a-time construction. Current practice prefers the use of butt joints over keyed joints because keyed joints usually do not perform well due to the occurrence of cracks along the key and they are also difficult to construct with slipform paving.

SUMMARY

This chapter discusses the stresses and deflections in rigid pavements, on the basis of Westergaard's theory. Westergaard viewed pavement as a plate on a liquid foundation

Downloaded From : www.EasyEngineering.net

Downloaded From : www.EasyEngineering.net

with full subgrade contact. Analyses based on partial contact and other types of foundation are presented in Chapter 5.

Important Points Discussed in Chapter 4

1. Curling stresses in an infinite slab are caused by the restraining effect of the slab and can be determined easily from Hooke's law by assuming plane strain.
2. Curling stresses in a finite slab are caused by the curling of the slab and are difficult to compute. Using Westergaard's theory, Bradbury developed a simple chart for determining the maximum warping stress in the interior and at the edge of a finite slab.
3. Whether curling stresses should be considered in rigid pavement design is controversial. The Portland Cement Association does not consider curling stresses in fatigue analysis because the very few number of stress reversals does not contribute to fatigue cracking and also the curling stresses may be added to or subtracted from the loading stresses to neutralize the effect. Others think that curling stresses should be combined with loading stresses, because past experience has shown that longer slabs with greater curling stresses always result in more cracking of the slab. A more reasonable approach is to consider the fatigue damage due to curling separately from that due to loading and then combine them.
4. Westergaard's closed-form formulas can be used to determine the maximum stresses and deflections in a concrete slab due to a circular loaded area applied at the corner, in the interior, or near to the edge. If the load is applied over a set of dual tires, the formulas can still be applied by using an equivalent circular area.
5. The stresses and deflections due to interior and edge loadings can also be determined by influence charts. When influence charts are employed, the actual tire imprints should be used, instead of assuming the imprints to be circular areas.
6. The design of steel reinforcements and tie bars is based on the stresses due to friction. These steel reinforcements, such as wire fabric and bar mats, do not increase the structural capacity of the slab but are used to increase the joint spacing and to tie the cracked concrete together to maintain load transfers through aggregate interlock.
7. The design of dowels is mostly based on experience. One rule of thumb is that the diameter of dowel be equal to $\frac{1}{8}$ of the slab thickness. However, a theoretical method is available to determine the bearing stress between dowel and concrete and check against the allowable bearing stress.
8. Joints should be provided in concrete pavements so that premature cracks due to temperature or moisture changes will not occur. As a rough guide, the joint spacing in feet for plain concrete pavements should not greatly exceed twice the slab thickness in inches, and the ratio of slab width to length should not be greater than 1.25. Contraction joints are usually placed at regular intervals perpendicular to the center line of pavements. However, skewed joints with randomized spacings have also been used. Expansion joints are used only at the connection between pavement and structure. Longitudinal joints are used to relieve curling and warping stresses, and different types may be used, depending on whether the construction is full width or lane-at-a-time.

Downloaded From : www.EasyEngineering.net

Downloaded From : www.EasyEngineering.net

PROBLEMS

In these problems the following data are assumed: modulus of elasticity of concrete = 4×10^6 psi, Poisson ratio of concrete = 0.15, modulus of elasticity of steel = 29×10^6 psi, Poisson ratio of steel = 0.3, modulus of dowel support = 1.5×10^6 pci, coefficient of thermal expansion of concrete = 5×10^{-6} in./in./°F, and coefficient of friction between slab and subgrade = 1.5.

4.1 Determine the curling stresses in an 8-in. slab during the day under a temperature gradient of 3°F per inch of slab for the following two cases: (a) at an interior point and at an edge point of an infinite slab, and (b) at points *A*, *B*, and *C* in a finite slab, as shown in Figure P4.1. The modulus of subgrade reaction is assumed to be 50 pci. [Answer: (a) 282.4 and 240 psi, (b) 211.4, 198.0, and 57.6 psi]

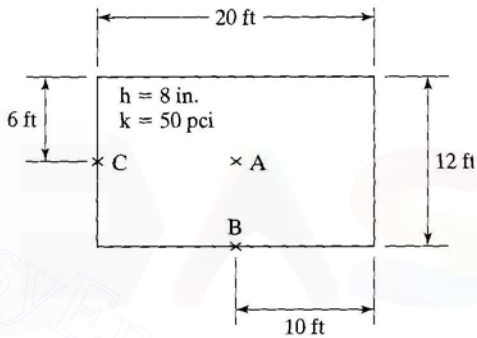


FIGURE P4.1

4.2 A concrete slab 10 in. thick is supported by a subgrade whose modulus of subgrade reaction is 200 pci. A 12,000-lb dual-wheel load (each wheel 6000 lb) spaced at 14 in. on centers is applied at the corner of the slab, as shown in Figure P4.2. The contact pressure is 80 psi. Determine the maximum stress in the concrete by Westergaard's equation with equivalent contact area. [Answer: 172.8 psi]

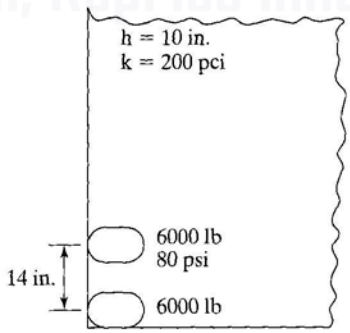


FIGURE P4.2

4.3 The pavement and loading are the same as in Problem 4.2, but the load is applied in the interior of an infinite slab, as shown in Figure P4.3. Determine the maximum stress in the concrete by (a) Westergaard's equation with equivalent contact area and (b) influence chart using dual tires. [Answer: 139.7 psi by equivalent area]

Downloaded From : www.EasyEngineering.net

Downloaded From : www.EasyEngineering.net

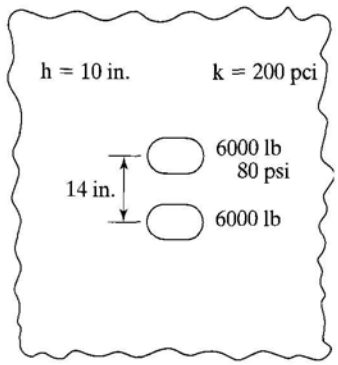


FIGURE P4.3

4.4 Same as Problem 4-3, except that the load is applied on the slab edge, as shown in Figure P4.4. [Answer: 252.5 psi by equivalent area]

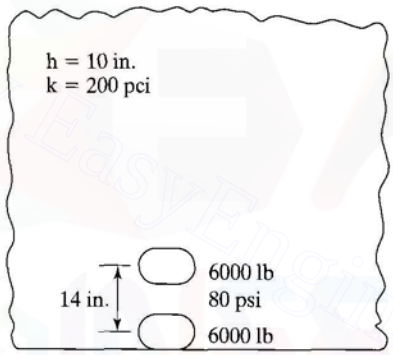


FIGURE 4.4

4.5 In Figure 4.12, what is the radius of relative stiffness of the pavement? If the thickness of slab is 11 in. and the contact pressure is 100 psi, determine the maximum stress due to the four tires under the center of one tire in the transverse, or n, direction. Estimate the maximum stress in the longitudinal direction under the center of one tire. [Answer: 57 in., 470 psi, 420 psi]

4.6 Figure P4.6 shows a set of dual-tandem wheels with a total weight of 40,000 lb (10,000 lb per wheel), a tire pressure of 100 psi, a dual spacing of 20 in., and a tandem spacing of 40 in. The concrete slab is 8 in. thick, and the modulus of subgrade reaction is 100 pci. Determine the interior stress in the y direction at point A under the center of the dual tandem wheels. [Answer: 279 psi]

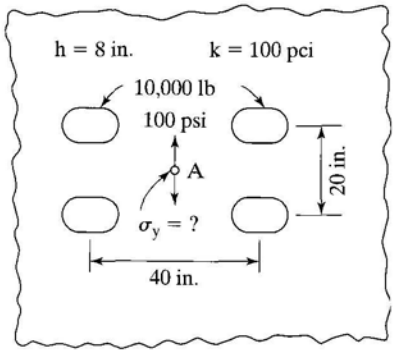


FIGURE 4.6

Downloaded From : www.EasyEngineering.net

Downloaded From : www.EasyEngineering.net

4.7 Same as Problem 4-6, except that the outside wheels are applied at the slab edge, as shown in Figure P4.7. Compute the edge stress at point A in an infinitely large slab by influence charts. [Answer: 317 psi]

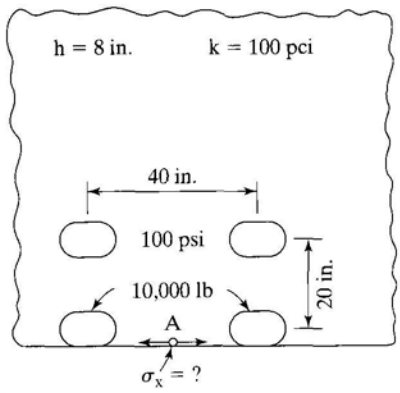


FIGURE P4.7

4.8 A concrete slab, 40 ft long, 11 ft wide, and 9 in. thick, is placed on a subgrade having a modulus of subgrade reaction of 200 pci. A 9000-lb single-wheel load is applied on the edge of the slab over a circular area with a contact pressure of 100 psi, as shown in Figure P4.8. Compute (a) the curling stress at the edge during the night when the temperature differential is 1.5°F per inch of slab, (b) the loading stress due to the 9000-lb wheel load, and (c) the combined stress at the edge beneath the load due to (a) and (b). [Answer: 140.4, 290.3, 149.9 psi]

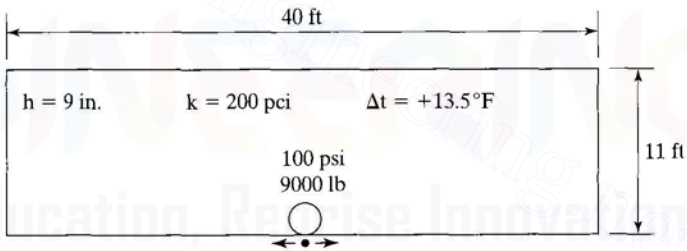


FIGURE P4.8

4.9 If the pavement in Problem 4-8 is one lane of a two-lane highway, as shown in Figure P4.9, design the welded wire fabric and tie bars. [Answer: area of fabric 0.0785 and 0.0432 in.^{2}/ft, $\frac{1}{2}$ in. tie bars, 2 ft long and 3 ft on centers]

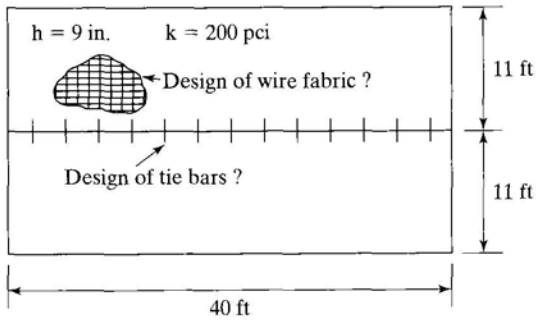


FIGURE P4.9

Downloaded From : www.EasyEngineering.net

Downloaded From : www.EasyEngineering.net

4.10 Develop a design chart for required area of temperature steel in terms of the thickness and length of slab, assuming an allowable tensile stress of 40,000 psi. [Answer: for 100-ft slab, steel areas are 0.1406, 0.1874, 0.2343, and 0.2812 in.^{2} for slab thicknesses of 6, 8, 10, and 12 in., respectively]

4.11 A concrete slab has a width of 12 ft, a thickness of 10 in., and a modulus of subgrade reaction of 300 pci. A 24,000-lb axle load with a wheel spacing of 6 ft is applied at the joint, with one wheel 6 in. from the edge, as shown in Figure P4.11. Determine the maximum bearing stress between concrete and dowel, assuming 100% load transfer, 0.25-in. joint opening, and 1-in. dowel bars at 12 in. on centers. The maximum negative moment is assumed to occur at a distance of 1.8ℓ from the load, where ℓ is the radius of relative stiffness. [Answer: 3160 psi]

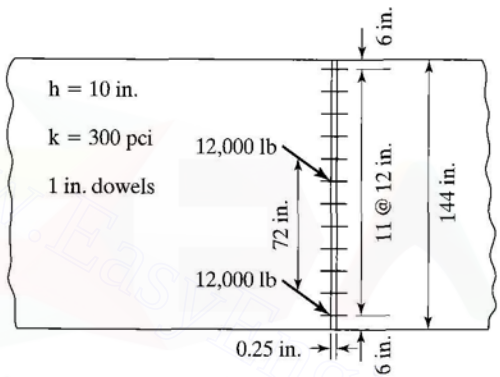


FIGURE P4.11

4.12 Repeat Problem 4-11 by assuming that the maximum negative moment occurs at a distance of 1.0ℓ from the load. [Answer: 4935 psi]

4.13 Same as Problem 4-11, except that one of the 12,000-lb wheels is placed 2.5 ft from the edge, as shown in Figure P4.13. [Answer: 2147 psi]

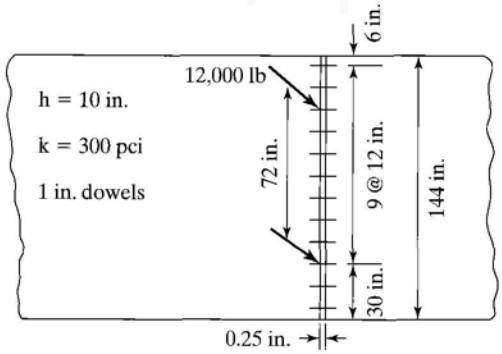


FIGURE P4.13

4.14 Repeat Problem 4-13 by assuming that the maximum negative moment occurs at a distance of 1.0ℓ from the load. [Answer: 3206 psi]

Downloaded From : www.EasyEngineering.net

Downloaded From : www.EasyEngineering.net

CHAPTER 5

KENSLABS Computer Program

5.1 THEORETICAL DEVELOPMENTS

The KENSLABS computer program (Huang, 1985) is based on the finite-element method, in which the slab is divided into rectangular finite elements with a large number of nodes. Both wheel loads and subgrade reactions are applied to the slab as vertical concentrated forces at the nodes.

5.1.1 Types of Foundation

Three different types of foundation can be assumed: liquid, solid, and layer. Westergaard's theory and most of the finite-element computer programs in use today are based on the liquid foundation. The use of liquid foundations results in a banded matrix for the simultaneous equations and requires very little computer time to solve. However, with the much faster speed and larger storage of personal computers, the more realistic solid and layer foundations should be used, if needed.

Liquid Foundation The liquid foundation is also called a Winkler foundation, with the force–deflection relationship characterized by an elastic spring. The term "liquid" does not mean that the foundation is a liquid with no shear strength, but simply implies that the deformation of the foundation under a slab is similar to that of water under a boat. According to Archimedes' principle, the weight of the boat is equal to the weight of water displaced. This is similar to the case where a slab is placed on an infinite number of springs and the total volume of displacement is proportional to the total load applied. The stiffness of a liquid foundation is defined by

$$k = \frac{p}{w} \tag{5.1}$$

Downloaded From : www.EasyEngineering.net

Downloaded From : www.EasyEngineering.net

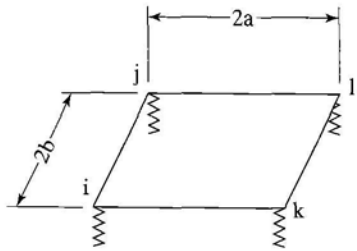


FIGURE 5.1
Liquid foundation under a plate element.

in which k is the modulus of subgrade reaction; p is the unit pressure, or force per unit area; and w is the vertical deflection. For water, $k = 62.4$ pcf $= 0.036$ pci (9.8 kN/m^3); for the subgrade, k can range from 50 to 800 pci (13.6 to 217 MN/m^3).

Figure 5.1 shows the replacement of the large number of springs under a rectangular plate element, with a length of $2a$ and a width of $2b$, by four identical springs at the corners. The force on each spring is equal to the unit pressure p multiplied by the area $a \times b$. From Eq. 5.1, $p = kw$, so the force at node i, F_{wi}, is related to the deflection at node i, w_i, by

$$F_{wi} = kabw_i \tag{5.2}$$

Equation 5.2 can be applied directly when the node is located at the corner of a slab. If the node is located at the edge or interior of a slab, superposition of two or four adjoining elements is required to obtain the force–displacement relationship. Equation 5.2 indicates that the vertical force at node i depends only on the vertical deflection at node i and is independent of the deflections at all other nodes, so the stiffness matrix of a liquid foundation is a diagonal matrix with zero entries everywhere except those relating the vertical force F_{wi} to the vertical deflection w_i itself.

Solid Foundation A solid foundation is more realistic than a liquid foundation because the deflection at any nodal point depends not only on the force at the node itself but also on the forces at all other nodes. This type of foundation is also called a Boussinesq foundation, because the Boussinesq equation for surface deflection is used for determining the stiffness matrix:

$$w_{i,j} = \frac{P_j(1 - \nu_f^2)}{\pi E_f d_{i,j}} \tag{5.3}$$

In this equation, $w_{i,j}$ is the deflection at node i due to a force at node j, P_j is the force at node j, ν_f is Poisson ratio of the foundation, E_f is the elastic modulus of the foundation, and $d_{i,j}$ is the distance between nodes i and j. The flexibility matrix of the foundation is defined as the deflection at a given node due to the forces at all nodes, including the node itself. If $i \neq j$, the flexibility coefficient can be obtained directly from Eq. 5.3 by assigning $P_j = 1$. If $i = j$, then $d_{i,j} = 0$, and Eq. 5.3 cannot be applied. It is therefore necessary to distribute the unit concentrated load over one-quarter of the area as a uniform pressure of $1/(4ab)$ and then integrate numerically. A five-point Gaussian quadrature formula in both the x and the y directions, with the responses computed at 25 points, as shown in Figure 5.2, was used by KENSLABS.

Downloaded From : www.EasyEngineering.net

Downloaded From : www.EasyEngineering.net

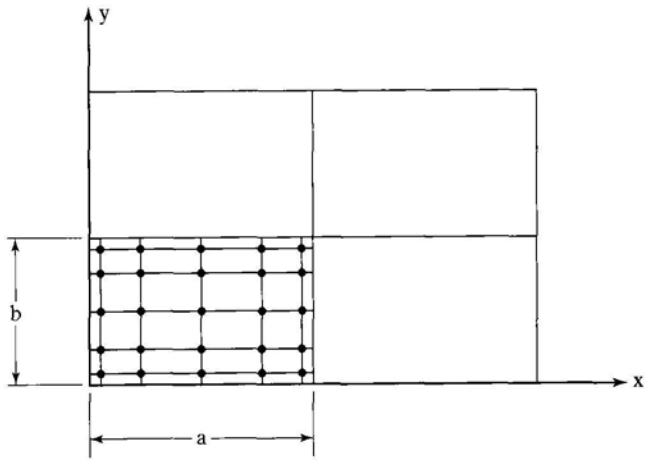


FIGURE 5.2
Solid foundation under a plate element.

For a total of n nodes on the foundation, the flexibility matrix of a solid foundation can be written as

$$\begin{Bmatrix} w_1 \\ w_2 \\ \cdot \\ w_i \\ \cdot \\ w_n \end{Bmatrix} = \begin{bmatrix} g_{11} & g_{12} & \cdot & g_{1i} & \cdot & g_{1n} \\ g_{21} & g_{22} & \cdot & g_{2i} & \cdot & g_{2n} \\ \cdot & \cdot & \cdot & \cdot & \cdot & \cdot \\ g_{i1} & g_{i2} & \cdot & g_{ii} & \cdot & g_{in} \\ \cdot & \cdot & \cdot & \cdot & \cdot & \cdot \\ g_{n1} & g_{n2} & \cdot & g_{ni} & \cdot & g_{nn} \end{bmatrix} \begin{Bmatrix} F_{w1} \\ F_{w2} \\ \cdot \\ F_{wi} \\ \cdot \\ F_{wn} \end{Bmatrix} \tag{5.4a}$$

in which g_{ij} is the flexibility coefficient. If $i \neq j$, then $g_{i,j}$ can be determined by

$$g_{i,j} = \frac{(1 - \nu_f^2)}{\pi E_f d_{i,j}} \tag{5.4b}$$

If $i = j$, then g_{ii} for each finite element must be integrated numerically and then superimposed over all the adjoining elements. It can be seen that the flexibility matrix of a solid foundation is fully populated because the deflection at a given node is affected by the force at any other node. Inversion of the flexibility matrix yields the stiffness matrix of the foundation.

Layer Foundation A layer foundation is also called a Burmister foundation, because Burmister's layered theory is used to form the flexibility matrix. In Burmister's theory, the load is distributed over a circular area, but can easily be converted to a concentrated load by letting the radius of contact approach zero, as illustrated in Section B.4. The procedure for a layer foundation is the same as that for a solid foundation, except that the relationship between deflection and force for the layer foundation is computed from Eq. B.20, instead of from Eq. 5.3 for the solid foundation. To avoid evaluating Eq. B.20 several thousand times, the deflections at 21 different radial distances are computed by Eq. B.20, and those at any given distance can be obtained by a three-point interpolation formula.

Downloaded From : www.EasyEngineering.net

Downloaded From : www.EasyEngineering.net

Relationships Between Solid and Liquid Foundations It is well known that the modulus of subgrade reaction k for a liquid foundation is a fictitious property not characteristic of soil behaviors. However, for simplicity in application, k values have been used most frequently for the design of concrete pavements. It is useful if the k value can be related to the elastic modulus E_f and the Poisson ratio ν_f of the solid foundation, so that a liquid foundation can be used to replace a solid foundation, thus resulting in a large saving of computer time and storage.

Vesic and Saxena (1974) indicated that the value of k depends on the relative flexibility of the slab with respect to the foundation and that there is no single value of k that can give stresses and deflections in a concrete pavement comparable to those obtained by considering the foundation as an elastic solid. For computing stresses, they suggested the use of

$$k = \left(\frac{E_f}{E}\right)^{1/3} \frac{E_f}{(1 - \nu_f^2)h} \tag{5.5}$$

in which E is the elastic modulus of concrete and h is the thickness of the slab. For computing deflections, they suggested that only 42% of the value obtained from Eq. 5.5 be used.

Huang and Sharpe (1989) found that Eq. 5.5 is applicable only to loads in the interior of a slab and not to loads near the slab edge. For edge loading, a factor of 1.75 must be applied to obtain the same edge stress:

$$k = 1.75\left(\frac{E_f}{E}\right)^{1/3} \frac{E_f}{(1 - \nu_f^2)h} \tag{5.6}$$

For corner loading at the transverse joint, a factor of 0.95 must be applied to Eq. 5.5 to obtain the same corner deflection:

$$k = 0.95\left(\frac{E_f}{E}\right)^{1/3} \frac{E_f}{(1 - \nu_f^2)h} \tag{5.7}$$

It should be noted that Eqs. 5.6 and 5.7 must be used only as a rough guide and are applicable only to slabs subjected to a single-axle load.

5.1.2 Two Layers of Slab

KENSLABS can have two layers of slab, either bonded or unbonded. The two layers can be an HMA on top of a PCC or a PCC over a cement-treated base. In the latter case, the cement-treated base can be considered as the second layer of slab or the first layer of the foundation. When it is considered to be the foundation, it is assumed that there is no bond between the concrete slab and the foundation.

Bonded Slabs Figure 5.3 shows a layer of hot mix asphalt with a thickness h_1, an elastic modulus E_1, and a Poisson ratio ν_1 that has been placed on a concrete slab with a thickness h_2, an elastic modulus E_2, and a Poisson ratio ν_2. The left figure is the original section with a unit width, and the right figure is the equivalent section in which the width of hot-mix asphalt is reduced to E_1/E_2. When the moment is taken at the bottom surface, the distance d from the neutral axis to the bottom of slab is

$$d = \frac{(E_1/E_2)h_1(0.5h_1 + h_2) + 0.5h_2^2}{(E_1/E_2)h_1 + h_2} \tag{5.8}$$

Downloaded From : www.EasyEngineering.net

Downloaded From : www.EasyEngineering.net

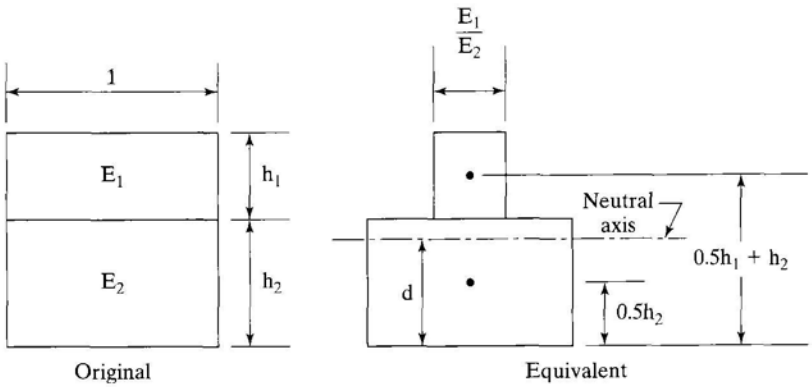


FIGURE 5.3

Original versus equivalent section of composite pavement.

The composite moment of inertia I_c about the neutral axis is

$$I_c = \left(\frac{E_1}{E_2}\right)\left[\frac{1}{12}h_1^3 + h_1(0.5h_1 + h_2 - d)^2\right] + \frac{1}{12}h_2^3 + h_2(d - 0.5h_2)^2 \quad (5.9)$$

Given the moment M, the flexural stress f at the bottom of the concrete slab is

$$f = \frac{Md}{I_c} \quad (5.10)$$

Equation 5.10 can also be used to determine the stress at any point in the composite section, by considering d as the distance from that point to the neutral axis. When two layers are bonded, KENSLABS will print the stresses at four different locations (i. e., at both the top and bottom of each layer).

Example 5.1:

A composite pavement with two bonded layers is subjected to a moment of 3000 in.-lb/in. of slab (13.4 kN-m/m). If $h_1 = 4$ in. (102 mm), $E_1 = 4 \times 10^5$ psi (2.8 GPa), $h_2 = 6$ in. (152 mm), and $E_2 = 4 \times 10^6$ psi (27.6 GPa), as shown in Figure 5.4, determine the maximum flexural stress in tension.

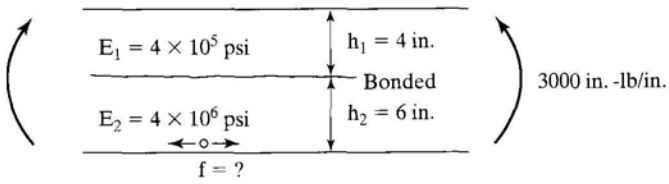


FIGURE 5.4

Example 5.1 (1 in. = 25.4 mm, 1 lb = 4.45 N, 1 psi = 6.9 kPa).

Downloaded From : www.EasyEngineering.net

Downloaded From : www.EasyEngineering.net

Solution: Given $E_1/E_2 = 0.1$, from Eq. 5.8, $d = [0.1 \times 4 \times (0.5 \times 4 + 6) + 0.5 \times 36]/(0.1 \times 4 + 6) = 3.31$ in. (84 mm). From Eq. 5.9, $I_c = 0.1[(4)^3/12 + 4(0.5 \times 4 + 6 - 3.31)^2] + (6)^3/12 + 6(3.31 - 0.5 \times 6)^2 = 27.91$ in.^{3} (4.57×10^5 mm^3). From Eq. 5.10, $f = 3000 \times 3.31/27.91 = 355.8$ psi (2.46 MPa). If there is no asphalt overlay, $d = 3$ in. (76.2 mm) and $I_c = (6)^3/12 = 18$ in.^{3} (2.95×10^5 mm^3), so $f = 3000 \times 3/18 = 500$ psi (3.45 MPa). Note that the overlay reduces the flexural stress in concrete from 500 to 355.8 psi (3.45 to 2.46 MPa), or by about 30%. This is based on the assumption that the moment is the same in both cases. In fact, under the same load, the moment in thicker pavements should be greater than that in thinner pavements, so the actual reduction caused by thicker pavement should be smaller.

In the finite-element method involving only one layer of slab, the stiffness matrix of a plate depends on the modulus of rigidity of the plate R, defined as

$$R = \frac{EI}{1 - \nu^2} = \frac{Eh^3}{12(1 - \nu^2)} \tag{5.11}$$

in which E, ν, I, and h are the modulus of elasticity, Poisson ratio, moment of inertia, and thickness of the plate. When the slabs are composed of two bonded layers, the stiffness matrix of each layer is computed independently, from the respective moduli of rigidity, and then added together to obtain the stiffness matrix of the slabs. The modulus of rigidity of each layer is computed as

$$R_1 = \frac{E_1\left[\frac{1}{12}h_1^3 + h_1(0.5h_1 + h_2 - d)^2\right]}{1 - \nu_1^2} \tag{5.12a}$$

$$R_2 = \frac{E_2\left[\frac{1}{12}h_2^3 + h_2(d - 0.5h_2)^2\right]}{1 - \nu_2^2} \tag{5.12b}$$

Unbonded Slabs If there is no bond between the two layers, each layer is considered an independent slab with the same displacements at the nodes. Therefore, the stiffness matrix of the slabs is the sum of the stiffness matrices of the two layers. After the displacements are determined, the moments at each node in each layer can be computed. After the moment M in each slab is found, the flexural stress f can be determined by

$$f = \frac{Md}{I} \tag{5.13}$$

in which d is the distance from neutral axis to the top or bottom of each layer and I is the moment of inertia of each layer.

Example 5.2:

Same as Example 5.1 except that the two slabs are unbonded. The Poisson ratios are assumed 0.4 for HMA and 0.15 for PCC, as shown in Figure 5.5.

Downloaded From : www.EasyEngineering.net

Downloaded From : www.EasyEngineering.net

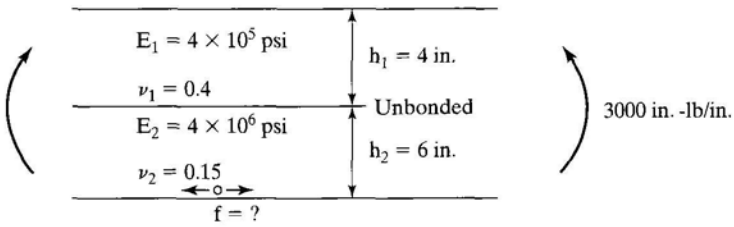


FIGURE 5.5

Example 5.2 (1 in. = 25.4 mm, 1 lb = 4.45 N, 1 psi = 6.9 kPa).

Solution: From Eq. 5.11, the modulus of rigidity of the asphalt layer is $4 \times 10^5 \times (4)^3/[12 \times (1 - 0.16)] = 2.54 \times 10^6$ in.^{2}-lb (7.3 m^2-kN) and that of the concrete is $4 \times 10^6 \times (6)^3/[12 \times (1 - 0.0225)] = 73.7 \times 10^6$ in.^{2}-lb (212 m^2-kN). Although the moments are not exactly proportional to the modulus of rigidity (because they are also affected slightly by the Poisson ratio), an approximate assumption can be made that the amount of moment carried by each layer is proportional to the modulus of rigidity. In the asphalt layer, the moment is $3000 \times 2.54/(2.54 + 73.7) = 100$ in.-lb/in. of slab (445 m-N/m) and, from Eq. 5.13, the flexural stress is $100 \times 2 \times 12/(4)^3 = 37.5$ psi (259 kPa). In the concrete slab, the moment is $3000 \times 73.7/(2.54 + 73.7) = 2900$ in.-lb/in. of slab (12.9 m-kN/m) and the flexural stress is $2900 \times 3 \times 12/(6)^3 = 483$ psi (3.33 MPa).

It can be seen that, if the hot-mix asphalt is not bonded to the concrete, it has very little effect in reducing the flexural stress in the concrete. This conclusion is also based on the assumption that the total moment remains the same after the overlay. However, the total moment would in fact increase after the overlay, so the actual effect should be even smaller. By the use of KENSLABS computer program, it was found that a stress of 500 psi (3.45 MPa) could be obtained in the 6-in. (152-mm) slab with no overlay when the foundation had a modulus of subgrade reaction equal to 100 pci (27.2 MN/m^3) while a concentrated load equal to 2715 lb (12.1 kN) was applied in the interior of the slab. Table 5.1 shows the effect of the 4-in. (102-mm) asphalt overlay on the maximum moments and tensile stresses in the concrete, as obtained by KENSLABS. It can be seen that the overlay increases the total moments by 5% in the bonded case and 1% in the unbonded case and that the decrease in concrete stress is 25% and 3%, respectively.

TABLE 5.1 Effect of Asphalt Overlay on Moments and Stresses in Concrete Slab

	Total moment		Stress in concrete	
Type	in.-lb/in.	%	psi	%
No overlay	3000	100	500	100
Bonded	3162	105	375	75
Unbonded	3032	101	485	97

Note. 1 lb = 4.45 N, 1 psi = 6.9 kPa.

Downloaded From : www.EasyEngineering.net

Downloaded From : www.EasyEngineering.net

5.1.3 General Procedures

The stiffness matrix of the slab is combined with the stiffness matrices of the foundation and the joint, if any, to form the overall stiffness matrix.

Stiffness Matrix of Slab Figure 5.6 shows a rectangular finite element with nodes *i*, *j*, *k*, and *l*. At each node there are three fictitious forces and three corresponding displacements. The three forces are a vertical force F_w, a moment about the *x* axis $F_{\theta x}$, and a moment about the *y* axis $F_{\theta y}$. The three displacements are the vertical deflection in the *z* direction *w*, a rotation about the *x* axis θ_x, and a rotation about the *y* axis θ_y. The positive direction of the coordinates is shown in the figure and the positive direction of moments and rotations can be determined by the right-hand rule. For each element, the forces and displacements are related by

$$\begin{Bmatrix} F_i \\ F_j \\ F_k \\ F_l \end{Bmatrix} = [K_p]^e \begin{Bmatrix} \delta_i \\ \delta_j \\ \delta_k \\ \delta_l \end{Bmatrix} \tag{5.14a}$$

in which $[K_p]^e$ is the element stiffness matrix of a plate having dimension 12×12. At any given node,

$$F_i = \begin{Bmatrix} F_{wi} \\ F_{\theta xi} \\ F_{\theta yi} \end{Bmatrix} \quad \delta_i = \begin{Bmatrix} w_i \\ \theta_{xi} \\ \theta_{yi} \end{Bmatrix} \tag{5.14b}$$

The stiffness matrix of a slab is obtained by superimposing the element stiffness matrix over all elements. By combining the stiffness matrices of slab, foundation, and joint and replacing the fictitious nodal forces with the statical equivalent of the externally applied wheel loads, a set of simultaneous equations is obtained for solving the

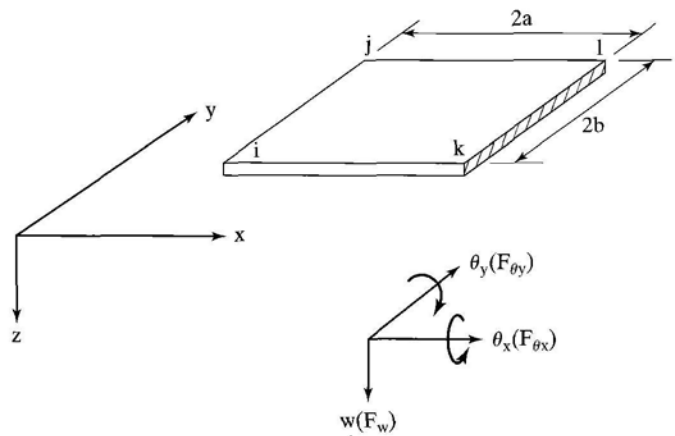


FIGURE 5.6
A rectangular plate element.

Downloaded From : www.EasyEngineering.net

Downloaded From : www.EasyEngineering.net

unknown nodal displacements:

$$[K]\{\delta\} = \{F\} \tag{5.15}$$

in which $[K]$ is the overall stiffness matrix, $\{\delta\}$ are the nodal displacements, and $\{F\}$ are the externally applied nodal forces. The overall stiffness matrix is symmetric, so only the upper half of the matrix need be considered. The nodal moments and stresses can then be computed from the nodal displacements by using the stress matrix tabulated by Zienkiewicz and Cheung (1967). Because the stresses at a given node computed by means of one element are different from those obtained from the neighboring elements, the stresses in all adjoining elements are computed and their average values obtained.

Stiffness of Joint The stiffness of joint is represented by a shear spring constant C_w and a moment spring constant C_θ, defined as

$$C_w = \frac{\text{Shear force per unit length of joint}}{\text{Difference in deflections between two slabs}} \tag{5.16}$$

$$C_\theta = \frac{\text{Moment per unit length of joint}}{\text{Difference in rotations between two slabs}} \tag{5.17}$$

It is generally agreed that load is transferred across a joint principally by shear, with $C_\theta = 0$. Ball and Childs (1975) reported that some moment may be transferred through the joints that remain closed, but moment transfer across joints with visible openings is negligible.

Figure 5.7 shows the shear transfer through a joint by aggregate interlock, as indicated by a spring having a spring constant C_w. After the load is applied, the left slab deflects an amount w_l, and the spring pushes the right slab down a distance w_r. The difference in deflection w_d is equal to $w_l - w_r$.

In the finite-element method, the shear forces are concentrated at the nodes along the joint. From Eq. 5.16,

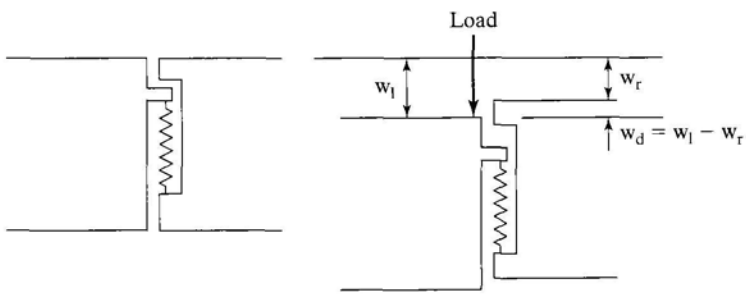


FIGURE 5.7

Shear transfer through joint by aggregate interlock.

Downloaded From : www.EasyEngineering.net

Downloaded From : www.EasyEngineering.net

$$F_w = LC_w w_d \tag{5.18}$$

in which F_w is the nodal force applied to both slabs through the spring and L is the average nodal spacing at the joint. The forces F_w can then be substituted into Eq. 5.15 to solve the nodal displacements.

When dowel bars are used to transmit shear, it is assumed that they are concentrated at the nodes. If the dowel spacing is s_b, the number of dowels at each node is L/s_b. The force F_w is divided by the number of dowels needed to obtain the force P_t on each dowel:

$$P_t = \frac{S_b F_w}{L} \tag{5.19}$$

A simple procedure to include the effect of dowel bars in the finite-element analysis was presented by Huang and Chou (1978). Figure 5.8 shows the shear transfer through a joint by a dowel bar. The difference in deflection w_d is caused by the shear deformation of the dowel ΔS and the deformation of concrete under the dowel y_0:

$$w_d = \Delta S + 2y_0 \tag{5.20}$$

The shear deformation of the dowel can be determined approximately as

$$\Delta S = \frac{P_t z}{GA} \tag{5.21}$$

in which P_t is the shear force on one dowel bar, z is the joint width, A is the area of the dowel, and G is the shear modulus of the dowel, which can be determined from

$$G = \frac{E_d}{2(1 + v_d)} \tag{5.22}$$

The deformation of concrete under the dowel can be determined from the formula

$$y_0 = \frac{P_t(2 + \beta z)}{4\beta^3 E_d I_d} \tag{4.42}$$

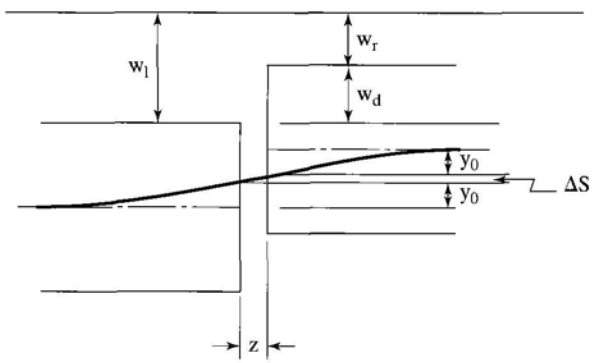


FIGURE 5.8

Shear transfer through joint by dowel bar.

Downloaded From : www.EasyEngineering.net

Downloaded From : www.EasyEngineering.net

Substituting Eqs. 5.21 and 4.42 into Eq. 5.20 yields

$$w_d = \left(\frac{z}{GA} + \frac{2 + \beta z}{2\beta^3 E_d I_d}\right) P_t \tag{5.23}$$

Substituting Eq. 5.19 into Eq. 5.23 and comparing with Eq. 5.18 gives

$$C_w = \frac{1}{S_b\left(\frac{z}{GA} + \frac{2 + \beta z}{2\beta^3 E_d I_d}\right)} \tag{5.24}$$

Equation 5.24 indicates that, given the spacing and diameter of dowels and the joint width, the shear spring constant can be determined. The above analysis is based on the assumption that there is no gap between the spring (or dowel) and the concrete. If a gap w_g exists, then Eq. 5.18 should be written as

$$F_w = LC_w(w_d - w_g) \tag{5.25}$$

Therefore, a term, $LC_w w_g$, should be subtracted from the force vector $\{F\}$ in Eq. 5.15. Because $F_w = 0$ when $W_d < W_g$, Eq. 5.25 is valid only when $W_d > W_g$. Because w_d varies along the joint and it is not known whether W_d is greater than w_g, a trial-and-error method must be used if a gap exists.

Example 5.3:

A 10-in. (254-mm) concrete pavement has joint width 0.2 in. (5 mm), dowel diameter 1 in. (25.4 mm), and dowel spacing 12 in. (305 mm). Determine the spring constant of the joint.

Solution: Assume that $K = 1.0 \times 10^6$ pci (271 GN/m^3) and $E_d = 29 \times 10^6$ psi (200 GPa). With $d = 1$ in. (25.4 mm), from Eq. 4.43, $I_d = \pi/64 = 0.0491$ in.^{4}, and from Eq. 4.44, $\beta = [1.0 \times 10^6 \times 1/(4 \times 29 \times 10^6 \times 0.0491)]^{0.25} = 0.647$ in. (16.4mm). Assuming that Poisson ratio of dowel = 0.3, from Eq. 5.22, $G = 0.5 \times 29 \times 10^6/(1 + 0.3) = 11.2 \times 10^6$ psi (76.9 GPa). With $s_b = 12$ in. (305mm) and $z = 0.2$in. (5mm), from Eq. 5.24,

$$C_w = \frac{1}{12\left(\frac{0.2}{11.2 \times 10^6 \times \pi} + \frac{2 + 0.647 \times 0.2}{2(0.647)^3 \times 29 \times 10^6 \times 0.0491}\right)}$$

$$= \frac{1}{12(5.68 \times 10^{-9} + 2.76 \times 10^{-6})} = 3.01 \times 10^4 \text{ psi (279 MPa)}$$

It can be seen that the term relating to the deformation of dowel is 5.68×10^{-9} while that relating to the deformation of concrete is 2.76×10^{-6}. Therefore, the deformation of concrete actually determines the spring constant of the joint.

Multiple Slabs Figure 5.9 shows a four-slab system with load transfer across the joints. For simplicity, only a limited number of finite elements is used. Slab 1 is divided into four rectangular elements, slabs 2 and 3 are divided into two elements each, and

Downloaded From : www.EasyEngineering.net

Downloaded From : www.EasyEngineering.net

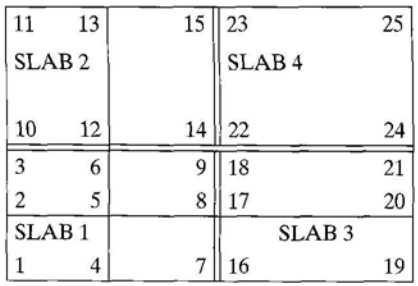


FIGURE 5.9
A four-slab system.

slab 4 is considered as one element. The slabs are numbered consecutively from bottom to top and from left to right. Starting from slab 1, the nodes are also numbered from bottom to top and from left to right and continue to the next slab.

The stiffness matrix of the slab is a banded matrix, because the forces at one node are affected by the displacements at another node only when the two nodes are located in the same element. For the system shown in Figure 5.9, the maximum difference between the two nodal numbers in the same element is 4 and each node has three degrees of freedom, so the minimum half-band width required is $(4 + 1) \times 3 = 15$. If the slabs are placed on liquid foundation with no load transfer across the joints, a half-band width of 15 is sufficient. The use of a small half-band width is highly desirable because it reduces both the computer time and storage in solving the simultaneous equations. If there is shear transfer across the joint, the maximum difference between the two nodes on the opposite side of a joint is 9, so that minimum half-band width required is $(9 + 1) \times 3 = 30$. If the slabs are placed on a solid or layer foundation, the stiffness matrix is fully populated and so has a half-band width of 75.

The procedure for computing the stiffness matrix of solid and layer foundations was described previously for a single slab. For multiple slabs, it is necessary to distribute the stiffness over those nodes meeting at the same point. Take Figure 5.9 for example. Although there are 25 nodes on the slab, only 16 nodes exist on the foundation, because many of the nodes, such as 9, 14, 18, and 22, are actually located at the same point and should be considered as one node. Therefore, the flexibility matrix of the foundation has dimension 16×16. After inversion, the 16×16 stiffness matrix must be enlarged to a 25×25 matrix by distributing the stiffness to all nodes sharing the same point. For instance, the stiffness entry (3, 9) is evenly divided among (3, 9), (3, 14), (3, 18), (3, 22), (10, 9), (10, 14), (10, 18), and (10, 22); the stiffness entry (9, 9) is evenly divided among (9, 9), (14, 14), (18, 18), and (22, 22); and the stiffness entry (3, 21) is evenly divided among (3, 21) and (10, 24). When two or more nodes meet at a joint, the deflections of the slab at the nodes are different but the deflection of the foundation is the same.

The stiffness of a joint is represented by a shear spring constant and a moment spring constant as described previously. Taking nodes 7 and 16 in Figure 5.9 as an example, the shear and moment transfer across the joint can be expressed as

$$F_{w7} = (w_{16} - w_7)C_w \tag{5.26a}$$

$$F_{\theta y7} = (\theta_{y16} - \theta_{y7})C_\theta \tag{5.26b}$$

Downloaded From : www.EasyEngineering.net

Downloaded From : www.EasyEngineering.net

$$F_{w16} = (w_7 - w_{16})C_w \tag{5.26c}$$

$$F_{\theta y16} = (\theta_{y7} - \theta_{y16})C_\theta \tag{5.26d}$$

in which F_w is the shear force across joint, w is the vertical deflection, $F_{\theta y}$ is the moment about the y axis, and θ_y is the rotation about the y axis. These forces and moments can be placed in the force vector on the right side of Eq. 5.15, and the vertical deflections and rotations are then transferred to the left to form the stiffness matrix of the joint.

Simultaneous Equations Equation 5.15 can be solved by the Gauss elimination method. For the system shown in Figure 5.9, the total number of equations is 75. If the foundation is a liquid, the half-band width is 30, instead of 15, due to the presence of joints, so the dimension for the stiffness matrix is $75 \times 30 = 2250$. If the foundation is solid or layer, the half-band width is 75, so the dimension for the stiffness matrix is $75 \times 75 = 5625$. In practical applications, the number of nodes is much greater than 25. The previous DOS version of KENSLABS could not have a memory exceeding 600K, so the dimension of the stiffness matrix was limited to 70,000 (equivalent to 280K of memory). The current Windows version does not have this limitation; the dimension of the stiffness matrix can be increased to 1,600,000 (equivalent to 6.4 MB of memory). With the maximum allowable 420 nodes, the dimension of the stiffness matrix for solid and layer foundations is $420 \times 3 \times 420 \times 3 = 1{,}587{,}600$. However, in analyzing the case of partial contact, only one-half of the dimension can be used to store the new matrix, while the other half is being used to store the previous matrix. If insufficient memory is a problem, an iteration method can be used (Huang, 1974b). In this method, an arbitrary half-band width can be assigned. Any entry in the stiffness matrix outside the half-band is stored and moved to the right side of Eq. 5.15:

$$[K_1]\{\delta\} = \{F\} - [K_2]\{\delta_a\} \tag{5.27}$$

Here, $[K_1]$ is the stiffness matrix within the assigned half-band, $[K_2]$ is the stiffness matrix outside the half-band, and $\{\delta_a\}$ are the assumed displacements outside the half-band. Because the stiffness matrix outside the half-band consists principally of the stiffness matrix of the foundation, eight-ninths of the entries are zeros, which need not be stored, so the storage required for $[K_2]$ is very small.

Equation 5.27 can be solved by an iteration method. First, a set of displacements $\{\delta_a\}$ is assumed and a new set of displacements $\{\delta\}$ is computed. Using $\{\delta\}$ as $\{\delta_a\}$, the process is repeated until the displacements converge to a specified tolerance. This iterative procedure can be applied to all three types of foundation. It was found that the solution converges quite rapidly if a large half-band width is assigned. If the half-band width is equal to the number of equations, no iteration will be required. However, if the half-band width is too small, the solution could diverge, so a larger half-band width should be used. In KENSLABS, the largest possible half-band width within the allowable dimension will be selected automatically for the stiffness matrix.

The use of the foregoing iteration method with a smaller half-band requires not only less memory, but also less time to run. For computers with insufficient memory, a separate program, providing only 100,000 as the dimension of the stiffness matrix, is available. It is suggested that this KENSLABS with small memory be run first. If an

Downloaded From : www.EasyEngineering.net

Downloaded From : www.EasyEngineering.net

error message about insufficient memory appears, then the KENSLABS with large memory can be used.

5.1.4 Temperature Curling

In analyzing temperature curling, it is assumed that each slab acts independently and is not restrained by the lubricated dowel bars. This assumption is reasonable if all the adjoining slabs are of the same size and thickness and curl the same amount at corresponding points along the joint.

General Formulation The general formulation involving curling is similar to that for loading. After the stiffness matrix is superimposed over all elements and the nodal forces are replaced with the statical equivalent of externally applied loads, the following simultaneous equations can be obtained for solving the nodal displacements:

$$[K_p]\{\delta\} = \{F\} + [K_f]\{\delta'\} \tag{5.28a}$$

In these equations, $[K_p]$ is the stiffness matrix of the slab including the joint, if any, $\{\delta\}$ are the nodal displacements of slab, $\{F\}$ are the nodal forces due to applied loads, $[K_f]$ is the stiffness matrix of foundation, and $\{\delta'\}$ are the nodal displacements of foundation. Note that the second term on the right side of Eq. 5.28*a* represents the nodal forces due to the foundation reaction. If the slab has a total of n nodes, then

$$\{\delta\} = \begin{Bmatrix} \delta_1 \\ \cdot \\ \delta_i \\ \cdot \\ \delta_n \end{Bmatrix} \quad \{F\} = \begin{Bmatrix} F_1 \\ \cdot \\ F_i \\ \cdot \\ F_n \end{Bmatrix} \quad \{\delta'\} = \begin{Bmatrix} \delta'_1 \\ \cdot \\ \delta'_i \\ \cdot \\ \delta'_n \end{Bmatrix} \tag{5.28b}$$

and

$$\delta_i = \begin{Bmatrix} w_i \\ \theta_{xi} \\ \theta_{yi} \end{Bmatrix} \quad F_i = \begin{Bmatrix} F_{wi} \\ 0 \\ 0 \end{Bmatrix} \quad \delta'_i = \begin{Bmatrix} c_i - w_i \\ 0 \\ 0 \end{Bmatrix} \tag{5.28c}$$

in which the subscript i indicates the ith node; w is the vertical deflection, downward positive; θ_x is the rotation about the x axis; θ_y is the rotation about the y axis; F_w is the vertical force due to externally applied load, downward positive; and c is the initial curling of a weightless and unrestrained slab due to a temperature differential between the top and the bottom, upward positive. The subgrade displacement indicated by Eq. 5.28*c* is based on Westergaard's assumption of full contact. If the slab curls up an amount c_i, the subgrade will pull it down an amount w_i, so the vertical deflection of the subgrade is $c_i - w_i$. The reason that F_i and δ'_i contain only one nonzero element is that the nodal forces are determined by statics and only vertical loads and reactions are involved. If there is no curling, then $c_i = 0$, so w_i can be moved to the left side of Eq. 5.28*a* and Eq. 5.15 is obtained.

Downloaded From : www.EasyEngineering.net

Downloaded From : www.EasyEngineering.net

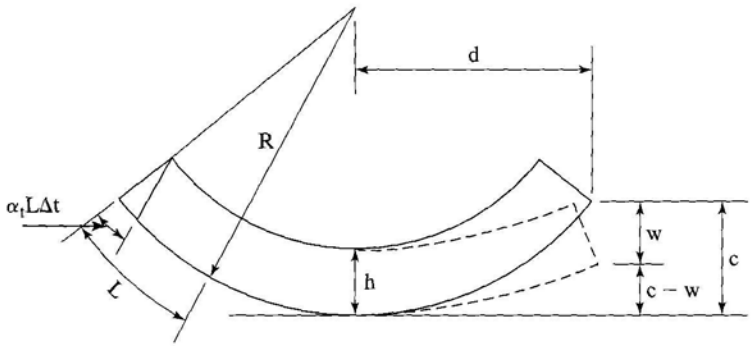


FIGURE 5.10
Curling of slab. (After Huang and Wang (1974).)

Initial Curling The determination of initial curling was presented by Huang and Wang (1974). Figure 5.10 shows, in an exaggerated scale, a thin slab subjected to a temperature differential Δt between the top and the bottom. If the slab is weightless and unrestrained, it will form a spherical surface with a radius R. Because the slab is only slightly curved, the length of the arc on the upper surface is practically the same as that on the lower surface, so the length L of the upper surface is shown as the length of the lower surface. The length is actually greater at the bottom than at the top by $\alpha_t L\Delta t$, where α_t is the coefficient of thermal expansion. Now, the radius R is much greater than the thickness h, and L is much greater than $\alpha_t L\Delta t$, so it can easily be shown by geometry that

$$R = \frac{h}{\alpha_t \Delta t} \tag{5.29}$$

and

$$c = \frac{d^2}{2R} \tag{5.30}$$

in which d is the distance to the center of slab, where curling is zero. Substituting Eq. 5.29 into Eq. 5.30 gives

$$c = \frac{\alpha_t \Delta t d^2}{2h} \tag{5.31}$$

Note that Δt is positive when the slab is curled up, with a temperature at the bottom greater than that at the top, but negative when it is curled down. The assumption that the slab remains in contact with the subgrade implies that the subgrade reaction always exists no matter how the slab is curled. If the slab is curled up, the subgrade will pull the slab down, and a deflection w is obtained, as shown in Figure 5.10. The displacement of the subgrade is thus $c - w$, as indicated by Eq. 5.28*c*. If w (within $\{\delta'\}$ in the second term on the right side of Eq. 5.28*a*) is moved to the left and combined with w on the

Downloaded From : www.EasyEngineering.net

Downloaded From : www.EasyEngineering.net

left, and if c is combined with $\{F\}$, Eq. 5.15 is obtained to solve the nodal displacements. After the displacements are obtained, the stresses can also be computed.

The above derivation for upward curling also applies to downward curling. When the slab is curled down, the temperature differential is negative. If the temperature differential is the same for downward curling as for upward curling, the stresses and deflections will be the same in magnitude, but opposite in sign.

5.1.5 Slab–Subgrade Contact

An important factor that affects the design of concrete pavements is the contact condition between slab and foundation. Both Westergaard's analysis for liquid foundations and Pickett's analysis for solid foundations (Pickett *et al.*, 1951) are based on the assumption that the slab and foundation are in full contact. This assumption is valid if there are no gaps between slab and foundation, because the weight of the slab naturally imposes a large precompression on the foundation, which will keep the slab and foundation in full contact. However, this is not true when the slab is subjected to curling or pumping, which results in a separation between slab and foundation. The KENSLABS computer program is particularly useful for evaluating the effect of contact conditions on stresses and deflections. The analysis of partial contact for liquid foundations was presented by Huang and Wang (1974) and will be described here. Three cases of contact are discussed: full contact, partial contact without initial gaps, and partial contact with initial gaps. The modifications of the procedure for solid and layer foundations are also discussed.

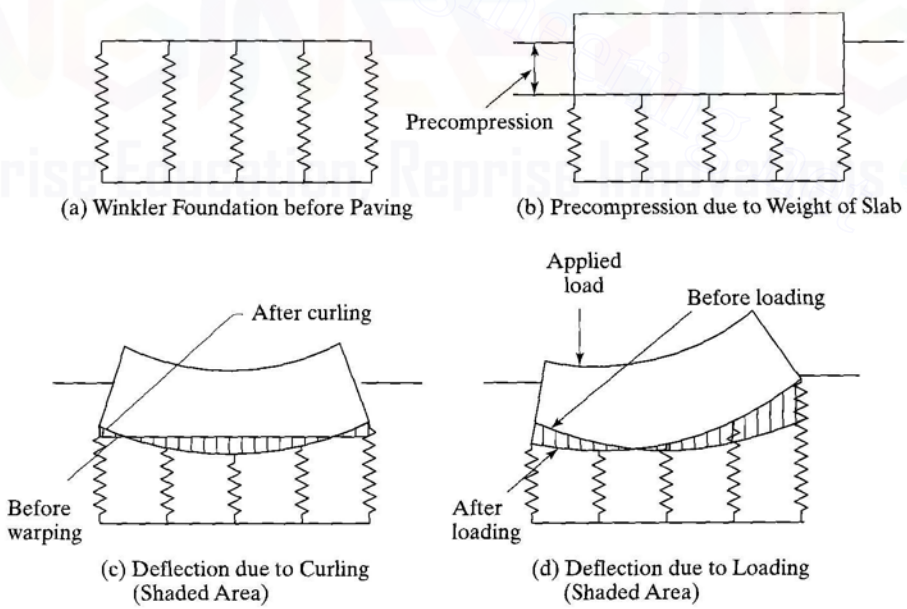


FIGURE 5.11

Spring analogy for full contact. (After Huang and Wang (1974).)

Downloaded From : www.EasyEngineering.net

Downloaded From : www.EasyEngineering.net

Full Contact Figure 5.11 shows a liquid or Winkler foundation consisting of a series of springs, each representing a nodal point in the finite-element analysis. When a slab is placed on the foundation, the weight of the slab will cause a precompression of the springs, as shown in Figure 5.11*b*. Because the slab is uniform in thickness, each spring will deform the same amount, and no stresses will be induced in the slab. The amount of precompression can be determined directly by dividing the weight of slab per unit area by the modulus of subgrade reaction.

When the temperature on top of the slab is colder than that at the bottom, as is usually the case at night, part of the slab will deflect upward, as shown in Figure 5.11*c*. However, the slab and the springs remain in contact because the upward deflections are smaller than the precompression. The deflection of the slab due to curling can be determined by subtracting the precompression due to the weight of the slab from the deflection due to the weight and the curling combined, as indicated by the shaded area in Figure 5.11*c*. The result is exactly the same as when considering the curling alone. The same is true when a load is applied to a curled slab, as shown in Figure 5.11*d*. Therefore, when the slab and the subgrade are in full contact, the principle of superposition applies. The stresses and deflections due to curling and loading can be determined separately, each independently of the other, disregarding the weight of the slab. This principle forms the basis of Westergaard's analysis.

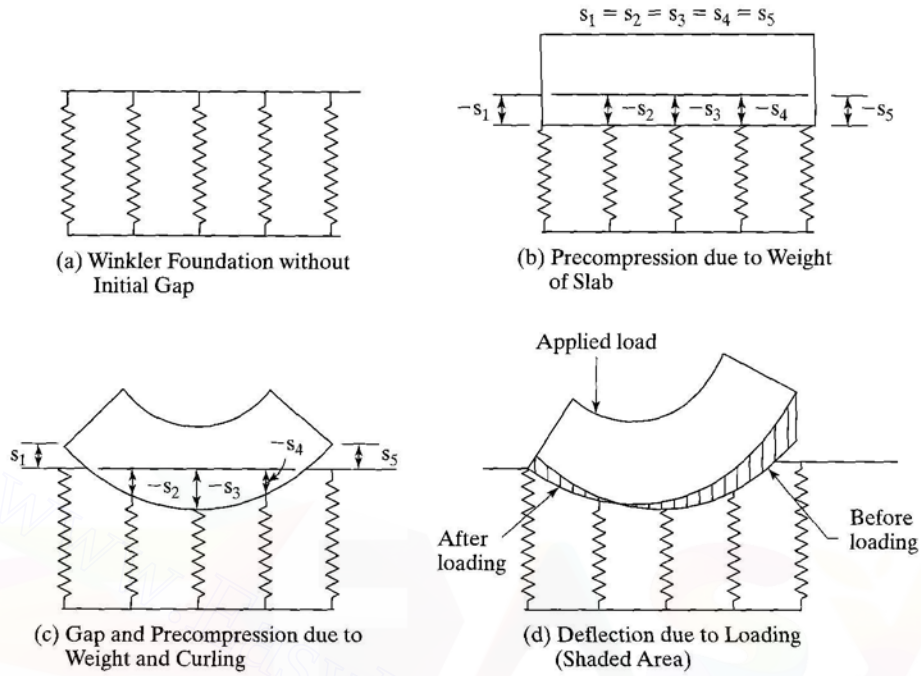
The major difference in procedure between full and partial contact is that, in the case of full contact, it is not necessary to consider the weight of the slab, whereas, in the case of partial contact, the weight of the slab must be considered. The latter case involves two steps. First, the gaps and precompressions of the subgrade due to the weight of the slab or due to the weight of the slab and the curling combined are determined. These gaps and precompressions are then used to determine the stresses and deflections due to applied loads.

It should be noted that full contact is a special case of partial contact. Every problem in partial contact is analyzed first by assuming the slab and the subgrade to be in full contact. If it turns out that they are actually in full contact, no iterations are needed. If some points are found out of contact, the reactive force at those points is set to zero. The process is repeated until the same contact conditions are obtained.

Partial Contact Without Initial Gaps This case applies to new pavements not subjected to significant amounts of traffic and where there is no pumping or plastic deformation of the subgrade. Each spring in the Winkler foundation is in good condition and, if the slab is removed, will rebound to the same elevation with no initial gaps, as shown in Figure 5.12*a*. Under the weight of the slab, each spring is subjected to a precompression, as shown in Figure 5.12*b*. If the slab is curled up, gaps will form at the exterior springs, as indicated by a positive s in Figure 5.12*c*, and precompressions will form at the interior springs, as indicated by a negative s. If the slab is curled down, all springs will be under precompression—similar to Figure 5.12*b*, except that the precompressions are not equal. For very stiff springs, a gap could also form at the interior springs. The displacements due to the weight of the slab and curling combined can be determined from Eq. 5.28, except that the

Downloaded From : www.EasyEngineering.net

Downloaded From : www.EasyEngineering.net



(a) Winkler Foundation without Initial Gap

(b) Precompression due to Weight of Slab

(c) Gap and Precompression due to Weight and Curling

(d) Deflection due to Loading (Shaded Area)

FIGURE 5.12

Partial contact without initial gap. (After Huang and Wang (1974).)

subgrade displacements are expressed as

$$\delta_i' = \begin{Bmatrix} c_i - w_i \\ 0 \\ 0 \end{Bmatrix} \quad \text{when } w_i > c_i \tag{5.32a}$$

$$\delta_i' = \begin{Bmatrix} 0 \\ 0 \\ 0 \end{Bmatrix} \quad \text{when } w_i < c_i \tag{5.32b}$$

Note that δ_i' in Eq. 5.32*a* is the same as that in Eq. 5.28*c* for full contact and will be used to start the iteration. After each iteration, a check is made on each node to find out whether any contact exists. If the deflection w is found to be smaller than the initial curling c, then the slab is not in contact with the subgrade, and the subgrade displacement is set to zero, as indicated by Eq. 5.32*b*. Thus, after each iteration, a new set of simultaneous equations is established. The process is repeated until the same equations are obtained. In most cases, this can be achieved by five or six iterations. After the deflections due to the weight and curling are determined, the gaps and precompressions can be computed for use later in computing the stresses and deflections due to the load alone.

Downloaded From : www.EasyEngineering.net

Downloaded From : www.EasyEngineering.net

To determine the stresses and deflections due to the load alone, the gaps and precompressions shown in Figures 5.12*b* or 5.12*c*, depending on whether curling exists, must first be determined. Using these gaps and precompressions as s, the deflections due to the load alone, as shown in Figure 5.12*d*, can be determined from Eq. 5.28, except that the subgrade displacements are expressed as

$$\delta_i' = \begin{Bmatrix} 0 \\ 0 \\ 0 \end{Bmatrix} \qquad \text{when } w_i < s_i \tag{5.33a}$$

$$\delta_i' = \begin{Bmatrix} s_i - w_i \\ 0 \\ 0 \end{Bmatrix} \qquad \text{when } w_i > s_i \text{ and } s_i > 0 \tag{5.33b}$$

$$\delta_i' = \begin{Bmatrix} -w_i \\ 0 \\ 0 \end{Bmatrix} \qquad \text{when } w_i > s_i \text{ and } s_i < 0 \tag{5.33c}$$

In checking w with s, downward deflection is considered positive, upward negative; likewise, the gap is considered positive and precompression negative. First, assume the slab and the subgrade to be in full contact, and determine the deflections of the slab due to the applied load. Second, check the deflections with s, and form a new set of equations based on Eq. 5.33. Repeat the process until the same equations are obtained.

When the slab and the subgrade are in partial contact, the principle of superposition no longer applies. To determine the stresses and deflections due to an applied load, the deformed shape of the slab immediately before the application of the load must be computed first. This deformed shape depends strongly on the condition of curling, so the stresses and deflections due to loading are affected appreciably by curling. This fact was borne out in both the Maryland (HRB, 1952) and the AASHO (HRB, 1962) road tests.

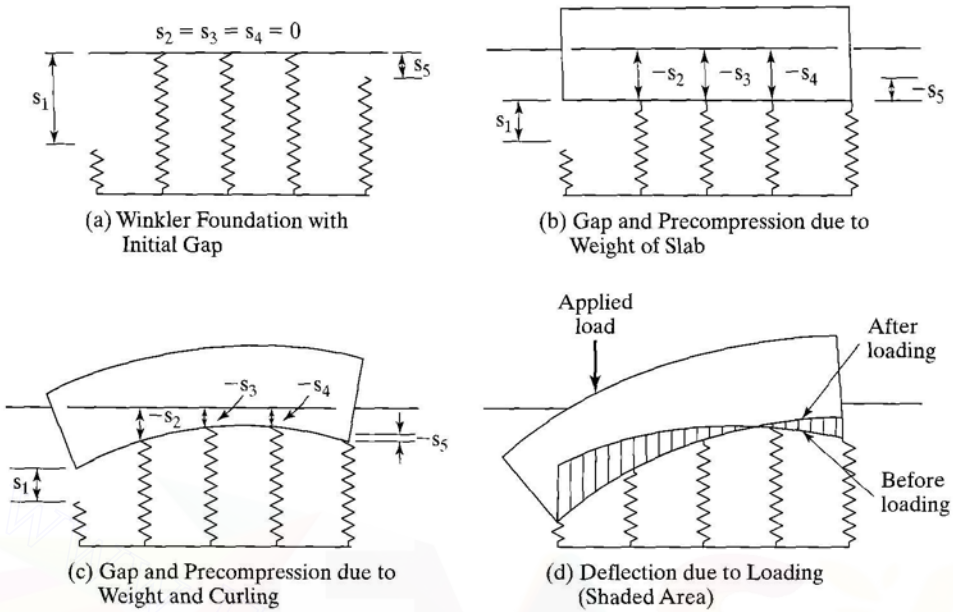
Partial Contact with Initial Gaps This case applies to pavements that have been subjected to a high intensity of traffic. Because of pumping or plastic deformation of the subgrade, some springs in the Winkler foundation become defective and, if the slab is removed, will not return to the original elevation. Thus, initial gaps are formed, as indicated by the two exterior springs in Figure 5.13*a*. These gaps s must be assumed before an analysis can be made. The displacements due to the weight of the slab, as shown in Figure 5.13*b*, can be determined from Eq. 5.28, except that the subgrade displacements are expressed as

$$\delta_i' = \begin{Bmatrix} s_i - w_i \\ 0 \\ 0 \end{Bmatrix} \qquad \text{when } w_i > s_i \tag{5.34a}$$

$$\delta_i' = \begin{Bmatrix} 0 \\ 0 \\ 0 \end{Bmatrix} \qquad \text{when } w_i < s_i \tag{5.34b}$$

Downloaded From : www.EasyEngineering.net

Downloaded From : www.EasyEngineering.net



(a) Winkler Foundation with Initial Gap

(b) Gap and Precompression due to Weight of Slab

(c) Gap and Precompression due to Weight and Curling

(d) Deflection due to Loading (Shaded Area)

FIGURE 5.13

Partial contact with initial gap. (After Huang and Wang (1974).)

First, assume that the slab and the subgrade are in full contact, and determine the vertical deflections of the slab from Eq. 5.28*a*. Next, check the deflection at each node against the gap *s*. If the deflection is smaller than the gap, as shown by the left-most spring in Figure 5.13*b*, then use Eq. 5.34*b*; if the deflection is greater than the gap, as shown by the other springs in Figure 5.13*b*, then use Eq. 5.34*a*. Repeat the process until the same equations are obtained. After the deflections are obtained, the gaps and precompressions can be computed and used later for computing the stresses and deflections due to loading, if no curling exists.

It can be seen that, if the springs are of the same length, as shown in Figure 5.12, the weight of the slab will result in a uniform precompression, and no stresses will be set up in the slab. However, if the springs are of unequal lengths, the deflections will no longer be uniform, and stressing of the slab will occur.

Figure 5.13*c* shows the combined effect of weight and curling when the slab is curled down. Downward, rather than upward, curling is considered here because the case of upward curling is similar to Figure 5.12*c* except that the gaps are measured from the top of the defective springs. Because the method is applicable to both upward and downward curling, the case of downward curling is used for illustration. The procedure for determining the deflections is similar to that involving the weight of the slab alone, except that the initial curling of the slab, as indicated by Eq. 5.31, is added to the gap shown in Figure 5.13*a* to form the total gap and precompression *s* for use in Eq. 5.34. Because the gap is either positive or zero and the initial curling may be positive or negative, depending on whether the slab is curled up or down, *s* may be positive or negative. After the deflections of the slab are obtained, the gaps and precompressions, as shown in Figure 5.13*c*, can be

Downloaded From : www.EasyEngineering.net

Downloaded From : www.EasyEngineering.net

determined. These gaps and precompressions will be used for computing the stresses and deflections due to the load alone, as shown in Figure 5.13*d*.

Modifications for Solid and Layer Foundations The above procedure for liquid foundations has to be modified when it is applied to solid or layer foundations. The actual criterion for deciding the contact condition is whether any tension exists between the slab and the foundation. In liquid foundations, tension is indicated if the slab moves up relative to the foundation, and compression is implied if the slab moves down. By merely comparing deflections, as indicated by Eqs. 5.32 and 5.33, the contact conditions can be ascertained. In solid or layer foundations, tension or compression at a given node is governed not only by the deflection of the node itself but also by the deflections of all other nodes. If the contact condition is purely based on the deflection at one node, there is the possibility that tension may develop due to the deflections at other nodes. Therefore, whether the slab and foundation are treated as being in contact at a given node should be based on whether the actual reactive force is in compression or tension, instead of on the deflections.

First, the slab and foundation are assumed to be in full contact and the reactive force at each node is determined. If the reactive force is in tension and the tension is greater than the precompression (note that the term precompression used in solid or layer foundations indicates a force, while that in liquid foundation indicates a displacement), the node is not in contact, and its reactive force is set to zero in the next iteration. When there is no reactive force at a given node, that node should be eliminated from the flexibility matrix and a new stiffness matrix for the foundation is formed. The process is repeated until the same contact conditions are obtained.

5.2 PROGRAM DESCRIPTION

KENSLABS, together with its input program SLABSINP and graphic programs SGRAPH and CONTOUR, is part of a computer package called KENPAVE. In its present dimensions, it can be applied to a maximum of 6 slabs, 7 joints, and 420 nodes. Each slab can have a maximum of 15 nodes in the x-direction and 15 nodes in the y-direction. Damage analysis can be made by dividing each year into a maximum of 12 periods, each with a maximum of 12 load groups.

Similar to LAYERINP, a program named SLABSINP can be used to create and edit data files. More about SLABSINP is presented in Appendix C.

5.2.1 General Features

The capabilities, limitations, and applications of the program, together with the automatic checking of contact between slab and foundation, are discussed in this section.

Capabilities The capabilities of the program are as follows:

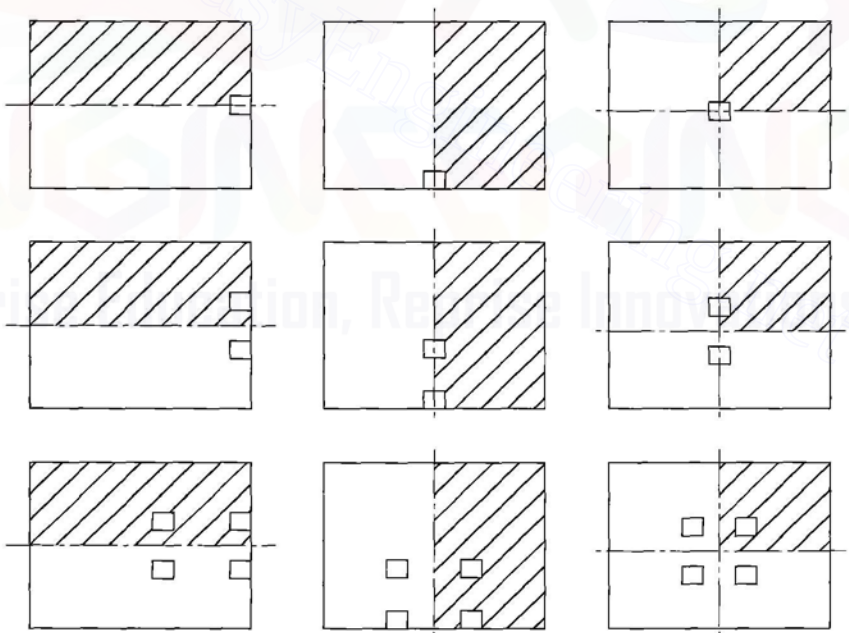
1. A maximum of six slabs with shear and moment transfer across the joints can be analyzed. Shear transfer can be effected by specifying a shear spring constant or by providing information on the size, spacing, Young's modulus, and Poisson ratio

Downloaded From : www.EasyEngineering.net

Downloaded From : www.EasyEngineering.net

of dowel bars together with the joint width and the modulus of the dowel support. Dowels can have nonuniform spacings by assigning zero, one, or more dowels at each node along a joint. Moment transfer is specified by a moment spring constant. The looseness of the dowel can be considered by specifying a gap between dowel and concrete. This gap can also be applied to the shear spring constant but not to the moment spring constant.

2. Each slab can have different thicknesses and sizes. In the same slab, thickness can vary from node to node. However, two adjoining slabs must have the same width, and all joints must be continuous throughout the slabs.
3. The slabs can have two rigid layers, either bonded or unbonded. Each layer has its own Young's modulus and Poisson ratio. The modulus of rigidity for determining the stiffness of the slabs is computed by Eq. 5.11 for unbonded layers and Eq. 5.12 for bonded layers. The stiffness matrix of the slabs is the sum of the stiffness matrices of both layers.
4. The load can be uniformly distributed over rectangular areas or concentrated at a given number of nodes. Each loaded area can have a different intensity of pressure.
5. If symmetry with respect to one or both axes exists, only one-half or one-quarter of the slab system need be considered (Huang, 1974b). This feature can save a great deal of computer time and storage. Figure 5.14 shows several cases of



(a) SYMMETRY WITH RESPECT TO x-AXIS

(b) SYMMETRY WITH RESPECT TO y-AXIS

(c) SYMMETRY WITH RESPECT TO BOTH x-AND y-AXES

FIGURE 5.14

Use part of slab for cases of symmetry.

Downloaded From : www.EasyEngineering.net

Downloaded From : www.EasyEngineering.net

symmetry under single, dual, and dual-tandem wheel loads. Although the part to be used for analysis is indicated by hatched lines, any quadrant or half can be used.

6. The effect of temperature curling and the gap between slab and foundation on the stresses and deflections can be analyzed.
7. The slab and foundation can be assumed to be in full contact at all nodes or not in contact at some designated nodes. The contact condition can also be evaluated automatically by iterations.
8. The program can analyze slabs on liquid, solid, or layer foundations.

Limitations

1. When one is considering temperature curling, each slab is assumed to curl into a spherical surface independent of the others. This occurs only when there is no moment transfer across the joints, and each slab can move up and down freely, as in the case of lubricated dowel joints. It might not be applicable to hinged or longitudinal joints, where the edges of adjoining slabs are held tightly together. Fortunately, the most critical area for a pavement is not in the vicinity of a longitudinal joint, so this inaccuracy should have very little effect on the final design. The analysis of temperature curling is based on the assumption that there is only one layer of slabs and that each slab is of uniform thickness. For slabs of nonuniform thickness, an average thickness must be assumed.
2. When slabs are composed of two layers, the joints through the two layers are at exactly the same locations. If the bottom layer has no joints and is much weaker than the top layer, this assumption should have very little effect on the stresses in the top layer.
3. The program does not permit the use of infinitely stiff joints, where the deflections or rotations on the two sides of the joint are equal. When a very large spring constant is applied to a joint, the equation for each node on the two opposite sides is identical and the system of simultaneous equations becomes singular. This situation will not occur in practice and can be detected easily if the printout shows that the sum of applied forces is significantly different from the sum of reactive forces. Methods based on the efficiency of load transfer (Chou, 1981; Huang and Deng, 1982) can be applied to infinitely stiff joints but are not used in KENSLABS because it is unreasonable to assume the same efficiency for all points along a joint.
4. The use of rectangular elements severely limits the size of elements to be employed. If small elements are used in the main slab, elements in the adjoining slabs will be of the same small width. The limitation that the length–width ratio of any element be not greater than 4 or 5 requires a lot of elements to be used throughout the slab system. If many slabs are involved, a relatively large grid should be used to save computer time and storage. Fortunately, a relatively large grid can still yield reasonable results.

Downloaded From : www.EasyEngineering.net

Downloaded From : www.EasyEngineering.net

5. The program can determine only the stresses in the concrete slabs and the deflections of the slab and the foundation. The stresses in the solid or layer foundation cannot be obtained.

Evaluation of Contact To check the contact condition between slab and foundation under a given load, it is necessary to know the contact condition before the load is applied. Therefore, the gaps at those nodes not in contact and the precompressions at those nodes in contact must be specified. Because these gaps and precompressions prior to the application of the load are difficult to determine, the best way is to divide the analysis into two steps.

First, determine the gaps and precompressions between slab and foundation under weight, temperature curling, and initial gaps, if any. The initial gap is the gap before the slab is constructed. In fact, there are no gaps between slab and foundation when the concrete is poured. Gaps develop only after pumping or plastic deformation of the foundation has taken place. Initial gaps can be visualized as a change in grade should the slabs be removed. Because these gaps are difficult to predict, a rough estimate of their possible occurrences near the pavement edges or joints is all that is needed. Nondestructive deflection tests can be used to detect the voids under concrete pavements (AASHTO, 1986) and the information obtained from these tests on existing pavements can be used as a guide. Next, using the gaps and precompression obtained in the first step, determine the stresses and displacements under the applied load. These two steps should be executed in the same run, one immediately after the other, so the gaps and precompressions determined in step 1 can be used in step 2.

The reasons that curling and loading are analyzed separately in two steps are because these two cases do not occur at the same frequency and because the modulus of the subgrade due to the slowly changing temperature gradient could be much smaller than that due to transient wheel loads. Although stresses due to temperature curling are significant in concrete pavements, many of the current design methods consider only the stresses due to loading, so a separation of loading and curling stresses is needed. However, the program can determine the combined effect of curling and loading, if desired.

Applications Before running KENSLABS, it is necessary to sketch a plan view of the slabs, divide them into rectangular finite elements of various sizes, and number the slabs, nodes, and joints. In dividing slabs into rectangular finite elements, it is not necessary to use very fine divisions. In most cases, elements of width 10 to 12 in. (254 to 305 mm) are sufficient for regions near the load or in the area of interest. Larger elements can be used when they are far away from the load. To obtain more accurate results, the length-to-width ratio of any element should not be greater than 5. To model an infinite slab, the boundary or edge of slab should be placed at least 10 ft (3.28 m) from the load.

Numbering of Slabs, Nodes, and Joints To facilitate programming, it is necessary to number the slabs in a systematic manner. First, consider the slab at the lower left corner as number 1, and proceed column-wise from bottom to top. When one column of slabs has been numbered, move to the right column and continue numbering from bottom to top until all slabs are numbered. In each slab, the nodes are numbered

Downloaded From : www.EasyEngineering.net

Downloaded From : www.EasyEngineering.net

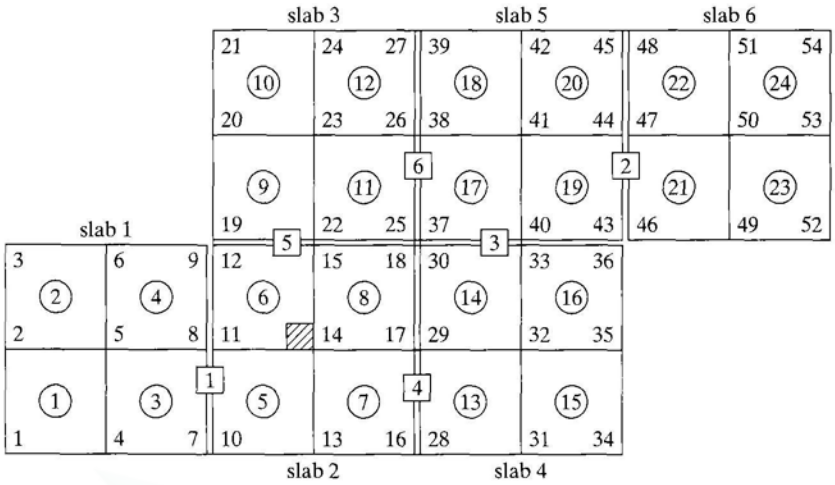


FIGURE 5.15

Numbering of slabs, nodes, and joints.

consecutively from bottom to top along the y axis, starting from the lower left corner, and then moving to the right until all nodes in the slab are numbered. The numbering is then continued on the next slab. The joints can be numbered in any arbitrary way. Figure 5.15 shows the numbering of slabs, nodes, and joints. Also shown within the circles are the element numbers to be used internally and the uniform load applied at the corner of element 6 to be used later for illustration.

The above method for numbering nodal points is not very efficient for multiple slabs on a liquid foundation because it usually results in a stiffness matrix with a larger half-band width. The half-band width is governed by the maximum difference between the nodal numbers on the opposite side of the joints. The maximum difference for the slabs shown in Figure 5.15 is 12 and occurs at joints 4 and 6. The half-band width is $(12 + 1) \times 3 = 39$. The half-band width can be reduced if the nodes are numbered vertically from bottom to top across the joints. For example, if nodes 19, 20, and 21 are changed to 13, 14, and 15 and nodes 13, 14, and 15 are changed to 16, 17, and 18, and the other nodes are changed accordingly, the maximum number of nodes in the vertical direction is 6, so the half-band width is reduced to $(6 + 2) \times 3 = 24$. To reduce the half-band width and to save computer time and storage for a liquid foundation, the program will renumber the nodes vertically from the bottom of one slab to the top of the other slab before forming the overall stiffness matrix. This change is done internally, and the nodal numbers are switched back to the original without the knowledge of the program user. This additional procedure is applied only to liquid foundations when the dimension of stiffness matrix is less than 100,000, so that the equations can be solved without iterations. If, after renumbering, the dimension of stiffness matrix is still greater than 100,000, the original numbering will be restored and the equations will be solved by iterations. For solid and layer foundations, it is not necessary to renumber the nodes, because the stiffness matrix is always fully populated no matter how the nodes are numbered.

Downloaded From : www.EasyEngineering.net

Downloaded From : www.EasyEngineering.net

An input parameter JONO(J,I) is used to relate the location of joints to the slabs, where the first subscript, J, indicates the four sides (left, right, bottom, and top) of a slab, and the second subscript, I, indicates the slab number. For example, the left side of slab 1 has no joint, so JONO(1,1) = 0; the right side is joint 1, so JONO(2,1) = 1; the bottom and top sides have no joints, so JONO(3,1) = 0 and JONO(4,1) = 0. Similarly, for slab 2, JONO(1,2) = 1, JONO(2,2) = 4, JONO(3,2) = 0, and JONO(4,2) = 5. The same rule applies to all other slabs.

Types of Problems to Be Solved The following input parameters are important for determining the type of problems to be solved:

INPUT = code indicating whether gaps and precompressions are obtained from a previous problem. Assign 0 for no and 1 for yes.

NCYCLE = maximum number of iteration cycles for checking subgrade contact. Assign I for full contact or when no iterations are required and 10 for partial contact or when iterations are required.

NOTCON = total number of nodes that are assumed not in contact or at which subgrade reactions are initially set to 0. If NCYCLE = 1, these nodes will never be in contact. If NCYCLE = 10, these nodes may or may not be in contact, depending on the computed results.

NWT = code indicating whether slab weight is considered. Assign 0 when weight is not considered, as in the case of full contact with NCYCLE = 1, and 1 when weight is considered.

These parameters can be used in combinations to analyze the following cases:

1. *Case 1*: Slab and foundation are in full contact as originally assumed by Westergaard. Set INPUT to 0, NCYCLE to 1, NOTCON to 0, and NWT to 0. This case does not require iterations for checking contact conditions.
2. *Case 2*: Slab and foundation are in full contact at some nodes but completely out of contact at other nodes. Set INPUT to 0, NCYCLE to 1, NOTCON to the number of nodes not in contact, and NWT to 0. This case does not require iterations for checking contact conditions.
3. *Case 3*: Partial contact under wheel loads should be analyzed in two steps. First, determine the gaps and the precompressions between slab and foundation under weight, temperature curling, and gaps, if any, by setting INPUT = 0, NCYCLE =10, and NWT = 1. Then, using the gaps and precompressions thus computed, determine the stresses and deflections under wheel loads by setting INPUT = 1, NCYCLE = 10, and NWT = 0.
4. *Case 4*: If there is no gap between slab and foundation and no temperature curling, an approximate method with a single step can be used to analyze partial contact under wheel loads by specifying INPUT = 0, NCYCLE = 10, and NWT = 1. The stresses and deflections thus determined are due to the combined effect of the weight of slab and the wheel loads. Because the stress induced by the weight of slab is 0 for liquid foundations and very small for solid and layer foundations, when

Downloaded From : www.EasyEngineering.net

Downloaded From : www.EasyEngineering.net

compared with the stresses due to wheel loads, the maximum stress obtained by this simplified procedure can be used directly for design purposes. However, this method cannot be used to determine the deflections under wheel loads, because the deflections induced by the weight of slab are quite significant.

Damage Analysis Much as with KENLAYER, damage analysis can be performed by dividing each year into a maximum of 12 periods, each with a maximum of 12 load groups. Because only the properties of foundation vary with the season, a foundation seasonal adjustment factor (FSAF) is assigned to each period. The modulus of subgrade reaction of a liquid foundation or the stiffness matrix of solid and layer foundations is multiplied by this factor to simulate the seasonal change in the stiffness of foundation.

Damage is based on fatigue cracking only and is defined by the cracking index (CI), which is the same as the damage ratio shown by Eq. 3.19. The allowable number of repetitions can be expressed as

$$\log N_f = f_1 - f_2\left(\frac{\sigma}{S_c}\right) \tag{5.35}$$

in which N_f is the allowable number of repetitions, σ is the flexural stress in slab, and S_c is the modulus of rupture of concrete. In the design of zero-maintenance jointed plain concrete pavements, Darter and Barenberg (1977) recommended the use of $f_1 = 16.61$ and $f_2 = 17.61$. The following fatigue equations are recommended by the Portland Cement Association (Packard and Tayabji, 1985):

$$\text{For } \frac{\sigma}{S_c} \geq 0.55: \quad \log N_f = 11.737 - 12.077\left(\frac{\sigma}{S_c}\right) \tag{5.36a}$$

$$\text{For } 0.45 < \frac{\sigma}{S_c} < 0.55: \quad N_f = \left(\frac{4.2577}{\sigma/S_c - 0.4325}\right)^{3.268} \tag{5.36b}$$

$$\text{For } \frac{\sigma}{S_c} \leq 0.45: \quad N_f = \text{unlimited} \tag{5.36c}$$

More about fatigue characteristics of concrete is presented in Section 7.3.2.

After the allowable number of repetitions is determined, the damage ratio, as defined by Eq. 3.19 for flexible pavements, can be used to compute the design life. Because only the fatigue cracking is involved, the cracking index, CI, which is the same as the damage ratio, D_r, is used for rigid pavements.

How damage analysis is to be performed is controlled by the input parameter NDAMA. If NDAMA = 0, no damage analysis will be made. If NDAMA = 1, Eq. 5.36, recommended by PCA, will be used. If NDAMA = 2, Eq. 5.35 will be used and the coefficients f_1 and f_2 must be specified by the users. To simplify programming, NCYCLE must be equal to one when the number of periods (NPY) or the number of load groups (NLG) is greater than one.

One question on fatigue cracking that needs to be resolved is whether the passage of one set of tandem-axle loads should be considered as one or two repetitions.

Downloaded From : www.EasyEngineering.net

Downloaded From : www.EasyEngineering.net

The PCA method (PCA, 1984) treats one tandem-axle load as one repetition, the zero-maintenance method (Darter and Barenberg, 1977) as two. Theoretically, the damage analysis of tandem axles is similar to that for flexible pavements, as explained in Figure 3.3, except that the tensile stress caused by the passage of the first axle load is σ_a and that from the second axle load is $\sigma_a - \sigma_b$. If $\sigma_a - \sigma_b$ is much smaller than σ_a, the stress ratio (the ratio between the flexural stress and the modulus of rupture) due to the second load is most probably smaller than 0.45 and, according to the PCA failure criteria, should have no effect on fatigue damage. Therefore, the assumption of one tandem-axle load as one repetition is more reasonable. This is in line with the erosion analysis based on corner deflection in which one tandem-axle load is considered as one repetition. By the same reasoning, the passage of a set of tridem-axle loads should still be counted as one repetition.

If the stress ratio due to $\sigma_a - \sigma_b$ is greater than 0.45, or Eq. 5.35 without such a limit is used, then the second and third axle loads will have some effect on fatigue damage. This additional damage can be analyzed by KENSLABS and is discussed in Section 6.4.5.

5.3 COMPARISON WITH AVAILABLE SOLUTIONS

It is generally agreed that the finite-element method is one of the most powerful tools for analyzing rigid pavements, particularly those with partial contact. Many studies (Huang and Wang, 1973, 1974; Huang, 1974a; Darter and Barenberg, 1977; Chou and Huang, 1981) were made comparing finite-element solutions with field measurements, and close agreements were reported. In this section, the solutions obtained by KENSLABS are compared with other theoretical solutions available.

5.3.1 Analytical Solutions

The analytical solutions to be compared include Westergaard's solutions for edge loading and the solutions for temperature curling by Westergaard and Bradbury.

Edge Loading The analytical solutions for a concentrated load applied at the edge of an infinite slab far from any corner were presented by Westergaard (1926b). In the finite-element method, the infinite slab can be approximated by a large slab, 20ℓ long by 10ℓ wide, where ℓ is the radius of relative stiffness. Because the problem is symmetrical with respect to the y axis, only one-half of the slab need be considered. The slab is divided into rectangular finite elements, as shown by the insert in Figure 5.16. The x coordinates are 0, $\pi\ell/8$, $\pi\ell/4$, $\pi\ell/2$, $\pi\ell$, 5ℓ, 7ℓ, and 10ℓ, and the y coordinates are 0, $\pi\ell/4$, $\pi\ell/2$, $\pi\ell$, $1.5\pi\ell$, $2\pi\ell$, $2.5\pi\ell$, and 10ℓ. The Poisson ratio of the concrete is 0.25, as was assumed by Westergaard.

Figure 5.16 shows a comparison between Westergaard's exact solutions, as indicated by the curves, and the finite-element solutions obtained by KENSLABS, as indicated by the small circles. The moment M and the deflection w along the edge of slab and the deflection at a distance of $\pi\ell/4$ and $\pi\ell/2$ from the edge are presented. It can be seen that the solutions by KENSLABS check very closely with Westergaard's results.

Temperature Curling Westergaard's solutions for a slab of infinite length and Bradbury's solutions for a finite slab can be used to compare with KENSLABS.

Downloaded From : www.EasyEngineering.net

Downloaded From : www.EasyEngineering.net

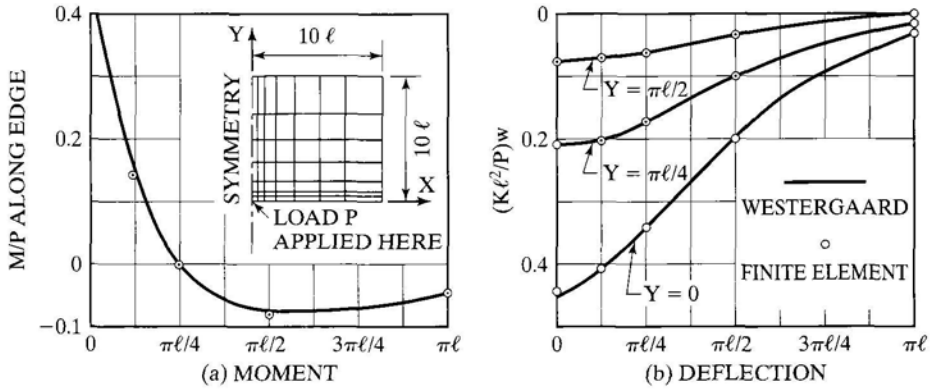


FIGURE 5.16

Comparison between KENSLABS and Westergaard's solutions. (After Huang and Wang (1974).)

Slab of Infinite Length Westergaard (1926a) presented exact solutions for the stress and deflection due to temperature curling in a concrete slab 4.2ℓ wide and infinitely long, where ℓ is the radius of relative thickness. His solutions for the stress and deflection along the y axis, which is perpendicular to the pavement edge, are shown by the two curves in Figure 5.17. The stress and deflection are expressed as dimensionless ratios in terms of σ_0 and w_0, respectively, where

$$\sigma_0 = \frac{E\alpha_t \Delta t}{2(1-\nu)} \tag{5.37a}$$

$$w_0 = \frac{(1+\nu)\alpha_t \ell^2}{h} \tag{5.37b}$$

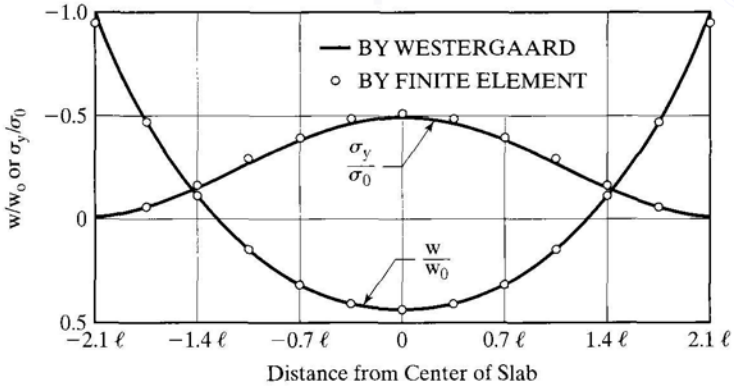


FIGURE 5.17

Stress and deflection along transverse direction. (After Huang and Wang (1974).)

Downloaded From : www.EasyEngineering.net

Downloaded From : www.EasyEngineering.net

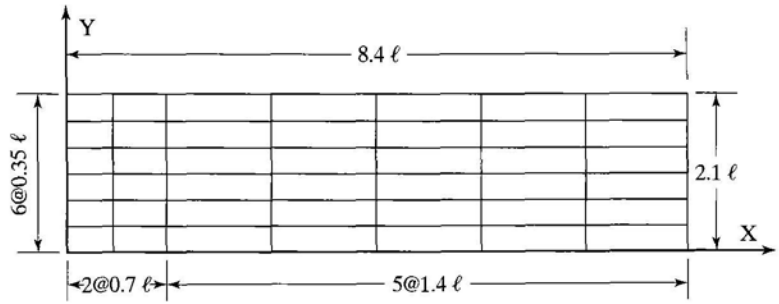


FIGURE 5.18

Division of slab into finite elements.

In the finite-element analysis, a long slab, 4.2ℓ wide and 16.8ℓ long, is employed. The slab is divided into finite elements, as shown in Figure 5.18. By symmetry, only the upper right quadrant of the slab is considered. It is assumed that $E = 3 \times 10^6$ psi (20.7 GPa), $k = 100$ pci (27.1 MN/m^3), $h = 9$ in. (229 mm), $\alpha_t = 5 \times 10^{-6}$/°F($9 \times 10^{-6}$/°C), and $\Delta t = 10$°F (5.6°C). The radius of relative stiffness ℓ is 36.95 in. (938.5 mm), which is used for determining the actual size of grid for computer input.

After the stress and deflection are computed, they are expressed as dimensionless ratios, as shown by the circles in Figure 5.17. It can be seen that the KENSLABS solutions check closely with Westergaard's exact solutions.

Westergaard's solutions are based on the assumption that the slab and the subgrade are in full contact. If the slab moves down, the subgrade will push it up; if the slab moves up, the subgrade will pull it down. This case is analyzed physically in KENSLABS by assuming that the slab is curled into a spherical surface and that the spring at each node will push or pull the slab up or down, depending on the movement of the slab. The close agreement in stress and deflection between the two solutions clearly indicates that the concept employed by KENSLABS is fundamentally correct.

Finite Slab To compare Bradbury's solutions with those obtained by KENSLABS, it is assumed that the slab is 20 ft (6.1 m) long and 12 ft (3.7 m) wide, with a Young's modulus of 5×10^6 psi (34.5 GPa), a Poisson ratio of 0.2, a coefficient of thermal expansion equal to 5×10^{-6}/°F (9×10^{-6}/°C), and a temperature differential of 3°F per in. (0.066°C per mm) of slab. Three different subgrade moduli—50, 200, and 500 pci (7.9, 31.4, and 78.6 kN/m^3) and three different thicknesses—8, 10, and 14 in. (203, 254, and 356 mm) are assumed. The results are shown in Table 5.2.

The stress shown in Table 5.2 is the maximum stress at the center of the slab. Bradbury's solutions are obtained by following the same procedure as was illustrated in Example 4.1. The solutions from KENSLABS are obtained by using one-quarter of the slab and dividing it into 1 ft × 1 ft (0.3 × 0.3 m) square elements. The agreement between the two solutions for a variety of thicknesses and subgrade moduli further validates KENSLABS for handling temperature warping with full subgrade contact.

The assumption of full contact for temperature curling is unreasonable because, when the slab curls up, there is no way that the subgrade will pull it down.

Downloaded From : www.EasyEngineering.net

Downloaded From : www.EasyEngineering.net

TABLE 5.2 Comparison of Curling Stress

Slab thickness (in.)	Method	Maximum curling stress (psi)		
		k = 50 pci	k = 200 pci	k = 500 pci
8	KENSLABS	248.8	361.3	391.8
	Bradbury	253.1	363.1	390.0
10	KENSLABS	224.5	394.4	466.4
	Bradbury	224.2	398.2	467.9
14	KENSLABS	158.3	382.4	538.5
	Bradbury	154.2	386.6	541.4

Note. 1 in. = 25.4 mm, 1 psi = 6.9 kPa, 1 pci = 271.3 kN/m^3.

Experience has shown that the curling stresses obtained by Westergaard or Bradbury's theory based on full contact are much larger than those from field measurements (Moore, 1956). As is shown in Section 5.3.3, the finite-element solutions based on partial contact result in much smaller stresses and check more closely with field measurements.

5.3.2 Influence Charts

The influence charts developed by Pickett and Ray (1951) for liquid foundations and by Pickett and Badaruddin (1956) for solid foundations can be used to compare with the solutions by KENSLABS.

Liquid Foundations Figure 5.19 shows an influence chart used by PCA (1969) for determining the moment at point O under a 36-kip (160-kN) tandem-axle load having an 11.5-in. (292-mm) dual spacing, a 49-in. (1.25-m) tandem spacing, and a 71-in. (1.80-m) spacing between the center of the two sets of dual tires. The radius of relative stiffness ℓ is 50 in. (1.77 m) and the number of blocks N covered by each tire is shown in the figure. When ℓ, N, and a tire contact pressure q of 67.2 psi (433 kPa) are known, the moment can be computed by Eq. 4.32a and compared with KENSLABS.

In the finite-element analysis by KENSLABS, each load was considered independently. The problem can be made symmetric by placing an image tire on the left corresponding to each tire on the right; therefore, only one-half of the slab is required. The moment thus determined must be divided by 2 to give the moment resulting from one tire only. A relatively large square grid was used near the loads, as shown in Figure 5.20.

Table 5.3 gives a comparison of the moments at point O due to six different tire positions. It can be seen that the solutions from KENSLABS check quite well with those from the influence chart, especially when the tire is close to point O. The large discrepancy for tire 7 is due to the fact that this tire straddles between positive and negative blocks and covers only two blocks. The percentage of discrepancy would become zero if the block enclosed were counted as 1.2 instead of as the two blocks counted by PCA.

Downloaded From : www.EasyEngineering.net

Downloaded From : www.EasyEngineering.net

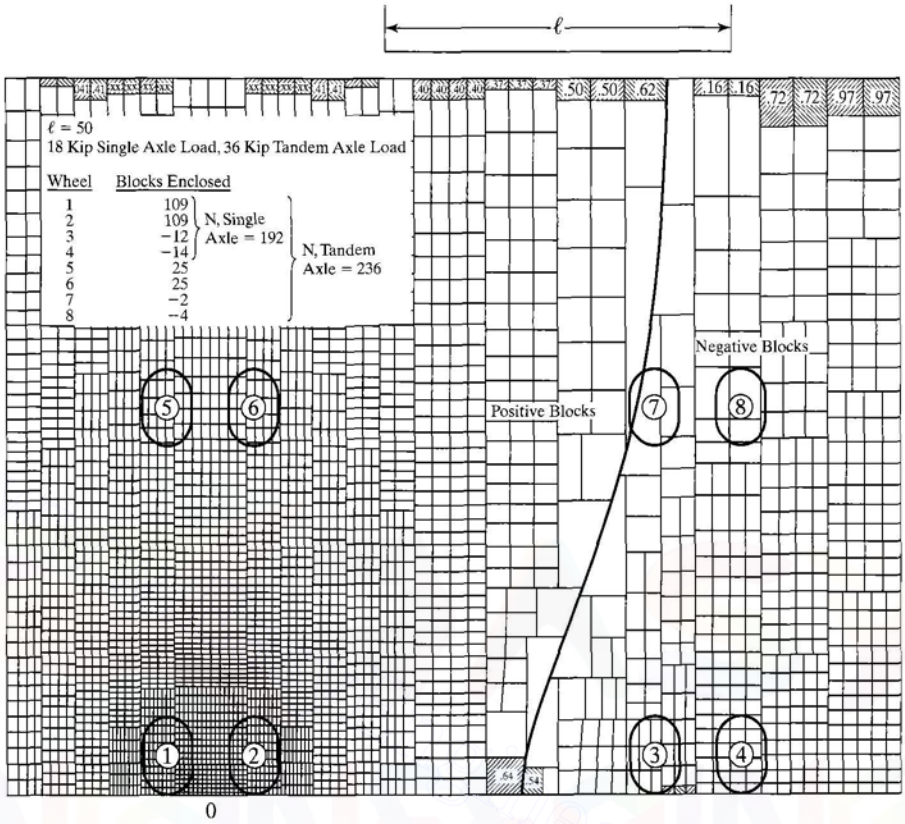


FIGURE 5.19

Contact imprints on influence chart based on liquid foundation. (After PCA (1969).)

Solid Foundation Pickett and Badaruddin (1956) developed analytical solutions for stresses at the edge of an infinite slab on a solid foundation due to a load near the edge. Figure 5.21 is an influence chart they developed. To use the chart, it is necessary to determine the modulus of relative stiffness for the solid foundation defined as

$$\ell = h\left[\frac{1}{6}\frac{E_c}{E_f}\frac{1-\nu_f^2}{1-\nu_c^2}\right]^{1/3} \tag{5.38}$$

The subscripts c and f denote the concrete slab and the solid foundation, respectively. After ℓ is determined, the loaded area can be plotted on the chart by using the scale on the top. The number of blocks N covered by the loaded area is counted, and the stress at point O can be obtained by Eq. 4.32. The number of blocks covered by the six contact areas, each having a size of $0.2\ell \times 0.2\ell$, was tabulated by Pickett and Badaruddin (1956) and is shown in Figure 5.21.

In the finite element analysis by KENSLABS, a slab 8 in. (203 mm) thick, 24 ft (7.32 m) long, and 12 ft (3.66 m) wide was assumed. The problem can be solved by

Downloaded From : www.EasyEngineering.net

Downloaded From : www.EasyEngineering.net

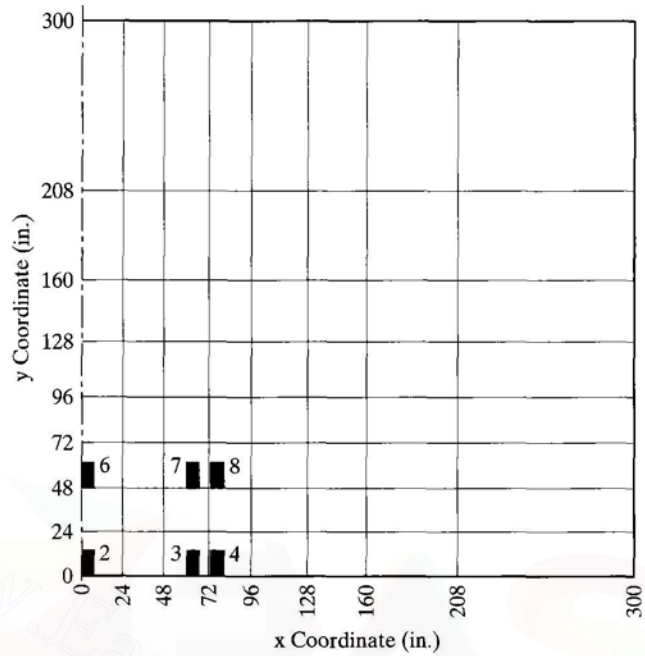


FIGURE 5.20

Finite-element mesh for liquid foundation (1 in. = 25.4 mm).

considering one-half of the slab, as in the case of liquid foundation described previously. The slab was divided into finite elements as shown in Figure 5.22. Assuming that $E_c = 4 \times 10^6$ psi (27.6 GPa), $E_f = 1 \times 10^4$ psi (69 MPa), $\nu_c = 0.15$, and $\nu_f = 0.475$, then from Eq. 5.38, $\ell = 30$ in. (762 mm).

Table 5.4 gives a comparison of edge stresses between the solutions by Pickett and Badaruddin's influence chart and those by KENSLABS. Both solutions check closely with an average discrepancy of about 5%.

TABLE 5.3 Comparison of Moments between Influence Chart and Kenslabs

Tire number	Moment (in.-lb)		Percentage of discrepancy
	Influence chart	KENSLABS	
2	1831	1861	+1.6
3	−202	−204	+1.0
4	−235	−260	+10.6
6	420	393	−6.4
7	−33	−20	−39.4
8	−67	−73	+9.0

Note. 1 in.-lb = 0.113 m-N.

Downloaded From : www.EasyEngineering.net

Downloaded From : www.EasyEngineering.net

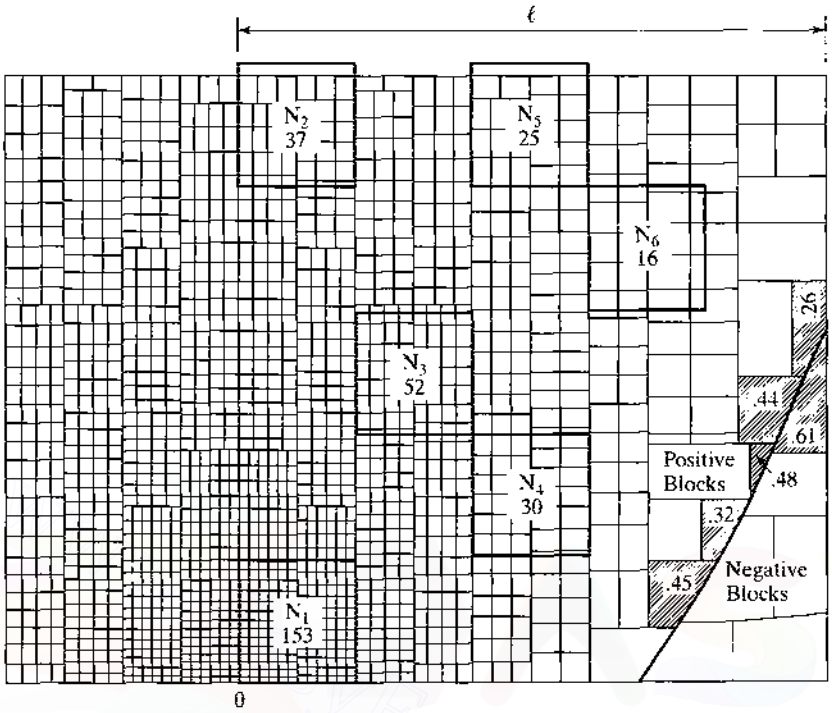


FIGURE 5.21

Contact areas on influence chart based on solid foundation.

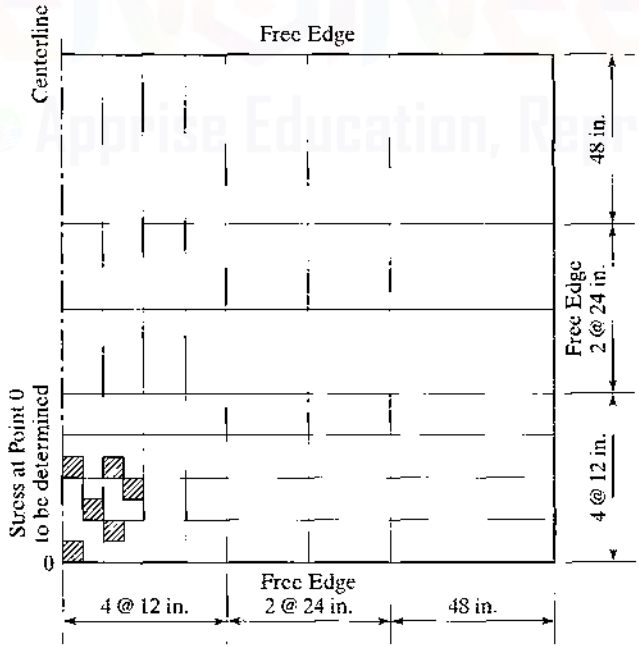


FIGURE 5.22

Finite element mesh for solid foundation (1 in. = 25.4 mm).

Downloaded From : www.EasyEngineering.net

Downloaded From : www.EasyEngineering.net

TABLE 5.4 Comparison of Stresses between Influence Chart and KENSLABS

Loading position	Edge stress/contact pressure, σ_e/q		Percentage of discrepancy
	Influence chart	KENSLABS	
1	2.580	2.653	+2.8
2	0.617	0.645	+4.5
3	0.870	0.909	+4.5
4	0.506	0.545	+7.7
5	0.417	0.443	+6.2
6	0.268	0.283	+5.6

5.3.3 ILLI-SLAB Computer Program

ILLI-SLAB was originally developed in 1977 for the structural analysis of one or two layers of slabs with or without mechanical load transfer systems at joints and cracks (Tabatabaie, 1977). It has since been continuously revised and expanded through several research studies to improve its accuracy and ease of application. Its capabilities are similar to KENSLABS, which was originally developed in 1973 and has been continuously updated and improved for classroom use.

Heinrichs *et al.* (1989) compared several available computer models for rigid pavements and concluded that both ILLI-SLAB or JSLAB, which is a similar finite-element program developed by the PCA, were efficient to use and could structurally model many key design factors of importance. They also indicated that ILLI-SLAB had had extensive checking, revisions, and verification by many researchers and was more nearly free of errors than any other available program. They presented the results of several cases by different models, with which KENSLABS can be compared.

Edge Loading Figure 5.23 shows the cross-section of a two-layer pavement with tied shoulders, which was analyzed by Heinrichs *et al.* In addition to the dimensions and material properties shown in the figure, other information includes joint width, 0.25 in. (6.4 mm); modulus of dowel support, 1.5×10^6 psi (10.4 GPa); Young's modulus of the dowel, 29×10^6 psi (200 GPa); Poisson ratio of the dowel, 0.3; single-axle load, 18 kip (80 kN); and contact pressure, 100 psi. The finite element grid and the loading position are shown in Figure 5.24.

Table 5.5 gives a comparison of results based on longitudinal edge loading. The slabs are assumed to be in full contact with the subgrade. This assumption is valid because there is no temperature curling and no initial gaps between the slab and the subgrade. The load-transfer system can be either aggregate interlock, with spring constants of 100,000 psi (690 MPa) at transverse joints and 31,570 psi (218 MPa) at longitudinal joints, or dowel and tie bars, with 1.25-in. (32-mm) dowel bars at 12-in. (305-mm) spacing and $\frac{5}{8}$-in. (16-mm) tie bars at 30-in. (76-mm) spacing. The interface between the two layers can be either unbonded or bonded. The joint efficiency is defined as the ratio of deflections between the unloaded and loaded slabs on the opposite side of the joint. The minimum longitudinal joint efficiency, as well as the maximum stress and deflection,

Downloaded From : www.EasyEngineering.net

Downloaded From : www.EasyEngineering.net

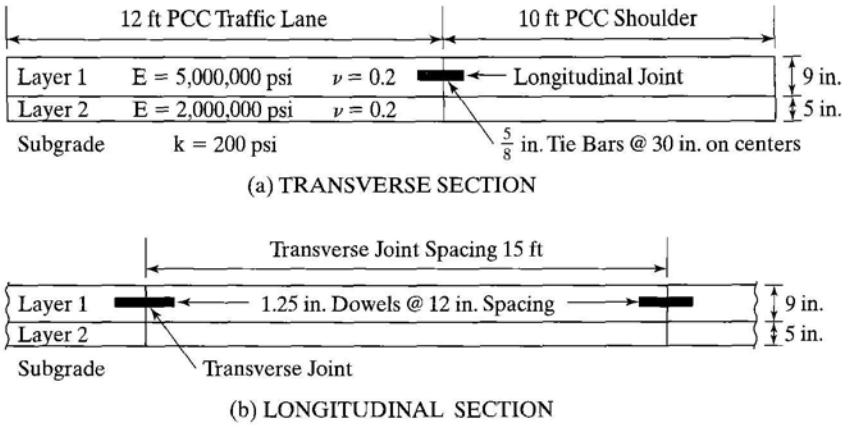


FIGURE 5.23

Cross-section of concrete pavement (1 ft = 0.305 m, 1 in. = 25.4 mm, 1 psi = 6.9 kPa, pci = 271.3 kN/m^3).

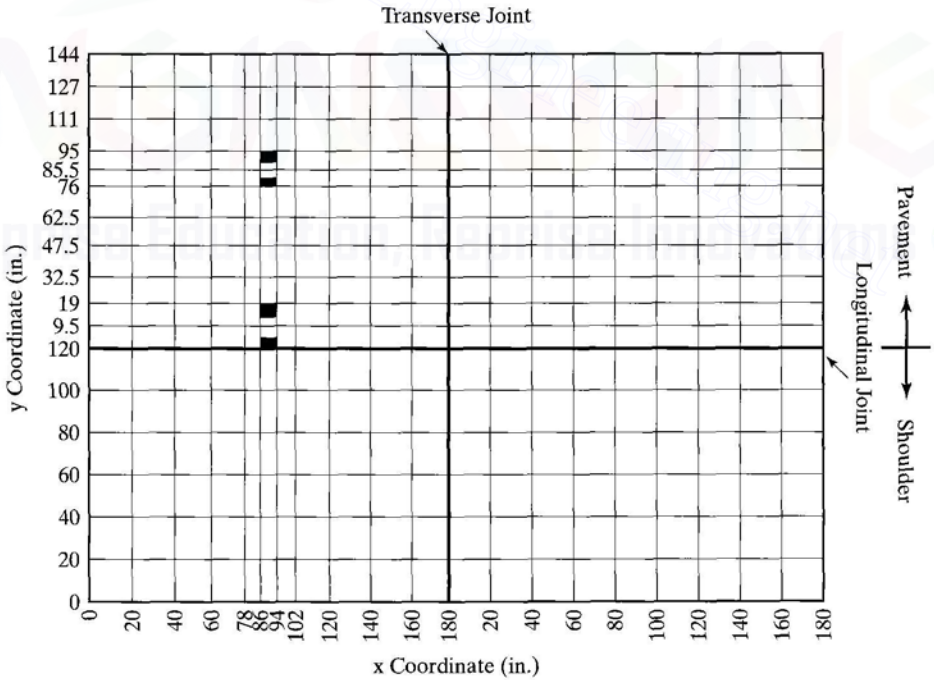


FIGURE 5.24

Finite-element grid for analyzing longitudinal edge loading (1 in. = 25.4 mm).

Downloaded From : www.EasyEngineering.net

Downloaded From : www.EasyEngineering.net

TABLE 5.5 Comparison of Results Based on Longitudinal Edge Loading

Load transfer	Type of interface	Model	Minimum longitudinal joint efficiency (%)	Maximum tensile stress at bottom of		Maximum deflection (10^{-3} in.)
				Slab (psi)	Base (psi)	
Aggregate interlock	Unbonded	KENSLABS	74	169.6	37.7	7.7
		ILLI-SLAB	74	172.3	38.3	7.9
		JSLAB	74	166.6	37.0	7.9
	Bonded	KENSLABS	72	66.7	67.4	6.2
		ILLI-SLAB	72	66.8	68.1	6.3
		JSLAB	72	66.9	68.3	6.3
Dowel and tie bars	Unbonded	KENSLABS	43	195.7	43.5	9.4
		ILLI-SLAB	60	185.7	41.3	8.6
		JSLAB	44	193.2	42.9	9.6
	Bonded	KENSLABS	41	77.0	78.5	7.8
		ILLI-SLAB	57	71.9	73.4	6.8
		JSLAB	42	77.1	78.7	7.7

Note. 1 in. = 25.4 mm, 1 psi = 6.9 kPa.

occurs under the wheel load at the longitudinal edge. It can be seen from Table 5.5 that the results obtained by KENSLABS, ILLI-SLAB, and JSLAB all check very well in the case of aggregate interlock. However, when dowel and tie bars are used, the ILLI-SLAB results in higher efficiencies of load transfer and smaller stresses and deflections compared to KENSLABS and JSLAB.

Corner Loading The same pavement was analyzed for corner loading with the grid shown in Figure 5.25. Table 5.6 is a comparison of results between KENSLABS and ILLI-SLAB. The data without parentheses were obtained by KENSLABS, while those within parentheses were obtained by ILLI-SLAB. The results of JSLAB are not shown because they were not reported by Heinrichs *et al.* (1989). As with edge loading, ILLI-SLAB checks well with KENSLABS in the case of aggregate interlock but results in higher joint efficiencies and slightly lower stresses and deflections when the dowel and tie bars are used. Therefore, the use of KENSLABS is on the safe side.

Temperature Curling In analyzing temperature curling, it is more reasonable to assume that the slab and subgrade are in partial contact. If the slab is weightless and the temperature at the top is colder than that at the bottom, the slab will curl up and form a spherical surface. There is no contact between the slab and the subgrade except at the very center. However, the weight of the slab will cause it to settle, and part of the slab in the interior will finally come in contact. If the temperature gradient is small, the entire slab may be in contact with the subgrade. In the finite-element method, the initial curling of a weightless slab at each node is first determined, and the deflection at each node due to the weight of slab is then computed. If the deflection of the slab is smaller

Downloaded From : www.EasyEngineering.net

Downloaded From : www.EasyEngineering.net

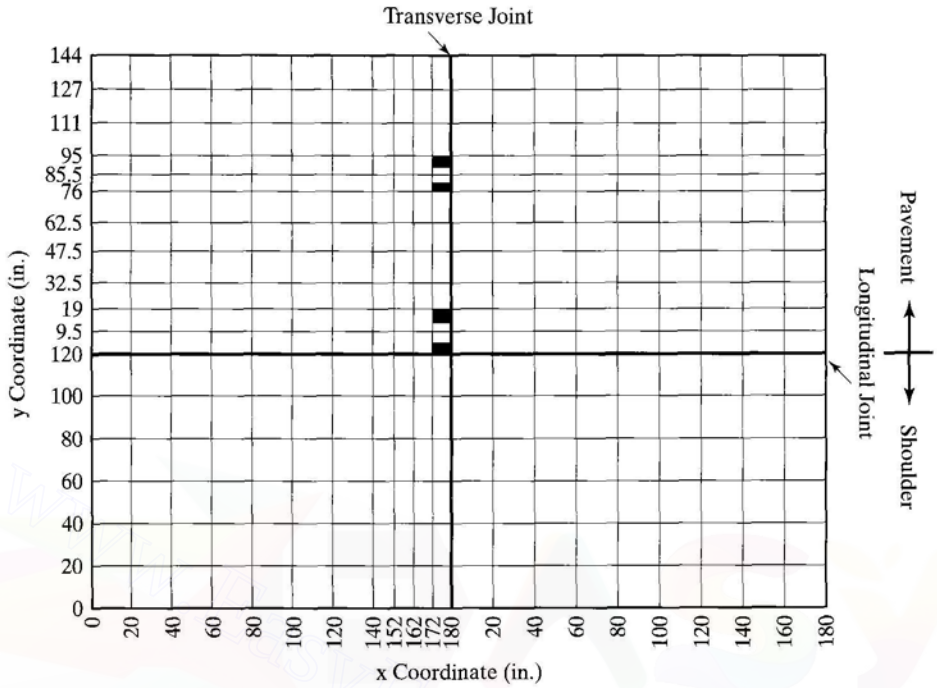


FIGURE 5.25

Finite element grid for analyzing corner loading (1 in. = 25.4 mm).

TABLE 5.6 Comparison of Results Based on Corner Loading

Load transfer	Type of interface	Minimum joint efficiency		Maximum principal tensile stress (psi)		Maximum subgrade stress (psi)	Maximum deflection (10^{-3} in.)
		Transverse (%)	Longitudinal (%)	Slab	Base		
Aggregate interlock	Unbonded	85	64	96.3	21.4	2.4	11.8
		(86)	(65)	(97.9)	(21.8)	(2.4)	(12.1)
	Bonded	84	60	52.9*	38.5	1.9	9.6
		(85)	(61)	(51.9*)	(37.1)	(1.9)	(9.7)
Dowel and tie bars	Unbonded	80	34	101.1	22.5	3.0	14.9
		(88)	(50)	(93.6)	(20.8)	(2.6)	(13.1)
	Bonded	79	31	67.0*	38.1	2.4	12.1
		(87)	(47)	(52.2*)	(35.2)	(2.1)	(10.5)

Note. Numbers without parentheses were obtained by KENSLABS and those within parentheses were obtained by ILLI-SLAB. Stresses are at the bottom of slab or base unless marked by*, when the critical tensile stress is at top. 1 in. = 25.4 mm, 1 psi = 6.9 kPa.

Downloaded From : www.EasyEngineering.net

Downloaded From : www.EasyEngineering.net

than the initial curling, the node is not in contact and its reactive force should be set to 0. The process is repeated until the same contact condition is obtained. Similar procedures can be applied when the slab curls down except that the interior of the slab may not be in contact.

Table 5.7 is a comparison of maximum curling stress based on partial contact. The slab is 20 ft (6.1 m) long and 12 ft (3.7 m) wide, which is similar to the case presented in Table 5.2 for full contact with the same material properties and the same mesh size of 1 ft × 1 ft (0.3 × 0.3 m). Two different temperature gradients of −3°F/in. (−0.066°C/mm) and 1.5°F/in. (0.033°C/mm) of slab were employed. The negative gradient indicates that the slab curls down and the positive gradient indicates that the slab curls up. The maximum curling stress occurs at the center of the slab.

As indicated in Table 5.7, the curling stresses obtained by KENSLABS are nearly the same as those by ILLI-SLAB when the slab curls up, but are slightly smaller when the slab curls down. However, the curling stresses obtained by JSLAB are much smaller than those by KENSLABS and ILLI-SLAB.

Recent Development ILLI-SLAB was later extended (and renamed ILLISLAB94) to overcome the typical limitations of 2-D programs (Khazanovich, 1994; Khazanovich and Yu, 1996). Features that distinguish ILLISLAB94 from other programs include a wide selection of subgrade models and the ability to analyze the effects of separation between pavement layers, linear and nonlinear temperature distribution, and partial-depth cracks in the concrete layer.

ILLISLAB94 was further improved by ERES (Khazanovich *et al.*, 2000) and renamed ISLAB2000, with many additional features, including analysis of mismatched joints and cracks, improved void-analysis model, convenient graphical input and output processors, automated mesh generator and load placement, batch processing of factorial runs, convenient handling of exceptions, and visualization of analysis results. ISLAB2000 was used for rigid pavement design in the forthcoming 2002 Pavement Design Guide.

TABLE 5.7 Comparison of Curling Stress Based on Partial Contact

Slab thickness (in.)	Computer model	Downward curling (−3°F/in.) Subgrade modulus (pci)			Upward curling (1.5°F/in.) Subgrade modulus (pci)		
		50	200	500	50	200	500
8	KENSLABS	219.6	270.2	284.6	120.4	165.3	182.1
	ILLI-SLAB	222.7	283.2	301.5	120.5	165.3	182.1
	JSLAB	180.2	225.0	233.8	94.0	127.4	133.5
10	KENSLABS	193.3	258.2	288.7	107.3	164.2	191.6
	ILLI-SLAB	198.7	276.6	315.2	107.2	164.5	191.9
	JSLAB	160.4	221.3	249.4	84.7	133.8	151.2
14	KENSLABS	139.1	203.3	223.6	76.1	133.0	163.6
	ILLI-SLAB	143.2	216.2	240.1	76.0	133.2	163.9
	JSLAB	116.0	184.2	204.9	60.1	114.6	141.7

Note. Curling stress is in psi. 1 in. = 25.4 mm, 1 psi = 6.9 kPa, 1 pci = 271.3 kN/m^3.

Downloaded From : www.EasyEngineering.net

Downloaded From : www.EasyEngineering.net

5.3.4 Layered Theory

Plate theory is used for the structural analysis of concrete pavements, and the layered theory is used to analyze asphalt pavements. When the modulus of elasticity of the pavement is much greater than that of the foundation and the load is applied in the interior of pavement far away from edges and corners, both theories should yield about the same results. Therefore, the results obtained by KENLAYER can be used to check those by KENSLABS.

In the following examples, a large slab, 24 ft (7.3 m) long, 24 ft (7.3 m) wide, and 8 in. (203 mm) thick, is assumed. The concrete has an elastic modulus of 4×10^6 psi (28 GPa) and a Poisson ratio of 0.15. The foundation is the solid type, with an elastic modulus of 10,000 psi (69 MPa) and a Poisson ratio of 0.4. A 9000-lb (40-kN) load with a contact pressure of 75 psi (518 kPa) is applied at the center of the slab. In applying KENLAYER, the contact area is a circle with a radius of 6.16 in. (157 mm); in KENSLABS, a square area with each side of 10.95 in. (278 mm) is assumed. Figure 5.26 shows the division of the slab into rectangular finite elements. By symmetry, only one-quarter of the slab need be considered.

Table 5.8 gives a comparison of stresses and deflection between KENSLABS and KENLAYER. In applying KENLAYER, the pavement is considered as a two-layer system with a frictionless interface between the concrete and the foundation, which is

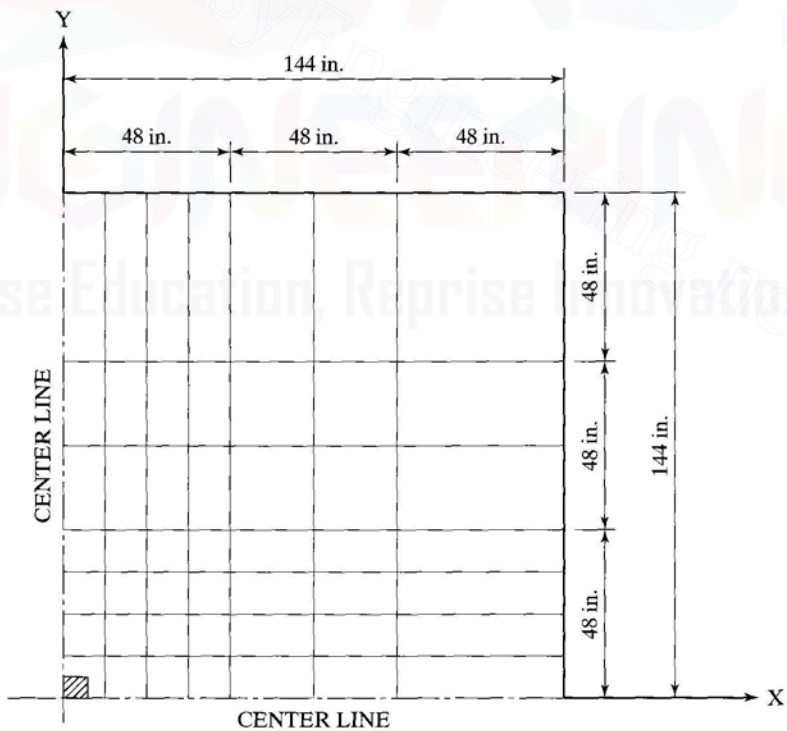


FIGURE 5.26

Finite-element grid of a large slab with an interior load (1 in. = 25.4 mm).

Downloaded From : www.EasyEngineering.net

Downloaded From : www.EasyEngineering.net

TABLE 5.8 Comparison of Stresses and Deflection.

Parameter	Distance (in.) 0	12	24	36	48
Radial stress (psi)					
KENSLABS	171.9	58.6	13.8	−3.6	−11.3
KENLAYER	176.0	60.2	14.5	−3.6	−11.2
Difference (%)	−2.3	−2.7	−5.1	0	1.0
Tangential stress (psi)					
KENSLABS	171.9	101.7	61.5	37.9	24.1
KENLAYER	176.0	109.9	63.0	38.9	24.8
Difference (%)	−2.3	−8.1	−2.4	−2.6	−2.9
Surface deflection (0.001 in.)					
KENSLABS	9.16	8.66	7.68	6.62	5.63
KENLAYER	9.53	8.82	7.78	6.65	5.64
Difference (%)	−4.0	−1.8	−1.3	−0.5	−0.2

Note. 1 in. = 25.4 mm, 1 psi = 6.9 kPa.

similar to a slab on a solid foundation. The radial and tangential stresses and the surface deflections are determined at distances of 0, 12, 24, 36, and 48 in. (0, 0.30, 0.61, 0.91, and 1.22 m) from the load, which correspond to the first five nodes in the finite-element grid. The difference is expressed as a percentage, using KENLAYER as a base. A negative difference implies that the solution by KENSLABS is smaller than that by KENLAYER. It can be seen that the solutions by KENSLABS check very well with those by KENLAYER.

5.4 SENSITIVITY ANALYSIS

With the use of KENSLABS, sensitivity analyses were made to determine the effect of finite-element mesh size and various design parameters on pavement responses.

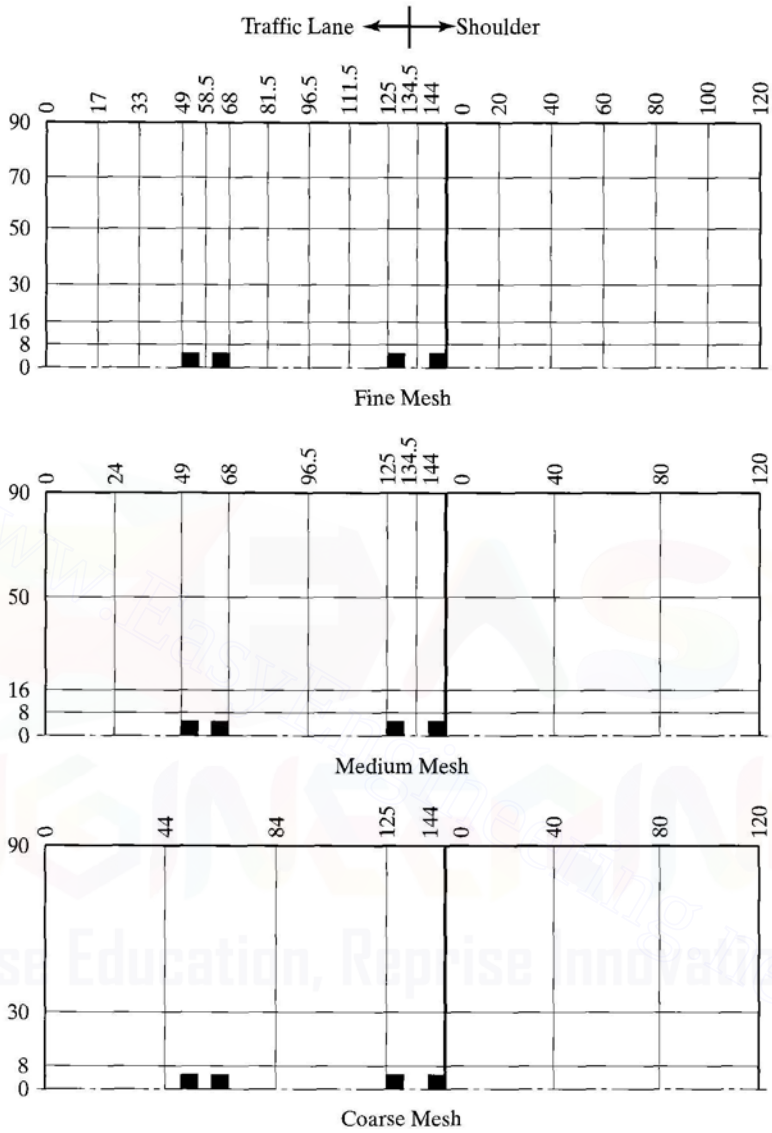
5.4.1 Mesh Size

The effect of mesh size is discussed separately for both edge and corner loadings. The two layers of unbonded slabs with aggregate interlock joints, as discussed in Section 5.3.3, were used for analysis. The cross section of the slabs is the same as shown in Figure 5.23, except that a spring constant of 100,000 psi (690 MPa) was used for the transverse joint and 31,570 psi (218 MPa) for the longitudinal joint.

Edge Loading Because transverse joints have practically no effect on the critical responses under edge loading, a two-slab system consisting of a main slab and a tied shoulder slab can be used to replace the four-slab system shown in Figure 5.24. Three different mesh sizes, designated as fine, medium, and coarse, were used, as shown in Figure 5.27. Because of symmetry, only one-half of the slabs need be considered. The fine mesh is similar to that shown in Figure 5.24, except that some adjustment was made near to the load. This is necessary because the x axis must pass through the centers of loaded areas in order to keep symmetry, whereas no such line was used in Figure 5.24.

Downloaded From : www.EasyEngineering.net

Downloaded From : www.EasyEngineering.net



Note: All Numbers Are Coordinates in inches.

FIGURE 5.27

Fine, medium, and coarse mesh for analysis of edge loading (1 in. = 25.4 mm).

It is well known that the maximum edge stress occurs under the center, rather than at the edge, of the loaded areas, so the division shown in Figure 5.27 is more reasonable than that in Figure 5.24 and results in a greater edge stress.

Table 5.9 shows the effect of mesh size on the responses under edge loading. Comparisons were made on the minimum longitudinal joint efficiency, the maximum tensile stress at bottom of slab and base, the maximum subgrade stress, and the maximum deflection. The values in parentheses are the ratios with respect to the fine mesh.

Downloaded From : www.EasyEngineering.net

Downloaded From : www.EasyEngineering.net

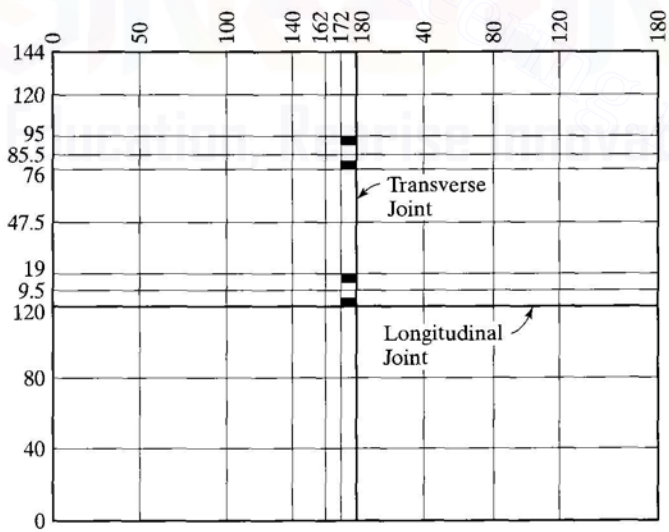
TABLE 5.9 Effect of Mesh Size on Responses Under Edge Loading.

Mesh size	No. of nodes	Minimum longitudinal joint efficiency	Maximum tensile stress (psi)		Maximum subgrade stress (psi)	Maximum deflection (10^{-3} in.)
			Slab	Base		
Fine	133	73	204.1 (1.00)	45.4 (1.00)	1.57 (1.00)	7.83 (1.00)
Medium	60	73	191.9 (0.94)	42.6 (0.94)	1.43 (0.91)	7.15 (0.91)
Coarse	36	73	178.5 (0.87)	39.7 (0.87)	1.35 (0.86)	6.75 (0.86)

Note. 1 in. = 25.4 mm, 1 psi = 6.9 kPa.

It can be seen that the coarser the mesh, the smaller the stresses and deflections, so the use of coarse mesh is on the unsafe side. Note that the maximum difference between the coarse mesh with 36 nodes and the fine mesh with 133 nodes is only 14%.

Corner Loading The fine mesh for corner loading is the same as that shown in Figure 5.25, while the medium and coarse meshes are shown in Figures 5.28 and 5.29. The comparisons are presented in Table 5.10. It can be seen that the results obtained by the medium and fine meshes check quite well but those obtained by the coarse mesh are unreasonably small. This is as expected, because one of the slabs is divided into six finite elements, which is certainly not enough.



Note: Numbers are coordinates in inches.

FIGURE 5.28

Medium finite-element mesh for corner loading (1 in. = 25.4 mm).

Downloaded From : www.EasyEngineering.net

Downloaded From : www.EasyEngineering.net

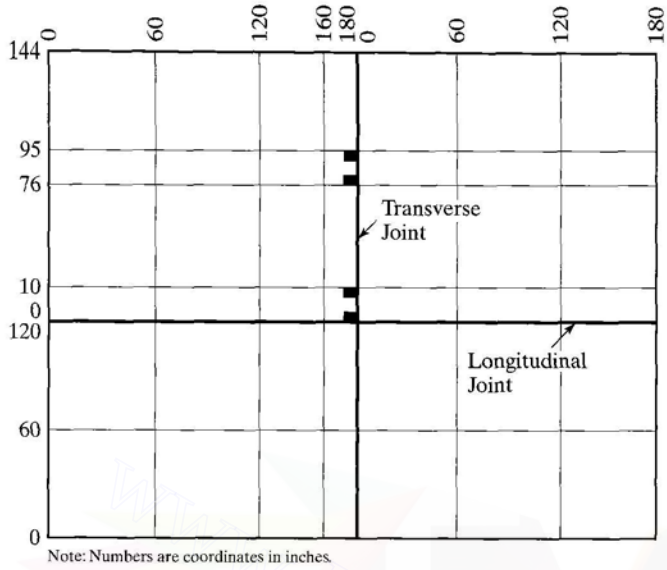


FIGURE 5.29

Coarse finite-element mesh for corner loading (1 in. = 25.4 mm).

5.4.2 Effect of Some Design Parameters

KENSLABS was used to determine the effect of various design parameters on pavement responses. The responses compared are the edge stress and the corner deflection, both of which have been used by PCA (1984) for the design of concrete pavements. The most critical edge stress occurs when the axle load is applied at the midspan of the slab far away from the joints, so without tied concrete shoulders, only one slab is needed for use in the analysis. The most critical corner deflection occurs when the axle load is applied at the joint, so a two-slab system with shear transfer across the joint is needed there. The slab is assumed to be 12 ft (3.66 m) wide. To show the effect of panel length on stress and deflection, two different lengths, one 15 ft (4.57 m) and the other 23 ft (7.0 m), were used.

TABLE 5.10 Effect of Mesh Size on Responses Under Corner Loading

Mesh size	Number of nodes	Minimum joint efficiency		Maximum principal tensile stress (psi)		Maximum subgrade stress (psi)	Maximum deflection (10^{-3} in.)
		Transverse (%)	Longitudinal (%)	Slab	Base		
Fine	418	85	64	96.3 (1.00)	21.4 (1.00)	2.4 (1.00)	11.8 (1.00)
Medium	156	83	64	91.2 (0.95)	20.3 (0.95)	2.1 (0.89)	10.6 (0.89)
Coarse	72	82	64	43.2 (0.45)	9.6 (0.45)	1.8 (0.75)	8.9 (0.75)

Note. 1 in. = 25.4 mm, 1 psi = 6.9 kPa.

Downloaded From : www.EasyEngineering.net

Downloaded From : www.EasyEngineering.net

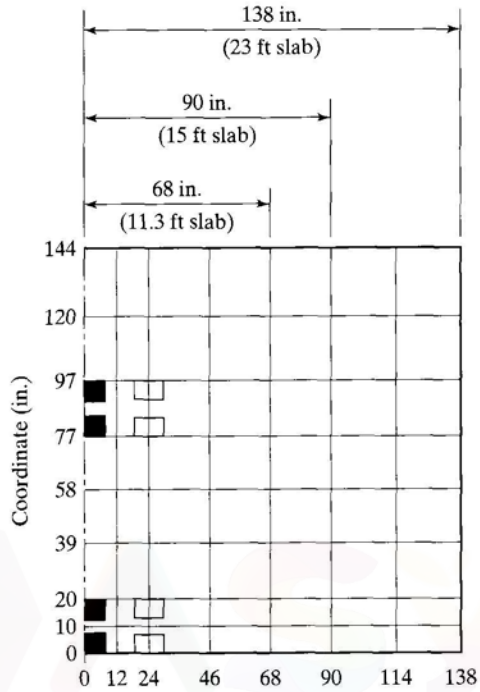


FIGURE 5.30

Analysis of edge stress by KENSLABS (1 in. = 25.4 mm, 1 ft = 0.305 m).

Edge Stress Figure 5.30 shows the division of slab into rectangular finite elements. By symmetry, only one-half of the slab need be considered. The standard case consists of an 18-kip (80-kN) single-axle load with a dual spacing of 13.5 in. (343 mm), a wheel spacing of 77 in. (1.96 m), and a contact pressure of 75 psi (517 kPa). The tire imprint is 9.3 × 6.5 in. (236 × 165 mm) and, because of symmetry, only one-half of the length is shown, as indicated by the shaded rectangles in the figure. The slab is 8 in. (203 mm) thick with a Young's modulus of 4×10^6 psi (27.6 GPa) and a Poisson ratio of 0.15. The foundation has a modulus of subgrade reaction of 100 pci (27.2 MN/m^3) and there is no temperature curling.

In addition to the standard case, eight more cases, each with only one parameter different from the standard case, were also analyzed. The results are presented in Table 5.11. In the table, the parameter ratio is the value of the parameter in the given case divided by that in the standard case. The stress is the edge stress directly under the axle load and the stress ratio is the ratio of the stresses between the case in question and the standard case. It can be seen that in all cases but case 4, the edge stress in the 23-ft (7.0-m) slab is smaller than that in the 15-ft (4.57-m) slab. A separate run of the standard case for a slab 11.3 ft (3.45 m) long results in an edge stress of 316.77 psi (2.19 MPa), indicating that the 15-ft (4.57-m) slab is the most critical with the largest edge stress.

Comments on Table 5.11

1. Increasing the slab thickness from 8 in. (203 mm) to 10 in. (254 mm) decreases the edge stress by 28%, indicating that thickness is very effective in reducing the edge stress.

Downloaded From : www.EasyEngineering.net

Downloaded From : www.EasyEngineering.net

TABLE 5.11 Sensitivity Analysis of Edge Stress

Case	Parameter ratio	15-ft slab		23-ft slab	
		Stress (psi)	Stress ratio	Stress (psi)	Stress ratio
Standard case	1.00	326.10	1.00	320.79	1.00
1. Slab thickness, 10 in.	1.25	233.13	0.72	231.26	0.72
2. Concrete modulus, 8×10^6 psi	2.00	365.53	1.12	363.69	1.13
3. Subgrade k, 300 pci	3.00	265.21	0.82	264.65	0.83
4. Warpup $\Delta t = 12°F$		321.89	0.99	322.02	1.00
5. Warpdown $\Delta t = -24°F$		354.56	1.09	330.63	1.03
6. Tandem		284.98	0.87	282.34	0.88
7. Solid foundation, 8-in. slab $E_f = 4000$ psi, $\nu_f = 0.35$		329.46	1.01	325.31	1.01
8. Solid foundation, 10-in. slab $E_f = 4720$ psi, $\nu_f = 0.35$		237.51	0.73	234.67	0.73

Note. 1 psi = 6.9 kPa, 1 in. = 25.4 mm, 1 pci = 271.3 kN/m^3, 1 ft = 0.305 m.

2. Increasing the Young's modulus of concrete from 4×10^6 psi (27.6 GPa) to 8×10^6 psi (55.2 GPa) increases the edge stress by only 12 to 13%. Because the increase in stress is much smaller than the increase in strength resulting from the higher modulus, the use of high-quality concrete for the slab has a beneficial effect.
3. Increasing the modulus of subgrade reaction from 100 pci (27.2 MN/m^3) to 300 pci (81.5 MN/m^3) decreases the edge stress by only 17 to 18%. It is uneconomical to improve the subgrade modulus just for the purpose of reducing the edge stress. The stress can be reduced more effectively by simply increasing the slab thickness.
4. When the temperature at the bottom of slab is 12°F (6.7°C) higher than that at the top, the slab curls up, causing the loss of subgrade contact at the slab edge. This loss of subgrade contact has a significant effect on the stresses due to loading in the transverse direction, but little effect on the edge stress in the longitudinal direction. In fact, the stress in the 15-ft (4.57-m) slab actually decreases, in response to the transfer of subgrade reaction from the edge to the interior of the slab.
5. When the temperature on the top of the slab is 24°F (13.3°F) higher than that at the bottom, the slab curls down, causing the loss of subgrade contact at the interior of the slab. The edge stress due to loading increases about 9% in the 15-ft (4.57-m) slab and 3% in the 23-ft (7.0-m) slab. This increase is caused by the transfer of subgrade reaction from the interior to the edge of slab, thus resulting in greater edge stress in the longitudinal direction.
6. When the slab is subjected to a 36-kip (160-kN) tandem-axle load, as indicated by the unshaded rectangles in Figure 5.30, the maximum edge stress occurs under the tandem axles. The negative moment caused by the other axle, makes the edge stress due to tandem axles smaller than that due to a single axle.
7. The standard case of liquid foundation is equivalent to a solid foundation with an elastic modulus of 4000 psi (27.6 MPa) and a Poisson ratio of 0.35, as indicated by Eq. 5.6. The edge stress obtained for the liquid foundation checks well with that for the solid foundation.

Downloaded From : www.EasyEngineering.net

Downloaded From : www.EasyEngineering.net

8. When the thickness of slab is increased by 10 in. (254 mm), the elastic modulus of solid foundation should be 4720 psi (32.6 MPa) according to Eq. 5.6. The edge stress based on the solid foundation also agrees reasonably well with case 1, based on the liquid foundation.

Corner Deflection Figure 5.31 shows the finite element mesh for a two-slab system under an 18-kip (80-kN) single-axle load applied at the joint, as indicated by the shaded rectangles. The standard case is the same as that for the analysis of edge stress with the following information on the doweled joint: dowel spacing, 12 in. (305 mm); dowel diameter, 1.0 in. (25.4 mm); modulus of dowel support, 1.5×10^6 pci (407 GN/m^3); and joint width, 0.125 in. (3.18 mm). In addition to the standard case, thirteen more cases were analyzed, with the results tabulated in Table 5.12. Unless noted otherwise, the results are based on the 15-ft (4.6-m) slabs. It was found that the same results were obtained for the 23-ft (7.0-m) slabs, indicating that the length of slab has practically no effect on corner deflections.

Comments on Table 5.12

1. Increasing the slab thickness by 25% decreases the corner deflection by only 18%, indicating that thickness is not as effective in reducing the corner deflection as in reducing the edge stress.
2. Increasing the Young's modulus of concrete decreases the corner deflection, which is in contrast to the increase in edge stress.
3. A threefold increase in the modulus of subgrade reaction reduces the corner deflection by 50%. Compared to the 18% reduction in edge stress, the improvement of subgrade is more effective in reducing the corner deflection.
4. Increasing the dowel diameter by 50% decreases the corner deflection by only 3%. However, large dowels reduce the bearing stress between dowel and concrete and prevent the faulting of joints.
5. Reducing the modulus of dowel support by one order of magnitude from 1.5×10^6 to 1.5×10^5 pci (407 to 40.7 GN/m^3) increases the corner deflection by 17%.
6. The looseness of dowels (a gap of 0.01 in. (0.25 mm) between dowel and concrete) increases the corner deflection by 14%.
7. The application of an additional 18-kip (80-kN) single-axle load, as indicated by the unshaded rectangles in Figure 5.31, to form a 36-kip (160-kN) tandem-axle load increases the corner deflection by 30%. The fact that the tandem-axle load decreases the edge stress by 13% but increases the corner deflection by 30% can well explain why single-axle loads are usually more critical in fatigue analysis and tandem-axle loads are more critical in erosion analysis (PCA, 1984).
8. The upward curling of the 15-ft (4.6-mm) slab by a temperature differential of 12°F (6.7°C) increases the corner deflection by 11%. The deflection is measured from the curled position. The actual deflection of the subgrade is only 0.0241 in. (0.61 mm) due to the existence of a gap of 0.0150 in. (0.38 mm) prior to loading.
9. It was originally suspected that longer slabs would have more curling at the corner and thus result in greater corner deflections due to loading. However, a comparison

Downloaded From : www.EasyEngineering.net

Downloaded From : www.EasyEngineering.net

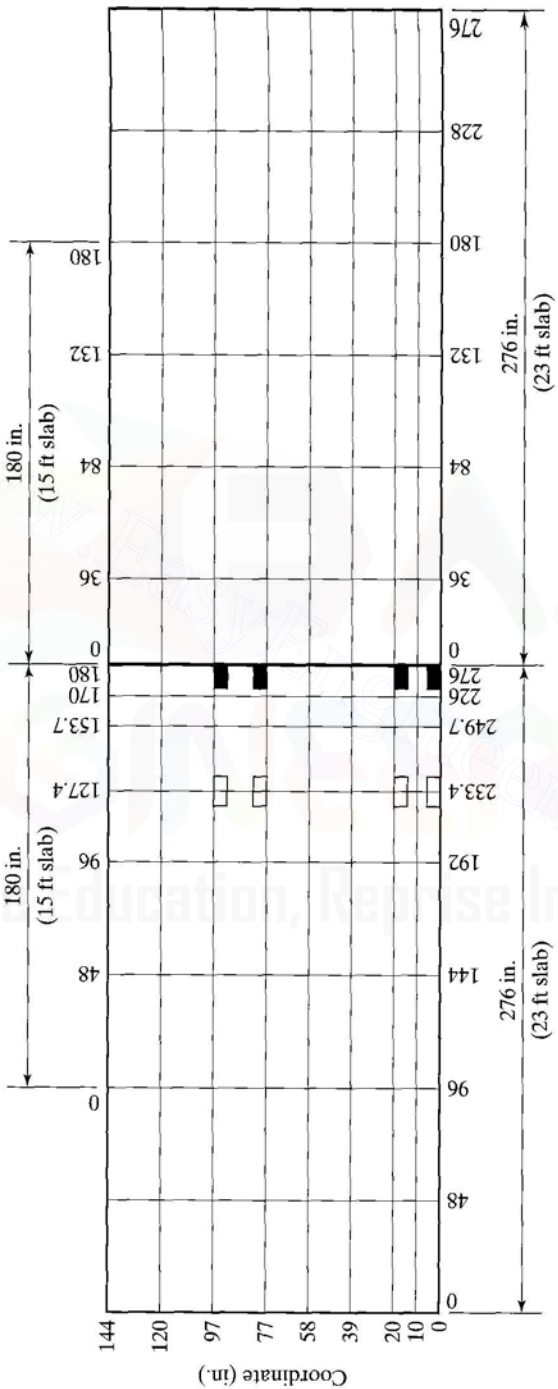


FIGURE 5.31
Analysis of corner deflection by KENSLABS (1 in. = 25.4 mm, 1 ft = 0.305 m).

Downloaded From : www.EasyEngineering.net

Downloaded From : www.EasyEngineering.net

TABLE 5.12 Sensitivity Analysis of Corner Deflection.

Case	Parameter ratio	Deflection (in.)	Deflection ratio
Standard case	1.00	0.0353	1.00
1. Slab thickness, 10 in.	1.25	0.0291	0.82
2. Concrete modulus, 8×10^6 psi	2.00	0.0289	0.82
3. Subgrade $k = 300$ pci	3.00	0.0177	0.50
4. Dowel diameter, 1.5 in.	1.50	0.0343	0.97
5. Modulus of dowel support, 1.5×10^5 pci	0.10	0.0413	1.17
6. Gap between dowel and concrete, 0.01 in.		0.0404	1.14
7. Tandem		0.0458	1.30
8. Warpup $\Delta t = 12°F$ (15-ft slab)		0.0391	1.11
9. Warpup $\Delta t = 12°F$ (23-ft slab)		0.0391	1.11
10. Warpdown $\Delta t = -24°F$ (15-ft slab)		0.0366	1.04
11. Warpdown $\Delta t = -24°F$ (23-ft slab)		0.0361	1.02
12. Solid foundation, 8-in. slab, $E_f = 6400$ psi, $\nu_f = 0.35$		0.0362	1.03
13. Solid foundation, 10-in. slab, $E_f = 7560$ psi, $\nu_f = 0.35$		0.0288	0.82

Note. 1 in. = 25.4 mm, 1 psi = 6.9 kPa, 1 pci = 271.3 kN/m^3, 1 ft = 0.305 m.

between cases 8 and 9 indicates that this is not true. Although the initial curling of a weightless slab is greater for longer slabs, the final curling is nearly the same due to the greater weight of longer slabs. Consequently, when the slabs curl up, the corner deflection is not affected by the length of slab.

10. When the slabs curl down under a temperature differential of 24°F (13.3°C), the corner deflection of the 15-ft (4.6-m) slab increases by 4%. This increase is caused by the loss of subgrade contact in the interior of the slab. Without the subgrade reaction to pull the slab down and counteract the corner loading, the deflection at the corner will increase.

11. Under the same temperature gradient as in case 10 for the 15-ft (4.6-m) slab, the corner deflection of the 23-ft (7.0-m) slab increases by only 2%. The smaller increase in longer slabs is reasonable, because the interior of longer slabs is farther from the corner and the loss of subgrade contact in the interior should have only a small effect on the corner deflection.

12. The standard case of liquid foundation is equivalent to a solid foundation with an elastic modulus of 6400 psi (44.2 MPa) and a Poisson ratio of 0.35, as indicated by Eq. 5.7. The corner deflection obtained by the liquid foundation checks reasonably with that by the solid foundation.

13. Based on Eq. 5.7, the elastic modulus of solid foundation should be 7560 psi (52.2 MPa) for a 10-in. (254-mm) slab. The corner deflection based on the solid foundation also checks really well with that in case 1 based on the liquid foundation.

SUMMARY

This chapter presents the finite-element method for analyzing concrete slabs on liquid, solid, or layer foundations and describes the KENSLABS computer program.

Downloaded From : www.EasyEngineering.net

Downloaded From : www.EasyEngineering.net

Important Points Discussed in Chapter 5

1. KENSLABS can be applied to three different types of foundation: liquid, solid, or layer. The liquid foundation, even though very unrealistic, has been used most frequently because of its simplicity and because it requires less computer time and storage. With the availability of personal computers, it is no longer necessary to use liquid foundations. The more realistic solid foundations should be used if the slabs are placed directly on the subgrade. If the slabs are placed on one or more layers of granular materials, the use of layer foundations is recommended.
2. The modulus of subgrade reaction k used in liquid foundations is a fictitious property not characteristic of soil behaviors. It is not possible to find a single k value that will match both the stresses and deflections in slabs on liquid foundations and those on solid foundations. However, if the design is based on the maximum stress or deflection under a single-axle load, it is possible to replace the solid foundation with a fictitious k, using Eq. 5.5 for interior stress, Eq. 5.6 for edge stress, and Eq. 5.7 for corner deflection, thus resulting in a large saving on computer time and storage.
3. The overall stiffness matrix is obtained by adding the stiffness matrices of slabs, foundation, and joints. The resulting simultaneous equations are solved by the Gauss elimination method. If the dimension of the overall stiffness matrix exceeds the limit, an iterative method is activated automatically to solve the simultaneous equations.
4. The stiffness of joint is computed from a shear spring constant and a moment spring constant. The moment spring constant should be specified as 0 if there is visible opening at the joint. The shear spring constant can be entered directly or computed from the size and spacing of dowel bars and other joint information. A gap can be specified between the spring or dowel and the concrete.
5. The stresses and deflections due to temperature curling can be obtained by assuming that the slab is initially curled into a spherical surface and then subjected to the subgrade reactions at the nodes.
6. The finite element method is particularly suited for analyzing slabs not in full contact with the subgrade by simply setting the reactive forces at those nodes not in contact to zero. For liquid foundations, whether a node is in contact with the subgrade is based on the deflection of the slab compared with the gap or precompression of the subgrade. However, for solid or layer foundations if the slab and subgrade are in contact, the reactive force should not be in tension.
7. The analysis of partial contact under wheel loads by KENSLABS involves two steps. First, determine the gaps and precompressions between slab and foundation due to weight, temperature curling, and gaps, if any. Then, using the gaps and precompressions thus computed, determine the stresses and deflections under the wheel loads.
8. KENSLABS can be applied to a maximum of 6 slabs, 7 joints, and 420 nodes. If the slabs and loadings exhibit symmetry, only one-half or one-quarter of the slab need be considered. Thus, a large amount of computer time can be saved.
9. Results obtained by KENSLABS compare favorably with those from analytical solutions, influence charts, and the ILLI-SLAB model. When the load is applied

Downloaded From : www.EasyEngineering.net

Downloaded From : www.EasyEngineering.net

in the interior of a slab, good agreement also exists between KENSLABS and KENLAYER solutions.

10. The size of finite element mesh has a significant effect on the results obtained. Therefore, the selection of an appropriate mesh requires careful consideration. It is really not necessary to use a very fine mesh. Satisfactory results can be obtained if a fine mesh is used near the load and a rather coarse mesh away from the load.
11. Sensitivity analyses were made to determine the effect of various parameters on the edge stress and corner deflections for slabs on liquid foundations. An interesting finding is that the upward curling of slab has only a small effect on the edge stress due to loading, but has a significant effect on the corner deflection, while downward curling causes a slight increase in both edge stress and corner deflection.

PROBLEMS

Note: On the Editor screen of KENPAVE, there is an Examples menu with six examples (SLA1 to SLA6). It is suggested that these examples be carefully studied before working on the following problems. Both English and SI units can be used, so it is suggested that some of these problems be converted to SI units and run with KENSLABS. The following material properties are assumed for problems 5-3 to 5-22: modulus of elasticity of concrete = 4×10^6 psi, Poisson ratio of concrete = 0.15, modulus of elasticity of steel = 29×10^6 psi, Poisson ratio of steel = 0.3, modulus of dowel support = 1.5×10^6 pci, and coefficient of thermal expansion of concrete = 5×10^{-6} in./in./°F.

5.1 A 7-in. concrete pavement with an elastic modulus of 4×10^6 psi psi is subjected to a wheel load with a bending stress of 400 psi, as shown in Figure P5.1*a*. What is the bending moment per in. width of the slab? Assuming that the moment remains the same after placing a 3-in. hot mix asphalt with an elastic modulus of 7×10^5 psi as an overlay, as shown in Figure P5.1*b*, what will be the maximum tensile stress in the concrete and the maximum compressive stress in the hot mix asphalt when both layers are bonded? [Answer: 3267 in.-lb/in., 305 psi, and 85.4 psi].

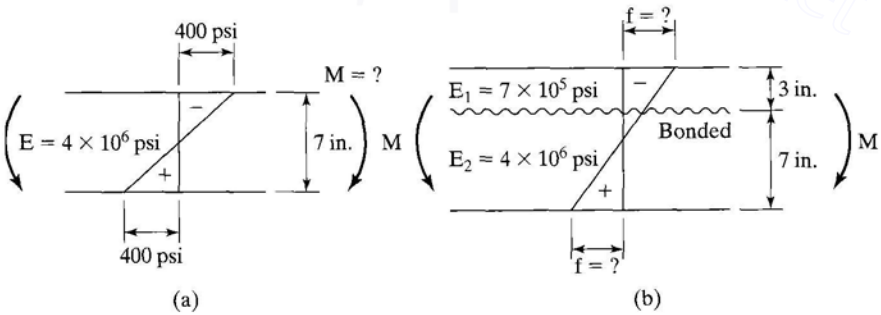


FIGURE P5.1

5.2 Same as Problem 5.1, except that both layers are unbonded, as shown in Figure P5.2, and the Poisson ratios are 0.4 for the hot mix asphalt and 0.15 for the concrete. What will be the maximum stress in the concrete and in the hot mix asphalt? [Answer: 394 and 34 psi].

Downloaded From : www.EasyEngineering.net

Downloaded From : www.EasyEngineering.net

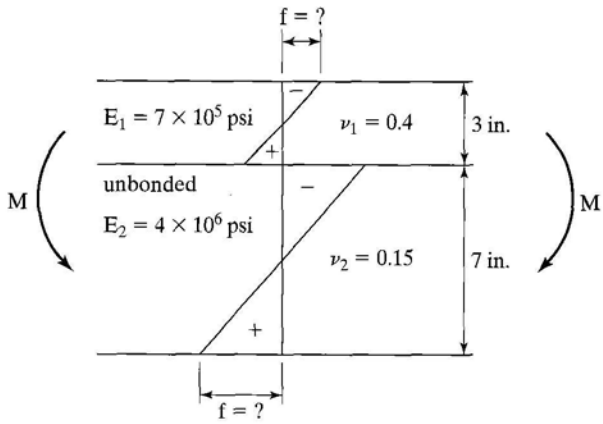


FIGURE P5.2

5.3 Determine the curling stresses during the day at points *A*, *B*, and *C* of a finite slab shown in Figure P5.3*a* using one-quarter of the slab. The slab has a thickness of 8 in. and is subjected to a temperature gradient of 3°F per inch of slab. The modulus of subgrade reaction is 50 pci. [Answer: 214.2, 207.4, and 57.8 psi based on the mesh shown in Figure P5.3*b*, which checks with Problem 4.1b]

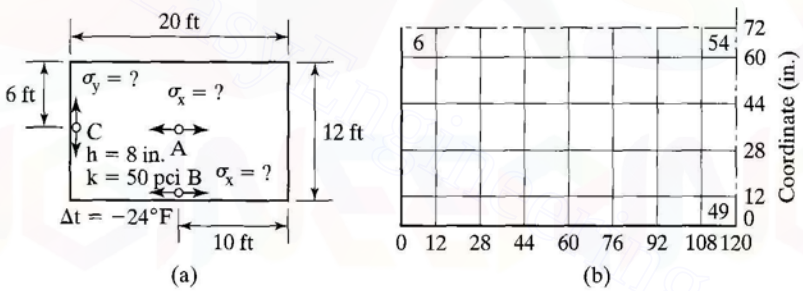


FIGURE P5.3

5.4 Figure P5.4*a* shows a concrete slab, 10 in. thick, supported by a subgrade with a modulus of subgrade reaction of 200 pci. A 12,000-lb dual-wheel load (each wheel 6000 lb) spaced at 14 in. on centers is applied at the corner of the slab. The contact pressure is 80 psi.

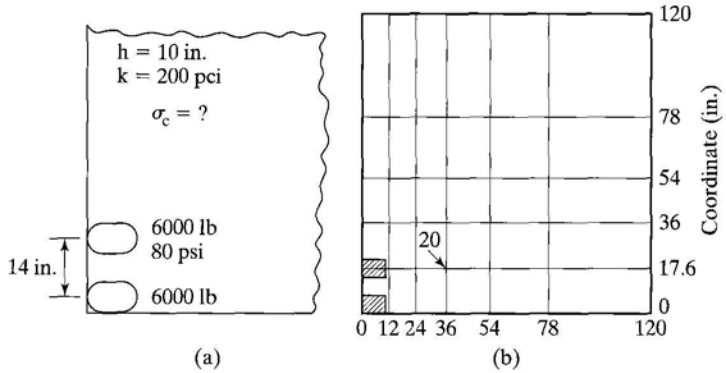


FIGURE P5.4

Downloaded From : www.EasyEngineering.net

Downloaded From : www.EasyEngineering.net

Determine the maximum stress in the concrete. [Answer: 174.6 psi at node 20 based on the mesh shown in Figure P5.4*b*, which checks with Problem 4.2]

5.5 The pavement and loading are the same as in Problem 5.4, but the load is applied in the interior of an infinite slab, as shown in Figure P5.5*a*. Determine the maximum stress in the slab using one-quarter of the slab. [Answer: 128.4 psi at node 2 based on the mesh shown in Figure P5.5*b*, which is slightly smaller than the 139.7 psi in Problem 4.3 based on equivalent area]

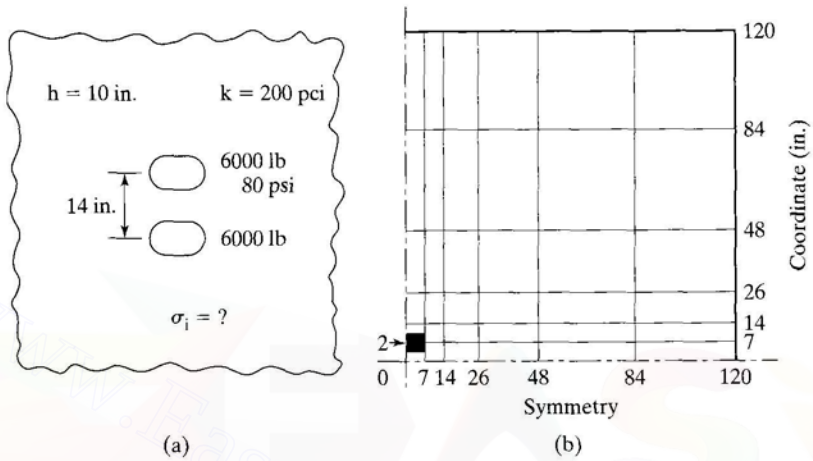


FIGURE P5.5

5.6 Same as Problem 5.4, except that the load is applied at the slab edge, as shown in Figure P5.6*a*. Determine the maximum stress using one-half of the slab. [Answer: 251.4 psi at node 1 based on the mesh shown in Figure P5.6*b*, which checks with Problem 4.4]

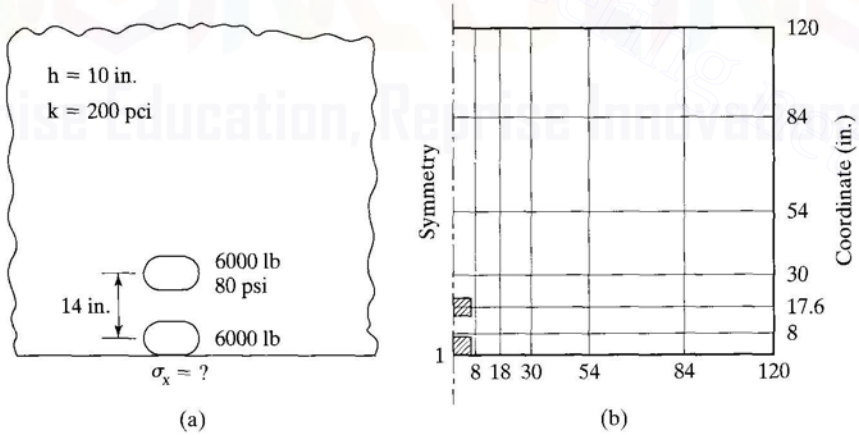


FIGURE P5.6

5.7 Figure P5.7*a* shows a set of dual-tandem wheels with a total weight of 40,000 lb (10,000 per wheel), a tire pressure of 100 psi, a dual spacing of 20 in., and a tandem spacing of 40 in. The concrete slab is 8 in. thick, with a modulus of subgrade reaction of 100 pci. Determine the interior stress at point *A* in the *y* direction under the center of the dual-tandem wheels

Downloaded From : www.EasyEngineering.net

Downloaded From : www.EasyEngineering.net

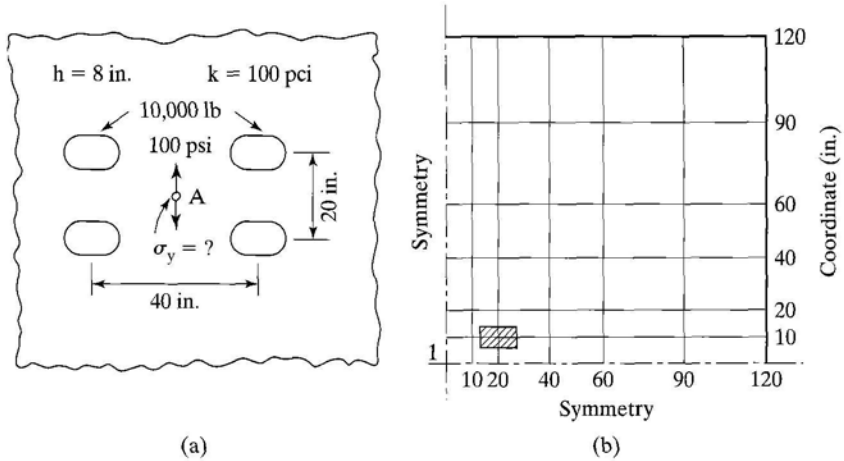


FIGURE P5.7

using one-quarter of the slab. [Answer: 299.3 psi in the y direction based on the mesh shown in Figure P5.7*b*, which checks with Problem 4.6]

5.8 Same as Problem 5.7, except that the outside wheels are applied at the slab edge, as shown in Figure P5.8*a*. Determine the edge stress at point A in an infinite slab using one-half of the slab. [Answer: 314.8 psi based on the mesh shown in Figure P5.8*b*, which checks with Problem 4.7].

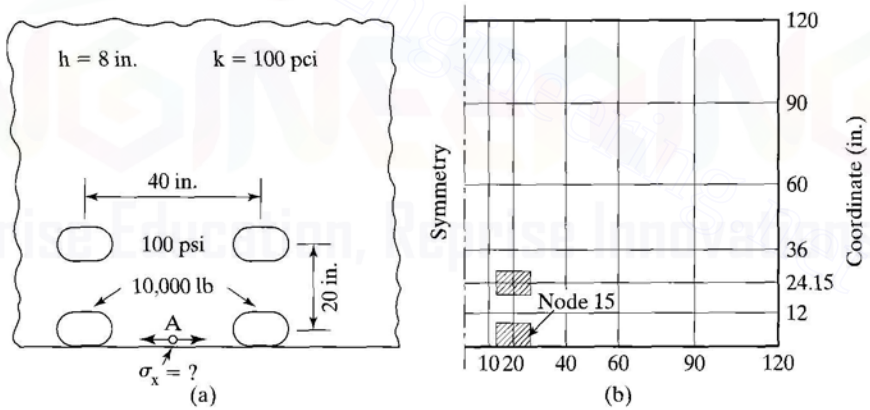


FIGURE P5.8

5.9 A concrete slab, 40 ft long, 11 ft wide, and 9 in. thick, is placed on a subgrade having a modulus of subgrade reaction of 200 pci. The pavement is subject to a temperature differential of 1.5°F per in. at night when a 9000-lb single-axle load is applied on the edge of the slab over a circular area with a contact pressure of 100 psi, as shown in Figure P5.9*a*. Determine the combined stress due to curling and loading at the edge beneath the load, using one-half of the slab. [Answer: 158.3 psi based on the mesh shown in Figure P5.9*b*, which checks with Problem 4.8c]

5.10 A concrete slab has a width of 12 ft, a thickness of 10 in., and a modulus of subgrade reaction of 300 pci. Two 1-ft × 1-ft loaded areas, each weighing 12,000 lb and spaced at

Downloaded From : www.EasyEngineering.net

Downloaded From : www.EasyEngineering.net

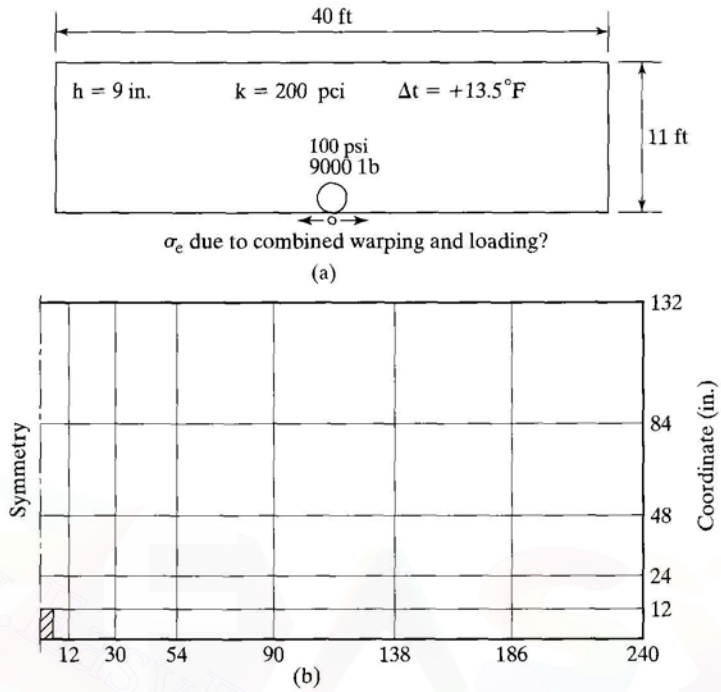


FIGURE P5.9

6 ft apart, are applied at the joint with the outside loaded area adjacent to the pavement edge, as shown in Figure P5.10*a*. Determine the maximum bearing stress between concrete and dowel. The joint has an opening of 0.25 in. and the dowels are 1 in. in

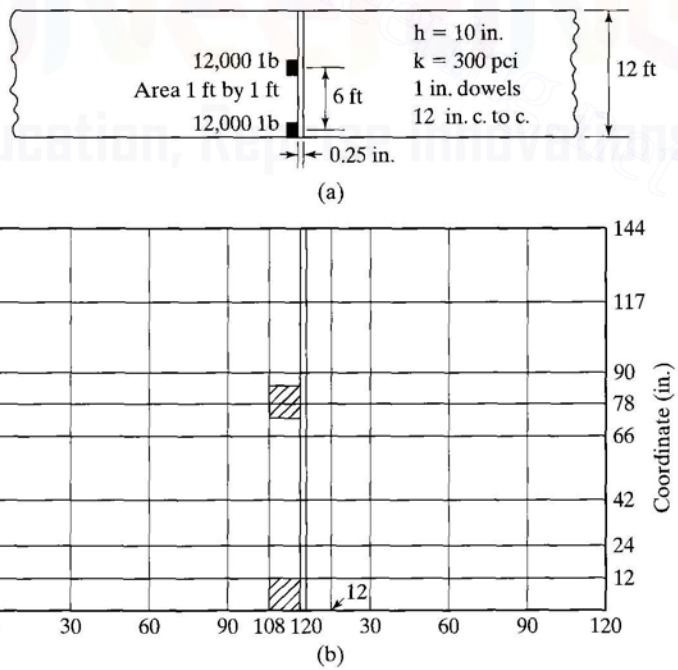


FIGURE P5.10

Downloaded From : www.EasyEngineering.net

Downloaded From : www.EasyEngineering.net

diameter and 12 in. on centers. [Answer: 4530 psi based on the mesh shown in Figure P5.10*b*].

5.11 Same as Problem 5.10, but using a mesh such that the location of the nodes are in line with the dowels, as shown in Figure P5.11. Determine the maximum bearing stress between dowel and concrete, the maximum bending stress in the concrete slab, and the maximum deflection of the slabs. [Answer: 4043 psi, 170.8 psi, 0.0228 in.]

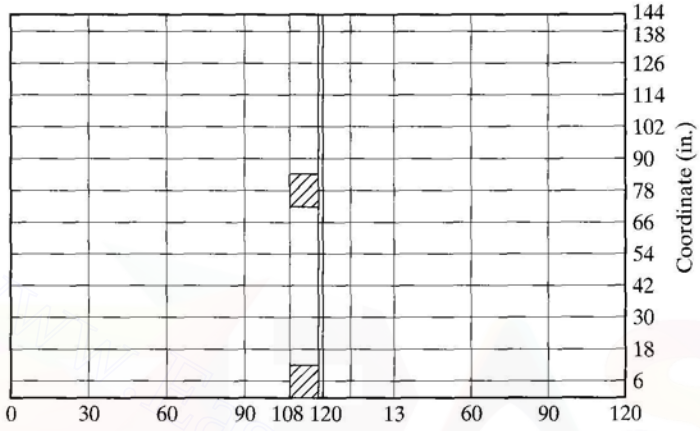
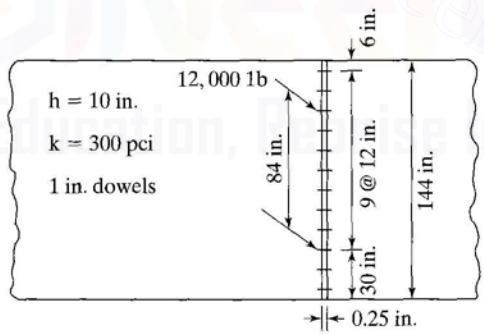


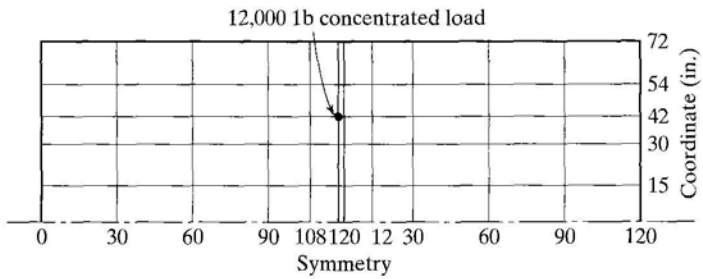
FIGURE P5.11

5.12 Same as Problem 5.10, except that a gap of 0.01 in. exists between dowel and concrete. [Answer: 3829 psi]

5.13 Same as Problem 5.10, except that each of the 12,000-lb wheels is considered as a concentrated load and placed at a distance of 2.5 ft from edge, as shown in Figure P5.13*a*.



(a)



(b)

FIGURE P5.13

Downloaded From : www.EasyEngineering.net

Downloaded From : www.EasyEngineering.net

Determine the maximum bearing stress between concrete and dowel using one-half of the slabs. [Answer: 2267 psi based on the mesh shown in Figure P5.13*b*]

5.14 Same as Problem 5.13, but using a mesh such that the location of the nodes is in line with the dowels, as shown in Figure P5.14. [Answer: 2284 psi]

5.15 Same as Problem 5.13, except that a gap of 0.01 in. exists between dowel and concrete. [Answer: 1656 psi]

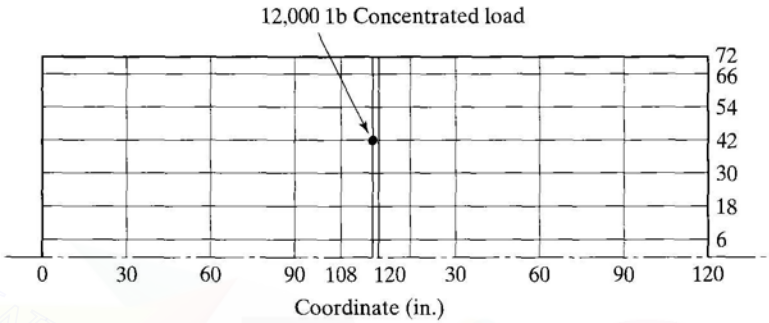


FIGURE P5.14

5.16 A slab track with an 8-in. continuous reinforced concrete is placed on a subgrade with a k value of 150 pci. The rail is supported on 7-in. × 12-in. pads. The design load consists of four wheels, each weighing 12,600 lb. By considering one-quarter of the slab, as shown in Figure P5.16, determine the maximum stress in the concrete. [Answer: 283.8 psi]

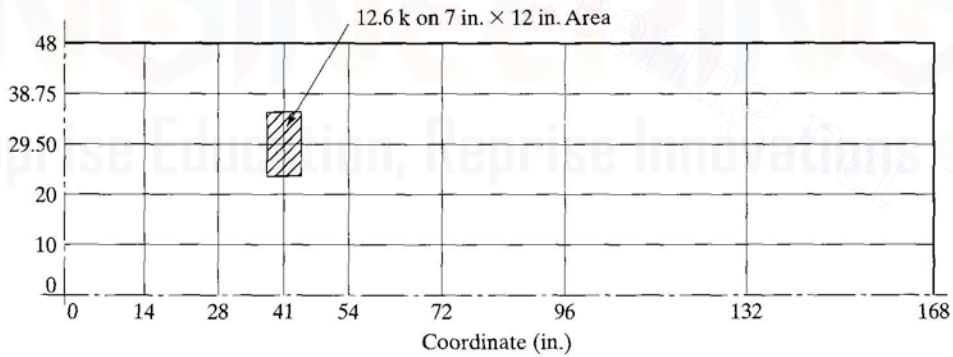


FIGURE P5.16

5.17 Similar to Problem 5.11, except that the liquid foundation is replaced by a solid foundation with an elastic modulus of 16,000 psi and a Poisson's ratio of 0.4. Compare the results with Problem 5.11, and comment on the results. [Answer: 3087 psi, 185.3 psi, 0.0225 in.]

5.18 As in Example 3, determine the maximum stress and deflection of the slab, assuming partial contact. Run KENSLABS in two steps. In the first step, consider the weight of slab only with INPUT = 0, NCYCLE = 10, and NWT = 1; in the second step, consider the load only with INPUT = 1, NCYCLE = 10, and NWT = 0. [Answer: 226.3 psi, 0.05384 in.]

Downloaded From : www.EasyEngineering.net

Downloaded From : www.EasyEngineering.net

5.19 Similar to Example 4: if the user-specified criteria are used with F2 = 17.61, what should be the value of F1 so that the same design life as in Example 4 can be obtained? What percentage of damage is contributed to the secondary cracking index? What conclusions can you draw from the analysis? [Answer: 14.75, less than 0.1%]

5.20 Rework Example 5, using two slabs, by considering symmetry with respect to the x axis along the joint. Use either the upper or lower part of the slabs and a reasonably fine finite-element grid to make the results more realistic. It is assumed that the subgrade pumping causes a gap of 0.05 in. along the pavement edge and the transverse joint. Determine the maximum flexural stress in the slab and the maximum bearing stress between dowel and concrete. [Answer: 459.4 psi and 2408 psi]

5.21 Same as Problem 5.13, but the liquid foundation is replaced by a solid foundation with an elastic modulus of 15,000 psi and a Poisson's ratio of 0.4. [Answer: 2050 psi]

5.22 Same as Problem 5.14, but the liquid foundation is replaced by a solid foundation with an elastic modulus of 15,000 psi and a Poisson's ratio of 0.4. [Answer: 2063 psi]

Downloaded From : www.EasyEngineering.net

Downloaded From : www.EasyEngineering.net

CHAPTER 6

Traffic Loading and Volume

6.1 DESIGN PROCEDURES

Traffic is the most important factor in pavement design. The consideration of traffic should include both the loading magnitude and configuration and the number of load repetitions. There are three different procedures for considering vehicular and traffic effects in pavement design: fixed traffic, fixed vehicle, and variable traffic and vehicle.

6.1.1 Fixed Traffic

In fixed traffic, the thickness of pavement is governed by a single-wheel load, and the number of load repetitions is not considered as a variable. If the pavement is subjected to multiple wheels, they must be converted to an equivalent single-wheel load (ESWL) so that the design method based on a single wheel can be applied. This method has been used most frequently for airport pavements or for highway pavements with heavy wheel loads but light traffic volume. Usually, the heaviest wheel load anticipated is used for design purposes. Although this method is rarely in use today for pavement design, the concept of converting multiple-wheel loads to a single-wheel load is important and is discussed in Section 6.2.

6.1.2 Fixed Vehicle

In the fixed vehicle procedure, the thickness of pavement is governed by the number of repetitions of a standard vehicle or axle load, usually the 18-kip (80-kN) single-axle load. If the axle load is not 18 kip (80 kN) or consists of tandem or tridem axles, it must be converted to an 18-kip single-axle load by an equivalent axle load factor (EALF). The number of repetitions under each single- or multiple-axle load must be multiplied by its EALF to obtain the equivalent effect based on an 18-kip (80-kN) single-axle load. A summation of the equivalent effects of all axle loads during the design period results in an equivalent single-axle load (ESAL), which is the single traffic parameter for design purposes. The great varieties of axle loads and traffic volumes and their intractable effects on pavement performance require that most of the design methods

Downloaded From : www.EasyEngineering.net

Downloaded From : www.EasyEngineering.net

in use today be based on the fixed-vehicle concept. Details about the equivalent axle load factor are discussed in Section 6.3.

6.1.3 Variable Traffic and Vehicle

For variable traffic and vehicles, both traffic and vehicle are considered individually, so there is no need to assign an equivalent factor for each axle load. The loads can be divided into a number of groups, and the stresses, strains, and deflections under each load group can be determined separately and used for design purposes. This procedure is best suited for the mechanistic methods of design, wherein the responses of pavement under different loads can be evaluated by using a computer. The method has long been employed by the PCA with the use of design charts and is discussed in Section 12.2.

6.2 EQUIVALENT SINGLE-WHEEL LOAD

The study of ESWL for dual wheels was first initiated during World War II when the B-29 bombers were introduced into combat missions. Because the design criteria for flexible airport pavements then available were based on single-wheel loads, the advent of these dual-wheel planes required the development of new criteria for this type of loading. Neither time nor economic considerations permitted the direct development of such criteria. It was necessary, therefore, to relate theoretically the new loading to an equivalent single-wheel load, so that the established criteria based on single-wheel loads could be applied.

The ESWL obtained from any theory depends on the criterion selected to compare the single-wheel load with multiple-wheel loads. Using Burmister's two-layer theory, Huang (1969c) conducted a theoretical study on the effect of various factors on ESWL by assuming that single and dual wheels have the same contact pressure. Similar studies were made by Gerrard and Harrison (1970) on single, dual, and dual-tandem wheels by assuming that all wheels have equal contact radii. It was found that the use of different criteria, based on stress, strain, or deflection, plays an important role in determining ESWL and, regardless of the criterion selected, the ESWL increases as the pavement thickness and modulus ratio increase or the multiple-wheel spacing decreases. In this section, some simple theoretical methods for determining ESWL of flexible pavements are presented. The determination of ESWL for rigid pavements can be made by comparing the critical flexural stress in the concrete and is not presented here.

The ESWL can be determined from theoretically calculated or experimentally measured stress, strain, or deflection. It can also be determined from pavement distress and performance such as the large-scale WASHO and AASHO road tests (HRB, 1955, 1962). Any theoretical method can be used only as a guide and should be verified by performance. This is particularly true for the empirical methods of design in which the ESWL analysis is an integral part of the overall design procedure. Erroneous results may be obtained if different ESWL methods are transposed for a given set of design curves.

6.2.1 Equal Vertical Stress Criterion

Working from a theoretical consideration of the vertical stress in an elastic half-space, Boyd and Foster (1950) presented a semirational method for determining ESWL, which had been used by the Corps of Engineers to produce dual-wheel design criteria from single-wheel criteria. The method assumes that the ESWL varies with the pavement

Downloaded From : www.EasyEngineering.net

Downloaded From : www.EasyEngineering.net

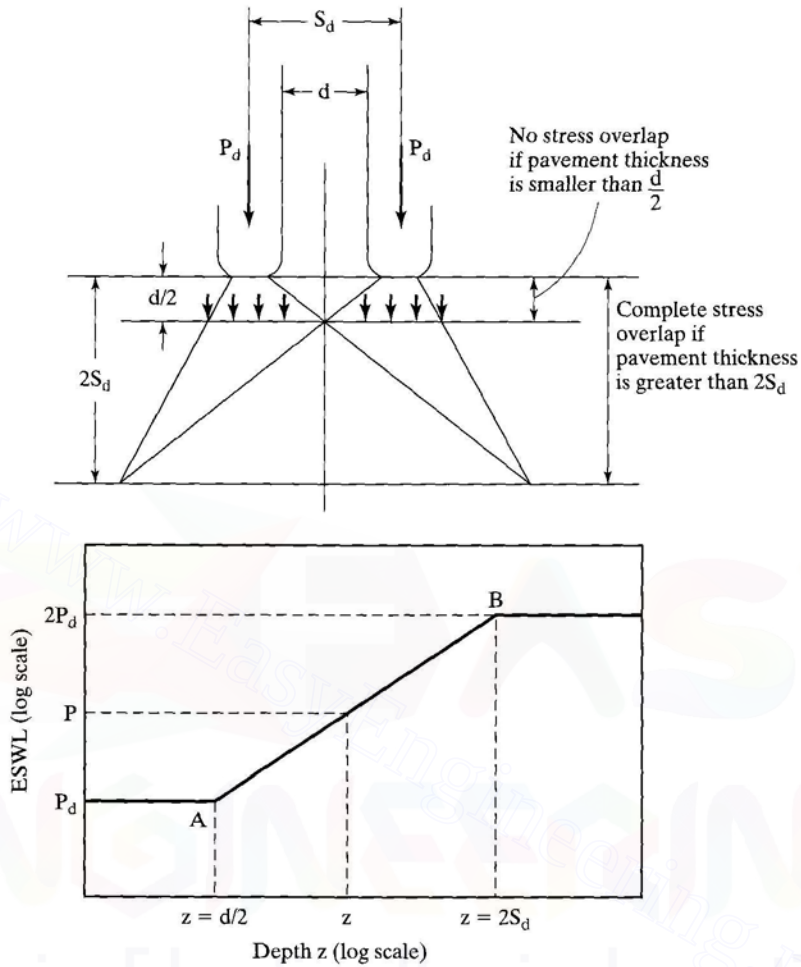


FIGURE 6.1

ESWL based on equal vertical subgrade stress.

thickness, as shown in Figure 6.1. For thicknesses smaller than half the clearance between dual tires, the ESWL is equal to one-half the total load, indicating that the subgrade vertical stresses caused by the two wheels do not overlap. For thicknesses greater than twice the center to center spacing of tires, the ESWL is equal to the total load, indicating that the subgrade stresses due to the two wheels overlap completely. By assuming a straight-line relationship between pavement thickness and wheel load on logarithmic scales, the ESWL for any intermediate thicknesses can be easily determined. After the ESWL for dual wheels is found, the procedure can be applied to tandem wheels.

Instead of plotting, it is more convenient to compute the ESWL by

$$\log(\text{ESWL}) = \log P_d + \frac{0.301 \log(2z/d)}{\log(4S_d/d)} \tag{6.1}$$

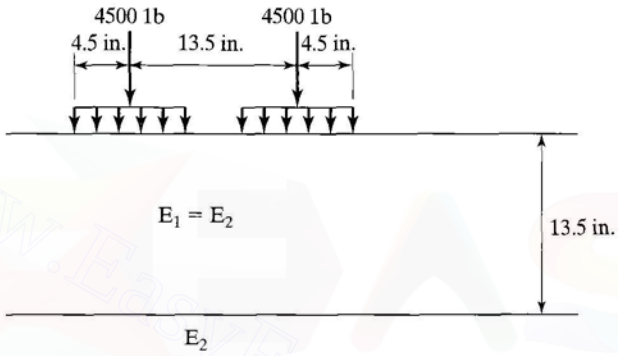
Downloaded From : www.EasyEngineering.net

Downloaded From : www.EasyEngineering.net

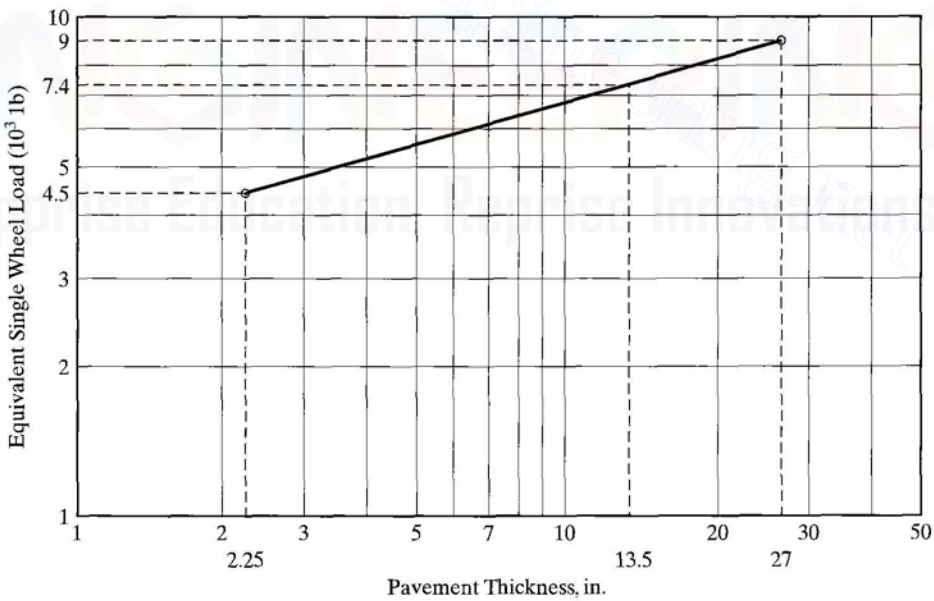
in which P_d is the load on one of the dual tires, z is the pavement thickness, d is the clearance between dual tires, and S_d is the center to center spacing between dual tires.

Example 6.1:

A set of dual tires has a total load $2P_d$ of 9000 lb (40 kN), a contact radius a of 4.5 in. (114 mm), and a center to center tire spacing S_d of 13.5 in. (343 mm), as shown in Figure 6.2*a*. Determine the ESWL by Boyd and Foster's method for a 13.5-in. (343-mm) pavement.



(a)



(b)

FIGURE 6.2

Example 6.1 (1 in. = 25.4 mm, 1 lb = 4.45 N).

Downloaded From : www.EasyEngineering.net

Downloaded From : www.EasyEngineering.net

Solution: Given S_d = 13.5 in. (343 mm) and a = 4.5 in. (114 mm), the clearance between the duals d = 13.5 − 9.0 = 4.5 in. (114 mm). When the thickness of pavement is equal to $d/2$, or 2.25 in. (57 mm), ESWL = P_d = 9000/2 = 4500 lb (20 kN). When the thickness is equal to $2S_d$ or 27 in. (689 mm), ESWL = $2P_d$ = 9000 lb (40 kN). After plotting thickness versus ESWL in Figure 6.2*b*, the ESWL for a 13.5 in. (343 mm) pavement is 7400 lb (32.9 kN). The ESWL can also be determined from Eq. 6.1 or log(ESWL) = log 4500 + 0.301 log(2 × 13.5/4.5)/log(4 × 13.5/4.5) = 3.87, or ESWL = 7410 lb (33.0 kN).

The vertical stress factor σ_z/q presented in Figure 2.2 can be used to determine the theoretical ESWL based on Boussinesq's theory. Figure 6.3 shows a pavement of thickness z under single and dual wheels that have the same contact radius a. The maximum subgrade stress under a single wheel occurs at point A with a stress factor of σ_z/q_s, where q_s is the contact pressure under a single wheel. The location of the maximum stress under dual wheels is not known and can be determined by comparing the stresses at three points: point 1 under the center of one tire, point 3 at the center between two tires, and point 2 midway between points 1 and 3. The stress factor at each point is obtained by superposition of the two wheels, and the maximum stress factor σ_z/q_d is found, where q_d is the contact pressure under dual wheels. To obtain the same stress,

$$q_s\left(\frac{\sigma_z}{q_s}\right) = q_d\left(\frac{\sigma_z}{q_d}\right) \tag{6.2}$$

For the same contact radius, contact pressure is proportioned to wheel load, or

$$\frac{P_s}{P_d} = \frac{\sigma_z/q_d}{\sigma_z/q_s} \tag{6.3}$$

in which P_s is the single-wheel load (which is the ESWL to be determined) and P_d is the load on each of the duals.

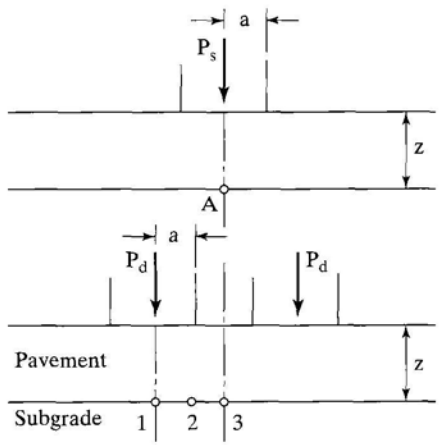


FIGURE 6.3
Location of maximum vertical stress or deflection on subgrade.

Downloaded From : www.EasyEngineering.net

Downloaded From : www.EasyEngineering.net

Example 6.2:

Same as Example 6.1 and Figure 6.2*a*. Determine the ESWL by Boussinesq's theory.

TABLE 6.1 Stress Factors Under Dual Wheels

	Left wheel		Right wheel		
Point no.	r/a	σ_z/q_s	r/a	σ_z/q_s	Sum σ_z/q_d
1	0	0.143	3	0.030	0.173
2	0.75	0.126	2.25	0.053	0.179
3	1.5	0.088	1.5	0.088	0.176

Solution: With $z/a = 13.5/4.5 = 3$, the stress factors can be obtained from Figure 2.2 and the results for dual wheels are presented in Table 6.1. It can be seen that the stresses at the three points are nearly the same with a maximum stress factor of 0.179 at point 2, which is slightly greater than the minimum of 0.173 at point 1. For a single wheel, the stress factor at point A is 0.143. From Eq. 6.3, ESWL $= P_s = 0.179/0.143 \times 4500 = 5630$ lb (25.1 kN), which differs significantly from the 7410 lb (32.9 kN) by Boyd and Foster's method. Although the original concept conceived by Boyd and Foster was based on the vertical subgrade stress, the method is more or less empirical in nature and, depending on the pavement thickness and the loading configuration, might not check well with the theoretical method based on Boussinesq stress distribution. However, the method gives an ESWL greater than the theoretical value and is therefore on the safe side.

6.2.2 Equal Vertical Deflection Criterion

After the application of Boyd and Foster's method and the subsequent completion of accelerated traffic tests, it was found that the design method was not very safe, and an improved method was developed by Foster and Ahlvin (1958). In this method, the pavement system is considered as a homogeneous half-space and the vertical deflections at a depth equal to the thickness of the pavement can be obtained from Boussinesq solutions. A single-wheel load that has the same contact radius as one of the dual wheels and results in a maximum deflection equal to that caused by the dual wheels is the ESWL.

The vertical deflection factor F presented in Figure 2.6 can be used to determine ESWL. Much as in the case of vertical stress, the deflection factors F_s at point A under the single wheel and F_d at points 1, 2, and 3 under the duals, as shown in Figure 6.3, are determined. The deflection can then be expressed as

$$w_s = \frac{q_s a}{E} F_s \tag{6.4a}$$

and

$$w_d = \frac{q_d a}{E} F_d \tag{6.4b}$$

in which the subscript s indicates single wheel and d indicates dual wheels. The deflection factor F_d is obtained by superposition of the duals. To obtain the same deflection,

Downloaded From : www.EasyEngineering.net

Downloaded From : www.EasyEngineering.net

$w_s = w_d$, or

$$q_s F_s = q_d F_d \tag{6.5}$$

For the same contact radius, contact pressure is proportional to wheel load:

$$\text{ESWL} = P_s = \frac{F_d}{F_s} P_d \tag{6.6}$$

Example 6.3:

Same as Example 6.1 and Figure 6.2*a*. Determine the ESWL by Foster and Ahlvin's method.

TABLE 6.2 Deflection Factors Under Dual Wheels for a Homogeneous Half-Space

	Left wheel		Right wheel		
Point no.	r/a	F_s	r/a	F_s	Sum F_d
1	0	0.478	3	0.263	0.741
2	0.75	0.443	2.25	0.318	0.761
3	1.5	0.390	1.5	0.390	0.780

Solution: The chart shown in Figure 2.6 can be used to determine vertical deflections. The deflection factors F at the three points shown in Figure 6.3 are calculated and presented in Table 6.2. The maximum deflection due to dual wheels occurs at point 3 with a deflection factor of 0.78. The maximum deflection due to a single wheel occurs under the center of the tire with a deflection factor of 0.478. From Eq. 6.6, ESWL = 0.78/0.478 × 4500 = 7340 lb (32.7 kN), which checks with the 7410 lb (32.9 kN) obtained in Example 6.1 by Boyd and Foster's method. The close agreement between the two methods is a coincidence. Depending on the pavement thickness and the geometry of wheel loads, Foster and Ahlvin's method may yield a much greater ESWL than Boyd and Foster's method.

Although the improved method by Foster and Ahlvin results in a larger pavement thickness, which is more in line with traffic data than the earlier method by Boyd and Foster, the assumption of a homogeneous half-space instead of a layered system is not logical from a theoretical viewpoint. From the data presented by Foster and Ahlvin (1958), Huang (1968b) indicated that the improved method was still not safe, as evidenced by the fact that some of the pavements with thicknesses greater than those obtained by the method were considered inadequate or on the borderline. Since the ESWL for layered systems is greater than that for a homogeneous half-space, Huang (1968b) suggested the use of layered theory and presented a simple chart for determining ESWL based on the interface deflection of two layered systems, as shown in Figure 6.4. Given contact radius a, pavement thickness h_1, modulus ratio E_1/E_2, and dual spacing S_d, the chart gives a load factor

$$L = \frac{\text{Total load}}{\text{ESWL}} = \frac{2P_d}{P_s} \tag{6.7a}$$

Downloaded From : www.EasyEngineering.net

Downloaded From : www.EasyEngineering.net

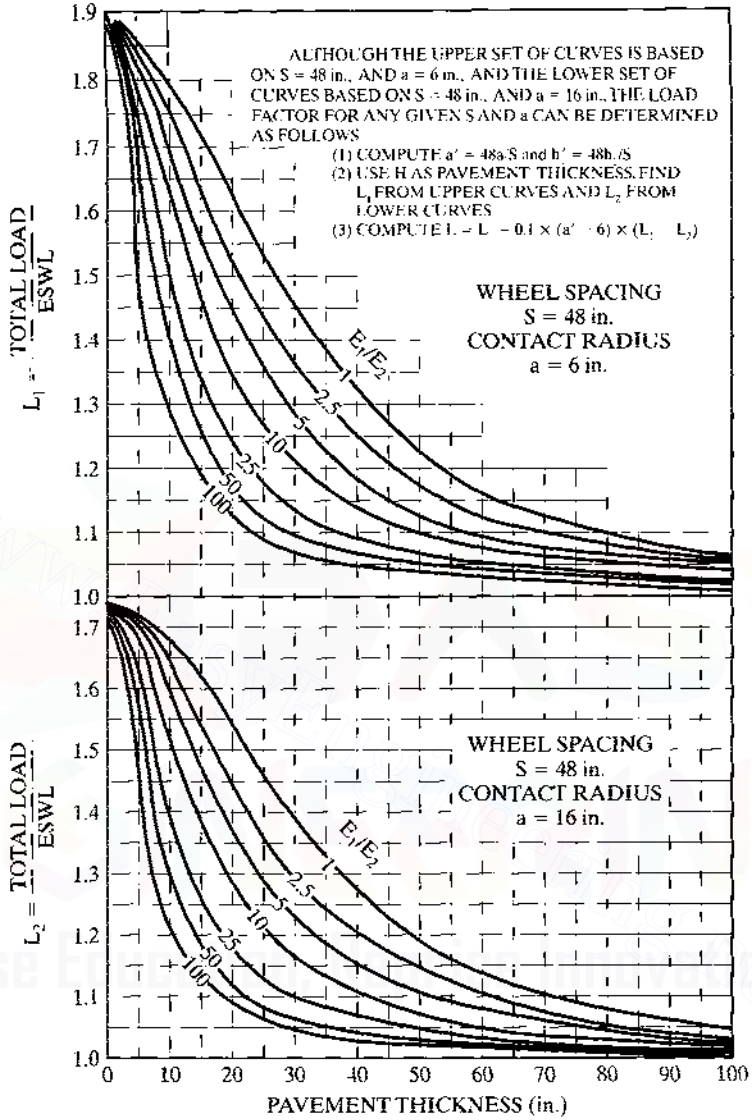


FIGURE 6.4

Chart for determining equivalent single-wheel load (1 in. = 25.4 mm). (After Huang (1968b).)

or

$$\text{ESWL} = \frac{2P_d}{L} \tag{6.7b}$$

Comparing Eq. 6.6 with Eq. 6.7*b* yields

$$L = \frac{2F_s}{F_d} \tag{6.8}$$

Equation 6.8 was used to develop the chart shown in Figure 6.4.

Downloaded From : www.EasyEngineering.net

Downloaded From : www.EasyEngineering.net

The ESWL can also be determined from the deflection factors presented in Figure 2.19 by following the same procedure illustrated in Example 6.3. However, the use of the chart shown in Figure 6.4 is much quicker. The chart is based on a dual spacing S_d of 48 in. (1.22 m). If the actual spacing is different, it must be changed to 48 in. (1.22 m), and the values of a and h_1 changed proportionally. As long as S_d/a and h_1/a remain the same, the load factor will be the same. The upper chart is for a contact radius of 6 in. (152 mm) and the lower chart is for a contact radius of 16 in. (406 mm). The load factor for any other contact radius can be obtained by a straight-line interpolation. The procedure can be summarized as follows:

1. From the given S_d, h_1, and a, determine the modified radius a' and the modified thickness h_1' by

$$a' = \frac{48}{S_d} a \tag{6.9a}$$

$$h_1' = \frac{48}{S_d} h_1 \tag{6.9b}$$

2. Using h_1' as the pavement thickness, find load factors L_1 and L_2 from the chart.
3. Determine the load factor L from

$$L = L_1 - (L_1 - L_2)\frac{a' - 6}{10} \tag{6.10}$$

and ESWL from Eq. 6.7*b*.

Example 6.4:

Same as Example 6.1 but the pavement is considered as a two-layer system, as shown in Figure 6.5. Determine the ESWL by equal interface deflection criterion for E_1/E_2 of 1 and 25, respectively.

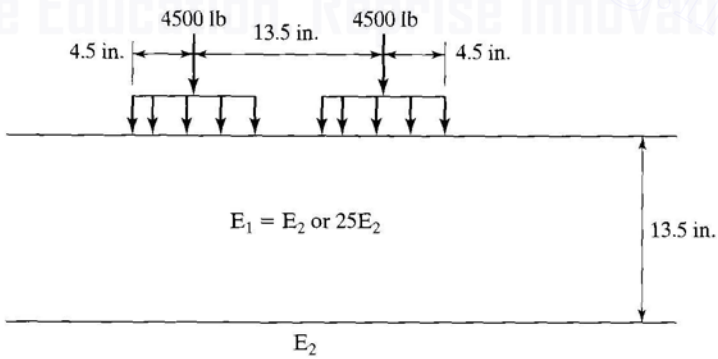


FIGURE 6.5

Example 6.4 (1 in. = 25.4 mm, 1 lb = 4.45).

Solution: Given S_d = 13.5 in. (343 mm), a = 4.5 in. (114 mm), and h_1 = 13.5 in. (343 mm), from Eq. 6.9, a' = 48/13.5 × 4.5 = 16 in. (406 mm) and h_1' = 48/13.5 × 13.5 = 48 in. (1.22 m).

Downloaded From : www.EasyEngineering.net

Downloaded From : www.EasyEngineering.net

Because the modified contact radius is exactly 16 in. (406 mm), no interpolation is needed. From the lower chart of Figure 6.4 $L = 1.22$ when $E_1/E_2 = 1$ and $L = 1.06$ when $E_1/E_2 = 25$. With $2P_d = 9000$ lb (40 kN), from Eq. 6.7b, ESWL = 9000/1.22 = 7380 lb (32.8 kN) when $E_1/E_2 = 1$ and ESWL = 9000/1.06 = 8490 lb (37.8 kN) when $E_1/E_2 = 25$. It can be seen that ESWL increases as the modulus ratio increases. An ESWL of 7380 lb (32.8 kN) for $E_1/E_2 = 1$ checks well with the 7340 lb (32.7 kN) obtained in Example 6.3.

6.2.3 Equal Tensile Strain Criterion

The conversion factors presented in Figures 2.23, 2.25, 2.26, and 2.27 can be used to determine ESWL. According to Eq. 2.17, the tensile strain e at the bottom of layer 1 under a single-wheel load is

$$e = \frac{q_s}{E_1} F_e \tag{6.11}$$

in which q_s is the contact pressure of a single wheel. The tensile strain under dual or dual-tandem wheels is

$$e = \frac{Cq_d}{E_1} F_e \tag{6.12}$$

in which C is the conversion factor and q_d is the contact pressure of dual or dual-tandem wheels. Equate Eqs. 6.11 and 6.12 to obtain the same tensile strain:

$$q_s = Cq_d \tag{6.13}$$

For equal contact radius, contact pressure is proportional to wheel load:

$$\text{ESWL} = P_s = CP_d \tag{6.14}$$

Example 6.5:

A full-depth asphalt pavement, 8 in. (203 mm) thick, is loaded by a set of dual wheels with a total load $2P_d$ of 9000 lb (40 kN), a contact radius a of 4.5 in. (114 mm), and a center to center wheel spacing S_d of 13.5 in. (343 mm), as shown in Figure 6.6. If $E_1/E_2 = 50$, determine ESWL by equal tensile strain criterion.

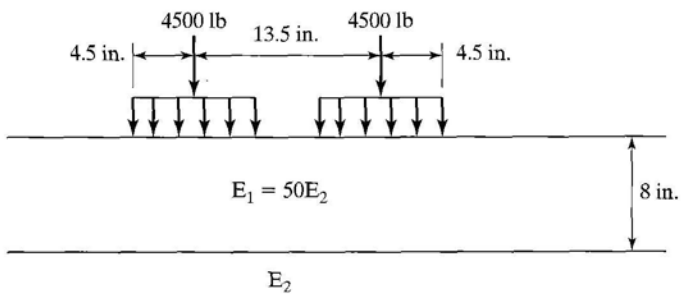


FIGURE 6.6

Example 6.5 (1 in. = 25.4 mm, 1 lb = 4.45 N).

Downloaded From : www.EasyEngineering.net

Downloaded From : www.EasyEngineering.net

Solution: Given $S_d = 13.5$ in. (343 mm), $a = 4.5$ in. (114 mm), and $h_1 = 8$ in. (203 mm), from Eq. 2.18, $a' = 24/13.5 \times 4.5 = 8$ in. (203 mm) and $h_1' = 24/13.5 \times 8 = 14.2$ in. (361 mm). Because the modified contact radius is exactly 8 in. (203 mm), no interpolation is needed. From the lower chart in Figure 2.23, $C = 1.50$. From Eq. 6.14, ESWL $= 1.50 \times 4500 = 6750$ lb (30.0 kN).

6.2.4 Criterion Based on Equal Contact Pressure

All of the above analyses of ESWL are based on the assumption that the single wheel has the same contact radius as each of the dual wheels. Another assumption, which has been frequently made, is that the single wheel has a different contact radius but the same contact pressure as the dual wheels. Although this assumption is more reasonable, its solution is much more complicated and cannot be presented by a simple chart.

According to Eq. 2.16, the interface deflections for single and dual wheels with the same contact pressure can be written as

$$w_s = \frac{qa_s}{E_2} F_s \tag{6.15a}$$

$$w_d = \frac{qa_d}{E_2} F_d \tag{6.15b}$$

in which the subscript s indicates single wheel and d indicates dual wheels. The deflection factor F_d is obtained by superposition of the duals. To obtain equal deflection, $w_s = w_d$, or

$$\frac{qa_s}{E_2} F_s = \frac{qa_d}{E_2} F_d \tag{6.16}$$

Because

$$a_s = \sqrt{\frac{P_s}{\pi q}} \tag{6.17a}$$

and

$$a_d = \sqrt{\frac{P_d}{\pi q}} \tag{6.17b}$$

Eq. 6.16 becomes

$$\text{ESWL} = P_s = \left(\frac{F_d}{F_s}\right)^2 P_d \tag{6.17c}$$

If P_d and q are given, a_d can be computed from Eq. 6.17*b*, and the maximum deflection factor F_d can be determined. However, the application of Eq. 6.17*c* presents a difficulty because F_s depends on the contact radius a, which varies with P_s according to Eq. 6.17*a*. Consequently, Eq. 6.17*c* can be solved only by a trial and error method.

Downloaded From : www.EasyEngineering.net

Downloaded From : www.EasyEngineering.net

Example 6.6:

A two-layer system with a thickness h_1 of 13.5 in. (343 mm) and a modulus ratio E_1/E_2 of 25 is loaded under a set of duals with a total load $2P_d$ of 9000 lb (40 kN), a contact pressure q of 70 psi (483 kPa), and a center to center tire spacing S_d of 13.5 in. (343 mm), as shown in Figure 6.7. Determine the ESWL based on the equal interface deflection criterion with equal contact pressure.

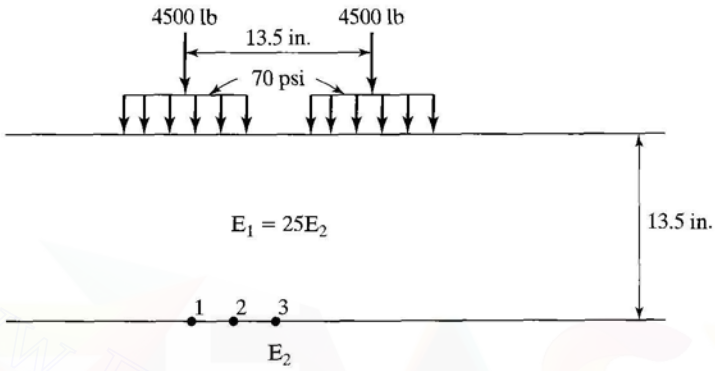


Figure 6.7

Example 6.6 (1 in. = 25.4 mm, 1 psi = 6.9 kPa, 1 lb = 4.45 N).

Solution: Given $P_d = 4500$ lb (20 kN) and $q = 70$ psi (483 kPa), from Eq. 6.17*b*, $a_d = \sqrt{4500/(\pi \times 70)} = 4.5$ in. (519 mm). With $h_1/a_d = 13.5/4.5 = 3.0$ and $E_1/E_2 = 25$, the deflection factors at points 1, 2, and 3, as shown in Figure 6.7, can be obtained from Figure 2.19 and the results are presented in Table 6.3. It can be seen that the same deflection factor of 0.36 is obtained at all three points, or $F_d = 0.36$.

TABLE 6.3 Deflection Factors Under Dual Wheels for a Layered System

	Left wheel		Right wheel		
Point no.	r/a	F_s	r/a	F_s	Sum F_d
1	0	0.19	3	0.17	0.36
2	0.75	0.19	2.25	0.17	0.36
3	1.5	0.18	1.5	0.18	0.36

Assume that $P_s = 8000$ lb (35.6 kN). From Eq. 6.17*a*, $a_s = \sqrt{8000/(\pi \times 70)} = 6.03$ in. (153 mm). With $h_1/a_s = 13.5/6.03 = 2.24$ and $E_1/E_2 = 25$, from Figure 2.19, $F_s = 0.26$. From Eq. 6.17*c*, $P_s = (0.36/0.26)^2 \times 4500 = 8630$ lb (38.4 kN). Because the deflection factor cannot be read accurately from Figure 2.19, a P_s of 8300 lb (36.9 kN), which is midway between 8000 lb (35.6 kN) and 8630 lb (38.4 kN), is taken as the final solution. The ESWL based on equal contact radius, as illustrated in Example 6.4, is 8490 (37.8 kN), which is not much different from the 8300 lb (36.9 kN) based on equal contact pressure.

Downloaded From : www.EasyEngineering.net

Downloaded From : www.EasyEngineering.net

Huang (1968b) compared the ESWL based on equal contact radius with that based on equal contact pressure for a variety of cases. He found that, unless the pavement is extremely thin and the modulus ratio close to unity, the differences between the two methods are not very significant.

Two-layer interface deflections based on equal contact pressure were also used by the Asphalt Institute to compute the ESWL for full-depth asphalt pavements. This procedure is applicable to aircraft having less than 60,000 lb (267 kN) gross weight. By the use of Figure 2.19, simplified charts were developed for determining the ESWL for dual wheels based on the CBR of the subgrade (AI, 1973).

6.2.5 Criterion Based on Equivalent Contact Radius

Instead of equal contact radius or equal contact pressure, loannides and Khazanovich (1993) proposed the use of an equivalent contact radius to determine the load equivalency and called this method equivalent single-axle radius (ESAR). The basic concept is to determine a single wheel load with an equivalent radius that would lead to the same response if loaded by the same total load as the dual-wheel assembly. For example, by the use of statistical regression techniques, they found that the maximum bending stress due to dual tires in the interior of a concrete slab would be the same as a single tire with the equivalent radius

$$a_{eq} = a\left[1 + 0.241683\left(\frac{S}{a}\right)\right] \tag{6.18}$$

in which a_{eq} = equivalent tire contact radius, a = contact radius of each of the dual tires, and S = center-to-center spacing between the dual. They maintained that it is possible to derive with reasonable accuracy an equivalent radius, a_{eq}, for any arbitrary loading configuration simply as a function of its geometry (i.e., size and spacing of tire imprints). Whether the same concept can be applied to flexible pavements needs to be investigated.

Example 6.7:

Same as Problem 4.3: determine the maximum stress in concrete, using equivalent contact radius instead of equivalent contact area.

Solution: $a = [6000/(\pi \times 80)]^{0.5} = 4.886$ in. (124 mm). From Eq. 6.18, $a_{eq} = 4.886(1 + 0.241683 \times 14/4.886 = 8.27$ in. (210 mm). From Eq. 4.19*b*, $b = [1.6 \times (8.27)^2 + 100]^{0.5} - 0.675 \times 10 = 7.722$ in. (196 mm). From Eq. 4.10, $\ell = [(4{,}000{,}000 \times 1000)/(12 \times 0.9775 \times 200)]^{0.25} = 36.135$ in. (0.92 m). From Eq. 4.20, $\sigma_i = 0.316 \times 12{,}000/100 \times [4 \log(36.135/7.722) + 1.069] = 142.2$ psi (980 kPa), which checks well with 139.7 psi (963 kPa) by the equivalent area.

6.3 EQUIVALENT AXLE LOAD FACTOR

An equivalent axle load factor (EALF) defines the damage per pass to a pavement by the axle in question relative to the damage per pass of a standard axle load, usually the

Downloaded From : www.EasyEngineering.net

Downloaded From : www.EasyEngineering.net

18-kip (80-kN) single-axle load. The design is based on the total number of passes of the standard axle load during the design period, defined as the equivalent single-axle load (ESAL) and computed by

$$\text{ESAL} = \sum_{i=1}^{m} F_i n_i \tag{6.19}$$

in which m is the number of axle load groups, F_i is the EALF for the ith-axle load group, and n_i is the number of passes of the ith-axle load group during the design period.

The EALF depends on the type of pavements, thickness or structural capacity, and the terminal conditions at which the pavement is considered failed. Most of the EALFs in use today are based on experience. One of the most widely used methods is based on the empirical equations developed from the AASHO Road Test (AASHTO, 1972). The EALF can also be determined theoretically based on the critical stresses and strains in the pavement and the failure criteria. In this section, the equivalent factors for flexible and rigid pavements are discussed separately.

6.3.1 Flexible Pavements

The AASHTO equations for computing EALF are described first, followed by a discussion of equivalent factor based on the results obtained from KENLAYER.

AASHTO Equivalent Factors The following regression equations based on the results of road tests can be used for determining EALF:

$$\log\left(\frac{W_{tx}}{W_{t18}}\right) = 4.79\log(18 + 1) - 4.79\log(L_x + L_2) + 4.33\log L_2 + \frac{G_t}{\beta_x} - \frac{G_t}{\beta_{18}} \tag{6.20a}$$

$$G_t = \log\left(\frac{4.2 - p_t}{4.2 - 1.5}\right) \tag{6.20b}$$

$$\beta_x = 0.40 + \frac{0.081(L_x + L_2)^{3.23}}{(\text{SN} + 1)^{5.19} L_2^{3.23}} \tag{6.20c}$$

In these equations, W_{tx} is the number of x-axle load applications at the end of time t; W_{t18} is the number of 18-kip (80-kN) single-axle load applications to time t; L_x is the load in kip on one single axle, one set of tandem axles, or one set of tridem axles; L_2 is the axle code (1 for single axle, 2 for tandem axles, and 3 for tridem axles); SN is the structural number, which is a function of the thickness and modulus of each layer and the drainage conditions of base and subbase; p_t is the terminal serviceability, which indicates the pavement conditions to be considered as failures; G_t is a function of P_t; and β_{18} is the value of β_x when L_x is equal to 18 and L_2 is equal to one. The method for

Downloaded From : www.EasyEngineering.net

Downloaded From : www.EasyEngineering.net

determining SN is presented in Section 11.3.4. Note that

$$\text{EALF} = \frac{W_{t18}}{W_{tx}} \tag{6.21}$$

Equation 6.20 can be used to solve EALF. The effect of p_t and SN on EALF is erratic and is not completely consistent with theory. However, under heavy axle loads with an equivalent factor much greater than unity, the EALF increases as p_t or SN decreases. This is as expected, because heavy axle loads are more destructive to poor and weaker pavements than to good and stronger ones. A disadvantage of using the above equations is that the EALF varies with the structural number, which is a function of layer thicknesses. Theoretically, a method of successive approximations should be used, because the EALF depends on the structural number and the structural number depends on the EALF. Practically, EALF is not very sensitive to pavement thickness, and SN = 5 may be used for most cases. Unless the design thickness is significantly different, no iterations will be needed. The AASHTO equivalent factors with $p_t = 2.5$ and SN = 5 are used by the Asphalt Institute, as shown in Table 6.4. The original table has single and tandem axles only, but the tridem axles are added to follow the AASHTO design guide (AASHTO, 1986). Tables of equivalent factors for SN values of 1, 2, 3, 4, 5, and 6 and p_t values of 2, 2.5, and 3 can be found in the AASHTO design guide.

Example 6.8:

Given $p_t = 2.5$ and SN = 5, determine the EALF for a 32-kip (151-kN) tandem-axle load and a 48-kip (214-kN) tridem-axle load.

Solution: For the tandem axles, $L_x = 32$ and $L_2 = 2$, from Eq. 6.20, $G_t = \log(1.7/2.7) = -0.201$, $\beta_x = 0.4 + 0.081\,(32 + 2)^{3.23}/[(5 + 1)^{5.19}(2)^{3.23}] = 0.470$, $\beta_{18} = 0.4 + 0.081\,(18 + 1)^{3.23}/(5 + 1)^{5.19} = 0.5$, and $\log(W_{tx}/W_{t18}) = 4.79 \log 19 - 4.79 \log(32 + 2) + 4.33 \log 2 - 0.201/0.47 + 0.201/0.5 = 0.067$, or $W_{tx}/W_{t18} = 1.167$. From Eq. 6.21, EALF = 0.857, which is exactly the same as that shown in Table 6.4.

For the tridem axles, $L_x = 48$, $L_2 = 3$, from Eq. 6.20, $\beta_x = 0.4 + 0.081(48 + 3)^{3.23}/[(5 + 1)^{5.19}(3)^{3.23}] = 0.470$, and $\log(W_{tx}/W_{t18}) = 4.79 \log 19 - 4.79 \log(48 + 3) + 4.33 \log 3 - 0.201/0.47 + 0.201/0.5 = -0.0139$, or $W_{tx}/W_{t18} = 0.968$. From Eq. 6.21, EALF =1.033, as shown in Table 6.4.

Theoretical Analysis In the mechanistic method of design, the EALF can be determined from the failure critera. The failure criterion for fatigue cracking was shown in Eq. 3.6 with f_2 of 3.291 by the Asphalt Institute and 5.671 by Shell:

$$N_f = f_1\,(\epsilon_t)^{-f_2}\,(E_1)^{-f_3} \tag{3.6}$$

Deacon (1969) conducted a theoretical analysis of EALF by layered theory based on an assumed f_2 of 4, or, from Eq. 3.6,

$$\text{EALF} = \frac{W_{t18}}{W_{tx}} = \left(\frac{\epsilon_x}{\epsilon_{18}}\right)^4 \tag{6.22}$$

Downloaded From : www.EasyEngineering.net

Downloaded From : www.EasyEngineering.net

TABLE 6.4 Asphalt Institute's Equivalent Axle Load Factors

Axle load (lb)	Equivalent axle load factor			Axle load (lb)	Equivalent axle load factor		
	Single axles	Tandem axles	Tridem axles		Single axles	Tandem axles	Tridem axles
1000	0.00002			41,000	23.27	2.29	0.540
2000	0.00018			42,000	25.64	2.51	0.597
3000	0.00072			43,000	28.22	2.76	0.658
4000	0.00209			44,000	31.00	3.00	0.723
5000	0.00500			45,000	34.00	3.27	0.793
6000	0.01043			46,000	37.24	3.55	0.868
7000	0.0196			47,000	40.74	3.85	0.948
8000	0.0343			48,000	44.50	4.17	1.033
9000	0.0562			49,000	48.54	4.51	1.12
10,000	0.0877	0.00688	0.002	50,000	52.88	4.86	1.22
11,000	0.1311	0.01008	0.002	51,000		5.23	1.32
12,000	0.189	0.0144	0.003	52,000		5.63	1.43
13,000	0.264	0.0199	0.005	53,000		6.04	1.54
14,000	0.360	0.0270	0.006	54,000		6.47	1.66
15,000	0.478	0.0360	0.008	55,000		6.93	1.78
16,000	0.623	0.0472	0.011	56,000		7.41	1.91
17,000	0.796	0.0608	0.014	57,000		7.92	2.05
18,000	1.000	0.0773	0.017	58,000		8.45	2.20
19,000	1.24	0.0971	0.022	59,000		9.01	2.35
20,000	1.51	0.1206	0.027	60,000		9.59	2.51
21,000	1.83	0.148	0.033	61,000		10.20	2.67
22,000	2.18	0.180	0.040	62,000		10.84	2.85
23,000	2.58	0.217	0.048	63,000		11.52	3.03
24,000	3.03	0.260	0.057	64,000		12.22	3.22
25,000	3.53	0.308	0.067	65,000		12.96	3.41
26,000	4.09	0.364	0.080	66,000		13.73	3.62
27,000	4.71	0.426	0.093	67,000		14.54	3.83
28,000	5.39	0.495	0.109	68,000		15.38	4.05
29,000	6.14	0.572	0.126	69,000		16.26	4.28
30,000	6.97	0.658	0.145	70,000		17.19	4.52
31,000	7.88	0.753	0.167	71,000		18.15	4.77
32,000	8.88	0.857	0.191	72,000		19.16	5.03
33,000	9.98	0.971	0.217	73,000		20.22	5.29
34,000	11.18	1.095	0.246	74,000		21.32	5.57
35,000	12.50	1.23	0.278	75,000		22.47	5.86
36,000	13.93	1.38	0.313	76,000		23.66	6.15
37,000	15.50	1.53	0.352	77,000		24.91	6.46
38,000	17.20	1.70	0.393	78,000		26.22	6.78
39,000	19.06	1.89	0.438	79,000		27.58	7.11
40,000	21.08	2.08	0.487	80,000		28.99	7.45

Note. 1 lb = 4.45 N.

Downloaded From : www.EasyEngineering.net

Downloaded From : www.EasyEngineering.net

in which ϵ_x is the tensile strain at the bottom of asphalt layer due to an x-axle load and ϵ_{18} is the tensile strain at the bottom of asphalt layer due to an 18-kip (80-kN) axle load. If W_{tx} is also a single axle, it is reasonable to assume that tensile strains are directly proportional to axle loads, or

$$\text{EALF} = \left(\frac{L_x}{18}\right)^4 \tag{6.23}$$

in which L_x is the load in kip on a single axle. Equation 6.23 is valid only when L_x is on a single axle. For tandem or tridem axles, a more general equation is

$$\text{EALF} = \left(\frac{L_x}{L_s}\right)^4 \tag{6.24}$$

in which L_s is the load in kip on standard axles which have the same number of axles as L_x. If the EALF for one set of tandem or tridem axles is known, that for other axles can be determined by Eq. 6.24.

Example 6.9:

Given $p_t = 2.5$ and SN = 5, determine the EALF for 5000-lb (22.3-kN) and 50,000-lb (223-kN) single axles by Eq. 6.23. If the EALF of a 32-kip (142-kN) tandem axle is 0.857, determine the EALF for 15,000-lb (66.8-kN) and 80,000-lb (356-kN) tandem axles by Eq. 6.24.

Solution: For a single axle with $L_x = 5$, from Eq. 6.23, EALF $= (5/18)^4 = 0.006$, which compares with 0.005 from Table 6.4. For a single axle with $L_x = 50$, EALF $= (50/18)^4 = 59.54$ compared with 52.88 from Table 6.4. For tandem axles with $L_x = 15$ and $L_s = 32$, from Eq. 6.24, the equivalent factor between 15-kip (66.8-kN) and 32-kip (142-kN) tandem axles is $(15/32)^4 = 0.0483$, which must be multiplied by 0.857 to obtain the equivalent factor between 15-kip (66.8-kN) tandem axles and an 18-kip (80-kN) single axle, so EALF $= 0.0483 \times 0.857 = 0.041$ compared with 0.036 from Table 6.4. For tandem axles with $L_x = 80$, EALF $= 0.857 \times (80/32)^4 = 33.48$ compared with 28.99 from Table 6.4. It can be seen that the equivalent factors based on tensile strains at the bottom of the asphalt layer check favorably with the AASHTO and Asphalt Institute's equivalent factors.

The other failure criterion is to control permanent deformation by limiting the vertical compressive strain on top of the subgrade, which can be expressed as

$$N_d = f_4 (\epsilon_c)^{-f_5} \tag{6.7}$$

Suggested values of f_5 are 4.477 by the Asphalt Institute, 4.0 by Shell, and 3.571 by the University of Nottingham. It can be seen that the use of 4 for f_5 is also reasonable. Therefore, when both L_x and L_s in Eq. 6.24 are of the same configuration, the EALF based on fatigue cracking may not be much different from that based on permanent deformation. However, this is not true when L_s is for a single axle but L_x is for multiple axles, because then the effect of additional axles on the tensile strains at the bottom of asphalt layer is quite different from that on the compressive strain at the top of the subgrade.

Table 6.5 shows the computation of EALF based on fatigue cracking; Table 6.6 shows that based on permanent deformation. The damage ratio D_r is caused by the

Downloaded From : www.EasyEngineering.net

Downloaded From : www.EasyEngineering.net

passage of one single axle or a set of tandem or tridem axles and can be obtained directly by KENLAYER. A full-depth asphalt pavement with two extreme HMA thicknesses of 2 and 12 in. (51 and 305 mm) and two extreme subgrade moduli of 5000 and 30,000 psi (35 and 207 MPa) is assumed. The single axle is a standard 18-kip (80-kN) axle with dual tires having a contact pressure of 100 psi (690 kPa) and a dual spacing of 13.5 in. (343 mm). Each of the tandem and tridem axles is the same as the single axle, so the total load on tandem axles is 36 kip (160 kN) and that on tridem axles is 54 kip (240 kN). The spacing between the two axles is 48 in. (1.2 m). The HMA has a resilient modulus of 450,000 psi (3.1 GPa) and a Poisson ratio of 0.35; the subgrade has a Poisson ratio of 0.45. The Asphalt Institute failure criteria were used for the analysis.

TABLE 6.5 Analysis of Damage Ratio for Fatigue Cracking by KENLAYER

HMA thickness (in.)	2		12	
Subgrade modulus (psi)	5000	30,000	5000	30,000
18*k* Single damage ratio	1.311×10^{-4}	7.030×10^{-6}	8.450×10^{-8}	1.974×10^{-8}
36*k* Tandem				
Primary D_f	1.282×10^{-4}	6.984×10^{-6}	6.740×10^{-8}	1.334×10^{-8}
Secondary D_f	1.138×10^{-4}	6.900×10^{-6}	6.199×10^{-10}	1.018×10^{-9}
Total D_f	2.420×10^{-4}	1.388×10^{-5}	6.802×10^{-8}	1.436×10^{-8}
EALF	1.85	1.97	0.80	0.73
54*k* Tridem				
Primary D_f	1.253×10^{-4}	6.939×10^{-6}	9.493×10^{-8}	8.555×10^{-9}
Secondary D_f	2.222×10^{-4}	1.371×10^{-5}	2.477×10^{-9}	7.034×10^{-10}
Total D_f	3.475×10^{-4}	2.065×10^{-5}	9.741×10^{-8}	9.258×10^{-9}
EALF	2.65	2.94	1.15	0.46

Note. 1 in. = 25.4 mm, 1 kip = 4.45 kN, 1 psi = 6.9 kPa.

TABLE 6.6 Analysis of Damage Ratio for Permanent Deformation by KENLAYER

HMA thickness (in.)	2		12	
Subgrade modulus (psi)	5000	30,000	5000	30,000
18*k* Single damage ratio	3.202×10^{-3}	4.843×10^{-5}	6.358×10^{-8}	4.408×10^{-9}
36*k* Tandem				
Primary D_f	3.178×10^{-3}	4.820×10^{-5}	9.634×10^{-8}	4.261×10^{-9}
Secondary D_f	3.178×10^{-3}	4.820×10^{-5}	1.456×10^{-9}	1.178×10^{-9}
Total D_f	6.356×10^{-3}	9.640×10^{-5}	9.780×10^{-8}	5.439×10^{-9}
EALF	1.99	1.99	1.54	1.23
54*k* Tridem				
Primary D_f	3.154×10^{-3}	4.797×10^{-5}	1.409×10^{-7}	4.118×10^{-9}
Secondary D_f	6.308×10^{-3}	9.594×10^{-5}	7.253×10^{-9}	2.250×10^{-9}
Total D_f	9.462×10^{-3}	1.439×10^{-4}	1.482×10^{-7}	6.368×10^{-9}
EALF	2.96	2.97	2.33	1.44

Note. 1 in. = 25.4 mm, 1 kip = 4.45 kN, 1 psi = 6.9 kPa.

Downloaded From : www.EasyEngineering.net

Downloaded From : www.EasyEngineering.net

For tandem-axle loads, the primary D_r is the damage ratio caused by the strain ϵ_a due to the passage of the first axle, the secondary D_r the damage ratio caused by the strain $\epsilon_a - \epsilon_b$, due to the passage of the second axle, as illustrated in Figure 3.3. For tridem-axle loads, the primary damage ratio is based on the loading position shown in Figure 3.4*a*, while the secondary damage ratio is based on two passages of the loading shown in Figure 3.4*b*. The total damage ratio is the sum of primary and secondary damage ratios. Dividing the total damage ratio due to tandem or tridem axles by the damage ratio due to a single axle gives the values of EALF shown in the tables.

Review of Tables 6.5 and 6.6

1. For the 2-in. (51-mm) pavement with a subgrade modulus of 5000 psi (35 MPa), the damage ratios due to permanent deformation are greater than those due to fatigue cracking, whereas the reverse is true for the 12-in. (305-mm) pavement with a subgrade modulus of 30,000 psi (207 MPa). Therefore, the design is controlled by fatigue cracking for stronger pavements but by permanent deformation for weaker pavements.
2. For the 2-in. (51-mm) pavement with a subgrade modulus of 30,000 psi (207 MPa), the strains due to one axle load are not affected by the other axle loads, so the damage ratios for tandem axles are nearly twice as large as those for a single axle, with an EALF close to 2, and those for tridem axles are three times as large, with an EALF close to 3. When the pavement becomes thicker or the subgrade modulus becomes smaller, the two or three axle loads begin to interact, and the EALF based on fatigue cracking can be quite different from that based on permanent deformation, as indicated by an EALF much smaller than 1 for fatigue cracking but much greater than 1 for permanent deformation.
3. The AASHTO equivalent factors for 36-kip (160-kN) tandem axles and 54-kip (240-kN) tridem axles, as obtained from Eq. 6.20, are practically independent of structural number. For a terminal serviceability of 2.5, the equivalent factor is 1.33 for 36-kip (160-kN) tandem axles and 1.66 for 54-kip (240-kN) tridem axles. However, the EALF obtained from KENLAYER could range from 0.73 to 1.99 for tandem axles and from 0.46 to 2.97 for tridem axles, depending on pavement geometry, material properties, and failure criteria.
4. The many factors involved make it impossible to select an appropriate EALF that can be applied to all situations. For a truly mechanistic design method, each load group should be considered individually, instead of using an equivalent single axle load.

6.3.2 Rigid Pavements

The AASHTO equations for computing EALF are described first, followed by a discussion of an equivalent factor based on the results obtained from KENSLABS.

AASHTO Equivalent Factors The AASHTO equations for determining the EALF of rigid pavements are as follows:

Downloaded From : www.EasyEngineering.net

Downloaded From : www.EasyEngineering.net

$$\log\left(\frac{W_{tx}}{W_{t18}}\right) = 4.62\log(18 + 1) - 4.62\log(L_x + L_2) + 3.28\log L_2 + \frac{G_t}{\beta_x} - \frac{G_t}{\beta_{18}} \tag{6.25a}$$

$$G_t = \log\left(\frac{4.5 - p_t}{4.5 - 1.5}\right) \tag{6.25b}$$

$$\beta_x = 1.00 + \frac{3.63(L_x + L_2)^{5.20}}{(D + 1)^{8.46}L_2^{3.52}} \tag{6.25c}$$

in which W_{tx}, W_{t18}, L_x, L_2, p_t, and β_{18} are as defined for Eq. 6.20 for flexible pavements and D is the slab thickness in inches. Note that Eqs. 6.20 and 6.25 are in the same form, but with different values of regression constants, and that the structural number SN in Eq. 6.20 is replaced by the slab thickness D in Eq. 6.25. The EALF can also be computed by Eq. 6.21. Table 6.7 shows the AASHTO equivalent factors for $p_t = 2.5$ and

TABLE 6.7 Equivalent Axle Load Factors for Rigid Pavements with $D = 9$ in. and $p_t = 2.5$

Axle load (kips)	Equivalent axle load factor			Axle load (kips)	Equivalent axle load factor		
	Single axles	Tandem axles	Tridem axles		Single axles	Tandem axles	Tridem axles
2	0.0002	0.0001	0.0001	48	56.8	7.73	2.49
4	0.002	0.0005	0.0003	50	67.8	9.07	2.94
6	0.01	0.002	0.001	52		10.6	3.44
8	0.032	0.005	0.002	54		12.3	4.00
10	0.082	0.013	0.005	56		14.2	4.63
12	0.176	0.026	0.009	58		16.3	5.32
14	0.341	0.048	0.017	60		18.7	6.08
16	0.604	0.082	0.028	62		21.4	6.91
18	1.00	0.133	0.044	64		24.4	7.82
20	1.57	0.206	0.067	66		27.6	8.83
22	2.34	0.308	0.099	68		31.3	9.9
24	3.36	0.444	0.141	70		35.3	11.1
26	4.67	0.622	0.195	72		39.8	12.4
28	6.29	0.850	0.265	74		44.7	13.8
30	8.28	1.14	0.354	76		50.1	15.4
32	10.7	1.49	0.463	78		56.1	17.1
34	13.6	1.92	0.596	80		62.5	18.9
36	17.1	2.43	0.757	82		69.6	20.9
38	21.3	3.03	0.948	84		77.3	23.1
40	26.3	3.74	1.17	86		86.0	25.4
42	32.2	4.55	1.44	88		95.0	27.9
44	39.2	5.48	1.74	90		105.0	30.7
46	47.3	6.53	2.09				

Note. 1 kip = 4.45 kN, 1 in. = 25.4 mm.

Source. After AASHTO (1986).

Downloaded From : www.EasyEngineering.net

Downloaded From : www.EasyEngineering.net

$D = 9$ in. (229 mm). If the thickness is not known in the design stage, the value $D = 9$ can be used. A comparison of Tables 6.4 and 6.7 shows that, for single-axle loads less than 18 kip, the equivalent factor is smaller for a rigid pavement than for a flexible pavement, but for heavier loads the reverse is true.

Example 6.10:

A flexible pavement with SN = 5 is subjected to a single-axle load of 12 kip (53.4 kN) and a tandem-axle load of 40 kip (178 kN). Based on a p_t of 2.5, what are the single- and tandem-axle loads on a 9-in. (229-mm) rigid pavement that are equivalent to those on the flexible pavements?

Solution: From Table 6.4 for flexible pavements, the equivalent factor for a single-axle load of 12 kip (53.4 kN) is 0.189 and that for a 40-kip (178-kN) tandem-axle load is 2.08. From an interpolation of Table 6.7, the single-axle load for a rigid pavement with an EALF of 0.189 is 12.2 kip (54.3 kN), which is slightly greater than the 12 kip (53.4 kN) for the flexible pavement. The tandem-axle load for an equivalent factor of 2.08 is 34.7 kip (154 kN), which is much smaller than the 40 kip (178 kN) for the flexible pavement. This may indicate that heavier axle loads are more destructive to rigid pavements than to flexible pavements, probably through the effect of pumping under heavier loads.

Theoretical Analysis For a terminal serviceability index of 2.5, the AASHTO equivalent factors obtained from Eq. 6.25 for a 6-in. (152-mm) slab are 2.29 for 36-kip (160-kN) tandem axles and 3.79 for 54-kip (240-kN) tridem axles, while those for a 14-in. (356-mm) slab are 2.53 and 4.34, respectively. These equivalent factors are quite different from those obtained from KENSLABS, because the AASHTO factors are based on the results of a road test, where the predominant type of failure is by pumping or the erosion of subbase, whereas the damage analysis by KENSLABS is based on fatigue cracking.

Table 6.8 shows the computation of EALF from the cracking index obtained by KENSLABS. Two extreme thicknesses of 6 and 14 in. (152 and 356 mm) and k values

TABLE 6.8 Computation of Equivalent Axle Load Factors Based on KENSLABS

Slab thickness (in.)	6		14	
Subgrade k value (pci)	50	500	50	500
18k Single cracking index	3.085	7.090×10^{-6}	1.741×10^{-12}	4.526×10^{-14}
36k Tandem				
Primary CI	3.478×10^{-2}	6.323×10^{-8}	7.969×10^{-12}	2.192×10^{-14}
Secondary CI	4.054×10^{-7}	6.323×10^{-8}	1.049×10^{-15}	1.733×10^{-15}
Total CI	3.478×10^{-2}	1.265×10^{-7}	7.970×10^{-12}	2.365×10^{-14}
EALF	0.011	0.018	4.58	0.52
54k Tridem				
Primary CI	5.119×10^{-4}	5.249×10^{-9}	2.702×10^{-11}	1.102×10^{-14}
Secondary CI	8.360×10^{-6}	1.050×10^{-8}	9.647×10^{-15}	5.949×10^{-15}
Total CI	5.202×10^{-4}	1.575×10^{-8}	2.703×10^{-11}	1.697×10^{-14}
EALF	0.00017	0.0022	15.5	0.37

Note. 1 in. = 25.4 mm, 1 kip = 4.45 kN, 1 pci = 271.3 kN/m^3.

Downloaded From : www.EasyEngineering.net

Downloaded From : www.EasyEngineering.net

of 50 and 500 pci (13.6 to 136 MN/m^3) are assumed. The 18-kip (80-kN) single axle, 36-kip (160-kN) tandem axles, and 54-kip (240-kN) tridem axles are the same as those used for the analysis of flexible pavements presented in Tables 6.5 and 6.6. The center to center spacing between the left and right dual wheels is 77 in. (1.96 m). The concrete has a modulus of rupture of 600 psi (4.1 MPa), an elastic modulus of 4×10^6 psi (28 GPa), and a Poisson ratio of 0.15. The allowable number of repetitions for fatigue cracking is based on Eq. 5.35 with $f_1 = 16.61$ and $f_2 = 17.61$.

The cracking index shown in Table 6.8 is the same as the damage ratio for fatigue cracking shown in Table 6.5 and is caused by the passage of a single axle or a set of tandem or tridem axles. The primary cracking index is based on the maximum stress, which occurs at the slab edge under either of the tandem axles or the central axle of the tridem. The secondary cracking index is caused by the stress differential due to the passage of one or two additional axles. Dividing the total cracking index of the tandem or tridem axles by the cracking index of a single axle gives the EALF.

It can be seen from Table 6.8 that the values of EALF vary a great deal and are very difficult to predict. For the 6-in. (152-mm) slab, the single axle is more destructive than the tandem axles, and the tandem axles are more destructive than the tridem axles. The same is true for the 14-in. (356-mm) slab with a subgrade k value of 500 pci (136 MN/m^3) because the flexural stress in the concrete is largest under a single axle and smallest under a set of tridem axles. However, for the 14-in. (356-mm) slab with a k value of 50 pci (13.6 MN/m^3), the reverse is true. The large EALF of 4.58 for tandem axles and 15.52 for tridem axles occurs because the maximum stresses are 187.8 psi (1.30 MPa) under tandem axles and 205.9 psi (1.42 MPa) under tridem axles, in contrast to the 165.3 psi (1.14 MPa) under a single axle. This analysis clearly indicates the sensitivity of EALF to the change in slab thickness and subgrade support and the difficulty of establishing an EALF based on empirical methods. The equivalent factor is valid only under the given conditions and is no longer applicable if any of the conditions are changed.

6.4 TRAFFIC ANALYSIS

To design a highway pavement, it is necessary to predict the number of repetitions of each axle load group during the design period. Information on initial traffic can be obtained from field measurements or from the W-4 form of a loadometer station that has traffic characteristics similar to those of the project in question. The initial daily traffic is in two directions over all traffic lanes and must be multiplied by the directional and lane distribution factors to obtain the initial traffic on the design lane. The traffic to be used for design is the average traffic during the design period, so the initial traffic must be multiplied by a growth factor. If n_i is the total number of load repetitions to be used in design for the ith load group, then

$$n_i = (n_0)_i(G)(D)(L)(365)(Y) \tag{6.26}$$

in which $(n_0)_i$ is the initial number of repetitions per day for the ith load group, G is the growth factor, D is the directional distribution factor, which is usually assumed to be 0.5 unless the traffic in two directions is different, L is the lane distribution factor

Downloaded From : www.EasyEngineering.net

Downloaded From : www.EasyEngineering.net

which varies with the volume of traffic and the number of lanes, and Y is the design period in years. If the design is based on the equivalent 18-kip (80-kN) single-axle load, then the initial number of repetitions per day for the ith load group can be computed from

$$(n_0)_i = (p_i F_i)(\text{ADT})_0(T)(A) \tag{6.27}$$

in which p_i is the percentage of total repetitions for the ith load group, F_i is the equivalent axle load factor (EALF) for the ith load group, $(\text{ADT})_0$ is the average daily traffic at the start of the design period, T is the percentage of trucks in the ADT, and A is the average number of axles per truck. Substituting Eq. 6.27 into 6.26 and summing over all load groups, the equivalent axle load for the design lane is

$$\text{ESAL} = \left(\sum_{i=1}^{m} p_i F_i\right)(\text{ADT})_0(T)(A)(G)(D)(L)(365)(Y) \tag{6.28}$$

In computing ESAL, it is convenient to combine the first and fourth terms in Eq. 6.28 to form a new term called the truck factor:

$$T_f = \left(\sum_{i=1}^{m} p_i F_i\right)(A) \tag{6.29}$$

T_f is the number of 18-kip (80-kN) single-axle load applications per truck. Thus, Eq. 6.28 becomes

$$\text{ESAL} = (\text{ADT})_0(T)(T_f)(G)(D)(L)(365)(Y) \tag{6.30}$$

6.4.1 Average Daily Truck Traffic

The minimum traffic information required for a pavement design is the average daily truck traffic (ADTT) at the start of the design period. The ADTT may be expressed as a percentage of ADT or as an actual value. This information can be obtained from the actual traffic counts on the existing roadway where the pavement is to be constructed or on nearby highways with similar travel patterns. Traffic volume maps showing the ADT, sometimes with the percentage of trucks, on various roadways within a given area may also be used, although they are far less accurate than the actual counts. The traffic counts must be adjusted for daily (weekday versus weekend) and seasonal (summer versus winter) variations to obtain the annual average daily traffic (AADT).

Traffic is the most important factor in pavement design. Every effort should be made to collect actual data on the project. This requires a portable device that can be taken to the project site. This device can be a static scale or the newer weigh in motion (WIM) scale. The WIM scale does not interrupt the traffic stream and can enhance the credibility of the data due to its concealment.

If actual traffic data are not available, Table 6.9 can be used as a guide to determine the distribution of ADTT on different classes of highways in the United States.

Downloaded From : www.EasyEngineering.net

TABLE 6.9 Distribution of Trucks on Different Classes of Highways in the United States[a]

Truck class	Percent trucks											
	Rural systems						Urban systems					
				Collectors								
	Interstate	Other Principal	Minor Arterial	Major	Minor	Range	Interstate	Other Freeways	Other Principal	Minor Arterial	Collectors	Range
Single-unit trucks												
2-axle, 4 tire	43	60	71	73	80	43–80	52	66	67	84	86	52–86
2-axle, 6-tire	8	10	11	10	10	8–11	12	12	15	9	11	9–15
3-axle or more	2	3	4	4	2	2–4	2	4	3	2	<1	<1–4
All single units	53	73	86	87	92	53–92	66	82	85	95	97	66–97
Multiple-unit trucks												
4-axle or less	5	3	3	2	2	2–5	5	5	3	2	1	1–5
5-axle[b]	41	23	11	10	6	6–41	28	13	12	3	2	2–28
6-axle or more[b]	1	1	<1	1	<1	<1–1	1	<1	<1	<1	<1	<1–1
All multiple units	47	27	14	13	8	8–47	34	18	15	5	3	3–34
All trucks	100	100	100	100	100		100	100	100	100	100	

[a] Compiled from data supplied by the Highway Statistics Division, U.S. Federal Highway Administration.
[b] Including full-trailer combinations in some states.
Source. After AI (1991).

Downloaded From : www.EasyEngineering.net
Downloaded From : www.EasyEngineering.net

Downloaded From : www.EasyEngineering.net

6.4.2 Truck Factor

A single truck factor can be applied to all trucks, or separate truck factors can be used for different classes of trucks. The latter case should be considered if the growth factors for different types of trucks are not the same. Table 6.10 shows the distribution of truck factors for different classes of highways and vehicles in the United States. Table 6.11 shows the computation of truck factors for trucks with five or more axles on a flexible pavement. The equivalent factors are based on an SN of 5 and a p_t of 2.5 and can be obtained from Table 6.4. The number of axles for each load group, plus the number of trucks weighed, can be found from the W-4 form. The sum of ESALs for all trucks weighed divided by the number of trucks weighed gives the truck factor.

6.4.3 Growth Factor

One simple way to project the growth factor is to assume a yearly rate of traffic growth and use the average traffic at the start and end of the design period as the design traffic:

$$G = \tfrac{1}{2}[1 + (1 + r)^Y] \tag{6.31}$$

The Portland Cement Association (1984) applies the traffic at the middle of the design period as the design traffic:

$$G = (1 + r)^{0.5Y} \tag{6.32}$$

Table 6.12 shows the growth factors for 20- and 40-year design periods based on Eq. 6.32.

The Asphalt Institute (AI, 1981a) and the AASHTO design guide (AASHTO, 1986) recommend the use of traffic over the entire design period to determine the total growth factor, as indicated by

$$\text{Total growth factor} = (G)(Y) = \frac{(1 + r)^Y - 1}{r} \tag{6.33}$$

Table 6.13 shows the total growth factor, which is the growth factor multiplied by the design period, as recommended by the Asphalt Institute. The same factor is used in the AASHTO design guide. If the growth rate is not uniform, different growth rates should be used for different load groups or types of vehicles.

To determine the annual growth rate, the following factors should be considered:

1. Attracted or diverted traffic due to the improvement of existing pavement
2. Normal traffic growth due to the increased number and usage of motor vehicles
3. Generated traffic due to motor vehicle trips that would not have been made if the new facility had not been constructed
4. Development traffic due to changes in land use as a result of the new facility

Downloaded From : www.EasyEngineering.net

TABLE 6.10 Distribution of Truck Factors for Different Classes of Highways and Vehicles in the United States[a]

	Truck factors											
	Rural systems						Urban systems					
				Collectors								
Vehicle type	Interstate	Other Principal	Minor Arterial	Major	Minor	Range	Interstate	Other Freeways	Other Principal	Minor Arterial	Collectors	Range
Single-unit trucks												
2-axle, 4-tire	0.003	0.003	0.003	0.017	0.003	0.003–0.017	0.002	0.015	0.002	0.006	—	0.006–0.015
2-axle, 6-tire	0.21	0.25	0.28	0.41	0.19	0.19–0.41	0.17	0.13	0.24	0.23	0.13	0.13–0.24
3-axle or more	0.61	0.86	1.06	1.26	0.45	0.45–1.26	0.61	0.74	1.02	0.76	0.72	0.61–1.02
All single units	0.06	0.08	0.08	0.12	0.03	0.03–0.12	0.05	0.06	0.09	0.04	0.16	0.04–0.16
Tractor semitrailers												
4-axle or less	0.62	0.92	0.62	0.37	0.91	0.37–0.91	0.98	0.48	0.71	0.46	0.40	0.40–0.98
5-axle[b]	1.09	1.25	1.05	1.67	1.11	1.05–1.67	1.07	1.17	0.97	0.77	0.63	0.63–1.17
6-axle or more[b]	1.23	1.54	1.04	2.21	1.35	1.04–2.21	1.05	1.19	0.90	0.64	—	0.64–1.19
All multiple units	1.04	1.21	0.97	1.52	1.08	0.97–1.52	1.05	0.96	0.91	0.67	0.53	0.53–1.05
All trucks	0.52	0.38	0.21	0.30	0.12	0.12–0.52	0.39	0.23	0.21	0.07	0.24	0.07–0.39

a Compiled from data supplied by the Highway Statistics Division, U.S. Federal Highway Administration.
b Including full-trailer combinations in some states.
Source. After AI (1991).

Downloaded From : www.EasyEngineering.net
Downloaded From : www.EasyEngineering.net

Downloaded From : www.EasyEngineering.net

TABLE 6.11 Computation of Truck Factor for Trucks with Five or More Axles

Axle load (lb)	EALF	Number of axles	ESAL
Single Axles			
Under 3000	0.0002	0	0.000
3000–6999	0.0050	1	0.005
7000–7999	0.0320	6	0.192
8000–11,999	0.0870	144	12.528
12,000–15,999	0.3600	16	5.760
16,000–29,999	5.3890	1	5.389
Tandem Axles			
Under 6000	0.0100	0	0.000
6000–11,999	0.0100	14	0.140
12,000–17,999	0.0440	21	0.924
18,000–23,999	0.1480	44	6.512
24,000–29,999	0.4260	42	17.892
30,000–32,000	0.7530	44	33.132
32,001–32,500	0.8850	21	18.585
32,501–33,999	1.0020	101	101.202
34,000–35,999	1.2300	43	52.890
ESALs for all trucks weighed			255.151

$$\text{Truck factor} = \frac{\text{18-kip ESALs for all trucks weighed}}{\text{Number of trucks weighed}} = \frac{255.151}{165} = 1.5464$$

Note. 1 lb = 4.45 N.

TABLE 6.12 Traffic Growth Factors

Annual growth rate (%)	20-Year design period	40-Year design period
1.0	1.1	1.2
1.5	1.2	1.3
2.0	1.2	1.5
2.5	1.3	1.6
3.0	1.3	1.8
3.5	1.4	2.0
4.0	1.5	2.2
4.5	1.6	2.4
5.0	1.6	2.7
5.5	1.7	2.9
6.0	1.8	3.2

Source. After PCA (1984).

Downloaded From : www.EasyEngineering.net

Downloaded From : www.EasyEngineering.net

TABLE 6.13 Total Growth Factor

Design period (years)	Annual growth rate (%)							
	No growth	2	4	5	6	7	8	10
1	1.0	1.0	1.0	1.0	1.0	1.0	1.0	1.0
2	2.0	2.02	2.04	2.05	2.06	2.07	2.08	2.10
3	3.0	3.06	3.12	3.15	3.18	3.21	3.25	3.31
4	4.0	4.12	4.25	4.31	4.37	4.44	4.51	4.64
5	5.0	5.20	5.42	5.53	5.64	5.75	5.87	6.11
6	6.0	6.31	6.63	6.80	6.98	7.15	7.34	7.72
7	7.0	7.43	7.90	8.14	8.39	8.65	8.92	9.49
8	8.0	8.58	9.21	9.55	9.90	10.26	10.64	11.44
9	9.0	9.75	10.58	11.03	11.49	11.98	12.49	13.58
10	10.0	10.95	12.01	12.58	13.18	13.82	14.49	15.94
11	11.0	12.17	13.49	14.21	14.97	15.78	16.65	18.53
12	12.0	13.41	15.03	15.92	16.87	17.89	18.98	21.38
13	13.0	14.68	16.63	17.71	18.88	20.14	21.50	24.52
14	14.0	15.97	18.29	19.16	21.01	22.55	24.21	27.97
15	15.0	17.29	20.02	21.58	23.28	25.13	27.15	31.77
16	16.0	18.64	21.82	23.66	25.67	27.89	30.32	35.95
17	17.0	20.01	23.70	25.84	28.21	30.84	33.75	40.55
18	18.0	21.41	25.65	28.13	30.91	34.00	37.45	45.60
19	19.0	22.84	27.67	30.54	33.76	37.38	41.45	51.16
20	20.0	24.30	29.78	33.06	36.79	41.00	45.76	57.28
25	25.0	32.03	41.65	47.73	54.86	63.25	73.11	98.35
30	30.0	40.57	56.08	66.44	79.06	94.46	113.28	164.49
35	35.0	49.99	73.65	90.32	111.43	138.24	172.32	271.02

Source. After AI (1981a).

Example 6.11:

For an annual growth rate of 3.5% and a design period of 30 years, compute the growth factors by Eqs. 6.31, 6.32, and 6.33.

Solution: From Eq. 6.31, $G = 0.5[1 + (1 + 0.035)^{30}] = 1.90$; from Eq. 6.32, $G = (1 + 0.035)^{0.5\times30} = 1.68$; and from Eq. 6.33, $G = [(1 + 0.035)^{30} - 1]/(0.035 \times 30) = 1.72$. It can be seen that the use of Eq. 6.31 by averaging the traffic at the start and the end of a design period is most conservative and results in the greatest growth factor, while the growth factor based on Eq. 6.33 is only slightly greater than that based on Eq. 6.32.

6.4.4 Lane Distribution Factor

For two-lane highways, the lane in each direction is the design lane, so the lane distribution factor is 100%. For multilane highways, the design lane is the outside lane. Table 6.14 shows the truck distribution on a multiple-lane highway based on 129 counts from 1982 to 1983 in six states (Darter et al., 1985). For four-lane highways with two lanes in each direction, the lane distribution factors range from 66 to 94%. For multiple-lane highways with three or more lanes in each direction, the lane distribution factors range from 49 to 82%.

Downloaded From : www.EasyEngineering.net

Downloaded From : www.EasyEngineering.net

TABLE 6.14 Truck Distribution for Multiple-Lane Highways

One-way ADT	Two lanes in each direction		Three or more lanes in each direction		
	Inner	Outer	Inner[a]	Center	Outer
2000	6	94	6	12	82
4000	12	88	6	18	76
6000	15	85	7	21	72
8000	18	82	7	23	70
10,000	19	81	7	25	68
15,000	23	77	7	28	65
20,000	25	75	7	30	63
25,000	27	73	7	32	61
30,000	28	72	8	33	59
35,000	30	70	8	34	58
40,000	31	69	8	35	57
50,000	33	67	8	37	55
60,000	34	66	8	39	53
70,000	—	—	8	40	52
80,000	—	—	8	41	51
100,000	—	—	9	42	49

[a] Combined inner one or more lanes.
Source. After Darter et al. (1985).

Based on the data in Table 6.14, the Portland Cement Association (PCA, 1984) developed a chart for determining the proportion of trucks in the design lane, as shown in Figure 6.8. The Asphalt Institute (AI, 1981a) combines the directional and lane distribution factors ($D \times L$) and determines the percentage of total truck traffic in the

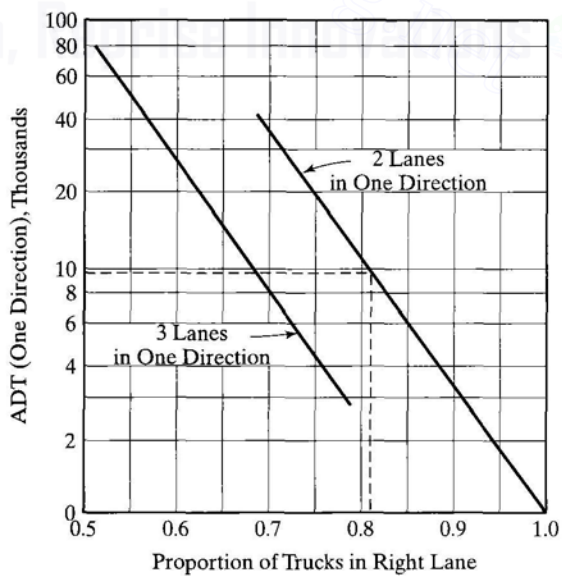


FIGURE 6.8
Proportion of trucks in design lane of multiple-lane highways. (After PCA (1984).)

Downloaded From : www.EasyEngineering.net

Downloaded From : www.EasyEngineering.net

TABLE 6.15 Percentage of Total Truck Traffic in Design Lane

Number of traffic lanes in two directions	Percentage of trucks in design lane
2	50
4	45 (35–48)[a]
6 or more	40 (25–48)[a]

[a] Probable range.
Source. After AI (1981a).

TABLE 6.16 Lane Distribution Factor

No. of lanes in each direction	Percentage of 18-kip ESAL in design lane
1	100
2	80–100
3	60–80
4	50–75

Source. After AASHTO (1986).

design lane by Table 6.15. A comparison of Table 6.15 and Figure 6.8 indicates that the lane distribution factors by the Asphalt Institute are about the same as those by PCA for an ADT of 3000 in one direction. The lane distribution factors recommended by the AASHTO design guide are shown in Table 6.16. Note that the percentage in Table 6.15 is based on total traffic, but the percentage in Table 6.16 is based on the traffic in one direction.

Example 6.12:

A two-lane major rural highway has an AADT of 4000 during the first year of traffic, 25% trucks, 4% annual growth rate, and 50% on the design lane. If the distribution of trucks is the same as shown in Table 6.9 and the distribution of truck factors is as shown in Table 6.10, compute the ESAL for a design period of 20 years.

Solution: For a growth rate of 4% and a design period of 20 years, from Table 6.13, or Eq. 6.33, $(G)(Y) = 29.78$. The truck factor for all trucks, as shown in Table 6.10, is the weighted average of the distribution of trucks shown in Table 6.9. If the distribution of trucks is given in Table 6.9, it is not necessary to break down the trucks into different classes; the use of $T_f = 0.38$ for all trucks in the "other principal" column of the rural systems, as shown in Table 6.10, is sufficient. From Eq. 6.30, ESAL $= 4000 \times 0.25 \times 0.38 \times 29.78 \times 0.5 \times 365 = 2{,}065{,}200$.

6.4.5 Other Design Considerations

In considering the number of load repetitions for pavement design, two important questions must be answered. The first question is whether the passage of a set of tandem or

Downloaded From : www.EasyEngineering.net

Downloaded From : www.EasyEngineering.net

tridem axles should be counted as one or more than one repetition. The second question is whether the effect of traffic wandering or lateral load placement should be considered in the design of highway pavements.

On the first question, if the design is based on the equivalent 18-kip (80-kN) single-axle load, the passage of a set of tandem or tridem axles should be counted as one repetition because the equivalent factor is based on one passage of the tandem- or tridem-axle loads. If the design is based on different load groups and the stresses or strains under single-, tandem-, or tridem-axle loads are used for damage analysis, the damage caused by the passage of a set of tandem or tridem axles should be analyzed by the method shown in Figure 3.3 or 3.4. The data presented in Tables 6.5 and 6.6 for flexible pavements and in Table 6.8 for rigid pavement can be used to determine the number of repetitions required. The number of repetitions can be computed from these tables by dividing the total damage ratio (or cracking index) by the primary damage ratio and the results are presented in Table 6.17.

As can be seen from Table 6.17, the required number of repetitions may range from 1 to 2 for tandem axles and from 1 to 3 for tridem axles, depending on the combined effect of pavement thickness and subgrade support. For flexible pavements, the passage of a set of tandem or tridem axles may be considered as one repetition for thicker pavements on a weak subgrade, but as two or three repetitions for thin pavements, regardless of the subgrade support. For rigid pavements with poor subgrade support, the passage of a set of tandem or tridem axles may be considered as one repetition, but the number of repetitions is increased as the subgrade support improved. However, it should be pointed out that these general trends are based on the input data assumed. The interactions among all the design variables are so complex that the best way is to analyze the damage directly by KENLAYER or KENSLABS, instead of applying a fixed number to tandem or tridem axles.

TABLE 6.17 Number of Repetitions for One Passage of Multiple Axles

Flexible Pavements				
HMA thickness (in.)	2		12	
Subgrade modulus (pci)	5000	30,000	5000	30,000
Tandem				
Fatigue cracking	1.89	1.99	1.01	1.08
Permanent deformation	2.00	2.00	1.02	1.28
Tridem				
Fatigue cracking	2.77	2.98	1.03	1.08
Permanent deformation	3.00	3.00	1.05	1.55

Rigid Pavements				
Slab thickness (in.)	6		14	
Subgrade k value (pci)	50	500	50	500
Tandem	1.00	2.00	1.00	1.08
Tridem	1.02	3.00	1.00	1.54

Note. 1 in. = 25.4 mm, 1 psi = 6.9 kPa, 1 pci = 271.3 kN/m^3.

Downloaded From : www.EasyEngineering.net

Downloaded From : www.EasyEngineering.net

As to the second question, traffic wandering certainly has a great effect on pavement damage. However, instead of reducing the number of load repetitions, the effect is incorporated in the failure criteria. For example, the damage coefficients for flexible pavement, such as f_1 in Eq. 3.6 and f_4 in Eq. 3.7, should include the wandering effect of traffic. In the PCA method of rigid pavement design, the wandering effect is considered in the fatigue analysis by reducing the edge stress and in the erosion analysis by increasing the allowable number of load repetitions, as described in Section 12.2.

SUMMARY

This chapter presents the load equivalent concept and the methods for traffic analysis.

Important Points Discussed in Chapter 6

1. The concept of load equivalency has been used most frequently in the empirical methods of pavement design. In the mechanistic methods, it is not necessary to apply the load equivalency concept because different loads can be considered separately in the design process. This is why the concept has been used more frequently on flexible pavements than on rigid pavements.
2. There are two types of load equivalency, one called the equivalent single-wheel load (ESWL) and the other called the equivalent axle load factor (EALF). The ESWL is based on the fixed traffic procedure of converting the most critical wheel loads, usually in multiple wheels, into an equivalent single-wheel load and using it for design purposes. The EALF is based on the fixed vehicle procedure of converting the number of repetitions of a given axle load, either single, tandem, or tridem, into an equivalent number of repetitions of an 18-kip (80-kN) single-axle load.
3. Various criteria have been used for determining the ESWL for a two-layer system, e.g., equal vertical interface stress, equal interface deflection, and equal tensile strain. The equivalency based on one criterion may be quite different from that based on other criteria. Also, the equivalency based on equal contact radius is different from that based on equal contact pressure.
4. The values of EALF depend on the failure criterion employed. The EALF based on fatigue cracking is different from that based on permanent deformation. The use of a single value for both modes of failure is approximate at best. The most widely used method for determining the EALF is that which uses the empirical equations developed from the AASHO Road Test. However, damage analyses by KENLAYER and KENSLABS indicate that the values of EALF vary a great deal and are difficult to predict. The complex interactions among a large number of variables make it impossible to select an appropriate EALF that can be applied to all situations. For a truly mechanistic design method, each load group should be considered individually, instead of via equivalent single-axle loads.
5. The traffic to be used in design is not the average traffic during the first year, but the average during the design period. Three different methods based on the compound rate are presented to compute the traffic growth factor. The use of average traffic at the start and the end of the design period gives the highest growth factor, while the use of the traffic at the middle of the design period results in the lowest growth factor.
6. Traffic is the most important factor in pavement design. Every effort should be made to collect actual traffic data. If actual data are not available, Tables 6.9 and

Downloaded From : www.EasyEngineering.net

Downloaded From : www.EasyEngineering.net

6.10, which give average values for different classes of highways in the United States, can be used as a guide.

7. In addition to the initial traffic and the growth factor, the directional and lane distribution factors must also be considered. Unless the traffic loading or volume is heavier in one direction than in the other due to some special reason, a directional distribution of 0.5 is assumed. The lane distribution factor varies with the number of lanes and the ADT and can be obtained from Figure 6.8 or Tables 6.15 and 6.16, although these tables do not consider ADT as a factor.
8. When the design is based on the equivalent 18-kip (80-kN) single-axle load, the use of a truck factor is very convenient. The method for computing truck factors based on the number of axles and trucks weighed, number of trucks counted, and the AASHTO equivalent factors is illustrated.
9. Damage analyses by KENLAYER and KENSLABS indicate that the passage of a set of tandem or tridem axles may be considered as one repetition in some cases, but as more than one repetition in other cases, depending on pavement thickness and subgrade support. The problem is so complex that it is best to analyze each load group, either tandem or tridem, directly, instead of applying a fixed number of repetitions.

PROBLEMS

6.1 A set of dual tires is spaced at 34 in. center to center and carries a total load of 45,000 lb with a tire pressure of 100 psi. Assuming the pavement to be a homogeneous half-space, determine the ESWL for a pavement of 25 in. using (a) the Boyd and Foster method, (b) the Foster and Ahlvin method, and (c) Huang's chart based on equal contact radius. [Answer: 32,200 lb, 32,800 lb, 32,800 lb]

6.2 A full-depth asphalt pavement is loaded by a set of dual wheels, each weighing 8000 lb and spaced at 20 in. on centers. The hot mix asphalt has a thickness of 10 in. and an elastic modulus of 250,000 psi; the subgrade has an elastic modulus of 10,000 psi. Both layers are incompressible with a Poisson ratio of 0.5. If the dual wheels and the equivalent single wheel have the same contact radius of 6 in., determine the ESWL based on (a) equal interface deflection and (b) equal tensile strain at the bottom of asphalt layer. [Answer: 13,800 lb, 10,900 lb]

6.3 A pavement is subjected to the single-axle loads shown in Table P6.3. Determine the ESAL for a design period of 20 years using (a) AI's equivalent axle load factors and (b) the equivalent axle load factors from Eq. 6.23. [Answer: 2.99×10^6, 3.07×10^6]

TABLE P6.3

Axle load (kip)	Number per day	Axle load (kip)	Number per day	Axle load (kip)	Number per day
12	200.0	20	47.2	28	2.9
14	117.4	22	21.4	30	1.2
16	84.5	24	12.9	32	0.7
18	61.4	26	6.1	34	0.3

Downloaded From : www.EasyEngineering.net

Downloaded From : www.EasyEngineering.net

6.4 Based on Eq. 6.25, discuss the effect of p_t on EALF.

6.5 Derive Eq. 6.33 and indicate the assumptions on which the equation is obtained. [*Hint*: $(G)(Y) = \int_0^Y (1 + r)^n$]

6.6 Estimate the equivalent 18-kip single-axle load applications (ESAL) for a four-lane pavement (two lanes in each direction) of a rural interstate highway with a truck count of 1000 per day (including 2-axle, 4-tire panel, and pickup trucks), an annual growth rate of 5%, and a design life of 20 years. [Answer: 2.82×10^6]

6.7 Table P6.7 is abstracted from a W-4 table on tractor semitrailer combinations for a loadometer station from July 16 to August 8. It is assumed that the traffic during the recorded period represents the average over the entire year. If the pavement to be constructed has

TABLE P6.7

Axle loads (lb)	3-axle	4-axle	5-axle	Tractor semitrailer combinations probable no.
Single axle under 3000	—	—	—	—
3000–6999	256	227	60	3188
7000–7999	148	243	85	2843
8000–11,999	345	939	363	9942
12,000–15,999	174	288	54	3111
16,000–17,999	67	225	12	1899
18,000–19,000	22	141	7	1078
19,001–19,999	8	54	5	423
20,000–21,999	5	80	9	598
22,000–23,999	1	29		144
24,000–25,999	—	1	—	6
26,000–29,999	—	1	—	6
Total single axles weighed	1026	2228	595	
Total single axles counted	5541	14,526	3171	23,238
Tandem axle under 6000	—	1	—	7
6000–11,999	—	237	173	2631
12,000–17,999	—	189	209	2541
18,000–23,999	—	218	150	2362
24,000–29,999	—	270	214	3103
30,000–31,500	—	62	52	703
31,501–31,999	—	11	11	141
32,000–33,999	—	36	43	503
34,000–35,999	—	26	35	388
36,000–37,999	—	16	28	280
38,000–39,999	—	12	27	247
40,000–41,999	—	10	19	183
42,000–43,999	—	14	11	160
44,000–45,999	—	2	6	51
46,000–49,999	—	5	5	64
50,000–53,999	—	1	—	7
Total tandem axles weighed		1110	983	—
Total tandem axles counted		7263	6135	13,398
Total vehicles counted	1847	7263	3087	12,197

Downloaded From : www.EasyEngineering.net

Downloaded From : www.EasyEngineering.net

a structural number SN of 5, estimate the ESAL of the tractor semitrailer combinations during the first year in two directions over all lanes based on a p_t of 2.5. [Answer: 192,000]

6.8 Same as Problem 6-7 but for a rigid pavement with a concrete thickness of 9 in. [Answer: 257,000]

6.9 Based on the axles weighed and the axles and vehicles counted, as shown in Table P6.7, determine the truck factor of all tractor semitrailer combinations for a flexible pavement with SN = 5 and p_t = 2.5. [Answer: 1.04]

6.10 Same as Problem 6-9 but for a rigid pavement with D = 9. [Answer: 1.38]

Downloaded From : www.EasyEngineering.net

Downloaded From : www.EasyEngineering.net

CHAPTER 7

Material Characterization

7.1 RESILIENT MODULUS

The resilient modulus is the elastic modulus to be used with the elastic theory. It is well known that most paving materials are not elastic, but experience some permanent deformation after each load application. However, if the load is small compared to the strength of the material and is repeated for a large number of times, the deformation under each load repetition is nearly completely recoverable (and proportional to the load) and can be considered elastic.

Figure 7.1 shows the straining of a specimen under a repeated load test. At the initial stage of load applications, there is considerable permanent deformation, as indicated by the plastic strain in the figure. As the number of repetitions increases, the plastic strain due to each load repetition decreases. After 100 to 200 repetitions, the strain is practically all recoverable, as indicated by ϵ_r in the figure.

The elastic modulus based on the recoverable strain under repeated loads is called the resilient modulus M_R, defined as

$$M_R = \frac{\sigma_d}{\epsilon_r} \tag{7.1}$$

in which σ_d is the deviator stress, which is the axial stress in an unconfined compression test or the axial stress in excess of the confining pressure in a triaxial compression test. Because the applied load is usually small, the resilient modulus test is a nondestructive test, and the same sample can be used for many tests under different loading and environmental conditions.

7.1.1 Loading Waveform

The type and duration of loading used in the repeated load test should simulate that actually occurring in the field. When a wheel load is at a considerable distance from a given point in the pavement, the stress at that point is zero. When the load is directly above the given point, the stress at the point is maximum. It is therefore

Downloaded From : www.EasyEngineering.net

Downloaded From : www.EasyEngineering.net

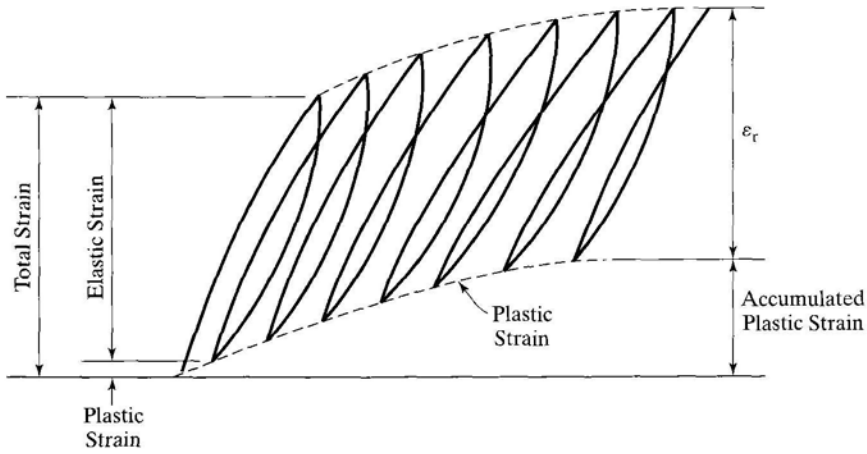


FIGURE 7.1
Strains under repeated loads.

reasonable to assume the stress pulse to be a haversine or triangular loading, the duration of which depends on the vehicle speed and the depth of the point below the pavement surface.

Barksdale (1971) investigated the vertical stress pulses at different points in flexible pavements. The stress pulse can be approximated by a haversine or a triangular function, as shown in Figure 7.2. After considering the inertial and viscous effects based on the vertical stress pulses measured in the AASHO Road Test, the stress pulse time can be related to the vehicle speed and depth, as shown in Figure 7.3. Because of these effects, the loading time is not inversely proportional to the vehicle speed.

Brown (1973) derived the loading time for a bituminous layer as a function of vehicle speed and layer thickness. The loading time is based on the average pulse time for stresses in the vertical and horizontal directions at various depths in the bituminous layer. For thicker layers, his loading times are slightly smaller than those obtained by Barksdale.

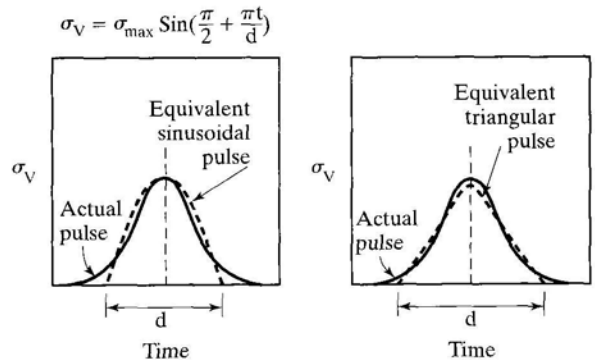


FIGURE 7.2
Equivalent haversine and triangular pulse.

Downloaded From : www.EasyEngineering.net

Downloaded From : www.EasyEngineering.net

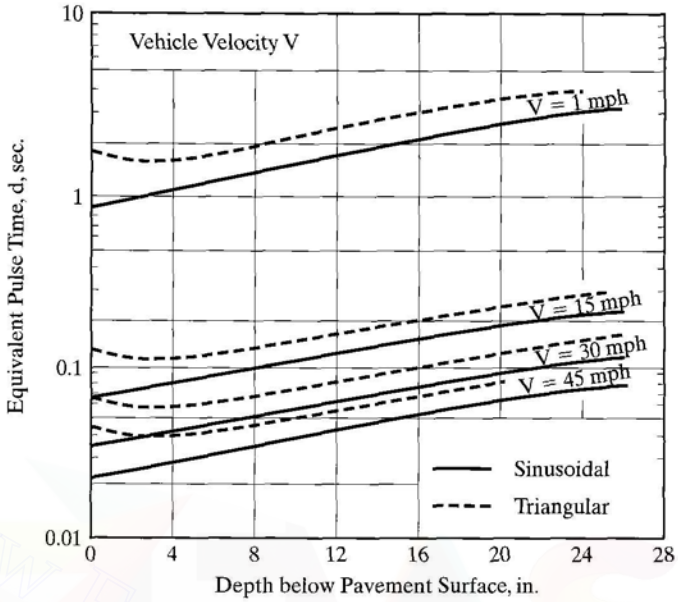


FIGURE 7.3

Vertical stress pulse time under haversine or triangular loading (1 in. = 25.4 mm. 1 mph = 1.6 km/h). (After Barksdale (1971).)

McLean (1974) determined the loading time for an equivalent square wave vertical pulse, as shown in Figure 7.4, on which the Barksdale's results for 30 mph (48 km/h) triangular loading are superimposed for comparison. It can be seen that the pulse time based on the square wave is shorter than that based on the triangular wave, which is as expected.

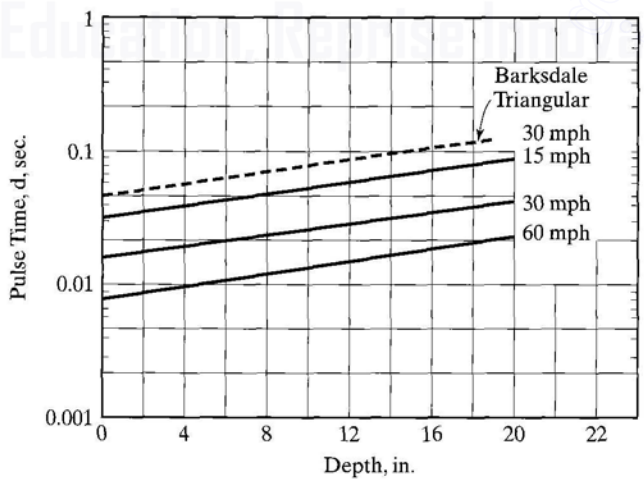


FIGURE 7.4

Vertical stress pulse time under square wave form (1 in. = 25.4 mm, 1 mph = 1.6 km/h). (After McLean (1974).)

Downloaded From : www.EasyEngineering.net

Downloaded From : www.EasyEngineering.net

Example 7.1:

Repeated load compression tests are employed to determine the resilient moduli of the surface, base, and subbase materials in a flexible pavement, as shown in Figure 7.5. The points at the midheight of each layer are used to determine the stress pulse times. If the vehicle speed is 40 mph (64 km/h), what should be the load durations of haversine and square wave loadings for each material?

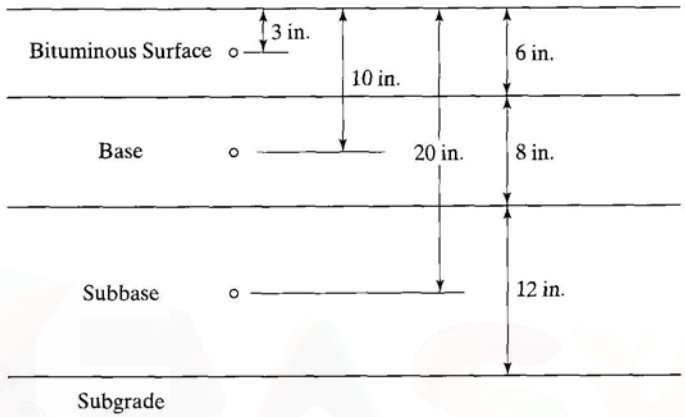


FIGURE 7.5
Example 7.1 (1 in. = 25.4 mm).

Solution: With a depth of 3 in. (76 mm) below the surface and a vehicle speed of 40 mph (64 km/h), the vertical stress pulse time is 0.028 s for a haversine load, as obtained from Figure 7.3, and 0.014 s for a square wave, as obtained from Figure 7.4. The results for all three materials are shown in Table 7.1.

It can be seen that the stress pulse time based on McLean's square wave loading is about one-half of that based on Barksdale's haversine loading. Note that a haversine pulse time of 0.028 to 0.064 s for a vehicle speed of 40 mph (64 km/h) is much smaller than the 0.1 s based on Eq. 2.55. The haversine pulse times indicated in Table 7.1 are based on $\sin(\pi/2 + \pi t/d)$, as shown in Figure 7.2; Eq. 2.55 is based on $\sin^2(\pi/2 + \pi t/d)$, as shown in Figure 2.40. The use of $\sin^2(\pi/2 + \pi t/d)$ in KENLAYER results in a reverse curve with a longer pulse time, which checks more closely with the actual stress pulse in pavements.

When the elastic theory is employed to analyze pavements, the duration of loading for determining the resilient modulus under repeated loading can be selected by using Figure 7.3 or 7.4 as a guide, depending on whether the loading is haversine or

TABLE 7.1 Vertical Stress Pulse Times for Materials at Various Depths

Material	Bituminous surface	Base course	Subbase course
Depth (in.)	3	10	20
Haversine wave	0.028 s	0.041 s	0.064 s
Square wave	0.014 s	0.020 s	0.031 s

Note. 1 in. = 25.4 mm.

Downloaded From : www.EasyEngineering.net

Downloaded From : www.EasyEngineering.net

square wave. In view of the fact that the vehicle speed varies a great deal and the depth of the material may not be known during the design stage, it is recommended that a haversine load of duration 0.1 s and rest period 0.9 s be used. It should be noted that load duration has very little effect on the resilient modulus of granular materials, some effect on fine-grained soils depending on moisture contents, and a considerable effect on bituminous materials. The effect of rest period is not known, but is probably insignificant.

7.1.2 Equipment

The resilient modulus of granular materials and fine-grained soils can be determined by the repeated load triaxial test. Figure 7.6 shows the test setup recommended by FHWA (1978). The sample is 4 in. (102 mm) in diameter and 8 in. (203 mm) in height. The triaxial cell is similar to most standard cells, except that it is larger to accommodate the internally mounted load and deformation measuring equipment and has additional outlets for the electrical leads from the measuring devices. With the internally mounted measuring devices, air, instead of water, should be used as the confining fluid. Other cells with suitable externally mounted load and deformation measuring equipment also may be used. However, the use of internal measuring equipment has the advantage that the effects of equipment deformation, end restraint, and piston friction can be eliminated.

The repetitive loading device can be an air-actuated piston assembly with electronic solenoid control or a sophisticated electrohydraulic testing machine with precise control on the shape of load pulse. The deformation measuring equipment consists of two linear variable differential transformers (LVDT) attached to the specimen by a pair of clamps at the upper and lower quarter points. In addition to the measuring devices, suitable signal excitation, conditioning, and recording equipment are needed.

The setup shown in Figure 7.6 can be used to determine the resilient modulus of asphalt mixtures. Unless the temperature or the level of stress is high, the confining pressure has very little effect on the resilient modulus, so the repeated load unconfined compression test without confining pressure, rubber membrane, and porous stones can be used. A temperature control system should be used to maintain a constant temperature in the specimen during the test.

The resilient modulus of asphalt mixtures can also be determined by the repeated load indirect tension test. A compressive load with a haversine or other suitable waveform is applied in the vertical diametric plane of a cylindrical specimen through a loading strip, and the resulting horizontal recoverable deformation is measured. The repetitive loading device is the same as that used in the compression test. The transducer arrangement to measure the resilient modulus is shown in Figure 7.7. The resilient modulus is computed from

$$M_R = \frac{P(\nu + 0.2734)}{\delta t} \tag{7.2}$$

in which P is the magnitude of the dynamic load in pounds, ν is Poisson ratio, δ is the total recoverable deformation in inches, and t is the specimen thickness in inches. The Poisson ratio is generally taken to be 0.35.

Downloaded From : www.EasyEngineering.net

Downloaded From : www.EasyEngineering.net

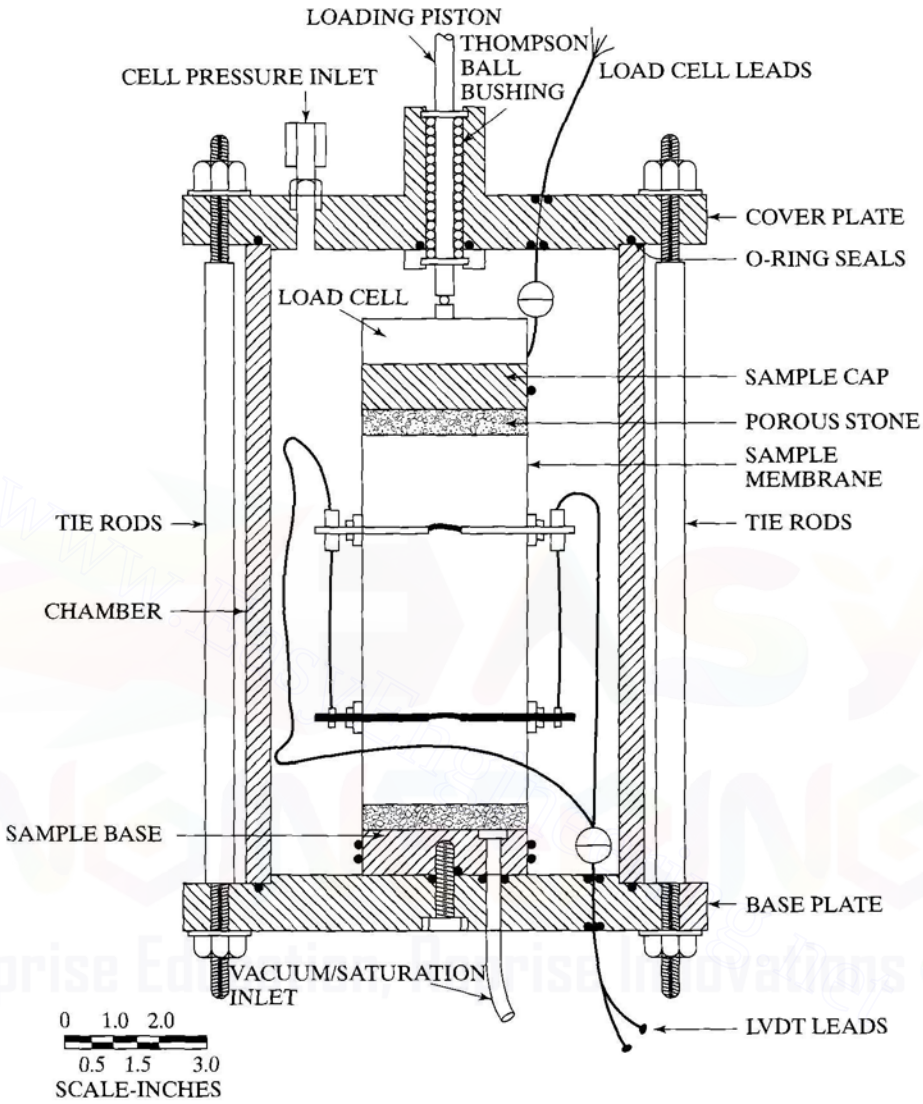


FIGURE 7.6

Triaxial cell for testing cylindrical specimens. (After FHWA (1978).)

7.1.3 Granular Materials

The resilient modulus test for granular materials and fine-grained soils is specified by AASHTO (1989) in "T274-82 Resilient Modulus of Subgrade Soils." Sample conditioning can be accomplished by applying various combinations of confining pressures and deviator stresses, as follows:

1. Set the confining pressure to 5 psi (35 kPa), and apply a deviator stress of 5 psi (35 kPa) and then 10 psi (69 kPa), each for 200 repetitions.

Downloaded From : www.EasyEngineering.net

Downloaded From : www.EasyEngineering.net

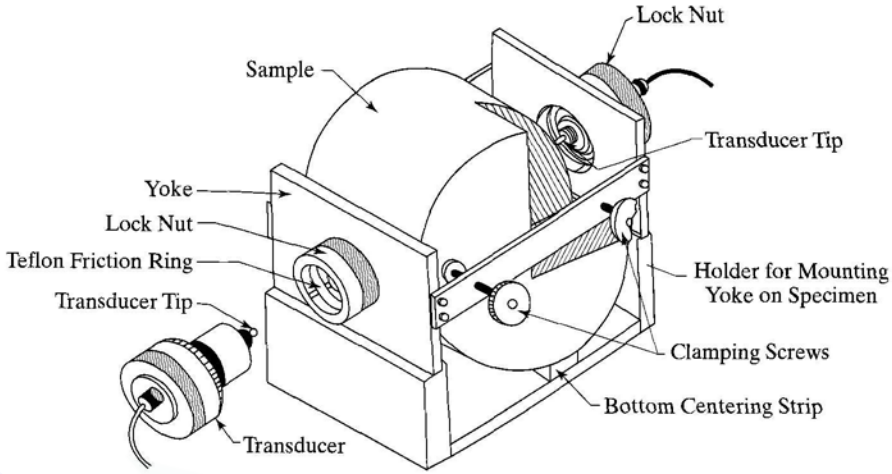


FIGURE 7.7

Transducer arrangement for indirect tensile test.

2. Set the confining pressure to 10 psi (69 kPa), and apply a deviator stress of 10 psi (69 kPa) and then 15 psi (104 kPa), each for 200 repetitions.
3. Set the confining pressure to 15 psi (104 kPa), and apply a deviator stress of 15 psi (104 kPa) and then 20 psi (138 kPa), each for 200 repetitions.

After sample conditioning, the following constant confining pressure–increasing deviator stress sequence is applied, and the results are recorded at the 200th repetition of each deviator stress:

1. Set the confining pressure to 20 psi (138 kPa), and apply deviator stresses of 1, 2, 5, 10, 15, and 20 psi (6.9, 14, 35, 69, 104, and 138 kPa).
2. Reduce the confining pressure to 15 psi (104 kPa), and apply deviator stresses of 1, 2, 5, 10, 15, and 20 psi (6.9, 14, 35, 69, 104, and 138 kPa).
3. Reduce the confining pressure to 10 psi (69 kPa), and apply deviator stresses of 1, 2, 5, 10, and 15 psi (6.9, 14, 35, 69, and 104 kPa).
4. Reduce the confining pressure to 5 psi (35 kPa), and apply deviator stresses of 1, 2, 5, 10, and 15 psi (6.9, 14, 35, 69, and 104 kPa).
5. Reduce the confining pressure to 1 psi (6.9 kPa), and apply deviator stresses of 1, 2, 5, 7.5, and 10 psi (6.9, 14, 35, 52, and 69 kPa). Stop the test after 200 repetitions of the last deviator stress level or when the specimen fails.

Example 7.2:

Table 7.2 shows the results of resilient modulus tests on a granular material. The distance between the LVDT clamps is 4 in. (102 mm). The average recoverable deformations measured by the two LVDTs after 200 repetitions of each deviator stress are shown in Table 7.2. Determine the nonlinear coefficient K_1 and exponent K_2 in Eq. 3.8.

Downloaded From : www.EasyEngineering.net

Downloaded From : www.EasyEngineering.net

TABLE 7.2 Computation of Resilient Modulus for Granular Materials

Confining pressure σ_3 (psi)	Deviator stress σ_d (psi)	Recoverable deformation (0.001 in.)	Recoverable strain ϵ_r ($\times 10^{-3}$)	Resilient modulus M_R ($\times 10^3$ psi)	Stress invariant θ (psi)
20	1	0.264	0.066	15.2	61
	2	0.496	0.124	16.1	62
	5	1.184	0.296	16.9	65
	10	2.284	0.571	17.5	70
	15	3.428	0.857	17.5	75
	20	4.420	1.105	18.1	80
15	1	0.260	0.065	15.4	46
	2	0.512	0.128	15.6	47
	5	1.300	0.325	15.4	50
	10	2.500	0.625	16.0	55
	15	3.636	0.909	16.5	60
	20	4.572	1.143	17.5	65
10	1	0.324	0.081	12.3	31
	2	0.672	0.168	11.9	32
	5	1.740	0.435	11.5	35
	10	3.636	0.909	11.0	40
	15	3.872	0.968	15.5	45
5	1	0.508	0.127	7.9	16
	2	0.988	0.247	8.1	17
	5	2.224	0.556	9.0	20
	10	3.884	0.971	10.3	25
	15	5.768	1.442	10.4	30
1	1	0.636	0.159	6.3	4
	2	0.880	0.220	9.1	5
	5	2.704	0.676	7.4	8
	7.5	3.260	0.815	9.2	10.5
	10	4.444	1.111	9.0	13

Note. 1 psi = 6.9 kPa, 1 in. = 25.4 mm.

Solution: The first three columns of data are given. The recoverable strains are obtained by dividing the recoverable deformation by an initial length of 4 in. (102 mm). The resilient modulus is obtained from Eq. 7.1. The stress invariant is obtained by

$$\theta = \sigma_1 + 2\sigma_3 = \sigma_d + 3\sigma_3 \tag{7.3}$$

The resilient modulus is plotted against the stress invariant on logarithmic scales, as shown in Figure 7.8. The least-square lines has an intercept of 3690 psi (25.5 MPa) at $\theta = 1$ psi (6.9 kPa), which is K_1, and a slope of log(18.58/3.69)/log(100/1) = 0.351, which is K_2, or

$$M_R = 3690\theta^{0.351} \tag{7.4}$$

Downloaded From : www.EasyEngineering.net

Downloaded From : www.EasyEngineering.net

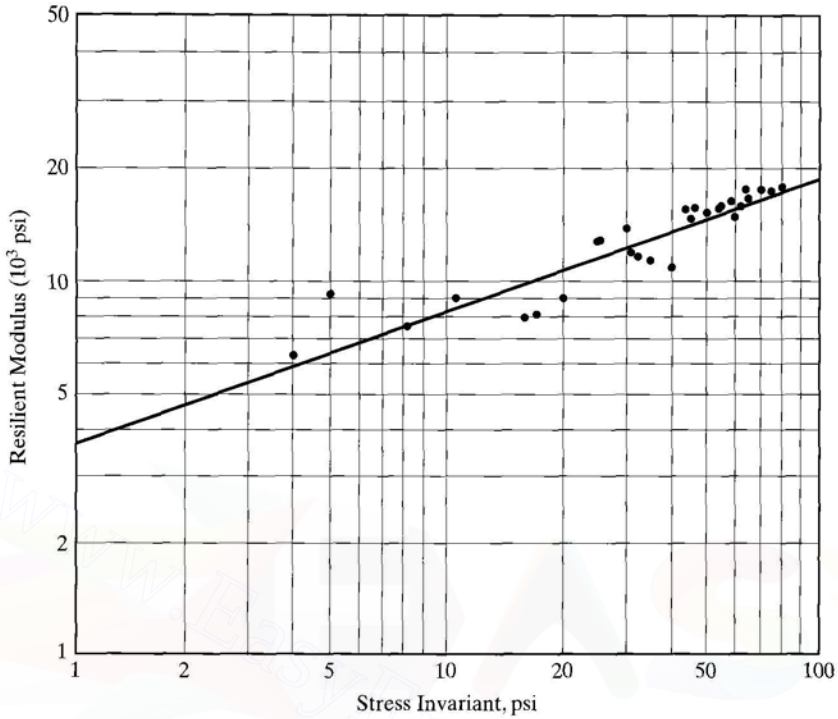


FIGURE 7.8
Example 7.2 (1 psi = 6.9 kPa).

7.1.4 Fine-Grained Soils

Sample conditioning for fine-grained soils is not as extensive as that for granular materials. AASHTO recommends the use of a confining pressure of 6 psi (41 kPa) followed by 200 repetitions each of deviator stresses of 1, 2, 4, 8, and 10 psi (6.9, 14, 28, 55, and 69 kPa). After sample conditioning, the following sequences of stresses are applied, and the results are recorded at the 200th repetition of each deviator stress:

1. Apply a deviator stress of 1 psi (6.9 kPa) under confining pressures of 6, 3, and 0 psi (41, 21, and 0 kPa).
2. Apply a deviator stress of 2 psi (14 kPa) under the same decreasing confining pressures of 6, 3, and 0 psi (41, 21, and 0 kPa).
3. Continue the constant deviator stress–decreasing confining pressure sequence for the deviator stresses 4, 8, and 10 psi (28, 48, and 69 kPa).

It is believed that a deviator stress of 10 psi is probably the largest that may occur in a subgrade. If the resilient moduli at higher deviator stresses are required, larger deviator stresses should be used until the unconfined compressive strength is reached.

Downloaded From : www.EasyEngineering.net

Downloaded From : www.EasyEngineering.net

Example 7.3:

Resilient modulus tests were made on a fine-grained soil. The distance between the LVDT clamps is 4 in. (102 mm). The average recoverable deformations measured by the two LVDTs after 200 repetitions of each deviator stress are shown in Table 7.3. The unconfined compressive strength of the soil is 15.5 psi (107 kPa). Determine the coefficients K_1, K_2, K_3, and K_4 in Eq. 3.13 and the maximum and minimum resilient modulus.

TABLE 7.3 Computation of Resilient Modulus for Fine-Grained Soils

Deviator stress σ_d (psi)	Confining pressure σ_3 (psi)	Recoverable deformation (0.001 in.)	Recoverable strain ϵ_r (10^{-3})	Resilient modulus M_R (10^3 psi)
1	6	0.392	0.098	10.2
	3	0.416	0.104	9.6
	0	0.456	0.114	8.8
2	6	0.816	0.204	9.8
	3	0.868	0.271	9.2
	0	1.040	0.260	7.7
4	6	2.052	0.513	7.8
	3	2.224	0.556	7.2
	0	3.020	0.755	5.3
8	6	5.712	1.428	5.6
	3	7.112	1.778	4.5
	0	9.412	2.353	3.4
10	6	7.692	1.923	5.2
	3	11.112	2.778	3.6
	0	16.000	4.000	2.5

Note. 1 psi = 6.9 kPa, 1 in. = 25.4 mm.

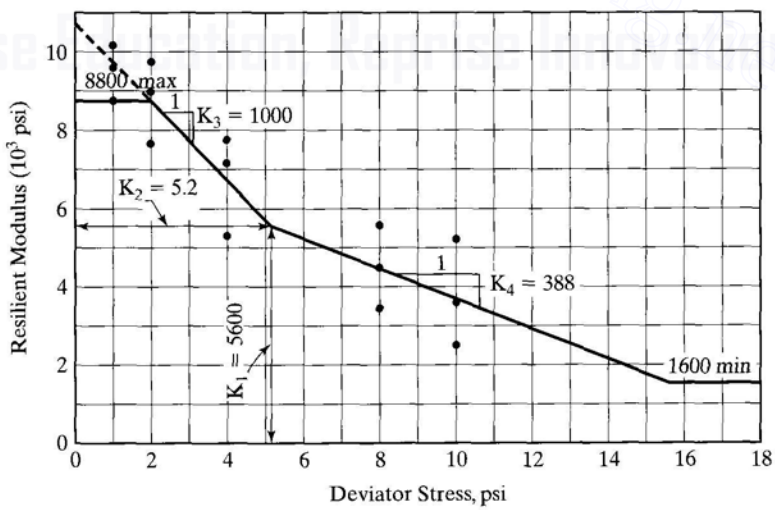


FIGURE 7.9
Example 7.3 (1 psi = 6.9 kPa).

Downloaded From : www.EasyEngineering.net

Downloaded From : www.EasyEngineering.net

Solution: The first three columns of data are given. The recoverable strains are obtained by dividing the recoverable deformation by an initial length of 4 in. (102 mm). The resilient modulus is computed by Eq. 7.1. The resilient modulus is plotted against the deviator stress on arithmetic scales, as shown in Figure 7.9. Two straight lines with the best fit are drawn. The intersection of the two lines gives $K_1 = 5600$ psi (38.6 MPa) and $K_2 = 5.2$ psi (36 kPa). The slopes of the lines are $K_3 = (10{,}800 - 5600)/5.2 = 1000$ and $K_4 = (5600 - 1600)/(15.5 - 5.2) = 388$. The maximum resilient modulus is 8800 psi (61 MPa), which corresponds to a deviator stress of 2 psi (14 kPa). The minimum resilient modulus is 1600 psi (11 MPa), which corresponds to an unconfined compressive strength of 15.5 psi (107 kPa).

It should be noted that the procedures specified in AASHTO T-274 for the testing of granular and fine-grained soils have many shortcomings and were modified by the Strategic Highway Research Program to produce more repeatable and less complicated test procedures (Claros *et al.*, 1990). The main changes are the use of external LVDTs for deformation measurements of all soil types and the complete modification of loading sequences, eliminating low deviator stresses, which produce high variability, and high deviator stresses, which cause sample failures.

Muhanna *et al.* (1999) found that the number of load applications, the rest period, and the load sequence have no significant effect on the measured resilient modulus of two different fine-grained soils. It was also demonstrated that a confining pressure in the range from 0 to 10 psi (from 0 to 69 kPa) has less than a 5 percent effect.

7.1.5 Asphalt Mixtures

The specimens used for compression tests are usually 4 in. (102 mm) in diameter and 8 in. (203 mm) high, while those for indirect tensile tests are 4 in. (102 mm) in diameter and 2.5 in. (64 mm) thick. The advantage of indirect tensile tests is to use specimens of Marshall size, which can be easily fabricated in the laboratory or cored from the pavements.

Sample conditioning is required before the recoverable deformation is recorded. The conditioning can be effected by applying a repeated load to the specimen without impact for a minimum period sufficient to obtain uniform deformation readout. Depending upon the loading frequency and temperature, a minimum of 50 to 200 load repetitions is typical; however, the minimum for a given situation must be determined so that the resilient deformations are stable. Tests on the same specimen are usually made at three temperatures—41, 77, and 104°F (5, 25, and 40°C)—to generate design values over the range of temperatures normally encountered in pavements.

The resilient modulus of compression specimens is determined from Eq. 7.1. A 20-psi (138-kPa) haversine loading with a duration of 0.1 s and a rest period of 0.9 s has been most frequently used. The resilient modulus of indirect tension specimens is computed by Eq. 7.2. Dynamic load amplitudes of 40 to 60 lb (180 to 270 kN) with a load duration of 0.1 s applied every 3 s are typical. The test is specified by ASTM (1989b) in "D4123-82 Standard Test Method for Indirect Tension Test for Resilient Modulus of Bituminous Mixtures."

Downloaded From : www.EasyEngineering.net

Downloaded From : www.EasyEngineering.net

7.1.6 Correlations with Other Tests

Various empirical tests have been used to determine the material properties for pavement design. Most of these tests measure the strength of the material and are not a true representation of the resilient modulus. An extensive study was made by Van Til *et al.* (1972) to relate the resilient modulus and other test parameters to the soil support value or the layer coefficient employed in the AASHO design equation. These correlations can be used as a guide if other, more reliable, information is not available. It should be noted that any empirical correlation is based on a set of local conditions. The correlation is not valid if the actual conditions are different from those under which the correlation is established. Therefore, great care must be exercised in the judicious selection of the resilient modulus from these correlations.

Subgrade Soils Figure 7.10 shows a correlation chart that can be used to estimate the resilient modulus of subgrade soils from the *R* value, CBR, Texas triaxial classification, and group index.

***R* Value** The *R* value is the resistance value of a soil determined by a stabilometer. The stabilometer test was developed by the California Division of Highways and measures basically the internal friction of the material; the cohesion for bonded materials is measured by the cohesiometer test. Figure 7.11 is a schematic diagram of

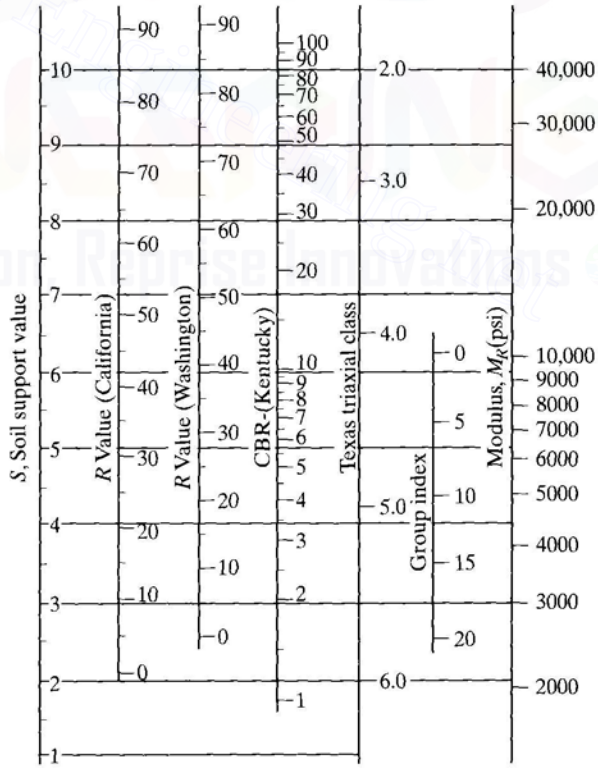


FIGURE 7.10

Correlation chart for estimating resilient modulus of subgrade soils (1 psi = 6.9 kPa). (After Van Til et al. (1972).)

Downloaded From : www.EasyEngineering.net

Downloaded From : www.EasyEngineering.net

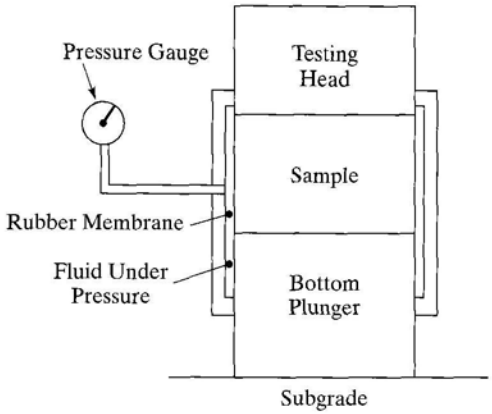


FIGURE 7.11
Schematic diagram of stabilometer

stabilometer, which is a closed-system triaxial test. A vertical pressure of 160 psi (1.1 MPa) is applied to a sample, 4 in. (102 mm) in diameter and about 4.5 in. (114 mm) in height, and the resulting horizontal pressures induced in the fluid within the rubber membrane are measured.

The resistance value is computed as

$$R = 100 - \frac{100}{(2.5/D_2)(p_v/p_h - 1) + 1} \tag{7.5}$$

in which R is the resistance value; p_v is the applied vertical pressure of 160 psi (1.1 MPa); p_h is the transmitted horizontal pressure at p_v of 160 psi (1.1 MPa); and D_2 is the displacement of stabilometer fluid necessary to increase horizontal pressure from 5 to 100 psi (35 to 690 kPa), measured in revolutions of a calibrated pump handle. The value of D_2 is determined after the maximum vertical pressure of 160 psi (1.1 MPa) is applied. If the sample is a liquid with no shear resistance, then $p_h = p_v$, or from Eq. 7.5, $R = 0$. If the sample is rigid with no deformation at all, then $p_h = 0$, or $R = 100$. Therefore, the R value ranges from 0 to 100. To ensure that the sample is saturated, California used an exudation pressure of 240 psi (1.7 MPa), whereas Washington used 300 psi (2.1 MPa).

CBR The California Bearing Ratio test (CBR) is a penetration test, wherein a standard piston, having an area of 3 in.^{2} (1935 mm^2), is used to penetrate the soil at a standard rate of 0.05 in. (1.3 mm) per minute. The pressure at each 0.1-in. (2.5-mm) penetration up to 0.5 in. (12.7 mm) is recorded and its ratio to the bearing value of a standard crushed rock is termed as the CBR. The standard values of a high-quality crushed rock are as follows:

Penetration	Pressure
0.1 in. (2.5 mm)	1000 psi (6.9 MPa)
0.2 in. (5.0 mm)	1500 psi (10.4 MPa)
0.3 in. (7.6 mm)	1900 psi (13.1 MPa)
0.4 in. (10.2 mm)	2300 psi (15.9 MPa)
0.5 in. (12.7 mm)	2600 psi (17.9 MPa)

Downloaded From : www.EasyEngineering.net

Downloaded From : www.EasyEngineering.net

In most cases, CBR decreases as the penetration increasees, so the ratio at the 0.1-in. (2.5-mm) penetration is used as the CBR. In some cases, the ratio at 0.2 in. (5.0 mm) will be greater than that at 0.1 in. (2.5 mm). If this occurs, the ratio at 0.2 in. (5.0 mm) should be used. In the Kentucky method, the specimen is molded at or near to the optimum moisture as determined by the standard proctor method. However, the sample is placed in a mold, 6 in. (152 mm) in diameter and 4.6 in. (117 mm) in height, and compacted in five equal layers, each subjected to 10 blows of a 10-lb (4.5-kg) hammer at 18 in. (457 mm) drop. The specimen is soaked for 4 days before testing.

Texas Triaxial Classification The Texas triaxial test is used to classify soils on the basis of the location of Mohr's envelope. The apparatus consists of a stainless cylinder with an inside diameter of $6\frac{3}{4}$ in. (171 mm) fitted with a tubular rubber membrane 6 in. (152 mm) in diameter. The lateral pressure σ_3 is applied by compressed air between the cylinder and the rubber membrane. The major principal stress σ_1 is the applied stress because the confining pressure is not applied to the top of the specimen. From the principal stresses at the time of failure, Mohr's circles for several tests with different confining pressures are constructed. Mohr's failure envelope is transferred to a classification chart, as shown in Figure 7.12, and the strength class of the material is determined to the nearest tenth.

Group Index The group index, which ranges from 0 to 20, is used in the AASHTO soil classification system. The values vary with the percentage passing through a No. 200 sieve, the plasticity index, and the liquid limit and can be found from charts or formulas.

Other Correlations In addition to Figure 7.10, other correlations between M_R, CBR, and R values are also available. These correlations could be quite different from those shown in Figure 7.10.

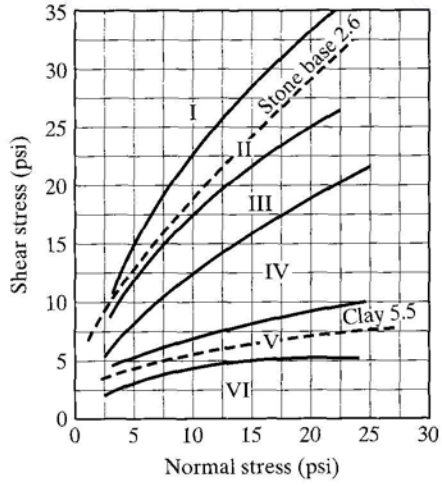


FIGURE 7.12

Chart for classification of subgrade and base by Texas triaxial test (1 psi = 6.9 kPa).

Downloaded From : www.EasyEngineering.net

Downloaded From : www.EasyEngineering.net

TABLE 7.4 Comparison of CBR, R Value, and Resilient Modulus

Soil description	CBR test		R value test		Triaxial test
	CBR	M_R (psi) by eq. 7.6	R	M_R (psi) by eq. 7.7	M_R (psi)
Sand	31	46,500	60	34,500	16,900
Silt	20	30,000	59	33,900	11,200
Sandy loam	25	37,500	21	12,800	11,600
Silt-clay loam	25	37,500	21	12,800	17,600
Silty clay	7.6	11,400	18	11,000	8200
Heavy clay	5.2	7800	<5	<3900	14,700

Note. 1 psi = 6.9 kPa.
Source: After AI (1982).

Heukelom and Klomp (1962) show that

$$M_R = 1500\,(\text{CBR}) \tag{7.6}$$

in which M_R is the resilient modulus in psi. The coefficient, 1500, could vary from 750 to 3000, with a factor of 2. Available data indicate that Eq. 7.6 provides better results at values of CBR less than about 20. In other words, the correlation appears to be more reasonable for fine-grained soils and fine sands than for granular materials.

The Asphalt Institute (1982) proposed the following correlation between M_R and the R value:

$$M_R = 1155 + 555R \tag{7.7}$$

Laboratory data obtained from six different soil samples were used by the Asphalt Institute (1982) to illustrate the relationships, as shown in Table 7.4. The R values were obtained at an exudation pressure of 240 psi (1.7 MPa). The CBR samples were compacted at optimum moisture content to maximum density and soaked before testing. The repeated load triaxial tests were performed at optimum conditions using a deviator stress of 6 psi (41 kPa) and a confining pressure of 2 psi (14 kPa).

It can be seen from Table 7.4 that the equations for estimating M_R from CBR and R values have a very limited range. The resilient moduli estimated from CBR values of 5.2 and 7.6 and R values of 18 and 21 generally conform to the guidelines for accuracy within a factor of 2. Estimates from CBR values of 25 or higher and R values above 60 would appear to overestimate M_R by Eqs. 7.6 and 7.7.

It should be noted that the M_R of granular materials increases with the increase in confining pressure, and that of fine-grained soils decreases with the increase in deviator stress. Therefore, a large variety of correlations might be obtained, depending on the confining pressure or the deviator stress to be used in the resilient modulus test.

Hot Mix Asphalt Figure 7.13 shows the relationships of the layer coefficient, Marshall stability, cohesiometer values, and resilient modulus.

Downloaded From : www.EasyEngineering.net

Downloaded From : www.EasyEngineering.net

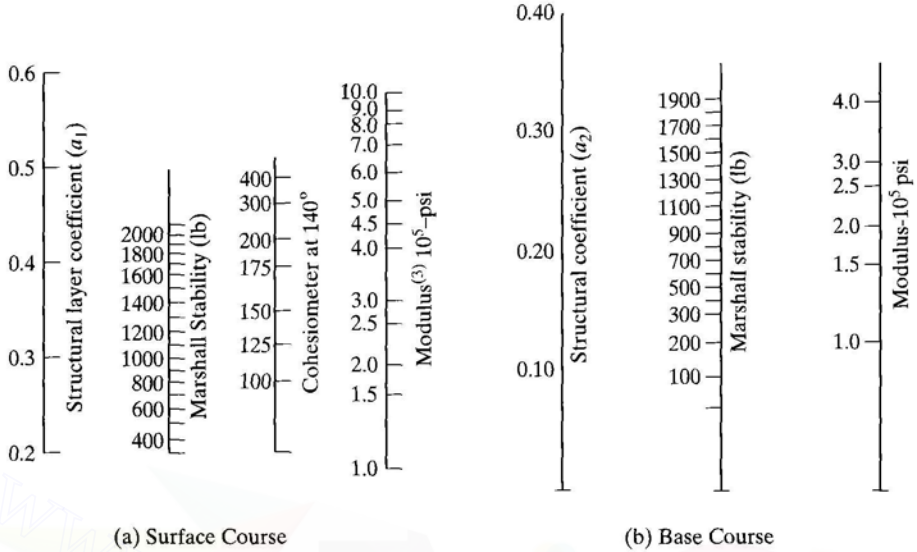


FIGURE 7.13

Correlation charts for estimating resilient modulus of HMA (1 lb = 4.45 N, 1 psi = 6.9 kPa). (After Van Til *et al.* (1972).)

Structural Layer Coefficient In the AASHTO design method, the quality of the HMA, base, and subbase is indicated by their structural layer coefficients. These correlation charts were originally developed to determine the layer coefficients, but can also be used to determine the resilient modulus. More about layer coefficients is presented in Section 11.3.4.

Marshall Test The Marshall test is performed on cylindrical specimens, 4 in. (102 mm) in diameter and 2.5 in. (64 mm) in height, at a temperature of 140°F (60°C) and a rate of loading of 2 in. (51 mm) per minute. Two values are measured: the stability, which is the required load to fail the specimen, and the flow index, which is the vertical distortion at the time of failure. Due to the very fast rate of loading, the stability is a measure of the cohesion, while the flow index is a measure of the internal friction.

Cohesiometer Test The cohesiometer test is used to measure the cohesion of HMA or rigidly cemented materials. Figure 7.14 is a schematic diagram of the cohesiometer setup. The load is applied at a control rate by the weight of shot until the sample breaks. The cohesiometer value is computed as

$$C = \frac{L}{W(0.2t + 0.044t^2)} \tag{7.8}$$

in which C is the cohesiometer value in grams per inch width corrected to 3 in. (76 mm) height, L is the weight of lead shot in grams, W is the diameter or width of specimen in

Downloaded From : www.EasyEngineering.net

Downloaded From : www.EasyEngineering.net

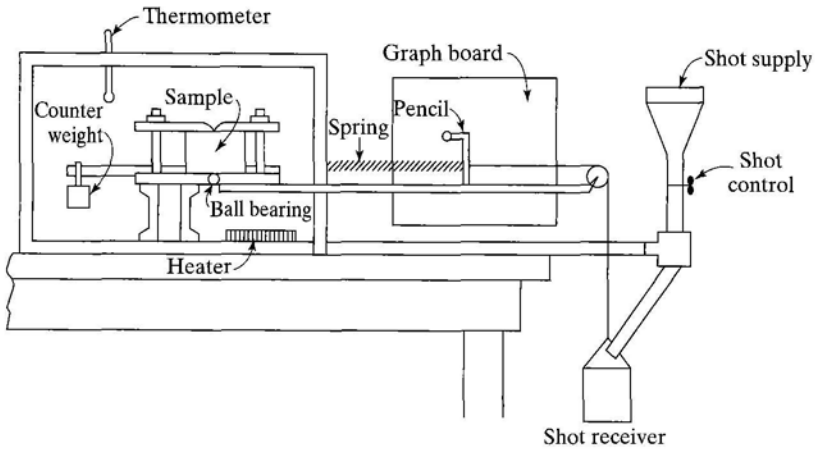


FIGURE 7.14
Schematic diagram of cohesiometer setup (After Yoder and Witczak (1975).)

inches, and t is the thickness of the specimen in inches. Note that when $t = 3$ in. (76 mm), $C = L/W$.

Bases Figure 7.15 shows the correlation charts for untreated granular base, bituminous-treated base, and cement-treated base. The resilient modulus of untreated bases is correlated with CBR, R value, and Texas triaxial classification, as shown in Figure 7.15*a*; the resilient modulus of bituminous-treated bases is correlated with the Marshall stability, as shown in Figure 7.15*b*; and that of cement-treated bases is correlated with the unconfined compressive strength, as shown in Figure 7.15*c*.

Subbases Figure 7.16 shows the correlation chart for estimating the resilient modulus of granular subbases from CBR, R values, and Texas triaxial classification. For the same untreated granular materials, the correlations for base, subbase, and subgrade are different, as is illustrated in the next example.

Example 7.4:

Given CBR values of 30 and 80, determine the corresponding R value, Texas classification, and resilient modulus when the materials are used as a base course, a subbase course, and a subgrade.

Solution: The correlations for base, subbase, and subgrade can be obtained from Figures 7.15*a*, 7.16, and 7.10. The results are tabulated in Table 7.5.

It can be seen from Table 7.5 that the correlations among CBR, R value, and Texas classification are practically the same no matter whether the material is used as a base, a subbase, or a subgrade. This is not true for the resilient modulus, where a large variation exists. This is reasonable, because the resilient modulus depends on the state of stresses, which varies with the location where the material is to be placed.

Downloaded From : www.EasyEngineering.net

Downloaded From : www.EasyEngineering.net

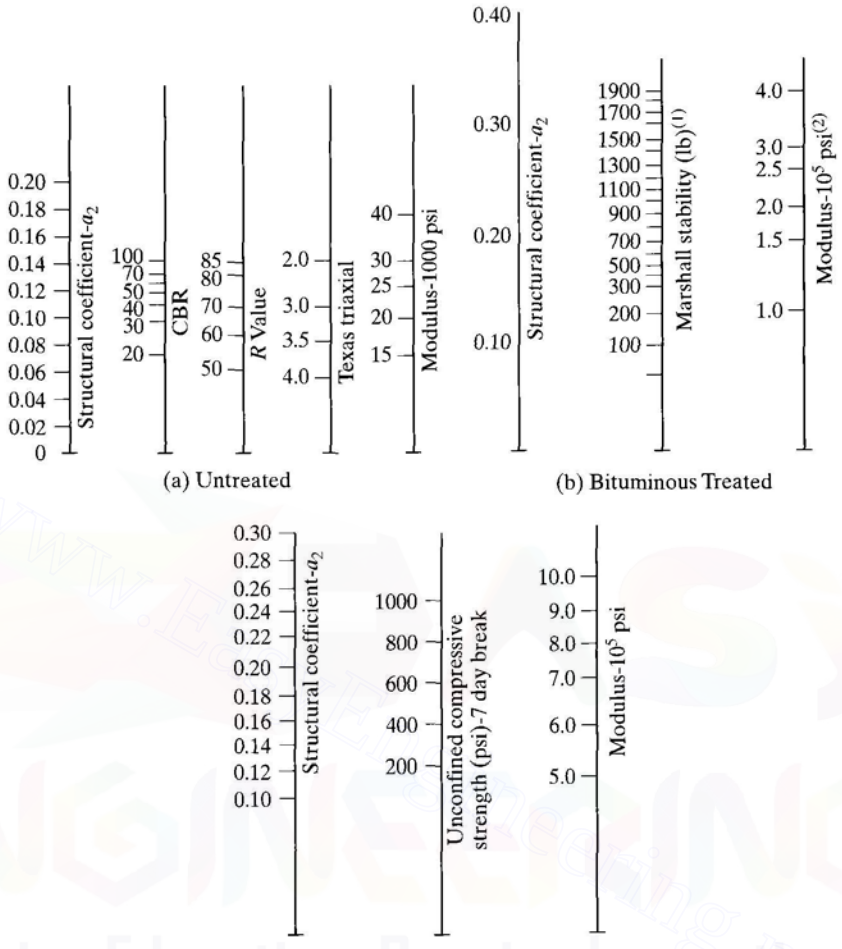


FIGURE 7.15

Correlation charts for estimating resilient modulus of bases (1 lb = 4.45 KN, 1 psi = 6.9 kPa). (After Van Til *et al.* (1972).)

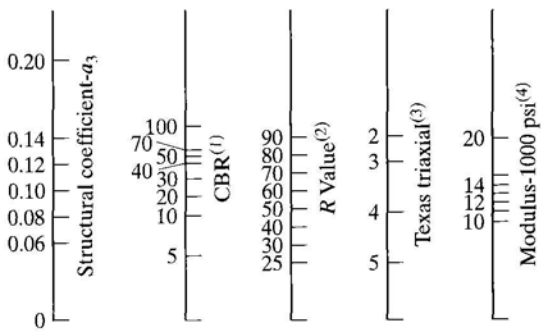


FIGURE 7.16

Correlation chart for estimating resilient modulus of subbases (1 psi = 6.9 kPa). (After Van Til *et al.* (1972).)

Downloaded From : www.EasyEngineering.net

Downloaded From : www.EasyEngineering.net

TABLE 7.5 Correlation Between CBR and Resilient Modulus

	CBR = 30			CBR = 80		
Location	*R* value	Texas classification	M_R (psi)	*R* value	Texas classification	M_R (psi)
Base	65	3.2	20,000	83	2.1	29,000
Subbase	61	3.4	14,700	85	2.3	20,000
Subgrade	64	3.2	19,000	83	2.1	39,000

Note. 1 psi = 6.9 kPa.

7.2 DYNAMIC MODULUS OF BITUMINOUS MIXTURES

In addition to the resilient modulus, the dynamic complex modulus and the dynamic stiffness modulus have also been used for pavement design.

7.2.1 Dynamic Complex Modulus

The difference between a resilient modulus test and a complex modulus test for bituminous mixtures is that the former uses loadings of any waveform with a given rest period, while the latter applies a sinusoidal or haversine loading with no rest period. The complex modulus is one of the many methods for describing the stress–strain relationship of viscoelastic materials. The modulus is a complex quantity, of which the real part represents the elastic stiffness and the imaginary part characterizes the internal damping of the materials. The absolute value of the complex modulus is commonly referred to as the dynamic modulus. The theory of complex modulus and Fourier transforms is presented in Appendix A.

The complex modulus test is usually conducted on cylindrical specimens subjected to a compressive haversine loading (Papazian, 1962). The same equipment described previously for the resilient modulus can be used for the complex modulus test. The dynamic modulus varies with the loading frequency. A frequency that most closely simulates the actual traffic load should be selected for the test, so that the dynamic modulus thus determined will be equivalent to the resilient modulus for design purposes. The dynamic modulus test is specified by ASTM (1989b) in "D3497-79 Standard Test Method for Dynamic Modulus of Asphalt Mixtures." In the ASTM method, a haversine compressive stress is applied to the specimen for a minimum of 30 s and not exceeding 45 s at temperatures of 41, 77, and 104°F (5, 25, and 40°C) and at load frequencies of 1, 4, and 16 Hz for each temperature. The axial strains are measured by bonding two wire strain gauges at midheight of the specimen opposite each other. The ratio between the axial stress and the recoverable axial strain is the dynamic modulus.

Most of the complex modulus tests are made by applying a compressive haversine loading to the specimens. If the specimens are truly viscoelastic, any other testing modes should yield the same results. Kallas (1970) investigated the complex modulus of HMA under a tension haversine loading and a tension–compression full sine loading. The dynamic modulus and phase angle in tension and tension–compression were

Downloaded From : www.EasyEngineering.net

Downloaded From : www.EasyEngineering.net

compared to those in compression. The following conclusions were drawn for dense-graded HMA with asphalt and air void contents within the normal ranges:

1. Differences in dynamic modulus are generally insignificant or relatively small among tension, tension–compression, and compression tests for temperatures ranging from 40 to 70°F (4 to 21°C) and loading frequencies from 1 to 16 Hz.
2. Differences in dynamic modulus are significant between the tension or tension–compression test and the compression test at a frequency of 1 Hz and temperatures ranging from 70 to 100°F (21 to 38°C). Under these conditions, the dynamic modulus in tension or tension–compression averages about one-half to two-thirds of that in compression.
3. Differences in phase angle are pronounced between tension and compression and are less pronounced between tension–compression and compression.
4. The phase angle is greatest in tension, least in compression, and intermediate in tension–compression. On the average, the phase angle in tension exceeds that in compression by about 50%, and the phase angle in tension–compression exceeds that in compression by about 25%.

The preceding conclusions might indicate that, if a design is based on the elastic theory with a given dynamic modulus for the HMA, any of the foregoing three testing modes may be used. However, if the design is based on the viscoelastic theory with both the dynamic modulus and phase angle as design variables, a testing mode consistent with the actual loading conditions should be used. This will probably be a tension–compression test, as suggested by Witczak and Root (1974).

The dynamic modulus can also be determined from a bending test. A two point bending apparatus was developed by Shell for determining the modulus of asphalt mixtures (Bonnaure *et al.*, 1977). In this test a trapezoidal specimen fixed at the bottom is subjected to a sinusoidal load at the free end. A continuous plot of load and deformation at the free end is obtained, and the stiffness modulus of the sample can be calculated. Another means is provided to calculate the stiffness modulus by measuring the strain on the surface at midlength of the beam with a strain gage. Due to the use of sinusoidal loads, the stiffness modulus obtained from Shell nomographs, described in Section 7.2.3, is actually the dynamic modulus. The test can also be used to determine the phase angle. From the stiffness modulus and the phase angle, the complex modulus can be obtained.

7.2.2 Dynamic Stiffness Modulus

In the fatigue testing of asphalt beam specimens, the elastic modulus at the initial stage must be determined, so that the initial strain can be computed. The elastic modulus based on the resilient deformation of the beam at the 200th repetition is called the dynamic stiffness modulus.

Test Method The fatigue testing equipment and procedures are described in Section 7.3.1. Repeated haversine loadings with a load duration of 0.1 s and a rest period of 0.4 s are applied at the third points, as shown in Figure 7.17. The size of specimens used by

Downloaded From : www.EasyEngineering.net

Downloaded From : www.EasyEngineering.net

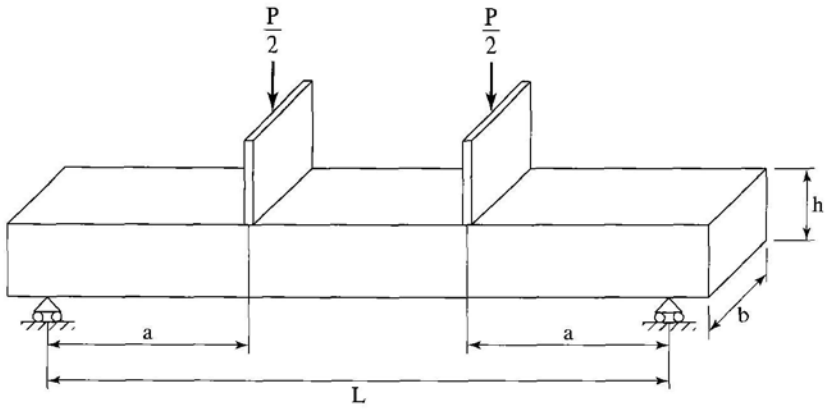


FIGURE 7.17

Third-point beam test for dynamic modulus.

the University of California at Berkeley (Deacon, 1965) was 1.5 in. (38 mm) in width and depth and 15 in. (381 mm) long. To reduce test variability, the width and depth of beams were increased to 3 in. (76 mm) by the Asphalt Institute (Kallas and Puzinauskas, 1972). The following formulas based on the elastic theory have frequently been used to compute the stress, stiffness modulus, and strain:

$$\sigma = \frac{3aP}{bh^2} \tag{7.9}$$

$$E_s = \frac{Pa(3L^2 - 4a^2)}{4bh^3\Delta} \tag{7.10}$$

$$\epsilon_t = \frac{\sigma}{E_s} = \frac{12h\Delta}{3L^2 - 4a^2} \tag{7.11}$$

in which σ is the extreme fiber stress, a is the distance between the load and the nearest support, P is the total dynamic load with $P/2$ applied at each third point, b is the specimen width, h is the specimen depth, E_s is the stiffness modulus based on center deflection, L is the span length between supports, Δ is the dynamic deflection at beam center, and ϵ_t is the extreme fiber tensile strain. When $a = L/3$, Eq. 7.10 becomes

$$E_s = \frac{23PL^3}{108bh^3\Delta} \tag{7.12}$$

After considering the shear deformation, Irwin and Gallaway (1974) suggested the use of the following equation for E_s:

$$E_s = \frac{23PL^3}{108bh^3\Delta}\left[1 + \frac{216h^2(1+\nu)}{115L^2}\right] \tag{7.13}$$

In this equation, ν is Poisson ratio of the beam. Note that the expression in the bracket is the correction factor for shear deformation. The correction factor varies with h/L.

Downloaded From : www.EasyEngineering.net

Downloaded From : www.EasyEngineering.net

For a beam with $L = 12$ in. (305 mm) and $\nu = 0.35$, the correction factor is 1.04 for $h = 1.5$ in. (38 mm) but increases to 1.16 for $h = 3.0$ in. (76 mm).

Example 7.5:

A beam with a span length of 12 in. (305 mm) and a width and depth of 3 in. (76 mm) is subjected to a dynamic load of 300 lb (1.34 kN) at third points. The dynamic deflection measured at the center of the beam is 6.25×10^{-4} in. (0.016 mm). Determine the extreme fiber stress and the stiffness modulus by Eqs. 7.12 and 7.13. In applying Eq. 7.13, a Poisson ratio of 0.35 may be assumed.

Solution: Given $P = 300$ lb (1.34 kN), $a = 4$ in. (102 mm), and $b = h = 3$ in. (76 mm), from Eq. 7.9, $\sigma = 3 \times 4 \times 300/(3 \times 9) = 133.3$ psi (920 kPa). Given $L = 12$ in. (305 mm) and $\Delta = 0.000625$ in. (0.016 mm), from Eq. 7.12, $E_s = 23 \times 300 \times (12)^3/(108 \times 3 \times 27 \times 0.000625) = 2.18 \times 10^6$ psi (15 GPa), and from Eq. 7.13, $E_s = 2.18 \times 10^6 \times 1.16 = 2.53 \times 10^6$ psi (17.5 GPa).

Relation to Dynamic Modulus All constant stress fatigue tests have shown that the dynamic stiffness modulus decreases with the increase in dynamic load, a pattern due to the relatively large strain in the flexural test. Witczak and Root (1974) indicated that a plot of log E_s versus σ results in a straight line:

$$E_s = E_0 A_1^{\sigma} \tag{7.14}$$

in which E_0 is the stiffness modulus when $\sigma = 0$, and A_1 is a regression constant depending upon the particular mix and test temperature. Figure 7.18 shows the typical plot of one type of asphalt mix at a temperature of 70°F (21°C). The value of E_0 for this case is 5.5×10^5 psi (38 GPa), which is the intercept of the regression line at zero flexural stress.

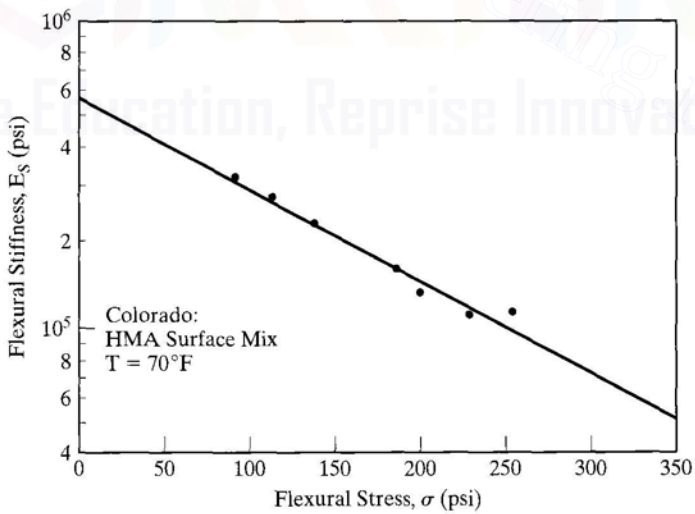


FIGURE 7.18

Relationship between stiffness modulus and flexural stress (1 psi = 6.9 kPa). (After Witczak and Root (1974).)

Downloaded From : www.EasyEngineering.net

Downloaded From : www.EasyEngineering.net

Because the stiffness modulus changes with the level of stresses, it cannot be used as a dynamic modulus in the linear elastic layer system. To define the relationship between E_0 and $|E^*|$, a regression analysis was conducted by Witczak and Root (1974) on the laboratory results of 17 different asphalt mix and temperature combinations that had been tested by both procedures. The loading used for determining the dynamic modulus was haversine in compression and that for the stiffness modulus was 0.1 s haversine and 0.5 s rest period. The regression equation can be represented by

$$|E^*| = 0.18089 f^{2.1456} E_0^{(14.6918/f^{0.01} - 13.5739)} \tag{7.15}$$

in which f is the frequency at which $|E^*|$ is desired.

Example 7.6:

For the results of dynamic stiffness shown in Figure 7.18, determine the dynamic modulus at a frequency of 8 Hz.

Solution: With $E_0 = 5.5 \times 10^6$ psi (38 GPa) and $f = 8$ Hz, from Eq. 7.15, $|E^*| = 0.18089(8)^{2.1456}(5.5 \times 10^6)^{[14.6918/(8)^{0.01} - 13.5739]} = 4.932 \times 10^6$ psi (34 GPa).

7.2.3 Nomographs and Formulas

Determination of the dynamic modulus of bituminous mixtures by laboratory tests not only is time-consuming, but also requires sophisticated equipment. It is highly desirable that the modulus be predictable by nomographs or formulas based on the property of the asphalt and the volume concentration of the aggregate. If actual test data are not available, the Shell nomographs (Bonnaure *et al.*, 1977) or the Asphalt Institute formulas (AI, 1982) can be used to determine the modulus without performing the modulus tests. Typical values of the dynamic modulus at different temperatures and frequencies are also presented.

Shell Nomographs The term "stiffness modulus" is used by Shell in lieu of the dynamic modulus. Two nomographs are used. The first nomograph is applied to determine the stiffness modulus of bitumen based on the temperature, the time of loading, and the characteristics of bitumen actually present in the mix. The second nomograph is then applied to determine the stiffness modulus of the bituminous mix based on the stiffness modulus of the bitumen, the percent volume of the bitumen, and the percent volume of the mineral aggregate.

The characteristics of bitumen are expressed as a penetration index, PI, defined as

$$\text{PI} = \frac{20 - 500A}{1 + 50A} \tag{7.16}$$

in which A is the temperature susceptibility, which is the slope of the straight line plot between the logarithm of penetration (abbreviated as pen) and temperature, or

$$A = \frac{\log(\text{pen at } T_1) - \log(\text{pen at } T_2)}{T_1 - T_2} \tag{7.17}$$

Downloaded From : www.EasyEngineering.net

Downloaded From : www.EasyEngineering.net

in which T_1 and T_2 are two temperatures at which penetrations are measured. When the penetration of the recovered bitumen at two different temperatures is known, the penetration index can be determined by Eqs. 7.16 and 7.17.

A convenient temperature to use is the temperature at the ring and ball softening point as specified by AASHTO (1989) in "T53-84 Softening Point of Asphalt (Bitumen) and Tar in Ethylene Glycol (Ring and Ball)." This is a reference temperature at which all bitumens have the same viscosity or penetration of about 800. Replacing T_2 in Eq. 7.17 by $T_{R\&B}$ and pen at T_2 by 800 yields

$$A = \frac{\log(\text{pen at } T) - \log 800}{T - T_{R\,\&\,B}} \tag{7.18}$$

Figure 7.19 shows the nomograph for determining the stiffness modulus of bitumens (Van der Poel, 1954). The three factors to be considered are the time of loading, temperature, and penetration index. The temperature to be used is the normalized temperature, which is the difference between the testing temperature and the temperature when the penetration is 800, or $T_{R\&B}$.

The stiffness modulus of bitumen can be determined by either a creep test with a loading time t or a dynamic test under a sinusoidal loading with a frequency f. It was found by Van Der Poel (1954) that the same stiffness modulus is obtained when t is related to f by

$$t = \frac{1}{2\pi f} \tag{7.19}$$

It has been suggested by Shell (1978) that a loading time of 0.02 s, which corresponds to a frequency of 8 Hz according to Eq. 7.19, is representative of the range of loading times occurring in practice and equivalent to a vehicle speed of 30 to 40 mph.

Example 7.7:

An asphalt cement recovered from a mix has a penetration of 22 at 25°C (77°F) and a ring and ball softening point of 64°C (147°F). Determine the stiffness modulus of the asphalt under a temperature of 11°C (52°F) and a loading time of 0.02 s.

Solution: Since SI units are used in the Shell nomographs, all computations will be based on SI units. From Eq. 7.18, $A = (\log 22 - \log 800)/(25 - 64) = 0.04$. From Eq. 7.16, $\text{PI} = (20 - 500 \times 0.04)/(1 + 50 \times 0.04) = 0$. The temperature below $T_{800\text{pen}} = 64 - 11 = 53$°C. As shown in Figure 7.19, a straight line is drawn from 0.02 s on the time of loading scale to 53°C below $T_{800\text{pen}}$ on the temperature difference scale and extended to intersect the horizontal line with a penetration index of 0. A stiffness modulus of 2×10^8 N/m^2 (2.9×10^4 psi) can be read from the curve.

Figure 7.20 shows the nomograph for determining the stiffness modulus of bituminous mixtures (Bonnaure *et al.*, 1977). The three factors to be considered are the stiffness modulus of bitumen, the percent volume of bitumen, and the percent volume of aggregate. The percent volumes of aggregate, bitumen, and air can be computed from the percentage by weight of bitumen, the specific gravities of bitumen and aggregate, and the bulk specific gravity of the mixture. The latter can be determined by the

Downloaded From : www.EasyEngineering.net

Downloaded From : www.EasyEngineering.net

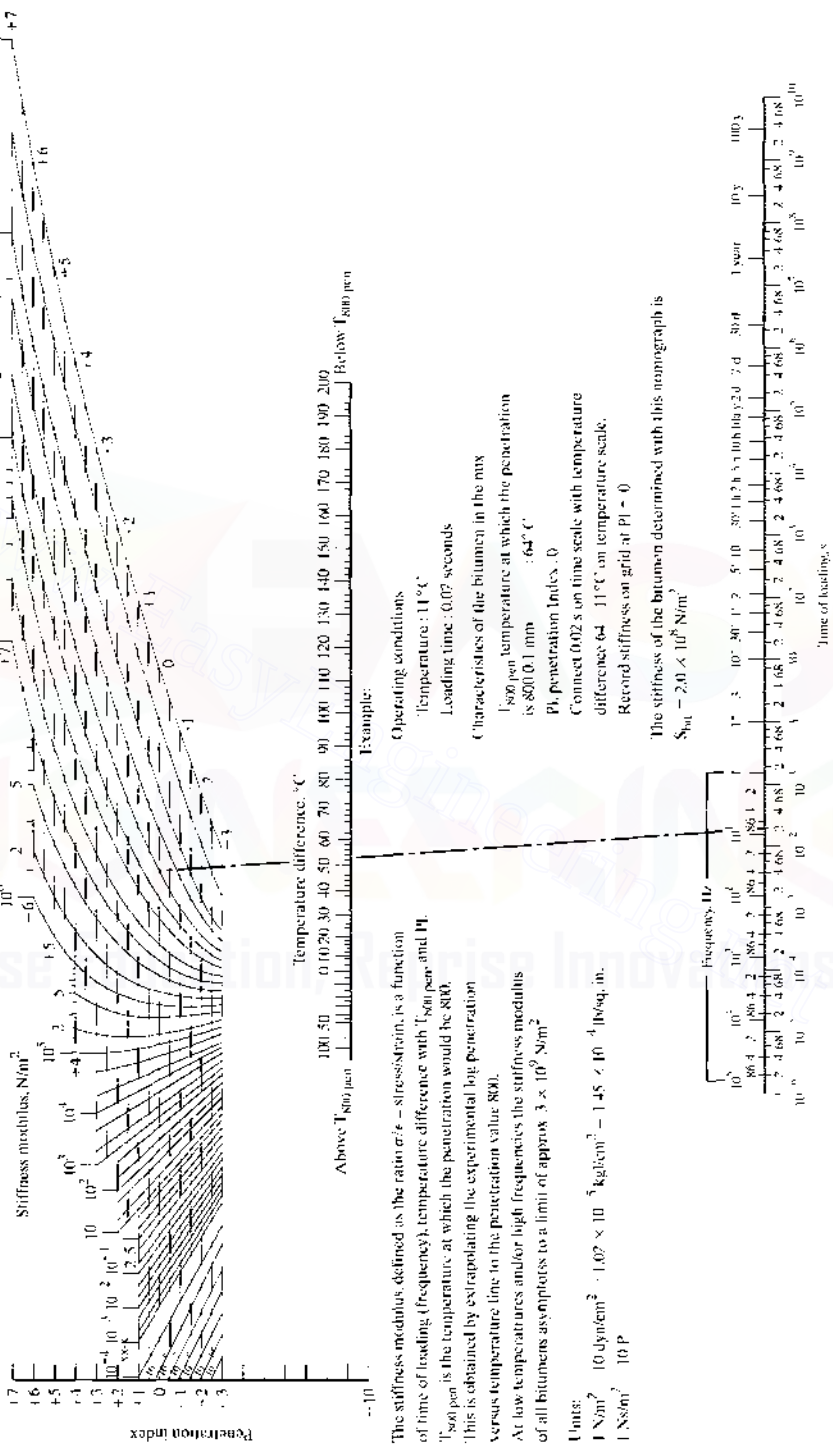


FIGURE 7.19

Nomograph for stiffness modulus of bitumens. (After Van der Poel (1954).)

Downloaded From : www.EasyEngineering.net

Downloaded From : www.EasyEngineering.net

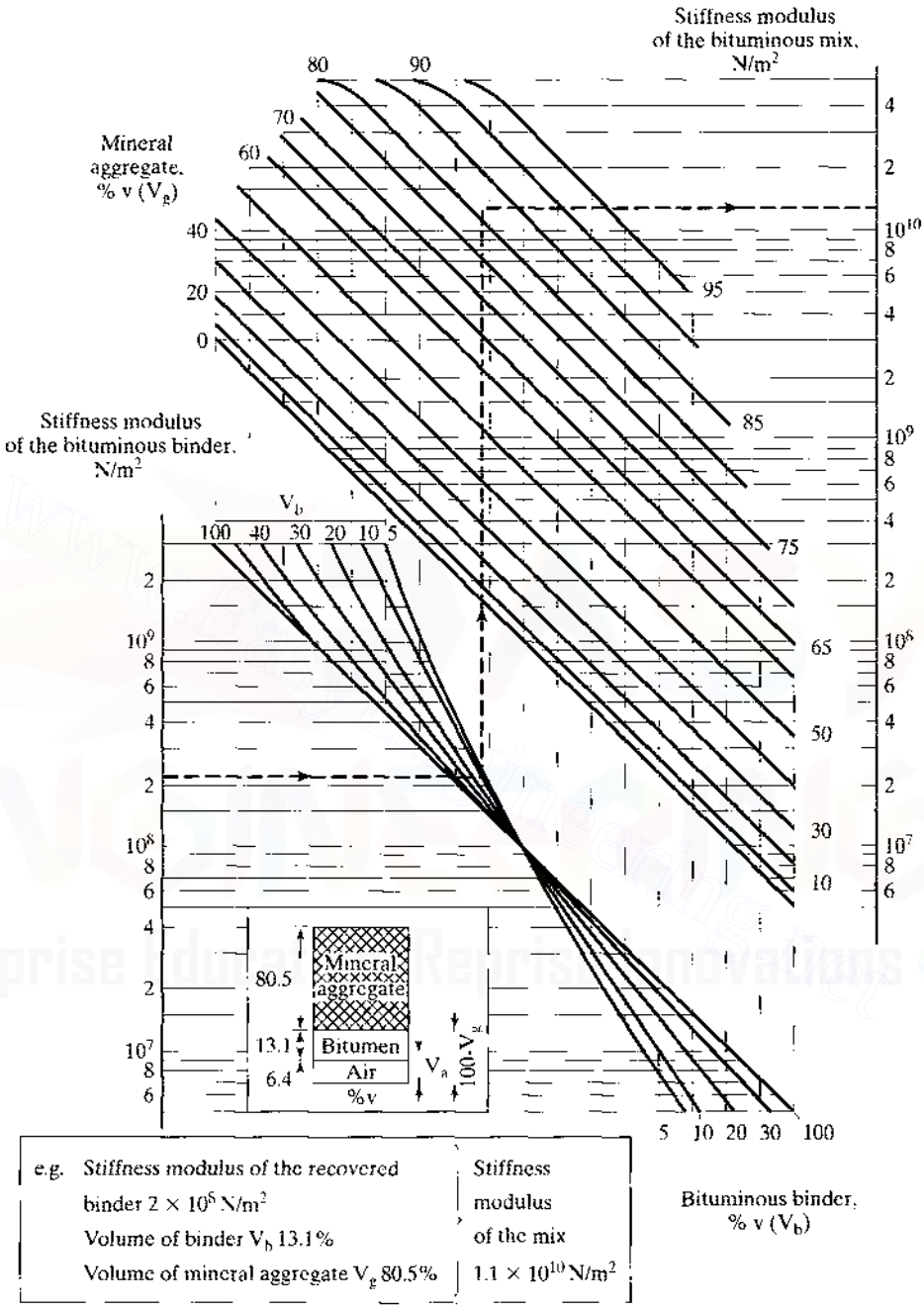


FIGURE 7.20

Nomograph for stiffness modulus of mixes. (After Shell (1978).)

Downloaded From : www.EasyEngineering.net

Downloaded From : www.EasyEngineering.net

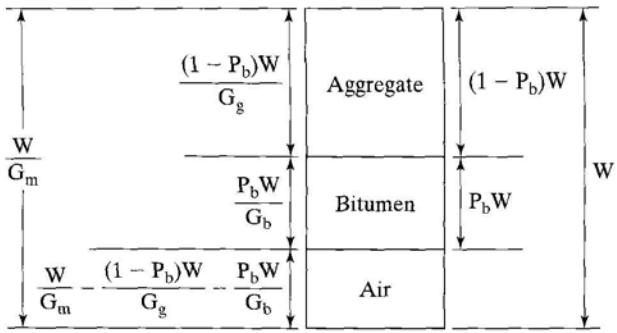


FIGURE 7.21
Phase diagram of bituminous mix.

water displacement method, as specified by AASHTO (1989) in "T166-83 Bulk Specific Gravity of Compacted Bituminous Mixtures."

Figure 7.21 shows the phase diagram of a bituminous mixture. Let W be the total weight of the mixture and P_b be the bitumen content expressed as a ratio of bitumen weight to total weight. The weight of bitumen is P_bW and the weight of aggregate is $(1 - P_b)W$, as shown on the right side of the diagram. For simplicity, it is assumed that no asphalt is absorbed by the aggregate. If the aggregate is porous and has a significant amount of absorption, the weight of asphalt absorbed should be deducted from W and not used for the computation.

If the specific gravity of the aggregate is G_g and that of the bitumen is G_b, the volumes of the aggregate and bitumen are $(1 - P_b)W/G_g$ and P_bW/G_b, respectively. If the bulk specific gravity of the mixture is G_m, the volume of the mixture is W/G_m. These volumes are shown on the left side of the diagram. By definition, the percent volume of aggregate V_g is

$$V_g = \frac{(1 - P_b)W/G_g}{W/G_m} \times 100 = \frac{100(1 - P_b)G_m}{G_g} \tag{7.20}$$

The percent volume of bitumen V_b is

$$V_b = \frac{P_bW/G_b}{W/G_m} \times 100 = \frac{100P_bG_m}{G_b} \tag{7.21}$$

The percent volume of air void V_a is

$$V_a = 100 - V_g - V_b \tag{7.22}$$

If the aggregate is a combination of several fractions, each with a different specific gravity, the average specific gravity of the aggregate is

$$G_g = \frac{100}{P_1/G_1 + P_2/G_2 + \ldots + P_n/G_n} \tag{7.23}$$

in which $P_1, P_2, \ldots, P_n$ is the percentage by weight of each fraction, and G_1, G_2, G_n is the specific gravity of each fraction. Note that the specific gravities to be used in the

Downloaded From : www.EasyEngineering.net

Downloaded From : www.EasyEngineering.net

above equations are the bulk specific gravity for the aggregates and the mixtures and the apparent specific gravity for the bitumen and the mineral filler. The apparent specific gravity, which is based on the solid volume only, is larger than the bulk specific gravity, which is based on the total volume including the air void.

Example 7.8:

An asphalt mixture has a bitumen content of 5.5% by weight and a bulk specific gravity of 2.43. The specific gravity of bitumen is 1.02 and that of aggregate is 2.85. If the stiffness modulus of bitumen is 2×10^8 N/m^2 (2.9×10^4 psi), estimate the stiffness modulus of the mixture.

Solution: From Eq. 7.20, $V_g = 100 \times (1 - 0.055) \times 2.43/2.85 = 80.6\%$. From Eq. 7.21, $V_b = 100 \times 0.055 \times 2.43/1.02 = 13.1\%$. The stiffness modulus of the mixture is 1.1×10^{10}N/m^2 (1.6×10^6 psi) and can be read from Figure 7.20, as indicated by the dashed lines.

Bonnaure *et al.* (1977) also developed the following equations for predicting the stiffness modulus of the mix S_m, based on V_g, V_b, and the stiffness modulus of the bitumen S_b:

$$\beta_1 = 10.82 - \frac{1.342(100 - V_g)}{V_g + V_b} \tag{7.24a}$$

$$\beta_2 = 8.0 + 0.00568V_g + 0.0002135V_g^2 \tag{7.24b}$$

$$\beta_3 = 0.6 \log\left(\frac{1.37V_b^2 - 1}{1.33V_b - 1}\right) \tag{7.24c}$$

$$\beta_4 = 0.7582\,(\beta_1 - \beta_2) \tag{7.24d}$$

For 5×10^6 N/m$^2 < S_b < 10^9$ N/m^2,

$$\log S_m = \frac{\beta_4 + \beta_3}{2}(\log S_b - 8) + \frac{\beta_4 - \beta_3}{2}|\log S_b - 8| + \beta_2 \tag{7.25a}$$

For 10^9 N/m$^2 < S_b < 3 \times 10^9$ N/m^2,

$$\log S_m = \beta_2 + \beta_4 + 2.0959(\beta_1 - \beta_2 - \beta_4)(\log S_b - 9) \tag{7.25b}$$

Equation 7.25 is based on SI units with S_m and S_b in N/m^2. If S_m and S_b are in psi, Eq. 7.26 should be used. For 725 psi $< S_b <$ 145,000 psi,

$$\log S_m = \frac{\beta_4 + \beta_3}{2}(\log S_b - 4.1612) + \frac{\beta_4 - \beta_3}{2}|\log S_b - 4.1612| + \beta_2 - 3.8383 \tag{7.26a}$$

For 145,000 psi $< S_b <$ 435,000 psi,

$$\log S_m = \beta_2 + \beta_4 + 2.0959(\beta_1 - \beta_2 - \beta_4)(\log S_b - 5.1612) - 3.8388 \tag{7.26b}$$

Downloaded From : www.EasyEngineering.net

Downloaded From : www.EasyEngineering.net

Example 7.9:

For the nine cases with values of S_b, V_b, and V_g shown in Table 7.6, determine the stiffness modulus of the mixtures by Eqs. 7.24 and 7.25 and compare with the nomograph solutions.

TABLE 7.6 Stiffness Modulus of Mixtures with Various Compositions

Case no.	S_b (N/m^2)	V_b (%)	V_g (%)	S_m (N/m^2) Equation	S_m (N/m^2) Nomograph
1	6×10^6	5	80	1.5×10^9	1.3×10^9
2	6×10^6	10	85	1.8×10^9	1.7×10^9
3	6×10^6	40	60	8.3×10^7	9.0×10^7
4	1×10^8	5	80	6.6×10^9	6.9×10^9
5	1×10^8	10	85	1.1×10^{10}	1.1×10^{10}
6	1×10^8	40	60	1.3×10^9	1.3×10^9
7	2×10^9	5	80	2.8×10^{10}	2.7×10^{10}
8	2×10^9	10	85	3.6×10^{10}	4.8×10^{10}
9	2×10^9	40	60	1.5×10^{10}	1.7×10^{10}

Note. 1 psi = 6900 N/m^2.

Solution: For case 1 with an extremely small S_b of 6×10^6 N/m^2 (870 psi), the detailed calculations by the formulas are shown below. From Eq. 7.24, $\beta_1 = 10.82 - 1.342\,(100 - 80)/(80 + 5) = 10.504$, $\beta_2 = 8.0 + 0.00568 \times 80 + 0.0002135(80)^2 = 9.821$, $\beta_3 = 0.6 \log [(1.37 \times 25 - 1)/(1.33 \times 5 - 1)] = 0.462$, $\beta_4 = 0.7582(10.504 - 9.821) = 0.518$. From Eq. 7.25*a*, $\log S_m = 0.5(0.518 + 0.462)[\log(6 \times 10^6) - 8] + 0.5(0.518 - 0.462)|\log(6 \times 10^6) - 8| + 9.821 = 9.188$, or $S_m = 1.5 \times 10^9$ N/m^2 (2.6×10^5 psi), which compares with 1.3×10^9 N/m^2 (1.9×10^5 psi) from the nomograph. The comparison of S_m obtained from the equations and the nomograph is shown at the right of Table 7.6. It can be seen that both solutions check quite well in most cases. However, for some extreme cases, a large discrepancy exists between the two solutions. Note that Eq. 7.25*a* should be used for cases 1 to 6 and Eq. 7.25*b* for cases 7 to 9.

According to Shell International Petroleum (1978), the accuracy of the nomograph, as checked by extensive measurements on a large number of different asphalt mixes, is a factor of 1.5 to 2, which is sufficient for practical design. Therefore, the use of Eqs. 7.24 and 7.25 to estimate the modulus in a computerized method of design should be considered acceptable.

Asphalt Institute Formulas In developing the DAMA computer program for the Asphalt Institute, Hwang and Witczak (1979) applied the following regression formulas to determine the dynamic modulus of HMA, $|E^*|$:

$$|E^*| = 100{,}000 \times 10^{\beta_1} \tag{7.27a}$$

$$\beta_1 = \beta_3 + 0.000005\,\beta_2 - 0.00189\,\beta_2 f^{-1.1} \tag{7.27b}$$

$$\beta_2 = \beta_4^{0.5}\,T^{\beta_5} \tag{7.27c}$$

Downloaded From : www.EasyEngineering.net

Downloaded From : www.EasyEngineering.net

$$\beta_3 = 0.553833 + 0.028829\,(P_{200}f^{-0.1703}) - 0.03476V_a + 0.070377\lambda + 0.931757f^{-0.02774} \quad (7.27d)$$

$$\beta_4 = 0.483V_b \quad (7.27e)$$

$$\beta_5 = 1.3 + 0.49825 \log f \quad (7.27f)$$

In these equations, β_1 to β_5 are temporary constants, f is the load frequency in Hz, T is the temperature in °F, P_{200} is the percentage by weight of aggregate passing through a No. 200 sieve, V_v is the volume of air void in %, λ is the asphalt viscosity at 70°F in 10^6 poise, and V_b is the volume of bitumen in %. If sufficient viscosity data are not available to estimate λ at 70°F, one may use the equation

$$\lambda = 29{,}508.2\,(P_{77°F})^{-2.1939} \quad (7.28)$$

in which $P_{77°F}$ is the penetration at 77°F (25°C). It can be seen that the factors considered by Asphalt Institute are mostly the same as those by Shell, with the following exceptions:

1. The percentage of fines passing through a No. 200 sieve is considered by AI but not by Shell.
2. The viscosity or penetration of asphalt considered by Shell is determined from the recovered asphalt, or the asphalt actually present in the mix, while that by AI is the original asphalt.
3. The temperature and the viscosity of asphalt are considered by AI, whereas the normalized temperature, which is the temperature above or below $T_{R\&B}$, and the penetration index, which indicates the temperature sensitivity of the asphalt, are used by Shell.

Example 7.10:

An asphalt cement has an original penetration of 70 at 77°F (25°C), a reduced penetration of 50 after being recovered from the mix, and a ring and ball softening point of 140°F (60°C). The mix containing the asphalt has an asphalt volume of 11%, an air void volume of 5%, and 6% of aggregates passing through a No. 200 sieve. Determine the dynamic modulus of the mix at a temperature of 77°F (25°C) and a frequency of 8 Hz by the AI equations and compare with the stiffness modulus of the mix by the Shell nomographs. What are the values of $|E^*|$ when the percentages passing through a No. 200 sieve are 1 and 11%, respectively.

Solution: First consider the AI method. With $P_{77°F} = 70$, from Eq. 7.28, $\lambda = 29{,}508.2 \times 70^{-2.1939} = 2.64 \times 10^6$ poise. Given $f = 8$ Hz, $T = 77°F$ (25°C), $P_{200} = 6\%$, $V_v = 5\%$, $\lambda = 2.64 \times 10^6$ poise and $V_b = 11\%$, from Eq. 7.27, $\beta_5 = 1.3 + 0.49825 \log 8 = 1.750$, $\beta_4 = 0.483 \times 11 = 5.313$, $\beta_3 = 0.553833 + 0.028829 \times 6 \times (8)^{-0.1703} - 0.03476 \times 5 + 0.070377 \times 2.64 + 0.931757 \times (8)^{-0.02774} = 1.567$, $\beta_2 = (5.313)^{0.5} \times (77)^{1.750} = 4613.5$, $\beta_1 = 1.567 + 0.000005 \times 0.000005 \times 4613.5 - 0.00189 \times 4613.5 \times (8)^{-1.1} = 0.705$, and $|E^*| = 100{,}000 \times (10)^{0.705} = 5.07 \times 10^5$ psi (3.5 GPa).

Next consider the Shell method. With $P_{77°F} = 50$ for recovered asphalt and $T_{R\&B} = 60°C$ (140°F), from Eq. 7.18, $A = (\log 50 - \log 800)/(25 - 60) = 0.0344$; from Eq. 7.16, PI $= (20 - 500 \times 0.0344)/(1 + 50 \times 0.0344) = 1.029$. With a frequency of 8 Hz, a temperature

Downloaded From : www.EasyEngineering.net

Downloaded From : www.EasyEngineering.net

difference of 60 − 25 = 35°C (95°F) and a penetration index of 1.029, from Figure 7.19, $S_b = 10^7$ N/m^2 (1450 psi). With $S_b = 10^7$ N/m^2 (1450 psi), $V_b = 11\%$, and $V_g = 100 - 11 - 5 = 84\%$, from Figure 7.20, $S_m = 2.1 \times 10^9$ N/m^2(3.1×10^5 psi), which compares with 3.5×10^9 N/m^2 (5.1×10^5 psi) from the AI equations.

If $P_{200} = 1\%$, from Eq. 7.27, $\beta_3 = 0.553833 + 0.028829 \times 1 \times (8)^{-0.1703} - 0.03476 \times 5 + 0.070377 \times 2.64 + 0.931757 \times (8)^{-0.02774} = 1.466$, $\beta_1 = 1.466 + 0.000005 \times 4613.5 - 0.00189 \times 4613.5 \times (8)^{-1.1} = 0.604$, and $|E^*| = 100{,}000 \times (10)^{0.604} = 4.0 \times 10^5$ psi (2.7 GPa). If $P_{200} = 11\%$, from Eq. 7.27, $\beta_3 = 1.668$, $\beta_1 = 0.806$, and $|E^*| = 6.4 \times 10^5$ psi (4.4 GPa).

It can be seen that the dynamic modulus increases with the increase in fine contents. An increase of the percentage passing through a No. 200 sieve from 1 to 11% increases the dynamic modulus from 4.0×10^5 to 6.4×10^5 psi (2.7 to 4.4 GPa). This change is quite small compared to other factors such as temperature, viscosity, frequency, and the volume concentration of bitumen and aggregate.

Typical Ranges Table 7.7 shows the typical ranges of an HMA modulus at different temperatures and load frequencies. As indicated previously, a frequency of 8 Hz is equivalent to a speed about 35 mph.

7.3 FATIGUE CHARACTERISTICS

Fatigue of bituminous mixtures and Portland cement concrete under repeated flexure is an important factor of pavement design. In this section, the use of laboratory fatigue tests, nomographs, and equations to predict the fatigue life is discussed.

7.3.1 Bituminous Mixtures

A variety of methods have been developed for the fatigue testing of bituminous mixtures. Most of the methods employ the bending of beams, although the bending of plates has also been used (Jimenez and Gallaway, 1962; Jimenez, 1972). In the beam tests, a simple beam with third-point (Deacon, 1965) or center-point loading (Franchen and Verstraeten, 1974) or a cantilever beam with rotating bending (Pell, 1962) has been used. The repeated load indirect tensile test has also been employed (Adedimila and Kennedy, 1976). In this section, only the beam test with third-point loading is described. The advantage of

TABLE 7.7 Typical Values of Dynamic Modulus for HMA

	Load frequency (Hz)					
	1		4		16	
Temperature (°F)	Range	Mean	Range	Mean	Range	Mean
40	6.0–18.0	12.0	9.0–27.0	16.0	10.0–30.0	18.0
70	2.0–6.0	3.0	4.0–9.0	5.0	5.0–11.0	7.0
100	0.5–1.5	0.7	0.7–2.2	1.0	1.0–3.2	1.6

Note. Modulus in terms of 10^5 psi, 1 psi = 6.9 kPa.

Downloaded From : www.EasyEngineering.net

Downloaded From : www.EasyEngineering.net

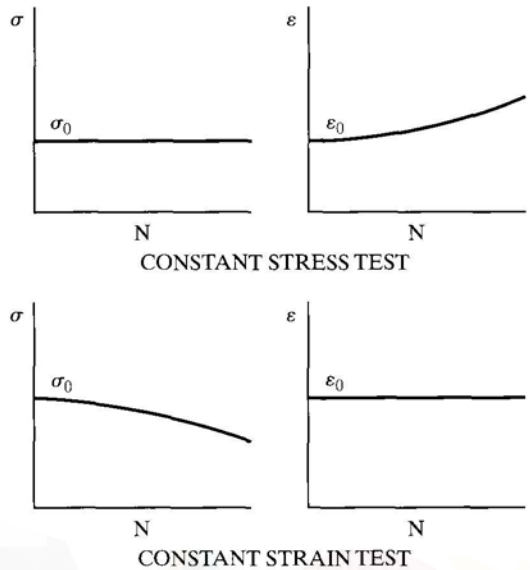


FIGURE 7.22
Two types of controlled loading for fatigue testing.

third-point loading over the center-point loading is the existence of a constant bending moment over the middle third of the specimen, so any weak spot due to nonuniform material properties will show up in the test results. In view of the fact that fatigue tests are expensive and require a large number of specimens, nomographs and equations for predicting fatigue life are also presented.

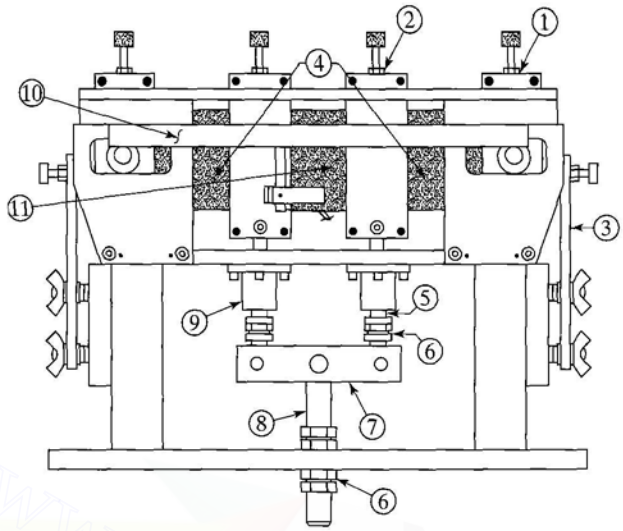
Test Procedures Two types of controlled loading can be applied: constant stress and constant strain, as shown in Figure 7.22. In the constant stress test, the stress remains constant but the strain increases with the number of repetitions. In the constant strain test, the strain is kept constant, and the load or stress is decreased with the number of repetitions. The constant stress type of loading is applicable to thicker pavements, wherein the HMA is more than 6 in. (152 mm) thick and is the main load-carrying component. As the HMA becomes weaker under repeated loads, the strain should increase with the number of repetitions. The constant strain type of loading is applicable to thin pavements with HMA less than 2 in. (51 mm) thick because the strain in the asphalt layer is governed by the underlying layers and is not affected by the decrease in stiffness of HMA. For intermediate thicknesses, a combination of constant stress and constant strain exists.

As can be seen in Figure 7.22, both stress and strain are larger in the constant stress test, so the use of constant stress is more conservative. The use of constant stress has the further advantage that failure occurs more quickly and can be more easily defined, while an arbitrary failure criterion, such as a stress equal to 50% of the initial stress, is frequently used for the constant strain test.

Figure 7.23 is a schematic diagram of the fatigue testing equipment. The load is applied upward through the piston rod to a beam specimen, 15 in. (310 mm) long with a width and depth not exceeding 3 in. An electrohydraulic or pneumatic testing machine

Downloaded From : www.EasyEngineering.net

Downloaded From : www.EasyEngineering.net



1. Reaction Clamp
2. Load Clamp
3. Restrainer
4. Specimen
5. Loading Rod
6. Stop Nuts
7. Load Bar
8. Piston Rod
9. Ball Bushing
10. LVDT Holder
11. LVDT

FIGURE 7.23
Fatigue testing equipment.

capable of applying repeated tension–compression loads in the form of haversine waves for 0.1-s duration with 0.4-s rest periods can be used. A sufficient load, approximately 10% of the upward load, is applied in the downward direction, forcing the beam to return to its original horizontal position and holding it at that position during the rest period. Adjustable stop nuts installed on the loading rods prevent the beam from bending below the initial horizontal position during the rest period. The dynamic deflection of the beam at the midspan is measured with a linear variable differential transformer (LVDT). The LVDT core is attached to a nut bonded with epoxy cement to the center of the specimen. The repeated flexure apparatus is enclosed in a controlled temperature cabinet.

A range of stresses should be selected so that the specimens will fail within a range from 1000 to 1,000,000 repetitions. Normally, 8 to 12 specimens are required to establish the fatigue relationship for a given temperature. Tests at several different temperatures are required so the effect of stiffness or temperature on the fatigue life can be evaluated.

Analysis The stiffness modulus and the initial strain of each test are determined at the 200th repetition by using Eqs. 7.10 and 7.11, respectively. The initial strains are plotted versus the number of repetitions to failure on log scales. The plot can be approximated by a straight line, as shown in Figure 7.24 and expressed by

$$N_f = c_2(\epsilon_t)^{-f_2} \tag{7.29}$$

in which N_f is the number of repetitions to failure, c_2 is a fatigue constant that is the value of N_f when $\epsilon_t = 1$, and f_2 is the inverse slope of the straight line. Under the same

Downloaded From : www.EasyEngineering.net

Downloaded From : www.EasyEngineering.net

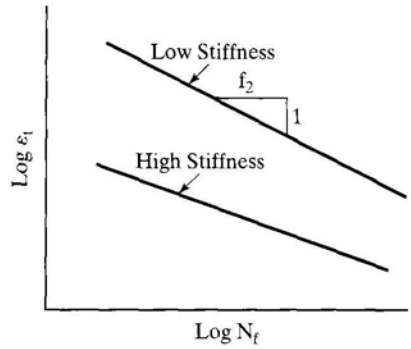


FIGURE 7.24
Relationship between strain and number of repetitions to failure.

initial strain, laboratory tests show that the number of repetitions to failure decreases with the increase in stiffness modulus, so Eq. 7.29 can also be written as

$$N_f = c_1(\epsilon_t)^{-f_2}(E_s)^{-f_3} \tag{7.30}$$

Note that Eq. 7.30 is similar to Eq. 3.6. However, Eq. 7.30 is based purely on laboratory fatigue tests, whereas Eq. 3.6 is the extension from laboratory specimens to actual prototype pavements. The factor f_1 for prototype pavements should be much greater than c_1 for laboratory specimens due to the fact that wheel loads on actual pavements do not apply at the same location and have longer rest periods, both of which increase the fatigue life. Also, for thicker pavements, it takes more repetitions for cracks to appear on the surface to be considered as failure. The Asphalt Institute's fatigue criterion is based on the assumption that f_1 is 18.4 times greater than c_1.

Example 7.11:

Fatigue tests were performed on 3-in. × 3-in. (75-mm × 75-mm) beams by the third-point loading with a span of 12 in. (305 mm). The deflection at the center of beam Δ and the number of repetitions to failure N_f are shown in Table 7.8. Develop an equation relating the number of repetitions to failure and the tensile strain.

TABLE 7.8 Results of Fatigue Tests on HMA Specimens

	Test no.							
	1	2	3	4	5	6	7	8
Δ (0.001 in.)	12.9	8.03	8.24	6.03	4.42	2.81	1.97	1.48
N_f	1110	3140	4115	6010	30,625	89,970	289,110	915,060

Note. 1 in. = 25.4 mm.

Solution: The tensile strain for each test can be determined from Eq. 7.11, or $\epsilon_t = 12 \times 3 \times \Delta/(3 \times 144 - 4 \times 16) = 0.0978\Delta$. The strains for the eight tests are 12.6, 7.85, 8.06, 5.90, 4.32, 2.75, 1.93, and 1.45×10^{-4}. Figure 7.25 is a plot of ϵ_t versus log N_f.

Downloaded From : www.EasyEngineering.net

Downloaded From : www.EasyEngineering.net

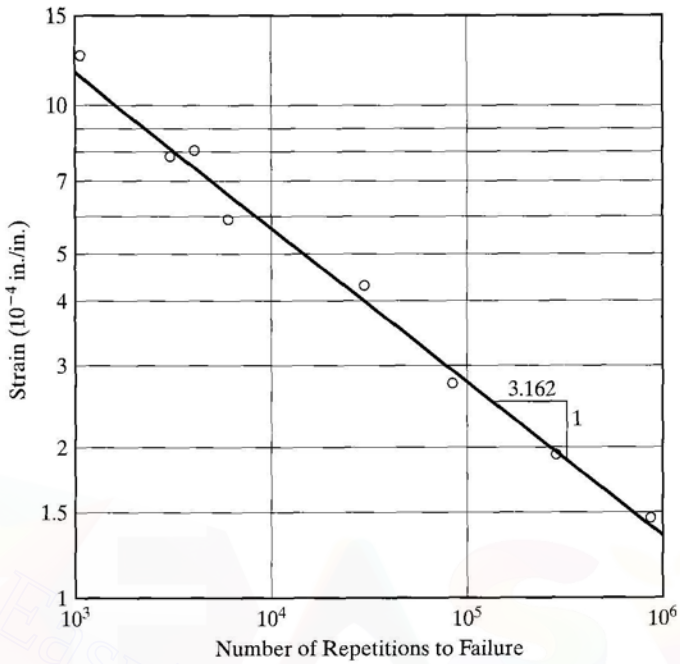


FIGURE 7.25
Example 7.11.

The inverse slope of the straight line $f_2 = 3/\log(11.9/1.34) = 3.162$. The intercept c_1 when $\epsilon_t = 1$ can be obtained from a given point ($\log \epsilon_t$, $\log N_f$) on the straight line by

$$f_2 = \frac{\log N_f - \log c_1}{\log 1 - \log \epsilon_t}$$

or

$$\log c_1 = \log N_f + f_2 \log \epsilon_t \tag{7.31}$$

Given $f_2 = 3.162$, $N_f = 1000$, and $\epsilon_t = 11.9 \times 10^{-4}$, from Eq. 7.31, $\log c_1 = \log(1000) + 3.162 \log(0.00119) = -6.247$ or $c_1 = 5.66 \times 10^{-7}$. Therefore, the fatigue equation is

$$N_f = 5.66 \times 10^{-7}(\epsilon_t)^{-3.162}$$

Nomographs and Equations The fatigue test is a destructive test and is much more time-consuming than the nondestructive resilient modulus test. To obtain Eq. 7.30, more than two dozen specimens need to be tested. There is a need to estimate the fatigue properties by simple nomographs and equations without actually performing the fatigue tests.

Based on 146 fatigue lines covering a wide range of mixes, bitumens, and testing conditions, Shell (Bonnaure *et al.*, 1980) developed separate equations for constant

Downloaded From : www.EasyEngineering.net

Downloaded From : www.EasyEngineering.net

stress and constant strain tests. For constant stress tests,

$$\epsilon_t = [36.43\text{PI} - 1.82\text{PI}(V_b) + 9.71V_b - 24.04] \times 10^{-6}\left(\frac{S_m}{5 \times 10^9}\right)^{-0.28}\left(\frac{N_f}{10^6}\right)^{-0.2} \tag{7.32}$$

in which ϵ_t is the tensile strain, PI is the penetration index defined by Eq. 7.16, V_b is the percentage of bitumen volume in the mix, S_m is the stiffness modulus of the mix in N/m^2 as determined from Figure 7.20, and N_f is the number of repetitions to failure. If S_m is in psi, Eq. 7.32 can be written as

$$N_f = [0.0252\text{PI} - 0.00126\text{PI}(V_b) + 0.00673V_b - 0.0167]^5\, \epsilon_t^{-5}\, S_m^{-1.4} \tag{7.33}$$

For constant strain tests,

$$\epsilon_t = [36.43\text{PI} - 1.82\text{PI}(V_b) + 9.71V_b - 24.04] \times 10^{-6}\left(\frac{S_m}{5 \times 10^{10}}\right)^{-0.36}\left(\frac{N_f}{10^6}\right)^{-0.2} \tag{7.34}$$

If S_m is in psi, Eq. 7.34 can be written as

$$N_f = [0.17\text{PI} - 0.0085\text{PI}(V_b) + 0.0454V_b - 0.112]^5\, \epsilon_t^{-5}\, S_m^{-1.8} \tag{7.35}$$

The solutions of the above equations can be presented in a nomograph, as shown in Figure 7.26. The accuracy of the equations for constant stress tests was reported within ±40% for 90% of the results and that for constant strain tests within ±50%.

Example 7.12:

Given $V_b = 13\%$, PI $= -0.7$, and $S_m = 3.3 \times 10^9$ N/m^2, determine the initial strains when failure occurs at 10^6 cycles of constant stress and 10^5 cycles of constant strain by using both the equations and the nomograph.

Solution: For constant stress tests, from Eq. 7.32, $\epsilon_t = [36.43(-0.7) - 1.82(-0.7) \times 13 + 9.71 \times 13 - 24.04] \times 10^{-6} \times [(3.3 \times 10^9)/(5 \times 10^9)]^{-0.28} \times (10^6/10^6)^{-0.2} = 1.1 \times 10^{-4}$. For constant strain tests, from Eq. 7.34, $\epsilon_t = [36.43(-0.7) - 1.82(-0.7) \times 13 + 9.71 \times 13 - 24.04] \times 10^{-6} \times [(3.3 \times 10^9)/(5 \times 10^{10})]^{-0.36} \times (10^5/10^6)^{-0.2} = 4.0 \times 10^{-4}$. The initial strains obtained from the nomograph shown in Figure 7.26 are 1.1×10^{-4} for the constant stress test and 4.2×10^{-4} for the constant strain test.

The laboratory fatigue equations developed by the Asphalt Institute (AI, 1982) are based on the constant stress criterion and can be expressed as

$$N_f = 0.00432C\epsilon_t^{-3.291}|E^*|^{-0.854} \tag{7.36}$$

in which

$$C = 10^M \tag{7.37a}$$

Downloaded From : www.EasyEngineering.net

Downloaded From : www.EasyEngineering.net

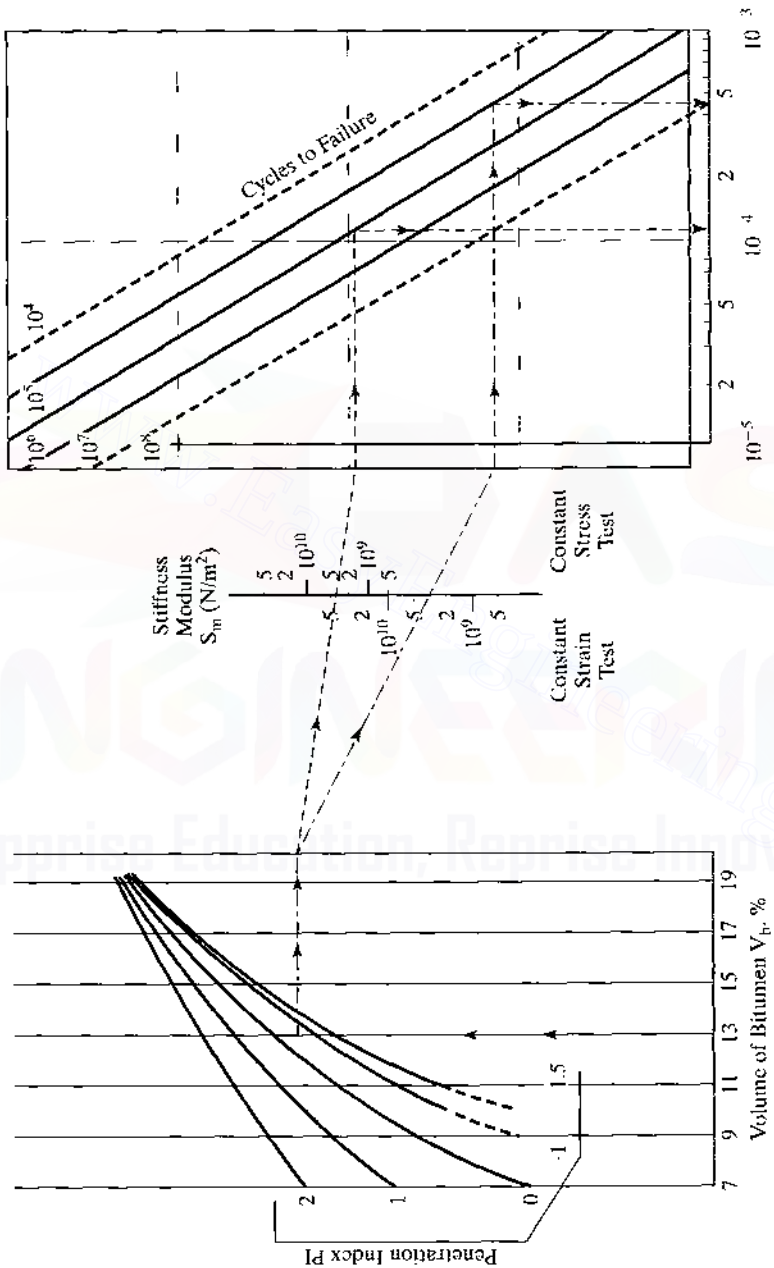


FIGURE 7.26
Nomograph for predicting fatigue life of bituminous mixes. (After Bonnaure *et al.* (1980).)

Downloaded From : www.EasyEngineering.net

Downloaded From : www.EasyEngineering.net

is the correction factor and

$$M = 4.84\left(\frac{V_b}{V_a + V_b} - 0.69\right) \tag{7.37b}$$

Note that, for a standard mix with an asphalt volume V_b of 11% and an air void volume of 5%, $M = 0$ or $C = 1$. This standard mix is used by the Asphalt Institute in the ninth edition of the design manual (AI, 1981a). After multiplying by a factor of 18.4 to account for the differences between laboratory and field conditions, the fatigue failure criterion becomes

$$N_f = 0.0796\epsilon_t^{-3.291}|E^*|^{-0.854} \tag{7.38}$$

in which $|E^*|$ is the dynamic modulus, which is equivalent to the elastic modulus of the asphalt layer in a layer system or the stiffness modulus in the Shell method. A comparison of Eq. 7.38 with Eq. 7.33 shows that the exponents in Eq. 7.38 are somewhat smaller than those in Eq. 7.33. This is not surprising in view of the large variability inherent in the fatigue tests.

7.3.2 Portland Cement Concrete

A fatigue test of portland cement concrete usually applies a repeated flexural loading on beam specimens 15 in. (381 mm) long, 3 in. (76 mm) wide, and 3 in. (76 mm) deep. Loading is generally applied at the third points, with a rate of 1 to 2 repetitions per second and a duration of 0.1 s. The extreme fiber stress in the beam is computed by Eq. 7.9. The number of repetitions to failure in log scale, log N_f, is plotted against the stress ratio, which is a quotient of the stress σ and the modulus of rupture of the concrete S_c. The modulus of rupture is determined by the same beam test, but with a steadily increasing static load, as specified by ASTM (1989a) in "C78-84 Standard Test Method for Flexural Strength of Concrete Using Simple Beam with Third Point Loading."

Figure 7.27 shows the fatigue data obtained by several investigators. It is speculated that concrete will not fail by fatigue when the stress ratio is smaller than 0.5, although no real limit has been found up to 10–20 million repetitions. The average line for 50% probability of failure is shown by the solid line in Figure 7.27 and expressed as

$$\log N_f = 17.61 - 17.61\left(\frac{\sigma}{S_c}\right) \tag{7.39}$$

Note that Eq. 7.39 is the same as Eq. 5.35 with $f_1 = 17.61$ and $f_2 = 17.61$. In the design of zero-maintenance pavements, Darter and Barenberg (1977) recommended the reduction of f_1 by one order of magnitude, to 16.61. The design curve used by the Portland Cement Association, as indicated by Eq. 5.36, is shown by the broken line. It can be seen that the PCA fatigue curve lies below most of the failure points and is very conservative.

7.4 PERMANENT DEFORMATION PARAMETERS

Permanent deformation is an important factor in flexible pavement design. With the increase in traffic load and tire pressure, most of the permanent deformation occurs in

Downloaded From : www.EasyEngineering.net

Downloaded From : www.EasyEngineering.net

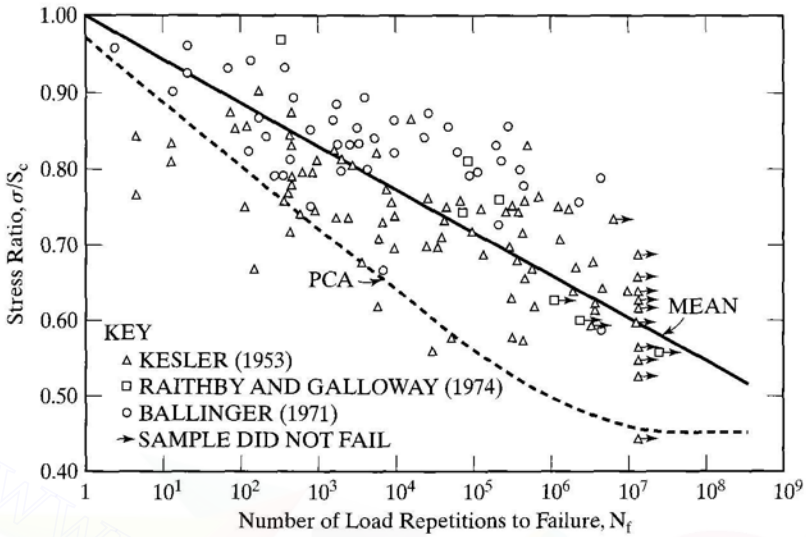


FIGURE 7.27

Results of fatigue tests on concrete from different sources.

the upper layers rather than in the subgrade. To estimate the rut depth, it is necessary to determine the permanent deformation parameters of the material for each layer.

Various methods have been used to determine the permanent deformation of paving materials. Most methods employ the repeated load test, which is similar to the resilient modulus test except that loads up to 100,000 repetitions have been applied and the permanent deformations at a number of designated cycles have been recorded.

7.4.1 Basic Principles

The permanent deformation of paving materials depends strongly on the testing methods and the procedures used for fabricating and testing the specimens. These variations, together with the uncertainty in traffic and environmental conditions, make the prediction of rut depth extremely difficult. Therefore, the use of simplified methods is warranted.

Direct Method When the load is applied over a circular area, the maximum deformation occurs directly under the center of the area. The rut depth on the pavement surface can be determined by the following direct method:

1. Divide the pavement and subgrade into a number of layers, and estimate the vertical and radial stresses at the midheight of each layer.
2. Using the vertical stress due to the applied load as the repeated deviator stress and the radial stress due to the applied load and the overburden combined as the confining pressure, conduct repeated load tests on laboratory specimens that represent the actual materials in the field and determine the permanent strains under a large number of load repetitions.

Downloaded From : www.EasyEngineering.net

Downloaded From : www.EasyEngineering.net

3. Compute the vertical deformation of each layer under any given number of repetitions by multiplying the permanent strains obtained from the laboratory tests with the thickness of the layer.
4. Sum the permanent deformation over all layers to obtain the rut depth on the surface.

Unless an equivalent single-axle load and an average set of material properties are used throughout the design period, it is not possible to apply the above method, because the stresses in each layer can be any values, depending on the axle loads and the environmental conditions throughout the year. A more practical approach is to perform a large number of permanent deformation tests under various stress and environment conditions and develop regression equations relating permanent strains to these conditions. These regression equations can then be incorporated into a multilayer computer program to compute the rut depth, as illustrated by Allen and Deen (1986).

The division of a pavement system into a large number of layers is cumbersome, and the development of regression equations for each paving material is expensive and time-consuming. The original VESYS program (FHWA, 1978) used the following simple method to characterize the permanent deformation properties, although a direct method was later added as another option.

VESYS Method The method incorporated in the VESYS computer program for the prediction of rut depth is based on the assumption that the permanent strain is proportional to the resilient strain by

$$\epsilon_p(N) = \mu\epsilon N^{-\alpha} \tag{7.40}$$

in which $\epsilon_p(N)$ is the permanent or plastic strain due to a single load application (i.e., at the Nth application); ϵ is the elastic or resilient strain at the 200th repetition; N is the load application number; μ is a permanent deformation parameter representing the constant of proportionality between permanent and elastic strains; and α is a permanant deformation parameter indicating the rate of decrease in permanent deformation as the number of load applications increases. The total permanent deformation can be obtained by integrating Eq. 7.40:

$$\epsilon_p = \int_0^N \epsilon_p(N)\, dN = \epsilon\mu \frac{N^{1-\alpha}}{1-\alpha} \tag{7.41}$$

Equation 7.41 indicates that a plot of $\log \epsilon_p$ versus $\log N$ results in a straight line, as shown in Figure 7.28. From Eq. 7.41,

$$\log \epsilon_p = \log\left(\frac{\epsilon\mu}{1-\alpha}\right) + (1-\alpha)\log N \tag{7.42}$$

So the slope of the straight line $S = 1 - \alpha$, or

$$\alpha = 1 - S \tag{7.43}$$

Downloaded From : www.EasyEngineering.net

Downloaded From : www.EasyEngineering.net

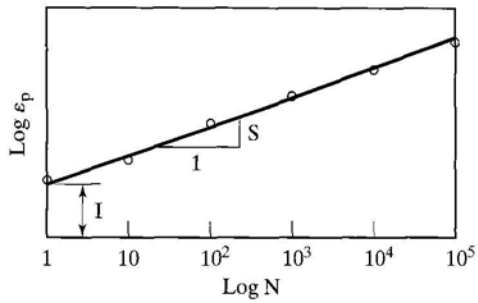


FIGURE 7.28
Log–log plot of permanent strain versus number of load repetitions.

The intercept occurs at $N = 1$, $I = \epsilon\,\mu/(1 - \alpha)$, so

$$\mu = \frac{IS}{\epsilon} \tag{7.44}$$

To determine the permanent deformation parameters of the layer system, α_{sys} and μ_{sys}, from those of the individual layers, it is further assumed that the sum of permanent and recoverable strains due to each load application is a constant and equals the elastic strain at the 200th repetition. This means that, after the 200th repetition,

$$\epsilon = \epsilon_p(N) + \epsilon_r(N) \tag{7.45}$$

in which $\epsilon_r(N)$ is the recoverable strain due to each load application. Substituting Eq. 7.40 into Eq. 7.45 yields

$$\epsilon_r(N) = \epsilon(1 - \mu N^{-\alpha}) \tag{7.46}$$

Under the same stresses, strains are inversely proportional to the moduli, so Eq. 7.46 can be written as

$$E_r(N) = \frac{E}{1 - \mu N^{-\alpha}} = \frac{EN^{\alpha}}{N^{\alpha} - \mu} \tag{7.47}$$

in which $E_r(N)$ is the elastic modulus due to unloading and E is the elastic modulus due to loading. Note that $E_r(N)$, which is the unloading modulus for each individual layer, is not a constant, but increases with the increase of load repetitions. These unloading moduli are used to determine the recoverable deformation $w_r(N)$ at different values of N. The permanent deformation $w_p(N)$ can then be computed by

$$w_p(N) = w - w_r(N) \tag{7.48a}$$

in which w is the elastic deformation due to loading. Similar to Eq. 7.40, $w_p(N)$ can be expressed by

$$w_p(N) = \mu_{sys} w N^{-\alpha_{sys}} \tag{7.48b}$$

Combining Eqs. 7.48*a* and *b* gives

$$1 - \frac{w_r(N)}{w} = \mu_{sys} N^{-\alpha_{sys}} \tag{7.49}$$

Downloaded From : www.EasyEngineering.net

Downloaded From : www.EasyEngineering.net

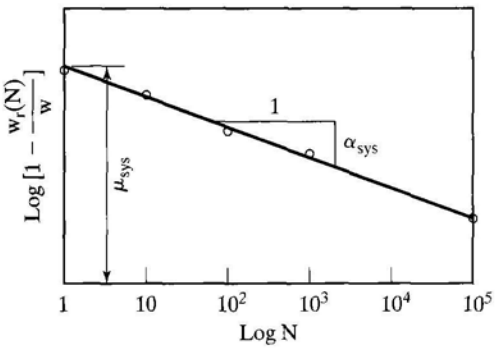


FIGURE 7.29

Log–log plot of $[1 - w_r(N)/w]$ versus number of load repetitions.

Equation 7.49 shows that a plot of $\log[1 - w_r(N)/w]$ versus $\log N$ results in a straight line, as shown in Figure 7.29. The slope of the straight line is α_{sys} and the intercept at $N = 1$ is $\log \mu_{sys}$.

The determination of α_{sys} and μ_{sys} from the α and μ of each layer can be summarized as follows:

1. Assume several values of N, say 1, 10, 10^2, 10^3, 10^4, and 10^5, and determine the unloading modulus $E_r(N)$ of each layer by Eq. 7.47.
2. Using the unloading moduli as the elastic moduli, determine the recoverable deformation $w_r(N)$ at the surface by the layered theory.
3. For each N, compute $1 - w_r(N)/w$ and plot it against N on log scales.
4. Fit the plotted points by a least-squares line. The slope of the line is α_{sys} and the intercept at $N = 1$ is μ_{sys}.
5. Determine the permanent deformation by Eq. 7.48*b*.

Because α and μ may change with the temperature of bituminous mixtures and the state of stresses, the VESYS IV-B program can input different values of α and μ for different temperatures and loadings to account for nonlinear effects.

Example 7.13:

A circular load of radius a and intensity q is applied on the surface of a homogeneous half-space with elastic modulus E, Poisson ratio ν, and permanent deformation parameters α and μ. Derive an equation for determining the permanent deformation at the center of the loaded area as a function of the number of load applications.

Solution: The elastic deformation can be obtained from Eq. 2.8:

$$w = \frac{2(1 - \nu^2)qa}{E}$$

From Eq. 7.47, the unloading modulus is

$$E_r(N) = \frac{EN^{\alpha}}{N^{\alpha} - \mu}$$

Downloaded From : www.EasyEngineering.net

Downloaded From : www.EasyEngineering.net

and the elastic deformation due to unloading is

$$w_r = \frac{2(1-\nu^2)qa(N^\alpha - \mu)}{EN^\alpha}$$

From Eq. 7.48*a*, the permanent deformation is

$$w_p(N) = \frac{2(1-\nu^2)qa}{E}\left(1 - \frac{N^\alpha - \mu}{N^\alpha}\right) = \frac{2(1-\nu^2)qa}{E}\mu N^{-\alpha}$$

Note that, for a homogeneous half-space, α_{sys} and μ_{sys} are the same as α and μ, because there is only one material.

Qi and Witczak (1998) used multiple regression to develop the following predictive equations relating α and μ to loading time and rest period, temperature, and stress levels:

$$\alpha = 0.751629 + 0.0438023 \log(t_l) + 0.0231006 \log(t_d) \quad (7.50a)$$

$$\mu = 0.00237082\,(t_l)^{0.0651478}\,(t_d)^{-0.107480}\,(T)^{1.01843}\,(s)^{0.320862} \quad (7.50b)$$

In these equations, t_l = loading time in sec, t_d = rest period in sec, T = temperature in °F, and s = stress in psi.

Field Calibration Because the performance of in-service pavements may deviate significantly from that predicted by use of laboratory calibrated performance models, the calibration of performance prediction models with data from in-service pavements is an important step in developing accurate rutting prediction models. In view of the fact that long-term data on rutting and traffic are not readily available, Ali and Tayabji (2000) proposed a method using transverse profile data now available under the LTPP program to back calculate permanent deformation parameters, α and m, for each component layer. The rutting observed on a pavement surface is an accumulation of the deformation caused by the vertical strains developed in each layer. If pavement layers are thin, the vertical strain at the middle of a layer can be assumed as the average of the layer. Given the lateral traffic load distribution and the cumulative traffic applications, the permanent deformation can be obtained by integrating it over all load groups and all pavement layers, resulting in the expression (similar to Eq. 7.41):

$$\rho_r = \sum_{j=1}^{L} h_j \left\{ \frac{\mu_j}{1-\alpha_j} \sum_{i=1}^{k} \left[\varepsilon_{i,j,r}\,(n_i)^{1-\alpha_j} \right] \right\} \quad (7.50c)$$

Here, ρ_r = permanent deformation at radial distance r from the load, h_j = thickness of layer j, $\varepsilon_{i,j,r}$ = vertical elastic strain at the center of layer j and a radial distance r from the center of load due to one load application of load group i, n_i = number of load applications for load group i, i = load group index from 1 to k, j = layer index from 1 to L, and r = radial distance index. Note that n_i varies from one point to the other along the transverse profile, thus making it possible to calibration α and μ , as illustrated in Figure 7.28.

Downloaded From : www.EasyEngineering.net

Downloaded From : www.EasyEngineering.net

The transverse profile data are measurements of rutting across the pavement travel lanes. If α and μ of each layer are known, the measured surface permanent deformation can be compared with the radial surface permanent deformation computed by Eq. 7.50*c*. Alternatively, α and μ of each layer can be back calculated by least square so that the difference between observed and computed permanent deformation will be minimum.

7.4.2 Types of Tests

Three different types of compression tests, *viz.*, incremental static, dynamic, and creep tests, are described. The test equipment and setup are the same as those used for the resilient modulus tests described previously. The specimens are usually 4 in. (101 mm) in diameter and 8 in. (203 mm) in height. The incremental static test is applicable only to bituminous mixtures and fine-grained soils that exhibit a predominant amount of viscous flow, while the dynamic and creep tests can be applied to all kinds of materials. In performing the tests, care should be taken to assure that test results reflect the effects of stress state, temperature, moisture content, and other conditions corresponding to those of the pavement in situ. The VESYS manual recommends the use of an unconfined test with an axial stress of 20 psi (138 kPa) for bituminous mixtures, a confined test with a confining pressure of 10 psi (69 kPa) and a deviator stress of 20 psi (138 kPa) for untreated granular materials, and a confined test with a confining pressure of 3 psi (21 kPa) and a deviator stress of 6 psi (41 kPa) for fine-grained soils. A haversine load with a duration of 0.1 s and a rest period of 0.9 s has been frequently used.

Incremental Static Test This is a simplified test and requires much less time to perform than the dynamic test. With a dynamic loading time of 0.1 s, a static load of t seconds is equivalent to $10t$ load repetitions. Therefore, the permanent deformation after a 1000-s creep test is equivalent to that of a dynamic test after 10,000 repetitions. The procedures for the testing of bituminous mixtures, as suggested in the VESYS manual (FHWA, 1978), are summarized as follows:

1. For preconditioning, apply two ramp loads of 20 psi (138 kPa) and hold each peak load for 10-min durations, with a minimum of unload time between them. A third load is then applied for 10 min, followed by a 10-min rest period.
2. Five different ramp loads, with durations of 0.1, 1, 10, 100, and 1000 s and rest periods of 2, 2, 2, 4, and 8 min, are applied successively, as shown in Figure 7.30. The total permanent strains at the end of each rest period are measured.
3. In the fifth ramp load or 1000-s creep test, measure the magnitude of creep deformations after 0.03, 0.1, 0.3, 1, 3, 10, 30, 100, and 1000 s. The 0.03-s creep strain is equivalent to the resilient strain ϵ under a dynamic haversine load of 0.1-s duration. The creep data should be extrapolated to obtain the strains at 0.001, 0.003, and 0.01 s so that the creep compliances at 11 time increments can be entered into VESYS or KENLAYER.
4. Plot the total permanent strain ϵ_p versus the incremental loading time and fit with a straight line, as shown in Figure 7.31.

Downloaded From : www.EasyEngineering.net

Downloaded From : www.EasyEngineering.net

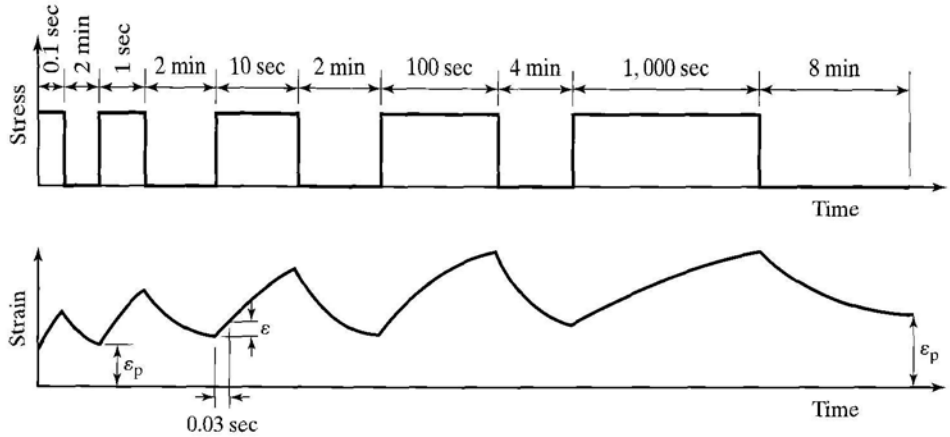


FIGURE 7.30

Stress and strain of incremental static test.

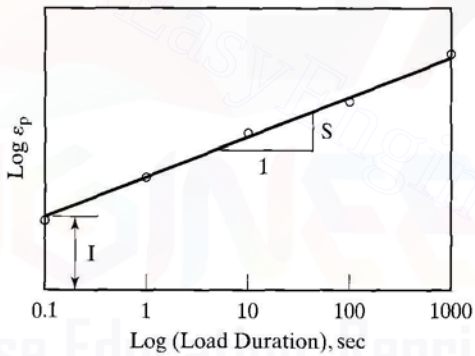


FIGURE 7.31

Log–log plot of incremental static test.

5. Determine the slope S and the intercept I of the straight line and compute α from Eq. 7.43 and μ from Eq. 7.44, in which ϵ is the creep strain at 0.03 s.

The same procedures can be applied to fine-grained soils except that a confining pressure of 3 psi (21 kPa) and a deviator stress of 6 psi (41 kPa) is used. Note that temperature control is needed for testing bituminous mixtures but not for soils.

Example 7.14:

A load of 20 psi (138 kPa) is applied to a HMA specimen. The average permanent deformations after the five ramp loads of 0.1-, 1-, 10-, 100-, and 1000-s duration, as measured by two LVDTs attached to the specimen by a pair of clamps, are 0.0012, 0.0035, 0.0117, 0.0317, and 0.0635 mm, respectively. The gauge length, or the distance between the LVDT clamps, is 4 in. (102 mm). The creep deformation at 0.03 s is 0.0031 mm. Determine the permanent deformation parameters α and μ.

Downloaded From : www.EasyEngineering.net

Downloaded From : www.EasyEngineering.net

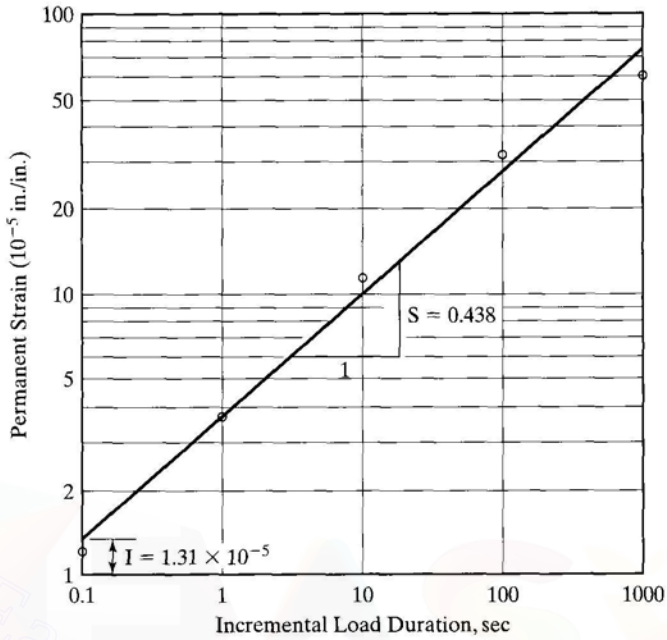


FIGURE 7.32
Example 7.14.

Solution: Dividing permanent deformation by a gauge length of 4 in. (102 mm) gives permanent strains of 1.2, 3.5, 11.5, 31.2, and 62.5 × 10^{-5} for the five ramp loads, respectively. The permanent strains are plotted versus the incremental loading times in log scales, as shown in Figure 7.32. The plot can be approximated by a straight line with a slope $S = (\log 74.3 - \log 1.31)/4 = 0.438$ and an intercept $I = 1.31 \times 10^{-5}$. From Eq. 7.43, $\alpha = 1 - 0.438 = 0.562$. The creep strain at 0.03 s $\epsilon = 0.0031/(4 \times 25.4) = 3.05 \times 10^{-5}$. From Eq. 7.44, $\mu = 1.31 \times 0.438/3.05 = 0.188$. It is interesting to note that both α and μ are dimensionless parameters not affected by the magnitude of applied load.

Dynamic Test The dynamic test can be performed immediately after the incremental static test without further sample conditioning. If the test is run independently, the sample must be preconditioned by applying a sufficient number of repeated loads until the resilient deformation becomes more stable.

The level of the repeated dynamic load and the confining pressure, if any, should simulate what actually occurs in the field. A minimum of 100,000 load applications is usually required, and the accumulated permanent deformation is measured at 1, 10, 100, 200, 1000, 10,000, and 100,000 repetitions. At the 200th repetition, both the permanent and the resilient deformations must be measured.

Example 7.15:

The resilient strain of a HMA specimen at the 200th repetition is 5.7 × 10^{-5} and the permanent strains at 1, 10, 100, 200, 1000, 10,000, and 100,000 repetitions are 4.5, 10.3, 18.4, 21.5, 41.5, 55.4, and 96.5 × 10^{-5}. Determine the permanent deformation parameters α and μ.

Downloaded From : www.EasyEngineering.net

Downloaded From : www.EasyEngineering.net

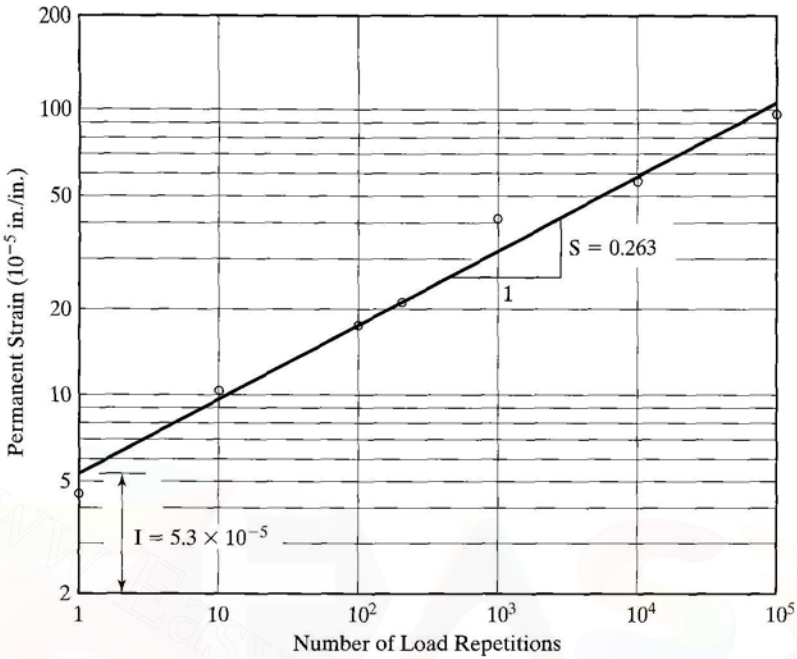


FIGURE 7.33
Example 7.15.

Solution: The permanent strains are plotted versus the number of load applications and fitted with a straight line, as shown in Figure 7.33. The slope of the straight line $S = (\log 109 - \log 5.3)/5 = 0.263$ and the intercept at 1 repetition $I = 5.3 \times 10^{-5}$. From Eq. 7.43, $\alpha = 1 - 0.263 = 0.737$. The resilient strain at the 200th repetition is 5.7×10^{-5}, so from Eq. 7.44, $\mu = 5.3 \times 0.263/5.7 = 0.245$.

Creep Test Creep test can be used not only to obtain the creep compliances at various times as an input for the analysis of viscoelastic systems, but also to estimate the rut depth due to the permanent deformation of bituminous layer. Van de Loo (1974, 1978) developed a method for estimating rut depth which was incorporated in the *Shell Pavement Design Manual*. The rut depth is computed from

$$\text{Rut depth} = C_m h_1 \left(\frac{\sigma_{av}}{S_{mix}} \right) \tag{7.51}$$

in which C_m is a correction factor for dynamic effect with values ranging from 1 to 2 depending on the type of mix, h_1 is the thickness of the asphalt layer, σ_{av} is the average vertical stress in the asphalt layer, and S_{mix} is the stiffness modulus of the mix. Because permanent deformation is caused by the viscous component of the mix while S_{mix} obtained from the creep test includes both the elastic and viscous components, a modification of S_{mix} based on the Van der Poel's nomograph and the viscosity of the bitumen is needed. Finn *et al.* (1983) suggested a simplified procedure in which S_{mix} is

Downloaded From : www.EasyEngineering.net

Downloaded From : www.EasyEngineering.net

determined directly from the creep test and C_m is assumed to be 1. If the number of load applications is N, then the creep time in seconds corresponding to N is $0.1N$, because the duration of each load application is 0.1 s.

Example 7.16:

Figure 7.34 shows a full-depth asphalt pavement 6 in. (305 mm) thick. A circular load with a radius of 6 in. (152 mm) and an intensity of 100 psi (690 kPa) is applied on the surface. The pavement has a modulus ratio E_1/E_2 of 100 and a Poisson ratio of 0.5 for both layers. If the HMA has a creep compliance of 2.1×10^{-5} in.^{2}/lb (3.0 mm^2/kN) at a loading time of 1000 s, estimate the rut depth after 10,000 load applications.

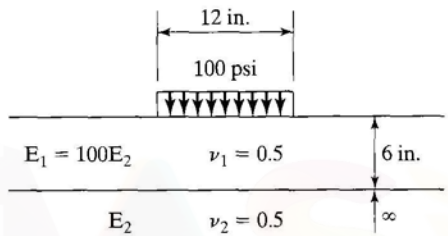


FIGURE 7.34
Example 7.16 (1 in. = 25.4 mm, 1 psi = 6.9 kPa).

Solution: The distribution of vertical stress in the asphalt layer can be found in Figure 2.14. For $E_1/E_2 = 100$, the average stress can be obtained quite accurately by averaging the stresses on the surface and at the interface, or $\sigma_{av} = (100 + 8)/2 = 54$ psi (373 kPa). With $S_{mix} = 1/(2.1 \times 10^{-5}) = 4.76 \times 10^4$ psi (328 MPa), $C_m = 1$, and $h_1 = 12$ in. (305 mm), from Eq. 7.51, rut depth $= 6 \times 54/(4.76 \times 10^4) = 0.0068$ in. (0.17 mm). Note that the rut depth is caused by the permanent deformation of the asphalt layer only, excluding that caused by the subgrade.

7.5 OTHER PROPERTIES

Some material properties that are related to pavement design but have not yet been discussed are presented here.

7.5.1 Modulus of Subgrade Reaction

The modulus of subgrade reaction k is determined from the loading test on a circular plate, 30 in. (762 mm) in diameter. To minimize bending, a series of stacked plates should be used. The load is applied to the plates by a hydraulic jack. A steel beam tied to heavy mobile equipment can be used as the reaction for the load. Deflections of the plate are measured by three dial gauges located at the outside edge about 120° apart. The support for the deflection dials must be located as far from the loaded area as possible, usually not less than 15 ft (4.5 m). Figure 7.35 is a schematic diagram of the plate loading test.

The load is applied at a predetermined rate until a pressure of 10 psi (69 kPa) is reached. The pressure is held constant until the deflection increases not more than 0.001 in. (0.025 mm) per minute for three consecutive minutes. The average of the three dial readings is used to determine the deflection. The modulus of subgrade

Downloaded From : www.EasyEngineering.net

Downloaded From : www.EasyEngineering.net

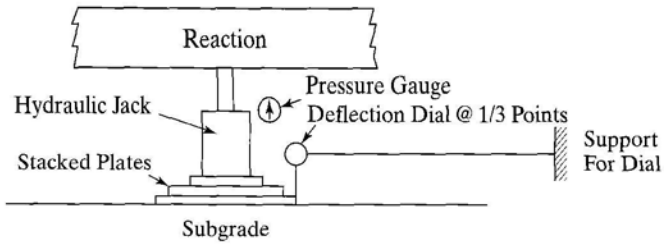


FIGURE 7.35

Schematic diagram of plate loading test.

reaction is given by

$$k = \frac{p}{\Delta} \tag{7.52}$$

in which p is the pressure on the plate, or 10 psi, and Δ is the deflection of plate in in.

Since the k value is determined from a field test, it cannot be conducted at various moisture contents and densities to simulate the different service conditions or the worst possible condition during the design life. To modify the k value for conditions other than those during the field test, laboratory specimens can be fabricated, one having the same moisture content and density as those in the field and the other having a different moisture content and density to simulate the service conditions. The specimens are subjected to a creep or consolidation test under a pressure of 10 psi (69 kPa), and the deformations d at various times are measured until the increase in deformation becomes negligibly small. The modified k value can be computed as

$$k_s = \frac{d_u}{d_s} k_u \tag{7.53}$$

in which subscript s indicates the service or saturated condition and u indicates the unsaturated or field condition.

The plate loading test is time-consuming and expensive, so the k value is instead usually estimated by correlation to simpler tests such as CBR and R value tests. Figure 7.36 shows the approximate relationship between the k value and other soil properties.

Hall *et al.* (1995) presented the results of research conducted to develop improved guidelines for selecting the k-values, together with a review of the evolution of k-value concepts and methods. A variety of methods were proposed to select the k-values, including correlations with soil types, soil properties, and other tests; deflection testing and back calculation methods; and plate-bearing test methods. Guidelines for seasonal adjustment to k and adjustments for embankments and for shallow, rigid layers were also developed.

7.5.2 Elastic Modulus

The ranges of K_1 and K_2 for untreated granular material are shown in Table 3.2 and those of the HMA dynamic modulus in Table 7.7. The modulus of fine-grained soil

Downloaded From : www.EasyEngineering.net

Downloaded From : www.EasyEngineering.net

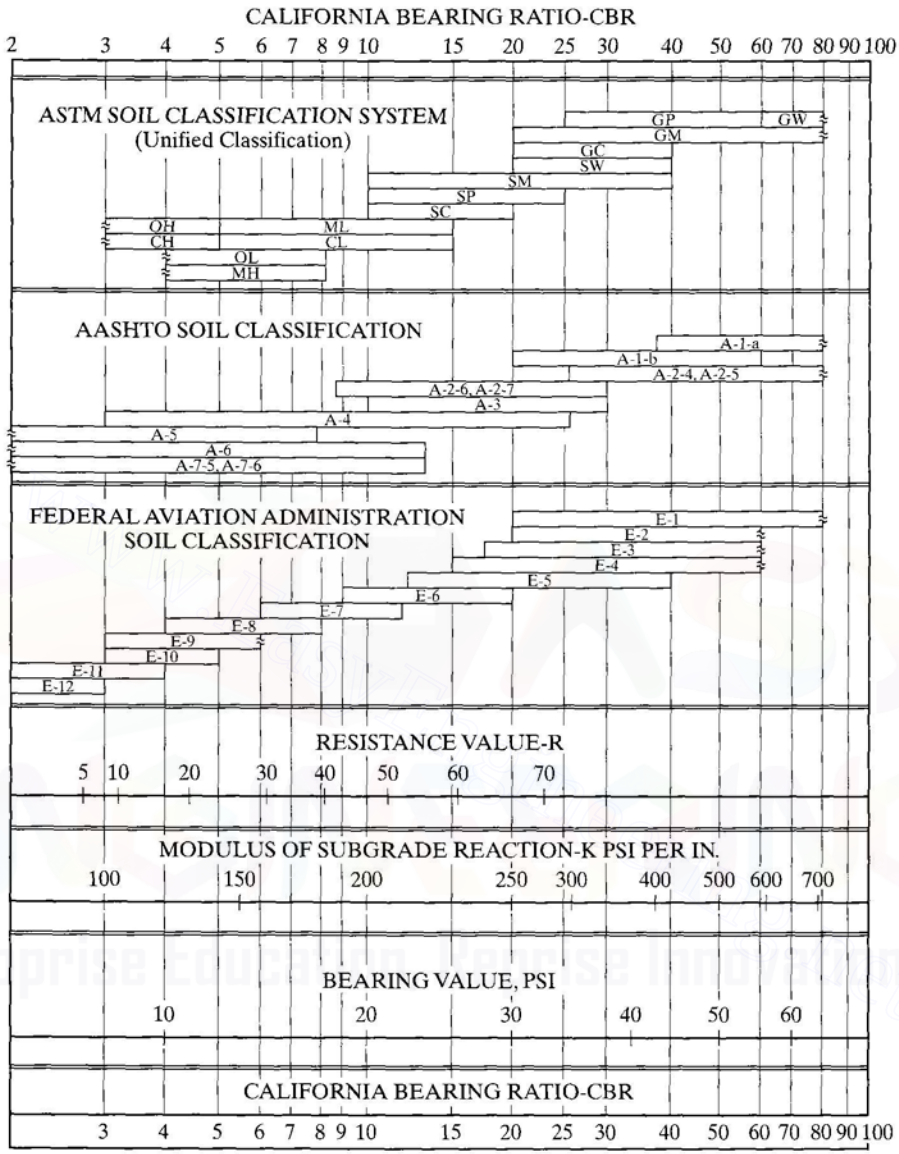


FIGURE 7.36

Approximate relationship between k values and other soil properties (1 psi = 6.9 kPa, 1 pci = 271.3 kN/m^3). (After PCA (1966).)

depends on the deviator stress. The maximum and minimum moduli shown in Figure 3.6 can be used as a guide. Table 7.9 shows the ranges of elastic modulus for different materials.

7.5.3 Poisson Ratio

The mechanistic method of pavement design requires information on the Poisson ratio. The Poisson ratio ν is defined as the ratio of the lateral strain to the axial strain.

Downloaded From : www.EasyEngineering.net

Downloaded From : www.EasyEngineering.net

TABLE 7.9 Elastic Moduli for Different Materials

Material	Range	Typical
Portland cement concrete	3×10^6 to 6×10^6	4×10^6
Cement-treated bases	1×10^6 to 3×10^6	2×10^6
Soil cement materials	5×10^4 to 2×10^6	1×10^6
Lime-flyash materials	5×10^5 to 2.5×10^6	1×10^6
Stiff clay	7600 to 17,000	12,000
Medium clay	4700 to 12,300	8000
Soft clay	1800 to 7700	5000
Very soft clay	1000 to 5700	3000

Note. Modulus in psi, 1 psi = 6.9 kPa.

TABLE 7.10 Poisson Ratios for Different Materials

Material	Range	Typical
Hot mix asphalt	0.30–0.40	0.35
Portland cement concrete	0.15–0.20	0.15
Untreated granular materials	0.30–0.40	0.35
Cement-treated granular materials	0.10–0.20	0.15
Cement-treated fine-grained soils	0.15–0.35	0.25
Lime-stabilized materials	0.10–0.25	0.20
Lime–flyash mixtures	0.10–0.15	0.15
Loose sand or silty sand	0.20–0.40	0.30
Dense sand	0.30–0.45	0.35
Fine-grained soils	0.30–0.50	0.40
Saturated soft clays	0.40–0.50	0.45

By measuring the axial and lateral strains during a resilient modulus test, the Poisson ratio can be determined. Because Poisson ratio has a relatively small effect on pavement responses, it is customary to assume a reasonable value for use in design, rather than to determine it from actual tests. Table 7.10 shows typical Poisson ratios for paving materials.

7.5.4 Portland Cement Concrete

The fatigue and modulus of rupture for portland cement concrete were discussed in Section 7.3.2. Some other concrete properties directly related to rigid pavement design are presented in this section.

The compressive strength is a universal measure of concrete quality and durability. As the information on compressive strength is readily available, studies have been made to correlate compressive strength with other properties. A general relationship between the modulus of rupture and the compressive strength is

$$S_c = 8\sqrt{f'_c} \quad \text{to} \quad 10\sqrt{f'_c} \tag{7.54}$$

in which S_c is the modulus of rupture in psi and f'_c is the compressive strength in psi. The relationship between the indirect tensile strength and the compressive strength, as

Downloaded From : www.EasyEngineering.net

Downloaded From : www.EasyEngineering.net

suggested by the American Concrete Institute, is

$$f_t = 6.5\sqrt{f'_c} \tag{7.55}$$

in which f_t is the indirect tensile strength in psi. The relationship between the modulus of elasticity and the modulus of rupture is (ERES, 1987)

$$S_c = \frac{43.5E_c}{10^6} + 488.5 \tag{7.56a}$$

or

$$E_c = (S_c - 488.5) \times 2.3 \times 10^4 \tag{7.56b}$$

For normal weight concrete, the American Concrete Institute suggested

$$E_c = 57{,}000\sqrt{f'_c} \tag{7.57}$$

The coefficient of thermal expansion ranges from 3 to 8×10^{-6}/°F (5.4 to 14.4×10^{-6}/°C), with 5×10^{-6}/°F(9×10^{-6}/°C) as typical. The coefficient of drying shrinkage ranges from 0.5 to 2.5×10^{-4}, with 1×10^{-4} as typical.

SUMMARY

This chapter describes the various methods for characterizing paving materials, including resilient and dynamic moduli, fatigue characteristics, and permanent deformation parameters.

Important Points Discussed in Chapter 7

1. In the analysis of layer systems under moving loads, the elastic modulus to be used for each layer is the resilient modulus obtained from the repeated load tests.
2. Theoretically, the load pulse for repeated load tests should vary with the vehicle speed and the location of the material below the pavement surface. Practically, a haversine load with a duration of 0.1 s and a rest period of 0.9 s has been frequently used.
3. Both the resilient and dynamic moduli have been used as the elastic modulus for bituminous mixtures. The difference between a resilient modulus and a dynamic modulus is that the resilient modulus is measured under a haversine pulse with a rest period, the dynamic modulus under a sinusoidal or haversine pulse with no rest period. The effect of rest period is insignificant, as evidenced by the fact that the same dynamic modulus is obtained no matter whether a sinusoidal or a haversine pulse is used.
4. The resilient modulus of untreated granular materials and fine-grained soils can be determined from the repeated load triaxial compression tests. Procedures for testing these materials are described, and the results are analyzed to determine the various parameters.
5. Correlations between the resilient modulus and other properties, such as CBR, *R* value, Texas triaxial classification, group index, Marshall stability, and cohesiometer

Downloaded From : www.EasyEngineering.net

Downloaded From : www.EasyEngineering.net

value, are presented. These correlations are only approximate and should be selected with great care, because the properties are related more to the shear strength than the resilient modulus. The dynamic modulus of bituminous mixtures can be predicted by Shell nomographs and AI equations.

6. The high tensile strains frequently used in the fatigue testing of bituminous mixtures make the dynamic stiffness modulus decrease with the increase in dynamic load, so it cannot be used as an elastic modulus. However, a correlation between the dynamic stiffness modulus and the dynamic modulus has been established for design purposes.
7. The fatigue testing of bituminous mixtures is time-consuming and expensive. To shorten the testing time, a haversine loading with a duration of 0.1 s and a rest period of 0.4 s, instead of the 0.9 s for the resilient modulus test, is usually used. Two types of fatigue test can be performed. The constant stress test, in which the strain increases with the increase in number of load repetitions, is applicable to thick pavements; the constant strain test, in which the strain is kept constant by reducing the stress as the number of load repetitions increases, is applicable to thin pavements. The use of the constant stress test for thin pavements is more conservative and results in a shorter design life. Nomographs and equations developed by Shell and AI can be used to predict the number of repetitions to failure.
8. The fatigue life of portland cement concrete depends on the stress ratio, which is a quotient between the flexural stress and the modulus of rupture. It is impractical to perform fatigue tests for a specific project because the variability of the test results requires a large number of tests and a great expense involved. Furthermore, a sufficient amount of data, as shown in Figure 7.27, is available and can be used for design purpose. The PCA design criterion is very conservative and results in a fatigue life much lower than the average life.
9. The permanent deformation properties of bituminous mixtures and fine-grained soils with sufficient viscous flow can be evaluated by the incremental static test, the dynamic test, and the creep test, whereas those of granular materials and fine-grained soils with little viscous flow can be evaluated only by the dynamic test. In conducting the permanent deformation test, care should be taken that the stresses used in the test be representative of those actually occurring in the in situ pavement, so that the effect of nonlinearity can be ignored.
10. The modulus of subgrade reaction k can be determined from a plate loading test using a circular plate 30 in. (762 mm) in diameter. Because the test is time-consuming and does not simulate the service conditions, it is customary to correlate the k value with other simpler tests such as CBR and R value, instead of performing the plate loading test.

PROBLEMS

7.1 The results of repeated load tests on a granular material are tabulated in Table P7.1. Develop an equation relating the resilient modulus to the first stress invariant or the sum of three principal stresses. [Answer: $M_R = 1750\theta^{0.711}$]

Downloaded From : www.EasyEngineering.net

Downloaded From : www.EasyEngineering.net

TABLE P7.1

Confining pressure (psi)	2	5	10	20	2
Deviator stress (psi)	6	15	30	60	6
Recoverable strain (10^{-4})	5.8	7.4	9.5	11.4	6.0

7.2 A fine-grained soil has an unconfined compressive strength of 2.3 tsf. The results of repeated load tests are tabulated in Table P7.2. Develop an equation relating the resilient modulus to the deviator stress. What should be the maximum and minimum resilient moduli for this soil? [Answer: $K_1 = 8300$, $K_2 = 7.9$, $K_3 = 1010$, $K_4 = 145$, $E_{max} = 14{,}200$ psi and $E_{min} = 4850$ psi]

TABLE P7.2

Deviator stress (psi)	2	4	7	14	20	28
Recoverable strain (10^{-4})	1.41	3.20	7.61	18.90	30.32	51.81

7.3 The flexural stresses and the initial moduli for a series of fatigue tests on HMA specimens are shown in Table P7.3. Determine the dynamic modulus for a frequency of 8 Hz by Eq. 7.15. [Answer: 8×10^5 psi]

TABLE P7.3

Test No.	1	2	3	4	5	6	7	8	9
Stress (psi)	278	254	228	197	185	165	137	115	91
Initial stiffness modulus (10^5 psi)	1.00	1.14	1.15	1.34	1.60	2.87	2.22	2.78	3.15

7.4 The results of fatigue test on an asphalt treated base are shown in Table P7.4. Develop an equation relating the number of repetitions to failure and the initial tensile strain. [Answer: $N_f = 6.66 \times 10^{-8}(\epsilon_t)^{-3.5}$]

TABLE P7.4

Test No.	1	2	3	4	5	6	7	8
Initial strain (10^{-3})	3.15	2.61	2.49	1.92	1.59	1.27	1.09	0.873
Fracture life (N_f)	35	75	100	294	340	970	1630	3573

7.5 An asphalt mixture has an asphalt content of 7% and a bulk specific gravity 2.24. The recovered asphalt has a specific gravity of 1.02, a ring and ball softening point of 120°F, and a penetration of 50 at 77°F. The specific gravity of the aggregate is 2.61. Determine the stiffness modulus of the mixture at a temperature of 74°F and a loading time of 0.02 s by

Downloaded From : www.EasyEngineering.net

Downloaded From : www.EasyEngineering.net

the Shell nomographs shown in Figures 7.19 and 7.20. Check the result by Eq. 7.25. [Answer: 2×10^9 N/m^2]

7.6 The asphalt mixture is the same as in Problem 7.5. The mineral aggregate has 5% passing through a No. 200 sieve, and the original asphalt has a penetration of 75 at 77°F. Determine the dynamic modulus at a temperature of 74°F and a loading frequency of 8 Hz by the AI equations. [Answer: 3.8×10^5 psi]

7.7 The asphalt mixture in Problem 7.5 is subjected to an initial tensile strain of 0.00015. Determine the number of repetitions to failure by the nomograph shown in Figure 7.26, using constant stress and constant strain tests, respectively, and check the results by using Eqs. 7.33 and 7.35. [Answer: 8.8×10^5 and 8.1×10^7]

7.8 The asphalt mixture in Problem 7-6 is subjected to an initial strain of 0.00015. Determine the number of repetitions to failure by Eqs. 7.36 and 7.37. [Answer: 6.4×10^5]

7.9 The results of incremental static test on a HMA specimen are shown in Table P7.9. If the creep strain at a time duration of 0.03 s is 3.045×10^{-5}, determine the permanent deformation parameters α and μ. [Answer: $\alpha = 0.558$ and $\mu = 0.186$]

TABLE P7.9

Load duration (s)	0.1	1	10	100	1000
Permanent strain (10^{-5})	1.158	3.474	11.533	31.172	62.483

7.10 The results of a dynamic test on a HMA specimen are shown in Table P7.10. If the elastic strain at the 200th repetition is 4.128×10^{-5}, determine the permanent deformation parameters α and μ. [Answer: $\alpha = 0.705$ and $\mu = 0.187$]

TABLE P7.10

No. of repetitions	1	10	100	200	1000	10,000	100,000
Accumulated permanent strain (10^{-5})	2.360	5.831	12.773	13.930	19.715	36.281	73.506

Downloaded From : www.EasyEngineering.net

Downloaded From : www.EasyEngineering.net

CHAPTER 8

Drainage Design

8.1 GENERAL CONSIDERATION

Drainage is one of the most important factors in pavement design. Until recently, this factor had not received the attention it merits. One misconception is that good drainage is not required if the thickness design is based on saturated conditions. This concept may have been true during the old days when the traffic loading and volume were small. As the weight and number of axle loads increase, water can cause more damage to pavements, such as by pumping and by degradation of paving materials, not merely by the loss of shear strength. Theoretically, an internal drainage system is not required if the infiltration into the pavement is smaller than the drainage capacity of the base, subbase, and subgrade. Because the infiltration and drainage capacity vary a great deal and are difficult to estimate, it is suggested that drainage layers be used for all important pavements, such as the premium or zero-maintenance pavements described in Section 1.2.3.

8.1.1 Detrimental Effects of Water

Water enters the pavement structure either by infiltration through cracks, joints, pavement surfaces, and shoulders or as groundwater from a high water table, interrupted aquifers, and localized springs. The detrimental effects of water, when entrapped in the pavement structure, can be summarized as follows:

1. It reduces the strength of unbounded granular materials and subgrade soils.
2. It causes pumping of concrete pavements, with subsequent faulting, cracking, and general shoulder deterioration.
3. Under high hydrodynamic pressure generated by moving traffic, pumping of fines in the base course of flexible pavements can also occur, with resulting loss of support.
4. In northern climates with a depth of frost penetration greater than the pavement thickness, a high water table causes frost heave and the reduction of load-carrying capacity during the frost melting period.

Downloaded From : www.EasyEngineering.net

Downloaded From : www.EasyEngineering.net

5. Water causes differential heaving over swelling soils.
6. Continuous contact with water causes stripping of asphalt mixture and induces durability (or "D") cracking of concrete.

8.1.2 Movement of Water

The movement of water in pavement structures can be caused by gravity, by capillary action, by vapor pressures, or by a combination of any of them. The flow in granular materials is basically due to gravity; that in fine-grained soil is mostly due to capillary action. In the absence of gravity and capillary flows, water moves primarily in the vapor phase in response to differences in vapor pressure.

The movements of water due to gravity obey Darcy's law of saturated flow,

$$v = ki \tag{8.1}$$

in which v is the discharge velocity, k is the coefficient of permeability (simply called permeability), and i is the hydraulic gradient, which is the head loss between two points divided by the distance between them. The discharge velocity can be used to determine the discharge as

$$Q = vA \tag{8.2}$$

in which Q is the discharge, or the volume of flow per unit time, and A is a cross-sectional area normal to the direction of flow. It can be seen that the discharge velocity is not the actual seepage velocity through the pores, but is an imaginary velocity for computing the discharge.

Darcy's law can be used in conjunction with the continuity equation to form the differential equation governing groundwater flow. A convenient and practical way to solve the equation is by drawing the flownets, as illustrated by Cedergren (1977). In many simple cases encountered in drainage design, Darcy's law can be applied directly to determine the amount of seepage.

Example 8.1:

Figure 8.1 shows a pavement with a thin granular drainage layer. The infiltration of surface water into the drainage layer is 0.5 $ft^3/day/ft^2$ (0.15 $m^3/day/m^2$). The drainage layer is placed on a 5-ft (1.5-m) sand layer with a permeability of 0.15 ft/day (5.3×10^{-5} cm/s). The sand layer is underlain by a very previous gravel deposit, and there is no water table in the sand layer. Estimate the required discharge capacity of the drainage layer.

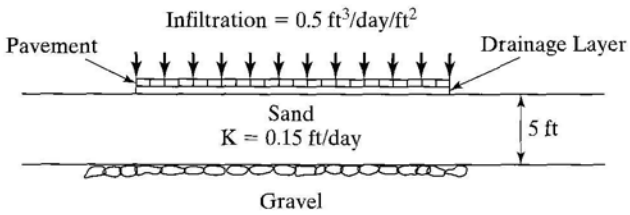


FIGURE 8.1
Example 8.1 (1 ft = 0.305 m).

Downloaded From : www.EasyEngineering.net

Downloaded From : www.EasyEngineering.net

Solution: Because the thickness of the sand layer is small compared to the width of the pavement, it is reasonable to assume that the flow of water through the sand is in the vertical direction, so Darcy's law can be applied directly. The thinness of the drainage layer allows the pressure head on the top of sand layer to be treated as zero. Both the top and the bottom of sand layer are subjected to the same atmospheric pressure, so the head loss between top and bottom is equal to the difference in elevations, or 5 ft (1.5 m). The distance between the top and the bottom is also 5 ft (1.5 m), so the hydraulic gradient is 5/5, or 1. Note that when the same atmospheric pressure exists at both top and bottom, the hydraulic gradient is always equal to 1, irrespective of the thickness of sand layer. From Eq. 8.1, $v = 0.15 \times 1 = 0.15$ ft/day (5.3×10^{-5} cm/s), which is the same as a discharge rate in $ft^3/day/ft^2$. Therefore, the required discharge capacity of the drainage layer is $0.5 - 0.15$, or 0.35 $ft^3/day/ft^2$ (0.11 $m^3/day/m^2$).

If the sand layer in this example is very thick, the flow channel becomes wider at greater depths. As more areas become open to the flow, the amount of seepage increases. Therefore, the use of Darcy's law for drainage design by assuming the flow lines to be vertical is on the conservative side. The analysis of unsaturated flow by capillary action is much more complicated. Both the permeability and the hydraulic gradient due to the change in capillary heads are functions of moisture content and are sometimes influenced by the past moisture conditions.

It is well known that moisture moves in vapor form from warmer to cooler regions. The vapor condenses under the pavement at night when the pavement becomes cool. In northern temperate climates, there is a downward migration of moisture vapor from the warmer surface to the cooler subsurface in the summer and a corresponding upward movement of moisture in the winter. This upward movement of water vapor is partially responsible for the high moisture content in granular bases.

8.1.3 Methods for Controlling Water in Pavements

The detrimental effects of water on pavements can be minimized by preventing it from entering the pavement, providing drainage to remove it quickly, or building the pavement strong enough to resist the combined effect of load and water.

Prevention The prevention of water from entering the pavement structure requires intercepting groundwater and sealing the pavement surface. The detrimental effects of groundwater have been well documented, and highway engineers have paid considerable attention to intercepting groundwater. Less attention has been given to sealing the surface to exclude infiltration from rain and snow melt. As a result, a considerable amount of water often enters the pavement structure. Because complete prevention is not possible during the useful life of a pavement, the installation of internal drainage systems to remove water could be needed.

To minimize the infiltration of surface water into the pavement, a good surface drainage is always required. Figure 8.2 shows typical cross sections for a two-lane and a multilane highway. To facilitate surface drainage, transverse slopes are introduced in all tangent sections of roadway. Except where super-elevation of curves directs all water toward the inside, two-lane highways usually have each lane sloping in a different direction. To make driving easier, each half of a divided highway is sloped individually,

Downloaded From : www.EasyEngineering.net

Downloaded From : www.EasyEngineering.net

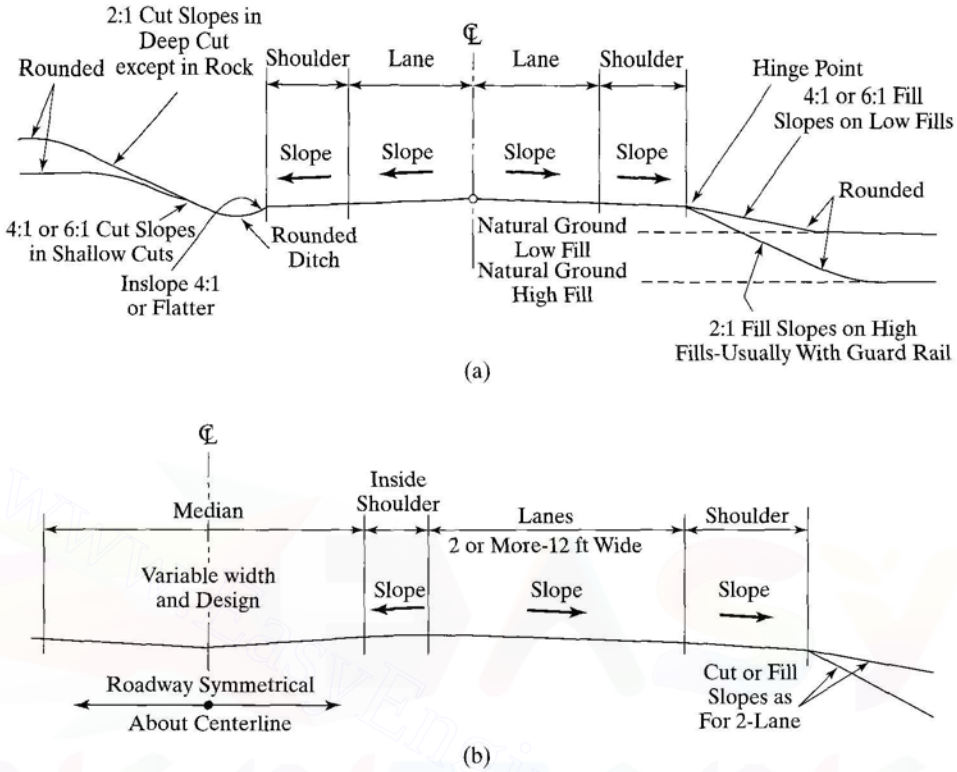


FIGURE 8.2

Cross sections of typical highways (1 ft = 0.305 m).

usually with the outside edges lower than the inside edges. Table 8.1 shows the transverse slopes of pavements, shoulders, and ditches.

Removal If water enters the pavement structure either through infiltration or as groundwater, it must be removed quickly before any damage can be initiated. Three different drainage installations, either individually or in combination, have been used most frequently for pavement design: drainage layer or blanket, longitudinal drain, and transverse drain.

TABLE 8.1 Transverse Slopes of Pavements, Shoulders, and Ditches

Feature	Pavement	Shoulder	Ditch
Slope (in./ft)	$\frac{3}{16}$–$\frac{3}{8}$	$\frac{3}{8}$–$\frac{3}{4}$	3–6
Slope (%)	1.5–3.0	3.0–6.0	25.0–50.0

Note. 1 in./ft = 82 mm/m.

Downloaded From : www.EasyEngineering.net

Downloaded From : www.EasyEngineering.net

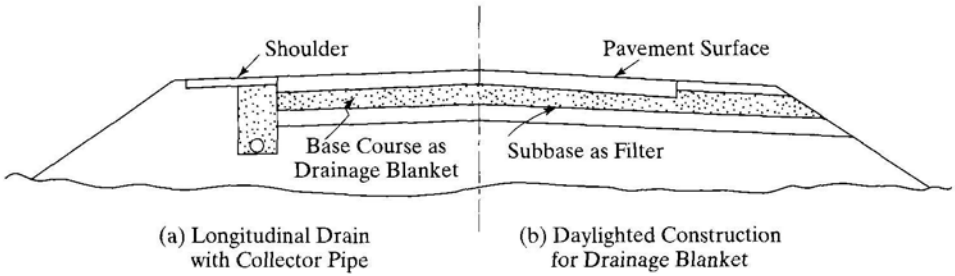


FIGURE 8.3

Drainage blanket with alternate longitudinal drain.

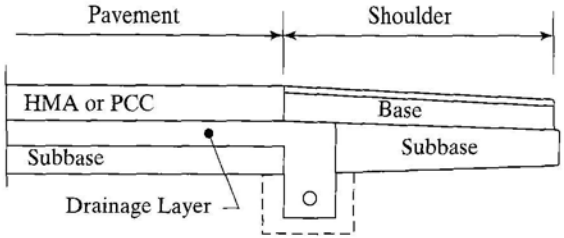
Figure 8.3 shows a drainage blanket for intercepting surface infiltration. The drainage blanket can be terminated with longitudinal drains and pipe outlets, as shown in (*a*), or daylighted by extending to the side slope, as shown in (*b*). To minimize the intrusion of fines, all materials surrounding the drainage blanket and the longitudinal drain must meet the filter criteria (discussed later). The use of longitudinal drains is more reliable and may be even more economical than the daylighted construction. The disadvantages of the daylighted construction are the propensity to contamination and clogging of the outlet at the side slope during construction and maintenance operations, the smaller hydraulic gradient caused by the wider blanket, and the possibility of carrying water from the side ditch to the pavement structure, instead of from the pavement structure to the side ditch. The longitudinal drains can be French drains without the perforated or slotted pipes. However, these pipes are usually used because they can accommodate larger flows and thus reduce the dimensions of French drains required.

Figure 8.4 shows the location of drainage layer in a pavement structure. In (*a*), the base course is used as a drainage layer and satisfies both the requirements of strength for a base course and the permeability for a drainage layer. In (*b*), the drainage layer is placed on the top of subgrade, either as an extra layer not considered in thickness design or as a part of the subbase. The placement of the drainage layer directly under the PCC or HMA is preferable because the water can be drained out more quickly, thus eliminating any chance for pumping to occur. However, it has the disadvantages that the deficiency of fines in the drainage layer could cause stability problems and that the water in the subbase cannot drain readily into the drainage layer. If the drainage layer is placed on the top of subgrade, the permeability of the base and subbase must be greater than the infiltration rate, so that water can flow freely to the drainage layer.

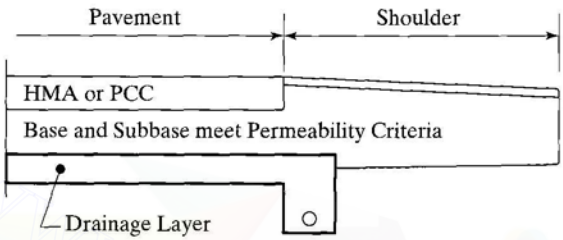
Another concept is to consider the subbase as a separation layer, instead of a filter (Mallela *et al.*, 2000). The separation layer is a dense-graded aggregate material (stabilized or unstabilized) placed between the permeable base and the subgrade. It has three main functions: to maintain separation between the permeable base and the subgrade and prevent them from intermixing; to form an impermeable barrier that deflects water from the permeable base horizontally toward the pavement edge; and to support construction and compactive effort of base and surface layers.

Downloaded From : www.EasyEngineering.net

Downloaded From : www.EasyEngineering.net



(a) Base as Drainage Layer



(b) Drainage Layer below Subbase or as Part of Subbase

NOTE: All Materials Surrounding Drainage Layer Must Meet Filter Criteria

FIGURE 8.4

Location of drainage layer and filter. (After Ridgeway (1982).)

Figure 8.5 shows the use of a longitudinal drain parallel to the roadway to lower the groundwater table. If the general direction of groundwater flow is parallel to the roadway, such as when the roadway is cut more or less perpendicular to the existing contours, then transverse drains can be more effective in intercepting the flow.

Longitudinal trench drains were used by Arkansas, Florida, Louisiana, and New Mexico for improving the drainage of existing rigid pavements (FHWA, 1986). The

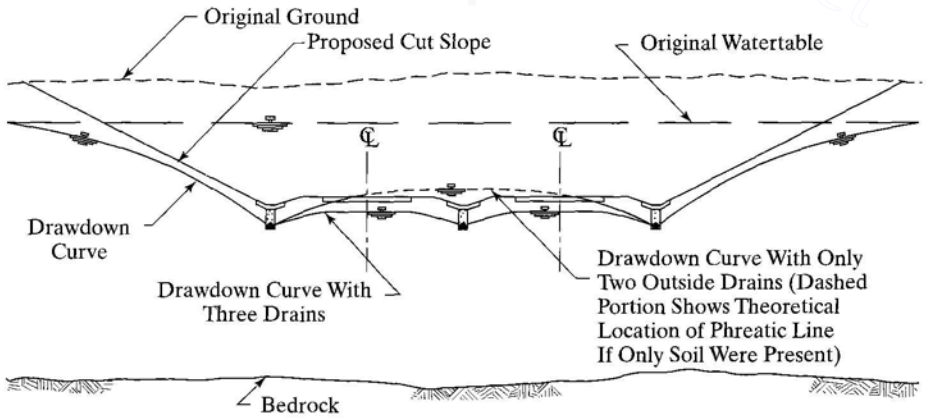


FIGURE 8.5

Longitudinal drains for lowering groundwater table. (After Moulton (1980).)

Downloaded From : www.EasyEngineering.net

Downloaded From : www.EasyEngineering.net

trench was placed adjacent to the concrete pavement and is therefore called an edge drain. Using similar designs with trench drains and collector pipes, these states reported that edge drains can remove water satisfactorily and are considered cost effective. A performance survey of five-year-old edge drains representing 120 miles (192 km) in Louisana indicated that 75% of the system continued to provide moderate to rapid drainage and the remaining 25% experienced clogging of the ends of lateral outlet pipes. Most of the clogged laterals began to drain upon cleaning, indicating no major problems in draining water from the trench. These pavements all contain cement-treated bases.

Stronger Pavement Sections The use of thicker HMA or PCC can greatly reduce the hydrodynamic pressure and its detrimental effects. The Asphalt Institute strongly advocates the use of full-depth asphalt pavements. According to AI (1984), vapor movement is probably a primary cause of moisture entering and saturating granular bases, and this problem can be eliminated by the construction of a full-depth asphalt pavement placed directly on the native soil. The same is true for PCC pavements with stabilized bases. Because water can still enter into the subgrade through cracks and joints and along the pavement edges, the thickness design should be based on a saturated subgrade, if no drainage layer is installed.

8.2 DRAINAGE MATERIALS

Drainage materials include aggregates, geotextiles, and pipes. Aggregates can be used as drainage layers and French drains or as filter materials for their protection. Geotextiles are used mainly to replace aggregates as filters. Pipes can be perforated, slotted, or open-jointed types to be placed inside the French drain to collect water, or the conventional type to convey water laterally to the outlet.

8.2.1 Aggregates

Aggregates to be used for drainage layers and French drains should consist of sound, clean, and open-graded materials. They must have a high permeability to accommodate the free passage of water and be protected from clogging by means of a filter.

Permeability Figure 8.6 shows the grain size curve and permeability of some typical open-graded bases and filter materials. The grain size is always plotted in log scale and the percent passing in arithmetic scale. The sizes in inches corresponding to the sieve numbers are also shown, to facilitate the determination of various sizes for filter design.

Effect of Fines It has long been recognized that proper gradation and density are vital to the stability of granular materials. The gradation required for stability usually ranges uniformly from coarse to fine. To obtain the desired permeability, the fine portions need be deleted; thus, the stability of the drainage layer can be adversely affected. This effect can be compensated for by stabilizing the drainage layer with a small amount of asphalt or portland cement. Table 8.2 shows the permeability of untreated and asphalt-treated open-graded aggregates. It can be seen that the use of 2% asphalt reduces the permeability only slightly.

Downloaded From : www.EasyEngineering.net

Downloaded From : www.EasyEngineering.net

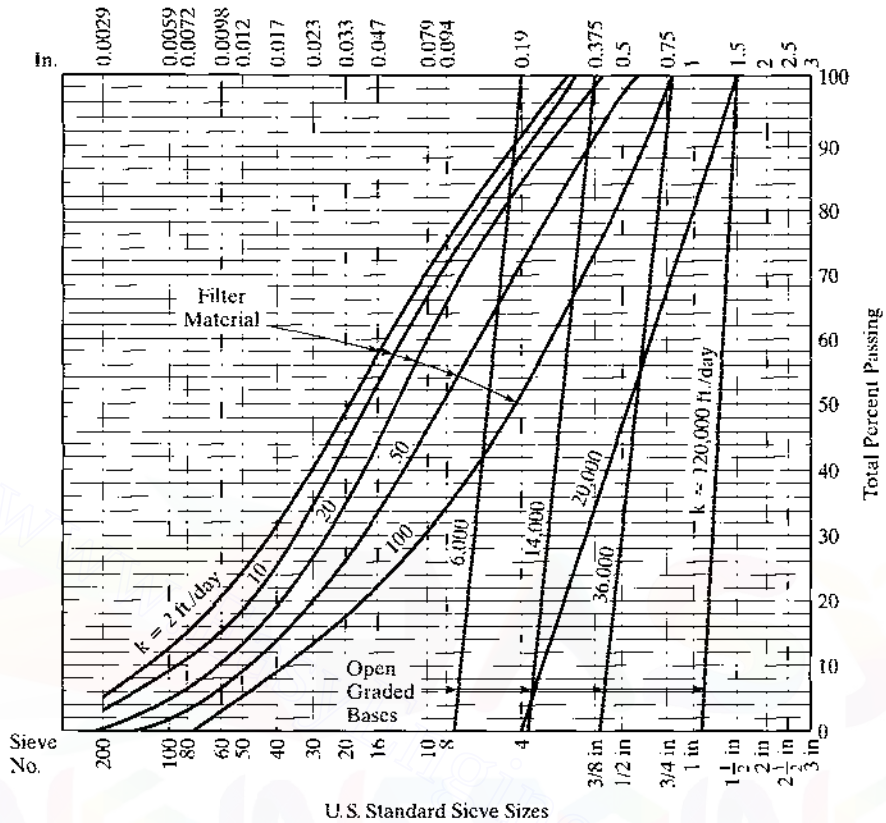


FIGURE 8.6

Typical gradations and permeabilities of open-graded bases and filter materials (1 in. = 25.4 mm, 1 ft/day = 3.5×10^{-4} cm/s. (After Cedergren *et al.* (1972).)

TABLE 8.2 Permeabilities of Untreated and Asphalt-Treated Open-Graded Aggregates

	Permeability (ft/day)	
Aggregate size	Untreated	Treated with 2% asphalt
$1\frac{1}{2}$ to 1 in.	140,000	120,000
$\frac{3}{4}$ to $\frac{3}{8}$ in.	38,000	35,000
No. 4 to No. 8	8000	6000

Note. 1 in. = 25.4 mm, 1 ft/day = 3.5×10^{-4} cm/s.
Source. After Lovering and Cedergren (1962).

Table 8.3 shows the permeability of graded aggregates with no fines. Sample 1 has a gradation similar to AASHTO grading C of soil aggregate mixtures for base course (AASHTO, 1989), except that grading C requires 5 to 15% passing No. 200. The other samples were obtained by successively eliminating small particles. As can be seen, the elimination of small particles significantly increases the permeability.

Downloaded From : www.EasyEngineering.net

Downloaded From : www.EasyEngineering.net

TABLE 8.3 Grain Size, Density, and Permeability of Graded Aggregates

% Passing	Sample 1	Sample 2	Sample 3	Sample 4	Sample 5	Sample 6
$\frac{3}{4}$ in.	100	100	100	100	100	100
$\frac{1}{2}$ in.	85	84	83	81.5	79.5	75
$\frac{3}{8}$ in.	77.5	76	74	72.5	69.5	63
No. 4	58.5	56	52.5	49	43.5	32
No. 8	42.5	39	34	29.5	22	5.8
No. 10	39	35	30	25	17	0
No. 20	26.5	22	15.5	9.8	0	0
No. 40	18.5	13.3	6.3	0	0	0
No. 60	13	7.5	0	0	0	0
No. 140	6	0	0	0	0	0
No. 200	0	0	0	0	0	0
Dry density (pcf)	121	117	115	111	104	101
k (ft/day)	10	110	320	1000	2600	3000

Note. 1 in. = 25.4 mm, 1 pcf = 157.1 N/m^3, 1 ft/day = 3.5×10^{-4} cm/s.
Source. After Barber and Sawyer (1952).

The effect of fines passing through a No. 200 sieve on the permeability of sample 1 is shown in Figure 8.7. The effect depends on the type of fines. The permeability is about 10 ft/day (3.5×10^{-3} cm/s) with no fines and decreases to 2×10^{-2} to 5×10^{-5} ft/day (7×10^{-6} to 1.7×10^{-8} cm/s) with 25% fines.

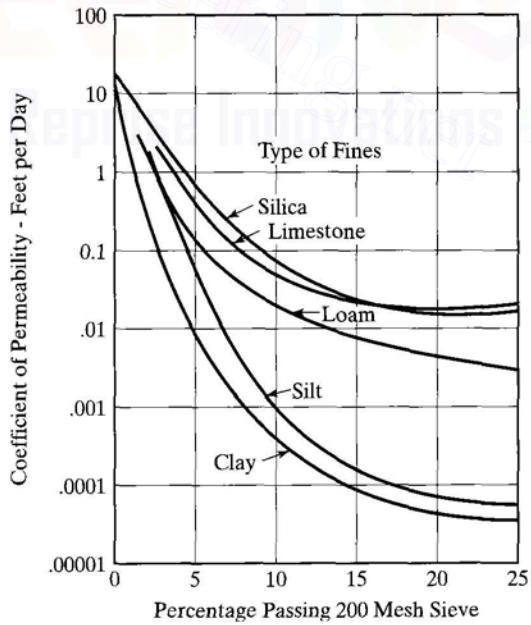


FIGURE 8.7
Effect of fines on permeability of sample 1 (1 ft/day = 3.5×10^{-4} cm/s). (After Barber and Sawyer (1952).)

Downloaded From : www.EasyEngineering.net

Downloaded From : www.EasyEngineering.net

Effect of Grain Size A number of approximate relationships have been suggested between permeability and grain size. The most frequently used approximation is the one suggested by Hazen for filter sands:

$$k = C_k D_{10}^2 \tag{8.3}$$

in which k is the permeability in mm/s, D_{10} is the effective size, or the grain size corresponding to 10% passing, and C_k is an experimental coefficient dependent on the nature of soil. Experimental evidence suggests that the acceptable approximate values for k can be obtained when Hazen's formula is applied over a wide range of soils. Table 8.4 gives the range of suggested values for the coefficient C_k.

In addition to the effective size D_{10}, other sizes, such as D_{15}, D_{50}, and D_{85}, have been used for the design of filters. If the values of percent passing, a and b, for two grain sizes, D_a and D_b, are given, then the size D_x for any percent passing x between a and b can be computed by linear interpolation, as shown in Figure 8.8:

$$\log D_x = \log D_a + \frac{x - a}{b - a} \log \frac{D_b}{D_a} \tag{8.4}$$

Example 8.2:

If 3% of minus 200 fines is added to sample 1 in Table 8.3, determine D_{10} of the sample.

Solution: The two successive sieves for determining D_{10} are No. 140, or $D_a = 0.105$ mm, and No. 60, or $D_b = 0.25$ mm. In the original sample, 6% pass No. 140 and 13% pass No. 60. After adding 3% fines, $a = (6 + 3)/1.03 = 8.7\%$ and $b = (13 + 3)/1.03 = 15.5\%$. From Eq. 8.4, $\log D_{10} = \log 0.105 + (10 - 8.7)/(15.5 - 8.7) \log(0.25/0.105) = -0.907$, or $D_{10} = 0.124$ mm.

TABLE 8.4 Values of Hazen's Coefficient

Soil type	D_{10} range (mm)	C_k (1/mm-s)
Uniform sand	0.06–3.0	8–12
Well-graded sands and silty sands	0.003–0.6	5–8

Source. After Whitlow (1990).

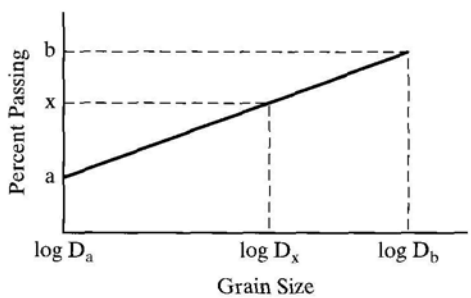


FIGURE 8.8
Interpolation between two grain sizes.

Downloaded From : www.EasyEngineering.net

Downloaded From : www.EasyEngineering.net

Moulton (1980) developed the following empirical equation for determining the permeability of granular drainage and filter materials:

$$k = \frac{6.214 \times 10^5 (D_{10})^{1.478} (n)^{6.654}}{(P_{200})^{0.597}} \tag{8.5a}$$

Here, k is the permeability in ft/day, D_{10} is the effective size in mm, which is the size at 10% passing, and n is the porosity, which can be computed from the dry unit weight as

$$n = 1 - \frac{\gamma_d}{62.4 G_s} \tag{8.5b}$$

in which γ_d is the dry unit weight in pcf and G_s is the specific gravity of solids. A major limitation of the formula is that it cannot be applied to materials with no fines passing the No. 200 sieve.

Example 8.3:

If 3% of minus 200 fines is added to sample 1 in Table 8.3, determine its permeability by Eq. 8.5. It is assumed that the specific gravity of solids is 2.7 and that the dry density increases by 3% due to the addition of fines.

Solution: With $\gamma_d = 1.03 \times 121 = 124.6$ pcf (19.6 kN/m^2) and $G_s = 2.7$, from Eq. 8.5*b*, $n = 1 - 124.6/(62.4 \times 2.7) = 0.260$. From Example 8.2, $D_{10} = 0.124$ mm and $P_{200} = 3/1.03 = 2.91$. From Eq. 8.5, $k = 6.214 \times 10^5 (0.124)^{1.478} (0.26)^{6.654}/(2.91)^{0.597} = 1.92$ ft/day.

Asphalt-Treated Bases Lindly and Elsayed (1995) developed the following regression equation for estimating the permeability of asphalt-treated bases:

$$k = 852.298 - 248.665\, P_b + 97.507\, V_a - 95.52\, P_{\#8} \tag{8.6}$$

In this equation, k = coefficient of permeability in feet per day, P_b = percent asphalt cement by total weight of sample, V_a = percent air voids by total volume of sample, $P_{\#8}$ = percent by weight passing no. 8 sieve (2.36 mm). This equation was based on 1.5-in. (38-mm) top size aggregates with 2 to 3 percent asphalt, as used by most highway agencies in the design of asphalt-treated drainage layers.

Filter Criteria Any aggregate used for drainage must satisfy the following filter criteria.

Clogging Criterion The filter material must be fine enough to prevent the adjacent finer material from piping or migrating into the filter material, as indicated by

$$\frac{D_{15}\ \text{filter}}{D_{85}\ \text{soil}} \le 5 \tag{8.7}$$

in which D_{15} and D_{85} are the grain size corresponding to 15 and 85% passing, respectively, and can be obtained from the grain size curves of each material. This criterion should be applied not only to the filter material but also to the drainage layer. For example, if the

Downloaded From : www.EasyEngineering.net

Downloaded From : www.EasyEngineering.net

subbase is designed as a filter, as shown in Figure 8.3, Eq. 8.7 should be applied first by considering the subbase as the filter and the subgrade as the soil and then by considering the drainage layer as the filter and the subbase as the soil. This will prevent migration of the subgrade material into the subbase and of the subbase material into the drainage layer.

Permeability Criterion The filter material must be coarse enough to carry water without any significant resistance, as indicated by

$$\frac{D_{15}\text{ filter}}{D_{15}\text{ soil}} \geq 5 \tag{8.8}$$

This criterion need be applied only to the filter or the subbase. The drainage layer is highly permeable, and this criterion can certainly be satisfied.

Additional Criteria Equations 8.7 and 8.8 were originally developed by Betram (1940), with the advice of Terzaghi and Casagrande. The work of Betram was later expanded by the U.S. Army Corps of Engineers (1955) and, to make the grain size curves of filters and protected soil materials somewhat parallel, an additional requirement, as indicated by Eq. 8.9, was added:

$$\frac{D_{50}\text{ filter}}{D_{50}\text{ soil}} \leq 25 \tag{8.9}$$

To minimize segregation, the Corps of Engineers further specified that filter materials must have a coefficient of uniformity, which is a ratio between D_{60} and D_{10}, not greater than 25. To prevent the fines in the filter from infiltrating into the drainage layer, Moulton (1980) recommended that the amount of fines passing through a No. 200 sieve be not greater than 5%, or D_5 of filter $\geq$ 0.0029 in. (0.074 mm). If the protected soil contains a large percentage of gravels, Sherard *et al.* (1963) indicated that the filter should be designed on the basis of material finer than 1 in. (25.4 mm).

Example 8.4:

Can the open-graded base with a permeability of 20,000 ft/day (70 mm/s), as shown in Figure 8.6, be placed directly on a subgrade soil with D_{15} = 0.0013 in. (0.033 mm), D_{50} = 0.0055 in. (0.038 mm), and D_{85} = 0.021 in. (0.53 mm)? If a subbase is to be placed between the subgrade and the open-graded base, which of the filter materials shown in Figure 8.6 can be used as a subbase?

Solution: When the base is placed directly on the subgrade, the base is considered as filter and the subgrade as soil. The D_{15} and D_{50} of base can be determined by Eq. 8.4. From the grain size curve in Figure 8.6, D_{15} is between D_a = 0.19 in. (4.8 mm) and D_b = 0.375 in. (9.5 mm) with a = 1% and b = 32%. From Eq. 8.4, $\log D_{15} = \log 0.19 + [(15 - 1)/(32 - 1)] \log(0.375/0.19) = -0.588$, or D_{15} = 0.26 in. (6.6 mm). By following the same procedure, $\log D_{50} = \log 0.5 + [(50 - 47)/(66 - 47)] \log(0.75/0.5) = -0.273$, or D_{50} = 0.53 in. (13.5 mm). From Eq. 8.7, (D_{15} of base)/(D_{85} of subgrade) = 0.26/0.021 = 12.4, which is greater than the maximum of 5 required, so the criterion is not satisfied. From Eq. 8.8, (D_{15} of base)/(D_{15} of subgrade) = 0.26/0.0013 = 200, which is greater than 5 and is considered satisfactory. From

Downloaded From : www.EasyEngineering.net

Downloaded From : www.EasyEngineering.net

Eq. 8.9, (D_{50} of base)/(D_{50} of subgrade) = 0.53/0.0055 = 96.4, which is greater than the maximum of 25 required, so the criterion is not satisfied. Therefore, the base should not be placed directly on the subgrade, because Eqs. 8.7 and 8.9 are not satisfied.

When a subbase is placed between the subgrade and the base, the analysis should be divided into two steps. First consider the subbase as filter and the subgrade as soil. From Eqs. 8.7, 8.8, and 8.9, the requirements of the subbase are as follows: $D_{15} \leq 5 \times 0.021 = 0.105$ in. (2.67 mm), $D_{15} \geq 5 \times 0.0013 = 0.0065$ in. (0.17 mm), and $D_{50} \leq 25 \times 0.0055 = 0.138$ in. (3.5 mm). Next consider the base as filter and the subbase as soil. Based on Eqs. 8.7, 8.8, and 8.9, the requirements of the subbase are $D_{85} \geq 0.26/5 = 0.052$ in. (1.32 mm), $D_{15} \leq 0.26/5 = 0.052$ in. (1.32 mm), and $D_{50} \geq 0.53/25 = 0.0212$ in. (0.54 mm). The preceding six requirements can be reduced to the following three:

$$0.0065 \text{ in. } (0.17 \text{ mm}) \leq D_{15} \leq 0.052 \text{ in. } (1.32 \text{ mm})$$

$$0.0212 \text{ in. } (0.54 \text{ mm}) \leq D_{50} \leq 0.138 \text{ in. } (3.5 \text{ mm})$$

$$D_{85} \geq 0.052 \text{ in. } (1.32 \text{ mm})$$

A review of the five filter materials in Figure 8.6 indicates that, except for the coarsest material—that having a D_{50} of 0.18 in. (4.6 mm)—all the foregoing requirements are satisfied. Because the finest filter material has slightly more than 5% passing No. 200 and is not considered acceptable, only the three intermediate materials, those having permeabilities of 10, 20, and 50 ft/day (3.5×10^{-3}, 7.0×10^{-3}, and 1.8×10^{-2} cm/s), can be used.

8.2.2 Geotextiles

Geotextiles are filter fabrics that can be used to protect the drainage layer from clogging. In addition to the two general requirements to retain soil and to allow water to flow, geotextiles must have sufficient opening areas to prevent them from clogging. They must be made from strong, tough, polyester, polypropylene, or other rot-proof polymeric fibers formed into a fabric of the woven or nonwoven type. They must be free of any treatment or coating that might significantly alter their physical properties. They must be dimensionally stable to keep the fibers at their relative position with respect to each other and provide adequate in-service performance.

Filter Criteria A variety of filter criteria have been developed by a number of organizations and researchers. From a review of these criteria, the Geotextile Engineering Manual (FHWA, 1989) suggested the use of more stringent criteria when the hydraulic loadings are severe or the performance of the drainage system is critical to the protection of roadways and pertinent structures. For less severe and less critical applications, cost savings can be realized by using the less stringent criteria. In view of the fact that the fabrics used for drainage are neither severe nor critical, only the less stringent criteria suggested by the manual are presented here.

Downloaded From : www.EasyEngineering.net

Downloaded From : www.EasyEngineering.net

The most important dimension of geotextiles is the apparent opening size, AOS, defined as the size of glass beads when 5% pass through the geotextile. The method for determining AOS is specified by the ASTM (1989a). There are two conflicting requirements for AOS. To achieve the maximum retention of soils, the smallest opening size (the largest AOS in terms of sieve number) should be used; yet, to minimize the clogging of fabrics, the maximum opening size (the lowest AOS) should be used.

Retention or Pumping Resistance Criteria

1. For fine-grained soils with more than 50% passing through a No. 200 sieve:

   Woven: $\text{AOS} \leq D_{85}$ (8.10*a*)

   Nonwoven: $\text{AOS} \leq 1.8D_{85}$ (8.10*b*)

   $\text{AOS} \geq$ No. 50 sieve or opening smaller than 0.297 mm (8.10*c*)

2. For granular materials with 50% or less passing through a No. 200 sieve:

   $$\text{AOS} \leq B \times D_{85} \tag{8.11}$$

   in which $B = 1$ when $C_u \leq 2$ or ≥ 8, $B = 0.5C_u$ when $2 \leq C_u \leq 4$, $B = 8/C_u$ when $4 < C_u < 8$, and C_u is the coefficient of uniformity $= D_{60}/D_{10}$.

3. When the protected soil contains particles from 1 in. (25.4 mm) to those passing through a No. 200 sieve, only the portion passing through a No. 4 sieve should be used to determine the grain size.

Permeability Criteria Methods for determining the permeability of fabric are specified by the ASTM. As with soils, both the constant and the falling head methods can be used. The result gives the permittivity of the fabric, which must be multiplied by the thickness of the fabric to obtain its permeability. To reduce hydraulic head loss in the filter and increase drainage efficiency, the fabric must be more permeable than the adjacent soil:

$$k(\text{fabric}) \geq k(\text{soil}) \tag{8.12}$$

Equation 8.12 can usually be satisfied unless the soil is extremely permeable.

Clogging Criteria

Woven: Percent open area $\geq 4\%$ (8.13*a*)

Nonwoven: Porosity $\geq 30\%$ (8.13*b*)

Example 8.5:

Figure 8.9 shows the grain size curves of two different soils, as indicated by the solid curves. Determine the required AOS of woven fabrics to retain the soils.

Downloaded From : www.EasyEngineering.net

Downloaded From : www.EasyEngineering.net

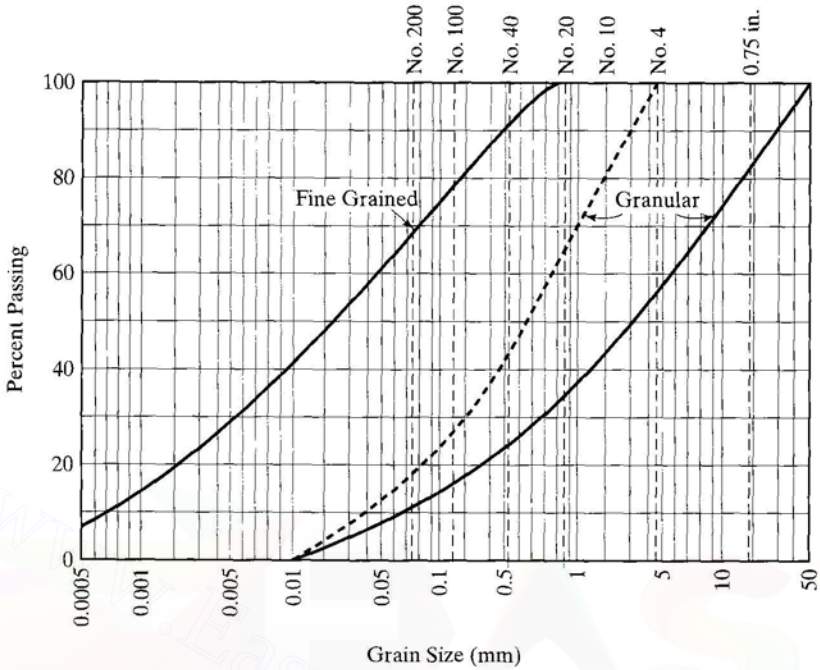


FIGURE 8.9

Example 8.5 (1 in. = 25.4 mm).

Solution: For the fine-grained soil, from Figure 8.9, $D_{85} = 0.24$ mm. From Eq. 8.10*a*, AOS ≤ 0.24 mm, so an AOS of No. 70, which corresponds to an apparent opening size of 0.21 mm, can be used. The selection of No. 70 also satisfies Eq. 8.10*c*.

For the granular material, only the fraction passing No. 4 is used for determining the grain size, as shown by the dashed curve in the figure. For any given grain size, the percent finer on the dashed curve can be obtained by dividing that on the solid curve by 0.57, which is the fraction passing through the No. 4 sieve. From the dashed curve, $D_{85} = 2.4$ mm, $D_{60} = 0.78$ mm, and $D_{10} = 0.042$ mm. From Eq. 8.11, with $C_u = 0.78/0.042 = 18.6$, $B = 1$, or AOS $\leq 1 \times 2.4 = 2.4$ mm. Therefore, an AOS greater than No. 16, which corresponds to an apparent opening size of 1.19 mm, can be used.

Applications Geotextiles for subsurface drainage may be used as an envelope of trench drains, a wrapping of pipe drains, or a filter of drainage layers. Figure 8.10 shows the various uses of geotextiles for pavement subdrainage.

In the design of subdrainage, geotextiles should be given consideration as an alternative design. Due to the relative ease of installation as compared to the difficulty of placing a filter aggregate and a coarse aggregate in separate layers without contamination, the use of geotextiles may be more cost effective.

Healey and Long (1972) described the use of prefabricated "fin" drains for longitudinal drains. These drains basically consist of a fin with vertical channels covered

Downloaded From : www.EasyEngineering.net

Downloaded From : www.EasyEngineering.net

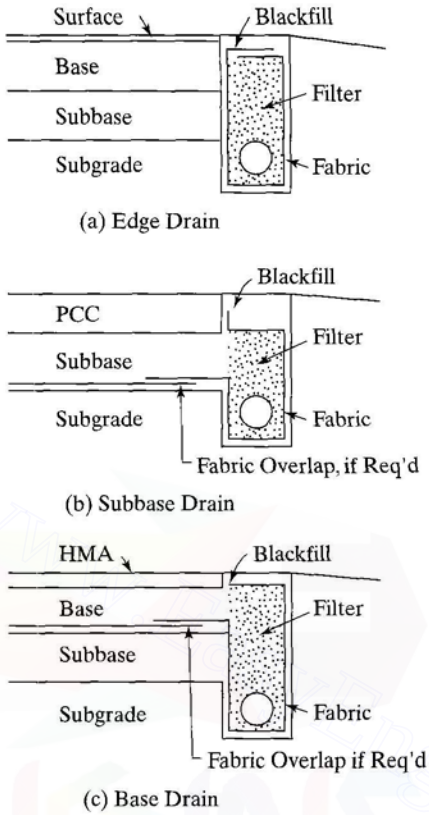


FIGURE 8.10
Use of geotextiles for subsurface drainage. (After Haliburton and Lawmaster (1981).)

with drainage fabric. The channels are connected to the pipe, as shown in Figure 8.11. Water enters through the drainage fabric, runs down the channels into the pipe, and is carried away from the site. This system can be installed in very narrow trenches and does not require any special fill, thus saving excavation and aggregate costs.

8.2.3 Pipes

The pipes to be used for subdrainage may be made of concrete, clay, bituminized fiber, metal, or various plastics with smooth or corrugated surfaces. When used as underdrains, most are perforated or slotted; a few have open joints, so that the water can flow freely into the pipes. They must be surrounded by suitable aggregates or fabrics as filter materials to prevent the openings from clogging. When used as outlet pipes, they do not need perforations, slots, or open joints and can be placed in a trench and backfilled with native soils.

Filter Criteria When perforated or slotted pipes are used for the collection and removal of water, the material in contact with the pipes must be coarse enough that no appreciable amount of this material can enter into the pipes. The criteria used by the U.S.

Downloaded From : www.EasyEngineering.net

Downloaded From : www.EasyEngineering.net

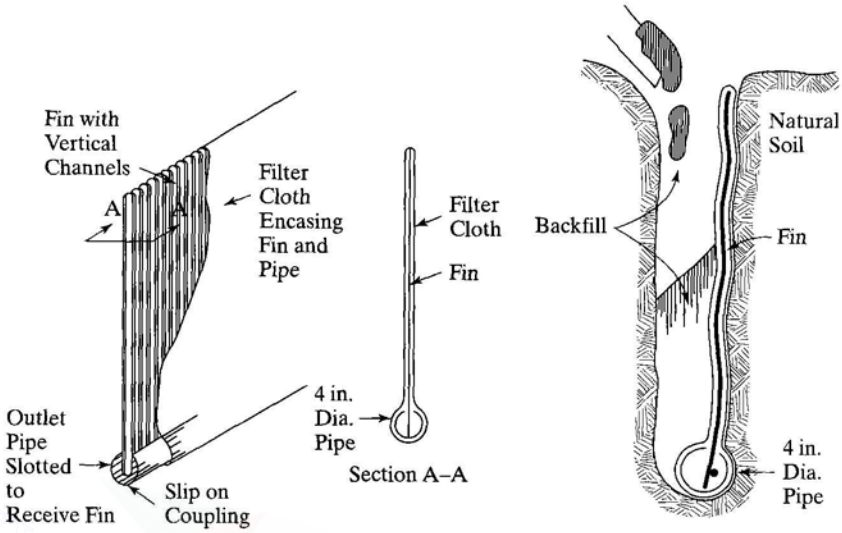


FIGURE 8.11

Use of prefabricated fin drain in trench. (1 in. = 25.4 mm). (After Healey and Long (1972).)

Army Corps of Engineers (1955) for pipes with slots and circular holes are as follows:

For slots:
$$\frac{D_{85} \text{ of filter material}}{\text{Slot width}} > 1.2 \tag{8.14}$$

For circular holes:
$$\frac{D_{85} \text{ of filter material}}{\text{Hole diameter}} > 1.0 \tag{8.15}$$

For open-jointed pipes, the U.S. Bureau of Reclamation (1973) specifies that

$$\frac{D_{85} \text{ of filter material}}{\text{Maximum opening of pipe}} \geq 2 \tag{8.16}$$

Applications Various types and sizes of pipes are available and can be used for the collection system. Physical strength is a major concern because the pipes could be subjected to heavy construction loading and rough handling. They must be durable under the physical and chemical environments to which they will be exposed. For example, metal pipes should not be used in areas of mine wastes and coal seams, to avoid corrosion by acid water. Some plastic pipes should not be placed in areas with gnawing rodents. Existing ASTM and AASHTO specifications and manufacturer's design recommendations should be consulted in selecting the proper types. Precedents based on past experience and history of performance together with economic considerations generally play an important role in the selection process.

Downloaded From : www.EasyEngineering.net

Downloaded From : www.EasyEngineering.net

Collector pipes are generally placed on compacted bedding material with perforations or slots down to reduce the possibility of sedimentation in the pipe and to lower the static water level in the trench. However, in extremely wet and muddy situations, where maintaining the trench and bedding materials in a free draining condition is difficult, it may be advisable to place collector pipes with the perforations and slots up or oriented somewhat laterally toward the direction of flow.

Outlet pipes should be installed at convenient intervals to convey the collected water to a suitable and safe exit point. The exit must be protected from natural and man-made hazards. This protection generally consists of a headwall and a combination of screens or valves and markers. Screens are usually adequate to prevent small animals or birds from nesting or depositing debris in the pipes. If high flows with a level above the outlet pipe are expected to occur in the outfall ditches, flap valves can be used to prevent backflow or deposition of debris. Suitable markers should be installed at each outlet site to facilitate inspection and maintenance.

8.3 DESIGN PROCEDURES

Figure 8.12 shows the cross section of a two-lane highway with asphalt shoulders. The concrete pavement is 9 in. (229 mm) thick with an open-graded subbase that also serves as a drainage layer. The drainage layer is 6 in. (152 mm) thick and is connected to the perforated or slotted collector pipes for lowering the water table and removing the inflow. This figure is used in the examples that follow to illustrate the design procedures.

8.3.1 Estimation of Inflow

The major sources of inflow are surface infiltration, groundwater seepage, and meltwater from ice lenses. Surface infiltration is the most important source of water and should always be considered in subdrainage design. Whenever possible, groundwater

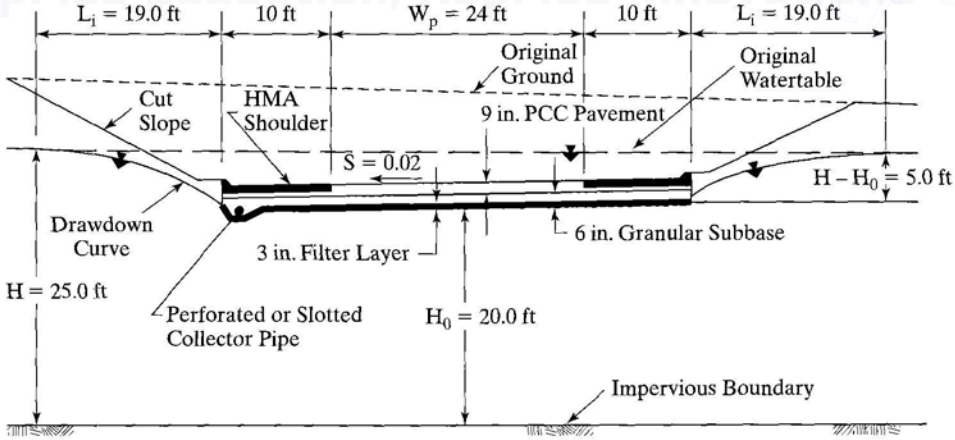


FIGURE 8.12

Subdrainage of rigid pavement in cut section (1 ft = 0.305 m, 1 in. = 25.4 mm).

Downloaded From : www.EasyEngineering.net

Downloaded From : www.EasyEngineering.net

should be lowered by deep longitudinal drains and should not be allowed to seep into the pavement structure, as shown in Figure 8.5. If this is not feasible, the amount of seepage entering the drainage layer should be estimated. The meltwater from ice lenses needs to be considered only in northern climates with frost heave. Because frozen fine-grained soils are very impermeable, it is unlikely that flow from both groundwater and meltwater would occur at the same time. Therefore, only the larger of the inflows need be considered.

Surface Infiltration When water table is at a considerable distance below the pavement surface, as in the case of a high fill, surface infiltration is probably the only water to be considered for subdrainage design. Cedergren *et al.* (1973) recommended that the design infiltration rate be found by multiplying the 1-h duration/1-yr frequency rain rate by a coefficient varying from 0.33 to 0.50 for asphalt pavements and 0.50 to 0.67 for concrete pavements. Figure 8.13 shows the 1-h duration/1-yr frequency precipitation rates in the United States.

Given the results of infiltration tests in Connecticut, Ridgeway (1976) indicated that the duration of rainfall is a more critical factor than the intensity. He found that the amount of infiltration can be related directly to cracking and suggested that an infiltration rate I_c of 2.4 ft^3/day/ft of crack (0.22 m^3/day/m) be used for design. The infiltration rate per unit area q_i can be expressed as

$$q_i = I_c\left(\frac{N_c}{W_p} + \frac{W_c}{W_p C_s}\right) + k_p \tag{8.17}$$

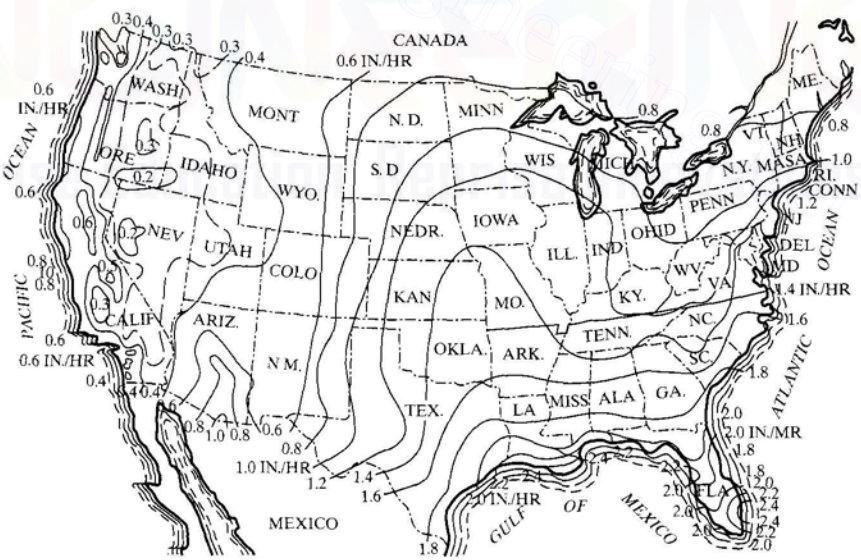


FIGURE 8.13

Maximum 1-h-duration/1-yr-frequency precipitation in the United States (1 in. = 25.4 mm). (After Cedergren *et al.* (1973).)

Downloaded From : www.EasyEngineering.net

Downloaded From : www.EasyEngineering.net

in which I_c is the crack infiltration rate, N_c is the number of longitudinal cracks, W_p is the width of pavement subjected to infiltration, W_c is the length of transverse cracks or joints, C_s is the spacing of transverse cracks or joints, and k_p is the rate of infiltration through uncracked pavement surface, which is numerically equal to the coefficient of permeability of HMA or PCC and is exceedingly small. By assuming that $N_c = N + 1$, where N is the number of traffic lanes, $W_c = W_p$, $k_p = 0$, and the infiltration rate is 0.1 ft^3/h/ft of crack, the inflow rate can be written as (Ridgeway, 1982)

$$q = q_i W_p = 0.1\left(N + 1 + \frac{W_p}{C_s}\right) \tag{8.18}$$

in which q is the inflow rate in ft^3/h/linear ft of pavement and C_s is the joint spacing for concrete pavements and is 40 ft (12.2 mm) for asphalt pavements.

Example 8.6:

The two-lane pavement shown in Figure 8.12 has a width of 24 ft (7.3 m) and a joint spacing of 15 ft (4.6 m). Compute the amount of surface infiltration q_i using Eq. 8.18. Assume that the pavement is located in Connecticut. Determine the surface infiltration by Cedergren's method.

Solution: Given $N = 2$, $W_p = 24$ ft (7.3 m), and $C_s = 15$ ft (4.6 m), from Eq. 8.18 $q = 0.1 \times (2 + 1 + 24/15) = 0.46$ ft^3/h/ft of pavement (0.042 m^3/h/m), or $q_i = 0.46/24 = 0.0192$ ft^3/h/ft^2 (0.00585 m^3/h/m^2), which is equivalent to 0.23 in./h (5.8 mm/h), or 0.46 ft/day (0.14 m/day). In determining q_i, the effect of paved shoulders is not considered. It is assumed that the infiltration through the shoulders is the same as that through the pavement. When the drainage layer extends over the entire roadway, the infiltration through the pavement per unit area is applied over the entire roadway, including the shoulders.

If the pavement is located in Connecticut, from Figure 8.13, the 1-h duration/1-yr frequency precipitation rate is 1.1 in. (28 mm). Cedergren's recommendation is to apply a coefficient of 0.50 to 0.67, so the surface infiltration ranges from 0.55 to 0.74 in./h (14.0 to 18.8 mm/h).

In this example, the infiltration obtained by Cedergren's method is much greater than that by Eq. 8.18. The results will check better in the western part of the United States, where there is less precipitation. It is recommended that Eq. 8.18 be used in the eastern part of the United States, because it is more rational and is based on field measurements. However, Cedergren's method can be used as a check, and, if necessary, the larger of the two can be used.

Groundwater Seepage If the drainage layer is used to lower the water table, in addition to providing drainage for surface infiltration, the chart shown in Figure 8.14 can be applied to determine the inflow from groundwater. The chart is applicable to the general case where an impervious boundary lies at a certain distance below the drainage layer. The inflow is divided into two parts. The inflow above the bottom of the drainage layer is q_1 and can be determined from

$$q_1 = \frac{k(H - H_o)^2}{2L_i} \tag{8.19}$$

Downloaded From : www.EasyEngineering.net

Downloaded From : www.EasyEngineering.net

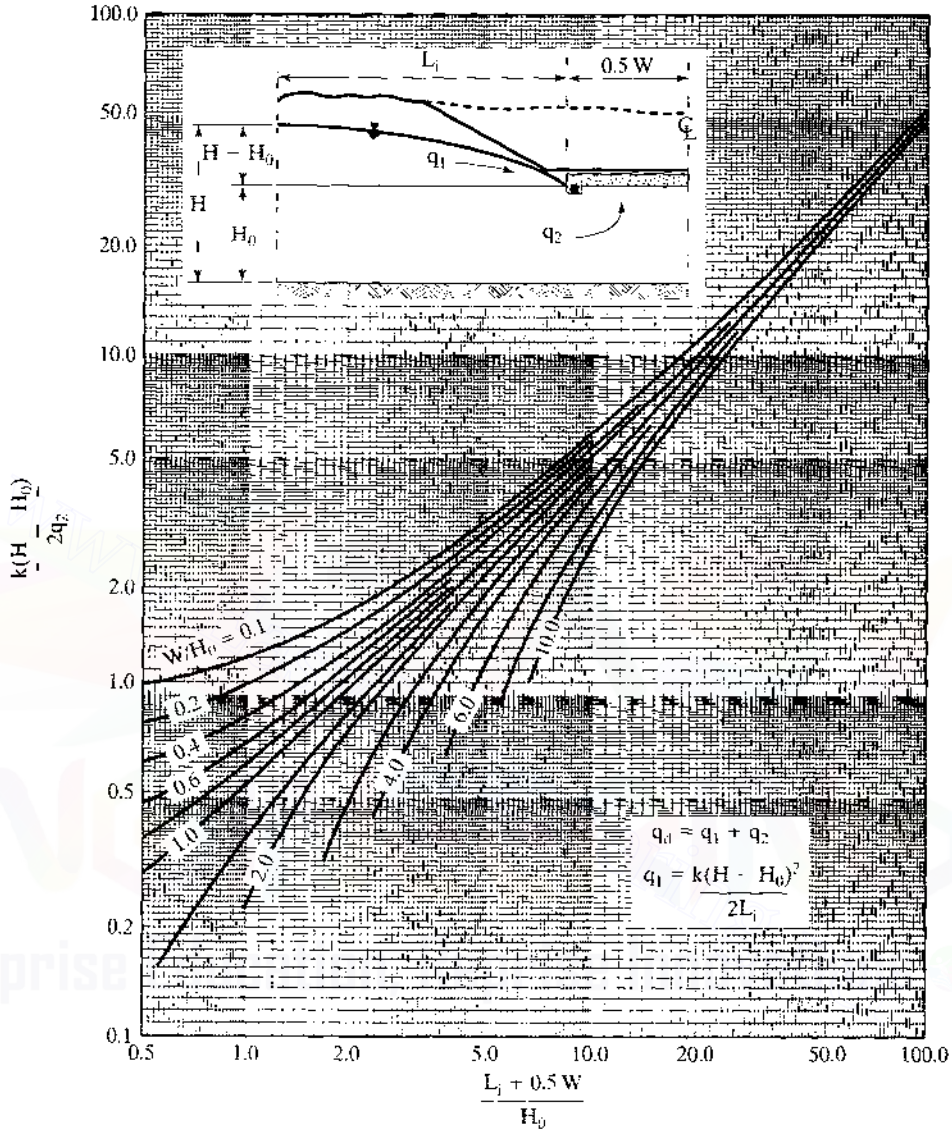


FIGURE 8.14

Chart for determining inflow of groundwater. (After Moulton (1980).)

in which k is the permeability of the soil in the cut slope or in the subgrade, H is the initial height of the groundwater table above the impervious layer, H_o is the vertical distance between the bottom of drainage layer and the impervious layer, and L_i is the distance of influence, which can be determined as

$$L_i = 3.8(H - H_o) \tag{8.20}$$

Downloaded From : www.EasyEngineering.net

Downloaded From : www.EasyEngineering.net

The inflow below the drainage layer is q_2 and can be determined from Figure 8.14. Note that q_1 and q_2 are the volume of flow per unit time per unit length of the longitudinal drain. The lateral flow is

$$q_L = q_1 + q_2 \tag{8.21}$$

The groundwater inflow to the drainage layer per unit area is

$$q_g = \frac{2q_2}{W} \tag{8.22}$$

in which W is the width of the roadway. However, if the pavement is sloped to one side and the collector pipes are installed only on one side, as shown in Figure 8.12, the lateral inflow per unit length of pipe is

$$q_L = 2(q_1 + q_2) \tag{8.23}$$

and

$$q_g = \frac{q_1 + 2q_2}{W} \tag{8.24}$$

Example 8.7:

For the situations shown in Figure 8.12, if the native soil is a silty sand with a permeability of 0.34 ft/day (1.2×10^{-4} cm/s), determine the inflow q_L to the longitudinal drain and q_g to the drainage layer.

Solution: Given $H = 25$ ft (7.6 m) and $H_o = 20$ ft (6.1 m), from Eq. 8.20, $L_i = 3.8 \times (25 - 20) = 19$ ft (5.8 m). From Eq. 8.19, $q_1 = 0.34 \times (25 - 20)^2/(2 \times 19) = 0.22$ ft^3/day/ft of longitudinal drain (0.021 m^3/day/m).

With $W/H_o = 44/20 = 2.2$ and $(L_i + 0.5W)/H_o = (19 + 0.5 \times 44)/20 = 2.05$, from Figure 8.14, $k(H - H_o)/(2q_2) = 0.74$, or $q_2 = 0.34 \times (25 - 20)/(2 \times 0.74) = 1.15$ ft^3/day/ft of drainage layer (0.107 m^3/day/m). From Eq. 8.23, $q_L = 2(0.22 + 1.15) = 2.74$ ft^3/day/ft (0.25 m^3/day/m). From Eq. 8.24, $q_g = (0.22 + 2 \times 1.15)/44 = 0.057$ ft^3/day/ft^2 (0.017 m^3/day/m^2). Compared to a q_i of 0.46 ft^3/day/ft^2 (0.14 m^3/day/m^2), the contribution by q_g is very small.

Meltwater from Ice Lenses From the theory of consolidation, Moulton (1980) developed a simple chart for estimating the inflow of meltwater from ice lenses, as shown in Figure 8.15. The rate of seepage from the consolidating soil is at maximum immediately following thawing and decreases rapidly as the time increases. The maximum rate of drainage exists for only a short period of time, so the design inflow rate q_m is taken as the average during the first day after thawing. The inflow q_m depends on the average rate of heave and the permeability k of subgrade soil as well as the consolidation pressure σ_p on the subgrade. The average rate of heave can be determined from laboratory tests or estimated by using Table 8.5. The value of σ_p can be determined simply by calculating the weight per unit area of pavement structure above the subgrade. In using the chart, the unit of q_m is ft^3/day/ft^2 and that of k is ft/day.

Downloaded From : www.EasyEngineering.net

Downloaded From : www.EasyEngineering.net

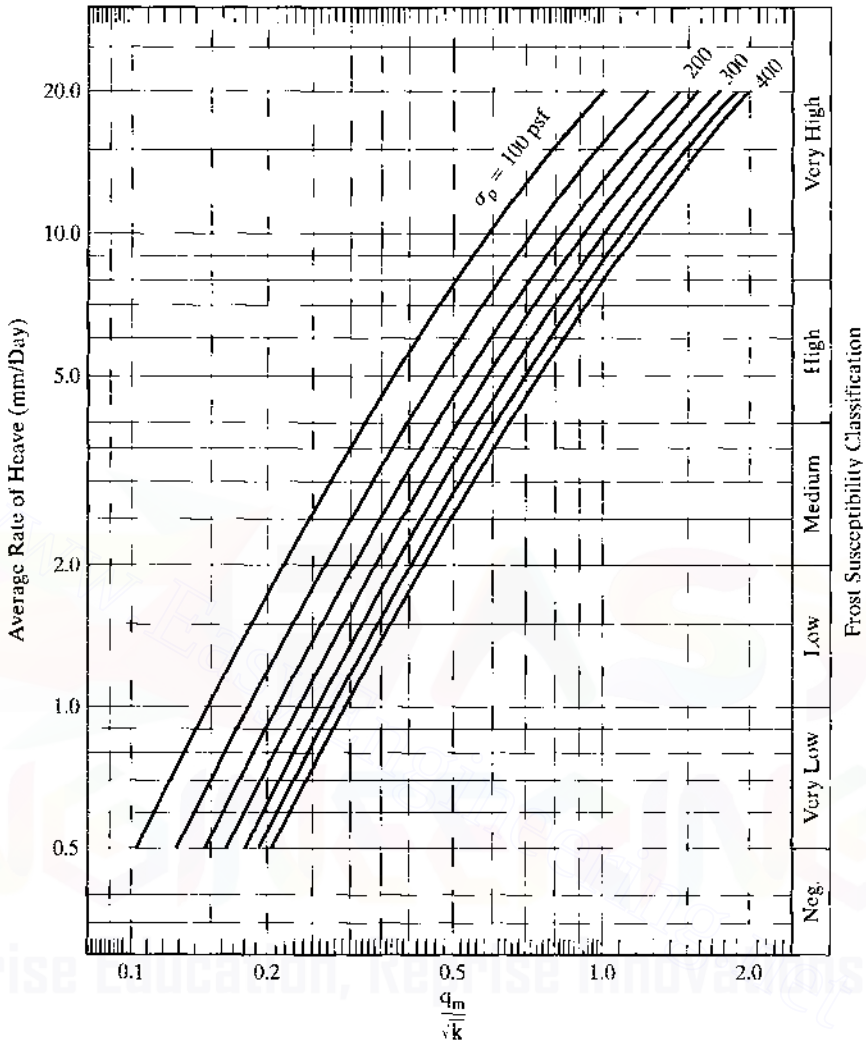


FIGURE 8.15

Chart for estimating inflow of meltwater from ice lenses (1 psf = 0.048 kPa). (After Moulton (1980).)

Example 8.8:

If the silty sand subgrade of the previous example has 9% of particles finer than 0.02 mm and is subjected to frost action, determine the inflow q_m to the drainage layer due to the melting of ice lenses.

Solution: The silty sand can be classified as SM. With 9% finer than 0.02 mm, from Table 8.5, the heave rate is 9 mm/day. If unit weights are 150 pcf (23.6 kN/m^3) for the concrete and 115 pcf (18.1 kN/m^3) for the drainage layer, then $\sigma_p = 150(9/12) + 115(6/12) = 170$ psf. From Figure 8.15,

Downloaded From : www.EasyEngineering.net

Downloaded From : www.EasyEngineering.net

$q_m/\sqrt{k} = 0.74$, or $q_m = 0.74 \times \sqrt{0.34} = 0.43$ ft^3/day/ft^2 (0.13 m^3/day/m^2). It can be seen that the value of q_m is as large as q_i in Example 8.5. In areas of seasonal frost, the meltwater from ice lenses constitutes an important part of the total inflow.

Design Inflow The design inflow is the sum of the inflows from all sources minus the outflow through the subgrade soil. The outflow through subgrade depends on the permeability of the soil and on the water table at the boundary and can be determined by the use of flownets or other simplified design charts, as presented by Moulton (1980). When the subgrade is not affected by any water table, a simple and conservative method to estimate the outflow capacity is to assume the hydraulic gradient to be 1, as illustrated in Example 8.1, so the outflow rate is equal to the permeability of the soil. In Example 8.6, the soil has a permeability of 0.34 ft/day (1.2×10^{-4} cm/s), so the outflow

TABLE 8.5 Guidelines for Selecting Heave Rate for Use with Figure 8.15

Unified classification		Percent passing 0.02 mm	Heave rate (mm/day)	Frost susceptibility classification
Soil type	Symbol			
Gravel and	GP	0.4	3.0	Medium
sandy gravel	GW	0.7–1.0	0.3–1.0	Negligible to low
		1.0–1.5	1.0–3.5	Low to medium
		1.5–4.0	3.5–2.0	Medium
Silty and	GP-GM	2.0–3.0	1.0–3.0	Low to medium
sandy gravel	GW-GM	3.0–7.0	3.0–4.5	Medium to high
	GM	7.0–10.0	4.5–3.0	High to medium
Clayey and	GW-GC	4.2	2.5	Medium
Silty gravel	GM-GC	15.0	5.0	High
	GC	15.0–30.0	2.5–5.0	Medium to high
Sand and	SP	1.0–2.0	0.8	Very low
gravelly sand	SW	2.0	3.0	Medium
Silty and	SP-SM	1.5–2.0	0.2–1.5	Negligible to low
gravelly sand	SW-SM	2.0–5.0	1.5–6.0	Low to high
	SM	5.0–9.0	6.0–9.0	High to very high
	SM	9.0–22.0	9.0–5.5	Very high to high
Clayey and	SM-SC	9.5–35.0	5.0–7.0	High
silty sand	SC	9.5–35.0	5.0–7.0	High
Silt and	ML-OL	23.0–33.0	1.1–14.0	Low to very high
organic silt	ML	33.0–45.0	14.0–25.0	Very high
	ML	45.0–65.0	25.0	Very high
Clayey silt	ML-CL	60.0–75.0	13.0	Very high
Gravelly and sandy clay	CL	38.0–65.0	7.0–10.0	High to very high
Lean clay	CL	65.0	5.0	High
	CL-OL	30.0–70.0	4.0	High
Fat clay	CH	60.0	0.8	Very low

Downloaded From : www.EasyEngineering.net

Downloaded From : www.EasyEngineering.net

rate will be 0.34 $ft^3/day/ft^2$ (0.10 $m^3/day/m^2$), which is quite large compared to the surface infiltration of 0.46 $ft^3/day/ft^2$ (0.14 $m^2/day/m^2$).

If the outflow through the subgrade is neglected, the design inflow can be determined by one of the following combinations:

1. If there in no frost action, the design inflow q_d is the sum of surface infiltration q_i and groundwater flow q_g:

$$q_d = q_i + q_g \tag{8.25}$$

   If there is no groundwater flow, then $q_g = 0$, so $q_d = q_i$.
2. If there is frost action, q_d is the sum of surface infiltration q_i and inflow from meltwater q_m:

$$q_d = q_i + q_m \tag{8.26}$$

If q_d obtained from Eq. 8.25 is greater than that from Eq. 8.26, then Eq. 8.25 should be used.

Example 8.9:

Given the results of the three previous examples, determine the design inflow q_d to the drainage layer and q_L to the longitudinal drain.

Solution: The inflows to the drainage layer are $q_i = 0.46\ ft^3/day/ft^2$ (0.14 $m^3/day/m^2$), $q_g = 0.057\ ft^3/day/ft^2$ (0.017 $m^3/day/m^2$), and $q_m = 0.43\ ft^3/day/ft^2$ (0.13 $m^3/day/m^2$), and the inflow to the longitudinal drain q_l is 0.22 $ft^3/day/ft$ (0.021 $m^3/day/m$). If there is no frost action, from Eq. 8.25, $q_d = 0.46 + 0.057 = 0.517\ ft^3/day/ft^2$ (0.158 $m^3/day/m^2$) and $q_L = 0.517 \times 44 + 0.22 = 23.0\ ft^3/day/ft$ (2.14 $m^3/day/m$). If there is frost action, from Eq. 8.26, $q_d = 0.46 + 0.43 = 0.89\ ft^3/day/ft^2$ (0.27 $m^3/day/m^2$) and $q_L = 0.89 \times 44 = 39.2\ ft^3/day/ft$ (3.64 $m^3/day/m$).

8.3.2 Determination of Drainage Capacity

The capacity of both the drainage layer and the collector pipe must be designed so that the outflow rate is greater than the inflow rate and the water can be carried out safely from the sources to the outlet sites.

Drainage Layer There are two design requirements for a drainage layer. First, the steady-state capacity must be greater than the inflow rate. Second, the unsteady-state capacity must be such that the water can be drained quickly after each precipitation event.

Steady-State Flow Figure 8.16 shows the dimensions of the drainage layer. The steady-state capacity of the drainage layer can be computed (Baber and Sawyer, 1952) as

$$q = kH\left(S + \frac{H}{2L}\right) \tag{8.27}$$

in which q is the discharge capacity of the drainage layer, k is the permeability of the drainage layer, S is the slope of the drainage layer, H is the thickness of the drainage

Downloaded From : www.EasyEngineering.net

Downloaded From : www.EasyEngineering.net

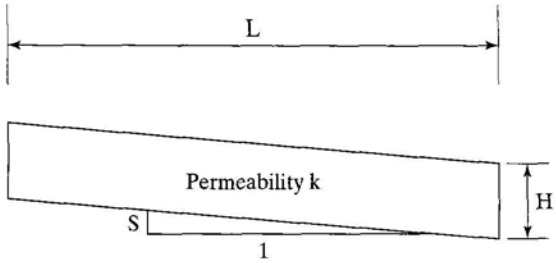


FIGURE 8.16
Dimension of drainage layer.

layer, and L is the length of the drainage layer. Equation 8.27 indicates that the discharge is composed of two terms. The first term is the discharge through area H caused by the hydraulic gradient S; the second term is that through area $H/2$ caused by the hydraulic gradient H/L. When $S = 0$, $q = 0.5k\,H^2/L$, which is a direct application of Darcy's law, assuming that the phreatic surface is at the top of the drainage layer on one end and at the bottom of the layer on the other end, with an average flow area of $H/2$. The drainage capacity q must be greater than $q_d L$. If the subgrade is permeable with significant outflow, then the capacity of the drainage layer must be greater than the design inflow minus the subgrade outflow.

Unsteady-State Flow The unsteady-state flow capacity is defined by the degree of drainage, which is a ratio between the volume of water drained since the rain stops and the total storage capacity of the drainage layer. Casagrande and Shannon (1952) showed that the time for a 50% degree of drainage can be computed as

$$t_{50} = \frac{n_e L^2}{2k(H + SL)} \tag{8.28}$$

in which t_{50} is the time for 50% drainage and n_e is the effective porosity, which is the porosity occupied by drainable water. For open-graded materials, all water is drainable, so the effective porosity is the same as the total porosity. Equation 8.28 was applied by Casagrande and Shannon to the design of the base course. They recommended that the time for 50% drainage of a saturated base not be greater than 10 days. This criterion is certainly inadequate for modern highways under heavy traffic. For example, the AASHTO (1986) design guide divides the quality of drainage into five categories: excellent, good, fair, poor, and very poor. If 50% of the water is removed within 10 days, several months will be required to remove most of the water, and the drainage is classified as very poor. For excellent drainage, AASHTO requires that water be removed within 2 h. For the design of drainage layer, the requirement that the time for complete or 95% drainage be less than 1 h, as used by Ridgeway (1982) to compare several different criteria, appears to be more appropriate.

In discussing the paper by Casagrande and Shannon (1952), Barber presented a simple chart to determine the time required for any degree of drainage, as shown in Figure 8.17. The degree of drainage U depends on a time factor T_f and a slope factor S_f, respectively defined as

$$T_f = \frac{kHt}{n_e L^2} \tag{8.29}$$

Downloaded From : www.EasyEngineering.net

Downloaded From : www.EasyEngineering.net

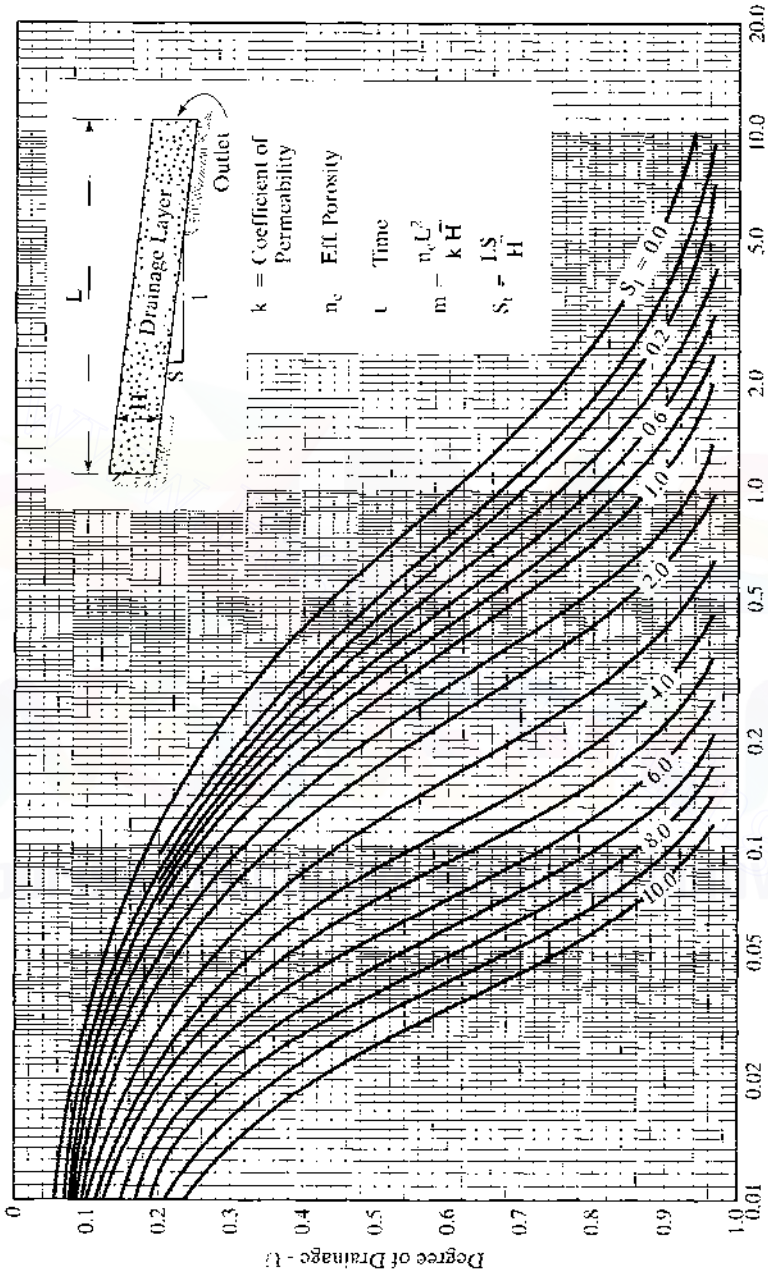


FIGURE 8.17
Time-dependent drainage of saturated layer. (After Barber and Sawyer (1952).)

Downloaded From : www.EasyEngineering.net

Downloaded From : www.EasyEngineering.net

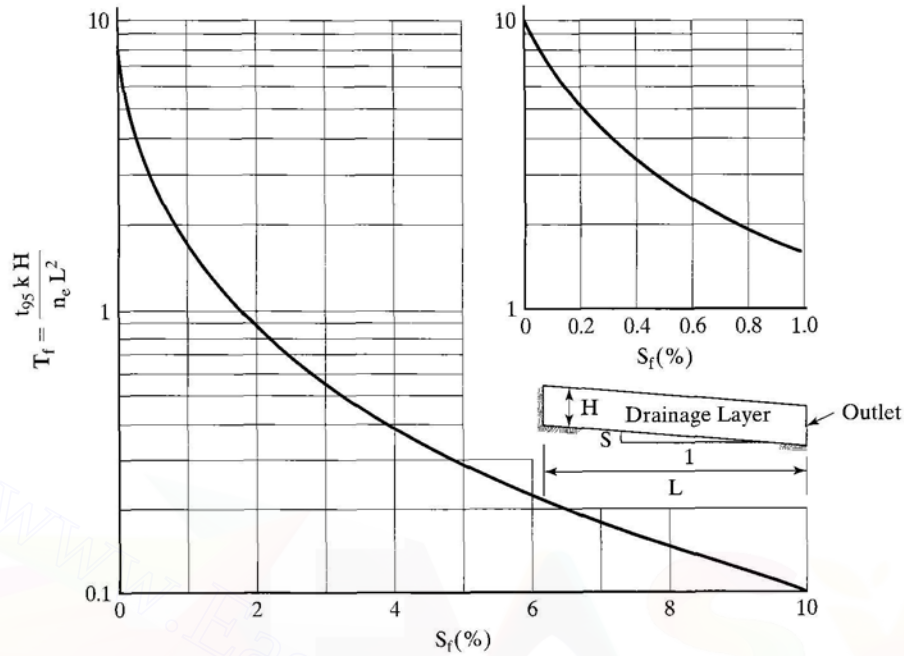


FIGURE 8.18

Relationship between time and slope factors for 95% drainage.

and

$$S_f = \frac{LS}{H} \tag{8.30}$$

in which t is the time since the rain stopped and drainage began. Given Figure 8.17, the relationship between the time factor for 95% drainage and the slope factor can be plotted in Figure 8.18 and used directly for design purposes.

Example 8.10:

For a drainage layer with $S = 0.02$, $H = 0.5$ ft (152 mm), $L = 22$ ft (6.7 m), a permeability k of 6000 ft/day (2.1 cm/s), and a porosity n_e of 20%, determine the steady-state capacity of the drainage layer and the time for 50% and 95% drainage, respectively.

Solution: The steady-state capacity can be determined from Eq. 8.27; $q = 6000 \times 0.5 \times (0.02 + 0.5/44) = 94.1$ ft^3/day/ft of drainage layer (8.7 m^3/day/m), which is 2.4 times greater than the maximum inflow of 39.2 ft^3/day/ft (3.64 m^3/day/m) obtained in Example 8.8.

The time for 50% drainage can be obtained either directly from Eq. 8.28 or from Figure 8.17. From Eq. 8.28, $t_{50} = 0.2 \times (22)^2/[2 \times 6000 \times (0.5 + 0.02 \times 22)] = 0.0086$ day, or 0.21 h. If Figure 8.17 is used, it can be found that the time factor T_f corresponding to $U = 0.5$ and $S_f = 22 \times 0.02/0.5 = 0.88$ is 0.265. From Eq. 8.29, $t_{50} = 0.265 \times 0.2 \times (22)^2/(6000 \times 0.5) = 0.0086$ day, or 0.21 h, which is exactly the same as the result obtained from Eq. 8.28.

Downloaded From : www.EasyEngineering.net

Downloaded From : www.EasyEngineering.net

The time for 95% drainage can be obtained from Figure 8.18. With $S_f = 0.88$, from Figure 8.18, $T_f = 1.8$, or $t_{95} = 1.8 \times 0.2 \times (22)^2/(6000 \times 0.5) = 0.058$ day, or 1.39 h. If the design is based on a maximum t_{95} of 1 h, the permeability of 6000 ft/day (2.1 cm/s) is not sufficient and should be increased to 1.39×6000, or 8340 ft/day (2.9 cm/s). If open-graded aggregates are used as drainage layers, the permeability will be much greater than the above value and there is no difficulty in satisfying the criterion that the time required for 95% drainage be less than 1 h.

The above example clearly illustrates that, if open-graded aggregates are used as drainage layers, the following two design criteria can be easily satisfied:

1. The lateral outflow rate, as computed by Eq. 8.27, must be greater than the inflow rate.
2. The time for 95% drainage, obtained from Figure 8.18, must be smaller than 1 h.

Collector Pipes A system of longitudinal collectors with some transverse collectors at critical points is generally used to remove the free water from the drainage layer (and from groundwater, if any). Transverse collectors may be used when the combination of transverse and longitudinal grades is such that flow tends to take place more in the longitudinal direction than in the transverse direction. The collection system consists of a set of perforated, slotted, or open-jointed pipes that are used to remove water from the pavement structure and to convey it to suitable outlets outside the roadway limits. The design of such systems should consider the type of pipe used, the location and depth of transverse and longitudinal collectors and their outlets, the slope and size of the collector pipes, and the provision of adequate filter protection for the pipes.

The longitudinal roadway grades or the cross slopes usually govern the slopes of the collector pipes. The pipes are simply set at a constant depth below the roadway surface. However, practical construction and operational factors dictate that slopes of collector pipes not be less than 1% for smooth bore pipes and 2% for corrugated pipes. Thus, in areas where the longitudinal grades or cross slopes are very flat, it may be necessary to steepen the grades of collector pipes to meet these minimum requirements. The size and flow capacity of the collector depend in part on the pipe gradient, so it might be necessary to steepen the pipe gradient to achieve a reduction in pipe size. Minimum recommended diameters are 3 in. (76 mm) for PVC pipes and 4 in. (102 mm) for all other pipes (Cedergren *et al.*, 1972).

Figure 8.19 shows the location and depth of longitudinal collectors. If there is no significant frost penetration and no groundwater, the longitudinal collector pipes may be placed in shallow trenches, as shown in (*a*). If there is significant frost penetration or it is desirable to draw down the groundwater table, deeper trenches should be used, as shown in (*b*). In either case, the longitudinal collector drain can be placed just outside the pavement edge, which is the most critical location for pumping. It can also be placed at the outer edge of the shoulder to provide drainage for the entire shoulder area. However, this will significantly increase the length of flow, or decrease the hydraulic gradient, in the drainage layer and so could cause an increase in the thickness required.

When deeper trenches are used, the trench backfill must have enough permeability that the water from the drainage layer can be freely transmitted to the collector pipe.

Downloaded From : www.EasyEngineering.net

Downloaded From : www.EasyEngineering.net

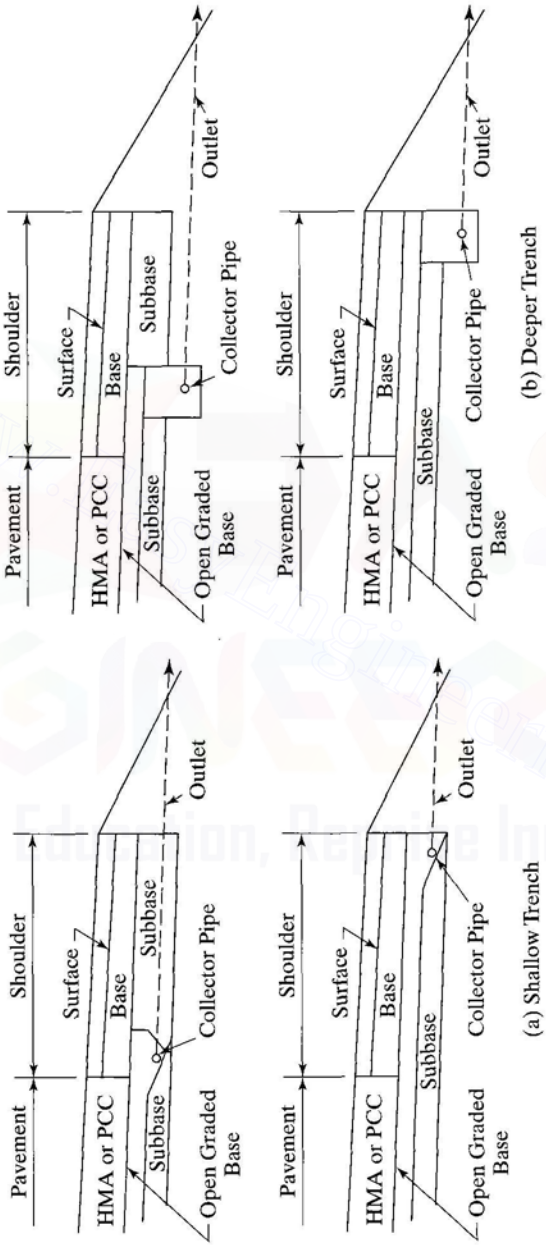


FIGURE 8.19
Location and depth of collector pipes. (After Cedergren *et al.* (1972).)

Downloaded From : www.EasyEngineering.net

Downloaded From : www.EasyEngineering.net

TABLE 8.6 Typical Roughness Coefficients for Underdrain

Clay drain tile	0.014–0.018
Concrete drain tile	0.011–0.015
Asbestos cement perforated drain tile	0.013
Bituminous fiber tile	0.012
Corrugated metal pipe	0.017–0.024
Corrugated polyethylene tubing	0.020
Smooth plastic pipe	0.008–0.012

The required permeability k can be determined directly from Darcy's law by assuming a hydraulic gradient of unity, or

$$k = \frac{\text{Discharge per unit length of trench}}{\text{Width of trench}} \tag{8.31}$$

Equation 8.31 can be used to determine the width of the trench if the permeability of the aggregate in the trench is given.

The discharge capacity of collector pipes can be calculated by Manning's formula for channel flow as

$$Q = 86{,}400\left(\frac{1.486}{n} A\, R^{2/3}\, S^{1/2}\right) \tag{8.32}$$

in which Q is the discharge in ft^3/day, n is the roughness coefficient, A is the area of pipe in ft^2, R is the hydraulic radius of pipe in ft, S is the slope of pipe in ft/ft. Table 8.6 shows typical roughness coefficients for underdrains.

The hydraulic radius is a ratio between flow area and wetted perimeter. When the flow in the pipe is full, $A = \pi D^2/4$ and the wetted perimeter $= \pi D$, so $R = D/4$, where D is the pipe diameter. Substituting the above A and R into Eq. 8.32 and noting that $Q = q_L L_o$, where L_o is the distance between two outlet points, yields

$$nq_L L_o = 53\, S^{0.5}\, D^{2.667} \tag{8.33}$$

in which n is the roughness coefficient, q_L is the lateral flow in ft^3/day/ft, L_o is the distance between outlets in ft, S is the slope in ft/ft, and D is the diameter of the pipe in inches. Equation 8.33 shows the relationships among n, q_L, L_o, S, and D. Given any four of the above values, the other one can be computed. To determine the diameter of the pipe, Eq. 8.33 can be written as

$$D = \left(\frac{nq_L L_o}{53 S^{0.5}}\right)^{0.375} \tag{8.34}$$

Example 8.11:

Corrugated metal pipe with a roughness coefficient of 0.024 is placed at 2% slope in a trench drain. Outlets are provided at every 500 ft (152 m), and the lateral flow is 39.2 ft^3/day/ft (3.64 m^3/day/m), as obtained in Example 8.8. Determine the diameter of the pipes required.

Downloaded From : www.EasyEngineering.net

Downloaded From : www.EasyEngineering.net

Solution: Given $n = 0.024$, $q_L = 39.2\ ft^3/day/ft$ ($3.64\ m^3/day/m$), $L_o = 500\ ft$ (152 m), and $S = 0.02$, from Eq. 8.34, $D = [0.024 \times 39.2 \times 500/(53 \times \sqrt{0.02})]^{0.375} = 4.72$ in. (120 mm). Use 5-in. (127-mm) pipes.

SUMMARY

Drainage is one of the most important factors in pavement design. Although highway engineers have long paid much attention to surface and groundwater drainage, very little has been done to provide drainage for surface infiltrations through joints and cracks, and, possibly, for the meltwater from ice lenses. The use of drainage layers and longitudinal drains to take care of surface infiltration and meltwater from ice lenses is the main theme of this chapter.

Important Points Discussed in Chapter 8

1. Water entrapped in the pavement structure not only weakens pavements and subgrades, but also generates high hydrodynamic pressures which pump out the fine materials under the pavement and result in loss of support.
2. The movement of water in pavements is governed by Darcy's law. In most instances, Darcy's law can be applied directly to the design of drainage systems.
3. The detrimental effects of water can be minimized by preventing it from entering the pavement, by providing drainage to remove it quickly, or by building the pavement strong enough to resist the combined effect of load and water. Of the above three methods, the first is difficult to achieve and the last is expensive, so the provision of drainage is the most practical and economical approach. All important highways should be provided with a drainage layer under the pavement.
4. The aggregates used for drainage purposes must satisfy the filter requirements. They must be fine enough to prevent the adjacent soil from piping or migrating into them but also coarse enough to carry water through them with no significant resistance. To meet the filter criteria, it could be necessary to use several different aggregates, one placed adjacent to the other. This procedure is difficult to construct without contamination and can be replaced by the use of geotextiles.
5. Geotextiles for subsurface drainage may be used as an envelope for trench drains, a wrapping for pipe drains, or a filter for drainage layers. A geotextile can easily be selected to satisfy the filter criteria without using one or more aggregates.
6. The most effective location for the drainage layer is directly under the HMA or PCC, but drainage layers may also be placed on the top of subgrade. To increase shear strength and facilitate compaction, the open-graded drainage material may be treated with a small amount of asphalt. The drainage layer is usually connected to longitudinal drains with collector pipes, although a daylighted construction extending over the entire roadway to the side slope may also be used.
7. The design inflow q_d for drainage layers should be based on either surface infiltration plus groundwater inflow, $q_i + q_g$, or on surface infiltration plus inflow from melting ice lenses, $q_i + q_m$, whichever is greater.

Downloaded From : www.EasyEngineering.net

Downloaded From : www.EasyEngineering.net

8. The lateral outflow from the drainage layer must satisfy two requirements. First, the steady-state outflow per unit width, as indicated by Eq. 8.27, should be greater than $q_d L$, where L is the length of drainage layer. Second, the unsteady-state flow after the cessation of rain should remove 95% of the initially saturated water within a very short time, say, 1 h.
9. Manning's formula, as indicated by Eq. 8.32, can be used to determine the discharge capacity of collector pipes. The diameter of the pipe required can be computed directly by Eq. 8.34, given lateral inflow q_L, distance between outlets L_o, roughness coefficient n, and slope of the pipe S.

PROBLEMS

8.1 Water is sprayed uniformly over a 400-ft^2 soil surface. If the soil has a permeability of 0.001 ft/min, what is the maximum spray rate in gal/min so that all water will be absorbed by the soil and there is no overland flow? [Answer: 2.99 gpm]

8.2 Determine D_{15} and D_{85} of sample 6 in Table 8.3. [Answer: 3.1 mm, 15 mm]

8.3 Figure P8.3 shows the grain-size curves for three different soils. Can soil A be used as a filter for soil C? If soil B is placed between soils A and C, can all the filter criteria be satisfied? [Answer: A and C no; A, B, and C yes]

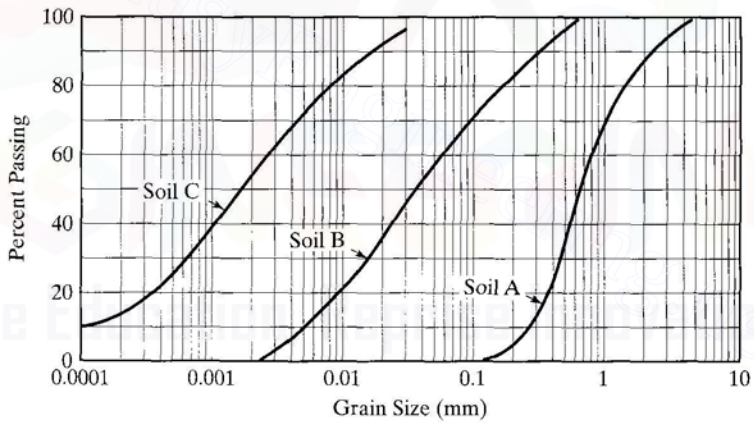


FIGURE P8.3

8.4 Can geotextiles be used as a filter for soil C in Figure P8.3? Why? If geotextiles are used for soils A and B, what AOS do you recommend? [Answer: no for C, greater than No. 60 for B, greater than No. 8 for A]

8.5 Estimate the permeability in ft/day of soil B in Figure P8.3 by Eq. 8.3. If the dry unit weight is 110 pcf, estimate its permeability in ft/day by Eq. 8.5a. [Answer: 0.037 to 0.059 ft/day by Eq. 8.3, 0.019 ft/day by Eq. 8.5a]

8.6 Figure P8.6 show a two-lane highway paved with HMA on the traffic lanes and the shoulders. Estimate the amount of surface infiltration in ft^3/h/ft^2 by Eq. 8.18. Assume that the pavement is located in Kentucky and estimate surface infiltration by Cedergren's method. [Answer: 0.016 ft^3/h/ft^2 by Eq. 8.18, 0.033 to 0.05 ft^{3}h/ft^2 by Cedergren]

Downloaded From : www.EasyEngineering.net

Downloaded From : www.EasyEngineering.net

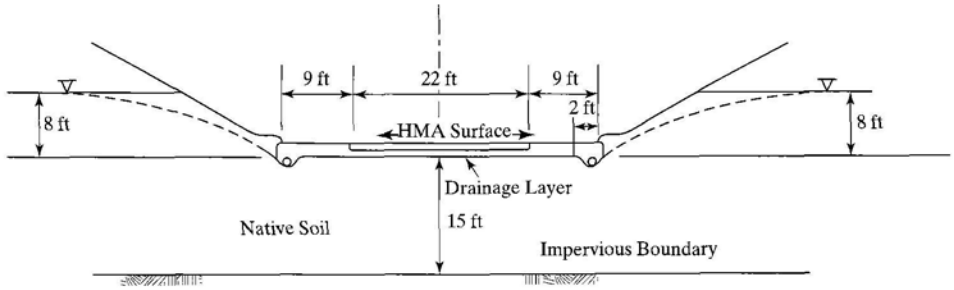


FIGURE P8.6

8.7 If the native soil above the impervious boundary, as shown in Figure P8.6, has a permeability of 0.5 ft/day, determine the groundwater inflow q_g into the drainage layer in $ft^3/day/ft^2$ and the lateral inflow q_L into the longitudinal drains in $ft^3/day/ft$. [Answer: 0.084 $ft^3/day/ft^2$, 2.2 $ft^3/day/ft$]

8.8 The highway in Figure P8.6 is located in a cold region with severe frost action and the subgrade consists of a well-graded clayey gravel, GW-GC, with 4% finer than 0.02 mm. Determine the inflow q_m to the drainage layer due to the melting of ice lenses. It is assumed that the HMA is 4 in. thick with a unit weight of 145 pcf, that the drainage layer, including the filter, is 10 in. thick and has an average unit weight of 120 pcf, and that the subgrade has a permeability of 0.05 ft/day. [Answer: 0.067 $ft^3/day/ft^2$]

8.9 The drainage layer shown in Figure P8.6 has a thickness H of 8 in., a cross slope S of 4%, a porosity n_e of 25%, and a permeability k of 10,000 ft/day. Determine the steady-state capacity of the drainage layer and the time for 50 and 95% drainage based on a drainage length L of 18 ft. [Answer: 390 $ft^3/day/ft$, 0.07 h, 0.44 h]

8.10 Smooth plastic pipe, 4 in. in diameter with a roughness coefficient of 0.01, is placed at 2.5% slope in a trench drain. If outlets are provided every 300 ft, what is the maximum allowable lateral inflow into the plastic pipe in $ft^3/day/ft$? [Answer: 112.7 $ft^3/day/ft$]

Apprise Education, Reprise Innovations

Downloaded From : www.EasyEngineering.net

Downloaded From : www.EasyEngineering.net

CHAPTER 9

Pavement Performance

9.1 DISTRESS

Distress is an important consideration in pavement design. In the mechanistic–empirical methods, each failure criterion should be developed separately to take care of each specific distress. Unfortunately, many of the distresses are caused by deficiencies in construction, materials, and maintenance and are not related directly to design. However, a knowledge of the various types of distress is important to pavement designers because it can help them to identify the causes of the distress. If distress is due to improper design, improvements in the design method can be made. Furthermore, the evaluation of pavement distress is an important part of the pavement management system by which a most effective strategy for maintenance and rehabilitation can be developed.

An excellent reference for identifying pavement distress is the *Highway Pavement Distress Identification Manual* published by the Federal Highway Administration (Smith *et al.*, 1979), in which each distress is described by its general mechanism, levels of severity (low, medium, and high), and measurement criteria. In this section, only the most significant types of distress directly related to design are described in detail and illustrated by photographs; other types of distress are discussed only briefly. The description and photographs presented herein are reproduced from the *Highway Pavement Distress Identification Manual.*

To provide a consistent, uniform basis for collecting distress data for the long-term pavement performance program, a distress identification manual was published by the Strategic Highway Research program (Smith *et al.*, 1987), was revised in 1990, and again revised in 1993 (SHRP, 1993). This 1993 manual is hereafter referred to as the SHRP manual. In addition to photographs and drawings to illustrate the various distress types, the SHRP manual also describes methods for measuring the size of distresses and for assigning severity levels. If the distresses described in the pages that follow are not included in or are in conflict with the SHRP manual, they will be noted in parenthesis.

Downloaded From : www.EasyEngineering.net

Downloaded From : www.EasyEngineering.net

9.1.1 Asphalt Pavements

Because many distresses in composite pavements or in asphalt overlays on concrete pavements are similar to those in asphalt pavements, both types of pavement are discussed in this section. A typical pattern of deterioration in asphalt pavements is rutting, which develops somewhat rapidly during the first few years and then levels off to a much slower rate. Fatigue or alligator cracking does not normally occur until after numerous loadings and then increases rapidly as the pavement weakens. In climates with either large variations in temperature or very cold temperatures, asphalt pavements develop transverse and longitudinal cracks from temperature stresses. These cracks usually break down and spall under traffic.

The most common problem with composite pavements is reflection cracking from joints and cracks in the underlying concrete slab. Infiltration of water into the cracks, along with freezing, thawing, and repeated loadings, usually results in break up and spalling of the asphalt surface. Typical load-associated fatigue cracking is not common on composite pavements. If fatigue cracking does occur, it usually initiates at the bottom of the concrete slab and can eventually deteriorate and spoil the asphalt overlay.

Alligator or Fatigue Cracking Alligator or fatigue cracking is a series of interconnecting cracks caused by the fatigue failure of an asphalt surface or a stabilized base under repeated traffic loading. The cracking initiates at the bottom of the asphalt surface or stabilized base, where the tensile stress or strain is highest under a wheel load. The cracks propagate to the surface initially as one or more longitudinal parallel cracks. After repeated traffic loading, the cracks connect and form many-sided, sharp-angled pieces that develop a pattern resembling chicken wire or the skin of an alligator, as shown in Figure 9.1. The pieces are usually less than 1 ft on the longest side. Alligator



FIGURE 9.1

Alligator cracking in wheel paths.

Downloaded From : www.EasyEngineering.net

Downloaded From : www.EasyEngineering.net

cracking occurs only in areas that are subjected to repeated traffic loadings. It would not occur over an entire area unless the entire area was subjected to traffic loading. Alligator cracking does not occur in asphalt overlays over concrete slabs. Pattern-type cracking, which occurs over an entire area that is not subjected to loading, is classified as block cracking, which is not a load-associated distress. Alligator cracking is considered a major structural distress. Alligator cracking is measured in square feet or square meters of surface area.

Block Cracking Block cracks divide the asphalt surface into approximately rectangular pieces, as shown in Figure 9.2. The blocks range in size from approximately 1 to 100 ft^2 (0.1 to 9.3 m^2). Cracking into larger blocks is generally categorized as longitudinal or transverse cracking. Block cracking is caused mainly by the shrinkage of hot mix asphalt and daily temperature cycling, which result in cyclic stress and strain. It is not load associated, although loads can increase the severity of the cracks. The occurrence of block cracking usually indicates that the asphalt has hardened significantly. Block cracking normally occurs over a large portion of pavement area, but sometimes will occur only in nontraffic areas. Block cracking is measured in square feet or square meters of surface area.

Joint Reflection Cracking from Concrete Slab This distress occurs only on pavements that have an asphalt surface over a jointed concrete slab. Cracks occur both at transverse joints and at the longitudinal joints where the old concrete pavement has been widened before overlay. This distress does not include the reflection cracking away from a joint or from any other types of stabilized bases, which is identified as longitudinal or transverse cracking. Joint reflection cracking is shown in Figure 9.3.

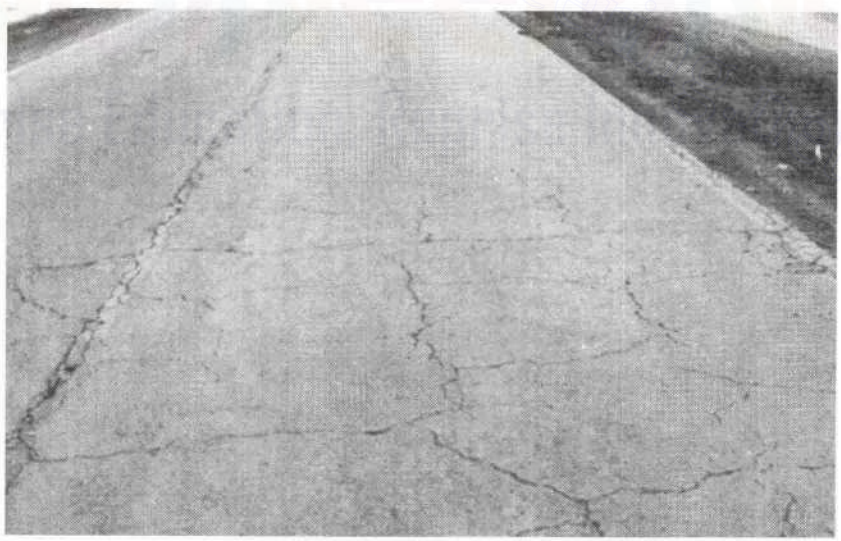


FIGURE 9.2
Block cracking.

Downloaded From : www.EasyEngineering.net

Downloaded From : www.EasyEngineering.net

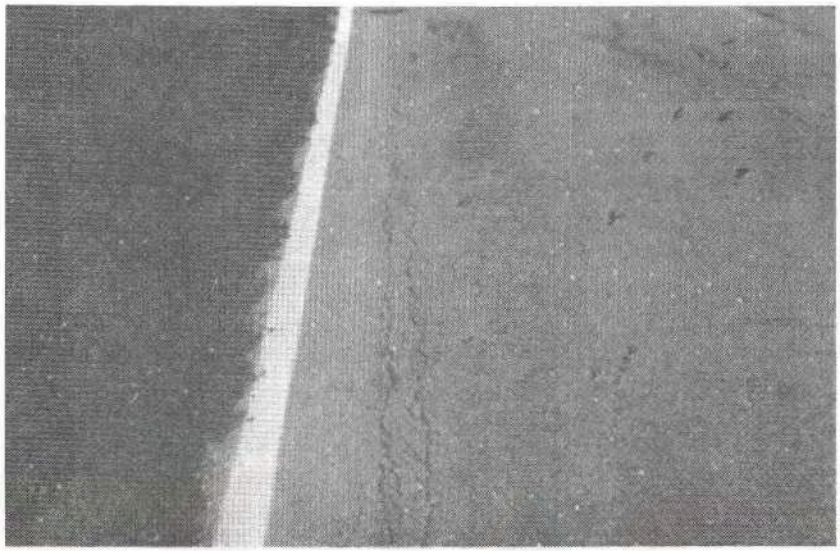


FIGURE 9.3
Joint reflection cracking from longitudinal widening joint.

Joint reflection cracking is caused mainly by the movement of concrete slab beneath the asphalt surface due to thermal or moisture changes and is generally not load initiated. However, traffic loading can cause a breakdown of the hot mix asphalt near the initial crack, resulting in spalling. A knowledge of slab dimensions beneath the asphalt surface will help to identify these cracks. Joint reflection cracking is measured in linear feet or linear meters. (In the SHRP manual, the transverse reflection cracking is recorded as the number and length in m (ft) together with the length in m (ft) with sealant in good condition; the longitudinal reflection cracking is recorded as the length in m (ft) together with the length in m (ft) with sealant in good condition.)

Lane/Shoulder Dropoff or Heave This distress occurs where there is a difference in elevation between traffic lane and shoulder, as seen in Figure 9.4. Typically, the outside shoulder settles in response to consolidation, settlement, or pumping of the underlying granular or subgrade material. Heave of the shoulder may be caused by frost action or swelling soils. Dropoff of granular or soil shoulder is generally caused by blowing away of shoulder material by passing trucks. Lane/shoulder dropoff or heave is measured every 100 ft (30 m) in inches (or mm) along the pavement edge. The mean difference in elevation is computed and is used to determine the severity level. (In the SHRP manual, this distress is recorded as mm (in.) to the nearest mm (0.04 in.) at intervals of 15 m (50 ft) along the lane-to-shoulder joint.)

Longitudinal and Transverse Cracking Longitudinal cracks are parallel to the pavement centerline, and transverse cracks extend across the centerline, as shown in

Downloaded From : www.EasyEngineering.net

Downloaded From : www.EasyEngineering.net

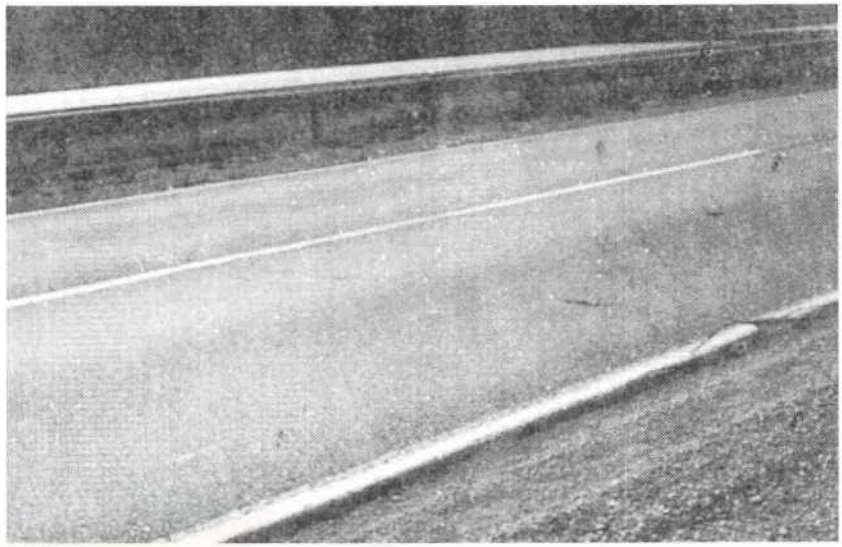


FIGURE 9.4
Lane/shoulder dropoff.



FIGURE 9.5
Transverse cracking.

Figure 9.5. They can be caused by a shrinkage of asphalt surface due to low temperatures or to asphalt hardening or can result from reflective cracks caused by cracks beneath the asphalt surface, including cracks in concrete slabs but not at the joints. Longitudinal cracks can also be caused by poorly constructed paving of a lane joint.

Downloaded From : www.EasyEngineering.net

Downloaded From : www.EasyEngineering.net

These types of cracks are not usually load associated. Longitudinal and transverse cracks are measured in linear feet or linear meters. (In the SHRP manual, longitudinal and transverse cracking are treated as two separate categories, and a new category, edge cracking, is added. The longitudinal cracking is further divided into wheel path longitudinal cracking and non-wheel path longitudinal cracking. The length in m (ft) of longitudinal cracking and the length in m (ft) with sealant in good condition within the defined wheel paths are recorded, along with those not located in the defined wheel paths. The number and length in m (ft) of transverse cracking and the length in m (ft) with sealant in good condition are also recorded. Edge cracking applies only to pavements with unpaved shoulders. It consists of crescent-shaped cracks or fairly continuous cracks which intersect the pavement edge and are located within 0.6 m (2 ft) of the pavement edge, adjacent to the shoulder. It also includes longitudinal cracks outside of the wheel path and within 0.6 m (2 ft) of the pavement edge. Edge cracking is recorded as the length in m (ft) of pavement edge affected.)

Pumping and Water Bleeding Pumping is the ejection of water and fine materials under pressure through cracks under moving loads, as shown in Figure 9.6. As the water is ejected, it carries fine materials, thus resulting in progressive material deterioration and loss of support. Surface staining or accumulation of material on the surface close to cracks is evidence of pumping. Water bleeding occurs where water seeps slowly out of cracks on the pavement surface. Pumping and water bleeding are measured by counting the number of cracks that exist. (In the SHRP manual, the number of occurrences of water bleeding and of pumping and the length in m (ft) of affected pavement are recorded.)

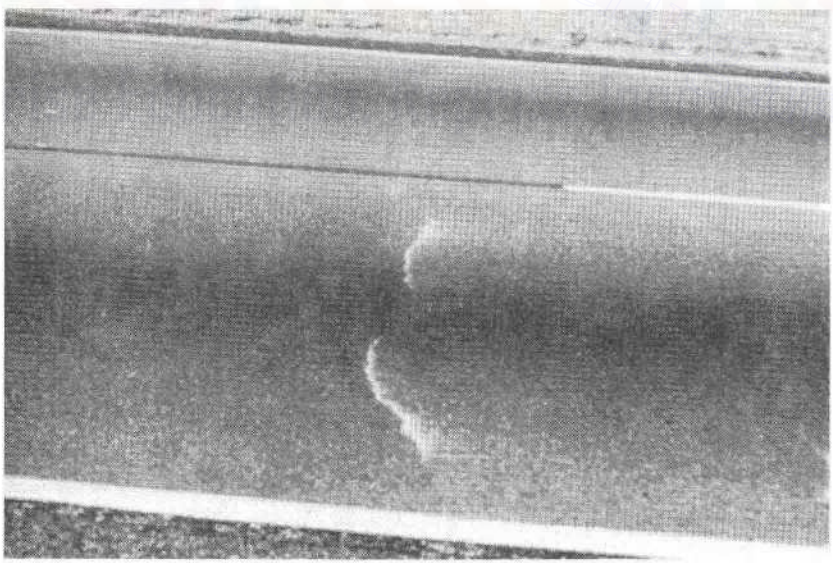


FIGURE 9.6

Pumping of stabilized base under asphalt pavement.

Downloaded From : www.EasyEngineering.net

Downloaded From : www.EasyEngineering.net

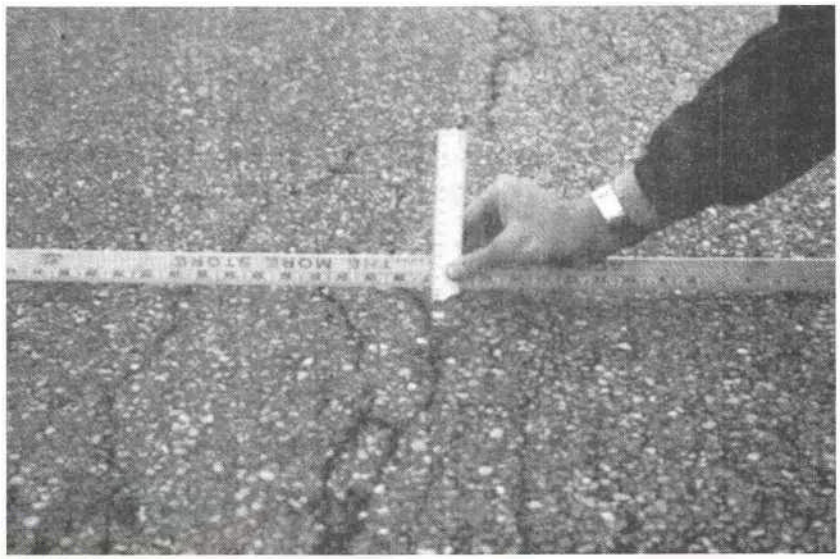


FIGURE 9.7
Rutting at the wheel path.

Rutting A rut is a surface depression in the wheel paths; see Figure 9.7. Pavement uplift might occur along the sides of the rut. However, in many instances, ruts are noticeable only after a rainfall, when the wheel paths are filled with water. Rutting stems from a permanent deformation in any of the pavement layers or in the subgrade, one usually caused by a consolidation or lateral movement of the materials due to traffic loads. Rutting can be caused by plastic movement of the asphalt mix either in hot weather or from inadequate compaction during construction. Significant rutting can lead to major structural failures and a potential for hydroplaning. Rutting is measured in square feet or square meters of surface area, for a given severity level based on rut depth. (In the SHRP manual, transverse profile is measured with a Dipstick profiler at 15 m (50 ft) intervals when it has not been measured in conjunction with photographic distress surveys.)

Swell Swell is characterized by an upward bulge on the pavement surface. A swell can occur sharply over a small area or as a long, gradual wave. Either type of swell can be accompanied by surface cracking. A swell is usually caused by frost action in the subgrade or by swelling soils, but a swell can also occur on the surface of an asphalt overlay on concrete pavement as a result of blowup in the concrete slab, as shown in Figure 9.8. Swell can often be identified by oil droppings due to the bumpy surface. Swells are measured in square feet or square meters of surface area. (This distress is not included in the SHRP manual.)

Other Types of Distress The following types of distress can be caused by deficiencies in construction, materials, or maintenance:

Downloaded From : www.EasyEngineering.net

Downloaded From : www.EasyEngineering.net

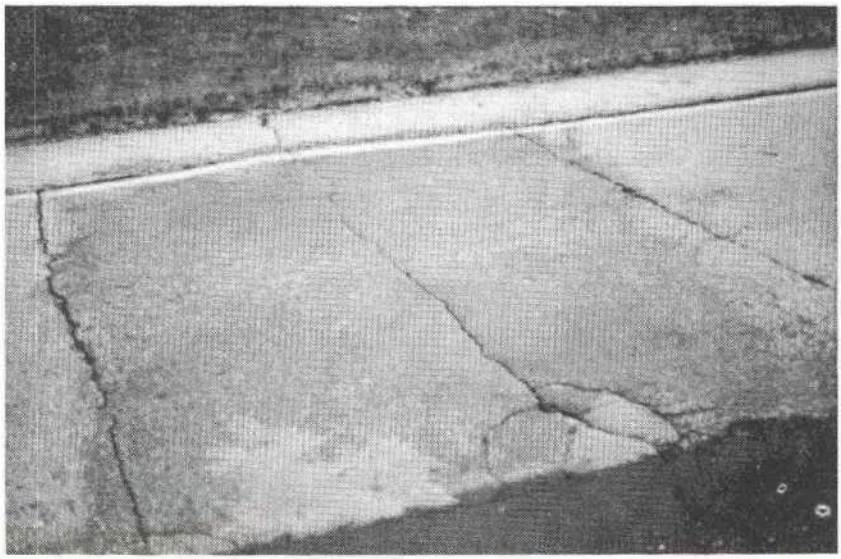


FIGURE 9.8

Swell at a patch due to buckling of concrete slab.

1. *Bleeding.* Bleeding is a film of bituminous material on the pavement surface, which creates a shiny, glass-like, reflecting surface that usually becomes sticky. It is caused by high asphalt content or low air void content. The bleeding process does not reverse during cold months, so asphalt will accumulate on the surface and lower the skid resistance.
2. *Corrugation.* Corrugation is a form of plastic movement typified by ripples across the asphalt surface. It usually occurs at bus stops and where vehicles accelerate or decelerate and is the result of shear action in the pavement surface or between the pavement surface and the base material. (This distress is not included in the SHRP manual.)
3. *Depression.* Depressions are localized pavement surface areas having elevations slightly lower than those of the surrounding pavement. They can be caused by settling of the foundation soil or can be "built in" during construction. Depressions cause roughness and, when filled with water of sufficient depth, could cause hydroplaning of vehicles. (This distress is not included in the SHRP manual.)
4. *Lane/shoulder joint separation.* The widening of the joint between the traffic lane and the shoulder is not considered a distress if the joint is well sealed and water cannot enter through it. (This distress is not included in the SHRP manual.)
5. *Patch deterioration.* Deteriorations occur in a patch, which is an area where the original pavement has been removed and replaced with either similar or different material. Traffic load, material, and poor construction practices can all cause patch deterioration.

Downloaded From : www.EasyEngineering.net

Downloaded From : www.EasyEngineering.net

6. *Polished aggregate.* A portion of the aggregates extending above the asphalt surface is either very small or without rough or angular particles to provide good skid resistance. This type of distress occurs mainly in the wheel path and is due to repeated traffic loads. (This distress is not included in the SHRP manual.)
7. *Potholes.* Potholes are bowl-shaped holes of various sizes on the pavement surface. They are caused by a broken pavement surface due to alligator cracking, localized disintegration, or freeze–thaw cycles.
8. *Raveling and weathering.* Raveling and weathering are the wearing away of the pavement surface caused by the dislodging of aggregate particles due to stripping and by the loss of asphalt binder due to hardening.
9. *Slippage cracking.* Slippage cracks are crescent- or half-moon-shaped, with both ends pointed into the direction of traffic. They are caused by the low strength of HMA or by a weaker bond between the surface course and the layer below. Part of the asphalt surface is moved laterally away from the rest of the surface by induced lateral and shear stresses caused by traffic loads.

Table 9.1 lists all possible types of distress or failure in asphalt pavements and indicates whether they are structural or functional failures and load-associated or non-load-associated distresses. Structural failure is associated with the ability of the pavement to carry the design load, whereas functional failure is associated with ride quality and safety. When structural failure increases in severity, it always results in functional failure as well. The non-load-associated distress is caused by climates, materials, or construction. A non-load-associated distress might be increased in severity by traffic loads.

9.1.2 Concrete Pavements

Concrete pavements include jointed plain concrete pavements (JPCP), jointed reinforced concrete pavements (JRCP), and continuous reinforced concrete pavements (CRCP). Common types of distress in these pavements are pumping, faulting, and cracking. Joint deterioration is a major problem in JRCP due to longer joint spacing; edge punchout is a major problem in CRCP due to the closely spaced cracks.

Blowup Blowups occur in hot weather at a transverse joint or crack that does not permit the expansion of concrete slabs. Insufficient width of a joint for expansion is usually caused by the infiltration of incompressible materials into the joint space. When the compressive expansive pressure cannot be relieved, either localized upward movement of the slab edges or shattering occurs in the vicinity of the joint; see Figure 9.9. Blowup can also occur at utility cut patches and at drainage inlets. Blowup is accelerated by a spalling away of the slab at the bottom that causes the reduction of contact areas between the two slabs. The presence of "D" cracking also weakens the concrete near the joint, thus resulting in increased spalling and blowup potential. Blowups are measured by counting the number that exist.

Corner Break A corner break is a crack that intersects the joint at a distance less than 6 ft (1.8 m) on either side measured from the corner of the slab, as shown in Figure 9.10. A corner break differs from a corner spall in that its crack extends vertically through

Downloaded From : www.EasyEngineering.net

Downloaded From : www.EasyEngineering.net

TABLE 9.1 Distresses in Asphalt Pavements

Types of Distress	Structural	Functional	Load associated	Non-load associated
Alligator or fatigue cracking	×		×	
Bleeding		×		×
Block cracking	×			×
Corrugation		×		×
Depression		×		×
Joint reflection cracking	×			×
Lane/shoulder dropoff or heave		×		×
Lane/shoulder separation		×		×
Longitudinal and transverse cracking	×			×
Patch deterioration	×	×	×	
Polished aggregate		×	× [a]	
Potholes	×	×	×	
Pumping and water bleeding	×	×	×	×
Raveling and weathering		×		×
Rutting		×	×	
Slippage cracking	×		×	
Swell	×	×		×

[a] Tire abrasion.

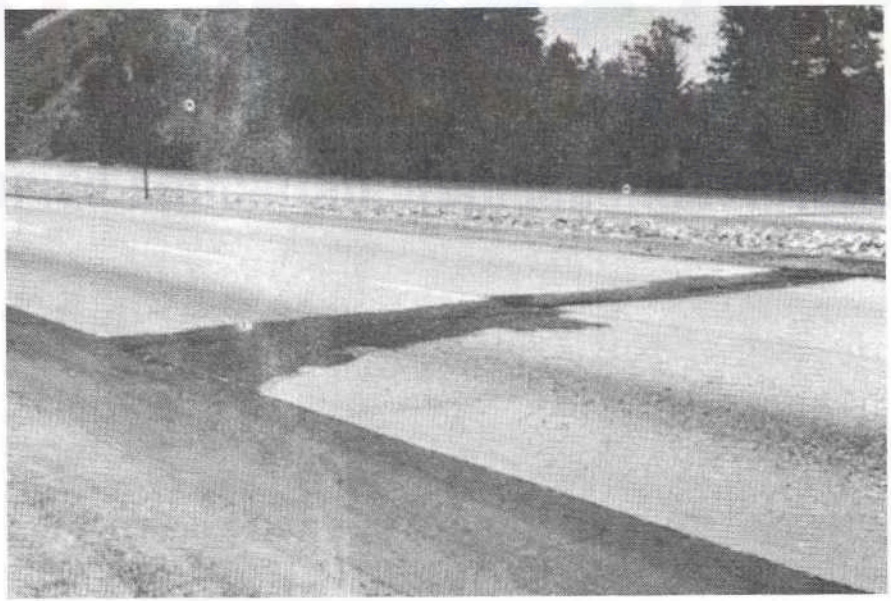


FIGURE 9.9
Blowup.

Downloaded From : www.EasyEngineering.net

Downloaded From : www.EasyEngineering.net

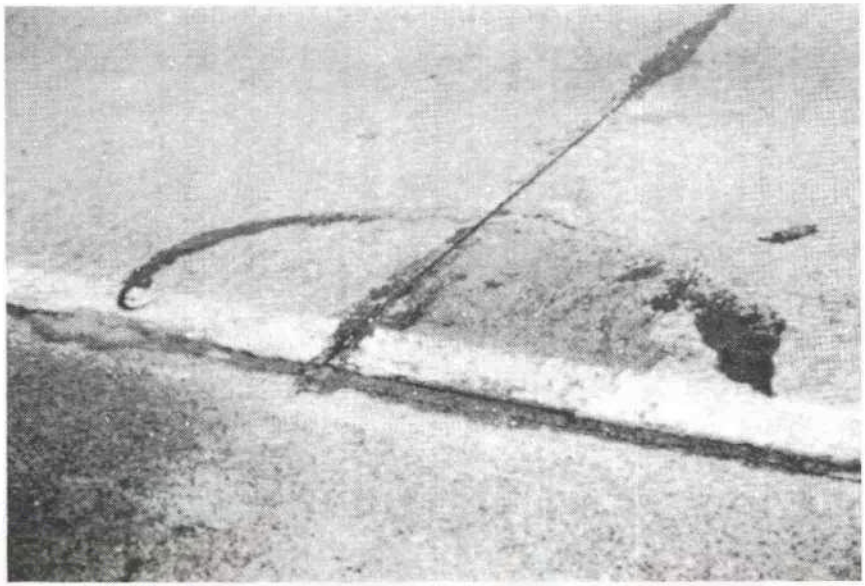


FIGURE 9.10
Corner break.

the entire slab thickness; that of a corner spall intersects the joint at an angle. Load repetitions combined with the loss of support, poor load transfer across the joint, and thermal curling and moisture warping stresses usually cause corner breaks. Corner breaks are measured by counting the number that exist.

Faulting of Transverse Joints and Cracks Faulting is a difference of elevation across a joint or crack; see Figure 9.11. Faulting is caused in part by a buildup of loose materials under the trailing slab near the joint or crack or by a depression of the leading slab. The buildup of eroded or infiltrated materials is caused by pumping due to heavy loadings. The upward warp and curl of the slab near the joint or crack due to moisture and temperature gradients contribute to the pumping condition. Lack of load transfer contributes greatly to faulting. Faulting is determined by measuring the difference in elevation of slabs 1 ft from the pavement edge. (In the SHRP manual, faulting in mm (in.) is measured to the nearest mm (0.04 in.) both at 0.3 m (1 ft) from the outside pavement edge and at 0.75 m (2.5 ft) from the outside lane edge (wheel path).)

Joint Load Transfer System Associated Deterioration This distress develops as a transverse crack a short distance from a transverse joint, usually at the end of joint load transfer dowels, as shown in Figure 9.12. This usually occurs when the dowel system fails to function properly, because of extensive corrosion or misalignment. It can also be caused by a combination of small-diameter dowels and heavy traffic loadings. The deterioration is measured by counting the number of deteriorated joints. (This distress is not included in the SHRP manual.)

Downloaded From : www.EasyEngineering.net

Downloaded From : www.EasyEngineering.net

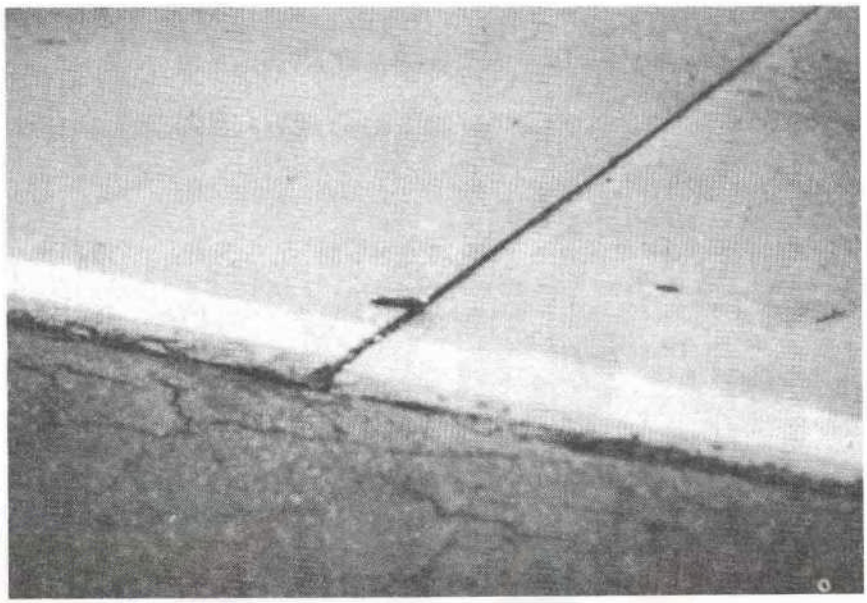


FIGURE 9.11
Joint faulting.



FIGURE 9.12
Joint load transfer system associated deterioration.

Downloaded From : www.EasyEngineering.net

Downloaded From : www.EasyEngineering.net

Lane/Shoulder Dropoff or Heave The description of this distress is the same as that for asphalt pavements. Lane/shoulder dropoff is shown in Figure 9.13.

Longitudinal Cracks Longitudinal cracks generally occur parallel to the centerline of the pavement; see Figure 9.14. They are often caused by a combination of heavy load repetition, loss of foundation support, and curling and warping stresses. Improper construction of longitudinal joints can also cause longitudinal cracks. Cracks are measured in linear feet or linear meters. (In the SHRP manual, not only the length in m (ft) of longitudinal cracking but also the length in m (ft) of longitudinal cracking with sealant in good condition are recorded.)

Longitudinal Joint Faulting Longitudinal joint faulting is a difference in elevation at the longitudinal joint between two traffic lanes, as shown in Figure 9.15. Where the longitudinal joint has faulted, the length of the affected area and the maximum joint faulting should be recorded. (This distress is not included in the SHRP manual.)

Pumping and Water Bleeding Pumping is the ejection of material by water through joints or cracks, caused by the deflection of slab under moving loads. As the water is ejected, it carries particles of gravel, sand, clay, or silt, resulting in a progressive loss of pavement support. Surface staining or accumulation of base or subgrade material on the pavement surface close to joints and cracks is evidence of

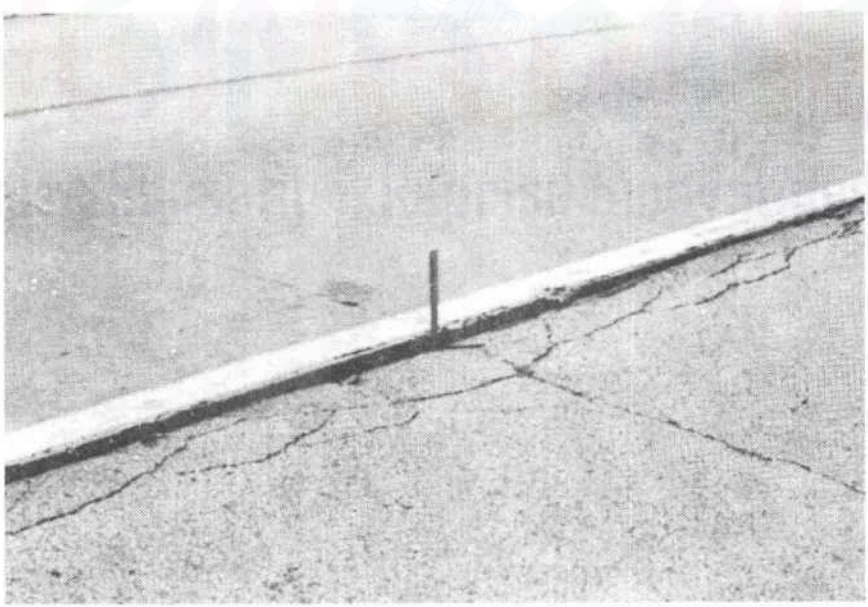


FIGURE 9.13
Lane/shoulder dropoff.

Downloaded From : www.EasyEngineering.net

Downloaded From : www.EasyEngineering.net



FIGURE 9.14
Longitudinal crack.

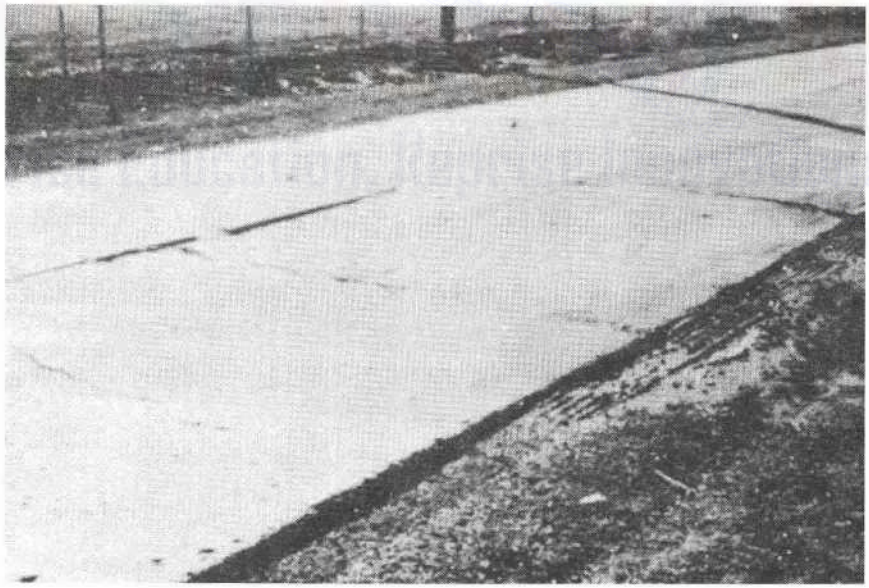


FIGURE 9.15
Longitudinal joint faulting.

Downloaded From : www.EasyEngineering.net

Downloaded From : www.EasyEngineering.net

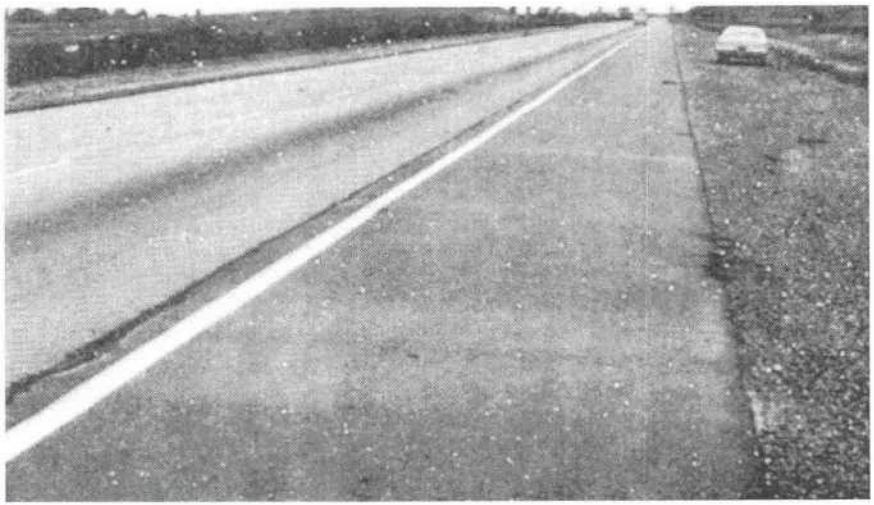


FIGURE 9.16
Pumping of fines at pavement edge and joint.

pumping; see Figure 9.16. Pumping can occur without such evidence, particularly when stabilized bases are used. The observation of water being ejected by heavy traffic loads after a rainstorm can also be used to identify pumping. Water bleeding occurs when water seeps out of joints or cracks. Pumping and water bleeding are measured by counting the number of occurences that exist. (In the SHRP manual, both the number of occurrences of water bleeding and pumping and the length in m (ft) of affected pavement are recorded.)

Spalling (Transverse and Longitudinal Joint or Crack) Spalling of cracks and joints is the cracking, breaking, or chipping of the slab edges within 2 ft (0.6 m) of the joint or crack. A joint spall, shown in Figure 9.17, usually does not extend vertically through the whole slab thickness, but instead extends to intersect the joint at an angle. Spalling usually results from excessive stresses at the joint or crack, caused by the infiltration of incompressible materials and by subsequent expansion or traffic loading. It can also be caused by the disintegration of concrete, by weak concrete at the joint caused by overworking, or by poorly designed or constructed load transfer devices. Spalling is measured by counting the number of spalls that exist. (In the SHRP manual, spalling of a longitudinal joint is recorded as the length in m (ft) of longitudinal joint spalling, and spalling of a transverse joint is recorded as the number of affected joints and the length in m (ft) of the spalled portion of the joint.)

Spalling (Corner) Corner spalling is the raveling or breakdown of the slab within approximately 2 ft (0.6 m) of the corner; see Figure 9.18. A corner spall differs from a corner break in that the spall usually angles downward at about 45° to intersect the joint, whereas a break extends vertically through the slab. Corner spalling can be caused by freeze–thaw conditions, by "D" cracking, or by other factors. Corner spalling

Downloaded From : www.EasyEngineering.net

Downloaded From : www.EasyEngineering.net

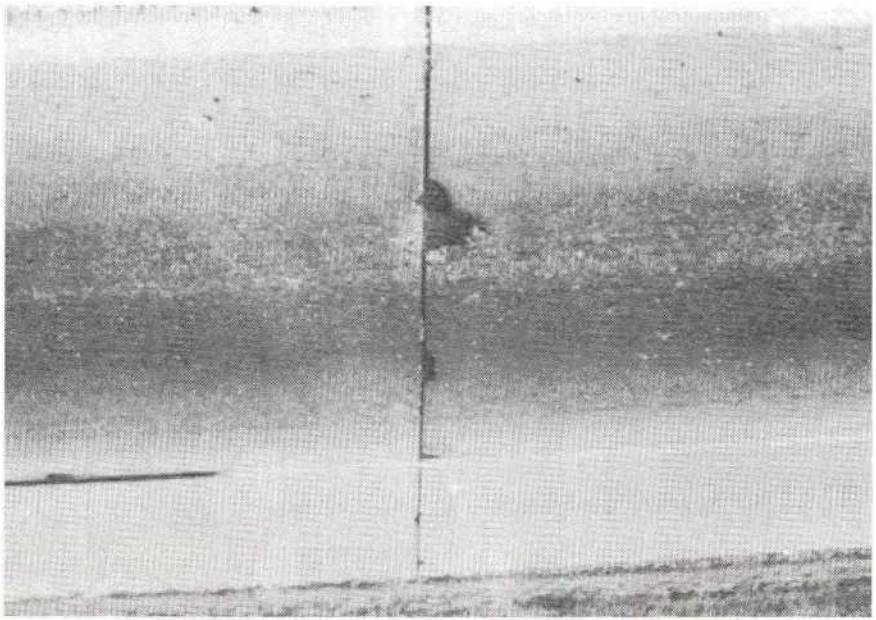


FIGURE 9.17
Joint spall.

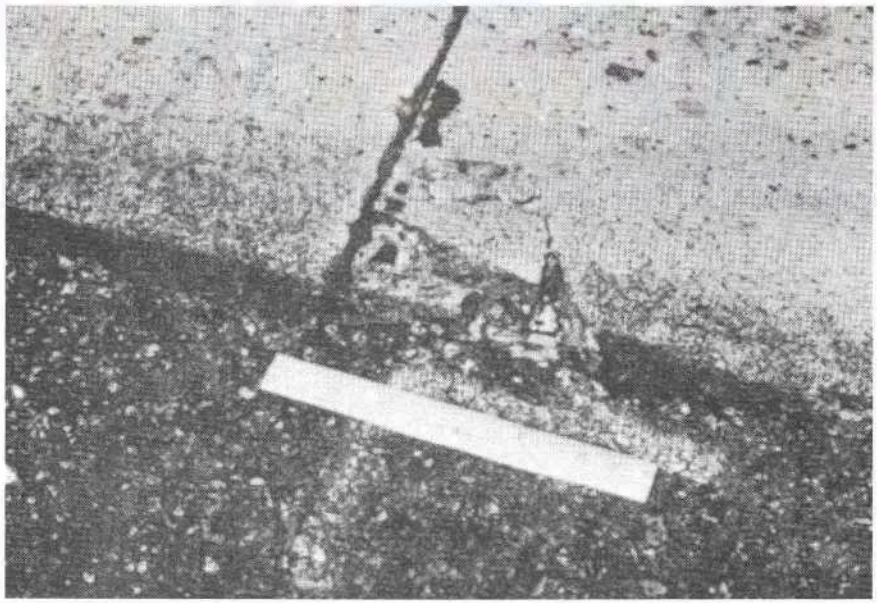


FIGURE 9.18
Corner spall.

Downloaded From : www.EasyEngineering.net

Downloaded From : www.EasyEngineering.net

is measured by counting the number that exist. (This distress is not included in the SHRP manual.)

Swell Swell is characterized by an upward bulge on the pavement surface. A swell can occur sharply over a small area or as a long, gradual wave. Either type of swell is usually accompanied by slab cracking. A swell is usually caused by frost action in the subgrade, as shown in Figure 9.19, or by swelling soils. Swells can often be identified by oil droppings due to the bumpy surface. Swells are counted by the number that exist. (This distress is not included in the SHRP manual.)

Transverse and Diagonal Cracks These cracks are usually caused by a combination of heavy load repetitions and stresses due to temperature gradient, moisture gradient, and drying shrinkage. A transverse crack is shown in Figure 9.20. Transverse and diagonal cracks are measured by counting the number that exist. Hairline cracks that are less than 6 ft (1.8 m) long are ignored. (In the SHRP manual, there are no diagonal cracks. A crack should be classified either as longitudinal or as transverse, depending on its orientation. Not only the number and length in m (ft) of transverse cracking but also the length in m (ft) of transverse cracking with sealant in good condition are recorded.)

Edge Punchout An edge punchout, a major structural distress of CRCP, is first characterized by a loss of aggregate interlock at one or two closely spaced, cracks, usually



FIGURE 9.19

Swell due to frost heave.

Downloaded From : www.EasyEngineering.net

Downloaded From : www.EasyEngineering.net

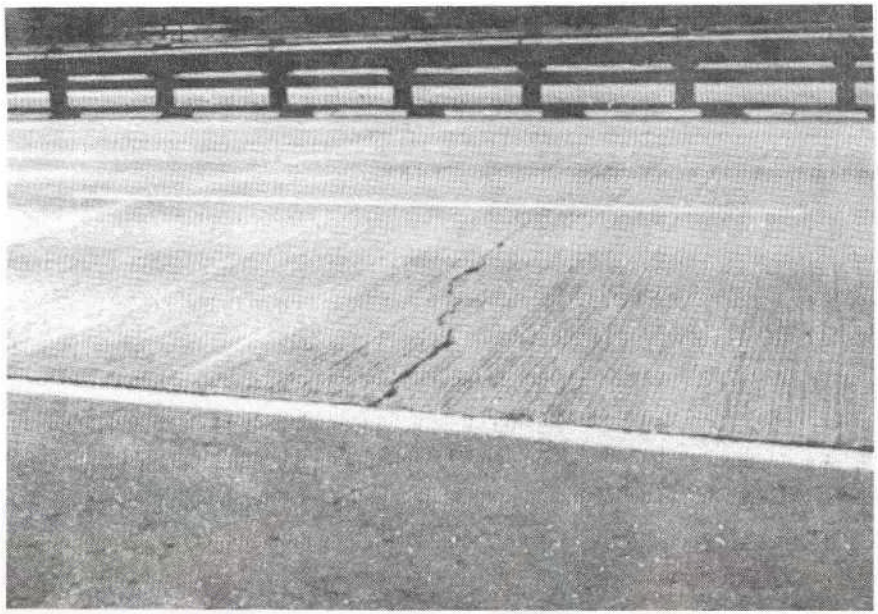


FIGURE 9.20
Transverse crack.

less than 2 ft (1.2 m) apart, at the edge. The crack or cracks begin to fault and spall slightly, causing the portion of the slab between the closely spaced cracks to act essentially as a cantilever beam. As the applications of heavy truck load continue, a short longitudinal crack forms between the two transverse cracks about 2 to 5 ft (0.6 to 1.5 m) from the pavement edge. Eventually the transverse cracks break down further, the steel ruptures, and pieces of concrete punch downward under load into the subbase and subgrade; see Figure 9.21. There is generally evidence of pumping near the edge punchouts, which is sometimes extensive. The distressed area will expand in size to adjoining cracks and develop into a very large area if not repaired. Edge punchouts are measured by counting the number that exist.

Localized Distress Localized distress occurs in CRCP where the concrete breaks up into pieces or spalls in a localized area, as shown in Figure 9.22. The localized distress takes many shapes and forms. It usually occurs within an area between intersecting, Y-shaped, or closely spaced cracks. Localized distress can occur anywhere on the slab surface, but is frequently located in the wheelpaths. Inadequate consolidation of concrete is often a primary cause of localized distress. Localized distress is measured by counting the number of occurrences. (This distress is not included in the SHRP manual.)

Other Types of Distress Other types of distress, caused possibly by the deficiencies in construction, materials, and maintenance, are as follows:

Downloaded From : www.EasyEngineering.net

Downloaded From : www.EasyEngineering.net

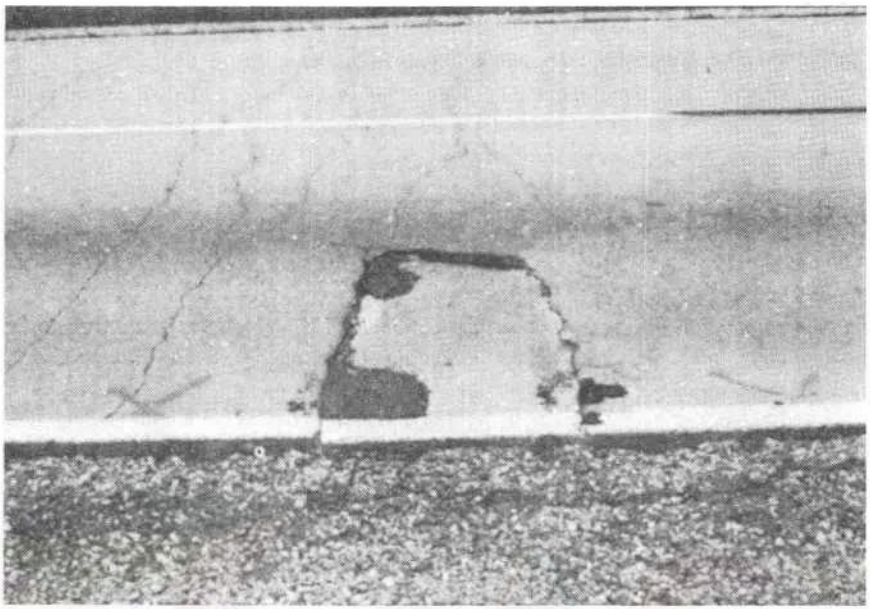


FIGURE 9.21
Edge punchout.

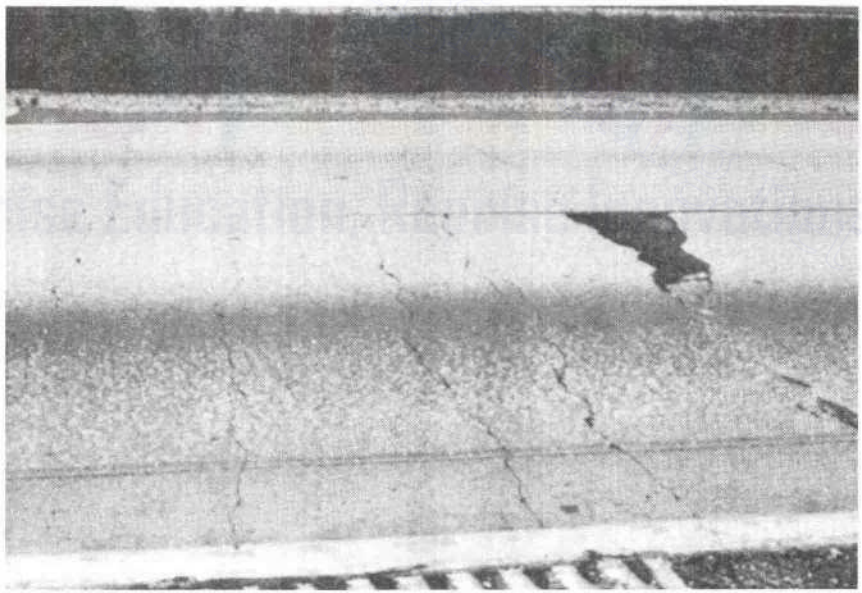


FIGURE 9.22
Localized distress.

Downloaded From : www.EasyEngineering.net

Downloaded From : www.EasyEngineering.net

1. *Depression.* As with asphalt pavements, depressions can be caused by the settlement of foundation soil or can be "built in" during construction. The exception is that depression in concrete pavements is generally associated with significant cracking. (This distress is not included in the SHRP manual.)
2. *Durability or "D" cracking.* "D" cracking is a series of closely spaced, crescent-shaped, hairline cracks that appear at the concrete surface adjacent to and roughly parallel to joints and cracks—and along the slab edge. The fine surface cracks contain calcium hydroxide residue, which causes a dark coloring of the crack in the immediate surrounding area. "D" cracking is caused by freeze–thaw expansive pressures of certain types of coarse aggregates.
3. *Joint seal damage of transverse joints.* Typical evidence of joint seal damage includes stripping and extrusion of joint sealant, weed growth, hardening of the filler, loss of bond to the slab edge, and lack or absence of sealant in the joint. (In the SHRP manual, a separate category of longitudinal joint seal damage is added.)
4. *Lane/shoulder joint separation.* The widening of the joint between the traffic lane and shoulder is not considered a distress if the joint is well sealed and water cannot enter through it.
5. *Patch deterioration.* A concrete patch is an area where a portion of the original concrete slab has been removed and replaced by concrete or other epoxy materials. Poor construction of the patch, loss of support, heavy load repetitions, lack of load transfer devices, improper or absent joints, and moisture or thermal gradients can all cause the distress.
6. *Patch adjacent slab deterioration.* This is similar to patch deterioration, except that the deterioration occurs in the original concrete slab adjacent to a permanent patch. (In the SHRP manual, this distress is combined with patch deterioration in Item 5 and called patch/patch deterioration.)
7. *Popouts.* A popout is a small piece of concrete that breaks loose from the surface. It can be caused by expansive, nondurable, or unsound aggregates or by freeze and thaw action.
8. *Reactive aggregate distress.* Reactive aggregates either expand in alkaline environments or develop prominent siliceous reaction rims in concrete. The reaction may be alkali–silica or alkali–carbonate. As the expansion occurs, the cement matrix is disrupted and cracks. It looks like a map-cracked area; however, the cracks go deeper into the concrete than does normal map cracking. (This distress is not included in the SHRP manual, but the manual adds a new category of polished aggregates described as surface mortar and texturing worn away to expose coarse aggregate.)
9. *Scaling, map cracking, or crazing.* Map cracking or crazing refers to a network of shallow, fine, or hairline cracks that extend only through the upper surface of the concrete. Map cracking or crazing is usually caused by overfinishing of the concrete and can lead to scaling of the surface, which is the breakdown of the slab surface to a depth of approximately $\frac{1}{4}$ to $\frac{1}{2}$ in. (6 to 13 mm). Scaling can be caused by deicing salts, by traffic, by improper construction, by freeze–thaw cycles, or by steel reinforcements too close to the surface. (In the SHRP manual, this category is separated into scaling and map cracking.)

Downloaded From : www.EasyEngineering.net

Downloaded From : www.EasyEngineering.net

10. *Construction joint deterioration.* Construction joint distress is a breakdown of the concrete or steel at a CRCP construction joint. It often results in a series of closely spaced transverse cracks near the construction joint or a large number of interconnecting cracks. The primary causes of construction joint distress are poorly consolidated concrete and inadequate steel content and placement.

Table 9.2 lists all possible types of distress for rigid pavements and indicates whether they are structural or functional, load associated or not load associated.

9.2 SERVICEABILITY

Serviceability is the ability of a specific section of pavement to serve traffic in its existing condition. There are two ways to determine serviceability. One method is to use the present serviceability index (PSI) developed at the AASHO Road Test, which is based both on pavement roughness and on distress conditions, such as rutting, cracking, and patching. The other method is to use a roughness index based on the roughness only.

TABLE 9.2 Distresses in Concrete Pavements

Types of distress	Structural	Functional	Load associated	Non-load associated
Blowup	×	×		×
Corner break	×	×	×	
Depression		×		×
Durability "D" cracking	×	×		×
Faulting of transverse joints and cracks		×	×	
Joint load transfer associated deterioration	×	×	×	×
Joint seal damage of transverse joints				×
Lane/shoulder dropoff and heave		×		×
Lane/shoulder joint separation		×		×
Longitudinal cracks		×		×
Longitudinal joint faulting		×		×
Patch deterioration	×	×	×	×
Patch adjacent slab deterioration	×	×	×	×
Popouts		×		×
Pumping and water bleeding	×	×	×	×
Reactive aggregate distress	×	×		×
Scaling, map cracking, and crazing	×			×
Spalling (transverse and longitudinal joints or cracks)	×	×		×
Spalling at corner	×	×		×
Swell	×	×		×
Transverse and diagonal cracks	×		×	×
Construction joint deterioration	×			×
Edge punchout	×		×	
Localized distress	×	×		×

Downloaded From : www.EasyEngineering.net

Downloaded From : www.EasyEngineering.net

9.2.1 Present Serviceability Index

The pavement serviceability–performance concept was developed during the AASHO Road Test (Carey and Irick, 1960). Prior to that time, there were no widely accepted definitions of performance that could be considered in the design of pavements. The inclusion of serviceability as a factor in pavement design was an outstanding feature of the AASHO design methods.

Definitions To correlate the subjective rating of pavement performance with objective measurements, the following terms need be defined:

1. *Present serviceability.* The ability of a specific section of pavement to serve high-speed, high-volume, mixed traffic in its existing condition.
2. *Individual present serviceability rating.* An independent rating by an individual of the present serviceability of a specific section of roadway. The ratings range from 0 to 5, as shown in Figure 9.23, which is the rating form used during the AASHO Road Test. The form also includes provision for the rater to indicate whether the pavement is acceptable as a primary highway. It was found that the 50th percentile for acceptability occurred when the PSR was in the neighborhood of 2.9, whereas the 50th percentile for unacceptability corresponded roughly to a PSR of 2.5.
3. *Present serviceability rating (PSR).* The mean of the individual ratings made by the members of a specific panel.
4. *Present serviceability index (PSI).* A mathematical combination of values obtained from certain physical measurements so formulated as to predict the PSR for those pavements within prescribed limits.
5. *Performance index (PI).* A summary of PSI over a period of time, which can be represented by the area under the PSI versus time curve, as shown in Figure 9.24. There are many possible ways in which the summary value can be computed. Perhaps the simplest summary consists in the mean ordinate of the curve of PSI against time.

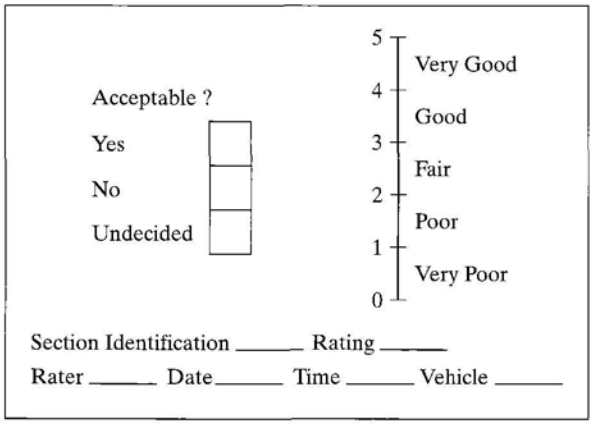


FIGURE 9.23
Individual present serviceability rating form. (After Carey and Irick (1960).)

Downloaded From : www.EasyEngineering.net

Downloaded From : www.EasyEngineering.net

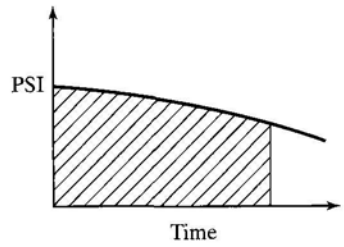


FIGURE 9.24
PSI as a function of time.

Steps in Formulating PSI The following procedures, which are general and can be applied to obtain similar indices for other purposes, represent the minimum requirements for the establishment, derivation, and validation of PSI:

1. *Establishment of definitions.* The precise meaning of terms and exactly what is to be rated and what should be included and excluded from consideration must be clearly understood by those involved in rating and in formulating and using the index.
2. *Establishment of rating group or panel.* Because the raters are to represent highway users, they should be selected from various segments of the users with divergent views and attitudes.
3. *Orientation and training of rating panel.* Members of the panel must understand the pertinent definitions and the rules of the game. Practice rating sessions may be conducted in which the raters can discuss their ratings.
4. *Selection of pavement for rating.* The pavements selected for rating should range from very poor to very good and contain all the various types and degrees of distress that are likely to influence serviceability. The minimum desirable length of a pavement to be rated shall be 1200 ft (366 m), so the raters can ride over the section at high speed and not be influenced by the condition of the pavement at both ends. A total of 74 sections of flexible pavements and 49 sections of rigid pavements in Illinois, Minnesota, and Indiana, plus some flexible pavements at the AASHO Road Test site, were used for developing the PSI equations.
5. *Field rating.* Members of the panel are taken in small groups to the sections to be rated. They are allowed to ride over each section in a vehicle of their choice and to walk and examine the pavement as they wish. Each rater works independently and no discussion between raters is permitted.
6. *Replication.* To determine the ability of the Road Test panel to rate the pavements consistently, many sections were rated twice within a short period of time so that the section did not change physically. It was found that the difference between two ratings ranged from 0 to 0.5 with an average of 0.2.
7. *Validity of rating panel.* The sections of flexible pavements in Illinois were also rated by two professional drivers based on the rides they obtained when driving their own fully loaded tractor semitrailers and by 20 Canadians, who were ordinary automobile drivers, not professionally associated with highways. It was found that the ratings given by the panel were similar to those given by the other user groups.

Downloaded From : www.EasyEngineering.net

Downloaded From : www.EasyEngineering.net

8. *Physical measurements.* The purpose of making physical measurements is to relate them to PSR, so that the tedious task of panel rating can be replaced by mechanical measurements. It was found that present serviceability was a function primarily of longitudinal and transverse profiles, with some likelihood that cracking, patching, and faulting would also contribute. Therefore, measurements can be divided into two categories: those that describe surface deformation and those that describe surface deterioration. Details about objective measurements are discussed in the next section.
9. *Summaries of measurements.* There are many different ways to summarize surface deformation and surface deterioration. For example, longitudinal profile may be expressed as mean slope variance, total deviation of the record from some baseline in in./mile (m/km), number of bumps greater than some minimum, a combination of several different measurements, or any other summary statistics involving variance of the record. Transverse profile may be summarized by mean rut depth, variance of transverse profile, or the variance of rut depth along the wheelpath. Cracking and deterioration occur in different levels of severity, and their measurements can be expressed in one unit or another.
10. *Derivation of PSI.* After PSRs and measurement summaries have been obtained for all the selected pavements, the final step is to combine the measurement summaries into a PSI formula that predicts the PSRs to a satisfactory approximation. The technique of multiple linear regression analysis may be used to arrive at the formula and to decide which measurements may be neglected. For example, if the longitudinal profile summary is found sensitive to faulting, then faulting measurements need not appear in the formula whenever the profile measure is included.

Objective Measurements Many measurements summaries were tried in the Road Test, but those finally selected were mean slope variance $\overline{SV}$ for the longitudinal profile, mean rut depth $\overline{RD}$ for the transverse profile, and cracking C and patching P for surface deterioration.

Mean Slope Variance The symbol $\overline{SV}$ is used for the summary statistics of wheelpath roughness as measured by the Road Test longitudinal profilometer. For each wheelpath, the profilometer produces a continuous record of the pavement slope between two points 9 in. apart, as shown by angle A in Figure 9.25. The slopes are generally sampled at 1-ft (0.3-m) intervals over the length of the record. A variance SV is

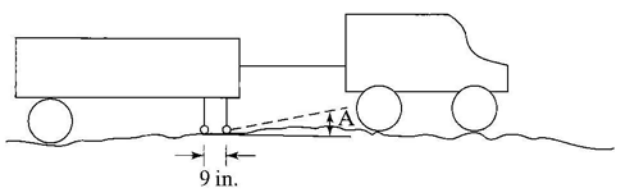


FIGURE 9.25
Measurement of slope variance by profilometer (1 in. = 25.4 mm).

Downloaded From : www.EasyEngineering.net

Downloaded From : www.EasyEngineering.net

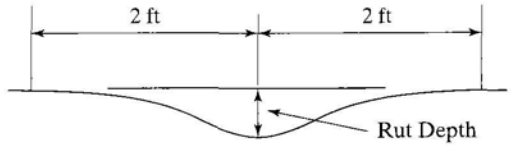


FIGURE 9.26
Measurement of rut depth by a gage (1 ft = 0.305 m).

computed for the sample slopes in each wheelpath from

$$SV = \frac{\Sigma(S - \bar{S})^2}{n - 1} \tag{9.1}$$

in which S is each sample slope, N is the number of samples, and $\bar{S}$ is the mean of all slopes, $\Sigma S/n$. The SVs of the two wheelpaths are averaged to give the mean slope variance $\overline{SV}$.

Mean Rut Depth The transverse profile of the flexible pavement sections was measured by a rut depth gage. The gage is used to determine the differential elevation between the wheelpath and a line connecting two points each 2 ft (0.6 m) away from the center of the wheelpath in the transverse direction, as shown in Figure 9.26. Rut depth measurements were obtained at 20-ft (6.1-m) intervals in both wheelpaths, which were averaged to give the mean rut depth $\overline{RD}$.

Cracking and Patching Cracking and patching were combined as a single variable. Cracking is expressed as linear feet and patching as square feet, both per 1000 ft^2 of pavement area.

Development of PSI Equation The basic equation is in the linear form

$$PSI = A_0 + (A_1R_1 + A_2R_2 + \cdots) + (B_1D_1 + B_2D_2 + \cdots) \tag{9.2}$$

in which $R_1, R_2, \ldots$ are functions of profile roughness and $D_1, D_2, \ldots$ are functions of surface deterioration. Note that PSI is an approximation of PSR within prescribed limits.

Choice of Functions Because the measurement summaries are not linearly related to PSR, a transformation must be applied to each of the summaries. This can be achieved by plotting the measurements versus PSR in various forms and finding out which plot results in a straight line. The following linearizing transformations can be used:

$$R_1 = \log(1 + \overline{SV}) \tag{9.3}$$

$$R_2 = \overline{RD}^2 \tag{9.4}$$

$$D_1 = \sqrt{C + P} \tag{9.5}$$

Figures 9.27, 9.28, and 9.29 show the plot of PSR versus R_1, R_2, and D_1 for the 74 flexible sections, and Figures 9.30 and 9.31 show the plot of PSR versus R_1 and D_1 for the 49 rigid sections. It can be seen that the data scatter a great deal, especially in

Downloaded From : www.EasyEngineering.net

Downloaded From : www.EasyEngineering.net

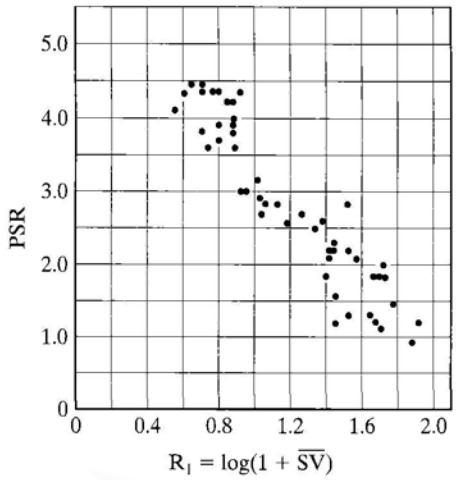


FIGURE 9.27
PSR versus $\log(1 + \overline{SV})$ for flexible pavements. (After Carey and Irick (1960).)

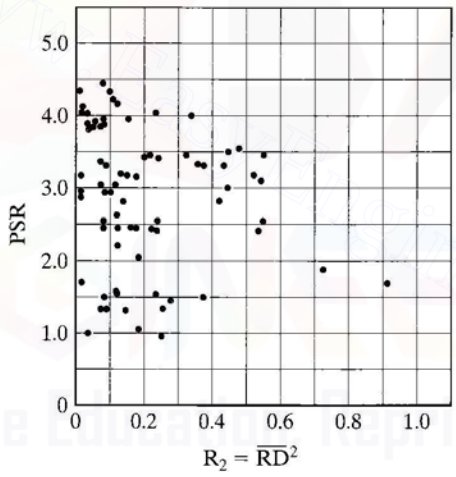


FIGURE 9.28
PSR versus $\overline{RD}^2$ for flexible pavements. (After Carey and Irick (1960).)

Figures 9.28 and 9.29. However, these plots were found to result in the best linearizing functions available. Therefore, the equation for flexible pavements can be written as

$$\begin{aligned} PSI &= A_0 + A_1R_1 + A_2R_2 + B_1D_1 \\ &= A_0 + A_1 \log(1 + \overline{SV}) + A_2\overline{RD}^2 + B_1\sqrt{C + P} \end{aligned} \tag{9.6}$$

For rigid pavements, there is no rut depth, so the equation becomes

$$PSI = A_0 + A_1R_1 + B_1D_1 = A_0 + A_1 \log(1 + \overline{SV}) + B_1\sqrt{C + P} \tag{9.7}$$

Determination of Coefficients The coefficients A_0, A_1, A_2, and B_1 in Eq. 9.6 and A_0, A_1, and B_1 in Eq. 9.7 can be determined by linear multiple regression. From

Downloaded From : www.EasyEngineering.net

Downloaded From : www.EasyEngineering.net

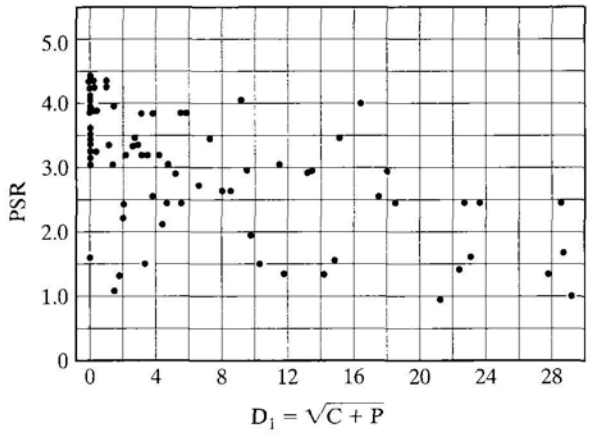


FIGURE 9.29

PSR versus $\sqrt{C + P}$ for flexible pavements. (After Carey and Irick (1960).)

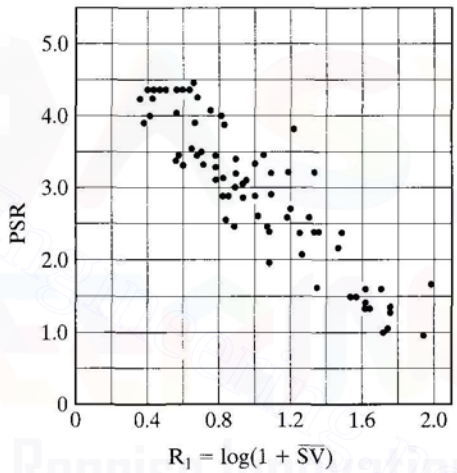


FIGURE 9.30

PSR versus $\log(1 + \overline{SV})$ for rigid pavements. (After Carey and Irick (1960).)

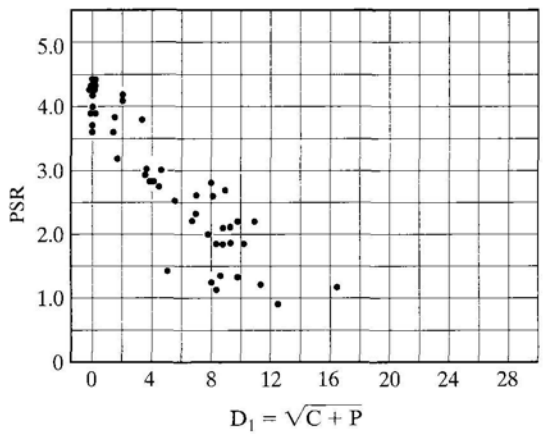


FIGURE 9.31

PSR versus $\sqrt{C + P}$ for rigid pavements. (After Carey and Irick (1960).)

Downloaded From : www.EasyEngineering.net

Downloaded From : www.EasyEngineering.net

Eq. 9.6, the error between PSR and PSI for all sections can be expressed as

$$E = \sum(\text{PSR} - \text{PSI})^2 = \sum(\text{PSR} - A_0 - A_1R_1 - A_2R_2 - B_1D_1)^2 \quad (9.8)$$

in which Σ is the summation over all sections (e.g., the 74 flexible pavement sections in the Road Test). The coefficients A_0, A_1, A_2, and B_1 must be selected so that the least error is obtained. The value of E can be minimized by taking partial derivatives with respect to each of the coefficients and setting them to zero. This results in four equations and four unknown coefficients, which can easily be solved. The derivation of these four equations is as follows: From Eq. 9.8,

$$\frac{\partial E}{\partial A_0} = -2\sum(\text{PSR} - A_0 - A_1R_1 - A_2R_2 - B_1D_1) = 0$$

or

$$\sum \text{PSR} - nA_0 - A_1\sum R_1 - A_2\sum R_2 - B_1\sum D_1 = 0$$

in which n is the number of pavement sections. Dividing by n and rearranging yields

$$\overline{\text{PSR}} = A_0 + A_1\overline{R}_1 + A_2\overline{R}_2 + B_1\overline{D}_1 \quad (9.9)$$

From Eq. 9.8,

$$\frac{\partial E}{\partial A_1} = -2\sum[(\text{PSR} - A_0 - A_1R_1 - A_2R_2 - B_1D_1)R_1] = 0$$

Replacing A_0 by Eq. 9.9 yields

$$\sum\{[\text{PSR} - \overline{\text{PSR}} - A_1(R_1 - \overline{R}_1) - A_2(R_2 - \overline{R}_2) - B_1(D_1 - \overline{D}_1)]R_1\} = 0$$

To make the equation more systematic, a constant term $\overline{R}_1$ can be added:

$$\sum\{[\text{PSR} - \overline{\text{PSR}} - A_1(R_1 - \overline{R}_1) - A_2(R_2 - \overline{R}_2) - B_1(D_1 - \overline{D}_1)](R_1 - \overline{R}_1)\} = 0 \quad (9.10)$$

This addition has no effect on the equation, because

$$\begin{aligned}
&\overline{R}_1\sum[\text{PSR} - \overline{\text{PSR}} - A_1(R_1 - \overline{R}_1) - A_2(R_2 - \overline{R}_2) - B_1(D_1 - \overline{D}_1)] \\
&= \overline{R}_1\left[\sum \text{PSR} - \sum\overline{\text{PSR}} - A_1\left(\sum R_1 - \sum\overline{R}_1\right) - A_2\left(\sum R_2 - \sum\overline{R}_2\right)\right. \\
&\quad \left. - B_1\left(\sum D_1 - \sum\overline{D}_1\right)\right] \\
&= 0
\end{aligned}$$

Downloaded From : www.EasyEngineering.net

Downloaded From : www.EasyEngineering.net

Equation 9.10 can be simplified to

$$A_1\sum(R_1 - \overline{R}_1)^2 + A_2\sum(R_2 - \overline{R}_2)(R_1 - \overline{R}_1) + B_1\sum(D_1 - \overline{D}_1)(R_1 - \overline{R}_1) = \sum(\text{PSR} - \overline{\text{PSR}})(R_1 - \overline{R}_1) \quad (9.11)$$

The remaining two equations can be obtained by taking partial derivatives of E with respect to A_2 and B_1 or by simply replacing the multiplier $(R_1 - \overline{R}_1)$ in Eq. 9.11 with $(R_2 - \overline{R}_2)$ and $(D_1 - \overline{D}_1)$, respectively:

$$A_1\sum(R_1 - \overline{R}_1)(R_2 - \overline{R}_2) + A_2\sum(R_2 - \overline{R}_2)^2 + B_1\sum(D_1 - \overline{D}_1)(R_2 - \overline{R}_2) = \sum(\text{PSR} - \overline{\text{PSR}})(R_2 - \overline{R}_2) \quad (9.12)$$

$$A_1\sum(R_1 - \overline{R}_1)(D_1 - \overline{D}_1) + A_2\sum(R_2 - \overline{R}_2)(D_1 - \overline{D}_1) + B_1\sum(D_1 - \overline{D}_1)^2 = \sum(\text{PSR} - \overline{\text{PSR}})(D_1 - \overline{D}_1) \quad (9.13)$$

Equations 9.9, 9.11, 9.12, and 9.13 can be used to solve the four coefficients.

The final PSI equation obtained by the Road Test based on 74 flexible sections is

$$\text{PSI} = 5.03 - 1.91\log(1 + \overline{\text{SV}}) - 1.38\overline{\text{RD}}^2 - 0.01\sqrt{C + P} \quad (9.14)$$

in which the units are 10^{-6} rad for $\overline{\text{SV}}$, in. for $\overline{\text{RD}}$, ft/1000 ft^2 for C, and ft^2/1000 ft^2 for P. The equation based on 49 rigid sections is

$$\text{PSI} = 5.41 - 1.71\log(1 + \overline{\text{SV}}) - 0.09\sqrt{C + P} \quad (9.15)$$

Example 9.1:

Table 9.3 gives the measurements and ratings on seven sections of rigid pavements. Find the regression equation for PSI.

TABLE 9.3 Measurements and Ratings on Rigid Pavement Sections

Section no.	Slope variance $\overline{\text{SV}}$ (10^{-6})	Cracking and patching $C + P$ (ft or ft^2/1000 ft^2)	Present serviceability rating (PSR)
1	52.0	60.8	2.0
2	6.5	4.0	4.2
3	22.2	53.5	2.6
4	26.2	53.3	2.3
5	47.8	130.0	1.2
6	25.5	16.0	2.8
7	3.2	0.0	4.4

Note. 1 ft = 0.305 m.

Downloaded From : www.EasyEngineering.net

Downloaded From : www.EasyEngineering.net

TABLE 9.4 Computation of Regression Equation for PSI

Section no.	$\log(1 + \overline{SV})$ R_1	$\sqrt{C + P}$ D_1	PSR	$R_1 - \overline{R}_1$	$D_1 - \overline{D}_1$	PSR $-$ $\overline{PSR}$	PSI check
1	1.72	7.80	2.00	0.42	2.11	−0.79	1.92
2	0.88	2.00	4.20	−0.42	−3.69	1.41	3.94
3	1.37	7.31	2.60	0.07	1.62	−0.19	2.43
4	1.43	7.30	2.30	0.13	1.61	−0.49	2.36
5	1.69	11.40	1.20	0.39	5.71	−1.59	1.34
6	1.42	4.00	2.80	0.12	−1.69	0.01	2.93
7	0.62	0.00	4.40	−0.68	−5.69	1.61	4.60
Average	1.30	5.69	2.79				

Solution: Consider $\log(1 + \overline{SV})$ as R_1 and $\sqrt{C + P}$ as D_1. The values of $R_1 - \overline{R}_1$, $D_1 - \overline{D}_1$, and PSR $-$ $\overline{PSR}$ are tabulated in Table 9.4.
From Eq. 9.9,

$$2.79 = A_0 + 1.30A_1 + 5.69B_1 \tag{9.16}$$

From Eq. 9.11, $[(0.42)^2 + (-0.42)^2 + (0.07)^2 + (0.13)^2 + (0.39)^2 + (0.12)^2 + (-0.68)^2]A_1 + [0.42 \times 2.11 + (-0.42)(-3.69) + 0.07 \times 1.62 + 0.13 \times 1.61 + 0.39 \times 5.71 + 0.12(-1.69) + (-0.68)(-5.69)]B_1 = 0.42(-0.79) + (-0.42) \times 1.41 + 0.07(-0.19) + 0.13 \times (-0.49) + 0.39(-1.59) + 0.12 \times 0.01 + (-0.68) \times 1.61$, or

$$1.004A_1 + 8.652B_1 = -2.715 \tag{9.17}$$

From Eq. 9.13, $8.652A_1 + [(2.11)^2 + (-3.69)^2 + (1.62)^2 + (1.61)^2 + (5.71)^2 + (-1.69)^2 + (-5.69)^2]B_1 = 2.11(-0.79) + (-3.69) \times 1.41 + 1.62(-0.19) + 1.61 \times (-0.49) + 5.71(-1.59) + (-1.69) \times 0.01 + (-5.69) \times 1.61$, or

$$8.652A_1 + 91.121B_1 = -26.223 \tag{9.18}$$

From Eqs. 9.17 and 9.18, $A_1 = -1.23$ and $B_1 = -0.17$. From Eq. 9.9, $A_0 = 5.36$. The regression equation is

$$PSI = 5.36 - 1.23 \log(1 + \overline{SV}) - 0.17\sqrt{C + P} \tag{9.19}$$

Values of PSI computed by Eq. 9.19 are tabulated in the last column of Table 9.4.

Deficiencies in PSI Equation The PSI equations developed by the AASHO Road Test have the following shortcomings:

1. They were based on the evaluations of the Road Test rating panel. Whether the public's perception of serviceability is the same today as 30 years ago is questionable because vehicles, highway characteristics, and travel speeds have changed significantly.
2. They include not only the rideability but also the surface defects. For the management of pavement inventory, it would be better to have separate measures of ride quality and surface defects. Therefore, there is a need to develop a new pavement rating scale to ensure that the objective pavement evaluations are directly and reasonably related to the public's perception of riding quality.

Downloaded From : www.EasyEngineering.net

Downloaded From : www.EasyEngineering.net

3. The profilometer used in the Road Test is no longer in use today. Errors are multiplied when the original AASHO PSI equation is used with a different method for measuring roughness. The best way to eliminate this problem is to form a new pavement rating panel and to correlate the result directly with the particular roughness instrument of interest.

Both pavement distress and ride quality are terms that describe the physical condition of pavements; it is frequently assumed that they will be highly correlated and that a relationship exists allowing a reliable estimate of one from a measure of the other. However, this relationship can rarely be found in the pavement performance data bases. The reason for the lack of correlation between distress and roughness is that, in reality, they are physically different attributes of pavement conditions.

9.2.2 Roughness

Although the physical measurements used for computing PSI include the distress data of rut depth, cracking, and patching, it is the longitudinal profile or roughness that provides the major correlation variable. The correlation coefficient between PSR and PSI is increased by only about 5% after the addition of distress data (Zaniewski *et al.*, 1985). Because of the relatively small contribution to PSI by physical distress and the difficulty in obtaining the distress data, many agencies rely only on roughness to estimate PSI.

Methods for Measuring Roughness Either direct or indirect methods can be used to measure roughness. Direct measures of longitudinal profile can be obtained from Class I or Class II devices. Class I devices include the traditional longitudinal surveys by rod and level or by some other labor-saving apparatus (such as the Face Dipstick, which is walked along the test path on two feet spaced 1 ft (0.305 m) apart). Class II devices include various types of profilometers, such as the chloe type rolling straightedge profilometer used in the AASHO Road Test, the Surface Dynamics Profilometer (SDP) designed by General Motors (Spangler and Kelly, 1964), the siometer employed by the Texas State Department of Highways and Public Transportation for measuring the serviceability index (Fernando *et al.*, 1990), and the profilometer and rut measuring device called PRORUT owned by FHWA (1987a). Indirect measures of longitudinal profile are those obtained from response-type road roughness meters (RTRRM), such as the Mays ridemeter. RTRRM systems are referred to as class III devices.

A survey of 48 states shows that the Mays ridemeter is the most popular device for roughness measurements and is used by 22 states (Epps and Monismith, 1986). The RTRRMs measure the relative movement in inches per mile (m/km) between the body of the automobile and the center of the rear axle. They are inexpensive, simple, and easy to operate at speeds of up to 50 mph (80 km/h). The recording systems are portable and can be installed in selected standard automobiles. The RTRRM measurements are sensitive to the type of tires, tire pressure, load, vehicle suspension system, speed of car, and factors that affect vehicle responses. Because of such sensitivity, they need to be calibrated when any of the foregoing factors changes significantly.

A recent survey of 37 states shows that most states are using laser-type profilometers (profilers) for roughness measurements, that only one state is still using

Downloaded From : www.EasyEngineering.net

Downloaded From : www.EasyEngineering.net

the Mays ridemeter, and that the international roughness index (IRI) is the one most widely used.

When the response-type road roughness meters are properly calibrated, the output from all the meters may be placed on a common scale. One primary advantage of this approach is that the subjective interpretation of road roughness can be eliminated and pavement engineers will have a common scale for describing the ride quality of a road. Once the common scale is accepted, each highway agency may define where good, fair, and poor ride quality should be located on the scale. Certainly, PSR values from large panels could be correlated with the roughness scale as a means for intepreting the roughnes data.

International Roughness Index To provide a common quantitative basis on which the different measures of roughness can be compared, the International Roughness Index (IRI) was developed at the International Road Roughness Experiment held in Brazil in 1982 under the sponsorship of the World Bank. The World Bank published guidelines for conducting and calibrating roughness measurements (Sayers *et al.*, 1986a); the IRI has been adopted as a standard for the FHWA Highway Performance Monitoring System (HPMS) data base (FHWA, 1987b).

The IRI summarizes the longitudinal surface profile in the wheelpath and is computed from surface elevation data collected by either a topographic survey or a mechanical profilometer. It is defined by the average rectified slope (ARS), which is a ratio of the accumulated suspension motion to the distance traveled obtained from a mathematical model of a standard quarter car transversing a measured profile at a speed of 50 mph (80 km/h). It is expressed in units of inches per mile (m/km). General methods for use in simulation are also specified in ASTM E 1170 "Standard Practices for Simulating Vehicular Response to Longitudinal Profiles of a Vehicular Traveled Surface."

Since no two RTRRMs are exactly alike, it is necessary to convert the measures to the standard IRI scale by using the relationships established through calibration. Calibration can be achieved by measuring the ARS of the RTRRM at a standard speed on special calibration sites of known IRI roughness values. The measured ARS values are plotted against the IRI values, and a line is fitted to the data points and used to estimate IRI from the RTRRM measurements in the field. A detailed discussion of this procedure was presented by Sayers et al. (1986b).

Riding Number Janoff *et al.* (1985) investigated the relationship between roughness and serviceability. They found that the riding number RN, as measured with a profilometer in the band of frequencies between 0.125 and 0.63 cycle/ft (10 to 15 Hz at 55 mph), is highly correlated with the mean panel rating MPR for all three types of pavements: asphalt, concrete, and composite. Note that RN, which ranges from 0 to 5, is equivalent to PSI and that MPR is equivalent to PSR. The resulting regression equation that transforms the longitudinal roughness in this frequency band into RN is

$$RN = -1.74 - 3.03 \log(PI) \tag{9.20}$$

in which RN is the riding number of a given pavement section, which gives the best estimate of MPR, and PI is the profile index, defined as the square root of the mean square

Downloaded From : www.EasyEngineering.net

Downloaded From : www.EasyEngineering.net

of the profile height in the specified frequency band. The MPR of a given test section is also an accurate predictor of the public's subjective perception of whether a specific test section needs repairs. The percentage of the driving public who feel that a given section requires repair is defined by

$$NR = 132.6 - 33.5\,MPR \tag{9.21a}$$

or

$$NR = 190.9 + 101.5\log(PI) \tag{9.21b}$$

in which NR is the percentage of drivers who think that the pavement needs repair. Therefore, given only longitudinal roughness measures, one can compute both the rideability number and the exact percentage of the driving population that thinks the road should be repaired.

Equations 9.20 to 9.21*b* were based on data from Ohio only. The data base was later extended to include 282 pavement sections in New Jersey, Michigan, New Mexico, and Louisiana. Given combined data from all five states, the equations were modified as follows (Janoff, 1988):

$$RN = -1.47 - 2.85\log(PI) \tag{9.22}$$

$$NR = 131.7 - 33.9\,RN \tag{9.23a}$$

$$NR = 181.5 + 96.6\log(PI) \tag{9.23b}$$

A nonlinear equation was also developed to compute RN:

$$RN = 5\exp[-11.72(PI)^{0.89}] \tag{9.24}$$

Equations 9.22 and 9.24 are both valid within the range of the data base collected. The nonlinear equation extends the prediction to the entire range of roughness, although it is no more accurate or valid than the linear equation within the range of the data base.

Relationship between PSI and IRI Relationships between PSR and IRI were developed by Al-Omari and Darter (1994) for flexible, rigid, and composite pavement types for the states of Louisiana, Michigan, New Jersey, New Mexico, and Indiana. They found that there were no significant differences between the models for different states and pavement types. The following nonlinear model that fits the boundary conditions is recommended:

$$PSR = 5 \times e^{(-0.0041 \times IRI)} \tag{9.25}$$

Here, PSR = present serviceability rating, IRI = international roughness index in in./mile. Gulen *et al.* (1994) indicated that the preceding equation was biased and was not statistically correct, because it was forced to pass through PSR = 5 when IRI = 0. They proposed a number of models for the state of Indiana and suggested that the selection of the model depended on the user's need.

Hall and Munoz (1999) developed models for estimating the present serviceability index (PSI) and the international roughness index (IRI) for asphalt and concrete pavements. These models were developed by first analyzing the correlation between

Downloaded From : www.EasyEngineering.net

Downloaded From : www.EasyEngineering.net

slope variance (SV) and PSI values using the AASHO Road Test data and then analyzing the correlation between SV and IRI for profiles representing a broad spectrum of road roughness levels. The following equations were obtained:

Asphalt Pavement:

$$\text{PSI} = 5 - 0.2397x^4 + 1.771x^3 - 1.4045x^2 - 1.5803x \tag{9.26a}$$

Concrete Pavement:

$$\text{PSI} = 5 + 0.6046x^3 - 2.2217x^2 - 0.0434x \tag{9.26b}$$

In both cases, $x = \log(1 + \text{SV})$ and $\text{SV} = 2.2704\ (\text{IRI})^2$.

9.3 SURFACE FRICTION

Adequate surface friction must be provided on a pavement, so that loss of control does not occur in normally expected situations when the pavement is wet. The skid accident reduction program issued by the Federal Highway Administration (FHWA, 1980) encourages each state highway agency to minimize wet weather skidding accidents by identifying and correcting sections of roadway with high or potentially high skid accident incidence and ensuring that new surfaces have adequate, durable skid-resistant properties.

9.3.1 Factors Affecting Skid Accidents

Pavement characteristics are only one element of a multiple-component system in which each component has a significant effect and interacts with the others to cause skid accidents. The four major elements are the driver, the roadway, the vehicle, and the weather.

Friction demands on a pavement vary greatly, depending on the speed of a vehicle, its design, and the design and condition of its braking system. The skill of the operator also affects the potential for loss of control or skidding. Weather, especially wet pavements and the thickness of water film on the pavement, also affects the available friction. If the water layer on the pavement is very thick and the tire moves at a high speed, hydroplaning occurs. This phenomenon is analogous to water skiing and makes the vehicle uncontrollable. The following are some of the surface conditions that are indicative of potential safety hazards:

1. Bleeding of asphalt, which covers the aggregates and obscures the effectiveness of their skid-resistant qualities.
2. Polished aggregate with smooth microtexture, which reduces friction between the aggregate and the tire.
3. Smooth macrotexture, which lacks suitable channels to facilitate drainage.
4. Rutting, which holds water in the wheelpaths after rain and causes hydroplaning.
5. Inadequate cross slope, which retains water on the pavement for a longer time, reduces friction, and increases the thickness of the water layer and the potential for hydroplaning.

Downloaded From : www.EasyEngineering.net

Downloaded From : www.EasyEngineering.net

9.3.2 Measurement of Surface Friction

Various methods have been used to determine the coefficient of friction between pavement and tire. The coefficient depends not only on pavement properties, but also on many other factors, such as tire type, tire wear, inflation pressure, vehicle speed, whether the wheel is rolling or locked, and whether the pavement is wet or dry. To obtain meaningful results, all the factors not related to the pavement must be fixed or clearly defined so that the only variables are the pavement properties.

Definition of Skid Number Surface friction is defined as the force developed when a tire that is prevented from rotating slides along the pavement surface. Surface friction can be computed as

$$F = \mu W \tag{9.27}$$

in which F is the tractive force applied to the tire at the tire–pavement contact, μ is the coefficient of friction, and W is the dynamic vertical load on the tire. The coefficient of friction determined from Eq. 9.27 is multiplied by 100 to obtain the skid number:

$$\text{SN} = 100\mu = 100\left(\frac{F}{W}\right) \tag{9.28}$$

Direct Measurement of Skid Number Pavement friction is measured most frequently by the locked wheel trailer procedure, as specified in ASTM E 274 "Standard Test Method for Skid Resistance of Paved Surfaces Using a Full-Scale Tire." The full-scale tire is usually a standard tire specified in ASTM E 501 "Standard Specification for Standard Rib Tire for Pavement Skid-Resistance Tests." The test tire is installed on the wheel or wheels of a single- or two-wheel trailer. The trailer is towed at a speed of 40 mph (64 km/h) over the dry pavement, and water is applied in front of the test wheel. The braking system is actuated to lock the test tire. Equipment is provided to measure the friction force generated when the tire is locked and the vehicle and trailer are moving at the prescribed speed. The results of the test are reported as a skid number, SN.

The ASTM E 274 method is used by more than forty states. Another method, which measures the coefficient of friction between tire and pavement in the yaw mode, is used by at least four states. A simple trailer called Mu Meter is commercially available, which measures the side force developed by two yawed wheels with smooth tires. The two wheels are yawed at equal but opposite angles to make the trailer travel in a straight line without requiring a restraining mechanism. The use of the Mu Meter is specified in ASTM E 670 "Standard Test Method for Side Force Friction on Paved Surfaces Using the Mu-Meter."

The most natural method for determining the skid resistance is to drive an automobile on a pavement, lock the wheels after the desired speed is reached, and measure how far the vehicle slides until it comes to a full stop. This method is specified in ASTM E 445 "Standard Test Method for Stopping Distance on Paved Surfaces Using a Passenger Vehicle Equipped with Full-Scale Tires." The coefficient of friction can then be

Downloaded From : www.EasyEngineering.net

Downloaded From : www.EasyEngineering.net

easily determined from mechanics by the formula

$$\mu = \frac{V^2}{2gS} \tag{9.29}$$

in which V is the initial vehicle speed, g is the acceleration of gravity, and S is the braking distance. If V is in mph and S in ft, then, from Eqs. 9.28 and 9.29,

$$\text{SDN} = 100\left(\frac{V^2}{30S}\right) \tag{9.30}$$

Note that the skid number obtained by the stopping distance method in ASTM E 445 is called the stopping distance number, SDN, instead of SN because values of SDN are numerically larger than those of SN. The reason is that wet pavement friction increases with decreasing speeds and the speed in stopping distance tests decreases from 40 to 0 mph (64 to 0 km/h), whereas the standard skid number is determined at 40 mph (64 km/h). The use of the stopping distance method is potentially hazardous, especially at high speeds. The hazard can be reduced by locking two diagonal wheels instead of all four wheels. The results, however, are questionable, because the stopping distance might not be representative of the actual value.

Relating Surface Texture to Skid Number Many methods have been used for measuring surface texture, such as tracing by stylus, measuring the outflow rate, and using putty to fill surface irregularities. One method that has been used frequently is the sand patch method, specified as ASTM E 965 "Standard Test Method for Measuring Surface Macrotexture Depth Using a Sand Volumetric Technique." The test procedure involves spreading a known volume of material on a clean and dry pavement surface, measuring the area covered, and calculating the mean texture depth MTD as a quotient between volume and area. This method is not suited for extensive field use because it requires the diversion of traffic. It is preferable to measure texture by some noncontact method from a vehicle moving at normal speed, as reported by Henry *et al.* (1984).

The macrotexture provides drainage paths for the water entrapped between pavement surface and tire imprint. After most of the water is expelled, some portion of the tire will make actual contact with the tips and plateaus of the pavement surface. Significant friction can be developed because the small-scale asperities of the aggregate particles penetrate whatever moisture may remain. This fine texture is referred to as microtexture. The division between macrotexture and microtexture is arbitrarily set at a texture depth of 0.5 mm, as defined in ASTM E 867 "Standard Definitions of Terms Relating to Traveled Surface Characteristics."

A new Road Surface Analyzer (ROSAN) was developed jointly by FHWA and private industry to provide measurements of pavement surface textures (Kuemmel *et al.*, 2000). It utilizes high-speed lasers to collect surface profile data, which are then converted to surface textural measurements by use of custom analysis software. Data acquisition and storage are accomplished by use of an onboard computer. The ROSAN system includes both vehicle-mounted and stationary measurement capabilities. The ROSAN_v (v for vehicle-mounted) uses a bumper-mounted 64-kHz laser sensor (operating at 32 kHz) for data collection at normal highway speeds. The ROSAN_b (b for beam-mounted) utilizes a trolley-mounted 16-kHz laser that traverses a 1-m metal beam and can be used for stationary measurements of localized pavement surface areas.

Downloaded From : www.EasyEngineering.net

Downloaded From : www.EasyEngineering.net

Unfortunately, no practical method has been developed to measure microtexture directly. A commonly used substitute is to measure low-speed friction by the British Pendulum Tester, as specified in ASTM E 303 "Standard Method for Measuring Surface Friction Properties Using the British Pendulum Tester." The tester is equipped with a standard rubber slider that is positioned to barely come in contact with the test surface prior to conducting the test. The pendulum is raised to a locked position, then released, thus allowing the slider to make contact with the test surface. A drag pointer is used to read the British Pendulum Number, BPN. The greater the friction between the slider and the test surface, the more the swing is retarded and the larger is the BPN reading. The test can be conducted either in the field or in the laboratory.

The relationship between skid number SN and speed V can be expressed by (Leu and Henry, 1978)

$$SN = SN_0 \exp\left[-\left(\frac{PNG}{100}\right)V\right] \tag{9.31}$$

in which SN_0 is the SN at zero speed and PNG is the percent normalized gradient of the SN versus V curve. Equation 9.31 shows that the skid number is contributed by microtexture in terms of SN_0 and macrotexture in terms of PNG. It can be easily proved from Eq. 9.31 that $PNG = -100(dSN/dV)/SN$, which is the percent gradient, $100(dSN/dV)$, normalized by dividing by SN.

Figure 9.32 shows the relationship between the zero intercept skid number, SN_0, and the BPN. The linear relationship can be expressed as (Meyer, 1991)

$$SN_0 = 1.32\,BPN - 34.9 \tag{9.32}$$

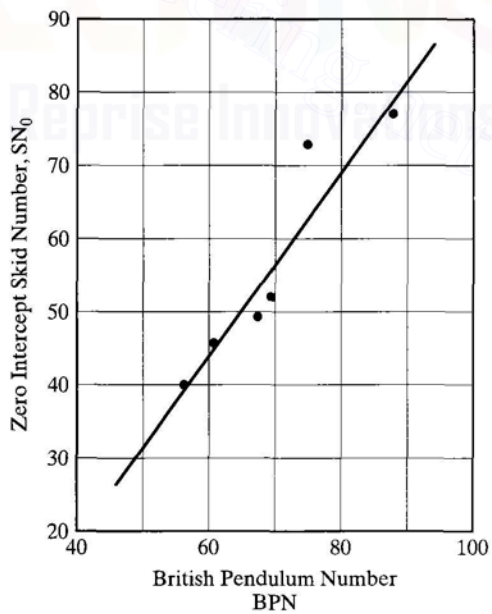


FIGURE 9.32

Relationship between SN_0 and BPN. (After Meyer (1991).)

Downloaded From : www.EasyEngineering.net

Downloaded From : www.EasyEngineering.net

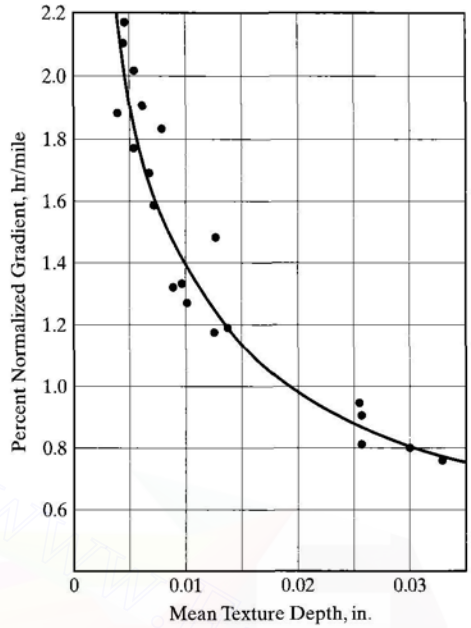


FIGURE 9.33

Relationship between PNG and MTD (1 h/mile = 0.63 h/km, 1 in. = 25.4 mm). (After Meyer (1991).)

Figure 9.33 shows the relationship between percent normalized gradient PNG and mean texture depth MTD. The relationship can be expressed as (Meyer, 1991)

$$\text{PNG} = 0.157(\text{MTD})^{-0.47} \tag{9.33}$$

in which PNG is in h/mile and MTD is in inches.

It should be pointed out that Eqs. 9.32 and 9.33 are based on limited data and that different regression equations were presented by Wambold *et al.* (1989). Values of PNG and SN_0 can also be obtained from the SN versus speed curve obtained from locked-wheel skid resistance tests at several speeds. From Eq. 9.31,

$$\log(\text{SN}) = \log(\text{SN}_0) - 0.00434(\text{PNG})V \tag{9.34}$$

Therefore, a plot of log(SN) versus V should result in straight line, as shown in Figure 9.34. The intercept at zero speed is SN_0 and the slope of the straight line is 0.00434 PNG.

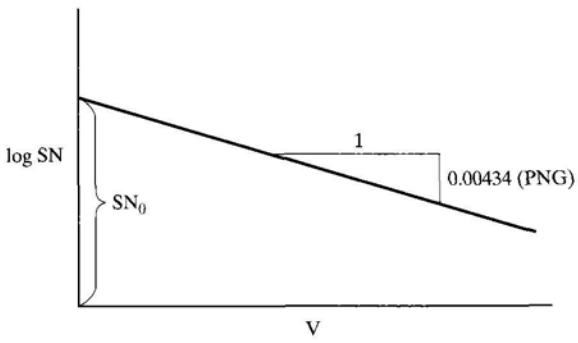


FIGURE 9.34

Method for determining SN_0 and PNG.

Downloaded From : www.EasyEngineering.net

Downloaded From : www.EasyEngineering.net

Example 9.2:

The skid numbers obtained from locked-wheel skid tests at various speeds are listed in Table 9.5. Determine the skid number SN_0 and the percent normalized gradient PNG. Estimate the probable BPN and the mean texture depth MTD of the pavement surface.

TABLE 9.5 Skid Numbers Measured at Various Speeds

Speed V (mph)	10	30	50	70
Skid number SN	52	44	34	29

Note. 1 mph = 1.6 km/h.

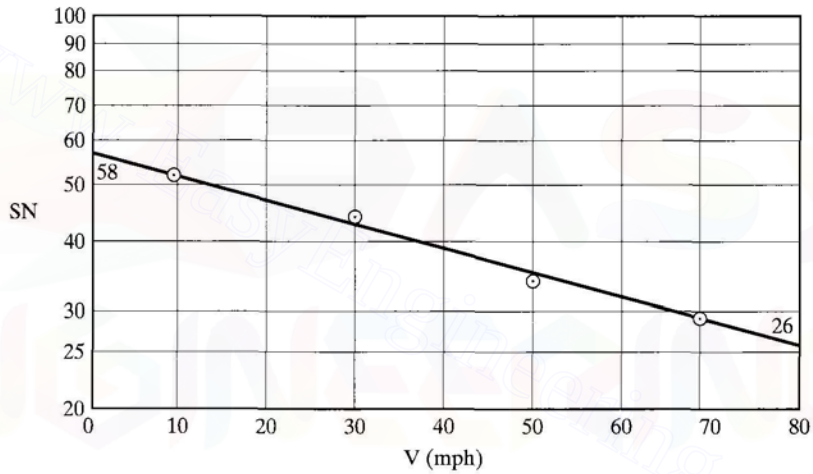


FIGURE 9.35
Example 9.2 (1 mph = 1.6 km/h).

Solution: Plot SN versus V on a semilog paper and draw a best-fit line passing through these four points, as shown in Figure 9.35. The intercept at $V = 0$ is $SN_0 = 58$ and the slope of the straight line is $0.00434(PNG) = (\log 58 - \log 26)/80 = 0.00436$, or PNG = 1.0%. From Eq. 9.32, BPN = (58 + 34.9)/1.32 = 70, and from Eq. 9.33, $1 = 0.157(MTD)^{-0.47}$, or MTD = 0.0195 in. (0.5 mm).

9.3.3 Control of Skid Resistance

The skid resistance of new and existing pavements must be properly controlled so that the minimum requirement can be met.

Minimum Required Skid Resistance The minimum skid resistance required for a pavement depends on the method of measurement and the traffic speed. Table 9.6

Downloaded From : www.EasyEngineering.net

Downloaded From : www.EasyEngineering.net

TABLE 9.6 Recommended Minimum Skid Number for Main Rural Highways

Traffic speed (mph)	SN measured at traffic speed	SN measured at 40 mph
30	36	31
40	33	33
50	32	37
60	31	41
70	31	46

Note. 1 mph = 1.6 km/h.
Source. After Kummer and Meyer (1967).

shows the minimum skid numbers, measured according to ASTM E 274, for main rural highways as recommended by the NCHRP Report 37 (Kummer and Meyer, 1967). For interstate highways, lower values of SN than those shown in the table could be sufficient, whereas certain sites will require higher values. For a mean traffic speed of 50 mph (80 km/h), NCHRP Report 37 recommended a SN of 37, measured at 40 mph (64 km/h), as the minimum permissible for standard main rural highways. Because there are no definite federal and state standards on the minimum SN required, most highway agencies follow the guidelines recommended by NCHRP Report 37.

Design of New Pavements The skid resistance of wearing surfaces depends both on the aggregate and on the mixture characteristics.

Aggregate Characteristics The most frequently sought after characteristics for a skid-resistant aggregate are its resistance to polish and wear and its texture, shape, and size:

1. The ability of an aggregate to resist the polish and wear actions of traffic has long been recognized as a most important characteristic. When an aggregate becomes smooth, it will have poor skid resistance.
2. Both the microtexture and the macrotexture have a great effect on skid resistance. Microtexture describes surface coarseness as governed by the size of individual mineral grains and the matrix in which they are cemented. Macrotexture refers to the angularity of the aggregate particles and the voids and pits in the pavement surface. An aggregate with larger than sand sizes of hard grains and weak cementation of the grains will wear under traffic and expose a continually renewed nonpolished surface. However, if the matrix of aggregate is strong, the individual grains will be tightly held and subsequently could be polished by traffic. For an aggregate to exhibit satisfactory skid resistance properties, it probably should contain at least two mineral constituents of different hardness in order to wear differentially and expose new surfaces.
3. The shape of an aggregate particle significantly affects its skid-resistant properties. Angular particles are more skid resistant as long as they remain angular. The

Downloaded From : www.EasyEngineering.net

Downloaded From : www.EasyEngineering.net

retention of angularity depends on such characteristics as mineralogical composition and the amount of polish and wear produced by traffic. Some minerals will crush into mostly flat and elongated particles, resulting in poor skid resistance.

4. The size of an aggregate has considerable effect on skid resistance. For HMA pavements, the quality of large-size aggregates has more effect on skid resistance than does that of small-size aggregates, whereas, for PCC pavements, the presence of cement mortar on the surface causes the sand-size aggregates to have more influence.

Mixture Characteristics Mixture characteristics can be controlled by the blending of aggregates, by the selection of proper aggregate size and gradation, by the use of appropriate binder content, and by the application of good construction practice:

1. Blending of aggregates to achieve the desired skid resistance is resorted to when superior quality aggregates are expensive or in limited supply. Blending may be accomplished by combining natural aggregates with a synthetic aggregate. Most frequently, one of the aggregates will constitute the entire coarse or fine aggregate. To provide good skid resistance, high-quality coarse aggregates should be used for HMA, but high-quality fine aggregates for PCC.
2. The maximum size of aggregate, as well as the mix gradation, may be varied to provide the desired surface texture. The skid resistance of asphalt pavements can be greatly increased by using an open-graded surface course or a porous pavement. In addition to reducing splash and spray and helping to maintain high friction levels between vehicle tires and wet pavements, porous asphalt pavements are recognized for their ability to reduce night reflectance and decrease tire and vehicle noise.
3. The binder content depends on the design criteria to be satisfied. The criteria for asphalt pavements include durability and stability; those for concrete pavements include durability, strength, and workability. This does not mean that binder content has no effect on skid resistance. For asphalt pavements, too much asphalt will cause bleeding and result in a slippery surface, whereas too little could lead to raveling and deterioration of the pavement surface. For concrete pavements, if the mortar is improperly balanced in the mix, rapid wear and early deterioration of the concrete surface can occur. The skid resistance will diminish as the pavement deteriorates.
4. The texture of concrete surface can be controlled by the finishing method. The mean texture depth and the initial skid number for some of the finishing methods are shown in Table 9.7.

Improvement of Existing Surface The correcting measure for a pavement surface of low skid resistance usually consists of modifying the existing surface rather than applying a new surface. The nature of the modification varies with the type of surface and the cause of low skid resistance. For example, grooving could be the answer for a concrete pavement, and bonding aggregates on the surface to form the desired texture could be the answer for a bituminous pavement.

Downloaded From : www.EasyEngineering.net

Downloaded From : www.EasyEngineering.net

TABLE 9.7 Mean Texture Depth and Initial Skid Number of Concrete Pavements with Different Finishing Methods

Method of finishing	Mean texture depth (in.)	Initial skid number (SN)		
		Minimum	Maximum	Mean
Burlap drag	0.019	38	64	52
Paving broom	0.031	46	72	58
Wire broom	0.042	51	72	61
Fluted float	0.045	40	72	61

Note. 1 in. = 25.4 mm.
Source. After NCHRP (1972).

Concrete Pavements For concrete pavements, surface modification can involve roughing, acid etching, grooving, or bonding a thin layer of aggregate:

1. Concrete surfaces may be roughened by mechanical means to improve their skid resistance. Steel shots and hand-operated machines have been used to cut into the pavement surface with varying degrees of success. The success of these methods depends on a number of variables, such as the hardness of the cement mortar and the type of aggregate in the concrete.
2. Concrete surfaces can also be roughened by acid etching. The chemicals most frequently used are concentrated hydrochloric or hydrofluoric acids that are diluted with water at the time of application. After the acid has reacted with the minerals of the aggregates and with the cement, the residue is flushed and an improved surface texture is obtained.
3. Grooving is the process of cutting shallow, narrow channels on the concrete surface by using a series of rotating diamond saw blades. It is used most often at locations where hydroplaning or wet pavement accidents are a problem. Although longitudinal grooving does not improve the drainage in the transverse direction, it is generally preferred over transverse grooving because the longitudinal grooving can be produced faster and the process does not require the closing of adjacent lanes.
4. Bonding a thin layer of aggregate to the surface is another method for improving skid resistance. The bonding medium may be an epoxy resin that is applied to the surface after it has been cleaned. The aggregate to be bonded should be extremely hard, highly angular, and free of fine material. Crushed quartz sand, synthetic aggregate, or slag can be used.

Bituminous Pavements The modification of bituminous surfaces to correct low skid resistance can be accomplished by grooving, by surface treatment or thin overlay, or by heater planer:

1. Grooving techniques for asphalt pavements are similar to those for concrete pavements. However, if the asphalt content is high and the weather is hot, grooves in asphalt pavements could flow together and lose their effectiveness.

Downloaded From : www.EasyEngineering.net

Downloaded From : www.EasyEngineering.net

2. Some types of surface treatment or thin overlay, such as the open-graded friction course, are specially designed to reduce hydroplaning and wet weather accidents. This can be achieved through careful selection of aggregate types and gradation and by improving the transverse slope to facilitate drainage.
3. A heater planer can be used to correct a surface with low skid resistance due to bleeding of the bituminous binder. The equipment consists essentially of a unit to heat the pavement surface and then remove the excess material by cutting or "planning" it away. After planing, stone chips or sand is spread and rolled into the surface while it is still hot. This method is most effective and economical in correcting isolated spots of bleeding, such as at high-volume intersections.

9.4 NONDESTRUCTIVE DEFLECTION TESTING

Deflection measurements have long been used to evaluate the structural capacity of in situ pavements. They can be used to backcalculate the elastic moduli of various pavement components, evaluate the load transfer efficiency across joints and cracks in concrete pavements, and determine the location and extent of voids under concrete slabs. Many devices are being used to perform nondestructive testing (NDT) on pavements. However, only the devices that measure deflections are discussed. Other nondestructive testing involving the use of wave propagation, impact hammer, ground-penetrating radar, and impedance devices are not presented.

9.4.1 Type of NDT Equipment

Based on the type of loading applied to the pavement, NDT deflection testing can be divided into three categories: static or slowly moving loads, steady-state vibration, and impulse loads.

Static or Slowly Moving Loads The Benkelman beam, California traveling deflectometer, and LaCroix deflectometer are the best known devices in this category.

The Benkelman beam, which was developed by A. C. Benkelman during the WASHO Road Test, is perhaps the best-known deflection measuring device in the world. It consists essentially of a measurement probe hinged to a reference beam supported on three legs, as shown in Figure 9.36. The deflection at one end of the probe is measured by a dial placed at the other end. The probe is placed between the rear dual tires of a loaded truck, normally with an 18-kip (80-kN) single-axle load, and the rebound deflection of the probe is measured after the truck is slowly driven away. By taking several dial readings as the tire passes a series of designated points at different distances from the probe, it is possible to measure the deflection basin by using the principle of reciprocal displacement. The test is easy to operate but is very slow. The beam finds limited use on stiff pavements when the legs of the reference beam are located within the influence of the deflection basin.

The traveling deflectometer, developed by the California Division of Highways, is used to measure deflections while a truck, generally with an 18-kip (80-kN) rear axle, is moving. The LaCroix deflectometer was developed in France and is used extensively in Europe. Like the California deflectometer, the system measures deflections under both rear wheels.

Downloaded From : www.EasyEngineering.net

Downloaded From : www.EasyEngineering.net

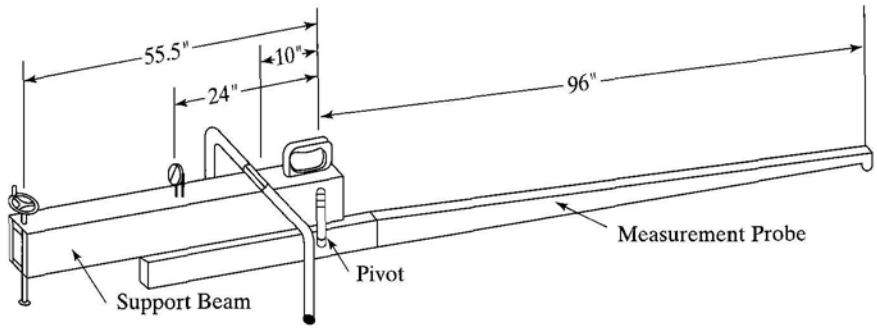


FIGURE 9.36

Benkelman beam (1 in. = 25.4 mm).

The most serious problem with these devices is the difficulty of obtaining an immovable reference for making deflection measurements. This makes the validity of their use on stiff pavements questionable. They also suffer from the disadvantage that the static or slowly moving loads do not represent the transient or impulse loads actually imposed on pavements. Therefore, they cannot be applied directly to any mechanistic method of pavement design and evaluation without extensive empirical correlations.

Steady-State Vibration Dynaflect and road rater are the best known devices in this category. The deflections are generated by vibratory devices that impose a sinusoidal dynamic force over a static force. The magnitude of the peak-to-peak dynamic force is less than twice that of the static force, so the vibratory device always applies a compressive force of varying magnitude on the pavement. The deflections are measured by accelerators or velocity sensors. These sensors are placed directly under the center of the load and at specified distances from the center, usually at 1-ft (0.3-m) intervals.

One advantage of this type of equipment over the static equipment is that a reference point is not required. An inertial reference is used so that the change in deflection can be compared to the magnitude of the dynamic force. The disadvantages of the method are that the actual loads applied to pavements are not in the form of steady-state vibration and that the use of relatively large static load could have some effect on the behaviors of stress sensitive materials.

Dynaflect Dynaflect was one of the first commercially available steady-state dynamic devices. It is trailer mounted and can be towed by a standard vehicle. A static weight of 2000 to 2100 lb (8.9 to 9.3 kN) is applied to the pavement through a pair of rigid steel wheels. A dynamic force generator is used to produce a 1000-lb (4.45-kN) peak-to-peak force at a frequency of 8 cycles per second. The dynamic force is superimposed on the static force, and the deflections due to the dynamic force are measured by five transducers.

The normal sequence of operations is to move the device to the test location and hydraulically lower the loading wheels and transducers to the pavement surface. A test is then conducted and the data are recorded. If the next test site is nearby, the device can be moved on the loading wheels at speeds up to 6 mph (9.6 km/h). After the last

Downloaded From : www.EasyEngineering.net

Downloaded From : www.EasyEngineering.net

test is completed, the loading wheels and transducers are hydraulically lifted and locked in a secure position. The fixed magnitude and frequency of the loading are the major limitations of the device.

Road Rater Road raters are commercially available in several models. The models vary primarily in the magnitude of the loads, with the static loads ranging from 2400 to 5800 lb (10.7 to 25.8 kN) and the peak-to-peak dynamic loads ranging from 500 to 8000 lb (2.2 to 35.6 kN). The loading frequency can be varied continuously from 5 to 70 cycles per second. Four sensors are used to measure the deflection basin. Earlier versions of the light model were mounted on vehicles; later versions are all trailer mounted.

In normal operation, the device is moved to the test location and the loading plate and deflection sensors are lowered to the pavement surface. After completing the test at selected loads and frequencies, the loading plate and sensors are lifted from the surface, and the device is ready to move to the next test location. The major limitations of this equipment include the small levels of load for the lighter models and the need for a heavy static load for the heavier models.

Rolling Dynamic Deflectometer The rolling dynamic deflectometer (RDD) is a relatively new tool for assessing the conditions of pavement (Bay *et al.*, 1999, 2000). Continuous deflection profiles, rather than deflections at discrete points, are measured with the RDD. The use of continuous profiles allows sections of pavement exhibiting large or anomalous deflections to be quickly and easily identified. Critical regions of pavement identified with the RDD for possible rehabilitation can be studied further via traditional discrete testing methods.

The RDD is a truck-mounted device consisting of a servohydraulic loading system and force and deflection measurement systems. The hydraulic actuator drives a 7500-lb (3400-kg) mass up and down, generating vertical dynamic forces up to 69.4 kips (308 kN) peak to peak, at frequencies from 5 to 100 Hz. The dynamic forces are applied to two loading rollers held in contact with the pavement by a static hold-down force. The combined static and dynamic forces applied to the pavement are measured with four load cells. Testing is performed by applying a sinusoidal dynamic force to the pavement while the RDD slowly drives along the pavement. Testing speeds of 0.6 to 1.5 ft/s (0.2 to 0.5 m/s) are typically used.

Impulse Loads All devices that deliver a transient force impulse to the pavement surface, such as the various types of falling weight deflectometers (FWD), are included in this category. By varying the amount of weight and the height of drop, different impulse forces can be generated. The normal operation is to move the trailer-mounted device to the test location, lower the loading plate and transducers hydraulically to the pavement surface, complete the test sequence by dropping the weight at each height selected, lift the loading plate and sensors, and tow the device to the next site. The major advantages of the impulse loading device are the ability to model a moving wheel load accurately in both magnitude and duration and the use of a relatively small static load compared with impulse loading. Three types of FWD are currently commercially available: Dynatest, KUAB, and Phoenix.

Downloaded From : www.EasyEngineering.net

Downloaded From : www.EasyEngineering.net

Dynatest Falling Weight Deflectometer The most widely used FWD in the United States is the Dynatest Model 8000 FWD system. The impulse force is created by dropping a weight of 110, 220, 440, or 660 lb (50, 100, 200, or 300 kg) from a height of 0.8 to 15 in. (20 to 381 mm). By varying the drop height and weight, a peak force ranging from 1500 to 24,000 lb (6.7 to 107 kN) can be generated. The load is transmitted to the pavement through a loading plate, 11.8 in. (300 mm) in diameter, to provide a load pulse in the form of a half sine wave with a duration from 25 to 30 ms. The magnitude of load is measured by a load cell.

Deflections are measured by seven velocity transducers mounted on a bar that can be lowered automatically to the pavement surface with the loading plate. One of the transducers is located at the center of the plate, while the remaining six can be placed at locations up to 7.4 ft (2.25 m) from the center. The Dynatest FWD is also equipped with a microprocessor-based control console that can fit on the passenger side of the front seat of a standard automobile.

KUAB Falling Weight Deflectometer The impulse force is created by dropping a set of two weights from different heights. By varying the drop height and weights, an impulse force ranging from 2698 to 35,000 lb (12 to 156 kN) can be generated. The load is transferred through a loading plate, 11.8 in. (300 mm) in diameter. A two-mass falling weight system is used to create a smoother rise of the force pulse on pavements with both stiff and soft subgrade support. Deflections are measured by five transducers.

Phoenix Falling Weight Deflectometer The Phoenix FWD is an earlier version of deflectometers now commercially available in Europe and in the United States. A single weight is dropped from different heights to develop impact loads from 2248 to 11,240 lb (10 to 50 kN). The load is transferred to the pavement through a plate, 11.8 in. (300 mm) in diameter. Deflections are measured by three transducers, one at the center of the loading plate and the others at 11.8 and 29.5 in. (300 and 750 mm) from the center.

9.4.2 Factors Influencing Deflections

The major factors that influence deflections include loading, climate, and pavement conditions. These factors must be carefully considered when conducting nondestructive tests.

Loading The magnitude and duration of loading have a great influence on pavement deflections. It is desirable that the NDT device be able to apply a load to the pavement similar to the actual design load (e.g., a 9000-lb (40-kN) wheel load). Unfortunately, not every commercially available NDT device is capable of simulating the design load. Some can simulate the magnitude of the design load but not its duration or frequency. It is generally agreed that the falling weight deflectometer is the best NDT device developed so far to simulate the magnitude and duration of actual moving loads (Lytton, 1989).

The nonlinear, or stress-sensitive, properties of most paving materials make pavement deflections fail to be proportional to load. Test results obtained for light loads must be extrapolated to those for heavy loads. Because extrapolation often leads to a significant error, the use of NDT devices that produce loads approximating those of heavy truck loads is strongly recommended.

Downloaded From : www.EasyEngineering.net

Downloaded From : www.EasyEngineering.net

Several agencies have developed correlations or regression equations relating the deflection under the lighter load of one device to that under the heavier load of another device. However, great caution should be exercised in applying these correlations, because the data from which these relationships were developed usually contain a large amount of scatter and a large error is always possible. Furthermore, the correlations for one type of pavement structure might not be applicable to a different structure. Even for the same pavement structure, considerable variation has been found between correlations developed by different agencies, due to differences in construction practice and to environmental conditions.

Climate Temperature and moisture are the two climatic factors that affect pavement deflections. For asphalt pavements, higher temperatures cause the asphalt binder to soften and increase deflections. For concrete pavements, temperature in the form of overall change or thermal gradient has a significant influence on the deflections near joints and cracks. The slab expands in warmer temperatures, causing tighter joints and cracks and resulting in greater efficiency of load transfer and smaller deflections. The curling of slab due to temperature gradients can cause a large variation in measured deflections. Measurements taken at night or early morning, when the top of slab is colder than the bottom, will result in higher corner and edge deflections than those taken in the afternoon, when the top of slab is much warmer than the bottom.

The season of the year has a great effect on deflection measurements. In cold regions, four distinct periods can be distinguished. The period of deep frost occurs during the winter season when the pavement is the strongest. The period of spring thaw starts when the frost begins to disappear from the pavement system and the deflection increases greatly. The period of rapid strength recovery takes place in early summer, when the excess free water from the melting frost leaves the pavement system and the deflection decreases rapidly. The period of slow strength recovery extends from late summer to fall when the deflection levels off slowly as the water content slowly decreases. For pavements in areas that do not experience freeze–thaw, the deflection generally follows a sine curve, with the peak deflection occurring in the wet season when the moisture content is high. In relatively dry areas, the period of maximum deflection could occur in the summer, when the asphalt surface softens due to the intense solar radiation (Poehl, 1971).

To compare and interpret deflection measurements, the time of the day and the season of the year when the measurements are made must be considered. Generally, deflection measurements are corrected to a standard temperature, say, 70°F (21°C) and to a critical period condition based on locally developed procedures.

Pavement Conditions Pavement conditions have significant effects on measured deflections. For asphalt pavements, deflections obtained in areas with cracking and rutting are normally higher than those in areas free of distress. For concrete pavements, voids beneath concrete slabs will cause increased deflections, and the absence or deterioration of load transfer devices will affect the deflections measured on both sides of the joint. Deflections taken near or over a culvert could be much higher, and pavements in cut or fill sections sometimes show significantly different deflections. These conditions must be carefully considered when one is selecting test locations.

Downloaded From : www.EasyEngineering.net

Downloaded From : www.EasyEngineering.net

9.4.3 Backcalculation of Moduli

One of the most useful applications of NDT testing is to backcalculate the moduli of pavement components, including the subgrade. The basic procedure is to measure the deflection basin and vary the set of moduli until a best match between the computed and measured deflections is obtained. A layer system program similar to KENLAYER can be used for computing the deflections of flexible pavement, and a finite element program similar to KENSLABS can be used for rigid pavements. If the load is applied in the interior of a slab on a solid or layer foundation, the layer system program can also be used for rigid pavements.

A variety of methods based on layer system programs have been used to backcalculate layer moduli. Unfortunately, none of the methods currently available is guaranteed to give reasonable modulus values for every deflection basin measured. It was reported that two agencies using the same computer program derived very different backcalculated results for the same pavement cross sections (Lytton and Chou, 1988). This is especially true for thin layers, because the deflection basin is insensitive to their moduli, and a good match between computed and measured deflections can be obtained even if totally unreasonable moduli are derived for these thin layers. Because engineering judgments play an important role in such situations, Chou *et al.* (1989) developed an expert system to serve as an intelligent preprocessor and postprocessor to the backcalculation program.

The Transportation Research Board (1992) conducted a symposium on "Capabilities and Limitations of Nondestructive Deflection Testing (NDT) and Backcalculation for Estimating Stiffness of Paving Materials" in August 1991. As part of that symposium, a workshop was held to reach consensus on current capabilities and limitations and on directions to pursue for improvements. Other than listing a number of limitations, it was reported that pavements suffered from too much variability, both in space and over time, and that we might need to lower our expectations for the technology and not expect more than it was able to provide.

Ullidtz and Coetzee (1995) presented an overview of typical procedures currently used for pavement evaluation, focusing primarily on backcalculation. There are more than 30 backcalculation softwares in use, mostly based on the multilayer elastic theory, and many new softwares continue to appear having little to differentiate from existing ones other than a name. Some of the more typical problems encountered in backcalculation including the fundamental theoretical assumptions of static loading, material continuity, homogeneity, and elastic behavior were also discussed.

Manual Method Figure 9.37 shows a three-layer system with the surface deflections measured by sensors at five locations. It is arbitrarily assumed that the load is distributed through the various layers according to the broken lines. Because sensors 4 and 5 are outside the stress zone of the HMA and granular base, the deflections at sensors 4 and 5 depend on the modulus of subgrade only and are independent of the moduli of HMA and granular base. Therefore, in applying the layer system program, any reasonable moduli can be assumed for the HMA and granular base, and the modulus of the subgrade can be varied until a satisfactory match between the computed and measured deflections at sensors 4 and 5 is obtained. The deflection at sensor 3 depends on the moduli of the granular base and the subgrade, independent of the modulus of the HMA. Because the modulus of the subgrade has been determined previously, the modulus of

Downloaded From : www.EasyEngineering.net

Downloaded From : www.EasyEngineering.net

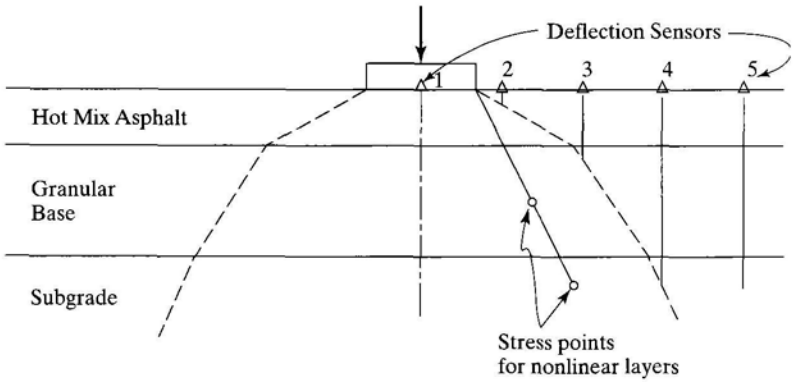


FIGURE 9.37

Stress zone within pavement structure.

the granular base can be varied until a satisfactory match between the computed and measured deflection at sensor 3 is obtained. The same applies to sensors 1 and 2, and so the modulus of the HMA can be determined.

The preceding explanation on how the layer moduli affect surface deflections is overly simplified. In reality, the deflection at any given sensor is affected by the moduli of all layers, each to a different degree. However, for a three-layer system, the following general principle always applies: The deflections of the sensors far away from the load are matched by adjusting the modulus of the bottom layer, those at intermediate distances from the load are matched by adjusting the modulus of the middle layer, and those near the load are matched by adjusting the modulus of the top layer.

The problem is more complicated if the granular base and the subgrade are nonlinear. Theoretically, to match the deflection at a given sensor, the stress points for computing the elastic moduli of all nonlinear layers should be located directly beneath that sensor. The use of different stress points for different sensors is not possible because the layer theory employs only one stress point in each layer. The best approach is to assume an average stress distribution, with the stress points shown by the smaller circles in Figure 9.37.

MODULUS Program MODULUS is a microcomputer program for backcalculating layer moduli (Uzan *et al.*, 1988, 1989; Scullion *et al.*, 1990). It can be applied to a two-, three-, or four-layer system with or without a rigid bedrock layer. A linear elastic program is used to generate a data base of deflection bowls by assuming different modulus ratios. Once the data base is generated for a particular pavement, the linear elastic program is not called again, no matter how many bowls are to be analyzed. In the case of a four-layer system, the elastic layer program is automatically run at least 27 times (3 surface × 3 base × 3 subbase modulus ratios). A pattern search routine is used to fit measured and calculated bowls.

The objective function to be minimized can be expressed as

$$\epsilon^2 = \sum_{i=1}^{s} \left(\frac{w_i^{\mathrm{m}} - w_i^{c}}{w_i^{\mathrm{m}}} \right)^2 = \sum_{i=1}^{s} \left(1 - \frac{w_i^{\mathrm{c}}}{w_i^{\mathrm{m}}} \right)^2 \tag{9.35}$$

Downloaded From : www.EasyEngineering.net

Downloaded From : www.EasyEngineering.net

in which ϵ^2 is the squared error, w^m is the measured deflection, w^c is the computed deflection, and i is a sensor number from 1 to s. The original equation contains a weighting factor for each sensor i. Because the same weighting factors are usually used, they are not shown in Eq. 9.35. Much as in Eq. 2.14, the computed deflection can be expressed as a function of modulus ratios:

$$w_i^c = \frac{qa}{E_n} f_i\left(\frac{E_1}{E_n}, \frac{E_2}{E_n}, \ldots, \frac{E_{n-1}}{E_n}\right) \tag{9.36}$$

In this equation, q is the contact pressure, a is the contact radius, and E is the elastic modulus with a subscript indicating the layer number. The value of f_i for sensor i can be obtained from the layer system program and used as a data base. By assuming $n - 1$ modulus ratios, w_i^c can be obtained from Eq. 9.36 and ϵ^2 from Eq. 9.35. As in any other backcalculation program, a set of seed moduli is required for the first trial. The following procedure is used to determine the seed modulus of subgrade E_n. When E_n and the modulus ratios are known, the modulus of each layer can be determined.

For a fixed set of modulus ratios, functions f_i can be considered as constants. To minimize the error, the value of E_n can be determined by taking the derivative of ϵ^2 with respect to E_n and setting the result to zero:

$$\frac{\partial \epsilon^2}{\partial E_n} = \sum_{i=1}^{s} 2\left(1 - \frac{w_i^c}{w_i^m}\right)\left(\frac{1}{w_i^m}\right)\left(\frac{\partial w_i^c}{\partial E_n}\right) = 0 \tag{9.37}$$

From Eq. 9.36,

$$\frac{\partial w_i^c}{\partial E_n} = -\frac{qaf_i}{E_n^2} = -\frac{w_i^c}{E_n}$$

so Eq. 9.37 can be reduced to

$$\sum_{i=1}^{s}\left(1 - \frac{w_i^c}{w_i^m}\right)\left(\frac{w_i^c}{w_i^m}\right) = 0$$

or

$$\sum_{i=1}^{s}\frac{w_i^c}{w_i^m} = \sum_{i=1}^{s}\left(\frac{w_i^c}{w_i^m}\right)^2 \tag{9.38}$$

When both sides are divided by w_1^c with $w_1^c = qaf_1/E_n$ and $w_i^c/w_1^c = f_i/f_1$, Eq. 9.38 becomes

$$\sum_{i=1}^{s}\frac{f_i}{f_1 w_i^m} = \sum_{i=1}^{s}\frac{qaf_i^2}{f_1 (w_i^m)^2 E_n}$$

or

$$E_n = \frac{qaf_1 \sum_{i=1}^{s}\left(\frac{f_i}{f_1 w_i^m}\right)^2}{\sum_{i=1}^{s}\left(\frac{f_i}{f_1 w_i^m}\right)} \tag{9.39}$$

Downloaded From : www.EasyEngineering.net

Downloaded From : www.EasyEngineering.net

where the functions of f_i are taken from the generated data base. The squared error ϵ^2 is computed by using the subgrade modulus from Eq. 9.39 and the modulus ratios of the data base points. A pattern search routine is used to find the optimum set of modulus ratios so that a minimum ϵ^2 is obtained.

Example 9.3:

A pressure of 80 psi (552 kPa) is applied to a pavement surface through a circular area 6 in. (152 mm) in radius. The measured deflections w_i^m at seven sensor locations and the deflection functions f_i generated from the data base for given modulus ratios are shown in Table 9.8. Determine the seed modulus of the subgrade E_n and the squared error ϵ^2.

TABLE 9.8 Deflection Data

	Point no.						
	1	2	3	4	5	6	7
w_i^m(in.)	0.0441	0.0334	0.0270	0.0219	0.0115	0.0085	0.0041
f_i	0.39156	0.33698	0.29917	0.19927	0.10906	0.07094	0.05125
$f_i/(f_1 w_i^m)$	22.676	25.767	28.298	23.238	24.220	21.314	31.924
w_i^c(in.)	0.0388	0.0334	0.0296	0.0197	0.0108	0.0070	0.0051
$(w_i^m - w_i^c)/w_i^m$	0.12018	0.00000	−0.09630	0.10046	0.06087	0.17647	−0.24390

Note. 1 in. = 25.4 mm.

Solution: Values of $f_i/(f_1 w_i^m)$ are calculated and shown in Table 9.8. If the calculated and measured deflections match exactly, then all points will have the same values of $f_i/(f_1 w_i^m)$. The degree of their variation is an indication of the amount of error.

From Eq. 9.39, $E_n = 80 \times 6 \times 0.39156\,[(22.676)^2 + (25.767)^2 + (28.298)^2 + (23.238)^2 + (24.220)^2 + (21.314)^2 + (31.924)^2]/[22.676 + 25.767 + 28.298 + 23.238 + 24.220 + 21.314 + 31.924] = 4850$ psi (33.5 MPa).

Values of w_i^c can be determined from Eq. 9.36 and are shown in Table 9.8. Also shown are values of $(w_i^m - w_i^c)/w_i^m$. From Eq. 9.35, $\epsilon^2 = (0.12018)^2 + (-0.09630)^2 + (0.10046)^2 + (0.06087)^2 + (0.17647)^2 + (-0.24390)^2 = 0.1282$.

WESDEF Program WESDEF (Van Cauwelaert *et al.*, 1989) is the backcalculation program developed by the U.S. Army Engineer Waterways Experiment Station (WES). The program is similar to the previous versions called CHVDEF (Bush, 1980), which used the CHEV n-layer program as a subroutine, and BISDEF (Bush and Alexander, 1985), which used the BISAR n-layer program. However, a new, fast, five-layer program called WESLEA is used in WESDEF to replace the BISAR program.

WESDEF contains a computer optimization routine to determine a set of modulus values that provide the best fit between a measured deflection basin and the computed deflection basin when given an initial estimate of the elastic modulus values and a limiting range of moduli. As in the collocation method described in Section 2.3.2, the number of deflections on the basin must be greater than the number of layer moduli to be determined.

Downloaded From : www.EasyEngineering.net

Downloaded From : www.EasyEngineering.net

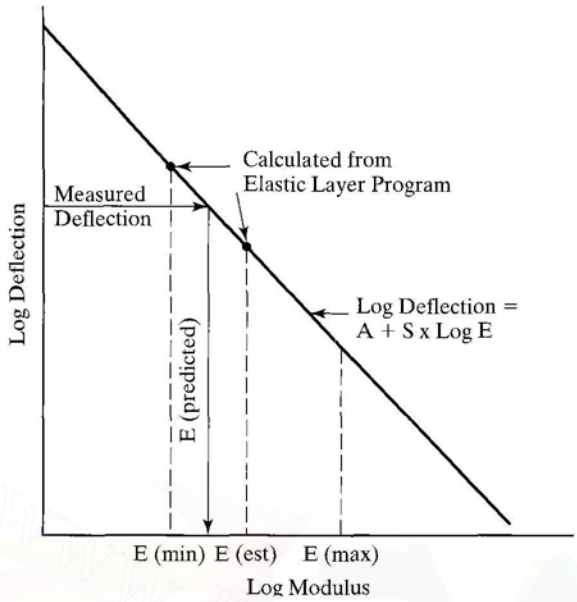


FIGURE 9.38
Relationship between deflection and modulus.

A set of E values is assumed, and the deflection is computed to correspond to the measured deflection. Each unknown E is varied individually, and a new set of deflections is computed for each variation. For each layer i and each sensor j, the intercept A_{ji} and the slope S_{ji}, as shown in Figure 9.38, are determined. For multiple deflections and layers, the solution is obtained by developing a set of equations that define the slope and intercept for each deflection and each unknown modulus:

$$\log(\text{deflection}_j) = A_{ji} + S_{ji}\,(\log E_i) \tag{9.40}$$

Normally, three iterations of the program can produce a set of modulus values that yield a deflection basin within an accuracy of 3%. Iterations will cease when the absolute sum of the percent differences between computed and measured deflections or the predicted change in modulus values becomes less than 10%.

ILL-BACK Program In contrast to the optimization programs that require the input of seed moduli, ILL-BACK can determine the moduli of rigid pavements directly without the use of a search routine (Ioannides *et al.*, 1989). The program can be applied to a concrete slab on a liquid or solid foundation with a circular load at the interior. The deflections at four sensors with distances of 0, 12, 24, and 36 in. (0, 305, 610, and 914 mm) from the center are measured, and the moduli of the slab and the foundation can be backcalculated.

For liquid foundations, Westergaard's equation for deflection at the center of loading was shown in Eq. 4.21 and can be expressed as

$$d_0 = \frac{w_0 k \ell^2}{P} = f\left(\frac{a}{\ell}\right) \tag{9.41}$$

Downloaded From : www.EasyEngineering.net

Downloaded From : www.EasyEngineering.net

in which d_0 is the normalized deflection under the center of loading and f is a function of a/ℓ. For a given contact radius a, d_0 is a function of the radius of relative stiffness ℓ only. Similar equations can be obtained for sensor i at a given distance from the center:

$$d_i = \frac{w_i k \ell^2}{P} = f_i(\ell) \tag{9.42}$$

Here, i can be 0, 1, 2, or 3. For a given ℓ, the normalized deflection d_i can be determined from theory. If the deflection w_i at any sensor i is measured, the modulus of subgrade reaction k can be computed by Eq. 9.42. Now the crucial question is how to determine ℓ. Once ℓ is known, the deflection measured by any one of the sensors can be used to determine k. A comparison of these k values can provide an evaluation of the agreement between theory and field measurements.

If two deflections, w_0 and w_1, are measured, then, from Eq. 9.42,

$$d_0 = \frac{w_0 k \ell^2}{P} = f_0(\ell) \tag{9.43a}$$

$$d_1 = \frac{w_1 k \ell^2}{P} = f_1(\ell) \tag{9.43b}$$

Dividing Eq. 9.43*b* by 9.43*a* gives

$$\frac{d_1}{d_0} = \frac{w_1}{w_0} = \frac{f_1}{f_0} = f(\ell) \tag{9.44}$$

Equation 9.44 indicates that ℓ can be determined from the deflection ratio, w_1/w_0. If four sensors are used, it is more reliable to use the average deflection of all four sensors, as indicated by the area of the deflection basin:

$$\text{AREA} = 6\left[1 + 2\left(\frac{w_1}{w_0}\right) + 2\left(\frac{w_2}{w_0}\right) + \left(\frac{w_3}{w_0}\right)\right] \tag{9.45}$$

Note that Eq. 9.45 is based on a sensor spacing of 12 in. (305 mm) and the unit of AREA is in inches.

Figure 9.39 shows the relationship between AREA and ℓ for both liquid and solid foundations, as obtained from theory. The solid curves are based on a circular load with a radius of 5.9 in. (150 mm), the broken curves on a concentrated load with a radius of zero. It can be seen that the effect of radius on the AREA versus ℓ relationship is not very significant.

After ℓ is determined from Figure 9.39, the normalized deflection d_i can be determined from Figure 9.40 for liquid foundations and Figure 9.41 for solid foundations. For liquid foundations, k can be determined from Eq. 9.42:

$$k = \frac{P d_i}{\ell^2 w_i} \tag{9.46}$$

Downloaded From : www.EasyEngineering.net

Downloaded From : www.EasyEngineering.net

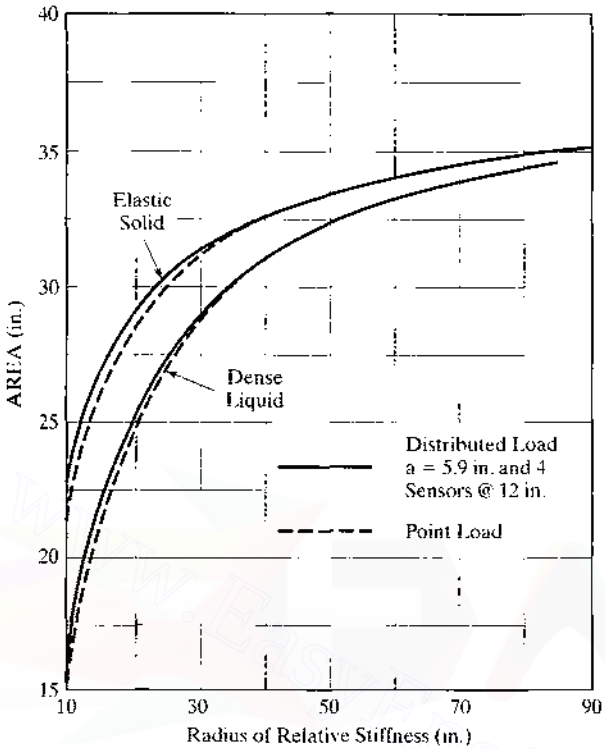


FIGURE 9.39

Relationship between AREA and ℓ (1 in. = 25.4 mm). (After Ioannides *et al.* (1989).)

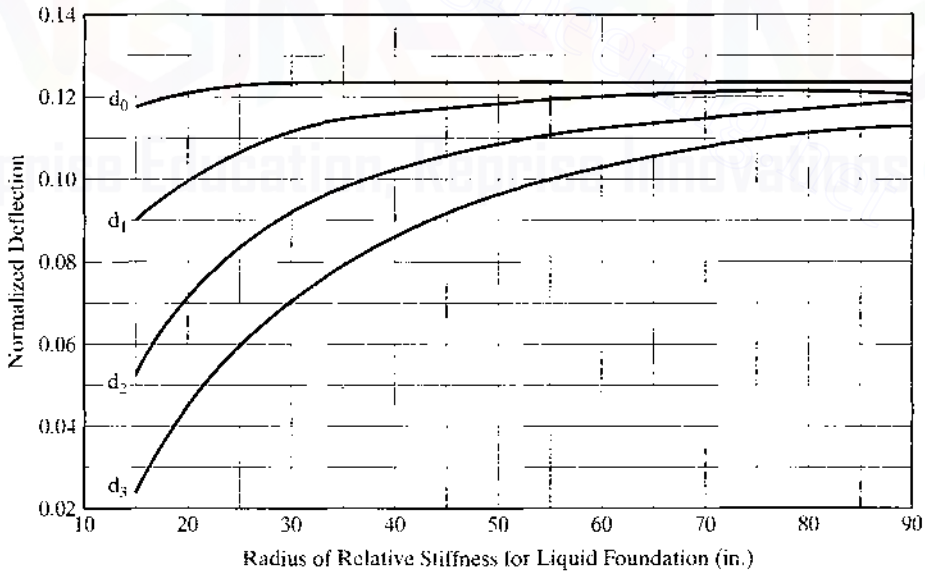


FIGURE 9.40

Relationship between normalized deflections and ℓ for liquid foundations (1 in. = 25.4 mm). (After Ioannides *et al.* (1989).)

Downloaded From : www.EasyEngineering.net

Downloaded From : www.EasyEngineering.net

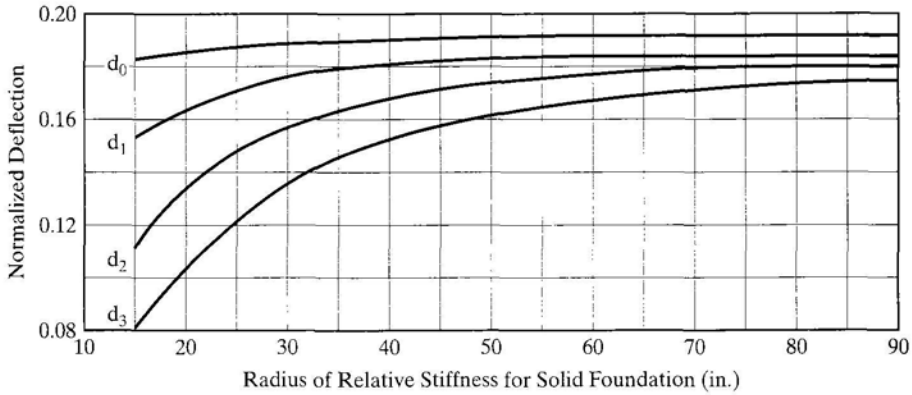


FIGURE 9.41

Relationship between normalized deflections and ℓ for solid foundations (1 in. = 25.4 mm). (After Ioannides *et al.* (1989).)

It can be shown that E_f for solid foundation can be determined from (Ioannides, 1990)

$$E_f = \frac{2(1 - \nu_f^2)Pd_i}{\ell w_i} \tag{9.47}$$

The radius of relative stiffness for liquid foundation is defined by Eq. 4.10, that for solid foundation by Eq. 5.38. These equations can be used to compute the elastic modulus of concrete E_c if the slab thickness h is known, or vice versa.

The elastic modulus of concrete E_c for liquid foundations can be computed from Eq. 4.10:

$$E_c = \frac{12(1 - \nu_c^2)k\ell^4}{h^3} \tag{9.48}$$

For solid foundations, from Eq. 5.38,

$$E_c = \frac{6(1 - \nu_c^2)E_f\ell^3}{(1 - \nu_f^2)h^3} \tag{9.49}$$

The procedure for backcalculating the moduli of concrete and foundation can be summarized as follows:

1. Measure deflections, w_0, w_1, w_2, and w_3.
2. Compute AREA by Eq. 9.45.
3. Determine ℓ from Figure 9.39.
4. For liquid foundations, determine the normalized deflection from Figure 9.40 and compute k by Eq. 9.46. Four k values, one for each sensor, are obtained and their average is taken. For solid foundations, determine the normalized deflection from Figure 9.41 and compute E_f by Eq. 9.47. The average of the four values is taken as E_f.
5. Based on the average k or E_f, compute E_c by Eq. 9.48 or 9.49.

Downloaded From : www.EasyEngineering.net

Downloaded From : www.EasyEngineering.net

Example 9.4:

An FWD test was conducted on a 10-in. (254-mm) concrete pavement. The radius of the loaded plate is 5.9 in. (300 mm) and the recorded load is 7792 lb (34.7 kN). Sensors were located at 0, 12, 24, and 36 in. (0, 305, 610, and 914 mm) and the corresponding deflections recorded are 0.0030, 0.0028, 0.0024, and 0.0021 in. (0.076, 0.071, 0.061, and 0.053 mm). It is assumed that the concrete has a Poisson ratio of 0.15. (a) If the subgrade is considered as a liquid foundation, determine k and E_c. (b) If the subgrade is considered as a solid foundation with a Poisson ratio of 0.45, determine E_f and E_c.

Solution: From Eq. 9.45, AREA = $6[1 + 2(2.8/3) + 2(2.4/3) + 2.1/3] = 31.0$ in. (787 mm). From Figure 9.39, $\ell = 39$ in. (991 mm) for liquid foundation and 28 in. (711 mm) for solid foundation.

(a) For a liquid foundation, from Figure 9.40, $d_0 = 0.123$, $d_1 = 0.115$, $d_2 = 0.102$, and $d_3 = 0.085$. From Eq. 9.46 and based on w_0 and d_0, $k = 7792 \times 0.123/[(39)^2 \times 0.0030] = 210$ pci (57.0 MN/m^3). The k values based on the other three sensors are 210, 218, and 207 pci (57.0, 59.1, and 56.2 MN/m^3). The mean of the four k values is 211 pci (57.3 kN/m^3). From Eq. 9.48, $E_c = 12[1 - (0.15)^2] \times 211 \times (39)^4/(10)^3 = 5.7 \times 10^6$ psi (39.3 GPa).

(b) For a solid foundation, from Figure 9.41, $d_0 = 0.188$, $d_1 = 0.174$, $d_2 = 0.152$, and $d_3 = 0.128$. From Eq. 9.47 and based on w_0 and d_0, $E_f = 2[1 - (0.45)^2] \times 7792 \times 0.188/(28 \times 0.0030) = 27{,}816$ psi (192 MPa). Values of E_f based on the other three sensors are 27,583, 28,111, and 27,055 psi (190, 194, and 187 MPa). The mean E_f is 27,641 psi (191 MPa). From Eq. 9.49, $E_c = 6 \times [1 - (0.15)^2] \times 27{,}641 \times (28)^3/\{[1 - (0.45)^2] \times (10)^3\} = 4.5 \times 10^6$ psi. Because of the incompatibility between liquid and solid foundations, it is to be expected that the elastic modulus of concrete based on a solid foundation is somewhat different from that based on a liquid foundation.

Multidepth Deflectometer System The multidepth deflectometer (MDD) was developed by the National Institute for Transport and Road Research (NITRR) in South Africa and can be used to backcalculate layer moduli (Basson *et al.*, 1981; DeBeer *et al.*, 1989; Yazdani and Scullion, 1990). The system consists of a number of LVDT modules installed vertically at various depths in the pavement, usually at the interfaces of pavement layers. A maximum of six MDD modules may be placed in a single 1.5-in.-(38-mm)-diameter hole. The modules are clamped against the sides of the hole and the center core is attached to an anchor located approximately 7 ft (2.1 m) below the pavement surface. The MDD can measure either the relative elastic deformation or the total permanent deformation of each layer in the pavement system. By matching the measured deflections against those computed by the layer system program, the modulus of each layer can be determined.

The use of MDD has an advantage over the use of a surface deflection basin because the sensors are placed at locations closer to the load, which are the most critical areas for design considerations. If the impulse loading has the same magnitude as the design wheel load, the moduli thus determined represent the actual field conditions and can be used directly with the linear elastic layer program, even when some of the materials are nonlinear. If the impulse loading is quite different from the design wheel load or the design is based on various load groups with widely different loading magnitudes, then a nonlinear layer program, such as KENLAYER, can be used to adjust the

Downloaded From : www.EasyEngineering.net

Downloaded From : www.EasyEngineering.net

nonlinear coefficients K_1 until a satisfactory match between the measured and computed deflections is obtained.

One disadvantage of using MDD is that a hole must be drilled in the pavement, so the test is actually a destructive test. The presence of the hole could change the stress and deflection regimes around the MDD hole, and so the measured deflections might not be representative of the actual deflections when the hole is not present.

Laboratory versus Backcalculated Moduli Several investigators made comparisons between laboratory and backcalculated moduli. Daleiden *et al.* (1994) analyzed roughly 700 experimental pavement sections from the Long Term Pavement Performance (LTPP) program. The subgrade soil moduli were determined from three methods: laboratory testing, backcalculation, and the equation in the 1986 AASHTO Guide. Unfortunately, a well-defined relationship between laboratory and backcalculated moduli could not be established. The same conclusions were presented by Akram *et al.* (1994) and Nazarian *et al.* (1995).

Mikhail *et al.* (1999) evaluated the laboratory and backcalculated resilient moduli from the WesTrack experiment in Northern Nevada. The backcalculated resilient modulus values were determined via the Washington State Department of Transportation's EVERCAL computer program (University of Washington, 1996); the FWD data was obtained from WesTrack pavement sections at the onset of trucking loading. The laboratory-based values use a combination of test results on remolded and recompacted WestTrack materials and the KENLAYER computer program to estimate the modulus under the state of stress created by the FWD during testing. As expected, they found significant differences between resilient moduli determined from backcalculation and those obtained through laboratory testing. They recommended that further improvements be required in backcalculation procedures to address the problem of multiple solutions and the sensitivity of the results to structural and environmentally related factors and that research be required to close the gap between laboratory-based and backcalculated resilient moduli or to derive an appropriate correction factor.

9.5 PAVEMENT PERFORMANCE

The evaluation of pavement performance is an important part of pavement design, rehabilitation, and management. It includes the evaluation of distress, roughness, friction, and structure, as described in Sections 9.1 through 9.4, and of traffic, materials, and drainage. The latter three are presented in Chapters 6, 7, and 8 for pavement design and can also be applied to pavement evaluation.

9.5.1 Expert Systems

Pavement evaluation and rehabilitation are not exact sciences; they depend to a large extent on past experiences and engineering judgments. They can be achieved by two different types of knowledge: deterministic, and heuristic. Deterministic knowledge is that body of factual information that is widely accepted and can be obtained from textbooks or published literature. Heuristic knowledge is the subjective or private knowledge possessed by each individual, which is largely characterized by beliefs, opinions,

Downloaded From : www.EasyEngineering.net

Downloaded From : www.EasyEngineering.net

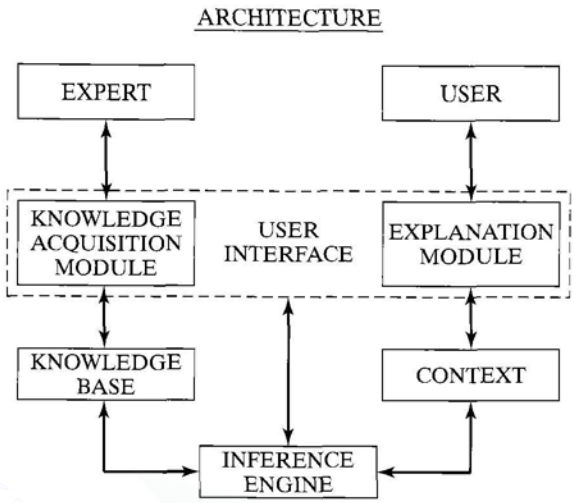


FIGURE 9.42

Basic architecture of an expert system. (Ritchie *et al.* (1986).)

and rules of thumb. Organizing and preserving the wealth of heuristic problem-solving knowledge forms the basis of a relatively new type of tool known as knowledge-based systems. These systems are computer programs in which heuristic knowledge is utilized to solve problems that are intractable under a purely deterministic approach. A subset of knowledge-based systems contains expert systems, which employ both the knowledge and reasoning methods of human experts to solve difficult problems in a narrowly defined problem domain.

Figure 9.42 shows the basic architecture of an expert system. The three main components are the knowledge base, the inference engine, and the context. The knowledge base contains all the empirical and factual information for the problem domain. The inference engine searches through the knowledge base or the context to find a conclusion for each subgoal and thus the entire problem. The context is the work space or short-term memory in which currently relevant facts and knowledge are placed successively by the inference engine. Finally, a user friendly interface contains an explanation module to explain the system's problem-solving strategy to the user and a knowledge-acquisition module to help experts articulate their knowledge in a form acceptable to the system's architecture.

SCEPTRE SCEPTRE is the acronym for Surface Condition Expert for Pavement Rehabilitation. It was developed for use by the Washington Department of Transportation to evaluate pavement surface distress and recommend feasible rehabilitation strategies for detailed analysis and design (Ritchie *et al.*, 1986). Currently, it is applicable only to flexible pavements.

The major task in building an expert system is to acquire and encode the expertise and knowledge of experts into the knowledge base. The factual and empirical information in the knowledge base can be represented in various ways. The most common is through "IF THEN" statements; for example, IF transverse cracking exists and crack width is greater than $\frac{1}{8}$ in. (3.2 mm), THEN fill cracks.

General purpose program languages, such as LISP and PROLOG, can be used to build expert systems. However, a much faster route is to use one of several knowledge

Downloaded From : www.EasyEngineering.net

Downloaded From : www.EasyEngineering.net

engineering tool kits, or shells, which comprise an inference engine, an empty knowledge base, and context structure. The system developer simply has to enter the rules into the knowledge base. SCEPTRE utilized a shell named EXSYS (EXSYS, 1985), which was developed for use with IBM personal computers and other compatibles. The types of surface distress to be considered include longitudinal cracking in wheelpaths, alligator cracking in wheelpaths, block cracking, transverse and longitudinal cracking outside wheelpaths, and rutting.

The following is a list of the rehabilitation and maintenance strategies (RAMs) from which a subset is drawn by SCEPTRE to form a feasible set for any particular combination of distress types:

1. Do nothing.
2. Fog seal.
3. Chip seal.
4. Double chip seal.
5. Thin HMA overlay, thickness $\leq$ 1.2 in. (31 mm).
6. Medium HMA overlay, 1.2 in. (31 mm) $<$ thickness $<$ 3 in. (76 mm).
7. Thick HMA overlay, thickness $\geq$ 3 in. (76 mm).
8. Friction course.
9. Fill cracks.
10. Reconstruct.
11. Recycled HMA.
12. Level up, mill, and make medium HMA overlay, 1.2 in. (31 mm) $<$ thickness $<$ 3 in. (76 mm).
13. Level up, mill, and make thick HMA overlay, thickness $\geq$ 3 in. (76 mm).

EXPEAR EXPEAR (Expert System for Pavement Evaluation and Rehabilitation) was developed by the University of Illinois for the Federal Highway Administration and the Illinois Department of Transportation (Hall *et al.*, 1989). It is an advisory program to assist practicing engineers in evaluating a specific pavement section and selecting rehabilitation alternatives. The evaluation part is an extension of COPES (Concrete Pavement Evaluation System) developed earlier (Darter *et al.*, 1985). Currently, the program can be used for only three types of rigid pavement: JPCP, JRCP, and CRCP.

Project level evaluation using EXPEAR begins with the collection of some basic design, construction, traffic, and climate data for the project in question, together with a visual condition survey. Back in the office, the design and condition data are entered into EXPEAR by the engineer. The program extrapolates the overall condition of the project from the distress data for one or more sample units.

EXPEAR evaluates the project in several key problem areas related to specific aspects of performance for that pavement type. For example, the problem areas for JPCP and JRCP are structural adequacy, roughness, drainage, joint deterioration, foundation movement, skid resistance, joint sealant condition, joint construction, concrete durability, load transfer, loss of support, and shoulders. The evaluation is performed via decision trees, which compare the pavement condition to predefined critical levels for

Downloaded From : www.EasyEngineering.net

Downloaded From : www.EasyEngineering.net

key design and distress variables. EXPEAR produces a summary of the deficiencies found and, by interacting with the engineer, formulates a rehabilitation strategy that will correct all the deficiencies. The major rehabilitation options are reconstruction of both lanes, reconstruction of the outer lane and restoration of the inner lane, bonded or unbonded PCC overlay, HMA overlay, crack and seat and HMA overlay, and restoration. Appropriate repair techniques for the shoulders, which are compatible with the rehabilitation strategy of mainline pavements, are also selected.

A large number of predictive models for concrete pavement performance with and without rehabilitation are incorporated into EXPEAR. Some of the models were developed from national data bases of new construction and rehabilitation projects; others were developed by using data from Illinois pavements. Some of these models are presented in Section 9.5.2. The models allow the engineer to predict the performance of the rehabilitation strategy developed. This information is then used, along with rehabilitation unit cost, to compute the cost of the strategy over the predicted life. EXPEAR produces a summary of the project's data file, the evaluation results, recommendations for physical testing, predictions of the pavement's future condition without rehabilitation, rehabilitation techniques, performance predictions, and cost estimates for as many rehabilitation strategies as the engineer wishes to investigate.

9.5.2 Predictive Models

Various equations, mostly based on regression analysis, were developed for predicting pavement performance. These equations illustrate the effect of various factors on pavement performance, but their usefulness in practice might be limited by the scope of the data base that was used in their development. Regression equations are valid only under certain conditions and should not be applied when the actual conditions are different. Because the regression constants vary with the units used, all equations are based on the U.S. customary unit, as specified for each variable.

Flexible Pavements The major failure modes for flexible pavements are fatigue cracking, rutting, and low-temperature cracking.

Fatigue Cracking The equations used in PDMAP for predicting the allowable number of load repetitions when crackings occur over 10 and 45% of the area in the wheelpath are (Finn *et al.*, 1986)

$$\log N_f(10\%) = 15.947 - 3.291 \log(\epsilon_t/10^{-6}) - 0.854 \log(E_1/10^3) \qquad (9.50a)$$

and

$$\log N_f(45\%) = 16.086 - 3.291 \log(\epsilon_t/10^{-6}) - 0.854 \log(E_1/10^3) \qquad (9.50b)$$

in which N_f is the allowable number of repetitions for fatigue cracking, ϵ_t is the horizontal tensile strain at the bottom of asphalt layer in in./in., and E_1 is the resilient modulus of asphalt layer in psi. Note that Eq. 9.50*b* is the Asphalt Institute's criterion presented in a different form and that 45% of the area in the wheelpath is equivalent to about 20% of the total area.

Downloaded From : www.EasyEngineering.net

Downloaded From : www.EasyEngineering.net

Example 9.5:

An asphalt pavement, after being subjected to one million load repetitions at a strain level of 10^{-4}, has experienced fatigue cracking over 10% of the area in the wheelpath. At the same strain level, what will be the number of load repetitions when cracking occurs over 45% of the area in the wheelpath? What should be the strain level to cause 45% cracking in the wheelpath after one million repetitions?

Solution: Subtracting Eq. 9.50*a* from Eq. 9.50*b* gives $\log[N_f(45\%)] - \log[N_f(10\%)] = 16.086 - 15.947 = 0.139$, or $\log[N_f(45\%)] = 0.139 + \log(10^6) = 6.139$. Therefore, $N_f(45\%) = 1.38 \times 10^6$, or the number of repetitions increases by 38% when the percentage of area cracked increases from 10 to 45%.

For the same number of repetitions at one million and subtracting Eq. 9.50*a* from Eq. 9.50*b*, $0 = 0.139 - 3.291 \log[\epsilon_t(45\%)/\epsilon_t(10\%)]$, or $\epsilon_t(45\%) = 1.102\epsilon_t(10\%) = 1.102 \times 10^{-4}$. Therefore, a 10% increase in strain causes an increase in area cracked from 10 to 45%.

Rutting In PDMAP, for conventional construction with HMA less than 6 in.,

$$\log \text{RR} = -5.617 + 4.343 \log w_0 - 0.167 \log(N_{18}) - 1.118 \log \sigma_c \quad (9.51a)$$

For full-depth construction with HMA equal to or greater than 6 in.,

$$\log \text{RR} = -1.173 + 0.717 \log w_0 - 0.658 \log(N_{18}) + 0.666 \log \sigma_c \quad (9.51b)$$

in which RR is the rate of rutting in microinches (1 μin. = 10^{-6} in.) per axle load repetition, w_0 is the surface deflection in mil (1 mil = 10^{-3} in.), σ_c is the vertical compressive stress under HMA in psi, and N_{18} is the equivalent 18-kip (80-kN) single-axle load in 10^5. For full-depth predictions, all traffic during frozen periods is neglected.

Example 9.6:

A full-depth asphalt pavement was constructed on a subgrade with a resilient modulus of 10,000 psi (69 MPa). The asphalt layer is 8 in. (203 mm) thick with a resilient modulus of 500,000 psi (3.45 GPa). Assuming that both HMA and subgrade are incompressible with a Poisson ratio of 0.5, estimate the rut depth after 1 million applications of a 9000-lb (40-kN) wheel load at contact pressure equal to 80 psi (552 kPa).

Solution: Contact radius $a = \sqrt{9000/(80\pi)} = 6$ in. (152 mm). With $h/a = \frac{8}{6} = 1.33$ and $E_1/E_2 = 500{,}000/10{,}000 = 50$, from Figure 2.17, $F_2 = 0.24$, or $w_0 = 1.5 \times 80 \times 6 \times 0.24/10{,}000 = 0.0173$ in. (0.44 mm). With $a/h = 0.75$ and $E_1/E_2 = 50$, from Figure 2.15, $\sigma_c/q = 0.075$, or $\sigma_c = 80 \times 0.075 = 6$ psi (41 kPa). From Eq. 9.51*b*, $\log \text{RR} = -1.173 + 0.717 \log(17.3) - 0.658 \log(10) + 0.666 \log(6) = -0.425$, or RR = 0.376 μin. per one repetition. For one million repetitions, rut depth = $0.376 \times 10^{-6} \times 10^6 = 0.376$ in.

Low-Temperature Cracking The cracking index due to low-temperature cracking can be computed by (Hajek and Haas, 1972)

$$10^I = 2.497 \times 10^{30} \times (0.1S_{bit})^{(6.7966 - 0.8740h + 1.3388a)} \times (7.054 \times 10^{-3})^d \times (3.193 \times 10^{-13})^{(0.1m)} \times d^{(0.06026s_{bit})} \quad (9.52a)$$

Downloaded From : www.EasyEngineering.net

Downloaded From : www.EasyEngineering.net

or

$$I = 30.3974 + (6.7966 - 0.8741h + 1.3388a)\log(0.1S_{bit}) - 2.1516d - 1.2496m + 0.06026S_{bit}\log d \quad (9.52b)$$

in which

I = cracking index (≥ 0) in terms of the number of full cracks plus one half of the half-transverse cracks per 500-ft section of two-lane road; cracks shorter than half-width are not due to low-temperature cracking and are not considered in the regression equation;

S_{bit} = stiffness modulus of the original asphalt in kg/cm^2, as determined from Van der Poel nomograph shown in Figure 7.20, using a loading time of 20,000 s and the winter design temperature; however, values of PI and $T_{R\&B}$ or bitumen should be determined from penetration at 77°F (25°C) and kinematic viscosity at 275°F (135°C) as suggested by McLeod (1970);

h = total thickness of asphalt layer in inches;

a = pavement age in years;

m = winter design temperature in −°C, neglect the negative sign and use positive value only;

d = subgrade type in terms of a dimensionless code with 5 for sand, 3 for loam, and 2 for clay.

Example 9.7:

Given thickness of asphalt layer, 4 in. (102 mm); stiffness of original asphalt cement, 205 kg/cm^2; winter design temperature, −27°C; and sand subgrade. Determine the cracking index I at 5 and 10 years after construction.

Solution: With $h = 4$ in. (102 mm), $a = 5$ years, $S_{bit} = 205$ kg/cm^2, $d = 5$, and $m = 27$°C, from Eq. 9.52*b*, $I = 30.3974 + (6.7966 - 0.8740 \times 4 + 1.3388 \times 5) \times \log(20.5) - 2.1516 \times 5 - 1.2496 \times 27 + 0.06026 \times 205 \times \log 5 = 7.6$. When $a = 10$ years, from Eq. 9.52*b*, $I = 16.4$.

Rigid Pavements A large number of models or regression equations have been developed for predicting pumping, joint faulting, joint deterioration, cracking, and present serviceability rating of both jointed plain concrete pavements (JPCP) and jointed reinforced concrete pavements (JRCP). These equations can be developed by using a combination of multiple linear regression and nonlinear regression techniques included in the SPSS statistical package (Nie *et al.*, 1975). Multiple linear regression is used to determine which independent variables are significant. Nonlinear regression is then used to compute the coefficients and exponents for the final predictive equation. Various forms of equations can be obtained, depending on the extent of the database. The presence or absence of certain variables in the data base will have a significant effect on the equation obtained.

Notable examples of regression models are the AASHTO design equation (AASHTO, 1986), the PEARDARP models (Purdue Economic Analysis of Rehabilitation and Design Alternative for Rigid Pavements, van Wiji, 1985), and the COPES models (Con-

Downloaded From : www.EasyEngineering.net

Downloaded From : www.EasyEngineering.net

crete Pavement Evaluation System, Darter *et al.*, 1985). The COPES models were also incorporated in the EXPEAR system, as described in Section 9.5.1, to formulate rehabilitation strategies (Hall *et al.*, 1989). A recent review of these models by ERES Consultants, Inc. (Smith *et al.*, 1990a) indicated that, when they were applied to 95 pavement sections located in four major climate zones, none could adequately predict the distress (such as faulting, cracking, joint deterioration, and pumping), serviceability, or roughness. From these 95 sections and the more than 400 sections from the COPES data base, new prediction models were developed and are presented below. It should be emphasized that the models are valid within the data base from which they were derived. There are many design, materials, climate, and construction variables, so it is extremely difficult to develop nationwide models. Regional models or general models calibrated to each state could be required.

Present Serviceability Rating The best way to predict PSR for a given pavement is by using roughness. However, to relate serviceability to physical deterioration, which may be modeled mechanistically, a PSR model based on key distress types is desirable. Models were developed for both JPCP and JRCP. Whereas all types of distress were initially included, only four were found significant.

For JPCP,

$$\text{PSR} = 4.356 - 0.0182\,\text{TFAULT} - 0.00313\,\text{SPALL} - 0.00162\,\text{TCRKS} - 0.00317\,\text{FDR} \tag{9.53a}$$

Statistics: $R^2 = 0.58$, SEE = 0.31, $n = 282$

in which

PSR = present serviceability rating (from 0 to 5);
TFAULT = cumulative transverse joint faulting in inches per mile;
SPALL = number of deteriorated joints (medium and high severity) per mile;
TCRKS = number of transverse cracks (all severity) per mile;
FDR = number of full-depth repair per mile;
R = correlation coefficient;
SEE = standard error of estimate;
n = number of sample points.

For JRCP,

$$\text{PSR} = 4.333 - 0.0539\,\text{TFAULT} - 0.00372\,\text{SPALL} - 0.00425\,\text{MHTCRKS} - 0.000531\,\text{FDR} \tag{9.53b}$$

Statistics: $R^2 = 0.64$, SEE = 0.37, $n = 434$

in which MHTCRKS is the number of medium and high severity cracks per mile.

Downloaded From : www.EasyEngineering.net

Downloaded From : www.EasyEngineering.net

Transverse Joint Faulting Two models, one for pavements with dowels and the other for pavements without dowels, were developed. Because of the mechanisms involved in faulting, it was not possible to combine these two design types into a single model. The models were developed using a combination of mechanistic and empirical approaches.

With dowels,

$$\begin{aligned}\text{FAULT} = \text{ESAL}^{0.5280}[&0.1204 + 0.04048(\text{BSTRESS}/1000)^{0.3388} - 0.007353 \\ &\times (\text{AVJSPACE}/10)^{0.6725} - 0.1492(\text{KSTAT}/100)^{0.05911} \\ &- 0.01868\,\text{DRAIN} - 0.00879\,\text{EDGESUP} \\ &- 0.00959\,\text{STYPE}]\end{aligned} \tag{9.54a}$$

Statistics: $R^2 = 0.67$

SEE = 0.0571 in.

$n = 559$

in which

FAULT = mean transverse joint faulting in inches;

ESAL = cumulative equivalent 18-kip (80-KN) single-axle loads per lane in millions;

BSTRESS = maximum concrete bearing stress in psi computed by Eq. 4.45, in which the load on each dowel P_t is computed by assuming that the 9000-lb (40-kN) wheel load is distributed over a length ℓ, where ℓ is the radius of relative stiffness, and that 45% of the load is transferred through the joint;

AVJSPACE = average transverse joint spacing in ft;

KSTAT = effective modulus of subgrade reaction on top of base in pci;

DRAIN = index for drainage condition: 0 without edge drain, 1 with edge drain;

EDGESUP = index for edge support: 0 without edge support, 1 with edge support;

STYPE = index for AASHTO subgrade soil classification, 0 for A-4 to A-7 and 1 for A-1 to A-3.

Without dowels,

$$\begin{aligned}\text{FAULT} = \text{ESAL}^{0.2500}[&0.000038 + 0.01830(100\,\text{OPENING})^{0.5585} \\ &+ 0.000619 \times (100\,\text{DEFLAMI})^{1.7229} + 0.0400(\text{FI}/1000)^{1.9840} \\ &+ 0.00565\,\text{BTERM} - 0.00770\,\text{EDGESUP} \\ &- 0.00263\,\text{STYPE} - 0.00891\,\text{DRAIN}]\end{aligned} \tag{9.54b}$$

Statistics: $R^2 = 0.81$

SEE = 0.028 in.

$n = 398$

Downloaded From : www.EasyEngineering.net

Downloaded From : www.EasyEngineering.net

in which

OPENING = average transverse joint opening in inches computed by Eq. 4.36 in which temperature change ΔT is equal to one-half of the annual temperature range;
DEFLAMI = Ioannides' corner deflection in inches (Ioannides *et al.*, 1985) $= P[1.2 - 0.88\sqrt{2}(a/\ell)]/(\text{KSTAT}\ell^2)$, where P is the wheel load and a is the contact radius;
FI = freezing index in degree days;
BTERM = base type factor, which can be computed by

$$\text{BTERM} = 10[\text{ESAL}^{0.2076}\,(0.04546 + 0.05115\,\text{GB} + 0.007279\,\text{CTB} + 0.003183\,\text{ATB} - 0.003714\,\text{OGB} - 0.006441\,\text{LCB} \quad (9.55)$$

in which GB = 1 for dense-graded aggregate base, 0 for others; CTB = 1 for cement-treated base, 0 for others; ATB = 1 for dense-graded asphalt-treated base, 0 for others; OGB = 1 for open-graded base, either untreated or asphalt-treated, and 0 for others; and LCB = 1 for lean concrete base, 0 for others.

Transverse Joint Spalling Predictive models were developed separately for JPCP and for JRCP. Extensive efforts to develop a single model for joint spalling were not successful. One reason might be that most of the joint spalling for JPCP was of medium severity, whereas a much greater proportion of joint spalling for JRCP was of high severity.

For JPCP,

$$\text{JTSPALL} = \text{AGE}^{2.178}[0.0221 + 0.5494\,\text{DCRACK} - 0.0135\,\text{LIQSEAL} - 0.0419\,\text{PREFSEAL} + 0.0000362\,\text{FI} \quad (9.56a)$$

Statistics: $R^2 = 0.59$
SEE = 15 joints per mile
$n = 262$

in which

JTSPALL = number of medium-and high-severity joint spalls per mile;
AGE = age since original construction in years;
DCRACK = 0 with no "D" cracking, 1 with "D" cracking;
LIQSEAL = 0 if no liquid sealant exists in joint, 1 if liquid sealant exists in joint;
PREFSEAL = 0 if no preformed compression seal exists, 1 if preformed compression seal exists;
FI = freezing index in degree days.

For JRCP,

$$\text{JTSPALL} = \text{AGE}^{4.1232}[0.00024 + 0.0000269\,\text{DCRACK} + 0.000307\,\text{REACTAGG} - 0.000033\,\text{LIQSEAL} - 0.0003\,\text{PREFSEAL} + 0.00000014\,\text{FI}] \quad (9.56b)$$

Downloaded From : www.EasyEngineering.net

Downloaded From : www.EasyEngineering.net

Statistics: $R^2 = 0.47$
SEE = 13 joints per mile
$n = 280$

in which REACTAGG = 0 if no reactive aggregate exists, 1 if reactive aggregate exists.

9.5.3 Effects of Design Features on Rigid Pavement Performance

The performance of rigid pavements is affected by a variety of design features, including slab thickness, base type, joint spacing, reinforcement, joint orientation, load transfer, dowel bar coatings, longitudinal joint design, joint sealant, tied concrete shoulders, and subdrainage. A study was made by ERES Consultants, Inc. under FHWA contract on the effects of these features on rigid pavement performance. Ninety-five pavement sections located in four major climatic regions were thoroughly evaluated. The following conclusions, which provide some revealing insights into pavement performance, are abstracted from the report (Smith *et al.*, 1990a).

Slab Thickness The effect of slab thickness on pavement performance was significant. It was found that increasing slab thickness reduced transverse and longitudinal cracking in all cases. This effect was much more pronounced for thinner slabs than for thicker slabs. It was not possible to compare the performance of the thinner slabs and the thicker slabs directly, because the thick slabs were all constructed directly on the subgrade and the thinner slabs were all constructed on a base course.

Increasing the thickness of slab did not appear to reduce joint spalling or joint faulting. Thick slabs placed directly on the subgrade, especially in wet climates and exposed to heavy traffic, faulted as much as thin slabs constructed on a base course.

Base Type Base types, including base/slab interface friction, base stiffness, base erodibility, and base permeability, seemed to have a great effect on the performance of jointed concrete pavements. The major performance indicators, which were affected by variations in base type, were transverse and longitudinal cracking, joint spalling, and faulting.

The worst performing base type, consisted of the cement-treated or soil cement bases, which tended to exhibit excessive pumping, faulting, and cracking. This is most likely due to the impervious nature of the base, which traps moisture and yet can break down and contribute to the movement of fines beneath the slab.

The use of lean concrete bases generally produced poor performance. Large curling and warping stresses have been associated with slabs constructed over lean concrete bases. These stresses result in considerable transverse and longitudinal cracking of the slab. The poor performance of these bases can also be attributed to a bathtub design, in which moisture is trapped within the pavement cross section.

Dense-graded asphalt-treated base courses ranged in performance from very poor to good. The fact that these types of bases were often constructed as a bathtub design contributed to their poor performance. This improper design often resulted in severe cracking, faulting, and pumping.

Downloaded From : www.EasyEngineering.net

Downloaded From : www.EasyEngineering.net

The construction of thicker slabs directly on the subgrade with no base resulted in a pavement that performed marginally. These pavements were especially susceptible to faulting, even under low traffic levels.

Pavements constructed over aggregate bases had varied performance, but were generally in the fair to very good category. In general, the more open-graded the aggregate, the better the performance. An advantage of aggregate bases is that they contribute the least to the high curling and warping stresses in the slab. Even though aggregate bases are not open-graded, they are more permeable and have a lower friction factor than stabilized bases.

The best bases in terms of pavement performance were the permeable bases. Typical base courses have permeabilities ranging from 0 to less than 1 ft/day (0.3 m/day); good permeable bases have permeabilities up to 1000 ft/day (305 m/day). Specific areas of concern were the high corner deflections and the low load transfer exhibited by the permeable bases. These can affect their long-term performance, so the use of dowel bars might be required. An unexpected benefit of using permeable bases was the reduction in "D" cracking on pavements susceptible to this type of distress.

Slab Length For JPCP, the length of slabs investigated ranged from 7.75 to 30 ft (2.4 to 9.1 m). It was found that reducing the slab length decreased both the magnitude of the joint faulting and the amount of transverse cracking. On pavements with random joint spacings, slabs with joint spacings greater than 18 ft (5.5 m) experienced more transverse cracking than did the shorter slabs.

For JRCP, the length of slabs investigated ranged from 21 to 78 ft (6.4 to 23.9 m). Generally, shorter joint spacings performed better, as measured by the deteriorated transverse cracks, joint faulting, and joint spalling. However, several JRCP with long joint spacings performed quite well. In particular, the long jointed pavements in New Jersey, which were constructed with expansion joints, displayed excellent performance.

An examination of the stiffness of foundation was made through the use of the radius of relative stiffness, ℓ. Generally speaking, when the ratio L/ℓ, where L is the length of slab, was greater than 5, transverse cracking occurred more frequently. This factor was further examined for different base types. It was found that stiffer base courses required shorter joint spacings to reduce or eliminate transverse cracking.

Reinforcement The amount of steel reinforcement appeared to have an effect in controlling the amount of deteriorated transverse cracking. Pavement sections with less than 0.1% reinforcing steel often displayed significant deteriorated transverse cracking. A minimum of 0.1% reinforcing steel is therefore recommended, with larger amounts required for more severe climate and longer slabs.

Joint Orientation Conventional wisdom has it that skewed joints prevent the application of two wheel loads to the joint at the same time and thus can reduce load-associated distresses. The results from the limited sample size in this study were ambiguous, but all of the nondoweled sections with skewed joints had a lower PSR than similar designs with perpendicular joints. The available data provide no definite conclusions on the effectiveness of skewing transverse joints for nondoweled slabs. Skewed joints are not believed to provide any benefit to doweled slabs.

Downloaded From : www.EasyEngineering.net

Downloaded From : www.EasyEngineering.net

Load Transfer Dowel bars were found to be effective in reducing the amount of joint faulting when compared with nondoweled sections of comparable designs. The diameter of dowels had an effect on performance, because larger diameter bars provided better load transfer and control of faulting under heavy traffic than did smaller dowels. It appeared that a minimum dowel diameter of 1.25 in. (32 mm) was necessary to provide good performance.

Nondoweled JPCP slabs generally developed significant faulting, regardless of pavement design or climate. This effect was somewhat mitigated by the use of permeable bases. However, the sections in this group had a much lower number of accumulated ESAL, so no definite conclusions can be drawn yet.

Dowel Bar Coatings Corrosion-resistant coatings are needed to protect dowels from the adverse effects of moisture and deicing chemicals. While most of the sections in this study did not contain corrosion-resistant dowel bars, those that did generally exhibited enhanced performance. Very little deteriorated transverse cracking was identified on these sections. In fact, one section in New Jersey with stainless steel-clad dowel bars was performing satisfactorily after 36 years of service.

Longitudinal Joint Design The longitudinal joint design was found to be a critical design element. Both inadequate forming techniques and insufficient depths of joint can contribute to the development of longitudinal cracking. There was evidence of the advantage of sawing the joints over the use of inserts. The depth of longitudinal joints is generally recommended to be one-third of the actual, not designed, slab thickness, but might have to be greater when stabilized bases are used.

Joint Sealant Joint sealing appeared to have a beneficial effect on performance. This was particularly true in harsh climates with excessive amounts of moisture. Preformed compression sealants were shown to perform well for more than 15 years under heavy traffic. Except where "D" cracking occurred, pavement sections containing preformed sealants generally exhibited little joint spalling and were in good overall conditions. Rubberized asphalt joint sealants showed good performance for 5 to 7 years.

Tied Concrete Shoulders It is generally believed that tied concrete shoulders can reduce edge stresses and corner deflections by providing more lateral supports to the mainline pavement, thus improving pavement performance. Surprisingly, this study showed that, although tied concrete shoulders performed better than asphalt shoulders, many of the tied shoulders were not designed properly and actually contributed to poor performance of the mainline pavement. The tiebars were spaced too far apart, sometimes at a spacing of 40 in. (1016 mm), and were not strategically located near slab corners to provide adequate support. In some cases, tied concrete shoulders were constructed over a stabilized dense-graded base in a bathtub design, resulting in the poor performance of mainline pavement.

Subdrainage The provision of positive subdrainage, either in the form of longitudinal edge drains or the combination of a drainage layer and edge drains, generally reduced the amount of faulting and spalling related to "D" cracking. With few exceptions, the

Downloaded From : www.EasyEngineering.net

Downloaded From : www.EasyEngineering.net

load-associated distresses, especially faulting and transverse cracking, decreased as the drainage characteristics improved. The overall pavement performance can be improved by using an open-graded base or restricting the percentage of fines. A filter layer must be placed below the permeable base, and regular maintenance of the outlets must be provided.

SUMMARY

Pavement performance is an important factor of pavement design because it provides a framework upon which a judgement on the success or failure of a design procedure or the need for further improvements can be made. This chapter discusses pavement performance, including distress, serviceability, skid resistance, nondestructive testing, and pavement evaluation.

Important Points Discussed in Chapter 9

1. Distress or failure can be divided into structural failure, which is associated with the ability of the pavement to carry the design load, and functional failure, which is concerned mainly with riding comfort and safety. Pavements that exhibit structural failures may finally end up in functional failure, whereas pavements with functional failures sometimes are structurally sound. Immediate attention must be paid to correct any structural failure so that damage to the pavement will not be accelerated.
2. Distress can be classified into load-associated distress and non-load-associated distress. This distinction is important because it identifies the causes of distress so that proper remedial measures can be taken. The non-load-associated distress is caused by climates, materials, or construction. A distress may begin as a non-load-associated distress and later become more severe as the number of load repetitions increases.
3. The types of distress that should be considered in the design of asphalt pavement are fatigue cracking, which is a load-associated structural failure, and rutting, which is a load-associated functional failure. In climates with large temperature variations or very cold temperatures, low-temperature cracking, which is a non-load-associated structural failure, should also be considered.
4. The most common problem with composite pavements is reflection cracking in the asphalt overlay above a joint or crack in the PCC slab. This is a non-load-associated structural failure caused mainly by movement of the concrete slab beneath the asphalt surface due to thermal or moisture changes.
5. Common types of distress in PCC pavements are pumping, faulting, and cracking. Joint deterioration is a major problem in JRCP, with its longer joint spacings, whereas edge punchout is a major problem in CRCP due to closely spaced cracks.
6. The pavement serviceability–performance concept was developed during the AASHO Road Test. Detailed procedures for developing the AASHO PSI equations relating physical measurements to panel ratings are presented. Changes in the public's perception of serviceability and the use of new equipment for physical measurements leave it doubtful that the AASHO equations developed more than 30 years ago are still applicable. One major deficiency of the AASHO equations is that they include both rideability and surface defects. For the management of

Downloaded From : www.EasyEngineering.net

Downloaded From : www.EasyEngineering.net

pavement inventory, it is preferable to have separate measures of ride quality and surface defects. Therefore, there is a need to develop new equations that reflect the public's perception of riding quality.

7. A variety of devices can be used to measure roughness and riding quality. The most popular is the response-type road roughness meter (RTRRM). RTRRMs measure the relative movement in inches per mile (m/km) between the body of the automobile and the center of the rear axle. Because the measurements are sensitive to the type and condition of the vehicle used, regular calibrations are required. To provide a common base for roughness measurements, the use of the international roughness index (IRI) is recommended.
8. Pavement friction is measured most frequently by the locked-wheel trailer procedure, specified in ASTM E 274. The skid number (SN), which is the measured coefficient of friction multiplied by 100, is determined when the vehicle travels at a speed of 40 mph (64 km/h).
9. Regression equations are available to relate the surface texture to the skid number determined by the ASTM E 274 method. The British Pendulum Number (BPN) can be used as an indicator for microtexture, which governs the surface friction at very low speeds, while the mean texture depth (MTD) is being used for macrotexture, which affects the surface drainage and friction at higher speeds.
10. Skid resistance of wearing surfaces depends both on the aggregate and on the mixture characteristics. The most frequently sought after characteristics for a skid-resistant aggregate are its resistance to polish and wear and its texture, shape, and size. The mixture characteristics can be controlled by blending of aggregates, selection of proper aggregate size and gradation, use of appropriate binder content, and application of good construction practice.
11. The surface friction of PCC pavement can be improved by roughing, acid etching, grooving, and bonding a thin layer of aggregate to the surface; that of bituminous pavement by grooving, surface treatment or thin overlay, and the use of a heater planer.
12. Nondestructive deflection tests can be conducted by three types of equipment, using static or slowly moving loads, steady-state vibration, or impulse loads. The falling weight deflectometer, which imposes an impulse load on the pavement surface, can simulate a moving wheel load in both magnitude and duration and is considered the best device for nondestructive testing.
13. Various computer programs are available to backcalculate the layer moduli. Because the solutions are not unique and depend on the initial moduli assumed, engineering judgments are needed in using these programs. The layer moduli can also be determined by a trial and error method using any layer system computer programs. The deflection of the sensor farthest from the load must be matched first by adjusting the modulus of the lowest layer. The process is then moved progressively inward by adjusting the moduli of the upper layers to match with the deflections of the inner sensors until the innermost sensor is reached. An exception to the above procedures is the ILL-BACK program for directly determining the composite modulus of the foundation and the elastic modulus of the PCC slab.
14. Pavement evaluation and rehabilitation are not exact sciences and depend to a large extent on past experiences and engineering judgments. Until recently, many

Downloaded From : www.EasyEngineering.net

Downloaded From : www.EasyEngineering.net

problems in this domain could be solved only by human experts with extensive practical experience and knowledge. The new technology of knowledge-based expert systems offers a powerful means for acquiring and organizing this human expertise so that it can be preserved and communicated to others. Two of the systems, SCEPTRE for flexible pavements and EXPEAR for rigid pavements, are briefly described.

15. A large number of regression equations can be found in the literature to predict pavement performance. These equations illustrate the effects of various factors on pavement performance, but their usefulness in practice can be limited by the scope of the data base that was used in their development. Some equations are presented for predicting fatigue cracking, rutting, and low-temperature cracking of flexible pavements, as well as the present serviceability rating, transverse joint faulting, and transverse joint spalling of rigid pavements.
16. An insight into the effects of various design features on the performance of jointed concrete pavements was presented. These features include slab thickness, base type, joint spacings, reinforcement, joint orientation, load transfer, dowel bar coatings, longitudinal joint design, joint sealant, tied concrete shoulders, and subdrainage.

PROBLEMS

9.1 It is assumed that the present serviceability index PSI of pavements is related to the roughness index RI by

$$\text{PSI} = A_0 + A_1 \log(\text{RI})$$

Derive the general equations for determining A_0 and A_1. Using the equations derived, find A_0 and A_1 based on the data shown in Table P9.1. [Answer: PSI = 9.50 − 2.98 log(RI)]

TABLE P9.1

Section no.	1	2	3	4	5
RI (in./mile)	800	300	200	150	80
PSR	1.0	2.0	2.5	3.0	4.0

9.2 Table P9.2 shows the measurements and ratings of five sections of flexible pavement. Develop the equation for the present serviceability index. [Answer: PSI = 5.51 − 1.70 log $(1 + \overline{\text{SV}})$ − 38.09$\overline{\text{RD}}^2$ − 0.004 $\sqrt{C + P}$]

TABLE P9.2

Section no.	Slope variance $\overline{\text{SV}}$ (10^{-6})	Rut depth $\overline{\text{RD}}$ (in.)	Cracking and patching $C + P$ (ft or ft²/1000 ft²)	PSR
1	2.8	0.06	0	4.3
2	5.8	0.10	1	3.8
3	10.9	0.11	13	3.2
4	16.8	0.16	23	2.4
5	56.0	0.19	31	1.1

Downloaded From : www.EasyEngineering.net

Downloaded From : www.EasyEngineering.net

9.3 Derive Eq. 9.29.

9.4 Glass beads are spread over a pavement surface to determine its mean texture depth. The volume of beads is 2 in.^{3} and the diameter of the patch area is 10 in. If the skid number of the pavement is 40 at a speed of 40 mph, estimate the skid number at speeds of 20 and 60 mph, respectively. [Answer: $SN_{20} = 47.7$ and $SN_{60} = 33.6$]

9.5 FWD deflection measurements were made on a pavement, as shown in Figure P9.5. A 9000-lb load was applied uniformly over a circular area with a radius of 6 in. The surface deflections at radial distances of 0, 8, 12, 24, 48, 72, and 96 in. were measured and found to be 23.7, 19.7, 17.1, 10.5, 5.4, 3.5, and 2.6 mil (1 mil = 10^{-3} in.) Assume the layer system to be linear elastic with the thicknesses and Poisson ratios shown in the figure, and backcalculate the layer moduli E_1, E_2, and E_3 by KENLAYER.

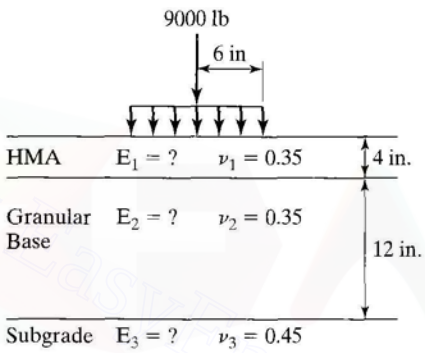


FIGURE P9.5

9.6 Same as Problem 9-5 except that the granular base is nonlinear elastic with the properties shown in Figure P9.6. Using method 3 with PHI = 40, backcalculate E_1, K_1, and E_3 via KENLAYER.

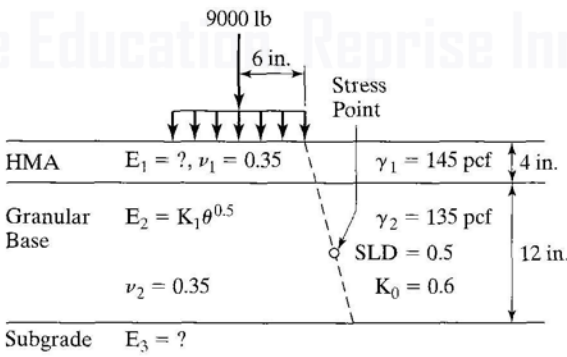


FIGURE P9.6

9.7 Same as Problem 9-6, but the granular base is divided into 6 layers, each 2 in. thick.

9.8 Figure P9.8 is a linear elastic three-layer system with the load, material properties, and layer thicknesses as shown. The deflection sensors are placed at 0, 12, 24, 36, and 48 in. from the axis of symmetry. Determine the functions f_1, f_2, f_3, f_4, and f_5, as shown in Eq. 9.36, by running KENLAYER. [Answer: 0.2971, 0.2427, 0.1907, 0.1530, 0.1125]

Downloaded From : www.EasyEngineering.net

Downloaded From : www.EasyEngineering.net

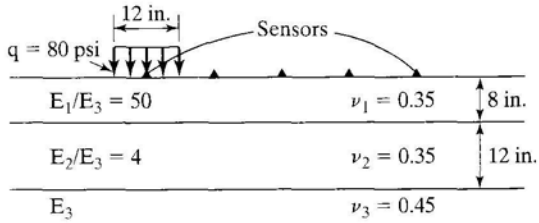


FIGURE P9.8

9.9 A FWD test was made on a concrete pavement. The radius of the load plate was 5.9 in. and the recorded load was 9000 lb. Sensors were located at 0, 12, 24, and 36 in. from the center of plate and the corresponding deflections recorded were 0.0047, 0.0040, 0.0035, and 0.0026 in. Laboratory tests on the cored samples indicated that the concrete has a modulus of elasticity of 4.7×10^6 psi. The foundation is assumed to be a dense liquid. Determine the modulus of subgrade reaction k and the thickness of the concrete slab. [Answer: 285 pci, 8 in.]

9.10 Same as problem 9-9, but the foundation is considered to be an elastic solid having Poisson ratio 0.4. [Answer: 37000 psi, 5.5 in.]

9.11 An asphalt pavement has a HMA thickness of 4 in., a stiffness of original asphalt of 200 kg/cm^2, and a loam type of subgrade. For a winter design temperature of $-20°$C and an age of 6 years, estimate the length of low-temperature cracks in ft per 1000 ft of two-lane road. [Answer: 39 ft/1000 ft]

9.12 A doweled concrete pavement has a joint spacing of 20 ft and no tied concrete shoulders for edge support. The subgrade soil is A-6, and there is no edge drain installed. The calculated bearing stress between dowel and concrete is 3000 psi, and the pavement is placed on a subbase with an effective modulus of subgrade reaction of 100 pci. Estimate the amount of transverse joint faulting after the pavement has been subjected to 20 million repetitions of an 18-kip equivalent single-axle load. [Answer: 0.089 in.]

9.13 No evidence of "D" cracking can be found on a 15-year-old jointed plain concrete pavement. If the freezing index at the pavement site is 1000 degree days, estimate the average number of medium- and high-severity joint spalls per mile if (a) liquid joint sealant is used or (b) preformed compressive seal is used. [Answer: 16.3 and 6.0 joints per mile]

Downloaded From : www.EasyEngineering.net

Downloaded From : www.EasyEngineering.net

CHAPTER 10

Reliability

10.1 STATISTICAL CONCEPTS

The variability of design factors has made the probabilistic method productive in the design of both flexible and rigid pavements (Lemer and Moavenzadeh, 1971; Darter *et al.*, 1973b; Kher and Darter, 1973; Darter, 1976). The method was also incorporated in the AASHTO design guide (AASHTO, 1986). The application of the method requires an understanding of some statistical concepts.

10.1.1 Definitions

Two of the most useful properties of a random variable are its expectation, or mean, and its variance. A random variable is a function that takes on a defined value for every point in a sample space. For example, consider the sample space generated by the tossing of two fair coins. The random variable x is defined as the total number of heads observed. The sample space consists of four points (0, 0), (0, 1), (1, 0) and (1, 1), and at these points x takes on the values 0, 1, 1, and 2, respectively. The probability that the random variable x takes these values is known as the probability function of x, often symbolized by $f(x)$. This can be expressed in tabular form:

x	0	1	2
$f(x)$	$\frac{1}{4}$	$\frac{1}{2}$	$\frac{1}{4}$

Note that the sum of $f(x)$ for all possible values of x must be equal to one. If the random variable is not discrete, but rather is continuous within the sample space, as shown in Figure 10.1, $f(x)$ is called the probability density function. For $f(x)$ to be a probability density function, it must satisfy the condition that $f(x) \geq 0$ for all x and that

$$\int_{-\infty}^{\infty} f(x)\,dx = 1 \tag{10.1}$$

Downloaded From : www.EasyEngineering.net

Downloaded From : www.EasyEngineering.net

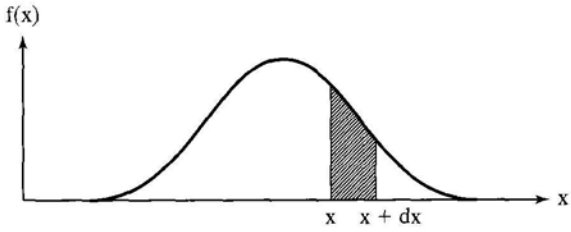


FIGURE 10.1
Probability density function.

Expectation The expectation, or mean, of a random variable x is defined as follows:

Discrete case
$$E[x] = \sum_{\text{all } x_i} x_i f(x_i) \tag{10.2a}$$

Continuous case
$$E[x] = \int_{-\infty}^{\infty} x f(x)\, dx \tag{10.2b}$$

If n independent observations of x are taken, each with the same probability $1/n$, the mean of the observations, $\bar{x}$, is obtained from Eq. 10.2*a*:

$$\bar{x} = \frac{\sum_{i=1}^{n} x_i}{n} \tag{10.3}$$

This value is called the sample mean and is the best estimate of the true or population mean μ.

Example 10.1:

Compute $E[x]$ for a random variable x with the following probability function:

x	1	2	3	4
$f(x)$	$\frac{1}{8}$	$\frac{1}{8}$	$\frac{1}{4}$	$\frac{1}{2}$

Solution: By Eq. 10.2a, $E[x] = 1(\frac{1}{8}) + 2(\frac{1}{8}) + 3(\frac{1}{4}) + 4(\frac{1}{2}) = 3.125$.

Example 10.2:

Compute $E[x]$ for a random variable x with the following probability density function:

$$f(x) = \begin{cases} \frac{1}{3}x & 0 \le x \le 1 \\ \frac{2}{3} & 1 < x \le 3 \end{cases}$$

Downloaded From : www.EasyEngineering.net

Downloaded From : www.EasyEngineering.net

Solution: By Eq. 10.2*b*,

$$E[x] = \int_0^1 \tfrac{1}{3}x^2 dx + \int_1^3 \tfrac{2}{3}x\, dx$$
$$= \tfrac{1}{9}x^3\Big|_0^1 + \tfrac{2}{6}x^2\Big|_1^3 = 2\tfrac{7}{9}$$

If c is a constant, then

$$E[c] = \int_{-\infty}^{\infty} cf(x)\, dx = c\int_{-\infty}^{\infty} f(x)\, dx = c \tag{10.4}$$

By using the definition shown in Eq. 10.2*b*, it can easily be proven that

$$E[cx] = cE[x] \tag{10.5}$$
$$E[g_1(x) + g_2(x)] = E[g_1(x)] + E[g_2(x)] \tag{10.6}$$

in which g_1 and g_2 are functions of x.

Variance The variance of a random variable x is defined as the expected value of the square of the deviation from its expectation:

$$V[x] = E[(x - E[x])^2] \tag{10.7a}$$

Discrete case
$$V[x] = \sum_{\text{all}x_i} (x_i - E[x])^2 f(x_i) \tag{10.7b}$$

Continuous case
$$V[x] = \int_{-\infty}^{\infty} (x - E[x])^2 f(x)\, dx \tag{10.7c}$$

If $E[x]$ is considered a constant, then Eq. 10.7*a* can be written as

$$V[x] = E[x^2 + (E[x])^2 - 2xE[x]] = E[x^2] + (E[x])^2 - 2(E[x])^2$$
$$= E[x^2] - (E[x])^2 \tag{10.8}$$

Equation 10.8 indicates that the variance of the random variable x is equal to the expectation of the square of x, abbreviated as square mean, minus the square of the expectation of x, abbreviated as mean square.

Example 10.3:

Compute $V[x]$ for the random variable x with the probability function shown in Example 10.1.

Solution: The variance can be calculated by either Eq. 10.7*b* or 10.8. From Eq. 10.7*b*, $V[x] = (1-3.125)^2(\frac{1}{8}) + (2 - 3.125)^2(\frac{1}{8}) + (3-3.125)^2(\frac{1}{4}) + (4 - 3.125)^2(\frac{1}{2}) = 1.109$. From Eq. 10.8, $V[x] = 1(\frac{1}{8}) + 4(\frac{1}{8}) + 9(\frac{1}{4}) + 16(\frac{1}{2}) - (3.125)^2 = 1.109$.

Downloaded From : www.EasyEngineering.net

Downloaded From : www.EasyEngineering.net

If n independent observations of x are taken, the variance of x is determined from

$$V[x] = \sum_{i=1}^{n} \frac{(x_i - \bar{x})^2}{n - 1} \tag{10.9}$$

The sum is divided by $n - 1$ rather than n because $\bar{x}$ is the sample mean rather than the true mean, so the degree of freedom is $n - 1$.

If a, b, and c are constants, it can be easily proved that

$$V[c] = 0 \tag{10.10}$$

$$V[cx] = c^2 V[x] \tag{10.11}$$

$$V[a + bx] = b^2 V[x] \tag{10.12}$$

The standard deviation s of a random variable x is defined as the square root of its variance:

$$s = \sqrt{V[x]} \tag{10.13}$$

The coefficient of variation is generally used in percentile form, but, for convenience, it can be expressed as a decimal by

$$C[x] = \frac{s}{\mu} \tag{10.14}$$

in which μ is the mean, $E[x]$.

Example 10.4:

Given the 10 values of x, 17, 19, 14, 11, 18, 16, 16, 10, 9, and 12, calculate the mean, variance, standard deviation, and coefficient of variation.

Solution: From Eq. 10.3, $\bar{x} = (17 + 19 + 14 + 11 + 18 + 16 + 16 + 10 + 9 + 12)/10 = 14.2$. From Eq. 10.9, $V[x] = [(17 - 14.2)^2 + (19 - 14.2)^2 + (14 - 14.2)^2 + (11 - 14.2)^2 + (18 - 14.2)^2 + (16 - 14.2)^2 + (16 - 14.2)^2 + (10 - 14.2)^2 + (9 - 14.2)^2 + (12 - 14.2)^2]/(10 - 1) = 12.4$. From Eq. 10.13, $s = \sqrt{12.4} = 3.52$. From Eq. 10.14, $C[x] = (3.52/14.2) \times 100 = 24.8\%$.

Covariance The covariance of two random variables x and y is defined as the expected value of the product of the deviations of x and y from their expected values:

$$\text{Cov}[x, y] = E[(x - E[x])(y - E[y])] \tag{10.15a}$$

Discrete case:

$$\text{Cov}[x, y] = \sum_{\text{all} x_i, y_i} (x_i - E[x])(y_i - E[y]) f(x_i, y_i) \tag{10.15b}$$

Continuous case:

$$\text{Cov}[x,y] = \int_{-\infty}^{\infty} \int_{-\infty}^{\infty} (x - E[x])(y - E[y]) f(x, y)\, dx\, dy \tag{10.15c}$$

Downloaded From : www.EasyEngineering.net

Downloaded From : www.EasyEngineering.net

From Eq. 10.15*a*,

$$\begin{aligned}\text{Cov}[x, y] &= E[xy - yE[x] - xE[y] + E[x]E[y]] \\ &= E[xy] - E[x]E[y] \end{aligned} \tag{10.16}$$

For actual computation of covariance, the use of Eq. 10.16 is more convenient than that of Eq. 10.15*a*.

If large positive deviations of x are associated with large positive deviations of y, or large negative deviations of x with large negative deviations of y, then the covariance will be positive. If positive deviations of x are associated with negative deviations of y, and vice versa, the covariance will be negative. On the other hand, if positive and negative deviations of x occur as frequently as positive and negative deviations of y, then the covariance will tend to 0. Therefore, the covariance is a measure of correlation between two random variables. It should be noted that variance is a special case of covariance of a random variable with itself:

$$\text{Cov}[x, x] = E[(x - E[x])(x - E[x])] = E[(x - E[x])^2] = V[x] \tag{10.17}$$

The correlation coefficient between random variables x and y is defined as

$$\rho(x, y) = \frac{\text{Cov}[x, y]}{\sqrt{V[x]\,V[y]}} \tag{10.18}$$

It can be shown that $-1 \leq \rho \leq 1$ and that

$$\rho = 1 \qquad \text{when } y = a + bx \tag{10.19}$$

and

$$\rho = -1 \qquad \text{when } y = a - bx \tag{10.20}$$

in which a and b are constants. The variance of $x + y$ can be expressed as

$$\begin{aligned} V[x + y] &= E[(x + y - E[x + y])^2] = E[(x - E[x] + y - E[y])^2] \\ &= E[(x - E[x])^2 + E[(y - E[y])^2] + 2E[(x - E[x])(y - E[y])] \\ &= V[x] + V[y] + 2\,\text{Cov}[x, y] \end{aligned} \tag{10.21}$$

If x and y are independent, $\text{Cov}[x, y] = 0$.

Example 10.5:

Compute $\text{Cov}[x, y]$ and $\rho(x, y)$ for the following probability functions of random variables x and y:

$$f(x,y) = \begin{cases} \frac{1}{4} & x = 1 \quad y = 3 \\ \frac{1}{8} & x = 2 \quad y = 6 \\ \frac{1}{2} & x = 3 \quad y = 9 \\ \frac{1}{8} & x = 4 \quad y = 12 \end{cases}$$

Solution: From Eq. 10.2*a*,

$$E[x] = (1)(\tfrac{1}{4}) + (2)(\tfrac{1}{8}) + (3)(\tfrac{1}{2}) + (4)(\tfrac{1}{8}) = 2.5$$

$$E[y] = (3)(\tfrac{1}{4}) + (6)(\tfrac{1}{8}) + (9)(\tfrac{1}{2}) + (12)(\tfrac{1}{8}) = 7.5$$

Downloaded From : www.EasyEngineering.net

Downloaded From : www.EasyEngineering.net

From Eq. 10.7*b*,

$$V[x] = (1 - 2.5)^2(\tfrac{1}{4}) + (2 - 2.5)^2(\tfrac{1}{8}) + (3 - 2.5)^2(\tfrac{1}{2}) + (4 - 2.5)^2(\tfrac{1}{8}) = 1$$

$$V[y] = (3 - 7.5)^2(\tfrac{1}{4}) + (6 - 7.5)^2(\tfrac{1}{8}) + (9 - 7.5)^2(\tfrac{1}{2}) + (12 - 7.5)^2(\tfrac{1}{8}) = 9$$

From Eq. 10.15*b*,

$$\text{Cov}[x, y] = (1 - 2.5)(3 - 7.5)(\tfrac{1}{4}) + (2 - 2.5)(6 - 7.5)(\tfrac{1}{8}) + (3 - 2.5)(9 - 7.5)(\tfrac{1}{2}) + (4 - 2.5)(12 - 7.5)(\tfrac{1}{8}) = 3$$

The covariance can also be determined from Eq. 10.16:

$$\text{Cov}[x, y] = (1)(3)(\tfrac{1}{4}) + (2)(6)(\tfrac{1}{8}) + (3)(9)(\tfrac{1}{2}) + (4)(12)(\tfrac{1}{8}) - (2.5)(7.5) = 3$$

From Eq. 10.18,

$$\rho(x, y) = \frac{3}{\sqrt{9}} = 1$$

This is as expected, because $y = 3x$.

Example 10.6:

Compute Cov[x, y] and $\rho(x, y)$ of the joint density function of random variables x and y:

$$f(x, y) = x + y \quad \text{when } 0 \le x \le 1 \text{ and } 0 \le y \le 1$$
$$= 0 \quad \text{otherwise}$$

Solution: To find the expectation involving two random variables, one is considered as a constant and the other as a variable. From Eq. 10.2*b*,

$$E[xy] = \int_{-\infty}^{\infty}\int_{-\infty}^{\infty} xy(x + y)\,dx\,dy = \int_0^1\int_0^1 (x^2y + xy^2)\,dx\,dy$$
$$= \int_0^1 \left[\frac{x^3}{3}y + \frac{x^2y^2}{2}\right]_0^1 dy = \int_0^1 \left[\frac{1}{3}y + \frac{1}{2}y^2\right] dy = \left[\frac{y^2}{6} + \frac{y^3}{6}\right]_0^1 = \frac{1}{3}$$

$$E[x] = \int_0^1\int_0^1 x(x + y)\,dx\,dy = \int_0^1 \left[\frac{x^3}{3} + \frac{x^2y}{2}\right]_0^1 dy = \left[\frac{y}{3} + \frac{y^2}{4}\right]_0^1 = \frac{7}{12}$$

$$E[y] = \int_0^1\int_0^1 y(x + y)\,dx\,dy = \frac{7}{12}$$

$$E[x^2] = \int_0^1\int_0^1 x^2(x + y)\,dx\,dy = \int_0^1 \left[\frac{x^4}{4} + \frac{x^3y}{3}\right]_0^1 dy = \left[\frac{y}{4} + \frac{y^2}{6}\right]_0^1 = \frac{5}{12}$$

$$E[y^2] = \int_0^1\int_0^1 y^2(x + y)\,dx\,dy = \frac{5}{12}$$

Downloaded From : www.EasyEngineering.net

Downloaded From : www.EasyEngineering.net

From Eq. 10.8, $V[x] = V[y] = \frac{5}{12} - (\frac{7}{12})^2 = \frac{11}{144}$. From Eq. 10.16, $\text{Cov}[x, y] = \frac{1}{3} - (\frac{7}{12})(\frac{7}{12}) = -\frac{1}{144}$. From Eq. 10.18, $\rho(x, y) = -\frac{1}{11}$.

10.1.2 Taylor's Expansion

Taylor's expansion for a function $f(x, y)$ about the point (a, b) can be expressed as

$$f(x, y) = f(a, b) + f_x(a, b)(x - a) + f_y(a, b)(y - b) + \tfrac{1}{2}[f_{xx}(a, b)(x - a)^2 + 2f_{xy}(a, b)(x - a)(y - b) + f_{yy}(a, b)(y - b)^2] + \cdots \quad (10.22)$$

in which the subscripts x and y indicate the partial differentiation with respect to x and y. Taylor's expansion and its extension into n random variables can be used to determine the mean and variance of a function (Benjamin and Cornell, 1970).

Mean If a and b are taken as the means of x and y, the expectation of $f(x, y)$ can be obtained from Eq. 10.22 by taking the expectation on both sides. When all terms higher than the second order are neglected, the following relation is obtained:

$$E[f(x, y)] = f(a, b) + \tfrac{1}{2}\{f_{xx}(a, b)\, V[x] + 2f_{xy}(a, b)\, \text{Cov}[x, y] + f_{yy}(a, b)\, V[y]\} \quad (10.23)$$

Note that $E[f_x(a, b)(x - a)] = f_x(a, b)\{E[x] - a\} = 0$ because $E[x] = a$. If $g(x_1, x_2, \ldots, x_n)$ is a function of n random variables x_i and μ is the mean value for each of these random variables, the second-order Taylor series approximation to the expected value of g is

$$E[g] = g(\mu) + \tfrac{1}{2}\sum_{i=1}^{n}\sum_{j=1}^{n}\left(\frac{\partial^2 g}{\partial x_i \partial x_j}\right)\text{Cov}[x_i, x_j] \quad (10.24)$$

in which μ is the set of mean values for x_i. If x_i and x_j are independent, then $\text{Cov}[x_i, x_j] = V[x_i]$ and $\text{Cov}[x_i, x_j] = 0$, so Eq. 10.24 becomes

$$E[g] = g(\mu) + \tfrac{1}{2}\sum_{i=1}^{n}\frac{\partial^2 g}{\partial x_i^2} V[x_i] \quad (10.25)$$

The second-order term may be neglected if the coefficients of variations of x_i are small, so

$$E[g] = g(\mu) \quad (10.26)$$

Equation 10.26 indicates that the mean value of g can be obtained simply by substituting the mean value of each random variable into the function.

Example 10.7:

The maximum surface deflection of a homogeneous and incompressible half-space under a circular loaded area, as indicated by Eq. 2.8, is

$$w_0 = \frac{1.5qa}{E} \quad (10.27)$$

Downloaded From : www.EasyEngineering.net

Downloaded From : www.EasyEngineering.net

If the contact pressure q, the contact radius a, and the elastic modulus E are independent with mean values of $q = 100$ psi (690 kPa), $a = 6$ in. (152 mm), and $E = 10{,}000$ psi (69 MPa) and coefficients of variation of $C[q] = 0.1$, $C[a] = 0.05$, and $C[E] = 0.2$, determine the mean of w_0 by the first- and second-order approximations.

Solution: By the first-order approximation, or Eq. 10.26, $E[w_0] = 1.5 \times 100 \times 6/10{,}000 = 0.09$ in. (2.29 mm). For the second-order approximation $\partial^2 w_0/\partial q^2 = 0$, $\partial^2 w_0/\partial a^2 = 0$, and $\partial^2 w_0/\partial E^2 = 3qa/E^3$, so the variance of q and a has no effect on $E[w_0]$. From Eqs. 10.13 and 10.14, $V[E] = (0.2 \times 10{,}000)^2 = 4 \times 10^6$ lb^2/in.^{4} (190 MN^2/m^4). From Eq. 10.25, $E[w_0] = 0.09 + 0.5 \times 3 \times 100 \times 6 \times 4 \times 10^6/10^{12} = 0.0936$ in. (2.38 mm).

Variance The first-order approximation for the variance of $f(x, y)$ can be determined from the first three terms on the right side of Eq. 10.22 by applying Eq. 10.21:

$$V[f(x,y)] = \{f_x(a,b)\}^2 V[x] + \{f_y(a,b)\}^2 V[y] + 2\{f_x(a,b)\}\{f_y(a,b)\}\text{Cov}[x,y] \tag{10.28}$$

Equation 10.28 can be extended to $g(x_1, x_2, \ldots, x_n)$ by

$$V[g] = \sum_{i=1}^{n}\sum_{j=1}^{n}\left(\frac{\partial g}{\partial x_i}\right)_\mu \left(\frac{\partial g}{\partial x_j}\right)_\mu \text{Cov}[x_i, x_j] \tag{10.29}$$

If $x_1, x_2, \ldots, x_n$ are independent, there are no cross product terms, and Eq. 10.29 becomes

$$V[g] = \sum_{i=1}^{n}\left(\frac{\partial g}{\partial x_i}\right)^2 V[x_i] \tag{10.30}$$

Example 10.8:

Compute $V[w_0]$ for the problem in Example 10.7.

Solution: With $V[q] = (0.1 \times 100)^2 = 100$ lb^2/in.^{4} (4.8 GN^2/m^4), $V[a] = (0.05 \times 6)^2 = 0.09$ in.^{2} (58.1 mm^2) and $V[E] = 4 \times 10^6$ lb^2/in.^{4} (190 MN^2/m^4), and applying Eq. 10.30 to Eq. 10.27, $V[w_0] = (1.5)^2\{(a/E)^2 V[q] + (q/E)^2 V[a] + (qa/E^2)^2 V[E]\} = 2.25\{(6/10{,}000)^2 \times 100 + (100/10{,}000)^2 \times 0.09 + (100 \times 6/10^8)^2 \times 4 \times 10^6\} = 4.25 \times 10^{-4}$ in.^{2}(0.274 mm^2).

10.1.3 Normal Distribution

The distribution function most frequently used as a probability model is called the normal or Gaussian distribution. Although this symmetrical and bell-shaped distribution is very important, it is not the only type of distribution to be used in the probabilistic method.

Basic Equation The mathematical equation of normal distribution expressing the frequency of occurrence of the random variable x is

$$f(x) = \frac{1}{s\sqrt{2\pi}}\exp\left[-\frac{1}{2}\left(\frac{x-\mu}{s}\right)^2\right] \tag{10.31}$$

in which s is the standard deviation and μ is the mean.

Downloaded From : www.EasyEngineering.net

Downloaded From : www.EasyEngineering.net

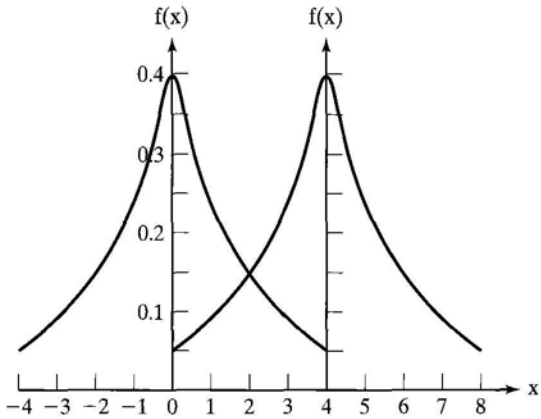


FIGURE 10.2
Normal distribution.

Figure 10.2 shows a plot of normal distribution with $s = 1$ and $\mu = 0$ and 4, respectively. Note that the two curves are similar, except that the x coordinate is displaced by a constant distance. If the x coordinate at the peak is not equal to zero, it can be made to zero by a simple displacement.

The cumulative distribution function for a normally distributed random variable x can be expressed as

$$\psi(x) = \int_{-\infty}^{x} \frac{1}{s\sqrt{2\pi}} \exp\left[-\frac{1}{2}\left(\frac{x-\mu}{s}\right)^2\right] dx \tag{10.32}$$

A simple way to eliminate μ and s in Eq. 10.32 is to introduce a normal deviate defined as

$$u = \frac{x-\mu}{s} \tag{10.33}$$

Replacing x in Eq. 10.32 by u gives

$$\psi(z) = \frac{1}{\sqrt{2\pi}} \int_{0}^{z} \exp\left(-\frac{u^2}{2}\right) du \tag{10.34}$$

in which $\psi(z)$ is the area under the standard normal distribution curve $f(u)$ between 0 and z, as indicated in Figure 10.3 and tabulated in Table 10.1. By using Eq. 10.34 and

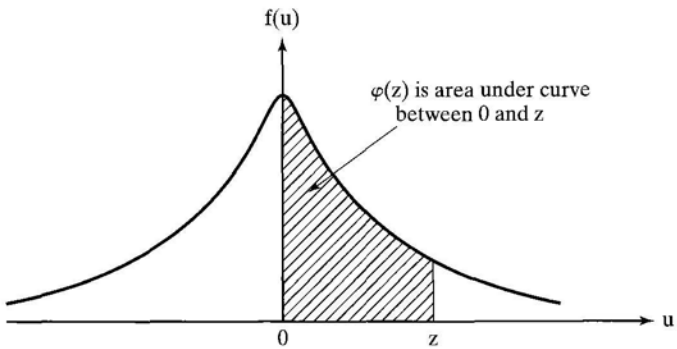


FIGURE 10.3
Area under normal curve.

Downloaded From : www.EasyEngineering.net

Downloaded From : www.EasyEngineering.net

TABLE 10.1 Area $\psi(z)$ Under Normal Curve

z	.00	.01	.02	.03	.04	.05	.06	.07	.08	.09
0	0	.003969	.007978	.011966	.015953	.019939	.023922	.027903	.031881	.035856
.1	.039828	.043795	.047758	.051717	.055670	.059618	.063559	.067495	.071424	.075345
.2	.079260	.083166	.087064	.090954	.094835	.098706	.102568	.106420	.110251	.114092
.3	.117911	.121720	.125516	.129300	.133072	.136831	.140576	.144309	.148027	.151732
.4	.155422	.159097	.162757	.166402	.170031	.173645	.177242	.180822	.184386	.187933
.5	.191462	.194974	.198466	.201944	.205401	.208840	.212260	.215661	.219043	.222405
.6	.225747	.229069	.232371	.235653	.234914	.242154	.245373	.248571	.251748	.254903
.7	.258036	.261148	.264238	.257305	.270350	.273373	.276373	.279350	.282305	.285236
.8	.288145	.291030	.293892	.296731	.299546	.302337	.305105	.307850	.310570	.313267
.9	.315940	.318589	.321214	.323814	.326391	.328944	.331472	.333977	.336457	.338913
1.0	.341345	.343752	.346136	.348495	.350830	.353141	.355428	.357690	.359929	.362143
1.1	.364334	.366500	.368643	.370762	.372857	.374928	.376976	.379000	.381000	.382977
1.2	.384930	.386861	.388768	.390651	.392512	.393350	.396165	.397958	.399727	.401475
1.3	.403200	.404902	.406582	.408241	.409877	.411492	.413085	.414657	.416207	.417736
1.4	.419243	.420730	.422196	.423641	.425066	.426471	.427855	.429219	.430563	.431888
1.5	.433193	.434476	.435745	.436992	.438220	.439429	.440620	.441792	.442947	.444083
1.6	.445201	.446301	.447384	.448449	.449497	.450529	.451543	.452540	.453521	.454486
1.7	.455435	.456367	.457284	.458185	.459070	.459941	.460796	.461636	.462462	.463273
1.8	.464070	.464852	.465620	.466375	.467116	.467843	.468557	.469258	.469946	.470621
1.9	.471283	.471933	.472571	.473197	.473610	.474412	.475002	.475581	.476148	.476705
2.0	.477250	.477784	.478308	.478822	.479325	.479818	.480301	.480774	.481237	.481691
2.1	.482136	.482571	.482997	.483414	.483823	.484222	.484614	.484997	.485371	.485738
2.2	.486097	.486447	.486791	.487126	.487455	.487776	.488089	.488396	.488696	.488989
2.3	.489276	.489556	.489830	.490097	.490358	.490613	.490863	.491106	.491344	.491576
2.4	.491802	.492024	.492240	.492451	.492656	.492857	.493053	.493244	.493431	.493613
2.5	.493790	.493963	.494132	.494297	.494457	.494614	.494766	.494915	.495060	.495201
2.6	.495339	.495473	.495604	.495731	.495855	.495975	.496093	.496207	.496319	.496427
2.7	.496533	.496636	.496736	.496833	.496928	.497020	.497110	.497197	.497282	.497365
2.8	.497445	.497523	.497599	.497673	.497744	.497814	.497882	.497948	.498012	.498074
2.9	.498134	.498193	.498250	.498305	.498359	.498411	.498462	.498511	.498559	.498605
3.0	.498650	.498694	.498736	.498777	.498817	.498856	.498893	.498930	.498965	.498999
3.1	.499032	.499065	.499096	.499126	.499155	.499184	.499211	.499238	.499264	.499289
3.2	.499313	.499336	.499359	.499381	.499402	.499423	.499443	.499462	.499481	.499499
3.3	.499517	.499534	.499550	.499566	.499581	.499596	.499610	.499624	.499638	.499651
3.4	.499663	.499675	.499687	.499698	.499709	.499720	.499730	.499740	.499749	.499758
3.5	.499767	.499776	.499784	.499792	.499800	.499807	.499815	.499822	.499828	.499835
3.6	.499841	.499847	.499853	.499858	.499864	.499869	.499874	.499879	.499883	.499888
3.7	.499892	.499896	.499900	.400904	.499908	.499912	.499915	.499918	.499922	.499925
3.8	.499928	.499931	.499933	.499936	.499938	.499941	.499943	.499946	.499948	.499950
3.9	.499952	.499954	.499956	.499958	.499959	.499961	.499963	.499964	.499966	.499967

recognizing that the area under half of the standardized normal curve is $\frac{1}{2}$, the probability associated with the value of the random variable being less or greater than any specified value can be determined.

Example 10.9:

Given a normally distributed random variable x with a mean of 135 and a variance of 125, determine the probability that x is greater than 150.

Downloaded From : www.EasyEngineering.net

Downloaded From : www.EasyEngineering.net

Solution: From Eq. 10.33, $z = (150 - 135)/\sqrt{125} = 1.34$. From Table 10.1, $\psi(z) = 0.41$, so there is a 0.09 chance, or 9% probability, that x is greater than 150.

Log Normal Distribution When a variable extends over several orders of magnitude, such as traffic volume, damage ratio, grain size, or permeability, it is necessary to present it in log scale and assume its distribution to be log normal, so that Eq. 10.33 becomes

$$u = \frac{\log x - \log \mu}{s_{\log x}} \tag{10.35}$$

in which $s_{\log x}$ is the standard deviation based on the log normal distribution of x. From Eq. 10.30,

$$V[\log x] = \left(\frac{\log e}{x}\right)^2 V[x] = \frac{0.1886}{x^2} V[x] \tag{10.36}$$

$$s_{\log x} = \frac{0.4343}{x} s = 0.4343C[x] \tag{10.37}$$

Equation 10.37 can be used to relate the standard deviation based on the normal distribution of x to that based on the log normal distribution of x.

Example 10.10:

If the distribution of x in Example 10.9 is log normal, determine the probability that x is greater than 150.

Solution: From Eq. 10.37, $s_{\log x} = (0.4343/135)\sqrt{125} = 0.036$. From Eq. 10.35, $u = (\log 150 - \log 135)/0.036 = 1.27$. From Table 10.1, $\psi(z) = 0.398$; so there is a 0.102 chance, or 10.2% probability, that x is greater than 150.

10.2 PROBABILISTIC METHODS

There are two methods of pavement design: deterministic and probabilistic. In the deterministic method, each design factor has a fixed value based on the factor of safety assigned by the designer. Using judgment, the designer usually assigns a higher factor of safety to those factors that are less certain or that have a greater effect on the final design. Application of this traditional approach based on the factors of safety can result in overdesign or underdesign, depending on the magnitudes of the safety factors applied and the sensitivity of the design procedures. A more realistic approach is the probabilistic method, in which each design factor is assigned a mean and a variance. The factor of safety assigned to each design factor and its sensitivity to the final design are automatically taken care of, and the reliability of the design can be evaluated. Reliability is defined as the probability that the design will perform its intended function over its design life.

Traffic, or the number of load repetitions, is one of the most important factors in pavement design. There are two types of load repetitions: the predicted number of load repetitions n and the allowable number of load repetitions N. In the deterministic

Downloaded From : www.EasyEngineering.net

Downloaded From : www.EasyEngineering.net

method, both n and N have fixed values, whereas in the probabilistic method, each has a mean and a variance. If the design is based on a single value of equivalent single-axle load (ESAL), n and N can be compared directly to evaluate the adequacy of the design. If the design is based on a variety of axle loads or on ESAL applications over two or more seasons, the concept of damage ratio, as indicated by Eq. 3.19, may be used.

The use of load repetitions as a failure criterion is only one of the general methods to evaluate the reliability of a design. Other failure criteria can also be used. For example, VESYS (FHWA, 1978) employed the serviceability index as a design criterion; traffic is treated as one of the many variables that affect the serviceability.

10.2.1 Method Based on Equivalent Single-Axle Load

For convenience, the determination of the predicted number of load repetitions and its variance is called traffic prediction, and the determination of the allowable number of load repetitions and its variance is called performance prediction.

Traffic Prediction The predicted ESAL during the design period is designated W_T and can be determined from Eq. 6.28 and rewritten as

$$W_T = \left(\sum_{i=1}^{m} p_i F_i\right)(\text{ADT}_0)(T)(A)(G)(D)(L)(365)(Y) \tag{10.38}$$

in which p_i is the percentage (decimal) of axles in the ith load group, F_i is the equivalent axle load factor (EALF) for the ith load group, m is the number of load groups, ADT_0 is the average daily traffic at the start of the design period, T is the percentage (decimal) of trucks in ADT, A is the average number of axles per truck, D is the percentage (decimal) of ADT in design direction, L is the percentage (decimal) of ADT in design lane, Y is the design period in years, and G is the growth factor, which can be computed by

$$G = \tfrac{1}{2}[1 + (1 + r)^Y] \tag{6.31}$$

in which r is the growth rate (decimal) per year. When the log operation is applied to both sides, Eq. 10.38 becomes

$$\begin{aligned}\log W_T = {} & \log(\Sigma p_i F_i) + \log(\text{ADT}_0) + \log G + \log T \\ & + \log A + \log D + \log L + \log Y + 2.562\end{aligned} \tag{10.39}$$

From Eq. 10.30, the variance of $\log W_T$ can be determined by

$$\begin{aligned}V[\log W_T] = {} & (\log e)^2\left\{\frac{V[\Sigma p_i F_i]}{(\Sigma p_i F_i)^2} + \frac{V[\text{ADT}_0]}{(\text{ADT}_0)^2} + \frac{V[G]}{G^2}\right. \\ & \left. + \frac{V[T]}{T^2} + \frac{V[A]}{A^2} + \frac{V[D]}{D^2} + \frac{V[L]}{L^2}\right\}\end{aligned} \tag{10.40}$$

Downloaded From : www.EasyEngineering.net

Downloaded From : www.EasyEngineering.net

Example 10.11:

The truck traffic on a flexible pavement is 55% 20-kip (90-kN) single-axle loads and 45% 36-kip (160-kN) tandem-axle loads. The average daily traffic at the start of the period is 5000 per day, with a coefficient of variation of 15%. The annual traffic growth rate is 6%, the percentage of trucks is 20%, and the number of axles per truck is 2.5, each having a coefficient of variation of 10%. The directional distribution factor is 50%, and the lane distribution factor is 100%, both being considered deterministic with no variations. If the coefficient of variation of p_iF_i, which is the product of axle load percentage and its equivalent factor, is 35% and the Asphalt Institute's equivalent factors are used, determine the mean and the variance of log W_T for a design period of 20 years.

TABLE 10.2 Mean, Coefficient of Variation, and Variance of Traffic Data

Design factor	ADT_0 (vehicles per day)	r (%)	T (%)	A (axles per truck)	D (%)	L (%)
Mean	5000	6	20	2.5	50	100
CV	15	10	10	10	0	0
Variance	562,500	0.000036	0.0004	0.0625	0	0

Solution: The given data and the computed variances are shown in Table 10.2.

From Table 6.4, the equivalent factors for 20-kip (90-kN) single-axle and 36-kip (160-kN) tandem-axle loads are 1.51 and 1.38, respectively, so $p_iF_i = 0.55 \times 1.51 + 0.45 \times 1.38 = 1.452$ and $V[p_iF_i] = (0.35 \times 1.452)^2 = 0.258$. From Eq. 6.31, $G = 0.5[1 + (1 + 0.06)^{20}] = 2.104$, and $V[G] = \{0.5Y(1 + r)^{Y-1}\}^2 V[r] = \{0.5 \times 20 \times (1.06)^{19}\}^2 \times 0.000036 = 0.033$. From Eq. 10.39, $\log W_T = \log 1.452 + \log 5000 + \log 2.104 + \log 0.2 + \log 2.5 + \log 0.5 + \log 1 + \log 20 + 2.562 = 7.445$. From Eq. 10.40, $V[\log W_T] = 0.1886[0.258/(1.452)^2 + 562{,}500/(5000)^2 + 0.033/(2.104)^2 + 0.0004/(0.2)^2 + 0.0625/(2.5)^2] = 0.1886(0.122 + 0.023 + 0.007 + 0.010 + 0.010) = 0.033$. It can be seen that the most important factor causing the variance is p_iF_i.

Performance Prediction The allowable ESAL during the design period is designated W_t and can be determined from design equations or computer programs. The AASHTO design equation for flexible pavement can be used as an example. Because of the empirical nature of this equation, only the English units will be shown. The equation is

$$\log W_t = 9.36 \log (SN + 1) - 0.2 + \frac{\log[(p_0 - p_t)/(4.2 - 1.5)]}{0.4 + 1094/(SN + 1)^{5.19}} + 2.32 \log M_R - 8.07 \quad (10.41)$$

in which p_0 is the initial serviceability index, p_t is the terminal serviceability index, M_R is the resilient modulus in psi, and SN is the structural number, defined as

$$SN = a_1D_1 + a_2D_2m_2 + a_3D_3m_3 \quad (10.42)$$

in which a_i is the ith layer coefficient, D_i is the ith layer thickness in inches, and m_i is the ith layer drainage coefficient. More about AASHTO design equations is presented in

Downloaded From : www.EasyEngineering.net

Downloaded From : www.EasyEngineering.net

Section 12.3.1. The variances of $\log W_t$ and SN are, respectively,

$$V[\log W_t] = \left(\frac{\partial \log W_t}{\partial \mathrm{SN}}\right)^2 V[\mathrm{SN}] + \left(\frac{\partial \log W_t}{\partial p_0}\right)^2 V[p_0] + \left(\frac{\partial \log W_t}{\partial M_\mathrm{R}}\right)^2 V[M_\mathrm{R}]$$

$$= \left\{\frac{9.36 \log e}{\mathrm{SN}+1} + \frac{\log[(p_0 - p_t)/(4.2-1.5)][(1094 \times 5.19)/(\mathrm{SN}+1)^{6.19}]}{[0.4 + 1094/(\mathrm{SN}+1)^{5.19}]^2}\right\}^2 V[\mathrm{SN}]$$

$$+ \left\{\frac{\log e/(4.2-1.5)}{[0.4 + 1094/(\mathrm{SN}+1)^{5.19}][(p_0 - p_t)/(4.2-1.5)]}\right\}^2 V[p_0]$$

$$+ \left\{\frac{2.32 \log e}{M_\mathrm{R}}\right\}^2 V[M_\mathrm{R}] \tag{10.43}$$

and

$$V[\mathrm{SN}] = D_1^2 V[a_1] + a_2^2 V[D_1] + (D_2 m_2)^2 V[a_2] + (a_2 m_2)^2 V[D_2] + (a_2 D_2)^2 V[m_2] + (D_3 m_3)^2 V[a_3] + (a_3 m_3)^2 V[D_3] + (a_3 D_3)^2 V[m_3] \tag{10.44}$$

Example 10.12:

Given the mean and coefficient of variation of the initial serviceability index, layer coefficients, drainage coefficients, layer thicknesses, and subgrade resilient modulus, as shown in Table 10.3, determine the mean and variance of the performance prediction for a terminal serviceability of 2.0.

TABLE 10.3 Mean and Coefficient of Variation of Pavement Variables

Design factor	p_0	a_1	D_1 (in.)	a_2	D_2 (in.)	m_2	a_3	D_3 (in.)	m_3	M_R (psi)
Mean	4.6	0.42	8.0	0.14	7.0	1.2	0.08	11.0	1.2	5700
CV	6.7	10.0	10.0	14.3	10.0	10.0	18.2	10.0	10.0	15.0

Note. 1 in. = 25.4 mm, 1 psi = 6.9 kPa.

Solution: From Eq. 10.42, $\mathrm{SN} = 0.42 \times 8 + 0.14 \times 7 \times 1.2 + 0.08 \times 11 \times 1.2 = 5.592$. From Eq. 10.41, $\log W_t = 9.36 \log 6.592 - 0.2 + \log[(4.6 - 2.0)/2.7]/[0.4 + 1094/(6.592)^{5.19}] + 2.32 \log 5700 - 8.07 = 8.074$. From Eq. 10.44, $V[\mathrm{SN}] = (8)^2 \times (0.42 \times 0.1)^2 + (0.42)^2 \times (8 \times 0.1)^2 + (7 \times 1.2)^2 \times (0.14 \times 0.143)^2 + (0.14 \times 1.2)^2 \times (7 \times 0.1)^2 + (0.14 \times 7)^2 \times (1.2 \times 0.1)^2 + (11 \times 1.2)^2 \times (0.08 \times 0.182)^2 + (0.08 \times 1.2)^2 \times (11 \times 0.1)^2 + (0.08 \times 11)^2 \times (1.2 \times 0.1)^2 = 0.341$. From Eq. 10.43, $V[\log W_t] = \{9.36 \times 0.4343/6.592 + [(\log 0.963) \times 5677.8/(6.592)^{6.19}]/[0.4 + 1094/(6.592)^{5.19}]^2\}^2 \times 0.341 + \{(0.4343/2.7)/[0.4 + 1094/(6.592)^{5.19}]/0.963\}^2 (4.6 \times 0.067)^2 + \{2.32 \times 0.4343/5700\}^2 (5700 \times 0.15)^2 = 0.128 + 0.012 + 0.023 = 0.163$.

Downloaded From : www.EasyEngineering.net

Downloaded From : www.EasyEngineering.net

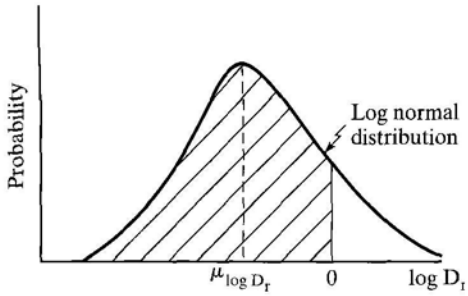


FIGURE 10.4
Reliability based on damage ratio.

Reliability When the mean and variance of log W_T and log W_t are known, the reliability of the design can be determined. Reliability is the probability that log W_T − log $W_t < 0$, or

$$\text{Reliability} = \text{Probability}\,(\log D_r = \log W_T - \log W_t < 0) \tag{10.45}$$

in which $D_r = W_T/W_t$ is the damage ratio. The variance of log D_r can be obtained by

$$V[\log D_r] = V[\log W_T] + V[\log W_t] \tag{10.46}$$

By assuming D_r to have a log normal distribution, the reliability of the design, as indicated by the shaded area in Figure 10.4, can be determined.

Example 10.13:

The results of the traffic prediction are shown in Example 10.11 and those of the performance prediction are shown in Example 10.12. Determine the reliability of the design.

Solution: From Example 10.11, log W_T = 7.445 and $V[\log W_T]$ = 0.033. From Example 10.12, log W_t = 8.074 and $V[\log W_t]$ = 0.163. The mean of log D_r = 7.445 − 8.074 = −0.629 and the variance of log D_r = 0.033 + 0.163 = 0.196, so $z = (0 + 0.629)/\sqrt{0.196} = 1.42$. From Table 10.1, the probability that log D_r is smaller than 0 is 0.5 + 0.422, or 92.2%.

The foregoing procedure for determining reliability is highly simplified for easy understanding. A more rigorous procedure (Irick *et al.*, 1987) defines reliability as

$$\text{Reliability} = \text{Probability}\,(\log N_T - \log N_t < 0) \tag{10.47}$$

in which N_T is the actual traffic and N_t is the actual performance. Both W_T and W_t can be predicted, but their actual values, N_T and N_t, can be known only after the pavement has been constructed and its traffic and performance have been observed. This can be explained by Figure 10.5, in which the performance is evaluated by the distress indicator d. The *predicted* number of load repetitions to cause the distress indicator to reach the terminal value is W_t, but the *actual* number is N_t. If the performance prediction is unbiased, with positive errors for some projects and negative errors for others, the mean of log N_t − log W_t should be zero. The same is true for traffic prediction with the

Downloaded From : www.EasyEngineering.net

Downloaded From : www.EasyEngineering.net

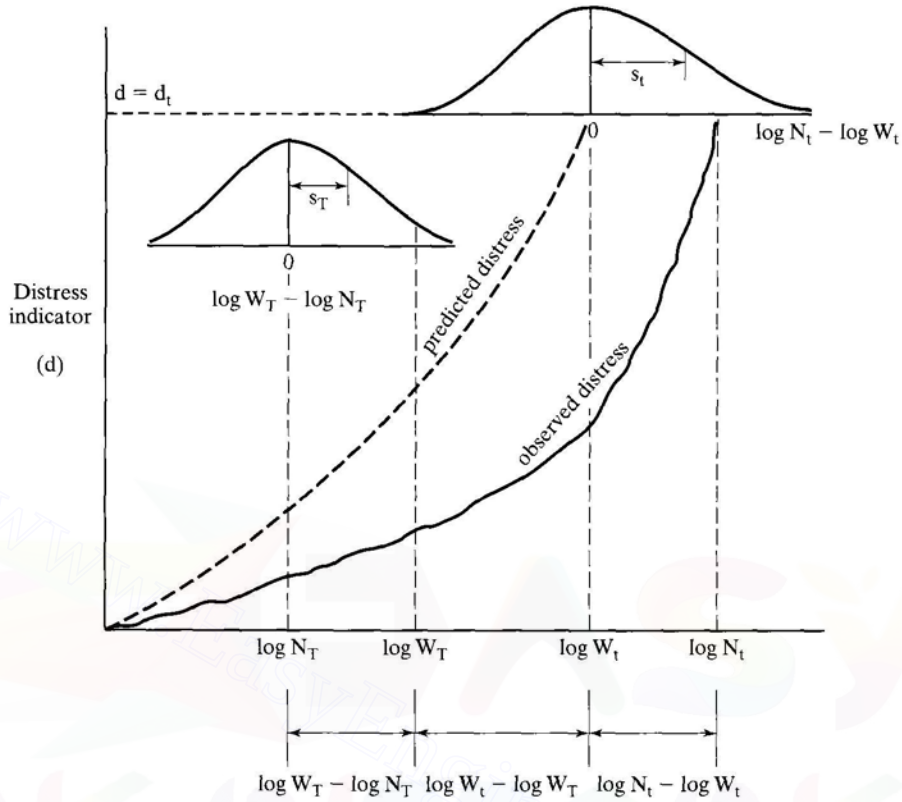


FIGURE 10.5

Probability distribution of traffic and performance. (After Irick *et al.* (1987).)

mean of $\log W_T - \log N_T$ equal to zero. The standard deviation for performance prediction is s_T, and that for the traffic prediction is s_t. Now,

$$\log N_t - \log N_T = (\log W_T - \log N_T) + (\log W_t - \log W_T) + (\log N_t - \log W_t) \tag{10.48}$$

and the first and third terms on the right side have a mean of zero, so Eq. 10.48 can be reduced to

$$\log N_T - \log N_t = \log W_T - \log W_t \tag{10.49}$$

Equation 10.49 implies that the mean of $\log N_T - \log N_t$ is the same as the mean of $\log W_T - \log W_t$. Because $\log W_t - \log W_T$ is a reliability interval selected by the designer and should be considered a constant, the variance of $\log N_t - \log N_T$ is

$$s^2 = V[\log N_t - \log N_T] = V[\log W_T - \log N_T] + V(\log N_t - \log W_t] = s_T^2 + s_t^2 \tag{10.50}$$

Downloaded From : www.EasyEngineering.net

Downloaded From : www.EasyEngineering.net

which is identical to Eq. 10.46. Therefore, the reliability determined from Eqs. 10.45 and 10.46 is the same as that determined from Eqs. 10.47 and 10.50.

10.2.2 Method Based on Different Axle Load Groups

If the design is based on a number of load groups, the damage ratio, indicated by Eq. 3.19, may be used. In the design of concrete pavements by the fatigue principle, a cracking index c, similar to the damage ratio, is usually used and is defined as

$$c = \sum_{i=1}^{m} \frac{n_i}{N_i} \tag{10.51}$$

in which m is the number of axle load groups, n_i is the predicted number of stress repetitions for load i during the design life, and N_i is the allowable number of stress repetitions for load i. The design is considered satisfactory if the cracking index is less than or equal to 1.

Traffic Prediction The procedure for predicting the mean and variance of n_i is similar to the method based on ESAL, except that each load group is considered separately. If $(n_0)_i$ is the number of the ith axle load group per day at the start of the design period, the predicted number of repetitions n_i for load group i during the design period is

$$n_i = 365(n_0)_i(G)(D)(L)(Y) \tag{10.52}$$

Note that the growth factor G, the percentage of axles in the design direction D, and the percentage of axles on the design lane L may be different for each load group. The variance is

$$V[n_i] = (365 \times Y)^2\{(GDL)^2V[(n_0)_i] + [(n_0)_iDL]^2V[G] + [(n_0)_i GL]^2V[D] + [(n_0)_i GD]^2V[L]\} \tag{10.53}$$

Example 10.14:

A rigid pavement is subjected to a combination of single-, tandem-, and tridem-axle loads. The means, coefficients of variation, and variances of the initial repetitions of each axle type, growth factor, directional distribution factor, and lane distribution factor are shown in Table 10.4. Determine the mean and variance of the number of repetitions of each axle type for a period of 20 years.

TABLE 10.4 Traffic Data for Each Axle Type

Design factor	$(n_0)_1$ Single per day	$(n_0)_2$ Tandem per day	$(n_0)_3$ Tridem per day	G	D (%)	L (%)
Mean	500	100	40	2.0	50	100
CV	30	80	100	20	0	0
Variance	22,500	6400	1600	0.16	0	0

Downloaded From : www.EasyEngineering.net

Downloaded From : www.EasyEngineering.net

Solution: For single-axle loads, from Eq. 10.52, $n_1 = 365 \times 500 \times 2 \times 0.5 \times 1 \times 20 = 3.65 \times 10^6$; from Eq. 10.53, $V[n_1] = (365 \times 20)^2[(2 \times 0.5)^2 \times 22{,}500 + (500 \times 0.5)^2 \times 0.16] = 1.73 \times 10^{12}$. For tandem-axle loads, $n_2 = 365 \times 100 \times 2 \times 0.5 \times 1 \times 20 = 7.3 \times 10^5$ and $V[n_2] = (365 \times 20)^2[(2 \times 0.5)^2 \times 6400 + (100 \times 0.5)^2 \times 0.16] = 3.62 \times 10^{11}$. For tridem-axle loads, $n_3 = 365 \times 40 \times 2 \times 0.5 \times 1 \times 20 = 2.92 \times 10^5$ and $V[n_3] = (365 \times 20)^2[(2 \times 0.5)^2 \times 1600 + (40 \times 0.5)^2 \times 0.16] = 8.87 \times 10^{10}$.

Performance Prediction In the design of concrete pavements, the allowable number of stress repetitions for load i depends on the stress ratio, which is a quotient of the stress σ and the modulus of rupture of the concrete S_c. For a given axle load, the average number of repetitions to cause fatigue failure is shown in Figure 7.27 and can be expressed as

$$\log N = 17.61 - 17.61\left(\frac{\sigma}{S_c}\right) \tag{7.39}$$

The variance of σ/S_c can be determined from

$$V\left[\frac{\sigma}{S_c}\right] = \left(\frac{1}{S_c}\right)^2 V[\sigma] + \left(\frac{\sigma}{S_c^2}\right)^2 V[S_c] \tag{10.54}$$

The variance of $\log N$ based on Eq. 7.39 is

$$V[\log N] = 310.11V\left[\frac{\sigma}{S_c}\right] \tag{10.55}$$

and, from Eq. 10.36,

$$V[N] = \frac{N^2}{0.1886}V[\log N] \tag{10.56}$$

It should be noted that the coefficients in the fatigue equations are not deterministic, but also exhibit a range of variations. Furthermore, σ and S_c are not completely independent because σ depends on the modulus of elasticity of concrete, which can be related to the modulus of rupture. Therefore, a variance due to the inadequacy of fatigue equations and other unexplained variances can be added to Eq. 10.56.

Example 10.15:

Given the means, coefficients of variation, and variances of critical stresses under single-, tandem-, and tridem-axle loads, as shown in Table 10.5, determine the means and variances of allowable stress repetitions for each load type.

TABLE 10.5 Mean and Variance of Concrete Stress and Modulus of Rupture

Design factor	Stress σ (psi)			Modulus of rupture S_c (psi)
	Single	Tandem	Tridem	
Mean	330	360	380	650
CV	30	30	35	10
Variance	9801	11,664	17,689	4225

Note. 1 psi = 6.9 kPa

Downloaded From : www.EasyEngineering.net

Downloaded From : www.EasyEngineering.net

Solution: For single-axle loads, $\sigma/S_c = 330/650 = 0.508$. From Eq. 10.54, $V[\sigma/S_c] = 9801/(650)^2 + [330/(650)^2]^2(4225) = 0.0258$. From Eq. 7.39, $\log N_1 = 17.61 - 17.61 \times 0.508 = 8.669$, or $N_1 = 4.67 \times 10^8$. From Eq. 10.55, $V[\log N_1] = 310.11 \times 0.0258 = 8.001$. From Eq. 10.56, $V[N_1] = (4.67 \times 10^8)^2 \times 8.001/0.1886 = 9.02 \times 10^{18}$.

For tandem-axle loads, $\sigma/S_c = 360/650 = 0.554$. From Eq. 10.54, $V[\sigma/S_c] = 11{,}664/(650)^2 + [360/(650)^2]^2 \times 4225 = 0.0307$. From Eq. 7.39, $\log N_2 = 17.61 - 17.61 \times 0.554 = 7.854$, or $N_2 = 7.15 \times 10^7$. From Eq. 10.55, $V[\log N_2] = 310.11 \times 0.0307 = 9.520$. From Eq. 10.56, $V[N_2] = (7.15 \times 10^7)^2 \times 9.520/0.1886 = 2.58 \times 10^{17}$.

For tridem-axle loads, $\sigma/S_c = 380/650 = 0.585$. From Eq. 10.54, $V[\sigma/S_c] = 17{,}689/(650)^2 + [380/(650)^2]^2 \times 4225 = 0.0453$. From Eq. 7.39, $\log N_3 = 17.61 - 17.61 \times 0.585 = 7.308$, or $N_3 = 2.03 \times 10^7$. From Eq. 10.55, $V[\log N_3] = 310.11 \times 0.0453 = 14.048$. From Eq. 10.56, $V[N_3] = (2.03 \times 10^7)^2 \times 14.048/0.1886 = 3.07 \times 10^{16}$.

In this example, it is assumed that the passage of a set of tandem or tridem axles is considered as one repetition. If the secondary damage due to the additional one or two axles is not negligible, it must be analyzed separately, as described in Section 6.4.5.

Reliability Given the predicted and allowable numbers of load repetitions n and N and their variances, the cracking index can be obtained from Eq. 10.51 and the variance of the cracking index from

$$V[c] = \sum_{i=1}^{m} \left\{ \left(\frac{1}{N_i} \right)^2 V[n_i] + \left(\frac{n_i}{N_i^2} \right)^2 V[N_i] \right\} \tag{10.57}$$

Because load repetitions are always expressed in log scale, it is reasonable to assume that the cracking index is also a log normal distribution. The variance of $\log c$ can be determined from the variance of c:

$$V[\log c] = \frac{0.1886}{c^2} V[c] \tag{10.58}$$

The standard deviation of $\log c$ is

$$S_{\log c} = \frac{0.4343}{c} \sqrt{V[c]} \tag{10.59}$$

When the mean and the standard deviation of $\log c$ are known, the reliability of the design, as indicated by the shaded area in Figure 10.6, can be defined as

$$\text{Reliability} = 1 - \text{Probability}\ (\log c \geq 0) \tag{10.60}$$

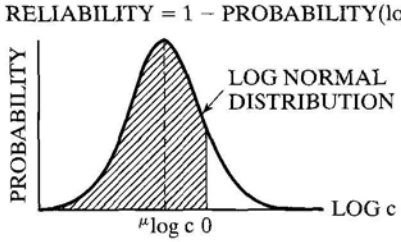


FIGURE 10.6
Reliability of cracking index.

Downloaded From : www.EasyEngineering.net

Downloaded From : www.EasyEngineering.net

Example 10.16:

The results of traffic prediction are shown in Example 10.14, those of performance prediction in Example 10.15. Determine the reliability of the design.

TABLE 10.6 Mean and Variance of Predicted and Allowable Repetitions

Axle load	Single	Tandem	Tridem
n_i	3.65×10^6	7.30×10^5	2.92×10^5
$V[n_i]$	1.73×10^{12}	3.62×10^{11}	8.87×10^{10}
N_i	4.67×10^8	7.15×10^7	2.03×10^7
$V[N_i]$	9.02×10^{18}	2.58×10^{17}	3.07×10^{16}

Solution: The means and variances of predicted and allowable repetitions for the three different axle loads are summarized in Table 10.6.

From Eq. 10.51, $c = 3.65 \times 10^6/(4.67 \times 10^8) + 7.30 \times 10^5/(7.15 \times 10^7) + 2.92 \times 10^5/(2.03 \times 10^7) = 0.0324$. From Eq. 10.57, $V[c] = 1.73 \times 10^{12}/(4.67 \times 10^8)^2 + [3.65 \times 10^6/(4.67 \times 10^8)^2]^2 \times 9.02 \times 10^{18} + 3.62 \times 10^{11}/(7.15 \times 10^7)^2 + [7.30 \times 10^5/(7.15 \times 10^7)^2]^2 \times 2.58 \times 10^{17} + 8.87 \times 10^{10}/(2.03 \times 10^7)^2 + [2.92 \times 10^5/(2.03 \times 10^7)^2]^2 \times 3.07 \times 10^{16} = 0.0235$. From Eq. 10.59, $s_{\log c} = 0.4343\sqrt{0.0235/0.0324} = 2.055$. With $\log c = \log 0.0324 = -1.489$, $z = (0 + 1.489)/2.055 = 0.725$, from Table 10.1, reliability = probability $(\log c < 0) = 0.5 + 0.261 = 0.761$, or 76.1%.

10.3 VARIABILITY

To determine the reliability of a design, the variances due to various sources must be known or estimated. This information can be obtained from field observations or laboratory tests or from past experience on similar projects.

10.3.1 Frequency Distribution

The frequency distribution of some design factors and their coefficients of variation are presented below.

Stiffness Coefficient of the Subgrade The stiffness coefficient of the subgrade, based on the surface curvature index measured by the Dynaflect, is an indication of the subgrade support. The in situ stiffness coefficients, which vary from about 0.2 for a weak clay to 1.0 for HMA, are calculated by means of a computer program. The theory and development of the stiffness coefficient are similar to those of the elastic modulus, with simplifying assumptions, as described by Scrivner and Moore (1968).

Figure 10.7 is a histogram showing typical distribution of the stiffness coefficient of subgrade within a project. The normal distribution curve fit to the plot is shown by the dotted line. The mean μ, the standard deviation s, and the number of measurements n are also shown in the figure. The average coefficient of variation within a project, based on a large number of projects, is about 10% (Darter, 1976).

Downloaded From : www.EasyEngineering.net

Downloaded From : www.EasyEngineering.net

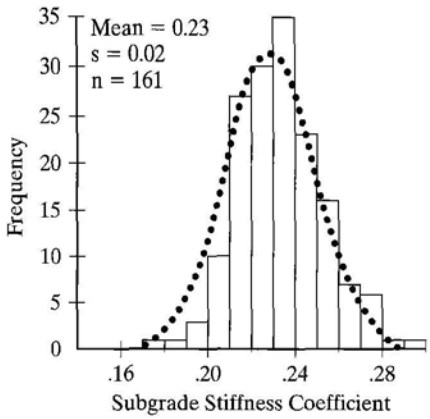


FIGURE 10.7

Frequency distribution of subgrade stiffness coefficient. (After Darter *et al.* (1973a).)

Stiffness Coefficient of Pavement Figure 10.8 shows a typical frequency distribution of stiffness coefficient for a pavement consisting of hot mix asphalt and cement-treated base. The stiffness coefficient of the pavement is much larger than that of the subgrade and has a greater coefficient of variation.

Thickness of Asphalt Surface Figure 10.9 shows a typical frequency distribution of asphalt surfacing thickness determined by individual cores. The coefficient of variation

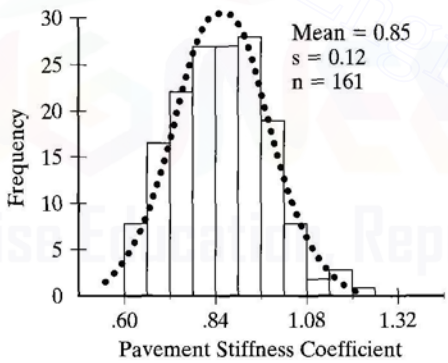


FIGURE 10.8

Frequency distribution of pavement stiffness coefficient. (After Darter *et al.* (1973a).)

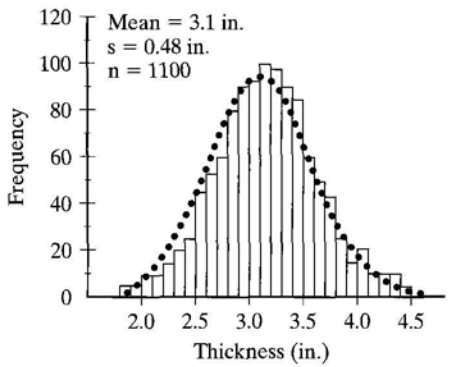


FIGURE 10.9

Frequency distribution of asphalt surfacing thickness (1 in. = 25.4 mm). (After Darter *et al.* (1973a).)

Downloaded From : www.EasyEngineering.net

Downloaded From : www.EasyEngineering.net

TABLE 10.7 Standard Deviations of Layer Thickness for Flexible Pavements

Material	Standard deviation
Hot mix asphalt	0.41 in.
Cement-treated base	0.68 in.
Aggregate base	0.79 in.
Aggregate subbase	1.25 in.

Note. 1 in. = 25.4 mm.
Source. After Darter *et al.* (1973a).

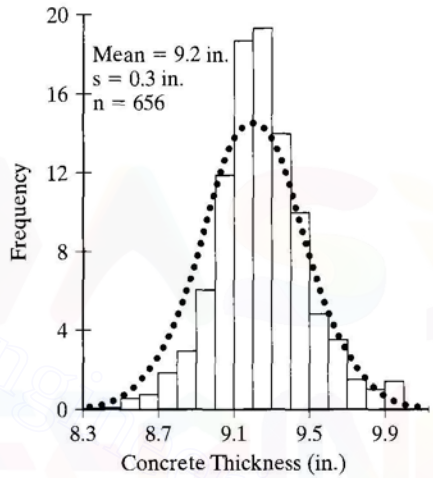


FIGURE 10.10
Frequency distribution of concrete slab thickness (1 in. = 25.4 mm). (After Kher and Darter (1973).)

is not a good representation of variance, because it increases with the decrease in thickness. Sherman (1971) presented results from California showing thickness variations in various pavement layers from 1962 to 1969. Based on over 8000 tests for each material, the standard deviations of thickness for four different paving materials are presented in Table 10.7. Using corresponding thicknesses of these layers, an average coefficient of variation of about 10% was obtained.

Thickness of Concrete Figure 10.10 shows a typical frequency distribution of concrete slab thickness, based on the measurement of individual cores. From the thicknesses obtained on 27 projects in four states, the standard deviations for three nominal pavement thicknesses are shown in Table 10.8. As can be seen, the standard deviation is not proportional to, or even dependent on, the average thickness of the pavement.

Modulus of Rupture of Concrete Figure 10.11 shows a typical frequency distribution of concrete modulus of rupture. The coefficient of variation for this particular project is 9.6%. The average coefficient of variation based on 15 projects is about 10.7% (Kher and Darter, 1973).

Downloaded From : www.EasyEngineering.net

Downloaded From : www.EasyEngineering.net

TABLE 10.8 Standard Deviations of Concrete Thickness for Rigid Pavements

Concrete thickness	Standard deviation	Number of projects
8 in.	0.32 in.	14
9 in.	0.29 in.	8
10 in.	0.29 in.	5

Note. 1 in. = 25.4 mm.
Source. After Kher and Darter (1973).

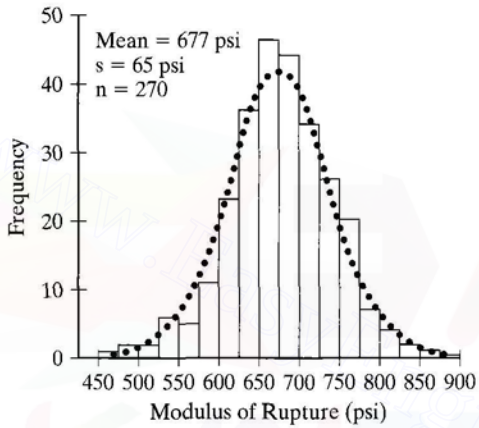


FIGURE 10.11
Frequency distribution of concrete modulus of rupture (1 psi = 6.9 kPa). (After Kher and Darter (1973).)

Initial Serviceability Index Figure 10.12 shows a typical frequency distribution for the initial serviceability index of a newly constructed flexible pavement and Figure 10.13 shows that of the AASHTO Road Test rigid pavements. Note that rigid pavements have a higher initial serviceability index and a lower coefficient of variation compared with flexible pavements.

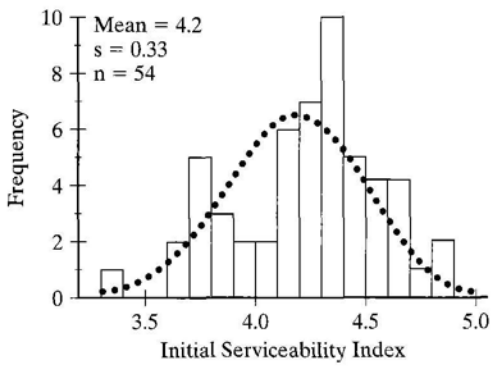


FIGURE 10.12
Initial serviceability index of flexible pavements (After Darter *et al.* (1973a).)

Downloaded From : www.EasyEngineering.net

Downloaded From : www.EasyEngineering.net

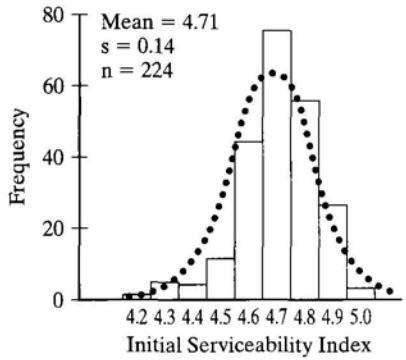


FIGURE 10.13

Initial serviceability index of concrete pavements. (After Kher and Darter (1973).)

10.3.2 Coefficients of Variation

The use of a coefficient of variation is a convenient way to specify the variability of design factors. Experience has shown that the standard deviations of most random variables are proportional to their average values. Therefore, a fixed coefficient of variation can be applied to a design factor regardless of its magnitude and dimensional unit. Even if the standard deviation is a constant and independent of the mean, such as pavement thickness, a coefficient of variation can still be easily figured out by simply dividing the standard deviation by the mean. Estimates on the coefficients of variation for some of the traffic and design factors are presented below (AASHTO, 1985).

Traffic Prediction Table 10.9 shows the coefficients of variation for design period traffic prediction. These coefficients fall in line with those originally suggested by Darter *et al.* (1973a). The overall coefficient of 42% is obtained as $[(35)^2 + (15)^2 + (10)^2 + (10)^2 + (10)^2]^{0.5}$.

Performance Prediction Table 10.10 shows the coefficients of variation of performance prediction for flexible pavements, Table 10.11 those for rigid pavements. The strength factor of each flexible layer is an indicator of its resilient modulus. The coefficients of variation of the resilient modulus vary from 10.0% for the asphalt surface layer to 18.2% for the subbase layer. If the concrete slab is placed on a solid or a layer foundation, a coefficient of variation of 15% may be assumed for the foundation. If the

TABLE 10.9 Coefficients of Variation for Design Period Traffic Prediction

Description	Symbol	Coefficient of variation (%)
Summation of EALF over % axle distribution	$\Sigma p_i F_i$	35
Initial average daily traffic	ADT_0	15
Traffic growth factor	G	10
Percentage of trucks	T	10
Average no. of axles per truck	A	10
Overall traffic prediction		42

Source. After AASHTO (1985).

Downloaded From : www.EasyEngineering.net

Downloaded From : www.EasyEngineering.net

TABLE 10.10 Coefficients of Variation for Performance Prediction of Flexible Pavements

Description	Symbol	Coefficient of variation (%)
Initial serviceability index	p_0	6.7
Surface strength factor	a_1	10.0
Surface thickness	D_1	10.0
Base strength factor	a_2	14.3
Base drainage factor	m_2	10.0
Base thickness	D_2	10.0
Subbase strength factor	a_3	18.2
Subbase drainage factor	m_3	10.0
Subbase thickness	D_3	10.0
Subgrade resilient modulus	M_R	15.0

Source. After AASHTO (1985).

TABLE 10.11 Coefficients of Variation for Performance Prediction of Rigid Pavements

Description	Symbol	Coefficient of variation (%)
Initial serviceability index	p_0	6.7
Slab thickness	D	4.0
Slab elastic modulus	E_c	10.0
Load transfer factor	J	5.0
Drainage factor	C_d	10.0
Modulus of subgrade reaction	k	35.0
Concrete modulus of rupture	S_c	10.0

Source. After AASHTO (1985).

slab is placed on a liquid foundation, a coefficient of variation of 35% may be assumed for the modulus of subgrade reaction, k.

10.3.3 Variances

All the variances discussed so far are caused by the variation of traffic and design factors. Other variances also have to be considered. The source and distribution of these variances are presented below.

Sources There are three sources of variance:

1. *Variances due to traffic or design factors.* Sampling errors in all traffic factors or construction errors in all design factors will increase the chance deviation between design and performance.
2. *Unexplained variance.* Many variables other than traffic and design factors give rise to chance deviations. For example, the allowable number of repetitions in concrete pavement design is governed by the stress ratio σ/S_c, according to Eq. 5.35. Even though the variation of σ/S_c caused by all the relevant design factors has been properly considered, the constants in the fatigue equations are

Downloaded From : www.EasyEngineering.net

Downloaded From : www.EasyEngineering.net

TABLE 10.12 Percentage Distribution of Overall Variance

Type of prediction	Source of variance		Flexible pavement		Rigid pavement
Traffic prediction	Traffic factor		14%		22%
	Unexplained		3%		4%
	Lack of fit		1%		1%
	Total variance	0.0429	18%	0.0429	27%
Performance prediction	Design factor		45%		42%
	Unexplained		5%		8%
	Lack of fit		32%		23%
	Total variance	0.1938	82%	0.1128	73%
Overall variance		0.2367	100%	0.1557	100%

Source. After AASHTO (1985).

actually not deterministic and can exhibit a range of variations. Disregarding these variations will increase the chance deviation between design and performance.

3. *Variance due to inadequacy of design procedure or lack of fit of design equation.* The application of a design procedure or equation always involves some degree of uncertainty, because of the use of simplifying assumptions or of neglect of certain design factors.

Distribution Table 10.12 shows the percentage distribution of overall variance when the AASHTO equations are used for pavement design. It can be seen that the variance due to performance prediction is much greater than that due to traffic prediction. The design equation for rigid pavements has a much smaller variance compared to that for flexible pavements. The large lack of fit variance in the performance prediction is due to the empirical nature of the AASHTO equations. This variance can be greatly reduced if mechanistic–empirical methods are used.

10.4 ROSENBLUETH METHOD

Taylor series expansion has been used for determining the mean and variance of a function. This method requires the knowledge of each term in the function and the existence and continuity of the first and second derivatives. Rosenblueth (1975) developed a simple method similar to the finite difference procedure that can be used directly to determine the mean and variance of any function without knowing its formulation.

10.4.1 Description of Method

In the design of concrete pavements by the probabilistic method, the most difficult part is to determine the maximum stress σ and its variance. From Eq. 10.8, the variance can be determined as

$$V[\sigma] = E[\sigma^2] - (E[\sigma])^2 \tag{10.61}$$

Downloaded From : www.EasyEngineering.net

Downloaded From : www.EasyEngineering.net

The expectations of σ and σ^2 can be determined by

$$E[\sigma^m] = \frac{1}{2}(\sigma_+^m + \sigma_-^m) \qquad \text{for one variable} \tag{10.62a}$$

$$E[\sigma^m] = \frac{1}{2^2}(\sigma_{++}^m + \sigma_{+-}^m + \sigma_{-+}^m + \sigma_{--}^m) \qquad \text{for two variables} \tag{10.62b}$$

$$E[\sigma^m] = \frac{1}{2^3}(\sigma_{+++}^m + \sigma_{++-}^m + \sigma_{+-+}^m + \sigma_{+--}^m + \sigma_{-++}^m + \sigma_{-+-}^m + \sigma_{--+}^m + \sigma_{---}^m) \qquad \text{for three variables} \tag{10.62c}$$

$$E[\sigma^m] = \frac{1}{2^4}(\sigma_{++++}^m + \sigma_{+++-}^m + \sigma_{++-+}^m + \sigma_{++--}^m + \sigma_{+-++}^m + \sigma_{+-+-}^m + \sigma_{+--+}^m + \sigma_{+---}^m + \sigma_{-+++}^m + \sigma_{-++-}^m + \sigma_{-+-+}^m + \sigma_{-+--}^m + \sigma_{--++}^m + \sigma_{--+-}^m + \sigma_{---+}^m + \sigma_{----}^m) \qquad \text{for four variables} \tag{10.62d}$$

The equation can be extended to any number of variables n by simply adding a plus sign and then a minus sign to the previous equation with a total of 2^n terms. Note that m is either 1 or 2, corresponding to $E[\sigma]$ and $E[\sigma^2]$.

If there are four random variables, it is necessary to determine the stress 16 times and then compute $E[\sigma]$ and $E[\sigma^2]$ by Eq. 10.62 and $V[\sigma]$ by Eq. 10.61.

10.4.2 Comparison with Taylor's Expansion

A comparison between Taylor's expansion and the Rosenblueth method can best be illustrated by a simple closed-form equation used previously by the U.S. Corps of Engineers (Turnbull and Ahlvin, 1957):

$$t = (0.231 \log n + 0.144)\sqrt{\frac{P}{8.1\,\text{CBR}} - \frac{A}{\pi}} \tag{10.63}$$

In this equation, t is the pavement thickness in inches, n is the number of passes or coverages, P is the wheel load in lb, CBR is the California bearing ratio of the subgrade, and A is the tire contact area in in.^2. Equation 10.63 can be written as

$$\log n = \frac{4.329t}{\sqrt{P/(8.1\,\text{CBR}) - A/\pi}} - 0.623 \tag{10.64}$$

Given that $t = 20$ in., $P = 30{,}000$ lb, CBR $= 4$, $A = 285$ in.^2 and that the coefficients of variations, $C[t]$, $C[P]$, $C[\text{CBR}]$, and $C[A]$, are all 0.1, determine the number of repetitions for 75% reliability. It is assumed that $\log n$ is normally distributed and that n is deterministic with no variations.

Taylor's Expansion We begin with the formula

$$E[\log n] = \frac{4.329 \times 20}{\sqrt{30{,}000/(8.1 \times 4) - 285/\pi}} - 0.623 = 2.373$$

Downloaded From : www.EasyEngineering.net

Downloaded From : www.EasyEngineering.net

The variances of $\log n$ due to the variances of t, p, CBR, and A can be computed by the first-order Taylor's expansion:

$$V[\log n]_t = \left(\frac{\partial \log n}{\partial t}\right)^2 V[t] = \left[\frac{4.329}{\sqrt{P/(8.1\ \text{CBR}) - A/\pi}}\right]^2 (t \times C[t])^2$$

$$= \frac{(4.329 \times 20 \times 0.1)^2}{30{,}000/(8.1 \times 4) - 285/\pi} = \frac{74.96}{835.21} = 0.0898$$

$$V[\log n]_p = \left\{ -\frac{1}{2}\frac{4.329t}{[P/(8.1\ \text{CBR}) - \text{A}/\pi]^{1.5}}\frac{1}{8.1\ \text{CBR}}\right\}^2 (P \times C[P])^2 = 0.0276$$

$$V[\log n]_{\text{CBR}} = \left\{\frac{1}{2}\frac{4.329t}{[P/(8.1\ \text{CBR}) - A/\pi]^{1.5}}\frac{P}{8.1(\text{CBR})^2}\right\}^2 (\text{CBR} \times C[\text{CBR}])^2 = 0.0276$$

$$V[\log n]_A = \left\{\frac{1}{2}\frac{4.329t}{[P/(8.1\ \text{CBR}) - A/\pi]^{1.5}}\frac{1}{\pi}\right\}^2 (A \times C[A])^2 = 0.0003$$

$$V[\log n] = 0.0898 + 0.0276 + 0.0276 + 0.0003 = 0.1453$$

$$S_{\log n} = \sqrt{0.1453} = 0.381$$

For 75% reliability, the area between the number of repetitions and the mean is 25%, as indicated in Figure 10.14. From Table 10.1, $z = -0.674$. From Eq. 10.35, $-0.674 = (\log n - 2.373)/0.381$, or $\log n = 2.373 - 0.674 \times 0.381 = 2.116$, so the allowable number of repetitions for 75% reliability is $n = 131$.

Rosenblueth's Procedure This procedure does not take derivatives on Eq. 10.64 with respect to t, P, CBR, and A, but instead requires the evaluation of $\log n$ 16 times. It is convenient to evaluate $\log n$ at plus and minus one standard deviation, and the results are presented in Table 10.13. The sum of $\log n$ is 38.1461, and the sum of $(\log n)^2$ is 93.3041. From Eq. 10.62*d*, $E[\log n] = 38.1461/16 = 2.3841$, which checks with the value 2.373 derived by Taylor's expansion, and $E[(\log n)^2] = 93.3041/16 = 5.8315$. From Eq. 10.61, $V[\log n] = 5.8315 - (2.3841)^2 = 0.1476$, which checks with the value 0.1453 derived by Taylor's expansion. For 75% reliability, $\log n = 2.3841 - 0.674 \times \sqrt{0.1476} = 2.125$, or $n = 133$, which checks with the value 131 derived by Taylor's expansion.

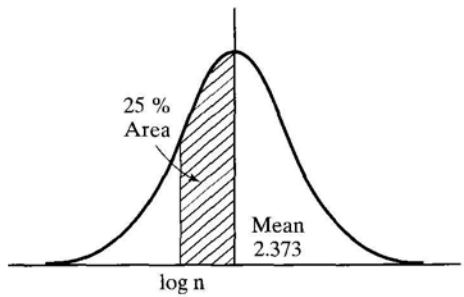


FIGURE 10.14
Allowable repetitions at 75% reliability.

Downloaded From : www.EasyEngineering.net

Downloaded From : www.EasyEngineering.net

TABLE 10.13 Computation of Log n and $(\log n)^2$ by Eq. 10.64

Term	t (in.)	P (lb)	CBR	A (in.)	log n	$(\log n)^2$
++++	22	33,000	4.4	313.5	2.6905	7.2387
+++−	22	33,000	4.4	256.5	2.6547	7.0474
++−+	22	33,000	3.6	313.5	2.3418	5.4839
++−−	22	33,000	3.6	256.5	2.3161	5.3643
+−++	22	27,000	4.4	313.5	3.0904	9.5504
+−+−	22	27,000	4.4	256.5	3.0402	9.2428
+−−+	22	27,000	3.6	313.5	2.6905	7.2387
+−−−	22	27,000	3.6	256.5	2.6547	7.0473
−+++	18	33,000	4.4	313.5	2.0880	4.3599
−++−	18	33,000	4.4	256.5	2.0587	4.2384
−+−+	18	33,000	3.6	313.5	1.8027	3.2498
−+−−	18	33,000	3.6	256.5	1.7817	3.1744
−−++	18	27,000	4.4	313.5	2.4152	5.8332
−−+−	18	27,000	4.4	256.5	2.3742	5.6366
−−−+	18	27,000	3.6	313.5	2.0880	4.3599
−−−−	18	27,000	3.6	256.5	2.0587	4.2384
				Sum	38.1461	93.3041

Note. 1 in. = 25.4 mm and 1 lb = 4.45 N.

SUMMARY

This chapter discusses the concept of reliability and its application to pavement design. Reliability is the probability of success. Depending on how the success or failure is defined, various design criteria, such as equivalent 18-kip single-axle loads, damage ratio or cracking index, and terminal serviceability index, may be used for computing reliability.

Important Points Discussed in Chapter 10

1. There are two methods of pavement design: deterministic and probabilistic. In the deterministic method, each design factor is assigned a fixed value, usually a value that is conservative compared with the mean. In the probabilistic method, each design factor has a mean and a variance. If any two of the design factors are correlated, their covariance must also be specified.
2. In the probabilistic method of design, the mean and variance of random variables can be determined by the Taylor series expansion. If the random variables are normally distributed, the second-order terms are small and can be neglected. Thus, Eq. 10.26 can be used to determine the mean and Eq. 10.29 or 10.30 can be used to determine the variance.
3. Various criteria can be used to evaluate the reliability of a design. The reliability can be obtained by comparing the mean value of the criterion with the required criterion. If the mean value is equal to the required value, the reliability of the design is 50%. To increase the reliability, the required criterion must be more stringent, depending on the variability of the mean value.
4. The most popular probabilistic method of pavement design is to compare the allowable number of load repetitions with the predicted number of load repetitions, all based on the mean values and each with its own coefficient of variation.

Downloaded From : www.EasyEngineering.net

Downloaded From : www.EasyEngineering.net

5. It is reasonable to assume that axle load repetitions have a log normal distribution. If an equivalent axle load is used for design purposes, the reliability is the probability that $\log D_r = \log W_T - \log W_t \leq 0$, in which D_r is the damage ratio or the ratio between the allowable number of load repetitions W_t and the predicted number of load repetitions W_T. When $\log D_r$ and its standard deviation are known, the probability that $\log D_r$ is not greater than 0 can be determined. If the axle loads are divided into a number of groups and a year is divided into several periods, each with a different W_t and W_T, the D_r is the summation of damage ratios for all load groups over all periods.
6. To apply the probabilistic method, it is necessary to know the coefficients of variation of various traffic and design factors. These coefficients depend on the method of construction and quality control and can be obtained only from past experiences and field measurements. In the absence of more definite information, the coefficients of variation presented in Tables 10.9, 10.10, and 10.11 can be used as a guide.
7. The Rosenblueth method can be used to determine the probabilistic solutions from the deterministic solutions. Any deterministic design method can easily be converted into a probabilistic method based solely on a number of deterministic solutions.

PROBLEMS

10.1 The probability function of a random variable x is

$$f(x) = \begin{cases} \frac{1}{3} & x = 0 \\ \frac{1}{2} & x = 1 \\ \frac{1}{6} & x = 2 \end{cases}$$

Find the mean and the variance of x. [Answer: 0.833, 0.472]

10.2 If $f(x) = t\exp(-t^2/2)$ when $t \geq 0$ and $f(x) = 0$ when $t < 0$, compute the mean and the variance of x. [Answer: 1.253, 0.429]

10.3 Two random variables, x and y, have the following probability functions:

$$f(x, y) = \begin{cases} \frac{1}{4} & x = 1 \quad y = 2 \\ \frac{1}{4} & x = 2 \quad y = 3 \\ \frac{1}{2} & x = 3 \quad y = 4 \end{cases}$$

Compute Cov$[x, y]$, $\rho(x, y)$, and $V[x + y]$. [Answer: 0.688, 1, 2.75]

10.4 The joint density function of two random variables, x and y, is

$$\begin{aligned} f(x, y) &= 6xy(2 - x - y) \quad \text{when } 0 \leq x \leq 1 \text{ and } 0 \leq y \leq 1 \\ &= 0 \quad \text{otherwise} \end{aligned}$$

Compute Cov$[x, y]$ and $\rho(x, y)$. [Answer: $-\frac{1}{144}, -\frac{5}{43}$]

10.5 The thickness of a full-depth asphalt pavement is determined by the equation

$$t = (0.25 + 0.125 \log n)\left[\sqrt{\left(\frac{75P}{\pi E}\right)^2 - a^2}\right]\sqrt[3]{\frac{E}{E_p}}$$

Downloaded From : www.EasyEngineering.net

Downloaded From : www.EasyEngineering.net

in which t is the thickness of asphalt concrete; n is the number of load repetitions; P is the wheel load; E is the modulus of the subgrade; a is the tire contact radius, and E_p is the modulus of asphalt concrete. Assume that $t = 6.5$ in., $n = 100{,}000$., $P = 9000$ lb, $E = 10{,}000$ psi, $a = 6$ in., and $E_p = 400{,}000$ psi and that the coefficients of variation of t, n, P, E, a, and E_p are all 10%. Also assume that t has a normal distribution and that the reliability is based on the required t obtained from the above equation versus the designed t of 6.5 in. Determine the reliability of the design based on Taylor series expansion. [Answer: 95.5%]

10.6 Solve Problem 10.5 by the Rosenblueth method. [Answer: 95.0%]

10.7 In Problem 10.5, it is assumed that $\log n$ is normally distributed and that the reliability is based on the n obtained from the equation and on the predicted n, namely, 100,000. Determine the reliability of the design based on Taylor series expansion. [Answer: 86.8%]

10.8 Solve Problem 10.7 by the Rosenblueth method. [Answer: 87.6%]

10.9 The number of load repetitions to induce the fatigue cracking of a certain hot mix asphalt is given by

$$N_f = f_1(\epsilon_t)^{-f_2}$$

For this problem, $f_1 = 0.00462$ with a coefficient of variation of 30%, $f_2 = 2.69$ with a coefficient of variation of 5%, the coefficient of correlation for f_1 and f_2 is -0.867, and the tensile strain ϵ_t is 0.0021 with a coefficient of variation of 10%. Compute the expectation and variance of N_f based on the first-order Taylor series expansion. [Answer: 73,770, 2.28×10^9]

10.10 The serviceability index of flexible pavements is determined as

$$\text{PSI} = \text{PSI}_0 - 1.91 \log(1 + \text{SV}) - 1.38\,\text{RD}^2 - 0.01\sqrt{C}$$

in which PSI_0 is the initial serviceability index, SV is the slope variance (10^{-6} rad), RD is the rut depth (in.), and C is the cracked area (sq ft/1000 sq ft). From the data shown in Table P10.11, determine (a) the expected value of PSI using second-order Taylor series expansion, (b) the variance of PSI, and (c) the terminal serviceability index for 95% reliability. [Answer: 3.21, 0.095, 2.7]

TABLE 10.11 Initial Serviceability and Physical Measurements

PSI_0		SV		RD		C
Mean	Variance	Mean (10^{-6} rad)	Variance (10^{-12} rad)	Mean (in.)	Variance (in.^{2})	Cracked area (ft^2/1000 ft^2)
4.2	0.06	1.572	0.32	0.284	0.003	120

10.11 Find $V[g]$ when $r = 1$, $C[r] = 0.2$ and

$$g = \frac{1 - 2r}{1 + r} + \frac{2 + r}{3 + 6r + r^2} + \frac{r}{(4 + r^2)(6 + r)}$$

[Answer: 0.01425]

10.12 Find $V[g]$ when $r = V[r] = 10$, $s = V[s] = 20$ and

$$g = \frac{1 - 2r - s}{1 + rs} + \frac{r + s}{3 + 6s + r^2} + \frac{rs}{(r + s)^2}$$

[Answer: 0.00139]

Downloaded From : www.EasyEngineering.net

Downloaded From : www.EasyEngineering.net

CHAPTER 11

Flexible Pavement Design

11.1 CALIBRATED MECHANISTIC DESIGN PROCEDURE

The design equations presented in the 1986 AASHTO design guide were obtained empirically from the results of the AASHO Road Test. To develop a mechanistic pavement analysis and design procedure suitable for future versions of AASHTO guide, a research project entitled "Calibrated Mechanistic Structural Analysis Procedures for Pavements" was awarded to the University of Illinois under NCHRP 1-26. The research included both flexible and rigid pavements, and a two-volume report, hereafter referred to as Report 1-26, was prepared for the National Cooperative Highway Research Program (NCHRP, 1990). Some of the information presented herein was obtained from Report 1-26.

The calibrated mechanistic procedure is a more specific name for the mechanistic–empirical procedure. It contains a number of mechanistic distress models that require careful calibration and verification to ensure that satisfactory agreement between predicted and actual distress can be obtained. The purpose of calibration is to establish transfer functions relating mechanistically determined responses to specific forms of physical distress. Verification involves the evaluation of the proposed models by comparing results to observations in other areas not included in the calibration exercise. This procedure has been used in several design methods, such as the Asphalt Institute method described in Section 11.2.6. However, these existing methods are based on many simplifying assumptions and are not as rigorous as is desirable. The recommended procedures presented in this section should be looked upon as the long-range goals to be accomplished in the future.

11.1.1 General Methodology

Figure 11.1 shows a general methodology for flexible pavement design. In the figure, it is assumed that the materials to be used for the pavement structure are known *a priori* and that only the pavement configuration is subjected to design iterations. If changing the pavement configuration does not satisfy the design requirements, it might be

Downloaded From : www.EasyEngineering.net

Downloaded From : www.EasyEngineering.net

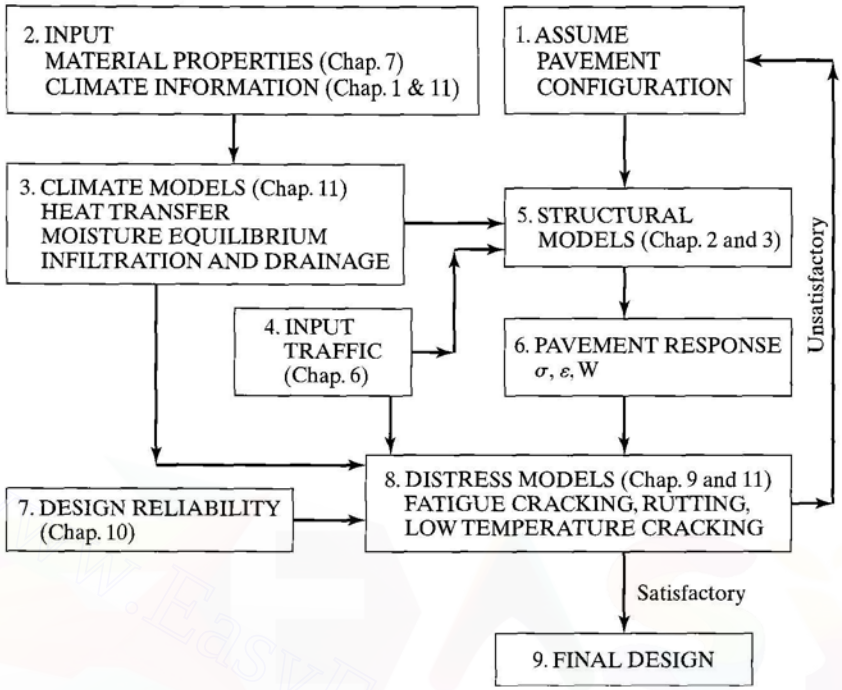


FIGURE 11.1

Methodology of calibrated mechanistic procedure for flexible pavement design.

necessary to change the types and properties of the materials to be used. Once a new material is selected, the process is repeated until a satisfactory design is obtained. Also shown in the figure are the chapters covering the appropriate subjects.

Explanation of Figure 11.1

1. Pavement configuration includes the number of layers, the thickness of each layer, and the type of materials.
2. The basic material properties for the structural models are the resilient moduli of HMA, base, subbase, and subgrade; those for the distress models involve the various failure criteria, one for each distress. If temperature and moisture at different times of the year vary significantly, it is unreasonable to use the same modulus for each layer throughout the entire year. Each year should be divided into a number of periods, each with a different set of moduli based on the climatic data specified.
3. Climatic models include the heat transfer model (Dempsey and Thompson, 1970) for determining the temperature distribution with respect to space and time, the moisture equilibrium model (Dempsey *et al.*, 1986) for determining the final moisture distribution in the subgrade, and the infiltration and drainage model (Liu and Lytton, 1984) for predicting the degree of saturation of granular bases. These models are described in Section 11.1.2.

Downloaded From : www.EasyEngineering.net

Downloaded From : www.EasyEngineering.net

4. Traffic should be divided into a number of load groups, each with different load magnitudes and configurations and different numbers of load repetitions. When the design is based on each type of distress, it is unreasonable to use an equivalent single-axle load, because the equivalent factor for one type of distress is different from that for others. The load magnitude and configuration—for example; wheel spacing, contact radius, and contact pressure—are used in the structural models, but the number of repetitions is used in the distress models.
5. The finite element models can analyze nonlinear pavement systems more realistically than any other structural model by considering the variation of modulus within each layer. More about structural models is presented in Section 11.1.3.
6. Pavement responses include stresses σ, strains ϵ, and deflections w. Theoretically, only those responses that contribute to each distress should be evaluated by the structural models and used in the distress models. However, if the responses can be related to surface deflections, it is possible to use surface deflections as input to the distress models. The most attractive feature of surface deflections is that they can be easily, rapidly, and inexpensively measured by utilizing automatic equipment.
7. Variabilities of materials, climate, traffic, and construction practice require the use of a probabilistic method to evaluate pavement distress. To determine the design reliability, the variances or coefficients of variation of some input parameters reflecting materials, climate, traffic, and even layer thicknesses must also be specified in steps 1 to 4 so that the variances of σ, ϵ, and w can be computed for use in the distress models.
8. Distress models include fatigue cracking, rutting, and low-temperature cracking. The roughness or performance model can also be included. If the reliability for a certain distress is less than the minimum level required, the assumed pavement configuration should be changed, and steps 5, 6, and 8 should be repeated, until the required level of reliability is met. More about distress models is presented in Section 11.1.4.
9. The final design is selected when the assumed pavement thicknesses satisfy the reliability requirement for each type of distress.

11.1.2 Climate Models

Temperature and moisture are significant climatic inputs for pavement design. The modulus of the HMA depends on pavement temperature; the moduli of the base, subbase, and subgrade vary appreciably with moisture content. Report 1-26 indicated that the current technology, as utilized in the climatic–materials–structural (CMS) model developed at the University of Illinois (Dempsey *et al.*, 1986), is adequate for characterizing the pavement temperature regime, but that the capabilities for moisture modeling are not as advanced as those for temperature modeling. The strength and modulus of cohesive soils (and of granular materials with a high percentage of fines) are very sensitive to even a small change in moisture content, say ±1%. Report 1-26 also indicated that the moisture equilibrium model in the CMS model for determining subgrade moisture is a reasonable and practical choice for design purpose.

Downloaded From : www.EasyEngineering.net

Downloaded From : www.EasyEngineering.net

Heat Transfer Model The heat transfer model was originally developed at the University of Illinois (Dempsey and Thompson, 1970) for evaluating frost action and temperature regime in multilayered pavement systems. The model applies the finite difference method to solve the following Fourier equation for one-dimensional heat flow:

$$\frac{\partial T}{\partial t} = \alpha \frac{\partial^2 T}{\partial z^2} \tag{11.1}$$

Here, T is the temperature, t is the time, z is the depth below surface, and α is the thermal diffusivity, which is related to the thermal conductivity and heat capacity of the pavement materials. Given the initial temperature distribution and the two boundary conditions (at the pavement surface and at a depth H below the surface), Eq. 11.1 can be solved.

Convection and radiation play a dominant role in transferring heat between the air and the pavement surface, whereas conduction plays a separate role in transferring heat within the pavement system. The total depth H is a variable input parameter in the heat transfer model. It can be determined from a study of deep soil temperatures at a given geographic location. For example, studies of soil temperatures in northern Illinois have indicated that the ground temperature is about 51°F (10.6°C) 12 ft (3.7 m) below surface. The temperature at this depth can be used as a boundary to solve Eq. 11.1.

Inputs to the heat transfer model are the climatic data and the thermal properties of paving materials and soils. The climatic data include maximum and minimum daily air temperatures, percent sunshine, and wind speed. The thermal properties include thermal conductivity, heat capacity, and latent heat of fusion. The model recognizes three sets of thermal properties, depending on whether the material is in an unfrozen, freezing, or frozen condition. To facilitate the application of the heat transfer model to various pavement-related problems, a comprehensive climate data base for the state of Illinois was developed by Thompson *et al.* (1987).

Moisture Equilibrium Model The moisture equilibrium model in the CMS model (Dempsey *et al.*, 1986) is based on the assumption that the subgrade cannot receive moisture by infiltration through the pavement. Any rainwater will drain out quickly through the drainage layer to the side ditch or longitudinal drain, so the only water in the subgrade is the capillary water caused by the water table. Because of the thermodynamic relationship between soil suction and moisture content, a simple way to determine the moisture content in a soil is to determine its suction, which is related to the pore water pressure.

Figure 11.2 shows the suction–moisture curves for five different soils with varying clay contents, as indicated by the numerals in parentheses under each soil title. These curves were obtained in the laboratory by drying tests, in which different levels of vacuum or suction were applied to a wet soil specimen until the moisture was reduced to an equilibrium value. The suction is expressed in the pF scale, which is the logarithm of water tension in cm, as defined by Schofield (1935). The corresponding values in terms of psi are shown on the left scale.

It can be seen that suction increases as the moisture content decreases or the clay content increases. The increase in suction is due to the smaller menisci formed between

Downloaded From : www.EasyEngineering.net

Downloaded From : www.EasyEngineering.net

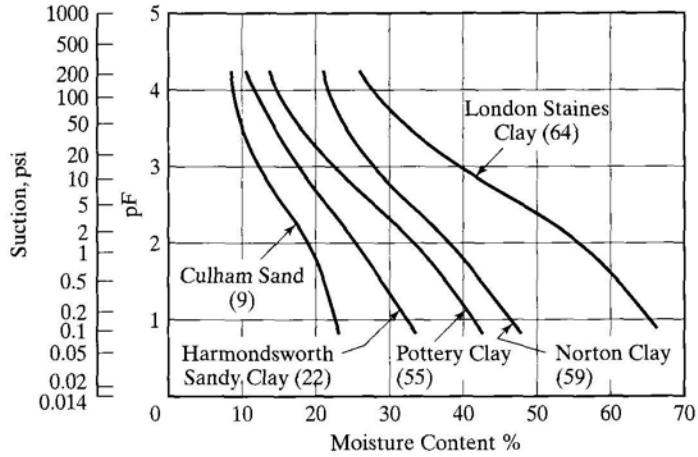


FIGURE 11.2

Soil suction–moisture content curves for different soils (1 psi = 6.9 kPa). (After Road Research Laboratory (1952).)

soil particles. In the CMS model, empirical relationships were used to define the suction–moisture curve based on the liquid limit, the plasticity index, and the saturated moisture content of the soil.

When there is no loading or overburden pressure, suction is equal to the negative pore pressure. When a load or overburden is applied to an unsaturated soil with a given moisture content or suction, the suction or moisture content remains the same but the pore pressure becomes less negative. The relationship between suction and pore pressure can be expressed as

$$u = S + \alpha p \tag{11.2}$$

in which u is the pore pressure when soil is loaded; S is the soil suction, which is a negative pressure; p is the applied pressure (or *overburden*), which is always positive; and α is the compressibility factor, varying from 0 for unsaturated, cohesionless soils to 1 for saturated soils. For unsaturated cohesive soils, α is related to the plasticity index PI by (Black and Croney, 1957)

$$\alpha = 0.03 \times \text{PI} \tag{11.3}$$

The pore pressure in a soil depends solely on its distance above the ground-water table:

$$u = -z\gamma_w \tag{11.4}$$

Here, z is the distance above the water table, and γ_w is the unit weight of water. This simple fact can be explained by considering soils as a bundle of capillary tubes with varying sizes. Water will rise in each of these capillary tubes to an elevation that depends on the size of the tube. At any distance z above the water table, a large number of menisci will form at the air–water interfaces, causing a tension at each elevation

Downloaded From : www.EasyEngineering.net

Downloaded From : www.EasyEngineering.net

corresponding to the height of capillary rise. Combining Eqs. 11.2 and 11.4 yields

$$S = -z\gamma_w - \alpha p \tag{11.5}$$

The procedures for determining the equilibrium moisture content at any point in a pavement system can be summarized as follows:

1. Determine the distance z from the point to the water table.
2. Determine the loading or overburden pressure p.
3. Determine the compressibility factor α from Eq. 11.3.
4. Determine the suction S from Eq. 11.5.
5. Determine the moisture content from the suction–moisture curve.

Example 11.1:

Figure 11.3 shows an 8-in. (203-mm) full-depth asphalt pavement on a subgrade composed of two different materials. The top 16 in. (406 mm) of subgrade is a Culham sand; below it is a Norton clay with a PI of 18. The relationship between the suction and moisture content of these two soils is shown in Figure 11.2. The water table is located 12 in. (305 mm) below the top of the clay. The unit weight γ of each material is shown in the figure. Predict the moisture contents at point A on top of the clay, point B at the bottom of the sand layer, and point C on top of the sand layer.

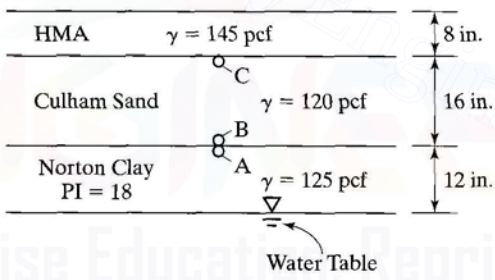


FIGURE 11.3
Example 11.1 (1 in. = 25.4 mm, 1 pcf = 157.1 N/m^3).

Solution: At point A, the overburden pressure $p = (8 \times 145 + 16 \times 120)/12 = 256.7$ psf. From Eq. 11.3, $\alpha = 0.03 \times 18 = 0.54$. From Eq. 11.5, $S = -1 \times 62.4 - 0.54 \times 256.7 = -201.0$ psf $= -1.40$ psi. From Figure 11.2, the moisture content is 38%.

At point B, $\alpha = 0$ and, from Eq. 11.5, $S = -62.4$ psf $= -0.43$ psi. From Figure 11.2, the moisture content is 21%.

At point C, from Eq. 11.5, $S = -(12 + 16) \times 62.4/12 = -145.6$ psf $= 1.01$ psi. From Figure 11.2, the moisture content is 19.5%.

Infiltration and Drainage Model The infiltration and drainage model developed by Texas A&M University (Liu and Lytton, 1984) can be used to evaluate the effects of rainfall on the degree of saturation and the resilient moduli of the base course and subgrade. The degree of saturation for the base and the subgrade is predicted daily by considering the probability distribution of the amount of rainfall, the probabilities of wet and dry days, the infiltration of water into the pavement through cracks and joints, the

Downloaded From : www.EasyEngineering.net

Downloaded From : www.EasyEngineering.net

drainage of the base course, and the wet and dry probabilities of pavement sublayers. Under a FHWA contract, Texas A&M University is in the process of upgrading the infiltration and drainage model. A research study has been initiated by the FHWA to combine the CMS model, the infiltration and drainage model, and the frost model, which is a mathematical model of coupled heat and moisture flow in soils developed by the Cold Regions Research and Engineering Laboratory (Johnson *et al.*, 1986).

11.1.3 Structural Models

Report 1-26 recommended the use of elastic layer programs (ELP) and the ILLI-PAVE finite element program for the development of a future AASHTO design guide. It suggested the use of the modulus–depth relationship obtained from ILLI-PAVE to establish the various moduli for the ELP, thus capitalizing on the stress-sensitive feature of ILLI-PAVE and the multiple wheel capability of ELP.

Finite Element Models The two finite element models, ILLI-PAVE and MICH-PAVE, are described in Section 3.3.2. One limitation of ILLI-PAVE and MICH-PAVE is the representation of wheel loading by a single circular area. As shown in Figure 3.24, the use of a single wheel to replace a set of duals is unsafe for thin asphalt pavements because the larger contact radius of a single wheel makes the tensile strain at the bottom of the asphalt layer smaller under a single wheel than under dual wheels. A finite element program capable of analyzing multiple wheels is highly desirable. Although the program will be very complex and will require an extensive interpolation and superposition of stresses, there is no reason that such a program cannot be developed. When the iteration method is used for nonlinear analysis, the superposition principle can still be applied. The system is considered linear during each iteration, and the stresses due to various wheel loads can be superimposed to determine the modulus of each element.

Elastic Layer Programs A large number of elastic layer programs are available. Three programs were used to compare results with KENLAYER: ELSYM5 in Table 3.3, VESYS in Table 3.5, and DAMA in Tables 3.6 and 3.7. KENLAYER (as presented in this book) is believed to be the most comprehensive structural model. It considers a variety of cases not available elsewhere and can be applied to layer systems consisting of linear elastic, nonlinear elastic, and viscoelastic materials under single- and multiple-wheel loads.

A major deficiency of KENLAYER is the nonlinear analysis, wherein a stress point must be specified for each nonlinear layer to compute its modulus for the state of the stresses. The assumption of a uniform modulus throughout each nonlinear layer is not theoretically correct, but its effects on the critical pavement responses are believed to be small. The most critical responses always occur near the loads, and the layer moduli near the loads have the most effect, so a stress point directly under the center of a single wheel or between the centers of dual wheels can reasonably be selected. It was demonstrated in Section 3.3.2 that, by dividing a nonlinear granular layer into a number of 2-in. (51-mm) layers, KENLAYER could yield critical strains very close to those obtained by MICH-PAVE.

Downloaded From : www.EasyEngineering.net

Downloaded From : www.EasyEngineering.net

11.1.4 Distress Models

Distress models are sometimes called transfer functions that relate structural responses to various types of distress. Distress models are the weak link in the mechanistic–empirical methods, and extensive field calibration and verification are needed to establish reliable distress predictions.

Usable transfer functions for HMA fatigue and subgrade rutting are available, but those for the rutting of HMA and granular materials are marginal and require further development. Report 1-26 indicated that the use of the "rutting rate" concept advanced by Ohio State University (Majidzadeh *et al.*, 1976) appears to be very promising, because it can be applied to all paving materials, including HMA, granular materials, and fine-grained soils. The report also recommended the use of the Shahin–McCullough thermal cracking model (1972) as a checking procedure to assess the thermal cracking potential after the thickness design is completed; if it is unsatisfactory, a softer asphalt cement should be used. Because HMA rutting is the major cause of permanent deformation on heavily traveled pavements with thick HMA, the design procedure may be simplified by checking the rutting potential after the thickness design is completed. If it is unsatisfactory, the selection of different mixture design procedures and practices should be made until the rut depth is reduced to the acceptable limit.

Fatigue Cracking Models Miner's (1945) cumulative damage concept has been widely used to predict fatigue cracking. It is generally agreed that the allowable number of load repetition is related to the tensile strain at the bottom of the asphalt layer. The amount of damage is expressed as a damage ratio between the predicted and the allowable number of load repetitions. Damage occurs when the sum of damage ratios reaches the value 1. Because of variabilities, damage will not occur all at once when the ratio reaches exactly 1. If mean parameter values are used for design, a damage ratio of 1 indicates that the probability of failure is 50%—that is, that 50% of the area will experience fatigue cracking. By assuming the damage ratio to have a log normal distribution, the probability of failure, or the percentage of area cracked, can be computed and checked against field performance.

The major difference in the various design methods is the transfer functions that relate the HMA tensile strains to the allowable number of load repetitions. In the Asphalt Institute and Shell design methods, the allowable number of load repetitions N_f to cause fatigue cracking is related to the tensile strain ϵ_t at the bottom of the HMA and to the HMA modulus E_1 by

$$N_f = f_1(\epsilon_t)^{-f_2}(E_1)^{-f_3} \tag{3.6}$$

For the standard mix used in design, the Asphalt Institute equation for 20% of area cracked is

$$N_f = 0.0796(\epsilon_t)^{-3.291}(E_1)^{-0.854} \tag{11.6}$$

and the Shell equation is

$$N_f = 0.0685(\epsilon_t)^{-5.671}(E_1)^{-2.363} \tag{11.7}$$

Downloaded From : www.EasyEngineering.net

Downloaded From : www.EasyEngineering.net

Because f_2 is much greater than f_3, the effect of ϵ_t on N_f is much greater than that of E_1. Therefore, the E_1 term may be neglected:

$$N_f = f_1(\epsilon_t)^{-f_2} \tag{11.8}$$

Equation 11.8 has been used by several agencies:

Illinois Department of Transportation (Thompson, 1987)

$$N_f = 5 \times 10^{-6} (\epsilon_t)^{-3.0} \tag{11.9}$$

Transport and Road Research Laboratory (Powell *et al.*, 1984)

$$N_f = 1.66 \times 10^{-10} (\epsilon_t)^{-4.32} \tag{11.10}$$

Belgian Road Research Center (Verstraeten *et al.*, 1982)

$$N_f = 4.92 \times 10^{-14} (\epsilon_t)^{-4.76} \tag{11.11}$$

It can be seen that the exponent f_2 of the fatigue equations varies from 3.0 to 5.671, but the coefficient f_1 varies over several orders of magnitude—from 5×10^{-6} to 4.92×10^{-14}. The exponents f_2 and f_3 are usually determined from fatigue tests on laboratory specimens, but f_1 must shift from laboratory to field values by calibration. Pell (1987) indicated that the shift factor can range from 5 to 700. Differences in materials, test methods, field conditions, and structural models imply that a large variety of transfer functions is expected. No matter what transfer function is used, it is important to calibrate the function carefully, by applying an appropriate shift factor, so that the predicted distress can match field observations.

Rutting Models Two procedures have been used to limit rutting: one to limit the vertical compressive strain on top of the subgrade, the other to limit the total accumulated permanent deformation on the pavement surface based on the permanent deformation properties of each individual layer. In the Asphalt Institute and Shell design methods, the allowable number of load repetitions N_d to limit rutting is related to the vertical compressive strain ϵ_c on top of the subgrade by

$$N_d = f_4 (\epsilon_c)^{-f_5} \tag{11.7}$$

Equation 3.7 is also used by several other agencies, with the values for f_4 and f_5 shown in Table 11.1.

As can be seen from Table 11.1, the exponent f_5 falls within a narrow range, but the coefficient f_4 varies a great deal. Both f_4 and f_5 should be calibrated by comparing the predicted performance with field observations.

In the subgrade strain method, it is assumed that, if the subgrade compressive strain is controlled, reasonable surface rut depths will not be exceeded. For example, designs by the Asphalt Institute method are expected not to have a rut depth greater than 0.5 in. (12.7 mm), and designs by the TRRL procedure are expected not to have a rut depth of more than 0.4 in. (10.2 mm). The Shell method has a suggested procedure for estimating permanent deformation, as shown by Eq. 7.51. Without such a procedure, HMA rutting can best be addressed by improving the material selection and mixture design.

Downloaded From : www.EasyEngineering.net

Downloaded From : www.EasyEngineering.net

TABLE 11.1 Subgrade Strain Criteria Used by Various Agencies

Agency	f_4	f_5	Rut depth (in.)
Asphalt Institute	1.365×10^{-9}	4.477	0.5
Shell (revised 1985)			
50% reliability	6.15×10^{-7}	4.0	
85% reliability	1.94×10^{-7}	4.0	
95% reliability	1.05×10^{-7}	4.0	
U.K. Transport & Road Research Laboratory (85% reliability)	6.18×10^{-8}	3.95	0.4
Belgian Road Research Center	3.05×10^{-9}	4.35	

Note. 1 in. = 25.4 mm.

Unless standard thicknesses and materials are used for design, the evaluation of surface rutting based on the subgrade strain does not appear to be reasonable. Under heavy traffic with thicker HMA, most of the permanent deformation occurs in the HMA, rather than in the subgrade. Because rutting is caused by the accumulation of permanent deformation over all layers, it is more reasonable to determine the permanent deformation in each layer and sum up the results, as described by the direct method in Section 7.4.1.

Many methods are available to determine rut depth. The VESYS method was described in Section 7.4.1. In VESYS-V, a new option similar to the direct method was added. In this section, only the Ohio State model, which was recommended in Report 1-26, is described.

Similar to VESYS, the Ohio State model also assumes a linear relationship between permanent strain ϵ_p and number of load repetitions N when plotted in log scales. However, instead of total rutting, the rutting rate is considered, as indicated by

$$\frac{\epsilon_p}{N} = A(N)^{-m} \tag{11.12}$$

in which A is an experimental constant depending on material type and state of stress and m is an experimental constant depending on material type. Figure 11.4 shows typical straight-line relationships between $\log(\epsilon_p/N)$ and $\log N$ of HMA specimens under different stress and temperature conditions. All lines are nearly parallel, indicating that the value of m, which is the slope of the straight lines, is a constant independent of the levels of stress and temperature.

Equation 11.12 can be written as

$$\epsilon_p = A(N)^{1-m} \tag{11.13}$$

Compared with Eq. 7.41 in VESYS,

$$m = \alpha \tag{11.14a}$$

and

$$A = \frac{\epsilon\mu}{1 - \alpha} \tag{11.14b}$$

Downloaded From : www.EasyEngineering.net

Downloaded From : www.EasyEngineering.net

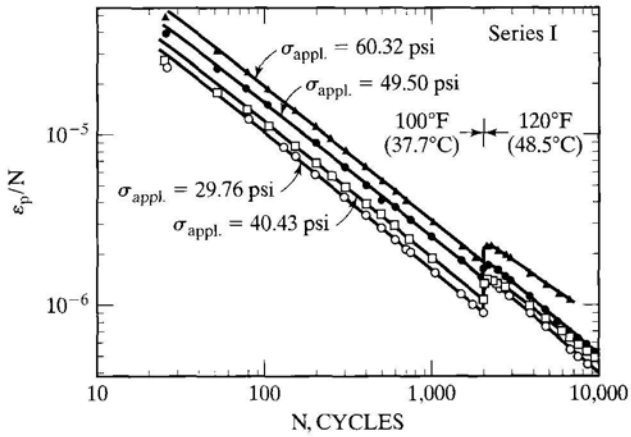


FIGURE 11.4

Typical relationship between ϵ_p/N and N for HMA specimens (1 psi = 6.9 kPa). (After Khedr (1986).)

VESYS calls the permanent deformation parameters α and μ; Ohio State calls them A and m. To facilitate the computation of permanent deformation without subdividing the system into a large number of layers, VESYS relates the permanent strain ϵ_p to the resilient strain ϵ; the Ohio State model applies the direct method and defines the parameter A directly as a material property. Khedr (1986) conducted a large number of repeated load tests on HMA specimens and found a straight-line relationship between log A and $\log(M_R/\sigma_d)$, as shown in Figure 11.5. Therefore, the value of A can be expressed as

$$A = a\left(\frac{M_R}{\sigma_d}\right)^{-b} = a(\epsilon)^b \tag{11.15}$$

in which a and b are material constants, ϵ is the resilient strain, M_R is the resilient modulus, and σ_d is the applied stress.

A comparison of Eqs. 11.14*b* and 11.15 shows that VESYS assumes that the parameter A is proportional to ϵ, whereas the Ohio State model assumes that A is proportional to $(\epsilon)^b$. It was reported that rut depths were generally seriously underpredicted by VESYS (Rauhut *et al.*, 1977). The addition of a new material constant, b, certainly gives the Ohio State model more flexibility in predicting rut depths. The final form of the Ohio State model is

$$\epsilon_p = a(\epsilon)^b (N)^{1-m} \tag{11.16}$$

Considerable experimental data (Majidzadeh *et al.*, 1976, 1978; Khedr, 1985) indicate that m varies within a narrow range for cohesive soils and granular materials. A typical value is 0.88 for cohesive soils and 0.8 for granular materials. The A term is quite variable and is dependent on material properties, repeated stress states, and environmental conditions. Several equations were developed to relate A to these parameters. When A and m are known for each material in the pavement, the rut depth, or the permanent deformation on the surface, can be determined by the direct method, as described in Section 7.4.1.

Downloaded From : www.EasyEngineering.net

Downloaded From : www.EasyEngineering.net

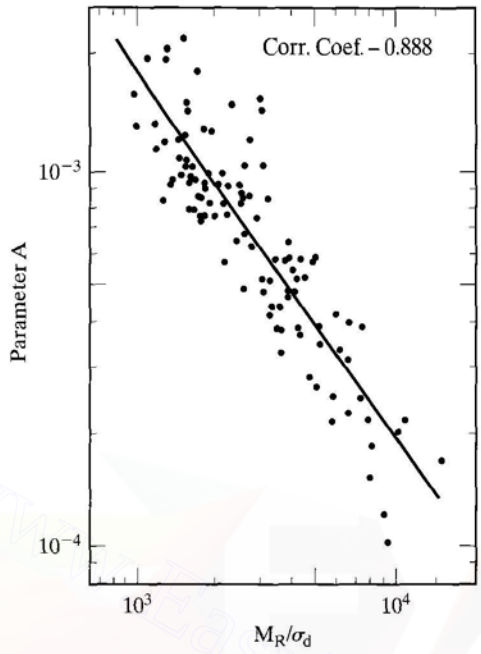


FIGURE 11.5

Relationship between parameter A and M_R/σ_d. (After Khedr (1986).)

Thermal Cracking Models There are two forms of thermal cracking in asphalt pavements: low-temperature cracking, and thermal fatigue cracking. The mechanism of low-temperature cracking is illustrated in Figure 11.6. When the pavement temperature decreases, the tensile stress always increases, but the tensile strength increases only to a maximum and then decreases. Low-temperature cracking occurs when the thermal tensile stress in the HMA exceeds its tensile strength. If the tensile stress is smaller

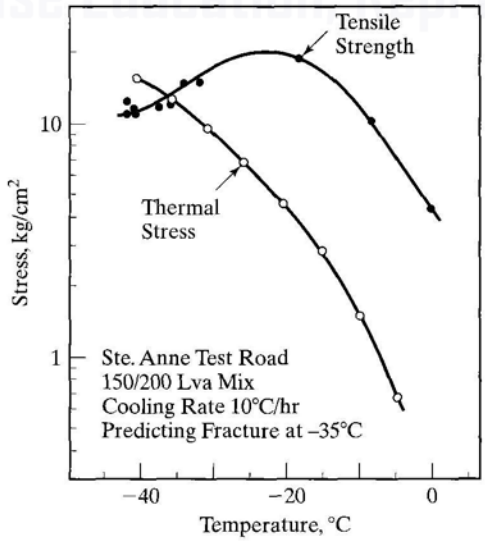


FIGURE 11.6

Mechanism of low-temperature cracking. (After McLeod (1970).)

Downloaded From : www.EasyEngineering.net

Downloaded From : www.EasyEngineering.net

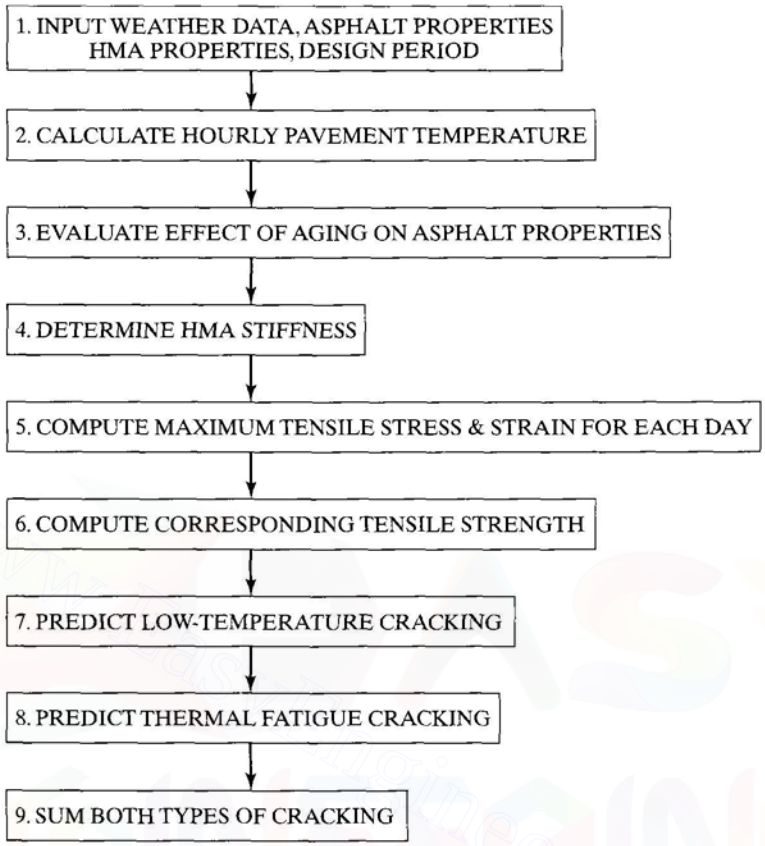


FIGURE 11.7

Analysis procedures for Shahin–McCullough model.

than the tensile strength, the pavement will not crack under a single daily temperature cycle but could still crack under a large number of cycles. This is called thermal fatigue cracking, which occurs when the fatigue consumed by daily temperature cycles exceeds the HMA fatigue resistance.

Several mechanistic thermal cracking models are available—for example, those developed by Finn *et al.* (1986), Ruth *et al.* (1982), Lytton *et al.* (1983), and Shahin and McCullough (1972). The latter two are the most comprehensive models that examine both low-temperature and thermal fatigue cracking and were recommended by Report 1-26 for further studies. They use the same basic structure to examine the accumulation of damage but with very different approaches. The model developed by Lytton *et al.* is more theoretical and is based on the principles of viscoelastic fracture mechanics, whereas that from Shahin and McCullough is more phenomenal and much easier to understand. Figure 11.7 shows how thermal cracking is analyzed in the Shahin–McCullough model.

Downloaded From : www.EasyEngineering.net

Downloaded From : www.EasyEngineering.net

Explanation of Figure 11.7

1. Weather data include mean annual air temperature, annual range in air temperature, daily range in air temperature, mean annual solar radiation, July average solar radiation, mean annual wind velocity, and surface absorptivity. Asphalt properties include original penetration, original softening point, and percentage of penetration after the thin film oven test. HMA properties include thermal conductivity, specific heat, density, mix composition, coefficient of thermal contraction, maximum tensile strength, and fatigue characteristics.
2. From the mean annual air temperature, the mean annual solar radiation, and the July average solar radiation, the mean daily air temperature and mean daily solar radiation can be estimated. For each day, the hourly temperatures at a designated point in the pavement, usually on the pavement surface where the thermal cracking initiates, can be computed by a modified version of Barber's equation (1957).
3. The effect of aging on penetration and the ring and ball softening point of the asphalt was considered by two empirical equations. The penetration at any time after HMA placement is a function of time duration, original penetration, percentage of void in HMA, and percentage of original penetration after the thin film oven test. The softening point is a function of time duration, original softening point, and the percentage of original penetration after the thin film test. Both equations were used in conjunction with the Van der Poel nomograph to estimate the asphalt stiffness as a function of time.
4. Van der Poel's nomograph, shown in Figure 7.19, was applied to estimate the stiffness of asphalt, which was then used to determine the stiffness of HMA, based on the volume concentration of the aggregate. Two techniques were established to computerize the nomograph. The first technique, which is more accurate but is limited to three loading times (0.01 s, 0.02 s, and 1 h), is to convert the nomograph to a computerized form. The second technique, which is less accurate but can be extended to other times of loading, is to develop predictive models through the use of regression.
5. Thermal stresses can be estimated by assuming the temperature drop to be uniform and dividing it into equal intervals ΔT of 1-h duration. Starting from the maximum temperature and going down on a hourly basis to the minimum temperature, estimate the stiffness at the middle of the temperature interval. The increase in thermal stress can be expressed as

$$\Delta\sigma(t, \Delta T) = \alpha_t \, \Delta T S_m(t, \overline{\Delta T}) \tag{11.17}$$

in which $\Delta\sigma(t, \Delta T)$ is the increase in thermal stress for a given time of loading t and temperature interval ΔT; α_t is the coefficient of thermal contraction; and S_m is the HMA stiffness at a given time of loading and at the mean value of ΔT. The increments of thermal stresses obtained from Eq. 11.17 are accumulated to estimate the maximum stress and strain for that day:

$$\sigma(t, T) = \alpha_t \sum \{\Delta T S_m(t, \overline{\Delta T})\} \tag{11.18}$$

Downloaded From : www.EasyEngineering.net

Downloaded From : www.EasyEngineering.net

In solving Eq. 11.18, it is assumed that the stress and strain are negligible at the end of each day and that the maximum daily stress occurs at the minimum daily pavement temperature as a result of accumulation of thermal stress increments during the day. Asphalt stiffness is affected strongly by the loading time, which is not the time corresponding to ΔT but depends on the rate of temperature drop. The time of loading was determined by matching the maximum thermal stress measured in a laboratory specimen under the given rate of temperature drop with that computed from Eq. 11.18.

6. The extent of low-temperature cracking is evaluated by comparing the maximum tensile stress σ with the tensile strength H of HMA at the corresponding temperature. The temperature–strength relationship can be specified directly or can be computed by Heukelom's procedure (1966) based on the maximum HMA tensile strength.
7. Given the coefficients of variation of α_t, T, and S_m, the variance of σ can be determined, which, in combination with the variance of H, results in the total variance. If both stress and strength are normally distributed random variables, the probability of failure, which indicates the percentage of area cracked, can be determined from

$$\text{Probability (failure)} = \text{Probability } (\sigma - H > 0) \tag{11.19}$$

The area of cracking can be converted to linear cracking by assuming that 1 ft (0.3 m) of linear cracking is equivalent to 5 ft^2 (0.46 m^2) of area cracking. Note that, in VESYS, 1 ft (0.3 m) of low-temperature cracking is equivalent to 3 ft^2 (0.28 m^2) of area cracking.

8. The analysis of thermal fatigue cracking is similar to that of fatigue cracking under repeated loading. Indeed, same fatigue equation can be used:

$$N_f = K_1 \left(\frac{1}{\epsilon_t}\right)^{K_2} \tag{10.68}$$

In this equation, N_f is the allowable number of cycles to cause fatigue cracking under tensile strain ϵ_t, and K_1 and K_2 are fatigue constants based on constant strain tests. Because K_1 and K_2 vary with the HMA stiffness, two sets of values, one at a very low stiffness and the other at a very high stiffness, must be specified; then the values at any intermediate stiffness can be interpolated. There is only one thermal cycle per day, so the damage ratio can be expressed as

$$c = \sum_{i=1}^{n} \frac{1}{N_i} \tag{11.20}$$

in which n is the number of days and N_i is the allowable number of repetitions for the ith day. If N is assumed to have a log normal distribution with a given standard deviation, then the probability of failure can be determined from

$$\text{Probability (failure)} = \text{Probability } (\log c > 0) \tag{11.21}$$

For easy understanding, the procedure described above is slightly different from the original report by Shahin and McCullough (1972), but the basic principle

Downloaded From : www.EasyEngineering.net

Downloaded From : www.EasyEngineering.net

is the same. The probability of failure is the percentage of cracked area, which can be converted to linear cracking by multiplying by 0.2.

9. Low-temperature cracking and thermal fatigue cracking can be summed to estimate total cracking for a specified time after construction.

Example 11.2:

Given a tensile stress σ of 100 psi (690 kPa) with a coefficient of variation of 0.3 and a tensile strength H of 150 psi (1.04 MPa) with a coefficient of variation of 0.2, estimate the length of crack in ft per 1000 ft^2.

Solution: The variance of $(\sigma - H)$ is $(0.3 \times 100)^2 + (0.2 \times 150)^2 = 1800\ (\text{psi})^2$ or the standard deviation of $(\sigma - H) = \sqrt{1800} = 42.4$ psi (293 kPa). The mean of $(\sigma - H)$ is $100 - 150 = -50$, so the normal deviate for $(\sigma - H) = 0$ is $z = [0 - (-50)]/42.4 = 1.18$. From Table 10.1, $\psi(z) = 0.381$, so there is 11.9% probability that $(\sigma - H)$ is greater than 0. The area cracked is $0.119 \times 1000 = 119$ ft^2/1000 ft^2, or the length cracked is 119/5 =23.8 ft/1000 ft^2 (78.1 m/1000 m^2).

11.2 ASPHALT INSTITUTE METHOD

From 1954 to 1969, eight editions of Manual Series No. 1 (MS-1) were published by the Asphalt Institute for the thickness design of asphalt pavements. The procedures recommended in these manuals were empirical. The seventh and eighth editions of MS-1 were based on data from the AASHO Road Test, the WASHO Road Test, and a number of British test roads and on comparisons with the design procedures of the U.S. Army Corps of Engineers and of some state agencies. In 1981, the ninth edition of MS-1 was published. Unlike previous editions, the ninth edition is based on mechanistic–empirical methodology and uses the mechanistic multilayer theory in conjuction with empirical failure criteria to determine pavement thicknesses. Based on the results from a computer program named DAMA, a series of design charts covering three different temperature regimes were developed. However, only the charts for one regime, which represents a large part of the United States, were included in MS-1. In 1991, a revision of the ninth edition of MS-1 was made, in which charts for all three temperature regimes were included (AI, 1991). Details about the DAMA program are presented in Section 3.3.4.

11.2.1 Design Criteria

As has been explained in previous chapters, two types of strains have frequently been considered the most critical for the design of asphalt pavements. One is the horizontal tensile strain ϵ_t at the bottom of the asphalt layer, which causes fatigue cracking; the other is the vertical compressive strain ϵ_c on the surface of the subgrade, which causes permanent deformation or rutting. These two strains are used as failure criteria in the Asphalt Institute method.

Fatigue Criterion The fatigue equation employed by the Asphalt Institute is discussed in Section 7.3.1. For a standard mix with an asphalt volume of 11% and an air

Downloaded From : www.EasyEngineering.net

Downloaded From : www.EasyEngineering.net

void volume of 5%, the equation is

$$N_f = 0.0796(\epsilon_t)^{-3.291}|E^*|^{-0.854} \tag{7.38}$$

in which N_f is the allowable number of load repetitions to control fatigue cracking and $|E^*|$ is the dynamic modulus of the asphalt mixture. If the asphalt or air void volume is different from 11 or 5%, a correction factor C, shown by Eq. 7.37, must be applied. However, Eq. 7.38, based on the standard mix, was used to develop the design charts. It was reported that the use of Eq. 7.38 would result in fatigue cracking of 20% of the total area, as observed on selected sections of the AASHO Road Test (AI, 1982).

Permanent Deformation Criterion The allowable number of load repetitions to control permanent deformation can be expressed as

$$N_d = 1.365 \times 10^{-9} (\epsilon_c)^{-4.477} \tag{11.22}$$

Equation 11.22 was used to develop the design charts. As long as good compaction of the pavement components is obtained and the asphalt mix is well designed, the use of Eq. 11.22 should not result in rutting greater than 0.5 in. (12.7 mm) for the design traffic.

11.2.2 Traffic Analysis

Methods for traffic analysis are discussed in Section 6.4. Load repetitions, expressed in terms of an 18-kip (80-kN) single-axle load, are determined from traffic estimates by using AASHTO equivalent factors for a structural number SN of 5 and a terminal serviceability index p_t of 2.5, as shown in Table 6.4.

Determination of Design ESAL The procedure for determining the design ESAL can be summarized as follows:

1. Estimate the number of vehicles of different types, such as passenger cars, single-unit trucks (including buses), and multiple unit trucks of various types, expected on the proposed facility. In the United States, traffic classification counts are made periodically by state highway and other agencies and should be available for use in pavement design. If the total number of trucks can be estimated but the classification is not known, Table 6.9 can be used as a guide.
2. Determine the number of each type of truck on the design lane during the first year of traffic. For two-lane highways, the design lane may be either lane of the pavement facility. Under some conditions, more trucks may travel in one direction than in the other. In many locations, heavily loaded trucks will travel in one direction, but empty trucks in the other. In the absence of specific data, Table 6.15 may be used for determining the relative proportion of trucks to be expected on the design lane.
3. Determine a truck factor for each vehicle type. Truck factor is defined as the number of 18-kip (80-kN) axle load applications contributed by one passage of a truck. The computation of the truck factor is described in Section 6.4.2 and illustrated in Table 6.11. Typical truck factors are given in Table 6.10. If only the total

Downloaded From : www.EasyEngineering.net

Downloaded From : www.EasyEngineering.net

number of trucks is known, it is not necessary to divide the number into different types according to Table 6.9. The equivalent 18-kip (80-kN) single-axle load applications can be obtained directly by multiplying the total number of trucks with the truck factor for all trucks shown at the bottom of Table 6.10.

4. For the given design period, select from Table 6.13 a single growth factor for all trucks or separate factors for each truck type, as appropriate.
5. Multiply the number of trucks of each type by the truck factor and the growth factor and sum the values determined to obtain the design ESAL.

Example 11.3:

Table 11.2 shows a four-lane rural highway with the number of trucks during the first year on the design lane shown in column 2 and the truck factor in column 3. If the annual growth rate is 4%, determine ESAL for a design period of 20 years.

TABLE 11.2 Example for Traffic Analysis

Vehicle type (1)	Number of vehicles (2)	Truck factor (3)	Growth factor (4)	ESAL (2 × 3 × 4) (5)
Single-unit trucks				
2 axles, 4 tires	78,800	0.003	29.8	7000
2 axles, 6 tires	13,200	0.25	29.8	98,300
3 axles or more	3900	0.86	29.8	100,000
All singles	95,900			205,300
Tractor semitrailers and combinations				
4 axles or less	3900	0.92	29.8	106,900
5 axles	30,200	1.25	29.8	1,125,000
6 axles or more	1300	1.54	29.8	59,700
All tractors, etc.	35,400		Subtotal	1,291,000
All trucks	131,300		Design ESAL =	1,496,900

Solution: With the annual growth rate being 4% and the design period being 20 years, from Table 6.13, the growth factor is 29.8, as shown by column 4 in Table 11.2. Column 5 is the product of columns 2, 3, and 4. The sum of column 5 is 1,496,900, which is the design ESAL.

It is interesting to note that column 2 is based on an AADT of 4000, 20% trucks, 45% in the design lane, and an average truck distribution shown in Table 6.9 under "Other Principal" of rural systems, and that column 3 is the average truck factor in Table 6.10 under the same category. Actually, the ESAL can be obtained directly by multiplying the total number of trucks by the truck factor for all trucks, or ESAL = 131,300 × 0.38 × 29.8 = 1,486,800 (which is slightly different from the 1,496,900 shown in Table 11.2, due to round-off error).

Simplified Procedure for Determining Design ESAL If detailed traffic data are not available, the Asphalt Institute recommends the use of Table 11.3 for estimating the design ESAL (AI, 1981b). This simplified procedure separates traffic into six classes, each associated with a type of highway or street and an average number of heavy trucks expected on the facility during the design period. Heavy trucks are defined as

Downloaded From : www.EasyEngineering.net

Downloaded From : www.EasyEngineering.net

TABLE 11.3 Traffic Classification

Traffic class	Type of street or highway	Range of heavy trucks expected in design period	ESAL
I	Parking lots, driveways Light traffic residential streets Light traffic farm roads	Less than 7000	5×10^3
II	Residential streets Rural farm and residential roads	7000 to 15,000	10^4
III	Urban minor collector streets Rural minor collector roads	70,000 to 150,000	10^5
IV	Urban minor arterial and light industrial streets Rural major collector and minor arterial highways	700,000 to 1,500,000	10^6
V	Urban freeways, expressways, and other principal arterial highways Rural interstate and other principal arterial highways	2,000,000 to 4,500,000	3×10^6
VI	Urban interstate highways Some industrial roads	7,000,000 to 15,000,000	10^7

Note. Whenever possible, more rigorous traffic analysis should be used for roads and streets in traffic category IV or higher.
Source. AI (1981b).

two-axle, six-tire trucks or larger. Pickup, panel, and light four-tire trucks are not included. The ESAL shown for each class can be used for design purposes.

11.2.3 Material Characterization

The material properties to be used for analysis include the resilient moduli and Poisson ratios of subgrade, granular base, and asphalt layer. Poisson ratios can be reasonably assumed as 0.45 for subgrade soils and 0.35 for all other materials.

Subgrade Soils The resilient modulus used in this design procedure is the normal resilient modulus, which is not representative of times when the subgrade is freezing or thawing. It can be determined from the resilient modulus test or correlated with other tests, such as CBR or R values, as described in Section 7.1.6. To determine a representative resilient modulus, substantial testing of subgrade materials within 2 ft (0.6 m) of the planned subgrade elevation is required. If significant variations are present, random sampling should be done to determine the controlling soil type or the boundaries between different soils. If the soil types are significantly different and each soil covers a sufficiently large area, consideration should be given to subdividing the project for separate designs.

At least six to eight test values are usually used to determine the design subgrade resilient modulus. The design subgrade resilient modulus is defined as the modulus value that is smaller than 60, 75, or 87.5% of all the test values. These percentages are known as percentile values and are related to traffic levels, as shown in Table 11.4.

Downloaded From : www.EasyEngineering.net

Downloaded From : www.EasyEngineering.net

TABLE 11.4 Design Subgrade Resilient Modulus

Traffic level ESAL	Design resilient modulus percentile value (%)
10^4 or less	60.0
Between 10^4 and 10^6	75.0
10^6 or more	87.5

Source. After AI (1981a).

Example 11.4:

The results of eight tests produced the following subgrade resilient modulus values; 6200, 7800, 8800, 9500, 10,000, 11,300, 11,900, and 13,500 psi (42.8, 53.8, 60.7, 65.6, 69.0, 78.0, 82.1 and 93.2 MPa). Determine the design subgrade resilient modulus for ESAL of 10^4, 10^5, and 10^6

TABLE 11.5 Computation of Percentile Value

Test value (psi)	Number equal to or greater than	Percent equal to or greater than
13,500	1	12.5
11,900	2	25.0
11,300	3	37.5
10,000	4	50.0
9500	5	62.5
8800	6	75.0
7800	7	87.5
6200	8	100.0

Note. 1 psi = 6.9 kPa.

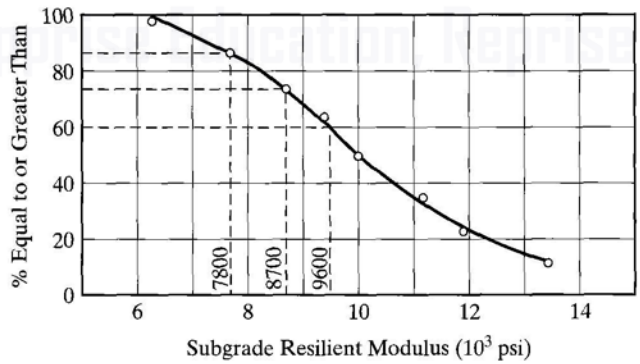


FIGURE 11.8
Graphical determination of design subgrade resilient modulus (1 psi = 6.9 kPa).

Solution: The percentile values are calculated in Table 11.5. From Table 11.4, the percentile values for ESAL of 10^4, 10^5, and 10^6 are 60, 75, and 87.5%, respectively. It can be estimated from Table 11.5 that the design resilient moduli corresponding to the 60, 75, and 87.5 percentile values are 9600, 8800, and 7800 psi (66.2, 60.7, and 53.8 MPa), respectively. For more accurate results, it is preferable to plot the percentile values versus the subgrade resilient moduli, as shown in Figure 11.8,

Downloaded From : www.EasyEngineering.net

Downloaded From : www.EasyEngineering.net

and to draw a smooth curve to correct any irregularities. Note that, at 75 percentile, the resilient modulus determined from Figure 11.8 is 8700 psi (60 MPa), which is slightly different from the original 8800 psi (60.7 MPa).

Untreated Granular Materials The effect of stresses on the resilient modulus of granular materials is indicated by Eq. 3.8. The coefficient K_1 was selected in the range from 8000 to 12,000 psi (55.2 to 82.8 MPa) and the exponent K_2 was set equal to 0.5. Instead of using an iterative method, as in KENLAYER, DAMA applies Eqs. 3.28 and 3.29 to determine the modulus of granular base.

When untreated aggregate base and subbase are used, it is recommended that they comply with ASTM Specification D 2940 "Graded Aggregate Material for Bases or Subbases for Highways and Airports," except that the requirements given in Table 11.6 should apply where appropriate.

Hot Mix Asphalt The resilient modulus is determined by Eq. 7.27. The design charts were developed with the following parameter values in Eq. 7.27: $P_{200} = 5\%$, $f = 10$ Hz, $V_a = 4\%$ for the surface course and 7% for the base course, and $V_b = 11\%$ for both courses. Three temperature regimes, representative of New York, South Carolina, and Arizona, were considered, with mean annual air temperatures (MAAT) of 45°, 60°, and 75°F (7°, 15.5°, and 24°C), respectively. The types of asphalt cement and their viscosities for use in the development of design charts are shown in Table 11.7.

Table 11.8 shows the mean monthly air temperatures for the three representative temperature regimes. The temperature T in Eq. 7.27 is the mean pavement temperature M_p, which can be computed from the mean monthly air temperature by Eq. 3.27.

TABLE 11.6 Quality Requirements for Untreated Aggregate Bases and Subbases

Test	Subbase	Base
CBR, minimum or	20	80
R value, minimum	55	78
Liquid limit, maximum	25	25
Plasticity index, maximum	6	NP
Sand equivalent, minimum	25	35
% passing No. 200, maximum	12	7

Source. After AI (1981a).

TABLE 11.7 Asphalt Grades and Viscosity for Different Temperature Regimes

Location	Mean annual air temperature (MAAT)	Asphalt grades	Viscosity λ at 70°F (10^6 poise)
New York	45°F (7°C)	AC-5, AC-10	0.6
South Carolina	60°F (15.5°C)	AC-10, AC-20	1.6
Arizona	75°F (24°)	AC-40	5.0

Source. After AI (1982).

Downloaded From : www.EasyEngineering.net

Downloaded From : www.EasyEngineering.net

TABLE 11.8 Variations of Mean Monthly Air Temperatures with MAAT

	Mean monthly air temperature (F°)											
MAAT	Jan	Feb	Mar	Apr	May	Jun	Jul	Aug	Sep	Oct	Nov	Dec
45°F	24	25	14	27	42	48	61	69	65	55	48	41
60°F	45	38	43	45	56	70	78	81	78	73	58	54
75°F	55	61	61	73	90	91	92	93	93	86	72	55

Note. °F = 32 + 1.8 × °C.
Source. After AI (1982).

Emulsified Asphalt Mixtures It is permissible to use emulsified asphalt mixtures for base courses. Depending on aggregate types, three types of mixes are specified:

1. *Type I*: mixes with processed dense graded aggregates, which should be mixed in a plant and have properties similar to HMA.
2. *Type II*: mixes with semiprocessed, crusher run, pit run, or bank run aggregates.
3. *Type III*: mixes with sands or silty sands.

Representative stiffness moduli at the time of placement and after full curing were used for each of the mix types, based on the results of 32 different mixes tested at 73°F (23°C) and 100°F (38°C). The moduli at other temperatures can be obtained by a straight-line interpolation. The effect of curing time on the stiffness modulus is represented by

$$E_t = E_f - (E_f - E_i)(\text{RF}) \tag{11.23}$$

in which E_t is the modulus at curing time t, E_f is the modulus in the fully cured state, E_i is the modulus in the uncured or initial state, and RF is the reduction factor representing the amount of cure at time t.

A six-month cure period was used to prepare the design charts; longer periods of curing (up to 30 months) do not have a significance influence on the thickness obtained from the design charts. The reduction factor for a six-month cure period is shown in Figure 11.9.

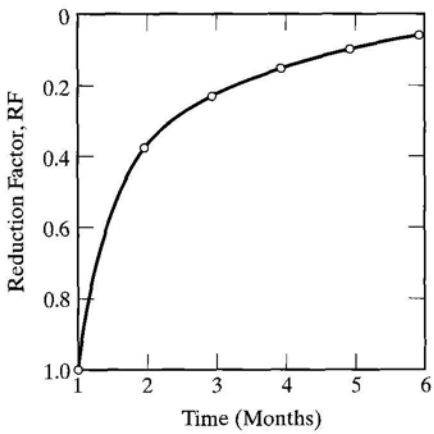


FIGURE 11.9
Reduction factor during six-month cure period. (After AI (1982).)

Downloaded From : www.EasyEngineering.net

Downloaded From : www.EasyEngineering.net

11.2.4 Environmental Effects

In addition to the effect of monthly temperature changes throughout the year on the stiffness moduli of HMA and emulsified asphalt mixtures, the design charts also take into consideration the effect of freezing and thawing on the resilient modulus of the subgrade and granular materials. This was accomplished by using an increased modulus to represent the freezing period and a reduced modulus to represent the thaw period. These adjustments are needed for regions with a MAAT of 45°F (7°C) or 60°F (15.5°C) but not for those of 75°F (24°C).

Subgrade Figure 11.10 shows the variations of a subgrade resilient modulus throughout a year. The diagram represents four distinct periods: freeze, thaw, recovery, and normal. When the subgrade is completely frozen, a frozen modulus of 50,000 psi (345 MPa) is assumed. The modulus is reduced during the thaw period and reaches a minimum thaw modulus, which is a small fraction of the normal modulus. The magnitude of the thaw modulus and the duration of each period are shown in Table 11.9 for the two temperature regimes. When the resilient moduli at the beginning and end of each period are known, those at any month during that period can be interpolated from Figure 11.10. Table 11.10 shows the monthly subgrade moduli used in DAMA for developing the design charts.

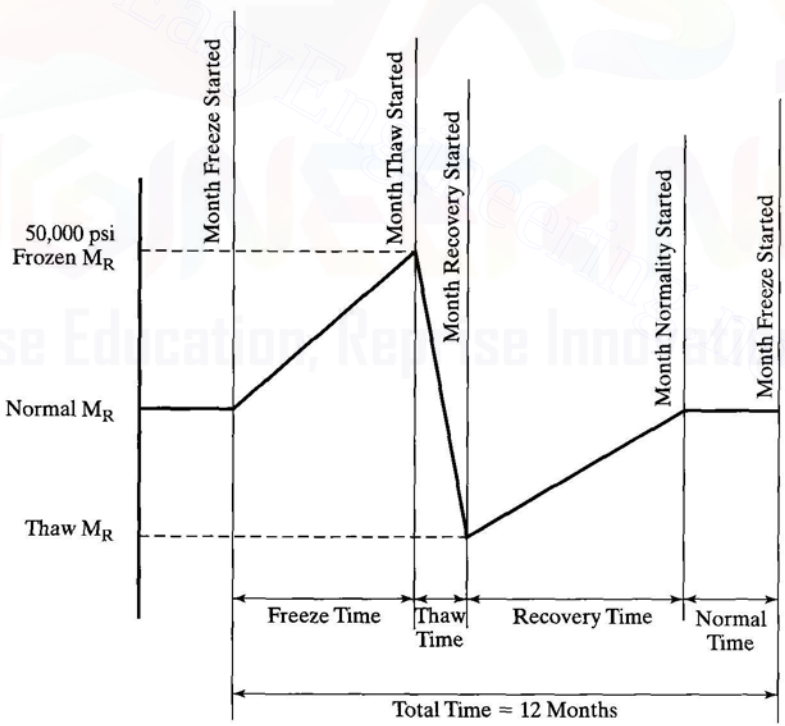


FIGURE 11.10

Seasonal variations of subgrade resilient modulus (1 psi = 6.9 kPa). (After AI (1982).)

Downloaded From : www.EasyEngineering.net

Downloaded From : www.EasyEngineering.net

TABLE 11.9 Conditions Used to Represent Frost Effects on Subgrade

MAAT	Normal modulus (psi)	Thaw modulus		Month freeze started	Duration (month)			
		% Normal	psi		Freeze	Thaw	Recovery	Normal
45°F	4500	20	900	Dec	4	1	5	2
	12,000	50	6000	Dec	4	1	5	2
(7°C)	22,500	70	15,800	Dec	4	1	5	2
60°F	4500	30	1350	Jan	2	1	4	5
	12,000	60	7200	Jan	2	1	4	5
(15.5°C)	22,500	80	18,000	Jan	2	1	4	5

Note. 1 psi = 6.9 kPa.
Source. After AI (1982).

Untreated Granular Materials A similar procedure was used to adjust the moduli of untreated granular sections. The coefficient K_1 in Eq. 3.28 was increased by a factor of 300% for the frozen condition and reduced during the spring thaw to 25% of the normal value. Table 11.11 contains a summary of the monthly K_1 values used. The value of K_2 was maintained constant at 0.5.

11.2.5 Design Procedure

The DAMA computer program was used to determine the minimum thickness required to satisfy both fatigue cracking and rutting criteria. For any given material and environmental conditions, two thicknesses were obtained, one by each criterion, and the larger of the two was used to prepare the design charts. For this reason, many of the design curves represent shapes associated with two different criteria.

Figures 11.11 through 11.20 are the design charts reproduced from the MS-1 manual. These charts are based on a mean annual air temperature of 60°F (15.5°C), which covers a major part of the continental United States. It is assumed that, if asphalt cements are selected according to Table 11.7, the resulting HMA modulus will not change significantly to affect the thickness design, even if the temperature is somewhat different. However, in a report (AI, 1982) documenting the research and development of MS-1 manual, charts for mean annual air temperatures of 45°F (7.0°C) and 75°F (24°C) were also presented. These charts were included in the 1991 version of MS-1. If the mean annual air temperature is significantly different from 60°F (15.5°C), it is recommended that these design charts be utilized. The Asphalt Institute has issued a computer program called HWY which can be used to determine the thickness for all three temperature regimes. The program can also be used for the design of overlay, as is discussed in Section 13.3, and of full-depth pavements for parking lots, service stations, and driveways.

Full-Depth HMA Figure 11.11 is the design chart for full-depth asphalt pavements. Given the subgrade resilient modulus M_R and the equivalent 18-kip single-axle load, ESAL, the total HMA thickness, including both surface and base courses, can be read directly from the chart.

Downloaded From : www.EasyEngineering.net

TABLE 11.10 Subgrade Modulus Used in the DAMA Program

MAAT	Normal modulus (psi)	Subgrade modulus by month (10^3 psi)											
		Dec	Jan	Feb	Mar	Apr	May	Jun	Jul	Aug	Sep	Oct	Nov
45°F	4500	4.5	15.9	27.3	38.7	50.0	0.9	1.62	2.34	3.06	3.78	4.5	4.5
	12,000	12.0	21.5	31.0	40.5	50.0	6.0	7.20	8.40	9.60	10.8	12.0	12.0
(7°C)	22,500	22.5	29.4	36.3	43.1	50.0	15.8	17.1	18.5	19.8	21.2	22.5	22.5
60°F	4500	4.5	4.5	27.3	50.0	1.35	2.14	2.93	3.71	4.5	4.5	4.5	4.5
	12,000	12.0	12.0	31.0	50.0	7.2	8.4	9.6	10.8	12.0	12.0	12.0	12.0
(15.5°C)	22,500	22.5	22.5	38.3	50.0	18.0	19.1	20.3	21.4	22.5	22.5	22.5	22.5

Note. 1 psi = 6.9 kPa.
Source. After AI (1982).

TABLE 11.11 Monthly K_1 Values for Granular Bases

MAAT	Normal K_1 (psi)	Monthly value for K_1 (10^3 psi)											
		Dec	Jan	Feb	Mar	Apr	May	Jun	Jul	Aug	Sep	Oct	Nov
45°F	8000	8.0	12.0	16.0	20.0	24.0	2.0	3.2	4.4	5.6	6.8	8.0	8.0
(7°C)	12,000	12.0	18.0	24.0	30.0	36.0	3.0	4.8	6.6	8.4	10.2	12.0	12.0
60°F	8000	8.0	8.0	16.0	24.0	2.0	3.5	5.0	6.5	8.0	8.0	8.0	8.0
(15.5°C)	12,000	12.0	12.0	24.0	36.0	3.0	5.25	7.50	9.75	12.0	12.0	12.0	12.0

Note. 1 psi = 6.9 kPa.
Source. After AI (1982).

Downloaded From : www.EasyEngineering.net
Downloaded From : www.EasyEngineering.net

Downloaded From : www.EasyEngineering.net

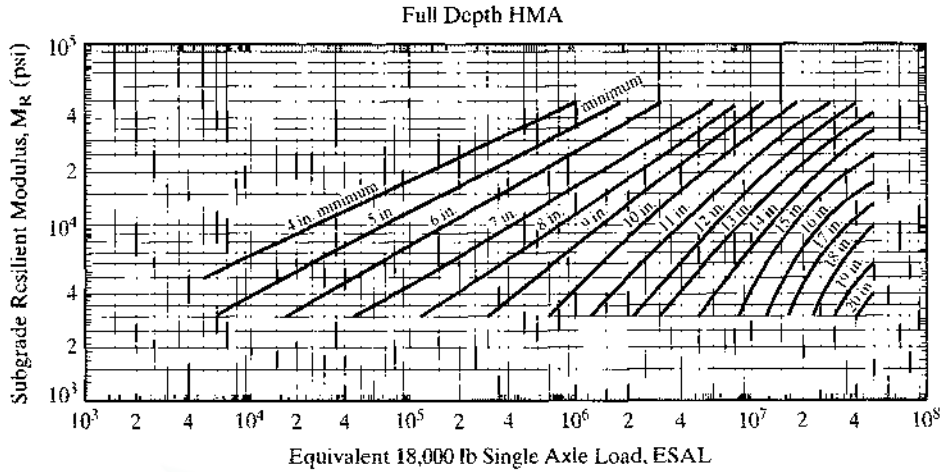


FIGURE 11.11

Design chart for full-depth HMA (1 psi = 6.9 kPa, 1 in. = 25.4 mm). (After AI (1981a).)

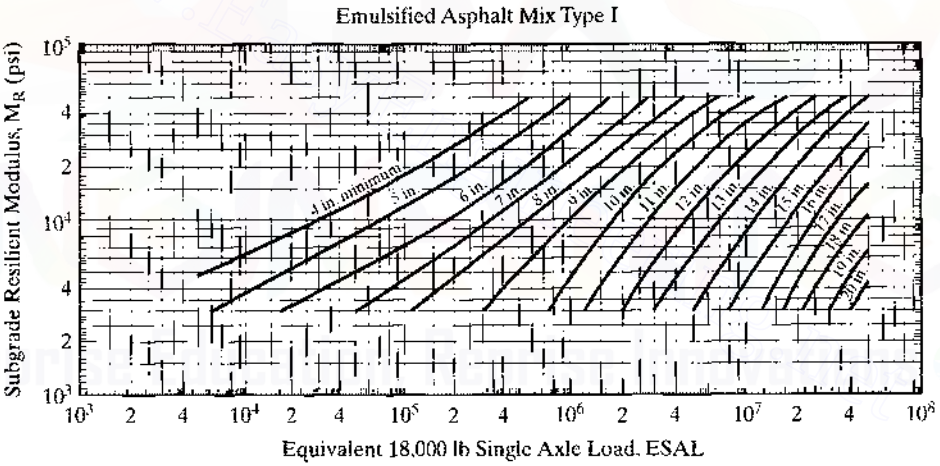


FIGURE 11.12

Design chart for type I emulsified asphalt mix (1 psi = 6.9 kPa, 1 in. = 25.4 mm). (After AI (1981a).)

Example 11.5:

Given M_R = 10,000 psi (69 MPa) and ESAL = 10^6, determine the thickness of HMA for a full-depth asphalt pavement.

Solution: On Figure 11.11, a horizontal line is drawn at $M_R = 10^4$ psi (69 MPa) and a vertical line from ESAL = 10^6. The intersection of these two lines gives a HMA thickness of 8.5 in. (216 mm).

HMA Over Emulsified Asphalt Base Figures 11.12, 11.13, and 11.14 are the design charts for types I, II, and III emulsified asphalt mixes, respectively. The chart gives the

Downloaded From : www.EasyEngineering.net

Downloaded From : www.EasyEngineering.net

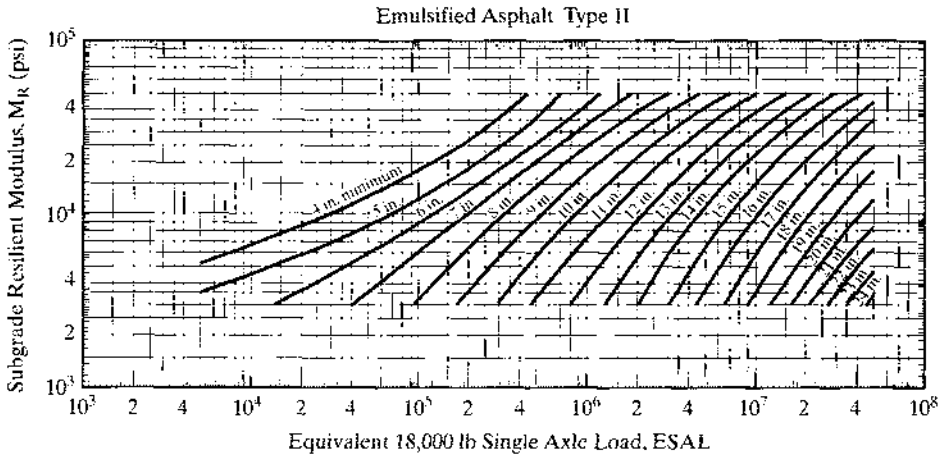


FIGURE 11.13

Design chart for type II emulsified asphalt mix (1 psi = 6.9 kPa, 1 in. = 25.4 mm). (After AI (1981a).)

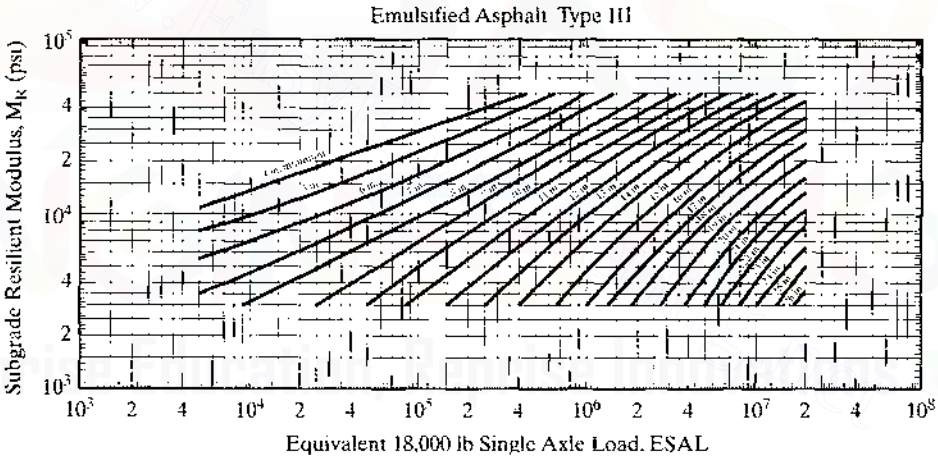


FIGURE 11.14

Design chart for type III emulsified asphalt mix (1 psi = 6.9 kPa, 1 in. = 25.4 mm). (After AI (1981a).)

combined thickness of HMA surface course and emulsified asphalt base course. The minimum thickness of HMA over the emulsified asphalt base varies with the traffic level, as shown in Table 11.12. The difference between the combined thickness and the HMA thickness is the thickness of emulsified asphalt required.

Example 11.6:

Given M_R = 10,000 psi (69 MPa) and ESAL = 10^6, design the thickness of a pavement with a HMA surface over a type II emulsified asphalt base.

Downloaded From : www.EasyEngineering.net

Downloaded From : www.EasyEngineering.net

Solution: With M_R = 10,000 psi (69 MPa) and ESAL = 10^6, from Figure 11.13, the combined thickness is 10.5 in. (267 mm). From Table 11.12, the minimum HMA thickness is 3 in. (76 mm). If the minimum HMA thickness is used, the thickness of the emulsified asphalt base is 10.5 − 3 = 7.5 in. (191 mm). Compared with Example 11.5, the total pavement thickness is increased by 2 in. (51 mm) when the emulsified asphalt base is used.

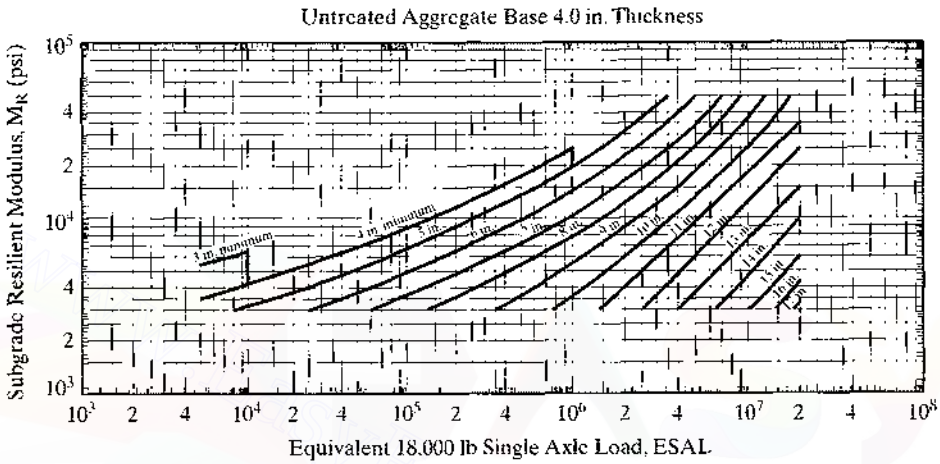


FIGURE 11.15

Design chart for HMA with 4-in. untreated aggregate base (1 psi = 6.9 kPa, 1 in. = 25.4 mm). (After AI (1981a).)

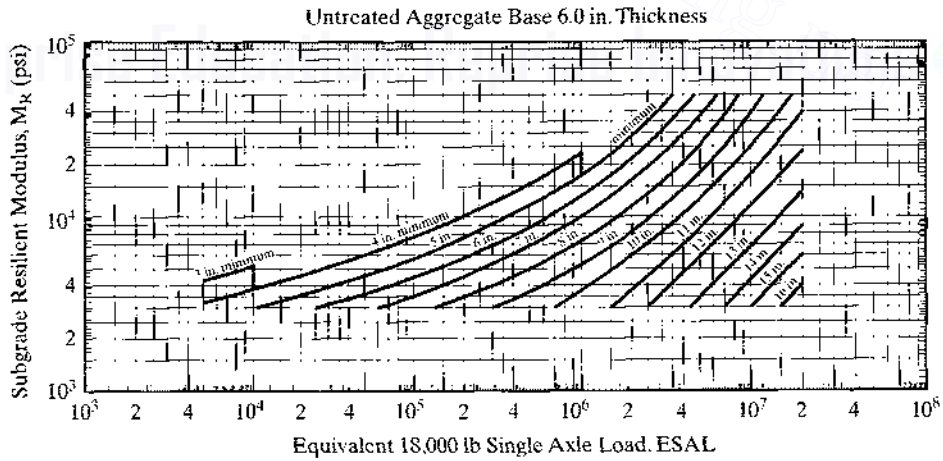


FIGURE 11.16

Design chart for HMA with 6-in. untreated aggregate base (1 psi = 6.9 kPa, 1 in. = 25.4 mm). (After AI (1981a).)

Downloaded From : www.EasyEngineering.net

Downloaded From : www.EasyEngineering.net

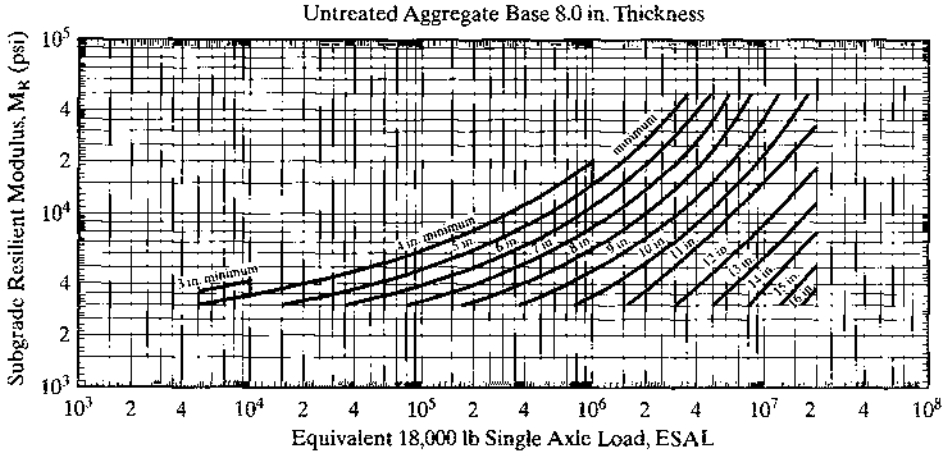


FIGURE 11.17

Design chart for HMA with 8-in. untreated aggregate base (1 psi = 6.9 kPa, 1 in. = 25.4 mm). (After AI (1981a).)

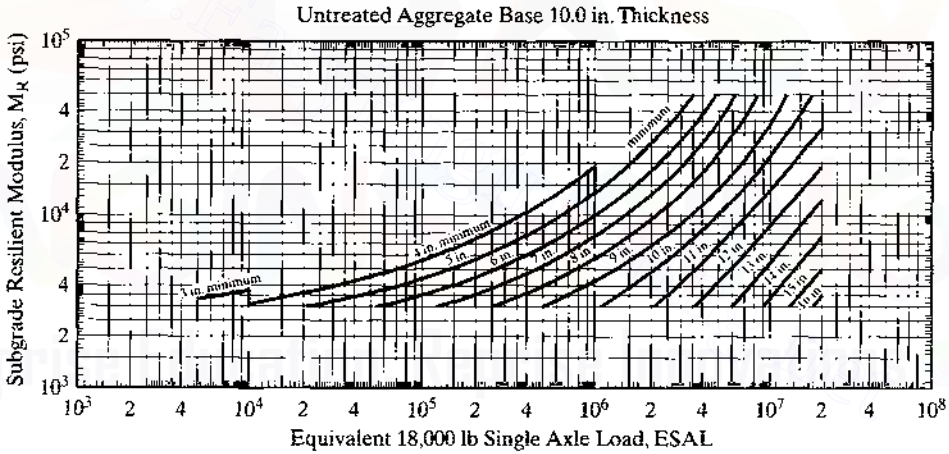


FIGURE 11.18

Design chart for HMA with 10-in. untreated aggregate base (1 psi = 6.9 kPa, 1 in. = 25.4 mm). (After AI (1981a).)

HMA Over Untreated Aggregate Base Figures 11.15 through 11.20 are the design charts for HMA surface courses on untreated aggregate base courses of 4, 6, 8, 10, 12, and 18 in. (102, 152, 203, 254, 305, and 457 mm), respectively. To accommodate the large number of charts needed to cover all three temperature regimes, charts for granular bases of 4, 8, 10, and 18 in. (102, 203, 252, and 457 mm) were not included in the 1991 version of MS-1. To use these charts, the designer must first determine what thickness of aggregate base is to be used and then select the appropriate design chart from which the HMA thickness can be found.

Downloaded From : www.EasyEngineering.net

Downloaded From : www.EasyEngineering.net

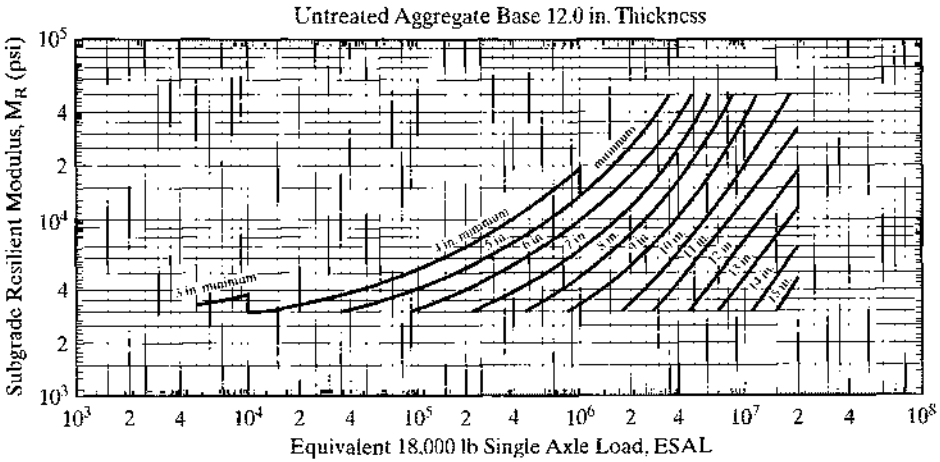


FIGURE 11.19

Design chart for HMA with 12-in. untreated aggregate base (1 psi = 6.9 kPa, 1 in. = 25.4 mm). (After AI (1981a).)

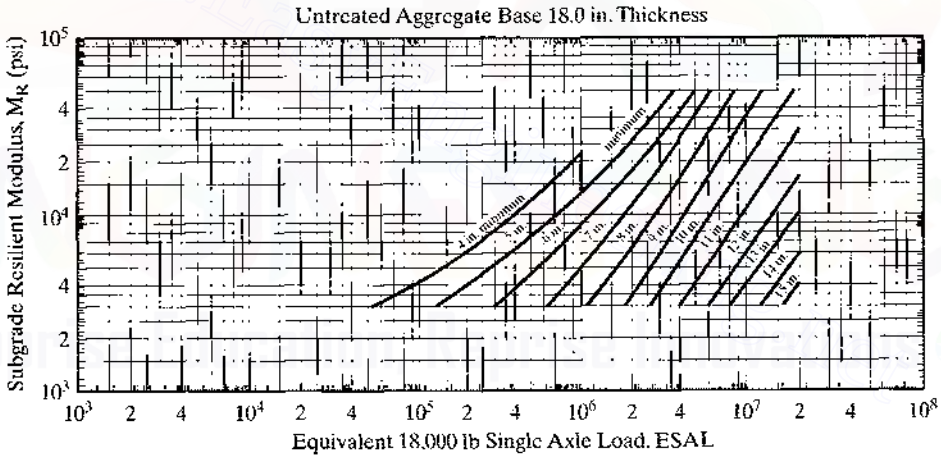


FIGURE 11.20

Design chart for HMA with 18-in. untreated aggregate base (1 psi = 6.9 kPa, 1 in. = 25.4 mm). (After AI (1981a).)

Example 11.7:

Given M_R = 10,000 psi (69 MPa), ESAL = 10^6, and an untreated aggregate base 8 in. (203 mm) thick, determine the thickness of HMA required.

Solution: With M_R = 10^4 psi (69 MPa) and ESAL = 10^6, from Figure 11.17, the thickness of HMA is 6.5 in. (165 mm). Compared with Example 11.5, the use of an 8-in. (203-mm) untreated base reduces the HMA thickness by 2 in. (51 mm).

Downloaded From : www.EasyEngineering.net

Downloaded From : www.EasyEngineering.net

TABLE 11.12 Minimum Thickness of HMA Over Emulsified Asphalt Bases

Traffic level ESAL	HMA thickness for type I mix (in.)	HMA thickness for type II and type III mixes (in.)
10^4	1	2
10^5	1.5	2
10^6	2	3
10^7	2	4
$>10^7$	2	5

Note. 1 in. = 25.4 mm.
Source. After AI (1981a).

HMA and Emulsified Asphalt Mix Over Untreated Aggregate Base Design charts for pavements consisting of a HMA surface, an emulsified asphalt base, and an untreated base are currently not available. The best alternative is to use the charts for full-depth HMA and emulsified asphalt mix to determine a substitution ratio, which indicates the thickness of emulsified asphalt mix required to substitute for a unit thickness of HMA. Then the chart for HMA over untreated aggregate base is applied to determine the thickness of HMA, part of which can be replaced by the emulsified asphalt mix according to the substitution ratio. The following method has been recommended by the Asphalt Institute:

1. Design a full-depth HMA pavement for the appropriate traffic and subgrade conditions. Assume a 2-in. (51-mm) surface course, and calculate the corresponding base thickness.
2. Design a pavement for the same traffic and subgrade conditions, using the selected emulsified mix type. Assume a 2-in. (51-mm) surface course, and calculate the corresponding base thickness.
3. Divide the thickness of the emulsified asphalt base in step 2 by the thickness of the HMA base in step 1 to obtain a substitution ratio.
4. Design a pavement for the same traffic and subgrade conditions, using HMA and untreated base.
5. Select a portion of the HMA thickness to be replaced by the emulsified asphalt mix, based on the minimum HMA thickness specified in Table 11.12.
6. Multiply the above thickness by the substitution ratio determined in step 3 to obtain the thickness of emulsified asphalt mix required.

Example 11.8:

Given M_R = 10,000 psi (69 MPa), ESAL = 10^6, and an 8-in. (203-mm) untreated aggregate base, design the thicknesses of HMA surface course and type II emulsified asphalt base course.

Solution:

1. The thickness for full-depth HMA is 8.5 in. (216 mm), as determined in Example 11.5. If the HMA surface is 2 in. (51 mm), then the thickness of the HMA base is 6.5 in. (165 mm).

Downloaded From : www.EasyEngineering.net

Downloaded From : www.EasyEngineering.net

2. The thickness for emulsified asphalt mix to be placed directly on the subgrade is 10.5 in. (267 mm), as obtained in Example 11.6. If the HMA surface is 2 in. (51 mm), then the thickness of the emulsified asphalt base is 8.5 in. (216 mm).
3. The substitution ratio is 8.5/6.5 = 1.31.
4. The thickness of HMA over an 8 in. (203 mm) untreated aggregate base is 6.5 in. (165 mm), as shown in Example 11.7.
5. From Table 11.12, the minimum HMA thickness is 3 in. (76 mm), so 3.5 in. (89 mm) of HMA base must be replaced by the emulsified asphalt base.
6. The thickness of the emulsified asphalt base is 3.5 × 1.31 = 4.5 in. (114 mm). The final design consists of 3 in. (76 mm) of HMA, 4.5 in. (114 mm) of emulsified asphalt base, and 8 in. (203 mm) of untreated aggregate base, or a total thickness of 15.5 in (394 mm).

The Asphalt Institute suggested the use of a 2-in. (51-mm) surface course to determine the substitution factor. If the actual thickness is 3 in. (76 mm), as shown in the above example, the substitution factor is $(10.5 - 3)/(8.5 - 3) = 1.36$, which is not too much different from the 1.31 used.

Planned Stage Construction Planned stage construction involves successive applications of HMA layers according to a predetermined time schedule. The procedure is based on the concept of remaining life, which implies that the second stage will be constructed before the first stage shows serious signs of distress. Stage construction is beneficial when funds are insufficient for constructing a pavement with a long design life. This approach is also desirable when there is a great amount of uncertainty in estimating traffic. The pavement can be designed for an initial traffic volume; then the next stage of construction can be designed with traffic projections based on the traffic in service. Finally, stage construction allows weak spots that develop in the first stage to be detected and repaired in the next stage.

If n_1 is the actual ESAL for stage 1 and N_1 is the allowable ESAL for the initial thickness h_1 selected for stage 1, then the damage ratio D_r at the end of stage 1 is

$$D_r = \frac{n_1}{N_1} \tag{11.24}$$

Note that D_r must be smaller than 1 because, when $D_r = 1$, the pavement fails. Therefore, the remaining life in the existing pavement at the end of stage 1 is $(1 - D_r)$. The thickness obtained from the design chart is based on a D_r of 1, with no remaining life. To keep some remaining life, the thickness h_1 should be determined from the design chart based on an adjusted design ESAL N_1, which is somewhat greater than the design ESAL n_1, depending on the D_r specified. If h_1 is based on N_1 and

$$N_1 = \frac{n_1}{D_r} \tag{11.25}$$

then the damage ratio after N_1 load applications is 1, so N_1 can be considered to be the allowable number of applications. Since n_1 is smaller than N_1, the damage ratio is smaller than 1; it can be determined from Eq. 12.24.

Downloaded From : www.EasyEngineering.net

Downloaded From : www.EasyEngineering.net

If n_2 is the design ESAL for stage 2 and N_2 is the allowable or adjusted ESAL for stage 2, then the damage incurred in stage 2 should not exceed the remaining life. That is,

$$\frac{n_2}{N_2} = 1 - D_r \tag{11.26}$$

or

$$N_2 = \frac{n_2}{1 - D_r} \tag{11.27}$$

Note that N_2 is an adjusted design ESAL to permit the selection of a thickness h_2 that will carry traffic n_2 and use the remaining life. The difference between h_2 and h_1 is the additional thickness required in stage 2.

Thus, in a stage construction analysis, the designer is required to select a stage time period and the amount of damage D_r to be incurred during this stage. Given D_r and n_1, the adjusted design ESAL N_1 can be computed by Eq. 11.25 and used for determining h_1. Given n_2 and D_r, the adjusted design ESAL N_2 can be computed by Eq. 11.27 and used for determining h_2. The MS-1 manual recommends the use of 5 to 10 years for the first stage, with a damage ratio of 60% at the end of the stage.

Example 11.9:

A full-depth HMA pavement with a subgrade resilient modulus of 10,000 psi (69 MPa) will be constructed in two stages. The first stage is 5 years with 150,000 ESAL repetitions, and the second stage is 15 years with 850,000 ESAL repetitions. Limiting the damage ratio to 0.6 at the end of stage 1, determine the thickness of HMA required for the first 5 years and the thickness of overlay required to accommodate the additional traffic expected during the next 15 years.

Solution: Given $n_1 = 150{,}000$ and $D_r = 0.6$, from Eq. 11.25, $N_1 = 150{,}000/0.6 = 2.5 \times 10^5$. From Figure 11.11, $h_1 = 6.5$ in. (165 mm)

Given $n_2 = 850{,}000$, from Eq. 11.27, $N_2 = 850{,}000/(1 - 0.6) = 2.1 \times 10^6$. From Figure 11.11, $h_2 = 10$ in. (254 mm).

The thickness for the first stage is 6.5 in. (165 mm) and the overlay for the second stage is 3.5 in. (89 mm). If the design is not divided into two stages, the thickness of the pavement is 8.5 in. (216 mm), as shown in Example 11.5. The use of stage construction decreases the thickness in the first stage by 2 in. (51 mm) but increases the total thickness by 1.5 in. (38 mm).

11.2.6 Comparison with Observed Performance

Extensive efforts were devoted by the Asphalt Institute to compare the predicted HMA thickness with the actual thickness. The predicted thickness was determined from the design charts (presented in MS-1) based on the estimated subgrade modulus, the thickness of untreated granular base, and the actual ESAL repetitions, which reduced the PSI level to 2.5. The actual thickness was the thickness of HMA incorporated in the pavement. The difference between predicted and actual thicknesses is Δh. If the predicted thickness is greater than the actual thickness, Δh is positive, and the use

Downloaded From : www.EasyEngineering.net

Downloaded From : www.EasyEngineering.net

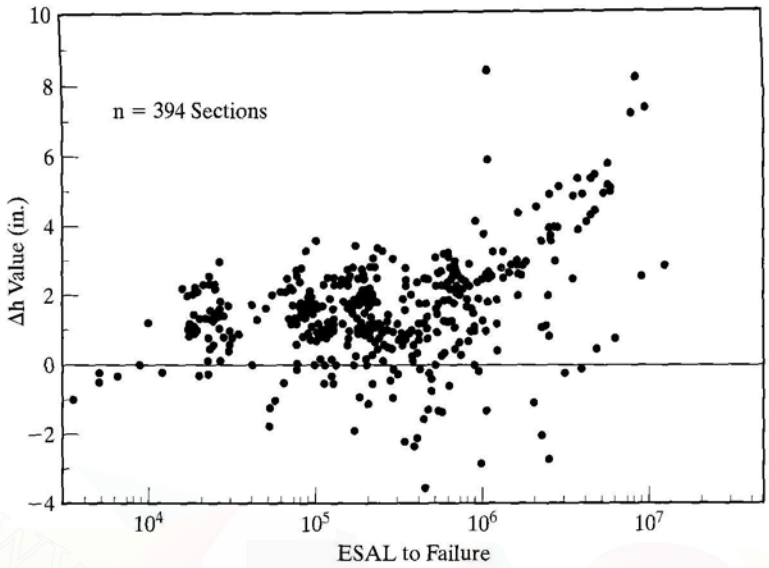


FIGURE 11.21

Thickness comparison for all pavement sections (1 in. = 25.4 mm). (After AI (1982).)

of the design charts is considered conservative. If the predicted thickness is smaller than the actual thickness, Δh is negative, and the design is unconservative.

Six separate sources of data, representing a total of 394 individual data points, were utilized. The studies include the San Diego Test Road in California, the Brampton Test Road in Canada, California investigation, Minnesota investigation, and the main factorial experiment and special base study of the AASHO Road Test in Illinois. The southern and eastern parts of the United States were excluded for lack of documented data.

Figure 11.21 is a plot of Δh for the 394 sections. The figure shows that the MS-1 design procedure yields conservative results, especially when ESAL is above 2×10^6. The mean Δh of the 394 sections is 1.61 in. (41 mm), with a standard deviation of 1.24 in. (31.5 mm).

Figure 11.22 shows the distribution of Δh and illustrates that the probability of achieving unconservative design with $\Delta h < 0$ is 12.7%. This percentage is based on the actual data. If the data are assumed to be normally distributed with a mean of 1.61 and a standard deviation of 1.24, then the normal deviate for $\Delta h = 0$ is $(0 - 1.61)/1.24 = 1.298$ and the probability that $\Delta h < 0$ is 40%.

11.3 AASHTO METHOD

The design procedure recommended by the American Association of State Highway and Transportation Officials (AASHTO) is based on the results of the extensive AASHO Road Test conducted in Ottawa, Illinois, in the late 1950s and early 1960s. The AASHO Committee on Design first published an interim design guide in 1961. It was

Downloaded From : www.EasyEngineering.net

Downloaded From : www.EasyEngineering.net

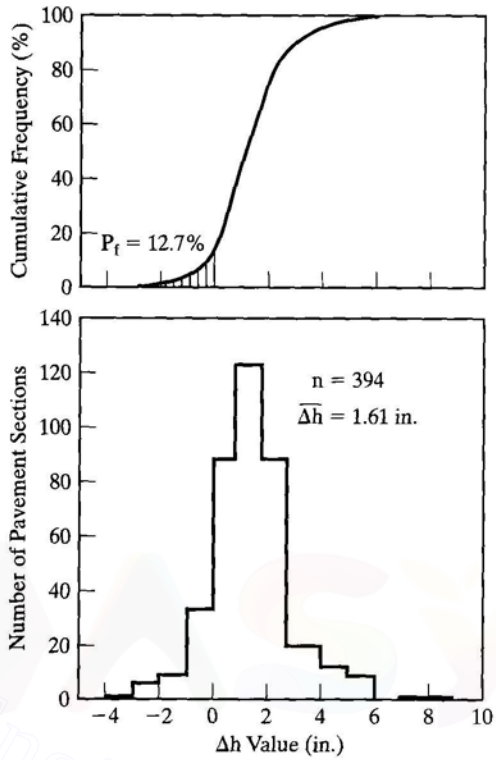


FIGURE 11.22
Distribution of Δh parameter for all pavement sections. (After AI (1982).)

revised in 1972 and 1981. In 1984–85, the Subcommittee on Pavement Design and a team of consultants revised and expanded the guide under NCHRP Project 20-7/24; they issued the guide in 1986. The guide was revised in 1993 with practically no change in the design method presented in this section.

The empirical performance equations obtained from the AASHO Road Test are still being used as the basic models in the current guide, but were modified and extended to make them applicable to other regions in the nation. It should be kept in mind that the original equations were developed under a given climatic setting with a specific set of pavement materials and subgrade soils. The climate at the test site is temperate with an average annual precipitation of about 34 in. (864 mm). The average depth of frost penetration is about 28 in. (711 mm). The subgrade soils consists of A-6 and A-7-6 that are poorly drained, with CBR values ranging from 2 to 4.

11.3.1 Design Variables

Several general design variables related to both flexible and rigid pavements are presented in this section. Other variables, such as the effective roadbed soil resilient modulus and the structural number, are presented in Sections 11.3.3 and 11.3.4, respectively.

Time Constraints To achieve the best use of available funds, the AASHTO design guide encourages the use of a longer analysis period for high-volume facilities, including

Downloaded From : www.EasyEngineering.net

Downloaded From : www.EasyEngineering.net

at least one rehabilitation period. Thus, the analysis period should be equal to or greater than the performance period, as described below.

Performance Period The performance period refers to the time that an initial pavement structure will last before it needs rehabilitation or the performance time between rehabilitation operations. It is equivalent to the time elapsed as a new, reconstructed, or rehabilitated structure deteriorates from its initial serviceability to its terminal serviceability. The designer must select the performance period within the minimum and maximum allowable bounds that are established by agency experience and policy. The selection of performance period can be affected by such factors as the functional classification of the pavement, the type and level of maintenance applied, the funds available for initial construction, life cycle costs, and other engineering considerations.

Analysis Period The analysis period is the period of time that any design strategy must cover. It may be identical to the selected performance period. However, realistic performance limitations may necessitate the consideration of staged construction or planned rehabilitation for the desired analysis period. In the past, pavements were typically designed and analyzed for a 20-year performance period. It is now recommended that consideration be given to longer analysis periods, because they can be better suited for the evaluation of alternative long-term strategies based on life cycle costs. Table 11.13 contains general guidelines for the length of the analysis period.

Traffic The design procedures are based on culmulative expected 18-kip (80-kN) equivalent single-axle load (ESAL). The determination of equivalent axle load factors (EALF) is discussed in Section 6.3.1 for flexible pavements and Section 6.3.2 for rigid pavements. The procedure for converting mixed traffic into ESAL is described in Section 6.4. The use of Table 6.13 for total growth factors and Table 6.16 for lane distribution factors is recommended.

If a pavement is designed for the analysis period without any rehabilitation or resurfacing, all that is required is the total ESAL over the analysis period. However, if stage construction is considered and rehabilitation or resurfacing is anticipated, a graph or equation of cumulative ESAL versus time is needed so that the ESAL traffic during any given stages can be obtained.

Reliability Reliability concepts for pavement design are discussed in Section 10.2. Basically, reliablity is a means of incorporating some degree of certainty into the

TABLE 11.13 Guidelines for Length of Analysis Period

Highway conditions	Analysis period (years)
High-volume urban	30–50
High-volume rural	20–50
Low-volume paved	15–25
Low-volume aggregate surface	10–20

Source. After AASHTO (1986).

Downloaded From : www.EasyEngineering.net

Downloaded From : www.EasyEngineering.net

TABLE 11.14 Suggested Levels of Reliability for Various Functional Classifications

Functional classification	Recommended level of reliability	
	Urban	Rural
Interstate and other freeways	85–99.9	80–99.9
Principal arterials	80–99	75–95
Collectors	80–95	75–95
Local	50–80	50–80

Note. Results based on a survey of AASHTO Pavement Design Task Force.
Source. After AASHTO (1986).

design process to ensure that the various design alternatives will last the analysis period. The level of reliability to be used for design should increase as the volume of traffic, difficulty of diverting traffic, and public expectation of availability increase. Table 11.14 presents recommended levels of reliability for various functional classifications.

Application of the reliability concept requires the selection of a standard deviation that is representative of local conditions. It is suggested that standard deviations of 0.49 be used for flexible pavements and 0.39 for rigid pavements. These correspond to variances of 0.2401 and 0.1521, which are nearly the same as those shown in Table 10.12.

When stage construction is considered, the reliability of each stage must be compounded to achieve the overall reliability; that is,

$$R_{\text{stage}} = (R_{\text{overall}})^{1/n} \tag{11.28}$$

in which n is the number of stages being considered. For example, if two stages are contemplated and the desired level of overall reliability is 95%, the reliability of each stage must be $(0.95)^{1/2}$, or 97.5%.

Environmental Effects The AASHO design equations were based on the results of traffic tests over a two-year period. The long-term effects of temperature and moisture on the reduction of serviceability were not included. If problems of swell clay and frost heave are significant in a given region and have not been properly corrected, the loss of serviceability over the analysis period should be estimated and added to that due to cumulative traffic loads. Figure 11.23 shows the serviceability loss versus time curves for a specific location. The environmental loss is a summation of losses from both swelling and frost heave. The chart may be used to estimate the serviceability loss at any intermediate period, for example, a loss of 0.73 at the end of 13 years. Of course, if only swelling or frost heave is considered, there will be only one curve on the graph. The shape of these curves indicates that the serviceability loss due to environment increases at a decreasing rate. This may favor the use of stage construction because most of the loss will occur during the first stage and can be corrected with little additional loss in later stages.

Downloaded From : www.EasyEngineering.net

Downloaded From : www.EasyEngineering.net

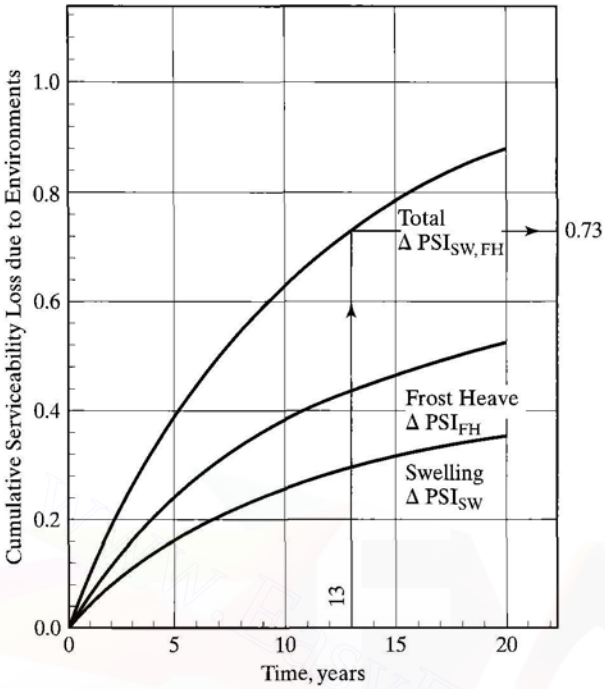


FIGURE 11.23

Environmental serviceability loss versus time for a specific location. (From the *AASHTO Guide for Design of Pavement Structures*. Copyright 1986. American Association of State Highway and Transportation Officials, Washington, DC. Used by permission.)

The serviceability loss due to roadbed swelling depends on the swell rate constant, the potential vertical rise, and the swell probability; that due to frost heave depends on the frost heave rate, the maximum potential serviceability loss, and the frost heave probability. Methods for evaluating these losses are described in Appendix G of the AASHTO design guide.

Serviceability Initial and terminal serviceability indexes must be established to compute the change in serviceability, ΔPSI, to be used in the design equations. The initial serviceability index is a function of pavement type and construction quality. Typical values from the AASHO Road Test were 4.2 for flexible pavements and 4.5 for rigid pavements. The terminal serviceability index is the lowest index that will be tolerated before rehabilitation, resurfacing, and reconstruction become necessary. An index of 2.5 or higher is suggested for design of major highways and 2.0 for highways with lower traffic. For relatively minor highways where economics dictate a minimum initial capital outlay, it is suggested that this be accomplished by reducing the design period or total traffic volume, rather than by designing a terminal serviceability index less than 2.0.

11.3.2 Design Equations

The original equations were based purely on the results of the AASHO Road Test but were modified later by theory and experience to take care of subgrade and climatic conditions other than those encountered in the Road Test.

Downloaded From : www.EasyEngineering.net

Downloaded From : www.EasyEngineering.net

Original Equations The following are the basic equations developed from the AASHO Road Test for flexible pavements (HRB, 1962):

$$G_t = \beta(\log W_t - \log \rho) \tag{11.29}$$

$$\beta = 0.40 + \frac{0.081\,(L_1 + L_2)^{3.23}}{(\mathrm{SN} + 1)^{5.19} L_2^{3.23}} \tag{11.30}$$

$$\log \rho = 5.93 + 9.36 \log(\mathrm{SN} + 1) - 4.79 \log(L_1 + L_2) + 4.33 \log L_2 \tag{11.31}$$

Here,

G_t = logarithm of the ratio of loss in serviceability at time t to the potential loss taken at a point where $p_t = 1.5$, or $G_t = \log[(4.2 - p_t)/(4.2 - 1.5)]$, noting that 4.2 is the initial serviceability for flexible pavements;

β = a function of design and load variables, as shown by Eq. 11.30, that influences the shape of ρ versus W_t curve;

ρ = a function of design and load variables, as shown by Eq. 11.31, that denotes the expected number of load applications to a p_t of 1.5, as can be seen from Eq. 11.29, where $\rho = W_t$ when $p_t = 1.5$;

W_t = axle load application at end of time t;

p_t = serviceability at end of time t;

L_1 = load on one single axle or a set of tandem axles, in kip;

L_2 = axle code—1 for single axle, 2 for tandem axle;

SN = structural number of pavement, which was computed as

$$\mathrm{SN} = a_1 D_1 + a_2 D_2 + a_3 D_3 \tag{11.32}$$

in which a_1, a_2, and a_3 are layer coefficients for the surface, base, and subbase, respectively, and D_1, D_2, and D_3 are the thicknesses of the surface, base, and subbase, respectively.

The procedure is greatly simplified if an equivalent 18-kip (80-kN) single axle load is used. By combining Eqs. 11.29, 11.30, and 11.31 and setting $L_1 = 18$ and $L_2 = 1$, we obtain the equation

$$\log W_{t18} = 9.36 \log(\mathrm{SN} + 1) - 0.20 + \frac{\log[(4.2 - p_t)/(4.2 - 1.5)]}{0.4 + 1094/(\mathrm{SN} + 1)^{5.19}} \tag{11.33}$$

in which W_{t18} is the number of 18-kip (80-kN) single-axle load applications to time t and p_t is the terminal serviceability index. Equation 11.33 is applicable only to the flexible pavements in the AASHO Road Test with an effective subgrade resilient modulus of 3000 psi (20.7 MPa).

Modified Equations For other subgrade and environmental conditions, Eq. 11.33 is modified to

Downloaded From : www.EasyEngineering.net

Downloaded From : www.EasyEngineering.net

$$\log W_{t18} = 9.36 \log(\text{SN} + 1) - 0.20 + \frac{\log[(4.2 - p_t)/(4.2 - 1.5)]}{0.4 + 1094/(\text{SN} + 1)^{5.19}} + 2.32 \log M_R - 8.07 \tag{11.34}$$

in which M_R is the effective roadbed soil resilient modulus. Note that when $M_R = 3000$ psi (20.7 MPa), Eq. 11.34 is identical to Eq. 11.33. To take local precipitation and drainage conditions into account, Eq. 11.32 was modified to

$$\text{SN} = a_1 D_1 + a_2 D_2 m_2 + a_3 D_3 m_3 \tag{11.35}$$

in which m_2 is the drainage coefficient of base course and m_3 is the drainage coefficient of subbase course.

Equation 11.34 is the performance equation that gives the allowable number of 18-kip (80-kN) single-axle load applications W_{t18} to cause the reduction of PSI to p_t. If the predicted number of applications W_{18} is equal to W_{t18}, the reliability of the design is only 50%, because all variables in Eq. 11.34 are based on mean values. To achieve a higher level of reliability, W_{18} must be smaller than W_{t18} by a normal deviate Z_R, as shown in Figure 11.24:

$$Z_R = \frac{\log W_{18} - \log W_{t18}}{S_0} \tag{11.36}$$

Here, Z_R is the normal deviate for a given reliability R, and S_0 is the standard deviation. Z_R can be determined from Table 10.1 or, more conveniently, from Table 11.15.

Combining Eqs. 11.34 and 11.36 and replacing $(4.2 - p_t)$ by ΔPSI yields

$$\log W_{18} = Z_R S_0 + 9.36 \log(\text{SN} + 1) - 0.20 + \frac{\log[\Delta\text{PSI}/(4.2 - 1.5)]}{0.4 + 1094/(\text{SN} + 1)^{5.19}} + 2.32 \log M_R - 8.07 \tag{11.37}$$

Equation 11.37 is the final design equation for flexible pavements. Figure 11.25 is a nomograph for solving Eq. 11.37. The DNPS86 computer program issued by AASHTO can also be used to solve Eq. 11.37 and perform the design procedure.

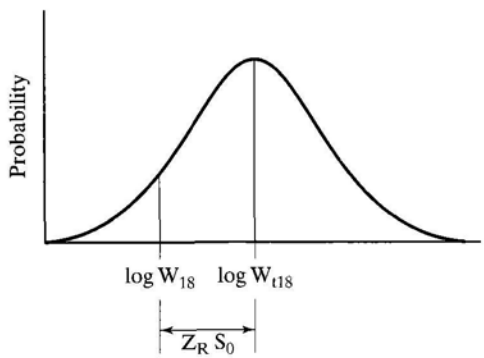


FIGURE 11.24
Reliability of design based on ESAL.

Downloaded From : www.EasyEngineering.net

Downloaded From : www.EasyEngineering.net

TABLE 11.15 Standard Normal Deviates for Various Levels of Reliability

Reliability (%)	Standard normal deviate (Z_R)	Reliability (%)	Standard normal deviate (Z_R)
50	0.000	93	−1.476
60	−0.253	94	−1.555
70	−0.524	95	−1.645
75	−0.674	96	−1.751
80	−0.841	97	−1.881
85	−1.037	98	−2.054
90	−1.282	99	−2.327
91	−1.340	99.9	−3.090
92	−1.405	99.99	−3.750

Example 11.10:

Given $W_{18} = 5 \times 10^6$, $R = 95\%$, $S_0 = 0.35$, $M_R = 5000$ psi (34.5 MPa), and $\Delta PSI = 1.9$, determine SN from Figure 11.25.

Solution: As shown by the arrows in Figure 11.25, starting from $R = 95\%$, a series of lines are drawn through $S_0 = 0.35$, $W_{18} = 5 \times 10^6$, $M_R = 5000$ psi (34.5 MPa), and $\Delta PSI = 1.9$ and finally intersect SN at 5.0, so SN = 5.0.

The chart is most convenient for determining SN, because the solution of SN by Eq. 11.37 is cumbersome and requires a trial and error process. If W_{18} is the unknown to be determined, the use of Eq. 11.37 is more accurate.

Example 11.11:

Given $R = 95\%$, SN = 5, $S_0 = 0.35$, $M_R = 5000$ psi (34.5 MPa), $\Delta PSI = 1.9$, determine W_{18} by Eq. 11.37.

Solution: For $R = 95\%$, from Table 11.15, $Z_R = -1.645$. From Eq. 11.37, $\log W_{18} = -1.645 \times 0.35 + 9.36 \log(5 + 1) - 0.2 + \log(1.9/2.7)/[0.4 + 1094/(6)^{5.19}] + 2.32 \log(5000) - 8.07 = 6.714$, or $W_{18} = 5.18 \times 10^6$, which checks with 5×10^6 in the previous example.

11.3.3 Effective Roadbed Soil Resilient Modulus

The effective roadbed soil resilient modulus M_R is an equivalent modulus that would result in the same damage if seasonal modulus values were actually used. The equation for evaluating the relative damage to flexible pavements u_f and the method for computing M_R are discussed next.

Relative Damage From Eq. 11.37, the effect of M_R on W_{18} can be expressed as

$$\log W_{18} = \log C - \log(1.18 \times 10^8 M_R^{-2.32}) \tag{11.38}$$

Downloaded From : www.EasyEngineering.net

Downloaded From : www.EasyEngineering.net

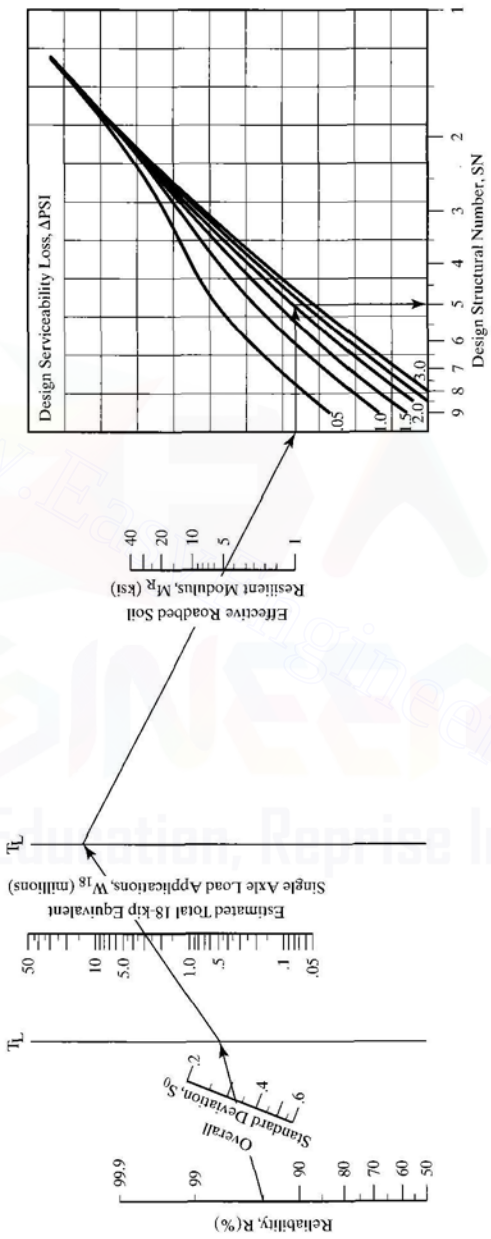


FIGURE 11.25
Design chart for flexible pavements based on mean values for each input (1 ksi = 6.9 MPa). (From the *AASHTO Guide for Design of Pavement Structures*. Copyright 1986. American Association of State Highway and Tranportation Officials, Washington, DC. Used by permission.)

Downloaded From : www.EasyEngineering.net

Downloaded From : www.EasyEngineering.net

in which log C is the sum of all but the last two terms in Eq. 11.37. Equation 11.38 can be written as

$$W_{18} = \frac{C}{1.18 \times 10^8 M_R^{-2.32}} \tag{11.39}$$

If W_T is the predicted total traffic, the damage ratio, which is a ratio between predicted and allowable number of load repetitions, can be expressed as

$$D_r = \frac{W_T}{C/(1.18 \times 10^8 M_R^{-2.32})} = \frac{W_T}{C}(1.18 \times 10^8 M_R^{-2.32}) \tag{11.40}$$

If W_T is uniformly distributed over n periods, the cumulative damage ratio is

$$D_r = \sum_{i=1}^{n} \frac{W_T/n}{C/(1.18 \times 10^8 M_{Ri}^{-2.32})} = \frac{W_T}{C}\frac{1}{n}\sum_{i=1}^{n}(1.18 \times 10^8 M_{Ri}^{-2.32}) \tag{11.41}$$

Equating Eq. 11.40 to Eq. 11.41 gives

$$1.18 \times 10^8 M_R^{-2.32} = \frac{1}{n}\sum_{i=1}^{n}(1.18 \times 10^8 M_{Ri}^{-2.32}) \tag{11.42}$$

Equation 11.42 can be used to determine the effective roadbed soil resilient modulus M_R in terms of seasonal moduli $M_{R\,i}$. Although the coefficient 1.18×10^8 can be canceled out to simplify the equation, the AASHTO design guide keeps the coefficient and defines the relative damage u_f as

$$u_f = 1.18 \times 10^8 M_R^{-2.32} \tag{11.43}$$

Computation of Effective Roadbed Soil Resilient Modulus Figure 11.26 is a worksheet for estimating effective roadbed soil resilient modulus, in which Eq. 11.43, together with a vertical scale for graphical solution of u_f, is also shown. A year is divided into a number of periods during which different roadbed soil resilient moduli are specified. The shortest time period is half a month. These seasonal moduli can be determined from correlations with soil moisture and temperature conditions or from nondestructive deflection testing.

In the worksheet, the 12 monthly subgrade moduli used in the DAMA program for a MAAT of 45°F (7.2°C) and a normal modulus of 4500 psi (31 MPa), as shown in Table 11.10, are used as an example. The relative damage during each month can be obtained from the vertical scale or computed from Eq. 11.43; the sum, 25.30, is shown at the bottom. The average relative damage = 25.30/12 = 2.11, which corresponds to an effective roadbed resilient modulus of 2200 psi (15.2 MPa).

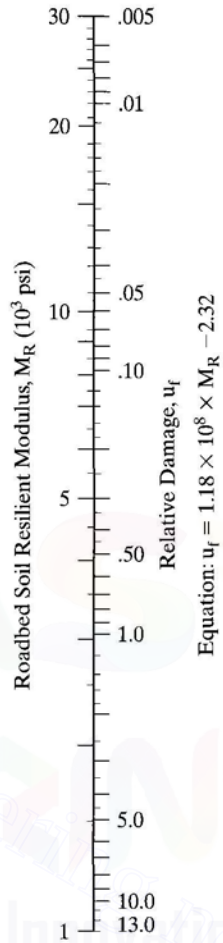
In the preceding example, there is a large variation in the monthly resilient modulus. The maximum and minimum values are outside the range of the vertical scale and must be computed from Eq. 11.43. About 65% of the damage is done in May alone. This is the reason that a very low effective modulus, 2200 psi (15.2 MPa), is obtained, one much lower than the normal modulus, 4500 psi (31.1 MPa).

Downloaded From : www.EasyEngineering.net

Downloaded From : www.EasyEngineering.net

Month	Roadbed Soil Modulus, M_R (psi)	Relative Damage, u_f
Jan.	15,900	0.02
Feb.	27,300	0.01
Mar.	38,700	0.00
Apr.	50,000	0.00
May	900	16.52
June	1,620	4.22
July	2,340	1.80
Aug.	3,060	0.97
Sept.	3,780	0.59
Oct.	4,500	0.39
Nov.	4,500	0.39
Dec.	4,500	0.39
Summation: $\Sigma u_f =$		25.30

Average: $\bar{u}_f = \frac{\Sigma u_f}{n} = 2.11$



Effective Roadbed Soil Resilient Modulus, M_R (psi) = 2,200 (corresponds to $\bar{u}_f$)

FIGURE 11.26

Worksheet for estimating effective roadbed soil resilient modulus (1 psi = 6.9 kPa).

11.3.4 Structural Number

Structural number is a function of layer thicknesses, layer coefficients, and drainage coefficients and can be computed from Eq. 11.35.

Layer Coefficient The layer coefficient a_i is a measure of the relative ability of a unit thickness of a given material to function as a structural component of the pavement. Layer coefficients can be determined from test roads or satellite sections, as was done in the AASHO Road Test, or from correlations with material properties, as was shown in Figures 7.13, 7.15, and 7.16. It is recommended that the layer coefficient be based on

Downloaded From : www.EasyEngineering.net

Downloaded From : www.EasyEngineering.net

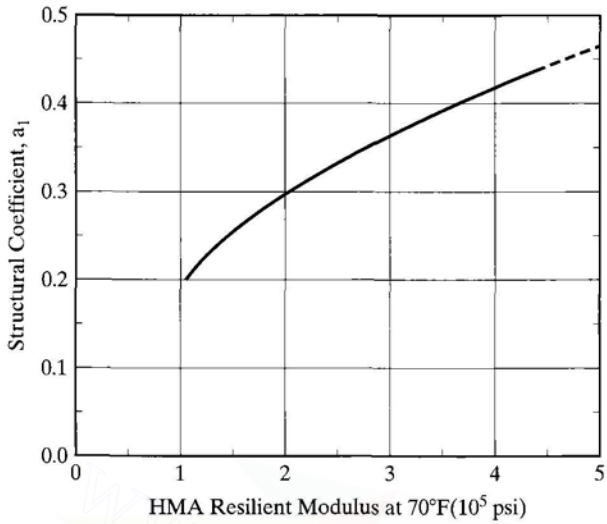


FIGURE 11.27

Chart for estimating layer coefficient of dense-graded asphalt concrete based on elastic modulus (1 psi = 6.9 kPa). (After Van Til et al. (1972).)

the resilient modulus, which is a more fundamental material property. The procedure for determining the resilient modulus of a particular material varies with its type. Except for the higher stiffness materials, such as HMA and stabilized bases, that may be tested by the repeated load indirect tensile test (ASTM D-4123), all materials should be tested by the resilient modulus test methods (AASHTO T274). Methods for determining the resilient modulus were described in Section 7.1.

In following the AASHTO design guide, the notation M_R, as used herein, refers only to roadbed soils, whereas E_1, E_2, and E_3 apply to the HMA, base, and subbase, respectively.

Asphalt–Concrete Surface Course Figure 11.27 is a chart relating the layer coefficient of a dense-graded HMA to its resilient modulus at 70°F (21°C). Caution should be used in selecting layer coefficients with modulus values greater than 450,000 psi (3.1 GPa), because the use of these larger moduli is accompanied by increased susceptiblity to thermal and fatigue cracking. The layer coefficient a_1 for the dense-graded HMA used in the AASHO Road Tests is 0.44, which corresponds to a resilient modulus of 450,000 psi (3.1 GPa).

Untreated and Stabilized Base Courses Figure 7.15 shows the charts that can be used to estimate the layer coefficient a_2 for untreated, bituminous-treated, and cement-treated base courses. In lieu of Figure 7.15*a*, the following equation can also be used to estimate a_2 for an untreated base course from its resilient modulus E_2:

$$a_2 = 0.249(\log E_2) - 0.977 \tag{11.44}$$

The layer coefficient a_2 for the granular base material used in the AASHO Road Test is 0.14, which corresponds to a base resilient modulus of 30,000 psi (207 GPa).

The resilient modulus of untreated granular materials depends on the stress state θ, as indicated by Eq. 3.8 and rewritten here as

$$E_2 = K_1 \theta^{K_2} \tag{11.45}$$

Downloaded From : www.EasyEngineering.net

Downloaded From : www.EasyEngineering.net

TABLE 11.16 Typical Values of K_1 and K_2 for Untreated Base Materials

Moisture condition	K_1	K_2
Dry	6000–10,000	0.5–0.7
Damp	4000–6000	0.5–0.7
Wet	2000–4000	0.5–0.7

Source. After AASHTO (1986).

TABLE 11.17 Typical Values of Stress State θ for Base Course

Asphalt concrete thickness (in.)	Roadbed soil resilient modulus (psi)		
	3000	7500	15,000
Less than 2	20	25	30
2–4	10	15	20
4–6	5	10	15
Greater than 6	5	5	5

Note. Unit of θ is in psi, 1 in. = 25.4 mm, 1 psi = 6.9 kPa.
Source. After AASHTO (1986).

Typical values of K_1 for base materials range from 3000 to 8000; those of K_2 range from 0.5 to 0.7. Values of K_1 and K_2 for each specific base material should be determined using AASHTO Method T274. In the absence of this information, the values shown in Table 11.16 can be used.

The resilient modulus of the base course is a function not only of K_1 and K_2, but also of the stress state θ. Values for the stress state within the base course vary with the roadbed soil resilient modulus and with the thickness of the surface layer. Typical values of θ are shown in Table 11.17. Given K_1, K_2, and θ, E_2 can be determined from Eq. 11.45.

Granular Subbase Course Figure 7.16 provides the chart that may be used to estimate layer coefficient a_3 of granular subbase courses. The relationship between a_3 and E_3 can be expressed as

$$a_3 = 0.227(\log E_3) - 0.839 \tag{11.46}$$

The layer coefficient a_3 for the granular subbase in the AASHO Road Test is 0.11, which corresponds to a resilient modulus of 15,000 psi (104 MPa). As with granular base courses, values of K_1 and K_2 for granular subbase courses can be determined from the resilient modulus test (AASHTO T274) or estimated from Table 11.18. Values of K_1, K_2, θ, and E_3 for the subbase in the AASHO Road Test are shown in Table 11.19.

Drainage Coefficient Depending on the quality of drainage and the availability of moisture, drainage coefficients m_2 and m_3 should be applied to granular bases and subbases to modify the layer coefficients, as shown in Eq. 11.35. At the AASHTO Road Test site, these drainage coefficients are all equal to 1, as indicated by Eq. 11.32.

Downloaded From : www.EasyEngineering.net

Downloaded From : www.EasyEngineering.net

TABLE 11.18 Typical Values of K_1 and K_2 for Granular Subbase Materials

Moisture condition	K_1	K_2
Dry	6000–8000	0.4–0.6
Damp	4000–6000	0.4–0.6
Wet	1500–4000	0.4–0.6

Source. After AASHTO (1986).

TABLE 11.19 Values of Resilient Modulus for AASHO Road Test Subbase Materials

			Stress state θ (psi)		
Moisture condition	K_1	K_2	5	7.5	10
Damp	5400	0.6	14,183	18,090	21,497
Wet	4600	0.6	12,082	15,410	18,312

Note. Resilient modulus is in psi; 1 psi = 6.9 kPa.
Source. After Finn *et al.* (1986).

TABLE 11.20 Recommended Drainage Coefficients for Untreated Bases and Subbases in Flexible Pavements

Quality of drainage		Percentage of time pavement structure is exposed to moisture levels approaching saturation			
Rating	Water removed within	Less than 1%	1–5%	5–25%	Greater than 25%
Excellent	2 hours	1.40–1.35	1.35–1.30	1.30–1.20	1.20
Good	1 day	1.35–1.25	1.25–1.15	1.15–1.00	1.00
Fair	1 week	1.25–1.15	1.15–1.05	1.00–0.80	0.80
Poor	1 month	1.15–1.05	1.05–0.80	0.80–0.60	0.60
Very poor	Never drain	1.05–0.95	0.95–0.75	0.75–0.40	0.40

Source. After AASHTO (1986).

Table 11.20 shows the recommended drainage coefficients for untreated base and subbase materials in flexible pavements. The quality of drainage is measured by the length of time for water to be removed from bases and subbases and depends primarily on their permeability. The percentage of time during which the pavement structure is exposed to moisture levels approaching saturation depends on the average yearly rainfall and the prevailing drainage conditions.

11.3.5 Selection of Layer Thicknesses

Once the design structural number SN for an initial pavement structure is determined, it is necessary to select a set of thicknesses so that the provided SN, as computed by Eq. 11.35, will be greater than the required SN. Note that Eq. 11.35 does not have a single unique solution. Many combinations of layer thicknesses are acceptable, so their cost effectiveness along with the construction and maintenance constraints must be considered

Downloaded From : www.EasyEngineering.net

Downloaded From : www.EasyEngineering.net

TABLE 11.21 Minimum Thickness for Asphalt Surface and Aggregate Base

Traffic (ESAL)	Asphalt concrete	Aggregate base
Less than 50,000	1.0	4
50,001–150,000	2.0	4
150,001–500,000	2.5	4
500,001–2,000,000	3.0	6
2,000,001–7,000,000	3.5	6
Greater than 7,000,000	4.0	6

Note. Minimum thickness is in in.; 1 in. = 25.4 mm.
Source. After AASHTO (1986).

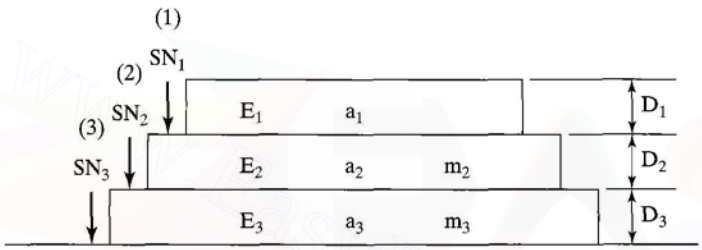


FIGURE 11.28
Selection of thicknesses.

to avoid the possibility of producing an impractical design. From a cost-effective viewpoint, if the ratio of costs for HMA and granular base is less than the corresponding ratio of layer coefficients times the drainage coefficient, then the optimum economical design is to use a minimum base thickness by increasing the HMA thickness.

Minimum Thickness It is generally impractical and uneconomical to use layers of material that are less than some minimum thickness. Furthermore, traffic considerations may dictate the use of a certain minimum thickness for stability. Table 11.21 shows the minimum thicknesses of asphalt surface and aggregate base. Because such minimums depend somewhat on local practices and conditions, they may be changed if needed.

General Procedure The procedure for thickness design is usually started from the top, as shown in Figure 11.28 and described as follows:

1. Using E_2 as M_R, determine from Figure 11.25 the structural number SN_1 required to protect the base, and compute the thickness of layer 1 from

$$D_1 \geq \frac{SN_1}{a_1} \tag{11.47}$$

2. Using E_3 as M_R, determine from Figure 11.25 the structural number SN_2 required to protect the subbase, and compute the thickness of layer 2 from

$$D_2 \geq \frac{SN_2 - a_1 D_1}{a_2 m_2} \tag{11.48}$$

Downloaded From : www.EasyEngineering.net

Downloaded From : www.EasyEngineering.net

3. Based on the roadbed soil resilient modulus M_R, determine from Figure 11.25 the total structural number SN_3 required, and compute the thickness of layer 3 from

$$D_3 \geq \frac{SN_3 - a_1D_1 - a_2D_2m_2}{a_3m_3} \tag{11.49}$$

Example 11.12:

Figure 11.29 is a pavement system with the resilient moduli, layer coefficients, and drainage coefficients as shown. If predicted ESAL = 18.6×10^6, $R = 95\%$, $S_0 = 0.35$, and $\Delta PSI = 2.1$, select thicknesses D_1, D_2, and D_3.

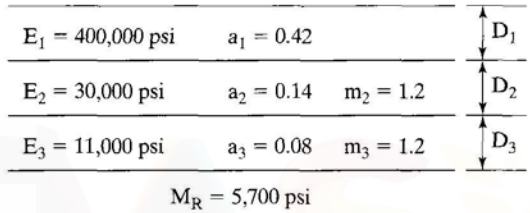


FIGURE 11.29
Example 11.12 (1 psi = 6.9 kPa).

Solution: With $M_R = E_2 = 30{,}000$ psi (207 MPa), from Figure 11.25, $SN_1 = 3.2$; from Eq. 11.47, $D_1 \geq 3.2/0.42 = 7.6$ in. (193 mm); use $D_1 = 8$ in. (203 mm).

With $M_R = E_3 = 11{,}000$ psi (76 MPa), from Figure 11.25, $SN_2 = 4.5$; from Eq. 11.48, $D_2 \geq (4.5 - 0.42 \times 8)/(0.14 \times 1.2) = 6.8$ in. (173 mm); use $D_2 = 7$ in. (178 mm). Note that a surface thickness of 8 in. (203 mm) and a base thickness of 7 in. (178 mm) meet the minimum thicknesses shown in Table 11.21.

With $M_R = 5700$ psi (39.3 MPa), from Figure 11.25, $SN_3 = 5.6$; from Eq. 11.49, $D_3 \geq (5.6 - 0.42 \times 8 - 0.14 \times 7 \times 1.20)/(0.08 \times 1.2) = 11.1$ in. (282 mm); use $D_3 = 11.5$ in. (292 mm).

11.3.6 Stage Construction

If the maximum performance period is less than the analysis period, any initial structure selected will require an overlay to last out the analysis period. The thickest recommended initial structure is that corresponding to the maximum performance period. Thinner initial structures, selected for the purpose of life cycle cost analyses, will result in shorter performance periods and require thicker overlays to last out the same analysis period. The design of the initial structure for stage construction works the same as that for new construction, except that the reliability must be compounded over all stages. The design of an overlay as a stage construction alternative is presented in Chapter 13.

If the loss of serviceability is caused by traffic loads alone, the length of the performance period, which is related to W_{18}, for a given serviceability loss can be determined from Figure 11.25 or directly from Eq. 11.37. However, if the serviceability loss is caused by both traffic loads and the environmental effects of roadbed swelling and frost heave, the performance period for a given terminal serviceability can be determined only by an iterative process, as illustrated by the following example.

Downloaded From : www.EasyEngineering.net

Downloaded From : www.EasyEngineering.net

Example 11.13:

Given the following design inputs, determine the length of the performance period required: structural number SN = 5.0, reliability R = 95%, standard deviation S_0 = 0.35, initial serviceability p_0 = 4.3, terminal serviceability p_t = 2.5, effective roadbed soil resilient modulus M_R = 5000 psi (35 MPa), ΔPSI due to both swelling and frost heave as shown in Figure 11.23, and traffic versus time relationship as

$$W_{18} = 10 \times 10^6 [(1.03)^Y - 1] \tag{11.50}$$

or

$$Y = 77.9 \log\left(\frac{W_{18}}{10 \times 10^6} + 1\right) \tag{11.51}$$

Solution: First, assume Y = 13 years. From Figure 11.23, ΔPSI due to environmental effects = 0.73; ΔPSI due to traffic = 4.3 − 2.5 − 0.73 = 1.07. From Eq. 11.37 or Figure 11.25, $W_{18} = 1.6 \times 10^6$. From Eq. 11.51, Y = 5.1 years, which is much smaller than the 13 years assumed.

Next assume Y as the average of 13 and 5.1 years, or 9.0 years. From Figure 11.23, ΔPSI due to environmental effects = 0.59; ΔPSI due to traffic = 4.3 − 2.5 − 0.59 = 1.21. From Eq. 11.37 or Figure 11.25, $W_{18} = 2.1 \times 10^6$. From Eq. 11.51, Y = 6.5 years.

Finally, assume Y = (9 + 6.5)/2 = 7.7 years. From Figure 11.23, ΔPSI due to environmental effects = 0.52; ΔPSI due to traffic = 4.3 − 2.5 − 0.52 = 1.28. From Eq. 11.37 or Figure 11.25, $W_{18} = 2.4 \times 10^6$. From Eq. 11.51, Y = 7.3, which is nearly equal to the 7.7 years assumed. When the difference between the assumed and calculated values is smaller than 1 year, no more iterations are needed and the average of the two values can be used as the performance period. Therefore, the performance period = (7.7 + 7.3)/2 = 7.5 years.

11.3.7 Comparison with Asphalt Institute Method

The difference in design variables makes it difficult to compare two different design methods. The AASHTO design method applies the reliability concept by using average values for all variables, including the effective roadbed soil resilient modulus. The Asphalt Institute method does not consider reliability and uses a normal subgrade resilient modulus that is smaller than 60 to 87.5% of all the test values, depending on the level of traffic. As shown by the example in Figure 11.26, a normal subgrade resilient modulus of 4500 psi (31 MPa) is equivalent to an effective roadbed soil resilient modulus of 2200 psi (15.2 MPa). Because the resilient modulus is based on the average value in the AASHTO method but on the 60 to 87.5 percentile value in the Asphalt Institute method, it is reasonable to assume that an effective roadbed soil resilient modulus of 3000 psi (20.7 MPa) in the AASHTO method is about equivalent to a normal modulus of 4500 psi (31 MPa) in the Asphalt Institute method. Other parameter values to be used in the AASHTO method are reliability R = 95%, standard deviation S_0 = 0.45, serviceability loss ΔPSI = 1.7, and layer coefficient for full-depth HMA a_1 = 0.44. These values are reasonable for use in the design of major highways.

Table 11.22 shows the thicknesses of full-depth HMA required by the AASHTO method versus those required by the Asphalt Institute method. Three HMA thicknesses,

Downloaded From : www.EasyEngineering.net

Downloaded From : www.EasyEngineering.net

TABLE 11.22 Comparison of Thickness Between AASHTO and AI Methods

AASHTO method			AI method
HMA thickness (in.)	SN	ESAL	HMA thickness (in.)
5.0	2.2	5.2×10^3	4.5
10.0	4.4	3.6×10^5	9.0
15.0	6.6	6.8×10^6	14.0

Note. 1 in. = 25.4 mm.

5, 10, and 15 in. (127, 254, and 381 mm), are assumed. The structural number SN is computed by multiplying the HMA thickness by 0.44. The ESAL based on the AASHTO method is determined from Eq. 11.37. Based on the ESAL thus obtained, the thickness by the Asphalt Institute method is obtained from Figure 11.11. It can be seen that the two methods check quite well. The thicknesses obtained by the Asphalt Institute method are 0.5 to 1 in. (127 to 254 mm) thinner than those from the AASHTO method.

11.4 DESIGN OF FLEXIBLE PAVEMENT SHOULDERS

As defined by AASHO (1968), a highway shoulder is the "portion of roadway contiguous with the traveled way for accommodation of stopped vehicles for emergency use, and for lateral support of base and surface courses." Shoulders also provide recovery space for errant vehicles, lateral clearance for signs and guardrails, improved sight distance in cuts, area for maintenance operations, and an additional lane for peak hour or detoured traffic.

11.4.1 Current Status of Shoulder Design

During the early years of highway construction, the need for first-class shoulders was of secondary importance. Therefore, the structural design of shoulder pavements has been developed mostly by experience rather than by rational methods. However, with the tremendous increase in both number and speed of vehicles, the need for adequate shoulders has greatly increased. In this section, a survey of state practices reported by the National Cooperative Highway Research Program (NCHRP, 1979) and a position paper on shoulder design prepared by the AASHTO Joint Task Force on Pavements (AASHTO, 1986) are presented.

Survey of State Practices A comprehensive survey of shoulder design, construction, and maintenance was conducted during 1967 by the Committee on Shoulder Design of the Highway Research Board and again during 1977 by NCHRP. It was found that nearly half of the states did not make any changes in their shoulder design standards during the ten-year period. Following is a summary of the findings reported by NCHRP:

1. The predominant criterion for selecting shoulder type, thickness, width, and slope is the combination of highway classification and traffic volume.
2. Although surface drainage can be provided by the cross slope of the shoulders, a significant number of states use some combination of dikes, catch basins, and gutters to

Downloaded From : www.EasyEngineering.net

Downloaded From : www.EasyEngineering.net

minimize slope erosion. For subsurface drainage, the predominant policy is to use underdrains or a free-draining base.

3. Shoulder conditions are evaluated in nearly all states through visual inspections, usually by a member of the maintenance team.
4. Most states use the same width and slope of shoulders for both rigid and flexible pavements. On interstate highways and freeways, nearly 80% of the states use a 10-ft (3-m) width for the outside shoulder. More than 40% of the states use a 4-ft (1.2-m) width for the median shoulder; the other states use a median shoulder of 3 to 10 ft (0.9 to 3.0 m), depending upon traffic volume and number of lanes. Shoulder slope is usually the same for both outside and median shoulders. The predominant slope is 4% or $\frac{1}{2}$ in./ft.
5. Only five states permit regular use of shoulders for slow-moving vehicles, although ten states permit such use under certain conditions.
6. All states use a 4-in. (102-mm) white reflectorized edge stripe to delineate the outside shoulder and a yellow edge stripe to delineate the median shoulder. However, a number of states supplement the edge stripe with contrasting color, texture, or rumble strips on the shoulder. Edge stripes are usually placed on the travel lane at or near the shoulder, but some states placed them on the paved shoulder.

Position Paper on Shoulder Design In view of the wide variety of practices related to shoulder design, a position paper was published as Appendix E in the AASHTO design guide. It was mentioned that California has a formal procedure for shoulder design, 14 other states have documented policies but no formal procedure, 28 states have no policy, and 5 states pave their shoulders integrally with the mainline pavements. Therefore, a definite need exists to develop criteria for a unified and widely accepted shoulder design guide.

The paper lists the following points that may need to be considered in shoulder design:

1. Shoulder thickness design as related to load-carrying requirements
2. Cost and service criteria for stabilization of shoulder aggregate base course
3. Problems associated with the interface of pavement edge and shoulder edge
4. Abrasive effects of traffic
5. Permeability or degree of imperviousness required for shoulder aggregate base course
6. Relationship between shoulder performance and subgrade support
7. Relationship of shoulder drainage subsystem to overall subsurface drainage system
8. Construction and maintenance methods and operations that result in adverse shoulder performance
9. Effect of environment on shoulder performance
10. Type and texture of shoulder surface for waterproofing and delineating purposes
11. Effects of shoulder geometrics on performance
12. Warrants for paved shoulders

Downloaded From : www.EasyEngineering.net

Downloaded From : www.EasyEngineering.net

Regarding the specific design of shoulders, the paper lists the following recommendations:

1. Design shoulder thickness to meet criteria reflecting the magnitude and frequency of loads to which the shoulder will be subjected.
2. Integrate shoulder drainage with the overall pavement subdrainage system.
3. Avoid the use of aggregate base courses having a significant amount of fine materials passing through a No. 200 sieve, to prevent frost heaving, pumping, clogging of the shoulder drainage system, and base instability.
4. Take advantage of the desirable performance features of plant-mixed bituminous and various stabilized shoulder materials as opposed to bituminous surface-treated, unbound shoulder aggregate bases.
5. Have a definite program of shoulder maintenance.
6. Take advantage of the desirable performance of rigid shoulders adjacent to rigid mainline pavements.
7. Develop criteria for paving shoulders.

The position paper was submitted to the states for comments in 1981. There was no general consensus expressed. However, the following comments are pertinent and reflect the preferences of individual agencies:

1. Design mainline and shoulder pavements as a single unit, to allow for future additions of new traveled lanes.
2. Use the same material for both mainline and shoulder pavements and tie concrete shoulders to the mainline concrete pavement.
3. Provide for means to seal the joint between the shoulder and the traveled way.
4. Develop shoulder design criteria for low-volume roads and investigate the advantage and economy of using a 28- to 30-ft (8.5- to 9.1-m) mainline section with aggregate shoulders.
5. Give proper consideration to a full-depth shoulder alternative.
6. Consider the use of shoulders for detouring traffic or as an extra lane during peak hours.

11.4.2 Prediction of Traffic for Shoulder Design

The factors affecting shoulder design are similar to those affecting mainline pavement design. The major difference is the amount of traffic. Traffic volume on shoulders is lower than on mainline pavements and more difficult to predict. Three types of traffic may be considered in shoulder design: encroaching traffic, parking traffic, and regular traffic. Regular traffic is considered only if the use of shoulder as an additional lane for peak hour or detoured traffic is anticipated. If there is no regular traffic, the sum of encroaching and parking traffic is used to design the inner edge of shoulder adjacent to the mainline pavement, and parking traffic is used to design the outer edge of shoulder. If a uniform thickness is used for shoulders, only the inner edge need be considered. However, this may not be true for rigid pavement shoulders, because the stresses and

Downloaded From : www.EasyEngineering.net

Downloaded From : www.EasyEngineering.net

deflections at the outer edge are much greater than those at the inner edge and may cause more damage even though the traffic volume is smaller.

Encroaching Traffic When there is a paved shoulder and no lateral obstruction within the shoulder area, trucks using the outer traffic lane tend to encroach on the shoulder as much as 12 in. (305 mm) and sometimes even more. In California (1972), shoulder sections are designed for 1% of the mainline traffic in the adjacent lane with a minimum traffic index of 5, which corresponds to approximately 10^4 equivalent 18-kip single-axle load applications. Results of a study in Georgia (Emery, 1975) showed that the use of 1% is low for some traffic flow conditions. In the absence of additional data, Barksdale and Hicks (1979) recommended that, for free flow traffic conditions in rural areas of the south, the inner edge of the shoulder should be designed for at least 2 to 2.5% of the truck traffic on the outer lane.

Because local conditions vary significantly, the best way to determine the percentage of encroaching traffic is to make an actual survey on a segment of highway with paved shoulders, which has the same traffic, geometric, and topographic conditions as the design case in question. For the study performed in Georgia, trucks were selected at random and followed by observers for 10 miles (16 km). Those trucks not completing the full 10-mile (16-km) trip were dropped from the analysis. The longitudinal distance for each encroachment is estimated from the prevailing speed and the time during which the truck encroaches on the shoulder. The percent encroaching traffic, which is the ratio of load applications on the shoulder to those on the adjacent lane, can be computed by

$$P_e = \frac{N_e L_e}{N_o L_o} \times 100 \tag{11.52}$$

in which P_e is the percent encroaching traffic, N_e is the total number of encroachments per day, L_e is the average length of each encroachment, N_o is the number of load applications per day on the outside lane, and L_o is the length of observed distance, such as 10 miles (16 km) used in the Georgia study. Note that $N_e L_e$ is the total length of encroachment for all trucks and $N_e L_e/N_o$ is the length of encroachment per truck, so P_e can also be defined as the length of encroachment per truck within an observed distance L_o.

Field observations indicate that P_e usually varies from 1 to 8% of the traffic volume on the adjacent lane. The percentage of parking traffic should be added to P_e, because any truck must encroach to park on the shoulder.

Example 11.14:

This example is the result of an actual survey on a 10-mile segment of I-75 at Perry, Georgia (Emery, 1975). Given the number of trucks on the outside lane per day $N_o = 2239$, the number of shoulder encroachments in the 10 mile (16 km) stretch $N_e = 7389$, and the average distance of each encroachment $L_e = 384$ ft (117 m), determine the percent encroachment P_e.

Solution: Given $N_e = 7839$, $L_e = 384$ ft (117 m), $N_o = 2239$, and $L_o = 52{,}800$ ft (16,100 m), from Eq. 11.52, $P_e = [(7389 \times 384)/(2239 \times 52{,}800)] \times 100 = 2.4\%$.

Downloaded From : www.EasyEngineering.net

Downloaded From : www.EasyEngineering.net

Parking Traffic Parking traffic is the number of load applications for trucks that park on the shoulder for emergencies or other purposes. This information can also be estimated for the design section by using traffic counts on an existing pavement with similar traffic and design characteristics. Parking traffic usually varies greatly along a given route, depending on geometric and interchange conditions. Because most trucks park near interchange ramps, it may be necessary to identify separate design sections for areas where parking is likely and for areas where minimum parking is expected. The parking survey should last at least one day and cover the early morning hours, during which more parking usually takes place.

Similar to percent encroaching traffic, the percent parking traffic can be computed by

$$P_p = \frac{N_p L_p}{N_o L_o} \times 100 \tag{11.53}$$

in which P_p is the percent parking traffic, which is the ratio between parking traffic and the traffic on the outside lane: N_p is the number of parked trucks per day; L_p is the average distance the trucks drive on the shoulder during a typical stop, which can be determined from a field survey; N_o is the number of trucks traveling on the outside lane per day; and L_o is the length of segment for the parking survey. Field observations indicate that P_p may range from 0.0005 to 0.02 percent. Note that the percent parking traffic is much smaller than the percent encroaching traffic and can usually be neglected.

Example 11.15:

Based on a limited field survey on I-80 in Illinois, the average number of trucks that might park on a 2-mile (3.2-km) stretch of shoulder during one day could range from 1 to 25 (Sawan and Darter, 1979). If the number of trucks on the outside lane is 2951 per day and a truck drives an average of 200 ft (61 m) during each parking manuever, determine the range of percent parking traffic.

Solution: Given $N_p = 1$, $L_p = 200$ ft (31 m), $N_o = 2951$, and $L_o = 2 \times 5280 = 10{,}560$ ft (1573 m), from Eq. 11.53, $P_p = [(1 \times 200)/(2951 \times 10{,}560)] \times 100 = 0.00064\%$. If $N_p = 25$, $P_p = 0.00064 \times 25 = 0.016\%$. The range of P_p is from 0.00064 to 0.016%.

Regular Traffic If it is anticipated that the shoulder will be used by regular traffic at any stage of its design life, this additional traffic should be added to the encroaching and parking traffic to form the total shoulder design traffic. The ultimate design is to consider the shoulder as an extra lane with the same traffic and cross section as that of the mainline outer lane.

11.4.3 Thickness Design Concepts

As indicated in the AASHTO position paper, many problems need to be solved before a unified and widely accepted shoulder design procedure can be developed. In this section, some of the design concepts are discussed.

Type of Shoulders The first decision to be made is the type of shoulder to be used. The Technical Advisory issued by FHWA (1982) recommends the use of similar materials for

Downloaded From : www.EasyEngineering.net

Downloaded From : www.EasyEngineering.net

mainline and shoulder pavements. Therefore, flexible shoulder pavements should be used with flexible mainline pavements, and rigid shoulder pavements should be used with rigid mainline pavements. If asphalt shoulders are placed adjacent to concrete mainline slabs, serious problems will occur at the longitudinal joint between slabs and shoulders because the difference in thermal expansion and contraction between dissimilar materials will introduce additional stresses on joint sealants that are already being stressed by differential vertical deflections across the joint. The problem is further compounded by the fact that few joint sealants are suited to bond dissimilar materials. Longitudinal joints between flexible shoulders and flexible mainline pavements generally do not exhibit serious problems and can easily be sealed, even if some separation takes place.

Configuration of Shoulder Section The thickness of shoulder can be uniform or nonuniform. Many agencies suggested that the same thickness be used for shoulder and mainline pavements to allow for maximum safety and performance, flexibility in shoulder use during periods of construction or congestion, and the potential for future additions of traffic lanes. Some suggested that the thickness at the inner edge of the shoulder pavement should be the same as the thickness of the mainline pavement, to avoid problems associated with varying support and volume change on both sides of the joint (ERES, 1987). Barksdale and Hicks (1979) recommended that shoulder sections be designed structurally for the expected amount of traffic due to encroachment, using currently accepted mainline design methods. Because virtually all truck encroachments and shoulder failures occur within 2 ft (0.61 m) of the longitudinal joint, Barksdale and Hicks suggested the use of a shoulder design having a variable structural strength, such as tapered sections or special support in the critical areas of heavy loading. On low-volume roads, the use of a 28- to 30-ft (8.5- to 9.1-m) mainline section with granular shoulders has special advantage. The mainline pavement can be striped to provide standard traffic lanes and reduce premature shoulder deterioration due to encroachment, while a sufficiently wide granular shoulder is provided to permit emergency use.

It can be seen that a variety of opinions exist on shoulder thickness design. If the thickness of the shoulder is the same as that of the mainline pavement and shoulder drainage is integrated with the overall pavement drainage design, as has been practiced by several states, there is no need to design shoulder thickness separately. The reason for using thinner pavements or tapered sections for shoulders is economy. It is difficult to find a consensus on shoulder design, so the final selection should be based on local experience, engineering judgment, and the availability of funds.

Environmental Effects The use of thinner shoulder sections makes environmental effects, such as roadbed swelling, frost heave, and drainage conditions, become more important, and they could govern the thickness of shoulder pavement required.

First, the foundation soil should be analyzed to determine its susceptibility to frost damage. If the average depth of frost penetration is more than 6 in. (152 mm), the thickness of the base and subbase must be selected to provide frost protection by using some appropriate methods, such as the procedure developed by the U.S. Army Corps of Engineers (1961).

Next, the need for proper drainage must be evaluated. A system for evaluating the moisture accelerated distress (MAD) was developed by Carpenter *et al.* (1981) and

Downloaded From : www.EasyEngineering.net

Downloaded From : www.EasyEngineering.net

may be used for shoulder design. If the MAD index, which is based on the climate of the area and the properties of the subgrade, indicates that drainage is required, a drainage layer is assumed, and its adequacy is checked by using the drainage evaluation criteria in the MAD system. If the assumed drainage is inadequate, a different design must be assumed and the process must be repeated, until a satisfactory design is obtained. The thickness of the drainage layer should then be compared with the minimum thickness required for frost penetration. If the drainage layer is thinner than what is required for frost protection, the thickness of drainage layer must be increased or a subbase added and the adequacy of the design reevaluated. The MAD system can also be used to determine the need for underdrains, if any.

Finally, based on the predicted traffic, material properties, and climate variables, a structural design can be conducted using the method for mainline pavements. The thicknesses thus determined must be checked against those required for frost penetration and drainage and modified as necessary to meet these criteria.

SUMMARY

This chapter presents several methods for flexible pavement design, including a calibrated mechanistic procedure, the Asphalt Institute method, the AASHTO design guide, and several methods for the design of shoulders.

Important Points Discussed in Chapter 11

1. The ideal design method, still under development, is the calibrated mechanistic procedure. It consists of a number of response models to evaluate the stresses and strains in the pavement system and a number of distress models using the pertinent stress or strain as an input. These distress models require careful calibration and verification to ensure that satisfactory agreements between predicted and observed distress can be obtained.
2. The response models include the heat transfer model, the moisture equilibrium model, the infiltration and drainage model, and the structural model. The finite element structural model can analyze nonlinear pavement systems more realistically by considering the variation of elastic modulus within each layer. If only critical stresses or strains are desired, the layer system program with an iterative scheme for nonlinear analysis might also serve the purpose.
3. The distress models include the fatigue cracking model, the rutting model, and the low-temperature cracking model. The roughness model and the performance model may also be included, if needed. When the design is based on each type of distress, it is preferable to use the various load groups for damage analysis, rather than an equivalent single-axle load, because the equivalent factor for each type of distress is different from that for the others.
4. From a theoretical view point, the use of the reliability concept to define the extent of distress is a much better approach than the use of the deterministic method. The variability of the design factors means that a pavement may or may not fail when the stress is exactly equal to the strength or when the damage ratio is exactly equal to one. However, the extent of distress depends on the probability

Downloaded From : www.EasyEngineering.net

Downloaded From : www.EasyEngineering.net

that the stress will exceed the strength or the damage ratio will exceed one. The thermal cracking model developed by Shahin and McCullough (1972) was described in details because it applies the reliability concept to predict both the low-temperature cracking and the thermal fatigue cracking. It is hoped that the same concept would be used in other distress models.

5. The design method from the Asphalt Institute is based on the equivalent 18-kip single-axle load. Two failure criteria are employed: (a) fatigue cracking based on the horizontal tensile strain at the bottom of the asphalt layer and (b) rutting based on the vertical compressive strain on top of the subgrade. The method applies the cumulative damage concept and assumes that failures occur when the damage ratio is equal to one. The variability of the design factors and the reliability of the design are not considered in the design procedure.
6. A computer program called DAMA was used by the Asphalt Institute to develop a series of design charts for full-depth HMA, HMA over aggregate base, and HMA over emulsified asphalt base. The program considers the asphalt layer and the subgrade as linear elastic and the granular base as nonlinear elastic. Each year was divided into 12 months, and the elastic moduli of the asphalt layer, the granular base, and the subgrade were varied monthly with assumed climatic conditions. Three temperature regimes (representing New York, South Carolina, and Arizona) were assumed, but only the charts for South Carolina, which represents the climate over a large part of the United States, were included in the 1981 version of MS-1 and reproduced here. Charts representing New York and Arizona were later added in the 1991 version of MS-1.
7. The Asphalt Institute devoted extensive effort to comparing the predicted thickness obtained from the charts with the actual thickness on pavements of known performance. Six separate sources of data were utilized, representing a total of 394 individual data points for pavements from California, Minnesota, Illinois, and Canada. It was found that the predicted thickness was about 1.61 in. (41 mm) greater than the actual thickness, so the use of the design charts is quite conservative. For lack of documented data, the southern and eastern parts of the United States were excluded from the comparison.
8. The AASHTO design method is based on the empirical regression equation obtained from the AASHO Road Test in Ottawa, Illinois. The design is based on the equivalent 18-kip single-axle load. The original equation is applicable only to the specific environmental and soil conditions at the test site. To make it applicable to other areas of the nation, the equation was modified by introducing an effective roadbed soil resilient modulus M_R and two drainage coefficients m_2 and m_3 for granular base and subbase, respectively. Although only one type of HMA, granular base, and subbase was used in the Road Test, the equation can be applied to other materials by varying the layer coefficients, which have been correlated empirically with the resilient moduli.
9. The effective roadbed resilient modulus is an equivalent modulus that would result in the same damage if seasonal modulus values were used. The equation for evaluating relative damage was derived from the AASHTO equation based on the cumulative damage concept. It has been demonstrated that most of the damage is done during the short period of spring breakup. As a result, the effective

Downloaded From : www.EasyEngineering.net

Downloaded From : www.EasyEngineering.net

roadbed resilient modulus is much smaller than the normal modulus usually taken during summer or fall.

10. A salient feature of the AASHTO design guide is the inclusion of reliability and standard deviation as design factors. The guide encourages the use of stage construction for high-traffic facilities by selecting a longer analysis period with an initial performance period plus at least one rehabilitation period. Because the Road Test lasted only about two years, the AASHTO equation does not include the loss of serviceability due to the environmental effects of roadbed swelling and frost heave. The consideration of these effects on stage construction was illustrated.
11. A definite need exists to develop criteria for a unified and widely accepted shoulder design guide. To avoid the difficulty of sealing the longitudinal joint between shoulder and mainline pavements, asphalt shoulders should be used for asphalt pavements but not for PCC pavements.
12. Factors affecting shoulder design are similar to those affecting mainline pavement design. Shoulders should be designed according to the amount of traffic anticipated, including encroaching traffic, parking traffic, and regular peak hour or detoured traffic, if any. When thinner sections are used for shoulders, the environmental effects, such as roadbed swelling, frost heave, and drainage conditions, become more important and could govern the thickness of shoulder required.

PROBLEMS

11.1 Figure P11.1*a* shows a thin pavement laid on a subgrade consisting of a layer of sand, 5 ft thick, underlain by a clay. The water table is 10 ft below the surface. The mass unit weight of sand is 120 pcf and that of clay is 100 pcf. The compressibility factor for the clay is 0.5. The soil suction–moisture content curves for each soil are shown in Figure P11.1*b*. Neglecting the weight of the pavement, determine the moisture content of the subgrade at the following two points: (a) point A, which is 7 ft above the water table, and (b) point B, which is 3 ft above the water table. [Answer; 10%, 21%]

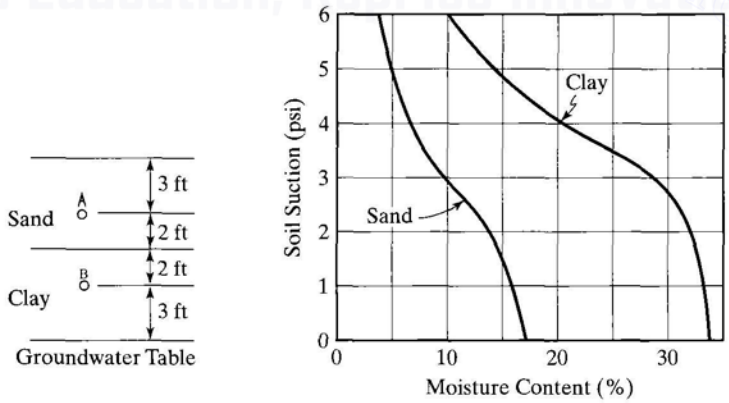


FIGURE P11.1

Downloaded From : www.EasyEngineering.net

Downloaded From : www.EasyEngineering.net

11.2 Based on the test results shown in Figures 11.4 and 11.5, estimate the coefficients of permanent deformation in the Ohio State model, as indicated by *a*, *b*, and *m* in Eq. 11.16. [Answer: 0.89, 0.91, 0.79]

11.3 The fatigue equation for an asphalt pavement is $N_f = 5 \times 10^{-6}(\epsilon_t)^{-3}$, in which ϵ_t is the tensile strain. If the pavement is subjected to 5000 thermal cycles with a maximum tensile strain of 0.0005 in./in. and the coefficient of variation of N_f, $C[N_f]$, is 0.8, estimate the percent area cracked that is due to thermal fatigue cracking. [Answer: 0.5%]

11.4 Figure P11.4 shows an asphalt pavement with the thicknesses and the resilient moduli of the granular base and subgrade as indicated. The hot mix asphalt has a viscosity of 2.5×10^6 poise at 70°F, a bitumen volume of 11%, and a fine content of 5% passing No. 200 and is subjected to a loading frequency of 8 Hz. The air void content is 4% for the surface course and 7% for the binder course. The mean monthly air temperature is 68°F. By the Asphalt Institute procedure, as used in the DAMA program, determine (a) temperatures for surface and binder courses using Eq. 3.27, (b) dynamic moduli of surface and binder courses using Eq. 7.27, and (c) the modulus of the untreated base using Eqs. 3.28 and 3.29. [Answer: (a) 81.3 and 78.3°F, (b) 4.2×10^5 and 3.8×10^5 psi, and (c) 20,700 psi]

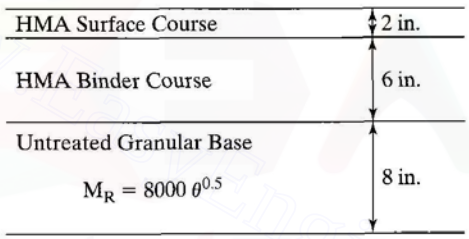


FIGURE P11.4

11.5 A six-lane (three in each direction) rural interstate highway has a truck count of 1885 per day (including two-axle, four-tire panel and pickup trucks) and an annual growth rate of 4%. The HMA will be laid on an untreated granular base, 8 in. thick, which is placed on a subgrade with a resilient modulus of 10,000 psi. (a) Referring to Tables 6.9 and 6.10, estimate ESAL for a design period of 20 years by the Asphalt Institute method. (b) Determine the HMA thickness required by the Asphalt Institute method. (c) If part of the HMA is replaced by emulsified asphalt mix type I, determine the thicknesses of HMA and of emulsified asphalt required. [Answer: (a) 4.26×10^6, (b) 10 in., (c) 2 in. and 8.5 in. or 3.5 in. and 7 in.]

11.6 A stage construction is planned for a full-depth asphalt pavement with a subgrade resilient modulus of 5000 psi. The design period is 30 years and is divided into three stages: the first 5 years, the middle 10, and the last 15. The first year traffic on the design lane is 20,000 equivalent 18-kip single-axle load applications, and the annual growth rate is 3.5%. If the damage ratios at the end of each stage are 0.5, 0.75, and 1.0, respectively, determine the thicknesses of HMA to be placed in each stage by the Asphalt Institute method. [Answer: 8.5, 2.5, and 1.5 in.]

11.7 From the properties given in Problem 11-4, estimate the structural number of the pavement shown in Figure P11.4, assuming that the drainage coefficient of the base is 1. [Answer: 4.6]

11.8 For a mean annual air temperature of 45°F and a normal modulus of 22,500 psi, determine the effective roadbed soil resilient modulus for the monthly moduli shown in Table 11.10 [Answer: 22,200 psi]

Downloaded From : www.EasyEngineering.net

Downloaded From : www.EasyEngineering.net

11.9 A 12-in. full-depth asphalt pavement is placed on a subgrade with an effective roadbed resilient modulus of 10,000 psi. Assuming a layer coefficient of 0.44 for the hot mix asphalt, a drop in PSI from 4.2 to 2.5, an overall standard deviation of 0.5, and a predicted ESAL of 3×10^7, determine the reliability of the design by the AASHTO equation, and check the result by the AASHTO design chart. [Answer: 88%]

11.10 An interstate highway pavement composed of a HMA surface course, a cement treated base course, and a sand–gravel subbase is to be designed for an ESAL of 1.2×10^6. The quality of drainage is considered fair because water can be removed from the subbase within a week. However, there is a large amount of precipitation, so more than 25% of the time the pavement will be exposed to moisture levels approaching saturation. The material properties are as follows: effective roadbed soil resilient modulus = 5500 psi, resilient modulus of subbase = 15,000 psi, unconfined compressive strength of cement-treated base at 7 days = 500 psi (see Figure 7.15*c* for correlation), and resilient modulus of HMA = 4.3×10^5 psi. Assuming a minimum thickness for HMA, determine the thicknesses of the surface, base, and subbase courses required. [Answer: 3 in., 6 in., and 9 in.]

11.11 The design ESAL for a mainline pavement is 5×10^6. The encroaching traffic on the shoulder is 2.5%, and the parking traffic is 0.02%. The subgrade resilient modulus is 8000 psi, and a full-depth construction is used for both mainline and shoulder pavements. By the Asphalt Institute method, determine the thicknesses of mainline and shoulder pavements required. [Answer: 12 in., 6.5 in.]

11.12 Given ESAL = 5×10^6, $P_e = 2.5\%$, $P_p = 0.02\%$, $\Delta PSI = 1.7$, and $M_R = 5000$ psi, determine the structural number SN of the mainline and shoulder pavement required for a reliability of 50%. [Answer: 4.2, 2.4]

Downloaded From : www.EasyEngineering.net

Downloaded From : www.EasyEngineering.net

CHAPTER 12

Rigid Pavement Design

12.1 CALIBRATED MECHANISTIC DESIGN PROCEDURE

As with flexible pavements, the calibrated mechanistic design procedure involves the application of structural models to calculate pavement responses, the development of distress models to predict pavement distress from structural responses, and the calibration of the predicted distress with the observed distress on in-service pavements. Figure 12.1 shows the general methodology for rigid pavement design. This figure is similar to Figure 11.1 for flexible pavements, except for step 5 on structural models and step 8 on distress models.

The structural models for rigid pavement analysis are more advanced than the distress models. Several finite element programs can be used as structural models, but most of the distress models are regression equations derived empirically with a large scatter of data. The major types of distress to be modeled include fatigue cracking, pumping, faulting, and joint deterioration for jointed concrete pavements and punchouts for continuous reinforced concrete pavements. Some steps in Figure 12.1 are described in Sections 11.1.1 and 11.1.2; only the steps involving these new models are discussed in this section. Most of the models presented herein were developed by the University of Illinois and described in Report 1-26 (NCHRP, 1990).

12.1.1 Structural Models

To analyze rigid pavement systems accurately, Report 1-26 (NCHRP, 1990) indicated that the structural models used must have the following minimum capabilities:

1. To analyze slabs of any arbitrary dimensions.
2. To analyze systems with two layers (slab and subbase), either bonded or unbonded, with the same or different material properties.
3. To analyze slab systems on either a liquid or a solid subgrade.

Downloaded From : www.EasyEngineering.net

Downloaded From : www.EasyEngineering.net

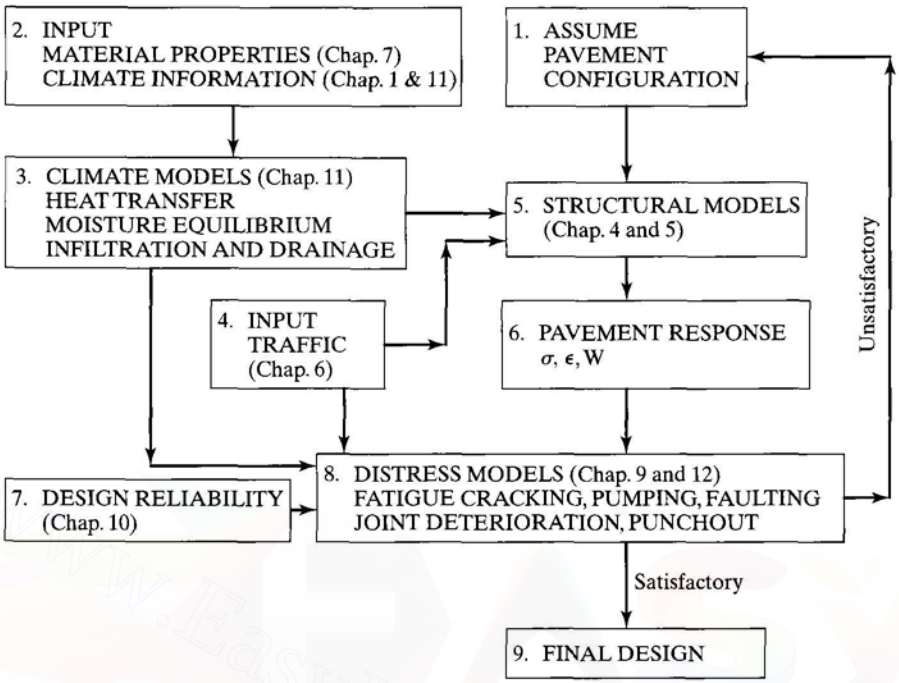


FIGURE 12.1

Methodology of calibrated mechanistic procedure for rigid pavement design.

4. To analyze slab systems with either uniform or nonuniform support, so that loss of support due to erosion or other causes can be taken into account.
5. To analyze multiple slabs with load transfer across the joints or cracks.
6. To consider slab warping and curling simultaneously with load responses.
7. To analyze slabs with variable crack spacings for CRCP design.
8. To analyze slabs with any arbitrary loading conditions, including single or multiple wheels, variable tire pressures, and loads applied at arbitrary assigned distances from cracks, joints, or slab edges.
9. To analyze pavement systems with arbitrary shoulder conditions, including asphalt shoulders, tied concrete shoulders, and extended driving lanes with asphalt or concrete shoulders beyond the extended slab.
10. To analyze systems with nonuniform slab or shoulder thicknesses.

After reviewing several finite element models, Report 1-26 recommended the use of ILLI-SLAB as the basic model for the analysis of rigid pavements. The KENSLABS program presented in this book also meets all the preceding requirements. In addition to liquid and solid foundations, KENSLABS can be applied to a layer subgrade consisting of up to six layers.

Report 1-26 also indicated that the finite element programs require a large computer core capacity, and conventional personal computers with a core capacity of 640 K

Downloaded From : www.EasyEngineering.net

Downloaded From : www.EasyEngineering.net

are not adequate to obtain reliable and accurate results. This statement was true at the time of the report. With the recent advance in personal computers and the introduction of the Windows operating system, core capacity is no longer a problem. However, a large finite-element program still requires a considerable time to run.

One way to reduce the computer time needed is to develop algorithms or regression equations to replace structural models for calculating pavement responses (Zollinger and Barenberg, 1989). These algorithms can be developed by running a finite element program thousands of times and fitting the results with regression equations. Tabulated values of the regression coefficients can be provided on a disk; the algorithms can be run on a PC. However, this method can be used only for typical designs with a limited number of variables that can be changed, such as PCC thickness, modulus of subgrade reaction, magnitude of single-axle load, and concrete modulus of elasticity. For unusual situations, such as axle loads with special configurations, voids under the slabs, two layers of slabs, and slabs of nonuniform thickness, the finite-element program must still be used.

12.1.2 Fatigue Cracking Models

The fatigue of PCC was described in Section 7.3.2. As with flexible pavements, the accumulation of fatigue damage can be expressed as a summation of damage ratios, defined as the ratio between predicted and allowable number of load repetitions. However, instead of relating to tensile strain, the allowable number of load repetitions is related to the stress ratio, which is the ratio between the flexural stress and the modulus of rupture. The same probability concept used to define percent area cracked can be used to define percent of slabs cracked.

Truck Load Placement The fatigue of concrete can cause both transverse cracking, which initiates at the pavement edge midway between transverse joints, and longitudinal cracking, which initiates in the wheelpaths at transverse joints, usually at the wheelpath nearest the slab centerline. Figure 12.2 shows the most critical loading and stress locations to be considered for fatigue analysis. Transverse cracking is caused by the midslab edge loading, and longitudinal cracking is caused by the joint loading.

The lateral distribution of traffic means that wheel loads are not applied at the same location, so only a fraction of the load repetitions need be considered for fatigue damage. Report 1-26 suggested the use of an equivalent damage ratio, EDR, for each critical loading position. EDR is the ratio of the traffic applied at a critical location that

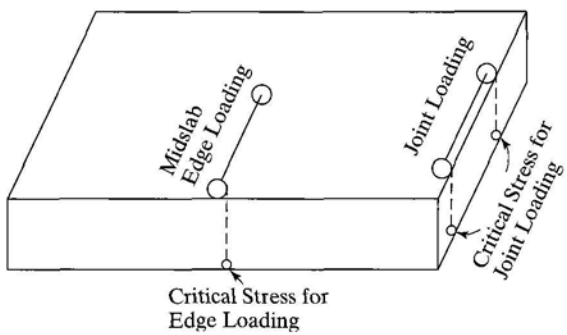


FIGURE 12.2
Critical loading and stress locations for fatigue analysis.

Downloaded From : www.EasyEngineering.net

Downloaded From : www.EasyEngineering.net

will produce the same accumulated fatigue damage as the total traffic distributed over all locations. It was demonstrated in Report 1-26 that an EDR of 0.05 to 0.06 can be used for the midslab edge loading with asphalt shoulders and that an EDR of 0.25 to 0.28 can be used for joint loading. For edge loading with tied concrete shoulders, the EDR ranges from 0.12 to 0.34. Therefore, the truck-load placement, which is not a factor in flexible pavement design, must be carefully considered in rigid pavement design.

Curling Stress Report 1-26 suggested the use of combined loading and curling stresses for determining the stress ratio and thus the allowable number of load repetitions. In addition to the number of periods and load groups, a new loop indicating curling conditions must be added to Eq. 3.19:

$$D_r = \sum_{i=1}^{p} \sum_{k=1}^{3} \sum_{j=1}^{m} \frac{n_{i,k,j}}{N_{i,k,j}} \tag{12.1}$$

In this equation, D_r is the accumulated damage ratio over the design period at the critical location, i is the counter for periods or subgrade support values, p is the total number of periods, k is the counter for three curing conditions (day, night, and zero temperature gradient), j is the counter for load groups, m is the total number of load groups, $n_{i,k,j}$ is the predicted number of load repetitions for the jth load group, kth curling condition, and ith period, and $N_{i,k,j}$ is the allowable number of load repetitions for the jth load group, kth curling condition, and ith period. The inclusion of curling stress complicates the computation, because the traffic has to be divided into three time periods, each with a different temperature gradient. It does not appear reasonable to combine loading and temperature stresses, since they do not occur at the same frequency. A pavement may be subject to thousands of load repetitions per day due to traffic, but the number of repetitions due to temperature curling is mostly only one a day. If curling stresses cannot be ignored and longer panel lengths have significant effects on fatigue cracking because of higher curling stresses, it is more reasonable to consider the damage ratios due to loading and curling separately and then combined, as illustrated by the Shahin–McCullough model for flexible pavements presented in Section 11.1.4.

Curling may not affect the fatigue life significantly because the curling stress may be subtracted from or added to the loading stress, thus neutralizing the effect. The edge stress is further reduced by moisture warping because the moisture contents at the bottom of slab are very frequently higher than those at the top. The curling stress should be much reduced when new pavements are to be constructed with reasonably short panel lengths. The calibration of the model can further minimize the effect of curling stress. For example, Figure 12.3 shows a plot of calibrated performance curves for jointed concrete pavements relating the percent slabs cracked to the accumulated damage ratio. The stress ratio used in calculating the fatigue relationships shown in the figure included both loading and curling stresses. If curling stresses were eliminated from this calculation, different performance curves would be obtained. However, the percent slabs cracked should not be significantly affected if the same procedure, either including or excluding the curling stress, is used in both design and calibration processes.

The performance curves shown in Figure 12.3 were based on field calibration. For 50% reliability, the theoretical percent slabs cracked at a damage ratio of 1 should be

Downloaded From : www.EasyEngineering.net

Downloaded From : www.EasyEngineering.net

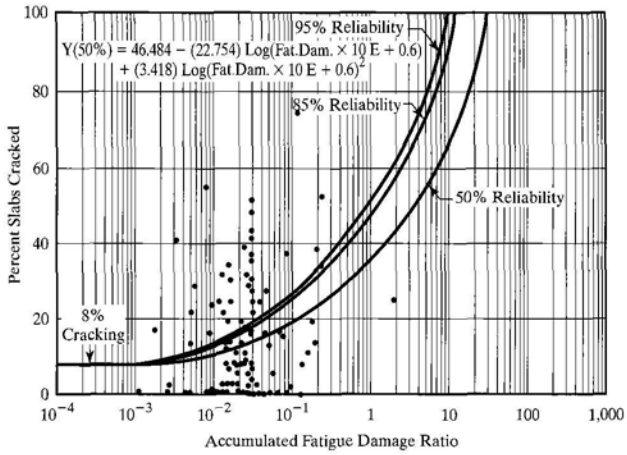


FIGURE 12.3
Calibrated performance curves based on Illinois COPES data. (After NCHRP (1990).)

50%, but the percentage shown in the figure is only 27%. One possible cause for the discrepancy is the difficulty of determining the concrete modulus of rupture during the entire evaluation period from the initial loading to the time of evaluation. Additional research needs to be done on the best method for estimating concrete strength in existing pavements and on how the observed cracking can be correlated with the damage ratio and the probability of cracking.

12.1.3 Pumping and Erosion Models

There is an important mode of distress in addition to fatigue cracking that needs to be addressed in the design of rigid pavements. This is the pumping and erosion of material beneath and beside the slab. In fact, most of the failures in the Maryland and AASHO road tests were the result of pumping.

Factors that influence pumping and erosion include the presence of water, the rate at which water is ejected under the slab, the erodibility of the subbase material, the magnitude and number of repeated loads, and the amount of deflection. No mechanistic models currently available take all of the above factors into account. The only available model is the one developed by PCA, which is described in Section 12.2. The PCA model was based primarily on the results of the AASHO Road Test, and only the corner deflection was taken directly into consideration. Because the subbase materials used in the AASHO Road Test are highly erodible and are currently not used by any of the highway agencies, the application of the model appears to be limited.

Attempts have been made to correlate erosion with rate of water ejection, traffic loads, and pavement deflection through an energy model (Dempsey, 1983; Phu *et al.*, 1986). The thrust of this approach is to calculate the amount of energy involved in the deflection of a pavement system and establish a correlation between the total energy absorbed for given levels of traffic and erosion. These attempts have been moderately successful for specified conditions, but there are other factors affecting erodibility that have not been duly considered. Additional work is needed before these models can be incorporated into a mechanistic-based pavement design procedure.

Downloaded From : www.EasyEngineering.net

Downloaded From : www.EasyEngineering.net

Report 1-26 also presented an empirically based pumping model that considers all factors believed to influence erosion and pumping of rigid pavements. The model, which can be applied to both JPCP and JRCP by including the type of load transfer as a variable, was developed by using nonlinear regression techniques from a data base of 927 pavement sections from seven states in every continental climatic zone. Because some of the regression constants in the model do not appear reasonable, the model is not presented here. Instead, the COPES pumping models (Darter *et al.*, 1985), which include separate equations for JPCP and JRCP, are presented below. Note that the erodibility of the base course, which is an important factor contributing to pumping and was considered in Report 1-26, was not included in the COPES models.

Jointed Plain Concrete Pavements

$$\text{PI} = (N_{18})^{0.443}[-1.479 + 0.255(1 - S) + 0.0605(P)^{0.5} + 52.65(H)^{-1.747} + 0.0002269(\text{FI})^{1.205}] \quad (12.2a)$$

Statistics: $R^2 = 0.68$, SEE = 0.42, $n = 289$

Here,

PI = pumping index rated on a scale of 0 to 3: 0 for no pumping, 1 for low-severity pumping, 2 for medium-severity pumping, 3 for high-severity pumping
N_{18} = number of equivalent 18-kip single-axle loads, in millions
S = soil type based on AASHTO classification: 0 for coarse-grained soils (A-1 to A-3), 1 for fine-grained soils (A-4 to A-7)
P = annual precipitation, in cm
H = slab thickness, in inches
FI = freezing index, in degree days

Jointed Reinforced Concrete Pavements

$$\text{PI} = (N_{18})^{0.670}[-22.82 + 26{,}102.2(H)^{-5.0} - 0.129(D) - 0.118(S) + 13.224(P)^{0.0395} + 6.834(\text{FI} + 1)^{0.00805} \quad (12.2b)$$

Statistics: $R^2 = 0.57$, SEE = 0.52, $n = 481$

Here, D is the indicator for the presence of subdrainage systems: 0 for no subdrainage system, 1 for subdrainage system.

A pumping prediction model was developed by Purdue University and incorporated in the PEARDARP computer program (Van Wiji, 1985; Van Wiji *et al.*, 1989). The model is based on field data from different sources and on the amount of deformation

Downloaded From : www.EasyEngineering.net

Downloaded From : www.EasyEngineering.net

energy in the pavement structure. The volume of pumped material is calculated as a function of the deformation energy produced by traffic. This volume is then adjusted to take into account the variations in subbase type, drainage conditions, load-transfer adequacy, subgrade conditions, and climate. The model can be used in the optimum design of rigid pavements by predicting the effect of different design alternatives on the development of pumping. As is true with any regression model, this model is valid only within the data base from which it was derived. It is hoped that more mechanistic-based models can be developed to replace the regression models.

12.1.4 Faulting Models

Faulting at transverse joints is a serious problem that can lead to severe roughness in jointed concrete pavements. The mechanisms of faulting distress in doweled pavements are quite different from those in undoweled pavements. Therefore, these two pavements are discussed separately.

Doweled Pavements Faulting of doweled pavements is caused by the erosion of concrete around the dowels under repeated loading. Because the design of dowels is based on the bearing stress between dowel and concrete, as described in Section 4.4.1, it is natural to assume that faulting is due to excessive bearing stress. It was found that, if the bearing stress is kept below approximately 1500 psi (10.4 MPa), faulting can be limited to an acceptable level.

The maximum bearing stress on dowel bars can be obtained directly by the finite-element computer programs. As an alternative, Report 1-26 recommended the use of Eq. 4.45 to compute the bearing stress. The procedure is the same as the one described in Example 4.12, Section 4.4.1, except that the load is distributed over an effective length of 1.0ℓ, instead of 1.8ℓ, and the load transferred through the joint is assumed to be $0.45W$ instead of $0.5W$, where W is the total load. Using the preceding method to calculate the bearing stress and assuming a modulus of dowel support K of 1.5×10^6 psi (10.4 GPa), the following regression equation based on 280 pavement sections in the COPES data base was obtained:

$$F = (N_{18})^{0.5377}\,[2.2073 + 0.002171(S)^{0.4918} + 0.0003292(\mathrm{JS})^{1.0793} - 2.1397(k)^{0.01305}] \tag{12.3}$$

In this equation,

F = pavement faulting, in inches
N_{18} = number of equivalent 18-kip single-axle loads, in millions
S = maximum bearing stress, in psi
JS = transverse joint spacing, in ft
k = estimated modulus of subgrade reaction on the top of the subbase, in pci

Several climatic variables, such as the precipitation and freezing indexes, were introduced originally but did not show any statistical significance and, therefore, were not included in the model. This is probably due to the limited number of climatic zones in the data base. Because of insufficient data, many other variables, such as permeable

Downloaded From : www.EasyEngineering.net

Downloaded From : www.EasyEngineering.net

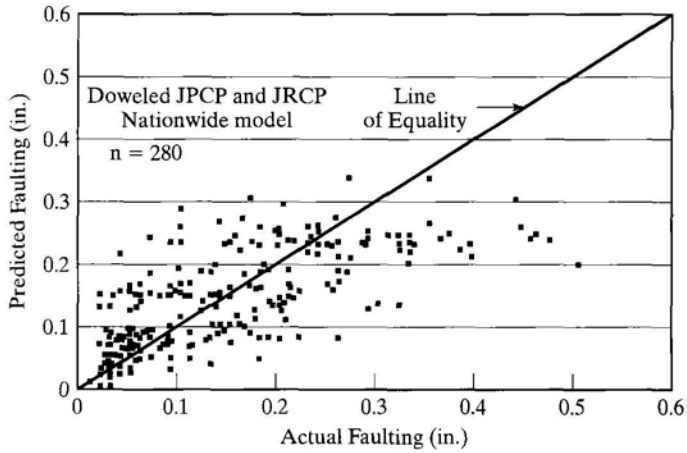


FIGURE 12.4

Predicted faulting versus observed faulting for doweled pavements (1 in. = 25.4 mm). (After NCHRP (1990).)

base, subgrade type, edge support, and sub-drainage are not included. This model must not be used to predict faulting by extrapolation beyond the data range used in its generation. This is particularly true for open-graded drainable bases, which were not included. Figure 12.4 is a plot of predicted faulting versus actual faulting for these 280 sections of doweled pavements. Note that Eq. 12.3 is quite different from Eq. 9.54*a*, which is a later model with a more extended data base and considers the effect of drainage condition, edge support, and soil type.

Figure 12.5 shows the effect of bearing stress on faulting, as obtained from Eq. 12.3, based on N_{18} = 10 million. Two different joint spacings and subgrade moduli

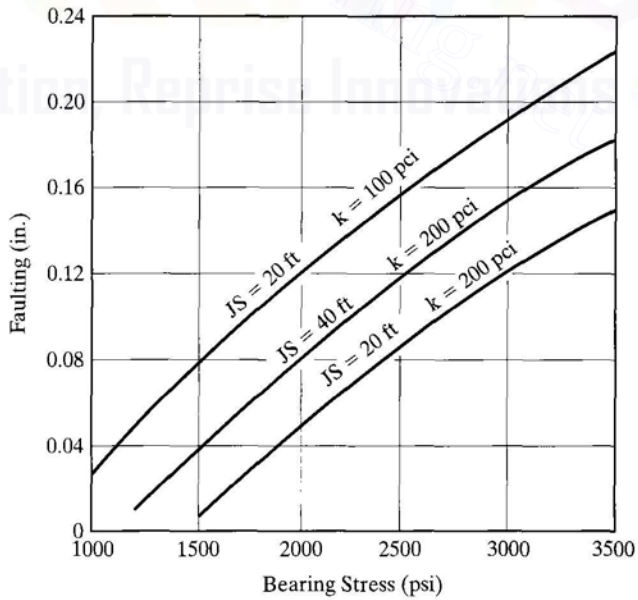


FIGURE 12.5

Effect of bearing stress on faulting. (1 in. = 25.4 mm, 1 ft = 0.305 m, 1 psi = 6.9 kPa, 1 pci = 271.3 kN/m^3).

Downloaded From : www.EasyEngineering.net

Downloaded From : www.EasyEngineering.net

were used. It can be seen that bearing stress has the most significant effect on faulting and joint spacing the least effect.

Undoweled Pavements To date, no mechanistic-based analyses have been attempted for undoweled pavements. The following regression equation was derived from 186 pavement sections in the COPES data base and presented in Report 1-26:

$$F = (N_{18})^{0.3157}[0.4531 + 0.3367(z)^{0.3322} - 0.5376(100w)^{-0.008437} + 0.0009092(\text{FI})^{0.5998} + 0.004654(B) - 0.03608(\text{ES}) - 0.01087(S) - 0.009467(D)] \quad (12.4)$$

Here,

F = faulting, in inches
N_{18} = number of equivalent 18-kip single-axle loads, in millions
z = joint opening, in inches, which can be determined from Eq. 4.36
w = corner deflection, in inches, which was determined from Eq. 4.16 based on a 9000-lb (40-kN) load with a contact pressure of 90 psi (621 kPa) applied at a free corner
FI = mean air freezing index, in degree days
B = erodibility factor for subbase materials: 0.5 for lean concrete subbase, 1.0 for cement-treated granular subbase, 1.5 for cement-treated nongranular subbase, 2.0 for asphalt-treated subbase, 2.5 for untreated granular subbase
ES = edge support condition: 0 for no edge support, 1 for tied edge beam or tied concrete shoulder
S = subgrade soil type: 0 for A-4 to A-7, 1 for A-1 to A-3
D = drainage index, with 0 for no edge drains and 1 for edge drains

Figure 12.6 is a plot of predicted faulting versus observed faulting for these 186 sections of undoweled pavements. Note that Eqs. 12.4 and 9.54*b* are of the same form and contain the same variables, but the regression constants are completely different and due to the scope of the data base.

Table 12.1 shows a sensitivity analysis of faulting in undoweled pavements based on Eq. 12.4. The parameter values shown in column 2 are used as the standard case. In the other seven cases, only the parameter shown in column 1 is changed in value from column 2 to column 3, while the other values remain the same as in column 2. For each case, the amount of faulting and its ratio to the standard case are tabulated.

A review of Table 12.1 indicates that, unless the freezing index is extremely high, edge support and the joint opening, which are directly related to the load transfer across the joint and edge, have the most effect on faulting and that corner deflection, which is related to slab thickness, is not very sensitive to faulting.

12.1.5 Joint Deterioration

Joint deterioration includes spalling and general breakup of the concrete near the joints. No mechanistic methods have been developed to analyze joint deterioration.

Downloaded From : www.EasyEngineering.net

Downloaded From : www.EasyEngineering.net

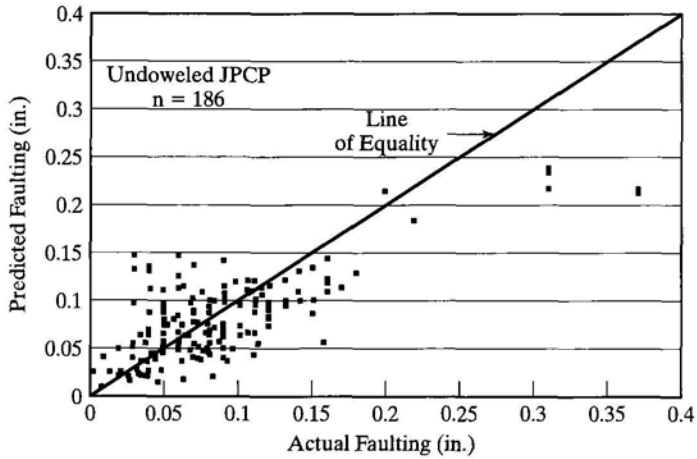


FIGURE 12.6

Predicted faulting versus observed faulting for undoweled pavements (1 in. = 25.4 mm). (After NCHRP (1990).)

TABLE 12.1 Sensitivity Analysis of Undoweled Pavements

Case	Change		Faulting	
	From	To	in.	Ratio
(1)	(2)	(3)	(4)	(5)
Standard case			0.118	1.00
ESAL, N_{18} (10^6)	10	20	0.147	1.25
Joint opening z (in.)	0.04	0.08	0.180	1.53
Corner deflection w (in.)	0.01	0.04	0.131	1.11
Freezing index FI (degree-days)	100	2000	0.268	2.27
Edge support ES	0	1	0.043	0.36
Base erodibility B	2.5	0.5	0.099	0.84
Subgrade soil type S	0	1	0.095	0.81
Drainage index D	0	1	0.098	0.83

Note. 1 in. = 25.4 mm.

The most important factor that causes joint deterioration is the "D" cracking of concrete, as described in Section 9.1.2. Therefore, the use of aggregates that do not cause "D" cracking is the first requisite to prevent joint deterioration.

A statistically based model was developed using the COPES data base. All pavements showing "D" cracking and reactive aggregate distress were removed from the data base, and nonlinear regression techniques were used on the remaining pavement sections. With over 501 pavement sections around the country, the following regression equation was obtained:

$$\text{DETJT} = (\text{AGE})^{2.3503}(N_{18})^{0.62974}\,[-0.0021443 + 3.6239 \times 10^{-6}\,(\text{FI}) + 7.08597 \times 10^{-5}\,(\text{JS}) + 3.5307 \times 10^{-5}\,(\text{SCTE})] \qquad (12.5)$$

Downloaded From : www.EasyEngineering.net

Downloaded From : www.EasyEngineering.net

In this equation,

DETJT = percentage of deteriorated joints
AGE = time in years since construction started
N_{18} = number of 18-kip equivalent single-axle loads, in millions
FI = mean air freezing index, in degree days
JS = transverse joint spacing, in ft
SCTE = Thornthwaite summer concentration of thermal energy

Table 12.2 shows a sensitivity analysis of Eq. 12.5. It can be seen that age and joint spacing have the most effect on joint deterioration, the summer concentration of thermal energy the least effect.

12.1.6 Punchout Models

Punchouts are the primary mode of distress in CRCP, as described in Section 9.1.2. If this type of distress could be eliminated, CRCP would have an outstanding performance record. A comprehensive study was made by Zollinger (1989) on punchout distress. He described four modes of distress that eventually lead to punchout, as illustrated in Figure 12.7.

When the concrete slab cracks, the tensile stress in the steel reinforcement causes the fracture of surrounding concrete, as shown in (*a*). The fracture of concrete reduces the stiffness of the slab and results in spalling on the crack surface, as shown in (*b*). The spalling on the crack surface makes the crack open wide and results in the loss of load transfer across the crack, as shown in (*c*). Without the load transfer, the slab between two cracks acts as a cantilever beam, and the tensile stress in the transverse direction due to the edge loading causes the slab to crack at the top, as shown in (*d*).

Figure 12.8 shows the stresses at two critical locations in a CRCP under an 18-kip (80-kN) single-axle load. The stresses are presented in terms of load transfer efficiency (LTE) and crack spacing. Based on the analysis by ILLI-SLAB, the figure shows that the maximum longitudinal tensile stress σ_B at the bottom of the slab is highly sensitive to crack spacing but is relatively unaffected by LTE across the crack. The transverse tensile stress σ_A on the top of the slab is highly sensitive to LTE whenever the crack

TABLE 12.2 Sensitivity Analysis of Joint Deterioration

	Change		Joint deterioration	
Case	From	To	%	Ratio
(1)	(2)	(3)	(4)	(5)
Standard case			7.426	1.00
AGE (year)	10	30	98.209	13.23
ESAL N_{18} (10^6)	10	30	14.833	2.00
FI (degree-day)	100	2000	14.002	1.89
JS (ft)	100	15	1.674	0.23
SCTE	70	35	6.246	0.84

Note. 1 ft = 0.305 m.

Downloaded From : www.EasyEngineering.net

Downloaded From : www.EasyEngineering.net

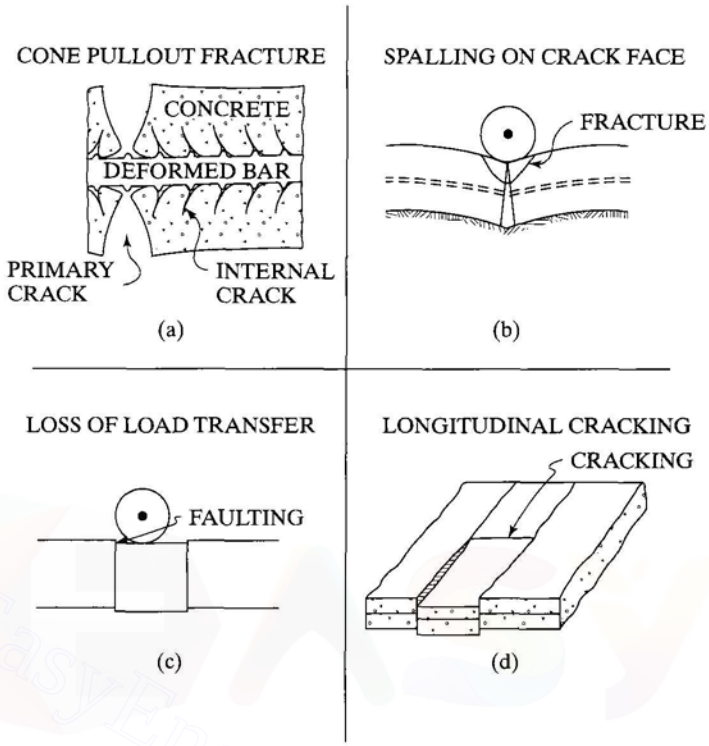


FIGURE 12.7

Failure modes leading to punchout distress. (After Zollinger and Barenberg (1990).)

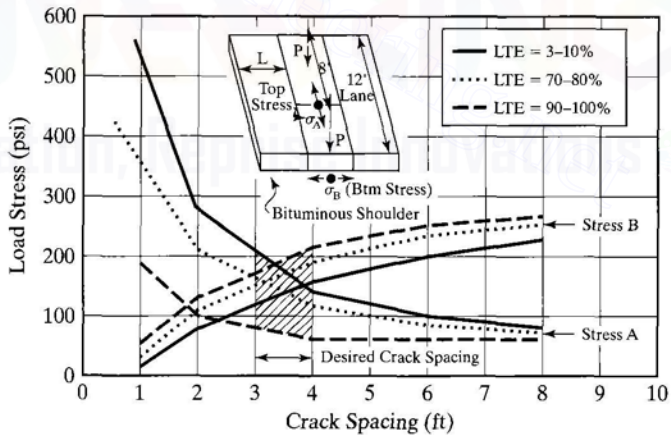


FIGURE 12.8

Comparison of σ_A and σ_B in CRCP for a 10-in. slab (1 psi = 6.9 kPa, 1 ft = 0.305 m). (After Zollinger and Barenberg (1990).)

spacing is less than 4 ft. These results indicate that, if the LTE can be maintained above 90%, the maximum transverse stress will remain relatively low even when the crack spacing is small. When the LTE drops to 70% or lower, the maximum transverse stress becomes increasingly large as the LTE and crack spacing decrease. When the tensile stress exceeds the tensile strength, a longitudinal crack will occur. The combination of

Downloaded From : www.EasyEngineering.net

Downloaded From : www.EasyEngineering.net

poor load transfer, voids around the reinforcing steel, longitudinal cracks, and so on, results in a punchout.

A mechanistic method of design to prevent punchout requires a knowledge of LTE, which depends on the level of shear stress across the crack and the crack width. The level of shear stress can be obtained from the finite element computer programs, but the determination of crack width requires an accurate prediction of crack spacing. Under normal construction conditions, crack spacings vary so widely that a reliable design procedure cannot be achieved. For the design approach to be reliable, some means of external control on the crack spacing is needed.

12.2 PORTLAND CEMENT ASSOCIATION METHOD

The Portland Cement Association's (PCA) thickness-design procedure for concrete highways and streets was published in 1984, superseding that published in 1966. The procedure can be applied to JPCP, JRCP, and CRCP. A finite element computer program called JSLAB (Tayabji and Colley, 1986) was employed to compute the critical stresses and deflections, which were then used in conjunction with some design criteria to develop the design tables and charts. The design criteria are based on general pavement design, performance, and research experience, including relationships to performance of pavements in the AASHO Road Test and to studies of pavement faulting. Design problems can be worked out by hand with tables and charts presented herein or by a microcomputer program available from PCA.

12.2.1 Design Criteria

One aspect of the new design procedure is the inclusion of an erosion analysis, in addition to the fatigue analysis. Fatigue analysis recognizes that pavements can fail by fatigue of concrete; in erosion analysis, pavements fail by pumping, erosion of foundation, and joint faulting.

Fatigue Analysis Fatigue analysis is based on the edge stress midway between the transverse joints, with the most critical loading position being shown in Figure 12.9. Because the load is near the midslab far away from the joints, the presence of the joints has practically no effect on the edge stress. When a concrete shoulder is tied onto the mainline pavement, the magnitude of the critical stress is reduced considerably.

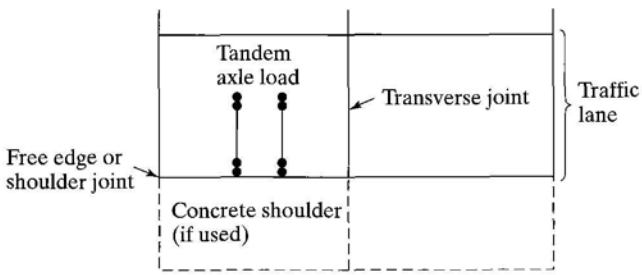


FIGURE 12.9
Critical loading position for fatigue analysis.

Downloaded From : www.EasyEngineering.net

Downloaded From : www.EasyEngineering.net

The cumulative damage concept, as described in Section 12.1.2, is used for fatigue analysis. However, only an average modulus of subgrade reaction k is used for the entire design period, and the stresses due to warping and curling are not considered. Warping and curling are excluded because the moisture content and temperature are usually higher at the bottom of the slab than at the top; thus, the combined effect of warping and curling stresses is subtractive from the loading stresses. Consequently, Eq. 12.1 is reduced to

$$D_r = \sum_{i=1}^{m} \frac{n_i}{N_i} \tag{12.6}$$

in which D_r is the damage ratio accumulated over the design period due to all load groups, m is the total number of load groups, n_i is the predicted number of repetitions for the ith load group, and N_i is the allowable number of repetitions for the ith load group, which can be determined from Eq. 5.36. The accumulated damage ratio at the end of the design period should be smaller than 1.

The placement of outside wheels at the pavement edge produces a critical stress higher than that at other locations. As the truck placement moves inward a few inches from the edge, the stress decreases significantly. At increasing distances inward from the edge, the frequency of load applications increases, but the magnitude of edge stress decreases. Theoretically, the distribution of load placement across the traffic lane must be known so that the damage ratio at the pavement edge caused by each load placement can be computed and summed toward the total damage. This procedure is too cumbersome for design purposes but was analyzed by PCA to develop a more easily applied method. In this method, fatigue at the pavement edge was computed by placing the load incrementally at different distances inward from the slab edge for typical distributions of truck placement. It was found that the same fatigue damage can be obtained by considering the edge loading only and placing 6% of the total number of load repetitions at the pavement edge. If the total number of repetitions is used for design, the edge stress must be reduced to obtain the same fatigue consumption. For 6% truck encroachment, the edge stress must be multiplied by an adjusting factor of 0.894, as shown in Figure 12.10. This factor was used in preparing the design tables.

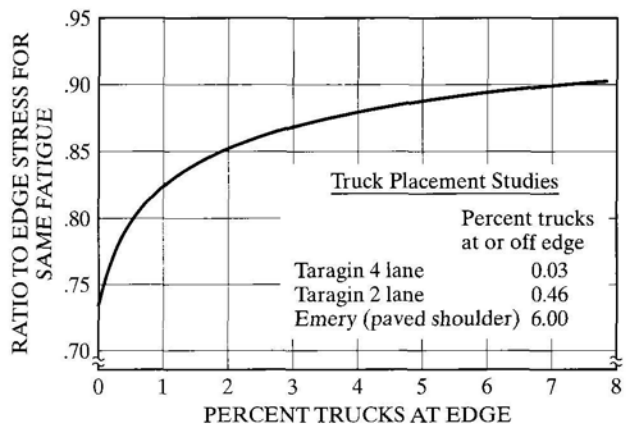


FIGURE 12.10

Equivalent stress factor versus percentage of trucks at edge. (After PCA (1984).)

Downloaded From : www.EasyEngineering.net

Downloaded From : www.EasyEngineering.net

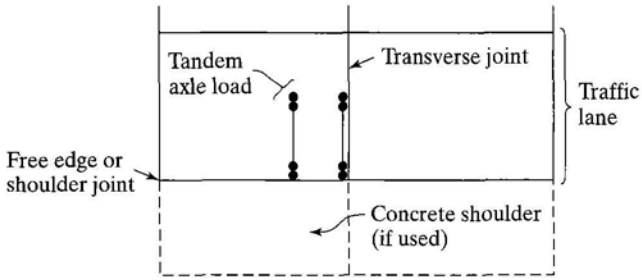


FIGURE 12.11
Critical loading position for erosion analysis.

Erosion Analysis Pavement distresses such as pumping, erosion of foundation, and joint faulting are related more to pavement deflections than to flexural stresses. The most critical pavement deflection occurs at the slab corner when an axle load is placed at the joint near the corner, as shown in Figure 12.11.

The principal mode of failure in the AASHO Road Test was pumping or erosion of the granular subbase from under the slabs. However, satisfactory correlations between corner deflections and the performance of these pavements could not be obtained. It was found that, to be able to predict their performance, different values of deflection criteria would have to be applied, depending on the slab thickness and, to a small extent, on the modulus of subgrade reaction. A better correlation was obtained by relating the performance to the rate of work, defined as the product of corner deflection w and pressure p at the slab–foundation interface, divided by the length of the deflection basin, which is a function of the radius of relative stiffness ℓ. The concept is that a thin slab with a shorter deflection basin receives a faster load punch than a thicker slab. The following equation was developed to compute the allowable load repetitions:

$$\log N = 14.524 - 6.777(C_1 P - 9.0)^{0.103} \tag{12.7}$$

In this equation, N is the allowable number of load repetitions (based on a PSI of 3.0), C_1 is an adjustment factor (with a value of 1 for untreated subbases and 0.9 for stabilized subbases), and P is the rate of work or power, defined by

$$P = 268.7\frac{p^2}{hk^{0.73}} \tag{12.8}$$

in which p is the pressure on the foundation under the slab corner in psi (which is equal to kw for a liquid foundation), h is the thickness of slab in inches, and k is the modulus of subgrade reaction in pci. The equation for erosion damage is

$$\text{Percent erosion damage} = 100\sum_{i=1}^{m}\frac{C_2 n_i}{N_i} \tag{12.9}$$

in which $C_2 = 0.06$ for pavements without concrete shoulders and 0.94 for pavements with tied concrete shoulders. With a concrete shoulder, the corner deflection is not significantly affected by the truck load placement, so a large C_2 should be used. The percent erosion damage should be less than 100%.

Downloaded From : www.EasyEngineering.net

Downloaded From : www.EasyEngineering.net

Example 12.1:

The sensitivity analysis of corner deflection presented in Table 5.12 shows that, for the standard case with $h = 8$ in. (203 mm) and $k = 100$ pci (27.1 MN/m^3), the corner deflection is 0.0353 in. (0.90 mm) under an 18-kip (80-kN) single-axle load and 0.0458 in. (1.16 mm) under a 36-kip (160-kN) tandem-axle load. If the predicted number of load repetitions is 5×10^6, compute the percent erosion damage under the single- and tandem-axle loads, respectively.

Solution: For the case of an 18-kip (80-kN) single-axle load, $p = kw = 100 \times 0.0353 = 3.53$ psi (24.4 kPa). From Eq. 12.8, $P = 268.7 \times (3.53)^2/[8 \times (100)^{0.73}] = 14.512$. Assuming that $C_1 = 1.0$, from Eq. 12.7, $\log N = 14.524 - 6.777(14.512 - 9.0)^{0.103} = 6.444$, or $N = 2.78 \times 10^6$. With $C_2 = 0.06$, from Eq. 12.9, percent erosion damage $= 100 \times 0.06 \times 5 \times 10^6/(2.78 \times 10^6) = 10.8\%$.

For the case of a 36-kip (160-kN) tandem-axle load, $p = 100 \times 0.0458 = 4.58$ psi (31.6 kPa); $P = 268.7 \times (4.58)^2/[8 \times (100)^{0.73}] = 24.429$; $\log N = 14.524 - 6.777(24.429 - 9.0)^{0.103} = 5.541$; $N = 3.47 \times 10^5$; and percent erosion damage $= 100 \times 0.06 \times 5 \times 10^6/(3.47 \times 10^5) = 86.5\%$.

12.2.2 Design Factors

After deciding whether doweled joints and concrete shoulders are to be used, the thickness design is governed by four design factors: concrete modulus of rupture, subgrade and subbase support, design period, and traffic. These factors are discussed below.

Concrete Modulus of Rupture The flexural strength of concrete is defined by the modulus of rupture, which is determined at 28 days by the method specified by ASTM in "C78-84 Standard Test Method for Flexural Strength of Concrete Using Simple Beam with Third Point Loading." The 28-day flexural strength is used as the design strength. The variability of strength and the gain in strength with age should be considered in the fatigue analysis.

In view of the fact that the variations in modulus of rupture have far greater effect on thickness design than do the usual variations in other material properties, it is recommended that the modulus of rupture be reduced by one coefficient of variation. A coefficient of variation of 15%, which represents good to fair quality control, was assumed and was incorporated into the design charts and tables. Also incorporated was the effect of strength gain after 28 days.

Subgrade and Subbase Support Subgrade and subbase support is defined by the modulus of subgrade reaction, k. Methods for determining the modulus of subgrade reaction are described in Section 7.5.1. Figure 7.36 can be used to correlate k values with other soil properties.

The PCA method does not consider the variation of k values over the year. The contention is that the reduced subgrade support during thaw periods has very little or no effect on the required thickness of concrete pavements, as evidenced by the results of AASHO Road Test. This is true because the brief periods when k values are low during spring thaws are more than offset by the longer freezing periods when k values are much higher than the design value. To avoid the tedious method of considering seasonal variations in k values, normal summer or fall k values can be used as reasonable mean values for design purposes.

Downloaded From : www.EasyEngineering.net

Downloaded From : www.EasyEngineering.net

TABLE 12.3 Effect of Untreated Subbase on k Values

Subgrade k value (pci)	Subbase k values (pci)			
	4 in.	6 in.	9 in.	12 in.
50	65	75	85	110
100	130	140	160	190
200	220	230	270	320
300	320	330	370	430

Note. 1 in. = 25.4 mm, 1 pci = 271.3 kN/m^3.
Source. After PCA (1984).

TABLE 12.4 Design k Values for Cement-Treated Bases

Subgrade k value (pci)	Subbase k values (pci)			
	4 in.	6 in.	8 in.	10 in.
50	170	230	310	390
100	280	400	520	640
200	470	640	830	—

Note. 1 in. = 25.4 mm, 1 pci = 271.3 kN/m^3.
Source. After PCA (1984).

It is not economical to use untreated subbases for the sole purpose of increasing k values. However, there are many reasons to use subbases, as described in Section 1.2.2. Where a subbase is used, there will be an increase in k that should be considered in the thickness design. If the subbase is composed of untreated granular materials, the approximate increase in k values can be taken from Table 12.3. For a cement-treated subbase, the design k values can be obtained from Table 12.4.

Design Period The term "design period" should not be confused with the term "pavement life," which is not subject to precise definition. "Design period" is more nearly synonymous with the term "traffic analysis period." Because traffic probably cannot be predicted with much accuracy for a longer period, a design period of 20 years has commonly been used in pavement design. However, there are cases where the use of a shorter or longer design period is economically justified. For example, a special-haul road that will be used only a few years requires a much shorter design period; a premium facility that must provide a high level of performance for a long time with little or no pavement maintenance can require a design period of up to 40 years.

Traffic The information presented in Section 6.4, such as Eq. 6.26, can be used to determine the design traffic. The growth factor can be determined from Table 6.12 and the lane distribution factor for multilane highways from Figure 6.8. Information on the average daily truck traffic (ADTT) and the axle-load distribution is needed in using the PCA design procedure. The ADTT includes only trucks with six tires or more and does not include panel and pickup trucks or other vehicles with only four tires.

Downloaded From : www.EasyEngineering.net

Downloaded From : www.EasyEngineering.net

TABLE 12.5 Axle Load Distribution for a Given Facility

Axle load kip (1)	Axles per 1000 trucks (2)	Adjusted axles per 1000 trucks (3)	Axles in design period (4)
Single axles			
28–30	0.28	0.58	6310
26–28	0.65	1.35	14,690
24–26	1.33	2.77	30,140
22–24	2.84	5.92	64,410
20–22	4.72	9.83	106,900
18–20	10.40	21.67	235,800
16–18	13.56	28.24	307,200
14–16	18.64	38.83	422,500
12–14	25.89	53.94	586,900
10–12	81.05	168.85	1,837,000
Tandem axles			
48–52	0.94	1.98	21,320
44–48	1.89	3.94	42,870
40–44	5.51	11.48	124,900
36–40	16.45	34.27	372,900
32–36	39.08	81.42	885,800
28–32	41.06	85.54	930,700
24–28	73.07	152.23	1,656,000
20–24	43.45	90.52	984,900
16–20	54.15	112.81	1,227,000
12–16	59.85	124.69	1,356,000

Note. 1 kip = 4.45 kN.
Source. After PCA (1984).

Axle Load Distribution Data on the axle load distribution of truck traffic is needed to compute the number of single and tandem axles of various weights expected during the design period. These data can be obtained from special traffic studies to establish the loadometer data for the specific project or from the W-4 table of a loadometer station representing truck weights and types that are expected to be similar to the project under design. If axle load distribution data are not available, the simplified design procedure described in Section 12.2.4 can be used.

Table 12.5 illustrates how the information in a W-4 table for a loadometer station can be used to determine the number of various axles based on the total number of trucks. In the W-4 table, axle loads are grouped by 2-kip (8.9-kN) increments for single axles and 4-kip (17.8-kN) increments for tandem axles, as shown in column 1. The axles per 1000 trucks shown in column 2 are obtained from the W-4 table. The table also shows 13,215 total trucks counted, with 6918 two-axle, four-tire trucks, which constitute 52% of total trucks. Because the trucks in column 2 include two-axle, four-tire trucks, which should be excluded from consideration, the data in column 2 must be divided by $(1 - 0.52)$ to obtain the adjusted axles per 1000 trucks shown in column 3. Column 4 is the number of load repetitions to be used for the sample problem in Figure 12.15 and can be obtained by the following formula: Column 4 = Column 3 × (Trucks on

Downloaded From : www.EasyEngineering.net

Downloaded From : www.EasyEngineering.net

design lane in design period)/1000. The number of trucks on the design lane in the design period is 10,880,000, as will be determined later in the sample problem.

Load Safety Factors In the design procedure, the axle load must be multiplied by a load-safety factor (LSF). The recommended load-safety factors are as follows:

1. For interstate highways and other multilane projects where there will be uninterrupted traffic flow and high volumes of truck traffic, LSF = 1.2.
2. For highways and arterial streets where there will be moderate volumes of truck traffic, LSF = 1.1.
3. For roads, residential streets, and other streets that will carry small volumes of truck traffic, LSF = 1.0.

In special cases, the use of a load safety factor as high as 1.3 might be justified for a premium facility to maintain a higher than normal level of pavement serviceability throughout the design period.

12.2.3 Design Procedure

The method presented in this section can be used when detailed axle-load distributions have been determined or estimated, as described in Section 12.2.2. If the axle load data are not available, the simplified method presented in Section 12.2.4 should be used.

Design Tables and Charts Separate sets of tables and charts are used to evaluate fatigue and erosion damages. The following parameter values are used in their development: elastic modulus of concrete = 4×10^6 psi (28 GPa), Poisson ratio of concrete = 0.15, diameter of dowels = $\frac{1}{8}$ in./in. of slab, spacing of dowels = 12 in. (305 mm), modulus of dowel support = 2×10^6 pci (543 GN/m^3), spring constant for aggregate interlock joints = 5000 psi (34.5 MPa), spring constant for tied concrete shoulder = 25,000 psi (173 MPa).

Fatigue Damage Fatigue damage is based on the edge stress. Because the edge stress on mainline pavements without concrete shoulders is much greater than that on those with tied concrete shoulders, two different tables are needed: Table 12.6 for slabs without concrete shoulders, Table 12.7 for slabs with concrete shoulders. The equivalent stresses shown in these tables are the edge stresses multiplied by a factor of 0.894. It is not known what axle load was used to generate these stresses. Based on the levels of stress, it appears that an 18-kip (80-kN) load was used for single axles and a 36-kip (160-kN) load was used for tandem axles. Both tables show that the equivalent stresses under 36-kip (160-kN) tandem-axle loads are smaller than those under 18-kip (80-kN) single-axle loads, which is as expected.

After the equivalent stress is determined, the stress ratio factor can be computed by dividing the equivalent stress by the design modulus of rupture, so that the allowable number of load repetitions can be obtained from Figure 12.12. Note that the reduction in the modulus of rupture by 15% and the increase in the modulus of rupture with age have been incorporated in the chart, so the user simply inputs the 28-day

Downloaded From : www.EasyEngineering.net

Downloaded From : www.EasyEngineering.net

TABLE 12.6 Equivalent Stresses for Slabs Without Concrete Shoulders

Slab thickness (in.)	k of Subgrade–subbase (pci)						
	50	100	150	200	300	500	700
4	825/679	726/585	671/542	634/516	584/486	523/457	484/443
4.5	699/586	616/500	571/460	540/435	498/406	448/378	417/363
5	602/516	531/436	493/399	467/376	432/349	390/321	363/307
5.5	526/461	464/387	431/353	409/331	379/305	343/278	320/264
6	465/416	411/348	382/316	362/296	336/271	304/246	285/232
6.5	417/380	367/317	341/286	324/267	300/244	273/220	256/207
7	375/349	331/290	307/262	292/244	271/222	246/199	231/186
7.5	340/323	300/268	279/241	265/224	246/203	224/181	210/169
8	311/300	274/249	255/223	242/208	225/188	205/167	192/155
8.5	285/281	252/232	234/208	222/193	206/174	188/154	177/143
9	264/264	232/218	216/195	205/181	190/163	174/144	163/133
9.5	245/248	215/205	200/183	190/170	176/153	161/134	151/124
10	228/235	200/193	186/173	177/160	164/144	150/126	141/117
10.5	213/222	187/183	174/164	165/151	153/136	140/119	132/110
11	200/211	175/174	163/155	154/143	144/129	131/113	123/104
11.5	188/201	165/165	153/148	145/136	135/122	123/107	116/98
12	177/192	155/158	144/141	137/130	127/116	116/102	109/93
12.5	168/183	147/151	136/135	129/124	120/111	109/97	103/89
13	159/176	139/144	129/129	122/119	113/106	103/93	97/85
13.5	152/168	132/138	122/123	116/114	107/102	98/89	92/81
14	144/162	125/133	116/118	110/109	102/98	93/85	88/78

Note. Number at left is for single axle and number at right is for tandem axle (single/tandem); 1 in. = 25.4 mm, 1 pci = 271.3 kN/m^3.
Source. After PCA (1984).

strength as the design modulus of rupture. Figure 12.12 can be applied to pavements both with and without concrete shoulders. If the allowable repetitions fall outside the range of the chart, the allowable number of repetitions is considered to be unlimited.

Example 12.2:

The sensitivity analysis presented in Table 5.11 shows an average edge stress of about 283 psi (1.95 MPa) under a 36-kip (160-kN) tandem-axle load when h = 8 in. (203 mm) and k = 100 pci (27.1 MN/m^3). Assuming a concrete modulus of rupture of 500 psi (4.5 MPa) and using the PCA fatigue equation, or Eq. 5.36, determine the allowable number of load repetitions. Compare the result with that obtained from Table 12.6 and Figure 12.12.

Solution: Because only a small portion of the wheel loads are applied at the pavement edge, the edge stress must be multiplied by an adjustment factor of 0.894; so the actual stress is $\sigma = 0.894 \times 283 = 253$ psi (1.75 MPa). With $\sigma/S_c = 253/500 = 0.506$, from Eq. 5.36*b*, $N_f = [4.2577/(0.506 - 0.43250)]^{3.268} = 5.8 \times 10^5$.

From Table 12.6, the equivalent stress for a tandem-axle load with a k value of 100 pci (27.1 MN/m^3) and a slab thickness of 8 in. (203 mm) is 249 psi (1.72 MPa),

Downloaded From : www.EasyEngineering.net

Downloaded From : www.EasyEngineering.net

TABLE 12.7 Equivalent Stresses for Slabs with Concrete Shoulders

Slab thickness (in.)	k of Subgrade–subbase (pci)						
	50	100	150	200	300	500	700
4	640/534	559/468	517/439	489/422	452/403	409/388	383/384
4.5	547/461	479/400	444/372	421/356	390/338	355/322	333/316
5	475/404	417/349	387/323	367/308	341/290	311/274	294/267
5.5	418/360	368/309	342/285	324/271	302/254	276/238	261/231
6	372/325	327/277	304/255	289/241	270/225	247/210	234/203
6.5	334/295	294/251	274/230	260/218	243/203	223/188	212/180
7	302/270	266/230	248/210	236/198	220/184	203/170	192/162
7.5	275/250	243/211	226/193	215/182	201/168	185/155	176/148
8	252/232	222/196	207/179	197/168	185/155	170/142	162/135
8.5	232/216	205/182	191/166	182/156	170/144	157/131	150/125
9	215/202	190/171	177/155	169/146	158/134	146/122	139/116
9.5	200/190	176/160	164/146	157/137	147/126	136/114	129/108
10	186/179	164/151	153/137	146/129	137/118	127/107	121/101
10.5	174/170	154/143	144/130	137/121	128/111	119/101	113/95
11	164/161	144/135	135/123	129/115	120/105	112/95	106/90
11.5	154/153	136/128	127/117	121/109	113/100	105/90	100/85
12	145/146	128/122	120/111	114/104	107/95	99/86	95/81
12.5	137/139	121/117	113/106	108/99	101/91	94/82	90/77
13	130/133	115/112	107/101	102/95	96/86	89/78	85/73
13.5	124/127	109/107	102/97	97/91	91/83	85/74	81/70
14	118/122	104/103	97/93	93/87	87/79	81/71	77/67

Note. Number at left is for single axle and number at right is for tandem axle (single/tandem); 1 in. = 25.4 mm, 1 pci = 271.3 kN/m^3.
Source. After PCA (1984)

which is slightly smaller than the 253 psi (1.75 MPa) obtained in the sensitivity analysis. This is as expected; the dual and tandem spacings and the tire contact pressure assumed by PCA are not known and could be quite different from those in the sensitivity analysis. Hence, the stress ratio factor = 249/500 = 0.498.

From Figure 12.12, a straight line is drawn starting from the 18-kip (80-kN) single-axle load on the left axis (which is the same as the 36-kip (160-kN) tandem-axle load), passing through a point on the middle axis with a stress-ratio factor of 0.498, and ending at the allowable load repetitions on the right axis. The allowable number of repetitions read from the right axis is 7×10^5, which is also slightly larger than the 5.8×10^5 obtained previously. Note that, in applying Eq. 5.36*b*, no adjustment was made to the modulus of rupture; yet, in the development of the chart, the modulus of rupture was reduced by 15% for variability and then increased by a certain amount for strength gain with age. It is not known how much gain in strength was assumed by PCA, so a discrepancy between the two results is expected.

Erosion Damage Because erosion damage occurs at the pavement corner and is affected by the type of joint, separate tables for doweled and aggregate interlock joints are needed. The erosion criteria also require two separate charts for slab with and without concrete shoulders.

Downloaded From : www.EasyEngineering.net

Downloaded From : www.EasyEngineering.net

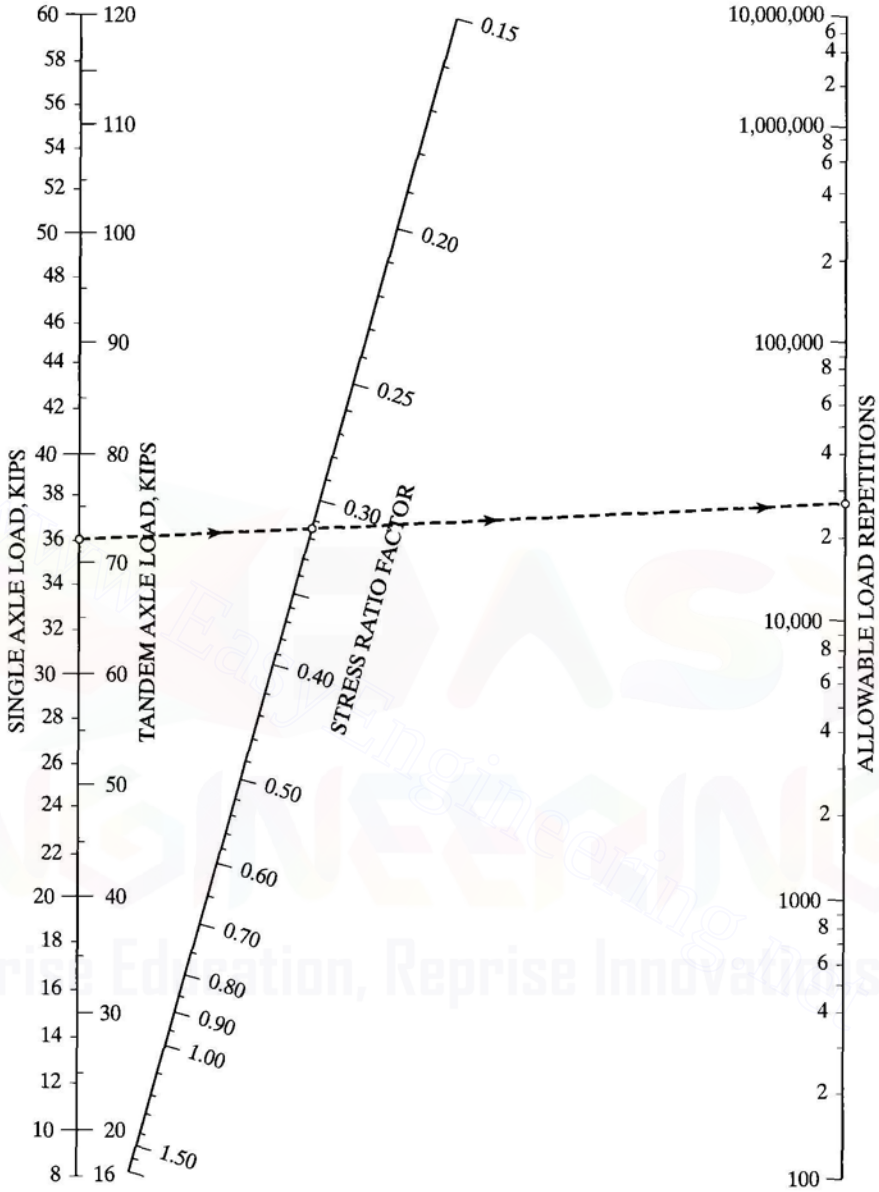


FIGURE 12.12

Stress ratio factors versus allowable load repetitions both with and without concrete shoulders (1 kip = 4.45 kN). (After PCA (1984).)

Table 12.8 shows the erosion factors for slabs with doweled joints and no concrete shoulders; Table 12.9 shows the erosion factors for slabs with aggregate interlock joints and no concrete shoulders. After the erosion factor is found, the allowable number of load repetitions can be obtained from Figure 12.13. Note that the allowable load

Downloaded From : www.EasyEngineering.net

Downloaded From : www.EasyEngineering.net

TABLE 12.8 Erosion Factors for Slabs with Doweled Joints and no Concrete Shoulders

Slab thickness (in.)	*k* of Subgrade-subbase (pci)					
	50	100	200	300	500	700
4	3.74/3.83	3.73/3.79	3.72/3.75	3.71/3.73	3.70/3.70	3.68/3.67
4.5	3.59/3.70	3.57/3.65	3.56/3.61	3.55/3.58	3.54/3.55	3.52/3.53
5	3.45/3.58	3.43/3.52	3.42/3.48	3.41/3.45	3.40/3.42	3.38/3.40
5.5	3.33/3.47	3.31/3.41	3.29/3.36	3.28/3.33	3.27/3.30	3.26/3.28
6	3.22/3.38	3.19/3.31	3.18/3.26	3.17/3.23	3.15/3.20	3.14/3.17
6.5	3.11/3.29	3.09/3.22	3.07/3.16	3.06/3.13	3.05/3.10	3.03/3.07
7	3.02/3.21	2.99/3.14	2.97/3.08	2.96/3.05	2.95/3.01	2.94/2.98
7.5	2.93/3.14	2.91/3.06	2.88/3.00	2.87/2.97	2.86/2.93	2.84/2.90
8	2.85/3.07	2.82/2.99	2.80/2.93	2.79/2.89	2.77/2.85	2.76/2.82
8.5	2.77/3.01	2.74/2.93	2.72/2.86	2.71/2.82	2.69/2.78	2.68/2.75
9	2.70/2.96	2.67/2.87	2.65/2.80	2.63/2.76	2.62/2.71	2.61/2.68
9.5	2.63/2.90	2.60/2.81	2.58/2.74	2.56/2.70	2.55/2.65	2.54/2.62
10	2.56/2.85	2.54/2.76	2.51/2.68	2.50/2.64	2.48/2.59	2.47/2.56
10.5	2.50/2.81	2.47/2.71	2.45/2.63	2.44/2.59	2.42/2.54	2.41/2.51
11	2.44/2.76	2.42/2.67	2.39/2.58	2.38/2.54	2.36/2.49	2.35/2.45
11.5	2.38/2.72	2.36/2.62	2.33/2.54	2.32/2.49	2.30/2.44	2.29/2.40
12	2.33/2.68	2.30/2.58	2.28/2.49	2.26/2.44	2.25/2.39	2.23/2.36
12.5	2.28/2.64	2.25/2.54	2.23/2.45	2.21/2.40	2.19/2.35	2.18/2.31
13	2.23/2.61	2.20/2.50	2.18/2.41	2.16/2.36	2.14/2.30	2.13/2.27
13.5	2.18/2.57	2.15/2.47	2.13/2.37	2.11/2.32	2.09/2.26	2.08/2.23
14	2.13/2.54	2.11/2.43	2.08/2.34	2.07/2.29	2.05/2.23	2.03/2.19

Note. Number at left is for single axle and number at right is for tandem axle (single/tandem);
1 in. = 25.4 mm, 1 pci = 271.3 kN/m^3.
Source. After PCA (1984).

repetitions shown in Figure 12.13 have already been divided by a C_2 of 0.06, so it is not necessary to multiply the predicted repetitions by C_2, as indicated by Eq. 12.9.

Example 12.3:

Same as Example 12.1, except that the percent erosion damages for the 18-kip (80-kN) single-axle and 36-kip (160-kN) tandem-axle loads are to be determined by Table 12.8 and Figure 12.13.

Solution: For the 18-kip (80-kN) single-axle load with a *k* value of 100 pci (27.1 MN/m^3) and a slab thickness of 8 in. (203 mm), from Table 12.8, erosion factor = 2.82, and, from Figure 12.13, allowable load repetitions = 3×10^7. Given predicted repetitions = 5×10^6, percent erosion damage = $100 \times (5 \times 10^6)/(3 \times 10^7) = 16.7\%$, compared with 10.8% in Example 12.1.

For the 36-kip (160-kN) tandem-axle load, from Table 12.8, erosion factor = 2.99; from Figure 12.13, allowable load repetitions = 6.2×10^6; percent erosion damage = $100 \times (5 \times 10^6)/(6.2 \times 10^6) = 80.6\%$, compared with 86.5% in Example 12.1. Allowable repetitions are very sensitive to corner deflections, so the agreement between the two examples is considered exceedingly good.

Downloaded From : www.EasyEngineering.net

Downloaded From : www.EasyEngineering.net

TABLE 12.9 Erosion Factors for Slabs with Aggregate Interlock Joints and no Concrete Shoulders

Slab thickness (in.)	*k* of Subgrade–subbase (pci)					
	50	100	200	300	500	700
4	3.94/4.03	3.91/3.95	3.88/3.89	3.86/3.86	3.82/3.83	3.77/3.80
4.5	3.79/3.91	3.76/3.82	3.78/3.75	3.71/3.72	3.68/3.68	3.64/3.65
5	3.66/3.81	3.63/3.72	3.60/3.64	3.58/3.60	3.55/3.55	3.52/3.52
5.5	3.54/3.72	3.51/3.62	3.48/3.53	3.46/3.49	3.43/3.44	3.41/3.40
6	3.44/3.64	3.40/3.53	3.37/3.44	3.35/3.40	3.32/3.34	3.30/3.30
6.5	3.34/3.56	3.30/3.46	3.26/3.36	3.25/3.31	3.22/3.25	3.20/3.21
7	3.26/3.49	3.21/3.39	3.17/3.29	3.15/3.24	3.13/3.17	3.11/3.13
7.5	3.18/3.43	3.13/3.32	3.09/3.22	3.07/3.17	3.04/3.10	3.02/3.06
8	3.11/3.37	3.05/3.26	3.01/3.16	2.99/3.10	2.96/3.03	2.94/2.99
8.5	3.04/3.32	2.98/3.21	2.93/3.10	2.91/3.04	2.88/2.97	2.87/2.93
9	2.98/3.27	2.91/3.16	2.86/3.05	2.84/2.99	2.81/2.92	2.79/2.87
9.5	2.92/3.22	2.85/3.11	2.80/3.00	2.77/2.94	2.75/2.86	2.73/2.81
10	2.86/3.18	2.79/3.06	2.74/2.95	2.71/2.89	2.68/2.81	2.66/2.76
10.5	2.81/3.14	2.74/3.02	2.68/2.91	2.65/2.84	2.62/2.76	2.60/2.72
11	2.77/3.10	2.69/2.98	2.63/2.86	2.60/2.80	2.57/2.72	2.54/2.67
11.5	2.72/3.06	2.64/2.94	2.58/2.82	2.55/2.76	2.51/2.68	2.49/2.63
12	2.68/3.03	2.60/2.90	2.53/2.78	2.50/2.72	2.46/2.64	2.44/2.59
12.5	2.64/2.99	2.55/2.87	2.48/2.75	2.45/2.68	2.41/2.60	2.39/2.55
13	2.60/2.96	2.51/2.83	2.44/2.71	2.40/2.65	2.36/2.56	2.34/2.51
13.5	2.56/2.93	2.47/2.80	2.40/2.68	2.36/2.61	2.32/2.53	2.30/2.48
14	2.53/2.90	2.44/2.77	2.36/2.65	2.32/2.58	2.28/2.50	2.25/2.44

Note. Number at left is for single axle and number at right is for tandem axle (single/tandem); 1 in. = 25.4 mm, 1 pci = 271.3 kN/m^3.
Source. After PCA (1984).

Similar tables and charts for slabs with concrete shoulders are shown in Tables 12.10 and 12.11 and Figure 12.14.

Sample Problem Figure 12.15 is the worksheet on a sample problem. The design involves a four-lane interstate pavement with doweled joints and no concrete shoulders. A 4-in. (102-mm) untreated subbase will be placed on a clay subgrade with a *k* value of 100 pci (27.2 MN/m^3). Other information include concrete modulus of rupture = 650 psi (4.5 MPa), design period = 20 years, current ADT = 12,900, annual growth rate = 4%, and ADTT = 19% of ADT.

On the worksheet, a trial thickness of 9.5 in. (241 mm) is selected. For a subgrade *k* value of 100 pci (27.1 MN/m^3) and a subbase thickness of 4 in. (102 mm), from Table 12.3, the *k* value for subbase–subgrade combination is 130 pci (35.3 MN/m^3). For an interstate highway, a load safety factor of 1.2 is recommended. With a thickness of 9.5 in. (241 mm) and a *k* value of 130 pci (35.3 MN/m^3), an equivalent stress of 206 psi (731 kPa) for single axles and 192 psi (1.32 MPa) for tandem axles can be obtained from Table 12.6 and entered as items 8 and 11 on the worksheet. The stress ratio factor is the

Downloaded From : www.EasyEngineering.net

Downloaded From : www.EasyEngineering.net

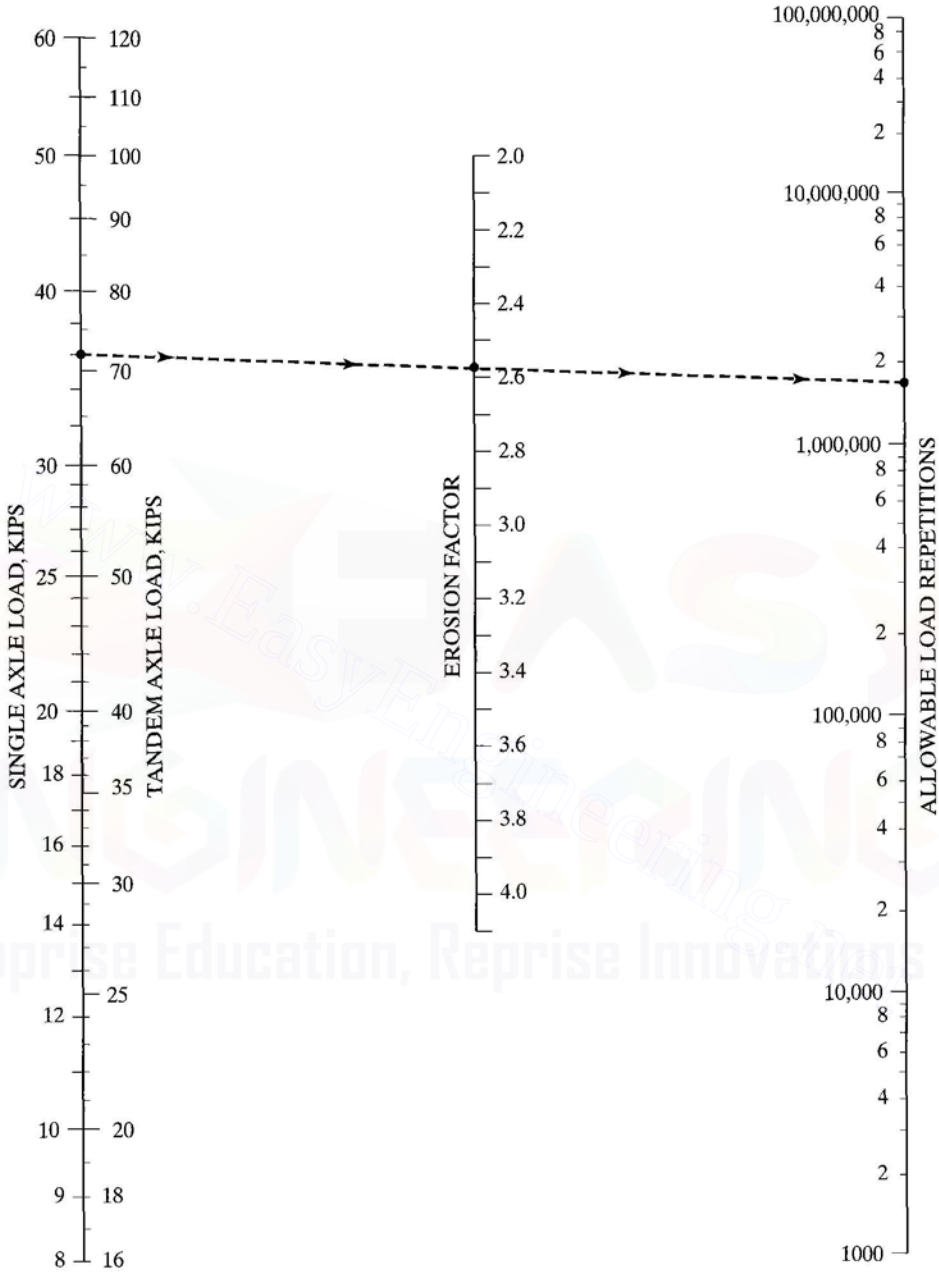


FIGURE 12.13

Erosion factors versus allowable load repetitions without concrete shoulders (1 kip = 4.45 kN). (After PCA (1984).)

Downloaded From : www.EasyEngineering.net

Downloaded From : www.EasyEngineering.net

TABLE 12.10 Erosion Factors for Slabs with Doweled Joints and Concrete Shoulders

Slab thickness (in.)	*k* of Subgrade–subbase (pci)					
	50	100	200	300	500	700
4	3.28/3.30	3.24/3.20	3.21/3.13	3.19/3.10	3.15/3.09	3.12/3.08
4.5	3.13/3.19	3.09/3.08	3.06/3.00	3.04/2.96	3.01/2.93	2.98/2.91
5	3.01/3.09	2.97/2.98	2.93/2.89	2.90/2.84	2.87/2.79	2.85/2.77
5.5	2.90/3.01	2.85/2.89	2.81/2.79	2.79/2.74	2.76/2.68	2.73/2.65
6	2.79/2.93	2.75/2.82	2.70/2.71	2.68/2.65	2.65/2.58	2.62/2.54
6.5	2.70/2.86	2.65/2.75	2.61/2.63	2.58/2.57	2.55/2.50	2.52/2.45
7	2.61/2.79	2.56/2.68	2.52/2.56	2.49/2.50	2.46/2.42	2.43/2.38
7.5	2.53/2.73	2.48/2.62	2.44/2.50	2.41/2.44	2.38/2.36	2.35/2.31
8	2.46/2.68	2.41/2.56	2.36/2.44	2.33/2.38	2.30/2.30	2.27/2.24
8.5	2.39/2.62	2.34/2.51	2.29/2.39	2.26/2.32	2.22/2.24	2.20/2.18
9	2.32/2.57	2.27/2.46	2.22/2.34	2.19/2.27	2.16/2.19	2.13/2.13
9.5	2.26/2.52	2.21/2.41	2.16/2.29	2.13/2.22	2.09/2.14	2.07/2.08
10	2.20/2.47	2.15/2.36	2.10/2.25	2.07/2.18	2.03/2.09	2.01/2.03
10.5	2.15/2.43	2.09/2.32	2.04/2.20	2.01/2.14	1.97/2.05	1.95/1.99
11	2.10/2.39	2.04/2.28	1.99/2.16	1.95/2.09	1.92/2.01	1.89/1.95
11.5	2.05/2.35	1.99/2.24	1.93/2.12	1.90/2.05	1.87/1.97	1.84/1.91
12	2.00/2.31	1.94/2.20	1.88/2.09	1.85/2.02	1.82/1.93	1.79/1.87
12.5	1.95/2.27	1.89/2.16	1.84/2.05	1.81/1.98	1.77/1.89	1.74/1.84
13	1.91/2.23	1.85/2.13	1.79/2.01	1.76/1.95	1.72/1.86	1.70/1.80
13.5	1.86/2.20	1.81/2.09	1.75/1.98	1.72/1.91	1.68/1.83	1.65/1.77
14	1.82/2.17	1.76/2.06	1.71/1.95	1.67/1.88	1.64/1.80	1.61/1.74

Note. Number at left is for single axle and number at right is for tandem axle (single/tandem); 1 in. = 25.4 mm, 1 pci = 271.3 kN/m^3.
Source. After PCA (1984).

ratio between the equivalent stress and the modulus of rupture, so ratios of 0.317 for single axles and 0.295 for tandem axles are entered as items 9 and 12. Erosion factors of 2.59 for single axles and 2.79 for tandem axles are obtained from Table 12.8 and entered as items 10 and 13. Each column, as numbered from 1 to 7 in the worksheet, is explained on page 622.

Explanation of Worksheet

1. Single-axle loads are incremented at 2-kip (8.9-kN) intervals, and tandem-axle loads are incremented at 4-kip (17.8-kN) intervals. The largest load in the single- or tandem-load group should be entered first. If the allowable number of repetitions for a given load is unlimited, it is not necessary to compute the damage for the remaining loads in the same group.
2. The axle loads in column 1 are multiplied by a load safety factor of 1.2.
3. The predicted or expected repetitions are obtained from Table 12.5. To be on the conservative side, the upper limit of the load in the range is used to represent the range. For example, all axle loads between 28 and 30 kip (125 and 134 kN) are considered as 30 kip (134 kN). With an annual growth rate of 4% and a design

Downloaded From : www.EasyEngineering.net

Downloaded From : www.EasyEngineering.net

TABLE 12.11 Erosion Factors for Slabs with Aggregate Interlock Joints and Concrete Shoulders

Slab thickness (in.)	k of Subgrade–subbase (pci)					
	50	100	200	300	500	700
4	3.46/3.49	3.42/3.39	3.38/3.32	3.36/3.29	3.32/3.26	3.28/3.24
4.5	3.32/3.39	3.28/3.28	3.24/3.19	3.22/3.16	3.19/3.12	3.15/3.09
5	3.20/3.30	3.16/3.18	3.12/3.09	3.10/3.05	3.07/3.00	3.04/2.97
5.5	3.10/3.22	3.05/3.10	3.01/3.00	2.99/2.95	2.96/2.90	2.93/2.86
6	3.00/3.15	2.95/3.02	2.90/2.92	2.88/2.87	2.86/2.81	2.83/2.77
6.5	2.91/3.08	2.86/2.96	2.81/2.85	2.79/2.79	2.76/2.73	2.74/2.68
7	2.83/3.02	2.77/2.90	2.73/2.78	2.70/2.72	2.68/2.66	2.65/2.61
7.5	2.76/2.97	2.70/2.84	2.65/2.72	2.62/2.66	2.60/2.59	2.57/2.54
8	2.69/2.92	2.63/2.79	2.57/2.67	2.55/2.61	2.52/2.53	2.50/2.48
8.5	2.63/2.88	2.56/2.74	2.51/2.62	2.48/2.55	2.45/2.48	2.43/2.43
9	2.57/2.83	2.50/2.70	2.44/2.57	2.42/2.51	2.39/2.43	2.36/2.38
9.5	2.51/2.79	2.44/2.65	2.38/2.53	2.36/2.46	2.33/2.38	2.30/2.33
10	2.46/2.75	2.39/2.61	2.33/2.49	2.30/2.42	2.27/2.34	2.24/2.28
10.5	2.41/2.72	2.33/2.58	2.27/2.45	2.24/2.38	2.21/2.30	2.19/2.24
11	2.36/2.68	2.28/2.54	2.22/2.41	2.19/2.34	2.16/2.26	2.14/2.20
11.5	2.32/2.65	2.24/2.51	2.17/2.38	2.14/2.31	2.11/2.22	2.09/2.16
12	2.28/2.62	2.19/2.48	2.13/2.34	2.10/2.27	2.06/2.19	2.04/2.13
12.5	2.24/2.59	2.15/2.45	2.09/2.31	2.05/2.24	2.02/2.15	1.99/2.10
13	2.20/2.56	2.11/2.42	2.04/2.28	2.01/2.21	1.98/2.12	1.95/2.06
13.5	2.16/2.53	2.08/2.39	2.00/2.25	1.97/2.18	1.93/2.09	1.91/2.03
14	2.13/2.51	2.04/2.36	1.97/2.23	1.93/2.15	1.89/2.06	1.87/2.00

Note. Number at left is for single axle and number at right is for tandem axle (single/tandem); 1 in. = 25.4 mm, 1 pci = 271.3 kN/m^3.
Source. After PCA (1984).

period of 20 years, from Table 6.12, growth factor $G = 1.5$. Design ADT = 12,900 $\times$1.5 = 19,350, or 9675 in one direction. ADTT = 19,350 $\times$0.19 = 3680, or 1840 in one direction. For an ADT of 9675 in one direction, from Figure 6.8, lane distribution factor $L = 0.81$. Therefore, the total number of trucks on the design lane during the design period is 1840 $\times$ 0.81 $\times$ 365 $\times$ 20 = 10,880,000, which was used to obtain the axle-load distribution in Table 12.5.

4. The allowable repetitions in fatigue analysis are obtained from Figure 12.12 and based on a stress-ratio factor of 206/650, or 0.317, for single axles and 192/650, or 0.295, for tandem axles.
5. The fatigue percentages are obtained by dividing column 3 by column 4 and multiplying by 100. The sum of fatigue percentages over all single- and tandem-axle loads is entered at the bottom.
6. The allowable repetitions in erosion analysis are obtained from Figure 12.13 and are based on an erosion factor of 2.59 for single axles, 2.79 for tandem axles.
7. The erosion percentages are obtained by dividing column 3 by column 6 and multiplying by 100. The sum of erosion percentages over all single- and tandem-axle loads is entered at the bottom.

Downloaded From : www.EasyEngineering.net

Downloaded From : www.EasyEngineering.net

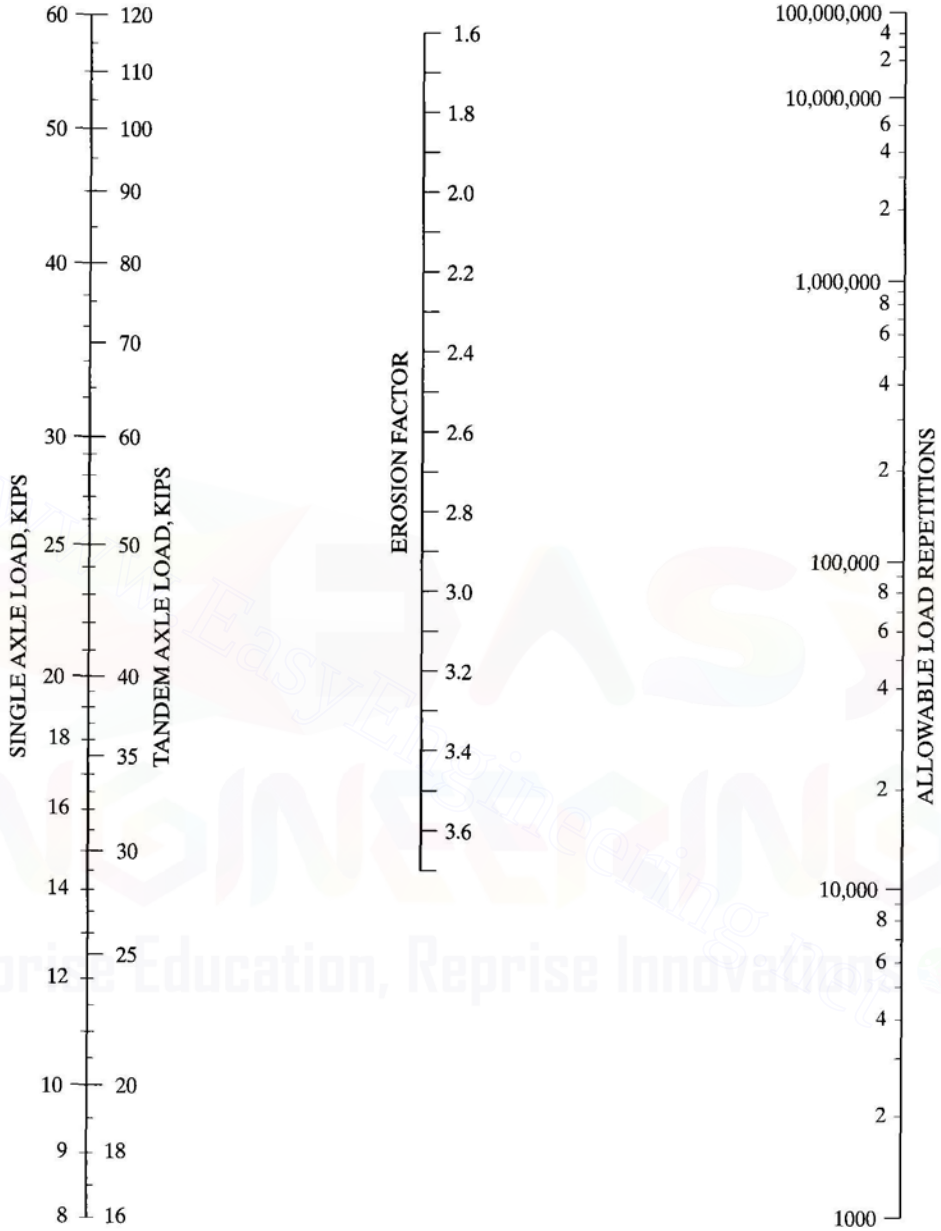


FIGURE 12.14

Erosion factors versus allowable load repetitions with concrete shoulders (1 kip = 4.45 kN). (After PCA (1984).)

Downloaded From : www.EasyEngineering.net

Downloaded From : www.EasyEngineering.net

Calculation of Pavement Thickness

Project *Design 1A, four-lane Interstate, rural*
Trial thickness *9.5* in.
Subbase-subgrade k *130* pci
Modulus of rupture. MR *650* psi
Load safety factor. LSF *1.2*
Doweled joints: yes ✓ no ____
Concrete shoulder: yes ____ no ✓
Design period *20* years
4 in. untreated subbase

Axle load, kips	Multiplied by LSF %2	Expected repetitions	Fatigue analysis		Erosion analysis	
			Allowable repetitions	Fatigue. percent	Allowable repetitions	Damage percent
1	2	3	4	5	6	7

8. Equivalent stress *206* 10. Erosion factor *2.59*
9. Stress ratio factor *0.317*

Single Axles

30	36.0	6,310	27,000	23.3	1,500,000	0.4
28	33.6	14,690	77,000	19.1	2,200,000	0.7
26	31.2	30,140	230,000	13.1	3,500,000	0.9
24	28.8	64,410	1,200,000	5.4	5,900,000	1.1
22	26.4	106,900	Unlimited	0	11,000,000	1.0
20	24.0	235,800	,,	0	23,000,000	1.0
18	21.6	307,200	,,	0	64,000,000	0.5
16	19.2	422,500			Unlimited	0
14	16.8	586,900			,,	0
12	14.4	1,837,000			,,	0

11. Equivalent stress *192* 13. Erosion factor *2.79*
12. Stress ratio factor *0.295*

Tandem Axles

52	62.4	21,320	1,100,000	1.9	920,000	2.3
48	57.6	42,870	Unlimited	0	1,500,000	2.9
44	52.8	124,900	,,	0	2,500,000	5.0
40	48.0	372,900	,,	0	4,600,000	8.1
36	43.2	885,800			9,500,000	9.3
32	38.4	930,700			24,000,000	3.9
28	33.6	1,656,000			92,000,000	1.8
24	28.8	984,900			Unlimited	0
20	24.0	1,227,000			,,	0
16	19.2	1,356,000				
			Total	62.8	Total	38.9

FIGURE 12.15

Worksheet for sample problem (1 in. = 25.4 mm, 1 psi = 6.9 kPa, 1 pci = 271.3 kN/m^3). (After PCA (1984).)

Downloaded From : www.EasyEngineering.net

Downloaded From : www.EasyEngineering.net

Figure 12.15 shows that damages caused by fatigue and erosion are 62.8 and 38.9, respectively. Both are less than 100%, so the use of a 9.5-in. (241-mm) slab is quite adequate. Separate calculations showed that a slab of 9.0-in. (229-mm) was not adequate, because the fatigue damage would increase to 142%. Therefore, this design is controlled by the fatigue analysis.

The fatigue analysis will usually control the design of pavements subjected to light traffic, whether the joints are doweled or not, or to medium traffic with doweled joints. The erosion analysis will usually control the design of pavements subjected to medium and heavy traffic with aggregate interlock joints or to heavy traffic with doweled joints. For pavements carrying a normal mix of axle weights, single-axle loads will cause more fatigue cracking, but tandem-axle loads will cause more erosion damage.

12.2.4 Other Features

The PCA design manual also includes a simplified design procedure to be used when axle load data are not available, an analysis of concrete pavements with a lean concrete subbase, and an analysis of tridem-axle loads. These features are described in this section.

Simplified Design Procedure A series of tables was developed by PCA to select the pavement thickness when specific axle load data are not available. The factors to be considered are traffic, subgrade–subbase strength, and the modulus of rupture of concrete.

Traffic Category Traffic is divided into four axle load categories, as shown in Table 12.12. The ADT and ADTT values should not be used as the primary criteria for selecting the axle load category. More reliance should be placed on word descriptions of the expected maximum axle loads. The axle load distributions used to prepare the simplified design tables for each traffic category are shown in Table 12.13. Each of these is the average of several W-4 tables representing pavement facilities in the appropriate category.

Subgrade–Subbase Strength Subgrade–subbase strength is characterized by the descriptive terms low, medium, high, and very high. These terms are related to the modulus of subgrade reaction k, as shown in Table 12.14. When a subbase is used, the increase in k value can be determined from Table 12.3 or 12.4, depending on whether the subbase is untreated or stabilized.

Design Tables The PCA design manual contains a series of tables showing the allowable ADTT for pavements with either doweled or aggregate interlock joints. Separate tables were developed for each axle load category. To illustrate the method, only the table for axle load category 3 with doweled joints is reproduced here, as shown in Table 12.15.

Three different moduli of rupture can be specified. The values 650 and 600 psi (4.5 and 4.1 MPa) on the upper portion of the tables are for good concrete with normal aggregates and are recommended for general design use; the value 550 psi (3.8 MPa) on the bottom portion is for a special case where high-quality aggregates are not available.

The allowable ADTT is based on a 20-year design period and does not include any two-axle, four-tire trucks. If the design period is not 20 years, the predicted ADTT must be changed proportionately. Incorporated in the tables are the load safety factors 1.0, 1.1, 1.2, and 1.2 for axle load categories 1, 2, 3, and 4, respectively. The tables were

Downloaded From : www.EasyEngineering.net

Downloaded From : www.EasyEngineering.net

TABLE 12.12 Axle Load Categories for Simplified Design Procedure

Axle-load category	Description	ADT	Traffic: ADTT %	Traffic: ADTT Per day	Traffic: Maximum axle loads (kips) Single axles	Traffic: Maximum axle loads (kips) Tandem axles
1	Residential streets Rural and secondary roads (low to medium)	200–800	1–3	Up to 25	22	36
2	Collector streets Rural and secondary roads (high) Arterial streets and primary roads (low)	700–5000	5–18	40–1000	26	44
3	Arterial streets and primary roads (medium) Expressways and urban and rural interstate highways (low to medium)	3000–12,000 2 lanes 3000–50,000+ 4 lanes or more	8–30	500–5000+	30	52
4	Arterial streets, primary roads expressways (high) Urban and rural interstate highways (medium to high)	3000–20,000 2 lanes 3000–150,000+ 4 lanes or more	8–30	1500–8000+	34	60

Note. The descriptors high, medium, or low refer to the relative weights of axle loads for the type of street or road; ADTT does not include two-axle, four-tire trucks; 1 kip = 4.45 kN.
Source. After PCA (1984).

developed by first assuming an ADTT and then determining the percentages of fatigue and erosion damage from the given slab thickness, concrete modulus of rupture, and subgrade–subbase k value. The allowable ADTT was then computed as

$$\text{Allowable ADTT} = \frac{100 \times (\text{assumed ADTT})}{\%\ \text{fatigue or erosion damage}}$$

Example 12.4:

The following information is given for a concrete pavement: arterial street, doweled joints, curb and gutter, design ADT = 6200, total trucks per day = 1440, ADTT = 630, concrete modulus of rupture = 650 psi (4.5 MPa), and 4 in. (102 mm) of untreated granular subbase on a subgrade with k = 150 pci(40.7 MN/m^3). Determine slab thickness by the simplified method.

Solution: Both ADT and ADTT fit well with axle-load category 3. From Table 12.3, the k value of the subgrade and subbase combined is about 170 pci (46.1 MN/m^3), so the subgrade–subbase support is classified as medium according to Table 12.14. From Table 12.15, a 7.5-in. (191-mm) slab gives an allowable ADTT of 1200; a 7-in. (178-mm) slab gives only 220. The predicted ADTT is 630, so the use of 7.5 in. (191-mm) is adequate.

Lean-Concrete Subbase The finite-element computer program can be used to analyze two layers of slab, either bonded or unbonded. If the bottom layer is a hardened lean

Downloaded From : www.EasyEngineering.net

Downloaded From : www.EasyEngineering.net

TABLE 12.13 Axle Load Distribution for Four Traffic Categories

Axle load (kips)	Axles per 1000 trucks			
	Category 1	Category 2	Category 3	Category 4
Single axles				
4	1693.31			
6	732.28			
8	483.10	233.60		
10	204.96	142.70		
12	124.00	116.76	182.02	
14	56.11	47.76	47.73	
16	38.02	23.88	31.82	57.07
18	15.81	16.61	25.15	68.27
20	4.23	6.63	16.33	41.82
22	0.96	2.60	7.85	9.69
24		1.60	5.21	4.16
26		0.07	1.78	3.52
28			0.85	1.78
30			0.45	0.63
32				0.54
34				0.19
Tandem axles				
4	31.90			
8	85.59	47.01		
12	139.30	91.15		
16	75.02	59.25	99.34	
20	57.10	45.00	85.94	
24	39.18	30.74	72.54	71.16
28	68.48	44.43	121.22	95.79
32	69.59	54.76	103.63	109.54
36	4.19	38.79	56.25	78.19
40		7.76	21.31	20.31
44		1.16	8.01	3.52
48			2.91	3.03
52			1.19	1.79
56				1.07
60				0.57

Note. 1 kip = 4.45 kN; all two-axle, four-tire trucks are excluded.
Source. After PCA (1984).

TABLE 12.14 Subgrade Soil Types and Approximate k Values

Type of soil	Support	k Values (pci)
Fine-grained soils in which silt and clay-size particles predominate	Low	75–120
Sands and sand-gravel mixtures with moderate amounts of silt and clay	Medium	130–170
Sands and sand-gravel mixtures relatively free of plastic fines	High	180–220
Cement-treated subbases	Very high	250–400

Note. 1 pci = 271.3 kN/m^3.
Source. After PCA (1984).

Downloaded From : www.EasyEngineering.net

TABLE 12.15 Allowable ADTT[a] for Axle Load Category 3 with Doweled Joints

No concrete shoulder or curb					Concrete shoulder or curb				
Slab thickness (in.)	Subgrade-subbase support				Slab thickness (in.)	Subgrade-subbase support			
	Low	Medium	High	Very high		Low	Medium	High	Very high
MR = 650 psi									
7.5				250	6.5			83	320
8		130	350	1300	7	52	220	550	1900
8.5	160	640	1600	6200	7.5	320	1200	2900	9800
9	700	2700	7000	11,500[b]	8	1600	5700	13,800	
9.5	2700	10,800			8.5	6900	23,700[b]		
10	9900								
MR = 600 psi									
					6.5				67
8			73	310	7			120	440
8.5		140	380	1500	7.5		270	680	2300
9	160	640	1700	6200	8	370	1300	3200	10,800
9.5	630	2500	6500		8.5	1600	5800	14,100	
10	2300	9300			9	6600			
10.5	7700								
MR = 550 psi									
					7				82
8.5			70	300	7.5			130	480
9		120	340	1300	8	67	270	670	2300
9.5	120	520	1300	5100	8.5	330	1200	2900	9700
10	460	1900	4900	19,100	9	1400	4900	11,700	
10.5	1600	6500	17,400		9.5	5100	18,600		
11	4900								

Note. [a]ADTT excludes two-axle, four-tire trucks.
[b]Erosion controls the design; otherwise fatigue controls. 1 in. = 25.4 mm, 1 psi = 6.9 kPa.
Source. After PCA (1984).

Downloaded From : www.EasyEngineering.net
Downloaded From : www.EasyEngineering.net

Downloaded From : www.EasyEngineering.net

concrete on which a layer of normal concrete is placed, the layers can be considered unbonded. If the two layers are built monolithically with the joints sawed deep enough to induce cracking through both layers, the case of two bonded layers applies. Design charts were developed by PCA for both bonded and unbonded cases. However, only the chart for the more popular unbonded case, which involves a normal concrete slab on a lean-concrete subbase, is presented here. In the finite-element analysis, the two layers of slab were assumed to have the same width. Because the lean-concrete subbase is usually built at least 2 ft (0.61 m) wider than the pavement on each side to support the tracks of the slipform paver, the assumption of equal width provides additional margin of safety to the design.

Figure 12.16 is the design chart for concrete pavements with lean-concrete subbases. To use the design chart, the slab thickness required for a conventional pavement without a lean-concrete subbase must be determined by the procedure described previously. For a given thickness of lean-concrete subbase, the thickness of concrete slab can be reduced, depending on the moduli of rupture of the two concrete materials. For

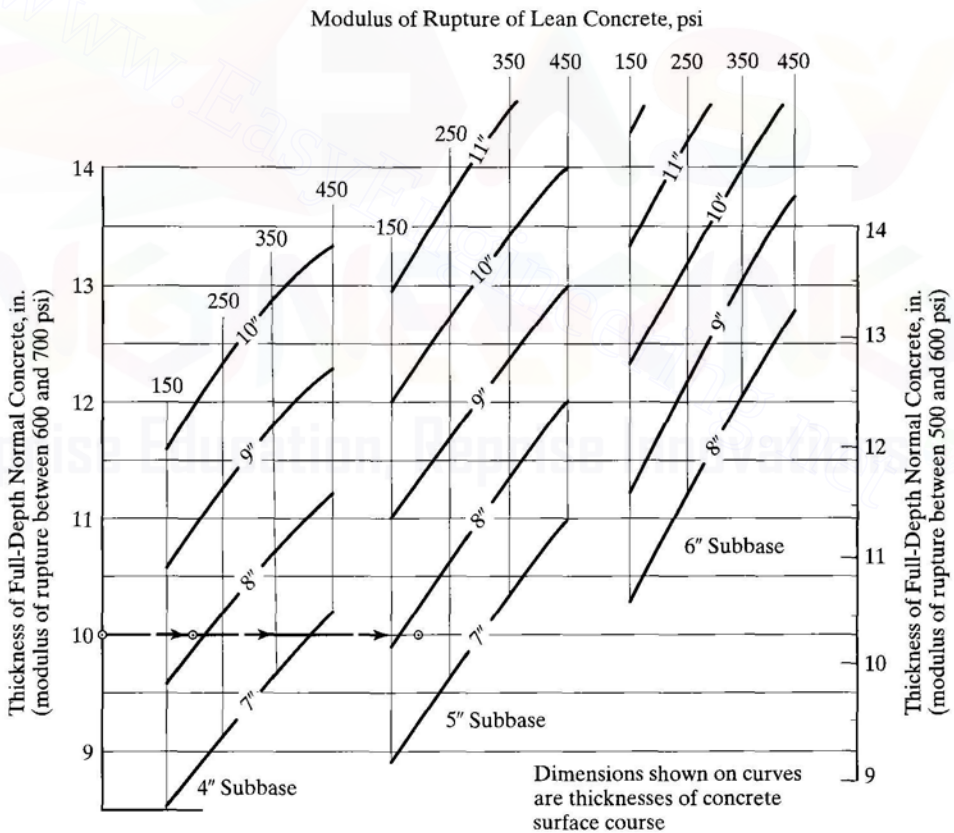


FIGURE 12.16

Design chart for concrete pavements with lean concrete subbase (1 in. = 25.4 mm, 1 psi = 6.9 kPa). (After PCA (1984).)

Downloaded From : www.EasyEngineering.net

Downloaded From : www.EasyEngineering.net

example, if the moduli of rupture are 650 psi (4.5 MPa) for normal concrete and 200 psi (1.4 MPa) for lean concrete, the design equivalent to the 10-in. (254-mm) pavement can be either a 7.7-in. (196-mm) concrete slab on a 5-in. (127-mm) lean-concrete subbase or an 8.1-in. (206-mm) concrete slab on a 4-in. (102-mm) lean-concrete subbase, as shown by the dashed line in Figure 12.16.

The normal practice has been to select a surface thickness about twice the subbase thickness. Therefore, either an 8-in. (203-mm) slab on a 5-in. (127-mm) subbase or an 8.5-in. (216-mm) slab on a 4-in. (127-mm) subbase can be used for practical design. The use of the design chart will ensure that the fatigue and erosion damage in the two layers of concrete does not exceed that in the conventional pavement. The use of a very low modulus of rupture, 200 psi (1.4 MPa), is recommended to minimize reflection cracking from the unjointed subbase through the concrete surface. If, contrary to current practice, joints are placed in the subbase at the same location as in the concrete surface, higher moduli of rupture for lean concrete may be used.

Tridem-Axle Loads Three more tables, one for equivalent stresses and two for erosion factors, were developed by PCA for tridem axles. One of the tables that can be used to determine erosion factors for slabs with doweled joints is shown in Table 12.16 for illustrative purposes. The procedure is similar to that for single and tandem axles. After the equivalent stress or erosion factor is obtained from the tables, Figure 12.12, 12.13, or 12.14 can be used to determine the allowable number of load repetitions. Although tridem-axle loads are not shown in these figures, the scale for single-axle loads can be used by dividing the tridem-axle load by three.

Example 12.5:

Given a concrete pavement with a thickness of 8 in. (203 mm), a k value of 100 pci (27.1 MN/m^3), doweled joints, and no concrete shoulders, determine the allowable repetitions under a 54-kip (240-kN) tridem-axle load based on erosion criteria.

Solution: From Table 12.16, erosion factor = 3.14. With a tridem-axle load of 54 kip (240 kN), or a single-axle load of 18 kip (80 kN), from Figure 12.13, the allowable number of repetitions is 2.3×10^6.

Some comments on the PCA method are in order. From Examples 12.3 and 12.5, the allowable repetitions based on erosion criteria are 3×10^7 for the 18-kip (80-kN) single-axle load, 6.2×10^6 for the 36-kip (160-kN) tandem-axle load, and 2.3×10^6 for the 54-kip (240-kN) tridem-axle load. Because erosion was the major distress in the AASHO Road Test, these allowable repetitions can be used to determine the equivalent axle load factor (EALF). The EALF for the 36-kip (160-kN) tandem-axle load is $(3 \times 10^7)/(6.2 \times 10^6)$, or 4.84, and that for the 54-kip (240-kN) tridem-axle load is $(3 \times 10^7)/(2.3 \times 10^6)$, or 13.0. These equivalent factors are much larger than the AASHTO factors of 2.42 and 4.0, as presented in Table 6.7. This is not surprising, because EALF values of 4.58 and 15.5 are also shown in Table 6.8 based on the fatigue analysis by KENLAYER. Under certain combinations of slab thickness and subgrade support, an extremely high or low EALF may be obtained.

Downloaded From : www.EasyEngineering.net

Downloaded From : www.EasyEngineering.net

TABLE 12.16 Erosion Factors for Slabs with Doweled Joints Under Tridem Axles

Slab thickness (in.)	*k* of Subgrade-subbase (pci)					
	50	100	200	300	500	700
4	3.89/3.33	3.82/3.20	3.75/3.13	3.70/3.10	3.61/3.05	3.53/3.00
4.5	3.78/3.24	3.69/3.10	3.62/2.99	3.57/2.95	3.50/2.91	3.44/2.87
5	3.68/3.16	3.58/3.01	3.50/2.89	3.46/2.83	3.40/2.79	3.34/2.75
5.5	3.59/3.09	3.49/2.94	3.40/2.80	3.36/2.74	3.30/2.67	3.25/2.64
6	3.51/3.03	3.40/2.87	3.31/2.73	3.26/2.66	3.21/2.58	3.16/2.54
6.5	3.44/2.97	3.33/2.82	3.23/2.67	3.18/2.59	3.12/2.50	3.08/2.45
7	3.37/2.92	3.26/2.76	3.16/2.61	3.10/2.53	3.04/2.43	3.00/2.37
7.5	3.31/2.87	3.20/2.72	3.09/2.56	3.03/2.47	2.97/2.37	2.93/2.31
8	3.26/2.83	3.14/2.67	3.03/2.51	2.97/2.42	2.90/2.32	2.86/2.25
8.5	3.20/2.79	3.09/2.63	2.97/2.47	2.91/2.38	2.84/2.27	2.79/2.20
9	3.15/2.75	3.04/2.59	2.92/2.43	2.86/2.34	2.78/2.23	2.73/2.15
9.5	3.11/2.71	2.99/2.55	2.87/2.39	2.81/2.30	2.73/2.18	2.68/2.11
10	3.06/2.67	2.94/2.51	2.83/2.35	2.76/2.26	2.68/2.15	2.63/2.07
10.5	3.02/2.64	2.90/2.48	2.78/2.32	2.72/2.23	2.64/2.11	2.58/2.04
11	2.98/2.60	2.86/2.45	2.74/2.29	2.68/2.20	2.59/2.06	2.54/2.00
11.5	2.94/2.57	2.82/2.42	2.70/2.26	2.64/2.16	2.55/2.05	2.50/1.97
12	2.91/2.54	2.79/2.39	2.67/2.23	2.60/2.13	2.51/2.02	2.46/1.94
12.5	2.87/2.51	2.75/2.36	2.63/2.20	2.56/2.11	2.48/1.99	2.42/1.91
13	2.84/2.48	2.72/2.33	2.60/2.17	2.53/2.08	2.44/1.96	2.39/1.88
13.5	2.81/2.46	2.68/2.30	2.56/2.14	2.49/2.05	2.41/1.93	2.35/1.86
14	2.78/2.43	2.65/2.28	2.53/2.12	2.46/2.03	2.38/1.91	2.32/1.83

Note. Number at left is without concrete shoulder and number at right is with concrete shoulder (without concrete shoulder/with concrete shoulder); 1 in. = 25.4 mm, 1 pci = 271.3 kN/m^3.
Source. After PCA (1984).

12.3 AASHTO METHOD

The design guide for rigid pavements was developed at the same time as that for flexible pavements and was published in the same manual. The design is based on the empirical equations obtained from the AASHO Road Test, with further modifications based on theory and experience. In this section, only the thickness design is presented. The design of steel reinforcements and tiebars is similar to that discussed in Section 4.3.2 and is not presented here.

A comprehensive survey conducted in 1994 and 1995 (Jiang *et al.*) showed that most state highway agencies used some version of the AASHTO pavement design procedures for rigid pavements. About 84 percent used either the 1972 or 1986/1993 AASHTO design procedures for rigid pavement design, about 4 percent (two states) used the PCA method, and the remaining states (12 percent) used their own design procedures.

12.3.1 Design Equations

The basic equations developed from the AASHO Road Test for rigid pavements are in the same form as those for flexible pavements, but with different values for the regression

Downloaded From : www.EasyEngineering.net

Downloaded From : www.EasyEngineering.net

constants. The equations were then modified to include many variables originally not considered in the AASHO Road Test.

Original Equations Much as with flexible pavements, the regression equations are

$$G_t = \beta(\log W_t - \log \rho) \tag{11.29}$$

$$\beta = 100 + \frac{3.63(L_1 + L_2)^{5.20}}{(D + 1)^{8.46} L_2^{3.52}} \tag{12.10}$$

$$\log \rho = 5.85 + 7.35 \log(D + 1) - 4.62 \log(L_1 + L_2) + 3.28 \log L_2 \tag{12.11}$$

in which

$G_t = \log[(4.5 - p_t)/(4.5 - 1.5)]$, where 4.5 is the initial serviceability for rigid pavement at the AASHO Road Test, which is different from the 4.2 for flexible pavements, and p_t is the serviceability at time t;

D = slab thickness in inches, which replaces SN for flexible pavements.

Using an equivalent 18-kip (80-kN) single axle load with $L_1 = 18$ and $L_2 = 1$ and combining Eqs. 11.29, 12.10, and 12.11 yields

$$\log W_{t18} = 7.35 \log(D + 1) - 0.06 + \frac{\log[(4.5 - p_t)/(4.5 - 1.5)]}{1 + 1.624 \times 10^7/(D + 1)^{8.46}} \tag{12.12}$$

in which W_{t18} is the number of 18-kip (80-kN) single axle load applications to time t. Equation 12.12 is applicable only to the pavements in the AASHO Road Test with the following conditions: modulus of elasticity of concrete $E_c = 4.2 \times 10^6$ psi (29 GPa), modulus of rupture of concrete $S_c = 690$ psi (4.8 MPa), modulus of subgrade reaction $k = 60$ pci (16 MN/m^3), load transfer coefficient $J = 3.2$, and drainage coefficient $C_d = 1.0$.

Modified Equations To account for conditions other than those that existed in the road test, it is necessary to modify Eq. 12.12, using experience and theory. After comparing stresses calculated from strain measurements on the Road Test pavements with theoretical solutions, the Spangler equation for corner loading (Spangler, 1942) was selected for its simplicity by AASHTO (1972) to extend Eq. 12.12 to other conditions. The Spangler equation is given as

$$\sigma = \frac{JP}{D^2}\left(1 - \frac{a_1}{\ell}\right) \tag{12.13}$$

in which σ is the maximum tensile stress in concrete in psi, J is the load transfer coefficient, P is the wheel load in lb, a_1 is the distance from corner of slab to center of load, and ℓ is the radius of relative stiffness defined by Eq. 4.10 and rewritten as

$$\ell = \left[\frac{ZD^3}{12(1 - \nu^2)}\right]^{0.25} \tag{12.14}$$

Downloaded From : www.EasyEngineering.net

Downloaded From : www.EasyEngineering.net

in which $Z = E_c/k$ and ν is the Poisson ratio of concrete. Assuming that $a_1 = 10$ in. (254 mm) and $\nu = 0.2$ and substituting Eq. 12.14 into 12.13 gives

$$\sigma = \frac{JP}{D^2}\left(1 - \frac{18.42}{Z^{0.25}D^{0.75}}\right) \tag{12.15}$$

Stresses were calculated for different combinations of Road Test variables by using Eq. 12.15. The ratio between the calculated stresses and the modulus of rupture, σ/S_c, was subsequently compared with axle-load applications. These comparisons indicated that, for any given load and terminal serviceability level p_t, the following relationship similar to the general fatigue equation exists:

$$\log W_t = a - (4.22 - 0.32p_t)\log\frac{\sigma}{S_c} \tag{12.16}$$

Assuming the same form of equation for other pavements with W'_t, σ, and S'_c yields

$$\log W'_t = a - (4.22 - 0.32p_t)\log\frac{\sigma'}{S'_c} \tag{12.17}$$

Combining Eqs. 12.16 and 12.17 and using the equivalent 18-kip (80-kN) single-axle load gives

$$\log W'_{t18} = \log W_{t18} + (4.22 - 0.32p_t)\log\left(\frac{S'_c}{S_c}\frac{\sigma}{\sigma'}\right) \tag{12.18}$$

From Eq. 12.15,

$$\frac{\sigma}{\sigma'} = \frac{J[1 - 18.42/(Z^{0.25}D^{0.75})]}{J'[1 - 18.42/(Z'^{0.25}D^{0.75})]} \tag{12.19}$$

Combining Eqs. 12.12, 12.18, and 12.19 results in

$$\log W'_{t18} = 7.35\log(D+1) - 0.06 + \frac{\log[(4.5 - p_t)/(4.5 - 1.5)]}{1 + 1.624 \times 10^7/(D+1)^{8.46}} + (4.22 - 0.32p_t)\log\left[\left(\frac{S'_cJ}{S_cJ'}\right)\left(\frac{D^{0.75} - 18.42/Z^{0.25}}{D^{0.75} - 18.42/Z'^{0.25}}\right)\right] \tag{12.20}$$

Letting $Z = E_c/k = 4.2 \times 10^6/60 = 70{,}000$, $S_c = 690$, and $J = 3.2$; adding a drainage coefficient C_d and a reliability term Z_RS_o; replacing the term $(4.5 - p_t)$ by ΔPSI; and removing the primes for simplicity, the final design equation for rigid pavements becomes

$$\log W_{18} = Z_RS_o + 7.35\log(D+1) - 0.06 + \frac{\log[\Delta PSI/(4.5 - 1.5)]}{1 + 1.624 \times 10^7/(D+1)^{8.46}} + (4.22 - 0.32p_t)\log\left\{\frac{S_cC_d(D^{0.75} - 1.132)}{215.63\,J[D^{0.75} - 18.42/(E_c/k)^{0.25}]}\right\} \tag{12.21}$$

Downloaded From : www.EasyEngineering.net

Downloaded From : www.EasyEngineering.net

Figure 12.17 is a nomograph for solving Eq. 12.21. Note that p_t does not appear in the nomograph because it was assumed that $p_t = 4.5 - \Delta PSI$. The DARWin computer program can also be used to solve Eq. 12.21 and perform the design procedure.

Example 12.6:

Given $k = 72$ pci (19.5 MN/m^3), $E_c = 5 \times 10^6$ psi (34.5 GPa), $S_c = 650$ psi (4.5 MPa), $J = 3.2$, $C_d = 1.0$, $\Delta PSI = 4.2 - 2.5 = 1.7$, $R = 95\%$, $S_o = 0.29$, and $W_t = 5.1 \times 10^6$, determine thickness D from Figure 12.17.

Solution: The required thickness D can be determined by the following steps:

1. Starting from Figure 12.17*a* with $k = 72$ pci (19.5 MN/m^3), a series of lines, as indicated by the arrows, are drawn through $E_c = 5 \times 10^6$ psi (34.5 GPa), $S_c = 650$ (4.5 MPa), $J = 3.2$, and $C_d = 1.0$ until a scale of 74 is obtained at the match line.
2. Starting at 74 on the match line in Figure 12.17*b*, a line is drawn through $\Delta PSI = 1.7$ until it intersects the vertical axis.
3. From the scale with $R = 95\%$, a line is drawn through $S_o = 0.29$ and then through $W_{18} = 5.1 \times 10^6$ until it intersects the horizontal axis.
4. A horizontal line is drawn from the last point in Step 2, a vertical line from that in Step 3. The intersection of these two lines gives a D of 9.75 in. (246 mm), which is rounded to 10 in. (254 mm).

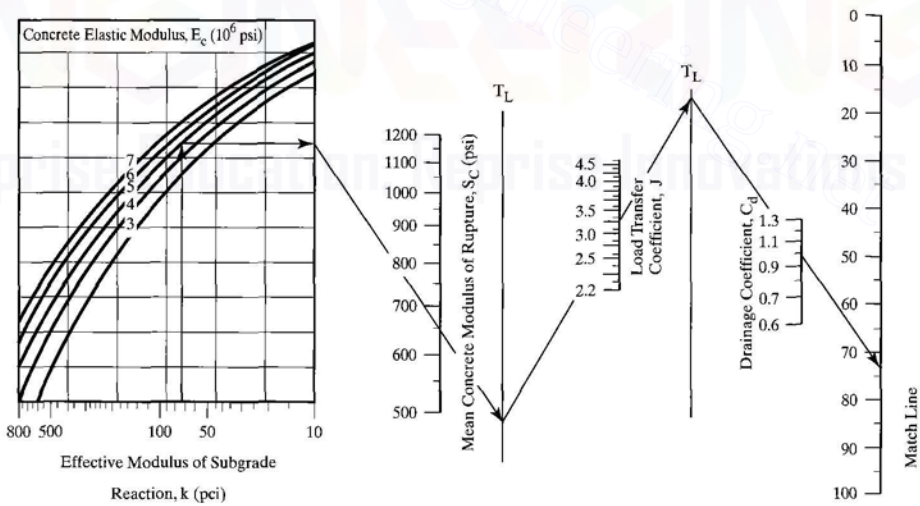


FIGURE 12.17

Design chart for rigid pavements based on mean values (1 in. = 25.4 mm, 1 psi = 6.9 kPa, 1 pci = 271.3 kN/m^3). (From the *AASHTO Guide for Design of Pavement Structures*. Copyright 1986. American Association of State Highway and Transportation Officials, Washington, DC. Used by permission.)

Downloaded From : www.EasyEngineering.net

Downloaded From : www.EasyEngineering.net

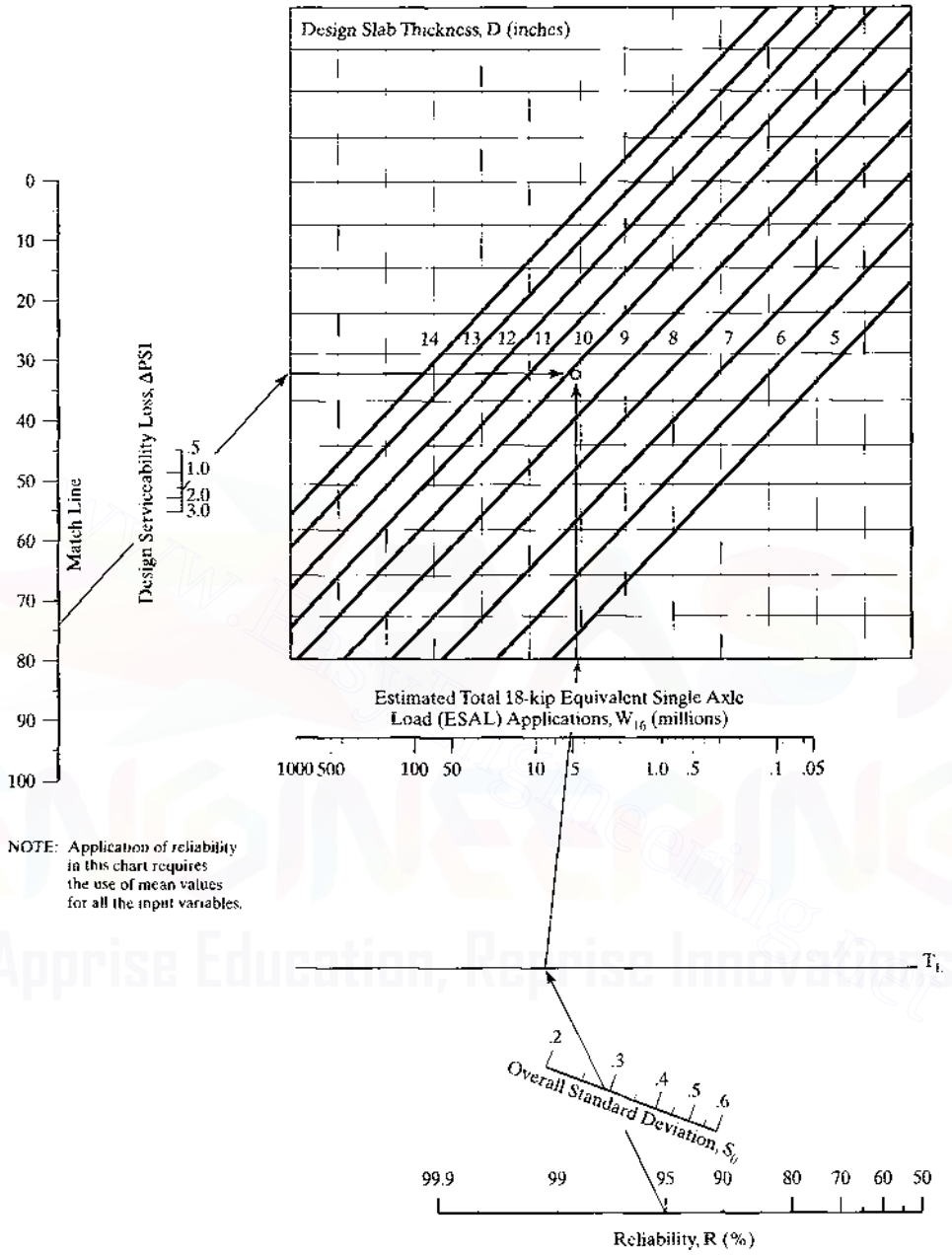


FIGURE 12.17 (Continued)

Downloaded From : www.EasyEngineering.net

Downloaded From : www.EasyEngineering.net

Example 12.7:

Same as Example 12.6, except that D is given as 9.75 in. (246 mm). Determine W_{18} by using Eq. 12.21.

Solution: For $R = 95\%$, from Table 11.15, $Z_R = -1.645$. From Eq. 12.21, $\log W_{18} = -1.645 \times 0.29 + 7.35 \log(9.75 + 1) - 0.06 + \log(1.7/2.7)/[1 + 1.624 \times 10^7/(9.75 + 1)^{8.46}] + (4.22 - 0.32 \times 2.5) \log\{[(650 \times 1.0)/(215.63 \times 3.2)][(9.75)^{0.75} - 1.132]/[(9.75)^{0.75} - 18.42/(5 \times 10^6/72)^{0.25}]\} = -0.477 + 7.581 - 0.06 - 0.195 - 0.088 = 6.761$, or $W_{18} = 5.8 \times 10^6$, which checks well with the 5.2×10^6 obtained from the chart.

12.3.2 Modulus of Subgrade Reaction

The property of roadbed soil to be used for rigid pavement design is the modulus of subgrade reaction k, rather than the resilient modulus M_R. It is therefore necessary to convert M_R to k. As with M_R, the values of k also vary with the season of the year, and the relative damage caused by the change of k needs to be evaluated.

Correlation with Resilient Modulus As discussed in Section 5.1.1, there is no unique correlation between the modulus of subgrade reaction for liquid foundation and the resilient modulus for solid foundation. Any relationship between k and M_R is arbitrary and depends on whether stresses or deflections are to be compared and on whether the loads are applied at the interior, edge, or corner of the slab.

Without Subbase If the slab is placed directly on the subgrade without a subbase, AASHTO suggested the use of the following theoretical relationship based on an analysis of a plate-bearing test:

$$k = \frac{M_R}{19.4} \tag{12.22}$$

Here, k is in pci and M_R is in psi. This equation gives a k value that is too large. For example, the resilient moduli equivalent to a k value of 100 pci (27.1 MN/m^3) are about 4000 psi (27.6 kPa) for an 8-in. (203-mm) slab and 4720 psi (32.6 MPa) for a 10-in. (254-mm) slab, based on the edge stress as shown in Table 5.13, while those based on the corner deflection are 6400 and 7560 psi (44.2 and 52.2 MPa), as shown in Table 5.14. For a k value of 100 pci (27.1 MPa), the resilient modulus obtained from Eq. 12.22 is only 1940 psi (13.4 MPa).

Equation 12.22 was based on the definition of k using a 30-in. (762-mm) plate. The deflection w_0 of a plate on a solid foundation can be determined by Eq. 2.10. The modulus of subgrade reaction, which is defined as the ratio between an applied pressure q and the deflection w_0, can be expressed as

$$k = \frac{q}{w_0} = \frac{2M_R}{\pi(1 - \nu^2)a} \tag{12.23}$$

in which ν is the Poisson ratio of the foundation and a is the radius of the plate. If $\nu = 0.45$ and $a = 15$ in. (381 mm), then Eq. 12.23 becomes

$$k = \frac{M_R}{18.8} \tag{12.24}$$

Downloaded From : www.EasyEngineering.net

Downloaded From : www.EasyEngineering.net

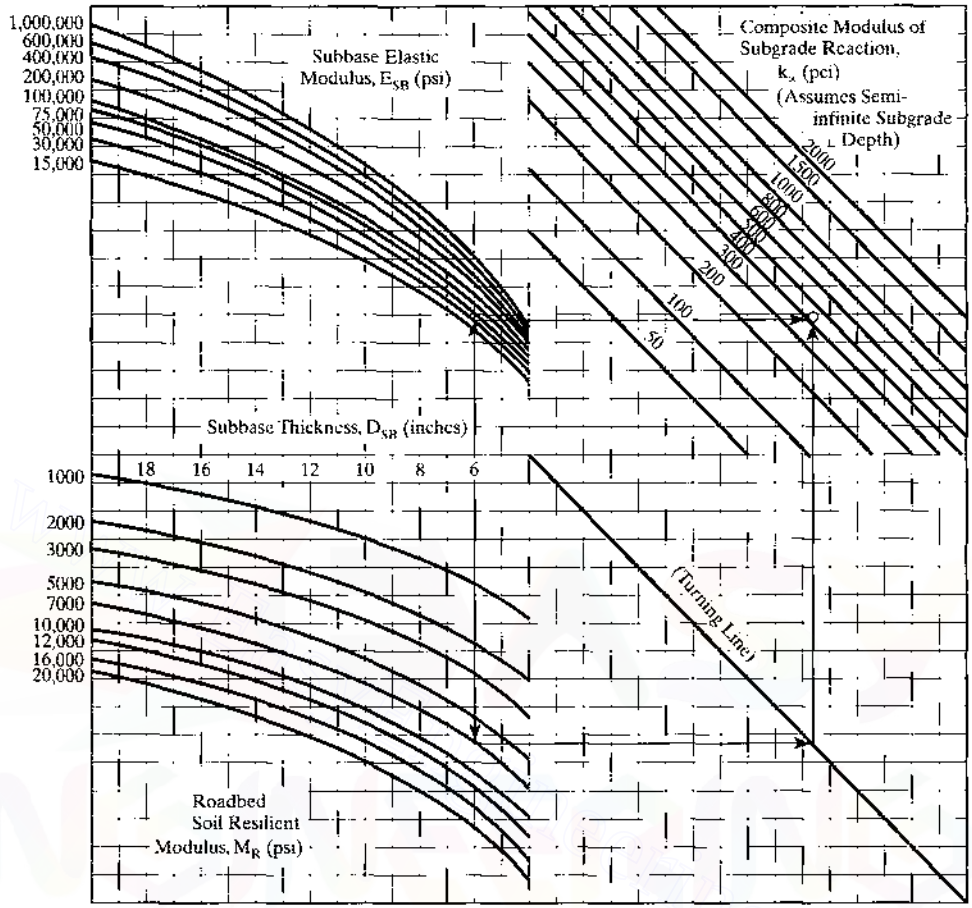


FIGURE 12.18

Chart for estimating modulus of subgrade reaction (1 in. = 25.4 mm, 1 psi = 6.9 kPa, 1 pci = 271.3 kN/m^3). (From the *AASHTO Guide for Design of Pavement Structures*. Copyright 1986. American Association of State Highway and Transportation Officials, Washington, DC. Used by permission.)

Equation 12.24 is a more exact solution compared to Eq. 12.22, which is an approximate solution using the average surface deflection under a flexible loaded area as w_0 (AASHTO, 1985). Equations 12.22 and 12.24 give a k value that is too large because k is inversely proportional to a, as indicated by Eq. 12.23. To correlate k with M_R, a very large plate should be used. The use of a 30-in. (762-mm) plate is arbitrary and is the only practical way to obtain a given value of k, because tests with larger plates will be more expensive and difficult to perform. Therefore, the use of Eq. 12.22 or 12.24 based on a 30-in. (762-mm) plate to compute k from M_R is misleading and will result in stresses and deflections that are too small compared with those based on M_R.

With Subbase If a subbase exists between the slab and the subgrade, the composite modulus of subgrade reaction can be determined from Figure 12.18. The modulus is

Downloaded From : www.EasyEngineering.net

Downloaded From : www.EasyEngineering.net

based on a subgrade of infinite depth and is denoted by k_∞. The chart was developed by using the same method as for a homogeneous half-space, except that the 30-in. (762-mm) plate is applied on a two-layer system. Therefore, the k values obtained from the chart are too large and do not represent what actually occurs in the field.

Example 12.8:

Given a subbase thickness D_{SB} of 6 in. (152 mm), a subbase resilient modulus E_{SB} of 20,000 psi (138 MPa), and a roadbed soil resilient modulus M_R of 7000 psi (48 MPa), determine the composite modulus of subgrade reaction k_∞.

Solution: The composite modulus of subgrade reaction can be determined as follows:

1. In Figure 12.18, a vertical line is drawn upward from the horizontal scale with a subbase thickness E_{SB} of 6 in. (152 mm) until it reaches a point with a subbase modulus E_{SB} of 20,000 psi (138 MPa).
2. The same line is drawn downward until it intersects the curve with a roadbed soil resilient modulus M_R of 7000 psi (48 MPa), and then the line is turned horizontally until it intersects the turning line.
3. A horizontal line is drawn from the point in Step 1, a vertical line from the point on the turning line in Step 2. The intersection of these two lines gives a k_∞ of 400 pci (108 MN/m^3).

Rigid Foundation at Shallow Depth Equation 12.22 and Figure 12.18 are based on a subgrade of infinite depth. If a rigid foundation lies below the subgrade and the subgrade depth to rigid foundation D_{SG} is smaller than 10 ft (3 m), then the modulus of subgrade reaction must be modified by the chart shown in Figure 12.19. The chart can be applied to slabs either with or without a subbase.

Example 12.9:

Given M_R = 4000 psi (27.6 MPa), D_{SG} = 5 ft (1.52 m), and k_∞ = 230 pci (62.4 MN/m^3), determine k.

Solution: In Figure 12.19, a vertical line is drawn from the horizontal scale with a M_R of 4000 psi (27.6 MPa) until it intersects the curve with a D_{SG} of 5 ft. The line is turned horizontally until it reaches a point with a k_∞ of 230 pci (62.4 MN/m^3) and then vertically until a k of 300 pci (81.4 MN/m^3) is obtained.

Effective Modulus of Subgrade Reaction The effective modulus of subgrade reaction is an equivalent modulus that would result in the same damage if seasonal modulus values were used throughout the year. The equation for evaluating the relative damage and the method for computing the effective k are discussed next.

Relative Damage From Eq. 12.21, the effect of k on W_{18} can be expressed as

$$\log W_{18} = \log C - \log\left[\left(D^{0.75} - \frac{18.42k^{0.25}}{E_c^{0.25}}\right)^{(4.22-0.32p_t)}\right]$$

Downloaded From : www.EasyEngineering.net

Downloaded From : www.EasyEngineering.net

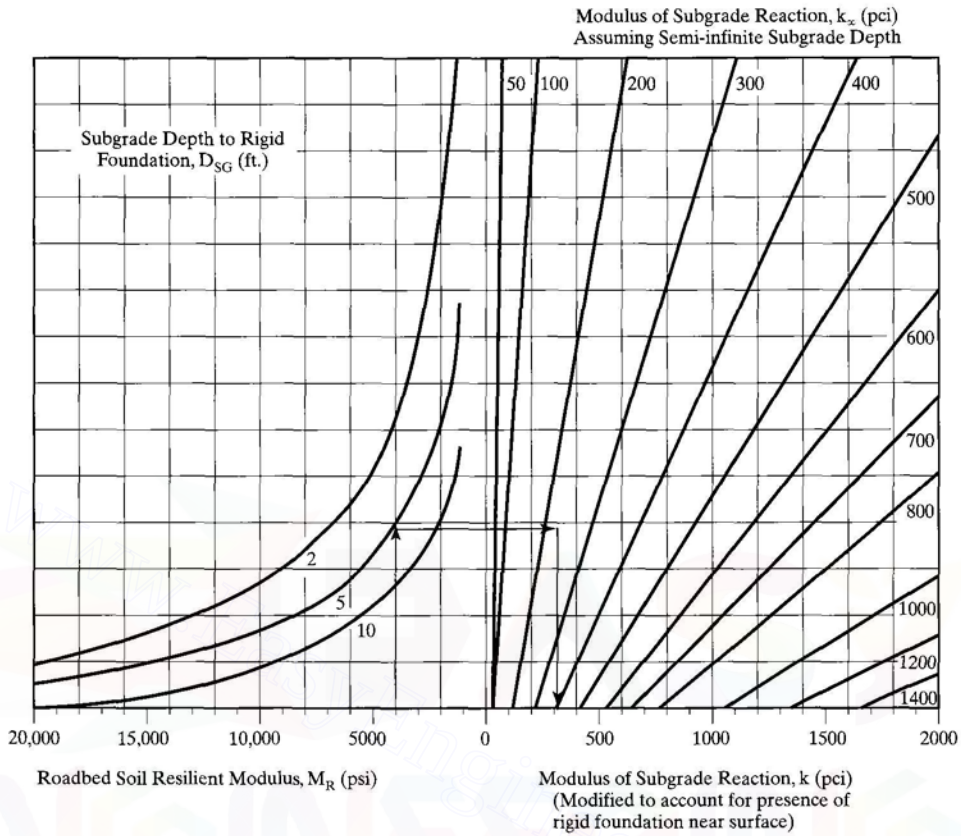


FIGURE 12.19

Chart for modifying modulus of subgrade reaction due to rigid foundation near surface (1 ft = 0.305 m, 1 psi = 6.9 kPa, 1 pci = 271.3 kN/m^3). (From the *AASHTO Guide for Design of Pavement Structures*. Copyright 1986. American Association of State Highway and Transportation Officials, Washington, DC. Used by permission.)

or

$$W_{18} = \frac{C}{(D^{0.75} - 18.42k^{0.25}/E_c^{0.25})^{(4.22-0.32p_t)}} \tag{12.25}$$

in which C is the sum of all terms except for those related to k. Because of the relatively small variation in E_c and p_t, Eq. 12.25 can be simplified by assuming that $E_c = 5 \times 10^6$ psi (34.5 GPa) and $p_t = 2.5$:

$$W_{18} = \frac{C}{(D^{0.75} - 0.39k^{0.25})^{3.42}} \tag{12.26}$$

If W_T is the predicted total traffic, then the damage ratio can be expressed as

$$D_r = \frac{W_T}{C}(D^{0.75} - 0.39k^{0.25})^{3.42} \tag{12.27}$$

Downloaded From : www.EasyEngineering.net

Downloaded From : www.EasyEngineering.net

If W_T is distributed uniformly over n periods, then the cumulative damage ratio is

$$D_r = \frac{W_T}{C}\frac{1}{n}\sum_{i=1}^{n}(D^{0.75} - 0.39k_i^{0.25})^{3.42} \tag{12.28}$$

Equating Eq. 12.27 to Eq. 12.28 gives

$$(D^{0.75} - 0.39k^{0.25})^{3.42} = \frac{1}{n}\sum_{i=1}^{n}(D^{0.75} - 0.39k_i^{0.25})^{3.42} \tag{12.29}$$

Equation 12.29 can be used to determine the effective modulus of subgrade reaction k in terms of seasonal moduli k_i. The relative damage to rigid pavements u_r is defined as

$$u_r = (D^{0.75} - 0.39k^{0.25})^{3.42} \tag{12.30}$$

Figure 12.20 is a chart for solving Eq. 12.30.

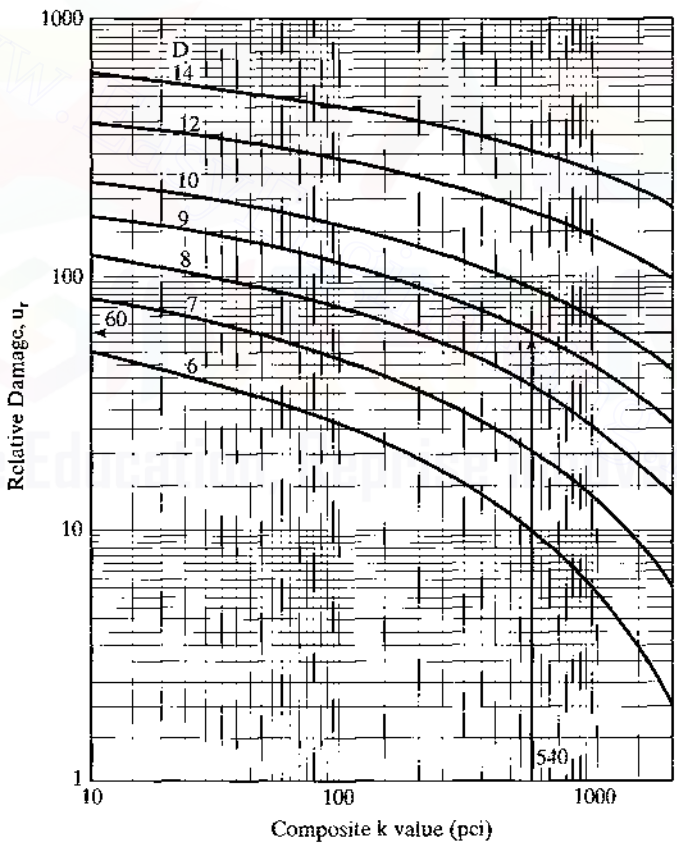


FIGURE 12.20

Chart for estimating relative damage to rigid pavements (1 in. = 25.4 mm, 1 pci = 271.3 kN/m^3). (From the *AASHTO Guide for Design of Pavement Structures*. Copyright 1986, American Association of State Highway and Transportation Officials, Washington, DC. Used by permission.)

Downloaded From : www.EasyEngineering.net

Downloaded From : www.EasyEngineering.net

Example 12.10:

Given $D = 9$ in. (229 mm) and $k = 540$ pci (147 MN/m^3), determine u_r by Eq. 12.30 and compare the result with Figure 12.20.

Solution: From Eq. 12.30, $u_r = [(9)^{0.75} - 0.39(540)^{0.25}]^{3.42} = 60.3$, which checks with a relative damage of 60 obtained from the chart.

Computation Table 12.17 shows the computation of the effective modulus of subgrade reaction for a slab thickness of 9 in. (229 mm). It is assumed that the slab is placed directly on a subgrade having the monthly resilient moduli shown in the table.

Explanation of Columns in Table 12.17

1. Each year is divided into 12 months, each with a different subgrade modulus.
2. The roadbed resilient moduli are the same as those used in the DAMA program for a MAAT of 60°F (15.5°C) and a normal modulus of 4500 psi (31 MPa), as shown in Table 11.10. The maximum modulus is 50,000 psi (345 MPa) and occurs in March when the subgrade is frozen.
3. The k values are obtained from Eq. 12.22. Because no corrections for rigid foundation are needed, these k values can be used for computing relative damage.
4. The relative damage can be obtained from Eq. 12.30 or Figure 12.20. The sum of relative damage is 988.7 and the average over the 12 months is 82.4, which is equivalent to an effective modulus of 263 pci (71.4 MN/M^3).

It is interesting to note the significant difference in behaviors between flexible and rigid pavements under freeze–thaw conditions. For the flexible pavement analyzed in Figure 11.26, the damage caused by the spring breakup in May constitutes about 65% of the total damage, and the effective roadbed soil modulus is 2200 psi (15 MPa), versus the normal value of 4500 psi (31 MPa). For the rigid pavement analyzed in Table 12.17, the damage caused by the spring breakup in April constitutes only 12% of the total damage, and the effective modulus of subgrade reaction is 263 pci (71.4 MN/m^3) versus the normal value of 232 pci (62.9 MN/m^3). The fact that the effective modulus is even greater than the normal modulus substantiates the claim by PCA (1984) that the normal summer or fall k values can be used for design purposes to avoid the tedious method of considering seasonal variations.

Loss of Subgrade Support To account for the potential loss of support by foundation erosion or differential vertical soil movements, the effective modulus of subgrade reaction must be reduced by a factor, LS. Figure 12.21 shows a chart for correcting the effective modulus of subgrade reaction due to the loss of foundation support. For example, if the effective modulus of subgrade reaction for full contact, LS = 0, is 540 pci (147 MN/m^3), the effective modulus of subgrade reaction for partial contact with LS = 1 is 170 pci (46 MN/m^3).

Figure 12.21 was developed by computing the maximum principal stress under a single-axle load for four different contact conditions with LS = 0, 1, 2, and 3. The best case is LS = 0, when the slab and foundation are assumed to be in full contact. The

Downloaded From : www.EasyEngineering.net

Downloaded From : www.EasyEngineering.net

TABLE 12.17 Computation of Effective Modulus of Subgrade Reaction

Month (1)	Roadbed modulus M_R (psi) (2)	k Value (pci) (3)	Relative damage u_r (%) (4)
Jan	4500	232	85.7
Feb	27,300	1407	34.2
Mar	50,000	2577	20.5
Apr	1350	70	121.4
May	2140	110	108.1
Jun	2930	151	98.7
Jul	3710	191	91.6
Aug	4500	232	85.7
Sep	4500	232	85.7
Oct	4500	232	85.7
Nov	4500	232	85.7
Dec	4500	232	85.7

Average $\bar{u}_r = \dfrac{\Sigma u_r}{n} = 82.4$ $\Sigma u_r = 988.7$

Effective modulus of subgrade reaction, $k = 263$ pci

Note. 1 psi = 6.9 kPa, 1 pci = 271.3 kN/m^3.

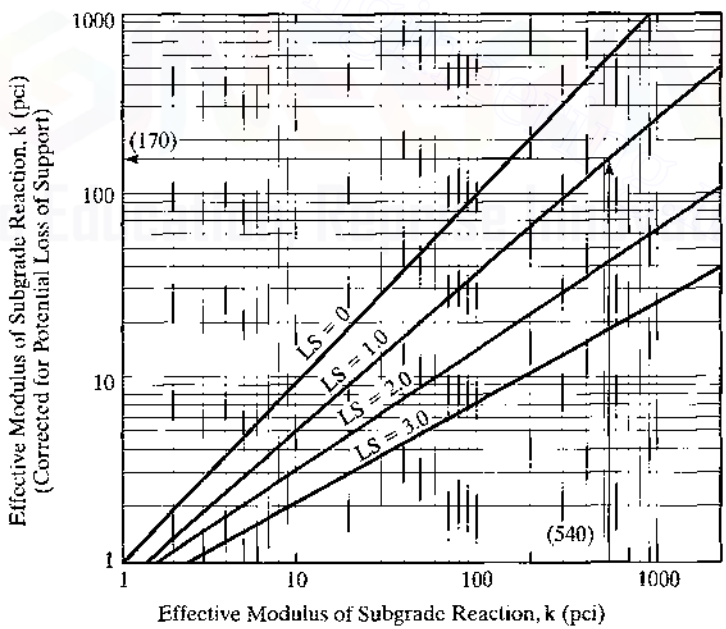


FIGURE 12.21

Correction of effective modulus of subgrade reaction due to loss of foundation contact (1 pci = 271.3 kN/m^3). (After McCullough and Elkins (1979).)

Downloaded From : www.EasyEngineering.net

Downloaded From : www.EasyEngineering.net

worst case is LS = 3, when an area of slab, 9 ft (2.7 m) long and 7.25 ft (2.2 m) wide along the pavement edge, is assumed not to be in contact with the subgrade. The area assumed not to be in contact for LS = 2 is smaller than that for LS = 3 but greater than that for LS = 1. The result of the AASHO Road Test indicates that the stresses produced in a concrete pavement are proportional to the number of load applications it can carry, so the equivalent k value for partial contact can be obtained by varying the k values until the maximum principal stress for full contact is equal to that for partial contact.

Table 12.18 provides some suggested ranges of LS for different types of subbase and subgrade materials. In the selection of LS factor, consideration should be given to differential vertical soil movements that may result in voids beneath the pavement. Even though a nonerosive subbase is used, LS values of 2.0 to 3.0 may still be used for active swelling clays or excessive frost heave.

12.3.3 Design Variables

The design variables presented in Sections 11.3.1 and 11.3.6 for flexible pavements, such as time constraints, traffic, reliability, environmental effects, serviceability, stage construction, and the analysis of swelling and frost heave, are the same as those for rigid pavements and are not repeated here. The effective modulus of subgrade reaction was discussed in Section 12.3.2, so only the elastic modulus of concrete E_c, the concrete modulus of rupture S_c, the load transfer coefficient J, and the drainage coefficient C_d are presented in this section.

Elastic Modulus of Concrete The elastic modulus of concrete can be determined according to the procedure described in ASTM C469 or correlated with the compressive strength. The following is a correlation recommended by the American Concrete Institute:

$$E_c = 57{,}000(f'_c)^{0.5} \tag{12.31}$$

in which E_c is the concrete elastic modulus in psi and f'_c is the concrete compressive strength in psi as determined by AASHTO T22, T140, or ASTM C39.

TABLE 12.18 Typical Ranges of LS Factors for Various Types of Materials

Type of material	Loss of support (LS)
Cement-treated granular base ($E = 1 \times 10^6$ to 2×10^6 psi)	0.0 to 1.0
Cement aggregate mixtures ($E = 500{,}000$ to 1×10^6 psi)	0.0 to 1.0
Asphalt-treated bases ($E = 350{,}000$ to 1×10^6 psi)	0.0 to 1.0
Bituminous-stabilized mixture ($E = 40{,}000$ to $300{,}000$ psi)	0.0 to 1.0
Lime-stabilized materials ($E = 20{,}000$ to $70{,}000$ psi)	1.0 to 3.0
Unbound granular materials ($E = 15{,}000$ to $45{,}000$ psi)	1.0 to 3.0
Fine-grained or natural subgrade materials ($E = 3000$ to $40{,}000$ psi)	2.0 to 3.0

Note. E in this table refers to the general symbol of the resilient modulus.
Source. After AASHTO (1986).

Downloaded From : www.EasyEngineering.net

Downloaded From : www.EasyEngineering.net

Concrete Modulus of Rupture The modulus of rupture required by the design procedure is the mean value determined after 28 days by using third-point loading, as specified in AASHTO T97 or ASTM C78. If center-point loading is used, a correlation should be made between the two tests.

Load Transfer Coefficient The load transfer coefficient J is a factor used in rigid pavement design to account for the ability of a concrete pavement structure to transfer a load across joints and cracks. The use of load transfer devices and tied concrete shoulders increases the amount of load transfer and decreases the load-transfer coefficient. Table 12.19 shows the recommended load transfer coefficients for various pavement types and design conditions. The AASHO Road Test conditions represent a J value of 3.2, because all joints were doweled and there were no tied concrete shoulders.

Drainage Coefficient The drainage coefficient C_d has the same effect as the load-transfer coefficient J. As indicated by Eq. 12.21, an increase in C_d is equivalent to a decrease in J, both causing an increase in W_{18}. Table 12.20 provides the recommended C_d values based on the quality of drainage and the percentage of time during which the pavement structure would normally be exposed to moisture levels approaching saturation. As with flexible pavements, the percentage of time is dependent on the average yearly rainfall and the prevailing drainage conditions.

TABLE 12.19 Recommended Load Transfer Coefficient for Various Pavement Types and Design Conditions

Type of shoulder	Asphalt		Tied PCC	
Load transfer devices	Yes	No	Yes	No
JPCP and JRCP	3.2	3.8–4.4	2.5–3.1	3.6–4.2
CRCP	2.9–3.2	N/A	2.3–2.9	N/A

Source. After AASHTO (1986).

TABLE 12.20 Recommended Values of Drainage Coefficients C_d for Rigid Pavements

Quality of drainage		Percentage of time pavement structure is exposed to moisture levels approaching saturation			
Rating	Water removed within	Less than 1%	1–5%	5–25%	Greater than 25%
Excellent	2 hours	1.25–1.20	1.20–1.15	1.15–1.10	1.10
Good	1 day	1.20–1.15	1.15–1.10	1.10–1.00	1.00
Fair	1 week	1.15–1.10	1.10–1.00	1.00–0.90	0.90
Poor	1 month	1.10–1.00	1.00–0.90	0.90–0.80	0.80
Very poor	Never drain	1.00–0.90	0.90–0.80	0.80–0.70	0.70

Source. After AASHTO (1986).

Downloaded From : www.EasyEngineering.net

Downloaded From : www.EasyEngineering.net

12.3.4 Comparison with PCA Method

It is difficult to compare results between the AASHTO and the PCA methods because the AASHTO method is based on reliability, using mean values for all variables, whereas the PCA method does not consider reliability, but incorporates load safety factors and more conservative material properties. The AASHTO method is based on the equivalent 18-kip (80-kN) single-axle load applications and does not distinguish the type of distress; the PCA method considers both fatigue cracking and foundation erosion, using actual single- and tandem-axle loads. In view of the fact that fatigue cracking is more critical under single-axle loads and foundation erosion is more critical under tandem-axle loads, it is unreasonable to use ESAL for rigid pavement design, because the conversion of a tandem-axle load to an equivalent single-axle load actually changes the failure mode from erosion at the joint to fatigue at midslab. In the following comparison, it is assumed that the pavement is subjected to only one type of axle load, that is, the same 18-kip (80-kN) single-axle load, so the predominant mode of distress is fatigue cracking.

In applying the AASHTO method, the following parameter values are assumed: reliability $R = 95\%$, standard deviation $S_o = 0.35$, serviceability loss $\Delta PSI = 2.0$ ($p_t = 2.5$), drainage coefficient $C_d = 1.0$, load transfer coefficient $J = 3.2$ without concrete shoulders and 2.5 with concrete shoulders, concrete modulus of rupture $S_c = 650$ psi (4.5 MPa), and modulus of subgrade reaction $k = 100$ pci (27.1 MN/m^3). In the PCA method, a load safety factor of 1.2 and the same S_c of 650 psi (4.5 MPa) and k of 100 pci (27.1 MN/m^3) are assumed. The PCA design chart has already taken into account the variation of S_c and the increase of S_c with time, so only the input of S_c at 28 days is required, which is the same as the S_c specified by AASHTO. The same k values are used in both methods because the normal summer or fall modulus of subgrade reaction specified by PCA is not too much different from the effective modulus of subgrade reaction specified by AASHTO, as illustrated by the example in Table 12.17. Table 12.21 shows a comparison of thickness design between the AASHTO and PCA methods.

In Table 12.21, comparisons are made for pavements both with and without tied concrete shoulders. The allowable ESAL for five different slab thicknesses are shown. The AASHTO ESAL was computed by the AASHTO design equation (Eq. 12.21); the PCA ESAL was obtained from the PCA design tables and charts based on the fatigue criterion (Table 12.6 or 12.7 and Figure 12.12) by using a single-axle load of 21.6 kip (96 kN), which

TABLE 12.21 Comparison of Thickness Between AASHTO and PCA Methods

Slab thickness (in.)	No concrete shoulder			With concrete shoulder		
	AASHTO ESAL	PCA ESAL	Thickness by PCA (in.)	AASHTO ESAL	PCA ESAL	Thickness by PCA (in.)
5	1.2×10^5	<100	7.5	2.8×10^5	350	6.6
6	3.2×10^5	500	7.9	7.4×10^5	4.0×10^4	6.9
7	7.4×10^5	3.0×10^4	8.1	1.7×10^6	1.0×10^6	7.1
8	1.6×10^6	5.0×10^5	8.2	3.7×10^6	$>10^7$	7.2
9	3.3×10^6	$>10^7$	8.3	7.7×10^6	$>10^7$	7.3

Note. 1 in. = 25.4 mm.

Downloaded From : www.EasyEngineering.net

Downloaded From : www.EasyEngineering.net

is the 18-kip (80-kN) load multiplied by a load safety factor of 1.2. It was found that, when the joints are doweled, the use of the erosion criterion is not as critical as the use of the fatigue criterion. The thickness by PCA, as shown in Table 12.21, is the slab thickness determined by the PCA method based on the AASHTO ESAL.

As can be seen from Table 12.21, a large difference in ESAL exists between the two methods. For slabs with a thickness smaller than 8 in. (203 mm) and no concrete shoulder or for slabs with a thickness smaller than 7 in. (178 mm) and a tied concrete shoulder, the ESAL determined by the AASHTO method is one or more orders of magnitude greater than that obtained by the PCA method. Therefore, the use of the AASHTO equation for thin pavements, such as concrete shoulders, is less conservative. For example, with an ESAL of 2.8×10^5 and a tied concrete shoulder, a thickness of 5 in. (122 mm) is sufficient by the AASHTO equation but the thickness required by the PCA method is 6.6 in. (168 mm).

It appears that the ESAL obtained by the PCA method is more reasonable, at least for thinner pavements. Consider the case of a 5-in. (127-mm) slab without a concrete shoulder. A run of KENSLABS shows that the critical edge stress under an 18-kip (80-kN) single-axle load is 641 psi (4.4 MPa), which is nearly equal to the concrete modulus of rupture. Thus, it is not possible that the pavement can withstand 120,000 applications of an 18-kip (80-kN) single-axle load as computed by the AASHTO equation.

12.4 CONTINUOUS REINFORCED CONCRETE PAVEMENTS

In both PCA and AASHTO design methods, the procedure for determining the thickness of CRCP is the same as that for JPCP and JRCP. According to PCA (1984), the analysis of CRCP by the JSLAB computer program indicated that the critical stresses and deflections in CRCP were about the same as those in conventional pavements, sometimes slightly larger and sometimes slightly smaller (depending on the crack spacing), so the use of the same thickness is recommended. The difference in thickness design between CRCP and conventional pavements in the AASHTO method is that CRCP allows the use of a slightly smaller load transfer coefficient, as shown in Table 12.19. If the load transfer coefficient in Example 12.6 is reduced from 3.2 to 2.9, the thickness of the slab can be reduced from 9.75 in. (248 mm) to 9 in. (229 mm).

In this section, only the design of longitudinal steel recommended by AASHTO (1986) is presented. The design of transverse steel is similar to that discussed in Example 4.10 and is not presented here. The AASHTO method for designing longitudinal reinforcements is the same as the method published by Austin Research Engineers, Inc. (McCullough and Elkins, 1979) and later adopted as a design procedure by the Associated Reinforcing Bar Producers–CRSI (McCullough and Cawley, 1981).

12.4.1 Design Variables

The input variables for the design of longitudinal reinforcement are discussed below.

Concrete Tensile Strength The concrete indirect tensile strength at 28 days, as determined by AASHTO T198 or ASTM C496, should be used for the design of longitudinal steel reinforcement. The indirect tensile strength f_t can be assumed to be 86% of the modulus of rupture S_c that is used for thickness design.

Downloaded From : www.EasyEngineering.net

Downloaded From : www.EasyEngineering.net

TABLE 12.22 Approximate Relationship Between Shrinkage and Indirect Tensile Strength of PCC

Indirect tensile strength (psi)	Shrinkage (in./in.)
300 or less	0.0008
400	0.0006
500	0.00045
600	0.0003
700 or greater	0.0002

Source. After AASHTO (1986).

Concrete Shrinkage Concrete shrinkage at 28 days, Z, is a significant factor in the reinforcement design. Shrinkage is strongly related to strength, because both depend on the water–cement ratio. Table 12.22 may be used as a guide in selecting a shrinkage value corresponding to the indirect tensile strength.

Concrete Thermal Coefficient The thermal coefficient of expansion for PCC, α_c, depends on many factors such as the water–cement ratio, concrete age, richness of the mix, relative humidity, and the type of aggregate in the mix. However, the type of coarse aggregate has the most influence. Recommended values of the thermal coefficient of PCC as a function of aggregate types is presented in Table 12.23.

Bar or Wire Diameter Typical No. 5 and No. 6 deformed bars are used for longitudinal reinforcement in CRCP. The nominal diameter of a reinforcing bar in inches is simply the bar number divided by 8. The No. 6 bar is the largest practical size that should be used to meet bond requirements and control crack widths. The relationship between longitudinal and transverse wire should conform to manufacturers' recommendations.

Steel Thermal Coefficient Unless specific knowledge of the thermal coefficient is known, the value 5×10^{-6}/°F (9×10^{-6}/°C) may be assumed for design purposes.

Design Temperature Drop The design temperature drop is the difference between the average concrete curing temperature and a design minimum temperature and can be computed as

$$DT_D = T_H - T_L \tag{12.32}$$

TABLE 12.23 Recommended Value of the Thermal Coefficient of PCC as a Function of Aggregate Types

Type of coarse aggregate	Concrete thermal coefficient (10^{-6}/°F)
Quartz	6.6
Sandstone	6.5
Gravel	6.0
Granite	5.3
Basalt	4.8
Limestone	3.8

Note. Value/°F must be multiplied by 1.8 to obtain value/°C.
Source. After AASHTO (1986).

Downloaded From : www.EasyEngineering.net

Downloaded From : www.EasyEngineering.net

in which DT_D is the design temperature drop, T_H is the average daily high temperature during the month the pavement is constructed, and T_L is the average daily low temperature during the coldest month of the year.

Wheel Load Tensile Stress Figure 12.22 can be used to estimate the wheel-load tensile stress developed during initial loading of the constructed pavement by either construction equipment or truck traffic. This stress depends on the design slab thickness,

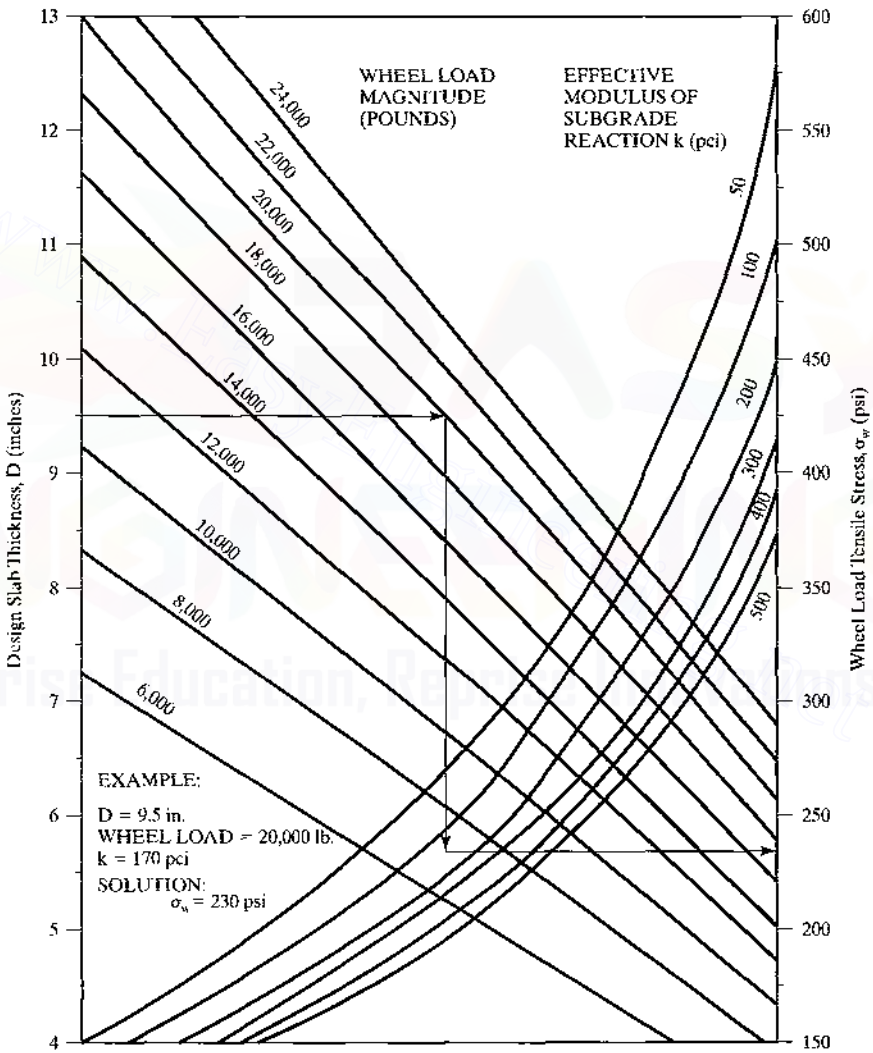


FIGURE 12.22

Chart for estimating wheel load tensile stress (1 in. = 25.4 mm, 1 lb = 4.45 N, 1 psi = 6.9 kPa, 1 pci = 271.3 kN/m^3). (From the *AASHTO Guide for Design of Pavement Structures*. Copyright 1986. American Association of State Highway and Transportation Officials, Washington, DC. Used by permission.)

Downloaded From : www.EasyEngineering.net

Downloaded From : www.EasyEngineering.net

the wheel load magnitude, and the effective modulus of subgrade reaction, as shown by the example in Figure 12.22.

12.4.2 Limiting Criteria

Three limiting criteria must be considered for the design of longitudinal steel: crack spacing, crack width, and steel stress.

Crack Spacing The limits on crack spacing are based on the possibility of spalling and punchout. To minimize spalling, the maximum spacing between consecutive cracks should be limited to 8 ft (2.4 m). To minimize the potential for punchout, the minimum desirable spacing is 3.5 ft (1.1 m).

Crack Width The limit on crack width is based on a consideration of spalling and water infiltration. The allowable crack width should not exceed 0.04 in. (1.0 mm). The crack width should be reduced as much as possible through the selection of a higher steel percentage or smaller diameter reinforcing bars.

Steel Stress A limiting stress of 75% of the ultimate tensile strength is recommended. Table 12.24 shows the mean steel working stress as a function of reinforcing-bar size and concrete strength. The indirect tensile strength of concrete should be determined according to AASHTO T198 or ASTM C496. The limiting steel working stresses in Table 12.24 are for Grade 60 steel meeting ASTM A615 specifications. Guidance for the allowable steel stress for other types of steel is provided by Majidzadeh (1978).

12.4.3 Design Nomographs and Equations

Figures 12.23, 12.24, and 12.25 show the nomographs for determining the percentage of longitudinal reinforcement to satisfy the criteria of crack spacing, crack width, and steel stress, respectively. Also shown in the figures are the equations for developing the

TABLE 12.24 Allowable Steel Working Stress

Indirect tensile strength of concrete at 28 days (psi)	Reinforcing bar size[a]		
	No. 4	No. 5	No. 6
300 or less	65,000	57,000	54,000
400	67,000	60,000	55,000
500	67,000	61,000	56,000
600	67,000	63,000	58,000
700	67,000	65,000	59,000
800 or greater	67,000	67,000	60,000

Note. Steel stress is in psi, 1 psi = 6.9 kPa.
[a] Proportional adjustments may be made for DWF based on wire diameter to bar diameter.
Source. After AASHTO (1986).

Downloaded From : www.EasyEngineering.net

Downloaded From : www.EasyEngineering.net

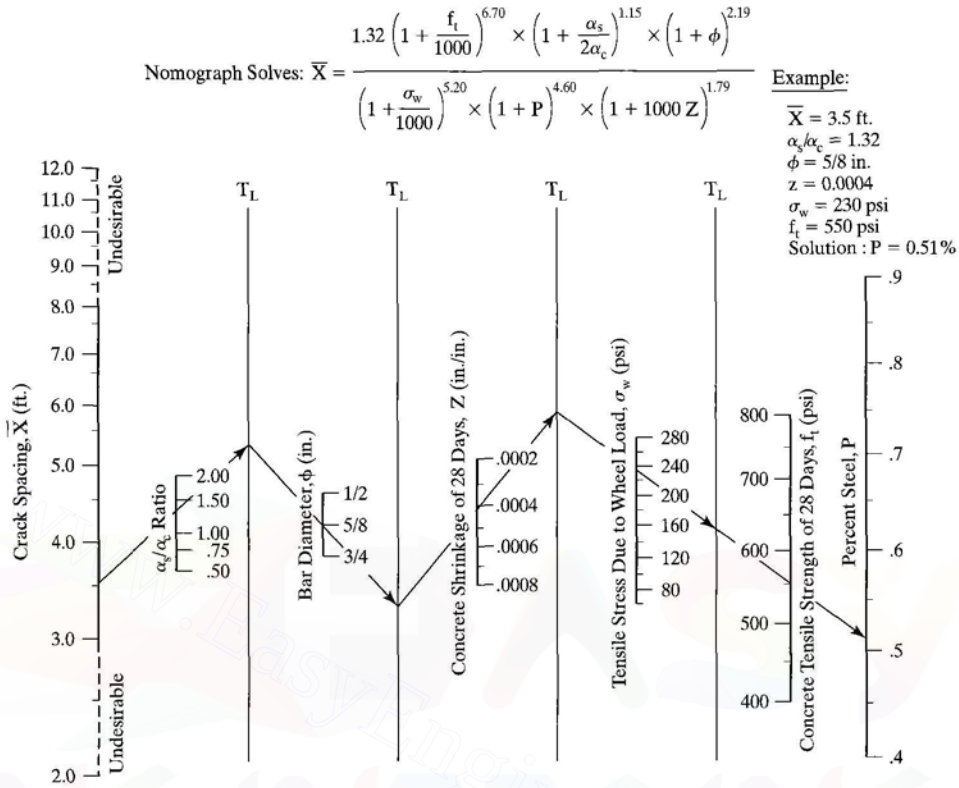


FIGURE 12.23

Percent steel to satisfy crack spacing criterion (1 ft = 0.305 m, 1 in. = 25.4 mm, 1 psi = 6.9 kPa). (From the *AASHTO Guide for Design of Pavement Structures*. Copyright 1986. American Association of State Highway and Transportation Officials, Washington, DC. Used by permission.)

nomographs. To facilitate the computation of percent steel P from the limiting criteria, the equations can be rewritten as presented below.

Crack Spacing Given the crack spacing, the percent steel can be determined by

$$P = \frac{1.062(1 + f_t/1000)^{1.457}(1 + \alpha_s/2\alpha_c)^{0.25}(1 + \phi)^{0.476}}{(\overline{X})^{0.217}(1 + \sigma_w/1000)^{1.13}(1 + 1000Z)^{0.389}} - 1 \qquad (12.33)$$

in which P is the amount of longitudinal steel in percent, $\overline{X}$ is the crack spacing in ft, f_t is the indirect tensile strength in psi, α_s/α_c is the thermal coefficient ratio, ϕ is the reinforcing bar or wire diameter in inches, σ_w is the wheel load stress in psi, and Z is the concrete shrinkage at 28 days in in./in. For the example shown in Figure 12.23, the percent steel computed by Eq. 12.33 is $P = [1.062(1.55)^{1.457}(1.66)^{0.25}(1.625)^{0.476}]/[(3.5)^{0.217}(1.23)^{1.13}(1.4)^{0.389}] - 1 = 0.52$, which checks with the 0.51% obtained from the chart.

Downloaded From : www.EasyEngineering.net

Downloaded From : www.EasyEngineering.net

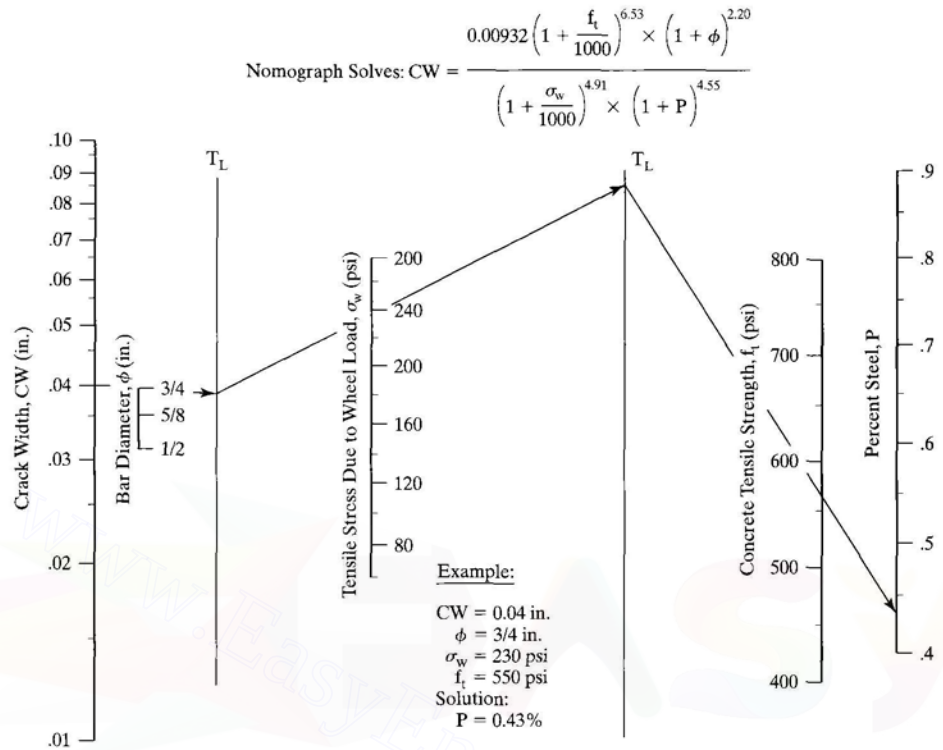


FIGURE 12.24

Minimum percent steel to satisfy crack width criterion (1 in. = 25.4 mm, 1 psi = 6.9 kPa). (From the *AASHTO Guide for Design of Pavement Structures*. Copyright 1986. American Association of State Highway and Transportation Officials, Washington, DC. Used by permission.)

Crack Width Given the crack width, the percent steel can be computed by

$$P = \frac{0.358(1 + f_t/1000)^{1.435}(1 + \phi)^{0.484}}{(\text{CW})^{0.220}(1 + \sigma_w/1000)^{1.079}} - 1 \tag{12.34}$$

in which CW is the crack width in inches. For the example shown in Figure 12.24, the percent steel computed by Eq. 12.34 is $P = [0.358(1.55)^{1.435}(1.75)^{0.484}]/[(0.04)^{0.22}(1.23)^{1.079}] - 1 = 0.43$, which is the same as that obtained from the chart.

Steel Stress Given the steel stress, the percent of steel can be computed by

$$P = \frac{50.834(1 + \text{DT}_\text{D}/100)^{0.155}(1 + f_t/1000)^{1.493}}{(\sigma_s)^{0.365}(1 + \sigma_w/1000)^{1.146}(1 + 1000Z)^{0.180}} - 1 \tag{12.35}$$

in which σ_s is the steel stress in psi and DT_D is the design temperature drop in °F. For the example shown in Figure 12.25, the percent steel computed by Eq. 12.35 is $P = [50.834(1.55)^{0.155}(1.55)^{1.493}]/[(57{,}000)^{0.365}(1.23)^{1.146}(1.4)^{0.18}] - 1 = 0.43$, which is slightly smaller than the 0.47% obtained from the chart.

Downloaded From : www.EasyEngineering.net

Downloaded From : www.EasyEngineering.net

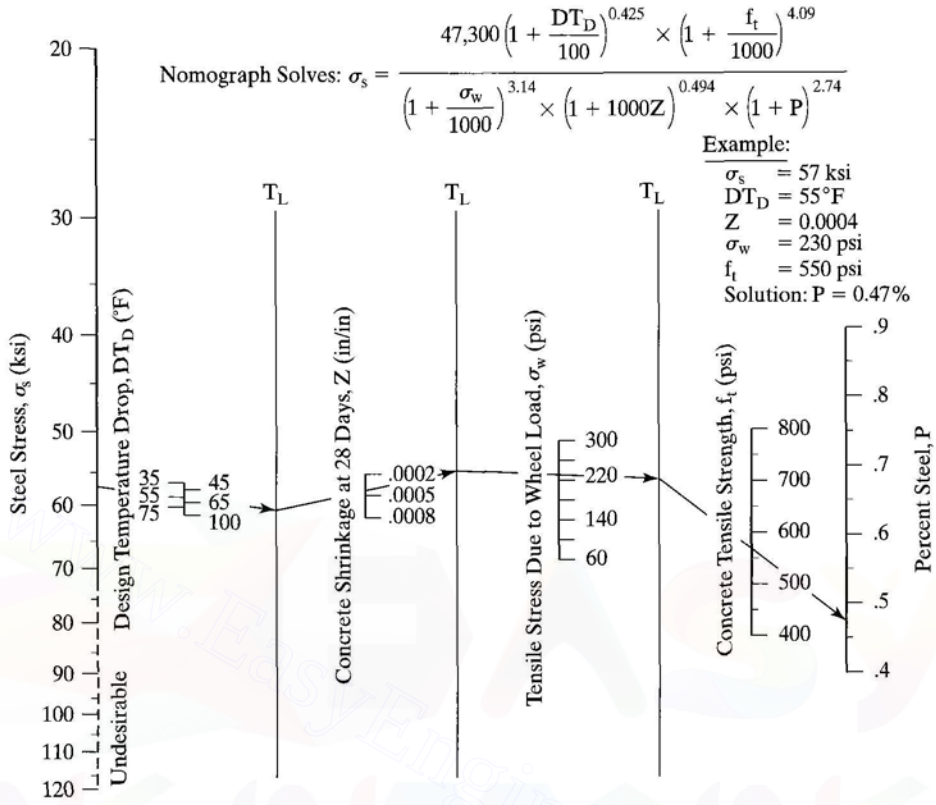


FIGURE 12.25

Minimum percent steel to satisfy steel stress criterion (1 psi = 6.9 kPa, 1°F = 0.56°C). (From the *AASHTO Guide for Design of Pavement Structures*. Copyright 1986. American Association of State Highway and Transportation Officials, Washington, DC. Used by permission.)

12.4.4 Design Procedure

The following design procedures may be used to determine the amount of longitudinal reinforcement required:

1. Determine the required amount of steel reinforcement to satisfy each limiting criterion, using Figures 12.23, 12.24, and 12.25 or Eqs. 12.33, 12.34, and 12.35. The minimum amount of steel P_{min} is selected as the largest among the three criteria: crack spacing of 8.0 ft (2.4 m), crack width, and steel stress; the maximum amount P_{max} is based solely on a crack spacing of 3.5 ft (1.1 m).
2. If P_{max} is less than P_{min}, the design is unsatisfactory, and some of the inputs must be revised until P_{max} is greater than P_{min}.
3. Determine the range in the number of reinforcing bars or wires required by

$$N_{min} = 0.01273 P_{min} W_s D/\phi^2 \tag{12.36}$$

$$N_{max} = 0.01273 P_{max} W_s D/\phi^2 \tag{12.37}$$

Downloaded From : www.EasyEngineering.net

Downloaded From : www.EasyEngineering.net

in which N_{min} and N_{max} are the minimum and maximum number of reinforcing bars or wires required, P_{min} and P_{max} are the minimum and maximum amount of steel in percent, W_s is the total width of pavement section in inches, D is the thickness of the concrete slab in inches, and ϕ is the reinforcing bar or wire diameter in inches, which may be increased if loss of cross section due to corrosion is foreseen.

4. Determine the final steel design by selecting the total number of bars or wires N such that N is a whole number between N_{min} and N_{max}. The appropriateness of the final design may be checked by converting N to P and working backward through the design charts or by using the equation at the top of each chart to estimate crack spacing, crack width, and steel stress.

Example 12.11:

Given the following information, determine the number of longitudinal steel bars per 12 ft (3.66 m) lane for a continuously reinforced concrete pavement: thickness of slab D = 9.5 in. (241 mm), magnitude of wheel load due to construction traffic = 20,000 lb (89 kN), effective modulus of subgrade reaction k = 170 pci (46.1 MN/m^3), concrete indirect tensile strength f_t = 550 psi (3.8 MPa), concrete shrinkage Z = 0.0004 in./in., thermal coefficient of steel $\sigma_s = 5 \times 10^{-6}$ in./in./°F (9×10^{-6} mm/mm/°C), thermal coefficient of concrete (limestone aggregate) $\alpha_c = 3.8 \times 10^{-6}$ in./in./°F (6.8×10^{-6} mm/mm/°C), and design temperature drop DT_D = 55°F (31° C).

TABLE 12.25 Worksheet for Longitudinal Reinforcement Design

Design inputs			
Input variable	Value	Input variable	Value
Reinforcing Bar/Wire Diameter ϕ (in.)	5/8 (No. 5)	Thermal Coefficient Ratio α_s/α_c	1.32
Concrete Shrinkage Z (in./in.)	0.0004	Design Temperature Drop DT_D(°F)	55
Concrete Tensile Strength, f_t(psi)	550	Wheel Load Stress σ_w(psi)	230

Design criteria and required steel percentage				
	Crack Spacing $\bar{x}$ (ft)	Allowable Crack Width, CW_{max} (in.)	Allowable Steel Stress, $(\sigma_s)_{max}$ (ksi)	Steel Range[b]
Value of Limiting Criteria	Max: 8.0 Min: 3.5	0.04	62	
Minimum Required Steel Percentage	<0.40%	<0.40%	<0.40%	0.40% (P_{min})[a]
Maximum Allowable Steel Percentage	0.51%			0.51% p_{max}

Note.[a]Enter the largest percentage across line.
[b]If $p_{max} < p_{min}$, reinforcement criteria are in conflict, design not feasible 1 in. = 25.4 mm, 1 ft = 0.305 m, 1 psi = 6.9 kPa.

Downloaded From : www.EasyEngineering.net

Downloaded From : www.EasyEngineering.net

Solution: Table 12.25 is a worksheet for longitudinal reinforcement design. The design inputs are entered at the top part of the table. It is assumed that No. 5 bars with a diameter of $\frac{5}{8}$ in. (16 mm) are used. The thermal coefficient ratio is $\alpha_s/\alpha_c = (5 \times 10^{-6})/(3.8 \times 10^{-6}) = 1.32$. The wheel load stress σ_w is 230 psi (1.6 MPa) and can be obtained from Figure 12.22.

The percentages of steel based on the limiting criteria are shown at the bottom part of Table 12.25. The percent steel for a crack spacing of 3.5 ft (1.1 m) is 0.51%, as shown in Figure 12.23, and that for a crack spacing of 8 ft (2.4 m) is less than 0.4% and outside the range of the chart (Eq. 12.33 gives P = 0.27%). The percent steel for a crack width of 0.04 in. (1 mm) can be determined from Figure 12.24 or computed by Eq. 12.34. A steel of 0.43%, as shown in Figure 12.24, is for $\frac{3}{4}$-in. bars. For $\frac{5}{8}$-in. bars, the percent steel computed by Eq. 12.34 is 0.38%, which is less than the minimum, 0.4%, required. For a No. 5 bar with a f_t of 550 psi (3.8 MPa), the allowable steel stress σ_s is 62,000 psi (428 MPa), as shown in Table 12.24. The example in Figure 12.25 is for No. 6 bars with a σ_s of 57 ksi (393 MPa). For No. 5 bars with a σ_s of 62 ksi (428 MPa), the percent steel obtained from Eq. 12.35 is 0.39%, which is smaller than 0.4% and outside the range of the chart. With $P_{min} = 0.4\%$ and $P_{max} = 0.51\%$, from Eq. 12.36, $N_{min} = 0.01273 \times 0.4 \times 12 \times 12 \times 9.5/(0.625)^2 = 17.8$; from Eq. 12.37, $N_{max} = 0.01273 \times 0.51 \times 12 \times 12 \times 9.5/(0.625)^2 = 22.7$. Using 18 No. 5 bars per lane, the longitudinal reinforcing bar spacing is 8 in. (203 mm).

From the equation at the top of each chart, the predicted crack spacing is 5.12 ft (1.56 m), which is between the required 3.5 to 8 ft (1.1 to 2.4 m); the predicted crack width is 0.037 in. (0.94 mm), which is smaller than the allowable 0.04 in. (1 mm); and the predicted steel stress is 60,200 psi (415 MPa), which is smaller than the allowable 62,000 psi (428 MPa).

12.4.5 Field Performance

A nationwide field investigation was made by Tayabji *et al.* (1995) under the sponsorship of FHWA to evaluate the performance of existing CRCP sections. Twenty-three in-service CRCP were investigated to study the effect of various design and construction features on pavement performance. Some of their findings are summarized below:

1. There is a strong correlation among percentage of steel, concrete strength, and crack spacing. For conventional concrete with a compressive strength at 28 days of about 3,000 psi (21 MPa), steel in the amount of 0.6 to 0.7 percent appears to provide desirable long-term average crack spacing in the range of 3 to 5 ft (0.9 to 1.5 m). The use of steel less than 0.6 percent may result in longer crack spacing and possible premature development of punchouts at closely spaced cracks adjacent to longer spaced cracks. The use of 0.65 percent as the minimum steel content is strongly recommended. If higher steel content is to be used, higher strength concrete should be specified to maintain appropriate crack spacing or a stabilized base must be specified.
2. The effect of a tied concrete shoulder could not be considered positive with respect to improving the structural response of CRCP, as indicated by deflection tests along the edges. The use of widened lanes appears to be promising and should be seriously considered as a design option.
3. The effect of base type on CRCP was not pronounced. The two sections with permeable bases exhibited higher crack spacing. However, both sections were young, and one was constructed with a small amount of steel. Also, a separate

Downloaded From : www.EasyEngineering.net

Downloaded From : www.EasyEngineering.net

evaluation of a 3-year-old Virginia CRCP constructed with cement-treated base (CTB) indicated that adequate crack spacing can develop in CRCP incorporating permeable CTB.

4. The use of epoxy-coated reinforcement resulted in no undesirable cracking pattern. The FHWA Technical Advisory T5080.14 dated June 5, 1990 recommended that the bond area be increased 15 percent if epoxy-coated steel reinforcement is used. This implies that 15 percent more steel should be used if epoxy-coated bars are employed. Based on the limited data, it appears that the use of 15 percent more steel may not be warranted provided the steel content is properly estimated. However, additional field data need to be compiled to verify those observations.
5. An attempt was made to determine why certain CRCP sections had cracking patterns significantly different from other sections with similar design factors. No explanation could be made other than that the ambient temperature and curing conditions might have contributed to the development of cracking pattern.
6. Load transfer efficiencies at transverse cracks of CRCP, even after many years of service, remain high, generally greater than 90 percent, provided an adequate amount of steel is used.
7. Further research and development for CRCP should focus on improving the crack patterns through improved construction and design technology. For many years, the design of CRCP has focused on the percent of steel reinforcement and the expected drop in pavement temperature over the course of a year. However, it is clear that crack patterns cannot be controlled by the steel design alone and that other considerations should be included in the design process, such as the type of aggregate, method of curing, concrete shrinkage potential, depth of steel cover, and rate of strength gain in the first 3 days, among others. Also, the design process for CRCP should continue through construction and not end as soon as the plans and specifications are prepared. A more active interaction between design process and actual ambient conditions during construction needs to be developed to achieve CRCP with acceptable cracking patterns. This may require the imposing of guidelines on acceptable ambient conditions for placing of CRCP.

12.5 DESIGN OF RIGID PAVEMENT SHOULDERS

Most of the information presented in Section 11.4 on the design of flexible pavement shoulders is also applicable to the design of rigid pavement shoulders. Some of the features of rigid pavement shoulders that are different from those of flexible pavement shoulders are presented here.

PCC shoulders have been used in urban expressways for many years, but their use on rural highways began only in the mid 1960s. The good performance of these pavements has made it the standard practice of many agencies to utilize PCC shoulders for rigid pavements.

12.5.1 Advantages of Tied Concrete Shoulders

Concrete shoulders must be tied to the mainline concrete pavements. The advantages of tied concrete shoulders are as follows:

Downloaded From : www.EasyEngineering.net

Downloaded From : www.EasyEngineering.net

1. The placement of a tied concrete shoulder next to the mainline pavement can substantially increase the load-carrying capacity of the pavement. The tied concrete shoulder provides support to the edge of the pavement and reduces stresses and deflections in the mainline slab. The shoulder is also benefited by receiving support from the mainline slab, so the damage due to encroaching traffic can be greatly reduced.
2. A tied longitudinal joint between mainline and shoulder pavements can be easily sealed to reduce the amount of surface runoff infiltrating into the pavement structure. Field studies conducted in Georgia and Illinois showed that sealing the longitudinal joint greatly reduced the amount of inflow from rainfall into the pavement structure (Dempsey *et al.*, 1982).
3. Pumping beneath the mainline slab is reduced through the reduction of edge and corner deflections, the reduction of water infiltration through the longitudinal joint, and the draining of water far away from the traffic lane.
4. Tied concrete shoulders can reduce differential movements at the longitudinal shoulder joint and do not experience the lane/shoulder dropoff type of distress that occurs so frequently in flexible shoulders.

12.5.2 Types of Rigid Pavement Shoulders

As with mainline pavements, three types of shoulder pavements are available: jointed plain concrete pavement (JPCP), jointed reinforced concrete pavement (JRCP), and continuous reinforced concrete pavement (CRCP). Generally, the type of shoulder should match the type of mainline pavement. However, some exceptions may be accepted:

1. For mainline JPCP, only JPCP shoulders with the same joint spacings as the mainline pavement are recommended, because of their low cost. If JRCP shoulders with longer joint spacings are used, the excessive joint movements may cause problems in the adjacent mainline slabs. All transverse joints should be provided with an adequate reservoir and sealed similarly to the mainline joints.
2. For mainline JRCP, either JRCP shoulders that match the mainline pavement in design or JPCP shoulders with closer joint spacings may be used. The use of JPCP shoulders is more cost effective, because no steel reinforcement is needed. They can be placed at the same time as the JRCP mainline pavement by leaving out the reinforcing steel and cutting transverse joints at shorter intervals.
3. For mainline CRCP, either CRCP shoulders that match the mainline pavement in design or JPCP shoulders with short joint spacings may be used. The use of short joint spacing for JPCP shoulders will reduce potential movements of the joints that might cause cracking in the mainline CRCP. The elimination of steel reinforcement in the JPCP shoulders can save construction cost.

12.5.3 Design of Longitudinal Shoulder Joint

Adequate load transfer across the longitudinal shoulder joint must be provided to reduce the stresses and deflections in both mainline and shoulder slabs. Tied and keyed joints have been used most frequently to ensure a high degree of load transfer. Colley

Downloaded From : www.EasyEngineering.net

Downloaded From : www.EasyEngineering.net

et al. (1978) investigated load transfers in laboratory slabs constructed with keyed, tied and keyed, and tied butt joints and concluded that all three were equally effective in reducing load-induced strains and deflections. However, the use of a keyed joint without tiebars was not recommended, because of the possibility of shoulder joint separation. The excellent performance of the tied butt joint suggests that this type of construction is feasible and can reduce costs. Malleable tiebars of No. 4 or No. 5 size spaced at 18 to 24 in. (457 to 610 mm) are preferable to stiffer short bars spaced at larger intervals. This will substantially reduce stress concentration and the possibility of joint spall in the vicinity of the bar.

When a PCC shoulder is to be constructed adjacent to an existing pavement, tiebars can be installed by drilling holes in the edge of the existing slab. This can be done by using a tractor-mounted drill that can drill several holes at one time. Tiebars are installed in the holes by using epoxy or cement grout. The bar should be inserted into the slab over such a length as to develop sufficient bond. To avoid spalling over the base, a minimum insertion of 9 in. (229 mm) is required.

In the case of new construction, tiebars can be inserted into the plastic concrete near the rear of the slip form paver. Bent bars can be installed manually or by mechanical means. The bent portion can be straightened later to tie the shoulder to the mainline pavement. In addition to tiebars, a keyway can be formed to provide additional load transfer capability.

The longitudinal joint between the traffic lane and the shoulder should be provided with a sealant reservoir and sealed with an effective sealant. This will minimize the possibility of foreign materials collecting inside the joint to cause joint spall and reduce the amount of water and deicing salts entering into the joint and corroding the tiebars.

12.5.4 Shoulder Thickness Design

The thickness design concepts presented in Section 11.4.3 for flexible pavement shoulders are also applicable to rigid pavement shoulders. One major difference is that the inner edge is always more critical for flexible shoulders, because of encroaching traffic, but the outer edge can be more critical for rigid shoulders, because of parking traffic. There is also some question about whether a separately designed shoulder is really needed. Lokken (1973) reviewed the performance of 16 projects located in 12 states and recommended the use of a 6-in. (152-mm) slab with an alternative tapered slab varying from roadway pavement depth at the longitudinal joint to 6 in. (152 mm) at the outside edge of the shoulder. Slavis (1981) reported on the performance review of these same projects in 1980 and indicated that the vast majority performed extremely well. The only notable deficiency identified in the field investigation was some faulting in one project due to inadequately covered tiebars. It is impossible to place the tiebars at the middepth both of a 6-in. (152-mm) shoulder and of a thicker mainline pavement, so it was recommended in the 1980 review that the shoulder thickness be equal to the mainline slab at the longitudinal joint. This thickness can be used for the entire width of the shoulder or tapered to 6 in. (152 mm) at the outside edge. The use of the same thickness for both mainline and shoulder pavements is not only easier to construct, especially in installing the longitudinal joint, but has the further advantages of improving drainage by the elimination of bathtub trench and reducing differential frost heave.

Downloaded From : www.EasyEngineering.net

Downloaded From : www.EasyEngineering.net

If it is necessary to use thinner shoulder sections, for economic or other reasons, the thickness of the inner edge can be based on the encroaching and parking traffic combined, that of the outer edge on the parking traffic alone. The design method used for the mainline pavement can also be used for the shoulder, except that the traffic on the shoulder is much lighter. The following example illustrates how the PCA method can be used for determining the thickness of shoulder. In applying the PCA method to real situations, various weights of single- and tandem-axle loads must be analyzed separately, because each has a different effect on the mode of failure. However, for simplicity, only the 18-kip (80-kN) single-axle loads will be used in the example.

Example 12.12:

The outside lane on a heavily traveled highway is subjected to 10 million applications of an 18-kip (80-kN) single-axle load during the design life. A JPCP shoulder with aggregate interlock transverse joints is tied onto the traffic lane. Assuming an encroaching traffic of 3.5%, a parking traffic of 0.02%, a load safety factor of 1.2, a concrete modulus of rupture of 650 psi (4.5 MPa), and a modulus of subgrade reaction of 100 pci (27.1 MN/m^3), determine the thickness of tied concrete shoulder by the PCA design method.

Solution: The outer edge of shoulder slab should be designed as aggregate interlock joints with no concrete shoulder, and the inner edge as aggregate interlock joints with concrete shoulder. Parking traffic on the outer edge = 10,000,000 × 0.0002 = 2000. Total traffic on the inner edge including both encroaching and parking traffic = 10,000,000 × 0.0352 = 352,000. Based on both fatigue and erosion analyses, the allowable repetitions for several assumed thicknesses are tabulated in Table 12.26.

In the fatigue analysis, the equivalent stress was found from Table 12.6 for the outer edge with no concrete shoulder and Table 12.7 for the inner edge with concrete shoulder. The stress ratio was computed by dividing the equivalent stress with 650, which is the concrete modulus of rupture. The allowable number of repetitions was obtained from Figure 12.12. In the erosion analysis, the erosion factor was found from Table 12.9 for the outer edge and Table 12.11 for the inner edge. The allowable number of repetitions was obtained from Figure 12.13 for the outer edge and from Figure 12.14 for the inner edge. The single-axle load to be used with the charts is 1.2 × 18, or 21.6 kip (96 kN).

TABLE 12.26 Computation of Allowable Load Repetitions by PCA Method

Assumed thickness (in.)	Fatigue analysis			Erosion analysis	
	Equivalent stress	Stress ratio	Allowable repetitions	Erosion sfactor	Allowable repetitions
Outer edge					
6.0	411	0.63	640	3.40	120,000
6.5	367	0.56	5000	3.30	240,000
Inner edge					
6.0	327	0.50	52,000	2.95	160,000
6.5	294	0.45	200,000	2.86	320,000
7.0	266	0.41	1,500,000	2.77	650,000

Note. 1 in. = 25.4 mm.

Downloaded From : www.EasyEngineering.net

Downloaded From : www.EasyEngineering.net

It can be seen from Table 12.26 that fatigue is more critical for 6 and 6.5 in. (152 and 165 mm) slabs, as indicated by the smaller allowable load repetitions compared with the erosion analysis, but erosion is more critical for the 7-in. (178-mm) slab. The required thickness is 6.5 in. (165 mm) for the outer edge and 7.0 in. (178 mm) for the inner edge. That fatigue prevails in thin pavements and erosion in thick pavements can be explained by the fact that the edge stress decreases more rapidly than the corner deflection as the thickness increases. Separate calculations also indicate that the thickness for the mainline slab with aggregate interlock joints is 8 in. (203 mm) based on fatigue analysis, but 9 in. (229 mm) based on erosion analysis.

The thickness of shoulder can be designed in several ways. The best, but most expensive, method is to use a uniform slab of 9 in. (229 mm). Another method is to use 9 in. (229 mm) at the longitudinal joint and taper to 6.5 in. (165 mm) at the outer edge. The last resort is to use a uniform thickness of 7 in. (178 mm). It is not worth the effort to taper the section from 7 to 6.5 in. (18 to 165 mm) because the saving is too small.

SUMMARY

This chapter presents several methods for rigid pavement design, including a calibrated mechanistic procedure, the Portland Cement Association method, and the AASHTO method, as well as methods for the design of shoulders.

Important Points Discussed in Chapter 12

1. The most nearly ideal design method, still under development, is the calibrated mechanistic procedure. As with flexible pavements, it consists of a number of response and distress models. The environmental response models, such as heat transfer, moisture equilibrium, and infiltration and drainage, can be applied to both flexible and rigid pavements. The structural response model based on the finite element plate theory and the fatigue cracking model based on the cumulative damage concept are quite advanced, but the other distress models are not adequate and need to be improved.
2. The distress models include fatigue cracking, erosion, faulting, and joint deterioration for JPCP and JRCP, and punchout for CRCP. One major problem of fatigue cracking is how temperature warping should be included in the analysis. The prospects of developing mechanistic erosion and punchout models are promising, but more work needs to be done to put them into practical use. The faulting and joint deterioration models currently available are not mechanistic; they are empirical regression equations valid only within the data base from which they were derived.
3. The PCA design method considers the fatigue of concrete caused by the edge stress at midslab and the erosion of foundation caused by corner deflection. The erosion criterion was developed primarily from the results of the AASHTO Road Test using a specific subbase and might not be applicable to situations where different types of subbase are used. Generally, the fatigue analysis controls the design of thinner pavements under lighter traffic, the erosion analysis that of thicker pavements under heavier traffic. For pavements carrying a normal mix of axle weights, single-axle loads will cause more fatigue cracking, and tandem-axle loads will cause more erosion damage.

Downloaded From : www.EasyEngineering.net

Downloaded From : www.EasyEngineering.net

4. The PCA method considers each load group individually and sums up the damage according to the cumulative damage concept. A slab thickness is assumed, and the damage ratios due to both fatigue and erosion are determined. If either ratio is greater than 1, the thickness is increased every 0.5 in. (127 mm) until both ratios are smaller than 1. The smallest thickness with both damage ratios smaller than 1 is the thickness to be used. The design variables include modulus of subgrade reaction, concrete modulus of rupture, load safety factors, types and weights of axle load, types of joint, and types of shoulder.
5. Design tables and charts were developed by PCA via a finite element computer program called JSLAB. The program was also used to develop the design charts for lean concrete lower course and the tables for equivalent stress under tridem-axle loads. A simplified design procedure was also recommended by PCA when specific axle load data are not available.
6. The AASHTO design method is based on the empirical equation obtained from the AASHO Road Test, which is similar in form to the flexible pavement equation, but has different regression constants. However, two additional terms are added, one relating to reliability and standard deviation, the other to several design variables not included in the original equation, such as concrete modulus of rupture, concrete modulus of elasticity, drainage coefficient, load transfer coefficient, and modulus of subgrade reaction. A comparison of results with the PCA method, as well as with the KENSLABS computer program, indicates that the AASHTO equation is unsafe for thin pavements and gives a performance traffic that is too large.
7. The effective modulus of subgrade reaction k is an equivalent modulus that would result in the same damage if seasonal k values are used. The equation for evaluating relative damage was derived from the AASHTO equation based on the cumulative damage concept. Unlike flexible pavements, the effective k values are not much different from the normal summer or fall k values. To avoid the tedious method of dividing a year into 12 months, each having a different k value, a mean normal k value may be used for design purposes. The correlations between the resilient moduli and k values, as recommended by AASHTO and shown in Eq. 12.22 and Figure 12.18, are questionable and result in a k value that is too large and does not check with theory.
8. The thickness of CRCP can be designed by the same methods used for JPCP and JRCP. Due to the stiffness of steel reinforcement which prevents the concrete from shrinkage, CRCP will always experience a large number of cracks. The amount of steel reinforcement should be selected so that the crack spacing lies between 3.5 and 8 ft (1.1 and 2.4 m), the crack width is less than 0.04 in. (1.0 mm), and the steel stress does not exceed 75% of the ultimate tensile strength. Empirical equations and design nomographs are available to predict crack spacing, crack width, and steel stress and can be used for design.
9. Concrete shoulders tied onto mainline slabs should be used for concrete pavements. It is preferable that the thickness of shoulders be the same as that of the mainline pavement for ease of construction, to facilitate drainage, and to provide additional lanes for possible future use. This is similar to the use of the same thickness for both inside and outside lanes in the mainline pavement, even though the

Downloaded From : www.EasyEngineering.net

Downloaded From : www.EasyEngineering.net

traffic on the inside lane is much lighter. If this cannot be done, at least the thickness at the longitudinal joint should be the same, so that tiebars can be installed at the middepth of both mainline and shoulder slabs. The thickness can be tapered to a minimum of 6 in. (152 mm) at the outer edge. The thickness at the outside edge can be designed according to the parking traffic.

10. If thinner shoulder sections have to be used due to economic or other reasons, shoulder slabs should be designed according to the traffic they will carry. The design methods for mainline pavement can also be applied to the design of shoulder pavement. The inner edge of the shoulder slab should be designed for encroaching and parking traffic, the outer edge for parking traffic alone. If the shoulder might be used as an additional lane for peak hour or detoured traffic, this traffic should also be estimated and added to the encroaching and parking traffic at the inner edge and the parking traffic at the outer edge.

PROBLEMS

12.1 A 10-in. concrete pavement without concrete shoulders is placed on an untreated subbase having the k value 150 pci. Estimate the allowable corner deflection by the PCA erosion criterion if the pavement is subjected to 2 million applications of a given axle load. [Answer: 0.0468 in.]

12.2 Same pavement as in Problem 12-1, but with concrete shoulders. Estimate the allowable corner deflection. [Answer: 0.0318 in.]

12.3 Determine the thickness of a concrete pavement for a two-lane highway by the PCA method. The pavement has doweled joints and no concrete shoulders. The modulus of subgrade reaction is 200 pci and the concrete modulus of rupture is 650 psi. Assume a load safety factor of 1.1 and a design period of 20 years. The average daily traffic during the design period is 2500, of which 35% are trucks. Truck weight distribution data for single (S) and tandem (T) loads are tabulated in Table P12.3. [Answer: 8.0 in.]

TABLE P12.3

Axle loads (kip)	No. axles per 1000 trucks	Axle loads (kip)	No. axles per 1000 trucks
16 S	130.9	24 T	80.2
18 S	110.8	28 T	34.4
20 S	65.4	32 T	24.0
22 S	15.6	36 T	17.2
24 S	2.3	40 T	16.8
26 S	1.9	44 T	10.5
28 S	0.9	48 T	9.6

12.4 A concrete pavement has doweled joints and tied concrete shoulders. Given a concrete modulus of rupture of 650 psi, a modulus of subgrade reaction of 150 pci, a load safety factor of 1.2, a design period of 20 years, an average daily truck traffic of 3460 (excluding all two-axle, four-tire trucks) on the design lane during the design life, and an axle load distribution shown by category 3 in Table 12.13. Determine the slab thickness by the PCA method using the procedure similar to the worksheet shown in Figure 12.15. Check the result by the simplified procedure using Table 12.15. [Answer: 8.5 in. versus 8.0 in.]

Downloaded From : www.EasyEngineering.net

Downloaded From : www.EasyEngineering.net

12.5 Same as Problem 12-4, but with no concrete shoulders. Determine the slab thickness by the regular PCA procedure, and check the result with the simplified procedure. [Answer: 9.5 in.]

12.6 The predicted traffic W_{18} and the serviceability loss due to frost heave ΔPSI_{FH} as a function of time can be expressed by

$$W_{18} = 5 \times 10^6 [(1.04)^Y - 1]$$

$$\Delta PSI_{FH} = 0.08(Y)^{0.6}$$

in which Y is the time in years. Determine the performance period for a rigid pavement with the following information: $R = 90\%$, $S_0 = 0.4$, $D = 8$ in., $\Delta PSI = 4.5 - 2.5 = 2.0$, $S_c = 600$ psi, $C_d = 1.05$, $J = 3.2$, $E_c = 5 \times 10^6$, and $k = 100$ pci. [Answer: 6.5 years]

12.7 Figure P12.7 shows a concrete pavement with the thicknesses and elastic moduli as indicated. Assume a modulus of rupture of 650 psi, a load transfer coefficient of 3.2, a serviceability loss from 4.5 to 2.0, and poor drainage with 5% of time near saturation. Determine the performance traffic by Eq. 12.21 without the reliability term and check the result by the AASHTO design chart. [Answer: 8.5×10^6]

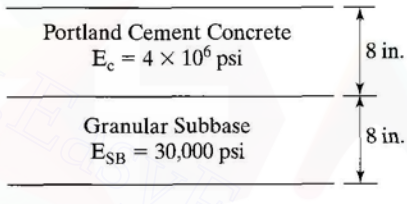


FIGURE P12.7

12.8 A 8.5-in. (216-mm) concrete slab is placed directly on a subgrade. The relationship between the resilient modulus and k value is indicated by Eq. 12.22. The monthly subgrade resilient moduli from January to December are 15,900, 27,300, 38,700, 50,000, 900, 1620, 2340, 3060, 3780, 4500, 4500, and 4500 psi. Determine the effective modulus of subgrade reaction. [Answer: 305 pci]

12.9 Same as Problem 12-8, except that the relationship between the resilient modulus and k value is indicated by Eq. 5.7. Assuming that the concrete has an elastic modulus of 4,000,000 psi and a Poisson ratio of 0.15 and the subgrade has a Poisson ratio of 0.45, determine the effective modulus of subgrade reaction. [Answer: 105 pci]

12.10 A continuous reinforced concrete pavement using limestone as coarse aggregate is subjected to 10^7 ESAL. Assume $k = 75$ pci, $E_c = 4 \times 10^6$ psi, $S_c = 650$ psi, $C_d = 1.05$, $J = 2.9$, $R = 95\%$, $S_o = 0.3$, $\Delta PSI = 2.0$, $DT_D = 60°F$, and wheel load due to construction traffic = 18,000 lb. Determine the thickness of concrete and the number of No. 5 bars per 12-ft lane required. [Answer: 9.5 in. and 18 to 24 bars]

12.11 The mainline pavement and traffic are the same as Problem 12-4. If dowels are also used for the shoulders and the parking traffic is 2% of the mainline traffic, determine the thickness of the outer pavement edge by the PCA method. [Answer: 8.5 in.]

12.12 The mainline pavement and traffic are the same as Problem 12-4. If dowels are also used for the shoulders and the encroaching and parking traffic combined is 2% of the mainline traffic, determine the thickness of the inner shoulder edge by the PCA method. [Answer: 7 in.]

Downloaded From : www.EasyEngineering.net

Downloaded From : www.EasyEngineering.net

CHAPTER 13

Design of Overlays

13.1 TYPES OF OVERLAYS

As the nation's highways age and deteriorate, some type of treatment is eventually required to provide a safe and serviceable facility for the users. The types of treatments can range from simple maintenance to complete reconstruction, depending on the circumstances. For pavements subjected to moderate and heavy traffic, the most prevalent treatment is to place an overlay on the existing pavement. Depending on the types of overlay and existing pavement, four possible designs may serve: HMA overlays on asphalt pavements, HMA overlays on PCC pavements, PCC overlays on asphalt pavements, and PCC overlays on PCC pavements.

13.1.1 HMA Overlays on Asphalt Pavements

HMA overlay is the predominant type of resurfacing on asphalt pavements. Design methods ranging from engineering judgment to mechanistic-empirical procedures have been used. If the existing pavement is adequately repaired prior to overlay, a satisfactory design can usually be achieved. The flexible types of materials used in the existing pavement and the overlay allow the elastic layer programs to be applied for design purposes.

13.1.2 HMA Overlays on PCC Pavements

Although HMA overlays have been used extensively on PCC pavements, this type of overlay is the most difficult to analyze mechanistically because it involves two different types of materials. Theoretically, the finite-element plate programs can be used by considering HMA as the top layer and PCC as the bottom layer. However, with cracks in the existing concrete slabs, it is difficult to model the bottom slab. This type of overlay can also be analyzed by an elastic layer program if the stress adjustment factors for edge and corner loads are known. These factors were obtained by the Austin Research Engineers, using the discrete element program called SLAB49, and incorporated into

Downloaded From : www.EasyEngineering.net

Downloaded From : www.EasyEngineering.net

the Pavement Overlay Design (POD) program developed for the Federal Highway Administration (Treybig *et al.*, 1977).

A major problem in the design of HMA overlays on PCC pavements is reflection cracking, defined as the fractures in an overlay or surface that reflect the crack or joint pattern in the underlying layer. It is imperative that such cracking be prevented or controlled to provide a smooth riding surface, maintain the structural integrity of the overlay, and prevent the intrusion of water into the pavement system. It is generally agreed that the primary mechanisms leading to the development of reflection cracks in a HMA overlay on a PCC pavement are the horizontal movement due to temperature and moisture changes and the differential vertical movement due to traffic loadings, both occurring at the joints and cracks in the PCC pavement; the horizontal movement is considered more critical.

Several methods can be used to minimize the reflection cracking in HMA overlays on PCC pavements:

1. Design a thicker HMA overlay.
2. Crack and seat the existing PCC slab into smaller sections.
3. Use a crack relief layer with drainage system.
4. Saw and seal joints in a HMA overlay.
5. Use a stress-absorbing membrane interlayer with an overlay.
6. Incorporate a fabric membrane interlayer with an overlay.

Method 1 may be used if the thickness of overlay to alleviate reflection cracking is less than 9 in. (229 mm). Normally, when an overlay approaches the 8- to 9-in. (203- to 229-mm) range, other methods should be used. Methods 5 and 6 are being used in some areas and appear to be effective in reducing reflection cracking. However, the available documentation on the performance of these interlayers is insufficient for indicating the proper thickness of overlay. Therefore, if method 5 or 6 is considered, the manufacturers of the interlayer materials should be consulted toward establishing the required overlay thickness. Methods 2, 3, and 4 are described below.

Cracking and Seating The crack and seat procedure, sometimes also called "break and seat" procedure, involves cracking the PCC slab into small segments, seating the segments with heavy rollers to eliminate underlying voids, and overlaying the PCC slab with HMA. The purpose is to create small pieces of concrete, so that slab movement by thermal or other causes is minimal, thereby reducing the reflection cracking in the HMA overlay. The segments, usually 4 to 6 ft^2 (0.37 to 0.56 m^2) in size, are still large enough to have some structural integrity due to aggregate interlock.

In the past, a major problem during the breaking of JRCP slabs has been the difficulty in rupturing the reinforcing steel. If the fragmented pieces are held together by the steel, not only is an effective seating not possible, but also, horizontal movements cannot be reduced. This problem has been solved recently by the availability of new cracking devices that can break the bond between the concrete and the steel.

There have been some controversies on the effectiveness of using cracking and seating. A report by FHWA (1987c) based on a review of 22 projects indicated that

Downloaded From : www.EasyEngineering.net

Downloaded From : www.EasyEngineering.net

cracking and seating could reduce reflection cracking during the first few years, but that after 4 to 5 years the cracking increased and was about the same as that in the control section without cracking and seating. The structural capacity of the existing pavement is reduced by cracking, and the condition of the crack and seat sections and the control sections seemed to be the same after some period of time, so the report raised questions about the justification for using the cracking and seating method. A recent study by Kilareski and Stoffels (1990) concurred with the above report that cracking and seating only delayed, rather than eliminated, the reflection cracking, but disagreed that cracking and seating reduced the structural capacity. Following are some of their conclusions:

1. Over the past 30 years, 24 states have experimented with the crack and seat method of overlay and have reported experiences that range from poor to excellent.
2. The crack and seat sections in California exhibited significantly less reflection cracking than the control sections. The use of a fabric interlayer further reduced the quantity of reflection cracking.
3. The crack and seat sections showed significantly less roughness than the corresponding control sections.
4. Analysis of FWD tests showed no significant loss of structural support or decrease in the modulus of elasticity on the crack and seat sections.
5. The crack and seat sections experienced significant increases in cracking with age.
6. The crack and seat sections displayed more medium- and high-severity cracking, but less total cracking, than the corresponding control sections.

The thickness design of HMA overlays on cracked and seated slabs is considered in the Asphalt Institute and AASHTO procedures and is discussed in Sections 13.3.2 and 13.5.4.

Crack Relief Layer The crack relief layer is designed specifically to minimize the reflection cracking from the old PCC pavement to the new asphalt overlay. It is placed as the first course of an overlay system. Typically, the crack-relief layer is a 3.5-in. (90-mm) layer of coarse open-graded HMA containing 25 to 35% interconnecting voids and made up of 100% crushed material. The large proportion of interconnecting voids provides the crack relief layer a medium through which differential movements of the underlying slab are not readily transmitted. The crack relief layer should be connected to a drainage system so that water can be drained out freely.

Before placing the crack relief layer, the existing pavement surface should be prepared so that it is as structurally sound and clean as possible; a tack coat is generally required. After the placing of the crack relief layer, a well-graded intermediate leveling or binder course from 2 to 4 in. (51 to 102 mm) thick is laid, followed by a dense-graded surface course about 1.5 in. (38 mm) thick. Figure 13.1 shows a typical cross section of overlay with a crack relief layer.

Table 13.1 gives the gradation recommended for the crack relief layer. Depending on the availability of the size of aggregate, three different gradings may be used. The use of a particular mix also should depend on the characteristics of the material

Downloaded From : www.EasyEngineering.net

Downloaded From : www.EasyEngineering.net

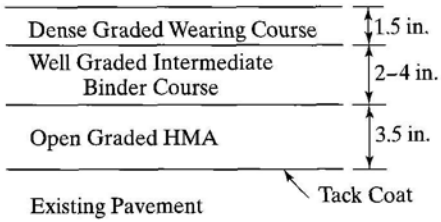


FIGURE 13.1
Typical cross section of overlay with crack relief layer (1 in. = 25.4 mm).

TABLE 13.1 Recommended Grading Limits for Crack Relief Layers

	Percent passing		
Sieve	Mix A	Mix B	Mix C
3 in.	100	—	—
$2\frac{1}{2}$ in.	95–100	100	—
2 in.	—	—	100
$1\frac{1}{2}$ in.	30–70	35–70	75–90
$\frac{3}{4}$ in.	3–20	5–20	50–70
$\frac{3}{8}$ in.	0–5	—	—
No. 4	—	—	8–20
No. 8	—	0.5	—
No. 100	—	—	0.5
No. 200	—	0.3	—
Asphalt cement content 1.5–3.0% (AC-40, 40–50 pen., or AR-16000)			

Note. 1 in. = 25.4 mm.
Source. After AI (1983).

used in the existing PCC pavement. Highly expansive PCC pavements, such as those constructed of washed silica gravel or having joint spacings exceeding 20 ft (6.1 m) should use mix A or B. Less expansive PCC pavements can be overlaid with mix C.

Sawing and Sealing of Joints Because of the difficulty in eliminating reflection cracking, one method is to control the cracking rather than eliminate it. This is effected by sawing a joint above each existing transverse joint immediately after the overlay. The joints are then sealed and subsequently maintained as typical pavement joints. A recent study by Kilareski and Bionda (1990) on the sawing and sealing of joints resulted in the following conclusions:

1. A total of 12 states, mostly in the northeastern part of the country, have used saw and seal HMA overlay as a routine rehabilitation procedure. Several states have prepared specifications and standards for the saw and seal overlay procedure. States that documented their experiments with sawing and sealing have reported marginal to good results with the technique.
2. The overall documented experience with saw and seal overlay is extremely limited. Information is generally lacking concerning measured field performance, traffic,

Downloaded From : www.EasyEngineering.net

Downloaded From : www.EasyEngineering.net

existing pavement condition, and characterization of the existing pavement in terms of joint width, load transfer efficiency, crack spacing, joint and crack opening under known temperature changes, and load deflection.

3. An important step in the construction process is to locate the saw cut above the existing joint properly. Secondary reflection cracking can occur unless the saw cut is made within 1 in. (25 mm) from the existing joint.
4. Saw and seal sections with thick overlay, say 5 in. (127 mm), performed better than sections with thin overlay, say 2.5 in. (64 mm), and had less roughness and reflection cracking.
5. If properly constructed, sawed and sealed joints in a HMA overlay of jointed PCC pavement can reduce the adverse effect of reflection cracking and extend the pavement life. A comparison between control sections and saw and seal sections for 15 pavement projects showed that saw and seal sections reduced pavement roughness by 20% and transverse reflection cracking by 64%.

13.1.3 PCC Overlays on Asphalt Pavements

The use of PCC overlays on asphalt pavements is somewhat uncommon. However, they have been used very successfully in the United States and other countries. This method can be used if the vertical clearance does not pose a problem. It can be cost effective if the asphalt pavement is severely distressed and must be used only as a foundation for the PCC overlay. The design procedure is similar to that of new pavements and uses the existing pavement as the foundation. The finite-element plate programs can be used for the mechanistic method of design. To prevent reflection cracking, all cracks of high severity in the existing asphalt pavement should be repaired and sealed. Because the existing asphalt pavement can be considered a nonerodible subbase, only fatigue cracking need be considered for determining the thickness of overlay required.

13.1.4 PCC Overlays on PCC Pavements

Three types of PCC overlay may be used for PCC pavements: unbonded, bonded, and partially bonded. Mechanistic designs can be carried out via the finite-element plate programs, in which somewhat lower elastic modulus should be specified for the old concrete, depending on the conditions of the existing pavement.

Unbonded or Separated Overlay Unbonded overlays are typically placed on pavements that are badly cracked. Prior to the overlay, the surface of the existing pavement must be cleaned of debris and excess sealing materials. A separation layer, usually consisting of HMA or sand asphalt of less than 2 in. (51 mm) thick, is then placed between the new overlay and the existing pavement to prevent reflection cracking. The separation layer can also serve as a leveling course so that a more uniform thickness of concrete can be obtained. In applying the finite-element plate programs, the plate is considered as two unbonded layers and the effect of separation layer is ignored.

Unbonded overlay may be plain, reinforced, continuously reinforced, or prestressed concrete. It is not necessary to match the location or type of joints in the overlay with those in the existing pavement. The minimum thickness of unbonded overlay is 6 in. (152 mm).

Downloaded From : www.EasyEngineering.net

Downloaded From : www.EasyEngineering.net

Bonded or Monolithic Overlay Bonded overlays should be used only when the existing pavement is in good condition or when serious distress has been repaired. To achieve a fully bonded overlay, it is necessary to carefully prepare the existing surface before placing the overlay. All oil, grease, paint, and surface contaminants must be removed by cold milling, sandblasting, or waterblasting. Then a thin layer of cement grout should be placed on the cleaned dry surface just in front of the concrete paver. A liquid epoxy resin of low viscosity may also be used as a bonding agent. The finite-element plate programs with two bonded layers can be used for the design of bonded overlays.

Irrespective of the type of existing PCC pavements, plain concrete is the most commonly used bonded overlay, although steel reinforcements may be used in thicker overlays to supplement the steel in the existing pavements. The location of the joints in the overlay must match that in the existing pavement. Use of dowel bars in bonded and partially bonded overlays is not recommended, because it could produce localized failures in the overlay directly above the dowel and could also cause the overlay to debond. For use over continuously reinforced pavements, the bonded overlay does not require the installation of joints.

Partially Bonded or Direct Overlay Partially bonded overlays are obtained when the fresh concrete is placed directly on relatively sound and clean existing slabs. Unless steps are taken to prevent bond, some degree of bonding can be assumed, so the overlay can be designed slightly thinner than unbonded overlays to take advantage of the resulting stress reduction.

If the existing pavement is jointed, a joint should be placed immediately above the existing joint to prevent reflection cracking. It is also important to keep the joint spacing of a partially bonded overlay as short as possible by providing additional joints in the overlay to minimize temperature stresses caused by the stiff underlying slabs.

13.2 DESIGN METHODOLOGIES

A variety of methods have been used by various agencies for the design of overlays. Prior to 1960, most agencies relied heavily on engineering judgment and experience in determining the thickness and type of overlay required. Since 1960, the use of nondestructive deflection testing has gained wide acceptance, and more rational methods based on deflection measurements to evaluate the in-situ pavement conditions have been gradually developed. As in the design of new pavements, most agencies now have their own methods for the design of overlays. Usually the procedure for the design of the overlay is similar to that for new pavement, except that the condition or remaining life of the existing pavement at the time of overlay is taken into consideration. By considering the existing pavement as new or as having 100% remaining life, the overlay design method can be applied to the design of new composite pavements as well. In this section, the basic concepts on overlay design are presented. Details about AI, PCA, and AASHTO design methods are described in subsequent sections.

Three methods can be used for overlay design: the effective thickness approach, the deflection approach, and the mechanistic–empirical approach. No matter what method is used, it is important to make a pavement condition survey and to subdivide the proposed project into one or more homogeneous analysis sections based on age,

Downloaded From : www.EasyEngineering.net

Downloaded From : www.EasyEngineering.net

traffic, design, and pavement conditions. Major distress in the existing pavement must be properly repaired before the placing of the overlay. If more than one analysis section is identified, practical construction and cost considerations must be used to decide whether separate overlay designs should be developed for each analysis section or which sections should be combined.

13.2.1 Effective Thickness Approach

The basic concept of this method is that the required thickness of the overlay is the difference between the thickness required for a new pavement and the effective thickness of the existing pavement:

$$h_{OL} = h_n - h_e \tag{13.1}$$

Here, h_{OL} is the thickness of the overlay, h_n is the thickness of the new pavement, and h_e is the effective thickness of the existing pavement. The procedure assumes that, as the pavement deteriorates and uses part of its total life, it behaves as if it were an increasingly thinner pavement (i.e., its effective thickness accounts less and less for the expended portion of the total life). Because the effective thickness is based on the type, condition, and thickness of each component layer, this method is also called the component analysis procedure. All thicknesses of new and existing materials must be converted into an equivalent thickness of HMA or PCC based on their types and conditions. If the overlay is HMA, all thicknesses in Eq. 13.1 are expressed in terms of HMA. If the overlay is PCC, all thicknesses are expressed in terms of PCC. This method is used by the Asphalt Institute, as described in Section 13.3.1, and by AASHTO, as described in Section 13.5.

A modified version of Eq. 13.1 was developed by the U.S. Corps of Engineers for the design of PCC overlays on PCC airport pavements. The equation, which was based on the results of full-scale traffic tests, is shown by Eq. 13.2:

$$h_{OL}^n = h_n^n - Ch_e^n \tag{13.2}$$

in this equation, h_e is the thickness of the existing pavement, which is different from the effective thickness shown in Eq. 13.1; $n = 2$ for unbonded overlays, 1.4 for directly placed overlays, 1 for fully bonded overlays; and C is a condition factor with suggested values as follows:

- $C = 1.0$ for existing pavement in good overall structural conditions with little or no cracking;
- $C = 0.75$ for existing pavements with initial transverse and corner cracking due to loading but without progressive structural distress or recent cracking;
- $C = 0.35$ for existing pavement that is badly cracked or shattered structurally.

For bonded overlays with $n = 1$ and $C = 1$, Eq. 13.2 is identical to Eq. 13.1 in form. Because h_e in Eq. 13.2 is the existing thickness rather than the effective thickness, the application of the Eq. 13.2 for bonded overlays with $n = 1$ and $C = 1$ implies that the concrete in the existing pavement has suffered no fatigue or other damage due

Downloaded From : www.EasyEngineering.net

Downloaded From : www.EasyEngineering.net

to traffic or weathering and is therefore as strong as the concrete in a new pavement. This assumption is contrary to the remaining life concept currently being used for the design of highway overlays.

13.2.2 Deflection Approach

The basic concept of this method is that larger pavement surface deflections imply weaker pavement and subgrade and thus require thicker overlays. The overlay must be thick enough to reduce the deflection to a tolerable amount. Usually, only the maximum deflection directly under the load is measured. This approach should not be confused with the estimate of in-situ material properties from multisensor deflection measurements for use in the effective thickness and the mechanistic-empirical methods. The deflection method is based on the empirical relationship between pavement deflection and overlay thickness and has been used by the Asphalt Institute (AI, 1983), the California Department of Transportation (1979), the Roads and Transportation Association of Canada (1977), and the Transport and Road Research Laboratory of Great Britain (Kennedy and Lister, 1978). Only the Asphalt Institute method is presented in Section 13.3.

13.2.3 Mechanistic-Empirical Approach

Similar to the design of new pavements, this method requires the determination of critical stress, strain, or deflection in the pavement by some mechanistic methods and the prediction of resulting damages by some empirical failure criteria. First, the condition or remaining life of the existing pavement must be evaluated. Based on the pavement condition or remaining life, the thickness of the overlay is then determined so that the damages in either the existing pavement or the new overlay will be within the allowable limits. This mechanistic design procedure has been used by PCA for the design of PCC overlays on PCC pavements, as described in Section 13.4.

The failure criteria that have been used most frequently for the design of flexible overlays are fatigue cracking and permanent deformation, but only fatigue cracking is considered for rigid overlays. The erosion criterion is usually not considered for the design of PCC overlays, because of the large increase in pavement thickness and the use of existing pavement as a nonerodible foundation. The following procedure can be used if the existing pavement has remaining fatigue life, as indicated by

$$\sum_{i=1}^{m} \frac{n_i}{N_i} < 1 \tag{13.3}$$

in which n_i is the actual number of load repetitions for the ith load group, N_i is the allowable number of load repetitions for the ith load group, and m is the number of load groups. If the existing pavement has no remaining life, the overlay should be considered as the top layer of a two-layer system with a modulus of subgrade depending on the conditions of the existing pavement.

Fatigue Cracking For ease of illustration, it is assumed that the design is based on the equivalent single-axle load. The method can be applied equally to various axle loads by

Downloaded From : www.EasyEngineering.net

Downloaded From : www.EasyEngineering.net

using the cumulative damage concept and summing the damage ratios over all load groups. First, the remaining life of existing pavement is estimated by

$$\frac{n_r}{N_a} = 1 - \frac{n_e}{N_a} \tag{13.4}$$

in which n_r is the additional number of load repetitions that can be applied to the existing pavement after the overlay, N_a is the allowable number of load repetitions on the existing pavement before overlay, and n_e is the actual number of load repetitions on the existing pavement before overlay. Next, based on the tensile stress or strain at the underside of the existing layer after the overlay, the allowable number of load repetitions on the overlaid pavement is determined. Because the existing pavement is not new and has a remaining life of n_r/N_a, the allowable repetitions must be multiplied by the ratio n_r/N_a to obtain the allowable repetitions after the overaly.

If the overlay and existing pavements are not bonded, the fatigue damage in the new overlay should also be checked.

Permanent Deformation It is assumed that the existing rut, if any, will be filled and that the development of rutting has nothing to do with the previous traffic but will be a function only of the additional traffic to be applied on the new pavement structure with the overlay. If the vertical compressive strain at the top of the subgrade is used to control the permanent deformation, the strain on the subgrade prior to the overlay is ignored, and only the strain after the overlay is used to determine the additional traffic allowed.

Example 13.1:

An asphalt overlay is placed on an existing asphalt pavement that has been subjected to an ESAL of 7×10^6. The horizontal tensile strain at the bottom of the asphalt layer is 1×10^{-4} before the placement of overlay, 7×10^{-5} after the overlay. By using the Asphalt Institute fatigue criteria and assuming an elastic modulus of 5×10^5 psi (3.5 GPa) for the HMA, determine the allowable number of ESAL on the overlaid pavement.

Solution: From Eq. 11.6, the allowable number of repetitions on the existing pavement $N_a = 0.0796 \times (0.0001)^{-3.291} \times (500{,}000)^{-0.854} = 15{,}677{,}000$. From Eq. 13.4, $n_r/N_a = 1 - 7{,}000{,}000/15{,}677{,}000 = 0.553$. The allowable number of repetitions on the overlaid pavement $= 0.553 \times 0.0796 \times (0.00007)^{-3.291} \times (500{,}000)^{-0.854} = 2.8 \times 10^7$.

13.3 ASPHALT INSTITUTE METHOD

Separate design procedures are used for asphalt overlay on asphalt pavement and asphalt overlay on concrete pavement. The design procedures are illustrated by a number of examples. Most of these examples are the same as those presented by the Asphalt Institute (AI, 1983), with only slight modifications.

Downloaded From : www.EasyEngineering.net

Downloaded From : www.EasyEngineering.net

13.3.1 Asphalt Overlay on Asphalt Pavement

Two methods are available: the effective thickness method and the deflection method. The effective thickness method is based on the condition of existing pavement at the time of overlay without the necessity of conducting deflection tests.

Effective Thickness Method To determine the effective thickness of existing pavement in terms of HMA thickness, one or more conversion factors must be found. If the existing pavement is full depth, method 1, based on the Present Serviceability Index (PSI) of the existing pavement, can be used to determine the conversion factor. Otherwise, method 2, based on the condition of each individual layer, should be used to determine the conversion factor of each layer.

Method 1 Figure 13.2 gives the conversion factors C (for full-depth asphalt pavements) based on the PSI of an existing pavement at the time of overlay. The two curves in the figure reflect the difference in performance after the placement of overlay. The upper curve, line A, represents pavements with a reduced rate of change in PSI, compared to their rate of change before overlay. The lower curve, line B, represents a projected rate of change in PSI about the same as before overlay and therefore is somewhat more conservative. The choice between the two curves is largely a matter of judgment and experience.

The conversion factors shown in Figure 13.2 are applicable only for HMA. If emulsifed asphalt mixes are used, the equivalency factors shown in Table 13.2 should be used. The effective thickness of each existing layer is calculated by multiplying the actual thickness of each layer by the product of the conversion factor and the appropriate equivalency factor. The total effective thickness is obtained by summing the individual effective thicknesses of all pavement layers:

$$h_e = \sum_{i=1}^{n} h_i C_i E_i \tag{13.5}$$

Here, h_i, C_i, and E_i are the thickness, conversion factor, and equivalency factor of layer i and n is the total number of layers.

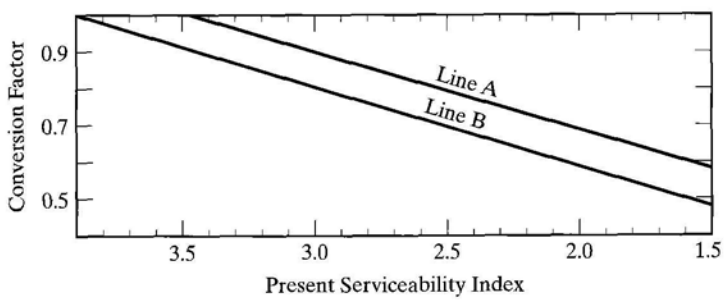


FIGURE 13.2

Conversion factors for full depth pavements. (After AI (1983).)

Downloaded From : www.EasyEngineering.net

Downloaded From : www.EasyEngineering.net

TABLE 13.2 Equivalent Factors for Emulsified Asphalt Bases

Material type	Equivalency factor (E)
Hot mix asphalt	1.00
Type I emulsified asphalt base	0.95
Type II emulsified asphalt base	0.83
Type III emulsified asphalt base	0.57

Source. After AI (1983).

Example 13.2:

A full-depth asphalt pavement consisting of a 2-in. (51-mm) HMA and a 6-in. type II emulsified asphalt base course is to be overlaid. Even though there are cracks on the surface, the cracks are not open, and the pavement appears to be stable. The pavement has a PSI of 2.0. Determine its effective thickness.

Solution: From Figure 13.2, $C = 0.7$ when based on line A, but 0.6 when based on line B. From Table 13.2, $E = 0.83$. From Eq. 13.5, $h_e = 2 \times 0.7 \times 1 + 6 \times 0.7 \times 0.83 = 4.9$ in. (124 mm) when based on line A, but $h_e = 2 \times 0.6 \times 1 + 6 \times 0.6 \times 0.83 = 4.2$ in. (107 mm) when based on line B. If average C is used, $h_e = 4.6$ in. (117 mm).

Method 2 In this method, the condition of each individual layer is evaluated, and the appropriate conversion factor C is selected from Table 13.3. As in Eq. 13.5, the effective thickness is computed as

$$h_e = \sum_{i=1}^{n} h_i C_i \tag{13.6}$$

Method 2 can also be used for full-depth pavements. If the PSI is known, it is suggested that both methods 1 and 2 be used and the two results compared. Although the ranges in values shown in Table 13.3 are based on subjective analysis, experience has shown that they are reasonable and are useful for overlay design.

Example 13.3:

Determine the effective thickness of a pavement consisting of a 4-in. (102-mm) HMA surface, a 6-in. (152-mm) cement-stabilized base, and a 4-in. (102-mm) untreated crushed-gravel subbase. The surface shows numerous transverse cracks and considerable alligator cracking in the wheelpath. The cement-stabilized base shows signs of pumping and loss of stability along the pavement edges, and the crushed-gravel subbase is in good condition, with a plasticity index smaller than 6.

Solution: The material classification for HMA surface is V(a) in Table 13.3. Because there are considerable transverse and alligator cracks, a lower bound of 0.5 is selected for C. The cement-stabilized base is classified as IV(c). Because there are signs of pumping and loss of stability, a lower bound of 0.3 is selected for C. The crushed-gravel subbase is classified as II. Because it is in good condition, with PI less than 6, an upper bound of 0.2 is selected for C. From Eq. 13.6, $h_e = 4 \times 0.5 + 6 \times 0.3 + 4 \times 0.2 = 4.6$ in. (117 mm).

Downloaded From : www.EasyEngineering.net

Downloaded From : www.EasyEngineering.net

TABLE 13.3 Conversion Factors for Determining Effective Thickness

Classification of material	Description of material	Conversion factors[a]
I	(a) Native subgrade in all cases. (b) Improved subgrade, predominantly granular materials, may contain some silt and clay but have P.I. of 10 or less. (c) Lime-modified subgrade constructed from high-plasticity soils, P.I. greater than 10.	0.0
II	Granular subbase or base, reasonably well-graded, hard aggregates with some plastic fines and CBR not less that 20. Use upper part of range if P.I. is 6 or less; lower part of range if P.I. is more than 6.	0.1–0.2
III	Cement or lime-fly ash stabilized subbases and bases constructed from low plasticity soils, P.I. of 10 or less.	0.2–0.3
IV	(a) Emulsified or cutback asphalt surfaces and bases that show extensive cracking, considerable raveling or aggregate degradation, appreciable deformation in the wheelpaths, and lack of stability. (b) Portland cement concrete pavements (including those under asphalt surfaces) that have been broken into small pieces 2 ft (0.6 m) or less in maximum dimension prior to overlay construction. Use upper part of range when subbase is present, lower part of range when slab is on subgrade. (c) Cement or lime-fly ash stabilized bases that have developed pattern cracking, as shown by reflected surface cracks. Use upper part of range when cracks are narrow and tight, lower part of range with wide cracks, pumping, or evidence of instability.	0.3–0.5
V	(a) Asphalt concrete surface and base that exhibit appreciable cracking and crack patterns. (b) Emulsified or cutback asphalt surface and bases that exhibit some fine cracking, some reveling or aggregate degradation, and slight deformation in the wheelpaths but remain stable. (c) Appreciably cracked and faulted portland cement concrete pavement (including such under asphalt surfaces) that cannot be effectively undersealed. Slab fragments, ranging in size from approximately 10 to 40 ft^2 (1 to 4 m^2), and have been well seated on the subgrade by heavy pneumatic-tired rolling.	0.5–0.7
VI	(a) Asphalt concrete surfaces and bases that exhibit some fine cracking, have small intermittent cracking patterns and slight deformation in the wheelpaths but remain stable. (b) Emulsified or cutback asphalt surface and bases that are stable, generally uncracked, show no bleeding, and exhibit little deformation in the wheelpaths. (c) Portland cement concrete pavements (including such under asphalt surfaces) that are stable and undersealed, have some cracking but contain no pieces smaller than about 10 ft^2 (1 m^2).	0.7–0.9
VII	(a) Asphalt concrete, including asphalt concrete base, generally uncracked, and with little deformation in the wheelpaths. (b) Portland cement concrete pavement that is stable, undersealed, and generally uncracked. (c) Portland cement concrete base, under asphalt surface, that is stable, nonpumping, and exhibits little reflected surface cracking.	0.9–1.0

[a]Originally meeting minimum strengths and compaction requirements specified by most state highway departments.
Source. After AI (1983).

Downloaded From : www.EasyEngineering.net

Downloaded From : www.EasyEngineering.net

Calculation of Overlay Thickness The required overlay thickness is the difference between the required thickness of a new full-depth pavement and the effective thickness of the existing pavement, as is shown by Eq. 13.1. The thickness of the new pavement can be determined from the design chart for full-depth pavements presented in Figure 11.11.

Example 13.4:

The existing pavement shown in Example 13.3 has a subgrade resilient modulus M_R of 10,000 psi (6.9 MPa). Determine the thickness of overlay required to carry an ESAL of 3×10^6.

Solution: From Example 13.3, $h_e = 4.6$ in. (117 mm). With $M_R = 10{,}000$ psi (6.9 MPa) and ESAL $= 3 \times 10^6$, from Figure 11.11, $h_n = 10.6$ in. (269 mm). From Eq. 13.1, the thickness of overlay required is $h_{OL} = 10.6 - 4.6 = 6$ in. (152 mm).

Deflection Method Pavement deflections are measured with the Benkelman beam by using a rebound test procedure. Condition survey and deflection data are used to establish the analysis section. At least 10 deflection measurements should be made for each analysis section, or else a minimum of 20 measurements per mile (13 measurements/km). Pavement temperatures are measured at the time of deflection measurements so that deflections can be adjusted to a standard temperature of 70°F (21°C). A random sampling technique is recommended for selecting the locations of deflection measurements.

Representative Rebound Deflection When the deflection tests on the analysis section are completed, the recorded pavement rebound deflections are used to determine a representative rebound deflection (RRD):

$$\delta_{rrd} = (\bar{\delta} + 2s)\text{Fc} \tag{13.7}$$

In this equation, δ_{rrd} is the representative rebound deflection, $\bar{\delta}$ is the mean deflection, s is the standard deviation, F is the temperature adjustment factor, and c is the critical period adjustment factor. The use of two standard deviations above the mean implies that 97% of the measurements are smaller than δ_{rrd}. Locations within the analysis section with deflections greater than δ_{rrd} are recommended for special treatment. It is suggested that additional deflections be measured to determine the extent of such weak areas. These locations could require replacement before overlay.

Figure 13.3 gives the temperature adjustment factors for various thicknesses of dense-graded aggregate bases. A base thickness of 0 in. corresponds to a full-depth asphalt pavement. Temperatures have their greatest effect on full-depth pavements; the effect decreases as the thickness of granular base increases.

The critical period is the interval during which the pavement is most likely to be damaged by heavy loads. In frost areas, this will normally be the period during or directly after the spring thaw. If the deflection measurements are made during the critical period, the adjustment factor c is equal to 1. If deflections are not measured in the critical period, c is greater than 1 and can be determined from a continuous record of

Downloaded From : www.EasyEngineering.net

Downloaded From : www.EasyEngineering.net

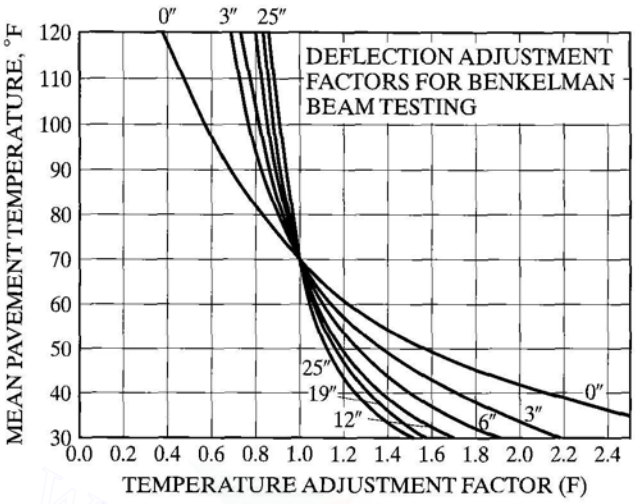


FIGURE 13.3

Temperature adjustment factors for various thicknesses of untreated granular bases (1 in. = 25.4 mm, 1°F = 0.56°C). (After AI (1983).)

measured deflections for a similar pavement. If no record of comparable deflection data is available, c should be selected by means of engineering judgment.

Example 13.5:

A series of deflection measurements by a Benkelman beam were made on a full-depth pavement during a critical period at pavement temperature of 55°F (13.3°C). The measured deflections are 0.033, 0.035, 0.040, 0.025, 0.028, 0.026, 0.020, 0.035, 0.034, and 0.027 in. (0.84, 0.89, 1.02, 0.64, 0.71, 0.66, 0.51, 0.89, 0.86, and 0.69 mm). Compute the representative rebound deflection δ_{rrd}.

Solution: $\bar{\delta} = (0.033 + 0.035 + 0.040 + 0.025 + 0.028 + 0.026 + 0.020 + 0.035 + 0.034 + 0.027)/10 = 0.030$ in. (0.77 mm). From Eq. 10.9, $V[\delta] = [(0.033 - 0.030)^2 + (0.035 - 0.030)^2 + (0.040 - 0.030)^2 + (0.025 - 0.030)^2 + (0.028 - 0.030)^2 + (0.026 - 0.030)^2 + (0.020 - 0.030)^2 + (0.035 - 0.030)^2 + (0.034 - 0.030)^2 + (0.027 - 0.030)^2]/(10 - 1) = 3.66 \times 10^{-5}$ in^2 (0.024 mm^2), or $s = 0.006$ in. (0.15 mm). At pavement temperature of 55°F (13.3°C) and without an untreated aggregate base, from Figure 13.3, the temperature adjustment factor $F = 1.38$. During the critical period, $c = 1$. From Eq. 13.7, $\delta_{rrd} = (0.030 + 2 \times 0.006) \times 1.38 \times 1 = 0.058$ in. (1.47 mm).

Deflection After Overlay In developing the design procedure, the overlaid pavement was considered as a two-layer system with the HMA overlay as layer 1 and the existing pavement as layer 2 (Finn and Monismith, 1984). The representative rebound deflection δ_{rrd} was used to determine the modulus of layer 2. By assuming the existing pavement to be a homogeneous half-space with a Poisson ratio of 0.5, from Eq. 2.8,

$$E_2 = \frac{1.5qa}{\delta_{rrd}} \tag{13.8}$$

Downloaded From : www.EasyEngineering.net

Downloaded From : www.EasyEngineering.net

in which q is the contact pressure, assumed to be 70 psi (483 kPa), and a is the radius of the equivalent single loaded area to represent the load on dual tires, assumed to be 6.4 in. (163 mm). The expected deflection after overlay is called the *design rebound deflection* δ_d and can be determined from the approximate equation

$$\delta_d = \frac{1.5qa}{E_2}\left(\left\{1 - \left[1 + 0.8\left(\frac{h_1}{a}\right)^2\right]^{-0.5}\right\}\frac{E_2}{E_1} + \left\{1 + \left[0.8\frac{h_1}{a}\left(\frac{E_1}{E_2}\right)^{1/3}\right]^2\right\}^{-0.5}\right) \tag{13.9}$$

in which h_1 is the thickness of the overlay and E_1 is the modulus of the overlay, assumed to be 500,000 psi (3.5 GPa).

Overlay Thickness Design It is assumed that there is a unique relationship between design rebound deflection in inches and the allowable ESAL, as shown in Figure 13.4 and represented by

$$\delta_d = 1.0363\ (\text{ESAL})^{-0.2438} \tag{13.10}$$

Given the ESAL for the overlay, δ_d can be determined from Eq. 13.10. Given the representative rebound deflection δ_{rrd}, E_2 can be obtained from Eq. 13.8. With δ_d and E_2 known and values of q, a, and E_1 assumed, the thickness of overlay h_1 can be computed from Eq. 13.9. Figure 13.5 shows the design chart relating ESAL and δ_{rrd} to overlay thickness.

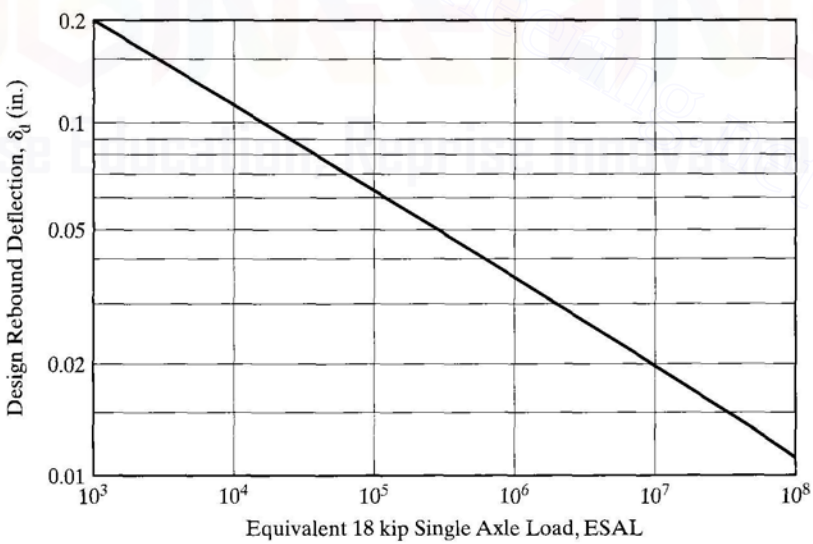


FIGURE 13.4

Relationship between design rebound deflection and ESAL (1 in. = 25.4 mm). (After AI (1983).)

Downloaded From : www.EasyEngineering.net

Downloaded From : www.EasyEngineering.net

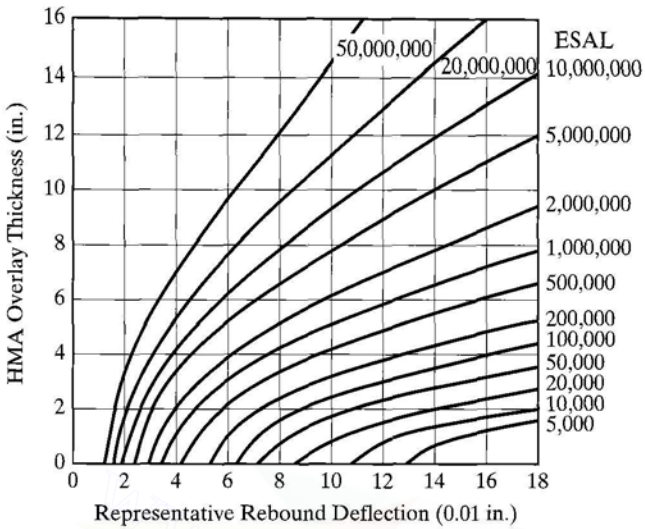


FIGURE 13.5

Overlay thickness design chart based on representative rebound deflection and design ESAL (1 in. = 25.4 mm). (After AI (1983).)

Example 13.6:

By the Asphalt Institute method, determine the allowable ESAL for a 2-in. (51-mm) overlay on an asphalt pavement with a representative rebound deflection δ_{rrd} of 0.062 in. (1.57 mm).

Solution: Based on Eq. 13.8 and the parameters assumed by the Asphalt Institute, $E_2 = 1.5 \times 70 \times 6.4/0.062 = 10{,}840$ psi (74.8 MPa). From Eq. 13.9,

$$\delta_d = \frac{1.5 \times 70 \times 6.4}{10{,}840}\left(\left\{1 - \left[1 + 0.8\left(\frac{2}{6.4}\right)^2\right]^{-0.5}\right\}\frac{10{,}840}{500{,}000} + \left\{1 + \left[0.8 \times \frac{2}{6.4}\left(\frac{500{,}000}{10{,}840}\right)^{1/3}\right]^2\right\}^{-0.5}\right) = 0.04621 \text{ in. } (1.17 \text{ mm})$$

From Eq. 13.10, $0.04621 = 1.0363\ (\text{ESAL})^{-0.2438}$, or ESAL = 347,000, which checks with the value obtained from Figure 13.5.

Remaining Life Figure 13.4 or Eq. 13.10 can also be used to estimate the remaining life of an existing pavement—how much time remains before an overlay is needed. The procedure is as follows:

1. Determine the representative rebound deflection δ_{rrd}.
2. Obtain remaining life (ESAL), from Figure 13.4 by assuming δ_{rrd} to be the design rebound deflection δ_d. A more convenient method is to use Eq. 13.10, which can be rewritten as

$$(\text{ESAL})_r = \left(\frac{1.0363}{\delta_{rrd}}\right)^{4.1017} \tag{13.11}$$

in which δ_{rrd} is in inches.

Downloaded From : www.EasyEngineering.net

Downloaded From : www.EasyEngineering.net

3. Estimate the design ESAL for the current year $(ESAL)_0$, and determine the growth factor by

$$\text{Growth factor} = \frac{(ESAL)_r}{(ESAL)_0} \tag{13.12}$$

4. Estimate the traffic growth rate in percent, and find the design period corresponding to the growth factor from Table 6.13. The design period is the estimated number of years before an overlay is needed.

Example 13.7:

Given $(ESAL)_0 = 68{,}000$ for the current year, $\delta_{rrd} = 0.042$ in. (1.07 mm), and traffic growth rate = 4%, estimate number of years before overlay.

Solution: From Eq. 13.11, $(ESAL)_r = (1.0363/0.042)^{4.1017} = 513{,}000$. From Eq. 13.12, growth factor = 513,000/68,000 = 7.54. From Table 6.13, estimated time before overlay = 6.5 years.

13.3.2 Asphalt Overlay on PCC Pavement

As with asphalt overlays on asphalt pavements, both effective thickness and deflection methods are available for asphalt overlays on PCC pavements.

Effective Thickness Method The procedure is the same as for asphalt overlays on asphalt pavements, and the conversion factors for existing PCC pavements are also shown in Table 13.3. However, there are certain distresses peculiar to rigid pavements that should be considered in design. Among the signals of distress to look for are pumping, cracking, spalling, faulting, and slab movement under traffic. Also, if the pavement is to be either undersealed or cracked and seated prior to overlay, this plan should be considered in selecting the proper conversion factor from Table 13.3. This component analysis procedure also can be applied to PCC pavements that have previously been overlaid with asphalt.

Example 13.8:

Given a design ESAL of 2×10^6, design an asphalt overlay for a pavement consisting of 8 in. (203 mm) of jointed PCC slabs and 4 in. (102 mm) of sand–gravel subbase. The rigid pavement is appreciably cracked and faulted, but the slab fragments have been broken and well seated on the subbase by heavy rollers prior to overlay. The sand–gravel subbase is of average quality. The subgrade has a resilient modulus of 8000 psi (55 MPa).

Solution: From Table 13.3, the PCC is classified as V(c) with a conversion factor of 0.5, and the sand–gravel subbase is classified as II with a conversion factor of 0.15. From Eq. 13.6, $h_e = 8 \times 0.5 + 4 \times 0.15 = 4.6$ in. (117 mm). With ESAL $= 2 \times 10^6$ and $M_R = 8000$ psi (55 MPa), from Figure 11.11, a 10.2-in. (259-mm) full-depth pavement is required. Therefore, thickness of overlay $= 10.2 - 4.6 = 5.6$ in. (142 mm), and the use of 5.5 in. (140 mm) should be adequate.

Deflection Method The deflection procedure presented by the Asphalt Institute emphasizes the identification and repair of distress areas prior to overlay. Pavement condition

Downloaded From : www.EasyEngineering.net

Downloaded From : www.EasyEngineering.net

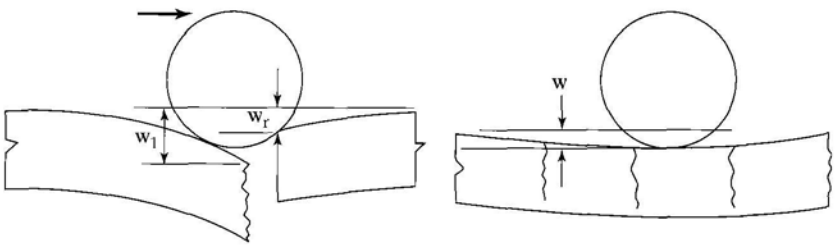
surveys in conjunction with deflection testing are helpful in identifying distress conditions. For two-lane highways, deflection measurements are made on the outside edge on both sides of the center line. For divided highways, deflections should be measured on the outermost edge only. Additional deflection measurements should be made at corners, joints, cracks, and deteriorated pavement areas to determine load transfer capability.

Allowable Deflections For JPCP and JRCP, vertical deflections at the joints are most important. As measured by the Benkelman beam, the differential deflection, $w_1 - w_r$, should be less than 0.002 in. (0.05 mm), and the mean deflection, $(w_1 + w_r)/2$ should be less than 0.014 in. (0.36 mm). Measurements of these deflections are shown in Figure 13.6*a*. Stabilization and undersealing are required if these criteria are not met.

Studies on CRCP indicate that Dynaflect deflections of 0.0006 to 0.0009 in. (15 to 23 μm) or greater lead to excessive cracking and deterioration. If the critical deflection w, shown in Figure 13.6*b*, exceeds 0.0006 in. (15 μm), undersealing or stabilization is required.

Dense-graded HMA can reduce deflections by 5%/in. (0.2%/mm). However, this varies with the mix type and the environmental conditions and may be as high as 10 to 12%/in. (0.4 to 0.5%/mm). If the deflection analysis indicates a desired reduction of 50% or more, overlays should not be used alone. It is more economical to reduce deflections by applying undersealing in conjunction with the overlay.

Overlay Thickness Design Chart Figure 13.7 is a design chart for selecting the thickness of an asphalt overlay over PCC pavements. The thicknesses of HMA were selected to minimize the reflection cracking by considering the effect both of the horizontal tensile strains and of the vertical shear stresses. In this procedure, overlay thicknesses are related to slab length and mean annual temperature differential, which is the difference between the highest normal daily maximum temperature and the lowest normal daily minimum temperature for the hottest and coldest months, based on a 30-year average. Maximum and minimum daily temperatures at locations throughout the United States can be found in MS-17 (AI, 1983). An abbreviated table for maximum annual temperature differential is presented in Table 13.4.



(a) Jointed Reinforced Concrete Pavement (b) Continuous R. C. Pavement

FIGURE 13.6

Deflections to be considered in overlay thickness design.

Downloaded From : www.EasyEngineering.net

Downloaded From : www.EasyEngineering.net

Slab Length (Ft)	TEMPERATURE DIFFERENTIAL (°F) 30	40	50	60	70	80	Slab Length (m)
10 or Less	100 mm (4 in.)	100 mm (4 in.)	100 mm (4 in.)	100 mm (4 in.)	100 mm (4 in.)	100 mm (4 in.)	3
15	100 mm (4 in.)	100 mm (4 in.)	100 mm (4 in.)	100 mm (4 in.)	100 mm (4 in.)	100 mm (4 in.)	4.5
20	100 mm (4 in.)	100 mm (4 in.)	100 mm (4 in.)	100 mm (4 in.)	125 mm (5 in.)	140 mm (5.5 in.)	6
25	100 mm (4 in.)	100 mm (4 in.)	100 mm (4 in.)	125 mm (5 in.)	150 mm (6 in.)	175 mm (7 in.)	7.5
30	100 mm (4 in.)	100 mm (4 in.)	125 mm (5 in.)	150 mm (6 in.)	175 mm (7 in.)	200 mm (8 in.)	9
35	100 mm (4 in.)	115 mm (4.5 in.)	150 mm (6 in.)	175 mm (7 in.)	215 mm (8.5 in.)	Use Alternative 2 or 3	10.5
40	100 mm (4 in.)	140 mm (5.5 in.)	175 mm (7 in.)	200 mm (8 in.)	Use Alternative 2 or 3	Use Alternative 2 or 3	12
45	115 mm (4.5 in.)	150 mm (6 in.)	190 mm (7.5 in.)	225 mm (9 in.)	Use Alternative 2 or 3	Use Alternative 2 or 3	13.5
50	125 mm (5 in.)	175 mm (7 in.)	215 mm (8.5 in.)	Use Alternative 2 or 3	Use Alternative 2 or 3	Use Alternative 2 or 3	15
60	150 mm (6 in.)	200 mm (8 in.)	Use Alternative 2 or 3	Use Alternative 2 or 3	Use Alternative 2 or 3	Use Alternative 2 or 3	18
	17	22	28	33	39	44	

TEMPERATURE DIFFERENTIAL (°C)

FIGURE 13.7

Thickness design chart for asphalt overlays on PCC pavements. (After AI (1983).)

The overlay thickness chart is divided into three sections, designated as A, B, and C, according to slab lengths and temperature differentials. In section A, a minimum thickness of 4 in. (100 mm) is recommended. This thickness should reduce the deflection by an estimated 20%. The overlay thickness of sections B and C may be used as given. However, the overlay thicknesses may be reduced if the PCC slabs are shortened by cracking and seating to reduce temperature effects. In section C, the thicknesses range upward to 8.5 in. (215 mm). Normally, when an overlay approaches the 8- to 9-in. (200- to 225-mm) range, other alternatives should be considered. Note that alternative 2 indicated in Figure 13.7 is crack and seat and that alternative 3 is a crack relief layer, both described in Section 13.1.2.

Downloaded From : www.EasyEngineering.net

Downloaded From : www.EasyEngineering.net

TABLE 13.4 Maximum Annual Temperature Differential

State	City	Temperature differential (°F)	State	City	Temperature differential (°F)
AL	Mobile	49	NV	Reno	73
AK	Juneau	46	NH	Concord	73
AZ	Phoenix	67	NJ	Atlantic City	61
AR	Little Rock	64	NM	Albuquerque	69
CA	Los Angeles	30	NY	Albany	71
	Sacramento	56		Buffalo	62
	San Francisco	32		New York	59
CO	Denver	71	NC	Charlotte	56
CT	Hartford	68		Raleigh	58
DE	Wilmington	62	ND	Bismark	87
DC	Washington	61	OH	Cincinnati	64
FL	Jacksonville	46		Cleveland	61
	Miami	31		Columbus	64
GA	Atlanta	53	OK	Okla City	67
HI	Honolulu	22	OR	Portland	47
ID	Boise	69	PA	Philadelphia	62
IL	Chicago	68		Pittsburgh	62
	Peoria	70	RI	Providence	61
IN	Indianapolis	66	SC	Columbia	58
IA	Des Moines	74	SD	Soiux Falls	81
KS	Wichita	71	TN	Memphis	60
KY	Louisville	63		Nashville	61
LA	New Orleans	47	TX	Dallas-Fort Worth	62
ME	Portland	67		El Paso	64
MD	Baltimore	62		Houston	53
MA	Boston	59	UT	Salt Lake City	74
MI	Detroit	64	VT	Burlington	73
	Sault Ste. Marie	69	VA	Norfolk	54
MN	Duluth	77		Richmond	61
	Minneapolis-St. Paul	79	WA	Seattle-Tacoma	42
MS	Jackson	57		Spokane	65
MO	Kansas City	69	WV	Charleston	60
	St. Louis	66	WI	Milwaukee	69
MT	Great Falls	72	WY	Cheyenne	69
NE	Omaha	76	PR	San Juan	19

Source. After AI (1983).

Example 13.9:

A JRCP has a joint spacing of 40 ft (12.2 m) and a temperature differential of 70°F (21°C). Measured Benkelman beam deflections are $w_1 = 0.035$ in. (0.89 mm) and $w_r = 0.025$ in. (0.64 mm). Determine the thickness of overlay required.

Solution:

1. *Alternative 1: Thick Overlay.* With a slab length of 40 ft (12.2 m) and a temperature differential of 70°F (21°C), from Figure 13.7, the required overlay thickness is greater than 9 in. (229 mm); therefore, use alternative 2 or 3.

Downloaded From : www.EasyEngineering.net

Downloaded From : www.EasyEngineering.net

2. *Alternative 2: Reduce Slab Length.*
   1. Break the slab into 20-ft (6.1-m) sections. With a slab length of 20 ft (6.1 m) and a temperature differential of 70°F (21°C), from Figure 13.7, the required overlay is 5 in. (125 mm).
   2. Check vertical mean deflection. Mean deflection before overlay = (0.025 + 0.035)/2 = 0.03 in. (0.76 mm). Assuming that each inch of HMA will reduce deflection by 5%, the mean deflection reduced by overlay = 5 × 0.03 × 0.05 × 0.05 = 0.0075 in. Mean deflection after overlay = 0.030 − 0.0075 = 0.0225 (0.56 mm) > 0.014 in. (0.36 mm) allowed. Therefore, undersealing is required.
   3. Check differential deflections. Differential deflection before overlay = 0.035 − 0.025 = 0.01 (0.25 mm). Differential deflection reduced by overlay = 5 × 0.01 × 0.05 = 0.0025 in. (0.064 mm). Differential deflection after overlay = 0.01 − 0.0025 = 0.0075 in. (0.19 mm) > 0.002 in. (0.051 mm) allowed. Therefore, undersealing is required.
3. *Alternative 3: Crack Relief Layer.* Use the layer thicknesses recommended in Figure 13.1. The design consists of a 3.5-in. (89-mm) mix A crack relief layer, a 2-in. (51-mm) dense-graded HMA leveling course, and a 1.5-in. (38-mm) dense-graded HMA surface. The total thickness is 7 in. (178 mm). A check of deflection indicates that undersealing is required.

13.4 PORTLAND CEMENT ASSOCIATION METHOD

There are three types of PCC overlays on PCC pavement: unbonded, bonded, and partially bonded. In this section, the PCA method of overlay design (including the evaluation of existing pavements and the design of unbonded and bonded overlays) is presented. Depending on the amount of bonding, the design of a partially bonded overlay can be interpolated between the two.

13.4.1 Evaluation of Existing Pavement

As a part of the design process, a comprehensive evaluation of the existing pavement must be made, including pavement condition survey, nondestructive deflection testing, and in-situ material evaluation.

Pavement Condition Survey The condition survey should identify the type, extent, and severity of pavement distress. These distresses are described in Section 9.1.2. The pavement is divided into survey sections based on the differences in design, construction, traffic, and location. For small projects, the entire length of each section should be surveyed. For larger projects, each section may be divided into sample units consisting of about 10 to 20 slabs. Sample units from each section are then randomly selected. The use of 25 to 50% of the sample is recommended. The exact sampling frequency should be based on site conditions. For each sample unit, the type, severity, and extent of distress are recorded. For high-severity distress, the cause of distress should be identified and corrective measures taken prior to the overlay.

Nondestructive Deflection Testing The need for deflection testing is based on site conditions and on the information obtained from the condition survey. If the condition survey indicates the existence of, or potential for, load-associated distress, then deflection

Downloaded From : www.EasyEngineering.net

Downloaded From : www.EasyEngineering.net

testing should be conducted to determine the severity of the problem. Deflection measurements should be taken at joints and cracks to learn whether loss of support exists and whether load transfer across the joints and cracks is adequate. The test should be performed by using a NDT device that delivers an 8000- to 10,000-lb (35.6- to 44.5-kN) load to the pavement. The use of lighter loads is not recommended.

In-Situ Material Evaluation An in-situ material evaluation should be performed to identify the subgrade and subbase materials and establish the design modulus of subgrade reaction at the top of the subbase to be used in different sections of the project. For bonded overlay projects, the strength related properties of the concrete must also be determined. The modulus of subgrade reaction at the top of the subbase may also be backcalculated from results of nondestructive testing, as described in Section 9.4.3.

The design of a bonded overlay requires a knowledge of the modulus of rupture and the modulus of elasticity of the concrete in the existing pavement. Because it is not practical to obtain beam specimens from the pavement, it is recommended that splitting tensile tests be made on cored specimens. The test should be conducted according to ASTM C 496 "Splitting Tensile Strength of Cylindrical Concrete Specimens." One core should be taken every 300 to 500 ft (91 to 152 m) at midslab and about 2 ft (0.6 m) from the edge of outside lane. Core diameter should not be less than 4 in. The bottoms of cores may be trimmed, but not more than $\frac{1}{2}$ in. (13 mm).

For each section, the effective splitting tensile strength is determined to be

$$f_{te} = \bar{f}_t - 1.65s \tag{13.13}$$

in which f_{te} is the effective splitting tensile strength, $\bar{f}_t$ is the average value of splitting tensile strength, and s is the standard deviation of splitting tensile strength. Equation 13.13 implies that only 5% of the samples in a section have a tensile strength less than the effective values. The modulus of rupture S_c is then obtained from the relationship

$$S_c = ABf_{te} \tag{13.14}$$

in which A is a regression constant based on local experience and B is the damage factor (equal to 0.9, to relate the strength of concrete specimens taken 2 ft (0.61 m) from the edge of outside lane to that near or at the edge). Values of A reported in the literature range from 1.35 to about 1.55; a reasonable value based on local experience should be selected for design purposes. In the absence of local information, an A value of 1.45 is suggested.

The modulus of elasticity of the concrete in the existing pavement can be determined by testing concrete cores in accordance with ASTM C 469 "Static Modulus of Elasticity and Poisson Ratio of Concrete in Compression" or by the approximate relationship

$$E_c = DS_c \tag{13.15}$$

in which D is a constant = 6000 to 7000.

13.4.2 Design of Unbonded Overlay

The JSLAB computer program was used by PCA to analyze both bonded and unbonded overlays.

Downloaded From : www.EasyEngineering.net

Downloaded From : www.EasyEngineering.net

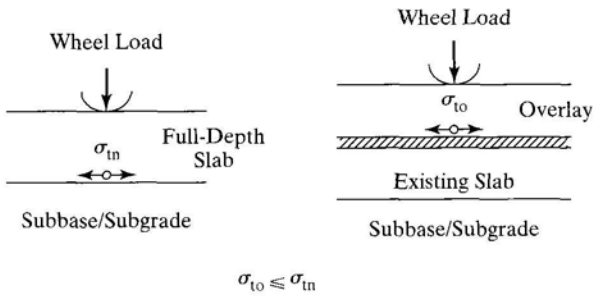


FIGURE 13.8
Stress equivalent concept for unbonded overlay.

Basic Concept The design concept is to provide an overlaid pavement that is structurally equivalent to a new full-depth pavement placed on the same subbase and subgrade. The premise of structural equivalency is based on fatigue cracking by ensuring that the edge stress in the unbonded overlay σ_{to} is equal to or less than the edge stress σ_{tn} in the new pavement, as indicated in Figure 13.8.

Cracks in the existing pavement were modeled by using soft elements. Wheel load was placed at the edge directly over a crack in the existing pavement, as shown in Figure 13.9. The effect of crack spacing in the existing pavement was determined for spacings of 5, 7, and 10 ft (1.5, 2.1, and 3.0 m). It was found that the edge stress is larger when a crack is present in the existing pavement, but that additional cracking does not further increase the edge stress.

Design Charts The edge stresses obtained from JSLAB were used to prepare design charts for determining the thickness of unbonded overlays. The following assumptions were made in the analysis: loading type, 18-kip (80-kN) single-axle load; modulus of elasticity, 5×10^6 psi (35 GPa) for overlays and 3×10^6 psi and 4×10^6 (21 and 28 GPa) for existing pavements; slab length, 20 ft (6.1 m).

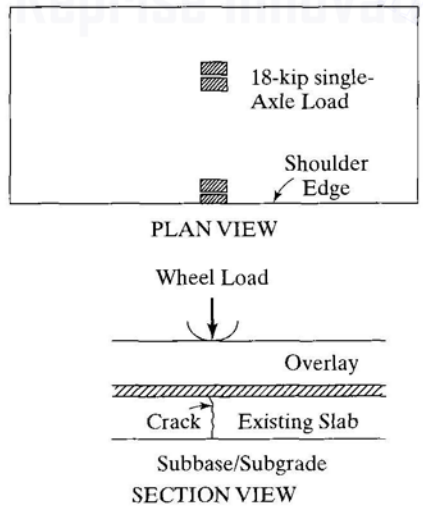


FIGURE 13.9
Loading position for stress analysis.

Downloaded From : www.EasyEngineering.net

Downloaded From : www.EasyEngineering.net

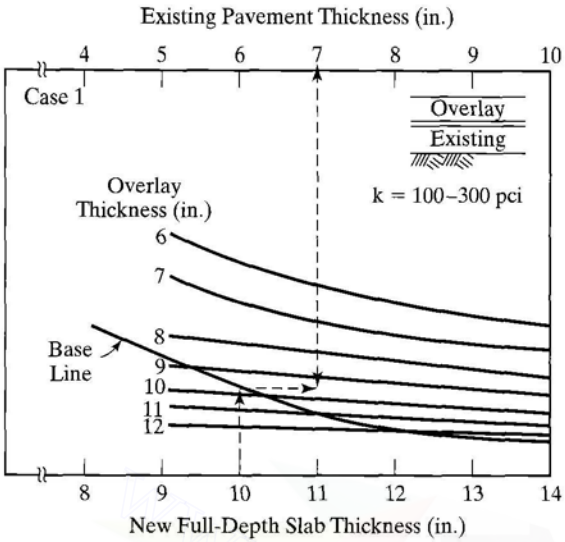


FIGURE 13.10

Design chart for case 1 condition of existing pavement (1 in. = 25.4 mm, 1 pci = 271.3 kN/m^3). (After Tayabji and Okamoto (1985).)

Design charts for three cases of existing pavement conditions are shown in Figures 13.10, 13.11, and 13.12. These charts are applicable to existing concrete pavements having modulus of elasticity from about 3×10^6 to 4×10^6 psi (21 to 28 GPa). The three cases are described next:

1. *Case 1.* Existing pavement exhibiting a large amount of midslab and corner cracking; poor load transfer across cracks and joints.
2. *Case 2.* Existing pavement exhibiting a small amount of both midslab and corner cracking; reasonably good load transfer across cracks and joints; localized repairs performed to correct distressed existing slabs.

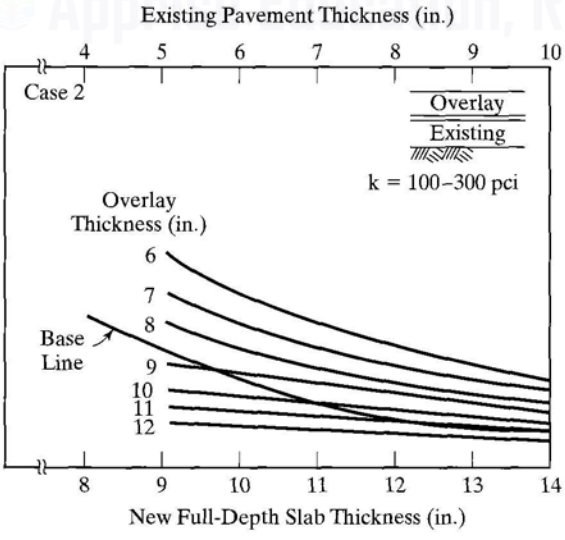


FIGURE 13.11

Design chart for case 2 condition of existing pavement (1 in. = 25.4 mm, 1 pci = 271.3 kN/m^3). (After Tayabji and Okamoto (1985).)

Downloaded From : www.EasyEngineering.net

Downloaded From : www.EasyEngineering.net

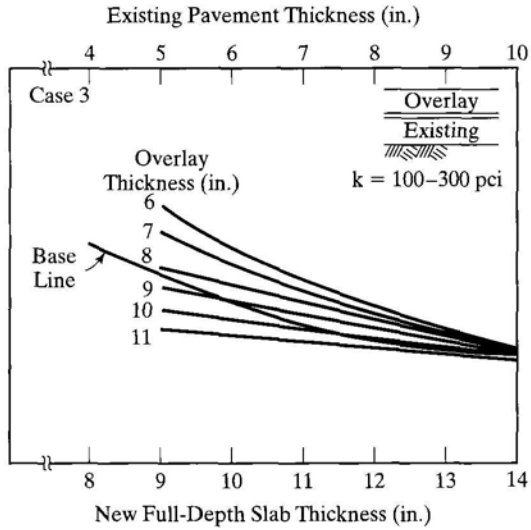


FIGURE 13.12

Design chart for case 3 condition of existing pavement (1 in. = 25.4 mm, 1 pci = 271.3 kN/m^3). (After Tayabji and Okamoto (1985).)

3. *Case 3.* Existing pavement exhibiting a small amount of midslab cracking; good load transfer across cracks and joints; loss of support corrected by undersealing.

The design chart for case 1 was based on the results when a crack was placed in the existing pavement directly under the edge load. The design chart for case 3 was based on the results when no cracking occurred in the existing pavement. The design chart for case 2 was interpolated between cases 1 and 3. The thicknesses of the overlays are based on concrete pavements without tied concrete shoulders. If a tied shoulder is used in conjunction with the overlay, the thickness of the overlay may be reduced by 1 in. (25 mm), provided that a minimum thickness of 6 in. (25 mm) is used.

Overlay Thickness The first step in the design process is to determine the thickness of a new full-depth concrete pavement to carry the anticipated traffic, as described in Section 12.2. Based on the condition of the existing pavement, the proper design chart is selected and the overlay thickness corresponding to a new pavement thickness is determined. Use of the design chart is illustrated in Figure 13.10 for an existing pavement of 7 in. (178 mm) and a new full-depth pavement of 10 in. (254 mm). A vertical line is drawn from the 10-in. (254-mm) thickness to intersect the base line and then to turn horizontally until it meets the vertical line through the 7-in. (178-mm) existing thickness. The intersection of these two lines gives an overlay thickness of 9.5 in. (241 mm). The minimum overlay thickness provided by the design charts is 6 in. (152 mm). The use of thinner overlays is not recommended.

Representative values of overlay thickness determined from the charts are summarized in Table 13.5 in terms of new pavement thickness h_n and existing pavement thickness h_e. To compare the results with Eq. 13.2 for the unbonded case with $n = 2$, overlay thicknesses were computed for C values of 0.35, 0.6, and 0.8. These results are presented in Table 13.6. It can be seen that the overlay thicknesses listed in Table 13.5 agree closely with those listed in Table 13.6. This indicates that cases 1, 2, and 3 are equivalent to the C values from 0.3 to 0.5, from 0.5 to 0.7, and from 0.7 to 0.9, respectively.

Downloaded From : www.EasyEngineering.net

Downloaded From : www.EasyEngineering.net

TABLE 13.5 Representative Values of Unbonded Overlay Thickness

		Overlay thickness (in.)		
h_n (in.)	h_e (in.)	Case 1	Case 2	Case 3
8	8	6.8	6.0[a]	6.0[a]
	7	7.2	6.0	6.0
	6	7.6	6.8	6.0
10	9	9.0	7.0	6.0[a]
	8	9.2	7.8	6.0
	7	9.4	8.8	8.0
12	9	11.5	10.4	9.0
	8	11.7	10.8	10.0
	7	11.8	11.2	10.8

Note. [a]Indicates minimum thickness; 1 in. = 25.4 mm.
Source. After Tayabji and Okamoto (1985).

TABLE 13.6 Thicknesses of Unbonded Overlay Based on Corps of Engineers' Equation

		Overlay thickness (in.)		
h_n (in.)	h_e (in.)	$C = 0.35$	$C = 0.6$	$C = 0.8$
8	8	6.5	6.0[a]	6.0[a]
	7	6.8	6.0[a]	6.0[a]
	6	7.2	6.5	6.0
10	9	8.5	7.2	6.0
	8	8.5	7.9	7.0
	7	9.1	8.4	7.8
12	9	10.8	9.8	8.9
	8	11.0	10.3	9.6
	7	11.3	10.7	10.2

Note. [a]Indicates minimum thickness; 1 in. = 25.4 mm.
Source. After Tayabji and Okamoto (1985).

13.4.3 Design of Bonded Overlay

Bonded overlay is used when the existing pavement is still in good condition but does not have the structural capacity to carry the anticipated future traffic.

Basic Concept The basic concept for bonded overlay is the same as that for unbonded overlay, but the location of the edge stress to be compared is different. In the unbonded case, the edge stress at the bottom of the full-depth slab is compared with that at the bottom of overlay, as shown in Figure 13.8. Since both are made of new concrete with the same modulus of rupture S_c, a comparison of edge stress is sufficient. If the edge stress σ_t is the same, the stress ratio σ_t/S_c will be the same, and so will the fatigue life. In the bonded case, the edge stress at the bottom of the full-depth slab is compared with that at the bottom of the existing slab, as shown in Figure 13.13. Because the new full-depth slab and the old existing slab have different moduli of rupture, the equivalency

Downloaded From : www.EasyEngineering.net

Downloaded From : www.EasyEngineering.net

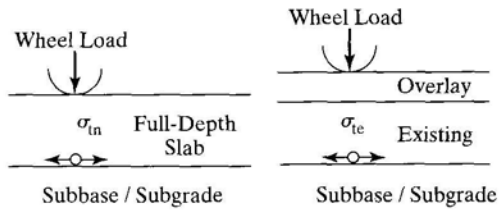


FIGURE 13.13
Equivalent concept for bonded overlay.

$$\frac{\sigma_{te}}{S_{ce}} \leq \frac{\sigma_{tn}}{S_{cn}}$$

should be based on the stress ratio rather than the stress alone. For both pavements to be equivalent, the stress ratio in the existing overlaid pavement must be equal to or smaller than that in the new full-depth pavement:

$$\frac{\sigma_{te}}{S_{ce}} \leq \frac{\sigma_{tn}}{S_{cn}} \tag{13.16}$$

Here, σ_{te} is the critical edge stress in the existing overlaid pavement, σ_{tn} is the critical edge stress in the new full-depth pavement, S_{ce} is the modulus of rupture of the existing concrete, and S_{cn} is the modulus of rupture of the new concrete.

Design Chart The JSLAB computer program was used to determine the critical tensile stresses due to edge loading in a full-depth concrete pavement and in an existing pavement with bonded overlay. The computed stresses together with the moduli of rupture were then used to prepare the design chart, as shown in Figure 13.14.

In the design chart, three different curves (representing different moduli of rupture of the existing concrete) are shown. Curve 1 is applicable for moduli of rupture

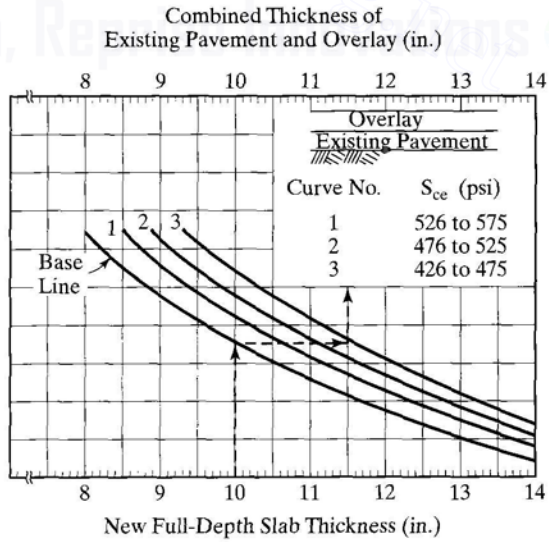


FIGURE 13.14
Design chart for bonded overlay (1 in. = 25.4 mm, 1 psi = 6.9 kPa). (After Tayabji and Okamoto (1985).)

Downloaded From : www.EasyEngineering.net

Downloaded From : www.EasyEngineering.net

from 526 to 575 psi (3.6 to 4.0 MPa), curve 2 from 476 to 525 psi (3.3 to 2.6 MPa), curve 3 from 426 to 475 psi (2.9 to 3.3 MPa). Given the thickness of the full-depth pavement and the curve number, the combined thickness of the existing pavement and the overlay can be read from the chart. The difference between the combined thickness and the thickness of the existing pavement is the overlay thickness required.

To develop the design chart, the moduli of elasticity of the existing concrete corresponding to the three curves were computed by Eq. 13.15 on D values from 6000 to 7000. The moduli of elasticity of the new concrete were assumed to be from 4×10^6 to 5×10^6 psi (28 to 25 GPa), the moduli of rupture from 600 to 650 psi (4.1 to 4.5 MPa).

The chart cannot be applied when the modulus of rupture of the existing concrete is lower than 426 psi (2.9 MPa) or higher than 575 psi (4.0 MPa). When the modulus of rupture is lower than 425 psi (2.9 MPa), the very large thickness required might not warrant the use of a bonded overlay. Furthermore, an existing pavement with such a low modulus of rupture could be in such a distressed condition that the use of an unbonded or directly placed overlay, rather than a bonded overlay, should be considered. For the case when the modulus of rupture of the existing concrete is greater than 575 psi (4.0 MPa), the existing pavement is considered as good as the new pavement, so the overlay thickness required is simply the difference between the full-depth pavement thickness and the existing pavement thickness plus the depth of surface milling or scarification.

It should be noted that the maximum bonded overlay thickness recommended is 5 in. (127 mm). When the bonded overlay thickness exceeds 5 in. (127 mm), the use of a directly placed or unbonded overlay might be more cost effective.

Example 13.10:

An existing concrete pavement is of a thickness 7.5 in. (191 mm) after milling. Tests on a number of cored samples taken from the existing pavement give an average splitting tensile strength of 440 psi (3.0 MPa) and a standard deviation of 50 psi (345 kPa). If the required thickness for a new full-depth pavement is 10 in. (254 mm) and the conditions used to develop the design chart are all satisfied, determine the thickness of the bonded overlay required.

Solution: From Eq. 13.13, $f_{te} = 440 - 1.65 \times 50 = 358$ psi (2.5 MPa). From Eq. 13.14 with a value of 1.45 for constant A, $S_c = 1.45 \times 0.9 \times 358 = 467$ psi (3.2 MPa). From Figure 13.14, the combined thickness of existing pavement and overlay is 11.5 in. (381 mm), so the thickness of bonded overlay = 11.5 − 7.5 = 4 in. (102 mm).

13.5 AASHTO METHOD

The overlay design procedures presented in Chapter 5 of the 1986 AASHTO Design Guide, as described in the first edition of this book, were avoided by most state highway agencies because the determination of the remaining life factor was complex and yielded conflicting results. Elliott (1989) examined the remaining life concept and revealed inconsistencies in overlay designs that use the AASHTO remaining life factor. Further investigation revealed that the remaining life factor should have a value of 1.0 for all overlay situations. He recommended that the AASHTO overlay design approach be

Downloaded From : www.EasyEngineering.net

Downloaded From : www.EasyEngineering.net

revised to exclude remaining life considerations. This recommendation was accepted by AASHTO, and a new design guide was published (AASHTO, 1993) in which chapter 5 was completely revised by not only eliminating the remaining life factor, but also adding more detailed guidelines and documentations to the new guide.

The following abbreviations for pavement are used in this section:

AC:	Asphalt concrete, same as HMA in the rest of this book
PCC:	Portland cement concrete
JPCP:	Jointed plain concrete pavement
JRCP:	Jointed reinforced concrete pavement
CRCP:	Continuous reinforced concrete pavement
AC/PCC:	AC-overlaid Portland cement concrete

13.5.1 Design Concepts

Pavement overlay projects can involve a number of pavement sections with length ranging from a few hundred feet to several miles. A crucial question to be asked at the outset is how to divide the project into analysis sections so that the thickness of overlay for each section can be designed. This concept will be described first, followed by a discussion of the structural deficiency concept.

Design of Overlay along Project There are two approaches to designing an overlay thickness for a project; each has advantages and disadvantages. The designers should select the approach that best fits the specific situations.

Uniform Section Approach The project is divided into sections of various lengths, each with relatively uniform characteristics. Each uniform section is considered independently and overlay design inputs representing the average of the section are obtained. To delineate an overlay length, the historical data should be consulted—construction and maintenance records, types and thicknesses of layer materials, subgrade, traffic, pavement conditions, and so on. If accurate records have been kept, the use of historical data has more merit in delineating unique units than does a procedure that relies on current observations of condition or performance indicators, because changes in one or more design factors are not always evident through observation.

If accurate historical data are not available, the designer must rely upon the analysis of a measured pavement response for unit delineation. Although deflection measurements by NDT are effective as a performance indicator, other responses, such as pavement condition, serviceability, and rut depth, can also be used. A plot of the measured response versus station number along an actual highway system may be used to delineate units using different analytical or statistical methods. This can be done manually or through computerized data analysis–graphics systems.

Point-By-Point Approach Overlay thicknesses are determined for specific points along the uniform design section—for example; every 300 ft (91 m). All required inputs are determined for each point, so that the overlay thickness can be designed. This approach produces a required overlay design thickness for each analysis point

Downloaded From : www.EasyEngineering.net

Downloaded From : www.EasyEngineering.net

along the entire project for a given reliability level. In the selection of one thickness for the uniform section, keep in mind that each overlay thickness has already been increased to account for the design reliability level. Selection of a thickness that is greater than the mean of these values will achieve a higher level of reliability, but might not be warranted. This approach can be used to divide the project into different design sections, or one design thickness may be used for the entire project. Areas having unusually large thicknesses could be targeted for additional field investigation, and extensive repair or reconstruction might be needed before overlay.

Structural Deficiency The overlay design procedures presented here provide an overlay thickness to correct the structural deficiency of a pavement and increase its ability to carry loads over a future design period. Figure 13.15 illustrates the decrease in serviceability and structural capacity of a pavement with the increase in load repetitions, N. Structural capacity, SC, is a general term that can be applied to flexible, rigid, and composite pavements. For flexible pavements, SC is expressed by a structural number, SN; for rigid pavements, by the PCC thickness, D; and for existing composite pavements, by an equivalent slab thickness. The original pavement has an initial serviceability of p_1 and a structural capacity of SC_o. As the number of load applications increases, the pavement gradually deteriorates, and its serviceability and structural capacity decrease. After N_p load repetitions, the pavement reaches an acceptable serviceability level of p_2. At this time, the pavement reaches a structural capacity of

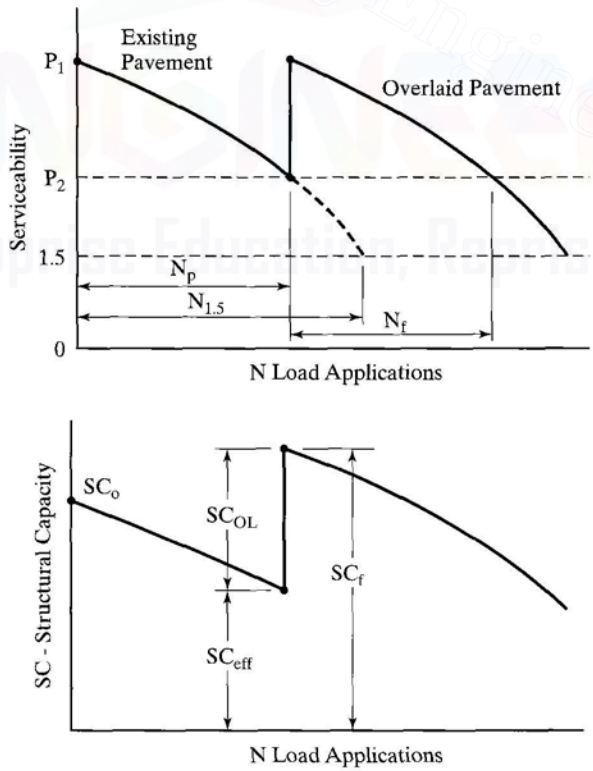


FIGURE 13.15

Effect of traffic on serviceability and structural capacity. (From the AASHTO Guide for Design of Pavement Structures. Copyright 1993. American Association of State Highway and Transportation Officials, Washington, DC. Used by permission.)

Downloaded From : www.EasyEngineering.net

Downloaded From : www.EasyEngineering.net

SC_{eff}, which is called the effective structural capacity of the existing pavement. Note that SC_{eff} is equal to SN_{eff} for flexible pavements, but to D_{eff} for rigid and composite pavements.

To upgrade the pavement condition to the serviceability p_1, additional structural capacity, SC_{OL}, in the form of an overlay is required. The sum of this added structural capacity and the structural capacity of the existing pavement, SC_{eff}, is equivalent to the structural capacity, SC_f, of a new pavement designed for the existing roadbed modulus and the projected future overlay traffic, N_f. Also shown in Figure 13.15 is the number of repetitions, $N_{1.5}$, on the existing pavement that will reduce the serviceability to 1.5. The basic equation for overlay design is

$$(SC_{OL})^n = (SC_f)^n - (SC_{eff})^n \tag{13.18}$$

in which n is a constant that depends on the type of pavement system used in the analysis. For unbonded rigid overlays on rigid pavements, $n = 2$; for all other types of pavements, $n = 1$. The 1986 design guide recommended $n = 1.4$ for partially bonded rigid overlays on rigid pavements, but this case was not included in the 1993 guide.

13.5.2 Evaluation of Effective Structural Capacity

The most difficult part of overlay design is the determination of SC_{eff}. Three alternative methods can be used: visual condition survey and material testing, nondestructive deflection testing, NDT, and remaining life from fatigue damage by traffic. There are uncertainties involved in each method, so the three cannot be expected to provide equivalent estimates. The designers should use all three methods whenever possible and select the best estimate through their own judgment. There is no substitute for experience and judgment.

Visual Survey and Materials Testing A key component in the determination of effective structural capacity is the visual survey of existing pavement conditions, beginning with a review of all available information regarding the design, construction, and maintenance history. This should be followed by a detailed survey to identify the type, amount of severity, and location of surface distresses, as described in Section 9.1. Coupled with the distress survey should be a drainage survey to identify moisture related problems and locations where drainage can be improved to reduce the influence of moisture on the performance of the pavement following the overlay.

Materials testing should include a coring and testing program to verify or identify the cause of the observed surface distress. The location for coring should be selected after the distress survey, to assure that all significant pavement conditions are represented. If NDT is performed, the data from that testing should also be used to help select the appropriate coring sites. Coring can also be used to determine the material thicknesses and conditions. A great deal of information can be obtained simply by a visual inspection of the cored materials. The testing program should aim at determining how the existing materials compare with those used in a new pavement, how the materials have changed since the pavement was constructed, and whether the materials function as expected. The types of tests needed depend on the types of materials and the types of distresses observed. Typical tests include strength tests for AC and PCC

Downloaded From : www.EasyEngineering.net

Downloaded From : www.EasyEngineering.net

cores, gradation tests to identify degradation or contamination of granular materials, and extraction tests to determine binder contents and gradation of AC mixes. PCC cores exhibiting durability problems could be examined by a petrographer to identify the cause of the problem.

Flexible Pavements The condition survey method for determining SN_{eff} involves a component analysis using the structural number equation:

$$SN_{eff} = a_1D_1 + a_2D_2m_2 + a_3D_3m_3 \tag{13.19}$$

This equation is the same as Eq. 11.35 for new pavements, and Table 11.20 can be consulted for selecting drainage coefficients m_2 and m_3. Depending on the types and amounts of deterioration, the layer coefficients assigned to in-service pavements should in most cases be smaller than those originally assigned to the new pavements, except for unbound granular materials that show no sign of degradation or contamination. Some suggested layer coefficients for existing materials are shown in Table 13.7.

TABLE 13.7 Layer Coefficients for Existing AC Pavements

Materials	Surface Condition	Coefficient
AC Surface	Little or no alligator cracking and/or only low-severity transverse cracking	0.35 to 0.40
	<10% low-severity alligator cracking and/or <5% medium- and high- severity transverse cracking	0.25 to 0.35
	>10% low-severity alligator cracking and/or <10% medium-severity alligator cracking and/or >5–10% medium- and high- severity transverse cracking	0.20 to 0.30
	>10% medium-severity alligator cracking and/or <10% high-severity alligator cracking and/or >10% medium- and high- severity transverse cracking	0.14 to 0.20
	>10% high-severity alligator cracking and/or >10% high- severity transverse cracking	0.08 to 0.15
Stabilized Base	Little or no alligator cracking and/or only low-severity transverse cracking	0.20 to 0.35
	<10% low-severity alligator cracking and/or <5% medium- and high- severity transverse cracking	0.15 to 0.25
	>10% low-severity alligator cracking and/or <10% medium-severity alligator cracking and/or >5–10% medium- and high- severity transverse cracking	0.15 to 0.20
	>10% medium-severity alligator cracking and/or <10% high-severity alligator cracking and/or >10% medium- and high- severity transverse cracking	0.10 to 0.20
	>10% high-severity alligator cracking and/or >10% high- severity transverse cracking	0.08 to 0.15
Granular Base or Subbase	No evidence of pumping, degradation, or contamination by fines	0.10 to 0.14
	Some evidence of pumping, degradation, or contamination by fines	0.00 to 0.10

Source. After AASHTO (1993).

Downloaded From : www.EasyEngineering.net

Downloaded From : www.EasyEngineering.net

The following notes apply to Table 13.7:

1. All the distresses are as observed at the pavement surface.
2. Patching all high-severity alligator cracking is recommended. The layer coefficients of the AC surface and stabilized base should reflect the amount of high-severity cracking remaining after patching.
3. In addition to evidence of pumping noted during condition survey, samples of base material should be obtained and examined for evidence of erosion, degradation, contamination by fines, and durability, and layer coefficients should be reduced accordingly.
4. The percentage of transverse cracking is the linear feet of cracking per square foot of pavement, expressed as a percentage.
5. Coring and testing are recommended for the evaluation of all materials, especially stabilized layers.
6. There may be other types of distresses (e.g., surface raveling or stripping of an AC layer, freeze-thaw damage to a cement-treated base) which, in the opinion of the engineer, would affect the performance of the overlay. These should be considered by decreasing the structural coefficient of the layer exhibiting the distress.

Rigid Pavements The effective thickness of the existing slab is computed by the equation

$$D_{eff} = (F_{jc})(F_{dur})(F_{fat})(D) \tag{13.20}$$

in which F_{jc} = joints and cracks adjustment factor, F_{dur} = durability adjustment factor, and F_{fat} = fatigue damage adjustment factor.

The joints and cracks adjustment factor depends on the number of deteriorated transverse joints and cracks per mile and can be determined by Figure 13.16. It is recommended that all deteriorated joints and cracks and any other major discontinuities in the existing slab be full-depth repaired prior to overlay, so $F_{jc} = 1$.

A durability adjustment factor is applied when the existing slab has durability problems, such as "D" cracking or reactive aggregate distress. Suggested durability adjustment factors are shown in Table 13.8.

The fatigue damage adjustment factor is determined by observing the extent of transverse cracking (JPCP, JRCP) and punchouts (CRCP) that could be caused primarily by repeated loading. Suggested fatigue adjustment factors are shown in Table 13.9.

Nondestructive Deflection Testing The NDT procedures used on flexible pavements are different from those used on rigid pavements. For flexible pavements, NDT is used to estimate the roadbed soil resilient modulus and to provide a direct estimate of SN_{eff}. Some agencies apply NDT to backcalculate the moduli of individual layers and then use these moduli to estimate SN_{eff}, but this approach was not recommended in the 1993 guide. For rigid pavements, NDT can be used to examine load transfer efficiency at joints and cracks, determine the effective modulus of subgrade reaction, or k-value, and estimate the modulus of elasticity of the concrete, which provides an estimate of strength.

Flexible Pavements To determine the modulus of the subgrade, the deflection of a sensor far from the load can be used. This is explained in Figure 9.37, where the

Downloaded From : www.EasyEngineering.net

Downloaded From : www.EasyEngineering.net

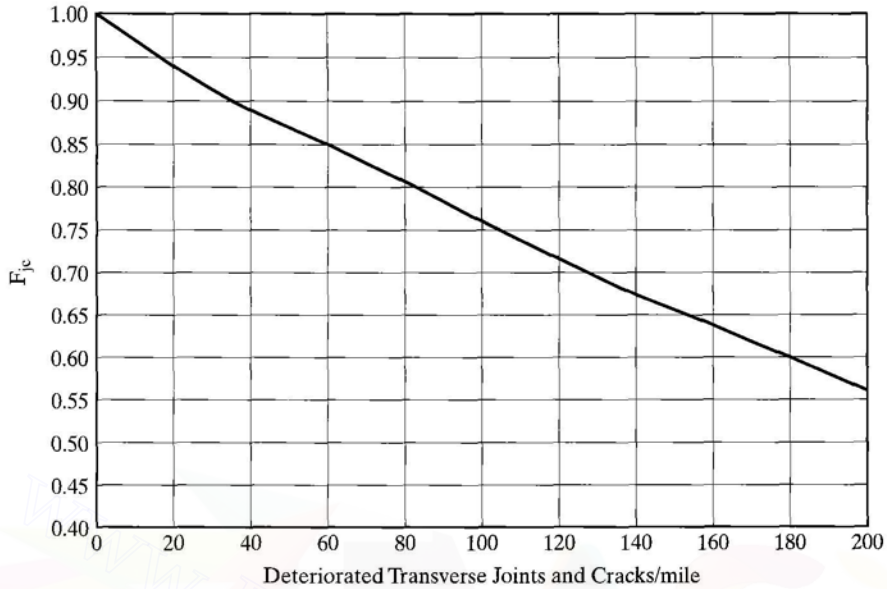


FIGURE 13.16

Joints and cracks adjustment factor F_{jc} (1 mile = 1.6 km). (From the AASHTO Guide for Design of Pavement Structures. Copyright 1993. American Association of State Highway and Transportation Officials, Washington, DC. Used by permission.)

TABLE 13.8 Durability Adjustment Factor for Existing PCC Pavements

Condition	Adjustment Factor
No sign of PCC durability problems	1.00
Some durability cracking but no spalling	0.96 to 0.99
Substantial cracking and some spalling	0.88 to 0.95
Extensive cracking and severe spalling	0.80 to 0.88

Source. After AASHTO (1993).

deflection at sensor 5 depends on the modulus of subgrade only and is independent of the modulus of overlying layers, thus permitting the backcalculation of the subgrade resilient modulus from a single measurement. According to the Boussinesq equation for a homogeneous half space,

$$d_r = \frac{P(1 - v^2)}{\pi r M_R} \tag{13.21}$$

in which d_r = surface deflection at a distance r from the load, P = point load, v = Poisson's ratio, r = distance from the load, and M_R = resilient modulus. Note that Eq. 13.21 is the same as Eq. 5.3 except for the change in notation. The deflection is independent of the size of the load plate, so the total load applied to the plate should

Downloaded From : www.EasyEngineering.net

Downloaded From : www.EasyEngineering.net

TABLE 13.9 Fatigue Adjustment Factor For Existing PCC Pavements

Condition	Adjustment Factor
Few transverse cracks/punchouts (none caused by "D" cracking or reactive aggregate distress) JPCP: <5 percent of slabs cracked JRCP: <25 working cracks per mile CRCP: <4 punchouts per mile	0.97 to 1.00
A significant number of transverse cracks/punchouts (none caused by "D" cracking or reactive aggregates) JPCP: 5–15 percent of slabs cracked JRCP: 25–75 working cracks per mile CRCP: 4–12 punchouts per mile	0.94 to 0.96
A large number of transverse cracks/punchouts (none Caused by "D" cracking or reactive aggregate distress) JPCP: >15 percent of slabs cracked JRCP: >75 working cracks per mile CRCP: >12 punchouts per mile	0.90 to 0.93

Source. After AASHTO (1993).

be used. By assuming a Poisson's ratio of 0.5, the following equation can be used:

$$M_R = \frac{0.24P}{d_r r} \tag{13.22}$$

To account for the difference between the backcalculated M_R and the design M_R, the M_R computed by Eq. 13.22 must be multiplied by an adjustment factor C. AASHTO recommends the use of a C value not greater than 0.33 in the following equation:

$$M_R = C\left(\frac{0.24P}{d_r r}\right) \tag{13.23}$$

The location selected to backcalculate the subgrade modulus must be far enough from the load to eliminate the effect of any layers above but also close enough that the deflection is not too small to be measured accurately. The minimum distance is given by the relationship

$$r = 0.7\sqrt{a^2 + \left\{D\sqrt[3]{\frac{E_p}{M_R}}\right\}^2} \tag{13.24}$$

in which a = radius of load plate, D = total thickness of pavement layers above the subgrade, and E_p = effective modulus of all pavement layers above the subgrade, as described below.

To estimate SN_{eff}, it is necessary to determine E_p first, from the formula

$$\frac{M_R d_0}{qa} = 1.5\left\{\frac{1}{\sqrt{1 + \left[\left(\frac{D}{a}\right)\sqrt[3]{\frac{E_p}{M_R}}\right]^2}} + \frac{1 - \frac{1}{\sqrt{1 + \left(\frac{D}{a}\right)^2}}}{\left(\frac{E_p}{M_R}\right)}\right\} \tag{13.25}$$

Downloaded From : www.EasyEngineering.net

Downloaded From : www.EasyEngineering.net

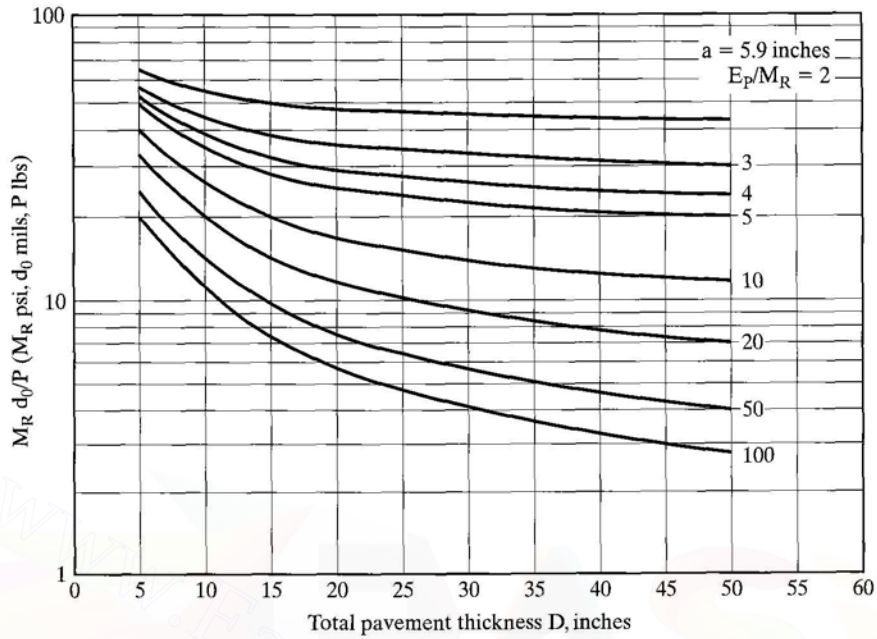


FIGURE 13.17

Chart for determining E_p/M_R, based on Eq. 13.25 (1 in. = 25.4 mm, 1 psi = 6.9 kPa, 1 lb = 4.45 N). (From the AASHTO Guide for Design of Pavement Structures. Copyright 1993. American Association of State Highway and Transportation Officials, Washington, DC. Used by permission.)

in which d_0 = deflection measured at the center of the load plate after adjustment to a standard pavement temperature of 68°F and q = pressure on load plate. Eq. 13.25 is based on a Poisson's ratio of 0.5, with E_p as the only unknown, and can be solved by iteration via a computer or spreadsheet. Figure 13.17 is a chart for determining E_p when a = 5.9 in. (150 mm). If a is not equal to 5.9 in. (150 mm), Eq. 13.25 must be used. Figure 13.18 can be used to determine the temperature adjustment factor for granular or asphalt-treated base, Figure 13.19 for cement- or pozzolanic-treated base. After E_p is determined, SN_{eff} can be computed by

$$SN_{eff} = 0.0045D\sqrt[3]{E_p} \tag{13.26}$$

Equation 13.26 is based on the assumption that the structural number is proportional to the cubic root of the modulus of rigidity, as defined by Eq. 5.11. Using the crushed stone base at the AASHO road test site as a standard with a layer coefficient of 0.14 and an elastic modulus of 30,000 psi (207 MPa), the constant of proportionality is $0.14/(30000)^{1/3} = 0.0045$.

It should be pointed out that a single chart can be easily developed and used for various plate radii, a, if dimensionless terms are used by plotting $M_R d_0/(qa)$ vs D/a. Furthermore, Eq. 13.25 is an approximate solution for a two-layer system developed by Odemark (1949), but not as accurate as Burmister's layered theory presented in Appendix B. Table 13.10 is a comparison between the solutions based on Eq. 13.25 and those computed by KENLAYER and so based on Burmister's theory. It can be seen that the deflections

Downloaded From : www.EasyEngineering.net

Downloaded From : www.EasyEngineering.net

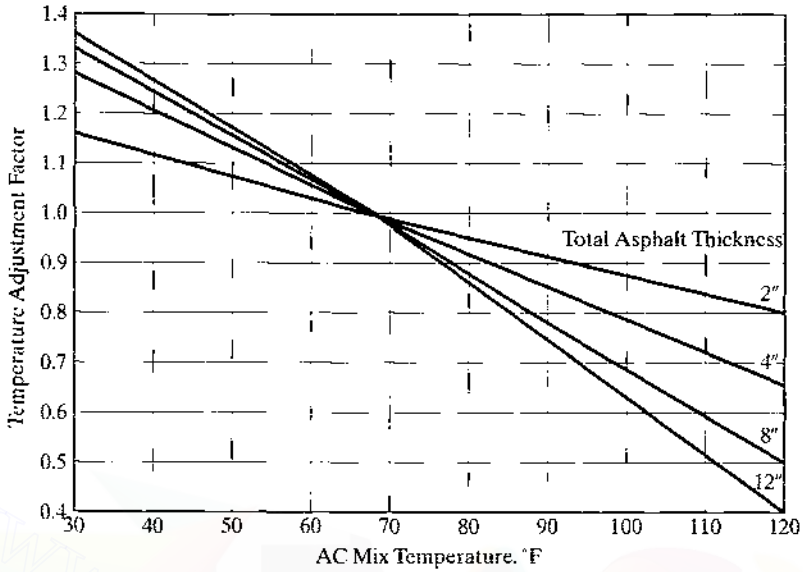


FIGURE 13.18

Adjustment of d_0 for asphalt pavement with granular or asphalt-treated base (1 in. = 25.4 mm). (From the AASHTO Guide for Design of Pavement Structures. Copyright 1993. American Association of State Highway and Transportation Officials, Washington, DC. Used by permission.)

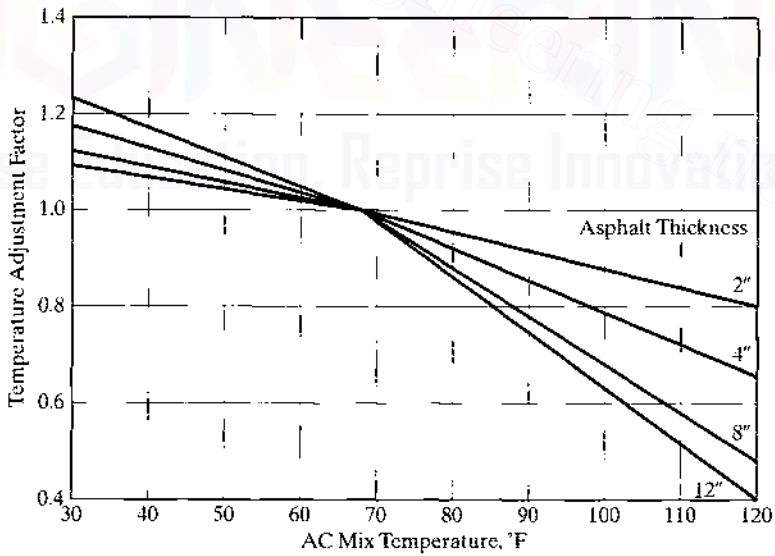


FIGURE 13.19

Adjustment of d_0 for asphalt pavement with cement- or pozzolanic-treated base (1 in. = 25.4 mm). (From the AASHTO Guide for Design of Pavement Structures. Copyright 1993. American Association of State Highway and Transportation Officials, Washington, DC. Used by permission.)

Downloaded From : www.EasyEngineering.net

Downloaded From : www.EasyEngineering.net

TABLE 13.10 Comparison of Dimensionless Deflection $M_R d_0/(qa)$

	Modulus ratio E_p/M_R								
	2			10			100		
$\frac{D}{a}$	Eq.13.25	KENLAYER	Percent	Eq.13.25	KENLAYER	Percent	Eq.13.25	KENLAYER	Percent
1	1.152	1.184	97.3	0.675	0.730	92.5	0.320	0.353	90.7
5	0.838	0.851	98.5	0.259	0.276	93.8	0.077	0.083	92.5
10	0.794	0.801	99.1	0.205	0.213	96.2	0.046	0.054	85.2

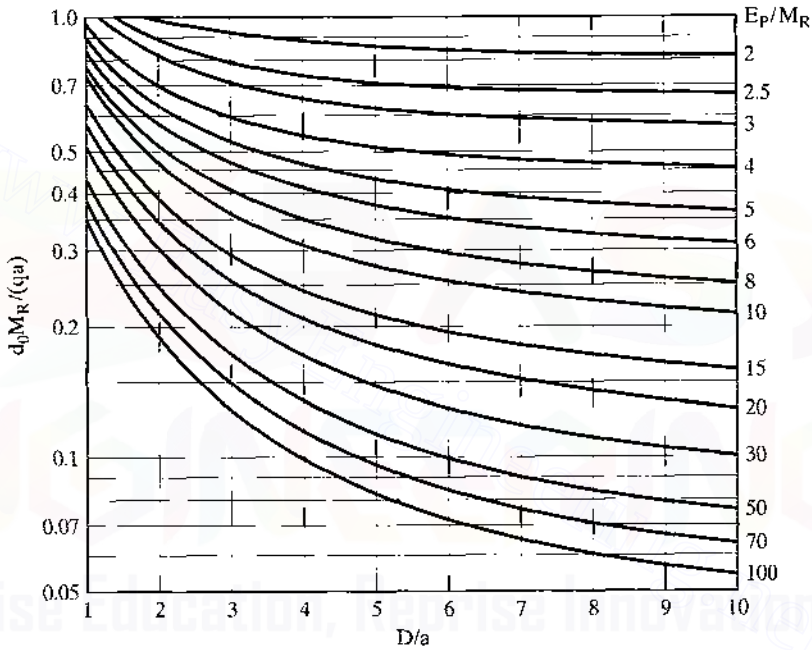


FIGURE 13.20

Chart for determining E_p/M_R, based on Burmister's Two-Layer Theory.

computed by Eq. 13.25 range from 85.2 to 99.1 percent of those computed by KENLAYER. The discrepancy between the two methods increases as the modulus ratio, E_p/M_R, increases. Figure 13.20 is a chart for determining E_p/M_R, based on KENLAYER and using dimensionless ratios. This chart is similar to Figure 2.17, but the maximum-modulus ratio is reduced to 100, with finer divisions for more accurate interpolation.

Example 13.11:

An NDT test was made on a flexible pavement using a 5.9 in. (150 mm) load plate. The thickness of AC is 4.25 in. (108 mm) and that of granular base is 8 in. (203 mm). The temperature of AC at the time of the test is 80°F. The total load applied on the plate is 9000 lb (40 kN). The deflection at the center of plate is 0.0139 in., or 13.9 mil (0.35 mm); that at a distance of 36 in. (0.91 m) is 0.00355 in. (0.09 mm). Estimate M_R and SN_{eff}.

Downloaded From : www.EasyEngineering.net

Downloaded From : www.EasyEngineering.net

Solution: From Eq. 13.22, $M_R = (0.24 \times 9000)/(0.00355 \times 36) = 16{,}900$ psi (117 MPa). Note that this is the modulus backcalculated from NDT, which must be multiplied by an adjustment factor of not greater than 0.33 to get the effective resilient modulus for use with the AASHTO equations and charts. Assuming that $C = 0.33$, from Eq. 13.23, $M_R = 0.33 \times 16{,}900 = 5580$ psi (38.5 MPa). With AC temperature of 80°F and AC thickness of 4.25 in. (108 mm), from Figure 13.18, the temperature adjustment factor for d_0 is 0.92, so $d_0 = 0.92 \times 0.0139 = 0.0128$ in. (0.33 mm). With $(M_R d_0)/P = (16900 \times 12.8)/9000 = 24.0$ and $D = 4.25 + 8 = 12.25$ in. (311 mm), from Figure 13.17, $E_p/M_R = 8.5$, or $E_p = 8.5 \times 16{,}900 = 143{,}650$ psi (991 MPa). From Eq. 13.26 $SN_{eff} = 0.0045 \times 12.25 \times (143{,}650)^{1/3} = 2.88$. The placement of the sensor at a distance of 36 in. (0.91 m) is sufficient, because it exceeds the minimum distance computed by Eq. 13.24, $r = 0.7 \times \{(5.9)^2 + [12.25 \times (8.5)^{1/3}]^2\}^{0.5} = 17.98$ in. (457 mm).

It is interesting to see the difference in E_p if Figure 13.20 is used. With $q = 9000/[\pi \times (5.9)^2] = 82.3$ psi (567 kPa), $M_R d_0/(qa) = (16{,}900 \times 0.0128)/(82.3 \times 5.9) = 0.45$, and $D/a = 12.25/5.9 = 2.08$, from Figure 13.20, $E_p/M_R = 10.0$, or $E_p = 10.0 \times 16{,}900 = 169{,}000$ psi (1.16 GPa), which is slightly greater than the 143,650 psi (991 MPa) obtained by Figure 13.17.

Rigid Pavements To examine the load transfer efficiency at joints and cracks, the load plate is placed on one side of the joint with the edge of the plate tangent to the joint. The deflections at two points, one at the center of the plate and the other at 12 in. (305 mm) from the center on the other side of the joint, are measured, and the load transfer efficiency is computed as

$$\Delta LT = 100B\left(\frac{\Delta_{ul}}{\Delta_l}\right) \tag{13.27}$$

in which ΔLT = deflection load transfer in percent, Δ_{ul} = unloaded side deflection, Δ_l = loaded side deflection, and B = slab bending correction factor, which is necessary because the deflections d_0 and d_{12} are not equal, even at the interior of the slab with no joints and cracks, so a correction factor of d_0/d_{12} measured in the interior of the slab must be applied at the joint. Typical values for B are between 1.05 and 1.15. The values of ΔLT are related to the load transfer coefficient J: if $\Delta LT > 70$, $J = 3.2$; if $\Delta LT = 50 - 70$, $J = 3.5$; and if $\Delta LT < 50$, $J = 4.0$.

The procedures for determining the effective modulus of subgrade reaction, k, and the elastic modulus of concrete, E_c, are similar to the ILL-BACK program described in Section 9.4.3. However, instead of going through the radius of relative stiffness, Figure 13.21 can be used directly to determine k and Figure 13.22 to determine E_c. The deflection basin area, AREA, used in these charts is similar to what is seen in Eq. 9.45 and can be rewritten as

$$AREA = 6\left[1 + 2\left(\frac{d_{12}}{d_0}\right) + 2\left(\frac{d_{24}}{d_0}\right) + \left(\frac{d_{36}}{d_0}\right)\right] \tag{13.28}$$

in which d_{12}, d_{24}, and d_{36} are deflections measured at 12, 24, and 36 in. (3.04, 6.10, and 9.14 m), respectively, from the plate center. Note that the k-value obtained from the

Downloaded From : www.EasyEngineering.net

Downloaded From : www.EasyEngineering.net

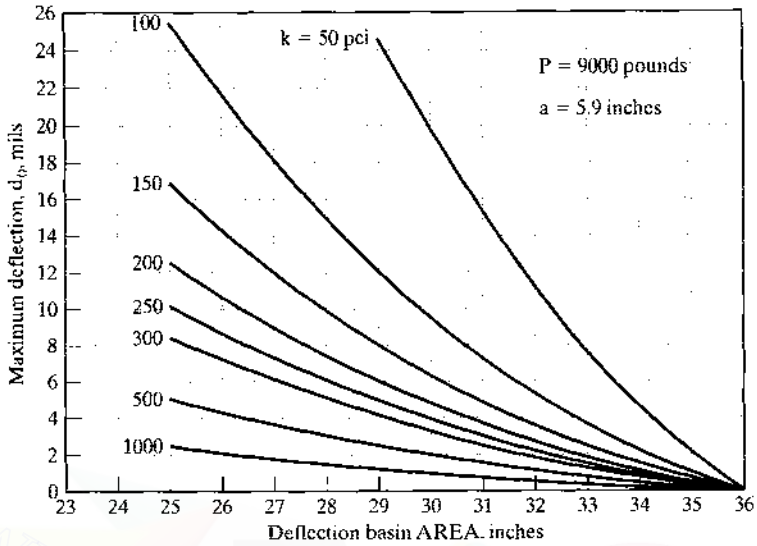


FIGURE 13.21

Determination of dynamic k-value from d_0 and AREA (1 in. = 25.4 mm, 1 lb = 4.45 N, 1 pci = 271.3 kN/m^3). (From the AASHTO Guide for Design of Pavement Structures. Copyright 1993, American Association of State Highway and Transportation Officials, Washington, DC. Used by permission.)

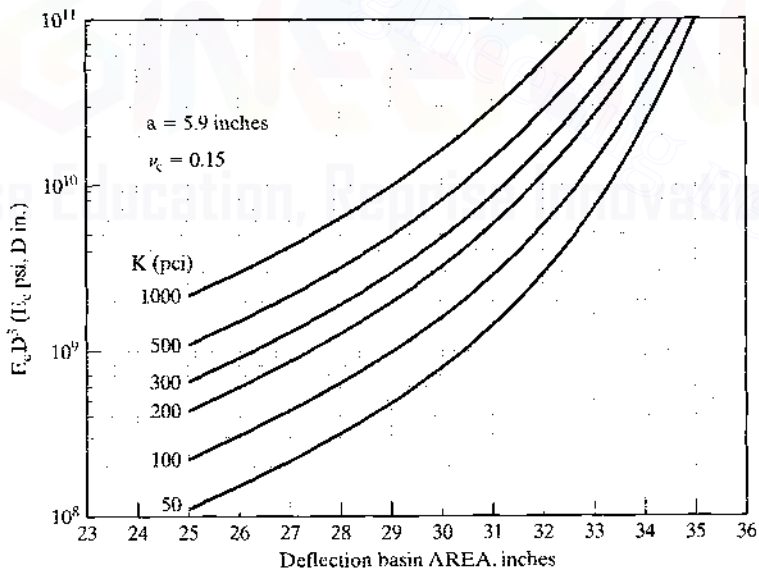


FIGURE 13.22

Determination of PCC modulus from k-value, AREA, and slab thickness. (1 in. = 25.4 mm, 1 lb = 4.45 N, 1 psi = 6.9 kPa, 1 pci = 271.3 kN/m^3). (From the AASHTO Guide for Design of Pavement Structures. Copyright 1993, American Association of State Highway and Transportation Officials, Washington, DC. Used by permission.)

Downloaded From : www.EasyEngineering.net

Downloaded From : www.EasyEngineering.net

chart is the dynamic k-value, whereas the k-value to be used with the AASHTO design equation and chart is the static k-value. The following relationship may be used for the conversion:

$$\text{Static } k\text{-value} = \frac{\text{Dynamic } k\text{-value}}{2} \tag{13.29}$$

Example 13.12:

Much as in example 9.4, determine the dynamic k-value and E_c by Figures 13.21 and 13.22.

Solution: In Example 9.4, $d_0 = 0.003$ in. = 3 mil (0.076 mm) and AREA = 31.0 in. (787 mm). From Figure 13.21, $k = 210$ pci (57 MN/m^3), which is the same as Example 9.4(a). With AREA = 31.0 in. (787 mm) and $k = 210$ pci (57 MN/m^3), from Figure 13.22, $E_c D^3 = 6 \times 10^9$. Since $D = 10$ in. (25 mm), $E_c = 6 \times 10^9/10^3 = 6 \times 10^6$ psi (41 GPa), which checks with the 5.7×10^6 (39 GPa) obtained in Example 9.4(a).

Remaining Life after Fatigue Damage by Traffic To compute the remaining life, the actual traffic in 18-kip ESAL the pavement has carried to date and the total traffic the pavement could be expected to carry to failure, as indicated respectively by N_p and $N_{1.5}$ in Figure 13.15, must be determined first. N_p may be estimated by the pavement design equations or nomographs in Section 11.3 or 12.3. To be consistent with the AASHTO Road Test and the development of these equations, a failure PSI equal to 1.5 and a reliability of 50 percent are recommended. The remaining life, RL in percent, can then be computed by

$$\text{RL} = 100\left(1 - \frac{N_p}{N_{1.5}}\right) \tag{13.30}$$

With RL known, a condition factor, CF, can be obtained from Figure 13.23, and the effective structural capacity can be calculated as

$$\text{SC}_{\text{eff}} = \text{CF} \times \text{SC}_{\text{o}} \tag{13.31}$$

Example 13.13:

A 10-in. (254-mm) concrete pavement with an initial PSI of 4.5 has been subjected to 14.5 million 18-kip (80-kN) ESAL before being overlaid. Given that $k = 72$ pci (19.5 MN/m^3), $E_c = 5 \times 10^6$ psi (34.5 GPa), $S_c = 650$ psi (4.5 MPa), $J = 3.2$, and $C_d = 1.0$, determine the effective structural capacity of the pavement by the remaining life approach.

Solution: With $N_p = 14{,}500{,}000$, it is now necessary to determine $N_{1.5}$. The data given in this example are the same as those in Example 12.6, except that, for failure to occur, $\Delta\text{PSI} = 4.5 - 1.5 = 3.0$, instead of 1.7, and R = 50%, instead of 95%. $N_{1.5}$ can be determined from Figure 12.17 by the following steps:

Downloaded From : www.EasyEngineering.net

Downloaded From : www.EasyEngineering.net

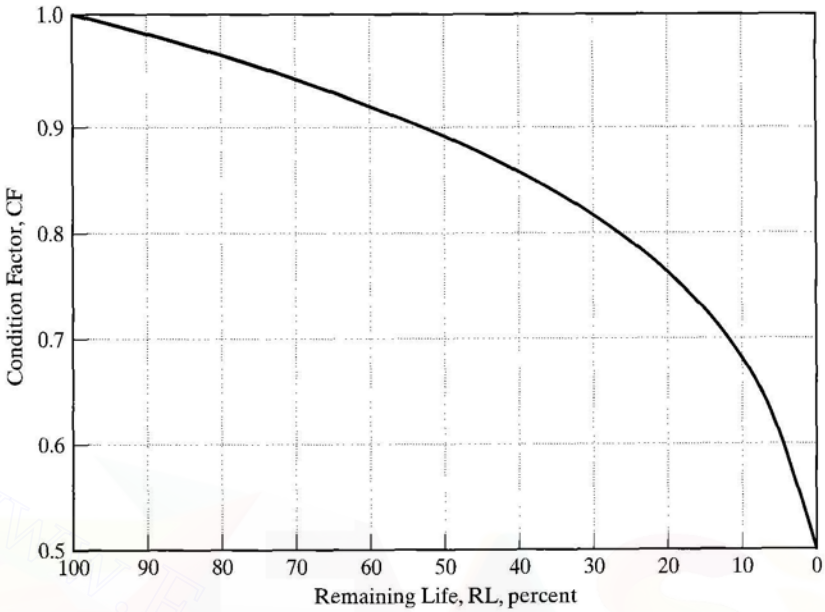


FIGURE 13.23

Relationship between condition factor and remaining life. (From the AASHTO Guide for Design of Pavement Structures. Copyright 1993. American Association of State Highway and Transportation Officials, Washington, DC. Used by permission.)

1. Same as Example 12.6.
2. Starting at 74 on the match line in Figure 12.17b, a line is drawn through $\Delta PSI = 3.0$ until it intersects the vertical axis, then turns horizontally until it intersects $D = 10$ in. (254 mm), and finally turns vertically until it intersects the horizontal axis.
3. From the reliability scale with $R = 50\%$, a line is drawn parallel and over the overall standard deviation scale until it intersects the TL line.
4. The intersection of a line connecting the last two points, the one in step 2 and the other in step 3, with the ESAL scale gives $N_{1.5} = 28$ millions.

A more accurate ESAL can be obtained from Eq. 12.21, or $\log N_{1.5} = 7.35 \log (10 + 1) - 0.06 + (4.22 - 0.32 \times 1.5) \log\{[(650 \times 1)/(215.63 \times 3.2)][(10)^{0.75} - 1.132]/[(10)^{0.75} - 18.42/(5 \times 10^6/72)^{0.25}]\} = 7.654 - 0.06 - 0.096 = 7.498$ or $N_{1.5} = 31{,}500{,}000$. From Eq. 13.30, $RL = 100(1 - 14.5/31.5) = 0.54$. From Figure 13.22, $CF = 0.9$. From Eq. 13.31, $D_{eff} = 0.9 \times 10 = 9$ in. (229 mm).

13.5.3 Future Structural Capacity Analysis

The major objective of future structural capacity analysis is to determine the total structural capacity of a new pavement required to carry N_f load repetitions during the overlay design period, as shown by SC_f in Figure 13.15. In other words, this step is simply a new pavement design for either a flexible or rigid pavement system based on the existing subgrade or foundation conditions. Consequently, the design procedures for

Downloaded From : www.EasyEngineering.net

Downloaded From : www.EasyEngineering.net

new pavements, as discussed in Section 11.3 or 12.3, can be used. However, some design factors, which may be slightly different from new construction, are discussed below.

Traffic Analysis The purpose of traffic analysis is to determine the 18-kip (80-kN) ESALs expected over the design life of the overlay in the design lane. The estimated ESALs must be calculated by using the appropriate equivalent factors for flexible or rigid pavements. Flexible pavement equivalent factors should be used if all layers are flexible with no any workable PCC layer underneath. Rigid pavement equivalent factors should be used if the overlay is PCC or if the existing pavement has a PCC layer that is not subjected to break and seat or rubblized procedures before overlay. This principle is based on the predominant effect of PCC over AC. If there is a PCC layer in the existing pavement, its effective structural capacity should be in terms of PCC thickness, D, so the future structural capacity should also be in terms of D, so that the structural deficiency, $D_f - D_{\text{eff}}$, can be determined. If AC is used for the overlay, this deficiency in PCC thickness can be converted to AC thickness by a conversion factor to be discussed later.

An approximate relationship exists between flexible pavement and rigid pavement equivalent factors. A factor of 0.67 can be used to convert rigid pavement ESALs to flexible pavement ESALs. For example, 15 million rigid pavement ESALs equal 10 million ESALs. Similarly, a factor of 1.5 can be used to convert flexible pavement ESALs to rigid pavement ESALs. Failure to use the correct type of ESALs will result in significant errors in the overlay design. Methods for traffic computations are presented in Chapter 6.

Subgrade The methods used for new pavements to determine the effective resilient modulus, M_R, or the effective modulus of subgrade reaction, k, can also be used for overlay design. However, if as-constructed soil data are used, their properties may have changed since construction, due to changes in moisture content or other factors.

If NDT procedures are used, the methods for calculating M_R or the k-value vary with the types of overlay and existing pavement as follows:

1. If both the overlay and the existing pavement are AC, use NDT for flexible pavements, as described in Section 13.5.2, to backcalculate M_R by Eq. 13.23.
2. If the existing pavement is PCC or AC/PCC, regardless of whether the overlay is AC or PCC, use NDT for rigid pavements, as described in Section 13.5.2, to backcalculate dynamic k-value by Figure 13.21. The dynamic k-value should be divided by 2 to obtain the static value for use in thickness design.
3. If the overlay is PCC and the existing pavement is AC or fractured PCC, use NDT for flexible pavements, as described in Section 13.5.2, to backcalculate M_R by Eq. 13.23 and E_p by Figure 13.17. Then, by considering E_p as E_{SB} and D as D_{SB}, the dynamic k-value can be found from Figure 12.18.

Reliability An overlay may be designed for different levels of reliability, as described in Section 11.3.1 for new pavements. However, reliability level has a large effect on overlay thickness. Varying reliability level to determine SN_f or D_f between 65 to 99 percent may yield a difference in overlay thickness of 6 in. (152 mm) or more. Based on field testing, it appears that a design reliability level of 95 percent and an overall standard deviation of 0.49 for any type of AC overlay and of 0.39 for any type of PCC overlay give overlay thicknesses consistent with those recommended for most projects by state highway agencies.

Downloaded From : www.EasyEngineering.net

Downloaded From : www.EasyEngineering.net

TABLE 13.11 Seven Cases of Overlay Design

Type of Overlay	Type of Existing Pavement	SC		NDT		Determination of SC_{eff}		
		SN	D	M_R	k	NDT	Condition Survey	Remaining Life
AC	AC	x		x		x	x	x
AC	Fractured PCC	x		x			x	
AC	PCC		x		x		x	x
AC	AC/PCC		x		x		x	
Unbonded PCC	PCC or AC/PCC		x		x		x	x
bonded PCC	PCC		x		x		x	x
PCC	AC		x	x				

Although the above values of standard deviations are the same as those recommended for new pavements, It should be pointed out that some sources of uncertainty for overlay design are different from those for new pavement design, thus requiring different overall standard deviations. The appropriate value may change with the overlay type and the uncertainty in evaluating SN_{eff} or D_{eff}. Some sources of variation, such as the estimation of future traffic, may be smaller in overlay design than in new pavement design. The use of a point-by-point approach should also result in a smaller standard deviation than that of the uniform section approach. To better establish the standard deviations for overlay design, additional research is needed.

13.5.4 Overlay Design Methodology

The 1993 AASHTO design guide discussed seven cases of overlays. Step-by-step procedures for each case were described, including feasibility, preoverlay repair, reflection crack control, subdrainage, and thickness design. These procedures were repeated for each case, even though many of them were about the same. In this book, only topics directly related to the thickness design are included, and procedures common to two or more cases are presented in the previous sections, so that they need not be repeated in a later section. Table 13.11 lists the seven cases of overlay design, indicating whether structural capacity is expressed as SN or D, whether NDT is used to determine M_R or k, and which methods can be used to determine SC_{eff}. These subjects have been discussed previously and are summarized in the table.

Some comments on Table 13.11:

1. As a general rule, when SC is defined by SN, NDT is used to determine M_R, whereas when SC is defined by D, NDT is used to determine k. The only exception is in the case of PCC overlay of AC pavement, where M_R and E_p are determined by NDT and then used to determine k by Figure 12.18.
2. When NDT is used to determine M_R, it is customary to determine E_p at the same time. For AC overlay of AC pavement, E_p is used directly to compute SN_{eff} by Eq. 13.26; for AC overlay of fractured PCC pavement, a comparison of E_p determined both before and after fracturing will insure that the PCC pavement has

Downloaded From : www.EasyEngineering.net

Downloaded From : www.EasyEngineering.net

been fractured sufficiently; and for PCC overlay of AC pavement, E_p is used to determine k.

3. When NDT is used to determine k, the elastic modulus of the slab, E_c, is also determined. E_c is not used directly to determine D_{eff}, but it can be used to estimate the modulus of rupture, S_c, by Eq. 7.56a.
4. To determine SC_{eff}, the only method applicable to all cases is the condition survey, and the only case to which all three methods can be applied is the AC overlay of existing AC pavement.
5. Flexible pavement ESALs should be used when SC = SN; rigid pavement ESALs should be used when SC = D.

In this section, each of the seven cases of overlay design will be discussed first, followed by a practical example. These examples are selected from a final report prepared for NCHRP by Darter *et al.* (1991a), in which a total of 74 examples were developed using actual in-service pavements located throughout the United States in five different regions identified as NE, SE, MW, NW, and SW. Except in Example 13.14, where all three methods were used to determine SN_{eff}, only the condition survey method was used in all the examples. To get more accurate results, the unknowns were solved directly from the original equations, instead of by using design charts. To save space and avoid confusion, these examples are presented in a different style. Instead of giving all the design data first and then the solution, the data are presented in groups just before a given item is computed. Note also that only English units are used.

AC Overlay of AC Pavement The required thickness of asphalt overlay, D_{OL}, can be determined as

$$D_{\text{OL}} = \frac{SN_{\text{OL}}}{a_{\text{OL}}} = \frac{SN_f - SN_{\text{eff}}}{a_{\text{OL}}} \tag{13.32}$$

in which a_{OL} = structural layer coefficient of the overlay material. It is suggested that all three methods, if available, be used to evaluate SN_{eff} and that the most appropriate value be selected, based on the engineering judgment of the designer and the past experience of the agency.

Example 13.14:

AC overlay of conventional AC pavement (NW1)

Existing pavement: AC surface 4.25 in., granular base 8 in., M_R = 5634 psi (by NDT, sandy silt, sandy gravel).

Find SN_f: N_f = 2,400,000 (flexible ESALs), R = 95%, S_o = 0.45, p_1 = 4.2, p_2 = 2.5, SN_f = 4.69 (by Eq. 11.37 using trial and error).

Find SN_{eff} by NDT: SN_{eff} = 2.88 (see Example 13.11).

Find SN_{eff} by condition survey: a_1 = 0.35, a_2 = 0.14 (see Table 13.7), m_1 = 1.00, m_2 = 1.00, $SN_{\text{eff}} = 0.35 \times 4.25 + 0.14 \times 8 = 2.61$ (by Eq. 13.19).

Downloaded From : www.EasyEngineering.net

Downloaded From : www.EasyEngineering.net

Find SN_{eff} by remaining life method: N_p = 400,000, a_1 = 0.44, a_2 = 0.14, SN = (0.44 × 4.25 + 0.14 × 8) = 2.99, R = 50%, p_1 = 4.2, p_2 = 1.5, $N_{1.5}$ = 1,140,161 (by Eq. 11.37). From Eq. 13.30, RL = 100(1 − 400,000/1,140,161) = 65. From Figure 13.23, CF = 0.93 or SN_{eff} = 0.93 × 2.99 = 2.78 in.

Find D_{OL}: It can be seen that the values of SN_{eff} by the three methods are not very much different. This is a coincidence, because in many cases they vary a great deal. If the smallest SN_{eff}, 2.61, is used, with a_{OL} = 0.44, from Eq. 13.32, D_{OL} = (4.69 − 2.61)/0.44 = 4.73 in. of AC.

AC Overlay of Fractured PCC Pavement This case covers AC overlay of PCC pavement that has been fractured by any of the following techniques: break/seat, crack/seat, and rubblize/compact.

Break/seat consists of breaking a JRCP into pieces larger than about 1 ft (0.3 m), rupturing the reinforcement or breaking its bond with the concrete, and seating the pieces firmly into the foundation.

Crack/seat consists of cracking a JPCP into pieces typically 1 to 3 ft (0.3 to 0.9 m) in size and seating the pieces firmly into the foundation. Seating typically consists of several passes of a 35- to 50- ton rubber-tired roller over a cracked or broken slab.

Rubblize/compact consists of completely rupturing any type of PCC slab, including JPCP, JRCP, or CRCP, into pieces smaller than 1 ft and then compacting the layer, typically with a 10-ton vibratory roller.

The same equation as Eq. 13.32 is used to determine the thickness of asphalt overlay. Although NDT can be used to evaluate M_R for the determination of SN_f, it cannot be used to evaluate SN_{eff}. The only method used to evaluate SN_{eff} is the component analysis given as

$$SN_{eff} = a_2 D_2 m_2 + a_3 D_3 m_3 \tag{13.33}$$

in which D_2, D_3 = thicknesses of fractured slab and base layers; a_2, a_3 = corresponding structural layer coefficients; and m_2, m_3 = corresponding drainage coefficients. Table 11.20 can be used as a guide for determining m_3. Because of the lack of information on drainage characteristics of fractured concrete, a default value of 1.0 for m_2 is recommended. Table 13.12 shows the suggested layer coefficients for fractured slab pavements.

Example 13.15:

AC overlay of break/seat JRCP (MW-4)

Existing pavement: rubblized PCC 8 in., granular subbase 6 in., M_R = 3090 psi (by NDT, A-6, from NDT E_p = 1,045,416 psi).

Find SN_f: N_f = 318,000 (20 years, flexible ESALs), R = 95%, S_o = 0.49, p_1 = 4.5, p_2 = 2.5 SN_f = 4.13 (by Eq. 11.37 using trial and error).

Find SN_{eff} by condition survey: a_2 = 0.25, a_3 = 0.14 (see Table 13.12), m_2 = 1.00, m_3 = 1.00, SN_{eff} = 0.25 × 8 + 0.14 × 6 = 2.84 (by Eq. 13.33).

Find D_{OL}: a_1 = 0.44, from Eq. 13.32, D_{OL} = (4.13 − 2.84)/0.44 = 2.93 in. of AC.

Downloaded From : www.EasyEngineering.net

Downloaded From : www.EasyEngineering.net

TABLE 13.12 Suggested Layer Coefficients for Fractured Pavements

Material	Slab Condition	Coefficient
Break/Seat JRCP	Pieces greater than 1 ft with ruptured reinforcement or steel/concrete bond broken	0.20 to 0.35
Crack/Seat JPCP	Pieces 1 to 3 ft	0.25 to 0.35
Rubblized PCC	Completely fractured slab with pieces <1 ft	0.14 to 0.30
Base/subbase Granular and stabilized	No evidence of degradation or intrusion of fines	0.10 to 0.14
	Some evidence of degradation and intrusion of fines	0.00 to 0.10

Source. After AASHTO (1993).

AC Overlay of PCC Pavement The required thickness of bonded PCC overlay can be determined simply as

$$D_{OL} = D_f - D_{eff} \tag{13.34}$$

in which D_{OL} is the thickness of PCC. If the overlay is AC, the required PCC thickness must be converted to an equivalent AC thickness by

$$D_{OL} = A(D_f - D_{eff}) \tag{13.35}$$

in which A = factor to convert PCC thickness to AC overlay thickness.

To investigate what A factor should be used in design of overlays of PCC pavements, the BISAR elastic layer program was used to compute stresses in PCC slabs with a range of bonded PCC overlay deficiencies and AC overlay thicknesses. The A factor is the ratio between the AC overlay thickness and the bonded AC overlay thickness when both types of overlay produce the same tensile stress at the bottom of the base slab. It was found that this A factor is a function of the PCC thickness deficiency and can be computed as

$$A = 2.2233 + 0.0099(D_f - D_{eff})^2 - 0.1534(D_f - D_{eff}) \tag{13.36}$$

in which D_{eff} can be computed by Eq. 13.20.

Example 13.16:

AC overlay of existing JRCP (NE-7)

Existing pavement: slab 10 in., subgrade k = 150 pci (CBR = 5, see Figure 7.36)

Find D_f: N_f = 10,050,000 (10 years, rigid ESALs), R = 95%, S_o = 0.35, p_1 = 4.2, p_2 = 3.0, J = 3.2, C_d = 1.00, $E_c = 4 \times 10^6$ psi, S_c = 650 psi, D_f = 11.40 in. (by Eq. 12.21).

Find D_{eff} by condition survey: F_{jc} = 0.95 (see Figure 13.16), F_{dur} = 0.98 (see Table 13.8) F_{fat} = 0.98 (see Table 13.9), $D_{eff} = 0.95 \times 0.98 \times 0.98 \times 10$ = 9.12 in.

Downloaded From : www.EasyEngineering.net

Downloaded From : www.EasyEngineering.net

Find D_{OL}: If the overlay is PCC instead of AC, from Eq. 13.34, $D_{OL} = 11.40 - 9.12 = 2.28$ in. of PCC. If the overlay is AC, from Eq. 13.36, $A = 1.93$. From Eq. 13.35, $D_{OL} = 1.93 \times 2.28 = 4.4$ in. of AC.

AC Overlay of AC/PCC Pavement Eqs. 13.35 and 13.36 can also be used for existing composite pavements, to determine the thickness of overlay. However, D_{eff} is computed as

$$D_{eff} = (F_{jc})(F_{dur})(D_{pcc}) + (D_{ac}/2)F_{ac} \tag{13.37}$$

in which D_{pcc} = thickness of existing PCC slab, F_{ac} = AC quality adjustment factor, and D_{ac} = thickness of existing AC surface. In the equation, the A factor to convert AC thickness to PCC thickness is assumed to be 2.

The joints and cracks adjustment factor, F_{jc}, can be determined from Figure 13.16, based on the total number of unrepaired deteriorated reflection cracks, punchouts, and other discontinuities per mile. The durability adjustment factor, F_{dur}, can be determined from Table 13.13.

The AC quality adjustment factor, F_{ac}, is based on the quality of the existing AC material and can be determined by Table 13.14. The value selected should depend only on distresses related to the AC layer, such as rutting, stripping, shoving, weathering, and raveling, if they are not removed by surface milling. Consideration should be given to complete removal of a poor-quality AC layer. If the AC surface is to be milled prior to overlay, the AC thickness remaining after milling should be used in determining D_{eff}.

TABLE 13.13 Durability Adjustment Factor for Existing AC/PCC Pavements

Condition	Adjustment Factor
No evidence or history of PCC durability problems	1.00
Pavement known to have PCC durability problems but no localized failures or related distress	0.96 to 0.99
Some durability distress and localized failures visible at pavement edge	0.88 to 0.95
Extensive durability distress and localized failures	0.80 to 0.88

Source. After AASHTO (1993).

TABLE 13.14 AC Quality Adjustment Factor for Existing AC/PCC Pavements

Condition	Adjustment Factor
No AC material distress	1.00
Minor AC material distress (weathering, raveling) not corrected by surface milling	0.96 to 0.99
Significant AC material distress (rutting, stripping, Shoving)	0.88 to 0.95
Severe AC material distress (rutting, stripping, shoving)	0.80 to 0.88

Source. After AASHTO (1993).

Downloaded From : www.EasyEngineering.net

Downloaded From : www.EasyEngineering.net

However, no adjustment need be made to D_{eff} if the depth of milling does not exceed the minimum necessary to remove surface ruts.

When NDT is performed on composite pavements to determine the dynamic subgrade k-value and the PCC modulus, the compression of AC under the loading plate must be estimated and deducted from the measured d_0. This compression depends both on the thickness and elastic modulus of AC and on the interface bonding condition between AC and PCC. Procedures for estimating this compression were described in the 1993 design guide and are not repeated here.

Example 13.17:

AC overlay of existing AC/JRCP (MW-15)

Existing pavement: $D_{\text{ac}} = 3$ in., $D_{\text{pcc}} = 10$ in., static k-value $= 164$ pci (by NDT).

Find D_f: $N_f = 10{,}000{,}000$ (20 years, rigid ESALs), $R = 95\%$, $S_o = 0.39$, $p_1 = 4.5$, $p_2 = 2.5$, $J = 3.2$, $C_d = 1.00$, $E_c = 2.7 \times 10^6$ psi (by NDT), $S_c = 606$ psi (by Eq. 7.56a), $D_f = 10.92$ in. (by Eq. 12.21 using trial and error).

Find D_{eff} by condition survey: $F_{\text{jc}} = 0.90$ (50 unrepaired areas per mile), $F_{\text{dur}} = 0.90$ (localized failures from "D" cracking), $F_{\text{ac}} = 0.95$ (fair AC mixture), thickness of AC to be milled $= 0.5$ in., $D_{\text{ac}} = 3 - 0.5 = 2.5$ in. From Eq. 13.37, $D_{\text{eff}} = 0.9 \times 0.9 \times 10 + (2.5/2) \times 0.95 = 9.29$ in.

Find D_{OL}: From Eq. 13.36, $A = 2.00$. From Eq. 13.35, $D_{\text{OL}} = 2.00 \times (10.92 - 9.29) = 3.26$ in. of AC.

Bonded PCC Overlay of PCC Pavement The thickness design procedure for bonded PCC overlay of PCC pavement is almost exactly the same as that for AC overlay of PCC pavement, but without the final step to convert PCC thickness to equivalent AC thickness. Therefore, Eq. 13.34 and Example 13.16 for AC overlay of PCC pavement can also be applied. The 2.28 in. of PCC obtained in Example 13.16 is the final answer if the bonded PCC overlay is used.

Bonded concrete overlays have been successfully constructed as thin as 2 in. (51 mm) and as thick as 6 in. (152 mm) or more. For most highway pavement overlays, thicknesses from 3 to 4 in. (76 to 101 mm) are typical. If the bonded overlay is placed only for functional purpose such as roughness or friction, a thickness of 3 in. (76 mm) should be adequate.

Unbonded PCC Overlay of PCC or AC/PCC Pavement The thickness of unbonded PCC overlay can be determined from

$$D_{\text{OL}} = \sqrt{D_f^2 - D_{\text{eff}}^2} \tag{13.38}$$

in which D_{eff} = effective thickness of an existing PCC or AC/PCC, which can be computed as

$$D_{\text{eff}} = (F_{\text{jcu}})D \tag{13.39}$$

Downloaded From : www.EasyEngineering.net

Downloaded From : www.EasyEngineering.net

in which D = existing PCC slab thickness and F_{jcu} = joints and cracks adjustment factor for unbonded concrete overlays, which may range from 1 to 0.9 depending on the number of deteriorated joints and cracks per mile. As a rough guide, adjustment factors of 0.98 can be used for 20 deteriorated joints and cracks per mile, 0.94 for 100 per mile, and 0.9 for 200 per mile. Note that the existing AC surface is disregarded in determining D_{eff} of an existing AC/PCC pavement.

Example 13.18:

Unbonded JPCP overlay of existing JPCP (SW-20)
Existing pavement: slab 8.2 in., subgrade k = 183 pci (by NDT)
Find D_f: N_f = 11,000,000 (rigid ESALs), R = 95%, S_o = 0.35, p_1 = 4.5, p_2 = 2.5, J = 4.0, C_d = 1.00, $E_c = 4.9 \times 10^6$ psi, S_c = 700 psi (by Eq. 7.56a), D_f = 11.50 in. (by Eq. 12.21).
Find D_{eff} by condition survey: Assume 100 deteriorated cracks per mile or F_{jcu} = 0.94. From Eq. 13.39, $D_{eff} = 0.94 \times 8.2 = 7.71$ in.
Find D_{OL}: From Eq. 13.38, $D_{OL} = [(11.50)^2 - (7.71)^2]^{1/2} = 8.53$ in. of PCC.

PCC Overlay of AC Pavement The thickness of PCC overlay is computed as

$$D_{OL} = D_f \tag{13.40}$$

The existing AC pavement is considered as a foundation for the new PCC pavement. A major problem is how to select a k-value that represents the combined effect of AC surface, granular base, and subgrade. The 1993 guide suggests the use of Figure 12.18 to estimate the k-value based either on NDT data or on soil data and the types and thicknesses of the pavement layers. The k-value obtained may need to be adjusted for seasonal effect.

When NDT is used, first backcalculate M_R and E_p, then enter Figure 12.18 with D_{SB} as the total thickness of pavement above the subgrade and E_p as E_{SB}, and determine the effective dynamic k-value. Divide the effective dynamic k-value by 2 to obtain the effective static k-value. Note that the backcalculated M_R to estimate the effective dynamic k-value should not be adjusted by the C factor.

The use of Figure 12.18 for determining the k-value was not recommended in the original NCHRP report (Darter *et al.*, 1991b) when these examples were prepared. To investigate the appropriate k-values for designing PCC overlays of existing AC pavements, theoretical analyses were made on a variety of pavement systems consisting of a PCC slab and an AC layer, each with a wide range of thicknesses and elastic moduli, and of subgrades with resilient moduli ranging from 5000 to 40,000 psi (34 to 276 MPa). The deflection basins at the top of PCC were first computed by the BISAR elastic layer program, which were then used with the ILLI-BACK software to backcalculate the effective k-value beneath the PCC slab. It was found that the dominant factor influencing the backcalculated k-value was the subgrade modulus, the effects of AC thickness and modulus were much less significant. A curve relating M_R to k-value was

Downloaded From : www.EasyEngineering.net

Downloaded From : www.EasyEngineering.net

plotted and is recommended for use in design. However, this recommendation was not included in the AASHTO design guide, because it contradicts the use of Figure 12.18. It is doubtful that the ILLI-BACK program can be applied to backcalculate the k-value of the subgrade and AC layer combined, because the AC layer may have to be considered as part of PCC layer, instead of the subgrade. Because of the much lower k-values recommended in the NCHRP report, it was cautioned in Appendix L of the 1993 design guide that Figure 12.18 was developed by using an elastic layer computer program, without verification from field deflection data. This shortcut might yield reasonable values in some instances, but it could yield unreasonably high values in other instances. Further research into support for PCC overlays, including deflection testing on in-service PCC/AC pavements and the backcalculating of effective k-values, is strongly encouraged.

Example 13.19:

JPCP overlay of AC pavement (NW-10)

Existing pavement: AC surface 4 in., crushed stone base 14 in.

Find k: From NDT, M_R = 14,218 psi (by Eq. 13.22), E_p = 21,611 psi (by Eq. 13.25). With M_R = 14,000 psi, D_{SB} = 18 in., E_{SB} = 22,000 psi, from Figure 12.18, dynamic k-value = 800 pci, or static k-value = 400 pci.

Find D_f: N_f = 2,300,000 (rigid ESALs), R = 95%, S_o = 0.35, p_1 = 4.5, p_2 = 2.5, k = 400 pci, J = 3.2, C_d = 1.00, $E_c = 4.2 \times 10^6$ psi and, S_c = 690 psi, from Figure 12.17, D_f = 7.4 in. If a k-value of 137 pci, as recommended in the NCHRP report, were used, D_f = 8.1 in.

Check with Eq. 12.21: $\log W_{18} = -1.645 \times 0.35 + 7.35 \log(7.4 + 1) - 0.06 + \log(2/3)/[1 + 1.624 \times 10^7/(7.4 + 1)^{8.46}] + (4.22 - 0.32 \times 2.5) \log \{[(690 \times 1)/(215.63 \times 3.2)][(7.4)^{0.75} - 1.132]/[(7.6)^{0.75} - 18.42/(4.2 \times 10^6/400)^{0.25}]\} = -0.576 + 6.793 - 0.06 - 0.141 + 0.341 = 6.357$ or W_{18} = 2,275,097 ok

Find D_{OL}: From Eq. 13.40, D_{OL} = 7.4 in. of PCC.

SUMMARY

This chapter presents several methods for overlay design, including the Asphalt Institute method, the Portland Cement Association method, and the AASHTO method.

Important Points Discussed in Chapter 13

1. Either HMA or PCC can be used as an overlay on an existing flexible or rigid pavement. If both the overlay and the existing pavement are flexible, then an elastic layer program can be used as a mechanistic design model. If either the overlay or the existing pavement is rigid, then a finite element plate program should be used. Applying stress adjustment factors for edge and corner loading has made possible the use of an elastic layer program for the design of HMA overlays on PCC pavements.
2. A major problem in the design of HMA overlays on PCC pavements is the occurrence of reflection cracking. The most common methods for minimizing reflection cracking include

Downloaded From : www.EasyEngineering.net

Downloaded From : www.EasyEngineering.net

using a thicker overlay, cracking and seating the existing PCC slabs, incorporating a crack relief layer, and sawing and sealing joints on the HMA overlay. However, there has been some controversy about the effectiveness of cracking and seating. It was reported that cracking and seating only delayed, rather than eliminated, the reflection cracking. Also, the AASHTO design method assumes that cracking and seating cause a decrease in the structural capacity of the existing pavement, but a recent study conducted by Pennsylvania State University indicated that there was no significant loss of structural support or decrease in the modulus of elasticity on the crack and seat pavement sections.

3. Three general methods can be used for overlay design: the effective thickness approach, the deflection approach, and the mechanistic–empirical approach. In the effective thickness approach, the thickness of the existing pavement is reduced to an effective thickness depending on the conditions of its component layers. The difference between the required thickness of a new pavement and the effective thickness of the existing pavement is the thickness of overlay required. In the deflection approach, the thickness of overlay should be sufficient to reduce the pavement deflection to a tolerable amount, usually derived empirically from the amount of traffic. In the mechanistic–empirical approach, the critical stresses or strains in the existing and the overlaid pavements are determined by mechanistic models, and the damage due to traffic loads and environmental causes is evaluated to ensure that failures will not occur.
4. The Asphalt Institute employs both the effective thickness and the deflection methods for the design of HMA overlays on both flexible and rigid pavements. In the effective thickness method, the conversion factors based on the conditions listed in Table 13.3 must be applied to each layer to obtain an effective thickness equivalent to the thickness of new HMA. The difference between the required thickness of a new full-depth pavement and the effective thickness of the existing pavement is the thickness of overlay required. If the existing pavement is of full depth, the PSI of the existing pavement at the time of overlay can also be used directly for determining the conversion factor, as shown in Figure 13.2. In the deflection method, separate procedures are used, depending on whether the existing pavement is flexible or rigid. For flexible pavements, the overlay thickness can be obtained from Figure 13.5 as a function of the representative rebound deflection, RRD, and of the ESAL repetitions during the overlay period. For rigid pavements, unless special techniques described in Section 13.1.2 are used to minimize reflection cracking, the thickness of HMA overlay depends on the slab length and the maximum annual temperature differential, as shown in Figure 13.7. Prior to the overlay, deflection measurements by Benkelman beam should be made at the joints to determine both the mean deflection and the differential deflection. After the overlay, the mean deflection must be reduced to less than 0.014 in. (0.36 mm), the differential deflection to less than 0.002 in. (0.05 mm). The decrease in deflection after the overlay can be estimated by assuming that each inch of HMA overlay will reduce the deflection by 5%. If the mean and differential deflections cannot be reduced below the specified values, undersealing or stabilization of the subgrade will be required.
5. The Portland Cement Association has published design charts for both unbonded and bonded PCC overlays on existing rigid pavements. The method is considered mechanistic–empirical because the JSLAB finite element computer program was used to prepare the design charts. The many arbitrary assumptions employed make the method more empirical than mechanistic. For example, the modulus of existing PCC pavement in the unbonded pavement system is arbitrarily assumed to be 3×10^6 to 4×10^6 psi (21 to 28 GPa), regardless of the actual fatigue damage caused by the load repetitions prior to the overlay. Furthermore, the concept of providing an overlaid pavement that is structurally equivalent to a new full-depth pavement is approximate at best, because the equivalency

Downloaded From : www.EasyEngineering.net

Downloaded From : www.EasyEngineering.net

depends on a large number of factors, such as the k value and the type of loading. Another inconsistency is the use of different load groups to design a new pavement but the use of equivalent 18-kip (80-kN) single-axle loads to relate the overlay thickness to the new pavement thickness. However, the PCA method does provide a simple procedure for the design of both unbonded and bonded overlays. Design charts for unbonded overlays are presented in Figures 13.10, 13.11, and 13.12 for three different cases. Some judgment on the condition of existing pavement is needed to select the appropriate chart for use. The design chart for bonded overlays is shown in Figure 13.14.

6. The AASHTO design procedure is based on the structural deficiency approach. The basic equation is

$$(SC_{OL})^n = (SC_f)^n - (SC_{eff})^n \tag{13.18}$$

in which SC_{OL} = required structural capacity of the overlay, SC_f = structural capacity of a new pavement to carry future ESALs during the overlay period, SC_{eff} = effective structural capacity of the existing pavement, and n = an exponent with the value 1 for all cases except for the unbonded PCC overlays on PCC pavements, where $n = 2$. If the overlay or the existing pavement has a rigid layer, the structural capacity is the thickness of PCC, D; if all layers are flexible, the structural capacity is the structural number, SN. Seven cases of overlay design (AC overlay of AC, AC overlay of fractured PCC, AC overlay of PCC, AC overlay of AC/PCC, bonded PCC overlay of PCC, unbonded PCC overlay of PCC or AC/PCC, and PCC overlay of AC) and three methods to evaluate SC_{eff} (condition survey, NDT, and remaining life) were discussed. However, the only method applicable to all cases is the condition survey, and the only case to which all three methods can be applied is the AC overlay of existing AC pavement. When the overlay design is based on SN, the condition survey method involves the evaluation of layer and drainage coefficients in their existing conditions; when the design is based on D, it involves the estimation of adjustment factors for joints and cracks, durability or "D" cracking, and/or fatigue cracking of the existing slab. The NDT method is recommended in all cases to determine the resilient modulus, M_R, or k-value of the subgrade, but its application to the evaluation of SC_{eff} is limited to AC overlay of existing AC pavement. The remaining life method can be applied when the existing pavement is preserved and used as a structural component, but only when the historical traffic data is available. The thickness design procedures for the seven cases are different; each is illustrated by a practical example.

PROBLEMS

13.1 A flexible pavement is composed of a 4-in. HMA surface and a 12-in. crushed stone base. Deflection measurements were made in the spring by using a Benkelman beam. The mean deflection was found to be 0.034 in., with a standard deviation of 0.0041 in. The mean pavement temperature during the test was 80°F. Determine the thickness of HMA overlay required for a design ESAL of 10 million, using the Asphalt Institute's equations, and compare it with the result from the design chart. [Answer: 4.5 in.]

13.2 The representative rebound deflection on a flexible pavement is 0.055 in. If the traffic growth rate is 6% and the pavement is to be used for five years before the placement of a new overlay, what is the maximum allowable ESAL during the current year? [Answer: 30,100]

13.3 A CRCP has a crack spacing of 10 ft and a temperature differential of 56°F. Measured edge deflection by Dynaflect is 0.0007 in. By the Asphalt Institute procedure, determine the required thickness of asphalt overlay and check for whether undersealing is required. [Answer: 4 in., undersealing not required]

Downloaded From : www.EasyEngineering.net

Downloaded From : www.EasyEngineering.net

13.4 An existing 8-in. PCC slab is in fairly good condition but does not have sufficient structural capacity to carry the anticipated traffic. Twelve core samples were taken from the existing pavement at midslab about 2 ft from the edge, and the following splitting tensile strengths were found: 500, 453, 554, 450, 513, 488, 512, 468, 532, 520, 420, and 556 psi. The thickness of a new slab to carry the anticipated traffic is 11 in. Determine the thickness of overlay required by the PCA method for both the bonded and the unbonded case. [Answer: 3.5 and 9 in.]

13.5 An AC overlay with $a_1 = 0.44$ is to be placed on an existing AC pavement. The existing pavement has an AC surface of 1.5 in. and a stabilized base of 6 in. Results of NDT with a 5.9 in. plate under a 9000-lb load give deflections of 0.0161 in. at the center of plate and 0.00608 in. at a distance of 36 in. from the center. (a) Assuming C factor for $M_R = 0.33$, future ESALs on design lane = 100,000, $R = 95\%$, $S_o = 0.45$, $p_1 = 4.2$, $p_2 = 2.5$, determine SN_f. (b) Determine D_{OL} by NDT method. (c) Assuming $a_1 = 0.35$ and $a_2 = 0.25$, determine D_{OL} by the condition survey method and describe the conditions of the existing AC surface and stabilized base. (d) Assuming past ESALs in design lane = 95,000, $p_1 = 4.2$, $p_2 = 1.5$, $a_1 = 0.44$ and $a_2 = 0.33$, determine D_{OL} by the remaining life method. [Answer: 3.47, 1.9 in., 3.3 in., and 3.2 in.]

13.6 An AC overlay with $a_1 = 0.44$ is to be constructed on a rubblized PCC pavement. The existing slab to be rubblized has a thickness of 10 in., and the granular base has a thickness of 6 in. Results of NDT on the PCC surface prior to rubblizing using a 5.9 in. plate under a 9000-lb load give deflections of 0.0041 in. at the center of the plate and 0.0027 in. at a distance of 36 in. from the center. (a) Determine E_p from Figure 13.17 and compare it with that from Figure 13.20. Why is the value so large? (b) Assuming C factor = 0.167 for effective M_R, future ESALs on design lane = 6,700,000, $R = 95\%$, $S_o = 0.49$, $p_1 = 4.5$, $p_2 = 2.5$, determine SN_f. (c) Assuming $a_1 = 0.25$ and $a_2 = 0.05$, determine D_{OL} and describe the conditions of the rubblized PCC and base. [Answer: 860,000 vs 1,100,000 psi, 6.0 and 7.3 in.]

13.7 An AC overlay is planned for an existing JRCP. The existing slab thickness is 8 in. NDT was performed to backcalculate the dynamic k-value and the modulus of concrete, E_c, under a dynamic load of 9000 lb. The deflections measured at distances of 0, 12, 24 and 36 in. are 5.2, 4.5, 3.5, and 2.9 mils, respectively. (a) Determine E_c and the static k-value. (b) Using E_c and the k-value determined in part (a), together with Eq. 7.56a and assuming future ESALs on design lane = 80,000,000, $R = 95\%$, $S_o = 0.30$, $p_1 = 4.5$, $p_2 = 2.5$, $C_d = 1$, $J = 2.2$, $F_{jc} = 0.95$, $F_{fat} = 0.95$, and $F_{dur} = 1.00$, determine D_{OL} and describe the conditions of existing PCC pavement. [Answer: 3.4×10^6 psi, 150 pci, and 7.6 in.]

13.8 An AC overlay is to be placed on an existing AC/CRCP pavement. The existing pavement has a 3-in. AC surface and a 7-in. slab. The average of four sets of NDT tests on the existing pavement results in a dynamic k-value of 362 pci and an E_c of 2.1×10^6 psi. Assuming future ESALs on design lane = 10,000,000, thickness of AC to be milled = 0.75 in., $R = 95\%$, $S_o = 0.35$, $p_1 = 4.5$, $p_2 = 2.5$, $C_d = 1$, $J = 2.6$, $F_{jc} = 0.80$, $F_{dur} = 0.80$, and $F_{ac} = 0.85$, determine D_{OL} and describe the conditions of existing pavement. [Answer: 7.2 in.]

13.9 Same as Problem 13-8, except that a PCC overlay and a joint and crack adjustment factor, F_{jcu}, of 0.9 are used, determine the thickness of PCC overlay required. [Answer: 7.2 in.]

13.10 A bonded PCC overlay is planned for an existing JPCP. The existing slab thickness is 8.2 in. NDT was performed to backcalculate the dynamic k-value and the modulus of concrete, E_c, under a dynamic load of 8500 lb. The deflections measured at distances of 0, 12, 24 and 36 in. are 3.68, 3.08, 2.64, and 2.23 mils, respectively. (a) Determine E_c and the static k-value, and (b) using the E_c and static k-value obtained from NDT and assuming future ESALs on design lane = 11,000,000, $R = 95\%$, $S_o = 0.35$, $p_1 = 4.5$, $p_2 = 2.5$, $C_d = 1$,

Downloaded From : www.EasyEngineering.net

Downloaded From : www.EasyEngineering.net

$J = 4.0$, $F_{jc} = 1.00$, $F_{fat} = 0.95$, and $F_{dur} = 1.00$, determine D_{OL} and describe the conditions of existing PCC pavement. [Answer: 4.6×10^6 psi, 190 pci, and 3.8 in.]

13.11 Same as Problem 13-10, except that the PCC overlay is unbonded and $F_{jcu} = 0.98$; determine the thickness of overlay required. [Answer: 8.4 in.]

13.12 A JPCP is to be placed on an existing AC pavement. The existing pavement has an AC surface of 5.5 in. and a crushed stone base of 12 in. Results of NDT with a 5.9 in. plate under a 9000-lb load give deflections of 0.0241 in. at the center of the plate and 0.00445 in. at a distance of 36 in. from the center. Assuming future ESALs on design lane = 4,200,000, $R = 95\%$, $S_o = 0.35$, $p_1 = 4.5$, $p_2 = 2.5$, $J = 3.2$, $C_d = 1$, $S_c = 690$ psi, and $E_c = 4.2 \times 10^6$ psi, determine the thickness of overlay required by using Figure 12.17. Substituting the thickness into Eq. 12.21, check W_{18} with the assumed ESALs. [Answer: 8.3 in.]

Downloaded From : www.EasyEngineering.net

Downloaded From : www.EasyEngineering.net

APPENDIX A

Theory of Viscoelasticity

This appendix is a supplement to Section 2.3 on viscoelastic solutions and Section 7.2.1 on dynamic complex modulus. It discusses the use of differential operators to characterize viscoelastic materials, the application of the elastic–viscoelastic correspondence principle with the use of Laplace transforms, the conversion from creep compliance to the mechanical model by the method of successive residuals, and the change from the complex modulus to creep compliance by Fourier transforms. Readers with only basic calculus and without prior knowledge of these transforms should have no difficulty in following the presentation. This appendix is presented to give an insight into the classical theory of viscoelasticity.

A.1 DIFFERENTIAL OPERATORS

To facilitate the application of Laplace transforms, the mechanical models may be converted to differential operators. Let $\partial/\partial t = D$ = differential operators.

For an elastic spring,
$$\sigma = E\epsilon \quad \text{or} \quad \frac{\sigma}{\epsilon} = E \tag{A.1}$$

For a viscous dashpot,
$$\sigma = \lambda\frac{\partial \epsilon}{\partial t} \quad \text{or} \quad \frac{\sigma}{\epsilon} = \lambda D \tag{A.2}$$

For a Maxwell model with a spring and a dashpot in series, the total strain is equal to the sum of the two:

$$\epsilon = \frac{\sigma}{E_0} + \frac{\sigma}{\lambda_0 D}$$

$$\frac{\sigma}{\epsilon} = \frac{1}{1/E_0 + 1/(\lambda_0 D)} = \frac{E_0 T_0 D}{T_0 D + 1} \tag{A.3}$$

In these equations, $T_0 = \lambda_0/E_0$. Note that E_0 and $\lambda_0 D$ are the stress–strain ratio of the spring and dashpot, respectively. When two models are connected in series, the stress–strain ratio is the reciprocal of the sum of the reciprocal of the two stress–strain

Downloaded From : www.EasyEngineering.net

Downloaded From : www.EasyEngineering.net

ratios. For a Kelvin model with a spring and a dashpot in parallel, the total stress is equal to the sum of the two:

$$\sigma = E_1\epsilon + \lambda D\epsilon$$

or

$$\frac{\sigma}{\epsilon} = E_1 + \lambda_1 D = E_1(T_1 D + 1) \tag{A.4}$$

For a generalized model with one Maxwell model and n Kelvin models in series, by the foregoing reciprocal principle,

$$\frac{\sigma}{\epsilon} = \frac{1}{\dfrac{T_0 D + 1}{E_0 T_0 D} + \displaystyle\sum_{i=1}^{n} \frac{1}{E_i(T_i D + 1)}} \tag{A.5}$$

Example A.1:

Express the stress–strain ratio of the model shown in Figure 2.35*a* as differential operators.

Solution: Given $E_0 = 2, T_0 = 5, E_1 = 10, T_1 = 10, E_2 = 5, T_2 = 1, E_3 = 1$, and $T_3 = 0.1$, from Eq. A.5, we obtain

$$\frac{\sigma}{\epsilon} = \frac{1}{\dfrac{5D + 1}{10D} + \dfrac{1}{10(10D + 1)} + \dfrac{1}{5(D + 1)} + \dfrac{1}{0.1D + 1}}$$

or

$$E = \frac{\sigma}{\epsilon} = \frac{10D^4 + 111D^3 + 111D^2 + 10D}{5D^4 + 158.6D^3 + 197.9D^2 + 29.1D + 1} \tag{A.6}$$

It can be seen that Young's modulus of viscoelastic materials can be expressed as the quotient of two polynomials in terms of the differential operator D. The use of differential operations to describe the stress–strain relationship is for convenience only. Otherwise, Eq. A.6 should be written as

$$5\frac{\partial^4\sigma}{\partial t^4} + 158.6\frac{\partial^3\sigma}{\partial t^3} + 197.9\frac{\partial^2\sigma}{\partial t^2} + 29.1\frac{\partial\sigma}{\partial t} + \sigma = 10\frac{\partial^4\epsilon}{\partial t^4} + 111\frac{\partial^3\epsilon}{\partial t^3} + 111\frac{\partial^2\epsilon}{\partial t^2} + 10\frac{\partial\epsilon}{\partial t} \tag{A.7}$$

Example A.2:

Figure A.1 shows a viscoelastic model. Derive the governing differential equation of the model by using differential operators. Integrate the equation for the following two cases: (a) find the strain–time relationship when a constant stress σ_0 is applied to the model and (b) find the stress–time relationship when a constant strain ϵ_0 is applied to the model.

Downloaded From : www.EasyEngineering.net

Downloaded From : www.EasyEngineering.net

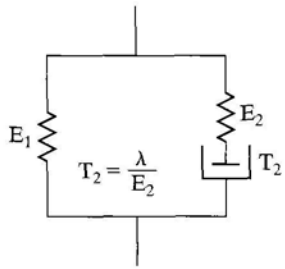


FIGURE A.1
Example A.2.

Solution: The stress–strain relationship of an elastic spring is indicated by Eq. A.1, that of a Maxwell model by Eq. A.3. When the two are connected in parallel, as shown in Figure A.1,

$$\frac{\sigma}{\epsilon} = E_1 + \frac{E_2 T_2 D}{T_2 D + 1} = \frac{T_2(E_1 + E_2)D + E_1}{T_2 D + 1} \tag{A.8}$$

The governing differential equation is

$$T_2 \frac{\partial \sigma}{\partial t} + \sigma = T_2(E_1 + E_2)\frac{\partial \epsilon}{\partial t} + E_1 \epsilon \tag{A.9}$$

(a) When a constant stress σ_0 is applied, the model experiences an instantaneous strain, $\sigma_0/(E_1 + E_2)$, due to the stretching of the two springs. If $\sigma = \sigma_0$, then, from Eq. A.9,

$$\sigma_0 = T_2(E_1 + E_2)\frac{d\epsilon}{dt} + E_1 \epsilon$$

$$\int_{\sigma_0/(E_1+E_2)}^{\epsilon} \frac{d\epsilon}{\sigma_0 - E_1 \epsilon} = \frac{1}{T_2(E_1 + E_2)} \int_0^t dt$$

$$-\frac{1}{E_1} \ln(\sigma_0 - E_1 \epsilon)\Big|_{\sigma_0/(E_1+E_2)}^{\epsilon} = \frac{t}{T_2(E_1 + E_2)}$$

$$\epsilon = \frac{\sigma_0}{E_1}\left\{1 - \frac{E_2}{E_1 + E_2} \exp\left[-\frac{E_1 t}{T_2(E_1 + E_2)}\right]\right\} \tag{A.10}$$

(b) When a constant strain ϵ_0 is applied, the model experiences an instantaneous stress, $(E_1 + E_2)\epsilon_0$. If $\epsilon = \epsilon_0$, then, from Eq. A.9,

$$\int_{(E_1+E_2)\epsilon_0}^{\sigma} \frac{d\sigma}{E_1 \epsilon_0 - \sigma} = \frac{1}{T_2} \int_0^t dt$$

$$-\ln(E_1 \epsilon_0 - \sigma)\Big|_{(E_1+E_2)\epsilon_0}^{\sigma} = \frac{t}{T_2}$$

$$\sigma = \epsilon_0\left[E_1 + E_2 \exp\left(-\frac{t}{T_2}\right)\right] \tag{A.11}$$

A.2 ELASTIC–VISCOELASTIC CORRESPONDENCE PRINCIPLE

Instead of using a Dirichlet series to fit the responses at various times, as presented in Section 2.3.2, the elastic–viscoelastic principle can be applied to obtain the viscoelastic

Downloaded From : www.EasyEngineering.net

Downloaded From : www.EasyEngineering.net

solutions from the elastic solutions. In this traditional method, a Laplace transform is applied to remove the time variable t with a transformed variable p, thus changing a viscoelastic problem into an associated elastic problem. The Laplace inversion of the associated elastic problem from the transformed variable p to the time variable t results in the viscoelastic solutions. For simple problems, this method can give the closed-form solutions directly. However, for viscoelastic layered systems, it is not possible to obtain Laplace inversion, and an approximate method of collocation must be used. Because the collocation with respect to the transformed variable p does not offer any advantage over that with respect to time t, the Laplace transform was not used in the development of KENLAYER.

A.2.1 Laplace Transform

Instead of stresses, strains, and loads, the Laplace transform of stresses, strains, and loads is considered in viscoelastic analysis. When the Laplace transform is applied, the time variable t is removed and is replaced by the transformed variable p, thus changing the viscoelastic problem into an elastic problem. The Laplace inversion of p to t results in the viscoelastic solution. The Laplace transform is defined as

$$L[F(t)] = \int_0^\infty F(t)e^{-pt}\,dt \tag{A.12}$$

in which $F(t)$ is a function of time t, and p is a transformed variable. After integration of Eq. A.12 and substitution of the limits of t, F becomes a function of p.

If the applied load q is a constant independent of time, the Laplace transform of q is

$$\bar{q} = L(q) = \int_0^\infty qe^{-pt}\,dt = -\frac{q}{p}e^{-pt}\Big|_0^\infty = \frac{q}{p} \tag{A.13}$$

in which p is a transformed variable. (A bar on top of a variable indicates the Laplace transform of the variable.)

The stress–strain relationship of viscoelastic materials can be expressed in the form shown by Eq. A.7. To remove the time variable t, Laplace transforms are applied to the stress or strain on each side of the equation. Take the first derivative, $d\sigma/dt$, for example:

$$L\left(\frac{d\sigma}{dt}\right) = \int_0^\infty \frac{d\sigma}{dt}e^{-pt}\,dt = \int_0^\infty e^{-pt}\,d\sigma$$
$$= \sigma\, e^{-pt}\Big|_0^\infty - \int_0^\infty \sigma\, d(e^{-pt})$$

If the material is initially undisturbed, or $\sigma = 0$ at $t = 0$, the first term is equal to zero, or

$$L\left(\frac{d\sigma}{dt}\right) = p\int_0^\infty \sigma\, e^{-pt}\,dt = p\bar{\sigma} \tag{A.14}$$

Equation A.14 indicates that the Laplace transform of $\partial\sigma/\partial t$, or $D\sigma$, is simply the replacement of D by p and σ by $\bar{\sigma}$. For the second derivative,

Downloaded From : www.EasyEngineering.net

Downloaded From : www.EasyEngineering.net

$$L\left(\frac{d^2\sigma}{dt^2}\right) = \int_0^\infty \frac{d^2\sigma}{dt^2} e^{-pt}\, dt = \int_0^\infty e^{-pt}\, d\left(\frac{d\sigma}{dt}\right)$$
$$= \frac{d\sigma}{dt} e^{-pt}\Big|_0^\infty - \int_0^\infty \frac{d\sigma}{dt} d(e^{-pt})$$

If the material is initially undisturbed, or $d\sigma/dt = 0$ at $t = 0$, the first term is equal to zero, or

$$L\left(\frac{d^2\sigma}{dt^2}\right) = p\int_0^\infty \frac{d\sigma}{dt} e^{-pt}\, dt = p^2\,\bar{\sigma} \tag{A.15}$$

As can be seen, the Laplace transform for the second derivative requires the replacement of D^2 by p^2. The same process can be applied to higher derivatives by replacing D^n by p^n. Consequently, the Laplace transform of Young's modulus, as indicated by Eq. A.6, becomes

$$E = \frac{\bar{\sigma}}{\bar{\epsilon}} = \frac{10p^4 + 111p^3 + 111p^2 + 10p}{5p^4 + 158.6p^3 + 197.9p^2 + 29.1p + 1} \tag{A.16}$$

When a viscoelastic material is characterized by a generalized model and a computer is used for the analysis, it is more convenient to apply Eq. A.5 directly:

$$\bar{E} = \frac{1}{\dfrac{T_0p + 1}{E_0T_0p} + \displaystyle\sum_{i=1}^{n} \frac{1}{E_i(T_ip + 1)}} \tag{A.17}$$

The Laplace transform of $e^{-t/T}$ is also of interest and can be calculated as

$$L\left(e^{-t/T}\right) = \int_0^\infty e^{-t/T} e^{-pt}\, dt = \int_0^\infty e^{-[(Tp+1)/T]t}\, dt$$
$$= -\frac{T}{Tp + 1} e^{-[(Tp+1)/T]t}\Big|_0^\infty = \frac{T}{Tp + 1} \tag{A.18}$$

Example A.3:

Figure A.2 shows a viscoelastic homogeneous half-space under a circular loaded area. The half-space has a Young's modulus characterized by a Kelvin model and a constant Poisson ratio ν. Derive an expression for the vertical deflection at the center of the loaded area as a function of time.

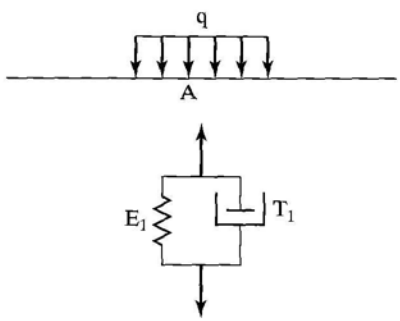


FIGURE A.2
Example A.3.

Downloaded From : www.EasyEngineering.net

Downloaded From : www.EasyEngineering.net

Solution: The elastic solution can be obtained from Eq. 2.8:

$$w_0 = \frac{2(1 - \nu^2)q\,a}{E} \tag{2.8}$$

Consider the Laplace transforms of deflection, load, and Young's modulus:

$$\overline{w}_0 = \frac{2(1 - \nu^2)\overline{q}\,a}{\overline{E}} \tag{A.19}$$

From Eq. A.13, $\overline{q} = q/p$, and from Eq. A.17, with only one Kelvin element, $\overline{E}_1 = E_1(T_1 p + 1)$, so Eq. A.19 becomes

$$\overline{w}_0 = \frac{2(1 - \nu^2)q\,a}{E_1 p(T_1 p + 1)} = \frac{2(1 - \nu^2)q\,a}{E_1}\left(\frac{1}{p} - \frac{T_1}{T_1 p + 1}\right) \tag{A.20}$$

Equation A.20 can be easily inverted from p to t, because $1/p$ can be inverted to 1, as indicated by Eq. A.13, and $T_1/(T_1 p + 1)$ can be inverted to e^{-t/T_1}, as indicated by Eq. A.18:

$$w_0 = \frac{2(1 - \nu^2)q\,a}{E_1}\left[1 - \exp\left(-\frac{t}{T_1}\right)\right] \tag{A.21}$$

When the Poisson ratio is a constant, Eq. A.21 indicates that the viscoelastic deflection is equal to the elastic deflection multiplied by $(1 - e^{-t/T_1})$, which is the expression for a Kelvin model. Because the stresses in a homogeneous half-space are independent of E, the same stresses will be obtained whether the half-space is elastic or viscoelastic. It can be shown that, if the half-space is characterized by the generalized model shown in Figure 2.33*f*, the surface deflection is

$$w_0 = 2(1 - \nu^2)q\,a\left[\frac{1}{E_0}\left(1 + \frac{t}{T_0}\right) + \sum_{i=1}^{n}\frac{1}{E_i}(1 - e^{-t/T_i})\right] \tag{A.22}$$

Example A.4:

If the model shown in Figure A.1 is used to characterize a homogeneous half-space subjected to a circular load of intensity q and radius a, as shown in Figure A.3, express the surface deflection at the center of the loaded area in terms of q, a, ν, E_1, E_2, and T_2 by the elastic–viscoelastic correspondence principle.

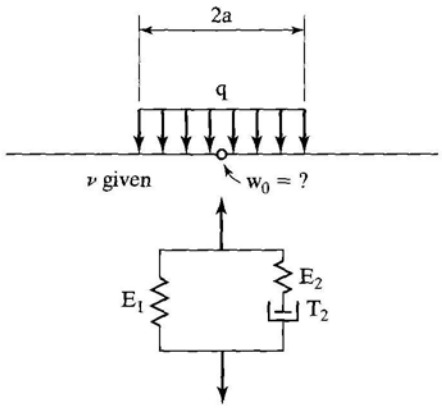


FIGURE A.3
Example A.4.

Downloaded From : www.EasyEngineering.net

Downloaded From : www.EasyEngineering.net

Solution: From Eq. A.8,

$$\overline{E} = \frac{\overline{\sigma}}{\overline{\epsilon}} = \frac{T_2(E_1 + E_2)p + E_1}{T_2 p + 1} \tag{A.23}$$

Substituting Eq. A.23 into Eq. A.19 gives

$$\overline{w}_0 = \frac{2(1 - \nu^2)q\, a(T_2 p + 1)}{p[T_2(E_1 + E_2)p + E_1]} \tag{A.24}$$

Equation A.24 can be split into two terms:

$$\overline{w}_0 = 2(1 - \nu^2)q\, a\left[\frac{x}{p} + \frac{y}{T_2(E_1 + E_2)p + E_1}\right] \tag{A.25}$$

When Eqs. A.24 and A.25 are compared for constant and p terms, it can easily be shown that $E_1 x = 1$, or $x = 1/E_1$ and $T_2(E_1 + E_2)x + y = T_2$, or $y = T_2 - T_2(E_1 + E_2)/E_1 = -T_2E_2/E_1$. Therefore, Eq. A.25 can be written as

$$\overline{w}_0 = \frac{2(1 - \nu^2)q\, a}{E_1}\left[\frac{1}{p} - \frac{T_2E_2}{T_2(E_1 + E_2)p + E_1}\right] \tag{A.26}$$

Laplace inversion of Eq. A.26 results in

$$w_0 = \frac{2(1 - \nu^2)q\, a}{E_1}\left\{1 - \frac{E_2}{E_1 + E_2}\exp\left[-\frac{E_1 t}{T_2(E_1 + E_2)}\right]\right\} \tag{A.27}$$

Note that the terms in the braces are the same as those of Eq. A.10, as is expected.

A.2.2 Collocation Method

The problem involving a layered system is not as simple as that of a homogeneous half-space. First, each layer has its own elastic modulus, and the complex interaction among these moduli means that the deflection cannot be expressed as a function of p in closed forms, as shown by Eq. A.20. Second, even if the deflection can be expressed as a polynomial of p, it is of such a high degree that it is difficult to invert. However, the Laplace inversion can be most conveniently accomplished by a collocation method (Huang, 1967).

In Section 2.3.2, it was shown that the viscoelastic response R can be expressed as a Dirichlet series:

$$R = \sum_{i=1}^{7} c_i \exp\left(-\frac{t}{T_i}\right) \tag{2.49}$$

The Laplace transform of Eq. 2.49 is

$$\overline{R} = \sum_{i=1}^{7} \frac{c_i T_i}{T_i p + 1} \tag{A.28a}$$

Multiplying Eq. A.28 by p yields

$$p\overline{R} = \sum_{i=1}^{n} \frac{c_i}{1 + 1/(T_i p)} \tag{A.28b}$$

Downloaded From : www.EasyEngineering.net

Downloaded From : www.EasyEngineering.net

For any given value of p, $p\overline{R}$ is simply the elastic solution having the elastic modulus expressed as a function of p, as indicated by Eq. A.17. If retardation times T_i of 0.01, 0.03, 0.1, 1, 10, 30, and ∞ are assumed, the coefficients c_i can be obtained by solving the following simultaneous equations:

$$\begin{bmatrix} \frac{1}{1+\frac{0.01}{0.01}} & \frac{1}{1+\frac{0.01}{0.03}} & \frac{1}{1+\frac{0.01}{0.1}} & \frac{1}{1+\frac{0.01}{1}} & \frac{1}{1+\frac{0.01}{10}} & \frac{1}{1+\frac{0.01}{30}} & 1 \\ \frac{1}{1+\frac{0.03}{0.01}} & \frac{1}{1+\frac{0.03}{0.03}} & \frac{1}{1+\frac{0.03}{0.1}} & \frac{1}{1+\frac{0.03}{1}} & \frac{1}{1+\frac{0.03}{10}} & \frac{1}{1+\frac{0.03}{30}} & 1 \\ \frac{1}{1+\frac{0.1}{0.01}} & \frac{1}{1+\frac{0.1}{0.03}} & \frac{1}{1+\frac{0.1}{0.1}} & \frac{1}{1+\frac{0.1}{1}} & \frac{1}{1+\frac{0.1}{10}} & \frac{1}{1+\frac{0.1}{30}} & 1 \\ \frac{1}{1+\frac{1}{0.01}} & \frac{1}{1+\frac{1}{0.03}} & \frac{1}{1+\frac{1}{0.1}} & \frac{1}{1+\frac{1}{1}} & \frac{1}{1+\frac{1}{10}} & \frac{1}{1+\frac{1}{30}} & 1 \\ \frac{1}{1+\frac{10}{0.01}} & \frac{1}{1+\frac{10}{0.03}} & \frac{1}{1+\frac{10}{0.1}} & \frac{1}{1+\frac{10}{1}} & \frac{1}{1+\frac{10}{10}} & \frac{1}{1+\frac{10}{30}} & 1 \\ \frac{1}{1+\frac{30}{0.01}} & \frac{1}{1+\frac{30}{0.03}} & \frac{1}{1+\frac{30}{0.1}} & \frac{1}{1+\frac{30}{1}} & \frac{1}{1+\frac{30}{10}} & \frac{1}{1+\frac{30}{30}} & 1 \\ 1 & 1 & 1 & 1 & 1 & 1 & 1 \end{bmatrix} \begin{Bmatrix} c_1 \\ c_2 \\ c_3 \\ c_4 \\ c_5 \\ c_6 \\ c_7 \end{Bmatrix} = \begin{Bmatrix} (p\overline{R})_{p=1/0.01} \\ (p\overline{R})_{p=1/0.03} \\ (p\overline{R})_{p=1/0.1} \\ (p\overline{R})_{p=1} \\ (p\overline{R})_{p=1/10} \\ (p\overline{R})_{p=1/30} \\ (p\overline{R})_{p=10^{10}} \end{Bmatrix} \tag{A.29}$$

The above procedure is very similar to that presented in Section 2.3.2. If the viscoelastic property is characterized by the creep compliance, the use of the method presented in Section 2.3.2 is more direct. If the elastic–viscoelastic correspondence principle is employed, it is necessary to convert the creep compliance into a mechanical model with the elastic modulus indicated by Eq. A.17. For this reason, the elastic–viscoelastic correspondence principle and the Laplace transform were not used in KENLAYER.

A.3 METHOD OF SUCCESSIVE RESIDUALS

This method is used to determine the constants E_i and T_i of a viscoelastic material directly from the creep curve, rather than arbitrarily assuming T_i and then computing E_i by the collocation method, as described in Section 2.3.2. First, the creep compliances D due to retarded strains are determined by deducting the instantaneous and viscous strains from the total strains, as shown in Figure A.4. The actual number of Kelvin models required is not known at this time but can be determined later. For illustration, it is assumed that three Kelvin models are needed to describe retarded strains:

$$D = \frac{1}{E_1}\left[1 - \exp\left(-\frac{t}{T_1}\right)\right] + \frac{1}{E_2}\left[1 - \exp\left(-\frac{t}{T_2}\right)\right] + \frac{1}{E_3}\left[1 - \exp\left(-\frac{t}{T_3}\right)\right] \tag{A.30}$$

Let

$$b = \frac{1}{E_1} + \frac{1}{E_2} + \frac{1}{E_3}$$

so that Eq. A.30 can be written as

$$S_1 = b - D = \frac{1}{E_1}\exp\left(-\frac{t}{T_1}\right) + \frac{1}{E_2}\exp\left(-\frac{t}{T_2}\right) + \frac{1}{E_3}\exp\left(-\frac{t}{T_3}\right) \tag{A.31}$$

Downloaded From : www.EasyEngineering.net

Downloaded From : www.EasyEngineering.net

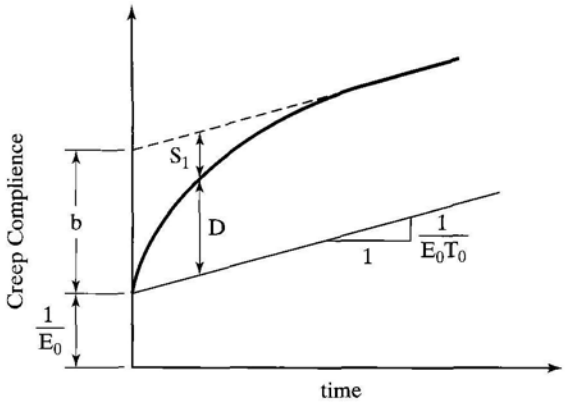


FIGURE A.4
Separation of creep compliances.

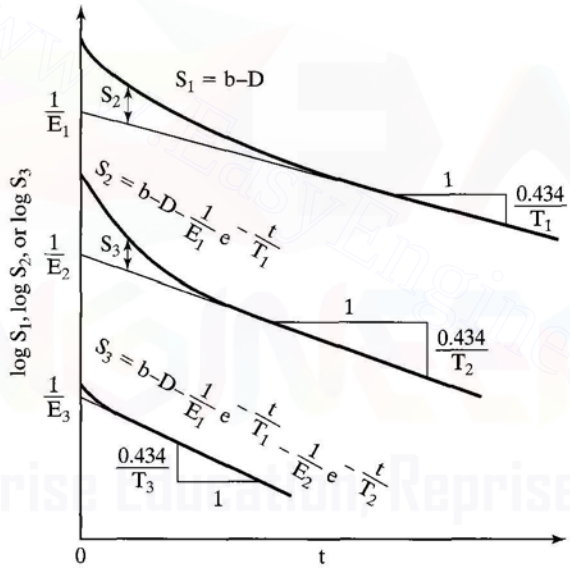


FIGURE A.5
Method of successive residuals.

If T_1 is much greater than T_2 and T_3, then, after a sufficient period of time, the last two terms on the right side of Eq. A.31 vanish:

$$S_1 = \frac{1}{E_1} \exp\left(-\frac{t}{T_1}\right) \tag{A.32}$$

Equation A.32 shows that a plot of log S_1 versus t results in a straight line, as indicated by Eq. A.33 and Figure A.5:

$$\log S_1 = \log\left(\frac{1}{E_1}\right) - \frac{0.434t}{T_1} \tag{A.33}$$

The slope of the straight line can be used to determine T_1, and the intercept at $t = 0$ can be used to determine E_1. After E_1 and T_1 are found, Eq. A.31 can be written as

Downloaded From : www.EasyEngineering.net

Downloaded From : www.EasyEngineering.net

$$S_2 = b - D - \frac{1}{E_1}\exp\left(-\frac{t}{T_1}\right) = \frac{1}{E_2}\exp\left(-\frac{t}{T_2}\right) + \frac{1}{E_3}\exp\left(-\frac{t}{T_3}\right) \quad \text{(A.34)}$$

in which S_2 is the vertical intercept between the curve and the straight line. If T_2 is much greater than T_3, a plot of log S_2 versus t should also finally become a straight line, so T_2 and E_2 can be determined. The process is continued until the intercept becomes negligibly small.

Example A.5:

The creep compliances of a viscoelastic material are shown in Table 2.4. Develop a mechanical model and determine its viscoelastic constants.

Solution: The generalized model is represented by Eq. 2.36. When $t = 0$, $D = 1/E_0$. From Table 2.4, $D = 0.5$ when $t = 0$, so $E_0 = 2$. At long loading times, only the viscous strains exist. The rate of change in compliance due to viscous strains is $1/(E_0T_0)$, as can be seen from Eq. 2.29 or 2.36. At $t = 40$, $D = 5.798$ and at $t = 50$, $D = 6.799$, so the change in compliance per unit time is $(6.799 - 5.798)/10 = 0.1$, and $E_0T_0 = 10$, or $T_0 = 5$.

Table A.1 shows the procedure for computing successive residuals. Column 2 is the compliance of the dashed line shown in Figure A.4 and can be computed by $6.799 - (50 - t) \times 0.1$. Column 3 is given in Table 2.4. Column 4 is the difference between columns 2 and 3. A plot of log S_1 versus t is shown in Figure A.6 and results in a

TABLE A.1 Computation of Successive Residuals

	Compliance						
Time (1)	Dashed line (2)	Total (3)	S_1 (4)	$\frac{\exp(-t/T_1)}{E_1}$ (5)	S_2 (6)	$\frac{\exp(-t/T_2)}{E_2}$ (7)	S_3 (8)
0	1.799	0.500	1.299	0.100	1.199	0.200	0.999
0.05	1.804	0.909	0.895	0.099	0.796	0.190	0.606
0.1	1.809	1.162	0.647	0.099	0.548	0.181	0.367
0.2	1.819	1.423	0.396	0.098	0.298	0.164	0.134
0.4	1.839	1.592	0.247	0.096	0.151	0.135	0.016
0.6	1.859	1.654	0.205	0.094	0.111	0.111	0.000
0.8	1.879	1.697	0.182	0.092	0.090		
1.0	1.899	1.736	0.163	0.090	0.073		
1.5	1.949	1.819	0.130	0.085	0.045		
2	1.999	1.891	0.108	0.081	0.027		
3	2.099	2.016	0.083	0.073	0.010		
4	2.199	2.129	0.070	0.066	0.004		
5	2.299	2.238	0.061	0.059	0.002		
10	2.799	2.763	0.036	0.035	0.001		
20	3.799	3.786	0.013				
30	4.799	4.795	0.004				
40	5.799	5.798	0.001				
50	6.799	6.799	0.000				

Downloaded From : www.EasyEngineering.net

Downloaded From : www.EasyEngineering.net

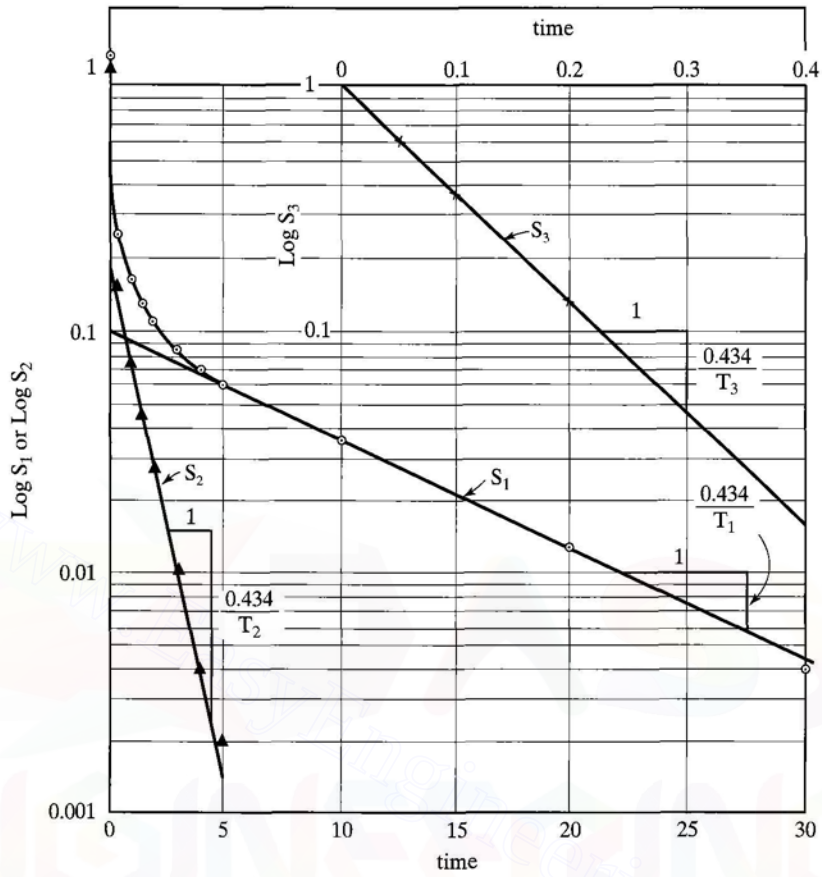


FIGURE A.6
Example A.5.

straight line. The slope of the straight line is

$$\frac{0.434}{T_1} = \frac{\log 0.1 - \log 0.01}{22} = 0.0455$$

or $T_1 = 9.54$. The intercept at $t = 0$ is $1/E_1 = 0.1$, or $E_1 = 10$. Column 5 can be calculated by $0.1 \exp(-t/9.54)$. Column 6 is the difference between columns 4 and 5. A plot of S_2 versus t results in a straight line. The slope of the straight line is

$$\frac{0.434}{T_2} = \frac{\log 0.2 - \log 0.0015}{5} = 0.426$$

or $T_2 = 1.02$. The intercept at $t = 0$ is $1/E_2 = 0.2$, or $E_2 = 5$. Column 7 can be calculated by $0.2 \exp(-t/1.02)$. Column 8 is the difference between columns 6 and 7. A plot of

Downloaded From : www.EasyEngineering.net

Downloaded From : www.EasyEngineering.net

S_3 versus t results in a straight line. The slope of the straight line is

$$\frac{0.434}{T_3} = \frac{\log 1 - \log 0.017}{0.4} = 4.424$$

or $T_3 = 0.098$. The intercept at $t = 0$ is $1/E_3 = 1$ or $E_3 = 1$. Because all points on S_3 lie practically on a straight line, three Kelvin models are sufficient to describe the creep-compliance curve. The equation for predicting the creep compliance is

$$D(t) = \frac{1}{2}\left(1 + \frac{t}{5}\right) + \frac{1}{10}\left[1 - \exp\left(-\frac{t}{9.54}\right)\right] + \frac{1}{5}\left[1 - \exp\left(-\frac{t}{1.02}\right)\right] + \left[1 - \exp\left(-\frac{t}{0.098}\right)\right] \tag{A.35}$$

Note that the values of E are the same as the original model shown in Figure 2.35*a*, but the values of T are slightly different, as a result of plotting error.

It can be seen that the stress–strain relationship of viscoelastic material can be characterized by a mechanical model or a creep curve. When one is known, the other can be determined.

A.4 COMPLEX MODULUS

The theory of complex modulus can be illustrated by the use of mechanical models. Figure A.7 shows a Kelvin model subjected to a sinusoidal loading. The sinusoidal loading can be represented by a complex number

$$\sigma = \sigma_0 \cos(\omega t) + i\sigma_0 \sin(\omega t) = \sigma_0 e^{i\omega t} \tag{A.36}$$

in which σ_0 is the stress amplitude and ω is the angular velocity, which is related to the frequency f by

$$\omega = 2\pi f \tag{A.37}$$

By assuming that the inertia effect is negligible, the governing differential equation can be written as

$$\lambda_1 \frac{\partial \epsilon}{\partial t} + E_1 \epsilon = \sigma_0 e^{i\omega t} \tag{A.38}$$

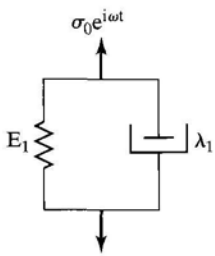


FIGURE A.7
Kelvin model under sinusoidal loading.

Downloaded From : www.EasyEngineering.net

Downloaded From : www.EasyEngineering.net

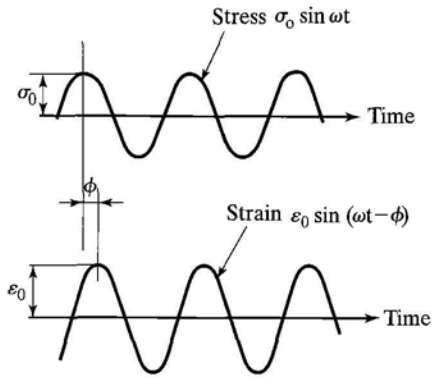


FIGURE A.8
Lag of strain behind stress.

The solution of Eq. A.38 can be expressed as

$$\epsilon = \epsilon_0 e^{i(\omega t - \phi)} \tag{A.39}$$

in which ϵ is the strain amplitude and ϕ is the phase angle by which the strain lags the stress, as shown in Figure A.8. Substituting Eq. A.39 into Eq. A.38 gives

$$i\lambda_1 \epsilon_0 \omega e^{i(\omega t - \phi)} + E_1 \epsilon_0 e^{i(\omega t - \phi)} = \sigma_0 e^{i\omega t} \tag{A.40}$$

After canceling $e^{i\omega t}$ on both sides of Eq. A.40 and equating the real terms to σ_0 and the imaginary terms to zero, we obtain the following two equations to solve for ϵ_0 and ϕ:

$$\lambda_1 \omega \epsilon_0 \sin \phi + E_1 \epsilon_0 \cos \phi = \sigma_0 \tag{A.41a}$$

$$\lambda_1 \omega \epsilon_0 \cos \phi - E_1 \epsilon_0 \sin \phi = 0 \tag{A.41b}$$

The solutions of Eq. A.41 are

$$\epsilon_0 = \frac{\sigma_0}{\sqrt{E_1^2 + (\lambda_1 \omega)^2}} \tag{A.42a}$$

$$\tan \phi = \frac{\lambda_1 \omega}{E_1} \tag{A.42b}$$

It can be seen from Eq. A.42*b* that, for elastic materials, $\lambda_1 = 0$, so $\phi = 0$; however, for viscous materials, $E_1 = 0$, so $\phi = \pi/2$. Therefore, the phase angle for viscoelastic materials ranges from 0 to $\pi/2$. The complex modulus E^* is defined as

$$E^* = \frac{\sigma}{\epsilon} = \frac{\sigma_0 e^{i\omega t}}{\epsilon_0 e^{i(\omega t - \phi)}}$$

or

$$E^* = \frac{\sigma_0}{\epsilon_0} \cos \phi + i \frac{\sigma_0}{\epsilon_0} \sin \phi \tag{A.43}$$

The dynamic modulus is the absolute value of the complex modulus

$$|E^*| = \sqrt{\left(\frac{\sigma_0}{\epsilon_0} \cos \phi\right)^2 + \left(\frac{\sigma_0}{\epsilon_0} \sin \phi\right)^2} = \frac{\sigma_0}{\epsilon_0} \tag{A.44}$$

Downloaded From : www.EasyEngineering.net

Downloaded From : www.EasyEngineering.net

It is interesting to note that the real part of Eq. A.43 is actually equal to the elastic stiffness E_1 and the imaginary part to the internal damping $\lambda_1\omega$.

Example A.6:

A sinusoidal loading with an amplitude of 50 psi (345 kPa) and a frequency of 5 Hz is applied to a specimen characterized by the Kelvin model shown in Figure A.9. Determine the strain amplitude ϵ_0, phase angle ϕ, and dynamic modulus $|E^*|$.

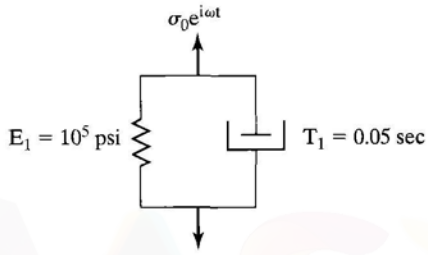


FIGURE A.9
Example A.6 (1 psi = 6.9 kPa).

Solution: Given $f = 5$ Hz, from Eq. A.37, $\omega = 2\pi \times 5 = 31.416$ rad/s. $\lambda_1 = T_1E_1 = 0.05 \times 10^5 = 5000$ lb-s/in.^{2} (35 MPa-s). From Eq. A.42*a*, $\epsilon_0 = 50/[(10^5)^2 + (5000 \times 31.416)^2]^{0.5} = 2.69 \times 10^{-4}$; from Eq. A.42*b*, $\tan\phi = 5000 \times 31.416/10^5 = 1.57$, or $\phi = 57°$; and from Eq. A.44, $|E^*| = 50/(2.69 \times 10^{-4}) = 1.85 \times 10^5$ psi (1.38 MPa).

Most viscoelastic materials cannot be simulated by a single Kelvin model; rather, they require a series of Kelvin models. The complex modulus of these models can be more easily obtained by the use of Fourier transform similar to the Laplace transform discussed in Section A.2.1. The Fourier transform is defined as

$$L[F(t)] = \int_{-\infty}^{\infty} F(t)e^{-i\omega t}\,dt \tag{A.45}$$

For simplicity, the same notations are used for the Fourier transform as for the Laplace transform. The Fourier transform of the first derivative $d\sigma/dt$ is

$$L\left(\frac{d\sigma}{dt}\right) = \int_{-\infty}^{\infty} \frac{d\sigma}{dt} e^{-i\omega t}\,dt = \int_{-\infty}^{\infty} e^{-i\omega t}\,d\sigma$$
$$= \sigma e^{-i\omega t}\Big|_{-\infty}^{\infty} - \int_{-\infty}^{\infty} \sigma d(e^{-i\omega t})$$

If the material is initially undisturbed, or $\sigma = 0$ when $t = -\infty$, then the first term is equal to 0, or

$$L\left(\frac{d\sigma}{dt}\right) = i\omega \int_{-\infty}^{\infty} \sigma e^{-i\omega t}\,dt = i\omega\bar{\sigma} \tag{A.46}$$

Downloaded From : www.EasyEngineering.net

Downloaded From : www.EasyEngineering.net

It can easily be proven that the Fourier transform of $\partial^n\sigma/\partial t^n$, abbreviated as $D^n\sigma$, is obtained by replacing D with $i\omega$ and σ with $\overline{\sigma}$, similar to the Laplace transform where D is replaced by p:

$$L(D^n\sigma) = (i\omega)^n\,\overline{\sigma} \tag{A.47}$$

The application of the Fourier transform to determine the dynamic modulus of a viscoelastic material characterized by a generalized model can best be illustrated by the following example.

Example A.7:

Figure A.10 shows a generalized model composed of one Maxwell model and two Kelvin models. If the model is subjected to a sinusoidal loading with a frequency of 10 Hz, determine the dynamic modulus of the material.

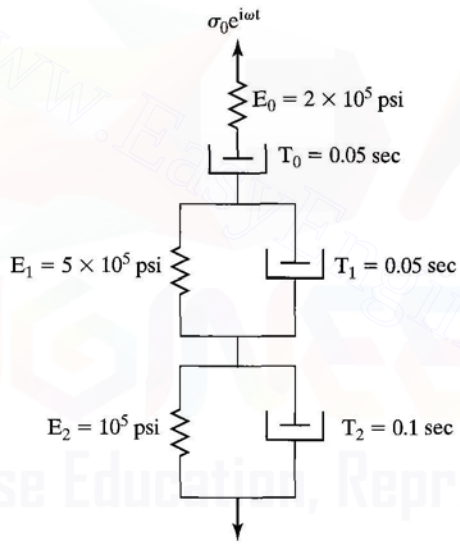


FIGURE A.10
Example A.7 (1 psi = 6.9 kPa).

Solution: From Eq. A.5, the stress-strain ratio of the model can be expressed as

$$\frac{\sigma}{\epsilon} = \left[\frac{0.05D + 1}{2 \times 10^5 \times 0.05D} + \frac{1}{5 \times 10^5(0.05D + 1)} + \frac{1}{10^5(0.1D + 1)}\right]^{-1} \tag{A.48}$$

From Eq. A.37, $\omega = 2\pi \times 10 = 62.83$. The complex modulus can be obtained by replacing D in Eq. A.48 by $62.83i$. We have

$$E^* = \frac{10^5}{\dfrac{(3.142i + 1)}{6.283i} + \dfrac{1}{5(3.142i + 1)} + \dfrac{1}{(6.283i + 1)}}$$

$$= \frac{10^5}{\dfrac{(3.142 - i)}{6.283} + \dfrac{(1 - 3.142i)}{54.361} + \dfrac{(1 - 6.283i)}{40.476}} = \frac{10^5}{0.543 - 0.372i}$$

Downloaded From : www.EasyEngineering.net

Downloaded From : www.EasyEngineering.net

$$= \frac{10^5(0.543 + 0.372i)}{0.433} = 10^5(1.254 + 0.859i)$$

$$|E^*| = 10^5\sqrt{(1.254)^2 + (0.859)^2} = 1.52 \times 10^5 \text{ psi } (1.05 \text{ GPa})$$

It was shown in Section 2.3.1 that the stress-strain relationship of viscoelastic materials can be represented by a mechanical model or a creep compliance curve. If one is known, the other can be determined. The complex modulus can also be obtained from the mechanical model, so the creep compliance and complex modulus should also be related. As long as the material is ideally viscoelastic, any type of test can be used. However, to describe the viscoelastic behavior over a large time range, various frequencies should be used to determine the complex modulus.

Downloaded From : www.EasyEngineering.net

Downloaded From : www.EasyEngineering.net

APPENDIX B

Theory of Elastic Layer Systems

This appendix derives the equations for determining the stresses and displacements in a multilayer system under a circular loaded area, as assumed in KENLAYER, and under a concentrated nodal force, as applied in KENSLABS.

B.1 DIFFERENTIAL EQUATIONS

As in the classical theory of elasticity, a stress function ϕ that satisfies the governing differential equation

$$\nabla^4 \phi = 0 \tag{B.1a}$$

is assumed for each of the layers. For systems with an axially symmetrical stress distribution,

$$\nabla^4 = \left(\frac{\partial^2}{\partial r^2} + \frac{1}{r}\frac{\partial}{\partial r} + \frac{\partial^2}{\partial z^2}\right)\left(\frac{\partial^2}{\partial r^2} + \frac{1}{r}\frac{\partial}{\partial r} + \frac{\partial^2}{\partial z^2}\right) \tag{B.1b}$$

in which r and z are the cylindrical coordinates for radial and vertical directions, respectively. After the stress function is found, the stresses and displacements can be determined by

$$\sigma_z = \frac{\partial}{\partial z}\left[(2 - \nu)\nabla^2 \phi - \frac{\partial^2 \phi}{\partial z^2}\right] \tag{B.2a}$$

$$\sigma_r = \frac{\partial}{\partial z}\left(\nu \nabla^2 \phi - \frac{\partial^2 \phi}{\partial r^2}\right) \tag{B.2b}$$

$$\sigma_t = \frac{\partial}{\partial z}\left(\nu \nabla^2 \phi - \frac{1}{r}\frac{\partial \phi}{\partial r}\right) \tag{B.2c}$$

Downloaded From : www.EasyEngineering.net

Downloaded From : www.EasyEngineering.net

$$\tau_{rz} = \frac{\partial}{\partial r}\left[(1-\nu)\nabla^2\phi - \frac{\partial^2\phi}{\partial z^2}\right] \tag{B.2d}$$

$$w = \frac{1+v}{E}\left[(1-2\nu)\nabla^2\phi + \frac{\partial^2\phi}{\partial r^2} + \frac{1}{r}\frac{\partial\phi}{\partial r}\right] \tag{B.2e}$$

$$u = -\frac{1+\nu}{E}\left(\frac{\partial^2\phi}{\partial r\,\partial z}\right) \tag{B.2f}$$

Because Eq. B.1 is a fourth-order differential equation, the stresses and displacements thus determined will consist of four constants of integration that must be determined from the boundary and continuity conditions.

Let $\rho = r/H$ and $\lambda = z/H$, in which H is the distance from the surface to the upper boundary of the lowest layer, as shown in Figure 3.1. It can be verified easily by substitution that

$$\phi_i = \frac{H^3 J_0(m\rho)}{m^2}[A_i e^{-m(\lambda_i-\lambda)} - B_i e^{-m(\lambda-\lambda_{i-1})} + C_i m\lambda e^{-m(\lambda_i-\lambda)} - D_i m\lambda e^{-(\lambda-\lambda_{i-1})}] \tag{B.3}$$

is a stress function for the ith layer which satisfies Eq. B.1, in which J_0 is a Bessel function of the first kind and order 0; m is a parameter; and A, B, C, D are constants of integration to be determined from boundary and continuity conditions. The subscript i varies from 1 to n and refers to the quantities corresponding to the ith layer.

Substituting Eq. B.3 into B.2 gives

$$(\sigma_z^*)_i = -mJ_0(m\rho)\{[A_i - C_i(1-2\nu_i - m\lambda)]\,e^{-m(\lambda_i-\lambda)} + [B_i + D_i(1-2\nu_i + m\lambda)]\,e^{-m(\lambda-\lambda_{i-1})}\} \tag{B.4a}$$

$$(\sigma_r^*)_i = \left[mJ_0(m\rho) - \frac{J_1(m\rho)}{\rho}\right]\{[A_i + C_i(1+m\lambda)]\,e^{-m(\lambda_i-\lambda)} + [B_i - D_i(1-m\lambda)] \times e^{-m(\lambda-\lambda_{i-1})}\} + 2\nu_i\, mJ_0(m\rho)[C_i e^{-m(\lambda_i-\lambda)} - D_i e^{-m(\lambda-\lambda_{i-1})}] \tag{B.4b}$$

$$(\sigma_t^*)_i = \frac{J_1(m\rho)}{\rho}\{[A_i + C_i(1+m\lambda)]\,e^{-m(\lambda_i-\lambda)} + [B_i - D_i(1-m\lambda)]\,e^{-m(\lambda-\lambda_{i-1})}\} + 2\nu_i\, mJ_0(m\rho)[C_i e^{-m(\lambda_i-\lambda)} - D_i e^{-m(\lambda-\lambda_{i-1})}] \tag{B.4c}$$

$$(\tau_{rz}^*)_i = mJ_1(m\rho)\{[A_i + C_i(2\nu_i + m\lambda)]\,e^{-m(\lambda_i-\lambda)} - [B_i - D_i(2\nu_i - m\lambda)]\,e^{-m(\lambda-\lambda_{i-1})}\} \tag{B.4d}$$

$$(w^*)_i = -\frac{1+\nu_1}{E_i}J_0(m\rho)\{[A_i - C_i(2-4\nu_i - m\lambda)]\,e^{-m(\lambda_i-\lambda)} - [B_i + D_i(2-4\nu_i + m\lambda)]\,e^{-m(\lambda-\lambda_{i-1})} \tag{B.4e}$$

Downloaded From : www.EasyEngineering.net

Downloaded From : www.EasyEngineering.net

$$(u^*)_i = \frac{1+\nu_i}{E_i} J_1(m\rho)\{[A_i + C_i(1+m\lambda)]\, e^{-m(\lambda_i-\lambda)} + [B_i - D_i(1-m\lambda)]e^{-m(\lambda-\lambda_{i-1})}\} \quad \text{(B.4}f\text{)}$$

in which σ_z is the stress in the vertical or z direction; σ_r is the stress in the radial or r direction; σ_t is the stress in the tangential or t direction; τ_{rz} is the shear stress; w is the displacement in the vertical or z direction; u is the displacement in the radial or r direction; and J_1 is a Bessel function of the first kind and of order one. The subscript i outside the parentheses indicates the ith layer. A star superscript is placed on these stresses and displacements because they are not the actual stresses and displacements due to a uniform load q distributed over a circular area of radius a, but are those due to a vertical load of $-mJ_0(m\rho)$, as can be seen from Eq. B.4a when the terms within the braces are set to 1.

B.2 CIRCULAR LOADED AREA

To find the stresses and displacements due to a constant load q distributed over a circular area of radius a, the Hankel transform method is employed. The Hankel transform of such load is

$$\bar{f}(m) = \int_0^{\alpha} q\rho J_0(m\rho)\, d\rho = \frac{q\alpha}{m} J_1(m\alpha) \quad \text{(B.5)}$$

in which $\alpha = a/H$. The Hankel inversion of $\bar{f}(m)$ is

$$q(\rho) = \int_0^{\infty} \bar{f}(m) m J_0(m\rho)\, dm = q\alpha \int_0^{\infty} J_0(m\rho)\, J_1(m\alpha)\, dm \quad \text{(B.6)}$$

If R^* is the stress or displacement in Eq. B.4 due to the loading $-mJ_0(m\rho)$ and R is that due to load q, and tension is considered negative, then

$$R = q\alpha \int_0^{\infty} \frac{R^*}{m} J_1(m\alpha)\, dm \quad \text{(B.7)}$$

The analysis of layered systems can therefore be summarized into the following steps:

1. Assign successive values of m, from 0 to a rather large positive number until R in Eq. B.7 converges.
2. For each value of m, determine the constants of integration, A_i, B_i, C_i, and D_i, from the boundary and continuity conditions, which are discussed later.
3. Substitute these constants into Eq. B.4 to obtain R^*.
4. Determine R from Eq. B.7 by numerical integration.

In the numerical integration, the zeros of $J_0(m\rho)$ and $J_1(m\alpha)$ are determined and the integral between these two zeros is evaluated by a four-point Gaussian formula. In view of the fact that the first cycle of integration has to be more finely divided, especially

Downloaded From : www.EasyEngineering.net

Downloaded From : www.EasyEngineering.net

when ρ is large, the interval between 0 and 2.40483, which is the first zero of J_0, is subdivided into six intervals, and that between 2.40483 and 3.83171, which is the first zero of J_1, is subdivided into two intervals. The integral for each subinterval is also evaluated by the four-point formula.

B.3 BOUNDARY AND CONTINUITY CONDITIONS

At the upper surface, $i = 1$ and $\lambda = 0$, the boundary conditions

$$(\sigma_z^*)_1 = -mJ_0(m\rho) \tag{B.8a}$$

$$(\tau_{rz}^*)_1 = 0 \tag{B.8b}$$

result in two equations:

$$\begin{bmatrix} e^{-m\lambda_1} & 1 \\ e^{-m\lambda_1} & -1 \end{bmatrix} \begin{Bmatrix} A_1 \\ B_1 \end{Bmatrix} + \begin{bmatrix} -(1-2\nu_1)e^{-m\lambda_1} & 1-2\nu_1 \\ 2\nu_1 e^{-m\lambda_1} & 2\nu_1 \end{bmatrix} \begin{Bmatrix} C_1 \\ D_1 \end{Bmatrix} = \begin{Bmatrix} 1 \\ 0 \end{Bmatrix} \tag{B.9}$$

All the solutions of layered systems presented in Chapter 2 are based on the assumption that the layers are fully bonded with the same vertical stress, shear stress, vertical displacement, and radial displacement at every point along the interface. Therefore, when $\lambda = \lambda_i$, the continuity conditions

$$(\sigma_z^*)_i = (\sigma_z^*)_{i+1} \tag{B.10a}$$

$$(\tau_{rz}^*)_i = (\tau_{rz}^*)_{i+1} \tag{B.10b}$$

$$(w^*)_i = (w^*)_{i+1} \tag{B.10c}$$

$$(u^*)_i = (u^*)_{i+1} \tag{B.10d}$$

result in four equations:

$$\begin{bmatrix} 1 & F_i & -(1-2\nu_i-m\lambda_i) & (1-2\nu_i+m\lambda_i)F_i \\ 1 & -F_i & 2\nu_i+m\lambda_i & (2\nu_i-m\lambda_i)F_i \\ 1 & F_i & 1+m\lambda_i & -(1-m\lambda_i)F_i \\ 1 & -F_i & -(2-4\nu_i-m\lambda_i) & -(2-4\nu_i+m\lambda_i)F_i \end{bmatrix} \begin{Bmatrix} A_i \\ B_i \\ C_i \\ D_i \end{Bmatrix}$$

$$= \begin{bmatrix} F_{i+1} & 1 & -(1-2\nu_{i+1}-m\lambda_i)F_{i+1} & 1-2\nu_{i+1}+m\lambda_i \\ F_{i+1} & -1 & (2\nu_{i+1}+m\lambda_i)F_{i+1} & 2\nu_{i+1}-m\lambda_i \\ R_iF_{i+1} & R_i & (1+m\lambda_i)R_iF_{i+1} & -(1-m\lambda_i)R_i \\ R_iF_{i+1} & -R_i & -(2-4\nu_{i+1}-m\lambda_i)R_iF_{i+1} & -(2-4\nu_{i+1}+m\lambda_i)R_i \end{bmatrix} \begin{Bmatrix} A_{i+1} \\ B_{i+1} \\ C_{i+1} \\ D_{i+1} \end{Bmatrix} \tag{B.11}$$

In these equations,

$$F_i = e^{-m(\lambda_i-\lambda_{i-1})} \tag{B.12a}$$

$$R_i = \frac{E_i}{E_{i+1}} \frac{1+\nu_{i+1}}{1+\nu_i} \tag{B.12b}$$

The stresses and displacements must vanish as λ approaches infinity, so it can be concluded from Eq. B.3 that, for the lowest layer with $i = n$,

Downloaded From : www.EasyEngineering.net

Downloaded From : www.EasyEngineering.net

$$A_n = C_n = 0 \tag{B.13}$$

For an n-layer system, there are $4n$ constants of integration. With $A_n = C_n = 0$, the remaining $4n - 2$ constants can be determined from the $4n - 2$ equations, two from Eq. B.9 and $4(n - 1)$ from Eq. B.11.

To save computer times in solving simultaneous equations, a procedure was developed by which only two equations need be solved, instead of $4n - 2$ equations. This can be achieved by transforming Eq. B.11 to

$$\begin{Bmatrix} A_i \\ B_i \\ C_i \\ D_i \end{Bmatrix} = \begin{bmatrix} 4 \times 4 \\ \text{matrix} \end{bmatrix} \begin{Bmatrix} A_{i+1} \\ B_{i+1} \\ C_{i+1} \\ D_{i+1} \end{Bmatrix} \tag{B.14}$$

By successive multiplications, the constants for the first layer can be related to those of the last layer by

$$\begin{Bmatrix} A_1 \\ B_1 \\ C_1 \\ D_1 \end{Bmatrix} = \begin{bmatrix} 4 \times 2 \\ \text{matrix} \end{bmatrix} \begin{Bmatrix} B_n \\ D_n \end{Bmatrix} \tag{B.15}$$

When Eq. B.15 is substituted into Eq. B.9, two equations with two unknowns, B_n and D_n, are obtained. After B_n and D_n are solved, they can be substituted into Eq. B.14, with $A_n = C_n = 0$, to obtain the constants for the $(n - 1)$th layer. The procedure is repeated until the constants for every layer up to the first layer are obtained.

If the ith interface, or $\lambda = \lambda_i$, is unbonded or frictionless, the continuation of shear stress and radial displacement must be replaced by zero shear stress on both sides of the interface:

$$(\sigma_z^*)_i = (\sigma_z^*)_{i+1} \tag{B.16a}$$

$$(w^*)_i = (w^*)_{i+1} \tag{B.16b}$$

$$(\tau_{rz}^*)_i = 0 \tag{B.16c}$$

$$(\tau_{rz}^*)_{i+1} = 0 \tag{B.16d}$$

Hence, Eq. B.11 must be replaced by

$$\begin{bmatrix} 1 & F_i & -(1 - 2\nu_i - m\lambda_i) & (1 - 2\nu_i + m\lambda_i)\, F_i \\ 1 & F_i & 1 + m\lambda_i & -(1 - m\lambda_i)\, F_i \\ 1 & -F_i & 2\nu_i + m\lambda_i & (2\nu_i - m\lambda_i)\, F_i \\ 0 & 0 & 0 & 0 \end{bmatrix} \begin{Bmatrix} A_i \\ B_i \\ C_i \\ D_i \end{Bmatrix}$$

$$= \begin{bmatrix} F_{i+1} & 1 & -(1 - 2\nu_{i+1} - m\lambda_i)F_{i+1} & 1 - 2\nu_{i+1} + m\lambda_i \\ R_i F_{i+1} & R_i & (1 + m\lambda_i)R_i F_{i+1} & -(1 - m\lambda_i)R_i \\ 0 & 0 & 0 & 0 \\ F_{i+1} & -1 & (2\nu_{i+1} + m\lambda_i)F_{i+1} & 2\nu_{i+1} - m\lambda_i \end{bmatrix} \begin{Bmatrix} A_{i+1} \\ B_{i+1} \\ C_{i+1} \\ D_{i+1} \end{Bmatrix} \tag{B.17}$$

Downloaded From : www.EasyEngineering.net

Downloaded From : www.EasyEngineering.net

Both Eqs. B.11 and B.17 are used in KENLAYER. If any interface is bonded, Eq. B.11 applies. If any interface is frictionless, Eq. B.17 applies. The program is more efficient when all interfaces are bonded, because only two equations are to be solved. If some interfaces are frictionless, the program is less efficient, because more time is needed to solve the $4n - 2$ equations. KENLAYER was originally developed for bonded interfaces only. When the frictionless interfaces were added, an existing subroutine for collocation was used to solve the $4n - 2$ equations. Because frictionless interfaces are very rarely used, the requirement of more computer time is not of major concern.

B.4 EXTENSION TO CONCENTRATED LOAD

In Burmister's theory, the load is applied over a circular area. In the finite-element method, the load is concentrated at each node. To find the stiffness of a foundation, it is necessary to determine the deflection at a given node i due to a concentrated load at a given node j. This can be obtained from Eq. B.7 by reducing the contact radius to zero, or

$$R = \frac{1}{\pi a^2}\frac{a}{H}\int_0^\infty \frac{R^*}{m} J_1(m\alpha)\, dm = \frac{1}{\pi H^2}\int_0^\infty \frac{J_1(m\alpha)}{m\alpha} R^* dm \tag{B.18}$$

Since

$$\lim_{\alpha \to 0} \frac{J_1(m\alpha)}{m\alpha} = 0.5 \tag{B.19}$$

Eq. C.2 becomes

$$R = \frac{1}{2\pi H^2}\int_0^\infty R^*\, dm \tag{B.20}$$

in which R is the dimensionless deflection and R^* is expressed by Eq. B.4*e* and involves the Bessel function $J_0(m\rho)$. To obtain more accurate results when ρ is large, a 32-point Gaussian quadrature formula is used for the first cycle of integration, and an 8-point formula is used for the remaining cycles until the specified maximum number of iterations is reached.

The analysis of layered systems under a unit concentrated load can be summarized into the following steps:

1. Assign successive values of m, starting from 0 to a rather large positive number until R in Eq. B.20 converges.
2. For each value of m, determine the constants of integration, A, B, C, and D, from the boundary and continuity conditions, as discussed previously.
3. Substitute these constants into Eq. B.4 to obtain R^*. In KENSLABS, only the vertical deflection w^*, or Eq. B.4e, need be considered.
4. Determine R from Eq. B.20 by numerical integration.

Downloaded From : www.EasyEngineering.net

Downloaded From : www.EasyEngineering.net

APPENDIX C

KENPAVE Software

The four separate computer programs, viz. LAYERINP, KENLAYER, SLABSINP, KENSLABS, together with some other graphics programs are combined together to form a new software called KENPAVE. KENPAVE was written in Visual Basic and can be run on computers with Windows 95 or higher. Details on the use of the software can be found on the computer screens, so only a brief summary of the most important features is presented in this appendix.

C.1 SOFTWARE INSTALLATION

The software is stored in a CD and consists of five files: SETUP.EXE, SETUP.LST, KENPAVE1.CAB, KENPAVE2.CAB, and KENPAVE3.CAB. It can be installed on any computer with Windows 95 or higher. The procedures to install KENPAVE are described below:

1. Insert disk into the CD Drive, say, Drive D. Click the Start button, then click Run, and an input box will be shown.
2. Type the drive first followed by SETUP (e.g. D:\SETUP), then click OK, and a setup screen with some instructions will appear.
3. It is suggested that all the installed files be stored in a default directory called C:\KENPAVE. However, you can override the default and store them in any directory you want.
4. Follow the instructions on the screen until the message "KENPAVE setup was completed successfully" appears. During the installation, if the message "A file being copied is older than the file in your system. Do you want to keep this file?" appears, simply click "Yes" as recommended. If an error message appears for a certain file, click the Ignore button and let the installation continue; your system might already have this file, or the destination file might be write protected.
5. Run KENPAVE by clicking the Start button, then pointing to Programs and KENPAVE, and finally clicking KENPAVE. A Main Screen of KENPAVE will appear.

Downloaded From : www.EasyEngineering.net

Downloaded From : www.EasyEngineering.net

For computers without a CD drive, the software can be installed by copying the five files in the CD into three 1.44MB floppy disks, using a computer with both CD and floppy disk drives. Copy SETUP.EXE, SETUP.LST, and KENPAVE1.CAB to disk 1, KENPAVE2.CAB to disk 2, and KENPAVE3 to disk 3. The installation procedures are the same as described above, except that the first two steps should be changed to "Insert disk 1 into Drive A and type A:\SETUP."

After installation, a total of 30 files will be stored in the KENPAVE directory, among them KENPAVE.EXE, KENLAYER.EXE, KENSLABS.EXE, LARGE.EXE (KENSLABS with a large memory), 12 data files in English units, 12 data files in SI units, DATAPATH for use by drop-down list box, and ST6UNST for software removal.

To remove the software from the computer, click Start, point to Settings, and click Control Panel. Then double-click the Add/Remove Programs icon, and a list box for all the installed programs, including KENPAVE, will be shown. After clicking on KENPAVE and then on the Add\Remove button, you will have deleted all the previously installed KENPAVE files, including .EXE files and .DAT files.

C.2 MAIN SCREEN

Figure C.1 shows the Main Screen of KENPAVE, consisting of two input boxes at the top and 11 command buttons at the bottom. The left three buttons are used for flexible or asphalt pavements, the right five for rigid or concrete pavements, and the remaining three for general purposes. Details on the use of these boxes and buttons can be viewed by clicking the Help button and therefore are not repeated in this appendix.

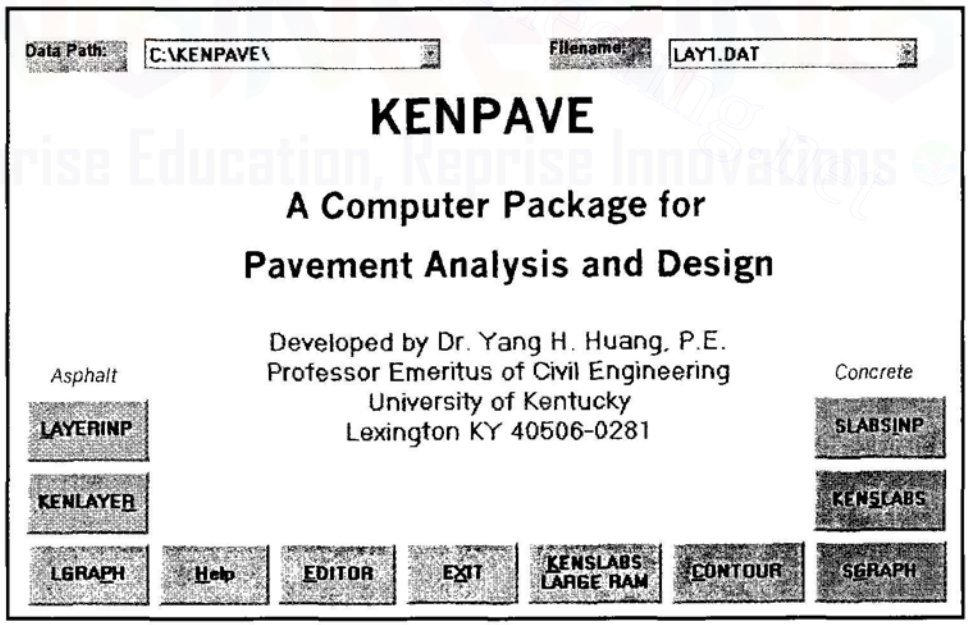


FIGURE C.1

Main Screen of KENPAVE.

Downloaded From : www.EasyEngineering.net

Downloaded From : www.EasyEngineering.net

File LAY1.DAT is the data file for example 1 of KENLAYER, which is stored in C:\KENPAVE directory. Clicking the KENLAYER button runs this example, and a graph can be obtained by clicking the LGRAPH button. Clicking the EDITOR button and then clicking Examples\KENLAYER\LAY1 menu displays an explanation of this example.

To run SLA1.DAT by KENSLABS, first click the downward arrow on the right side of Filename input box; a drop-down list box will be shown. Then click SLA1.DAT, and this file will appear in the Filename input box. Click KENSLABS, then SGRAPH, and finally CONTOUR. Because this example does not require large memory, there is no need to click KENSLABS LARGE RAM.

C.3 LAYERINP

Detailed instructions on the use LAYERINP can be viewed on the computer screens and therefore are not repeated here. Figure C.2 shows the location of input parameters on various screens in LAYERINP. All input parameters are in upper case; the menus in

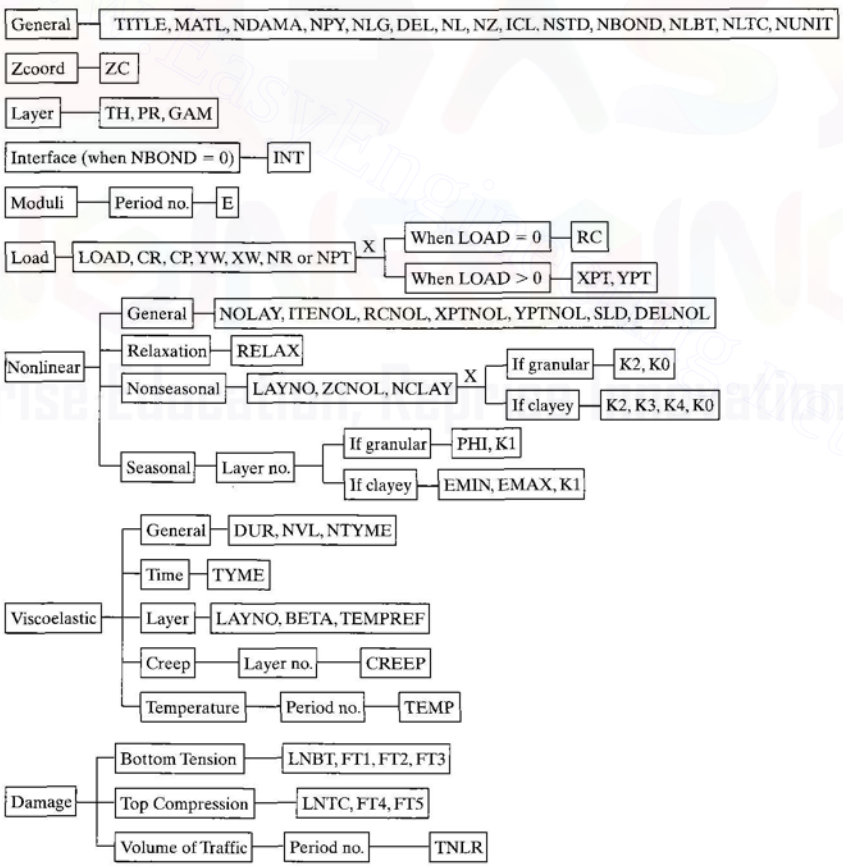


FIGURE C.2

Location of input parameters by various menus in LAYERINP.

Downloaded From : www.EasyEngineering.net

Downloaded From : www.EasyEngineering.net

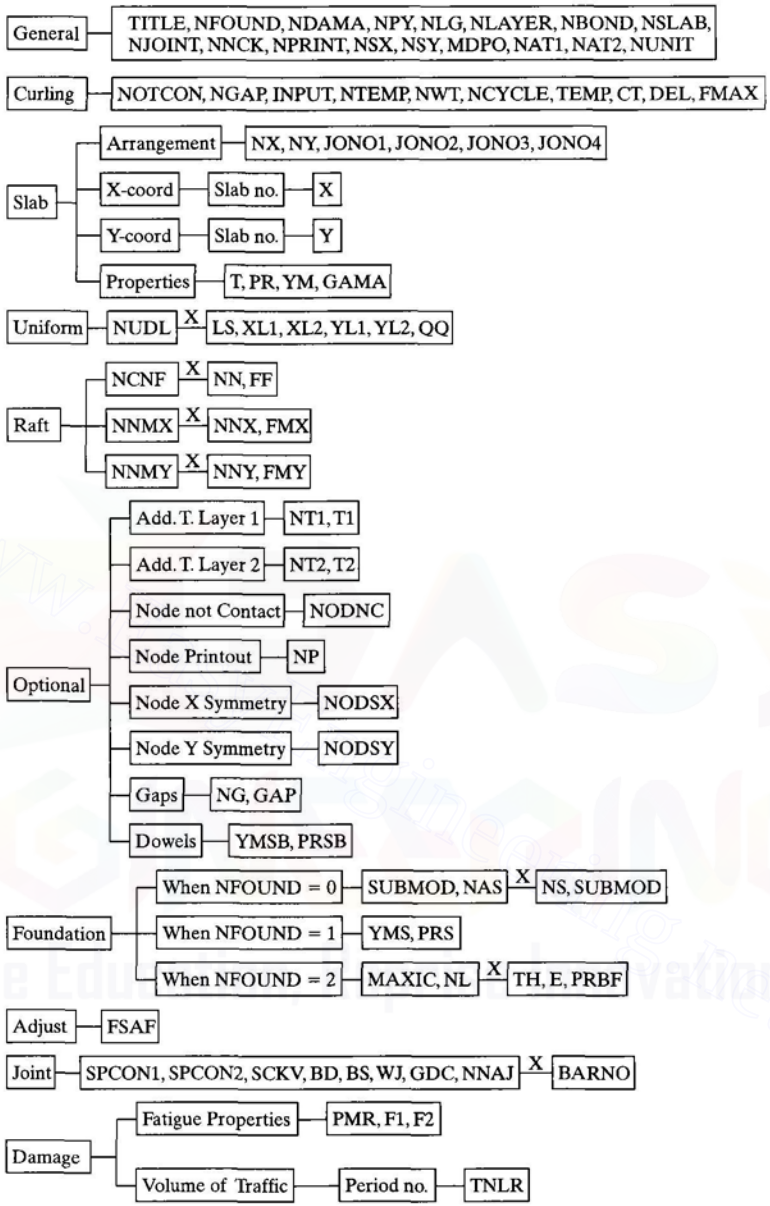


FIGURE C.3

Location of input parameters by various menus in SLABSINP.

which the input parameters are located are in lower case, except for the first letter of each menu. The letter X indicates the existence of an auxiliary screen, which will appear automatically when a certain input parameter in the previous screen is typed. For example, Figure C.2 shows that there are nine menus on the Main Screen of LAYERINP. When

Downloaded From : www.EasyEngineering.net

Downloaded From : www.EasyEngineering.net

the "Load" menu is clicked, a screen with one or more lines, each representing a given load group, will be shown. On each line are six input parameters. When the entry to the last parameter NR or NPT is typed, an auxiliary screen with input parameters RC or XPT and YPT will appear. This auxiliary screen can also be reached by double-clicking anywhere on the line where NR or NPT for the given load group is located.

C.4 SLABSINP

Detailed instructions on the use of SLABSINP can be viewed on the computer screens and therefore are not repeated here. Figure C.3 shows the location of input parameters on various screens in SLABSINP. There are 10 menus on the Main Screen of SLABSINP and seven auxiliary screens, as indicated by the seven X's.

Downloaded From : www.EasyEngineering.net

Downloaded From : www.EasyEngineering.net

APPENDIX D

An Introduction to Superpave

by Kamyar C. Mahboub, Ph.D., P.E.

Superpave is a product of the Strategic Highway Research Program (SHRP). This research effort led to a new system for design of hot mix asphalt based upon mechanistic concepts. The Superpave™ has been fully implemented by most of the state highway agencies. Superpave is an acronym for Superior Performing Asphalt Pavements. The Superpave system accounts for materials characteristics in light of climatic and traffic considerations (AI, 2001, 1996, 1997). Perhaps the most significant component of Superpave is its new asphalt binder grading system, which is designed to link with pavement performance. The Superpave methodology is believed to be the best available at this time. However, it is an evolving methodology, and as such there are various asphalt characterization routines that are under consideration as future additions to the Superpave (Witczak, *et al.* 2002).

D.1 ASPHALT BINDER GRADING SYSTEM

The asphalt binder grading system in Superpave is called the performance grading (PG) system. This system is a radical departure from the previous viscosity or penetration based systems. All PG binders are characterized based upon fundamental engineering parameters. Additionally, Superpave accounts for the impact of climatic factors on binder characteristics at both hot and cold temperature regimes. This is a major improvement over previous systems of asphalt binder grading. In addition to climatic conditions, traffic and aging control the performance of the asphalt pavement. To simulate climate conditions, testing is conducted at three pavement temperatures: hot, intermediate, and cold pavement temperatures. These temperatures are derived from weather data for various geographical locations. The climatic data is further transformed to represent the pavement temperature. To simulate traffic conditions, an average rate of loading was assumed for normal highway traffic speeds. Heavy traffic conditions may be addressed by selecting a binder corresponding to higher temperature regimes. To simulate binder aging, a new rolling thin-film oven procedure was

Downloaded From : www.EasyEngineering.net

Downloaded From : www.EasyEngineering.net

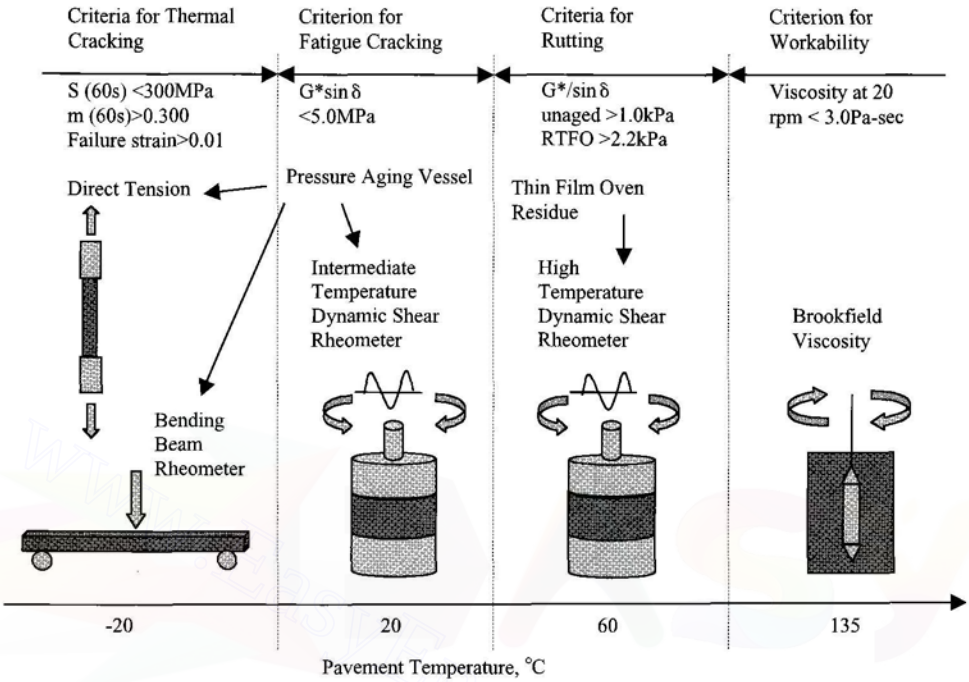


FIGURE D.1

A summary of mechanical tests related to asphalt binder PG grading.

developed under Superpave, which allows for rapid aging/oxidation of an asphalt binder under simulated conditions.

The Superpave binder grading tests are based upon engineering properties that control three major modes of distress in asphalt pavements: rutting, fatigue cracking, and thermal cracking. The contribution of the asphalt binder to these modes of distress is characterized through a battery of rheological tests which are outlined in Figure D1. The test data are analyzed in light of climatic conditions for determining the asphalt binder grade. For example, a PG 64-28 is suitable for an environment where the maximum pavement temperature will not exceed 64°C, and the minimum pavement temperature will not drop below −28°C.

Figure D.1 presents a summary of mechanical tests related to asphalt binder PG grading. The direct tension (DT) test is intended to determine the resistance of asphalt to thermal cracking. Similarly, the Bending Beam Rheometer (BBR) is designed to measure the critical stiffness (S) at which the asphalt becomes brittle and susceptible to thermal cracking (m=slope of stiffness courve). In order to simulate the most severe case, the thermal-cracking analysis is conducted using the asphalt which has gone through the accelerated aging process using the pressurized aging vessel (PAV). The Dynamic Shear Rheometer (DSR) is the device that is used for fatigue and rutting characterization. The rheometer protocols are designed to measure elastic and damping properties of the asphalt binder via the complex shear modulus parameter (G^*). The rutting parameter is $G^*/\sin\delta$,

Downloaded From : www.EasyEngineering.net

Downloaded From : www.EasyEngineering.net

where δ is the phase angle and is related to damping. On the other hand, the $G^*\sin\delta$ is used to characterize the fatigue-cracking potential of asphalt. The fatigue characterization is conducted on asphalt, which is aged via the PAV process, while the rutting characterization is conducted on the asphalt binder that is aged using a Rolling Thin-Film Oven (RTFO) test. Superpave binder grading protocols are outlined in AASHTO MP1 specifications (AASHTO, 1999a). Tables D.1 through D.4 present Superpave Performance grade CPG binder specifications.

D.2 AGGREGATES IN HMA

Experience has shown that aggregates play a key role in HMA performance, and this was realized by SHRP researchers, which led to the refining of existing procedures to fit within the Superpave system. SHRP researchers produced an aggregate gradation specification without the benefit of experimentation to support or verify its formulation. Thus, in lieu of experimentally verifiable protocols, a panel of SHRP experts developed a set of recommendations for Superpave aggregate specifications (NCHRP Project 9-14, 1997). This led to a number of controversial issues including flat and elongated aggregates, and the restricted zone.

D.2.1 Flat and Elongated Aggregates

The recommendation for flat and elongated aggregate content was that, for high traffic (greater than 10^6 equivalent single axle loads—ESALs), no more than 10% of the aggregate particles retained on the 4.75 mm sieve should have a ratio of maximum-to-minimum dimension greater than 5:1 (Cominsky *et al.*, 1994).

Vavrik *et al.* (1999) recommended performance based testing as a requirement to establish if the use and breakdown of F&E particles had a detrimental effect on mixture performance. Brown *et al.* (1997) evaluated the effect of flat and elongated particles on SMA mixes. Stephens and Sinha (1978) studied the significance of flat and elongated particles on the characteristics of bituminous mixtures. In a mix design, they recommended 40–70 % cubical aggregates, 5–45 % flat aggregates and 5–45 % elongated aggregates. Oduroh *et al.* (2000) reported that coarse aggregates of 3:1 size ratio at 40% and higher had the highest tendency to lie flat (horizontally) during HMA compaction. Overall, Superpave laboratory mixture performance tests did not show any significant changes in mixture properties due to the presence of up to 40% of 3:1 flat and elongated aggregates.

D.2.2 Coarse Aggregate Angularity

The aggregate interlock and internal friction is responsible for the HMA rutting resistance. Aggregate angularity is quantified as the percent by weight of aggregates larger than 4.75 mm with one or more fractured faces. The standard test for measuring coarse aggregate angularity is ASTM D 5821: *Standard Test Method for Determining the Percentage of Fractured Particles in Coarse Aggregate*. Superpave specifies a higher degree of aggregate angularity for higher traffic. This is illustrated in Table D.5.

Downloaded From : www.EasyEngineering.net

Downloaded From : www.EasyEngineering.net

Table D.1 Superpave Specifications for Rutting

Superpave Binder Specifications
Average 7-day Maximum Pavement Design Temperature, °C
Minimum Pavement Design Temperature, °C
Flash Point Temp, T48: minimum, °C
Viscosity, ASTM D 4402: Maximum, 3-Pa-s (3000 cP). Test Temp, °C
Dynamic Shear, TP5 **G*/sin δ, Minimum, 1.00 kPa** Test Temperature@ 10 rad/s,°C
Rolling Thin Film Oven (T240)
Mass Loss, Maximum, %
Dynamic Shear, TP5: **G*/sin δ, Minimum, 2.20 kPa** Test Temp @ 10 rad/sec,°C

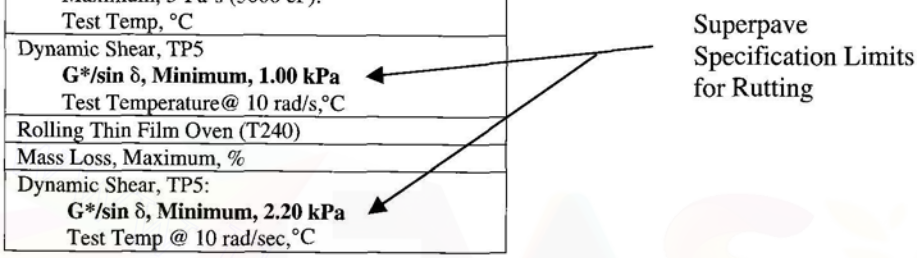
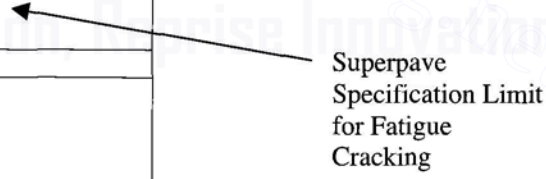


Table D.2 Superpave Specifications for Fatigue Cracking

Superpave Binder Specifications
PAV Aging Temp,°C
Dynamic Shear, TP5: **G*sin δ, Maximum, 5000 kPa** Test Temperature@ 10 rad/s,°C
Physical Hardening
Creep Stiffness, TP1: S, Maximum, 300 MPa m-value, Minimum, 0.300 Test Temperature@ 60sec,°C
Direct Tension, TP3: Failure Strain, Minimum, 1.0% Test Temperature@ 1.0mm/min, °C



Downloaded From : www.EasyEngineering.net

Downloaded From : www.EasyEngineering.net

Table D.3 Superpave Specifications for Thermal Cracking

Superpave Binder Specifications
PAV Aging Temp,°C
Dynamic Shear, TP5: G*sin δ, Maximum, 5000 kPa Test Temperature@ 10 rad/s,°C
Physical Hardening
Creep Stiffness, TP1: **S, Maximum, 300 MPa** m-value, Minimum, 0.300 Test Temperature@ 60sec,°C
Direct Tension, TP3: **Failure Strain, Minimum, 1.0%** Test Temperature@ 1.0mm/min, °C

Superpave Specification Limits for Thermal Cracking

Table D.4 Superpave Asphalt Binder Grades

High Temperature Grades (°C)	**Low Temperature Grades (°C)**
46	-34, -40, -46
52	-10, -16, -22, -28, -34, -40, -46
58	-16, -22, -28, -34, -40
64	-10, -16, -22, -28, -34, -40
70	-10, -16, -22, -28, -34, -40
76	-10, -16, -22, -28, -34
80	-10, -16, -22, -28, -34

Performance Grade Designation:

PG **Hot Temp** **Cold Temp**

Example: **PG 64-22**

Downloaded From : www.EasyEngineering.net

Downloaded From : www.EasyEngineering.net

TABLE D.5 Superpave Coarse Aggregate Angularity Requirements

Traffic, million ESALs	Minimum Fractured Surface Requirements (%)	
	$D < 100$ mm	$D > 100$ mm
<0.3	55/–	–/–
<1	65/–	–/–
<3	75/–	50/–
<10	85/80	60/–
<30	95/90	80/75
<100	100/100	95/90
≥100	100/100	100/100

Note. "85/80" means that 85% of the coarse aggregate has one fractured face, and 80% has two fractured faces. D = depth from surface

D.2.3 Fine Aggregate Angularity

Fine aggregate contribution to the internal friction of HMA is quantified as the percent of air voids present in loosely compacted fine aggregates (smaller than 2.36 mm). Higher void content in this case reflects a more textured fine aggregate. The standard test for measuring this property is AASHTO T 304: *Uncompacted Void Content–Method A*. Superpave specifies a higher degree of fine aggregate angularity for higher traffic. This is illustrated in Tables D.6.

D.2.4 Aggregate Clay Content

Clay is a highly undesirable material in HMA. The clay content is characterized via a suspension in the water test: AASHTO T 176: *Plastic Fines in Graded Aggregates and Soils by Use of the Sand Equivalent Test*. The clay content is controlled using a minimum sand equivalent criteria. Superpave requires higher sand equivalent (i.e. lower clay content) for higher traffic. This is illustrated in Table D.7.

TABLE D.6 Superpave Fine Aggregate Angularity Requirements

Traffic, million ESALs	Minimum Uncompacted Fine Aggregate Air Voids Requirements (%)	
	$D < 100$ mm	$D > 100$ mm
<0.3	–	–
<1	40	–
<3	40	40
<10	45	40
<30	45	40
<100	45	45
≥100	45	45

Note. Air voids criteria are presented as percent air voids in loosely compacted fine aggregate. D = depth from surface

Downloaded From : www.EasyEngineering.net

Downloaded From : www.EasyEngineering.net

TABLE D.7 Superpave Fine Aggregate Angularity Requirements

Traffic, million ESALs	Sand Equivalent, minimum
<0.3	40
<1	40
<3	40
<10	45
<30	45
<100	50
≥100	50

D.2.5 Aggregate Toughness

Toughness is characterized using the Los Angeles Abrasion test. The procedure is described in AASHTO T 96: *Resistance to Abrasion of Small Size Coarse Aggregate by Use of the Los Angeles Machine*. This test simulates the resistance of coarse aggregate to abrasion and mechanical impact during handling, construction, and in service. The test is based upon comparing the coarse aggregate gradation before and after subjecting the aggregate to a mechanical degradation test. The test measures the percent loss in the coarse aggregate. The percent loss should be less than 35–45%.

D.2.6 Aggregate Soundness

Soundness is the percent loss of materials from an aggregate blend during the sodium or magnesium sulfate soundness test. The procedure is stated in AASHTO T 104: *Soundness of Aggregate by Use of Sodium Sulfate or Magnesium Sulfate*. This test estimates the resistance of aggregate to weathering while in service. It can be performed on both coarse and fine aggregate. The test is performed alternately by exposing an aggregate sample to repeated immersions in saturated solutions of sodium or magnesium sulfate each followed by oven drying. One immersion and drying process is considered one soundness cycle. During the drying phase, salts precipitate in the permeable void space of the aggregate. Upon re-immersion, the salt rehydrates and exerts internal expansive forces that simulate the expansive forces of freezing water. The test result is the total percent loss over various sieve intervals for a required number of cycles. Maximum-loss values range from approximately 10–20% for five cycles.

D.2.7 Aggregate Gradation

Superpave aggregate gradation requirements posed several controversial issues. For example, the initial versions of Superpave included a "restricted zone" in the gradation. This zone was identified on a 0.45-power gradation chart to define a permissible gradation. The 0.45-power chart (Figure D2) is a common format for plotting aggregate gradation, because it can easily illustrate the maximum density line as depicted in Figure D2. It was initially hypothesized that gradations that violate the restricted zone possess weak aggregate skeletons which may exhibit tenderness during construction and poor performance. However, recent research (TRB, 2002) suggests that "Independent results from the literature

Downloaded From : www.EasyEngineering.net

Downloaded From : www.EasyEngineering.net

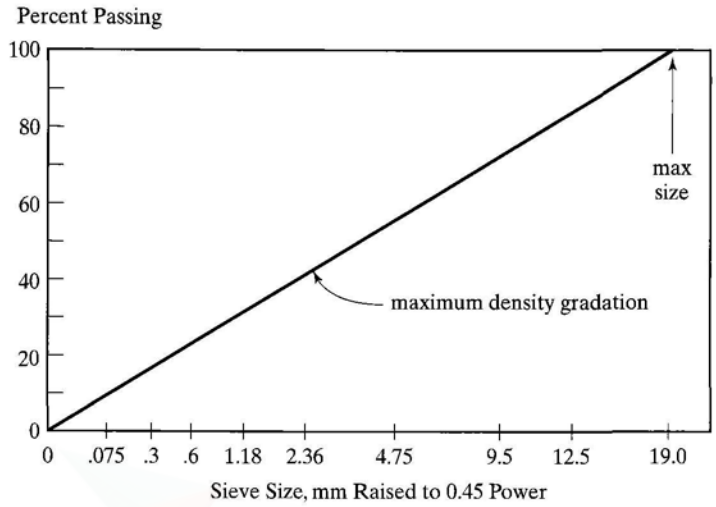


FIGURE D.2
0.45-Power curve.

clearly indicated that no relationship exists between the Superpave restricted zone and HMA rutting or fatigue performance." This report further recommends that perhaps all references to the restricted zone should be deleted from AASHTO MP2 (1999b) and AASHTO PP28 (1999c).

The maximum density gradation represents a tight aggregate packing. This type of gradation does not necessarily produce the best performing HMA. Superpave gradations are recommended to have a strong aggregate interlock, which is common in more open mixes.

D.3 ASPHALT MIX DESIGN

The Superpave mix design is based upon mixture volumetric properties at a specified level of compaction. These volumetric properties are assumed to produce well performing mixtures (AASHTO MP2: *Superpave Volumetric Mix Design*). Advanced Superpave protocols are available for mixture performance analysis: *Standard Test Method for Determining the Permanent Deformation and Fatigue Cracking Characteristics of Hot Mix Asphalt (HMA) Using the Simple Shear Test (SST) Device*, AASHTO TP7 Provisional Standards, 1998.

The mixture compaction is accomplished via the Superpave gyratory compactor (SGC), and the resulting volumetric properties are used to select the optimum asphalt content. The Superpave volumetric terms are defined in Table D.8.

D.3.1 Superpave Laboratory Compaction

The Superpave gyratory compactor (SGC) is designed to produce specimens in the laboratory which exhibit particle orientation similar to the field compacted mixtures.

Downloaded From : www.EasyEngineering.net

Downloaded From : www.EasyEngineering.net

TABLE D.8 Superpave Volumetric Terminology

Constituent	Abbreviated Term	Parameter
Aggregate	P—mass percent G—specific gravity s—stone (aggregate) b—bulk a—apparent e—effective	P_s—percent of mixture which is stone G_{sb}—bulk specific gravity of stone G_{sa}—apparent specific gravity of stone G_{se}—effective specific gravity of stone
Asphalt binder	P—mass percent G—specific gravity b—binder (asphalt) a—absorbed e—effective	P_b—percent of mixture which is binder P_{be}—percent effective binder P_{ba}—percent binder absorbed G_b—specific gravity of binder
Mixture	G—specific gravity b—bulk m—maximum m—mixture V—volume percent	G_{mb}—bulk gravity of mix G_{mm}—maximum theoretical gravity of mix V_a—volume of air in compacted mix VMA—voids in mineral aggregate VFA—voids filled with asphalt D:B ratio—dust to binder ratio

This is achieved with a mold gyrating 30 revolutions per minute at 1.25-degree pivot angle at the compaction pressure of 600 kPa. The number of revolutions are adjusted to produce a target density.

There are a number of issues surrounding the Superpave laboratory compaction. The main concern is the relationship between laboratory and field compaction (Blankenship, et al., 1994). For example, Peterson *et al.* (2003) have suggested a number of modifications in order to improve upon the existing Superpave compaction protocols. These modifications include revisiting the angle of gyration and compaction pressure. Additionally, there are standardization tools and techniques which are becoming available for the calibration of the angle of gyration.

D.3.2 Mix Design Criteria

Once the proper aggregate and grade of asphalt binder have been selected, the next step is to produce a mixture that meets the Superpave criteria. The goal of the mix design process is to determine the optimum asphalt content corresponding to a set of Superpave volumetric criteria. The most critical criterion is a 4% air content in the laboratory compacted specimens. Additionally, voids in the mineral aggregate (VMA) and voids filled with asphalt (VFA) are checked. Superpave volumetric characteristics are determined at various compaction levels, which correspond to various traffic levels in the field. AASHTO reports the required compactive effort for various traffic (AASHTO, 1999b and 1999c).

Downloaded From : www.EasyEngineering.net

Downloaded From : www.EasyEngineering.net

The mixtures are compacted to N_i, N_d and N_f in accordance with the following:

N_i—Number of initial gyrations: This parameter indicates a potential for tenderness in the mix during construction.
N_d—Design number of gyrations: The number of gyrations for which the mix is designed to produce 4% air content.
N_f—Final number of gyrations: The final number of gyrations is designed to simulate the post-compaction densification due to traffic. A mixture demonstrating less than 2 % air content at this point would be susceptible to rutting.
N_m—Maximum number of gyrations that should never be exceeded.

The volumetric properties of trial batches at 0.5% asphalt content increments are measured, and the optimum asphalt content is selected based upon an air content of 4 % (AASHTO MP-2).

Finally, the moisture sensitivity of the mixture is determined in accordance with AASHTO T283. This test is designed to measure the effect of moisture and cycles of freeze–thaw on a mixture containing 7 % air. The indirect tensile strength test is used to quantify the laboratory-simulated moisture damage. A strength ratio of 80% or higher is normally required. A strength ratio below 80% hints at a potential susceptibility to stripping.

Example D.1:

A Superpave mixture was prepared using for trial batches at 0.5% asphalt content increments. All volumetric and compaction data are presented in the table below:

	Batch #1	Batch #2	Batch #3	Batch #4
1- AC (%)	4.5	5.0	5.5	6.0
2- Air (%) at N_d	6.1	4.1	3.0	2.0
3- G_{mm}	2.467	2.444	2.430	2.410
4- VMA (%)	15.6	15.1	15.2	15.3
5- VFA (%)	62.1	72.7	81.5	89.1
6- % G_{mm} at N_i	84.1	86.1	87.0	88.1
7- % G_{mm} at N_m	95.4	97.1	98.6	99.5

Solution: Using an interpolation routine or a graphical solution will reveal that 5.1% would be the optimum asphalt content at which the 4% air content requirement is satisfied. As a cross check, all other volumetric properties are reviewed at this optimum asphalt content to ensure their compliance with Superpave requirements.

SUMMARY

Superpave has put the asphalt mix design and analysis on a rational platform. There are many who may argue that Superpave is not purely mechanistic. However, most

Downloaded From : www.EasyEngineering.net

Downloaded From : www.EasyEngineering.net

would agree that features such as the PG binder systems and mixture analysis protocols, are major improvements over the empirical methods of the past. The PG binder system incorporates the climatic information in the binder selection process. The volumetric properties of HMA are used for Superpave mix design. Many of these properties lend themselves to quality control measurements.

Protocols related to Superpave aggregates were developed based upon literature review rather than sound experimentation. This resulted in many early, less-than-perfect aggregate specifications, which were later adjusted. Additionally, there are new procedures being developed in order to do a better job with addressing modified binders, recycled asphalt, and waste materials in HMA.

A mechanistic mix design methodology provides us with the opportunity to integrate asphalt mix design and flexible pavement structural design (Mahboub and Little, 1990). Superpave is hoped to link with the latest AASHTO pavement design guide in a mechanistic manner.

PROBLEMS

D.1 What is Superpave? Why is it innovative?

D.2 What is the PG system? Why is it considered an improvement over the viscosity and penetration systems?

D.3 What are the critical factors affecting asphalt performance in pavements?

D.4 What are the engineering parameters used in rating the asphalt binders? How are these parameters tested in Superpave?

D.5 For an asphalt pavement, the maximum consecutive seven day pavement temperature is 66°C and single event coldest temperature is −20°C. The design ESALs for this pavement is 10,000,000, and traffic speed is standard. Select a PG grade for this pavement.

D.6 Can Superpave be used for both base and surface mixes?

D.7 Use the maximum gradation chart in Figure D.3, and draw a typical Superpave surface mix gradation.

D.8 List the steps in the Superpave mix design.

Downloaded From : www.EasyEngineering.net

Downloaded From : www.EasyEngineering.net

APPENDIX E

Pavement Management Systems

by Kamyar C. Mahboub, Ph.D., P.E.

Pavement management systems (PMS) have been defined by AASHTO as a set of tools or methods that assist decision-makers in finding optimum strategies for providing, evaluating, and maintaining pavements in a serviceable condition over a period of time (AASHTO, 2001, 1993; Delaware DOT, 2000). Pavement management provides a rational and cost-effective approach to pavement maintenance operations. Pavement management systems that evaluate various alternatives use the expected impact of maintenance and rehabilitation treatments on the future performance of pavements. They also provide the information needed to support fund requests and justify maintenance and rehabilitation programs. In recent years, state highway agencies have attempted to integrate their separate management functions in areas such as pavements and bridges within a geographic information systems framework.

E.1 PMS ACTIVITY LEVELS

Pavement management activities are conducted at two distinctive levels: network level, and project level (Haas, *et al.* 1994). The network level is a global view of the pavement infrastructure and addresses the overall budget and planning issues. The project level has a local focus on a limited component of the larger network. The project level is where specific decisions on maintenance strategies and funding allocations are made. The following section describes these two types of activities in more detail.

E.1.1 Network-Level Activities

The purpose and goals of the network-level management process are normally related to the budget process and include:

Downloaded From : www.EasyEngineering.net

Downloaded From : www.EasyEngineering.net

1. Identifying pavement maintenance, reconstruction, and rehabilitation needs;
2. Determining funds needed to address these needs;
3. Selecting feasible funding options and strategies to be tested;
4. Determining the impact of these funding options on the pavement performance as well as the overall safety of the driving public; and
5. Developing optimum pavement budget recommendations.

Generally, the PMS offers support for the planning, programming, budgeting, and analysis phases. The primary areas of network-level analysis include maintenance and rehabilitation needs, funding needs, forecasting future impacts for various funding options considered, and the prioritized listing of candidate projects needing repair. These results can be used to provide support to legislative, administration, and technical users.

E.1.2 Project-Level Activities

The overall network-level PMS is comprised of several project-level PMS activities. At the project level, the purpose of PMS is to provide the most cost-effective, feasible, and optimum design, maintenance, rehabilitation, or reconstruction strategy possible for a selected section of pavement within available funds and other constraints. This generally includes:

1. An assessment of the need for construction or cause of deterioration;
2. Identifying feasible design, maintenance, rehabilitation, and reconstruction strategies;
3. Analysis of the cost-effectiveness of various alternatives;
4. Definition of imposed constraints; and
5. Selection of the most cost-effective strategy within imposed constraints.

This generally provides support at the design level, and the results primarily are used by technical users. Some agencies call this stage preliminary design; preliminary because it dose not include the final development of plans and specification. Depending on the detail of the analysis, it can include the complete alternative selection and design process.

E.2 NETWORK-LEVEL ELEMENTS

The basic elements of a network-level PMS include an inventory, a condition assessment, determination of needs, prioritization of projects needing maintenance and rehabilitation, a method to determine the impact of funding decisions, and a feedback process (AASHTO 1990; FHWA 1995). This overall system is generally composed of two major subsystems. The information management system collects, stores, and manages the data. The decision support system is the collection of algorithms that analyzes the data and provides recommendation to managers. However, both of these are required to assist with the effective management of pavement systems, and they are seldom separated during discussions. In this section, a PMS will be assumed to include both the

Downloaded From : www.EasyEngineering.net

Downloaded From : www.EasyEngineering.net

information management and decision support components unless explicitly expressed otherwise. Briefly, network-level elements include:

1. Defining the limits of the network;
2. Developing an inventory of the streets within the network;
3. Developing a condition survey which identifies different pavement distresses;
4. Developing maintenance strategies, cost estimates, and life expectancy;
5. Determining PMR&R (pavement management rehabilitation and reconstruction) needs;
6. Analyzing costs of PMR&R;
7. Determining overall needs of the network;
8. Prioritizing PMR&R needs based on limited funds;
9. Forecasting the future condition of the network and impact of funding. An interactive process to: select candidate projects and analyze impact of decision on future projects; and
10. Implementing a feedback system to: update costs and life expectancies, revise PMR&R strategies, and improve reliability of the system.

E.2.1 Inventory

Inventory information is needed as the basis of decisions supported within a PMS program. The network-level inventory, or database of basic information, includes information on the pavements the agency is responsible for managing. The inventory generally includes information that defines the type of pavement sections. Additionally, it includes information about the location, limits, size, connectivity to other sections, number of traffic lanes, route designations, and functional classification for each management section. This type of data normally is entered into the database once, and it is changed only when some significant change occurs in the data.

Management sections generally have similar pavement layers, material types, past rehabilitation activities, past maintenance activities, and past traffic loadings. This type of information is often stored in a database for each individual management section. Since this can be changed over time, and the previous information may be useful to later decisions, the data is often stored in history type files and subsequent information is added over time providing a "history" of activities

E.2.2 Pavement Condition Assessment

Pavement condition assessment begins with collecting data to determine the type, amount, and severity of surface distress, structural integrity, ride quality, and skid resistance of the pavement. Pavement condition data is necessary to determine maintenance and rehabilitation needs, project future condition, and identify the impacts of treatment. It is also used to identify feasible maintenance and rehabilitation strategies, prioritize work, and help optimize maintenance and rehabilitation fund expenditures. Pavement condition is normally measured using the following factors as described below (AASHTO 1990; Peterson 1987):

Downloaded From : www.EasyEngineering.net

Downloaded From : www.EasyEngineering.net

Surface Distress Distress surveys are performed to determine the type, severity, and quantity of observable surface distress. This information is often used to determine a pavement condition index (PCI), which can be used to compute a rate of deterioration and is often used to project future pavement condition. Surface distress and the current or future PCI values are often used to help identify the timing of maintenance and rehabilitation, as well as the fund needs in the PMS process.

Structural Capacity Structural analysis normally is conducted to determine the current pavement load-carrying capacity that can be compared to the capacity needed to accommodate projected traffic. Non-destructive deflection testing of the pavement is a simple and reliable method to assist in making this evaluation; however, coring and component analysis techniques may be used as well.

Ride Quality Roughness is often converted into an index such as the present serviceability index (PSI) or the international roughness index (IRI). Pavement roughness is considered the most important indicator of pavement condition by the driving public, and it is especially important on pavement with higher speed limits, like those above 70 kph (45 mph). It is also needed to calculate vehicle-operating costs.

Surface Friction Skid resistance is the ability of the pavement surface to provide sufficient friction to avoid skid-related safety problems, especially in wet weather. Skid resistance is of high importance for pavements where vehicles operate at higher speeds. It generally is considered a separate measure of the condition of the pavement surface, and it may be used to determine the need for remedial maintenance by itself to address safety. These pavement condition measures can be used to determine the overall pavement condition and to identify the most cost-effective and optimum maintenance and rehabilitation treatments.

Determination of Needs Once the pavement network has been defined, and the condition data has been colleted, most agencies then want to know what work is needed and the resources that are needed to complete that work. This process should identify the work needed over some defined analysis period to support the level of service that the agency wants to provide to their highway users and its associated costs. This provides a base value of the needs that can be used to show the work and resources needed to meet the agency goals.

In general, this requires that the condition of the individual pavement management sections, without maintenance or rehabilitation, be projected to a common period and into the future in terms of individual distress, PCI, PSI, or some combination index as illustrated in Figure E.1. The projected condition of all sections in the network can then be used to determine the overall condition of the network at any time with or without treatment. The project condition, without treatment, gives a base condition of pavement sections being analyzed or the network as a whole.

A common method used to identify sections that need work is to compare the condition of each management section during each year over the analysis period to establish decision criteria (or commonly known as trigger values) that normally are based on condition, surface type, functional classification, and traffic loading. Figure E.2 shows a

Downloaded From : www.EasyEngineering.net

Downloaded From : www.EasyEngineering.net

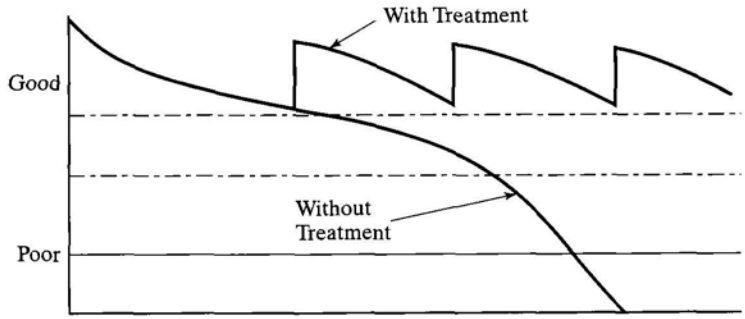


FIGURE E.1

Projected condition with and without treatment.

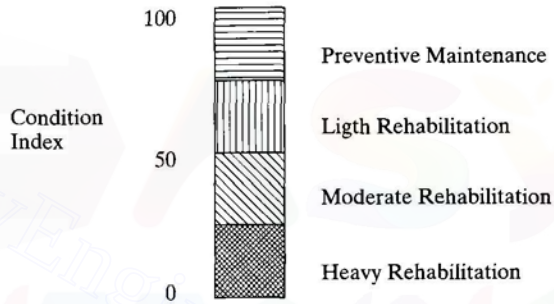


FIGURE E.2

Trigger value example ranges.

condition index scale with four different network-level treatment categories: preventive maintenance, light rehabilitation, moderate rehabilitation, and heavy rehabilitation (or reconstruction). The dividing lines between preventive maintenance and light rehabilitation, between light rehabilitation and moderate rehabilitation, and between moderate rehabilitation/reconstruction would be the trigger values. When the condition of a pavement is projected to cross from one level to another, a specific treatment is identified or triggered.

Prioritizing Candidate Sections Once the agency identifies the section of pavement needing work and determines the funds needed to provide the desired level of services, it must prioritize and fund work for those sections. In most cases, the available funds are less than those needed to complete all identified work. Even when adequate funds are available, they generally must be allocated over a number of years to match the work with the available resources. Generally, the goal of prioritization is to provide the greatest benefits to the driving public for funds expended; however, the pavement on highways with the greatest traffic generally are given a higher priority than those with a lower traffic level.

Determine the Impact of Funding Decisions The general goal of government agencies is to provide the maximum social benefit for the money provided to them by the

Downloaded From : www.EasyEngineering.net

Downloaded From : www.EasyEngineering.net

public. However, funds usually are allocated to a managing agency by elected officials who must run for election every few years. These elected officials are often more interested in solutions that show immediate impacts for their districts rather than long-term solutions that do not show immediate results, even if the long-term solutions are more cost-effective. It generally requires considerable justification to get funds for long-term solutions that either do not show immediate impacts or that cost more than short-term solutions. One of the best ways to justify funding is to show the impact of alternate funding levels and strategies on the overall condition of the network, the backlog of needs, future fund needs, and user costs.

Feedback Process Many of the pavement management systems currently being used were implemented with projection techniques, assignment management processes, and costs based on limited information. For a system to fully become adopted and used, it must be reliable and robust. The feedback process provides information on how well past estimates have matched observed values and provides information to improve future estimates. Managers use the feedback process to compare projections to actual observed information and modify the projection techniques to make them more reliable. These feedback and updating processes may not be a part of PMS software, but rather a manual process by which the personnel responsible for operating the PMS update projection algorithms, assignment processes, and costs on a recurring basis (see Figure E.3)

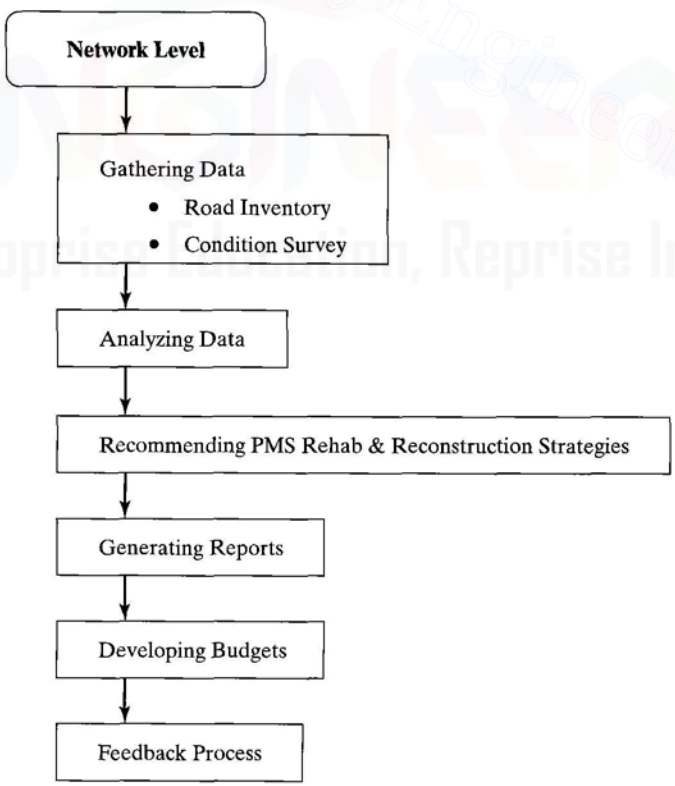


FIGURE E.3
Network-level data elements.

Downloaded From : www.EasyEngineering.net

Downloaded From : www.EasyEngineering.net

E.3 PROJECT-LEVEL ELEMENTS

Project-level pavement management is process of analysis and design to determine the layer material types and thickness needed for a pavement structure to serve the public. Although computer programs may be used in designing the layer thickness of specific materials and in economic analysis, much of the process must be completed outside a computer program. The complete project-level analysis can require considerable materials sampling and testing both in-situ and in laboratories. Project-level pavement management activities usually include new design, rehabilitation design, reconstruction design, and programmed maintenance that require some level of design (see Figure E.4)

E.3.1 New Design

The impetus for a new design may be the congestion management, planning activities, or other management processes. Although engineers often consider pavements one of the simplest types of structures, the design is quite complex. Most pavements are constructed using layers of materials, and eventually, all of the imposed traffic loads are transmitted to the underlying natural soils. A rational design procedure forces the designer to consider each of the major factors that affect pavement performance. This process leads to a better design compared to selecting a standard thickness of a single material that does not consider the important design variables, even when many of the design variables are estimated. One of the most commonly used pavement design procedures which is used by most state agencies is the AASHTO. Some state highway

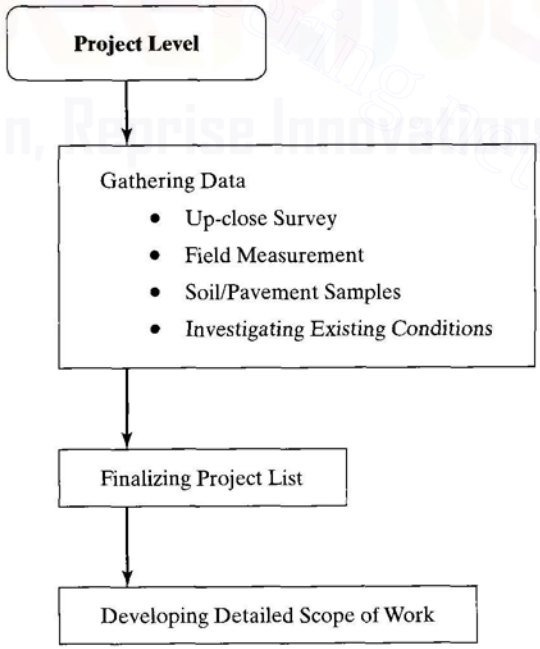


FIGURE E.4
Project-level data elements.

Downloaded From : www.EasyEngineering.net

Downloaded From : www.EasyEngineering.net

agencies use their own design procedures. All pavement design procedures should address several basic factors that are known to affect pavement including:

1. Support provided by the in-place soil (subgrade);
2. Traffic loads expected to be applied (primarily trucks and other heavy loads);
3. Environmental factors (especially the impact of rainfall, changing moisture levels, extreme temperatures, and freeze-thaw cycles);
4. Drainage;
5. Available materials;
6. Capabilities of construction forces; and
7. Cost.

E.3.2 Developing Maintenance, Rehabilitation, and Reconstruction Plans

Rehabilitation, reconstruction, and programmed maintenance needs should be generated from the network-level PMS functions, or some other management process, such as the safety management process.

Like initial pavement construction, rehabilitation and reconstruction are costly construction activities. The design of maintenance, rehabilitation, and reconstruction can take more time, effort, and funds than the design of a new pavement, because the properties of existing pavement layer materials are needed as well as the complex interactions of different options possible to address existing problems. An analysis of the existing pavement to determine the cause of deterioration is necessary to identify cost-effective maintenance, rehabilitation, or reconstruction treatments that can correct the problem. This can be approached as a series of steps to determine the cause of deterioration and identify relevant constrains. The answers to a set of questions are then used to identify feasible treatments. A question-answer oriented project-level evaluation should include the following questions (AASHTO, 1993):

1. Is the pavement structurally adequate for future traffic?
2. Is the pavement functionally adequate?
3. Is the rate of deterioration abnormal?
4. Are the pavement materials durable?
5. Is the drainage adequate?
6. Has previous maintenance been effective?
7. Does the condition vary substantially along the length of the project or between lanes?
8. Do the environmental factors require special consideration?
9. What traffic control options are available?
10. What geometric factors will impact the design?
11. What is the condition of the shoulders?

One of the difficulties associated with this process is deciding which and how much data to collect. It is difficult to know what kind and how much data are needed to

Downloaded From : www.EasyEngineering.net

Downloaded From : www.EasyEngineering.net

answer all of these questions until some of the data is available and has been analyzed. AASHTO (1993) recommends a series of steps for a staged project-level data collection, including:

1. Office data collection;
2. Field survey;
3. Data evaluation and determination of additional data needed;
4. Laboratory testing of samples; and
5. Final field and office data analysis.

The size of the project and importance of the highway to the agency also influences the amount of time and funds that will be expended in project-level evaluation. Pavements on high-volume major highways generally will be subjected to more testing and evaluation than those on low-volume roads.

There are a large number of maintenance, rehabilitation, and construction alternatives available for both flexible and rigid pavements, and recycling has increased that number of options. Surface seals such as aggregate seals and slurry seals combined with localized repairs are often used as preventive maintenance treatment for flexible pavement, and they are also used as rehabilitation treatments on lower volume flexible pavements when structural improvements are not required. Overlays have become more versatile by combining them with inter-layers such as fabric, milling full or partial widths, and recycling part of an existing layer prior to applying the overlay. Other types of rehabilitation and reconstruction for flexible pavements include the following:

1. Cold in-place recycling followed by a new surface;
2. Hot in-place recycling with or without an overlay;
3. Reworking and stabilization of foundation materials followed by a new surface;
4. Partial or full depth removal and replacement;
5. Full depth recycling; and
6. Overlay with PCC.

Other types of rehabilitation for rigid pavements may include:

1. A series of maintenance treatments such as partial depth patching, full depth repair, surface grinding, and joint sealing, often referred to as concrete pavement restoration (CPR);
2. Break and seat with a concrete/asphalt overlay; and
3. Bonded or unbonded PCC overlay.

E.3.3 Thickness Design

Since most rehabilitation is in the form of overlays, most engineers will think of overlay design when they determine the layer thickness for the rehabilitation of pavements. Overlay design procedures are used when a new layer is to be added to an existing

Downloaded From : www.EasyEngineering.net

Downloaded From : www.EasyEngineering.net

pavement. When the existing bound layers (asphalt concrete, portland cement concrete, or stabilized material) of a pavement are to be removed and replaced, or are to be reworked completely (such as with cold in-place recycling), new design procedures can be used to design the required layer thickness.

E.3.4 Selecting the Best Strategy

The process of selecting the combination of treatments, materials, and thicknesses for the new design, maintenance, rehabilitation, or reconstruction is an integral step of the project design process. The approach followed in project-level analysis should include completing a preliminary thickness design using all of the available materials and treatments that are considered feasible under the circumstances. The designer should then try to identify the combination of treatments, material types, layer thickness, and future maintenance and rehabilitation activities that give the least life-cycle costs for the design period analyzed while providing the design condition. Life-cycle costing concepts should be used to determine the differences in costs of the different strategies to account for the time value of funds spent. The total cost should include construction costs, traffic control costs, and other costs to the agency. The analysis should also consider the impact of the construction and future maintenance and rehabilitation operation on users.

Collection of data at the project level may include:

1. Up-close survey of each street to investigate all pavement distresses;
2. Field measurements to determine extent of work area;
3. Soil and pavement samples; and
4. Investigation of existing drainage facilities, etc.

The network-level analysis is the first phase of the project-level analysis, and the project-level analysis should build on the network-level analysis.

E.4 LIFE-CYCLE COST ANALYSIS

Life-cycle cost analysis is a process for evaluating the total economic worth of a usable project segment by analyzing initial costs and discounted future cost, such as maintenance, user, reconstruction, rehabilitation, restoring, and resurfacing costs, over the life of the project. A usable project segment is defined as a portion of a highway that, when completed, could be opened to traffic independent of some larger overall project (FHWA, 1998).

In simple terms, LCCA is an analysis technique that supports more informed and better investment decisions. It builds on well-founded principles of economic analysis that have been used to evaluate highway and other public works investment for years. It incorporates discounted long-term agency, user, and other relevant costs over the life of a highway or bridge to identify the best value for investment expenditures (i.e., the lowest long-term cost that satisfies the performance objective sought). LCCA can be applied to a wide variety of investment-related decision levels to evaluate the economic worth of various designs, projects, alternatives, or system strategies to get the best return on the funds.

Downloaded From : www.EasyEngineering.net

Downloaded From : www.EasyEngineering.net

E.4.1 Pavement Design

Pavement design is a project-level activity where detailed engineering and economic considerations are given to alternate combinations of sub-base, base, and surface materials which will provide adequate load-carrying capacity. Factors that are considered include: materials, traffic, climate, maintenances, drainage, and life-cycle costs.

E.4.2 User Costs

User costs are costs incurred by highway users traveling on the facility and the excess costs incurred by those who cannot use the facility because of either agency imposed or detour requirements. User costs typically are an aggregation of three separate components: Vehicle operating costs (VOC), crash costs, and user delay costs.

E.4.3 Benefit/Cost (B/C) Analysis or Ratio

The B/C represents the net discounted benefits of an alternative divided by net discounted costs. B/C ratios greater than 1.0 indicate that benefits exceed cost. The B/C ratio approach is generally not recommended for pavement analysis because of the difficulty in sorting out benefits and costs for use in developing B/C ratios.

E.4.4 Internal Rate of Return (IRR)

The IRR, primarily used in private industry, represents the discount rate necessary to make discounted cost and benefit equal. While the IRR does not generally provide an acceptable decision criterion, it does provide useful information, particularly when budgets are constrained or there is uncertainty about the appropriate discount rate.

E.4.5 Net Present Value (NPV)

NPV is the discounted monetary value of expected net benefits (i.e., benefits minus costs). The basic formula for computing NPV is:

$$\text{NPV} = \text{PV}_{\text{benefits}} - \text{PV}_{\text{costs}} \tag{E.1}$$

Because the benefits of keeping the roadway above some pre-established terminal level are the same for all design alternatives, the benefits component drops out and the formula reduces to:

$$\text{NPV} = \text{InitialCost} + \sum_{k=1}^{N} \text{RehabCost}_k \left[\frac{1}{(1+i)^{n_k}}\right] \tag{E.2}$$

in which N = number of rehabilitations, i = discount rate, and n = year of expenditure.

To simplify the calculations, the term in the brackets in Eq. E.2 is referred to as the discount factor. Table E.1 lists some common discount factors.

E.4.6 Cost Estimates

Estimates of future costs and benefits can be made using constant or nominal dollars. Constant dollars, often called real dollars, reflect dollars with the same or constant

Downloaded From : www.EasyEngineering.net

Downloaded From : www.EasyEngineering.net

TABLE E.1 Present Value Discount Factors: Single Future Payment

	Discount Factor				Discount Factor		
Year	3%	4%	5%	Year	3%	4%	5%
1	0.970874	0.961538	0.952381	21	0.537549	0.438834	0.358942
2	0.942596	0.924556	0.907029	22	0.521893	0.421955	0.34185
3	0.915142	0.888996	0.863838	23	0.506692	0.405726	0.325571
4	0.888487	0.854804	0.822702	24	0.491934	0.390121	0.310068
5	0.862609	0.821927	0.783526	25	0.477606	0.375117	0.295303
6	0.837484	0.790315	0.746215	26	0.463695	0.360689	0.281241
7	0.813092	0.759918	0.710681	27	0.450189	0.346817	0.267848
8	0.789409	0.73069	0.676839	28	0.437077	0.333477	0.255094
9	0.766417	0.702587	0.644609	29	0.424346	0.320651	0.242946
10	0.744094	0.675564	0.613913	30	0.411987	0.308319	0.231377
11	0.722421	0.649581	0.584679	31	0.399987	0.29646	0.220359
12	0.70138	0.624597	0.556837	32	0.388337	0.285058	0.209866
13	0.680951	0.600574	0.530321	33	0.377026	0.274094	0.199873
14	0.661118	0.577475	0.505068	34	0.366045	0.263552	0.190355
15	0.641862	0.555265	0.481017	35	0.355383	0.253415	0.18129
16	0.623167	0.533908	0.458112	36	0.345032	0.243669	0.172657
17	0.605016	0.513373	0.436297	37	0.334983	0.234297	0.164436
18	0.587395	0.493628	0.415521	38	0.325226	0.225285	0.156605
19	0.570286	0.474642	0.395734	39	0.315754	0.216621	0.149148
20	0.553676	0.456387	0.376889	40	0.306557	0.208289	0.142046

purchasing power over time. In such cases, the cost of performing an activity would not change as a function of the future year in which it would be accomplished. For example, if hot-mixed asphalt (HMA) costs $20/ton today, then $20 should be used for future year HMA cost estimates.

Nominal dollars, on the other hand, reflect dollars that fluctuate in purchasing power as a function of time. When using nominal dollars, the estimated cost of an activity would change as a function of the future year in which it is accomplished. In this case, if HMA costs $20/ton today, and inflation were estimated at 5%, the HMA cost estimate for 1 year from today would be $21/ton.

E.4.7 Discount Rates

Similar to costs, LCCA can use either real or nominal discount rates. Real discount rates reflect the true-time value of money with no inflation premium and should be used in conjunction with non-inflated dollar cost estimates of future investments. Nominal discounts rates include an inflation component and should only be used in conjunction with inflated future dollar cost estimates of future investments.

Data on the historical trends over a very long period indicate that the real value of money is approximately 4%. In 1995 and 1996, the FHWA Office of Engineering, Pavement Division, conducted a national pavement design review and found that the discount rates currently employed by SHAs to conduct LCCA in pavement design showed a distribution of values clustering in the 3–5% range. Good practice suggests

Downloaded From : www.EasyEngineering.net

Downloaded From : www.EasyEngineering.net

using a real discount rate, one that does not reflect an inflation premium, of 3–5% in conjunction with real/constant dollar cost estimates.

E.4.8 Alternative Strategies

The primary purpose of the LCCA is to quantify both the long-term as well as the short-term implication of various alternative strategies. A pavement design strategy is the combination of initial pavement design and necessary supporting maintenance and rehabilitation activities. Analysis period is the time horizon over which life-cycle costs are evaluated. The first step in conducting an LCCA of alternative pavement design is to identify the alternative pavement design strategies for the analysis period under consideration.

Generally, the LCCA analysis period should be sufficiently long to reflect long-term consequences of various alternatives and strategies. This means that the analysis period should always be longer than the pavement design period, except in the case of extremely long-lived pavement. As a rule of thumb, the analysis period should be long enough to incorporate at least one rehabilitation activity. The FHWA (1995) recommends an analysis period of at least 35 years for all pavement projects, including new or total reconstruction projects, as well as rehabilitation, restoration, and resurfacing projects. Regardless of the analysis period selected, the analysis period used should be the same for all alternatives. Typically, each design alternative will have an expected initial design life, periodic maintenance treatment, and, possibly, a series of rehabilitation activities. It is important to identify the scope, timing, and cost of these activities.

E.4.9 Performance Periods and Activity Timing

Performance life for the initial pavement design and subsequent rehabilitation activities has a major impact on LCCA results. It directly affects the frequency of agency intervention on the highway facility, which in turn affects the frequency of agency cost, as well as user costs during the period of construction and maintenance activities. SHAs can determine specific performance information for various pavement strategies through the analysis of pavement management data and historical experience.

Work zone requirements for initial construction, maintenance, and rehabilitation directly affect highway user costs and should be estimated along with pavement strategy development. The frequency, duration, severity, and year of work zone requirements are critical factors in developing user costs for the alternative being considered.

E.4.10 Agency Costs

Construction quantities and costs are related directly to the initial design and subsequent rehabilitation strategy. The first step in estimating agency costs is to determine construction quantities/unit price. LCCA needs only consider differential costs between alternatives. Costs common to all alternatives cancel out.

Agency costs include all costs incurred directly by the agency over the life of the project. They typically include initial preliminary engineering, contract administration,

Downloaded From : www.EasyEngineering.net

Downloaded From : www.EasyEngineering.net

construction supervision and construction costs, as well as future routine and preventive maintenance, resurfacing and rehabilitation cost, and the associated administrative cost. Agency costs also include the maintenance of traffic cost and can include operating costs such as pump station energy costs, tunnel lighting, and ventilation. At all times, the salvage value, the remaining value of the investment at the end of the analysis period, is included as a negative cost. Salvage value represents the value of an investment alternative at the end of the analysis period.

Serviceable life represents the more significant salvage value component and is the remaining life in a pavement alternative at the end of the analysis period. It is used primarily to account for differences in remaining pavement life between alternative pavement design strategies at the end of the analysis period.

E.4.11 User Costs

In LCCA, highway user costs of concern are the apparent and hidden costs incurred by the motoring public. User costs are an aggregation of three separate cost components: vehicle operating costs (VOC), user delay costs, and crash costs. In the LCCA of pavement design alternatives, there are user costs associated with both normal operations and work zone operations.

The normal operations category reflects highway user costs associated with a facility during periods free of construction activities. User costs in this category are a function of the differential pavement performance (roughness) of various pavement alternatives. Some researches indicate that VOC will increase with the increase of pavement roughness. The additional operating costs (as compared to a smooth road baseline) begin to accrue around IRI = 170 in/mi (PSR = 2.5). Typically, a pavement with a PSR = 2.5 will be considered as having reached its terminal serviceability index and should be scheduled for some rehabilitation.

The work zone operations category, however, reflects highway user costs associated with using a facility during periods of construction, maintenance, and/or activities that generally restrict the capacity of the facility and disrupt normal traffic flow. The work zone user costs are quantified by the following approach:

1. Project future year traffic demand;
2. Calculate work zone directional hourly demand;
3. Determine roadway capacity;
4. Identify the user cost components;
5. Quantify traffic affected by each component;
6. Compute reduced speed delay;
7. Select and assign VOC cost rates;
8. Select and assign delay cost rates;
9. Assign traffic to vehicle classes;
10. Compute individual user cost components by vehicle class;
11. Sum total work zone user costs; and
12. Address the crash costs.

Downloaded From : www.EasyEngineering.net

Downloaded From : www.EasyEngineering.net

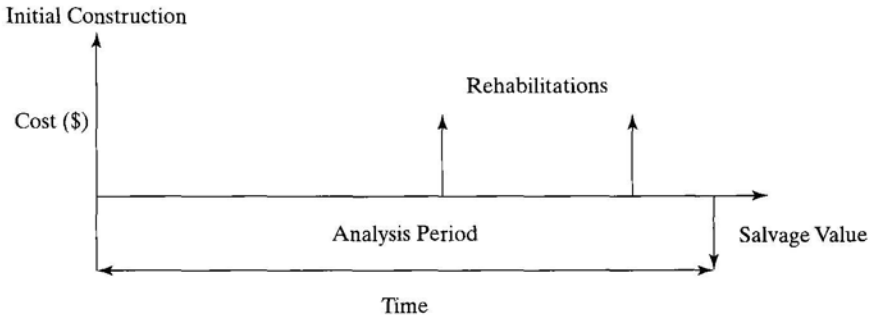


FIGURE E.5

Typical expenditure stream diagram.

E.4.12 Expenditures Stream

Expenditure stream diagrams are graphical representations of expenditure over time. They generally are developed for each pavement design strategy to help visualize the extent and timing of expenditures. Figure E.5 shows a typical expenditure stream diagram. Normally, costs are depicted as upward arrows at the appropriate time they occur during the analysis period, and benefits are represented as negative costs or downward arrows. In LCCA of pavement design alternatives, the benefits of providing the specific level of pavement condition are considered to be the same for all pavement design strategies. As a result, the only concerns are the differential costs among alternatives. The only negative cost would be the cost associated with any salvage value. Under these conditions, the LCCA objective becomes finding the alternative pavement design strategy that meets the performance requirements at the lowest life-cycle cost.

In its broadest sense, LCCA is a form of economic analysis used to evaluate the long-term economic efficiency between alternative investment options. Economic analysis focuses on the relationship between costs, timing of costs, and discount rates employed. Once all costs and their schedule have been developed, future costs must be discounted to the base year and added to the initial cost to determine the NPV for the LCCA alternative. As noted earlier, NPV is the economic indicator of choice (see Eqs. E.1 and E.2).

Example E.1:

The initial design will cost $1,100, $1,100,000 and have an associated work zone cost of $300,000 at year 0. Additional rehabilitation costs of $325,000 will be incurred in years 15 and 30. Associated work zone user costs in years 15 and 30 will be $269,000 and $361,000, respectively. The salvage value at year 35, based on a prorated cost of the year-30 rehabilitation design and remaining life, will be $216,000 (10/15 of $325,000). The expenditure stream diagram is shown in Figure E.6. The results of PV computations using 4% PV factors for single future amounts for the example expenditure stream diagram are shown in Table E.2.

Downloaded From : www.EasyEngineering.net

Downloaded From : www.EasyEngineering.net

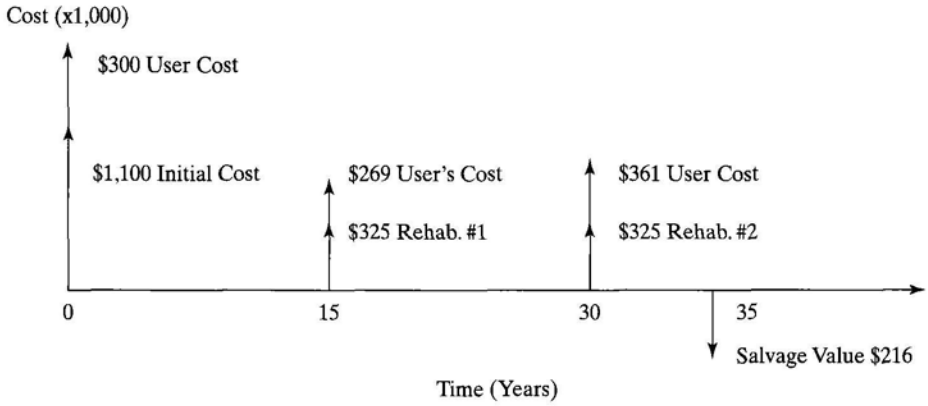


FIGURE E.6

Expenditure stream diagram for an NPV computation example.

TABLE E.2 Results of PV Computation

Cost Component Activity	Years	Costs ($1,000)	Discount Factor	Discounted Cost ($1,000)
Initial Construction	0	1100.0	1.0000	1100
Initial Work Zone User Cost	0	300.0	1.0000	300
Rehab 1	15	325.0	0.5553	180
Rehab 1 Work Zone User Cost	15	269.0	0.5553	149
Rehab 2	30	325.0	0.3083	100
Rehab 2 Work Zone User Cost	30	361.0	0.3083	111
Salvage Value	35	−216	0.2534	−55
		Total NPV		1885

E.4.13 Analysis of Results

Once completed, all LCCA should, at a minimum, be subjected to a sensitivity analysis. Sensitivity analysis is a technique used to determine the influence of major LCCA input assumptions, projections and estimates on LCCA results. In a sensitivity analysis, major input values are varied (either within some percentage of the initial value or over a range of values) while all other input values remain constant and the amount of changes in results is noted. The input variables may be ranked according to their effect on results. Sensitivity analysis allows the analyst to subjectively get a feel for the impact of the variability of individual inputs on overall LCCA results.

Tables E.3 and E.4 present the results of a sensitivity analysis on two pavement design strategies at discount rates ranging from 2–6% for a 35-year period. Alternative 1 has a lower initial agency cost, and, because of a shorter construction period, a lower user cost than Alternative 2. However, Alternative 1 requires three identical 10-year design rehabilitations compared to an identical 15-year design rehabilitation for Alternative 2.

Downloaded From : www.EasyEngineering.net

Downloaded From : www.EasyEngineering.net

TABLE E.3 Sensitivity Analysis-Alternative 1

			NPV				
Activity (a)	Year (b)	Cost (c)	2.00%	3.00%	4.00%	5.00%	6.00%
Construction	0	975	975	975	975	975	975
User Cost	0	200	200	200	200	200	200
Rehab 1	10	200	164	149	135	123	112
User Cost 1	10	269	220	200	182	165	150
Rehab 2	20	200	135	111	91	75	62
User Cost 2	20	361	243	200	165	136	113
Rehab 3	30	200	110	82	62	46	35
User Cost 3	30	485	268	200	150	122	85
Salvage	35	−100	−50	−36	−25	−18	−13
Total NPV			2265	2081	1935	1824	1719
Agency Cost			1334	1281	1238	1201	1171
User Cost			932	800	696	613	547

TABLE E.4 Sensitivity Analysis-Alternative 2

			NPV				
Activity (a)	Year (b)	Cost (c)	2.00%	3.00%	4.00%	5.00%	6.00%
Construction	0	1100	1100	1100	1100	1100	1100
User Cost	0	300	300	300	300	300	300
Rehab 1	15	325	241	209	180	156	136
User Cost 1	15	269	200	173	149	129	112
Rehab 2	30	325	179	134	100	75	57
User Cost 2	30	361	199	149	111	84	63
Salvage	35	−217	−108	−77	−55	−39	−28
Total NPV			2111	1988	1885	1805	1740
Agency Cost			1413	1366	1326	1292	1264
User Cost			699	621	561	513	475

Out-year user costs for Alternative 1 increase as a result of increased traffic level over time; out-year user costs for Alternative 2 decrease first due to a shorter work zone period and then as a result of increased traffic levels over time. Both alternatives have a remaining service life at year 35. The salvage value, as a prorated share of the last rehabilitation, is 50% of its last rehab cost for Alternative 1 ($100,000). The salvage value of Alternative 2, on the other hand, is 66.6% of its last rehab cost ($217,000).

The sensitivity analysis reveals that the NPV of both alternatives decreases as the discount rate increase. This results from the reduced present value of future costs at higher discount rates. Because the amount and timing of future costs differ between alternatives, the effect of discounts on the NPV is different for each alternative. In this example, Alternative 1 is more expensive than Alternative 2 at discount rates of 5% and lower, while Alternative 2 is more expensive than Alternative 1 at a discount rate of 6% or more.

The sensitivity analysis also reveals that Alternative 2 has a higher agency cost than Alternative 1 at all discount rates considered. Further, Alternative 2 has a lower

Downloaded From : www.EasyEngineering.net

Downloaded From : www.EasyEngineering.net

user cost than Alternative 1 at all discount rates considered. Similar sensitivity analysis could be conducted using other input variables such as agency cost, user costs, pavement performance lives, and the hourly dollar value of user delay. In addition to conducting a sensitivity analysis, the analyst should examine the implication of contractor work hours on queuing costs, as well as the anticipated maximum queue lengths and delay times. A primary drawback of the sensitivity analysis is that the analysis assigns an equal weight to all input value assumptions, regardless of the likelihood of occurring. This may be addressed by using a probabilistic approach.

E.4.14 Final Design Strategy

Once the NPVs have been computed for each alternative and limited sensitivity analysis performed, the analyst needs to step back and reevaluate the competing design strategies. As noted, the overall benefit of conducting a LCCA is not necessarily the LCCA results themselves, but rather how the designer can use the information resulting from the analysis to modify the proposed alternatives and develop more cost-effective strategies. For example, if user costs dwarf agency costs for all of the alternatives, the analysis may indicate that none of the alternative analyzed are viable. It could indicate that the designer needs to evaluate the current design strategies' impact on the future maintenance of traffic.

It is important to note that LCCA results are just one of many factors that influence the ultimate selection of a pavement design strategy. The final decision may include a number of additional factors outside of the LCCA process, such as local politics, availability of funding, industry capability to perform the required construction, and agency experience with a particular pavement type.

E.5 PMS DATA AND SOFTWARE

Pavement management is a process to cost effectively manage the roadway system. The formal process includes a systematic, consistent approach to gathering and analyzing data and generating recommendations and reports so those who control road maintenance budgets can make informed investment decisions. PMS uses computer software for storing and analyzing data, and providing information and recommendations to assist in road-related decision making. Most PMS software consists of three general components:

1. A database containing an inventory of the physical data, history of repairs, repair costs and life of repairs, and other data such as truck volume or accident history.
2. A data analysis package that makes recommendations about how and when to allocate resources to potential PMR&R projects. It analyzes and sorts data, generates reports and provides recommendations based on a prioritization equation. The analysis can show a single year or forecast future years based on pavement performance models.
3. A feedback process to verify and improve the reliability of the PMS. For a PMS to be truly effective, it requires the support of everyone involved in the process. As more data is collected and analyzed, the system is fine-tuned and calibrated.

Downloaded From : www.EasyEngineering.net

Downloaded From : www.EasyEngineering.net

Three different types of data go into the PMS software program. They are a road inventory, pavement condition survey and various PMR&R strategies and options.

The purpose of the road inventory is to define the physical characteristics for each road. This information is stored in road inventory files in the PMS database. Each road is divided into manageable sections called "road segments".

The purpose of the condition survey is to determine the condition of each road segment based upon pavement distress. The condition survey is a critical part of pavement management, since specific distresses are very much related to certain causes of pavement deterioration. Due to this direct correlation, PMS software programs link distress types to strategies. An accurate condition survey is critical in helping determine appropriate PMR&R strategies to restore a deteriored pavement to an acceptable level. Common distresses in asphalt pavement include: alligator cracking, environmental cracking, block cracking, patch potholes, and raveling. Common distresses in concrete pavement include: patching, joint deterioration, slab cracking, and alkali-silica reactivity. It is imperative that the correct repair alternative be selected for the specific condition on each road segment. This is accomplished using the predetermined PMR&R strategies in the software program. There are five different PMR&R strategies.

1. Routine maintenance;
2. Prevention maintenance;
3. Deferred maintenance;
4. Rehabilitation; and
5. Reconstruction.

Trained personnel gather information for the PMS database in a variety of ways, including observation or the collection of pavement samples by automated collection equipment. The PMS software contains analysis tools that will:

1. Identify potential repair alternatives for each segment;
2. Calculate the associated estimated repair costs; and
3. Select the most cost-effective solution for each road segment.

It will also rank and prioritize the segments most worthy of funding for a single year (see Figure E.7), based on common ranking criteria such as:

1. Pavement condition;
2. Initial cost;
3. Life-cycle cost; and
4. Benefit versus cost.

All project maps and data are linked through a geographic information system (GIS). Since the software's analysis component produces tremendous amounts of information, it is important that all information be presented clearly to decision makers.

Downloaded From : www.EasyEngineering.net

Downloaded From : www.EasyEngineering.net

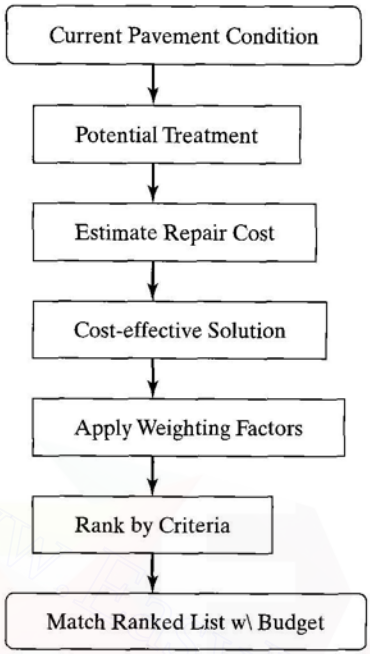


FIGURE E.7
Single year prioritization process.

E.6 INFRASTRUCTURE AND ASSET MANAGEMENT

Infrastructure management systems were developed to help integrate individual management systems. Pavement and bridge management were some of the first decision support systems developed in highway agencies for their physical infrastructure. Most of these various decision support systems have been developed independently. For them to truly be effective, they need to be integrated (at least coordinated) to provide the information needed by administration and funding authorities to support their strategic planning and budgeting activities.

Asset management is a systematic process of maintaining, updating, and operating physical assets cost effectively (FHWA 1995). It combines engineering principles with sound business practice and economic theory, and it provides tools to facilitate a more organized, local approach to decision making. Thus, asset management provides a framework for handling both short- and long-range planning.

There are similarities and differences among pavement, infrastructure, and asset managements. Pavement management focuses on pavements, infrastructure management focuses on physical facilities, and asset management can include all of the elements managed by the agency, including many nonphysical assets (financial capabilities, methods, and technologies). However, the basic management concepts are the same in all three (i.e., to provide the best return for the funds available). As asset management matures, it appears that it will attempt to better integrate the management of physical assets and, possibly, nonphysical assets. Pavement management is one of the tools most transportation agencies have in place, and it should be one of the first that is integrated into an overall management approach.

Downloaded From : www.EasyEngineering.net

Downloaded From : www.EasyEngineering.net

E.7 PAVEMENT PRESERVATION

Pavement preservation is a program of activities aimed at preserving the investment in the nation's highway system, enhancing pavement performance, extending pavement life, and meeting the driver's needs. It is the sum of all activities undertaken to provide and maintain serviceable roadways; this includes corrective maintenance and preservative maintenance, as well as minor and major rehabilitation. It excludes structural capacity improvements and new or reconstruction pavements.

Pavement preservation is an inclusive program that identifies the treatment for each section of pavement in the management network that will give the greatest pavement life for the least money. The treatments include corrective maintenance, pavement maintenance, and rehabilitation. A method to identify appropriate treatments for each section of pavements is required. A database of information about each pavement section is necessary to identify candidate projects and select the right treatment at the right time.

SUMMARY

Pavement management is a methodology by which the resources are applied in the most efficient manner to provide a desirable level of service to the driving public. Pavement management systems (PMS) activities are conducted at two distinctive levels: namely, network level and project level. The network level is a global view of the pavement infrastructure and addresses the overall budget and planning issues. The project level has a local focus on a limited component of the larger network. The project level is where specific decisions on maintenance strategies and funding allocations are made. From an operations point of view, the PMS must be capable of collecting, analyzing and summarizing a large amount of data on a periodic basis. Common PMS analytical tools include: pavement performance models, economic analysis models, and forecasting models. All PMS data are often linked with other agency maps and data through a geographic information systems platform.

PROBLEMS

E.1 What is PMS? What are the purposes of the network-level and project-level activities? Show the process of both the network level and project level by diagrams.

E.2 What pavement condition factors enter into a PMS database?

E.3 What is the advantage of using life-cycle cost analysis (LCCA) in pavement design? What are user costs? Give a definition to the net present value (NPV) of a pavement project.

E.4 Assume that hot-mixed asphalt (HMA) costs \$25/ton, and the inflation rate is 4%. What is the HMA cost estimate for 5 years from today:

1. If real dollars are used in the LCCA analysis;
2. If nominal dollars are used in the LCCA analysis.

E.5 For a pavement design project, two design strategy alternatives are proposed. For Alternative 1, the initial design will cost \$1 million and have an associated work

Downloaded From : www.EasyEngineering.net

Downloaded From : www.EasyEngineering.net

zone cost of $220,000 at year 0. Three additional rehabilitations, at a cost of $250,000, will be incurred in years 10, 20, and 30. Associated work zone user costs in years 10, 20, and 30 will be $220,000, $330,000 and $440,000, respectively. For Alternative 2, the initial design will cost $1.2 million and have an associated work zone cost of $240,000 at year 0. Two additional rehabilitations, at a cost of $300,000, will be incurred in years 15 and 30. Associated work zone user costs in years 15 and 30 will be $220,000 and $330,000, respectively. Over a 35-year analysis period,

1. Calculate the salvage value of the two alternatives.
2. Develop an expenditure stream diagram for Alternative 1.
3. Compute the NPV for each alternative (discount rate is 4%).
4. If LCCA results are the only factors that influence the ultimate selection of this pavement design strategy, which strategy would you like select? Account for your decision.

E.6 What are the three main components of the PMS software? What are the three different types of input data that are entered into the PMS software program.

E.7 Explain how to rank and prioritize the segments most worthy of funding for a single year, based on common ranking?

E.8 Describe a PMS software you have used. Describe all input and output parameters.

Downloaded From : www.EasyEngineering.net

Downloaded From : www.EasyEngineering.net

APPENDIX F

A Preview Of 2002 Pavement Design Guide

An effort to develop an improved *Pavement Design Guide* (referred to as the 2002 Guide) by the year 2002 was initiated by the AASHTO Joint Task Force on Pavements (JTFP), which is responsible for the development and implementation of pavement design technologies. As part of this effort, a workshop was held in March 1996 in Irvine, California, to discuss the framework for improving the Guide. At the conclusion of that workshop, a major long-term goal identified by the JTFP was the development of a design guide based as fully as possible on mechanistic principles. The work was later contracted to several private consultants and universities under NCHRP Project 1-37A. The target date for the delivery of the final report to JTFP, including the 2002 Guide, was by the end of 2001. Due to unexpected delays, the Guide was still not available more than one year later at the time of this writing. In view of the fact that the new Guide is mechanistic–empirical and is such a deviation from the current guide, approval by several AASHTO standing committees and all fifty states are required. It will take several years after 2002 before the Guide can be implemented. The information presented in this appendix was provided mostly by the research team as posted on the Internet. It must be cautioned that what appears in this preview is not necessarily indicative of what will appear in the final version of the Guide.

F.1 GENERAL FEATURES

The *2002 Guide for Design of New and Rehabilitated Pavement Structures* will constitute a significant revision to the pavement design and analysis procedure currently used throughout the world. Some general features of the Guide are summarized below:

1. The Guide presents procedures for the design and analysis of all commonly used new and rehabilitated pavement systems. Particular emphasis is placed on pavement rehabilitation including procedures for life-cycle cost analysis (LCCA) and

Downloaded From : www.EasyEngineering.net

Downloaded From : www.EasyEngineering.net

evaluations of existing pavements, as well as recommendations on rehabilitation treatments, subdrainage, and foundation improvements for problem soils.

2. The Guide uses the calibrated mechanistic design procedure that allows the full integration of material characterization, climate condition, and traffic loading into pavement design. The basic concept is the same as that described in Sections 11.1 and 12.1. The structural models for flexible pavements include both a layer system program for linear analysis and a finite element program for nonlinear analysis. For rigid pavements, a two-dimensional finite element program called ISLAB2000, which is a later version of ILLI-SLAB, will be used. Various distress models will be selected and calibrated against the long-term pavement performance (LTPP) and other available databases.
3. The Guide integrates the design methodologies for the various types of pavements whenever feasible. The same design parameters, such as material and soil characterization, climate factors, traffic analysis, and reliability, will be used across all pavement types. This integration of input parameters puts all types of pavements on an equitable basis and allows the use of alternate pavement types for comparison.
4. The Guide uses a hierarchical approach for determining the design inputs. Three levels of input can be selected depending on the importance of the project and the availability of data. Level 1 is based on site-specific measurements, level 2 on regional values or regression equations, and level 3 on default values or educated guess. Level 1 is the most accurate because it uses the actual measurements on or near the project sites, while level 3 is the least accurate. This approach allows the use of current procedures and provides for inclusion of improved procedures in the future.
5. The Guide eliminates the equivalent single axle load (ESAL) approach and use the full spectra of axle loads applied to a pavement structure by the prevailing or projected traffic stream. However, an ESAL conversion capability is included so that earlier mathematical models based on ESAL can still be used.
6. Separate programs for flexible and rigid pavements will be developed and then integrated with a common interface. The software will be based upon existing mechanistic–empirical models and will utilize existing software implementations of those models. It allows the user to input trial layer thicknesses in addition to various input parameters. The software predicts the expected performance parameters (i.e., fatigue cracking, roughness, etc.) at different ages of the pavement. The user then has the option to make changes in layer thicknesses and/or other input parameters until the design criteria are satisfied. The software can be run on computers with Windows 98, 2000, NT, and XP.

F.2 DESIGN INPUTS

The four categories of inputs to be discussed are: traffic, material characterization, climate, and reliability.

F.2.1 Traffic

The traffic data required by the 2002 Guide are consistent with the practices outlined in the *Traffic Monitoring Guide* (TMG) (FHWA, 2001b). State highway agencies that

Downloaded From : www.EasyEngineering.net

Downloaded From : www.EasyEngineering.net

currently collect data according to the TMG have already met the requirements. The traffic analysis subroutine in the 2002 pavement design software will assist users in collecting and organizing the required data. Agencies will be able to import much of the required data directly from their existing traffic database.

Two types of traffic data are usually collected: weigh-in-motion (WIM), which provide information about the number and configuration of axles observed within a series of load groups, and automatic vehicle classification (AVC), which counts over a period of time the number and types of vehicles that use a given roadway. The associated error and variability of the inputs will be considered in determining the reliability of the design. To facilitate this analysis, traffic data supplied for pavement design will require an estimate of quality including the hierarchical level used, along with the number of days of WIN, AVC, and traffic counting data used in the analysis. The three levels of traffic inputs are described below:

Level 1 Level 1 uses volume/classification and axle-load spectra data directly related to the project. It requires the agency to gather and analyze facility-specific traffic volume and load data. The traffic data measured along a facility including counting and classifying the number of trucks traveling over the roadway, along with the breakdown by lane and direction, and measuring the axle loads for each truck class to reliably determine the truck traffic for the first year after construction. To determine the traffic variations over time, the following additional information is needed:

1. Average annual daily truck traffic (AADTT) for the base year.
2. Truck traffic distribution factor (TTDF), which is the percent of the AADTT for each vehicle classification.
3. Monthly truck traffic adjustment factors by class, which are used to adjust the AADTT into monthly average daily truck traffic (MADTT) volume.
4. Hourly distribution factors, which are used to distribute the monthly MADTT volumes by hour of the day. The average hourly distribution of traffic is needed for computing the incremental damage on rigid pavements due to different thermal gradients during the day.
5. Lane distribution factor, which accounts for the percentage of trucks in the total traffic population in the design lane.

Level 2 The traffic data required for level 2 are the same as level 1, except that the regional axle load spectra data, instead of the facility-specific axle load spectra data, are used. Level 2 requires the collection of enough truck volume information on a facility to accurately measure truck volumes, including any weekday/weekend volume variation and any significant seasonal trends in truck load. Vehicle weight is taken from regional weight summaries maintained by each state that are used to differentiate between routes with heavy weights and those with light weights.

Level 3 Level 3 uses regional or default classification and axle-load spectra data. It is used when the designer has only a value for average annual daily traffic (AADT) and a truck percentage for the roadway in question. A regional or statewide average load

Downloaded From : www.EasyEngineering.net

Downloaded From : www.EasyEngineering.net

distribution, default distributions developed by the agency, or the default load distribution tables provided in the 2002 Guide are used for a level 3 analysis.

F.2.2 Material Characterization

Two categories of material properties are considered: response properties and distress properties. The response properties, such as elastic modulus and Poisson ratio, are required to predict the states of stress, strain, and displacement within the structure. The distress properties are used through transfer functions to predict the major modes of distress associated with a particular material, such as fatigue, low-temperature cracking, permanent deformation of asphalt pavements, and repeated load fatigue and joint faulting of rigid pavements.

Asphalt Materials The elastic modulus of asphalt mixtures is the dynamic modulus, discussed in Sections 7.2.1 and A.4. The dynamic modulus of AC is known to vary with temperature, rate of loading, and age. In the 2002 Guide, a relationship was developed between the dynamic modulus, the time rate of loading, and mixture temperature. This is referred to as the master curve. The master curve, coupled with an asphalt binder aging model, can be used to select mixture modulus values at incremental points in the design analysis period. This time–temperature superposition principle was discussed in Section 2.3.2 and applied in KENLAYER to convert the creep compliances from one temperature to the other. Table F.1 shows the three levels of inputs for asphalt materials.

PCC Materials PCC materials can be divided into two major groups: intact and fractured slabs. A great deal of information is available on the material properties, major distress functions, and strength of intact slabs. The recommended test procedure for determining the elastic modulus and Poisson ratio of concrete using cylindrical specimens is specified in ASTM Standard C 469. The test provides a stress–strain ratio value, E_c, and a Poisson ratio based on the lateral to longitudinal strains. Fractured slabs are used in PCC rehabilitation involving the reduction of slab length to minimize the influence of reflective cracking in subsequent overlays. As the degree of fracture is increased, the effective moduli of the PCC slab decreases and finally might approach to that of a high-quality stone base. One of the most reliable ways for determining moduli of these

TABLE F.1 Three Levels of Inputs for Asphalt Materials

Design Type	Input Level	Description
New	1	Conduct laboratory dynamic modulus test, perform tests on binder, simulate aging of mix, develop mix master curve
	2	Use predictive equation for dynamic modulus, perform tests on binder, develop mix master curve
	3	Use predictive equation for dynamic modulus, develop mix master curve
Rehabilitation	1	Backcalculate by FWD, develop mix master curve with aging, test cores in laboratory
	2	Determine mix properties from cores, develop mix master curve
	3	Develop undamaged mix master curve from typical mix properties, adjust for damage based on distress surveys

Downloaded From : www.EasyEngineering.net

Downloaded From : www.EasyEngineering.net

TABLE F.2 Three Levels of Inputs for PCC Materials

Design Type	Input Level	Description
New	1	Lab determined elastic modulus at 7, 14, 28, and 90 days
	2	Modulus estimated from compressive strength
	3	Modulus selected from typical values based on agency experience
Rehabilitation of intact slabs	1	FWD backcalculation or coring and lab testing (see 1 above)
	2	Same as 2 above
	3	Same as 3 above
Rehabilitation of fractured slabs	1	FWD backcalculation of fractured slabs
	2	Modulus selected from table based on slab condition
	3	Modulus selected from table based on nominal fractured slab size

systems is through backcalculation from FWD data. Table F.2 shows the three levels of inputs for PCC materials.

Unbound Materials In the 2002 Guide, the following nonlinear model is used to characterize the resilient modulus of unbound bases, subbases, and subgrades:

$$M_R = k_1 p_a \left(\frac{\theta}{p_a}\right)^{k_2} \left(\frac{\tau_{oct}}{p_a} + 1\right)^{k_3} \tag{F.1}$$

in which M_R = resilient modulus, p_a = atmospheric pressure to normalize stresses and modulus; k_1, k_2, k_3 = regression constants which are functions of material types and properties; θ = stress invariant, or the sum of the three principal stresses; and τ_{oct} = octahedral shear stress. The octahedral stress can be expressed as

$$\tau_{oct} = \frac{\sqrt{(\sigma_1 - \sigma_2)^2 + (\sigma_2 - \sigma_3)^2 + (\sigma_1 - \sigma_3)^2}}{3} \tag{F.2}$$

In using triaxial tests to determine M_R, $\sigma_3 = \sigma_2$, so $\tau_{oct} = 0.471\ (\sigma_1 - \sigma_2)$. It can be seen that the octahedral shear stress is related directly to the deviator stress. This universal model, applicable to all types of unbound paving materials ranging from very plastic clays to clean granular bases, is currently being studied in an ongoing NCHRP Project 1-28A on the development of a harmonized M_R test protocol. For purely cohesive clays, the k_2 term will approach a value of 0; while for a cohesionless granular material, k_3 approaches 0.

Table F.3 shows the three levels of inputs for determining the resilient modulus of unbound materials. In the 2002 Guide, each of the three input levels is further subdivided, so there are actually eight levels of inputs for new pavements and also eight levels for rehabilitated pavements. However, these subdivisions are included in the main division and not separately shown in Table F.3.

F.2.3 Climate

The climate factors that affect pavement design include temperature and moisture. The properties of asphalt materials are highly temperature dependent. Temperature gradients

Downloaded From : www.EasyEngineering.net

Downloaded From : www.EasyEngineering.net

TABLE F.3 Three Levels of Inputs for Determining M_R of Unbound Materials

Design Type	Input Level	Description
New	1	Use k_1, k_2, k_3 nonlinear coefficients, which can be determined by direct tests, predictive equations, or tabular summary based on soil classification group
	2	Correlate M_R from predictive equations, CBR or R values, or plasticity/gradation properties
	3	Correlate M_R from soil classification
Rehabilitation	1	Backcalculate M_R using direct FWD measurements or tabular summary of backcalculated values by soil group
	2	Correlate M_R from predictive equations, CBR, R values, dynamic cone penetration test, plasticity/gradation properties or layer coefficients
	3	Select typical M_R as default based on soil classification and design conditions

on PCC slabs cause curling, while moisture gradients cause warping, both affecting the contact conditions between slab and foundation. The properties of unbound materials are affected by moisture and frost. The effects of temperature and moisture regimes should be considered on a project basis using site-specific environmental factors. Of the several procedures available to establish site-specific variations, the one showing the most promise for integration within the 2002 Guide is the FHWA's Integrated Climate Model (ICM). The ICM is a comprehensive environmental-effect model that consists of four primary sub-models: precipitation, infiltration and drainage, climate–material–structure, frost heave and thaw settlement. The model was enhanced by the research team and renamed as the Enhanced Integrated Climate Model (EICM). With the input of hourly climatic data, the model can produce hourly temperature profiles through the PCC slab and the seasonal moduli of base and subgrade. The nonlinear hourly temperature profiles can be converted to equivalent linear temperature differences for computational efficiency.

F.2.4 Reliability

Due to the large numbers of inputs, it was indicated by the research team at the outset that the Monte Carlo simulation method would be used in the 2002 Guide. However, it was later found that the number of calculations for the performance prediction over the entire design life for even a deterministic analysis is just too long, especially for flexible pavements, thus making the Monte Carlo simulation approach practically infeasible. Although the Monte Carlo procedure theoretically could have been used for rigid pavements, as their structural analysis is a bit simpler and has been optimized in a very fast neural network, NCHRP and the project team thought it essential to keep the reliability approach the same for both pavement types. After some careful studies, the residuals of distress models i.e. the differences between measured and predicted distresses are being used for both flexible and rigid pavement reliability. This residual method is based on the contention that the residuals represent the accuracy of the distress prediction model and smaller residuals indicate a more reliable design. A major

Downloaded From : www.EasyEngineering.net

Downloaded From : www.EasyEngineering.net

drawback of this method is that the residuals are obtained from the results of calibration, which itself may not be reliable. By assuming the residuals as normal distribution with a mean and a standard deviation, the predicted distress at any level of reliability can be determined.

The Monte Carlo method has not been discussed anywhere in this book. The potential use of the method in future pavement design makes it worthwhile to describe briefly here.

The Monte Carlo Method is a statistical method quite different from the numerical methods discussed in this book. In many applications of the Monte Carlo method, the physical process is simulated directly, and there is no need to even write down the equations that describe the behavior of the system. The only requirement is that the system be described by probability density functions (PDFs) from which the Monte Carlo simulation can proceed by random sampling. Many simulations are then performed and the desired result is taken as an average over the number of observations. In many practical applications, one can predict the statistical error or the variance of this average result and, therefore, an estimate of the number of Monte Carlo trials needed to achieve a given error.

In the case of pavement design, each input parameter has a PDF such as the normal distribution with a mean and a variance, as discussed in Section 10.1.3. By random sampling, an input value is picked from each of the PDFs. These input values, which are somewhat different from the given mean values, will be processed through the computer program, and an outcome is predicted. After n number of trials, n number of outcomes can be obtained. These outcomes can be used to determine the mean and variance of the outcome, and thus, the reliability of the design can be evaluated.

It can be seen that the Monte Carlo method is somewhat similar to the Rosenblueth method described in Section 10.4. However, the number of trials and the input values in the Rosenblueth method are predetermined, but those in the Monte Carlo method are arbitrary or randomly selected. The problem with the Rosenblueth method is that it can be applied only to simple problems with a limited number of variables. If there are n input variables, the Rosenblueth method requires 2^n trials, which is practically impossible if n is large. This problem can be easily overcome by the Monte Carlo method because, regardless of the large number of inputs, only a limited number of trials are needed. With the great increase in speed of personal computers and the complexity of problems to be solved, it is expected that the Monte Carlo method will gain popularity in the years to come.

F.3 DISTRESS PREDICTION MODELS

The mechanistic–empirical method of design used in the 2002 Guide consists of two parts. The first part involves the use of mechanistic structural models to determine the stresses, strains, and displacements in the pavement structure, and the second part involves the use of mechanistic or empirical distress models to predict the type and extent of damage at various times. When each type of damage exceeds the allowable limit, the proposed design of a new pavement must be revised or appropriate rehabilitation of an existing pavement will be needed.

Downloaded From : www.EasyEngineering.net

Downloaded From : www.EasyEngineering.net

Most of the distress models are regression equations consisting of a number of constants, which must be carefully calibrated so a best fit between the predicted distresses and the actual field measurements can be obtained. A major problem with a regression model is that it may not include all of the factors that affect the predicted distress. As long as these unaccounted factors remain unchanged, the regression model can be applied with confidence. However, if the same model is applied to another region where the unaccounted factors are quite different, the prediction may no longer be valid and a recalibration of the model is needed.

F.3.1 AC Pavements

The methodology of calibrated mechanistic procedure presented in Figure 11.1 is similar to that used by the 2002 Guide, with two exceptions. First, the 2002 Guide considers not only the alligator fatigue cracking from bottom up but also the longitudinal fatigue cracking from top down. Second, the 2002 Guide predicts the pavement roughness using the International Roughness Index (IRI), which is not included in Figure 11.1.

Fatigue Cracking The basic fatigue equation used in the 2002 Guide to determine the allowable number of load repetitions is the same as Eq. 3.6 with three coefficients. Fatigue beam tests with constant stress or constant strain control, as described in Section 7.31, can be used to determine these three coefficients in the laboratory. However, these coefficients must be adjusted to represent the actual field conditions. Damage ratio, which is a ratio between the actual number of load repetitions and the allowable number of load repetitions, is computed for each load in each season and accumulated over the years. The accumulated damage ratio is then correlated to the percentage of pavement cracking by area using regression equations that are calibrated as part of the field calibration/validation process.

Most of the fatigue cracking occurs at or near the wheel path where the tensile strain at the bottom of HMA is the greatest. However, some longitudinal cracking may occur between the two wheel paths where the top of HMA is under tension. Although longitudinal cracks are few in number, they contribute to the integrity of the pavement and should be controlled by proper design.

Rutting The repeated load tests on cylindrical specimens of asphalt mixtures or unbound materials can be used to determine the permanent deformation parameters of each material, as described in Section 7.4. For asphalt mixtures, it is assumed that the permanent strain is proportional to the resilient strain as represented by the following equation:

$$\frac{\varepsilon_p}{\varepsilon_r} = 0.0007\beta_{r1}T^{1.734\beta_{r2}}N^{0.39937\beta_{r3}} \tag{F.3}$$

in which ε_p = permanent strain; ε_r = resilient strain; T = AC temperature; N = number of load repetitions; and β_{r1}, β_{r2}, β_{r3} = calibration factors. The numerical coefficients are obtained from laboratory tests and should be adjusted in the field by the calibration factors.

Downloaded From : www.EasyEngineering.net

Downloaded From : www.EasyEngineering.net

Eq. F.3 is similar to Eq. 7.41 and indicates that a plot of log ε_p versus log N results in a straight line, as shown in Figure 7.28. Substituting the average vertical compressive strain, ε_r, in the asphalt layer computed by the software program into Eq. F.3, the permanent vertical strain, ε_p, can be determined. Multiplying ε_p by the thickness of the layer gives the rut depth caused by permanent deformation of the AC layer.

The equation for permanent deformation of unbound materials was originally proposed by Tseng and Lytton (1998) and can be expressed as

$$\delta_a = \beta_{s1}\varepsilon_v h\left(\frac{\varepsilon_0}{\varepsilon_r}\right)\left[e^{-\left(\frac{e}{N}\right)^{\beta}}\right] \tag{F.4}$$

in which δ_a = permanent deformation of the unbound layer; β_{s1} = field calibration factor; e = base of natural logarithm with a value of 2.71828; N = number of load repetitions; ε_v = average vertical resilient strain obtained from the software program; h = thickness of the layer; β, ρ, and ε_o = regression constants representing material properties; and ε_r = resilient strain imposed in the laboratory test to obtain the three regression constants. The ratio $\varepsilon_o/\varepsilon_r$ is usually combined to represent a material property. It can be seen that, similar to AC layers, the permanent deformation of unbonded layers is also proportional to the resilient deformation.

Thermal Fracture The indirect tensile test can be used to predict thermal fracture. The thermal cracking model is basically the same as in the SHRP Superpave Performance Models (Lytton, et al., 1993). The equation used for calibration is

$$C_f = \beta_{t1}\beta_1 N_0\left(\frac{\log C/h_{ac}}{\sigma}\right) \tag{F.5}$$

in which C_f = observed amount of thermal cracking in ft (m); β_1 = calibration factor based on LTPP data; N_0 = standard normal distribution evaluated at 0; C = predicted crack depth by a crack propagation model; h_{ac} = thickness of AC layer; σ = standard deviation of the log crack depth; and β_{t1} = field calibration factor.

Roughness The International Roughness Index (IRI), as described in Section 9.2.2, is used to evaluate roughness. The IRI is evaluated by increments as indicated by

$$\text{IRI} = \text{IRI}_0 + \Delta\text{IRI} \tag{F.6a}$$

$$\Delta\text{IRI} = \text{Function}\,(D_j, S_f) \tag{F.6b}$$

in which IRI_0 = pavement smoothness when it is newly constructed, D_j = effect of surface distress, and S_f = effect of non-distress variables or site factor.

F.3.2 PCC Pavements

The design procedure generally follows that presented in Figure 12.1. The distress models for JPCP include fatigue cracking, joint faulting, and roughness while those for CRCP are punchouts and roughness.

Downloaded From : www.EasyEngineering.net

Downloaded From : www.EasyEngineering.net

Fatigue The number of allowable repetitions varies with the stress ratio, which is a ratio between the tensile stress, σ, and the modulus of rupture, S_c. Since S_c increases with age, the following strength-gain model can be used to determine S_c at various ages.

$$\text{STRATIO} = 1 + 0.1249 \log(\text{AGE}/0.0767) - 0.01566 [\log(\text{AGE}/0.0767)]^2 \quad \text{(F.7)}$$

in which STRATIO = ratio of PCC strength at a given age to 28-day strength, AGE = PCC age in years. The model gives a strength gain of 1.12 at 10 years and 1.21 at 20 years. In contrast to the PCA equation, which limits the maximum stress ratio to 1, Eq. F.8 which allows the stress ratio as high as 2, can be used in the field. Keep in mind that the probability of cracking at a stress ratio of 1 is 50%. If the probability of failure is greater than 50%, the stress ratio should be greater than 1.

$$\text{Log } N = \left[\frac{-\left(\frac{\sigma}{S_c}\right)^{-\beta} \text{Log}(1 - P)}{\alpha} \right]^{\gamma} \quad \text{(F.8)}$$

in which N = allowable number of stress repetitions; P = probability of cracking; and α, β, and γ = fatigue coefficients obtained from fatigue tests with P = 0.5. In applying Eq. F.8 to field conditions, P also serves as a calibration factor to match the field data.

Similar to AC pavements, both bottom-up and top-down crackings are considered. The fatigue damage is determined by

$$D_r = \sum \frac{n_{ijklmn}}{N_{ijklmn}} \quad \text{(F.9)}$$

in which D_r = damage ratio, n_{ijklmn} = actual number of load repetitions, N_{ijklmn} = allowable number of load repetitions computed by Eq. F.8, i = age with 4 categories, j = season with 2 to 4 categories, k = axle combination with 3 categories, l = load level with 5 to 10 categories, m = temperature gradient with 7 categories, and n = traffic path with 4 to 8 categories. Eq. F.9 is very similar to Eq. 3.19 incorporated in KENSLABS, which only considers season (period) and load (both axle combination and load level), but the 2002 Guide also considers age, season, temperature gradient, and traffic path.

In calibrating the fatigue model, the percentage of slab cracking, as observed in the field, is plotted against the damage ratio based on P = 0.5, and the following characteristic fatigue curve is used to get the best fit:

$$\% \text{ Slab Cracking} = \left(\frac{D_r^b}{a^b + D_r^b} \right) \times 100 \quad \text{(F.10)}$$

in which a and b are the calibration factors. From this fatigue curve, the damage ratio at 50% slab cracking can be determined. Because the damage ratio at 50% slab cracking, obtain from this fatigue curve, is most probably not equal to 1, the curve must be shifted horizontally by changing P so that 50% slab cracking occurs at D_r = 1. The percentage of slabs cracked can be predicted by successive applications of Eqs. F.7 through F.10.

Downloaded From : www.EasyEngineering.net

Downloaded From : www.EasyEngineering.net

Faulting Incremental faulting is computed for each month using the following model:

$$\text{DFAULT} = \text{A}(\text{FAULTMAX} - \text{FAULT})^2 \sum_{ij} (n_{ij}\text{DE}_{ij}) \tag{F.11}$$

in which DFAULT = incremental faulting; FAULTMAX = maximum potential faulting (which is a function of corner deflection, erodibility, number of wet days, and overburden pressure); FAULT = current cumulative faulting at month beginning, DE_{ij} = differential energy (which varies with axle type i and load level j); n_{ij} = number of load repetitions, and A = a calibration constant.

Summation of all the previous incremental faulting gives the faulting at any given time.

Punchout Punchout is the major distress in CRCP and consists of an area enclosed by two closely spaced transverse cracks, a short longitudinal crack, and the edge of the pavement or a longitudinal joint. The short longitudinal crack is located between the two wheel paths and caused by the critical tensile stress at the top of the slab. The mechanics of punchouts are described in Section 12.1.6. Crack spacing, crack width, and loss of load transfer efficiency (LTE) across the cracks are the major factors that contribute to punchouts. These factors must be evaluated so that the critical stress can be computed and the fatigue damage determined. The following transfer function is then used to relate the fatigue damage to the number of punchouts.

$$PO_y = e^{-e^{[b+m-\text{Ln}(D_y)]}} * [5280 * P(L \leq 2\text{ ft})/\overline{L}] \tag{F.12}$$

in which PO_y = number of punchouts per mile at the end of the yth year; e = base of natural logarithm; D_y = accumulated fatigue damage at the end of the yth year; b and m = punchout calibration constants; $\overline{L}$ = mean crack spacing in inches; and $P(L \leq 2\text{ ft})$ = probability of crack spacing of 2 ft or less as a fraction. Note that D_y is the damage ratio similar to Eq. F.9 (with only two indexes of time increment and load level), and that $\overline{L}$ and $P(L \leq 2\text{ ft})$ can be computed from close-form formulas.

Roughness Similar to AC pavements, roughness is measured by IRI. The IRI at any given time depends on the initial IRI and the change in IRI, as indicated by the following regression equations:

$$\text{IRI} = \text{IRI}_0 + C_1\,\text{CRK} + C_2\,\text{SPALL} + C_3\,\text{TF} + C_4\,\text{SF} \tag{F.13}$$

in which IRI_0 = initial IRI; CRK = cracked slabs in%; SPALL = spalled joints in%; TF = total joint faulting in inches per mile; and SF = site factor (which is a function of age, freezing index, and the percent of fines (minus 200) in the subgrade). The variance of IRI can be determined from the variance of each component. From Eq. 10.11:

$$V[\text{IRI}] = V[\text{IRI}_0] + C_1^2 V[\text{CRK}] + C_2^2 V[\text{SPALL}] + C_3^2 V[\text{TF}] + S_e^2 \tag{F.14}$$

in which S_e^2 = variance of model residual error. The predicted IRI at a given reliability R is

$$\text{IRI}_R = \text{IRI} + \sigma_{\text{IRI}} Z_R \tag{F.15}$$

Downloaded From : www.EasyEngineering.net

Downloaded From : www.EasyEngineering.net

in which IRI_R = predicted IRI at reliability R; IRI = predicted IRI based on mean inputs corresponding to 50% reliability; σ_{IRI} = standard deviation of IRI; and Z_R = standard deviate (see Table 11.15),

SUMMARY

This appendix provides a brief introduction to the 2002 Design Guide. This Guide, when completed, will be a comprehensive procedure that addresses the design of the total pavement structure, not just layer thickness. However, only the information related directly to the thickness design was presented here. It should be borne in mind that the purpose of this appendix is not to cover every aspect of the Guide but is merely to shed some light on the design principles and general approach. Detailed procedures are not available currently and, even if available, might be subject to changes in the immediate future through the various review and implementation processes.

From the information posted on the Internet, it appears that the procedure for the design of rigid pavements has been well established and is ready for implementation. However, this is not the case for flexible pavements, where very little information on the field calibration of fatigue cracking and thermal fracture was presented, and the method used for reliability was not even mentioned. One difficulty in the implementation of the 2002 Guide is the calibration of the distress models. Calibration requires good and reliable traffic and performance data, which may not be readily available. The use of level 3 inputs by default or engineering guessing is not warranted because it defeats the very purpose of the calibrated mechanistic method. Even after the Guide is published, great efforts are needed on the part of users to collect performance data and calibrate the distress prediction models before putting it into practical use. Some modifications and improvements of the 2002 Guide are expected for many years to come.

Apprise Education, Reprise Innovations

Downloaded From : www.EasyEngineering.net

Downloaded From : www.EasyEngineering.net

APPENDIX G

List of Symbols

A	a/h_2 of a three-layer system; or area of dowel; or average number of axles per truck; or temperature susceptibility of bitumen; or cross-section area normal to direction of flow; or area of pipe; or area cracked; or permanent deformation parameter in the Ohio State model; or regression constant relating effective indirect tensile strength to modulus of rupture of concrete; or factor to convert PCC thickness to AC overlay thickness.
AC	asphalt concrete
AC/PCC	asphalt concrete overlaid Portland cement concrete
ADT	average daily traffic
$(ADT)_0$	average daily traffic at start of design period
ADTT	average daily truck traffic
AOS	apparent opening size of fabric
A_c	tire contact area
A_i	constant of integration for layer i; or coefficients of PSI equation
A_{ji}	intercept of log deflection versus log E
A_s	area of steel per unit width of slab
A_1	area of one tie bar at longitudinal joint; or regression constant in stiffness modulus test
a	contact radius; or half-length of rectangular finite element; or a constant; or distance from support to third point of beam; or pavement age in years
a'	modified contact radius
a_{OL}	structural layer coefficient of asphalt overlay
a_T	time-temperature shift factor
a_d	contact radius of dual tires
a_{eq}	equivalent tire contact radius
a_s	contact radius of single tire
a_1	distance from corner of slab to center of load
a_1, a_2, a_3	layer coefficients for asphalt surface, base, and subbase courses, respectively

Downloaded From : www.EasyEngineering.net

Downloaded From : www.EasyEngineering.net

B	a coefficient for determining AOS; or a pavement roughness property; or a damage factor; or slab bending correction factor
BPN	British Pendulum Number
B_i	constant of integration for layer i; or coefficients of PSI equation
b	total compliance due to retarded strain; or half-width of rectangular element; or a constant; or width of beam
C	conversion factor for dual or dual-tandem wheels; or correction factor for warping stress in finite slab with length L; or coefficient of variation; or area cracked; or adjustment factor due to slab-subbase friction; or cohesiometer value; or fatigue correction factor due to different mixes; or a pavement roughness property; or a constant; or adjustment factor from backcalculated M_R to design M_R
CBR	California Bearing Ratio
CF	condition factor
CRCP	continuous reinforced concrete pavement
CTB	cement-treated base
CW	crack width
C_d	drainage factor for rigid pavements
C_i	constant of integration for layer i
C_k	Hazen's coefficient relating effective size to permeability
C_m	correction factor for dynamic effect
COV	covariance
C_s	spacing of transverse cracks or joints
C_u	uniformity coefficient
C_w	shear spring constant of joint
C_x	correction factor for finite slab with length L_x
C_y	correction factor for finite slab with length L_y
C_1	an adjustment factor for erosion: 1 for untreated subbases, 0.9 for stabilized subbases
C_2	equivalent damage ratio: 0.06 for edge loading, 0.94 for corner loading
C_θ	moment spring constant of joint
c	side length of a square contact area; or initial curling of slab; or a constant; or cracking index; or critical period correction factor
c_i	coefficients of Dirichlet series for viscoelastic response; or initial curling of slab at node i
c_1	fatigue coefficient of laboratory specimen
D	creep compliance; or differential operator $\partial/\partial t$; or depth of sealant reservoir; or thickness of concrete slab by AASHTO method; or percentage of ADT in design direction; or diameter of pipe; or constant relating modulus of rupture to modulus of elasticity of concrete; or total thickness of pavement layers above subgrade
DETJT	percentage of deteriorated joints
DT_D	design temperature drop
D_{OL}	required thickness of overlay
D_{SB}	thickness of subbase under concrete slab

Downloaded From : www.EasyEngineering.net

Downloaded From : www.EasyEngineering.net

D_{SG}	thickness of subgrade above a rigid foundation
D_a, D_b	grain sizes corresponding to a and b % passing
D_{ac}	thickness of existing AC surface
D_{eff}	effective thickness of in situ PCC pavement prior to overlay
D_f	PCC thickness required to support overlay traffic
D_i	creep compliance at time i; or constant of integration for layer i; or functions of surface deterioration in PSI equation
D_{pcc}	thickness of existing PCC slab
D_r	damage ratio at end of year; or damage ratio at the end of design period
D_x	grain size corresponding to x% passing
D_1, D_2, D_3	thickness of hot mix asphalt, base, and subbase by AASHTO method
D_2	amount of displacement in stabilometer test
D_{15}, D_{50}, D_{85}	grain size corresponding to 15, 50, and 85% passing, respectively
d	distance from neutral axis to bottom of slab; or duration of moving load; or clearance between dual tires; or diameter of steel bar; or distance to the center of slab where curling is zero; or a constant; or distress indicator; or subgrade type
d_{ij}	distance between node i and node j
d_r	surface deflection at a distance r from the load
d_s	deformation of saturated specimen
d_u	deformation of unsaturated specimen
d_0	deflection measured at the center of the load plate
d_{12}	deflection measured at 12 in. from the load
d_{24}	deflection measured at 24 in. from the load
d_{36}	deflection measured at 36 in. from the load
E	elastic modulus; or elastic modulus of concrete; or expectation; or error between PSR and PSI; or equivalent factor for emulsified asphalt base
$\overline{E}$	Laplace transform of E
E^*	complex modulus
$\|E^*\|$	dynamic modulus
EALF	equivalent axle load factor
EDR	equivalent damage ratio
ELP	elastic layer program
ESAL	equivalent single-axle load, which is the total number of repetitions of a standard 18-kip axle load during the design period
E_{SB}	resilient modulus of subbase for concrete pavement
ESWL	equivalent single-wheel load
E_c	elastic modulus of concrete
E_d	Young's modulus of dowel
E_f	elastic modulus of solid foundation; or modulus in fully cured state
E_i	elastic modulus of Kelvin model; or modulus in uncured or initial state
E_o	initial elastic modulus for nonlinear soil; or elastic modulus of Maxwell model; or stiffness modulus when $\sigma = 0$

Downloaded From : www.EasyEngineering.net

Downloaded From : www.EasyEngineering.net

E_p	effective modulus of all pavement layers above the subgrade
$E_r(N)$	elastic modulus due to unloading at Nth repetition
E_s	stiffness modulus
E_t	modulus at curing time t
E_1	elastic modulus of layer 1 or HMA layer; or elastic modulus of Kelvin model
E_2	elastic modulus of layer 2 or base course
E_3	elastic modulus of layer 3, which may be a subbase or a subgrade
E_4	elastic modulus of subgrade for a four-layer system
E_{1a}, E_{1b}	elastic moduli of 1st and 2nd asphalt layers, respectively
e	critical tensile strain at the bottom of layer 1
F	deflection factor; or a function; or a force vector; or tractive force at tire-pavement contact; or a probability function; or faulting; or temperature adjustment factor
FWD	falling weight deflectometer
F_{ac}	AC quality adjustment factor
F_d	deflection factor under dual wheels
F_{dur}	durability adjustment factor
F_e	strain factor
F_{fat}	fatigue damage adjustment factor
F_i	EALF for ith load group
F_{jc}	joints and cracks adjustment factor
F_{jcu}	joints and cracks adjustment factor for unbonded concrete overlays
F_s	deflection factor under single wheels
$F(t)$	function of t
F_w	vertical force
$F_{\theta x}$	moment about x axis
$F_{\theta y}$	moment about y axis
F_2	deflection factor for two-layer system used in Figure 2.17
f	flexural stress; or probability function
f_a	average coefficient of friction between slab and subgrade
f_b	allowable bearing stress between dowel and concrete
f'_c	ultimate compressive strength of concrete
f_s	allowable stress in steel
f_t	concrete indirect or splitting tensile strength
f_{te}	effective indirect tensile strength of concrete
f_1, f_2, f_3	coefficients of fatigue criterion
f_4, f_5	coefficients of permanent deformation criterion
G	shear modulus of dowel; or traffic growth multiplier; or specific gravity
G_b	specific gravity of bitumen
G_g	specific gravity of aggregate
G_i	coefficient of Dirichlet series for creep compliance
G_m	specific gravity of mixture
G_s	specific gravity of soil solid
G_t	function of terminal serviceability index p_t
g	function of random variables; or acceleration of gravity

Downloaded From : www.EasyEngineering.net

Downloaded From : www.EasyEngineering.net

g_{ij}	flexibility coefficient for deflection at i due to force at j
H	h_1/h_2 of three-layer system; or thickness of all layers combined; or initial height of groundwater table above impervious layer; or thickness of drainage layer; or tensile strength of HMA
HMA	hot mix asphalt
H_o	vertical distance between bottom of drainage layer and impervious layer
h	thickness; or thickness of concrete slab; or thickness of beam
h_{OL}	thickness of overlay
h_e	effective thickness; or thickness of existing pavement
h_i	thickness of slab at node i
h_n	thickness of new pavement
h_1	thickness of layer 1 or asphalt surface course
h_2	thickness of layer 2 or granular base
h_{1a}, h_{1b}	thickness of 1st and 2nd asphalt layers, respectively
h_1'	modified thickness of layer 1
I	moment of inertia; or intercept of log ϵ_p versus log N curve at $N = 1$; or low-temperature cracking index
IRI	international roughness index
I_c	composite moment of inertia of two layers; or crack infiltration rate
I_d	moment of inertia of dowel
i	an index for Kelvin models, Dirichlet series, load groups, loading times, layer numbers, design periods, or nodal points; or hydraulic gradient
J	load transfer factor for rigid pavements
JPCP	jointed plain concrete pavement
JRCP	jointed reinforced concrete pavement
JS	joint spacing
J_0	Bessel function of first kind and of order 0
J_1	Bessel function of first kind and of order 1
K	modulus of dowel support; or overall stiffness of slab system
K_f	stiffness matrix of foundation
K_0	coefficient of earth pressure at rest
K_p	stiffness matrix of slab or plate
K_1	nonlinear coefficient of granular materials; or breakpoint resilient modulus of non-linear fine-grained soils; or stiffness matrix within assigned half band; or coefficient of fatigue equation
K_2	nonlinear exponent of granular materials; or deviator stress at breakpoint for nonlinear fine-grained soils; or stiffness matrix outside the assigned half-band; or exponent of fatigue equation
K_3	slope of first straight line for nonlinear fine-grained soils
K_4	slope of second straight line for nonlinear fine-grained soils
k	modulus of subgrade reaction; or permeability
k_i	modulus of subgrade reaction at node i
k_p	permeability of pavement surface
k_s	saturated modulus of subgrade reaction
k_u	unsaturated modulus of subgrade reaction

Downloaded From : www.EasyEngineering.net

Downloaded From : www.EasyEngineering.net

k_1	E_1/E_2 of a three-layer system
k_2	E_2/E_3 of a three-layer system
k_∞	modulus of subgrade reaction when D_{SG} is greater than 10 ft
L	length of tire contact area; or load factor defined as $2P_d/P_s$; or Laplace transform; or length of slab; or average nodal spacing at joint; or percentage of ADT in design lane; or weight of lead shot in cohesiometer test; or length of beam between supports; or length of drainage layer; or Fourier transform
L'	distance from longitudinal joint to the free edge of slab
LS	factor indicating loss of subgrade support
LSF	load safety factor
LTE	load transfer efficiency
L_e	average length of each encroachment
L_i	distance of groundwater influence
L_o	distance between outlets; or length of observed distance
L_p	average distance traveled during parking
L_s	load in kip on standard axles
$L(t)$	moving load function
L_x	load in kip on one single axle, one set of tandem axles, or one set of tridem axles; or length of slab in x direction
L_y	length of slab in y direction
L_1	load factor for $a = 6$ in. (152 mm); or distance measured on grain size curve; or load on one single axle or a set of tandem or tridem axles
L_2	load factor for $a = 16$ in. (406 mm); or axle code, 1 for single axle, 2 for tandem axles, and 3 for tridem axles; or distance measured on grain size curve
M	moment
MAAT	mean annual air temperature
MAD	moisture accelerated distress
MDD	multidepth deflectometer
MPR	mean panel rating
MTD	mean texture depth
M_a	mean monthly air temperature
M_p	mean monthly pavement temperature
M_R	resilient modulus; or effective roadbed soil resilient modulus
m	number of axle load groups; or parameter for layered system; or number of periods in a year; or permanent deformation exponent in the Ohio State model
m_2, m_3	drainage coefficients for base and subbase courses, respectively
N	allowable number of load repetitions; or number of blocks in influence chart; or number of load repetitions; or number of traffic lanes
NDT	nondestructive testing
NR	percentage of drivers indicating that pavement needs repair
N_T	actual traffic during design period
N_a	allowable number of load repetitions on existing pavement before overlay
N_c	number of longitudinal cracks

Downloaded From : www.EasyEngineering.net

Downloaded From : www.EasyEngineering.net

N_d	allowable number of load repetitions to limit permanent deformation
N_e	encroaching traffic; or number of load repetitions on existing pavement before overlay
N_f	allowable number of load repetitions to prevent fatigue cracking; or number of load repetitions expected on a new overlay
N_i	allowable number of load repetitions due to ith axle load; or allowable number of load repetitions during ith period; or allowable number of load repetitions during ith stage
N_{max}	maximum number of steel bars per traffic lane
N_{min}	minimum number of steel bars per traffic lane
N_o	number of load applications on the outside lane
N_p	number of parked trucks per day; or number of load repetitions at which the payment reaches a serviceability that requires overlay
N_t	actual performance traffic
$N_{1.5}$	total traffic a pavement could be expected to carry to failure
N_{18}	number of equivalent 18-kip single-axle loads
n	number of Kelvin models; or number of terms in Dirichlet series; or number of layers; or predicted number of load repetitions; or direction of moment in influence chart; or number of observations; or number of random variables; or roughness coefficient in Manning formula; or porosity; or number of construction stages; or an exponent in overlay equation
n_e	effective porosity
n_i	number of passes of ith axle load; or predicted number of load repetitions during ith period; or predicted number of repetitions during ith stage
$(n_0)_1$, $(n_0)_2$, $(n_0)_3$	number of single-, tandem-, and tridem-axle loads per day at start of design period, respectively
n_r	additional number of load repetitions that can be applied to existing pavement after overlay
P	a concentrated load; or percent by weight; or area patched; or rate of work for erosion; or percentage of steel
PCC	portland cement concrete
PI	penetration index; or profile index; or plasticity index; or pumping index
PMS	pavement management system
PNG	percent normalized gradient
PSI	present serviceability index
PSI_f	final or terminal serviceability index
PSI_i	present serviceability index at point i
PSI_0	initial serviceability index
PSR	present serviceability rating
P_b	bitumen content

Downloaded From : www.EasyEngineering.net

Downloaded From : www.EasyEngineering.net

P_d load on each of dual wheels
P_e percent encroaching traffic
P_h transmitted horizontal pressure in stabilometer test
P_j force at node j
P_{max} maximum percent steel
P_{min} minimum percent steel
P_p percent parking traffic
P_r permanent deformation at radial distance r from the load
P_s load on single wheel
P_t load on one dowel
P_v applied vertical pressure in stabilometer test
P_{200} percent passing 200 sieve
P_{77F} penetration at 77°F
$P_{\#8}$ percent by weight passing no. 8 sieve
p transform variable; or unit pressure; or shear force per length of joint; or number of periods per year
p_f ultimate failure serviceability
p_i ith transform variable; or percentage of axles in ith load group
p_0 initial serviceability index
p_1 initial serviceability of existing pavement
p_2 serviceability of existing pavement that requires overlay
p_t terminal serviceability index
Q discharge
q uniform contact pressure; or discharge
q Laplace transform of contact pressure
q_L total inflow to longitudinal collector
q_d contact pressure of dual tire; or design discharge
q_g inflow to drainage layer from groundwater
q_i inflow to drainage layer from surface infiltration
q_m inflow to drainage layer from melting of ice lenses
q_s contact pressure of single tire
$q(r)$ pressure under a rigid plate as a function of r
q_1 inflow to longitudinal collector from groundwater
q_2 inflow to drainage layer from groundwater
R response due to q expressed as stress, strain, or displacement; or radius of a warped slab; or modulus of rigidity; or resistance value; or hydraulic radius; or level of reliability
R^* response due to $-mJ_0(m\rho)$
RD rut depth
RDD rolling dynamic deflectometer
$\overline{RD}$ mean rut depth
RF reduction factor indicating the degree of curing
RL remaining life of existing pavement, in percent
RN roughness number
RR rate of rutting
RR1 radial stress factor at bottom of layer 1

Downloaded From : www.EasyEngineering.net

Downloaded From : www.EasyEngineering.net

RR2	radial stress factor at bottom of layer 2
RTRRM	response-type road roughness meter
R_i	functions of profile roughness in PSI equation
r	radial coordinate; or a random variable; or traffic growth rate; or distance from load
S	slope of straight line in permanent deformation test; or slope of pipe; or slope of drainage layer; or slope of load distribution for nonlinear analysis; or braking distance; or pavement slope measured by a profilometer; or soil suction
$\overline{S}$	mean of all slopes measured by a profilometer
SC	structural capacity
SC_{eff}	effective structural capacity of existing pavement
SC_f	structural capacity of new pavement for future overlay traffic
SC_{OL}	required structural capacity of overlay
SC_0	initial structural capacity of existing pavement
SDN	stopping distance number
SN	structural number; or skid number
SN_{OL}	required structural number of overlay
SN_{eff}	total effective structural number of existing pavement prior to overlay
SN_f	total structural number to support overlay traffic
SN_0	skid number at zero speed
SV	slope variance
$\overline{SV}$	mean slope variance
S_b	stiffness modulus of bitumen
S_{bit}	stiffness modulus of original asphalt for analyzing low-temperature cracking
S_c	modulus of rupture of concrete
S_{ce}	modulus of rupture of existing concrete
S_{cn}	modulus of rupture of new pavement
S_d	dual spacing
S_f	slope factor
S_{ji}	slope of log deflection versus log E
S_m	stiffness modulus of mixture
S_{mix}	stiffness modulus of mixture determined directly from creep test
S_o	overall standard deviation in AASHTO design guide
S_t	tandem spacing
S_1, S_2, S_3	vertical intercepts for use in method of successive residuals
s	vehicle speed; or standard deviation; or a random variable; or shear strength; or number of sensors; or stress
s_T	standard deviation for traffic prediction
s_b	spacing of dowel bars
s_i	gap or precompression at node i: gap is positive, precompression is negative
s_t	standard deviation for performance prediction
T	temperature; or percentage of trucks in ADT
T_H	average daily high temperature during the month the pavement is constructed

Downloaded From : www.EasyEngineering.net

Downloaded From : www.EasyEngineering.net

T_L average daily low temperature during the coldest month of the year
$T_{R\&B}$ temperature at ring and ball softening point
T_f truck factor; or time factor for drainage
T_i retardation time of ith Kelvin model
T_0 relaxation time of Maxwell model; or reference temperature
T_1 relaxation time of Kelvin model
T_1, T_2 two temperatures at which penetrations are measured
t time; or length of tie bar; or thickness of specimen
t_d rest period
t_l loading time
t_T time to obtain creep compliance at temperature T
t_{T_0} time to obtain creep compliance at reference temperature T_0
t_i time at ith increment
t_{50} time for 50% drainage
U degree of drainage
u radial displacement; or normal deviate $(x - \mu)/s$; or ratio $d/2T$; or pore pressure
u_f relative damage to flexible pavement
u_r relative damage to rigid pavement
V variance; or vehicle speed
V_a volume of void
V_b volume of bitumen
V_g volume of aggregate
v discharge velocity
W wheel load; or width of slab; or width of specimen; or total weight of bituminous mixture; or width of roadway; or vertical load on tire
W_T predicted ESAL during design period
W_c length of transverse cracks or joints
W_p width of pavement
W_s width of slab
W_t allowable ESAL during design period
W_{tx} number of x axle load applications at end of time t
W_{t18} number of 18-kip axle load applications at end of time t
W_{18} allowable 18-kip single-axle load applications for a given reliability
w vertical deflection; or elastic deformation; or width of sealant reservoir
w^c computed deflection
w_d difference in deflection between left and right slab
w_g amount of gap in spring or dowel at joint
w_i vertical deflection at node i
w_{ij} deflection of node i due to force at node j
w_l deflection of left slab
w^m measured deflection
w_0 surface deflection
$\overline{w}_0$ Laplace transform of surface deflection
w_p permanent or plastic deformation
w_r deflection of right slab; or rebound deflection
$\overline{X}$ crack spacing

Downloaded From : www.EasyEngineering.net

Downloaded From : www.EasyEngineering.net

x	coordinate axis; or distance from a diagonal cross section to the corner of slab; or a random variable
$\bar{x}$	average of x
Y	design period in years
y	coordinate axis; or a random variable
y_0	deformation of dowel at the face of joint
Z	ratio between concrete modulus and modulus of subgrade reaction; or concrete shrinkage
Z_R	normal deviate for a given reliability R
ZZ1	vertical stress factor at interface 1
ZZ2	vertical stress factor at interface 2
z	vertical coordinate; or distance below surface; or thickness of pavement considered as homogeneous half-space; or width of joint; or normal deviate; or distance above water table
α	contact area/total thickness, a/H; or angle between a line and x axis; or permanent deformation parameter; or thermal diffusivity; or compressibility factor
α_c	coefficient of thermal expansion for concrete
α_s	coefficient of thermal expansion for steel
α_{sys}	permanent deformation parameter of pavement system
α_t	coefficient of thermal expansion
β	soil constant indicating the increase in E per unit increase in θ; or slope of log a_T versus temperature; or relative stiffness of a dowel embedded in concrete
β_x	function of SN, L_x, and L_2
β_1	to β_5 constants to evaluate stiffness or dynamic modulus of HMA
β_{18}	value of β_x when L_x is equal to 18 and L_2 to 1
γ	unit weight; or shear strain
γ_c	unit weight of concrete
γ_d	dry unit weight of soil
γ_i	unit weight of layer i
γ_w	unit weight of water
Δ	deflection at beam center; or deflection of plate loading test
ΔL	joint opening due to temperature change ΔT and drying shrinkage
ΔLT	deflection load transfer in percent
Δ_l	loaded side deflection
Δ_{ul}	unloaded side deflection
ΔPSI	serviceability loss
ΔS	shear deformation of dowel
ΔT	temperature range, which is the temperature at placement minus the lowest mean monthly temperature; or temperature increment
Δ_c	corner deflection
Δ_e	deflection due to edge loading
Δ_i	deflection due to interior loading
Δt	temperature differential between top and bottom of slab
$\Delta\sigma$	stress increment

Downloaded From : www.EasyEngineering.net

Downloaded From : www.EasyEngineering.net

δ	displacement vector of slab; or recoverable deformation in indirect tension specimen
δ_{rrd}	representative rebound deflection
δ'	displacement vector of foundation
δ_a	assumed displacement vector of slab by the iterative method
δ_d	design rebound deflection
ℓ	length of hypotenuse; or radius of relative stiffness
ϵ	normal strain; or drying shrinkage coefficient of concrete; or elastic strain
$\bar{\epsilon}$	Laplace transform of strain
ϵ_a	strain due to load a
ϵ_b	strain due to load b
ϵ_c	vertical compressive strain on the surface of subgrade
ϵ_0	initial strain in fatigue test; or strain amplitude
ϵ_p	permanent strain
ϵ_r	radial strain; or recoverable strain
ϵ_t	tangential strain; or tensile strain at bottom of asphalt layer
ϵ_x	tensile strain due to x axle load; or strain in x direction
ϵ_y	strain in y direction
ϵ_z	vertical strain
ϵ^2	squared error
$\epsilon_1, \epsilon_2, \epsilon_3$	major, intermediate and minor principal strains
ϵ_{18}	tensile strain due to 18-kip single-axle load
θ	stress invariant
θ_x	rotation about x axis
θ_y	rotation about y axis
λ	viscosity; or dimensionless vertical distance, z/H
λ_0	viscosity of Maxwell model
λ_1	viscosity of Kelvin model
μ	allowable bond stress between concrete and tie bar; or mean; or permanent deformation parameter; or coefficient of friction
μ_{sys}	permanent deformation parameter of pavement system
ν	Poisson ratio
ν_c	composite Poisson ratio of two layers; or poisson's ratio of concrete
ν_d	Poisson ratio of dowel
ν_f	Poisson ratio of foundation
ν_1	Poisson ratio of layer 1
ν_2	Poisson ratio of layer 2
ρ	dimensionless radial distance, r/H; or correlation coefficient
Σo	bar perimeter
σ	normal stress; or tensile stress in concrete slab; or tensile stress in beam test
$\bar{\sigma}$	Laplace transform of σ
σ_a	stress due to load a
σ_b	bearing stress between dowel and concrete; or stress due to load b
σ_c	vertical compressive stress on subgrade; or stress in concrete slab due to corner loading; or tensile stress in concrete slab due to friction

Downloaded From : www.EasyEngineering.net

Downloaded From : www.EasyEngineering.net

σ_d	deviator stress $\sigma_1 - \sigma_3$
σ_e	stress in concrete slab due to edge loading
σ_h	combined horizontal stress, including both loading and geostatic stresses
σ_i	stress in concrete slab due to interior loading
σ_o	initial stress on Maxwell model; or initial stress in fatigue test; or stress amplitude
σ_p	consolidation pressure on subgrade
σ_r	radial stress
σ_{r1}	radial stress at bottom of layer 1
σ'_{r1}	radial stress at top of layer 2
σ_{r2}	radial stress at bottom of layer 2
σ'_{r2}	radial stress at top of layer 3
σ_s	steel stress
σ_t	tangential stress; edge stress
σ_{te}	edge stress in existing overlaid pavement
σ_{tn}	edge stress in new pavement
σ_{to}	edge stress in new overlay
σ_v	vertical stress; or vertical combined stress including loading and geostatic stresses
σ_w	wheel load stress
σ_x	stress in x direction
σ_y	stress in y direction
σ_z	vertical stress
σ_{z1}	vertical stress at interface 1
σ_{z2}	vertical stress at interface 2
$\sigma_1, \sigma_2, \sigma_3$	three principal stresses
σ'_1	maximum allowable major principal stress
τ	shear stress
τ_{rz}	shear stresses on r plane in z direction
Ψ	cumulative distribution functions
ϕ	stress function; or angle of internal friction; or reinforcing bar or wire diameter; or phase angle
ϕ_i	stress function for layer i
ω	angular velocity

Downloaded From : www.EasyEngineering.net

Downloaded From : www.EasyEngineering.net

APPENDIX H

References

AASHO, 1968. *AASHO Highway Definitions*; Special Committee on Nomenclature, American Association of State Highway officials.

AASHTO, 1972. *AASHTO Interim Guide for Design of Pavement Structures*; American Association of State Highway and Transportation Officials.

AASHTO, 1985. *Proposed AASHTO Guide for Design of Pavement Structures*, NCHRP Project 20-7/24, Vol. 2, American Association of State Highway and Transportation Officials.

AASHTO, 1986. *Guide for Design of Pavement Structures*; American Association of State Highway and Transportation Officials.

AASHTO, 1989. *Standard Specifications for Transportation Materials and Methods of Sampling and Testing*, Part II, *Methods of Sampling and Testing*; American Association of State Highway Officials.

AASHTO, 1990. *Guidelines for Pavement Management System*; American Association of State Highway and Transportation Officials.

AASHTO, 1993. *Guide for Design of Pavement Structures*; American Association of State Highway and Transportation Officials.

AASHTO, 1998. *Standard Test Method for Determining the Permanent Deformation and Fatigue Cracking Characteristics of Hot Mix Asphalt (HMA) Using the Simple Shear Test (SST) Device*, TP7 Provisional Standards; American Association of State Highway and Transportation Officials.

AASHTO, 1999a. *MP1 Standard Specifications for Performance Graded Asphalt Binder*; American Association of State Highway and Transportation Officials.

AASHTO, 1999b. *MP2 Standard Specifications for Volumetric Mix Design*; American Association of State Highway and Transportation Officials.

AASHTO, 1999c. *PP28 Standard Specifications for asphalt Mix Design*; American Association of State Highway and Transportation Officials.

ASHTO, 2001. *Pavement Management Guide*, PMG-1; American Association of State Highway and Transportation Officials.

ABAQUS, 1993. *Users Manual*, Version 5.2; Hibbitt, Karlsson, and Sorensen, Inc., Pawtucket, RI.

ADEDIMILA, A. S., and T. W. KENNEDY, 1976. "Repeated-Load Indirect Tensile Fatigue Characteristics of Asphalt Mixtures," *Transportation Research Record 595*, pp. 25–33; Transportation Research Board.

Downloaded From : www.EasyEngineering.net

Downloaded From : www.EasyEngineering.net

AHLVIN, R. G., and H. H. ULERY, 1962. "Tabulated Values for Determining the Complete Pattern of Stresses, Strains and Deflections Beneath a Uniform Circular Load on a Homogeneous Half Space," *Bulletin 342*, pp. 1–13; Highway Research Board.

AI, 1973. *Full-Depth Asphalt Pavements for General Aviation Aircraft, IS–154*; Asphalt Institute.

AI, 1981a. *Thickness Design—Asphalt Pavements for Highways and Streets*, Manual Series No. 1; Asphalt Institute.

AI, 1981b. *Asphalt Pavement Thickness Design*, Information Series No. 181; Asphalt Institute.

AI, 1982. *Research and Development of The Asphalt Institute's Thickness Design Manual (MS-1)*, 9th ed., *Research Report 82-2*; Asphalt Institute.

AI, 1983. *Asphalt Overlays for Highway and Street Rehabilitation*, Manual Series No. 17; Asphalt Institute.

AI, 1984. *Drainage of Asphalt Pavement Structures*, Manual Series No. 15; Asphalt Institute.

AI, 1987. *Thickness Design, Asphalt Pavements for Air Carrier Airports*, Manual Series No. 11; Asphalt Institute.

AI, 1989. *The Asphalt Handbook*, Manual Series No. 4; Asphalt Institute.

AI, 1991. *Thickness Design-Asphalt Pavements for Highways & Streets*, Manual Series No. 1; Asphalt Institute.

AI, 1996. *Superpave Mix Design*, Superpave Series No. 2 (SP-2); Asphalt Institute.

AI, 1997. *Superpave Mix Design*, Superpave Series No. 2 (SP-2); Asphalt Institute.

AI, 1998. *Superpave: Performance Graded Asphalt, Binder Specification and Testing*, Superpave Series No. 1 (SP-1), 2nd edition; Asphalt Institute.

AI, 2001. *Superpave Mix Design*, Superpave Series No. 2 (SP-2), 3rd edition; Asphalt Institute.

AKRAM, T., T. SCULLION, and R. E. SMITH, 1994. *Comparing Laboratory and Backcalculated Layer Moduli on Instrumented Pavement Sections*, Special technical Publication 1198; ASTM, Philadelphia, Pa.

ALI, H. A., and S. D. TAYABJI, 2000. "Using Transverse Profile Data to Compute Plastic deformation Parameters for Asphalt Concrete pavements," *Transportation Research Record 1716*, pp. 89–97; Transportation Research Board.

ALLEN, J. J., 1973. *The Effect of Non-Constant Lateral Pressures on the Resilient Response of Granular Materials*, Ph. D. Dissertation; University of Illinois at Urbana–Champaign.

ALLEN, D. L., and R. C. DEEN, 1986. "A Computerized Analysis of Rutting Behavior of Flexible Pavement," *Transportation Research Record 1095*, pp. 1–10; Transportation Research Board.

AL-Omari, B., and M. I. DARTER, 1994. "Relationships between International Roughness Index and Present Serviceability Rating," *Transportation Research Record 1435*, pp. 130–136; Transportation Research Board.

AMERICAN CONCRETE INSTITUTE, 1956. "Structural Design Considerations for Pavement Joints," Report of ACI Committee 325, ACI Journal, July 1956.

ASTM, 1989a. *Annual Books of ASTM Standards, Concrete and Aggregates*, Vol. 04.02; American Society for Testing and Materials.

ASTM, 1989b. *Annual Books of ASTM Standards, Road and Paving Materials: Traveled Surface Characteristics*, Vol. 04.03; American Society for Testing and Materials.

BAKER, R. F., 1973. "New Jersey Composite Pavement Project," *Highway Research Record 434*, pp. 16–23; Highway Research Board.

BALL, C. G., and L. D. CHILDS, 1975. *Tests of Joints for Concrete Pavements*, Bulletin RD026.01P; Portland Cement Association.

BALLINGER, C. A., 1971. "Cumulative Fatigue Damage Characteristics of Plain Concrete," *Highway Research Record 370*, pp. 48–60; Highway Research Board.

BARBER, E. S., 1946. "Application of Triaxial Compression Test Results to the Calculation of Flexible Pavement Thickness," *Proceedings, Highway Research Board*, pp. 26–39.

Downloaded From : www.EasyEngineering.net

Downloaded From : www.EasyEngineering.net

BARBER, E. S., 1957. "Calculation of Maximum Pavement Temperatures from Weather Report," *Bulletin 168*, pp. 1–8; Highway Research Board.

BARBER, E. S., and C. L. SAWYER, 1952. "Highway Subdrainage," *Proceedings, Highway Research Board*, pp. 643–666.

BARKSDALE, R. G., 1971. "Compressive Stress Pulse Times in Flexible Pavements for Use in Dynamic Testing," *Highway Research Record 345*, pp. 32–44; Highway Research Board.

BARKSDALE, R. G., and R. G. HICKS, 1979. *Improved Pavement-Shoulder Joint Design*, NCHRP Report 202; Transportation Research Board.

BASSON, J. E. B., O. J. WIJNBERGER, and J. SKULTETY, 1981. *The Multidepth Deflectometer: A Multistage Sensor for the Measurement of Deflections and Permanent Deformations at Various Depths in Road Pavements*, Technical Report RP/3/81; Institute of Transportation and Road Research, Pretoria, South Africa.

BAY, J. A., K. H. STOKOE II, M. T. MCNERNEY, B. F. MCCULLOUGH, and D. R. ALEXANDER, 1999. "Profiling Flexible Highway Pavements Continuously with the Rolling Dynamic Deflectometer and at Discrete Points with Falling Weight Deflectometer," *Transportation Research Record 1655*, pp. 74–85; Transportation Research Board.

BAY, J. A., K. H. STOKOE II, M. T. MCNERNEY, S. SORALUMP, D. A. VAN VLEET, and D. K. ROZYCKI, 2000. "Evaluating Runway Pavements at Seattle–Tacoma International Airport, Continuous Deflection Profiles Measured with the Rolling Dynamic Deflectometer," *Transportation Research Record 1716*, pp. 1–9; Transportation Research Board.

BENJAMIN, J. R., and C. A. CORNELL, 1970. *Probability, Statistics and Decision for Civil Engineers*; McGraw-Hill, New York.

BETRAM, G. E., 1940. *An Experimental Investigation of Protective Filters*, Publication No. 267; Graduate School of Engineering, Harvard University.

BLACK, W. P. M., and D. CRONEY, 1957. "Pore Water Pressure and Moisture Content Studies under Experimental Pavements," *Proceedings, 4th International Conference on Soil Mechanics and Foundation Engineering*, Vol. 2, pp. 94–103.

BLANKENSHIP, P. B., K. C. MAHBOUB, and G. A. HUBER, 1994. "Rational Method for Laboratory Compaction of Hot-Mix Asphalt," *Transportation Research Record 1454*, pp. 144–153; Transportation Research Board.

BONNAURE, F., G. GEST, A. GRAVOIS, and P. UGE, 1977. "A New Method of Predicting the Stiffness of Asphalt Paving Mixtures," *Proceedings, Association of Asphalt Paving Technologists*, Vol. 46, pp. 64–100.

BONNAURE, F., A. GRAVOIS, and J. UDRON, 1980. "A New Method for Predicting the Fatigue Life of Bituminous Mixes," *Proceedings, Association of Asphalt Paving Technologists*, Vol. 49, pp. 499–524.

BOUSSINESQ, J., 1885. *Application des Potentiels a l'etude de l'equilibre et du Mouvement des Solids Elastiques*; Gauthier-Villars, Paris.

BOYCE, J. R., S. F. BROWN, and P. S. PELL, 1976. "The Resilient Behavior of a Granular Material Under Repeated Loading," *Proceedings*; Australian Road Research Board.

BOYD, W. K., and C. R. FOSTER, 1950. "Design Curves for Very Heavy Multiple-Wheel Assemblies, Development of CBR Flexible Pavement Design Methods for Airfield, A Symposium," *Transactions, ASCE*, Vol. 115, pp. 534–546.

BRADBURY, R. D., 1938. *Reinforced Concrete Pavements*; Wire Reinforcement Institute, Washington, DC.

BRADEMEYER, B., 1988. *VESYS Modification*, Final Report to FHWA, Work Order DTFH61-87-P-00441.

BROWN, E. R., J. E. HADDOCK, R. B. MALLICK, and T. A. LYNN, 1997. "Development of Mixture Design Procedure for Stone Matrix Asphalt (SMA)," *Proceedings, Association of Asphalt Paving Technologists*, Vol. 66, pp. 1–30.

Downloaded From : www.EasyEngineering.net

Downloaded From : www.EasyEngineering.net

BROWN, S. F., 1973. "Determination of Young's Modulus for Bituminous Materials in Pavement Design," *Highway Research Record 431*, pp. 38–49; Highway Research Board.

BROWN, S. F., P. S. PELL, and A. F. STOCK, 1977. "The Application of Simplified, Fundamental Design Procedures for Flexible Pavement," *Proceedings, 4th International Conference on the Structural Design of Asphalt Pavements*, Vol. 1, pp. 321–341.

BRUNNER, R. J., 1975. "Prestressed Pavement Demonstration Project," *Transportation Research Record 535*, pp. 62–72; Transportation Research Board.

BURMISTER, D. M., 1943. "The Theory of Stresses and Displacements in Layered Systems and Applications to the Design of Airport Runways," *Proceedings, Highway Research Board*, Vol. 23, pp. 126–144.

BURMISTER, D. M., 1945. "The General Theory of Stresses and Displacements in Layered Soil Systems," *Journal of Applied Physics*, Vol. 16, pp. 84–94, 126–127, 296–302.

BURMISTER, D. M., 1958. "Evaluation of Pavement Systems of the WASHO Road Test by Layered Systems Method," *Bulletin 177*, pp. 26–54; Highway Research Board.

BUSH, A. J., 1980. *Nondestructive Testing of Light Aircraft Pavements, Phase II, Development of the Nondestructive Evaluation Methodology*, Report No. FAA-RD-80-9-II; Federal Aviation Administration.

BUSH, A. J., and D. R. ALEXANDER, 1985. "Pavement Evaluation Using Deflection Basin Measurements and Layered Theory," *Transportation Research Record 1022*, pp. 16–28; Transportation Research Board.

CALIFORNIA DEPARTMENT OF PUBLIC WORKS, 1972. *Highway Design Manual.*

CALIFORNIA DEPARTMENT OF TRANSPORTATION, 1979. *Asphalt Concrete Overlay Design Manual.*

CAREY, W. N., and P. E. IRICK, 1960. *The Pavement Serviceability Performance Concept*, Bulletin 250; Highway Research Board.

CARPENTER, S. H., M. I. DARTER, and B. J. DEMPSEY, 1981. *A Pavement Moisture Accelerated Distress Identification System, User's Manual*, Vol. 2, Report No. FHWA/RD-81/080; Federal Highway Administration.

CASAGRANDE, A., and W. L. SHANNON, 1952. "Base Course Drainage for Airport Pavements," *Transactions, American Society of Civil Engineering*, pp. 792–814.

CEDERGREN, H. R., 1974. *Drainage of Highway and Airfield Pavements*; Wiley, New York.

CEDERGREN, H. R., 1977. *Seepage, Drainage, and Flow Nets*; Wiley, New York.

CEDERGREN, H. R., 1988. "Why All Important Pavements Should Be Well Drained," *Transportation Research Record 1188*, pp. 56–62; Transportation Research Board.

CEDERGREN, H. R., J. A. ARMAN, and K. H. O'BRIEN, 1972. *Guidelines for the Design of Subsurface Drainage Systems for Highway Pavement Structural Sections*, Report No. FHWA-RD-72-30; Federal Highway Administration.

CEDERGREN, H. R., J. A. ARMAN, and K. H. O'BRIEN, 1973. *Development of Guidelines for the Design of Subsurface Drainage Systems for Highway Pavement Structural Sections*, Report No. FHWA-RD-73-14; Federal Highway Administration.

CHEN, D. H., Z. MUSHARRAF, J. LAGUROS, and ALAN SOLTANI, 1995. "Assessment of Computer Programs for Analysis of Flexible Pavement Structure," *Transportation Research Record 1482*, pp. 123–133; Transportation Research Board.

CHEUNG, Y. K., and O. C. ZIENKIEWICZ, 1965. "Plates and Tanks on Elastic Foundations—An Application of Finite Element Method," *International Journal of Solids and Structures*, Vol. 1, pp. 451–461.

CHOU, Y. J., J. UZAN, and R. L. LYTTON, 1989. "Backcalculation of Layer Moduli from Nondestructive Pavement Deflection Data Using the Expert System Approach," *STP 1026*, pp. 341–354; American Society for Testing and Materials.

CHOU, Y. T., 1981. *Structural Analysis Computer Programs for Rigid Multicomponent Pavement Structures with Discontinuities—WESLIQID and WESLAYER*, Technical Report GL-81-6, Reports 1, 2, and 3; U.S. Army Engineer Waterways Experiment Station.

Downloaded From : www.EasyEngineering.net

Downloaded From : www.EasyEngineering.net

CHOU, Y. T., 1987. *Probabilistic and Reliability Design Procedures for Flexible Airfield Pavements—Elastic Layered Method*, Technical Report GL-82-24; U.S. Army Engineer Waterways Experiment Station.

CHOU, Y. T., and Y. H. HUANG, 1979. "A Computer Program for Slabs with Discontinuities," *Proceedings, International Air Transportation Conference*, Vol. 1, pp. 121–136.

CHOU, Y. T., and Y. H. HUANG, 1981. "A Computer Program for Slabs with Discontinuities on Layered Elastic Solids," *Proceedings, 2nd International Conference on Concrete Pavement Design*, pp. 78–85; Purdue University.

CHOU, Y. T., and Y. H. HUANG, 1982. "A Finite Element Method for Concrete Pavements," *Proceedings, International Conference on Finite Element Methods*, Shanghai, China, pp. 348–353.

CHOU, Y. T., and H. G. LAREW, 1969. "Stresses and Displacements in Viscoelastic Pavement Systems Under a Moving Load," *Highway Research Record 282*, pp. 25–40; Highway Research Board.

CHRISTISON, J. T., D. W. MURRAY, and K. O. ANDERSON, 1972. "Stress Prediction and Low Temperature Fracture Susceptibility of Asphalt Concrete Pavements," *Proceedings, Association of Asphalt Paving Technologists*, Vol. 41, pp. 494–523.

CHUA, K. M., and R. L. LYTTON, 1985. "Load Rating of Light Pavement Structures," *Transportation Research Record 1043*, pp. 89–102; Transportation Research Board.

CLAROS, G., W. R. HUDSON, and K. H. STOKOE, 1990. "Modifications to Resilient Modulus Testing Procedure and Use of Synthetic Samples for Equipment Calibration," *Transportation Research Record 1278*, pp. 51–62; Transportation Research Board.

CLAUSSEN, A. I. M., J. M. EDWARDS, P. SOMMER, and P. UGE, 1977. "Asphalt Pavement Design—The Shell Method," *Proceedings, 4th International Conference on the Structural Design of Asphalt Pavements*, Vol. 1, pp. 39–74.

CLEMMER, H. F., 1923. "Fatigue of Concrete," *Proceedings, ASTM*, Vol. 22, II, pp. 408–419.

COLLEY B. E., C. G. BALL, and P. ARRIYAVAT, 1978. "Evaluation of Concrete Pavements with Tied Shoulders or Widened Lanes," *Transportation Research Record 666*, pp. 39–45; Transportation Research Board.

COMINSKY, R. J., G. A. HUBER, and R. M. ANDERSON, 1994. *The Superpave Mix Design Manual for New Construction and Overlays,* SHRP Report A-407; National Research Council, Washington, DC.

CRAUS, J., R. YUCE, and C. L. MONISMITH, 1984. "Fatigue Behavior of Thin Asphalt Concrete Layers in Flexible Pavement Structures," *Proceedings, Association of Asphalt Paving Technologists*, Vol. 53, pp. 559–582.

DALEIDEN, J. F., B. M. KILLINGSWORTH, A. L. SIMPSON, and R. A. ZAMORA, 1994. "Analysis of Procedures for Establishing In Situ Subgrade Moduli," *Transportation Research Record 1462*, pp. 102–107; Transportation Research Board.

DARTER, M. I., 1976. "Application of Statistical Methods to the Design of Pavement Systems," Transportation Research Record 575, pp. 39–55; Transportation Research Board.

DARTER, M. I., and E. J. BARENBERG, 1977. *Design of Zero-Maintenance Plain Jointed Concrete Pavement*, Report No. FHWA-RD-77-111, Vol. 1; Federal Highway Administration.

DARTER, M. I., J. M. BECKER, M. B. SNYDER, and R. E. SMITH, 1985. *Portland Cement Concrete Pavement Evaluation System (COPES)*, NCHRP Report 277; Transportation Research Board.

DARTER, M. I., R. P. ELLIOTT, and K. T. HALL, 1991a. *Revision of AASHTO Pavement Overlay Design Procedures*, Appendix: Overlay Design Examples, NCHRP Project 20-7/task 39, Final Report.

DARTER, M. I., R. P. ELLIOTT, and K. T. HALL, 1991b. *Revision of AASHTO Pavement Overlay Design Procedures*, Appendix: Documentation of Design Procedures, NCHRP Project 20-7/task 39, Final Report.

DARTER, M. I., W. R. HUDSON, and J. L. BROWN, 1973a. "Statistical Variations of Flexible Pavement Properties and Their Consideration in Design," *Proceedings, Association of Asphalt Paving Technologists*, Vol. 42, pp. 589–613.

Downloaded From : www.EasyEngineering.net

Downloaded From : www.EasyEngineering.net

DARTER, M. I., B. F. MCCULLOUGH, and J. L. BROWN, 1973b. "Reliability Concepts Applied to the Texas Flexible Pavement System," *Highway Research Record 407*, pp. 180–190; Highway Research Board.

DEACON, J. A., 1965. *Fatigue of Asphalt Concrete*, Doctoral Dissertation; University of California, Berkeley.

DEACON, J. A., 1969. "Load Equivalency in Flexible Pavements," *Proceedings, Association of Asphalt Paving Technologists*, Vol. 38, pp. 465–491.

DE BEER, M., E. HORAK, and A. T. VISSER, 1989. "The Multidepth Deflectometer (MDD) System for Determining the Effective Elastic Moduli of Pavement Layers," *STP 1026*, pp. 70–89; American Society for Testing and Materials.

DE JONG, D. L., M. G. F. PEATZ, and A. R. KORSWAGEN, 1973. *Computer Program Bisar Layered Systems Under Normal and Tangential Loads*, External Report AMSR.0006.73; Konin Klijke Shell-Laboratorium, Amsterdam,

DELAWARE DEPARTMENT OF TRANSPORTATION, FEDERAL HIGHWAY ADMINISTRATION, 2000. *Pavement Management: A Guide for Elected Officials*.

DEMPSEY, B. J., 1983. "Laboratory and Field Studies of Channeling and Pumping in Pavement Systems," Paper presented at PIARC Seminar; Paris, France.

DEMPSEY, B. J., M. I. DARTER, and S. H. CARPENTER, 1982. *Improving Subdrainage and Shoulders of Existing Pavements, State of the Art*, Report No. FHWA-RD-81-077; Federal Highway Administration.

DEMPSEY, B. J., W. A. HERLACHE, and A. J. PATEL, 1986. "Climatic-Materials-Structural Pavement Analysis Program," *Transportation Research Record 1095*, pp. 111–123; Transportation Research Board.

DEMPSEY, B. J., and M. R. THOMPSON, 1970. "A Heat Transfer Model for Evaluating Frost Action and Temperature Related Effects in Multilayered Pavement Systems," *Highway Research Record 342*, pp. 39–56; Highway Research Board.

DORMON, G. M., and C. T. METCALF, 1965. "Design Curves for Flexible Pavements Based on Layered System Theory," *Highway Research Record 71*, pp. 69–84; Highway Research Board.

DUNCAN, J. M., C. L. MONISMITH, and E. L. WILSON, 1968. "Finite Element Analysis of Pavements," *Highway Research Record 228*, pp. 18–33; Highway Research Board.

ELLIOTT, J. F., and F. MOAVENZADEH, 1971. "Analysis of Stresses and Displacements in Three-Layer Viscoelastic Systems," *Highway Research Record 345*, pp. 45–57; Highway Research Board.

ELLIOTT, R. P., 1989. "An Examination of the AASHTO Remaining Life Factor," *Transportation Research Record 1215*, pp. 53–59; Transportation Research Board.

EMERY, D. K., 1975. "A Preliminary Report on the Paved Shoulder Encroachment and Transverse Lane Displacement for Design Trucks on Rural Freeways," *Proceedings, ASCE Specialty Conference on Pavement Design for Practicing Engineers*, pp. 6:10–6:15.

EPPS, J. A., and C. L. MONISMITH, 1986. "Equipment for Obtaining Pavement Condition and Traffic Loading Data," *NCHRP Synthesis of Highway Practice No. 126*; Transportation Research Board.

ERES Consultant, Inc., 1987. *Pavement Design, Principles and Practices, A Training Course Participant Notebook*; Federal Highway Administration.

EXSYS, Inc., 1985. *EXSYS Expert System Development Package, User's Manual*; Albuquerque, NM.

FAA, 1988. *Airport Pavement Design and Evaluation*, Consolidated Reprint, AC 150/5320-6C; Federal Aviation Administration.

FERNANDO, E. G., R. S. WALKER, and R. L. LYTTON, 1990. "Evaluation of the Siometer as a Device for Measurement of Pavement Profiles," *Transportation Research Record 1260*, pp. 112–124; Transportation Research Board.

FHWA, 1978. *Predictive Design Procedures, VESYS Users Manual*, Report No. FHWA-RD-77-154; Federal Highway Administration.

Downloaded From : www.EasyEngineering.net

Downloaded From : www.EasyEngineering.net

FHWA, 1980. *Skid Accident Reduction Program*, Technical Advisory T-5040.17; Federal Highway Administration.

FHWA, 1982. *Pavement Shoulders*, Technical Advisory T5040.18; Federal Highway Administration.

FHWA, 1986. *Longitudinal Edge Drains in Rigid Pavement Systems*, Report No. FHWA-TS-86-208; Federal Highway Administration.

FHWA, 1987a. *Reference Manual for the UMTRI/FHWA Road Profiling (PRORUT) System*, Report FHWA/RD-87/042; Federal Highway Administration.

FHWA, 1987b. *Highway Performance Monitoring System Field Manual for the Continuing Analytical and Statistical Database, Appendix J*, FHWA Order M5600.1A, OMB No. 2125–0028; Federal Highway Administration.

FHWA, 1987c. *Crack and Seat Performance*, Review Report, Demonstration Projects Division and Pavement Division; Federal Highway Administration.

FHWA, 1989. *Geotextile Engineering Manual, Course Text*, Publication No. FHWA-HI-89-050; Federal Highway Administration.

FHWA, 1995. "Pavement and Road Surface Management for Local Agencies," *Participant's Manual*; Federal Highway Administration.

FHWA, 1998. *Life-Cycle Cost Analysis in Pavement Design*, Pavement Division Interim Technical Bulletin; Federal Highway Administration.

FHWA, 2001a. *Highway Statistics*; Federal Highway Administration.

FHWA, 2001b. *Traffic Monitoring Guide*; Office of Highway Policy Information, Federal Highway Administration.

FINN, F. N., and C. L. MONISMITH, 1984. *Asphalt Overlay Design Procedures*, Synthesis of Highway Practice 116; National Cooperative Highway Research Program.

FINN, F. N., C. L. MONISMITH, and N. J. MARKEVICH, 1983. "Pavement Performance and Asphalt Concrete Mix Design, *Proceedings, Association of Asphalt Paving Technologists*, Vol. 52, pp. 121–144.

FINN, F., C. L. SARAF, R. KULKARNI, K. NAIR, W. SMITH, and A. ABDULLAH, 1986. *Development of Pavement Structural Subsystems*, NCHRP Report 291; Transportation Research Board.

FITCH, M., 1996. "Bellefontaine, Ohio: Home of America's Oldest Concrete Pavement," Summer 1996, pp. 4–6; Ohio T2 Center, Ohio State University.

FOSTER, C. R., and R. G. AHLVIN, 1954. "Stresses and Deflections Induced by a Uniform Circular Load," *Proceedings, Highway Research Board*, Vol. 33, pp. 467–470.

FOSTER, C. R., and R. G. AHLVIN, 1958. "Development of Multiple-Wheel CBR Design Criteria," *Journal of the Soil Mechanics and Foundations Division*, ASCE, Vol. 84, No. SM2, May, pp. 1647–1 to 1647–12.

FRANCHEN, L., and J. VERSTRAETEN, 1974. "Methods for Predicting Modulus and Fatigue Laws of Bituminous Mixes under Repeated Bending," *Transportation Research Record 515*, pp. 114–123; Transportation Research Board.

FREEME, C. R., and C. P. MARAIS, 1973. "Thin Bituminous Surfaces: Their Fatigue Behavior and Prediction," *Special Report 140*, pp. 158–179; Highway Research Board.

FRIBERG, B. F., 1940. "Design of Dowels in Transverse Joints of Concrete Pavements," *Transactions, ASCE*, Vol. 105, pp. 1076–1095.

GAGE, R. B., 1932. "Discussion on Joints in Concrete Pavements," *Proceedings, Highway Research Board*, Part I, pp. 137–141.

GERRARD, C. M., and W. J. HARRISON, 1970. "A Theoretical Comparison of the Effects of Dual-Tandem and Dual-Wheel Assemblies on Pavements," *Proceedings, Fifth Conference; Australian Road Research Board*.

GOLDBECK, A. T., 1919. "Thickness of Concrete Slabs," *Public Roads*, pp. 34–38.

Downloaded From : www.EasyEngineering.net

Downloaded From : www.EasyEngineering.net

GOMEZ-ACHECAR, M., and M. R. THOMPSON, 1986. "ILLI-PAVE-Based Response Algorithms for Full-Depth Asphalt Concrete Flexible Pavements," *Transportation Research Record 1095*, pp. 11–18; Transportation Research Board.

GROENENDIJK, J., C. H. VOGELZANG, A. MARIDI, A. A. A. MOLENAAR, and L. J. M. DOHMEN, 1997. "Rutting Development in Linear Tracking Test Pavements to Evaluate Shell Subgrade Strain Criterion," *Transportation Research Record 1570*, pp. 23–29; Transportation Research Board.

GULEN, S., R. WOODS, J. WEAVER, and V. L. ANDERSON, 1994. "Correlation of Present Serviceability Ratings with International Roughness Index," *Transportation Research Record 1435*, pp. 27–37; Transportation Research Board.

HAAS, R., W. R. HUDSON, and J. ZANIEWSKI, 1994. *Modern Pavement Management*; Krieger Publishing Company, Malabar, FL.

HAJEK, J. J., and R. C. G. HAAS, 1972. "Predicting Low-Temperature Cracking Frequency of Asphalt Concrete Pavements," *Transportation Research Record 407*, pp. 39–54; Transportation Research Board.

HALIBURTON, T. A., and J. D. LAWMASTER, 1981. *Training Manual on Use of Engineering Fabrics*, Contract No. DTFH 61-80-C-0094; Federal Highway Administration.

HALL, K. T., C. E. C. MUNOZ, 1999. "Estimation of Present Serviceability Index from International Roughness Index," *Transportation Research Record 1655*, pp. 93–99; Transportation Research Board.

HALL, K. T., M. I. DARTER, and C. M. KUO, 1995. "Improved Methods for Selection of k Value for Concrete Pavement Design," Transportation Research Record 1505, pp. 128–136; Transportation Research Board.

HALL, K. T., J. M. CONNOR, M. I. DARTER, and S. H. CARPENTER, 1989. *Rehabilitation of Concrete Pavements*, Vol. 3, *Concrete Pavement Evaluation and Rehabilitation System*, Report No. FHWA-RD-88-073; Federal Highway Administration.

HANNA, A. M., P. J. NUSSBAUM, P. ARRIYAVAT, J. J. TSENG, and B. F. FRIBERG, 1976. *Technological Review of Prestressed Pavements*, Report No. FHWA-RD-77-8; Federal Highway Administration.

HARICHANDRAN, R. S., N. BUCH, and G.Y. BALADI, 2001. "Flexible Pavement Design in Michigan: Transition from Empirical to Mechanistic Methods," Transportation Research Record 1778, pp. 100–106; Transportation Research Board.

HARICHANDRAN, R. S., G. Y. BALADI, and M. YEH, 1989. *Development of a Computer Program for Design of Pavement Systems Consisting of Bound and Unbound Materials*; Department of Civil and Environmental Engineering, Michigan State University.

HARIK, I. E., P. JIANPING, H. SOUTHGATE, and D. ALLEN, 1994. "Temperature effects on Rigid Pavements," Journal of Transportation Engineering, Vol. 120, No. 1, pp. 127–143; ASCE.

HEALEY, K. A., and R. P. LONG, 1972. "Prefabricated Filter Fin for Subsurface Drains," *Journal of Irrigation and Drainage Division, ASCE*, Vol. IR4, pp. 543–552.

HEINRICHS, K. W., M. J. LIU, M. I. DARTER, S. H. CARPENTER, and A. M. IOANNIDES, 1989. *Rigid Pavement Analysis and Design*, Report No. FHWA-RD-88-068; Federal Highway Administration.

HENRY, J. J., J. C. WAMBOLD, and H. XUE, 1984. *Evaluation of Pavement Texture*, Report No. FHWA-RD-84-016; Federal Highway Administration.

HEUKELOM, W., 1966. "Observations on the Rheology and Fracture of Bitumens and Asphalt Mixes," *Proceedings, Association of Asphalt Paving Technologists*, Vol. 35, pp. 358–399.

HEUKELOM, W., and A. J. G. KLOMP, 1962, "Dynamic Testing as a Means of Controlling Pavements During and After Construction," *Proceedings, (1st) International Conference on the Structural Design of Asphalt Pavements*, pp. 667–685.

HICKS, R. G., 1970. *Factors Influencing the Resilient Properties of Granular Materials*, Ph. D. Dissertation; University of California, Berkeley.

HICKS, R. G., and F. N. FINN, 1970. "Analysis of Results from the Dynamic Measurements Program on the San Diego Test Road," *Proceedings, Association of Asphalt Paving Technologists*, Vol. 39, pp. 153–185.

Downloaded From : www.EasyEngineering.net

Downloaded From : www.EasyEngineering.net

HOFFMAN, M. S., and M. R. THOMPSON, 1982. "Comparative Study of Selected Nondestructive Testing Devices," *Transportation Research Record 852*, pp. 32–41; Transportation Research Board.

HOGENTOGLER, C. A., and C. TERZAGHI, 1929. "Interrelationship of Load, Road and Subgrade," *Public Roads*, May, pp. 37–64.

HRB, 1945. "Report of Commitee on Classification of Materials for Subgrades and Granular Type Roads," *Proceedings, Highway Research Board*, Vol. 25, pp. 376–384.

HRB, 1952. *Final Report on Road Test One MD*, Special Report 4; Highway Research Board.

HRB, 1955. *The WASHO Road Test*, Part 2; *Test Data Analysis and Findings*, Special Report 22; Highway Research Board.

HRB, 1962. *The AASHO Road Test*, Report 5; *Pavement Research*; Report 6; *Special Studies*; and Report 7: *Summary Report*, Special Reports 61E, 61F, and 61G; Highway Research Board.

HUANG, Y. H., 1967. "Stresses and Displacements in Viscoelastic Layered Systems Under Circular Loaded Areas," *Proceedings, 2nd International Conference on the Structural Design of Asphalt Pavements*, pp. 225–244.

HUANG, Y. H., 1968a. "Stresses and Displacements in Nonlinear Soil Media," *Journal of the Soil Mechanics and Foundation Division, ASCE*, Vol. 94, No. SM1, pp. 1–19.

HUANG, Y. H., 1968b. "Chart for Determining Equivalent Single-Wheel Loads," *Journal of the Highway Division, ASCE*, Vol. 94, No. HW2, pp. 115–128.

HUANG, Y. H., 1969a. "Finite Element Analysis of Nonlinear Soil Media," *Proceedings, Symposium on Application of Finite Element Methods in Civil Engineering*, pp. 663–690; Vanderbilt University, Nashville, TN.

HUANG, Y. H., 1969b. "Influence Charts for Two-Layer Elastic Foundations," *Journal of the Soil Mechanics and Foundation Division, ASCE*, Vol. 95, No. SM2, March, pp. 709–713.

HUANG, Y. H., 1969c. "Computation of Equivalent Single-Wheel Loads Using Layered Theory," *Highway Research Record 291*, pp. 144–155; Highway Research Board.

HUANG, Y. H., 1971. "Deflection and Curvature as Criteria for Flexible Pavement Design and Evaluation," *Highway Research Record 345*, pp. 1–11; Highway Research Board.

HUANG, Y. H., 1972. "Strain and Curvature as Factors for Predicting Pavement Fatigue," *Proceedings, 3rd International Conference on the Structural Design of Asphalt Pavements*, Vol. 1, pp. 622–628.

HUANG, Y. H., 1973a. "Critical Tensile Strain in Asphalt Pavements," *Transportation Engineering Journal, ASCE*, Vol. 99, No. TE3, pp. 553–569.

HUANG, Y. H., 1973b. "Stresses and Strains in Viscoelastic Multilayer Systems Subjected to Moving Loads," *Highway Research Record 457*, pp. 60–71; Highway Research Board.

HUANG, Y. H., 1974a. "Finite Element Analysis of Slabs on Elastic Solids," *Transportation Engineering Journal, ASCE*, Vol. 100, No. TE2, pp. 403–416.

HUANG, Y. H., 1974b. "Analysis of Symmetrically Loaded Slabs on Elastic Solid," *Transportation Engineering Journal, ASCE*, Vol. 100, No. TE2, pp. 537–541.

HUANG, Y. H., 1985. "A Computer Package for Structural Analysis of Concrete Pavements," *Proceedings, 3rd International Conference on Concrete Pavement Design and Rehabilitation*, pp. 295–307; Purdue University.

HUANG, Y. H., and Y. T. CHOU, 1978. "Discussion on Finite Element Analysis of Jointed or Cracked Pavements," *Transportation Research Record 671*, pp. 17–18; Transportation Research Board.

HUANG, Y. H., and X. DENG, 1982. "A Simplified Method for Analyzing Concrete Pavements Composed of Jointed Slabs," *Proceedings, International Conference on Finite Element Methods*, Shanghai, China, pp. 376–381.

HUANG, Y. H., C. LIN, X. DENG, and J. G. ROSE, 1984b. *KENTRACK: A Computer Program for Hot-Mix Asphalt and Conventional Ballast Railway Trackbeds*, Report No. RR-84-1; The Asphalt Institute, College Park, Maryland.

HUANG, Y. H., C. LIN, X. DENG, and J. G. ROSE, 1986b. *KENTRACK, A Finite Element Computer Program for the Analysis of Railroad Tracks, User's Manual*; Department of Civil Engineering, University of Kentucky, Lexington, KY.

Downloaded From : www.EasyEngineering.net

Downloaded From : www.EasyEngineering.net

HUANG, Y. H., C. LIN, and J. G. ROSE, 1984a. "Asphalt Pavement Design: Highway versus Railroad," *Journal of Transportation Engineering, ASCE*, Vol. 110, pp. 276–282.

HUANG, Y. H., J. G. ROSE, and C. J. KHOURY, 1986a. "Hot-Mix Asphalt Railroad Trackbeds," *Transportation Research Record 1095*, pp. 102–110, Transportation Research Board.

HUANG, Y. H., J. G. ROSE, and C. J. KHOURY, 1987. "Thickness Design for Hot-Mix Asphalt Railroad Trackbeds," *Proceedings, Association of Asphalt Paving Technologists*, Vol. 56, pp. 427–451.

HUANG, Y. H., J. G. ROSE, and C. LIN, 1985. "Structural Design of Hot Mix Asphalt Underlayments for Railroad Trackbeds," *Proceedings, Association of Asphalt Paving Technologists*, Vol. 54, pp. 502–528.

HUANG, Y. H., and G. W. SHARPE, 1989. "Thickness Design of Concrete Pavements by Probabilistic Method," *Proceedings, 4th International Conference on Concrete Pavement Design and Rehabilitation*, pp. 251–265; Purdue University.

HUANG, Y. H., and S. T. WANG, 1973. "Finite Element Analysis of Concrete Slabs and Its Implications for Rigid Pavement Design," *Highway Research Record 466*, pp. 55–69; Highway Research Board.

HUANG, Y. H., and S. T. WANG, 1974. "Finite-Element Analysis of Rigid Pavements with Partial Subgrade Contact," *Transportation Research Record 485*, pp. 39–54; Transportation Research Board.

HUDSON, W. R., and H. MATLOCK, 1966. "Analysis of Discontinuous Orthotropic Pavement Slabs Subjected to Combined Loads," Highway Research Record 131, pp. 1–48; Highway Research Board.

HWANG, D., and M. W. WITCZAK, 1979. *Program DAMA (Chevron), User's Manual*; Department of Civil Engineering, University of Maryland.

IOANNIDES, A. M., 1990. "Dimensional Analysis in NDT Rigid Pavement Evaluation," *Journal of Transportation Engineering*, Vol. 116, No. 1, pp. 23–36.

IOANNIDES, A. M. and M. I. HAMMONS, 1996. "Westergaard-Type Solution for Edge Load Transfer Problem," *Transportation Research Record 1525*, pp. 28–34; Transportation Research Board.

IOANNIDES, A.M. and L. KHAZANOVICH, 1993. "Load Equivalency Concepts: A Mechanistic Reappraisal," *Transportation Research Record 1388*, pp. 42–50; Transportation Research Board.

IOANNIDES, A. M., E. J. BARENBERG, and J. A. LARY, 1989. "Interpretation of Falling Weight Deflectometer Results Using Principles of Dimensional Analysis," *Proceedings, 4th International Conference on Concrete Pavement Design and Rehabilitation*, pp. 231–247; Purdue University.

IOANNIDES, A. M., M. R. THOMPSON, and E. J. BARENBERG, 1985. "Westergaard Solutions Reconsidered," *Transportation Research Record 1043*, pp. 13–23; Transportation Research Board.

IRICK, P., W. R. HUDSON, and B. F. MCCULLOUGH, 1987. "Application of Reliability Concepts to Pavement Design," *Proceedings, 6th International Conference on the Structural Design of Asphalt Pavements*, Vol. 1, pp. 163–179.

IRWIN, L. H., and B. M. GALLAWAY, 1974. "Influence of Laboratory Test Method on Fatigue Test Results for Asphalt Concrete," *STP 561*, pp. 12–46; American Society for Testing and Materials.

JANOFF, M. S., 1988. *Pavement Roughness and Rideability Field Evaluation*, NCHRP Report 308; Transportation Research Board.

JANOFF, M. S., J. B. NICK, and P. S. DAVIT, 1985. *Pavement Roughness and Rideability*, NCHRP Report 275; Transportation Research Board.

JIANG, Y., M.I. DARTER, and E. OWUSU-ANTWI, 1996. "Analysis of Current State Rigid Pavement Design Practices in the United States," *Transportation Research Record 1525*, pp. 72–82; Transportation Research Board.

JIMENEZ, R. A., 1972. "Fatigue Testing of Asphaltic Concrete Slabs," *STP 508*, pp. 3–17; American Society for Testing and Materials.

Downloaded From : www.EasyEngineering.net

Downloaded From : www.EasyEngineering.net

JIMENEZ, R. A., and B. M. GALLAWAY, 1962. "Behavior of Asphalt Concrete Diaphragms to Repetitive Loadings," *Proceedings, (1st) International Conference on the Structural Design of Asphalt Pavements*, pp. 339–344.

JOHNSON, T. C., R. L. BERG, E. J. CHAMBERLAIN, and D. M. COLE, 1986. *Frost Action Predictive Techniques for Roads and Airfields*, Report DOT/FAA/PM-85-23; Federal Aviation Administration.

JONES, A., 1962. "Tables of Stresses in Three-Layer Elastic Systems," *Bulletin 342*, pp. 176–214. Highway Research Board.

JORDAHL, P. R., and J. B. RAUHUT, 1983. *Flexible Pavement Model VESYS IV-B*, Report prepared for Federal Highway Administration under Contract DTFH61-C-00175.

KALCHEFF, I. V., and R. G. HICKS, 1973. "A Test Program for Determining the Resilient Properties of Granular Materials," *Journal of Testing and Evaluation, ASTM*, Vol. 1, No. 6, pp. 472–479.

KALLAS, B. F., 1970. "Dynamic Modulus of Asphalt Concrete in Tension and Tension-Compression," *Proceedings, Association of Asphalt Paving Technologists*, Vol. 39, pp. 1–20.

KALLAS, B. F., and V. P. PUZINAUSKAS, 1972. "Flexure Fatigue Tests on Asphalt Paving Mixtures," *STP 508*, pp. 47–65; American Society for Testing and Materials.

KANSAS STATE HIGHWAY COMMISSION, 1947. *Design of Flexible Pavement Using the Triaxial Compression Test*, Bulletin 8; Highway Research Board.

KENIS, W. J., 1977. "Predictive Design Procedures, a Design Method for Flexible Pavements Using the VESYS Structural Subsystem," *Proceedings, 4th International Conference on the Structural Design of Asphalt Pavements*, Vol. 1, pp. 101–147.

KENIS, W., and W. WANG, 1997. "Calibrating Mechanistic Flexible Pavement Rutting Models from Full Scale Accelerated Tests," *Proceedings, 8th International Conference on Asphalt Pavement*, pp. 663–672; University of Washington.

KENNEDY, C. K., and N. W. LISTER, 1978. *Prediction of Pavement Performance and the Design of Overlay*, TRRL Report No. 833; Transport and Road Research Laboratory, Great Britain.

KERKHOVEN, R. E., and G. M. DORMON, 1953. *Some Considerations on the California Bearing Ratio Method for the Design of Flexible Pavement*, Shell Bitumen Monograph No. 1.

KESLER, C. E., 1953. "Effect of Speed of Testing on Flexural Strength of Plain Concrete," *Proceedings, Highway Research Board*, Vol. 32, pp. 251–258.

KHAZANOVICH, L., 1994. *Structural Analysis of Multi-Layered Concrete Pavement Systems*, Ph.D. Thesis; University of Illinois, Urbana, Illinois.

KHAZANOVICH, L., and A.M. IOANNIDES, 1995. "DIPLOMAT: Analysis Program for Bituminous and Concrete Pavements, *Transportation Research Record 1482*, pp. 52–60; Transportation Research Board.

KHAZANOVICH, L., and T. YU, 1998, "Determination of Critical Stresses in Concrete Pavements," *Proceedings, International Conference on Computational Engineering Science*, Atlanta, Georgia, vol. 1, pp. 1695–1700.

KHAZANOVICH, L., H.T. YU, S. RAO, K. GALASOVA, E. SHATS, and R. JONES, 2000. *ISLAB2000—Finite Element Analysis Program for Rigid and Composite Pavements*, User's Guide; ERES, Inc., Champaign, IL.

KHEDR, S. A., 1985. "Deformation Characteristics of Granular Base Course in Flexible Pavements," *Transportation Research Record 1043*, pp. 131–138; Transportation Research Board.

KHEDR, S. A., 1986. "Deformation Mechanism in Asphalt Concrete," *Journal of Transportation Engineering, ASCE*, Vol 112, No. 1, pp. 29–45.

KHER, R. K., and M. I. DARTER, 1973. "Probabilistic Concepts and Their Applications to AASHTO Interim Guide for Design of Rigid Pavements," *Highway Research Record 466*, pp. 20–36; Highway Research Board.

Downloaded From : www.EasyEngineering.net

Downloaded From : www.EasyEngineering.net

KILARESKI, W. P., and R. A. BIONDA, 1990. *Structural Overlay Strategies for Jointed Concrete Pavements*, Vol. 1, *Sawing and Sealing of Joints in AC Overlay of Concrete Pavements*, Report No. FHWA-RD-89-142; Federal Highway Administration.

KILARESKI, W. P., and S. M. STOFFELS, 1990. *Structural Overlay Strategies for Jointed Concrete Pavements*, Vol. II, *Cracking and Seating of Concrete Slabs Prior to AC Overlay*, Report No. FHWA-RD-89-143; Federal Highway Administration.

KIM, H. B., N. BUCH, and D. Y. PARK, 2000. "Mechanistic–Empirical Rut Prediction Model for In-Service Pavements," *Transportation Research Record 1730*, pp. 99–109; Transportation Research Board.

KOPPERMAN, S., G. TILLER, and M. TSENG, 1986. *ELSYM5, Interactive Microcomputer Version, User's Manual*, Report No. FHWA-TS-87-206; Federal Highway Administration.

KUEMMEL, D. A., R. C. SONNTAG, J. R. JAECKEL, J. A. CROVETTI, Y. Z. BECKER, and A. SATANOVSKY, 2000. "Using a Road Surface Analyzer to Explain Noise Characteristics of Portland Cement Concrete Pavement Surface Texture," *Transportation Research Record 1716*, pp. 144–153; Transportation Research Board.

KUMMER, H. W., and W. E. MEYER, 1967. *Tentative Skid-Resistance Requirements for Main Rural Highways*, NCHRP Report 37; Highway Research Board.

LAI, J. S., 1977. *VESYS-G, a Computer Program for Analysis of N-layered Flexible Pavement*, Report No. FHWA-77-117; Federal Highway Administration.

LEMER, A. C., and F. MOAVENZADEH, 1971. "Reliability of Highway Pavements," *Highway Research Record 362*, pp. 1–8; Highway Research Board.

LEU, M. C., and J. J. HENRY, 1978. "Prediction of Skid Resistance as a Function of Speed from Pavement Texture," *Transportation Research Record 666*, pp. 38–43; Transportation Research Board.

LINDLY, J. K., and A. S. ELSAYED, 1995. "Estimating Permeability of Asphalt-Treated Bases," *Transportation Research Record 1504*, pp. 103–111; Transportation Research Board.

LIU, S. J., and R. L. LYTTON, 1984. "Rainfall Infiltration, Drainage, and Load-Carrying Capacity of Pavements," *Transportation Research Record 993*, pp. 28–35; Transportation Research Board.

LOKKEN, E. C., 1973. "What We Have Learned to Date from Experimental Concrete Shoulder Projects," *Highway Research Record 434*, pp. 43–53; Highway Research Board.

LOVERING, W. R., and H. R. CEDERGREN, 1962. "Structural Section Drainage," *Proceedings, (1st) International Conference on the Structural Design of Asphalt Pavements*, pp. 773–784.

LYTTON, R. L., 1989. "Backcalculation of Pavement Layer Properties," *STP 1026*, pp. 7–38; American Society for Testing and Materials.

LYTTON, R. L., and Y. J. CHOU, 1988. "Modulus Backcalculation Exercise," *Informal report to TRB Committee A2B05, Strength and Deformation Characteristics*; Transportation Research Board.

LYTTON, R. L., F. P. GERMANN, Y. J. CHOU, and S. M. STOFFELS, 1990. *Determining Asphalt Concrete Pavement Structural Properties by Non-destructive Testing*, NCHRP Report 327; Transportation Research Board.

LYTTON, R. L., U. SHANMUGHAM, and B. D. GARRETT, 1983. *Design of Asphalt Pavements for Thermal Fatigue Cracking*, Research Report No. 284-4; Texas Transportation Institute, Texas A&M University.

LYTTON, R. L., J. UZAN, E. G. FERNANCO, R. ROGUE, D. HILTUMEN, and S. M. STOFFEL, 1993. *Development and Validation of Performance Prediction Models and Specifications for Asphalt Binders and Paving Mixes*, Report No. SHRP-A-357; Strategic Highway Research Program.

MAHBOUB, K. C., and D. N. LITTLE, 1990. "An Improved Asphalt Concrete Mix Design Procedure", *Proceedings, Association of Asphalt Paving Technologists*, V. 59, pp. 138–175.

MAHONEY, J. P., and N. C. JACKSON, 1990. "Guidelines on When to Apply and Remove Seasonal Load Restrictions—Development Through Implementation," *Proceedings, 3rd International Conference on Bearing Capacity of Roads and Airfields*, Vol. 1, pp. 75–84; The Norwegian Institute of Technology, Trondheim.

Downloaded From : www.EasyEngineering.net

Downloaded From : www.EasyEngineering.net

MAJIDZADEH, K., 1978. *Observations of Field Performance of Continuously Reinforced Concrete Pavements in Ohio*, Report No. Ohio-DOT-12-77; Ohio Department of Transportation.

MAJIDZADEH, K., F. BAYOMY, and S. KHEDR, 1978. "Rutting Evaluation of Subgrade Soils in Ohio," *Transportation Research Record 671*, pp. 75–84; Transportation Research Board.

MAJIDZADEH, K., G. J. ILVES, and H. SKLYUT, 1984. *Mechanistic Design of Rigid Pavements*, Vol. 1, *Development of the Design Procedure*, Report No. FHWA-RD-86-124, Vol. 2, *Design and Implementation Manual*, Report No. FHWA-RD-86-235; Federal Highway Administration.

MAJIDZADEH, K., S. KHEDR, and H. GUIRGUIS, 1976. "Laboratory Verification of a Mechanistic Subgrade Rutting Model," *Transportation Research Record 616*, pp. 34–37; Transportation Research Board.

MALLELA, J., L. TITUS-GLOVER, and M. I. DARTER, 2000. "Considerations for Providing Subsurface Drainage in Jointed Concrete Pavements," *Transportation Research Record 1709*, pp. 1–10; Transportation Research Board.

MAMLOUK, M. S., 1987. "Dynamic Analysis of Multilayer Pavement Structures—Theory, Significance and Verification," *Proceedings, 6th International Conference on the Structural Design of Asphalt Pavements*, Vol. 1, pp. 466–474.

MCCULLOUGH, B. F., and M. L. CAWLEY, 1981. "CRCP Design Based on Theoretical and Field Performance," *Proceedings, 2nd International Conference on Concrete Pavement Design*, pp. 239–251; Purdue University.

MCCULLOUGH, B. F., and G. E. ELKINS, 1979. *CRC Pavement Design Manual*; Austin Research Engineers.

MCLEAN, D. B., 1974. *Permanent Deformation Characteristics of Asphalt Concrete*, Ph. D. Dissertation; University of California, Berkeley.

MCLEOD, N. W., 1953. "Some Basic Problems in Flexible Pavement Design," *Proceedings, Highway Research Board*, pp. 91–118.

MCLEOD, N. W., 1970. "Influence of Hardness of Asphalt Cement on Low Temperature Transverse Pavement Cracking," *Proceedings, Canadian Good Roads Association*.

MEYER, W. E., 1991. "Pavement Texture Significance and Measurement," *Standardization News, ASTM*, February, pp. 28–31.

MIKHAIL, M. Y., S. B. SEEDS, H. A. SIROUS, and C. O, WESTON, 1999. "Evaluation of laboratory and Backcalculated Resilient Moduli from WesTrack Experiment," *Transportation Research Record 1687*, pp. 55–65; Transportation Research Board.

MINER, M. A., 1945. "Cumulative Damage in Fatigue," *Transactions of the ASME*, Vol. 67, pp. A159-A164.

MOAVENZADEH, F., J. E. SOUSSOU, H. K. FINDAKLY, and B. BRADEMEYER, 1974. *Synthesis for Rational Design of Flexible Pavements*, Part 3, *Operating Instructions and Program Documentation*, Reports prepared for Federal Highway Administration under Contract FH 11-776.

MOHAMED, A. R. and W. HANSEN, 1997. "Effect of Nonlinear Temperature Gradient on Curling Stress in Concrete Pavements," *Transportation Research Record 1568*, pp. 65–71; Transportation Research Board.

MONISMITH, C. L., J. SOUSA, and J. LYSMER, 1988. "Modern Pavement Design Technology Including Dynamic Loading Conditions," *Vehicle/Pavement Interaction, Where the Truck Meets the Road*, SP-765, pp. 33–52; Society of Automotive Engineers, Inc.

MONISMITH, C. L., and M. W. WITCZAK, 1982. "Moderator's Report, Section 1," *Proceedings, Fifth International Conference on the Structural Design of Asphalt Pavements*, Vol. 2, pp. 2–59.

MOORE, J. H., 1956. "Thickness of Concrete Pavements," with discussions by E. C. Sutherland and W. Harwood, *Transactions, ASCE*, Vol. 121, pp. 1125–1152.

MOREELL, B., 1958. "Prestressing Promises Nearly Joint-Free Highways," *Civil Engineering*, Vol. 28, No. 8, pp. 34–37.

MOULTON, L. K., 1980. *Highway Subdrainage Design*, Report No. FHWA-TS-80-224; Federal Highway Administration.

Downloaded From : www.EasyEngineering.net

Downloaded From : www.EasyEngineering.net

MUHANNA, A. S., M. S. RAHMAN, and P.C. LAMBE, 1999. "Resilient Modulus Measurement of Fine-Grained Subgrade Soils," *Transportation Research Record 1687*, pp. 1–12; Transportation Research Board.

NAZARIAN, S., D. YUAN, and M.R. BAKER, 1995. *Rapid determination of Pavement Moduli with Spectral-Analysis-of-Surface-Wave Method*, Research Report 1243-1F, Center for Geotechnical and Highway Materials Research; University of Texas at El Paso.

NCHRP, 1972. *Skid Resistance*, Synthesis of Highway Practice 14; National Cooperative Highway Research Program.

NCHRP, 1979. *Design and Use of Highway Shoulders*, Synthesis of Highway Practice 63; National Cooperative Highway Research Program.

NCHRP, 1990. *Calibrated Mechanistic Structural Analysis Procedures for Pavement*, NCHRP 1–26, Vol. 1, *Final Report;* Vol. 2, *Appendices*; University of Illinois at Urbana–Champaign.

NCHRP, 1997. "Investigation of the Restricted zone in the Superpave Aggregate Gradation Specification," *Research Project Statement*, Project 9–14; National Cooperative Highway Research Program.

NIE, N. H. et al., 1975. *Statistical Package for the Social Sciences*, 2d ed.; McGraw-Hill, New York.

NUSSBAUM, P. J., and E. C. LOKKEN, 1978. *Portland Cement Concrete Pavements, Performance Related to Design–Construction–Maintenance*, Report No. FHWA-TS-78-202, Prepared by PCA for Federal Highway Administration.

ODEMARK, N., 1949. "Investigations as to the Elastic Properties of Soils and Design of pavements According to the Theory of Elasticity," Meddlande 77, Statens Vaginstitut; Stockholm, Sweden.

ODUROH, P. K., K.C MAHBOUB, and R. M. ANDERSON, 2000. "Flat and Elongated Aggregates in Superpave Regime," ASCE Journal of Materials Engineering, Vol. 12, No. 2, pp. 124–130.

OLDER, C., 1924. "Highway Research in Illinois," *Transactions, ASCE*, Vol. 87, pp. 1180–1222.

PACKARD, R. G., and S. D. TAYABJI, 1985. "New PCA Thickness Design Procedure for Concrete Highway and Street Pavements," *Third International Conference on Concrete Pavement Design and Rehabilitation*, pp. 225–236; Purdue University.

PAGEN, C. A., 1965. "Rheological Response of Bituminous Concrete," *Highway Research Record 67*, pp. 1–26; Highway Research Board.

PAPAZIAN, H. S., 1962. "The Response of Linear Viscoelastic Materials in the Frequency Domain with Emphasis on Asphaltic Concrete," *(1st) International Conference on the Structural Design of Asphalt Pavements*, pp. 454–463.

PASKO, T. J., 1972. "Prestressed Concrete Pavement at Dulles Airport for Transpo 72," *Journal of the Prestressed Concrete Institute*, Vol. 17, No. 2, pp. 46–54.

PCA, 1951. *Concrete Pavement Design*; Portland Cement Association.

PCA, 1955. *Design of Concrete Airport Pavement*; Portland Cement Association.

PCA, 1966. *Thickness Design for Concrete Pavements*; Portland Cement Association.

PCA, 1969. *Load Stresses at Pavement Edge, a Supplement to Thickness Design for Concrete Pavements*; Portland Cement Association.

PCA, 1975. *Join Design for Concrete Highway and Street Pavements*; Portland Cement Association.

PCA, 1984. *Thickness Design for Concrete Highway and Street Pavements*; Portland Cement Association.

PCA, 1991. *Design and Construction of Joints for Concrete Highways*, Concrete Paving Technology; Portland Cement Association.

PEATTIE, K. R., 1962. "Stress and Strain Factors for Three-Layer Elastic Systems," *Bulletin 342*, pp. 215–253; Highway Research Board.

PELL, P. S., 1962. "Fatigue Characteristics of Bituminous Mixes," *(1st) International Conference on the Structural Design of Asphalt Pavements*, pp. 310–323.

PELL, P. S., 1987. "Keynote Lecture—Pavement Materials," *Sixth International Conference on the Structural Design of Asphalt Pavements*, Vol. 2, pp. 36–70.

Downloaded From : www.EasyEngineering.net

Downloaded From : www.EasyEngineering.net

PERLOFF, W. H., and F. MOAVENZADEH, 1967. "Deflection of Viscoelastic Medium Due to Moving Load," *Proceedings, 2nd International Conference on the Structural Design of Asphalt Pavements*, pp. 269–276; University of Michigan.

PETERSON, D. E., 1987. *Pavement Management Practices*, NCHPR Synthesis 122; Transportation Research Board.

PETERSON, R. L., K. C. MAHBOUB, R. M. ANDERSON, E. MASAD, and L. TASHMAN, 2003. "Superpave Laboratory Compaction Versus Field Compaction", to be published in Transportation Research Record; *Transportation Research Board*.

PEZO, R. F., 1993. *A General Method of Reporting Resilient Modulus Tests of Soils—A Pavement Engineer's Point of View*, presented at the 72nd Annual Meeting of the Transportation Research Board.

PEZO, R. F., G. J. CLAROS, W. R. HUDSON, and K. H. STOKOE, 1992. *Development of a Reliable Resilient Modulus Test for Subgrade and Non-Granular Subbase Materials for Use in Routine Pavement design*, Research Report 1177-4F; Center for Transportation Research, The University of Texas at Austin.

PHU, N. C., J. P. CHRISTORY, and J. RAY, 1986. *The Hydromechanics of Pumping in Concrete Pavements: Modeling and Prevention*, Appendix I, *Combatting Concrete Pavement Pumping: State-of-the-Art and Recommendations*; PIARC Technical Committee on Concrete Roads.

PICKETT, G., and S. BADARUDDIN, 1956. "Influence Chart for Bending of a Semi-infinite Pavement Slab," *Proceedings, Ninth International Congress on Applied Mechanics*, Vol. 6, pp. 396–402.

PICKETT, G., M. E. RAVILLE, W. C. JANES, and F. J. MCCORMICK, 1951. "Deflections, Moments and Reactive Pressures for Concrete Pavements," *Bulletin No. 65*; Engineering Experiment Station, Kansas State College.

PICKETT, G., and G. K. RAY, 1951. "Influence Charts for Concrete Pavement." *Transactions, ASCE*, Vol. 116, pp. 49–73.

POEHL, R., 1971. *Seasonal Variations of Pavement Deflections in Texas*, Research Report 136–1; Texas Transportation Institute, Texas A & M University.

PORTER, O. J., 1950. "Development of the Original Method for Highway Design: Symposium on Development of CBR Flexible Pavement Design Method for Airfields," *Transactions, ASCE*, pp. 461–467.

POWELL, W. D., et al., 1984. *The Structural Design of Bituminous Pavements*, TRRL Laboratory Report 1132; Transportation and Road Research Laboratory, U.K.

QI, X., and M. W. WITCZAK, 1998. "Time-Dependent Permanent Deformation Models for Asphaltic Mixtures," *Transportation Research Record 1639*, pp. 83–93; Transportation Research Board.

RAAD, L., and J. L. FIGUEROA, 1980. "Load Response of Transportation Support Systems," *Transportation Engineering Journal, ASCE*, Vol. 106, No. TE1, pp. 111–128.

RADA, G., and M. W. WITCZAK, 1981. "Comprehensive Evaluation of Laboratory Resilient Moduli Results for Granular Materials," *Transportation Research Record 810*, pp. 23–33; Transportation Research Board.

RAITHBY, K. D., and J. W. GALLOWAY, 1974. "Effects of Moisture Condition, Age, and Rate of Loading on Fatigue of Plain Concrete," *SP-41*, pp. 15–34; American Concrete Institute.

RAUHUT, J. B., R. C. G. HAAS, and T. W. KENNEDY, 1977. "Comparison of VESYS IIM Predictions to Brampton/AASHO Performance Measurements," *Proceedings, 4th International Conference on the Structural Design of Asphalt Pavements*, Vol. 1, pp. 131–147.

RAUHUT, J. B., and P. R. JORDAHL, 1979. *Effects on Flexible Pavements of Increased Legal Vehicle Weights Using VESYS-IIM*, Report No. FHWA-77-116; Federal Highway Administration.

RICHARDSON, J. M., and J. M. ARMAGHANI, 1987. "Stress Caused by Temperature Gradient in Portland Cement Pavements," *Transportation Research Record 1121*, pp. 14–22; Transportation Research Board.

Downloaded From : www.EasyEngineering.net

Downloaded From : www.EasyEngineering.net

RIDGEWAY, H. H., 1976. "Infiltration of water through the Pavement Surface," *Transportation Research Record 616*, pp. 98–100; Transportation Research Board.

RIDGEWAY, H. H., 1982. *Pavement Subsurface Drainage Systems*, Synthesis of Highway Practice 96; Transportation Research Board.

RITCHIE, S. G., C. YEH, J. P. MAHONEY, and N. C. NEWTON, 1986. "Development of an Expert System for Pavement Rehabilitation Decision Making," *Transportation Research Record 1070*, pp. 90–103; Transportation Research Board.

ROAD RESEARCH LABORATORY, 1952. *Soil Mechanics for Road Engineers*; Her Majesty Stationery Company.

ROADS AND STREETS, 1971. "Prestressed Concrete Pavement in Service," Vol. 114, No. 10, p. 56.

ROADS AND TRANSPORTATION ASSOCIATION OF CANADA, 1977. *Pavement Management Guide*.

ROSENBLUETH, E., 1975. "Point Estimates for Probability Moments," *Proceedings, National Academy of Sciences, Mathematics*, Vol. 72, No. 10, pp. 3812–3814.

RUTH, B. E., L. A. K. BLOY, and A. A. AVITAL, 1982. "Prediction of Pavement Cracking at Low Temperatures," *Proceedings, Association of Asphalt Paving Technologists*, Vol. 51, pp. 53–90.

RYELL, J., and J. T. CORKILL, 1973. "Long Term Performance of an Experimental Composite Pavement," *Highway Research Record 434*, pp. 1–15; Highway Research Board.

SAAL, R. N. J., and P. S. PELL, 1960. *Kolloid-Zeitschrift MI*, Heft 1, pp. 61–71.

SAWAN, J. S., and M. I. DARTER, 1979. "Structural Design of PCC Shoulders," *Transportation Research Record 725*, pp. 80–88; Transportation Research Board.

SAXENA, S. K., 1973. "Pavement Slabs Resting on Elastic Foundation," *Highway Research Record 466*, pp. 163–178; Highway Research Board.

SAYERS, M. W., T. D. GILLESPIE, and W. D. PATERSON, 1986a. *Guidelines for the Conduct and Calibration of Road Roughness Measurements*, Technical Paper 46; The World Bank, Washington, DC.

SAYERS, M. W., T. D. GILLESPIE, and C. A. QUEIROZ, 1986b. *The International Road Roughness Experiment: Establishing Correlation and a Calibration Standard for Measurements*, Technical Paper 46; The World Bank, Washington, DC.

SCHOFIELD, R. K., 1935. "The PF of the Water in Soil," *Transactions, 3rd International Congress on Soil Science*, Oxford, 1935, Vol. 2, pp. 37–48.

SCRIVNER, F. H., and W. M. MOORE, 1968. *Standard Measurements for Satellite Road Test Program*, NCHRP Report No. 59; National Cooperative Highway Research Program.

SCRIVNER, F. H., R. POEHL, W. M. MOORE, and M. B. PHILLIPS, 1969. *Detecting Seasonal Changes in Load-Carrying Capacities of Flexible Pavements*, NCHRP Report No. 76; National Cooperative Highway Research Program.

SCULLION, T., J. UZAN, and M. PAREDES, 1990. "Modulus: A Microcomputer-Based Backcalculation System," *Transportation Research Record 1260*, pp. 180–191; Transportation Research Record.

SEBAALY, B. E., M. S. MAMLOUK, and T. G. DAVIES, 1986. "Use of Falling Weight Deflectometer Data," *Transportation Research Record 1070*, pp. 63–68; Transportation Research Board.

SELIG, E. T., H. LIN, L. J. DOYER, S. DUANN, and H. TZENG, 1986. *Layered System Performance Evaluation, Phase II*, Final Report, Report No. DOT/OST/P-34/86/047.

SHAHIN, M. Y., and B. F. MCCULLOUGH, 1972. *Prediction of Low-Temperature and Thermal-Fatigue Cracking in Flexible Pavements*, Report No. CFHR 1-8-69-123-14; The University of Texas.

SHELL, 1978. *Shell Pavement Design Manual—Asphalt Pavements and Overlays for Road Traffic*; Shell International Petroleum, London.

SHERARD, J. L., R. J. WOODWARD, S. F. GIZIENSKI, and W. A. CLEVENGER, 1963. *Earth and Earth-Rock Dams*; Wiley, New York.

SHERMAN, G. B., 1971. "In Situ Materials Variability," *Special Report 126*, pp. 180–188; Highway Research Board.

SHOOK, J. F., F. N. FINN, M. W. WITCZAK, and C. L. MONISMITH, 1982. "Thickness Design of Asphalt Pavements—The Asphalt Institute Method," *Proceedings, 5th International Conference on the Structural Design of Asphalt Pavements*, Vol. 1, pp. 17–44.

Downloaded From : www.EasyEngineering.net

Downloaded From : www.EasyEngineering.net

SHRP, 1993. *Distress Identification Manual for the Long-term Pavement Performance Project*, Report SHRP-P-338, Strategic Highway Research Program.

SKARLATOS, M. S., 1949. *Deflections and Stresses in Concrete Pavements of Airfields with Continuous Elastic Joints*, Report AD628501; Ohio River Division Laboratories, U.S. Army Corps of Engineers.

SLAVIS, C., 1981. "Portland Cement Concrete Shoulder Performance in the United States," *Proceedings, 2nd International Conference on Concrete Pavement Design*, pp. 331–341; Purdue University.

SMITH, B. E., and M. W. WITCZAK, 1981. "Equivalent Granular Base Moduli: Prediction," *Transportation Engineering Journal, ASCE*, Vol. 107, No. TE6, pp. 635–652.

SMITH, K. D., M. I. DARTER, J. B. RAUHUT, and K. T. Hall, 1987. *Distress Identification Manual for the LTPP Studies*; Strategic Highway Research Program, National Research Council.

SMITH, K. D., D. G. PESHKIN, M. I. DARTER, A. L. MUELLER, and S. H. CARPENTER, 1990a. *Performance of Jointed Concrete Pavements*, Vol. 1, *Evaluation of Concrete Pavement Performance and Design Features*, Report No. FHWA-RD-89-136; Federal Highway Administration.

SMITH, K. D., D. G. PESHKIN, M. I. DARTER, and A. L. MUELLER, 1990b. *Performance of Jointed Concrete Pavements*, Vol. 2, *Evaulation and Modification of Concrete Pavement Design and Analysis Models*, Report No. FHWA-RD-89-137; Federal Highway Administration.

SMITH, K. D., D. G. PESHKIN, M. I. DARTER, A. L. MUELLER, and S. H. CARPENTER, 1990c. *Performance of Jointed Concrete Pavements*, Vol. 5, *Appendix B: Data Collection and Analysis Procedures*, Report No. FHWA-RD-89-140; Federal Highway Administration.

SMITH, R. E., M. I. DARTER, and S. M. HERRIN, 1979. *Highway Pavement Distress Identification Manual for Highway Condition and Quality of Highway Construction Survey*, Contract DOT-FH-11-9175/NCHRP 1–19; Federal Highway Administration.

SPANGLER, E. B., and W. J. KELLY, 1964. *GMR Road Profilometer—A Method for Measuring Road Profiles*, Research Publication GMR-452; General Motor Corporation.

SPANGLER, M. G., 1942. *Stresses in the Corner Region of Concrete Pavements*, Bulletin 157; Iowa State College.

STEELE, D. J., 1945. "Application of the Classification and Group Index in Estimating Desirable Subbase and Total Pavement Thickness," (a discussion), *Proceedings, Highway Research Board*, pp. 388–392.

STEPHENS, J. E., and K. C. SINHA, 1978 "Effect of Aggregate Shape on Bituminous Mix Character," Proceedings, Association of Asphalt Paving Technologists, Vol. 47, pp. 434–456.

TABATABAIE, A. M., 1977. *Structural Analysis of Concrete Pavement Joints*, Ph.D. Thesis; University of Illinois.

TABATABAIE, A. M., and E. J. BARENBERG, 1979. *Longitudinal Joint Systems in Slip-Formed Rigid Pavements*, Vol. 3; *User's Manual*, Report FAA-RD-79-4, III; U.S. Department of Transportation.

TABATABAIE, A. M., and E. J. BARENBERG, 1980. "Structural Analysis of Concrete Pavement Systems," *Transportation Engineering Journal, ASCE*, Vol. 106, No. TE5, pp. 493–506.

TAYABJI, S. D., and B. E. COLLEY, 1986. *Analysis of Jointed Concrete Pavement*, Report No. FHWA-RD-86-041; Federal Highway Administration.

TAYABJI, S. D., and P. A. OKAMOTO, 1985. "Thickness Design of Concrete Resurfacing," *Proceedings, 3rd International Conference on Concrete Pavement Design and Rehabilitation*, pp. 367–379; Purdue University.

TAYABJI, S. D., P. J. STEPHANOS, and D. G. ZOLLINGER, 1995. "Nationwide Field Investigation of Continuously Reinforced Concrete Pavements," *Transportation Research Record 1482*, pp. 7–18; Transportation Research Board.

TELLER, L. W., and E. C. SUTHERLAND, 1935–1943. *The Structural Design of Concrete Pavements*, Reprints from *Public Roads*, Vols. 16, 17, and 23.

TERZAGHI, K., 1943. *Theoretical Soil Mechanics*; Wiley, New York.

Downloaded From : www.EasyEngineering.net

Downloaded From : www.EasyEngineering.net

THOMPSON, M. R., 1987. "ILLI-PAVE Based Full-Depth Asphalt Concrete Pavement Design Procedure," *Proceedings, Sixth International Conference on Structural Design of Asphalt Pavements*, Vol. 1, pp. 13–22.

THOMPSON, M. R., B. J. DEMPSEY, H. HILL, and J. VOGEL, 1987. "Characterizing Temperature Effects for Pavement Analysis and Design," *Transportation Research Record 1121*, pp. 14–22; Transportation Research Board.

THOMPSON, M. R., and R. P. ELLIOT, 1985. "ILLI-PAVE-Based Response Algorithms for Design of Conventional Flexible Pavements," *Transportation Research Record 1043*, pp. 50–57; Transportation Research Board.

TIMOSHENKO, S., and I. N. GOODIER, 1951. *Theory of Elasticity*; McGraw-Hill, New York.

TRB, 1992. *Nondestructive Deflection Testing and Backcalculation of Pavements*, Transportation Research Record 1377; Transportation Research Board.

TRB, 2002. *Significance of Restricted Zone in Superpave Aggregate Gradation Specification*, Circular E-C043; Transportation Research Board.

TREYBIG, H. C., B. F. MCCULLOUGH, P. SMITH, H. VONQUINTUS, and P. JORDAHL, 1977. *Flexible and Rigid Pavement Overlay Design Procedures*, Report No. FHWA-RD-77-133; Austin Research Engineers, Inc., Austin, TX.

TSENG, K. H., and LYTTON, R. L., 1998. "Prediction of Permanent Deformation in Flexible Pavement Materials," ASTM STP 1016, pp. 154–172; American Society for Testing and Materials.

TURNBULL, W. J., and R. G. AHLVIN, 1957. "Mathematical Expression of the CBR (California Bearing Ratio) Relations," *Proceedings, 4th International Conference on Soil Mechanics and Foundation Engineering*, Vol. 2, pp. 178–180.

UDDIN, W., R. M. HACKETT, A. JOSEPH, Z. PAN, and A. B. CRAWLEY, 1995. "Three-Dimensional Finite-Element Analysis of Jointed Concrete Pavement with Discontinuities," *Transportation Research Record 1482*, pp. 26–32; Transportation Research Board.

ULLIDTZ, P., 1987. *Pavement Analysis*; Elsevier Science, New York.

ULLIDTZ, P., and R. N. STUBSTAD, 1985. "Analytical-Empirical Pavement Evaluation Using the Falling Weight Deflectometer," *Transportation Research Record 1022*, pp. 36–44; Transportation Research Board.

UNIVERSITY OF WASHINGTON, 1996. *User's Guide to EVERCALC 5.0*; Civil Engineering Department, University of Washington, Seattle.

U.S. ARMY CORPS OF ENGINEERS, 1955. *Drainage and Erosion Control—Subsurface Drainage Facilities for Airfields*, Part XIII, Chapter 2, *Engineering Manual*, Military Construction.

U.S. ARMY CORPS OF ENGINEERS, 1961. *Revised Method of Thickness Design of Flexible Highway Pavements at Military Installations*, Technical Report No. 3-582; Waterways Experimental Station.

U.S. BUREAU OF RECLAMATION, 1973. *Design of Small Dams*; U.S. Government Printing Office, Washington, DC.

U.S. NAVY, 1953. Airfield Pavement, Bureau of Yards and Docks, Technical Publication, NAV-DOCKS TP-PW-4.

UZAN, J., 1985. "Characterization of Granular Material," *Transportation Research Record 1022*, pp. 52–59; Transportation Research Board.

UZAN, J., R. L. LYTTON, and F. P. GERMANN, 1989. "General Procedure for Backcalculating Layer Moduli," *STP 1026*, pp. 217–228; American Society for Testing and Materials.

UZAN, J., T. SCULLION, C. H. MICHALEK, M. PAREDES, and R. L. LYTTON, 1988. *A Microcomputer Based Procedure for Backcalculating Layer Moduli from FWD Data*, Research Report 1123-1; Texas Transportation Institute.

VAN CAUWELAERT, F. J., D. R. ALEXANDER, T. D. WHITE, and W. R. BAKER, 1989. Multilayer Elastic Program for Backcalculating Layer Moduli in Pavement Evaluation, *STP 1026*, pp. 171–188; American Society for Testing and Materials.

Downloaded From : www.EasyEngineering.net

Downloaded From : www.EasyEngineering.net

VAN DE LOO, P. J., 1974. "Creep Testing, a Simple Tool to Judge Asphalt Mix Stability," *Proceedings, Association of Asphalt Paving Technologists*, Vol. 43, pp. 253–281.

VAN DE LOO, P. J., 1978. "The Creep Test: A Key Tool in Asphalt Mix Design and in the Prediction of Pavement Rutting," *Proceedings, Association of Asphalt Paving Technologists*, Vol. 47, pp. 522–554.

VAN DER POEL, C., 1954. A General System Describing the Visco-Elastic Properties of Bitumens and Its Relation to Routine Test Data, *Journal of Applied Chemistry*, Vol. 4, 1954, pp. 221–236.

VAN TIL, C. J., B. F. MCCULLOUGH, B. A. VALLERGA, and R. G. HICKS, 1972. *Evaluation of AASHO Interim Guides for Design of Pavement Structures*, NCHRP 128; Highway Research Board.

VAN WIJI, A. J., 1985. *Purdue Economic Analysis of Rehabilitation and Design Alternatives for Rigid Pavements: A User's Manual for PEARDARP*, Final Report, FHWA Contract DTFH61-82-C-00035.

VAN WIJI, A. J., J. LARRALDE, C. W. LOVELL, and W. F. CHEN, 1989. "Pumping Prediction Model for Highway Concrete Pavements," *Journal of Transportation Engineering*, Vol. 115, No. 2, pp. 161–175.

VAVRIK, W. R., S. H. CARPENTER, and R. J. FRIES, 1999. "Effect of Flat and Elongated Coarse Aggregate on Characteristics of Gyratory Compacted Samples," Transportation Research Record 1761, pp. 26–31; Transportation Research Board.

VERSTRAETEN, J., V. VEVERKA, and L. FRANCKEN, 1982. "Rational and Practical Designs of Asphalt Pavements to Avoid Cracking and Rutting," *Proceedings, Fifth International Conference on the Structural Design of Asphalt Pavements*.

VESIC, A. S., and L. DOMASCHUK, 1964. *Theoretical Analysis of Structural Behavior of Road Test Flexible Pavements*, NCHRP Report No. 10; Highway Research Board.

VESIC, A. S., and K. SAXENA, 1974. *Analysis of Structural Behavior of AASHO Road Test Rigid Pavements*, NCHRP Report No. 97; Highway Research Board.

VON QUINTUS, H. L., F. N. FINN, W. R. HUDSON, and F. L. ROBERTS, 1980. *Flexible and Composite Structures for Premium Pavements*, Report Nos. FHWA-RD-81-154 and -155 Vols. 1 and 2; Federal Highway Administration.

WAMBOLD, J. C., J. J. HENRY, C. E. ANTLE, J. W. BUTTON, and D. A. ANDERSON, 1989. *Pavement Friction Measurement Normalized for Operational, Seasonal, and Weather Effects*, Report No. FHWA-RD-88-069; Federal Highway Administration.

WARREN, H., and W. L. DIECKMANN, 1963. *Numerical Computation of Stresses and Strains in a Multiple-Layer Asphalt Pavement System*, Internal Report; Chevron Research Corporation, Richmond, CA.

WESTERGAARD, H. M., 1926a. "Analysis of Stresses in Concrete Pavement Due to Variations of Temperature," *Proceedings, Highway Research Board*, Vol. 6, pp. 201–215.

WESTERGAARD, H. M., 1926b. "Stresses in Concrete Pavements Computed by Theoretical Analysis," *Public Roads*, Vol. 7, pp. 25–35.

WESTERGAARD, H. M., 1927. "Theory of Concrete Pavement Design," *Proceedings, Highway Research Board*, Part I, pp. 175–181.

WESTERGAARD, H. M., 1933. "Analytical Tools for Judging Results of Structural Tests of Concrete Pavements," *Public Roads*, Vol. 14, No. 10, pp. 185–188.

WESTERGAARD, H. M., 1939. "Stresses in Concrete Runways of Airports," *Proceedings, Highway Research Board*, Vol. 19, pp. 197–202.

WESTERGAARD, H. M., 1943. "Stress Concentrations in Plates Loaded over Small Areas," *Transactions, ASCE*, Vol. 108, pp. 831–856.

WESTERGAARD, H. M., 1948. "New Formulas for Stresses in Concrete Pavements of Airfields," *Transactions, ASCE*, Vol. 113, pp. 425–444.

WHITLOW, R., 1990. *Basic Soil Mechanics*; Wiley, New York.

WINTER, G., and A. H. NILSON, 1979. *Design of Concrete Structures*; McGraw-Hill, New York.

Downloaded From : www.EasyEngineering.net

Downloaded From : www.EasyEngineering.net

WITCZAK, M. W., and R. E. ROOT, 1974. "Summary of Complex Modulus Laboratory Test Procedures and Results," *STP 561*, pp. 67–94; American Society for Testing and Materials.

WITCZAK, M. W., K. KALOSH, T. PELLINEN, M. EL- BASYOUNY, and H. VON QUINTUS, 2002, NCHRP Report No. 465, National Cooperative Highway Research Program.

WRI, 1975. *Jointed Concrete Pavements Reinforced with Welded Wire Fabric*; Wire Reinforcement Institute, Inc.

YAZDANI, J. I., and T. SCULLION, 1990. "Comparing Measured and Theoretical Depth Deflections Under a Falling Weight Deflectometer Using a Multidepth Deflectometer," *Transportation Research Record 1260*, pp. 216–225; Transportation Research Board.

YODER, E. J., 1959. *Principles of Pavement Design*; Wiley, New York.

YODER, E. J., and M. W. WITCZAK, 1975. *Principles of Pavement Design*; Wiley, New York.

ZAGHLOUL, S. M. and T. D. WHITE, 1994. "Use of a Three-Dimensional, Dynamic, Nonlinear Analysis to Develop Load Equivalency Factors for Composite Pavements", *Transportation Research Record 1449*, pp. 199–208; Transportation Research Board.

ZANIEWSKI, J. P., W. R. HUDSON, R. HIGH, and S. W. HUDSON, 1985. *Pavement Rating Procedures*, Contract No. DTFH61-83-C-00153; Federal Highway Administration.

ZIENKIEWICZ, O. C., and Y. K. CHEUNG, 1967. *The Finite Element Method in Structrual and Continuum Mechanics*; McGraw-Hill, New York.

ZOLLINGER, D. G., 1989. *Investigation of Punchout Distress of Continuously Reinforced Concrete Pavements*, Ph.D. Thesis; Department of Civil Engineering, University of Illinois at Champaign-Urbana.

ZOLLINGER, D. G., and E. J. BARENBERG, 1989. *Proposed Mechanistic Based Design Procedure for Jointed Concrete Pavements*, Civil Engineering Studies, Transportation Engineering Series No. 57; Illinois Cooperative Highway Research Program,

ZOLLINGER, D. G., and E. J. BARENBERG, 1990. "Mechanistic Design Considerations for Punchout Distress in Continuously Reinforced Concrete Pavement," *Transportation Research Record 1286*, pp. 25–37; Transportation Research Board.

Downloaded From : www.EasyEngineering.net

Downloaded From : www.EasyEngineering.net

Author Index

A

AASHTO, 5, 8, 37, 38, 176, 209, 257, 258, 263, 273, 284, 302, 305, 309, 341, 359, 429, 441, 464–466, 505–522, 526, 568–591, 628, 684, 686, 689, 690, 694, 701, 702
ABAQUS, 7
Adedimila, A. S., 309
Ahlvin, R. G., 45–48, 249, 250, 467
AI, 3, 11, 25, 30, 98, 256, 267–269, 271–273, 293, 301, 316, 340, 487–505, 603, 607, 608, 617, 682, 683
Akram, T. T., 424
Alexander, D. R., 418
Ali, H. A., 321
Allen, D. L., 318
Allen, J. J., 101
Al-Omari, B., 400
American Concrete Institute, 172
Armaghani, J. M., 149
ASTM, 289, 297, 316, 347, 402
Asphalt binder grading system, 682

B

Badaruddin, S., 7, 216, 217
Baker, R. F., 17
Ball, C. G., 194
Ballinger, C. A., 317
Barber, E. S., 2, 342, 358, 360, 485
Barenberg. E. J., 7, 153, 167, 178, 212, 213, 316, 535, 544
Barksdale, R. G., 280, 281, 525, 527
Basson, J. E. B., 423
Bay, J. A., 412
Benjamin, J. R., 447
Betram,. G. E., 345
Bionda, R. A., 603
Black, W. P. M., 476
Blankenship, P. B., 690
Bonnaure, F., 298,301, 302, 306, 313, 315
Boussinesq, J., 2, 45, 187
Boyce, J. R., 101
Boyd, W. K., 245
Bradbury, R. D., 150
Brademeyer, B., 5, 215
Brown, E. R., 684
Brown, S. F., 98, 280
Brunner, R. J., 16
Burmister, D. M., 2, 45, 57, 58, 60
Bush, A. J., 418

C

California Highway Department, 2, 525, 607
Carey, W. N., 5. 389, 393
Carpenter, S. H., 527
Casagrande. A., 359
Cawley. M. L., 583
Cedergren, H. R., 14, 335, 341, 352, 362, 363
Chen, D. H., 122
Cheung. Y. K., 7, 194
Childs, L. D., 194

Downloaded From : www.EasyEngineering.net

Downloaded From : www.EasyEngineering.net

Chou, Y. J., 415
Chou, Y. T., 7, 87, 195, 208, 213
Christison, J. T., 35
Chua, K. M., 120
Charos. G., 289
Claussen, A. I. M., 3, 35, 98
Clemmer, H. F., 7
Collley, B. E., 7, 545, 593
Cominsky, R. J., 684
Corkill,. J. T., 17
Cornell, C. A., 447
Craus, J. R., 98
Croney, D., 476

D

Darter. M. I., 2, 5, 8, 153, 167, 178, 212, 213, 272, 316, 400, 426, 430,441, 460–464, 538, 644, 649
Daleiden, J. F., 424
Deacon, J. A., 256, 299, 309
DeBeer, M., 423
Deen, R. C., 318
De Jong, D. L., 4
Delaware Department of Transportation, 694
Dempsey, B. J., 473–475, 537, 593
Deng, X., 208
Dieckmann, W. L., 4
Domaschuk, L., 54
Dormon, G. M., 3
Duncan, J. M., 4

E

Elkins, G. E., 583
Elliot, J. F., 87
Elliot, R. P., 4, 102, 112, 113, 627
Elsayed, A. S., 344
Emery, D. K., 525
Epps, J. A., 398*
ERES Consultant, Inc., 135, 330, 527
EXSYS, Inc., 426

F

FAA, 39
Fermando, E. G., 398
FHWA, 1, 5, 35, 83, 85, 283, 284, 318, 322, 346, 398, 399, 526, 601, 703, 706, 717
Figueroa, J. L., 4, 105, 110
Finn, F. N., 4, 35, 86, 100, 101, 325, 427, 484, 518, 613
Fitch, M., 5
Foster, C. R., 45, 46, 47, 48, 245, 249, 250
Franchen, L., 309
Freeme, C. R., 131
Friberg, B. F., 172, 174

G

Gage. R. B., 8
Gallaway, B. M., 299, 309
Galloway, J. W., 317
Gerrard, C. M., 245
Goldbeek, A. T., 6, 154
Gomez-Achecar, M., 4
Goodier, I. N., 94
Groenendijk, J., 98
Gulen, S., 400

H

Haas, R., 428
Hajek. J. J., 428
Haliburton, T. A., 349
Hall, K. T., 2, 327, 400, 426
Hammons, M. I., 158
Hanna, A. M., 17
Hansen W., 149
Harichandran, R. S., 4, 35, 114
Harik, I. E., 149
Harrison, W. J., 245
Healey, K. A., 348, 350
Heinrichs, K. W., 176, 220, 222
Henry, J. J., 403, 404
Heukelom, W., 293, 486
Hick, R. G., 101, 525, 527
Hogentogler, C. A., 2,
HRB, 2, 19, 21, 23, 152, 204, 245, 510
Huang, Y. H., 7, 8, 39, 40, 53, 54, 57–59, 61, 64, 66–69, 87, 186, 189, 195, 198, 200, 201, 203, 205, 207, 208, 213, 214, 245, 250, 251, 256

Downloaded From : www.EasyEngineering.net

Downloaded From : www.EasyEngineering.net

Hudson, W. R., 7
Hwang, D., 4, 307

I

Ioannides, A. M., 4, 155, 157, 158, 256, 419, 421, 423, 432
Irick. P., 5, 389, 393, 394, 455, 456
Irwin, L. H., 299

J

Janoff, M. S., 399
Jiang, Y., 568
Jimenez, R. S., 309
Johnson, T. C., 478
Jones, A., 71, 73
Jordahl, P. R., 5, 99

K

Kalcheff, I. V., 101
Kallas, B. F., 297, 299
Kansas State Highway commission, 2, 45
Kelly, W. J., 398
Kenis, W. J., 5, 122
Kennedy, C. K., 607
Kennedy, T. W., 309
Kerkhoven, R. E., 3
Kesler, C. E., 317
Khazanovich, L., 4, 224, 256
Khedr, S. A., 482, 483
Kher, R. K., 8, 441, 462–464
Kilareski, W. P., 602, 603
Klomp, A. J. G., 293
Kopperman, S. G., 4, 109, 135
Kuemmel, D. A., 403
Kummer, H. W., 407

L

Lai, J. S., 5
Larew. H. G., 87
Lawmaster, J. D., 349
Lemer, A. C., 5, 441
Leu, M. C., 404
Lindly, J. K., 344
Lister, N. W., 607
Little, D. N., 692
Liu, S. J., 473, 477
Lokken, E. C., 15, 594
Long, R. P., 348, 350
Lovering, W. R., 341
Lytton, R. L., 120, 413, 415, 473, 477, 484, 724

M

Mahboub, K. C., 692
Majidzadeh, K., 7, 482, 586
Mallela, J. L., 338
Mamlouk, M. S., 5
Marais. C. P., 131
Matlock, H., 7
MeCullough, B. F., 479, 484, 486, 529, 583
McLean, D. B., 281
McLeod, N. W., 2, 429, 483
Metcalf, C. T., 3
Meyer, W. E., 404, 405, 407
Mikhail, M. Y., 424
Miner, M. A., 39, 479
Moavenzadeh, F., 5, 87, 441
Mohamed, A. R., 149
Monismith, C. L., 5, 101, 398, 613
Moore, W. M., 460
Moreell, B., 16
Moulton, L. K., 339, 344, 345, 354, 356, 357
Muhanna, A. S., 269
Munoz, E. C., 400

N

Nazarian, S., 424
NCHRP, 409, 472, 522, 533, 537, 540, 542, 684
Nie, N. H., 429
Nilson, A. H., 166
Nussbaum, P. J., 15

O

Odemark, N., 635
Odurah, P. K., 684
Okamoto, P. A., 623–626
Older,C., 6, 154

Downloaded From : www.EasyEngineering.net

Downloaded From : www.EasyEngineering.net

P

Packard, R. G, 212
Pagen, C. A, 85
Papazian, H. S., 297
Pasko, T. J, 16.,
PCA, 6, 28, 30, 36, 160, 171, 172, 177, 178, 201, 213, 216, 217, 229, 232, 268, 270, 272, 328, 545–568, 578, 583
Peattie, K. R., 74, 75
Pell, P. S., 3, 309, 480
Perloff, W. H., 87
Peterson, D. E., 690
Pezo, R. F., 54
Phu, N. C., 537
Pickett, G., 6, 7, 153, 160–165, 201, 212, 216, 217
Poehl, R., 414
Porter, O. J., 2
Powell, W. D., 480
Puzinauskas, V. P., 299

Q

Qi, X., 321

R

Raad, L., 4, 105, 110, 111
Rada, G., 101
Raithby, K. D., 317
Rauhut, J. B., 5, 99, 482
Ray, G. K., 153, 160–165, 216
Richardson, J. M., 149
Ridgeway, H. H., 33, 339, 352, 353, 359
Ritchie, S. G., 425
Road Research Laboratory, 476
Roads and Streets, 16
Roads and Transportation Association of Canada, 607
Root, R. E., 298, 300, 301
Rosenblueth, E., 466
Ruth., B. E., 484
Ryell, J. T., 17

S

Saal, R. N. J., 3
Sawyer, C. L., 342, 358, 360
Saxena, S. K., 7, 189
Sayers, M. W., 399
Schofield. R. K., 475
Scrivner, F. H., 460
Scullion, T., 416, 423
Selig, E. T., 104
Shahin, M. Y., 479, 484, 486, 529
Shannon, W. L., 359
Sharpe, G. W., 8
Shell Petroleum International, 3, 35, 302, 304, 307
Sherard, J. L., 345
Sherman, G. B., 462
Shook, J. F., 3, 35, 98, 101
SHRP, 368
Sinha, K. C., 684
Skarlatos, M. S., 158
Slavis, C., 594
Smith, B. E., 124
Smith, K. D., 430, 433
Smith, R. E., 368
Spangler, E. B., 398
Spangler, M. G., 569
Steele, D. J., 2
Stephens, J. E., 684
Stoffels, S. M., 602
Sutherland, E. C., 6, 152

T

Tabatabaie, A. M., 7, 212, 220
Tayabji, S. D., 7, 212, 321, 545, 623, 624–626
Teller, L. W., 6, 152
Terzaghi, K., 2
Thompson, M. R., 4, 102, 112, 113, 149, 473, 475, 480
Timoshenko, S., 94
TRB, 688
Treybig, H. C., 601
Tseng, K. H., 724
Turnbull, W. J., 467

Downloaded From : www.EasyEngineering.net

Downloaded From : www.EasyEngineering.net

U

Uddin, W., 7
Ulery, H. H., 46
Ullidtz, P., 51
University of Washington, 424
U. S. Army Corps of Enginners, 2, 345, 350, 527
U. S. Bureau of Reclamation, 350
U. S, Navy, 2
Uzan, J. T., 54, 416

V

Van Cauwelaert, F. J., 418
Van der Loo, P. J., 325
Van der Poel, C., 302, 303
Van Til, C. J., 290, 294, 296, 516
Van Wiji, A. J., 429, 538
Vavrik, W. R., 684
Verstraeten, J., 309, 480
Vesic. A. S., 54, 189
Von Quintus, H. L., 5, 17

W

Wambold, J. C., 405
Wang, S. T., 7, 200, 201, 203, 205, 213, 214
Warren, H., 4
Westergaard, H. M., 6, 7, 147, 155–157, 213, 214
White, T. D., 7
Whitlow, R., 343
Winter, G., 166
Witczak, M. W., 2, 4, 52, 101, 124, 295, 298, 300, 301, 307, 321, 682
WRI, 168, 169

Y

Yazdani, J. I., 423
Yoder, E. J., 2, 52, 295
Yu, T., 224

Z

Zaghloul, S. M., 7
Zaniewski, J. P., 398
Zienkiewiez, O. C, 7, 194
Zollinger, D. G., 535, 543, 544

Downloaded From : www.EasyEngineering.net

Downloaded From : www.EasyEngineering.net

Subject Index

A

AASHTO
- design equations and nomographs, 511, 513, 570, 571, 586
- design of overlay, 627
- equivalent axle load factors, 257, 259, 263
- flexible pavement design, 505
- rigid pavement design, 568
- road test, 23, 152
- 2002 pavement design guide, 716

ABAQUS program, 7, 122
AC quality adjustment factor, 647
AI
- equivalent axle load factors, 259
- failure criteria, 98, 260, 316, 488
- design methods, 487
- formulas for dynamic modulus, 307
- formulas for fatigue of bituminous mixtures, 314, 316
- overlay design, 608

Airport pavement, 16, 37, 160
Analysis period, 507, 520, 549, 568, 706
Angle of internal friction, 2, 104–106, 111, 112
Apparent opening size, 347
Area under normal curve, 450
Arlington Experimental Farm, 6, 152
Asphalt concrete, *see* Hot mix asphalt
Asphalt mix design 689
Asphalt pavement, *see* Flexible pavement
Asphalt performance grading specification, 685
Asphalt-treated bases, 296, 344, 432, 433
Average daily truck traffic, 266, 490, 563
Axle load distribution, 267, 564

B

Bates Road Test, *see* Road tests
Backcalculation of modulus, 120, 321, 415, 437
Base course, 10, 11, 295, 433, 492, 496, 516
- minimum thickness, 519

Bearing stress, 173, 431
Bending of plate, 147,150
Benefit/cost ratio, 704
Benkelman beam, 411, 612, 617
Binder course, 9
BISAR program, 4, 418, 646, 649
Block cracking, 370
Blowup, 376
Boltzmann's superposition principle, 88
Bonded slabs, 189, 625
British Pendulum Number, 404
Burgers model, 79

C

Calibrated mechanistic design procedure, 472, 533, 717
California bearing ratio, 2, 291, 293
- related to resilient modulus, 293

Downloaded From : www.EasyEngineering.net

Downloaded From : www.EasyEngineering.net

Cement-treated base, 296, 432, 592
CHEV program, 4, 418
Climate models, 474, 527, 720
  heat transfer model, 475
  moisture equilibrium model, 475
  infiltration and drainage model, 477
  integrated climate model, 721
Coefficient of variation, 444, 464
  frequency distribution, 460
  performance prediction, 465
  traffic prediction, 464
Cohesion, 113
Cohesiometer test, 294
Collector pipe, 362
Collocation method, 81, 661
  creep compliances , 83
  viscoelastic solutions, 86
Combined stresses, 152
Comparison of solutions
  KENLAYER and DAMA, 126, 128
  KENLAYER and ELSYM5, 111
  KENLAYER and MICH-PAVE, 116, 119, 121
  KENLAYER and VESYS, 123
  KENSLABS and Bradbury, 216
  KENSLABS and influence charts, 216, 218, 220
  KENSLABS and ILLI-SLAB, 222–224
  KENSLABS and JSLAB, 222, 224
  KENSLABS and Westergaard, 213
  KENSLABS and KENLAYER, 226
Complex modulus, *see* Dynamic modulus
Composite pavements, 17
Concrete pavement, *see* Rigid pavement
Condition factor, 640, 641
Continuous reinforced concrete pavement, 15
  field performance, 591
  first pavement, 15
Conversion factors
  effective thickness, 609, 611
  dual-tandem wheels, 68
  dual wheels, 66
COPES program, 2, 426, 430, 538
Corner loading, 154, 222, 547
Corner break, 376
Covariance, 444
Cracking and seating, 601, 618
Crack relief layer, 19, 602, 603, 645
Creep compliance, 80, 662
Creep test, 83, 325
Critical tensile strain, *see* Tensile strain
Curling stresses, 147, 150, 536

D

Damage analysis, 97, 122
  failure criteria, 98, 212, 260
  multiple axles, 99
DAMA program, 4, 109, 122, 123, 478, 492, 495
  nonlinear analysis, 124
Damage ratio, 108, 725
Darcy's law, 335, 364
DARWin program, 571
Deflection basin, 120, 639, 649
Degree of drainage, 360
Design inflow, 357
Design period, 549, 616
DIPLOMAT program, 4
Dirichlet series, 82, 86, 88, 661
Discount rate, 705
Discrete element method, 7
Distress, 368, 377, 388, 479, 697
Distress models, 479, 480, 483, 535, 537, 539, 541, 543, 722
Dowel bars
  allowable bearing stress, 172
  bearing stress on one dowel, 172, 431, 539
  dowel group action, 173
  recommended size and length, 172
  weights and dimensions, 168
Drainage coefficient, 518, 581
Drainage layer, 18, 338, 358
  steady-state flow, 358
  unsteady-state flow, 359
Dual tires, 158
Durability adjustment factor, 632, 633, 647
Durability or "D" cracking, 387, 652, 632
Duration of moving loads, 88, 302
Dynaflect, 411, 617
Dynamic loads, 5

Downloaded From : www.EasyEngineering.net

Downloaded From : www.EasyEngineering.net

Dynamic modulus
complex modulus, 297, 666
dynamic modulus by AI, 307
dynamic stiffness modulus, 298
relationship between dynamic stiffness modulus and dynamic modulus, 300
stiffness modulus by Shell, 301, 304
typical ranges, 309
Dynamic test, 283, 298, 324

E

Edge drain, 338, 340, 431, 435, 541
Edge loading, 213, 220
Edge punchout, 384, 386, 543, 726
Effective modulus of subgrade reaction, 575
Effective roadbed soil resilient modulus, 512
Effective structural capacity, 630
Effective thickness, 606, 609, 616
Elastic layer program, 416, 478
Elastic moduli for different materials, 329, 580
Elastic modulus of viscoelastic layer, 108
Elastic-viscoelastic correspondence principle, 77, 655, 657
ELSYM5 program, 4, 109, 135, 478
Empirical methods, 2, 245, 275, 505, 568
Emulsified asphalt mixtures, 493, 497
Environmental effect, 30, 494, 508, 527
Equivalent axle load factor, 244, 256, 262
Equivalent contact radius for dual tires, 159
Equivalent single axle load, 266, 452, 488, 490, 614
Equivalent single-axle radius, 256
Equivalent single wheel load, 245
equal contact pressure criterion, 254
equal tensile strain criterion, 253
equal vertical deflection criterion, 249
equal vertical stress criterion, 245
equivalent single-axle radius, 256
Erosion analysis, 547, 557
EXPEAR program, 2, 426, 430, 438
Expectation, 442, 467
Expenditure stream diagram, 708
Expert system, 415, 424, 426

F

Failure criteria, 3, 28, 33, 34, 316
AI, 98, 260, 316, 488
PCA, 212
Shell, 98, 260
University of Nottingham, 98, 260
Falling weight deflectometer, 120, 413
Faulting, 378, 380, 431, 539, 726
Fatigue adjustment factor, 632, 634
Fatigue cracking, 3, 4, 6, 34, 35, 369, 427, 479, 487, 545, 607, 723, 725
Fatigue of bituminous mixtures, 309, 315
Fatigue of concrete, 7, 212, 316
Field calibration, 321
Field-molded sealants, 178
Filter criteria, 344, 346, 350
Fine-grained soils, 287, 289
nonlinear coefficients, 102
universal model, 720
Finite element method, 4, 7, 193, 478
Flexible pavements
asphalt grade and viscosity, 492
design methods, 1, 472, 487, 505
first pavement, 1
full depth, 10
minimum thickness, 519
pavement types, 8
Flexibility matrix, 188
Flexible plate, 50
Foundations
layer foundation, 188
liquid foundation, 6, 186
relationships between E and k-value, 189, 573, 574
rigid foundation at shallow depth, 576
solid foundation, 6, 187
Fourier transform, 668
Freezing index, 31, 432, 538, 541, 543
Frost action, 13, 358, 371, 374, 475, 508
Frost penetration, 31
Full-depth asphalt pavement, 10, 495

G

General pavement studies, 26
Generalized model, 79

Downloaded From : www.EasyEngineering.net

Downloaded From : www.EasyEngineering.net

Geotextiles, 346
Goldbeck's formula, 6, 154
Granular materials, 284
  nonlinear coefficients K^1 and K^2, 101, 492, 495, 517
  universal model, 720
Groundwater inflow, 354
Groundwater table, 33
Group index, 2, 292
Growth factor, 268, 270, 271, 274

H

Haversine function, 88, 280, 322
Hazen's formula, 343
Homogeneous half space, 45
  approximate method, 54
  nonlinear mass, 52
  solutions at axis of symmetry, 50
    solutions by charts, 45
  surface deflection under rigid plate, 51
Horizontal principal strain, 64, 97
Hot mix asphalt
  binder course, 9
  definition, 3
  dynamic modulus, 297, 309, 492
  fatigue, 309, 315
  minimum thickness, 519
  minimum thickness over emulsified asphalt base, 502
  overlay, 226, 609, 616

I

ILL-BACK program, 419, 437, 649
ILLI-PAVE algorithms, 112
ILLI-PAVE program, 4, 105, 122, 478
  stress modification, 111
ILLI-SLAB program, 7, 220, 534, 543
ILLISLAB94 program, 224
ILLISLAB2000 program, 224
Incremental static test, 322
Indirect tension test, 283, 285
Influence charts
  edge loading, 163
  interior loading, 160
Initial curing, 200
Interface deflection, 61
Interior loading, 156, 225
Internal rate of return, 704
International roughness index, 399, 437, 697, 707, 724, 726
  related to PSI, 400
ISTEA, 25
Iterative method, 53, 198

J

Joint and crack adjustment factor, 632, 633
Joint deterioration, 36, 541
Joint opening, 167, 432, 541
Jointed plain concrete pavements, 14
Jointed reinforced concrete pavements, 15
Joints for concrete pavement
  construction joint, 179
  contraction joint, 176
  expansion joint, 179
  joint spacing, 15, 434, 618
  longitudinal joint, 179, 435
  recommended maximum spacing, 15, 434
  sealant, 177, 435
Jones' tables, 72, 545
JSLAB program, 7, 220, 545, 621, 650

K

Kelvin model, 78
KENLAYER program, 47, 56, 88, 94, 122, 635, 662
  comparison with available solutions, 109
  comparison with KENSLABS, 226
  damage analysis, 97, 107, 261
  effect of layer modulus, 132
  effect of layer thickness, 131
  general features, 106
  loads, 109
  materials, 107
  nonlinear analysis, 137
  number of period per year, 108
  three methods for nonlinear analysis, 105
  sensitivity analysis, 130

Downloaded From : www.EasyEngineering.net

Downloaded From : www.EasyEngineering.net

KENPAVE program
installation, 677
main screen, 678
LAYERINP, 679
SLABSINP, 681
KENSLABS program, 186, 192
capabilities, 206
comparison with available solutions, 213
comparison with KENLAYER, 226
damage analysis, 212, 264
effect of mesh size, 226, 228, 229
evaluation of contact, 209
factors affecting corner deflection, 232
factors affecting edge stress, 230
limitations, 208
numbering of slabs, nodes, and joints, 209
sensitivity analysis, 226, 231, 234
KENTRACK program, 39
Keyed joints, 180, 593
k-value, *see* Modulus of subgrade reaction

L

Lane-at-a-time construction, 180
Lane distribution factor, 271, 272, 273
Lane/should dropoff or heave, 371, 380
Laplace transform, 77, 658
Layer coefficients, *see* Structural layer coefficients
Layered systems, 57
four-layer system,134, 139
multilayer system, 94
nonlinear layer system, 110
three-layer system, 70, 130, 137
two-layer system, 57
viscoelastic layer system, 120
Layered theory, 245, 672, 637
LAYERINP program, 94, 106, 679
Lean concrete subbase, 563, 566
LGRAPH, 106
Life-cycle costs, 37, 703
Limiting deflection methods, 2
Limiting shear failure methods, 2
Liquid foundation, *see* Foundations
Loading waveform, 279
Load safety factor, 551
Load transfer, 170, 222, 378, 435, 581, 639
Logarithmic spirals, 2
Log normal distribution, 451, 470, 486
Longitudinal and transverse cracking, 371, 380
Longitudinal drain, 338, 339, 435
Low-temperature cracking, 35, 428, 483, 683, 724
LTPP, 25, 321

M

Manning's formula, 364
Marshall test, 294
Material characterization, 33, 279, 719
Maxwell model, 78
Mean monthly air temperature, 493
Mean texture depth, 405
Mechanical models, 77
Mechanistic-empirical methods, 3, 30, 33, 34, 37, 472, 533, 607
Meltwater from ice lenses, 355
Method of successive residuals, 662
MFPDS program, 114
MICH-PAVE program, 4, 35, 105, 109, 114, 122, 478
DOS versus Windows, 115
linear analysis, 114
nonlinear analysis, 117
Modulus of dowel support, 173
Modulus of rigidity, 191
Modulus of rupture, 316, 330, 462, 548, 581
related to compressive strength 329
related to modulus of elasticity, 330
Modulus of subgrade reaction, 326, 331, 431, 539, 549, 564, 573
loss of subgrade support, 578
related to other soil properties, 328
related to resilient modulus 573, 574
related to soil types, 564
relationship between static and dynamic *k*-values, 640
MODULUS program, 416
Mohr-Coulomb theory, 104
Moisture warping, 153, 433, 536

Downloaded From : www.EasyEngineering.net

Downloaded From : www.EasyEngineering.net

Monte Carlo method, 722
Moving loads, 87, 120
Multidepth deflectometer, 423
Multiple axles, 98, 261, 274
Multiple slabs, 196
Multiple wheels, 109

N

Net present value, 704
Nomographs
  continuous reinforced concrete pavement, 586
  fatigue of bituminous mixtures, 315
  flexible pavement, 513
  rigid pavement, 571
  stiffness modulus of bitumen, 303
  stiffness modulus of bituminous mixtures, 304
Nondestructive deflection testing, 410, 437, 607, 620, 632
Nonlinear coefficients K^1 and K^2, 101
Nonlinear analysis, 100
  stress adjustment, 103
  stress point, 103
Nonlinear materials
  fine-grained soils, 101
  granular materials, 100, 124, 492, 496, 517
Normal distribution, 448, 512
NPPDB, 25
Number of load repetitions, 27

O

Octahedral shear stress, 720
Overlays
  AC overlay of AC pavement, 600, 609, 644
  AC overlay of AC/PCC pavement, 647
  AC overlay of fractured PCC pavement, 645
  AC overlay of PCC pavement, 600, 616, 646
  bonded PCC overlay of PCC or AC/PCC pavement, 605, 625, 648
  design methodology, 605, 643
  minimum thickness, 616, 624
  PCC overlay of AC pavement, 604, 649
  unbonded PCC overlay of PCC or AC/PCC pavement, 604, 621, 648
  unit delineation, 628

P

Pavement condition survey, 621, 696
Pavement management systems, 36, 694
  data and software, 711
  life-cycle cost analysis, 703
  network level, 694, 695
  project level, 695, 700
Pavement performance, 368, 433, 424, 433, 438, 591
Pavement temperature, 123, 682
PCA
  failure criteria, 212
  overlay design, 620
  rigid pavement design, 545
  simplified design procedure, 562
PDMAP program, 4, 35, 427, 428
PEARDARP program, 429, 538
Peattie's charts, 74
Penetration index, 301, 314
Percent normalized gradient, 405
Performance period, 458, 507, 706
Performance prediction, 453, 458
Permanent deformation, *see* Rutting
Permanent deformation parameters, 316, 683
Permeability of aggregates, 343, 344
  open-graded bases and filters, 341
  graded aggregates, 342
  effect of fines, 342
  asphalt-treated bases, 344
Plate loading test, 327
Poisson ratios for different materials, 329
Portland cement concrete
  Compressive strength, 330
  elastic modulus, 330, 580, 621
  fatigue, 316
  indirect tensile strength, 330, 583, 621
  modulus of rupture, 330, 548, 581, 621
  shrinkage, 584
  strength gain, 725
  thermal coefficient, 584

Downloaded From : www.EasyEngineering.net

Downloaded From : www.EasyEngineering.net

Portland cement concrete pavement, *see* Rigid pavement
Precipitation, 33, 352
Predictive models, 427, 535, 537, 539, 541, 543
Preformed sealant, 178, 435
Present serviceability index, 5, 37, 389, 463, 509
  related to IRI, 400
Present serviceability rating, 389, 430, 707
Prestressed concrete pavement, 16
  first pavement, 16
Prime coat, 9
Principal stresses and strains, 97
Probabilistic method, 8, 451, 466, 721
Profilometer, 391, 398
PRORUT, 398
Pumping, 8, 12, 25, 36, 373, 380, 537, 547
Punchout, *see* Edge punchout

R

Radius of relative stiffness, 151, 217
Railroad trackbeds, 39
Reflection cracking, 17, 370, 436, 567
Regression methods, 2
Relative damage, 512, 577
Reliability, 5, 36, 455, 459, 507, 642, 721
  suggested levels, 508
Remaining life, 503, 607, 640
Representative rebound deflection, 612
Resilient modulus
  asphalt-treated bases, 295, 296
  cement-treated bases, 295, 296
  fine-grained soils, 287
  granular materials, 284
  hot mix asphalt, 289, 293, 294
  laboratory modulus versus backcalculated modulus, 424
  loading waveform 279
  subbases, 295, 296
  subgrade soils, 290, 293
  untreated bases, 296
Resolution of stresses into *x* and *y* components, 96
Response-type road roughness meter, 398, 399, 437
Riding number, 399
Rigid pavements, 11
  design methods, 533, 545, 568
  concrete stress due to volume change, 165
  corner loading, 154, 222
  edge loading, 157, 220
  effect of design feature on performance, 433
  first pavement, 5
  interior loading, 156
  steel stress due to volume change, 167
  temperature curling, 222, 414, 433
  types, 14
  use of base course, 12
Rigid plate, 51
RISC program, 7
Road Surface Analyzer, 403
Road rater, 412
Road tests, 1, 2, 19, 35
  AASHO Road Test, 23, 36, 100, 152, 153, 204
  Arlington Road Test, 152
  Bates Road Test, 6, 7
  Maryland Road Test, 19, 204
  WASHO Road Test, 21
Rolling Dynamic Deflectometer, 412
Rosenblueth method, 466
Roughness, 398, 697, 724, 726
Roughness coefficients for underdrains, 364
Rut depth, 34, 35, 98, 325, 392, 480
Rutting, 4, 24, 35, 98, 374, 428, 480, 488, 608, 723
  criteria by various agencies, 481
R-value, 290, 293, 492
  related to resilient modulus, 293

S

SAPIV program, 4
Sawing and sealing of joints, 603
SCEPTRE program, 425, 438
Seal coat, 9
Sensitivity analysis, 130, 226, 710
Separation layer, 338
Shell nomographs, 301, 315

Downloaded From : www.EasyEngineering.net

Downloaded From : www.EasyEngineering.net

Shoulder design, 522, 592
Simultaneous equations, 198
Skid number, 402
  recommended minimum skid number, 406
  related to BPN, 404
  related to concrete finishing methods, 408
Skid resistance, 406
SLABSINP program, 206, 681
Slab-subgrade contact, 201, 578
  full contact, 202
  modifications for solid and layer foundations, 206
  partial contact with initial gaps, 204
  partial contact without initial gaps, 202
Slope variance, 391, 401
Soil classification systems, 2
Solid foundation, *see* Foundation
Spalling, 36, 382, 432
Spring constants of dowel bars, 196
Stage construction, 503, 520
Standard deviation, 444, 462, 463
Standard normal deviate, 450, 512
Steel reinforcements
  allowable stress, 168, 586
  weights and dimensions, 168
  welded wire fabric, 169
Stiffness matrix
  foundation, 188, 199
  joint, 194
  multiple slabs, 196
  slab, 193
Stiffness modulus, *see* Dynamic modulus
Stopping distance number, 403
Strategic Highway Research Program, 24, 682
Stress adjustment or modification, 105, 111
Stresses due to friction, 164
Stress invariant, 53, 100, 517
Stress point, 103, 416
Structural deficiency, 629
Structural layer coefficient, 294, 515, 631
  related to resilient modulus, 516
Structural models, 478, 533
Structural number, 515, 453
Subbase, 10, 295, 517
Subdrainage, 351, 435, 538
Subgrade, 10, 290, 460, 490, 494, 512, 642
Superpave, 25, 682
  aggregate requirements, 684
  asphalt binder grading system, 682
  laboratory compaction, 689
  mix design, 689
  types of tests, 683
Superposition of wheel loads, 95
Surface friction, 401, 697
Surface infiltration, 352
Surface or wearing course, 9
Surface texture, 403
Swell, 14, 374, 384, 508

T

Tack coat, 9
Taylor's expansion, 447, 467
Temperature adjusting factor, 612, 613, 636
Temperature curling, 199, 222
Temperature differentials, 152, 619
Temperature effects, 30
Tensile strain
  horizontal principal versus overall principal, 97
  under dual-tandem wheels, 67
  under dual wheels, 65
  under single wheel, 64
Texas triaxial classification, 292
Thermal cracking, *see* Low-temperature cracking
Tie bars, 170
Tied concrete shoulder, 435, 592
Time-temperature superposition, 84, 120
Tire contact area, 28
Traffic analysis, 245, 488, 549, 642, 717
Traffic prediction, 452, 457
Traffic prediction for shoulder design, 524
Transverse slope of highway cross section, 337
Triaxial compression test, 283, 284
Truck factor, 268, 269

U

User costs, 704, 707
Unbonded slabs, 191
Unconfined compressive strength, 102

Downloaded From : www.EasyEngineering.net

Downloaded From : www.EasyEngineering.net

V

Variance, 443, 448, 460, 465
percentage distribution, 466
Vehicle speed, 30
Vertical surface displacement, 48, 60
Vertical interface displacement, 61
Vertical stress, 46, 58
VESYS program, 5, 88, 99, 109, 318, 322, 452, 478, 481, 482, 486
Viscoelastic materials, 77
Viscoelastic solutions, 76
Visual survey, 630

W

Water bleeding, 373, 380
WESDEF program, 418
WESLAYER program, 7
WESLIQID program, 7
Westergaard's analysis, 6
Wire fabric, 168

Z

Zero-maintenance or premium pavements, 18, 153, 316

Downloaded From : www.EasyEngineering.net